USGS
science for a changing world

Prepared in cooperation with the
Hampton Roads Planning District Commission,
Virginia Department of Environmental Quality, and
National Aeronautics and Space Administration Langley Research Center

Studies of the Chesapeake Bay Impact Structure—The USGS-NASA Langley Corehole, Hampton, Virginia, and Related Coreholes and Geophysical Surveys

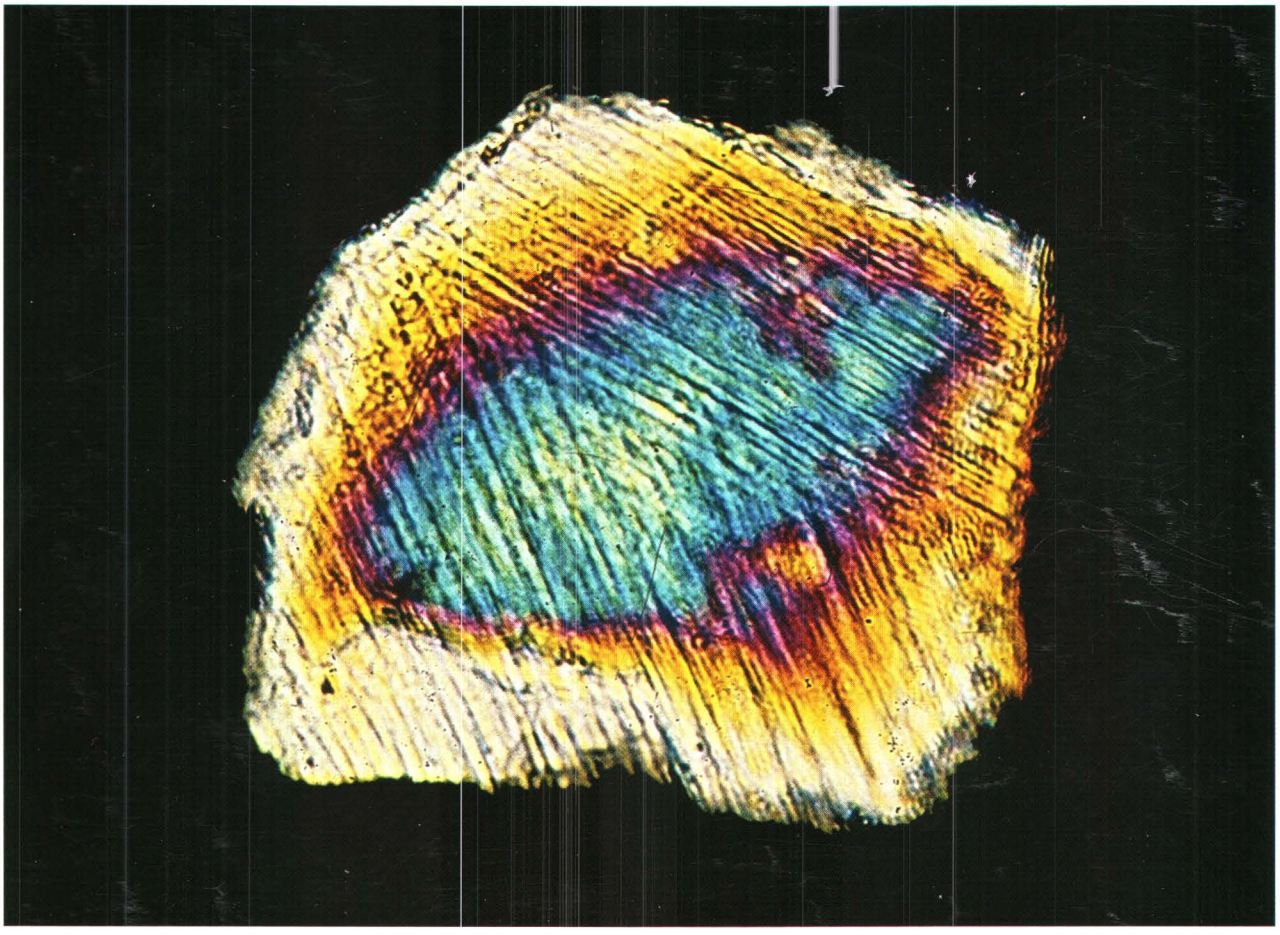

Professional Paper 1688

U.S. Department of the Interior
U.S. Geological Survey

Core samples of the Exmore beds from the USGS-NASA Langley corehole from depths of 266.3 to 262.8 meters (873.53 to 862.15 feet). A variety of sediment and rock clasts are suspended in a matrix of muddy quartz-glauconite sand. The Exmore beds are interpreted as debris-flow deposits produced by ocean resurge into the crater. See chapter C of this volume, figure C10*A*. Photograph by David S. Powars, U.S. Geological Survey.

Front cover. This quartz grain from the matrix of the Exmore beds in the USGS-NASA Langley core contains two sets of shock-induced planar deformation features, providing unequivocal evidence for the impact of an asteroid or comet nucleus near the mouth of the present Chesapeake Bay. The grain is 0.13 millimeter (0.005 inch) in diameter and is from a depth of 250.1 meters (820.6 feet); it is also shown in chapter E of this volume (figure E2*E*). Photomicrograph (cross-polarized light) by Glen A. Izett (College of William and Mary and Emeritus, U.S. Geological Survey).

Back cover. Conceptual model for sequential stages in the formation of the Chesapeake Bay impact crater as presented in chapter A of this volume. Schematic cross sections show the western half of the crater along a west-to-east profile. From figureA7, which has the complete caption and discussion.

Studies of the Chesapeake Bay Impact Structure—The USGS-NASA Langley Corehole, Hampton, Virginia, and Related Coreholes and Geophysical Surveys

Edited by J. Wright Horton, Jr., David S. Powars, and Gregory S. Gohn

Prepared in cooperation with the
Hampton Roads Planning District Commission,
Virginia Department of Environmental Quality, and
National Aeronautics and Space Administration Langley Research Center

This volume is published as chapters A through K.
The chapters are also available separately on the World Wide Web.

Professional Paper 1688

U.S. Department of the Interior
U.S. Geological Survey

U.S. Department of the Interior
Gale A. Norton, Secretary

U.S. Geological Survey
P. Patrick Leahy, Acting Director

U.S. Geological Survey, Reston, Virginia: 2005

For product and ordering information:
World Wide Web: http://www.usgs.gov/pubprod
Telephone: 1–888–ASK–USGS

For more information on the USGS—the Federal source for science about the Earth,
its natural and living resources, natural hazards, and the environment:
World Wide Web: http://www.usgs.gov
Telephone: 1–888–ASK–USGS

Suggested citation:
Edwards, L.E., Barron, J.A., Bukry, David, Bybell, L.M., Cronin, T.M., Poag, C.W., Weems, R.E., and Wingard, G.L., 2005, Paleontology of the upper Eocene to Quaternary postimpact section in the USGS-NASA Langley core, Hampton, Virginia, chap. H *of* Horton, J.W., Jr., Powars, D.S., and Gohn, G.S., eds., Studies of the Chesapeake Bay impact structure—The USGS-NASA Langley corehole, Hampton, Virginia, and related coreholes and geophysical surveys: U.S. Geological Survey Professional Paper 1688, p. H1–H47, 9 fossil plates, 2 oversize figures. (Also available online at http://pubs.usgs.gov/pp/2005/1688/ak/)

Library of Congress Cataloging-in-Publication Data

Studies of the Chesapeake Bay impact structure: the USGS-NASA Langley corehole, Hampton, Virginia, and related coreholes and geophysical surveys / edited by J. Wright Horton, Jr., David S. Powars, and Gregory S. Gohn; prepared in cooperation with the Hampton Roads Planning District Commission, Virginia Department of Environmental Quality, and National Aeronautics and Space Administration Langley Research Center.
p. cm. – (U.S. Geological Survey professional paper ; 1688)
Includes bibliographical references.
ISBN 0-607-98598-4
1. Meteorite craters–Chesapeake Bay (Md. and Va.). 2. Geology, Structural–Virginia. 3. Geology, Stratigraphic–Tertiary. 4. Geology, Stratigraphic–Quaternary. I. Horton, J. Wright, Jr. II. Powars, David S. III. Gohn, Gregory S. IV. Hampton Roads Planning District Commission (Va.). V. Virginia. Dept. of Environmental Quality. VI. Langley Research Center. VII. Series.
QE613.5.C48S78 2005
551.3'97'0916347–dc22

2005050400

Volume Contents

[Letters designate the chapters]

Conversion Factors and Datums

Multiply	By	To obtain
	Length	
micrometer (μm)	0.00003937	inch (in.)
millimeter (mm)	0.03937	inch (in.)
centimeter (cm)	0.3937	inch (in.)
meter (m)	3.281	foot (ft)
kilometer (km)	0.6214	mile (mi)
	Area	
square centimeter (cm^2)	0.1550	square inch (in^2)
	Volume	
milliliter (mL)	0.0338	fluid ounce
liter (L)	0.2642	gallon
	Mass	
milligram (mg)	0.00003527	ounce avoirdupois
gram (g)	0.03527	ounce avoirdupois
kilogram (kg)	2.205	pound avoirdupois

Temperature in degrees Celsius (°C) may be converted to degrees Fahrenheit (°F) as follows:

$$°F = (1.8 \times °C) + 32$$

Vertical coordinate information is referenced to the North American Vertical Datum of 1988 (NAVD 88).

Horizontal coordinate information is referenced to the North American Datum of 1983 (NAD 83).

Equipment used to drill the USGS-NASA Langley corehole at the NASA Langley Research Center in Hampton, Va., in 2000. Photograph by E. Randolph McFarland, U.S. Geological Survey.

Studies of the Chesapeake Bay Impact Structure—Introduction and Discussion

By J. Wright Horton, Jr., David S. Powars, and Gregory S. Gohn

Chapter A of
Studies of the Chesapeake Bay Impact Structure—The USGS-NASA Langley Corehole, Hampton, Virginia, and Related Coreholes and Geophysical Surveys

Edited by J. Wright Horton, Jr., David S. Powars, and Gregory S. Gohn

Prepared in cooperation with the
Hampton Roads Planning District Commission,
Virginia Department of Environmental Quality, and
National Aeronautics and Space Administration Langley Research Center

Professional Paper 1688

U.S. Department of the Interior
U.S. Geological Survey

Contents

Figures

Table

Studies of the Chesapeake Bay Impact Structure—Introduction and Discussion

By J. Wright Horton, Jr.,[1] David S. Powars,[1] and Gregory S. Gohn[1]

Abstract

The late Eocene Chesapeake Bay impact structure on the Atlantic margin of Virginia is the largest known impact crater in the United States, and it may be the Earth's best preserved example of a large impact crater that formed on a predominantly siliciclastic continental shelf. The 85-kilometer-wide (53-mile-wide) crater also coincides with a region of saline ground water. It has a profound influence on ground-water quality and flow in an area of urban growth.

The USGS-NASA Langley corehole at Hampton, Va., is the first in a series of new coreholes being drilled in the crater, and it is the first corehole to penetrate the entire crater-fill section and uppermost crystalline basement rock. The Langley corehole is located in the southwestern part of the crater's annular trough. A comprehensive effort to understand the crater's materials, architecture, geologic history, and formative processes, as well as its influence on ground water, includes the drilling of coreholes accompanied by high-resolution seismic-reflection and seismic-refraction surveys, audio-magnetotelluric surveys, and related multidisciplinary research.

The studies of the core presented in this volume provide detailed information on the outer part of the crater, including the crystalline basement, the overlying impact-modified and impact-generated sediments (physical geology, paleontology, shocked minerals, and crystalline ejecta), and the upper Eocene to Quaternary postimpact sedimentary section (stratigraphy, paleontology, and paleoenvironments).

The USGS-NASA Langley corehole has a total depth below land surface of 635.1 meters (m; 2,083.8 feet (ft)). The deepest unit in the corehole is the Neoproterozoic Langley Granite. The top of this granite at 626.3 m (2,054.7 ft) depth is overlain by 390.6 m (1,281.6 ft) of impact-modified and impact-generated siliciclastic sediments. These crater-fill materials are preserved beneath a 235.6-m-thick (773.12-ft-thick) blanket of postimpact sediments.

A high-resolution seismic-reflection and seismic-refraction profile that crosses the Langley drill site is tied to the core by borehole geophysical logs, and it reveals the details of extensional collapse structures in the western annular trough. Electrical cross sections based on audio-magnetotelluric (AMT) soundings image a nearly vertical zone of high resistivity at the outer margin of the annular trough, possibly indicating fresh ground water at that location, and they show impedance trends that match the curvature of the structure. They also image the subsurface contact between conductive sediments and resistive crystalline basement, showing that the depth to crystalline basement is relatively constant in the western part of the annular trough.

Chemical and isotopic data indicate that saline ground water of the Virginia inland saltwater wedge or bulge is a mixture of freshwater and seawater, and evidence for a mixing zone at the crater's outer margin supports the concept of differential flushing of residual seawater to create the bulge. Ground-water brine in the central part of the crater was produced by evaporation, and brine production from the heat of the impact is at least theoretically possible.

Introduction

This chapter begins with an overview of the Chesapeake Bay impact structure, including its geologic setting, the history of previous work, and the status of current research. This overview provides an introduction to more detailed studies reported in the volume. These reports contain data and interpretations from the USGS-NASA Langley corehole at Hampton, Va., which is the first corehole to basement in the structure, and from related coreholes and geophysical surveys.

This chapter also explains some style conventions used in this volume. Discussions highlight some important results of each chapter, as well as scientific results and issues that transcend the scope of individual chapters.

The impact event.—Although our understanding of the impact event is likely to improve as investigations continue, researchers currently agree on the following scenario. The

[1]U.S. Geological Survey, Reston, VA 20192.

impact event occurred 35 million to 36 million years ago, when the area that became eastern Virginia was covered by the Atlantic Ocean. An asteroid or comet fragment about 3 kilometers (km; about 2 miles (mi)) in diameter collided with Earth at a velocity on the order of 20 km (12 mi) per second (Crawford, 2002). It blasted through the shallow ocean, wet sediments, and rocks to leave a cavity about 38 km (24 mi) wide in the sea floor.

This explosion, approximately 100 times greater than a detonation of Earth's entire nuclear arsenal (Poag, 2002d), vaporized the projectile and billions of tons of water, sediment, and rock (Edwards and Powars, 2003). Some rocks and sediments melted instantly, and droplets solidified in the air before raining down as tektites as far away as Texas. The shock wave left extreme deformation features similar to those caused by nuclear explosions. Enormous volumes of water, sediment, and rock shot ballistically outward and upward to high altitudes, leaving a giant short-lived cavity in the water in addition to the hole in the seabed.

Rebound of the crater floor was followed by gravitational collapse; the inward slumping and faulting of poorly consolidated, wet sediments extended the crater to a width of about 85 km (53 mi). Ejected material fell back to Earth, and the ocean water surged violently back into the open cavity, carrying a chaotic mixture of debris ranging from damaged microorganisms to house-size blocks (Edwards and Powars, 2003). Tsunamis spread outward in all directions. Fallout particles settled on the seabed, and a thick pile of sediments accumulated on top of the crater, preserving the evidence beneath the present mouth of Chesapeake Bay until the human needs for drinkable ground water led to its discovery in recent decades (Powars and Bruce, 1999).

The impact crater location and name.—The Chesapeake Bay impact crater underlies the southern part of Chesapeake Bay, its surrounding peninsulas, and a small part of the western Atlantic Ocean (fig. A1). This buried, late Eocene complex crater is the largest known impact crater in the United States and the seventh largest known on Earth (Earth Impact Database, 2003). It may be the Earth's best preserved and best studied example of a large impact structure formed in a predominantly siliciclastic continental-shelf environment. The Chesapeake Bay impact crater coincides closely with an unusual region of saline ground water originally called the Virginia inland saltwater wedge (Sanford, 1913). The impact structure, therefore, has a profound influence on ground-water flow and quality, including salinity, across one of the fastest growing urban centers on the east coast of North America that increasingly depends on ground-water resources (Hampton Roads Planning District Commission, 1999).

In this volume, the terms "Chesapeake Bay impact crater" and "Chesapeake Bay crater" refer to the actual crater depression, whereas "Chesapeake Bay impact structure" is used in a broader sense to include outlying impact-related structures, such as faults in the outer fracture zone (fig. A1). The terms can be used interchangeably where this distinction is irrelevant to the context.

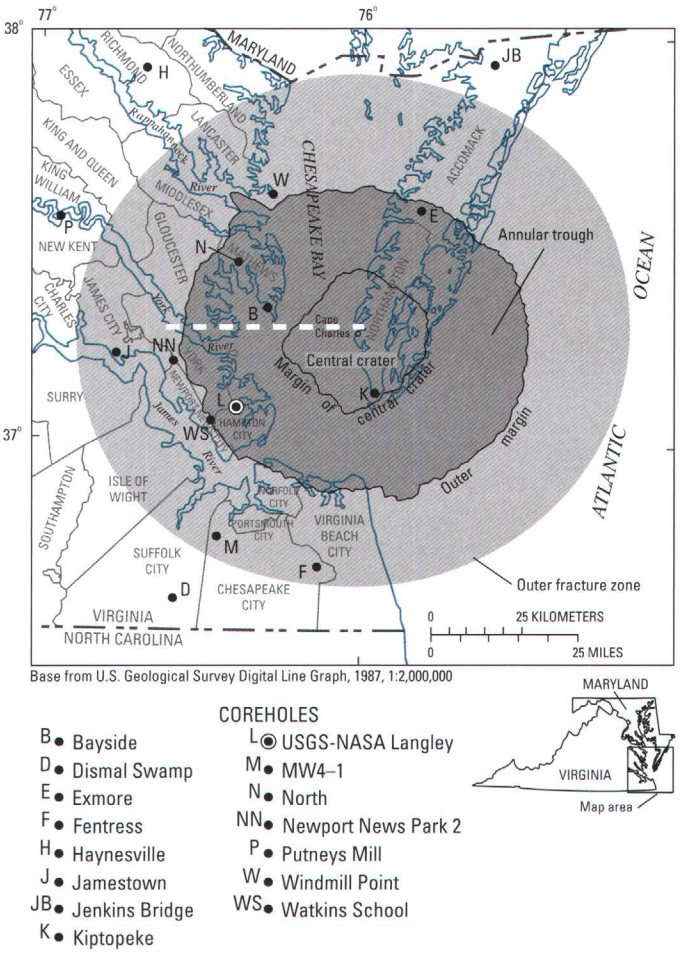

Figure A1. Regional map showing the location of the Chesapeake Bay impact structure, the USGS-NASA Langley corehole at Hampton, Va., and some other coreholes in southeastern Virginia. White dashed line indicates approximate location of schematic cross sections in figure A7. Locations of the central crater and outer margin are from Powars and Bruce (1999). The extent of the outer fracture zone (light gray) is based on Powars (2000) and Johnson and others (2001); the eastern part is speculative. Illustration modified from Powars, Johnson, and others (2002) and Edwards and Powars (2003).

The Chesapeake Bay Impact Crater Project.—The Chesapeake Bay Impact Crater Project is a multidisciplinary research collaboration begun in 2000 to understand the physical characteristics, geologic history, formative processes, and hydrologic implications of this buried structure. The project collaborators are described in the "Acknowledgments" section.

Most of the chapters in this Professional Paper discuss studies of samples from the USGS-NASA Langley corehole (fig. A1) or geophysical studies in the vicinity. This corehole was the first of four coreholes drilled for this project during the years 2000 through 2002, and it was the first corehole to penetrate the entire sedimentary section and reach uppermost crys-

talline basement rock within the crater's annular trough (fig. A1). Related studies of samples from additional coreholes, although mentioned in several chapters, are still in progress.

The four coreholes drilled for the Chesapeake Bay Impact Crater Project during 2000 through 2002 are listed below and are plotted in figures A1 and A2:

1. USGS Bayside corehole, in the western annular trough on the Middle Peninsula at Bayside, Va. (728.5 m, 2,390.2 ft total depth, year 2001)
2. USGS-NASA Langley corehole, in the western annular trough in Hampton, Va. (635.1 m, 2,083.8 ft total depth, year 2000)
3. USGS North corehole, in the western annular trough on the Middle Peninsula, Va. (435.1 m, 1,427.5 ft total depth, year 2001)
4. USGS Dorothy R. Watkins Elementary School corehole, just outside the outer margin in Newport News, Va. (300.3 m, 985.3 ft total depth, year 2002)

The Bayside, Langley, North, and Watkins School coreholes are located approximately 8, 19, 24, and 27 km (5, 12, 15, and 17 mi), respectively, outside the central crater (fig. A2). All four cores penetrated impact-generated sediments of the Exmore beds, and the cores from Bayside and Langley sampled complete postimpact and crater sections down to Neoproterozoic granites of a peri-Gondwanan basement terrane (Horton and others, this volume, chap. B). The short names "Bayside corehole," "Langley corehole," "North corehole," and "Watkins School corehole" are used in this volume.

The USGS-NASA Langley corehole is described in online drilling reports (Gohn, Clark, and others, 2001; Powars, Bruce, and others, 2001). The Langley corehole is located at lat 37°05'44.28" N., long 76°23'08.96" W. (North American Datum of 1927), at a ground-surface altitude of 2.4 m (7.9 ft) above the North American Vertical Datum of 1988. The corehole was drilled at the National Aeronautics and Space Administration (NASA) Langley Research Center in Hampton, Va. Drilling by the U.S. Geological Survey (USGS) and cooperators (see "Acknowledgments") took place in July–October 2000, and geophysical logs were run in the hole on three occasions.

Measurements in this volume.—Geophysical, paleontologic, and petrologic studies routinely use metric units for physical parameters. However, coastal plain stratigraphic and hydrologic studies, as well as the drilling industry, routinely use feet and fractions thereof as length units for stratigraphic thickness and depth. Borehole geophysical logs typically measure depth in feet, although unit systems for the measured parameters vary. To accommodate this mixture, this volume uses metric units for all measurements, with the following exceptions. Stratigraphic positions and thicknesses and general references to depths in cores and coreholes are made in meters or decimal fractions of meters with equivalent values in feet or decimal fractions of feet listed in parentheses, as in the example 73.3 m (240.6 ft). Similarly, horizontal distances are given in kilometers or meters with miles or feet in parentheses, as in the example 11.7 km (7.3 mi). Data collected in metric units are given in the text only in metric units, whereas data collected in feet and inches (in.) are given using both systems of measurement, as in the example 25 cm (10 in.). Conversion factors are given after the volume table of contents.

Previous Work

Sanford (1913) was the first to recognize and name the Virginia inland saltwater wedge, and D.J. Cederstrom's reports included a more comprehensive delineation of this feature and attributed it to differential flushing of seawater related to an Eocene basin fill north of the James River. Cederstrom conducted a series of comprehensive regional hydrogeologic investigations of the York-James Peninsula (Cederstrom, 1945a, 1957) and related studies in the southeastern Virginia Coastal Plain (Cederstrom, 1945b,c), providing lithologic logs of wells, biostratigraphic data analyzed by J.A. Cushman (USGS), and water-quality data (Cederstrom, 1943, 1946).

Cederstrom's (1957) subsurface Mattaponi Formation (term abandoned by Ward, 1984) included what we now recognize as crater-fill deposits (the Exmore beds), as well as additional undisturbed sediments outside the crater beneath most of the central to outer Virginia Coastal Plain (Powars and Bruce, 1999). Cederstrom proposed the "James River fault zone" to account for his interpretation of the erratic distribution and abrupt changes in thickness of strata. Knowledge of subsurface geology beneath the southeastern Virginia Coastal Plain was based mostly on water-well cuttings and geophysical logs until the late 1980s (Brown and others, 1972; Laczniak and Meng, 1988; Meng and Harsh, 1988), at which time the surficial deposits had already been mapped in considerable detail (Johnson and others, 1987, and references therein).

From 1986 to 1992, the analysis of samples from coreholes drilled by the USGS and the Virginia Department of Environmental Quality (VDEQ) significantly advanced the understanding of subsurface geology in southeastern Virginia (Powars and others, 1987, 1990, 1992; Poag and others, 1992). This work, combined with results of offshore drilling at Deep Sea Drilling Project Site 612, led to the initial recognition that an offshore layer of late Eocene impact ejecta (containing coesite, glass, and shocked quartz) had a likely source in the mid-Atlantic region (Bohor and others, 1988; Glass, 1989; Obradovich and others, 1989; Poag and others, 1991, 1992).

Subsequently, the analysis of marine seismic-reflection data, in the context of borehole data, revealed the existence of a large crater (Powars and others, 1993; Poag and others, 1994).

Figure A2. Map of southeastern Virginia showing locations of recently completed coreholes and geophysical surveys in relation to the Chesapeake Bay impact structure. AMT data are described by Pierce (this volume, chap. J), and seismic data collected near the Langley corehole are described by Catchings and others (this volume, chap. I). Seismic data (blue lines) collected on the Middle and Delmarva Peninsulas by the USGS in 2002 are being processed.

The seismic-reflection data were donated to the USGS by Texaco, Inc., and Exxon Exploration Co. in 1993 and 1994.

Structural and stratigraphic documentation of the Chesapeake Bay impact structure followed (Poag and Aubry, 1995; Koeberl and others, 1996, 2001; Poag, 1996, 1997, 2000; Poag, Hutchinson, and others, 1999; Poag, Plescia, and Molzer, 1999; Powars and Bruce, 1999; Powars, 2000). In 2000, the Virginia Museum of Natural History Foundation awarded the Thomas Jefferson Medal for Outstanding Contributions to Natural Science jointly to C.W. Poag (USGS), D.S. Powars (USGS), and T.S. Bruce (VDEQ) for their combined efforts to map, elucidate, and bring to public awareness the Chesapeake Bay impact structure.

Detailed, nontechnical accounts of the crater and its discovery are presented in Poag's (1999) book and Tennant's (2001) series of articles. Tennant's articles received the Walter Sullivan Award for Excellence in Science Journalism from the American Geophysical Union in 2002.

Significantly, until the crater was discovered, there was no satisfactory explanation for the anomalous saltwater wedge (Powars, Bruce, Poag, and Mixon, 1994; Powars and Bruce, 1999) or the region's stratigraphic and structural complexities (Powars and Bruce, 1999; Powars, 2000). The literature on the Chesapeake Bay impact structure has included interpretations based on conceptual models of craters and crater processes (Melosh, 1989), analogies to other craters, and interpretations of seismic-reflection profiles. Some of the fundamental concepts of this crater's morphology, internal structure, and formative processes, although widely cited, have remained untested hypotheses.

Accordingly, the Chesapeake Bay Impact Crater Project was undertaken in 2000 as a coordinated, multiagency effort to better understand the physical characteristics, geologic history, formative processes, hydrologic effects, and water-resource implications of this buried structure. Among specific interests are the structure's influence on ground-water quality and availability in southeastern Virginia and planetary-science implications for understanding impacts in a continental-shelf environment.

As described above, four deep coreholes for this project were completed in 2000 through 2002 (fig. A2). Various mineralogical, geochemical, isotopic, petrographic, sedimentologic, structural, and other methods of core-sample analysis are described in this volume. Nearly 23 km (14 mi) of land-based, high-resolution seismic-reflection and seismic-refraction surveys were conducted on the York-James Peninsula in 2001 and on the Middle Peninsula in 2002, both crossing the outer annular trough and outer margin, and some short surveys were conducted across parts of the central crater and its rim on the Delmarva Peninsula (fig. A2). Publications highlighting the recent studies include those by Catchings, Saulter, and others (2001), Gohn, Clark, and others (2001), Powars, Bruce, and others (2001), Poag (2002c), Poag, Plescia, and Molzer (2002), Edwards and Powars (2003), Sanford (2003), Self-Trail (2003), and Poag and others (2004); see also the abstracts listed in appendix A1.

The Chesapeake Bay Impact Structure

The following sections provide an overview of the Chesapeake Bay impact structure's complex form and structure, asymmetric layered marine target, and spatially associated land surface features. The term "target" is used for the area that was hit by the asteroid or comet fragment.

Form and Structure

An impact crater can be classified either as a *simple crater*, implying a bowl-shaped depression, or as a *complex crater*, implying a more complicated form that commonly includes a central uplift, a generally flat floor, and an inward collapse around its rim. Craters on Earth that exceed a diameter of about 4 km (2.5 mi) are complex craters (French, 1998).

The complex crater beneath Chesapeake Bay has an average width of about 85 km (53 mi), ranging from about 80 to 95 km (50 to 59 mi), and it contains an excavated central crater also termed the inner basin (Poag, Hutchinson, and others, 1999; Powars and Bruce, 1999; Powars, 2000). The central crater is variously interpreted on the basis of geophysical data to be approximately 30–38 km (19–24 mi) in diameter and subquadrate in shape (Powars and Bruce, 1999; Powars and others, 2003) or about 35–40 km (22–25 mi) in diameter and irregular in shape (Poag, Hutchinson, and others, 1999). Interpretations of seismic-reflection data suggest that the floor of the central crater penetrated crystalline basement about 1.3 km (0.8 mi) deeper than the lip of the outer rim and 1.6 km (1.0 mi) below sea level and that a mass of crystalline rock has a diameter of 15–20 km (9–12 mi) and rises as a central peak (uplift) about 900 m (2,950 ft) above the central crater floor (Poag, Plescia, and Molzer, 2002).

The central crater is surrounded by a flat-floored annular trough about 24 km (15 mi) in width (Poag and others, 1994). The margin of the central crater is characterized by uplifted basement rocks and has been interpreted by Poag, Plescia, and Molzer (2002) as an irregular peak ring. The outer margin of the annular trough is roughly circular and is characterized by a terraced zone of inwardly slumped fault blocks (Poag, 1996; Powars and Bruce, 1999). An outer escarpment ranges in relief from ~300 m (~1,000 ft) on the northwest to ~1,000 m (~3,300 ft) or more on the southeast (Poag, 1996; Poag, Hutchinson, and others, 1999). The outer margin of the annular trough is delineated by seismic profiles, which cross it at 61 locations (Poag, Plescia, and Molzer, 2002, p. 1083), and is generally considered to be the edge of the crater.

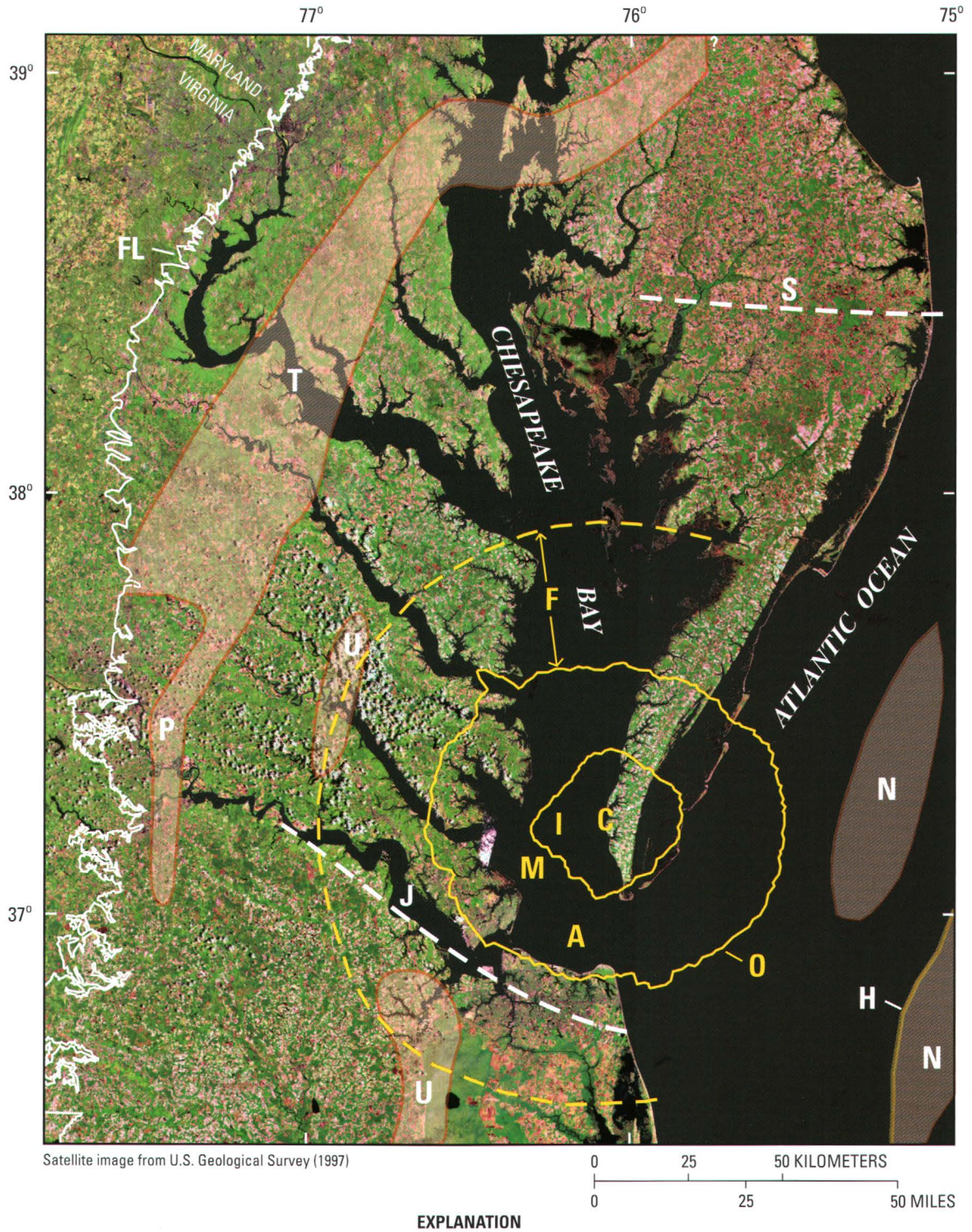

Figure A3. Satellite image of Chesapeake Bay showing location of the buried impact structure and nearby Mesozoic to Cenozoic tectonic features. Tectonic features modified from Powars and Bruce (1999, fig. 1) and Powars (2000, fig. 1).

The crater is surrounded by an outer fracture zone (F in fig. A3) about 35 km (22 mi) in width that contains discontinuous, concentric faults (Powars, 2000; Powars, Johnson, Edwards, and others, 2002) and radial faults (Johnson and others, 2000; Powars, 2000). All of the crater features are well preserved beneath a blanket of postimpact sediments that is about 150–400 m (490–1,300 ft) thick (Poag and others, 1994; Powars and Bruce, 1999).

The initial interpretations of crater structure and form relied on the seismic-reflection profiles donated to the USGS by Texaco and Exxon (Powars and others, 1993; Poag and others, 1994; Poag, 1996, 1997, 1999; Powars and Bruce, 1999). These profiles were generated from 48-fold, multichannel data collected in Chesapeake Bay and its estuaries by Teledyne Exploration in 1986. The USGS and the National Geographic Society generated more than 1,200 km (750 mi) of additional marine seismic-reflection profiles in 1996 from data acquired in a single-channel digital format using an air-gun seismic source. Poag, Hutchinson, and others (1999) based their interpretations of the crater architecture on these data as well as the earlier Texaco and Exxon data, noting that the single-channel seismic system did not resolve the basement surface in the deeper, eastern part of the crater.

Character of the Target

When the Chesapeake Bay impact structure formed on the Atlantic continental shelf of eastern North America, the marine target had three main components arranged as stacked layers: crystalline rocks, clastic sediments, and seawater. The uppermost target component consisted of seawater, estimated to have been in the range of 0–340 m (0–1,115 ft) deep at the impact site; water depths increased eastward across the structure as discussed below under the heading, "Water Depths—Impact and Postimpact."

The middle target component consisted of stratified, unconsolidated, mostly Lower and Upper Cretaceous siliciclastic deltaic sediments capped by thinner, Upper Cretaceous to lower Tertiary shallow-shelf marine sediments. These preimpact target sediments formed an eastward-thickening wedge ranging in thickness from about 400 m (about 1,300 ft) on the west side of the structure to about 1,500 m (about 4,900 ft) on the east side (Powars and others, 2003). Beneath the coastal plain north of the impact structure in Maryland, preimpact sediments dip toward the trough of the tectonic downwarp known as the Salisbury embayment (fig. A3), where they thicken to as much as 1,800 m (5,900 ft) about 90 km (60 mi) from the outer margin (Powars and Bruce, 1999). Preimpact Cretaceous and Cenozoic deformation of the target sediments is suggested by coastal plain subsurface mapping at the northern end of the Cape Fear-Norfolk structural block (J in fig. A3), south of the crater (Powars, 2000).

The lowermost target component consisted of crystalline metamorphic and igneous rocks ranging in age from Paleozoic to Proterozoic and similar in general character to rocks exposed in the Appalachian Piedmont (Daniels and Leo, 1985; Horton and others, 1991). The tectonic significance of this crystalline basement in the Chesapeake Bay target region has been controversial because of limited information, as exemplified by the wide range of interpretations as part of Laurentia (Sheridan and others, 1999), Gondwana (Lefort and Max, 1991), or an intervening volcanic arc (Horton and others, 1991).

The Paleozoic and Proterozoic rocks beneath the coastal plain and continental shelf, like those of the Piedmont, contain local rift basins of Triassic and Jurassic age. The outer margin of the Chesapeake Bay impact crater lies about 70 km (40 mi) east of the Petersburg-Studley rift basin, northeast of an unnamed basin, and just west of the offshore Norfolk rift basin (fig. A3). The crater lies west of a basement hinge zone, along which the upper surface of basement beneath sediments of the continental shelf deepens abruptly seaward from about 2 km (1 mi) to more than 8 km (5 mi) below sea level (Klitgord and others, 1988; Glover and Klitgord, 1995). The hinge zone is characterized by a series of half grabens bounded by seaward-dipping faults, tilted blocks bounded by landward-dipping faults, and associated sedimentary wedges, which are attributed to Jurassic rifting that preceded the opening of the Atlantic Ocean (Klitgord and others, 1988). Seismic-reflection interpretations in the region must distinguish extensional features associated with the late Eocene impact structure from those formed by the earlier rifting.

Land Surface Features

Although the Chesapeake Bay impact crater has no surface outcrops and can be sampled only by drilling, some features of the land surface are spatially associated with the buried crater. The surface geology at the USGS-NASA Langley corehole consists of shallow bay sediments that were deposited on an ancestral Chesapeake Bay floor when the late Pleistocene sea level was 5.5 m (18 ft) higher than the present sea level (Johnson, 1969). These bay-floor deposits form a flat land surface known as the Hampton flat (Coch, 1971), and their associated shoreline is the Big Bethel scarp shown in figure A4. The Big Bethel scarp is about 4 km (2.5 mi) west of the Langley drill site. The Hampton flat and similar surfaces are commonly described as terraces.

The geological literature characterizes the Virginia Coastal Plain geomorphology as a succession of terraces that descend in elevation toward the Chesapeake Bay, the Atlantic Ocean, and the large rivers (Oaks and Coch, 1973; Johnson and others, 1987; Mixon and others, 1989; Johnson and others, 2001). Each terrace is composed of a terrace tread (or flat) that terminates in a landward scarp. The terrace treads are aggradational surfaces that formed by fluvial-estuarine, bay, and shallow-marine depositional processes (Johnson, 1969; Johnson and others, 1987, 2001). The valley-facing scarps formed by fluvial and estuarine erosion, and the coast-facing scarps formed by shoreline erosion.

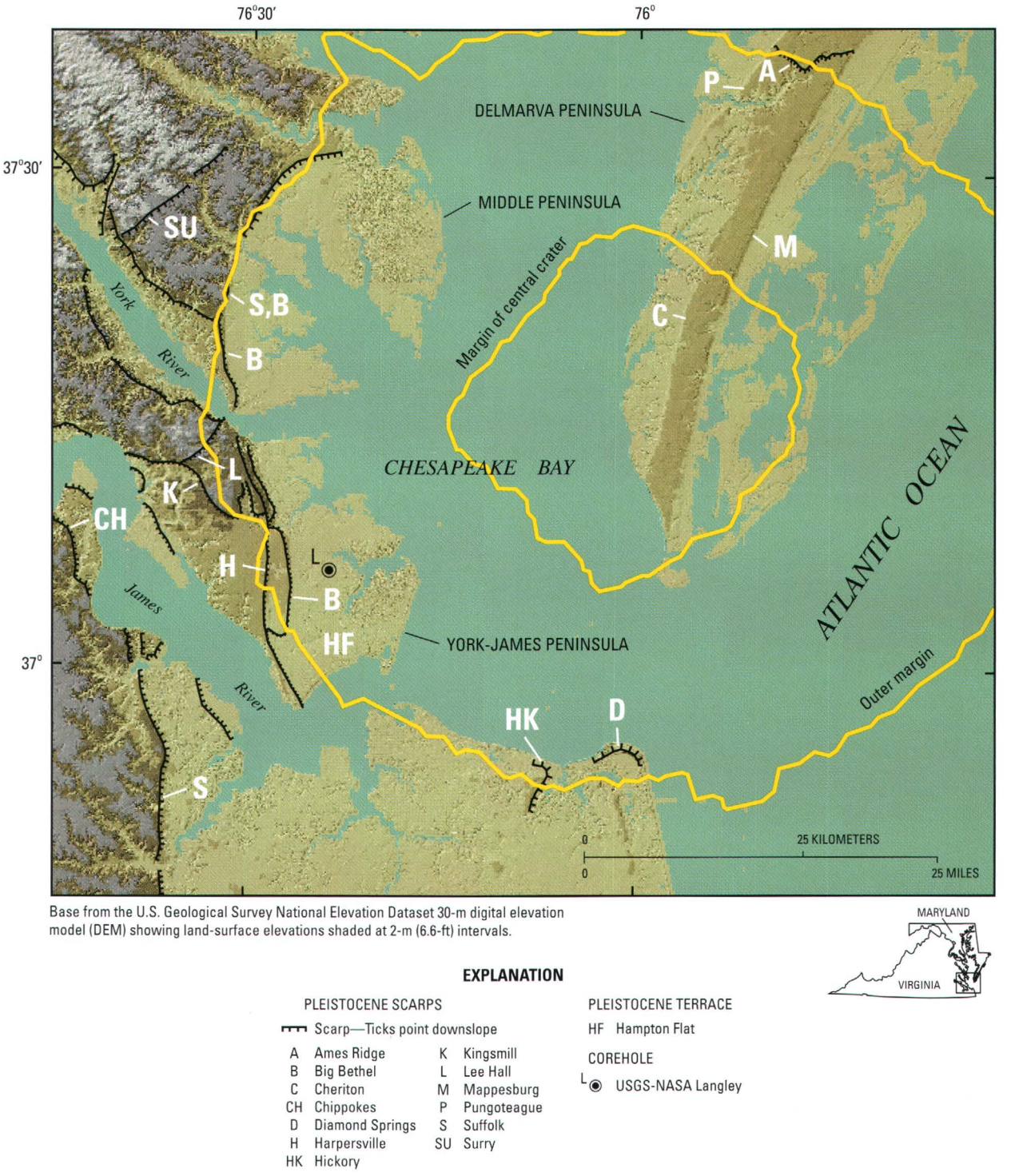

Base from the U.S. Geological Survey National Elevation Dataset 30-m digital elevation model (DEM) showing land-surface elevations shaded at 2-m (6.6-ft) intervals.

Figure A4. Map of the lower Chesapeake Bay showing Pleistocene scarps and terraces in relation to the buried Chesapeake Bay impact structure and the USGS-NASA Langley corehole. Valley-facing scarps formed by fluvial and estuarine erosion, and coast-facing scarps formed by shoreline erosion. Sources: Johnson (1969), Coch (1971), Oaks and Coch (1973), Johnson and others (1987), Mixon and others (1989), Powars and Bruce (1999), Powars (2000), and Johnson and others (2001).

The Big Bethel, Diamond Springs, Harpersville, and Ames Ridge scarps and the northern part of the Suffolk scarp approximately overlie the outer margin of the buried crater and mimic its curvature at different locations as shown in figure A4. Johnson and others (1998) found that Miocene, Pliocene, and Pleistocene strata show draping and other evidence of differential movement near the scarps, possibly related to compaction around the buried crater's margin.

The USGS-NASA Langley Core

Table A1 and figure A5 show the stratigraphic framework of the outer annular trough as revealed by the 635.1-m-deep (2,083.8-ft-deep) USGS-NASA Langley corehole at Hampton, Va. (L in figs. A1 and A2). The crystalline basement at this location consists of Neoproterozoic granite (Horton and others, 2001; Horton, Aleinikoff, and others, 2002; Horton, Kunk and others, 2002; Horton and others, this volume, chap. B). The top of the granite at 626.3 m (2,054.7 ft) depth is overlain by 390.6 m (1,281.6 ft) of impact-modified and impact-generated siliciclastic sediments. These crater-fill materials are preserved beneath a 235.6-m-thick (773.12-ft-thick) blanket of postimpact sediments.

Cretaceous sediments that were variably disturbed by the late Eocene asteroid or comet impact include crater units A and B; crater unit A is block faulted, locally fluidized, and gradational upward into crater unit B, which shows extensive fluidization, infiltration, and mixing (Gohn and others, this volume, chap. C). These impact-modified sediments were scoured and covered by ocean-water resurge deposits of the Exmore beds (polymict, matrix-supported diamicton). The Exmore beds consist of mixed Lower Cretaceous to upper Eocene sediment clasts (up to boulder size) and minor crystalline-rock clasts floating in a matrix of glauconitic, quartz-rich, muddy sand that contains Cretaceous, Paleocene, and Eocene fossils (Edwards and Powars, 2003; Self-Trail, 2003). The Exmore beds and their crystalline clasts are discussed in chapters C (Gohn and others), D (Frederiksen and others), and E (Horton and Izett).

The oldest postimpact stratigraphic unit, the upper Eocene Chickahominy Formation, is discussed by Poag and Norris (this volume, chap. F). Chapter G by Powars and others and chapter H by Edwards and others describe the entire postimpact (upper Eocene to Quaternary) stratigraphic section.

The stratigraphic framework in figure A5 and table A1 is used throughout this volume with one exception, chapter F, in which Poag and Norris use the stratigraphic framework of Poag,

Table A1. Stratigraphic units, ages, and contact depths below ground surface at the USGS-NASA Langley corehole, Hampton, Va.

[The USGS-NASA Langley corehole has a total depth below ground surface of 635.1 meters (2,083.8 feet). The ground-surface altitude of 2.4 m (7.9 ft) is given relative to the National Geodetic Vertical Datum of 1988]

Age	Stratigraphic unit	Base (ft)	Top (ft)	Base (m)	Top (m)
late Pleistocene	Tabb Formation, Lynnhaven Member	7.2	0.0	2.2	0.0
Pliocene	Yorktown Formation	76.3	7.2	23.3	2.2
late Miocene	Eastover Formation	224.5	76.3	68.4	23.3
late Miocene	St. Marys Formation	405.5	224.5	123.6	68.4
early and middle Miocene	Calvert Formation	470.9	405.5	143.5	123.6
middle Miocene	Calvert Beach Member	456.1	405.5	139.0	123.6
middle Miocene	Plum Point Member	461.1	456.1	140.5	139.0
early Miocene	Newport News beds	470.9	461.1	143.5	140.5
late Oligocene	Old Church Formation	577.4	470.9	176.0	143.5
late early Oligocene	Drummonds Corner beds*	601.3	577.4	183.3	176.0
late Eocene	Chickahominy Formation	773.12	601.3	235.65	183.3
late Eocene	Exmore beds	884.0	773.12	269.4	235.65
Early Cretaceous (+infiltration zones)	crater unit B	1,451.7	884.0	442.5	269.4
Early Cretaceous	crater unit A	2,054.7	1,451.7	626.3	442.5
Neoproterozoic	Langley Granite*	—	2,054.7	—	626.3

*Units named and defined in this volume.

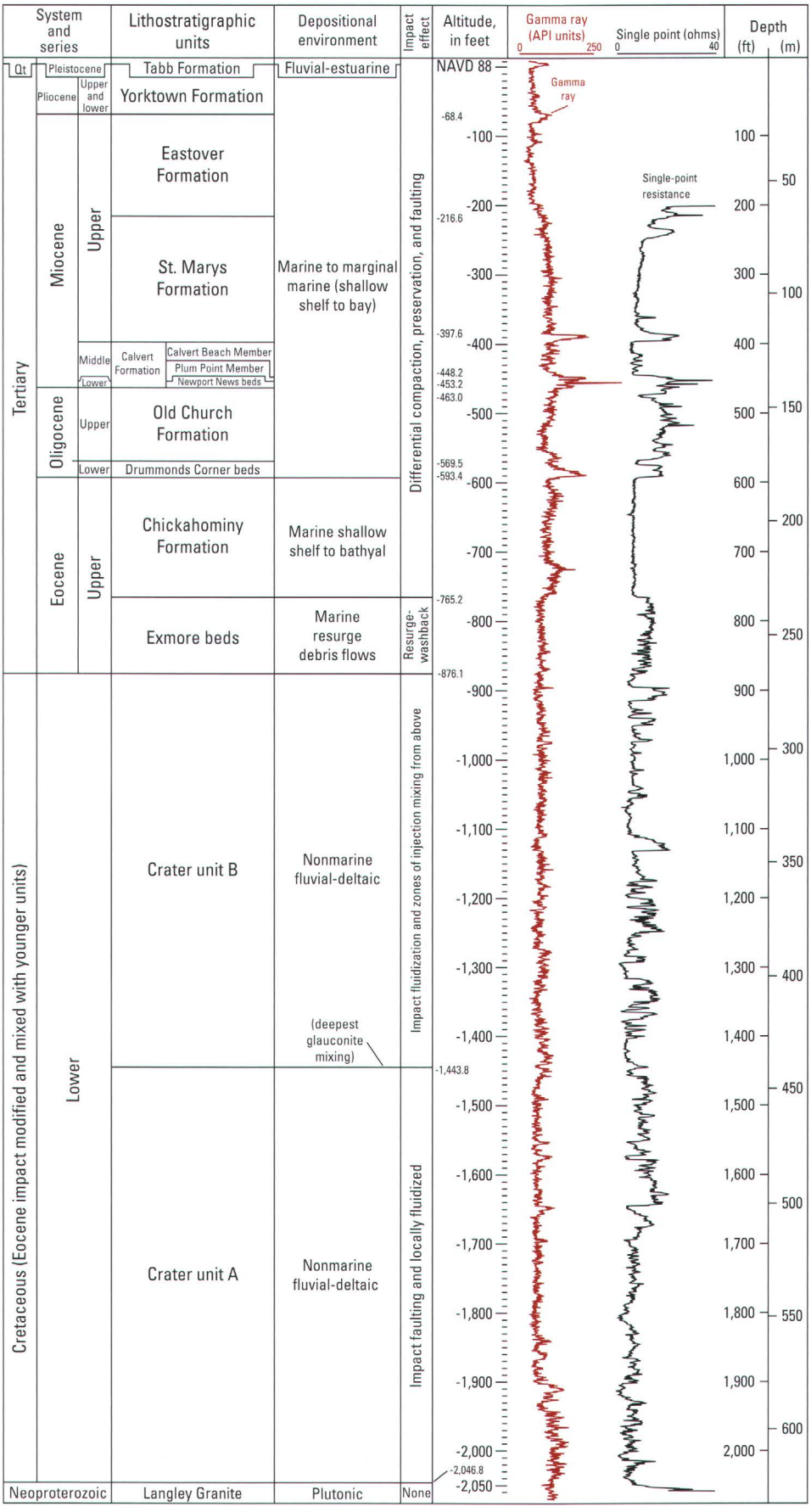

Figure A5. Stratigraphic column of the USGS-NASA Langley corehole, Hampton, Va., showing selected geophysical logs. Definitions: ft, feet; m, meters; NAVD 88, North American Vertical Datum of 1988; Qt, Quaternary.

Koeberl, and Reimold (2004). A correlation diagram for part of the USGS-NASA Langley core (fig. A6) shows the distinction between the informal Exmore beds of Gohn and others (this volume, chap. C) and the informal Exmore breccia of Poag and Norris (this volume, chap. F). Poag and Norris (p. F2) use the term "Exmore breccia" for "the brecciated sedimentary crater-fill deposits (underlain by either displaced sedimentary megablocks or crystalline basement rocks, and overlain by the fallout layer)" including all but the very top of the Exmore beds as well as crater unit B. Poag and Norris also treat thin units (their "fallout layer" and "dead zone") as a transitional interval distinct from the underlying Exmore breccia and overlying Chickahominy Formation. In summary, the "Exmore breccia" of Poag and Norris is a general term for impact breccias of any type anywhere in the crater, whereas the "Exmore beds" of Gohn and others is a term restricted in order to distinguish matrix-supported polymict sedimentary breccias that formed as water-resurge deposits from other kinds of impact breccias.

Significant Results

Of the ten chapters (B–K) on the Chesapeake Bay impact structure that follow this introduction, the first seven (B–H) present the results of multidisciplinary investigations of samples from the USGS-NASA Langley corehole. In chapter B, Horton and others discuss the petrography, structure, age, and thermal history of granitic basement rock beneath the Atlantic Coastal Plain at this location. The next three chapters (C–E) concentrate on impact-generated and impact-modified sediments in the Langley core. These include Gohn and others' analysis of the physical geology in chapter C, Frederiksen and others' interpretation of the paleontology in chapter D, and Horton and Izett's investigation of shocked minerals and crystalline-rock ejecta in chapter E. Three additional chapters (F–H) address the postimpact sediments in the USGS-NASA Langley core. In chapter F, Poag and Norris interpret the record of early postimpact deposition and paleoenvironments in the upper Eocene Chickahominy Formation. Powars and others discuss the physical stratigraphy of the postimpact, upper Eocene to Quaternary sedimentary section in chapter G. In chapter H, Edwards and others present the paleontology of the upper Eocene to Holocene stratigraphic section.

Two chapters (I and J) use recent geophysical investigations to decipher the subsurface geology in the western annular trough and outer margin of the impact structure. In chapter I, Catchings and others interpret the data from a land-based, high-resolution seismic-reflection and seismic-refraction profile on the York-James Peninsula. In chapter J, Pierce discusses subsurface information gained from audio-magnetotelluric soundings across the marginal area of the structure on the York-James Peninsula and the Middle Peninsula in southeastern Virginia.

The volume concludes with chapter K by McFarland and Bruce on the distribution, origin, and relations to flow of ground-water salinity along the western margin of the Chesapeake Bay impact crater in eastern Virginia. These hydrologic studies show how the structure, distribution and properties of materials, and formative processes of the impact crater directly influence ground-water flow and quality in a region of major urban development that depends heavily on ground-water resources.

Crystalline Basement Rocks

The stratigraphic section revealed by the USGS-NASA Langley corehole at Hampton, Va. (fig. A5), includes the basement rock concealed beneath 626.3 m (2,054.7 ft) of sedimentary deposits and designated the Langley Granite of Horton and others (this volume, chap. B). The Langley Granite, newly described in that chapter and discussed in related abstracts (Horton and others, 2001; Horton, Aleinikoff, and others, 2002; Horton, Kunk, and others, 2002), is a peraluminous monzogranite of Neoproterozoic age that is pervasively chloritized and nonfoliated. In chapter B, Horton and others point out that the absence of shocked minerals and discernible impact heating in the Langley Granite at this location provides boundary constraints for computational models of the impact. The top of the granite is weathered, but not saprolitized, and is nonconformably overlain by the Cretaceous sediments.

Recent tectonic models of eastern North America have interpreted little-known basement rocks in the Chesapeake Bay target region alternatively as a northern extension of the Roanoke Rapids volcanic-arc terrane (Horton and others, 1991), as a remnant of Gondwanan Archean crust now in northwest Africa that was left behind when the Atlantic Ocean opened (Lefort and Max, 1991), or as Mesoproterozoic (Grenvillian) basement of Laurentia (Sheridan and others, 1999). Horton and others (this volume, chap. B) present evidence that the Langley Granite is Neoproterozoic in age and that it formed in a peri-Gondwanan magmatic arc.

Impact-Modified and Impact-Generated Sediments

The Lower Cretaceous fluvial sediments are nearly pristine just above the granite. The study by Gohn and others (this volume, chap. C) indicates that, as confining pressure due to the thickness of overburden decreased upward, the water-saturated sand beds became increasingly fluidized, and the clay beds became more intensely fractured. Preimpact Upper Cretaceous and lower Tertiary marine sediments are missing from their normal stratigraphic position, but their disaggregated remnants are mixed into the upper part of the Lower Cretaceous sedimentary section. The overlying Exmore beds contain a mixture of clasts, including re-sedimented Cretaceous and Tertiary sediment clasts as well as sparse shocked minerals and crystalline ejecta.

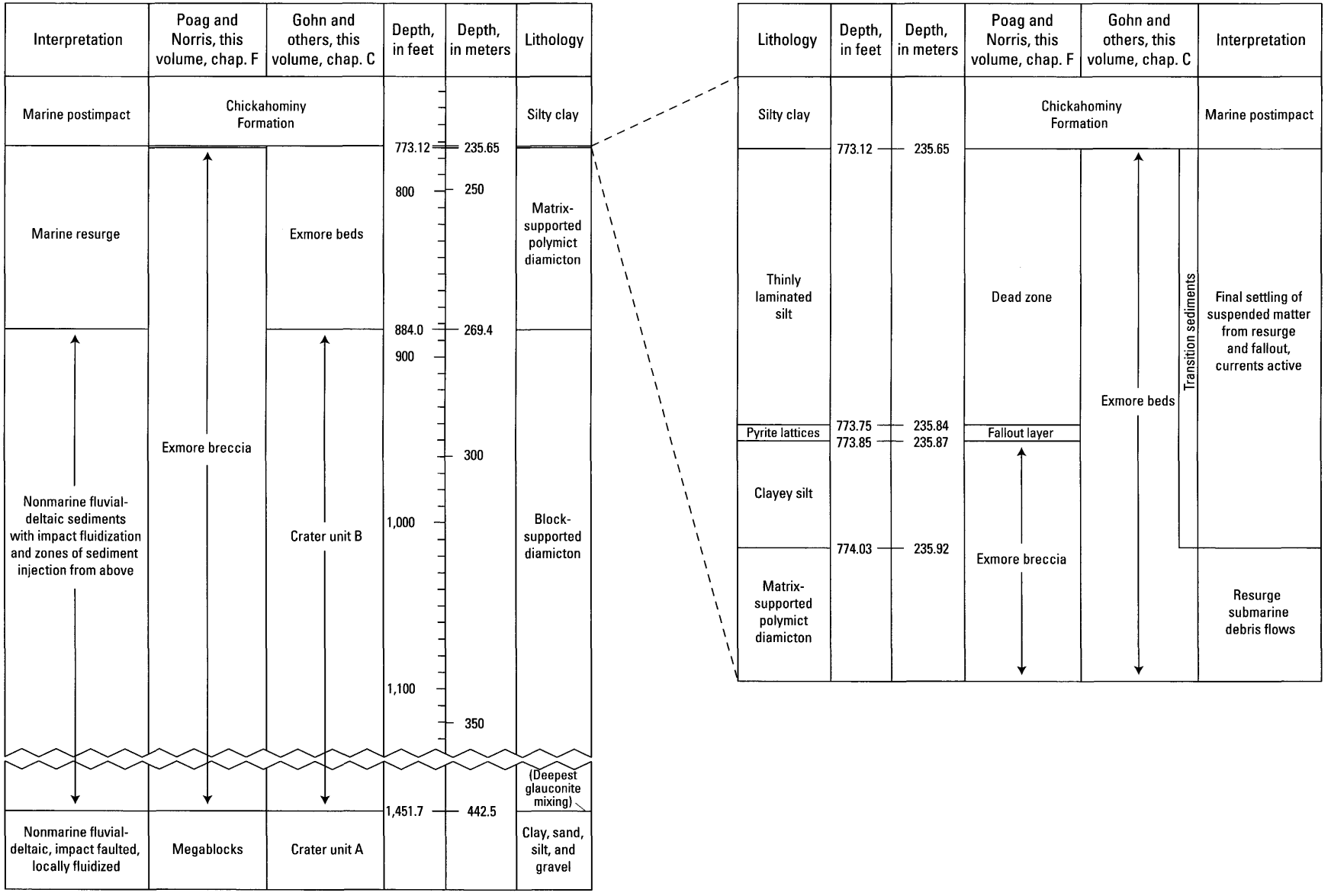

Figure A6. Correlation diagram for part of the USGS-NASA Langley core comparing informal usage of the terms "Exmore beds" and "Exmore breccia" in relation to lithology and interpretation of ocean-water resurge deposits. The stratigraphic terms defined in chapter C (Gohn and others) are used throughout this volume except in chapter F (Poag and Norris), which follows the stratigraphy of Poag, Koeberl, and Reimold (2004).

The mixture suggests scouring and erosion of the nearfield ejecta and underlying sediments by the resurge of seawater and debris flows into the crater.

The study by Frederiksen and others (this volume, chap. D) indicates that spore-pollen samples from crater units A and B are derived from the Cretaceous Potomac Group and that the upper part of crater unit B also contains microfossils derived from lower Tertiary formations. Their study of microfossils shows that the Exmore beds contain clasts that range in age from Early Cretaceous to late Eocene. Significantly, the Exmore contains microfossil species known only from the lower part of the middle Eocene and others known only from the uppermost middle Eocene and lowermost upper Eocene. Strata of these ages have never been recovered in the subsurface of the Virginia Coastal Plain but were once present and possibly have since been eroded away. In addition, some dinoflagellate cysts from the Exmore are fused, curled, fragmented, or otherwise degraded, and this damage is attributed to heat and abrasion during the oceanic impact, as also discussed by Edwards and Powars (2003). Some calcareous nannofossils appear to have impact-induced fractures (Self-Trail, 2003).

Horton and Izett (this volume, chap. E) confirm the presence of rare shocked quartz grains in the sandy matrix of the Exmore beds and in reworked crystalline-rock clasts in and just below the Exmore in the Langley core. Some crystalline-rock clasts are interpreted to be derived from ejecta because they contain shocked quartz and associated cataclastic fabrics. In the Langley core, nearly all of these clasts consist of variably porphyritic felsite. The contrast between relatively uniform crystalline-ejecta compositions at this site and more varied compositions at the Bayside and North sites suggests that the ejecta were distributed unevenly, perhaps in rays (Horton and Izett, this volume, chap. E). The impact event provided a remarkable sampling tool by excavating an enormous volume of target rock, including little-known basement terranes (Horton and others, 1991; Rankin, 1994; Sheridan and others, 1999), and scattering fragments where they can be retrieved at shallower levels.

Resurge deposits of the Exmore beds apparently were injected and mixed into variably liquefied, slumped sediments in the upper part of crater unit B, where Horton and Izett (this volume, chap. E) found shocked quartz in a single clast of felsic impact breccia (at 275.8 m (905.0 ft) depth), and where Frederiksen and others (this volume, chap. D) reported the only two matrix samples from crater unit B found to contain Tertiary microfossils. These include one dinocyst sample (at 278.4 m (913.4 ft) depth) and one calcareous nannofossil sample (at 298.5 m (979.3 ft) depth) that contain specimens of mixed Paleocene and Eocene ages (Frederiksen and others, this volume, chap. D), although the nannofossil sample is from the top of a drilling run and could be contaminated (Gohn and others, this volume, chap. C). However, zones containing glauconite of marine origin, presumably of Late Cretaceous and Tertiary age, occur at irregular intervals throughout crater unit B in the matrix between blocks derived from the older Cretaceous Potomac Formation.

Postimpact Sediments

Three chapters decipher the depositional environments, physical stratigraphy, and paleontology of postimpact sediments in the Langley core. In chapter F, Poag and Norris use stable-isotope, foraminifera, and bolboformid analyses of cores from several sites inside the crater (including the USGS-NASA Langley, Bayside, and North cores) and a variety of geophysical data to interpret the regional record of early postimpact deposition and paleoenvironments of the upper Eocene Chickahominy Formation. They also propose that the uppermost and latest syn-impact fallout deposit is contained in a thin, pyrite-bearing layer overlain by a thin postimpact "dead zone" as illustrated in figure A6. The oxygen and carbon isotopic data characterize three warm pulses that occurred during the deposition of the Chickahominy Formation. They interpret this climate history as possible evidence for the Chesapeake Bay impact and other late Eocene impacts collectively exerting long-term influence on global climate that led to the early Oligocene mass extinction event.

In chapter G, Powars and others use borehole geophysical logs to correlate lithostratigraphy of the Langley core with the land-based, high-resolution seismic-reflection data. They apply the correlated lithologic and geophysical data to characterize the physical stratigraphy of the postimpact, upper Eocene to Quaternary sedimentary section of the Langley core. Their correlation with the seismic data indicates that the postimpact units have distinct seismic signatures and that they are faulted. Significantly, most of the postimpact deposits are fine-grained sediments that slowly filled and buried the crater and therefore preserved several upper Eocene to lower Miocene stratigraphic units not found in the Virginia Coastal Plain outside the structure. A newly recognized Oligocene stratigraphic unit, the Drummonds Corner beds (informal name) (fig. A5), is described in chapter G by Powars and others.

In chapter H, Edwards and others present the paleontology of the postimpact upper Eocene to Quaternary stratigraphic section in the Langley core and include data on dinoflagellates, diatoms, mollusks, silicoflagellates, calcareous nannofossils, ostracodes, foraminifera and bolboformids, and vertebrate remains. They characterize the depositional and paleoenvironmental record of the postimpact sediments and discuss sediment accumulation rates, the paleontology of the newly recognized Drummonds Corner beds (informal name), and the reworking of impact-damaged microfossils into postimpact units. Variations in the rate of sediment accumulation indicate at least two episodes of rapid filling at about 20 meters per million years (~20 m/m.y.; ~66 ft/m.y.) during the late Eocene and late Miocene and several unconformities during the early and middle Miocene at this site.

Water Depths—Impact and Postimpact

The impact target was located on a gently sloping continental shelf where water depths increased seaward. Interpreted water depths for the western outer margin of the crater and estimated seabed gradients are used to project water depths at the eastern outer margin.

Target-water depth at the western outer margin of the crater.—At the crater's western outer margin near Newport News, Va. (fig. A1, locality NN), the estimated late Eocene water depth of the target is between minimum and maximum limits of about 0 and 170 m (0 and 560 ft). This depth range is interpreted on the basis of data from three coreholes: one updip of the crater at Putneys Mill, Va. (P in fig. A1), one updip at Haynesville, Va. (H in fig. A1), and one north of the crater at Solomons Island, Md. (north of the area shown in fig. A1). Benthic and planktonic foraminifera from the uppermost preimpact unit, the Piney Point Formation, in these cores indicate middle Eocene paleodepths of about 20–150 m (about 60–490 ft) (Poag, 1989; Bybell and Gibson, 1994; Gibson and Bybell, 1994). Projections from these locations (because the Piney Point is not intact in the crater) along the paleoshelf slope indicate middle Eocene water depths of about 20–170 m (about 60–560 ft) at the western outer margin. Subtracting 0–50 m (0–164 ft) from the middle Eocene depths to account for eustatic sea-level decline (Haq and others, 1988; Kominz and others, 1998) indicates late Eocene target-water depths of about 0–170 m (about 0–560 ft) at the western outer margin.

Target-seabed gradient.—The target seabed probably had a gradient between minimum and maximum limits of about 1:1,000 and 1:500; this range of gradients is based on Tertiary and modern analogs. A continental shelf gradient of 1:1,000 is approximately equivalent to the landward part of Tertiary reconstructions (for example, by Pekar and others, 2001) and the modern shelf as measured from Emery and Uchupi (1972). A gradient of 1:500 is approximately equivalent to the steeper, seaward part of Tertiary reconstructions (for example, by Steckler and others, 1999; Pekar and others, 2001).

Projected water depths across impact target.—The seabed gradients are used here to project target-water depth limits from the western outer margin to the center and to the eastern outer margin of the 85-km-diameter (53-mi-diameter) impact target. Projection of water paleodepths of 0–170 m (0–560 ft) from the western outer margin along a 1:1,000 gradient across the target yields paleodepths of 42.5–212.5 m (139–697 ft) at the center and 85–255 m (279–837 ft) at the eastern outer margin, whereas projection along a 1:500 gradient yields paleodepths of 85–255 m (279–837 ft) at the center and 170–340 m (560–1,115 ft) at the eastern outer margin. The metric numbers are rounded in 10-m increments and summarized below.

On the basis of these projections, the estimated target-water depths are in the range of about 0–170 m (0–560 ft) (mean value 85 m, 280 ft) at the western outer margin, about 40–260 m (131–853 ft) (mean value 150 m, 492 ft) at the center, and about 80–340 m (263–1,115 ft) (mean value 210 m, 689 ft) at the eastern outer margin of the crater target. If the paleoshelf steepened abruptly at an undetermined clinoform rollover point between a landward gradient approaching 1:1,000 and a seaward gradient approaching 1:500 as in some Tertiary reconstructions (Steckler and others, 1999; Pekar and others, 2001), the water depths would be within these limits.

Water depth after impact.—The postimpact Chickahominy Formation was deposited in a circular depression over the crater as illustrated on the isopach map in chapter F (Poag and Norris, this volume, chap. F, fig. F11), and so the water paleodepth probably exceeded that of the preimpact target seabed. Benthic and planktonic foraminiferal assemblages in the Chickahominy indicate a seabed paleodepth of about 300 m (984 ft), which is the outer neritic to upper bathyal environment (150–500 m (500–1,600 ft) depth) with restricted oxygen availability and high flux of organic carbon (Poag and Norrris, this volume, chap. F). Ostracodes also indicate that the Chickahominy Formation was mainly outer neritic to upper bathyal (Edwards and others, this volume, chap. H).

Dating the Impact Event

Chapters D, F, and H on paleontology of the Langley core agree that the age of the late Eocene Chesapeake Bay impact event is approximately 35.7 to 35.8 Ma (million years before the present). However, in chapter E, Horton and Izett present a weighted mean total fusion $^{40}Ar/^{39}Ar$ age of 35.3 Ma (±0.1 Ma at 1σ, ±0.2 Ma at 2σ) for 19 analyses of 4 North American tektites, and they interpret this as the age of the impact event.

Frederiksen and others (this volume, chap. D) determined from calcareous nannofossils that the Exmore beds belong to Zone NP 19/20 and that the impact occurred during the early part of the time represented by that zone at approximately 35.7–35.8 Ma. Poag and Norris (this volume, chap. F) give an extrapolated age of impact of about 35.78 Ma in their figures F6 and F26, while recognizing a range of uncertainty from 35.2 to 36.0 as shown in gray in their figure F3.

Edwards and others, in chapter H, independently calculated limits on sediment accumulation rates in the postimpact Chickahominy Formation based on zone boundaries and the Eocene-Oligocene boundary from the time scale of Berggren and others (1995); they note that Poag and Norris (this volume, chap. F) arrived at nearly identical rates by using slightly different assumptions. Then, as shown in figure H10, Edwards and others projected the base of the Chickahominy Formation in the Langley core into the time scale of Berggren and others (1995), using these zone boundaries and sediment accumulation rates to yield a value of 35.7–35.8 Ma for the age of impact. They note that this value is ultimately based on the geomagnetic reversal time scale of Cande and Kent (1995), which is calibrated to iso-

topic ages of 33.7±0.4 and 46.8±0.5 Ma; the calibration uses a cubic spline fit that does not take the age uncertainties into account (M.J. Kunk, USGS, written commun., 2003).

For ages determined by different methods and having various accuracies, the age of impact of 35.7–35.8 Ma based on microfossil zones calibrated to Berggren and others' (1995) time scale is not significantly different from the 35.3±0.2 Ma (2σ) age of tektites reported in chapter E by Horton and Izett.

Structural Interpretation of Seismic Data

The first parts of the crater to be subjected to more intensive study in the current phase of deep coring and high-resolution seismic-reflection surveying are the outer annular trough and its outer margin. In 2001, the USGS completed a 9-km-long (5.6-mi-long) high-resolution, land-based seismic-reflection and seismic-refraction survey (common-depth-point interval 2.5 m (8.2 ft)) on the York-James Peninsula (Catchings, Powars, and others, 2001; Catchings, Saulter, and others, 2001; Catchings and others, 2002). This seismic survey is linked to the adjacent Langley and Watkins School coreholes shown in figure A2 by borehole geophysical logs. The USGS investigators completed a similar 9-km-long (5.6-mi-long), high-resolution seismic survey along the Middle Peninsula (also crossing the outer annular trough and outer margin) in 2002 and obtained 4.6 km (2.9 mi) of data on the southern Delmarva Peninsula across the inner rim and central part of the crater (fig. A2). The data processing and interpretation of these profiles are still in progress.

In chapter I, Catchings and others (this volume) correlate a 1-km-long (0.62-mi-long) high-resolution seismic-reflection and seismic-refraction profile with lithologic and geophysical logs from the adjacent Langley corehole to decipher subsurface stratigraphic and structural details in the western annular trough. A stratabound, extensional collapse structure in that part of the impact-disturbed sedimentary section is generally confined to crater units A and B, with only a few minor offsets in the top of the Langley Granite, as shown by Catchings and others (this volume, chap. I). The abundance of faults in this interval increases upward, suggesting that extension increased in proportion to the decrease in overburden confining pressure. The top of the stratabound extensional fault system appears to be truncated at the base of the Exmore beds, except for a few faults that may be younger or reactivated, implying that formation of the extensional collapse structure largely preceded deposition of the water-resurge debris flows. More structural analysis of the faults is needed to determine if they formed by vertical extension due to rebound or lateral extension associated with inward slumping of sediments in the annular trough.

The high-resolution seismic data also provide guidance for interpreting the lower resolution marine seismic data, enabling the recognition of numerous collapse structures across the western annular trough (Powars and others, 2003). Most of these structures disrupt parautochthonous Cretaceous sediments, ocean-water resurge sediments, and postimpact sediments, thereby suggesting detachment zones within the sedimentary section. Many extensional collapse structures are formed by abundant short-displacement faults rather than a few normal faults of large displacement.

The marine seismic data and preliminary interpretation of the high-resolution land-based seismic data can be used to distinguish the discontinuous, locally inclined or offset reflectors interpreted to be slumped fault blocks from overlying resurge deposits of the Exmore beds; these data can also be used to distinguish the more continuous horizontal reflectors that represent little-disturbed Cretaceous sediments outside the crater (Powars and others, 2003). These sediments appear to be faulted to a much lesser degree than the slump blocks. Inward-dipping normal faults and antithetic faults define the typically rotated slump blocks. A few major normal faults displace the sediment-crystalline rock contact, indicating that they are relatively deep seated.

Resurge-tsunami and overlying postimpact sediments buried the irregular upper surface of the slump blocks. Observed thickness variations, dip reversals, and fault displacements of these sediments probably result from differential compaction across the underlying irregular surface. The impact-generated resurge deposits are up to 100 m (330 ft) thick in the annular trough but abruptly thin to 7.5 m (24.6 ft) just outside the outer margin in the Watkins School corehole (Powars and others, 2003).

Interpretation of Audio-Magnetotelluric (AMT) Soundings

Pierce (this volume, chap. J) discusses 18 tensor audio-magnetotelluric soundings that were collected in 2000 and 2001 to provide cross-section images of the electrical-response variations in traverses across the western outer margin of the crater (fig. A2). These soundings use the electromagnetic signals from distant lightning or atmospheric disturbances to determine variations in electrical resistivity of the earth as a function of depth (Vozoff, 1991). The orthogonal magnetic and electrical fields are measured to determine impedance tensors that account for anisotropy. Chapter J explains how resistivities were calculated from these impedances and used to construct two cross sections that show electrical-response variations in the structure as a function of depth on the York-James Peninsula and on the Middle Peninsula.

The audio-magnetotelluric soundings and resultant electrical cross sections of the York-James Peninsula and Middle Peninsula in Pierce's chapter J show a nearly vertical zone of high resistivity at the outer margin of the annular trough, which can be used to map the structure. The high resistivity may be caused

by fresh ground water discharging from the Lower Cretaceous sediments at the outer margin, by cementation along the fault zone, or by compaction of the sediments as a result of the impact event. Impedance trends to the northwest on the York-James Peninsula and to the northeast on the Middle Peninsula match the curvature of the structure. The electrical cross sections also image the lateral contact between conductive sediments and resistive basement, which is close to the technique's depth limit of resolution.

Hydrologic Effects and Water-Resources Implications

The Chesapeake Bay impact crater coincides approximately with Virginia's inland saltwater wedge in which saline ground water extends about 50 km (30 mi) landward of its normally expected position along the coast of southeastern Virginia. Powars and others (this volume, chap. G) describe it as a bulge rather than a wedge, because the saline ground water extends into shallower depths than in the region surrounding the crater. McFarland and Bruce (2002; this volume, chap. K) studied chemical analyses of water squeezed from sediment cores and pumped out of water wells in order to understand the relations between crater structure and ground-water salinity. These analyses included chloride, bromide, and chlorine-36, as well as stable hydrogen and oxygen isotopes and specific conductance.

In chapter K, McFarland and Bruce present chemical and isotopic analyses of ground-water samples from the USGS-NASA Langley, Bayside, and North cores and from water wells on the western margin of the impact structure. These analyses indicate that the high ground-water salinities of the Virginia inland saltwater wedge, or bulge, were more likely produced by mixing of freshwater and seawater than by other possible mechanisms. Vertical profiles of specific conductance and chloride concentrations indicate a zone of mixing along the western margin of the structure. These profiles also support the concept that the crater structure has caused differential flushing of residual seawater, older than 2 Ma and possibly as old as 35 Ma, to create the saltwater bulge.

Some chloride concentrations in ground water from the interior part of the crater (Kiptopeke well) exceed those of modern seawater. Stable hydrogen and oxygen isotopic ratios indicate that these brines probably were produced by evaporation (McFarland and Bruce, this volume, chap. K). Sanford (2002, 2003) has demonstrated that brine production from the escape of steam caused by the heat of the impact is at least theoretically possible. Future discovery of hydrothermal mineralization along pathways for escaping steam would favor this interpretation, whereas discovery of ground-water brines beneath the Atlantic Coastal Plain outside the crater would favor alternative explanations.

Ground water is expected during the next several decades to provide much of the required increase in water supply for southeastern Virginia, one of the most rapidly growing areas on the Atlantic Coast. The potential influence of the Chesapeake Bay impact crater on the future of this region's ground-water resource is profound.

Conceptual Model

A conceptual model of the Chesapeake Bay crater formation in stages, illustrated in figure A7, is derived from a synthesis of the chapters in this volume and concepts of the cratering process as summarized by French (1998). The preimpact target on the Atlantic continental shelf consisted of three main components as illustrated in figure A7*A*: (1) crystalline basement rocks deepening eastward; (2) poorly consolidated, water-saturated siliciclastic sediments, including nonmarine Upper Cretaceous and Lower Cretaceous beds and a veneer of marine Upper Cretaceous and Paleocene to upper Eocene beds; and (3) ocean water ranging in depth from about 0–170 m (0–560 ft) on the west side to about 80–340 m (263–1,115 ft) on the east side. Contact of the projectile produced shock waves in the target and projectile, vaporizing the projectile and causing vaporization, melting, and shock deformation in the target.

Figure A7*B* illustrates the crater excavation stage in which shock-wave expansion into the target forced material outward, upward (ejecting high-velocity particles), and downward to form a bowl-shaped *transient cavity* or *transient crater*. The shock wave also caused shock deformation and associated faults and fractures, melts lining the transient cavity, outward excavation flow of material forming an ejecta curtain, and an uplifted rim.

The transient *water cavity* is interpreted to have had about the same diameter as the transient cavity in underlying rocks and sediments on the basis of numerical simulations of marine-target craters (Ormö and others, 2002; Shuvalov and others, 2002). The numerical models indicate that the growing crater rim and ejecta curtain pushed the water aside to form a water surge, which eventually broke up and initiated tsunamis.

As soon as the transient cavity ceased to expand, crater modification by gravity-driven processes occurred as illustrated in figure A7*C*. Rebound and collapse of the central crater and central uplift were accompanied by inward slumping of water-saturated sediments within the annular trough beyond the central crater and by the resurge of seawater and submarine debris flows into the cavity as documented in other marine craters (von Dalwigk and Ormö, 2001). The collapse structures are illustrated by images of seismic profiles in chapters F and I, and the impact-modified and impact-generated sediments are described and illustrated in chapters C, D, and E. The high-energy resurge debris flows were followed by settling of fallout particles and

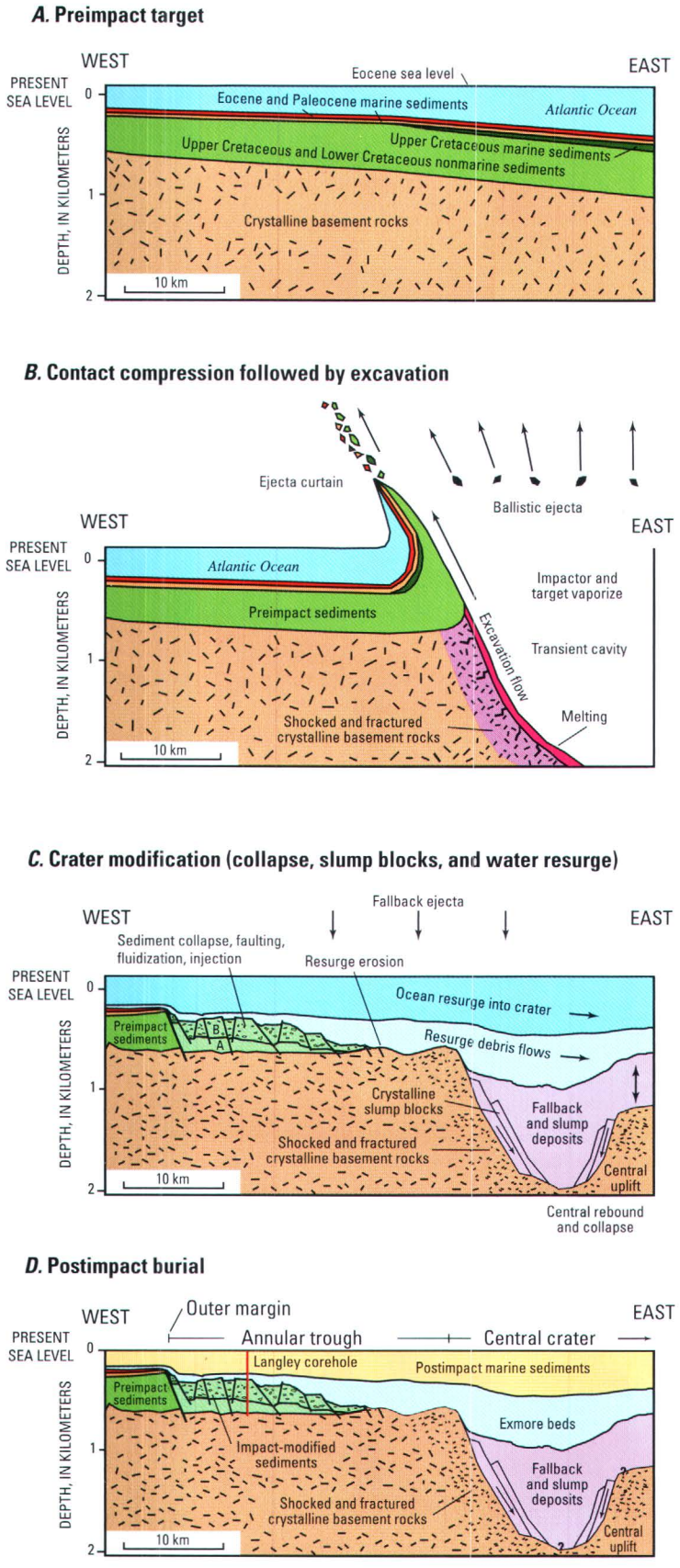

Figure A7. Schematic cross sections illustrating stages in a conceptual model of Chesapeake Bay crater formation. Diagrams show western half of crater along west-to-east profile as located approximately in figure A1. Modified from Edwards and Powars (2003). ***A*, Preimpact target:** Before the projectile hit, the ocean site consisted of three main layers: crystalline basement rocks (deepening eastward), siliciclastic sediments (thickening eastward), and ocean water deepening eastward from about 0–170 m (0–560 ft) to about 80–340 m (263–1,115 ft). ***B*, Contact compression followed by excavation:** Contact of the projectile produced shock waves, vaporizing the projectile and causing vaporization, melting, and shock metamorphism in the target. Expansion of the shock wave excavated a bowl-shaped transient cavity in the target, producing shock metamorphism, melts, ejecta, and an ejecta curtain (drawn approximately as modeled to occur in about 30 seconds; Crawford, 2002). ***C*, Crater modification (collapse, slump blocks, and water resurge):** Collapse of the transient cavity was accompanied by inward collapse of slump blocks in poorly consolidated sediments of the annular trough (for example, to form crater units A and B; see A and B in diagram). The collapse expanded the crater beyond the central excavation to a total width of about 85 km (53 mi). A violent resurge of ocean water and submarine debris flows filled the open cavity with water and debris. ***D*, Postimpact burial:** After the resurge currents deposited the Exmore beds, the crater was buried by marine sediments. The USGS-NASA Langley corehole is projected onto the section line.

other material suspended in the water column, which led to a resumption of normal marine sedimentation. Figure A7*D* illustrates subsequent burial of the crater by postimpact sedimentation as documented in chapters F, G, and H.

The studies in this volume are consistent with a model for internal structure of the sedimentary section of the annular trough of the Chesapeake Bay impact crater as consisting of slumped, normal-fault-bounded megablocks overlain by water-resurge debris flows (Exmore beds). This model likely remains accurate for the large slump blocks at the outer margin. The shallow collapse structures are similar to shallow extensional features recently observed in the Silverpit crater of the North Sea (Stewart and Allen, 2002).

Acknowledgments

This Professional Paper is a contribution to the Chesapeake Bay Impact Crater Project. Investigations of the Chesapeake Bay impact structure under this project are conducted by the U.S. Geological Survey (USGS) in cooperation with the Hampton Roads Planning District Commission, the Virginia Department of Environmental Quality, and the National Aeronautics and Space Administration (NASA) Langley Research Center. The Hampton Roads Planning District Commission and the USGS provided funds for the drilling of the USGS-NASA Langley corehole. The NASA Langley Research Center provided extensive operational and logistical support for the drilling operation. The Virginia Department of Environmental Quality and the Department of Geology of the College of William and Mary provided extensive operational support at the drill site.

We wish to acknowledge USGS organizational units of both the Geology Discipline and the Water Resources Discipline for their contributions to the project. Those from the Geology Discipline include the Eastern Earth Surface Processes Team (geology, paleontology, drilling, project management), the Eastern Mineral Resources Team (audio-magnetotelluric electrical sounding), the Central Mineral Resources Team (uranium-lead geochronology), the Crustal Imaging and Characterization Team (argon geochronology), the Coastal and Marine Geology Team (geology, paleontology), the Western Earthquake Hazards Team (seismic reflection and refraction surveys), and the Astrogeology Research Program (geophysics). Participants from the USGS Water Resources Discipline include the Virginia District (hydrology, project management), the Maryland District (geophysical logging), the Rocky Mountain Drilling Unit (core drilling), and the Central Regional Research Branch (geophysical logging). The principal USGS funding sources are the National Cooperative Geologic Mapping Program, the Coastal and Marine Geology Program, and the Cooperative Water Program.

Reviewers (all USGS) for chapters in this volume include Robert A. Ayuso, Thomas M. Brocher, Harry J. Dowsett, Joseph S. Duval, Lucy E. Edwards, Norman O. Frederiksen, Jeffrey N. Grossman, Michael J. Kunk, James E. Landmeyer, E. Randolph McFarland, Daniel J. Milton, Charles W. Naeser, Wayne L. Newell, Douglas J. Nichols, C. Wylie Poag, Douglas W. Rankin, Nicholas M. Ratcliffe, Ward E. Sanford, J. Stephen Schindler, Jean M. Self-Trail, Joseph P. Smoot, C. Scott Southworth, and Jeffrey C. Wynn. These individuals contributed significantly to the scientific quality of the book. We thank Lucy E. Edwards, E. Randolph McFarland, and Charles W. Naeser for reviewing earlier drafts of this chapter, and we are particularly grateful to Edwards for encouragement and assistance on the estimates of target-water depth. We thank Theodore B. Samsel, R. Brent Banks, Anita M. Cotton, and Peter G. Chirico (all USGS) for help with the computer graphics in this chapter and other chapters in the volume.

References Cited

Berggren, W.A., Kent, D.V., Swisher, C.C., III, and Aubry, M.-P., 1995, A revised Cenozoic geochronology and chronostratigraphy, *in* Berggren, W.A., Kent, D.V., Aubry, M.-P., and Hardenbol, Jan, eds., Geochronology, time scales and global stratigraphic correlation: SEPM (Society for Sedimentary Geology) Special Publication 54, p. 129–212.

Bohor, B.F., Betterton, W.J., and Foord, E.E., 1988, Coesite, glass, and shocked quartz at DSDP Site 612; Evidence for nearby impact in the late Eocene [abs.]: Lunar and Planetary Science Conference, 19th, Houston, Tex., March 14–18, 1988, Abstracts, p. 114–115.

Brown, P.M., Miller, J.A., and Swain, F.M., 1972, Structural and stratigraphic framework and spatial distribution of permeability of the Atlantic Coastal Plain, North Carolina to New York: U.S. Geological Survey Professional Paper 796, 79 p.

Bybell, L.M., and Gibson, T.G., 1994, Paleogene stratigraphy of the Putneys Mill, New Kent County, Virginia, corehole: U.S. Geological Survey Open-File Report 94–217, 38 p.

Cande, S.C., and Kent, D.V., 1995, Revised calibration of the geomagnetic polarity timescale for the Late Cretaceous and Cenozoic: Journal of Geophysical Research, v. B100, no. 4, p. 6093–6095.

Catchings, R.D., Powars, D.S., Gohn, G.S., and Goldman, M.R., 2002, High-resolution seismic reflection survey of the southwestern margin of the Chesapeake Bay impact structure, Virginia [abs.]: Eos, Transactions, American Geophysical Union, v. 83, no. 19, spring meeting supplement of 7 May 2002, Abstract T21A–05, p. S352. (Also available online at http://www.agu.org/meetings/waissm02.html)

Catchings, R.D., Powars, D.S., Gohn, G.S., Goldman, M.R., Gandhok, G., and Johnson, G.H., 2001, Subsurface images of

the annular trough of the Chesapeake Bay impact structure, Virginia, from seismic reflection/refraction data [abs.]: Lunar and Planetary Science Conference, 32d, Houston, Tex., March 12–16, 2001, Abstract 1937, available online at http://www.lpi.usra.edu/meetings/lpsc2001/pdf/1937.pdf

Catchings, R.D., Saulter, D.E., Powars, D.S., Goldman, M.R., Dingler, J.A., Gohn, G.S., Schindler, J.S., and Johnson, G.H., 2001, High-resolution seismic reflection/refraction images near the outer margin of the Chesapeake Bay impact crater, York-James Peninsula, southeastern Virginia: U.S. Geological Survey Open-File Report 01–407, 18 p., available only online at http://geopubs.wr.usgs.gov/open-file/of01-407/

Cederstrom, D.J., 1943, Chloride in ground water in the coastal plain of Virginia: Virginia Geological Survey Bulletin 58, 36 p.

Cederstrom, D.J., 1945a, Geology and ground-water resources of the coastal plain in southeastern Virginia: Virginia Geological Survey Bulletin 63, 384 p.

Cederstrom, D.J., 1945b, Selected well logs in the Virginia Coastal Plain north of James River: Virginia Geological Survey Circular 3, 81 p.

Cederstrom, D.J., 1945c, Structural geology of southeastern Virginia: American Association of Petroleum Geologists Bulletin, v. 29, no. 1, p. 71–95.

Cederstrom, D.J., 1946, Chemical character of ground water in the coastal plain of Virginia: Virginia Geological Survey Bulletin 68, 62 p.

Cederstrom, D.J., 1957, Geology and ground-water resources of the York-James Peninsula, Virginia: U.S. Geological Survey Water-Supply Paper 1361, 237 p.

Coch, N.K., 1971, Geology of the Newport News South and Bowers Hill quadrangles, Virginia: Virginia Division of Mineral Resources Report of Investigations 28, 26 p., 2 oversize maps.

Crawford, D.A., 2002, A computational model of the Chesapeake Bay impact [abs.]: Geological Society of America Abstracts with Programs, v. 34, no. 6, p. 465.

Daniels, D.L., and Leo, G.W., 1985, Geologic interpretation of basement rocks of the Atlantic Coastal Plain: U.S. Geological Survey Open-File Report 85–655, 45 p., 4 oversize pls.

Earth Impact Database, 2003 [a resource maintained by the Planetary and Space Science Centre at the University of New Brunswick, Canada]: available online at http://www.unb.ca/passc/ImpactDatabase/ (Accessed June 2, 2003.)

Edwards, L.E., Frederiksen, N.O., Self-Trail, J.M., and Poag, C.W., 2002, Paleontology of crater-fill deposits, Chesapeake Bay impact structure, Virginia [abs.]: Geological Society of America Abstracts with Programs, v. 34, no. 6, p. 465–466.

Edwards, L.E., and Powars, D.S., 2003, Impact damage to dinocysts from the late Eocene Chesapeake Bay event: Palaios, v. 18, no. 3, p. 275–285. (Also available online at http://www.bioone.org/pdfserv/i0883-1351-018-03-0275.pdf)

Edwards, L.E., and Self-Trail, J.M., 2002, Shocking news—Impact effects on marine microfossils, Chesapeake Bay impact structure, Virginia [abs.]: Eos, Transactions, American Geophysical Union, v. 83, no. 19, spring meeting supplement of 7 May 2002, Abstract T21A–04, p. S351. (Also available online at http://www.agu.org/meetings/waissm02.html)

Emery, K.O., and Uchupi, Elazar, 1972, Western North Atlantic Ocean; Topography, rocks, structure, water, life, and sediments: American Association of Petroleum Geologists Memoir 17, 532 p.

Emry, Scott, McFarland, E.R., and Powars, D.S., 2002, Societal implications of an impact crater—Chesapeake Bay impact structure, Virginia [abs.]: Eos, Transactions, American Geophysical Union, v. 83, no. 19, spring meeting supplement of 7 May 2002, Abstract T21A–01, p. S351. (Also available online at http://www.agu.org/meetings/waissm02.html)

French, B.M., 1998, Traces of catastrophe; A handbook of shock-metamorphic effects in terrestrial meteorite impact structures: Houston, Tex., Lunar and Planetary Institute, LPI Contribution No. 954, 120 p.

Gibson, T.G., and Bybell, L.M., 1994, Paleogene stratigraphy of the Solomons Island, Maryland corehole: U.S. Geological Survey Open-File Report 94–708, 39 p.

Glass, B.P., 1989, North American tektite debris and impact ejecta from DSDP Site 612: Meteoritics, v. 24, no. 4, p. 209–218.

Glass, B.P., 2002, Distal impact ejecta from the Chesapeake Bay impact structure [abs.]: Geological Society of America Abstracts with Programs, v. 34, no. 6, p. 466.

Glover, Lynn, III, and Klitgord, K.D., chief compilers, 1995, Continent-ocean transect E–3, southwestern Pennsylvania to Baltimore Canyon trough: Boulder, Colo., Geological Society of America, 78-p. pamphlet, 2 sheets, scale about 1:625,000.

Gohn, G.S., Bruce, T.S., Catchings, R.D., Emry, S.R., Johnson, G.H., Levine, J.S., McFarland, E.R., Poag, C.W., and Powars, D.S., 2001, Integrated geologic, hydrologic, and geophysical investigations of the Chesapeake Bay impact structure, Virginia, USA; A multi-agency program [abs.]: Lunar and Planetary Science Conference, 32d, Houston, Tex., March 12–16, 2001, Abstract 1901, available online at http://www.lpi.usra.edu/meetings/lpsc2001/pdf/1901.pdf

Gohn, G.S., Clark, A.C., Queen, D.G., Levine, J.S., McFarland, E.R., and Powars, D.S., 2001, Operational summary for the USGS-NASA Langley corehole, Hampton, Virginia: U.S. Geological Survey Open-File Report 01–87–A, 21 p., available online at http://pubs.usgs.gov/of/2001/of01-087/

Gohn, G.S., Powars, D.S., Bruce, T.S., Quick, J.E., and Catchings, R.D., 2002, Geologic constraints on modeling of complex-crater collapse; Data from the Chesapeake Bay impact structure, Virginia [abs.]: Eos, Transactions, American Geophysical Union, v. 83, no. 19, spring meeting supplement of 7 May 2002, Abstract T21A–07, p. S352. (Also available online at http://www.agu.org/meetings/waissm02.html)

Gohn, G.S., Powars, D.S., Bruce, T.S., Self-Trail, J.M., Weems, R.E., Edwards, L.E., Horton, J.W., Jr., Izett, G.A., and Johnson, G.H., 2001, Preliminary interpretation of the USGS-NASA Langley corehole, Chesapeake Bay impact

structure, York-James Peninsula, Hampton, VA [abs.]: Geological Society of America Abstracts with Programs, v. 33, no. 2, p. A–24.

Gohn, G.S., Powars, D.S., Quick, J.E., Horton, J.W., Jr., and Catchings, R.D., 2002, Variation of impact response with depth and lithology, outer annular trough of the Chesapeake Bay impact structure, Virginia Coastal Plain [abs.]: Geological Society of America Abstracts with Programs, v. 34, no. 6, p. 465.

Hampton Roads Planning District Commission, 1999, 35 million year-old meteor crater affects the region's ground water: Chesapeake, Va., Hampton Roads Planning District Commission, Environmental Planning Special Report, Issue 2, October 1999, p. 2–5. (Also available online at http://www.hrpdc.org/publications/specialreports/groundwater.pdf)

Haq, B.U., Hardenbol, Jan, and Vail, P.R., 1988, Mesozoic and Cenozoic chronostratigraphy and cycles of sea-level change, *in* Wilgus, C.K., Hastings, B.S., Ross, C.A., Posamentier, H.W., Van Wagoner, John, and Kendall, C.G.St.C., eds., Sea-level changes—An integrated approach: Society of Economic Paleontologists and Mineralogists Special Publication 42, p. 71–108.

Horton, J.W., Jr., Aleinikoff, J.N., Izett, G.A., Naeser, C.W., and Naeser, N.D., 2001, Crystalline rocks from the first corehole to basement in the Chesapeake Bay impact structure, Hampton, Virginia [abs.]: Geological Society of America Abstracts with Programs, v. 33, no. 6, p. A–448.

Horton, J.W., Jr., Aleinikoff, J.N., Izett, G.A., Naeser, N.D., Naeser, C.W., and Kunk, M.J., 2002, Crystalline basement and impact-derived clasts from three coreholes in the Chesapeake Bay impact structure, southeastern Virginia [abs.]: Eos, Transactions, American Geophysical Union, v. 83, no. 19, spring meeting supplement of 7 May 2002, Abstract T21A–03, p. S351. (Also available online at http://www.agu.org/meetings/waissm02.html)

Horton, J.W., Jr., Drake, A.A., Jr., Rankin, D.W., and Dallmeyer, R.D., 1991, Preliminary tectonostratigraphic terrane map of the central and southern Appalachians: U.S. Geological Survey Miscellaneous Investigations Series Map I–2163, scale 1:2,000,000.

Horton, J.W., Jr., Gohn, G.S., Edwards, L.E., Self-Trail, J.M., Powars, D.S., Kunk, M.J., and Izett, G.A., 2003, Recent research in the Chesapeake Bay impact crater, USA—Part 2. Reworked ejecta and impact debris [abs.]: International Conference on Large Meteorite Impacts, 3d, Noerdlingen, Germany, August 5–7, 2003, Abstract 4051, available online at http://www.lpi.usra.edu/meetings/largeimpacts2003/pdf/4051.pdf

Horton, J.W., Jr., Kunk, M.J., Naeser, C.W., Naeser, N.D., Aleinikoff, J.N., and Izett, G.A., 2002, Petrography, geochronology, and significance of crystalline basement rocks and impact-derived clasts in the Chesapeake Bay impact structure, southeastern Virginia [abs.]: Geological Society of America Abstracts with Programs, v. 34, no. 6, p. 466.

Johnson, G.H., 1969, Guidebook to the geology of the lower York-James Peninsula and south bank of the James River: Williamsburg, Va., College of William and Mary, Department of Geology Guidebook 1, 33 p.

Johnson, G.H., Kruse, S.E., Vaughn, A.W., Lucey, J.K., Hobbs, C.H., III, and Powars, D.S., 1998, Postimpact deformation associated with the late Eocene Chesapeake Bay impact structure in southeastern Virginia: Geology, v. 26, no. 6, p. 507–510.

Johnson, G.H., Powars, D.S., and Bruce, T.S., 2000, Stratigraphic and geohydrologic anomalies around the Chesapeake Bay impact structure, eastern Virginia [abs.]: Geological Society of America Abstracts with Programs, v. 32, no. 2, p. A–28.

Johnson, G.H., Powars, D.S., Bruce, T.S., Beach, T.A., Harris, M.S., and Goodwin, B.K., 2001, Post-impact effects of the Eocene Chesapeake Bay impact, lower York-James Peninsula, Virginia: Virginia Geological Field Conference, 31st, Williamsburg, Virginia, October 19 and 20, 2001 [Guidebook], 40 p.

Johnson, G.H., Ward, L.W., and Peebles, P.C., 1987, Stratigraphy and paleontology of Pliocene and Pleistocene deposits of southeastern Virginia, *in* Whittecar, G.R., ed., Geological excursions in Virginia and North Carolina—Geological Society of America, Southeastern Section, 36th Annual Meeting, 1987, Guidebook, Field Trips nos. 1–7: Norfolk, Va., Old Dominion University, Department of Geological Sciences, p. 189–218.

Klitgord, K.D., Hutchinson, D.R., and Schouten, Hans, 1988, U.S. Atlantic continental margin; Structural and tectonic framework, *in* Sheridan, R.E., and Grow, J.A., eds., The Atlantic continental margin, U.S., v. I–2 *of* The geology of North America: Boulder, Colo., Geological Society of America, p. 19–56.

Koeberl, Christian, Kruger, F.J., and Poag, C.W., 2001, Geochemistry of surficial sediments near the Chesapeake Bay impact structure and the search for source rocks of the North American tektites [abs.]: Lunar and Planetary Science Conference, 32d, Houston, Tex., March 12–16, 2001, Abstract 1333, available online at http://www.lpi.usra.edu/meetings/lpsc2001/pdf/1333.pdf

Koeberl, Christian, Poag, C.W., Reimold, W.U., and Brandt, Dion, 1996, Impact origin of the Chesapeake Bay structure and the source of the North American tektites: Science, v. 271, no. 5253, p. 1263–1266.

Kominz, M.A., Miller, K.G., and Browning, J.V., 1998, Long-term and short-term global Cenozoic sea-level estimates: Geology, v. 26, no. 4, p. 311–314.

Laczniak, R.J., and Meng, A.A., III, 1988, Ground-water resources of the York-James Peninsula of Virginia: U.S. Geological Survey Water-Resources Investigations Report 88–4059, 178 p.

Lefort, J.-P., and Max, M.D., 1991, Is there an Archean crust beneath Chesapeake Bay?: Tectonics, v. 10, no. 1, p. 213–226.

McFarland, E.R., 2002, Hydrochemical evidence for the origin of the elevated ground-water salinity in the Chesapeake Bay impact structure, southeastern Virginia [abs.]: Geological Society of America Abstracts with Programs, v. 34, no. 6, p. 466.

McFarland, E.R., and Bruce, Scott, 2002, Distribution, origin, and relations to flow of salty ground water along the western margin of the Chesapeake Bay impact structure in eastern Virginia [abs.]: Eos, Transactions, American Geophysical Union, v. 83, no. 19, spring meeting supplement of 7 May 2002, Abstract T21A–08, p. S352. (Also available online at http://www.agu.org/meetings/waissm02.html)

Melosh, H.J., 1989, Impact cratering—A geologic process: New York, Oxford University Press, 245 p.

Meng, A.A., III, and Harsh, J.F., 1988, Hydrogeologic framework of the Virginia Coastal Plain: U.S. Geological Survey Professional Paper 1404–C, p. C1–C82, 4 oversize pls.

Mixon, R.B., Berquist, C.R., Newell, W.L., Johnson, G.H., Powars, D.S., Schindler, J.S., and Rader, E.K., 1989, Geologic map and generalized cross sections of the Coastal Plain and adjacent parts of the Piedmont, Virginia: U.S. Geological Survey Miscellaneous Investigations Series Map I–2033, 2 sheets, scale 1:250,000.

Oaks, R.Q., Jr., and Coch, N.K., 1973, Post-Miocene stratigraphy and morphology, southeastern Virginia: Virginia Division of Mineral Resources Bulletin 82, 135 p.

Obradovich, J.D., Snee, L.W., and Izett, G.A., 1989, Is there more than one glassy impact layer in the late Eocene? [abs.]: Geological Society of America Abstracts with Programs, v. 21, no. 6, p. A134.

Ormö, Jens, Shuvalov, V.V., and Lindström, Maurits, 2002, Numerical modeling for target water depth estimation of marine-target impact craters: Journal of Geophysical Research, v. 107, no. E12, 9 p. (5120). (Also available online at http://www.agu.org/pubs/crossref/2002/2002JE001865.shtml)

Pekar, S.F., Christie-Blick, Nicholas, Kominz, M.A., and Miller, K.G., 2001, Evaluating the stratigraphic response to eustasy from Oligocene strata in New Jersey: Geology, v. 29, no. 1, p. 55–58.

Poag, C.W., 1989, Foraminiferal stratigraphy and paleoenvironments of Cenozoic strata cored near Haynesville, Virginia, chap. D *of* Mixon, R.B., ed., Geology and paleontology of the Haynesville cores—Northeastern Virginia Coastal Plain: U.S. Geological Survey Professional Paper 1489, p. D1–D20, 5 pls.

Poag, C.W., 1996, Structural outer rim of Chesapeake Bay impact crater—Seismic and borehole evidence: Meteoritics & Planetary Science, v. 31, no. 2, p. 218–226.

Poag, C.W., 1997, The Chesapeake Bay bolide impact; A convulsive event in Atlantic Coastal Plain evolution: Sedimentary Geology, v. 108, no. 1–4, p. 45–90.

Poag, C.W., 1999, Chesapeake invader; Discovering America's giant meteorite crater: Princeton, N.J., Princeton University Press, 183 p.

Poag, C.W., 2000, Nature and distribution of deposits derived from the Chesapeake Bay submarine impact [abs.]: Geological Society of America Abstracts with Programs, v. 32, no. 7, p. A–163.

Poag, C.W., 2002a, Biospheric consequences of the Chesapeake Bay bolide impact [abs.]: Geological Society of America Abstracts with Programs, v. 34, no. 6, p. 467.

Poag, C.W., 2002b, Structure and morphology of the Chesapeake Bay submarine impact crater [abs.]: Geological Society of America Abstracts with Programs, v. 34, no. 6, p. 465.

Poag, C.W., 2002c, Synimpact-postimpact transition inside Chesapeake Bay crater: Geology, v. 30, no. 11, p. 995–998.

Poag, C.W., 2002d, Tsunamis and hypercanes; Late-stage impact depositional systems at Chesapeake Bay [abs.]: Eos, Transactions, American Geophysical Union, v. 83, no. 19, spring meeting supplement of 7 May 2002, Abstract T21A–06, p. S352. (Also available online at http://www.agu.org/meetings/waissm02.html)

Poag, C.W., and Aubry, M.-P., 1995, Upper Eocene impactites of the U.S. East Coast; Depositional origins, biostratigraphic framework, and correlation: Palaios, v. 10, no. 1, p. 16–43.

Poag, C.W., and the Chesapeake Coring Team, 2001, Drilling to basement inside the Chesapeake Bay crater [abs.]: Lunar and Planetary Science Conference, 32d, Houston, Tex., March 12–16, 2001, Abstract 1203, available online at http://www.lpi.usra.edu/meetings/lpsc2001/pdf/1203.pdf

Poag, C.W., Gohn, G.S., and Powars, D.S., 2001, From shocked basement to fallout spherules; The coring record at the Chesapeake Bay crater [abs.]: Geological Society of America Abstracts with Programs, v. 33, no. 6, p. A–433.

Poag, C.W., Gohn, G.S., and Powars, D.S., 2002, Chesapeake Bay impact crater; Seismostratigraphy and lithostratigraphy of displaced sedimentary megablocks [abs.]: Lunar and Planetary Science Conference, 33d, League City, Tex., March 11–15, 2002, Abstract 1019, available online at http://www.lpi.usra.edu/meetings/lpsc2002/pdf/1019.pdf

Poag, C.W., Hutchinson, D.R., Colman, S.M., and Lee, M.W., 1999, Seismic expression of the Chesapeake Bay impact crater; Structural and morphologic refinements based on new seismic data, *in* Dressler, B.O., and Sharpton, V.L., eds., Large meteorite impacts and planetary evolution; II: Geological Society of America Special Paper 339, p. 149–164.

Poag, C.W., Koeberl, Christian, and Reimold, W.U., 2004, The Chesapeake Bay crater—Geology and geophysics of a late Eocene submarine impact structure: New York, Springer-Verlag, 522 p. plus CD-ROM.

Poag, C.W., Plescia, J.B., and Molzer, P.C., 1999, Chesapeake Bay impact structure; Geology and geophysics [abs.], *in* Gersonde, Rainer, and Deutsch, Alexander, eds., Oceanic impacts; Mechanisms and environmental perturbations; ESF–IMPACT Workshop, April 15–April 17, 1999, Alfred Wegener Institute for Polar and Marine Research, Bremerhaven, Germany, Abstracts: Berichte zur Polarforschung (Reports on Polar Research), v. 343, p. 79–83.

Poag, C.W., Plescia, J.B., and Molzer, P.C., 2002, Ancient impact structures on modern continental shelves; The Chesa-

peake Bay, Montagnais, and Toms Canyon craters, Atlantic margin of North America: Deep-Sea Research Part II—Topical Studies in Oceanography, v. 49, no. 6, p. 1081–1102.

Poag, C.W., Powars, D.S., Mixon, R.B., Edwards, L.E., Folger, D.W., Poppe, L.J., and Bruce, Scott, 1991, An upper Eocene impact-wave(?) deposit beneath Chesapeake Bay [abs.]: Geological Society of America Abstracts with Programs, v. 23, no. 5, p. A460.

Poag, C.W., Powars, D.S., Poppe, L.J., and Mixon, R.B., 1994, Meteoroid mayhem in Ole Virginny—Source of the North American tektite strewn field: Geology, v. 22, no. 8, p. 691–694.

Poag, C.W., Powars, D.S., Poppe, L.J., Mixon, R.B., Edwards, L.E., Folger, D.W., and Bruce, Scott, 1992, Deep Sea Drilling Project Site 612 bolide event—New evidence of a late Eocene impact-wave deposit and a possible impact site, U.S. East Coast: Geology, v. 20, no. 9, p. 771–774.

Powars, D.S., 2000, The effects of the Chesapeake Bay impact crater on the geologic framework and the correlation of hydrogeologic units of southeastern Virginia, south of the James River: U.S. Geological Survey Professional Paper 1622, 53 p., 1 oversize pl. (Also available online at http://pubs.usgs.gov/prof/p1622/)

Powars, D.S., and Bruce, T.S., 1999, The effects of the Chesapeake Bay impact crater on the geological framework and correlation of hydrogeologic units of the lower York-James Peninsula, Virginia: U.S. Geological Survey Professional Paper 1612, 82 p., 9 oversize pls. (Also available online at http://pubs.usgs.gov/prof/p1612/)

Powars, D.S., Bruce, T.S., Bybell, L.M., Cronin, T.M., Edwards, L.E., Frederiksen, N.O., Gohn, G.S., Horton, J.W., Jr., Izett, G.A., Johnson, G.H., Levine, J.S., McFarland, E.R., Poag, C.W., Quick, J.E., Schindler, J.S., Self-Trail, J.M., Smith, M.J., Stamm, R.G., and Weems, R.E., 2001, Preliminary geologic summary for the USGS-NASA Langley corehole, Hampton, Virginia: U.S. Geological Survey Open-File Report 01–87–B, 20 p., available online at http://pubs.usgs.gov/of/2001/of01-087/

Powars, D.S., Bruce, Scott, Poag, C.W., and Mixon, R.B., 1994, Virginia's coastal plain inland saltwater wedge; A geohydrologic response to the Chesapeake Bay bolide impact [abs.]: Geological Society of America Abstracts with Programs, v. 26, no. 7, p. A–410.

Powars, D.S., Gohn, G.S., Bruce, T.S., Johnson, G.H., Catchings, R.D., Frederiksen, N.O., Edwards, L.E., Self-Trail, J.M., and Pierce, H.A., 2002, Distribution and origin of impact-generated debris; Western annular trough, Chesapeake Bay impact crater [abs.]: Eos, Transactions, American Geophysical Union, v. 83, no. 19, spring meeting supplement of 7 May 2002, Abstract T21A–02, p. S351. (Also available online at http://www.agu.org/meetings/waissm02.html)

Powars, D.S., Gohn, G.S., Catchings, R.D., Horton, J.W., Jr., and Edwards, L.E., 2003, Recent research in the Chesapeake Bay impact crater, USA—Part 1. Structure of the western annular trough and interpretation of multiple collapse structures [abs.]: International Conference on Large Meteorite Impacts, 3d, Noerdlingen, Germany, August 5–7, 2003, Abstract 4053, available online at http://www.lpi.usra.edu/meetings/largeimpacts2003/pdf/4053.pdf

Powars, D.S., Gohn, G.S., Catchings, R.D., McFarland, E.R., Bruce, T.S., Johnson, G.H., Izett, G.A., Emry, S.R., and Edwards, L.E., 2001, Deep corehole and seismic reflection data provide insights into crater-filling processes and the hydrogeology of the outer margin of the Chesapeake Bay impact structure, eastern Virginia Coastal Plain, USA [abs.]: Lunar and Planetary Science Conference, 32d, Houston, Tex., March 12–16, 2001, Abstract 2183, available online at http://www.lpi.usra.edu/meetings/lpsc2001/pdf/2183.pdf

Powars, D.S., Gohn, G.S., Edwards, L.E., Bruce, T.S., Catchings, R.D., Emry, S.R., Johnson, G.H., Levine. J.S., Poag, C.W., and Pierce, H.A., 2001, Structure and composition of the southwestern margin of the buried Chesapeake Bay impact structure, Virginia [abs.]: Geological Society of America Abstracts with Programs, v. 33, no. 6, p. A–203.

Powars, D.S., Gohn, G.S., Edwards, L.E., Catchings, R.D., Bruce, T.S., Johnson, G.H., and Poag, C.W., 2002, Lithostratigraphic framework of the crater-fill deposits; Western annular trough, Chesapeake bay impact crater [abs.]: Geological Society of America Abstracts with Programs, v. 34, no. 6, p. 465.

Powars, D.S., Johnson, G.H., Bruce, T.S., and Edwards, L.E., 2001, The relation between the Chesapeake Bay impact structure and the structure and stratigraphy of Cenozoic deposits in eastern Virginia [abs.]: Geological Society of America Abstracts with Programs, v. 33, no. 2, p. A–76.

Powars, D.S., Johnson, G.H., Edwards, L.E., Horton, J.W., Jr., Gohn, G.S., Catchings, R.D., McFarland, E.R., Izett, G.A., Bruce, T.S., Levine, J.S., and Pierce, H.A., 2002, An expanded Chesapeake Bay impact structure, eastern Virginia; New corehole and geophysical data [abs.]: Lunar and Planetary Science Conference, 33d, League City, Tex., March 11–15, 2002, Abstract 1034, available online at http://www.lpi.usra.edu/meetings/lpsc2002/pdf/1034.pdf

Powars, D.S., Mixon, R.B., and Bruce, Scott, 1992, Uppermost Mesozoic and Cenozoic geologic cross section, outer coastal plain of Virginia, *in* Gohn, G.S., ed., Proceedings of the 1988 U.S. Geological Survey Workshop on the Geology and Geohydrology of the Atlantic Coastal Plain: U.S. Geological Survey Circular 1059, p. 85–101.

Powars, D.S., Mixon, R.B., Edwards, L.E., Andrews, G.W., and Ward, L.W., 1987, Evidence for Paleocene and lower Eocene pinch-outs on the north flank of the Norfolk arch, Eastern Shore of Virginia [abs.]: Geological Society of America Abstracts with Programs, v. 19, no. 2, p. 124.

Powars, D.S., Mixon, R.B., Edwards, L.E., Poag, C.W., and Bruce, Scott, 1990, Cross section of Cretaceous and Cenozoic strata, Norfolk arch to Salisbury basin, outer coastal plain of Virginia [abs.]: Geological Society of America Abstracts with Programs, v. 22, no. 4, p. 57.

Powars, D.S., Poag, C.W., and Mixon, R.B., 1993, The Chesapeake Bay "impact crater," stratigraphic and seismic evi-

dence [abs.]: Geological Society of America Abstracts with Programs, v. 25, no. 6, p. A–378.

Powars, D.S., Quick, J.E., Bruce, T.S., Catchings, R.D., Emry, S.R., Gohn, G.S., Izett, G.A., Johnson, G.H., Levine, J.S., McFarland, E.R., and Poag, C.W., 2001, Structure and composition of the southwestern margin of the buried Chesapeake Bay impact structure [abs.], *in* Morgan, M.L., and Warme, J.E., Bolide impacts on wet targets: Geological Society of America Field Forum, Nevada and Utah, April 2001, not paginated.

Rankin, D.W., 1994, Continental margin of the eastern United States; Past and present, *in* Speed, R.C., ed., Phanerozoic evolution of North American continent-ocean transitions—The Decade of North American Geology summary volume to accompany the DNAG continent-ocean transect series: Boulder, Colo., Geological Society of America, p. 129–218.

Reimold, W.U., Koeberl, Christian, and Poag, C.W., 2002, Chesapeake Bay impact crater; Petrographic and geochemical investigations of the impact breccia fill [abs.]: Geological Society of America Abstracts with Programs, v. 34, no. 6, p. 466.

Sanford, Samuel, 1913, The underground water resources of the Coastal Plain Province of Virginia: Virginia Geological Survey Bulletin 5, 361 p., 1 pl.

Sanford, W.E., 2002, Possible hydrothermal activity following the Chesapeake Bay bolide impact [abs.]: Geological Society of America Abstracts with Programs, v. 34, no. 6, p. 466.

Sanford, W.E., 2003, Heat flow and brine generation following the Chesapeake Bay bolide impact: Journal of Geochemical Exploration, v. 78–79, p. 243–247.

Self-Trail, J.M., 2003, Shock-wave-induced fracturing of calcareous nannofossils from the Chesapeake Bay impact crater: Geology, v. 31, no. 8, p. 697–700.

Sheridan, R.E., Maguire, T.J., Feigenson, M.D., Patino, L.C., and Volkert, R.A., 1999, Grenville age of basement rocks in Cape May, N.J. well—New evidence for Laurentian crust in U.S. Atlantic Coastal Plain basement Chesapeake terrane: Journal of Geodynamics, v. 27, no. 4–5, p. 623–633.

Shuvalov, V.V., Dypvik, H., and Tsikalas, F., 2002, Numerical modeling of the Mjølnir marine impact event [abs]: Lunar and Planetary Science Conference, 33d, League City, Tex., March 11–15, 2002, Abstract 1038, available online at http://www.lpi.usra.edu/meetings/lpsc2002/pdf/1038.pdf

Steckler, M.S., Mountain, G.S., Miller, K.G., and Christie-Blick, Nicholas, 1999, Reconstruction of Tertiary progradation and clinoform development on the New Jersey passive margin by 2-D backstripping: Marine Geology, v. 154, no. 1–4, p. 399–420.

Stewart, S.A., and Allen, P.J., 2002, A 20-km-diameter multi-ringed impact structure in the North Sea: Nature, v. 418, no. 6897, p. 520–523.

Tennant, Diane, 2001, A cosmic tale, reprinted from The Virginian-Pilot, June 24–30, 2001: Hampton Roads, Va., The Virginian-Pilot, 16 p.

U.S. Geological Survey, 1997, The Chesapeake Bay watershed [an image mosaic compiled from Landsat Thematic Mapper images collected from 1990 through 1994]: Reston, Va., U.S. Geological Survey poster, 1 sheet. (Also available online at http://chesapeake.usgs.gov/poster.html)

von Dalwigk, Ilka, and Ormö, Jens, 2001, Formation of resurge gullies at impacts at sea; The Lockne crater, Sweden: Meteoritics & Planetary Science, v. 36, no. 3, p. 359–369.

Vozoff, Keeva, 1991, The magnetotelluric method, chapter 8 *in* Nabighian, M.N., and Corbett, J.D., eds., Electromagnetic methods in applied geophysics: Society of Exploration Geophysicists Investigations in Geophysics no. 3, v. 2 (Applications), pt. A, p. 641–712.

Ward, L.W., 1984, Stratigraphy of outcropping Tertiary beds along the Pamunkey River, central Virginia Coastal Plain, *in* Ward, L.W., and Krafft, Kathleen, eds., Stratigraphy and paleontology of the outcropping Tertiary beds in the Pamunkey River region, central Virginia Coastal Plain—Guidebook for Atlantic Coastal Plain Geological Association Field Trip, October 6–7, 1984: Atlantic Coastal Plain Geological Association, p. 11–77, 12 pls.

Appendix A1. Abstracts of Research on the Chesapeake Bay Impact Structure, 2001–2003

Citations for the listed abstracts are in the "References Cited."

Year 2001

Catchings, Powars, and others (2001)
Gohn, Bruce, and others (2001)
Gohn, Powars, and others (2001)
Horton and others (2001)
Poag and the Chesapeake Coring Team (2001)
Poag, Gohn, and Powars (2001)
Powars, Gohn, Catchings, and others (2001)
Powars, Gohn, Edwards, Bruce, and others (2001)
Powars, Johnson, Bruce, and Edwards (2001)
Powars, Quick, and others (2001)

Year 2002

Catchings, Powars, Gohn, and Goldman (2002)
Crawford (2002)
Edwards and Self-Trail (2002)
Edwards and others (2002)
Emry and others (2002)
Glass (2002)
Gohn, Powars, Bruce, and others (2002)
Gohn, Powars, Quick, Horton, and Catchings (2002)
Horton, Aleinikoff, and others (2002)
Horton, Kunk, and others (2002)
McFarland (2002)
McFarland and Bruce (2002)
Poag (2002a,b,d)
Poag, Gohn, and Powars (2002)
Powars, Gohn, Bruce, and others (2002)
Powars, Gohn, Edwards, Catchings, and others (2002)
Powars, Johnson, Edwards, and others (2002)
Reimold and others (2002)
Sanford (2002)

Year 2003

Horton and others (2003)
Powars and others (2003)

Petrography, Structure, Age, and Thermal History of Granitic Coastal Plain Basement in the Chesapeake Bay Impact Structure, USGS-NASA Langley Core, Hampton, Virginia

By J. Wright Horton, Jr., John N. Aleinikoff, Michael J. Kunk, Charles W. Naeser, and Nancy D. Naeser

Chapter B of
Studies of the Chesapeake Bay Impact Structure—The USGS-NASA Langley Corehole, Hampton, Virginia, and Related Coreholes and Geophysical Surveys

Edited by J. Wright Horton, Jr., David S. Powars, and Gregory S. Gohn

Prepared in cooperation with the
Hampton Roads Planning District Commission,
Virginia Department of Environmental Quality, and
National Aeronautics and Space Administration Langley Research Center

Professional Paper 1688

U.S. Department of the Interior
U.S. Geological Survey

Contents

Figures

Tables

Petrography, Structure, Age, and Thermal History of Granitic Coastal Plain Basement in the Chesapeake Bay Impact Structure, USGS-NASA Langley Core, Hampton, Virginia

By J. Wright Horton, Jr.,[1] John N. Aleinikoff,[2] Michael J. Kunk,[2] Charles W. Naeser,[1] and Nancy D. Naeser[1]

Abstract

The USGS-NASA Langley corehole at Hampton, Va., was drilled in 2000 and was the first corehole to reach coastal plain basement in the late Eocene Chesapeake Bay impact structure. The Langley core provided samples of granite that had been concealed by 626.3 meters (2,054.7 feet) of preimpact, synimpact, and postimpact sediments. The granite, here named the Langley Granite, is pale red, medium grained, massive, and homogeneous in composition and fabric. It has a peraluminous composition (alumina saturation index 1.1) and a seriate-inequigranular, hypidiomorphic, isotropic fabric.

A pervasive secondary mineral assemblage of chlorite + albite + clinozoisite is consistent with either deuteric alteration or lower greenschist-facies metamorphism. Chlorite, the principal mafic mineral, occurs as tabular masses that suggest pseudomorphous replacement of biotite. The top of the granite is weathered but not saprolitized and is nonconformably overlain by Lower Cretaceous clastic sediments.

A SHRIMP $^{206}Pb/^{238}U$ weighted average zircon age of 612±10 Ma (2σ) indicates Neoproterozoic crystallization of the Langley Granite. The $^{40}Ar/^{39}Ar$ ages of microcline and plagioclase are consistent with regional cooling and uplift after the late Paleozoic Alleghanian orogeny. Zircon and apatite fission-track cooling ages of 375±44 Ma and 184±32 Ma (2σ), respectively, indicate no discernible impact-related thermal disturbance at the Langley corehole location in the annular trough of the structure about 19 kilometers (12 miles) outside the margin of the central crater.

Modeling the apatite fission-track data places upper limits on the impact-related heating at this location. For an impact-related thermal disturbance equivalent to a modeled thermal spike having a duration of 1 to 0.1 million years, temperatures in this part of the impact structure could not have been higher than about 100°C–120°C.

Most fractures, faults, and veins in the Langley Granite contain lower greenschist-facies minerals and are inferred to predate the impact. No shock-metamorphosed minerals or other features clearly attributable to the impact were found in the granite. Studies of the granite provide a glimpse into the nature of crystalline terranes beneath the Atlantic Coastal Plain and Chesapeake Bay and provide limits on the geographic extent of impact-generated shock and thermal effects.

Introduction

The USGS-NASA Langley corehole at Hampton, Va., was drilled in 2000 and was the first corehole to reach coastal plain basement in the late Eocene Chesapeake Bay impact structure. This structure is near the mouth of Chesapeake Bay, where it lies buried beneath postimpact sediments of the Atlantic Coastal Plain (fig. B1); it was described in earlier reports (Poag and others, 1992, 1994; Poag, 1996, 1997, 1999; Powars and Bruce, 1999; Powars, 2000). The Chesapeake Bay impact structure is one of the largest on Earth and is one of the few fully marine impact structures that have been extensively studied by seismic reflection and drilling (Reimold and others, 2002).

These studies reveal that the buried structure is a complex impact crater 85 kilometers (km; 53 miles (mi)) wide. It consists of an excavated central crater, which is 30–38 km (18–24 mi) wide and 1–2 km (0.6–1.2 mi) deep, surrounded by a flat-floored annular trough, which is 21–31 km (13–19 mi) wide and

[1]U.S. Geological Survey, Reston, VA 20192.
[2]U.S. Geological Survey, Denver, CO 80225.

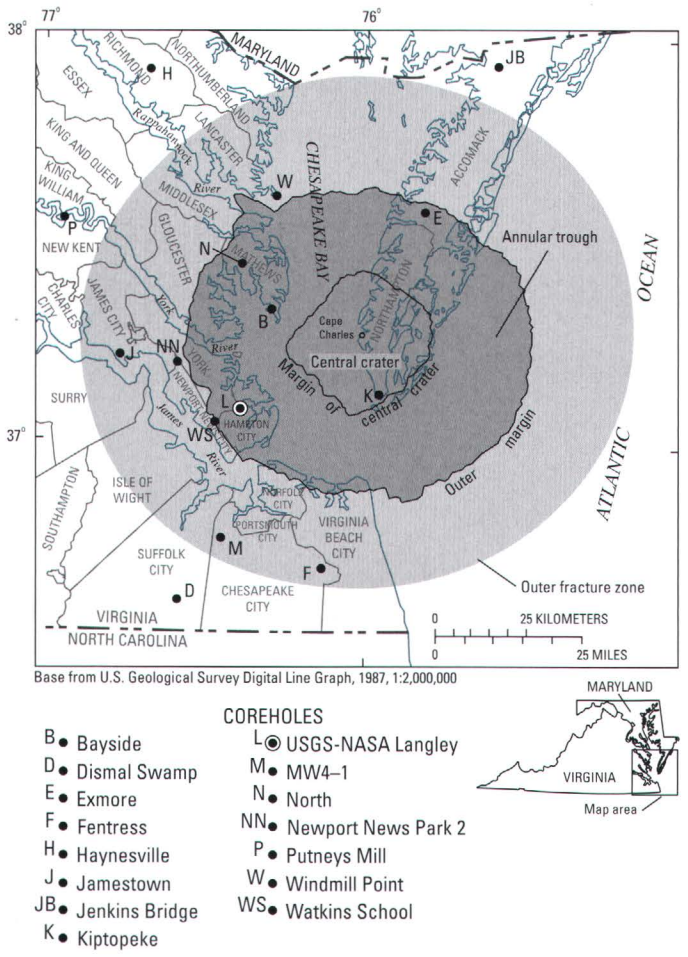

Figure B1. Regional map showing the location of the Chesapeake Bay impact structure, the USGS-NASA Langley corehole at Hampton, Va., and some other coreholes in southeastern Virginia. Locations of the central crater and outer margin are from Powars and Bruce (1999). The extent of the outer fracture zone (light gray) is based on Powars (2000) and Johnson and others (2001); the eastern part is speculative. Illustration modified from Powars, Johnson, and others (2002) and Edwards and Powars (2003).

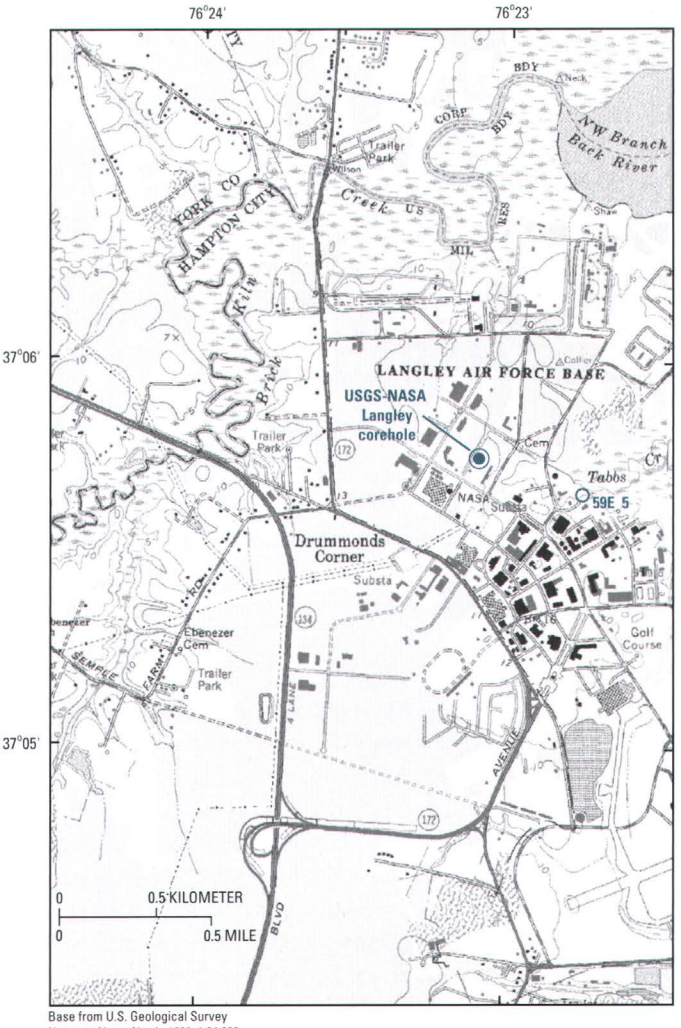

Figure B2. Detailed map showing the locations of the USGS-NASA Langley corehole (59E 31) and the 1974 NASA Langley test well (59E 5) at the NASA Langley Research Center, Hampton, Va. In 2000, the corehole provided samples of granite; for the 1974 well, "granite" was also reported beneath sediments of the coastal plain (Johnson, 1975).

contains disrupted sediments, a slumped terrace zone, and an eroded escarpment (Poag, 2002; Powars, Gohn, and others, 2002; Powars, Johnson, and others, 2002). This annular trough is encircled by a 35-km-wide (22-mi-wide) outer fracture zone of concentric faults (Powars, Gohn, and others, 2002; Powars, Johnson, and others, 2002).

The innermost part of the annular trough is interpreted by some workers (Poag, Hutchinson, and others, 1999; Poag, 2002; Poag and Norris, this volume, chap. F) to be underlain by a crystalline-rock peak ring that surrounds the central crater. In Poag's (2002) interpretation, a peak ring was inferred to be about 9 km (5.6 mi) wide and to have about 126 meters (m; 413 feet (ft)) of relief, and the central crater was inferred to contain a 5-km-wide (3-mi-wide) central peak having about 620 m (2,034 ft) of relief.

The USGS-NASA Langley corehole is on the York-James Peninsula at the National Aeronautics and Space Administration (NASA) Langley Research Center in Hampton, Va., about 19 km (12 mi) outside the margin of the central crater and about 8 km (5 mi) inside the outer margin of the annular trough as mapped by Powars and Bruce (1999) (figs. B1 and B2). The hole was drilled by the U.S. Geological Survey (USGS) and cooperators (see "Acknowledgments"). Preliminary descriptions of the core are available in Gohn, Clark, and others (2001), Gohn, Powars, and others (2001), Horton and others (2001), and Powars and others (2001).

The core shows a weathered granite below 626.3 m (2,054.7 ft) depth. This granite is overlain by weakly to strongly impact-disturbed preimpact sediments (crater units A and B of Gohn and others, this volume, chap. C), followed by a crater-fill unit informally known as the Exmore beds (Powars and others, 1992; Gohn and others, this volume, chap. C) and by postimpact sediments (Powars and others, this volume, chap. G).

The impact-disturbed sediments include a basal crater unit A, consisting of autochthonous Lower Cretaceous sediments of the Potomac Formation, which Gohn and others (this volume, chap. C) divide into lower beds (nonfluidized) and upper beds (variably fluidized). Crater unit A is present in the Langley core between depths of 626.3 and 442.5 m (2,054.7 and 1,451.7 ft) and is 183.8 m (603.0 ft) thick.

The overlying crater unit B consists of Lower Cretaceous sediments that have zones of extensive fluidization, injection, and mixing (Powars, Gohn, and others, 2002; Gohn, Powars, and others, 2001 and this volume, chap. C). Crater unit B is present in the Langley core between depths of 442.5 and 269.4 m (1,451.7 and 884.0 ft) and is 173.0 m (567.7 ft) thick.

The overlying unit known as the Exmore beds is a polymict diamicton composed of mixed sediments previously interpreted as tsunami deposits (Powars and Bruce, 1999; Powars, 2000) and reinterpreted as mainly seawater-resurge deposits (Gohn and others, this volume, chap. C). The Exmore beds in the Langley core extend from 269.4 to 235.65 m (884.0 to 773.12 ft) depth and have a thickness of 33.8 m (110.9 ft).

Crystalline rocks hidden under the thick blanket of Atlantic Coastal Plain and continental margin sediments make up one of the most poorly understood areas of geology in the United States (LeVan and Pharr, 1963; Denison and others, 1967; Daniels and Leo, 1985; Russell and others, 1985; Pratt and others, 1988; Horton and others, 1991; Rankin, 1994; Glover and others, 1997; Sheridan and others, 1999). Initial results of investigations on crystalline basement and impact-derived clasts from the most recent coreholes in the Chesapeake Bay impact structure were summarized in Horton and others (2001), Horton, Aleinikoff, and others (2002), and Horton, Kunk, and others (2002).

Studies of granite in the USGS-NASA Langley core, presented below, provide insight into the nature of crystalline basement terranes beneath the Atlantic Coastal Plain and Chesapeake Bay. They also provide boundary constraints on the geographic extent of impact-generated shock and thermal effects for numerical models of the late Eocene impact event.

Langley Granite (Here Named)

The Langley Granite is here named for the NASA Langley Research Center in Hampton, Va., where it was recovered in drill core from the USGS-NASA Langley corehole. The corehole site (fig. B2) is designated the type locality. It is "a short distance north of Langley Boulevard and southwest of Building 1190 in an open grassy area" (Powars and others, 2001, p. 3). The corehole is at lat 37°05'44.28" N., long 76°23'08.96" W. (North American Datum of 1927), at a ground-surface altitude of 2.4 m (7.9 ft) above the North American Vertical Datum of 1988.

Chloritized granite in the core extends from the upper contact at a depth of 626.3 m (2,054.7 ft) to the end of the core at 635.1 m (2,083.8 ft) below the ground surface (fig. B3*A*). In the corehole, the Langley Granite is overlain by clastic sediments of crater unit A, which are derived from the Cretaceous Potomac Formation; the upper contact of the granite is visible in the core as a sharp nonconformity (figs. B3*B* and B3*C*). The uppermost granite is highly weathered and crumbly, but no saprolite is present. Of the 8.9 m (29.1 ft) of granite core recovered, only the lowest ~0.9 m (~3 ft) is mostly unweathered except along fractures. The core shows a weathering profile in granite that appears to have been essentially homogeneous in original composition and grain size. The progressive decrease in weathering with increasing depth below the upper contact is conspicuous.

The top of the coastal plain basement in this area is characterized on seismic-reflection profiles by a distinct pair of reflectors (Catchings and others, this volume, chap. I), which we interpret as the top of the weathered granite (or other crystalline rock) and the base of the underlying transition from weathered to unweathered rock. The thickness of the weathering profile based on these data is about 40 m (about 130 ft).

Rounded pebbles of the granite in overlying Cretaceous sediments are present within about 2 m (6 ft) of the contact in the Langley core (fig. B3*B*,*C*); the pebbles diminish upward in size and abundance. The upper contact of the granite in the core is not faulted, although irregularly spaced faults were observed in the Langley core through the overlying Cretaceous sediments.

The areal extent of the Langley Granite beyond the USGS-NASA Langley corehole is undetermined because the body is concealed by coastal plain sediments. The Langley Granite was apparently drilled in 1974 in well 59E 5 (fig. B2), where "granite" cuttings were reported from a depth of about 636 m (2,088 ft) (table 1 of Johnson, 1975); a full description of the rock in these cuttings is unavailable. The location of this well in figure B2 is from unpublished USGS drilling records provided by Gregory S. Gohn (USGS, written commun., 2001) and is consistent with Powars and Bruce (1999, appendix 1A); it is at lat 37°05'38" N., long 76°22'43" W. Both the 59E 5 well and the newer USGS-NASA Langley corehole are located within a poorly defined 28-milligal gravity low, which was interpreted as evidence for a buried granitoid pluton in the vicinity of the NASA Langley Research Center before the Langley corehole was drilled (Daniels and Leo, 1985; Horton and others, 1991).

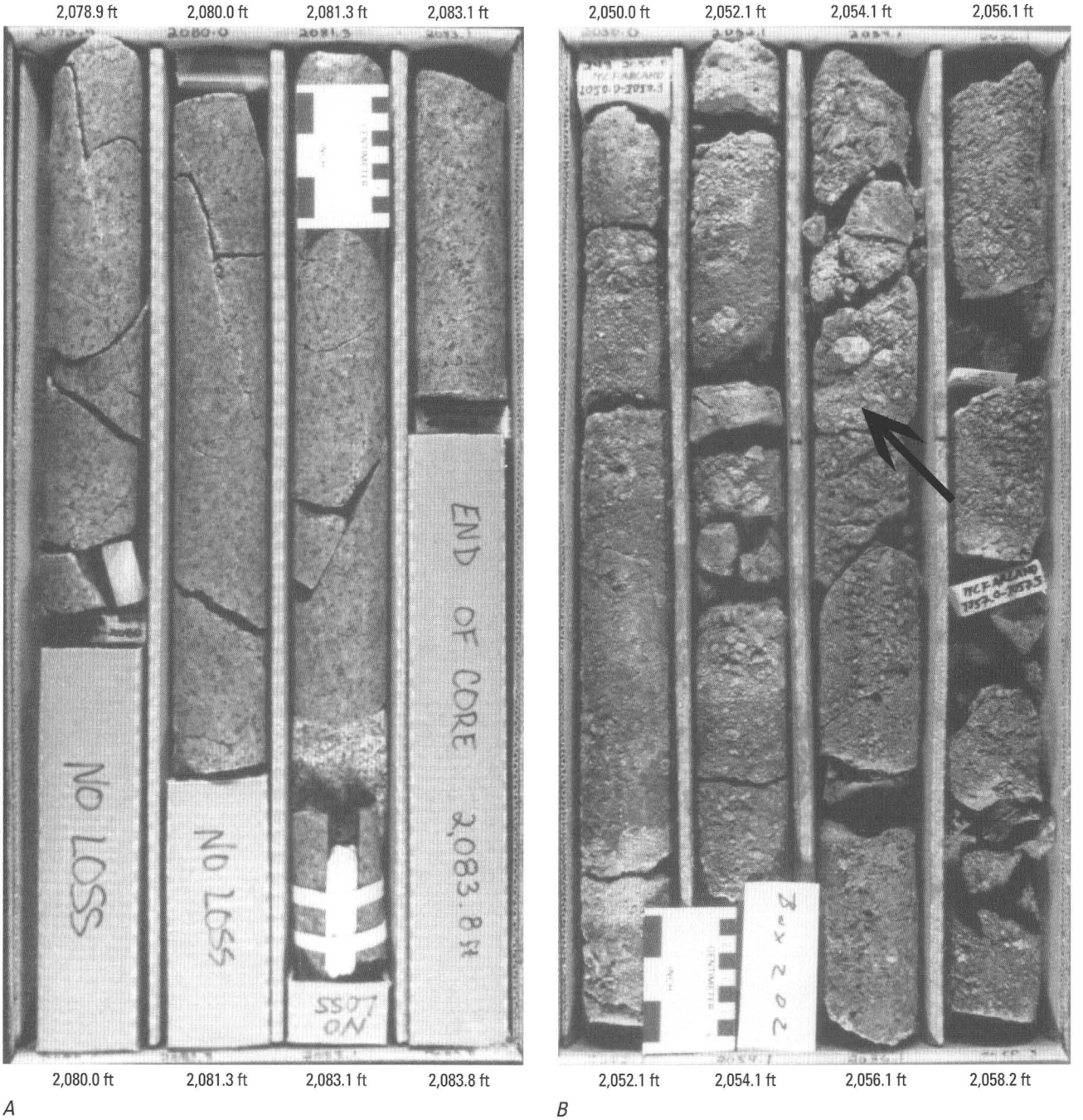

Figure B3. Photographs of sections of the USGS-NASA Langley core showing the Langley Granite and its upper contact. In core boxes, depth increases from left to right and top to bottom. Depths handwritten on the core boxes in feet are repeated in type for clarity. *A*, Core box 206 showing the deepest, least weathered section of Langley Granite core from 633.6 to 635.1 m (2,078.9 to 2,083.8 ft) depth; the granite is massive, medium grained, homogeneous in composition and fabric, nonfoliated, and mostly unweathered except along fractures. White spacer in the third column replaces slab from which sample NL2083.1 was taken. The scales are in centimeters (right side) and inches (left side). *B*, Upper contact of the Langley Granite in core box 202. Arrow points to the nonconformable contact between the weathered Langley Granite and overlying sediments of crater unit A derived from the Cretaceous Potomac Formation; the contact was drilled at 626.3 m (2,054.7 ft) depth. The contact was in the third column from left, 1.5 cm (0.59 in.) above the tick mark on the cardboard divider when the photograph was taken. The scales are in centimeters (right side) and inches (left side). *C*, Same nonconformable contact (at arrow) in closeup view. The centimeter scale has millimeter subdivisions.

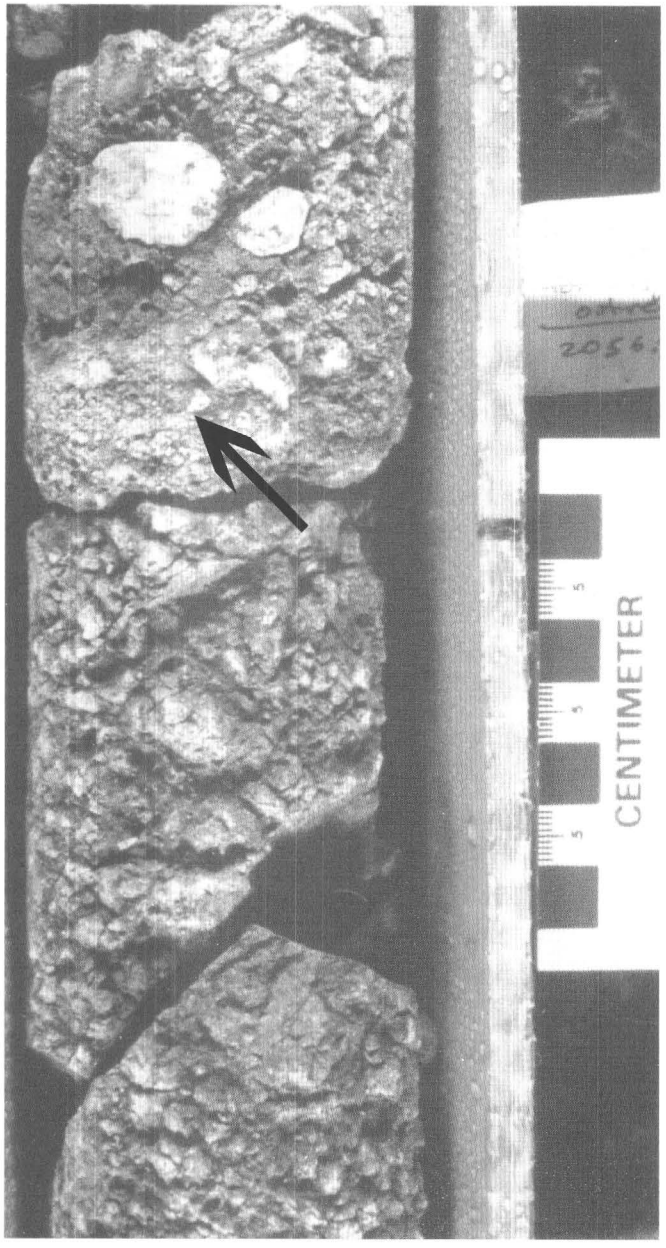

C

Figure B3. Continued.

Petrography, Mineralogy, and Texture

The Langley Granite in the USGS-NASA Langley core is pale red, medium grained, massive, homogeneous in composition and fabric, and nonfoliated (fig. B3*C*; see sample descriptions in appendix B1). The fabric is seriate-inequigranular, hypidiomorphic, homogeneous, and isotropic. The granite consists of oligoclase and albite (33–35 percent by volume), microcline (21–25 percent including perthite), quartz (32–40 percent), greenish-black chlorite (4–8 percent), and less than 1 percent opaque minerals (table B1). The rocks in all four of the thin sections examined are classified as monzogranite. Trace minerals identified by optical microscope, scanning-electron microscope (SEM), and X-ray diffraction include monazite, clinozoisite, titanite (within chlorite), hematite, iron-titanium oxides, apatite, and zircon. No amphibole, biotite, muscovite, garnet, or cordierite were found.

The microcline is mostly perthitic, having albite intergrowths and clean albite-free rims (fig. B4*A*). Plagioclase crystals are euhedral to subhedral, have concentric zones accentuated by differences in saussuritization, and locally coalesce as glomerocrysts. Both oligoclase and albite are present. In thin section under transmitted light, the oligoclase and albite appear cloudy, whereas quartz is clear. Quartz commonly has undulatory extinction, and some of the largest crystals have deformation bands. Disseminated micrographic (granophyric) intergrowths of microcline, quartz, and plagioclase make up about 10 percent of the rock. This granophyre, formed by the simultaneous crystallization of feldspars and quartz, is interpreted to represent the last fraction of granite to crystallize from a water-saturated melt.

Chlorite, the principal mafic mineral, occurs as tabular masses (fig. B4*B*), suggesting pseudomorphous replacement of biotite. The chlorite is magnesium-rich (as indicated by SEM backscatter data) clinochlore (as determined by X-ray diffraction). SEM backscatter imaging indicates that the chlorite has abundant inclusions of other minerals, including albite, an epidote mineral (clinozoisite?), titanite, and a low-titanium iron oxide. Trace amounts of magnetite evident in hand samples are associated with chlorite.

The granite has been pervasively chloritized, as evidenced by the abundant chlorite in shapes suggesting pseudomorphous replacement of biotite and by the apparent absence of igneous biotite or amphibole. The secondary assemblage of chlorite + albite + clinozoisite is consistent with either (1) subsolidus deuteric alteration of igneous minerals by hydrothermal solutions residual from the magma when the granite was still hot and water saturated (autometamorphism) or (2) lower greenschist-facies regional metamorphism. The lack of foliation or other ductile fabrics suggests essentially static conditions during the chloritization. An apparent lack of pegmatite and aplite may not be meaningful because of the limited amount of granite drill core.

Chemical analyses show that concentrations of major and trace elements in a Langley Granite sample are typical of monzogranite (table B2 and Horton and Izett, this volume, chap. E, table E2). The granite is slightly peraluminous, having an alumina saturation index (A/CNK = $Al_2O_3/[CaO+Na_2O+K_2O]$, mol proportion) of 1.1 and corundum in the CIPW norm. The inferred primary mafic and accessory mineral assemblage of biotite (now totally replaced by chlorite), monazite, and iron-titanium oxides is also consistent with peraluminous rocks.

Chemical analyses were also obtained for a rhyolite clast (NL790.9) from the Exmore beds of the Langley core (table B2). This clast, which is interpreted to be impact derived, is slightly peraluminous and is similar in composition to the granite (Horton and others, 2001; Horton and Izett, this volume, chap. E).

Table B1. Modal composition and rock classification of the Langley Granite from the USGS-NASA Langley core.

[Mineral percentages were estimated visually from thin sections in transmitted light. Plagioclase includes oligoclase + albite, microcline includes perthite, and chlorite has trace-mineral inclusions. The rock classification was based on proportions of quartz (Q), alkali feldspar (A), and plagioclase (P) in the diagram by Streckeisen (1973, 1976). tr, trace amount (less than 1 percent)]

A, Modal composition (volume percent)

Sample no.	NL2080.1		NL2083.1		Mean	Range
Thin section	1	2	1	2		
Quartz	32	35	36	40	35.75	32–40
Plagioclase	35	33	35	35	34.50	33–35
Microcline	25	25	25	21	24.00	21–25
Chlorite	8	7	4	4	5.75	4–8
Opaque minerals	tr	tr	tr	tr	tr	tr
Other minerals	tr	tr	tr	tr	tr	tr
Total	100	100	100	100	100.00	

B, Rock classification

Sample no.	NL2080.1	NL2083.1
Q	36	40
A	27	24
P	37	36
(P/[P+A]) x 100	58	60
Name	Monzogranite	Monzogranite

Figure B4. Photographs of pieces of the USGS-NASA Langley core and photomicrographs of thin sections of the core showing mineralogy, texture, and structure of the Langley Granite. *A*, *B*, and *D* are photomicrographs of thin sections in plane-polarized light; *C*, *E*, *F*, and *G* are photographs of core. *A*, Typical Langley Granite composed of cloudy plagioclase (P) that includes both albite and oligoclase, quartz (Q), perthitic microcline (M) having albite intergrowths and albite-free rims, and chlorite (C) (sample NL2083.1, stained thin section 1, plane-polarized light; vertical dimension is 4 millimeters (mm; 0.16 in.)). *B*, Chlorite (C), in euhedral, tabular shape suggesting pseudomorphous replacement of biotite, contains inclusions of albite (A) and opaque minerals (sample NL2083.1, thin section 2, plane-polarized light). *C*, Joint surface coated by white albite crystals from 633.1 m (2,077.2 ft) depth. *D*, Fracture filled by albite (A) and smaller amounts of chlorite (C) (NL2080.1, thin section 2, plane-polarized light; vertical dimension is 2 mm (0.078 in.)). *E*, Fault surface coated by slickensided chlorite from 631.2 m (2,071.0 ft) depth. *F*, Clinozoisite vein from 631.3 m (2,071.3 ft) depth (see arrow point). *G*, Fracture having open cavities coated by drusy quartz crystals from 631.3 m (2,071.2 ft) depth.

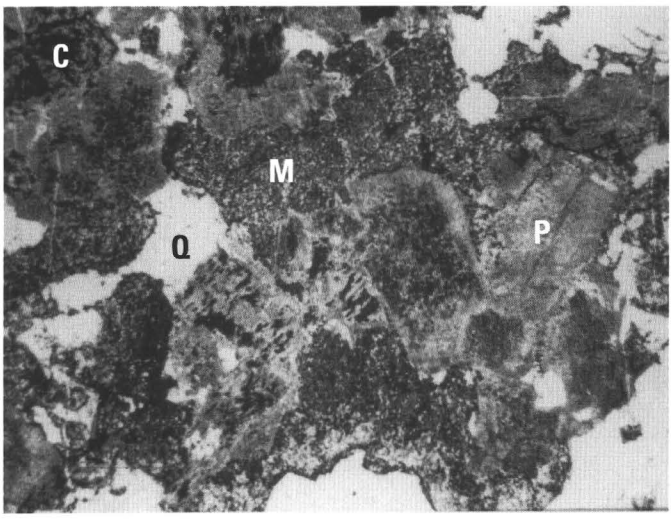

A

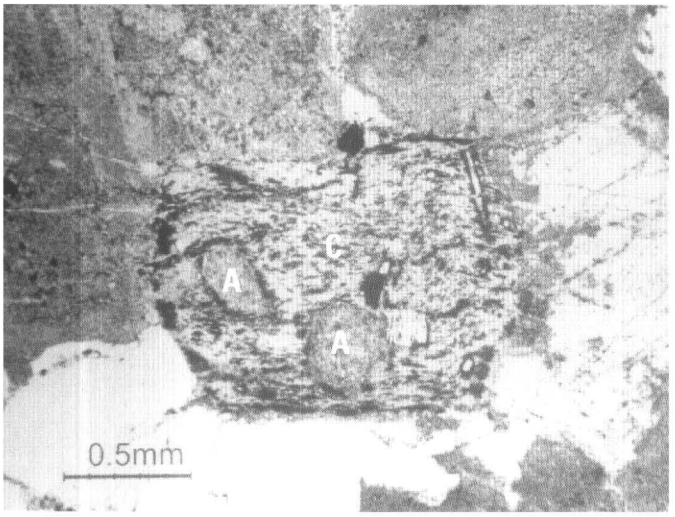

B

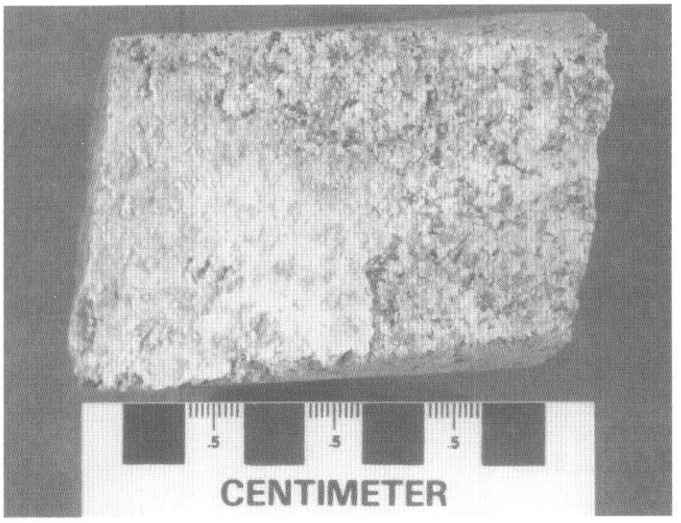

C

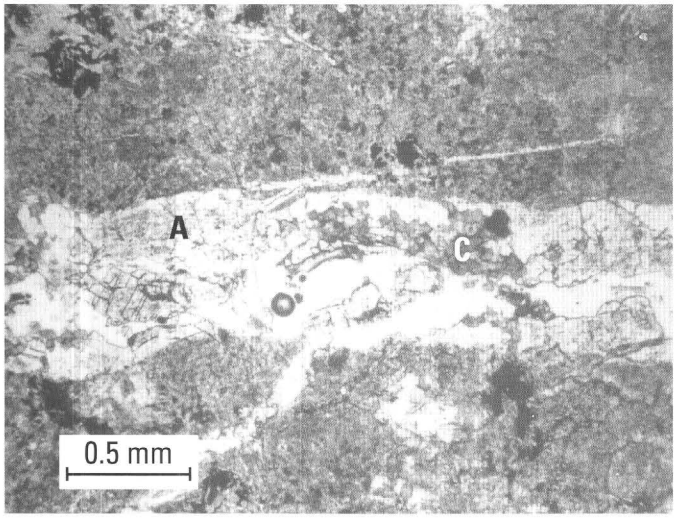

D

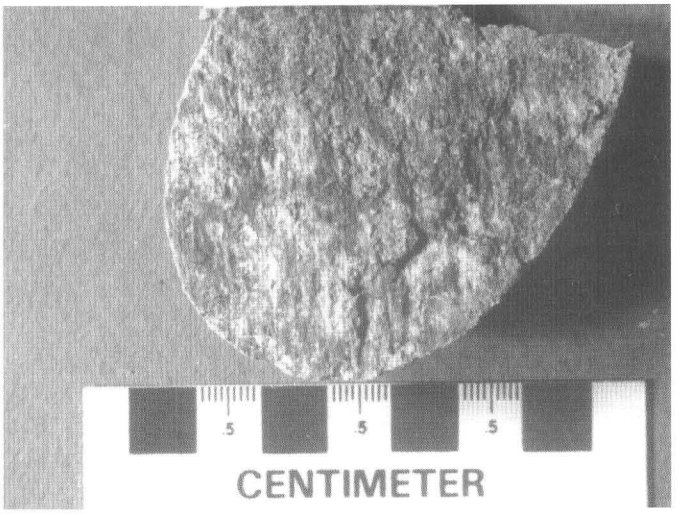

E

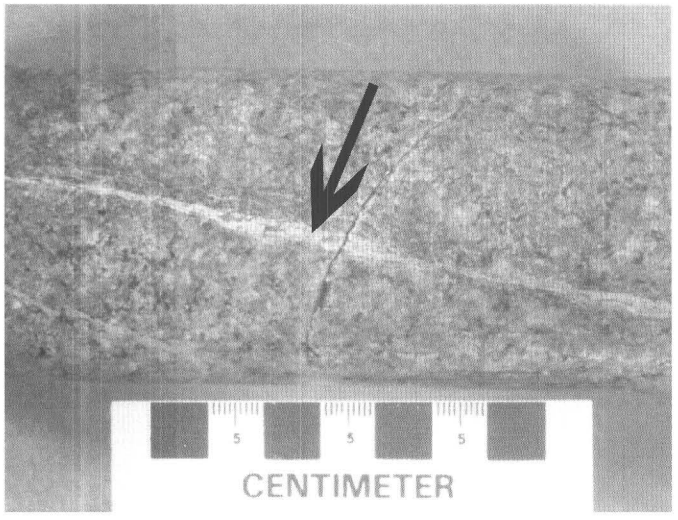

F

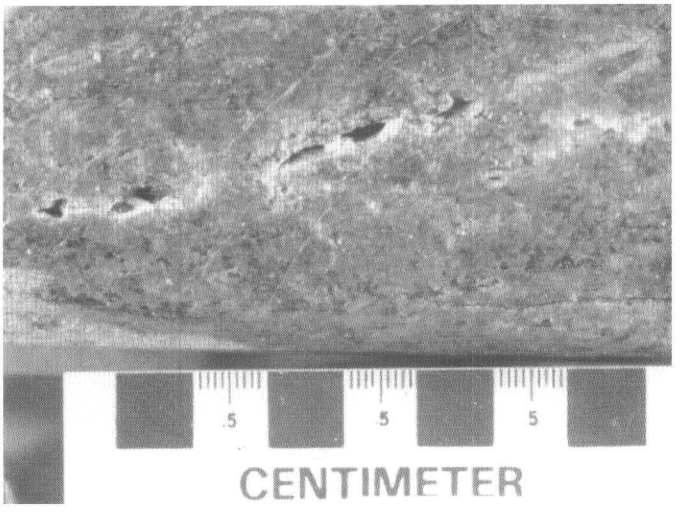

G

Figure B4. Continued.

Table B2. Chemical and normative mineral compositions of two samples of crystalline rocks from the USGS-NASA Langley core.

[Complete analyses and details are in Horton and Izett (this volume, chap. E)]

Sample no.....	NL2083.1	NL790.9
Rock type.....	monzogranite	rhyolite clast
Unit.....	Langley Granite	Exmore beds
Chemical composition, in weight percent		
SiO_2.....	71.0	74.9
Al_2O_3.....	14.2	12.8
Fe_2O_3.....	1.90	.83
FeO.....	1.03	.97
MgO.....	.77	.64
CaO.....	1.29	.91
Na_2O.....	3.98	4.11
K_2O.....	3.48	2.69
H_2O+.....	.9	.8
H_2O-.....	.1	.1
TiO_2.....	.38	.25
P_2O_5.....	.13	.11
MnO.....	.06	.06
CO_2.....	<.01	.14
S.....	.42	.18
F.....	.04	.02
Total.....	99.7	99.5
Normative mineral composition (CIPW norms), in weight percent		
Quartz.....	30.98	37.74
Orthoclase.....	20.56	15.90
Albite.....	33.67	34.77
Anorthite.....	5.55	3.80
Hypersthene.....	1.92	2.39
Magnetite.....	2.41	1.20
Ilmenite.....	.72	.47
Hematite.....	.24	.00
Corundum.....	1.85	1.74
Apatite.....	.30	.25
Total.....	98.2	98.26
Oxides for alumina saturation index, in mol percent		
Al_2O_3.....	9.1	12.6
CaO.....	1.5	1.6
Na_2O.....	4.2	6.6
K_2O.....	2.4	2.9
A/CNK*.....	1.1	1.1

*The alumina saturation index A/CNK = $Al_2O_3/[CaO+Na_2O+K_2O]$.

Petrologic studies of the chemical and physical parameters that controlled the genesis and evolution of the Langley Granite (including the history of melt production, ascent, and emplacement conditions) and regional geochemical comparisons would require additional rock analyses. Having less than 1 m (3 ft) of granite core that is mostly unweathered is a current limitation.

Fractures, Faults, and Veins

Most of the fractures, faults, and veins in the Langley Granite are coated or filled by chlorite, albite, and clinozoisite, which are typical of lower greenschist-facies metamorphic or similar deuteric alteration conditions, and by quartz. Figure B4*C* shows a joint surface coated by albite, figure B4*D* shows a similar fracture filled by albite and smaller amounts of chlorite, figure B4*E* shows a fault surface coated by chlorite, and figure B4*F* shows a clinozoisite vein. These fracture-fill minerals probably formed at temperatures higher than the effective closure temperature of about 90°C–100°C for fission tracks in apatite, which yield an age (presented below) far older than the late Eocene impact event. An attempt to directly date albite on a joint surface by the $^{40}Ar/^{39}Ar$ method is described below.

Figure B4*G* shows a quartz-filled fracture in which open cavities are coated by drusy, comb quartz crystals. Similar dilational fractures are commonly associated with early Mesozoic extensional faults in eastern North America (Garihan and others, 1993). Whether the quartz-filled fractures in the Langley Granite are related to the early Mesozoic continental rifting, earlier deuteric alteration or lower greenschist-facies mineralization, and (or) the late Eocene impact event is undetermined. Fractures in the granite core do not appear unusually abundant in comparison to fractures in drill cores from the Piedmont of the southeastern United States.

The variably mineralized joints in the granite have a wide range of dip angles. Dips were measured for 24 joints (excluding freshly broken surfaces) in the least weathered core section from 633.6 to 635.1 m (2,078.9 to 2,083.8 ft) depth (shown in fig. B3*A*). Dips for the 24 joints are grouped as follows:

- 8 percent are horizontal to subhorizontal (0°–10° dip)
- 21 percent are gently inclined (11°–30° dip)
- 29 percent are moderately inclined (31°–60° dip)
- 38 percent are steeply inclined (61°–80° dip)
- 4 percent are subvertical to vertical (81°–90° dip)

Faults in the overlying Cretaceous sediments are irregularly spaced in the core, where they are clearly recognizable as planes or planar zones of offset. Although not studied in detail, they include moderately dipping normal faults (identified on the basis of slickensides and rotation of adjacent material) and a few subhorizontal faults, which are visible in the core as local slickensided detachments (J.W. Horton, Jr., unpub. data).

Careful examination of the core revealed no such faults at the upper contact of the weathered granite. There is no evidence from this study of the granite, or from studies of the overlying Cretaceous sediments in the Langley core (Gohn and others, this volume, chap. C), to indicate a major décollement zone just above the granite. Such a zone had been suggested after a preliminary examination of this core (Poag and others, 2001) in order to explain earlier seismic evidence that most normal faults in the overlying sediments do not extend into the crystalline basement (Poag, Plescia, and Molzer, 1999). However, décollements may be found higher in the sedimentary section along the deepest subhorizontal fluidized zone at 558.1 m (1,831.0 ft) depth and in the upper fluidized part of crater unit A (Gohn and others, this volume, chap. C). The seismic-reflection data are more consistent with numerous small-displacement faults than a few large-displacement faults in the preimpact sediments (Catchings and others, this volume, chap. I).

Seismic-reflection data from parts of the Chesapeake Bay impact structure indicate that the top of coastal plain basement is locally offset by high-angle normal faults and low-angle reverse faults, although broad areas of the basement surface appear relatively flat and unfaulted (Poag, Hutchinson, and others, 1999). Catchings and others' (2002) 13.6-km-long (8.5-mi-long) seismic-reflection profile, which is linked to the core samples and to the sonic velocity log from the USGS-NASA Langley corehole, shows nearly 200 m (nearly 650 ft) of relief on the top of basement. Numerous diffractions on the unmigrated profile suggest that inhomogeneities such as the variably mineralized fractures, veins, and faults observed in the granite core are widespread throughout the Langley Granite. Other possible diffractions due to multiple injections, pegmatites, country-rock screens, or xenoliths were not observed in the core but cannot be ruled out because the granite core section is so short. The seismic profile also shows faults in the overlying sedimentary section, which are interpreted to be related to the late Eocene impact event. A few of these faults are inferred to penetrate and slightly offset the top of the Langley Granite in the general vicinity of the USGS-NASA Langley corehole (Catchings and others, this volume, chap. I). The impact-related faults anticipated from regional seismic-reflection data were not found in the Langley Granite core samples, but the small section (8.9 m or 29.1 ft) of granite core limited the chance of intersecting such faults.

Neoproterozoic Uranium-Lead (SHRIMP) Zircon Age

About 2 kilograms (about 4.4 pounds) of slightly weathered granite from a sawed half of the USGS-NASA Langley core from 633.98 m to 634.81 m (2,080.0 ft to 2,082.7 ft) depth made up sample NL2081; the sample was processed for zircons by standard mineral separation procedures, including crushing, pulverizing, and concentrating heavy minerals by use of a Wilfley table, methylene iodide, and a magnetic separator. Zircons to be dated by sensitive high resolution ion microprobe (SHRIMP) were hand picked, mounted in epoxy, ground to about half-thickness using 1,500-grit wet-dry sandpaper, and polished with 6-micrometer (μm) and 1-μm diamond suspensions. All grains were imaged in cathodoluminescence and were photographed in both transmitted and reflected light prior to SHRIMP measurements to identify pristine areas for analysis and to determine whether components having multiple ages (such as cores and overgrowths) were present (fig. B5).

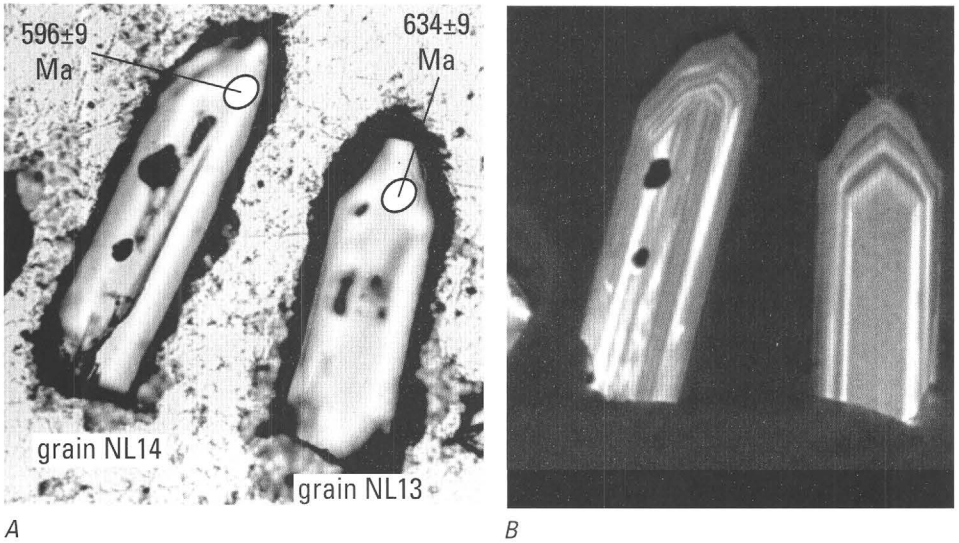

Figure B5. Transmitted-light photomicrograph and matching cathodoluminescence image of zircon crystals analyzed to determine a SHRIMP U-Pb zircon age of the Langley Granite in sample NL2081 from the USGS-NASA Langley core. *A,* Transmitted-light photomicrograph showing external morphology; age data are in table B3. *B,* Matching cathodoluminescence image showing oscillatory internal zones of relatively high (lighter) and low (darker) uranium content. SHRIMP spot diameter is ~25 micrometers.

The USGS/Stanford sensitive high resolution ion microprobe-reverse geometry (SHRIMP-RG) at Stanford University was used to date this sample. Analytical procedures followed the methods described in Compston and others (1984) and Williams and Claesson (1987). Zircon standard R33 was used to correct Pb/U ratios for instrumental fractionation. Standard R33 is zircon from monzodiorite of the Braintree Complex, Vermont, that has been dated at 419 Ma (Roland Mundil, Berkeley Geochronology Center, and Sandra L. Kamo, University of Toronto, unpub. data).

Concentrations of U and Th (table B3) are believed to be accurate to about 20 percent. A Tera-Wasserburg plot of ^{204}Pb-corrected isotopic data (plotted as 2σ error ellipses, fig. B6) was used only for visual assessment of the data array to determine which points to include in the age calculation. The age of the sample NL2081 was determined by calculating the weighted average of the $^{206}Pb/^{238}U$ ages (using the ^{207}Pb-common Pb correction method of Compston and others, 1984), shown in the figure B6 inset (2σ error bars).

Zircons from the granite are light brown, are euhedral, have length/width ratios of about 3 to 4, and contain fine concentric, oscillatory zoning in cathodoluminescence (fig. B5). A total of 15 grains were analyzed with one analysis per grain. Except in grain NL1, U concentrations are relatively low and have a limited range (129–269 parts per million, ppm) (table B3).

The $^{206}Pb/^{238}U$ ages range from 589±9 Ma to 634±9 Ma. The weighted average age from all 15 analyses is 611.6±9.5 Ma (mean square of the weighted deviates (MSWD)=2.5). Excluding five analyses that give ages of 600 Ma or younger results in an age of 621.2±7.6 Ma (MSWD=0.81). However, exclusion of these data based on age alone is subjective and possibly inappropriate. It is possible that these five $^{206}Pb/^{238}U$ ages are somewhat low due to a small loss of Pb, but there is no observable evidence in the images of the grains to substantiate this possibility. Thus, the preferred age of igneous zircon, combining isotopic data from all analyzed grains, is rounded to 612±10 Ma (2σ), which is interpreted to indicate a Neoproterozoic crystallization age for the granite.

Thermal History from Argon and Fission-Track Geochronology

Mineral ages that record different closure temperatures collectively provide information on the cooling history of the Langley Granite at the USGS-NASA Langley corehole. Newly determined $^{40}Ar/^{39}Ar$ ages of microcline and plagioclase and fission-track ages of zircon and apatite are presented below.

Both the microcline and the plagioclase are altered and have a cloudy appearance in thin section. The alteration is probably to clay or sericite and could be a result of the lower greenschist-facies metamorphism and (or) chemical weathering evident in the core samples.

$^{40}Ar/^{39}Ar$ Analysis of Feldspars

Methods

Three feldspar separates were dated from the USGS-NASA Langley corehole by using the $^{40}Ar/^{39}Ar$ age-spectrum dating technique (fig. B7, table B4). Microcline and plagioclase were separated from the Langley Granite in half the core from 633.98 m to 634.81 m (2,080.0 ft to 2,082.7 ft) depth; this material made up sample NL2081, the same sample from which zircons were also separated, as described above. Albite (sample NL2083) was scraped from a joint surface in the core between 634.81 m and 634.93 m (2,082.7 ft and 2,083.1 ft) depth.

All three mineral concentrates were prepared by using standard techniques, including magnetic separation, density separation, ultrasonic cleaning, and hand picking, to an apparent purity of >99 percent for the microcline and plagioclase and >99.9 percent for the albite. The samples were then re-sieved to remove fine material and were washed in acetone, in alcohol, and three times in deionized water, all in an ultrasonic cleaner.

The $^{40}Ar/^{39}Ar$ age-spectrum dating of the three feldspars was done at the U.S. Geological Survey's thermochronology laboratory in Denver, Colo. The samples were packaged in Cu foil capsules and sealed under vacuum into fused silica vials before irradiation in the U.S. Geological Survey's TRIGA reactor (Dalrymple and others, 1981) to convert a portion of their ^{39}K to ^{39}Ar. To monitor this conversion, packets of the standard MMhb–1 hornblende were intercalated with the samples. MMhb–1 has an age of 519.4±2.4 Ma (Alexander and others, 1978; Dalrymple and others, 1981).

The samples dated for this study were analyzed with a VG mm1200b or a MAP 216 mass spectrometer using the $^{40}Ar/^{39}Ar$ age-spectrum dating method. Data from procedural blanks were subtracted from the analytical results prior to data reduction. All data reduction for these samples was accomplished by using a modified version of the computer program ArAr* (Haugerud and Kunk, 1988). All estimates of analytical precision are at the 1σ level. Decay constants used are those recommended by Steiger and Jäger (1977). Corrections for the production of interfering reactor-produced argon isotopes from Ca, K, and Cl are those given in Dalrymple and others (1981) and Roddick (1983). Details of the argon analytical technique are in Haugerud and Kunk (1988).

Inverse-isotope-correlation diagrams were prepared by using the method of York (1969). For inverse-isotope-correlation age results to be considered meaningful, we require an MSWD (a goodness-of-fit indicator for the fit of the data to the line) $\leq$2.5, an initial $^{40}Ar/^{36}Ar$ ratio $\geq$295.5 (the ratio in the modern atmosphere), and contiguous regression points.

Microcline from Granite Sample NL2081

Sample NL2081 microcline has the most straightforward results of the three feldspars dated by the $^{40}Ar/^{39}Ar$ age-spectrum technique (fig. B7, table B4). The first four steps in the microcline age spectrum (600°C–900°C) decrease in apparent

Table B3. SHRIMP U-Th-Pb data for zircons from sample NL2081 of the Langley Granite from the USGS-NASA Langley core.

[The USGS/Stanford sensitive high resolution ion microprobe-reverse geometry (SHRIMP-RG) at Stanford University was used to date 15 igneous zircon grains (one analysis per grain). Analyst: J.N. Aleinikoff. Analytical procedures are discussed in the text. Definitions of terms: %, percent; ppm, parts per million; Ma, millions of years before present; —, not detected]

Zircon grain analysis	Measured $\frac{^{206}Pb}{^{204}Pb}$	Measured $\frac{^{207}Pb}{^{206}Pb}$	Common ^{206}Pb (weight %)	U (ppm)	Th/U	Age from $\frac{^{206}Pb}{^{238}U}$ (Ma)	Error, 1σ (Ma)	$\frac{^{238}U^{\dagger}}{^{206}Pb}$	Error, 1σ (%)	$\frac{^{207}Pb^{\dagger}}{^{206}Pb}$	Error, 1σ (%)
NL1	2,658.0	0.0627	0.38	741	0.89	589	9	10.49	1.50	0.0572	2.51
NL2	—	.0590	—	176	.75	600	9	10.27	1.54	.0590	2.09
NL3	—	.0624	.28	184	.73	608	9	10.09	1.54	.0624	2.06
NL4	17,872	.0608	.02	269	.98	629	9	9.77	1.49	.0600	1.86
NL5	—	.0615	.17	149	.72	608	10	10.09	1.75	.0615	2.22
NL6	14,415	.0586	—	222	1.14	598	9	10.32	1.51	.0576	1.99
NL7	4,305.1	.0630	.32	155	1.03	619	10	9.93	1.58	.0596	2.96
NL8	—	.0626	.36	230	.93	590	10	10.39	1.81	.0626	1.79
NL9	3,531.7	.0621	.21	160	.95	618	12	9.97	1.92	.0580	2.48
NL10	—	.0615	.12	129	.79	621	11	9.87	1.85	.0615	2.71
NL11	6,138.2	.0600	—	142	.87	619	9	9.95	1.57	.0577	2.88
NL12	—	.0591	—	140	.78	623	10	9.87	1.56	.0591	2.28
NL13	—	.0611	.03	197	.67	634	9	9.68	1.52	.0611	1.91
NL14	10,086	.0616	.22	154	.70	596	9	10.31	1.59	.0602	2.42
NL15	—	.0611	.05	239	.78	629	9	9.74	1.50	.0611	1.74

†Radiogenic ratios corrected for common Pb on the basis of the model by Stacey and Kramers (1975).

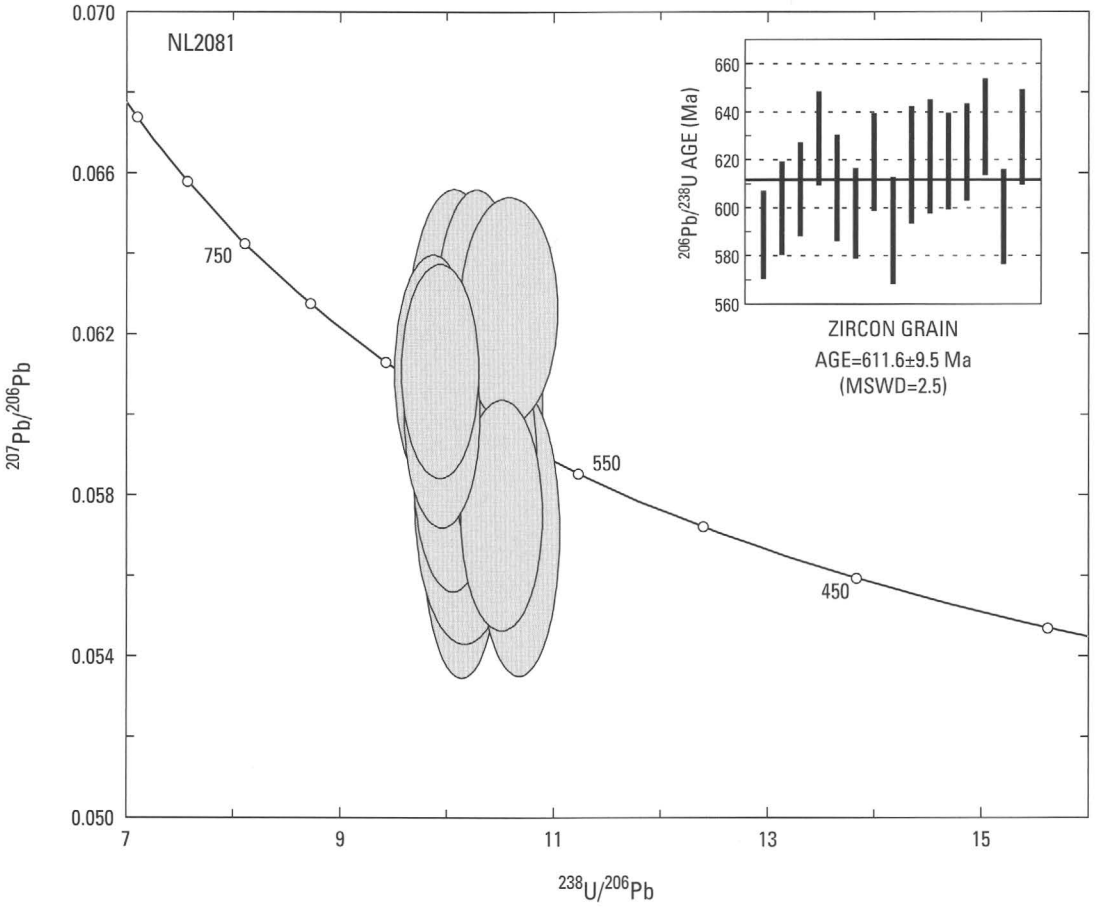

Figure B6. Graph showing SHRIMP U-Pb ages of zircon from the Langley Granite in sample NL2081 from the USGS-NASA Langley core. The main figure is a Tera-Wasserburg concordia diagram with 2σ error ellipses. The inset shows the SHRIMP $^{206}Pb/^{238}U$ ages with 2σ error bars. MSWD, mean square of the weighted deviates. The weighted average age from all 15 analyses is 611.6±9.5 Ma (MSWD=2.5). This age is rounded to 612±10 Ma (2σ) and is interpreted to indicate a Neoproterozoic crystallization age for the Langley Granite. See text for discussion.

Figure B7 (facing page). Graphs of $^{40}Ar/^{39}Ar$ age spectra (left) and inverse-isotope-correlation diagrams (right) for three feldspars from samples NL2081 and NL2083 of the Langley Granite from the USGS-NASA Langley core. Data are in table B4. The first step and the last two steps of sample NL2081 plagioclase do not fit in the age-spectra diagram because of the scale used. Height of horizontal boxes indicates 2σ error. For inverse-correlation ages, we require that the mean square of the weighted deviates (MSWD) be ≤2.5, that the initial $^{40}Ar/^{36}Ar$ ratio be ≥295.5 (the ratio in the modern atmosphere), and that the regressed points be contiguous. Only the regression results presented in the diagrams for microcline and plagioclase meet these criteria. See text for discussion.

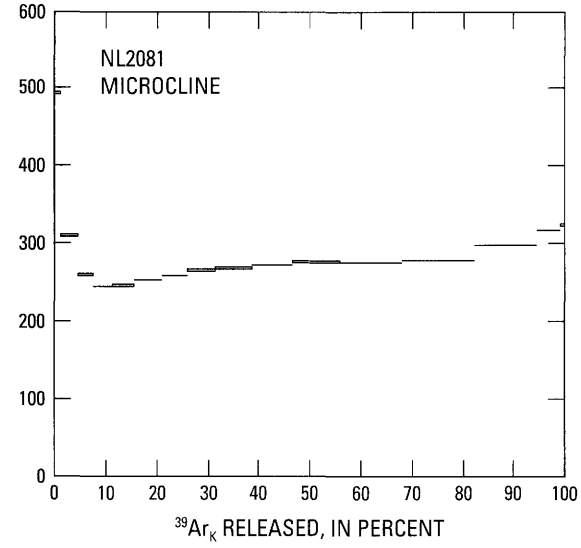
NL2081
MICROCLINE
600
500
400
300
200
100
0
0 10 20 30 40 50 60 70 80 90 100
$^{39}Ar_K$ RELEASED, IN PERCENT

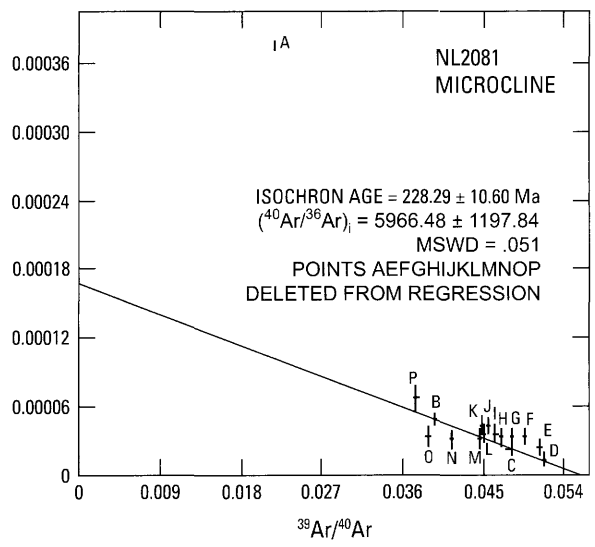
NL2081
MICROCLINE
ISOCHRON AGE = 228.29 ± 10.60 Ma
$(^{40}Ar/^{36}Ar)_i$ = 5966.48 ± 1197.84
MSWD = .051
POINTS AEFGHIJKLMNOP
DELETED FROM REGRESSION
0.00036
0.00030
0.00024
0.00018
0.00012
0.00006
0
0 0.009 0.018 0.027 0.036 0.045 0.054
$^{39}Ar/^{40}Ar$

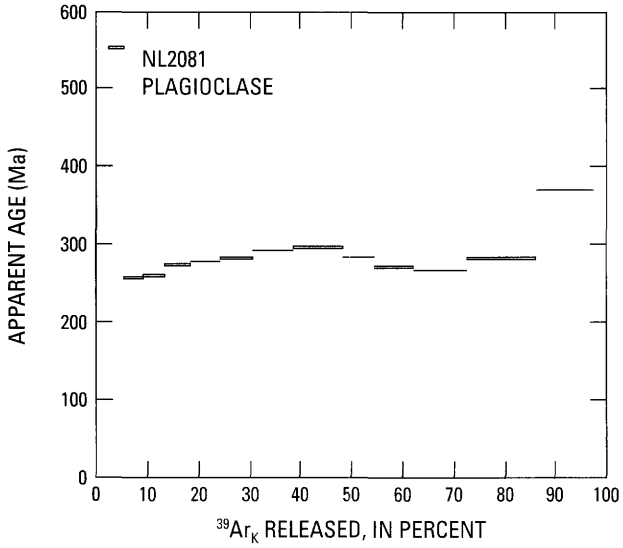
NL2081
PLAGIOCLASE
APPARENT AGE (Ma)
600
500
400
300
200
100
0
0 10 20 30 40 50 60 70 80 90 100
$^{39}Ar_K$ RELEASED, IN PERCENT

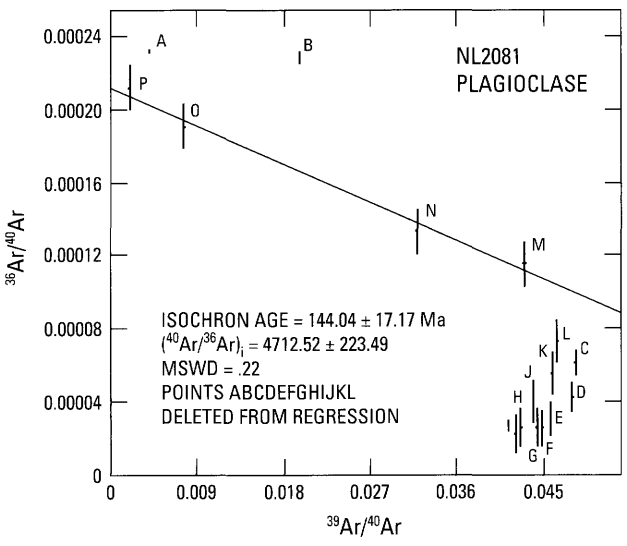
NL2081
PLAGIOCLASE
$^{36}Ar/^{40}Ar$
0.00024
0.00020
0.00016
0.00012
0.00008
0.00004
0
ISOCHRON AGE = 144.04 ± 17.17 Ma
$(^{40}Ar/^{36}Ar)_i$ = 4712.52 ± 223.49
MSWD = .22
POINTS ABCDEFGHIJKL
DELETED FROM REGRESSION
0 0.009 0.018 0.027 0.036 0.045
$^{39}Ar/^{40}Ar$

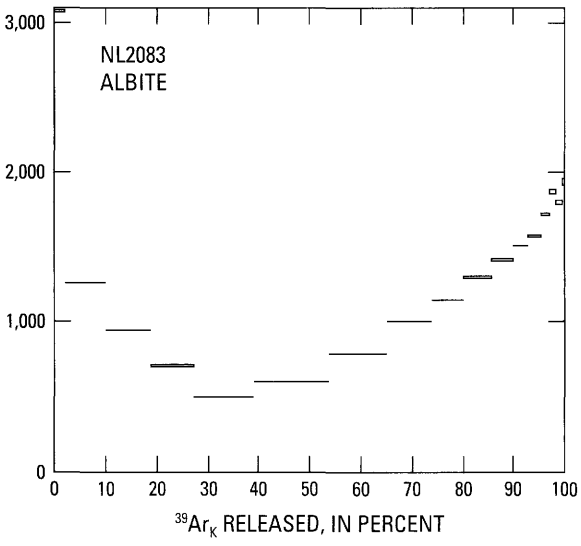
NL2083
ALBITE
3,000
2,000
1,000
0
0 10 20 30 40 50 60 70 80 90 100
$^{39}Ar_K$ RELEASED, IN PERCENT

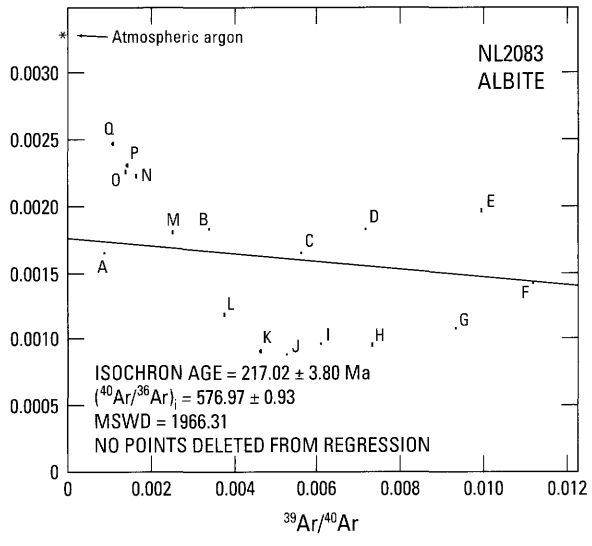
Atmospheric argon
NL2083
ALBITE
0.0030
0.0025
0.0020
0.0015
0.0010
0.0005
0
ISOCHRON AGE = 217.02 ± 3.80 Ma
$(^{40}Ar/^{36}Ar)_i$ = 576.97 ± 0.93
MSWD = 1966.31
NO POINTS DELETED FROM REGRESSION
0 0.002 0.004 0.006 0.008 0.010 0.012
$^{39}Ar/^{40}Ar$

Table B4. $^{40}Ar/^{39}Ar$ age results for three feldspars from samples NL2081 and NL2083 of the Langley Granite from the USGS-NASA Langley core.

[The $^{40}Ar/^{39}Ar$ age-spectrum dating of the three feldspars was done at the U.S. Geological Survey's thermochronology laboratory in Denver, Colo. Analyst: M.J. Kunk. The methods used are discussed in the text. Inverse-isotope-correlation diagrams for these data are in figure B7. Definitions of terms: Temp, temperature; °C, degrees Celsius; %, percent; $^{40}Ar^*$, radiogenic yield, which is the percentage of ^{40}Ar that was derived from decay of ^{40}K; $^{39}Ar_K$, the ^{39}Ar derived from ^{39}K produced during the irradiation of the sample; Ma, millions of years before present; *J*, a conversion factor, which is a measure of the fraction of ^{39}K converted to ^{39}Ar by the fast neutron reaction ($^{39}K(n,p)^{39}Ar$)]

Step	Temp (°C)	^{39}Ar (% total)	$^{40}Ar^*$ (%)	$^{39}Ar_K$ (x 10^{-12} mol)	$^{40}Ar^*/^{39}Ar_K$	K/Ca	K/Cl	Apparent age (Ma)	Error, ±1σ (Ma)
Microcline from sample NL2081 [0.0286 grams, age spectrum 9KD19, *J*=0.007534±0.25%]									
A	600	1.1	89.1	0.039199	41.886	14.80	21	494.78	0.89
B	700	3.4	98.6	.121731	24.832	40.10	206	309.38	.82
C	800	3.1	99.3	.111704	20.644	34.75	686	260.79	.74
D	900	3.8	99.6	.137321	19.268	45.09	2,120	244.53	.60
E	1,000	4.0	99.3	.146344	19.388	19.72	1,314	245.96	.71
F	1,100	5.8	99.0	.210381	19.945	10.94	759	252.55	.16
G	1,125	4.6	99.0	.168561	20.518	20.28	572	259.31	.30
H	1,150	5.6	99.0	.203593	21.072	27.29	457	265.82	.16
I	1,175	7.2	98.9	.260340	21.321	25.38	409	268.73	.34
J	1,200	7.9	98.7	.285571	21.627	24.00	372	272.32	.08
K	1,225	9.5	98.7	.343665	21.998	29.78	147	276.65	.14
L	1,250	12.0	99.0	.434244	21.990	44.31	311	276.55	.10
M	1,275	14.5	99.1	.525724	22.210	73.10	350	279.12	.15
N	1,300	12.0	99.1	.436300	23.846	81.45	362	298.06	.20
O	1,325	4.5	99.0	.164820	25.530	67.47	368	317.36	.23
P	1,350	1.0	98.0	.037128	26.108	15.42	285	323.94	.80
Total gas		100.0	98.9	3.626626	22.195	43.65	482	278.94	
No plateau									
Plagioclase from sample NL2081 [0.2725 grams, age spectrum 5KD19, *J*=0.007558±0.25%]									
A	650	2.3	93.2	0.045288	236.379	5.16	5	1,848.75	1.84
B	700	2.9	93.3	.056942	47.487	5.86	37	553.25	.70
C	750	3.8	98.2	.074788	20.321	4.38	294	257.75	.45
D	800	4.3	98.7	.082818	20.547	4.52	418	260.42	.41
E	850	5.1	99.1	.098523	21.691	6.47	574	273.86	.34
F	900	5.8	99.2	.113019	22.082	8.04	795	278.44	.28
G	950	6.4	99.2	.124015	22.407	4.56	839	282.24	.26
H	1,000	8.0	99.2	.156203	23.242	3.95	816	291.95	.25
I	1,050	9.5	99.4	.184779	23.594	2.92	873	296.02	.28
J	1,100	6.6	98.8	.128125	22.479	1.72	404	283.08	.27
K	1,150	7.5	98.4	.145397	21.449	2.39	305	271.03	.52
L	1,200	10.3	97.8	.199574	21.052	2.19	50	266.37	.26
M	1,250	13.7	96.6	.266530	22.438	2.34	142	282.60	.27
N	1,300	11.2	96.1	.217501	30.137	2.07	74	370.19	.22
O	1,350	2.0	94.4	.038967	123.251	.90	11	1,187.60	.47
P	1,400	.7	93.7	.014592	492.026	.62	2	2,798.98	.62
Total gas		100.0	97.8	1.947061	34.282	3.42	389	415.65	
No plateau									

Table B4. $^{40}Ar/^{39}Ar$ age results for three feldspars from samples NL2081 and NL2083 of the Langley Granite from the USGS-NASA Langley core.—Continued

Step	Temp (°C)	^{39}Ar (% total)	$^{40}Ar^*$ (%)	$^{39}Ar_K$ (x 10^{-12} mol)	$^{40}Ar^*/^{39}Ar_K$	K/Ca	K/Cl	Apparent age (Ma)	Error, ±1σ (Ma)
Albite from sample NL2083 [0.0094 grams, age spectrum 10KD19, J=0.007528±0.25%]									
A	825	2.0	51.3	0.000572	598.471	0.44	1	3,077.10	2.48
B	950	8.0	46.0	.002243	134.994	.75	3	1,265.03	2.22
C	1,050	8.9	51.2	.002483	91.566	.71	6	945.88	1.41
D	1,150	8.3	45.9	.002317	64.060	.78	10	709.98	1.76
E	1,250	11.9	42.0	.003318	42.101	.95	18	496.66	1.36
F	1,300	14.5	58.2	.004039	52.076	1.11	23	596.69	.98
G	1,320	11.6	68.1	.003243	72.865	.85	20	788.90	.92
H	1,340	8.8	71.9	.002455	98.427	.62	16	1,000.20	1.00
I	1,360	6.3	71.7	.001761	117.923	.51	13	1,146.21	1.26
J	1,380	5.2	73.9	.001455	140.442	.46	11	1,301.35	1.37
K	1,400	4.2	73.2	.001182	158.587	.41	10	1,417.32	1.46
L	1,450	3.2	65.0	.000893	173.499	.39	8	1,507.35	2.02
M	1,500	2.3	46.8	.000632	186.013	.39	5	1,579.58	3.89
N	1,550	1.8	34.3	.000514	210.816	.33	3	1,714.72	4.46
O	1,575	1.3	33.5	.000355	241.463	.28	3	1,868.82	5.42
P	1,600	1.0	32.1	.000281	226.286	.30	3	1,794.15	5.38
Q	1,650	.7	27.0	.000200	255.220	.28	2	1,933.94	7.77
Total gas		100.0	56.9	.027943	108.417	.73	13	1,076.49	
No plateau									

age from 495 Ma to 245 Ma with increasing temperature of release, suggesting the presence of excess argon represented by this part of the age spectrum. The gas represented by the remainder of the age spectrum climbs in apparent age from 245 Ma in the 900°C step to a maximum of 324 Ma in the 1,350°C step. This climbing pattern is almost certainly the result of slow cooling through argon closure in the microcline.

Inverse-isotope-correlation analysis of the age-spectrum data, regressing only points B, C, and D, indicates an apparent age of 228.3±10.6 Ma (1σ). This is not different from the minimum age of 245 Ma in the 900°C step of the age spectrum at the 2σ level of uncertainty. We interpret the maximum age in the age spectrum of 324 Ma to represent cooling through a temperature of about 250°C and the minimum age of 245 Ma to represent cooling through a temperature of about 150°C (McDougall and Harrison, 1999). These ages are consistent with slow cooling following the late Paleozoic Alleghanian metamorphic event. However, it is possible that these ages represent very slow cooling from an earlier Acadian metamorphic event or Alleghanian uplift following Acadian metamorphism.

Plagioclase from Granite Sample NL2081

Sample NL2081 plagioclase has a more complex age spectrum than the microcline has (fig. B7, table B4). The apparent age decreases in the first three steps from 1,849 Ma to 258 Ma, indicating the presence of some excess argon. The apparent ages then increase to 296 Ma in the 1,050°C step, before declining to 266 Ma in the 1,200°C step, and finally climbing to 2,799 Ma in the 1,400°C step. The climb in apparent ages in the high-temperature parts of the age spectrum is again the result of the inclusion of excess argon in the sample. The bulk of the gas was released between the 750°C and 1,250°C steps and has apparent ages ranging from 258 Ma to 296 Ma. Although we do not understand the convex upward shape of the age spectrum in this temperature range, which may be the result of alteration or weathering of the sample, the age results are consistent with those of NL2081 microcline and suggest cooling through closure following the late Paleozoic Alleghanian orogenic event.

Inverse-isotope-correlation analysis of the age-spectrum data from this sample produces an interesting apparent age result. By regressing only the last four steps in the age spectrum

(points M, N, O and P), a very imprecise apparent age of 144±17 Ma can be calculated. Regional palynological data (Doyle and Robbins, 1977; Reinhardt and others, 1980) indicate that the sediments deposited directly on crystalline basement in the vicinity of the Langley corehole are Aptian in age (about 121 to 112 Ma), suggesting that the weathering profile observed in the granite developed in the Aptian or earlier. The apparent age of 144±17 Ma is consistent with that timing for weathering. No other acceptable apparent ages were resolvable from the inverse-isotope-correlation diagram.

Albite from Joint-Surface Sample NL2083

The age spectrum of sample NL2083 albite from a joint surface is dominated by the effects of excess argon (fig. B7, table B4). Apparent ages decrease from 3,077 Ma in the 825°C step to a minimum of 497 Ma in the 1,250°C step and then climb to 1,934 Ma in the 1,650°C step. The age spectrum has a classic U-shape that is indicative of the presence of excess argon.

Inverse-isotope-correlation analysis of the age-spectrum data from this sample does not provide a meaningful age. The pattern of the points in the correlation diagram suggests that the isotopic composition of excess argon could have been changing in the geologic environment of the joint as the albite was crystallizing. We interpret the minimum apparent age in the age spectrum of 497 Ma as the maximum possible age for the formation of this albite. It is important to note that it could have formed hundreds of millions of years after this time.

Fission-Track Analysis of Zircon and Apatite

Fission tracks in a mineral result from spontaneous fission of ^{238}U present in trace amounts in the mineral. The age of a mineral can be calculated from the number of tracks and amount of uranium it contains. However, when a mineral containing fission tracks is heated at a sufficiently high temperature, the tracks shorten and ultimately disappear. The thermal annealing (shortening) of fission tracks and resulting reduction in fission-track age and track lengths provide information on the temperature history of rocks (Naeser, 1979; Gleadow and others, 1986). In a relatively stable geologic environment, apatite undergoes significant annealing between about 60°C and 110°C (Fitzgerald and others, 1995) and has an effective closure temperature (Dodson, 1979) of about 90°C–100°C. Higher temperatures would be required to produce annealing during relatively short-term, impact-related thermal disturbances. The annealing temperatures of zircon are not as well known but are significantly higher than those of apatite; in zircon damaged by natural alpha radiation, the fission-track closure temperature is probably in the range of ~235°C±25°C (Brandon and others, 1998).

Apatite and zircon were separated from the Langley Granite in sample NL2081 (see appendix B1) of the USGS-NASA Langley core; the sample came from a depth of 633.98 m to 634.81 m (2,080.0 ft to 2,082.7 ft). Separation methods are described above in the section on "Neoproterozoic Uranium-Lead (SHRIMP) Zircon Age."

Fission-track ages were determined by using the external detector method (Naeser, 1976, 1979; Naeser and others, 1989), as follows. The apatite separate was mounted in epoxy, polished, and etched in 7 percent nitric acid for 40 seconds at 23°C. Zircons were mounted in Teflon, polished, and etched in a eutectic KOH-NaOH melt (Gleadow and others, 1976) for 32 hours at about 214°C. The grain mounts were irradiated with low-uranium-content-muscovite external detectors. Grain mounts and external detectors were counted at x1,250 magnification using a x100 oil immersion lens. Ages were calculated by using the zeta calibration method (Hurford and Green, 1982, 1983) (table B5). All fission-track ages are reported at 2σ.

Apatite fission-track lengths were measured in the apatite grain mount in transmitted light at x1,875 magnification by using a x100 oil-immersion lens, a digitizing tablet, and a projection tube calibrated against a stage micrometer (1 unit = 0.01 millimeter). Only well-etched horizontal confined tracks in grains with polished surfaces approximately parallel to the crystallographic *c* axis were measured. Reported track lengths (table B5) are actual measurements, not corrected for length-measurement bias (Laslett and others, 1982).

The apatite fission-track age of sample NL2081 is 184±32 Ma (table B5); this age is consistent with the regional pattern of apatite fission-track ages northwest of the Langley corehole that record regional Mesozoic to present-day relatively slow cooling of the Piedmont and spatially related early Mesozoic basins (Roden and Miller, 1991; Hulver, 1997; Naeser and others, 2001). For example, the NL2081 apatite age is statistically indistinguishable (at ±2σ) from, or older than, apatite fission-track ages determined for exposed to shallowly buried (<1 km or <0.6 mi) Proterozoic and Paleozoic metamorphic and igneous rocks and Triassic sedimentary and igneous rocks in the Potomac River area of northern Virginia, Maryland, and the District of Columbia (Naeser and others, 2001) and the Taylorsville basin-Richmond basin area of east-central Virginia (Roden and Miller, 1991). The similarity of the apatite fission-track age for the Langley Granite in the Langley corehole to regional apatite fission-track ages suggests that there was little, if any, impact-related apatite annealing in NL2081.

The mean fission-track length in apatite from sample NL2081 is 13.84±0.59 μm at ±1σ and is generally statistically indistinguishable from, or somewhat longer than, reported track lengths from Piedmont and early Mesozoic basin rocks in the area (Roden and Miller, 1991; Hulver, 1997; C.W. Naeser and N.D. Naeser, unpub. data); the length data are consistent with relatively slow, undisturbed cooling of the rocks (Gleadow and others, 1986). However, the length data for apatite from sample NL2081 should be considered very preliminary. The low yield of apatite and low spontaneous track density (related to a uranium content of only ~3 ppm) resulted in an inadequate number

Table B5. Apatite and zircon fission-track ages and apatite track lengths for sample NL2081 of the Langley Granite from the USGS-NASA Langley core.

[Analysts: C.W. Naeser and N.D. Naeser. Definitions of terms: Lab. no., laboratory number; tr/cm^2, tracks per square centimeter; %, percent; Ma, millions of years before present; µm, micrometer; —, not determined]

Lab. no. DF	Mineral	No. of grains counted	ρ_s* x10^6 (tr/cm^2)	No. of tracks counted	ρ_i** x10^6 (tr/cm^2)	No. of tracks counted	ρ_d*** x10^5 (tr/cm^2)	No. of tracks counted	P(χ^2)† (%)	Age†† (Ma± 2σ)	Mean track length (µm±σ)	No. of tracks measured	Standard deviation of the track-length distribution††† (µm)
6895	Apatite	10	0.375	245	1.04	340	0.482	2,930	P	184±32	13.84±0.59	6	1.44
6899	Zircon	9	20.1	1,980	7.88	388	4.73	3,450	P	375±44	—	—	—

*ρ_s, spontaneous track density in tracks per square centimeter (tr/cm^2) in the sample for the number of tracks counted; see next column.

**ρ_i, induced track density (reported induced track density = 2 x measured value).

***ρ_d, track density in muscovite detector covering National Institutes of Standards and Technology (NIST) standard glass SRM 963 (for apatite) or standard glass SRM 962 (for zircon) (Carpenter and Reimer, 1974).

†P(χ^2), measure of probability that all individual grains counted in a sample are from a single age population; P ("pass") indicates P(χ^2) values >5%, F ("fail") indicates P(χ^2) values <5%; P(χ^2) values <5% are generally taken as an indication of a real spread in single-grain ages (Galbraith, 1981; Green and others, 1989).

††Age calculated from the fission-track age equation of Hurford and Green (1982, 1983) by using the sums of the spontaneous and induced track counts obtained for all grains counted in the sample and the following values: $\lambda_D = 1.551 \times 10^{-10}$/year, $g = 0.5$, zeta = 10,752 for apatite (based on SRM 963) and 319.6 for zircon (based on SRM 962).

†††Standard deviation calculated by combining Poisson errors on spontaneous and induced counts and on counts in detector covering glass standard NIST SRM 963 or SRM 962 (McGee and others, 1985).

of track-length measurements for thermal-history modeling or other quantitative track-length analysis.

The fission-track age of zircon from sample NL2081 is 375±44 Ma. As would be predicted from the apatite age data, there is no indication of impact-related annealing in zircon. The few zircon fission-track ages that have been determined from eastern Piedmont and early Mesozoic basin rocks in Virginia, Maryland, and the District of Columbia (Roden and Miller, 1991; Kohn and others, 1993; Naeser and others, 2001) are all statistically younger than the NL2081 zircon fission-track age.

An anomalous feature of the $^{40}Ar/^{39}Ar$ and fission-track data remains unexplained. Zircon fission tracks and argon in potassium feldspar have similar closure temperatures and, thus, typically yield similar cooling ages. However, the $^{40}Ar/^{39}Ar$ age of potassium feldspar (microcline) from sample NL2081 (324 Ma maximum age; see above section "Microcline from Granite Sample NL2081") is significantly younger than the zircon fission-track age, possibly because of the presence of alteration products within the microcline.

In summary, the fission-track data for the granite from about 634.3 m (2,081 ft) depth in the Langley corehole indicate that at 19 km (12 mi) from the margin of the central crater, the impact-related thermal disturbance was not sufficient to cause detectable annealing of fission tracks in zircon or apatite.

The lack of annealing in apatite from sample NL2081 can be used to set an upper limit on the impact-related thermal disturbance at this location in the crater; the limit is based on the maximum temperature that could have been attained without affecting the apatite fission-track age. A preliminary estimate of the maximum temperature was obtained by the following steps. First, the thermal history of NL2081 was modeled for regional cooling with the assumption of no impact-related heating (fig. B8). As noted above, the long-term cooling history of NL2081 cannot be modeled directly because of the low number of measurable apatite track lengths, but for the purpose of this exercise, it was approximated by using track-length data imported from another Piedmont "basement" sample that yielded apatite age and track-length data statistically indistinguishable from data for sample NL2081 (C.W. Naeser and N.D. Naeser, unpub. data). Next, forward modeling was used to predict the reduction in apatite fission-track age that would result from impact-related heating, modeled as the simplest case of a thermal spike of varying maximum temperature and duration superimposed at 35 Ma (time of impact) on the long-term cooling history (fig. B9).

Figure B10 summarizes the predicted reduction in apatite fission-track age that would result from including a thermal spike of 0.1–1 million year (m.y.) total duration and 60°C–140°C maximum temperature in the time-temperature history of

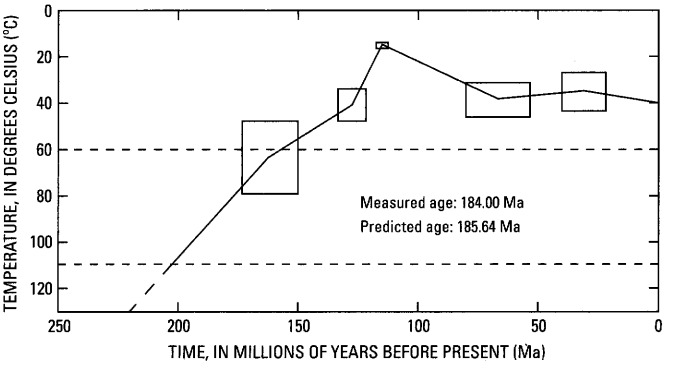

Figure B8. Graph showing modeled Mesozoic to present-day thermal history of sample NL2081 of the Langley Granite from the USGS-NASA Langley core. The plotted curve is the average of a family of thermal-history curves, each of which predicts a statistical match with the measured apatite fission-track age and track-length data. Boxes shown on the plotted curve are ±1σ bounds on the average time-temperature points that were calculated by the computer model. The dashed horizontal lines at 60°C and 110°C mark the boundaries of the apatite partial-annealing zone in a relatively stable geologic environment. The model was generated by using Kerry Gallagher's (1995; written commun., 1996) genetic algorithm time-temperature modeling program, Laslett and others' (1987) annealing model for Durango apatite (from Cerro de Mercado, Durango, Mexico), the measured apatite fission-track age of NL2081, and apatite track-length data from a Piedmont sample with statistically indistinguishable age and mean track length (C.W. Naeser and N.D. Naeser, unpub. data; see text). An annealing model based on Durango apatite is considered appropriate because the mean pit widths of apatite tracks in the analyzed samples indicate an annealing susceptibility comparable to that of Durango apatite. The time-temperature model was constrained to allow NL2081 to be in near-surface conditions in the Aptian (about 121–112 Ma), when deposition of overlying Potomac Formation sediments probably began in this area. This age is poorly constrained in the Langley core (Frederiksen and others, this volume, chap. D) and is inferred from regional information (Doyle and Robbins, 1977; Reinhardt and others, 1980).

NL2081. The plot indicates that for an impact-related thermal disturbance with an effective heating time equivalent to the modeled 1-m.y. thermal spike, temperatures in this part of the crater could not have been higher than about 100°C without producing a significant (at 1σ) reduction in apatite fission-track age. If the thermal disturbance was equivalent to the 0.1-m.y. thermal spike, temperatures as high as about 120°C are possible.

With data from additional coreholes, it may be possible to refine these preliminary estimates of the impact-related thermal structure in the crater.

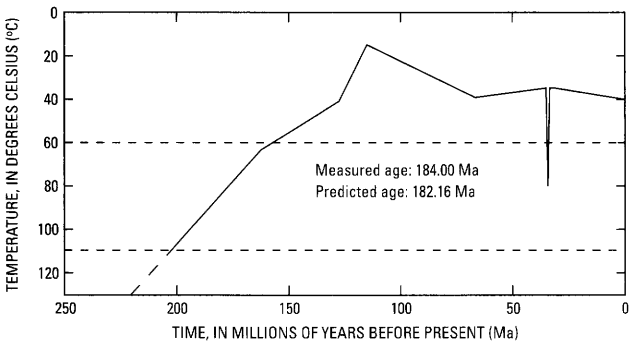

Figure B9. Graph showing an example of forward modeling (by using the program by Kerry Gallagher, 1995; written commun., 1996) of the estimated long-term thermal history of sample NL2081 (from fig. B8) with a superimposed impact-related thermal "spike" beginning at 35 Ma and, in this example, lasting 1 m.y. with a maximum temperature of 80°C. The resulting predicted apatite fission-track age (182.2 Ma) is statistically indistinguishable (at ±1σ) from the measured age of NL2081 (184±16 Ma), suggesting that an impact-related temperature increase of this magnitude in the part of the crater near the Langley corehole would not have produced a significant reduction in fission-track age.

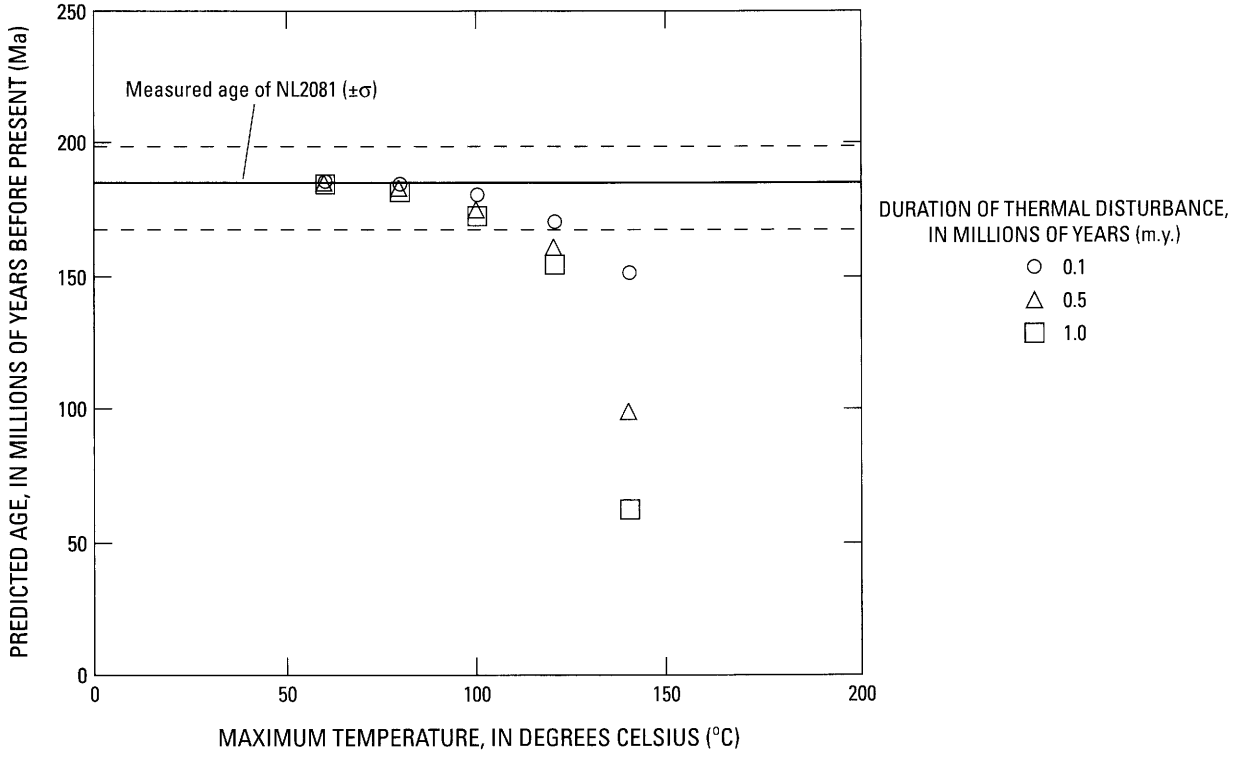

Figure B10. Graph showing a summary of the predicted reduction in apatite fission-track age of sample NL2081 that would result from impact-related heating of varying magnitude and duration (see fig. B9). Horizontal solid and dashed lines indicate the measured age (±1σ) of NL2081 (184±16 Ma). The plot suggests that, as a first approximation, temperatures in excess of 100°C would be required to produce a significant (at 1σ) decrease in age for effective heating times equivalent to a thermal spike of 1-m.y. duration beginning at 35 Ma. For heating times of ≤0.1 m.y., temperatures greater than 120°C would be required.

Discussion

Regional Comparisons

Crystalline rocks beneath the Atlantic Coastal Plain in the vicinity of Chesapeake Bay are poorly known, and so a comparison of the Langley Granite with other rocks in the region may help to constrain regional correlations and tectonic interpretations. The Langley Granite differs in age from Neoproterozoic igneous rocks associated with Laurentia (ancestral North America), such as the Crossnore Plutonic Suite (Su and others, 1994; Fetter and Goldberg, 1995) or Catoctin Formation (Aleinikoff and others, 1995). However, igneous rocks of similar age (table B6) are found in magmatic-arc terranes of the Appalachian Piedmont and beneath the Atlantic Coastal Plain of the eastern United States.

Figure B11 shows the position of the Langley corehole and the Chesapeake Bay impact structure on a tectonostratigraphic map (Horton and others, 1991) that was prepared before the structure was recognized. The Langley Granite is similar in age to some of the older igneous rocks in the Carolina, Spring Hope, and Roanoke Rapids terranes of the Appalachian Piedmont, and in the Hatteras terrane beneath the Atlantic Coastal Plain (table B6, fig. B11), and it is comparable in appearance to some of the plutonic rocks. For example, granite in the central part of the Chapel Hill pluton in the Carolina terrane also has micrographic feldspar-quartz intergrowths and chloritization accompanied by an apparent lack of foliation (Mann and others, 1965). Geochemical studies indicate that most of these igneous rocks were derived from magmas generated in a subduction zone, although cordierite-bearing granite at Stumpy Point, N.C., in the Hatteras terrane appears to be an exception (Speer, 1981; McSween and others, 1991).

On the basis of limited geochemical data, Horton and Izett (this volume, chap. E) suggest that the Langley Granite was emplaced in a volcanic arc setting, unlike chemically distinct granitoids of similar age within the Goochland terrane (fig. B11, table B6). Additional geochemical data are required for regional comparisons of the Langley Granite, the granite at Bayside, Va. (Horton, Aleinikoff, and others, 2002), and Neoproterozoic igneous rocks of similar age in the Carolina, Spring Hope, Roanoke Rapids, and Hatteras terranes (table B6).

Neoproterozoic igneous rocks are also found in Avalonian terranes of the northern Appalachians and Europe (summarized in Nance and Thompson, 1996) and in the Pan-African orogenic belts of West Africa (Dallmeyer and Villeneuve, 1987; Dallmeyer, 1989). The Langley Granite is similar in age to relatively undeformed intrusive rocks in New England, such as the Dedham, Milford, and Esmond Granites in Massachusetts and Rhode Island (Zartman and Naylor, 1984; Thompson and others, 1996), and to metavolcanic and metaplutonic rocks in Connecticut (Wintsch and Aleinikoff, 1987; Wintsch and others, 1992).

Preimpact target rocks of the Chesapeake Bay impact structure are considered to be a likely source for tektites of the North American strewn field (Poag and others, 1994; Koeberl and others, 1996, 2001; Glass, 2002). Furthermore, late Eocene tektites and microtektites from several sites in this field have Nd model ages of 620 to 670 Ma (Shaw and Wasserburg, 1982) and 630 Ma (Ngo and others, 1985), indicating that they were derived from Neoproterozoic source materials similar in age to, or slightly older than, the Langley Granite. The compositions of these tektites, including bediasites, georgiaites, and microtektites, were summarized by Koeberl (1990) and Koeberl and others (2001).

Koeberl and others (2001) compared major-element, trace-element, and Nd and Sr isotopic compositions of some lower Tertiary sediments in the Chesapeake Bay target area with tektite compositions and found "no immediate similarity between the tektite compositions and the sediments" that they analyzed. We compared data for microtektites from Koeberl (1990, tables 1 and 2) with new data for the Langley Granite (table B2 and Horton and Izett, this volume, chap. E); the Langley Granite is similar in the major elements Si, Al, Fe, Mg, Ca, and K, is higher in Na and lower in Ti, but shows virtually no similarity in trace elements. Elements such as Na may be too volatile and mobile during melting for simple comparisons to be meaningful. More detailed chemical comparisons constrained by volumetric considerations and mass balance were not attempted at this stage because of the apparent dissimilarity in less mobile trace elements.

Tectonic Implications for Terranes beneath the Atlantic Coastal Plain

In the tectonic interpretation shown in figure B11, the USGS-NASA Langley corehole and the Chesapeake Bay impact structure are within the Chesapeake block. The southern margin of this block is shown as a suture, which was proposed by Lefort (1988, 1989) and Lefort and Max (1991) on the basis of geophysical data. They interpreted the Chesapeake block as the remnant of a tectonic indenter of Archean(?) African crust, left behind when the Atlantic Ocean opened. Similarities in age (table B6) between the Langley Granite and Neoproterozoic igneous rocks, including granites, in terranes to the south and southwest, raise doubts about the proposed suture. If the proposed suture (Lefort, 1989; Lefort and Max, 1991) is nonexistent, then the Roanoke Rapids and (or) Hatteras terrane may extend northward beneath the coastal plain into the target area of the impact structure (fig. B11). Testing these relations will require information on the age and character of host rocks that were intruded by the Langley Granite, new geochronology in the Roanoke Rapids and Hatteras terranes (where published dates in table B6 are too imprecise), and more geochemistry to support detailed chemical comparisons of igneous rocks in terranes beneath the coastal plain.

Table B6. Isotopic ages of selected Neoproterozoic igneous rocks for comparison with the age of the Langley Granite.

[Terranes are shown in figure B11]

Unit dated	Age (Ma)	Isotopic system and method	Reference*
	Chesapeake block		
Langley Granite, Hampton, Va.	612±10	$^{206}Pb/^{238}U$ SHRIMP zircon	1, 5
Granite at Bayside, Va.	625±11	$^{206}Pb/^{238}U$ SHRIMP zircon	5
	Carolina terrane		
Granite of Flat River complex, N.C.	613.4+2.8/–2	U-Pb zircon, upper intercept	7
Diorite of Flat River complex, N.C.	613.9+1.6/–1.5	U-Pb zircon, upper intercept	7
Osmond granite gneiss, N.C.	612.4+5.2/–1.7	U-Pb zircon, upper intercept	7
Granodiorite near Clarkesville, Va.	602±9	U-Pb zircon, upper intercept	4
Granite of Chapel Hill pluton, N.C.	633+2/–1.5	U-Pb zircon, upper intercept	7
Felsic gneiss of Hyco Formation, N.C.	619.9+4.5/–3	U-Pb zircon, upper intercept	7
Metarhyolite of Hyco Formation, N.C.	615.7+3.7/–1.9	U-Pb zircon, upper intercept	7
Felsic metatuff of Hyco Formation, Va.	621±8	U-Pb zircon, upper intercept	4
Felsic crystal metatuff of Hyco Formation, Va.	616±4	U-Pb zircon, upper intercept	4
	Spring Hope terrane		
Gneiss at Mill Creek, N.C.	620±9	U-Pb zircon, upper intercept	2
Felsic crystal tuff near Spring Hope, N.C.	590±3	U-Pb zircon, upper intercept	2
	Roanoke Rapids terrane		
Metatonalite of Roanoke Rapids complex, N.C.	668	$^{207}Pb/^{206}Pb$ zircon, discordant	3
Metatonalite intruding(?) Easonburg Formation, N.C.	607	$^{207}Pb/^{206}Pb$ zircon, discordant	3
	Hatteras terrane		
Amphibole quartz monzonite at Camp Lejeune, N.C.	630±39	Rb/Sr whole rock	6
Garnet-cordierite-biotite granite at Stumpy Point, N.C.	583±46	Rb/Sr whole rock	6
	Goochland terrane		
Fine Creek Mills granite, Va. (A-type)	629+4/–5	U-Pb zircon, lower intercept	8
Granite (SF98–2), Va. (A-type)	630+9/–10	U-Pb zircon, lower intercept	8
Granite (SF99–11), Va. (A-type)	600+7/–9	U-Pb zircon, lower intercept	8
Granite (SF99–20), Va. (A-type)	588+9/–12	U-Pb zircon, lower intercept	8

*References: 1, this chapter; 2, Goldberg (1994); 3, Horton and Stern (1994); 4, Horton and others (1999); 5, Horton, Kunk, and others (2002); 6, Russell and others (1981); 7, Wortman and others (2000); 8, Owens and Tucker (2003).

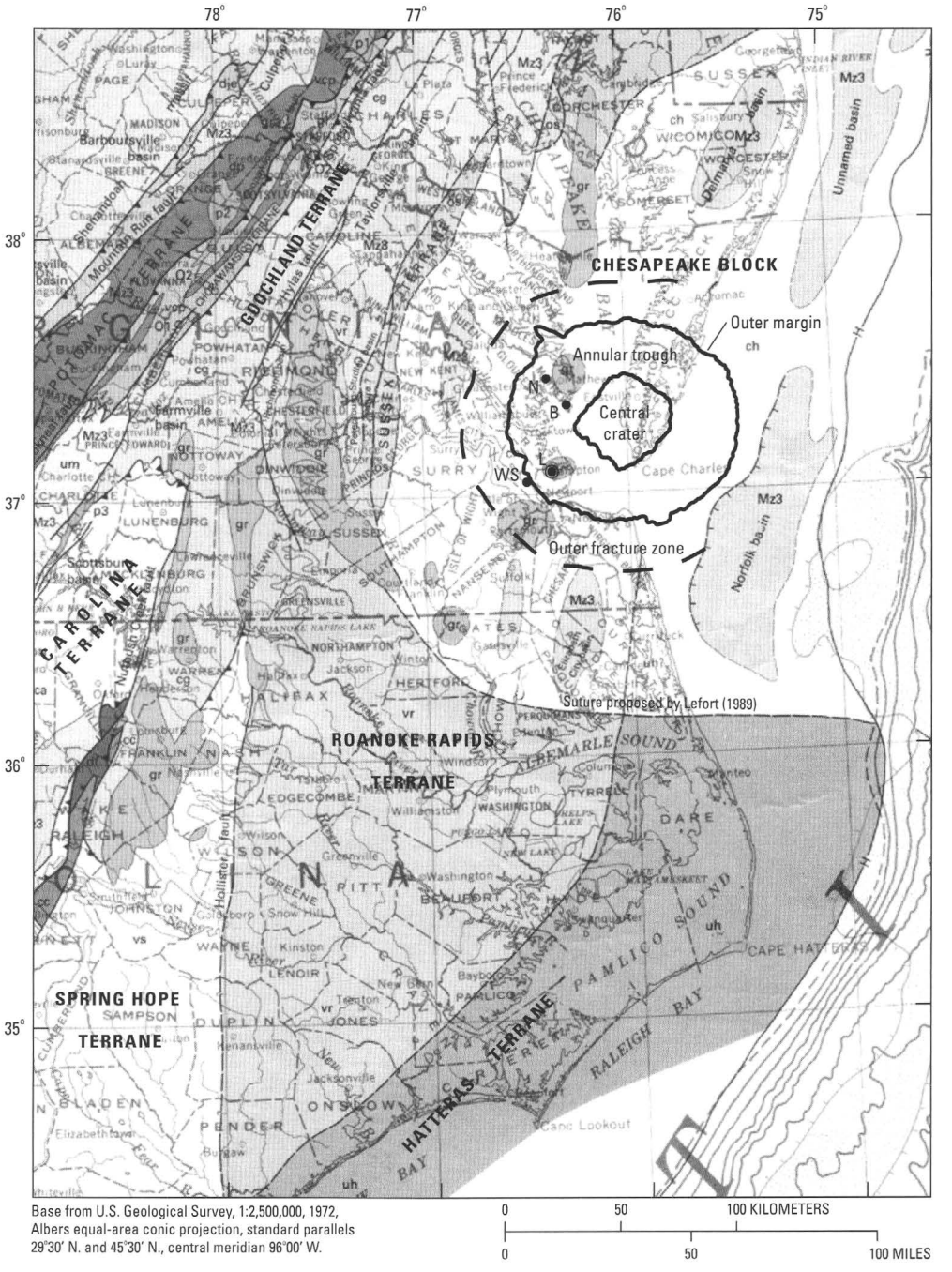

Figure B11. Map showing the location of the USGS-NASA Langley corehole (L), Hampton, Va., and the Chesapeake Bay impact structure in relation to a tectonostratigraphic terrane map (Horton and others, 1991) prepared before the structure was recognized. Other coreholes for this project are also shown: B, Bayside; N, North; WS, Watkins School. Features of the impact structure are modified from Powars and Bruce (1999), Powars (2000), Johnson and others (2001), Powars, Johnson, and others (2002), and Edwards and Powars (2003).

If Mesoproterozoic Laurentian crust underlies the New Jersey Coastal Plain in the northern part of the Chesapeake block, as suggested by Rb/Sr geochronology (Sheridan and others, 1999), then an intervening suture is proposed here to separate those rocks from terrane(s) to the south that contain the Langley Granite and similar Neoproterozoic igneous rocks. However, that interpretation depends on a single Rb/Sr isochron age of 1.025±0.036 Ga for metagabbro, hornblende, and quartzofeldspathic gneiss cuttings from a deep well at Cape May, N.J. (Sheridan and others, 1999); the geologic significance of a single isochron for such diverse rocks is questionable.

The age of the Langley Granite strongly suggests that coastal plain basement in the vicinity of the impact is related to peri-Gondwanan magmatic arc terranes such as the Carolina, Roanoke Rapids, and Avalon terranes, rather than Laurentia. Some peri-Gondwanan terranes, notably Avalon and Cadomia (not shown in fig. B11), have igneous rocks older than 650 Ma that have not yet been found in similar terranes of the southeastern United States (Secor and others, 1983; Samson and others, 1999; Wortman and others, 2000). Modern high-precision geochronology and geochemistry of exposed rocks in the Roanoke Rapids terrane are needed to determine whether rocks similar in age and composition to the Langley Granite and (or) rocks older than 650 Ma are present.

Lack of Discernible Impact-Related Deformation or Heating

No shock-metamorphosed minerals, shatter cones, or other features clearly attributable to the impact were seen in the Langley Granite in the Langley core, although crystalline-rock ejecta in the overlying impact-related sediments contain shock-metamorphosed quartz (Horton and others, 2001; Horton Aleinikoff, and others, 2002; Horton, Kunk, and others, 2002; Horton and Izett, this volume, chap. E). The argon and fission-track cooling ages of minerals show no discernible impact-related thermal disturbance in granite at this location near the outer margin of the impact structure. The apatite fission-track age of 184±32 Ma is typical of cooling that followed the early Mesozoic rifting event throughout the region (Roden and Miller, 1991; Hulver, 1997; Naeser and others, 2001).

Seismic-reflection data suggest that impact-related faults penetrate crystalline basement beneath the coastal plain in the vicinity of the USGS-NASA Langley corehole (Catchings and others, this volume, chap. I). No such faults were documented in the core, but the chance of intersecting them was limited by having <9 m (<30 ft) of granite core.

Conclusions

The Langley Granite is peraluminous, nonfoliated, and highly chloritized. Fractures in the granite from the USGS-NASA Langley core are no more abundant than those in many Piedmont cores, and most have lower greenschist-facies minerals suggesting that they predate the impact. The $^{206}Pb/^{238}U$ weighted average age of igneous zircon at 612±10 Ma indicates a Neoproterozoic age for the granite. The $^{40}Ar/^{39}Ar$ ages of microcline and plagioclase may be related to regional cooling and uplift following the late Paleozoic Alleghanian orogeny. Apatite and zircon fission-track ages and apatite track lengths determined for sample NL2081 from the granite show no discernible impact-related thermal disturbance at this location about 19 km (12 mi) beyond the margin of the central crater. The granite has not yielded any shock-metamorphosed minerals or shatter cones or any evidence of an impact-related thermal event. Impact-generated faults were not detected in the granite core, although seismic-reflection data suggest that they penetrate coastal plain basement rocks in the general vicinity.

Acknowledgments

U.S. Geological Survey (USGS) investigations of the Chesapeake Bay impact structure are conducted in cooperation with the Hampton Roads Planning District Commission, the Virginia Department of Environmental Quality, and the National Aeronautics and Space Administration (NASA) Langley Research Center. The Hampton Roads Planning District Commission and the USGS provided funds for the drilling of the USGS-NASA Langley corehole. The NASA Langley Research Center provided extensive operational and logistical support for the drilling operation. The Virginia Department of Environmental Quality and the Department of Geology of the College of William and Mary provided extensive operational support at the drill site.

We thank Wendy Hodges (USGS) for mineral separations, Harvey Belkin (USGS) for assistance with the scanning-electron microscope, John Jackson (USGS) for assistance with the X-ray diffractometer, Glen A. Izett (College of William and Mary and USGS Emeritus) and Daniel J. Milton (USGS Emeritus) for consultations on shock-metamorphic criteria, and Yolanda Fong-Sam (USGS) for help in preparing figure B11. Reviews by Douglas W. Rankin (USGS) and Robert A. Ayuso (USGS) significantly improved the quality of this manuscript.

References Cited

Aleinikoff, J.N., Zartman, R.E., Walter, Marianne, Rankin, D.W., Lyttle, P.T., and Burton, W.C., 1995, U-Pb ages of metarhyolites of the Catoctin and Mount Rogers Formations, central and southern Appalachians—Evidence for two pulses of Iapetan rifting: American Journal of Science, v. 295, no. 4, p. 428–454.

Alexander, E.C., Jr., Mickelson, G.M., and Lanphere, M.A., 1978, MMhb–1; A new $^{40}Ar/^{39}Ar$ dating standard, *in* Zartman, R.E., ed., Short papers of the Fourth International Conference, Geochronology, Cosmochronology, Isotope Geol-

ogy, 1978: U.S. Geological Survey Open-File Report 78–701, p. 6–8.

Brandon, M.T., Roden-Tice, M.K., and Garver, J.I., 1998, Late Cenozoic exhumation of the Cascadia accretionary wedge in the Olympic Mountains, northwest Washington State: Geological Society of America Bulletin, v. 110, no. 8, p. 985–1009.

Carpenter, B.S., and Reimer, G.M., 1974, Standard reference materials—Calibrated glass standards for fission track use: National Bureau of Standards Special Publication 260–49, 16 p.

Catchings, R.D., Powars, D.S., Gohn, G.S., and Goldman, M.R., 2002, High-resolution seismic reflection survey of the southwestern margin of the Chesapeake Bay impact structure, Virginia [abs.]: Eos, Transactions, American Geophysical Union, v. 83, no. 19, spring meeting supplement of 7 May 2002, Abstract T21A–05, p. S352. (Also available online at http://www.agu.org/meetings/waissm02.html)

Compston, W., Williams, I.S., and Meyer, C.E., 1984, U-Pb geochronology of zircons from lunar breccia 73217 using a sensitive high mass-resolution ion microprobe: Journal of Geophysical Research, v. 89B, suppl., p. 525–534.

Dallmeyer, R.D., 1989, Contrasting accreted terranes in the southern Appalachian orogen and Atlantic-Gulf Coastal Plains and their correlations with West African sequences, *in* Dallmeyer, R.D., ed., Terranes in the circum-Atlantic Paleozoic orogens: Geological Society of America Special Paper 230, p. 247–267.

Dallmeyer, R.D., and Villeneuve, Michael, 1987, $^{40}Ar/^{39}Ar$ mineral age record of polyphase tectonothermal evolution in the southern Mauritanide orogen, southeastern Senegal: Geological Society of America Bulletin, v. 98, no. 5, p. 602–611.

Dalrymple, G.B., Alexander, E.C., Jr., Lanphere, M.A., and Kraker, G.P., 1981, Irradiation of samples for $^{40}Ar/^{39}Ar$ dating using the Geological Survey TRIGA reactor: U.S. Geological Survey Professional Paper 1176, 55 p.

Daniels, D.L., and Leo, G.W., 1985, Geologic interpretation of basement rocks of the Atlantic Coastal Plain: U.S. Geological Survey Open-File Report 85–655, 45 p., 4 oversize pls.

Denison, R.E., Raveling, H.P., and Rouse, J.T., 1967, Age and descriptions of subsurface basement rocks, Pamlico and Albemarle Sound areas, North Carolina: American Association of Petroleum Geologists Bulletin, v. 51, no. 2, p. 268–272.

Dodson, M.H., 1979, Theory of cooling ages, *in* Jäger, E., and Hunziker, J.C., eds., Lectures in isotope geology: New York, Springer-Verlag, p. 194–202.

Doyle, J.A., and Robbins, E.I., 1977, Angiosperm pollen zonation of the continental Cretaceous of the Atlantic Coastal Plain and its application to deep wells in the Salisbury embayment: Palynology, v. 1, p. 43–78.

Edwards, L.E., and Powars, D.S., 2003, Impact damage to dinocysts from the late Eocene Chesapeake Bay event: Palaios, v. 18, no. 3, p. 275–285. (Also available online at http://www.bioone.org/pdfserv/i0883-1351-018-03-0275.pdf)

Fetter, A.H., and Goldberg, S.A., 1995, Age and geochemical characteristics of bimodal magmatism in the Neoproterozoic Grandfather Mountain rift basin: Journal of Geology, v. 103, no. 3, p. 313–326.

Fitzgerald, P.G., Sorkhabi, R.B., Redfield, T.F., and Stump, Edmund, 1995, Uplift and denudation of the central Alaska Range—A case study in the use of apatite fission track thermochronology to determine absolute uplift parameters: Journal of Geophysical Research, v. 100, no. B10, p. 20,175–20,191.

Galbraith, R.F., 1981, On statistical models for fission track counts: Mathematical Geology, v. 13, no. 6, p. 471–478.

Gallagher, Kerry, 1995, Evolving temperature histories from apatite fission-track data: Earth and Planetary Science Letters, v. 136, no. 3–4, p. 421–435.

Garihan, J.M., Preddy, M.S., and Ranson, W.A., 1993, Summary of mid-Mesozoic brittle faulting in the Inner Piedmont and nearby Charlotte belt of the Carolinas, *in* Hatcher, R.D., Jr., and Davis, T.L., eds., Studies of Inner Piedmont geology with a focus on the Columbus promontory—Carolina Geological Society annual field trip, November 6–7, 1993: Carolina Geological Society, p. 55–65.

Glass, B.P., 2002, Distal impact ejecta from the Chesapeake Bay impact structure [abs.]: Geological Society of America Abstracts with Programs, v. 34, no. 6, p. 466.

Gleadow, A.J.W., Duddy, I.R., Green, P.F., and Lovering, J.F., 1986, Confined fission track lengths in apatite—A diagnostic tool for thermal history analysis: Contributions to Mineralogy and Petrology, v. 94, no. 4, p. 405–415.

Gleadow, A.J.W., Hurford, A.J., and Quaife, R.D., 1976, Fission track dating of zircon—Improved etching techniques: Earth and Planetary Science Letters, v. 33, no. 2, p. 273–276.

Glover, Lynn, III, Sheridan, R.E., Holbrook, W.S., Ewing, John, Talwani, Manik, Hawman, R.B., and Wang, Ping, 1997, Paleozoic collisions, Mesozoic rifting and structure of the Middle Atlantic States continental margin; An "EDGE" Project report, *in* Glover, Lynn, III, and Gates, A.E., eds., Central and southern Appalachian sutures—Results of the EDGE Project and related studies: Geological Society of America Special Paper 314, p. 107–135.

Gohn, G.S., Clark, A.C., Queen, D.G., Levine, J.S., McFarland, E.R., and Powars, D.S., 2001, Operational summary for the USGS-NASA Langley corehole, Hampton, Virginia: U.S. Geological Survey Open-File Report 01–87–A, 21 p., available online at http://pubs.usgs.gov/of/2001/of01-087/

Gohn, G.S., Powars, D.S., Bruce, T.S., Self-Trail, J.M., Weems, R.E., Edwards, L.E., Horton, J.W., Jr., Izett, G.A., and Johnson, G.H., 2001, Preliminary interpretation of the USGS-NASA Langley corehole, Chesapeake Bay impact structure, York-James Peninsula, Hampton, VA [abs.]: Geological Society of America Abstracts with Programs, v. 33, no. 2, p. A–24.

Goldberg, S.A., 1994, U-Pb geochronology of volcanogenic terranes of the eastern North Carolina Piedmont—Preliminary results, *in* Stoddard, E.F., and Blake, D.E., eds., Geology and field trip guide, western flank of the Raleigh meta-

morphic belt, North Carolina—Carolina Geological Society field trip guidebook, November 5–6, 1994: Raleigh, N.C., North Carolina Geological Society, p. 13–17. (Also available online at http://carolinageologicalsociety.org/gb%201994.pdf)

Green, P.F., Duddy, I.R., Gleadow, A.J.W., and Lovering, J.F., 1989, Apatite fission-track analysis as a paleotemperature indicator for hydrocarbon exploration, *in* Naeser, N.D., and McCulloh, T.H., eds., Thermal history of sedimentary basins—Methods and case histories: New York, Springer-Verlag, p. 181–195.

Haugerud, R.A., and Kunk, M.J., 1988, ArAr*, a computer program for reduction of ^{40}Ar-^{39}Ar data: U.S. Geological Survey Open-File Report 88–261, 68 p.

Horton, J.W., Jr., Aleinikoff, J.N., Burton, W.C., Peper, J.D., and Hackley, P.C., 1999, Geologic framework of the Carolina slate belt in southern Virginia—Insights from geologic mapping and U-Pb geochronology [abs.]: Geological Society of America Abstracts with Programs, v. 31, no. 7, p. A–476.

Horton, J.W., Jr., Aleinikoff, J.N., Izett, G.A., Naeser, C.W., and Naeser, N.D., 2001, Crystalline rocks from the first corehole to basement in the Chesapeake Bay impact structure, Hampton, Virginia [abs.]: Geological Society of America Abstracts with Programs, v. 33, no. 6, p. A–448.

Horton, J.W., Jr., Aleinikoff, J.N., Izett, G.A., Naeser, N.D., Naeser, C.W., and Kunk, M.J., 2002, Crystalline basement and impact-derived clasts from three coreholes in the Chesapeake Bay impact structure, southeastern Virginia [abs.]: Eos, Transactions, American Geophysical Union, v. 83, no. 19, spring meeting supplement of 7 May 2002, Abstract T21A–03, p. S351. (Also available online at http://www.agu.org/meetings/waissm02.html)

Horton, J.W., Jr., Drake, A.A., Jr., Rankin, D.W., and Dallmeyer, R.D., 1991, Preliminary tectonostratigraphic terrane map of the central and southern Appalachians: U.S. Geological Survey Miscellaneous Investigations Series Map I–2163, scale 1:2,000,000.

Horton, J.W., Jr., Kunk, M.J., Naeser, C.W., Naeser, N.D., Aleinikoff, J.N., and Izett, G.A., 2002, Petrography, geochronology, and significance of crystalline basement rocks and impact-derived clasts in the Chesapeake Bay impact structure, southeastern Virginia [abs.]: Geological Society of America Abstracts with Programs, v. 34, no. 6, p. 466.

Horton, J.W., Jr., and Stern, T.W., 1994, Tectonic significance of preliminary uranium-lead ages from the eastern Piedmont of North Carolina [abs.]: Geological Society of America Abstracts with Programs, v. 26, no. 4, p. 21.

Hulver, M.L., 1997, Post-orogenic evolution of the Appalachian Mountain system and its foreland: Chicago, University of Chicago, Ph.D. dissertation, 1,055 p.

Hurford, A.J., and Green, P.F., 1982, A users' guide to fission track dating calibration: Earth and Planetary Science Letters, v. 59, no. 2, p. 343–354.

Hurford, A.J., and Green, P.F., 1983, The zeta age calibration of fission-track dating: Isotope Geoscience, v. 1, p. 285–317.

Johnson, G.H., Powars, D.S., Bruce, T.S., Beach, T.A., Harris, M.S., and Goodwin, B.K., 2001, Post-impact effects of the Eocene Chesapeake Bay impact, lower York-James Peninsula, Virginia: Virginia Geological Field Conference, 31st, Williamsburg, Virginia, October 19 and 20, 2001 [Guidebook], 40 p.

Johnson, S.S., 1975, Bouger gravity in southeastern Virginia: Virginia Division of Mineral Resources Report of Investigations 39, 42 p.

Koeberl, Christian, 1990, The geochemistry of tektites—An overview: Tectonophysics, v. 171, no. 1–4, p. 405–422.

Koeberl, Christian, Kruger, F.J., and Poag, C.W., 2001, Geochemistry of surficial sediments near the Chesapeake Bay impact structure and the search for source rocks of the North American tektites [abs.]: Lunar and Planetary Science Conference, 32d, Houston, Tex., March 12–16, 2001, Abstract 1333, available online at http://www.lpi.usra.edu/meetings/lpsc2001/pdf/1333.pdf

Koeberl, Christian, Poag, C.W., Reimold, W.U., and Brandt, Dion, 1996, Impact origin of the Chesapeake Bay structure and the source of the North American tektites: Science, v. 271, no. 5253, p. 1263–1266.

Kohn, B.P., Wagner, M.E., Lutz, T.M., and Organist, G., 1993, Anomalous Mesozoic thermal regime, central Appalachian Piedmont—Evidence from sphene and zircon fission-track dating: Journal of Geology, v. 101, no. 6, p. 779–794.

Laslett, G.M., Green, P.F., Duddy, I.R., and Gleadow, A.J.W., 1987, Thermal annealing of fission tracks in apatite—2. A quantitative analysis: Chemical Geology (Isotope Geoscience Section), v. 65, no. 1, p. 1–13.

Laslett, G.M., Kendall, W.S., Gleadow, A.J.W., and Duddy, I.R., 1982, Bias in measurement of fission-track length distributions: Nuclear Tracks and Radiation Measurements, v. 6, no. 2–3, p. 79–85.

Lefort, J.P., 1988, Imprint of the Reguibat uplift (Mauritania) onto the central and southern Appalachians of the U.S.A.: Journal of African Earth Sciences, v. 7, no. 2, p. 433–442.

Lefort, J.P., 1989, Basement correlation across the North Atlantic: Berlin, Springer-Verlag, 148 p.

Lefort, J.P., and Max, M.D., 1991, Is there an Archean crust beneath Chesapeake Bay?: Tectonics, v. 10, no. 1, p. 213–226.

LeVan, D.C., and Pharr, R.F., 1963, A magnetic survey of the coastal plain in Virginia: Virginia Division of Mineral Resources Report of Investigations 4, 17 p., 3 oversize pls.

Mann, V.I., Clarke, T.G., Hayes, L.D., and Kirstin, D.S., 1965, Geology of the Chapel Hill quadrangle, North Carolina: Raleigh, North Carolina Division of Mineral Resources Special Publication 1, 35 p., 1 oversize pl.

McDougall, Ian, and Harrison, T.M., 1999, Geochronology and thermochronology by the ^{40}Ar/^{39}Ar method, (2d ed.): New York, Oxford University Press, 269 p.

McGee, V.E., Johnson, N.M., and Naeser, C.W., 1985, Simulated fissioning of uranium and testing of the fission-track dating method: Nuclear Tracks and Radiation Measurements, v. 10, no. 3, p. 365–379.

McSween, H.Y., Jr., Speer, J.A., and Fullagar, P.D., 1991, Plutonic rocks, *in* Horton, J.W., Jr., and Zullo, V.A., eds., The geology of the Carolinas, Carolina Geological Society fiftieth anniversary volume: Knoxville, University of Tennessee Press, p. 109–126.

Naeser, C.W., 1976, Fission track dating: U.S. Geological Survey Open-File Report 76–190, 58 p.

Naeser, C.W., 1979, Fission-track dating and geologic annealing of fission tracks, *in* Jäger, E., and Hunziker, J.C., eds., Lectures in isotope geology: New York, Springer-Verlag, p. 154–169.

Naeser, C.W., Naeser, N.D., Kunk, M.J., Morgan, B.A., III, Schultz, A.P., Southworth, C.S., and Weems, R.E., 2001, Paleozoic through Cenozoic uplift, erosion, stream capture, and depositional history in the Valley and Ridge, Blue Ridge, Piedmont, and Coastal Plain provinces of Tennessee, North Carolina, Virginia, Maryland, and District of Columbia [abs.]: Geological Society of America Abstracts with Programs, v. 33, no. 6, p. A312.

Naeser, N.D., Naeser, C.W., and McCulloh, T.H., 1989, The application of fission-track dating to the depositional and thermal history of rocks in sedimentary basins, *in* Naeser, N.D., and McCulloh, T.H., eds., Thermal history of sedimentary basins—Methods and case histories: New York, Springer-Verlag, p. 157–180.

Nance, R.D., and Thompson, M.D., 1996, Avalonian and related peri-Gondwanan terranes of the circum-North Atlantic—An introduction, *in* Nance, R.D., and Thompson, M.D., eds., Avalonian and related peri-Gondwanan terranes of the circum-North Atlantic: Geological Society of America Special Paper 304, p. 1–7.

Ngo, H.H., Wasserburg, G.J., and Glass, B.P., 1985, Nd and Sr isotopic compositions of tektite material from Barbados and their relationship to North American tektites: Geochimica et Cosmochimica Acta, v. 49, no. 6, p. 1479–1485.

Owens, B.E., and Tucker, R.D., 2003, Geochronology of the Mesoproterozoic State Farm Gneiss and associated Neoproterozoic granitoids, Goochland terrane, Virginia: Geological Society of America Bulletin, v. 115, no. 8, p. 972–982.

Poag, C.W., 1996, Structural outer rim of Chesapeake Bay impact crater—Seismic and bore hole evidence: Meteoritics & Planetary Science, v. 31, no. 2, p. 218–226.

Poag, C.W., 1997, The Chesapeake Bay bolide impact; A convulsive event in Atlantic Coastal Plain evolution: Sedimentary Geology, v. 108, no. 1–4, p. 45–90.

Poag, C.W., 1999, Chesapeake invader; Discovering America's giant meteorite crater: Princeton, N.J., Princeton University Press, 183 p.

Poag, C.W., 2002, Structure and morphology of the Chesapeake Bay submarine impact crater [abs.]: Geological Society of America Abstracts with Programs, v. 34, no. 6, p. 465.

Poag, C.W., and the Chesapeake Coring Team, 2001, Drilling to basement inside the Chesapeake Bay crater [abs.]: Lunar and Planetary Science Conference, 32d, Houston, Tex., March 12–16, 2001, Abstract 1203, available online at http://www.lpi.usra.edu/meetings/lpsc2001/pdf/1203.pdf

Poag, C.W., Hutchinson, D.R., Colman, S.M., and Lee, M.W., 1999, Seismic expression of the Chesapeake Bay impact crater; Structural and morphologic refinements based on new seismic data, *in* Dressler, B.O., and Sharpton, V.L., eds., Large meteorite impacts and planetary evolution; II: Geological Society of America Special Paper 339, p. 149–164.

Poag, C.W., Plescia, J.B., and Molzer, P.C., 1999, Chesapeake Bay impact structure; Geology and geophysics [abs.], *in* Gersonde, Rainer, and Deutsch, Alexander, eds., Oceanic impacts; Mechanisms and environmental perturbations; ESF–IMPACT Workshop, April 15–April 17, 1999, Alfred Wegener Institute for Polar and Marine Research, Bremerhaven, Germany, Abstracts: Berichte zur Polarforschung (Reports on Polar Research), v. 343, p. 79–83.

Poag, C.W., Powars, D.S., Poppe, L.J., and Mixon, R.B., 1994, Meteoroid mayhem in Ole Virginny—Source of the North American tektite strewn field: Geology, v. 22, no. 8, p. 691–694.

Poag, C.W., Powars, D.S., Poppe, L.J., Mixon, R.B., Edwards, L.E., Folger, D.W., and Bruce, Scott, 1992, Deep Sea Drilling Project Site 612 bolide event—New evidence of a late Eocene impact-wave deposit and a possible impact site, U.S. East Coast: Geology, v. 20, no. 9, p. 771–774.

Powars, D.S., 2000, The effects of the Chesapeake Bay impact crater on the geologic framework and the correlation of hydrogeologic units of southeastern Virginia, south of the James River: U.S. Geological Survey Professional Paper 1622, 53 p., 1 oversize pl. (Also available online at http://pubs.usgs.gov/prof/p1622)

Powars, D.S., and Bruce, T.S., 1999, The effects of the Chesapeake Bay impact crater on the geological framework and correlation of hydrogeologic units of the lower York-James Peninsula, Virginia: U.S. Geological Survey Professional Paper 1612, 82 p., 9 oversize pls. (Also available online at http://pubs.usgs.gov/prof/p1612/)

Powars, D.S., Bruce, T.S., Bybell, L.M., Cronin, T.M., Edwards, L.E., Frederiksen, N.O., Gohn, G.S., Horton, J.W., Jr., Izett, G.A., Johnson, G.H., Levine, J.S., McFarland, E.R., Poag, C.W., Quick, J.E., Schindler, J.S., Self-Trail, J.M., Smith, M.J., Stamm, R.G., and Weems, R.E., 2001, Preliminary geologic summary for the USGS-NASA Langley corehole, Hampton, Virginia: U.S. Geological Survey Open-File Report 01–87–B, 20 p., available online at http://pubs.usgs.gov/of/2001/of01-087/

Powars, D.S., Gohn, G.S., Edwards, L.E., Catchings, R.D., Bruce, T.S., Johnson, G.H., and Poag, C.W., 2002, Lithostratigraphic framework of the crater-fill deposits; Western annular trough, Chesapeake Bay impact crater [abs.]: Geological Society of America Abstracts with Programs, v. 34, no. 6, p. 465.

Powars, D.S., Johnson, G.H., Edwards, L.E., Horton, J.W., Jr., Gohn, G.S., Catchings, R.D., McFarland, E.R., Izett, G.A.,

Bruce, T.S., Levine, J.S., and Pierce, H.A., 2002, An expanded Chesapeake Bay impact structure; eastern Virginia: New corehole and geophysical data [abs.]: Lunar and Planetary Science Conference, 33d, League City, Tex., March 11–15, 2002, Abstract 1034, available online at http://www.lpi.usra.edu/meetings/lpsc2002/pdf/1034.pdf

Powars, D.S., Mixon, R.B., and Bruce, Scott, 1992, Uppermost Mesozoic and Cenozoic geologic cross section, outer coastal plain of Virginia, *in* Gohn, G.S., ed., Proceedings of the 1988 U.S. Geological Survey Workshop on the Geology and Geohydrology of the Atlantic Coastal Plain: U.S. Geological Survey Circular 1059, p. 85–101.

Pratt, T.L., Coruh, Cohit, Costain, J.K., and Glover, Lynn, III, 1988, A geophysical study of the Earth's crust in central Virginia; Implications for Appalachian crustal structure: Journal of Geophysical Research, v. 93, no. B6, p. 6649–6674.

Rankin, D.W., 1994, Continental margin of the eastern United States; Past and present, *in* Speed, R.C., ed., Phanerozoic evolution of North American continent-ocean transitions—The Decade of North American Geology summary volume to accompany the DNAG continent-ocean transect series: Boulder, Colo., Geological Society of America, p. 129–218.

Reimold, W.U., Koeberl, Christian, and Poag, C.W., 2002, Chesapeake Bay impact crater; Petrographic and geochemical investigations of the impact breccia fill [abs.]: Geological Society of America Abstracts with Programs, v. 34, no. 6, p. 466.

Reinhardt, Juergen, Christopher, R.A., and Owens, J.P., 1980, Lower Cretaceous stratigraphy of the core, *in* Geology of the Oak Grove core: Virginia Division of Mineral Resources Publication 20, pt. 1, p. 31–52, 1 pl.

Roddick, J.C., 1983, High precision intercalibration of ^{40}Ar-^{39}Ar standards: Geochimica et Cosmochimica Acta, v. 47, no. 5, p. 887–898.

Roden, M.K., and Miller, D.S., 1991, Tectono-thermal history of Hartford, Deerfield, Newark, and Taylorsville Basins, eastern United States, using fission-track analysis: Schweizerische Mineralogische und Petrographische Mitteilungen, v. 71, p. 187–203.

Russell, G.S., Russell, C.W., Speer, J.A., and Glover, Lynn, III, 1981, Rb-Sr evidence of latest Precambrian to Cambrian and Alleghanian plutonism along the eastern margin of the subcoastal plain Appalachians, North Carolina and Virginia [abs.]: Geological Society of America Abstracts with Programs, v. 13, no. 7, p. 543.

Russell, G.S., Speer, J.A., and Russell, C.W., 1985, The Portsmouth Granite, a 263 Ma postmetamorphic biotite granite beneath the Atlantic Coastal Plain, Suffolk, Virginia: Southeastern Geology, v. 26, no. 2, p. 81–93.

Samson, S.D., Secor, D.T., and Stern, R., 1999, Provenance and paleogeography of Neoproterozoic circum-Atlantic arc-terranes—Constraints from U-Pb ages of detrital zircons [abs.]: Geological Society of America Abstracts with Programs, v. 31, no. 7, p. 429.

Secor, D.T., Jr., Samson, S.L., Snoke, A.W., and Palmer, A.R., 1983, Confirmation of the Carolina slate belt as an exotic terrane: Science, v. 221, no. 4611, p. 649–651.

Shaw, H.F., and Wasserburg, G.J., 1982, Age and provenance of the target materials for tektites and possible impactites as inferred from Sm-Nd and Rb-Sr systematics: Earth and Planetary Science Letters, v. 60, no. 2, p. 155–177.

Sheridan, R.E., Maguire, T.J., Feigenson, M.D., Patino, L.C., and Volkert, R.A., 1999, Grenville age of basement rocks in Cape May, N.J. well—New evidence for Laurentian crust in U.S. Atlantic Coastal Plain basement Chesapeake terrane: Journal of Geodynamics, v. 27, no. 4–5, p. 623–633.

Speer, J.A., 1981, Petrology of cordierite- and almandine-bearing granitoid plutons of the southern Appalachian Piedmont, U.S.A.: Canadian Mineralogist, v. 19, pt. 1, p. 35–46.

Stacey, J.S., and Kramers, J.D., 1975, Approximation of terrestrial lead isotope evolution by a two-stage model: Earth and Planetary Science Letters, v. 26, no. 2, p. 207–221.

Steiger, R.H., and Jäger, E., comps., 1977, Subcommission on geochronology—Convention on the use of decay constants in geo- and cosmochronology: Earth and Planetary Science Letters, v. 36, no. 3, p. 359–362.

Streckeisen, A.L., chairman, 1973, Plutonic rocks—Classification and nomenclature recommended by the IUGS Subcommission on the Systematics of Igneous Rocks: Geotimes, v. 18, no. 10, p. 26–30.

Streckeisen, A.L., 1976, To each plutonic rock its proper name: Earth-Science Reviews, v. 12, no. 1, p. 1–33.

Su, Qi, Goldberg, S.A., and Fullagar, P.D., 1994, Precise U-Pb zircon ages of Neoproterozoic plutons in the southern Appalachian Blue Ridge and their implications for the initial rifting of Laurentia: Precambrian Research, v. 68, no. 1–2, p. 81–95.

Thompson, M.D., Hermes, O.D., Bowring, S.A., Isachsen, C.E., Besancon, J.R., and Kelly, K.L., 1996, Tectonostratigraphic implications of late Proterozoic U-Pb zircon ages in the Avalon Zone of southeastern New England, *in* Nance, R.D., and Thompson, M.D., eds., Avalonian and related peri-Gondwanan terranes of the circum-North Atlantic: Geological Society of America Special Paper 304, p. 179–191.

United States Geological Survey, 1986, [Topographic map of the] Newport News North, Virginia [7.5-minute quadrangle showing photorevisions of the 1965 map]: Reston, Va., U.S. Geological Survey, scale 1:24,000.

Williams, I.S., and Claesson, S., 1987, Isotopic evidence for the Precambrian provenance and Caledonian metamorphism of high grade paragneisses from the Seve Nappes, Scandinavian Caledonides, II. Ion microprobe zircon U-Th-Pb: Contributions to Mineralogy and Petrology, v. 97, no. 2, p. 205–217.

Wintsch, R.P., and Aleinikoff, J.N., 1987, U-Pb isotopic and geologic evidence for late Paleozoic anatexis, deformation, and accretion of the late Proterozoic Avalon terrane, south-

central Connecticut: American Journal of Science, v. 287, no. 2, p. 107–126.

Wintsch, R.P., Sutter, J.F., Kunk, M.J., Aleinikoff, J.N., and Dorais, M.J., 1992, Contrasting P-T-t paths—Thermochronologic evidence for a late Paleozoic final assembly of the Avalon composite terrane in the New England Appalachians: Tectonics, v. 11, no. 3, p. 672–689.

Wortman, G.L., Samson, S.D., and Hibbard, J.P., 2000, Precise U-Pb zircon constraints on the earliest magmatic history of the Carolina terrane: Journal of Geology, v. 108, no. 3, p. 321–338.

York, D., 1969, Least squares fitting of a straight line with correlated errors: Earth and Planetary Science Letters, v. 5, no. 5, p. 320–324.

Zartman, R.E., and Naylor, R.S., 1984, Structural implications of some radiometric ages of igneous rocks in southeastern New England: Geological Society of America Bulletin, v. 95, no. 5, p. 522–539.

Appendix B1. Descriptions of Samples from the Langley Granite in the USGS-NASA Langley Core

Samples from the USGS-NASA Langley core that are described in this chapter were taken from core box 206 (fig. B3*A*). Samples are identified by the letters NL followed by a number indicating depth in feet. Parts of the core shown in figure B4*C,E,F,G* were not sampled for analysis.

The thin sections were studied by Horton and also were examined by Glen A. Izett (College of William and Mary and USGS Emeritus) and Daniel J. Milton (USGS Emeritus). These examinations revealed no shock-metamorphic features.

Sample NL2080.1

[2 thin sections (fig. B4*D*)]

Depth.—634.01 m (2,080.1 ft); core box 206.

Description.—Sample NL2080.1 consists of granite from the extreme upper end of the interval contained in sample NL2081 (described below). The granite is massive, pale red, medium grained, and nonfoliated; albite and chlorite fill fractures and faults. The fabric is seriate-inequigranular, hypidiomorphic, and isotropic. Mineral percentages are in table B1.

Sample NL2081

Depth.—In sawed half of the drill core from 633.98 to 634.81 m (2,080.0 to 2,082.7 ft) depth; core box 206.

Description.—Sample NL2081 consists of granite that is massive, pale red, medium grained, and nonfoliated. About 2 kilograms (about 4.4 pounds) of granite was processed for mineral separates of zircon (fig. B5) for SHRIMP U-Pb geochronology (fig. B6, table B3), microcline and plagioclase for $^{40}Ar/^{39}Ar$ geochronology (fig. B7, table B4), and zircon and apatite for fission-track geochronology (table B5). The presence of clinochlore, quartz, titanite, hematite, and clinozoisite was confirmed by X-ray diffraction of a mineral separate having a specific gravity between 3.17 and 3.32. NL2080.1 thin sections are from the extreme upper end of the interval contained in this larger sample. Data from NL2080.1 served as a guide for collecting this larger geochronology sample, which encompasses and extends beyond it.

Sample NL2083

Depth.—634.81 to 634.93 m (2,082.7 to 2,083.1 ft); core box 206.

Description.—White albite coating a single joint surface from 634.81 to 634.93 m (2,082.7 to 2,083.1 ft) depth in the granite core. The albite was confirmed by X-ray diffraction and dated by the $^{40}Ar/^{39}Ar$ age-spectrum method (fig. B7, table B4). NL2083.1 thin sections, which do not include the joint, are from rock adjacent to the lower end of this sample.

Sample NL2083.1

[2 thin sections (fig. B4*A,B*)]

Depth.—634.93 m (2,083.1 ft); core box 206.

Description.—Sample NL2083.1 consists of granite from just below the lower end of sample NL2083 (described above). The granite is massive, pale red, medium grained, and nonfoliated. The fabric is seriate-inequigranular, hypidiomorphic, and isotropic. Mineral percentages are in table B1, and chemical composition is in table B2.

Gray minerals were separated by color from part of the same rock sample; the gray minerals were determined by X-ray diffraction to be quartz, albite, and microcline. Semi-quantitative mineral compositions based on scanning-electron microscopy (SEM) follow:

- K-feldspar—66.6 percent SiO_2, 18.7 percent Al_2O_3, 13.2 percent K_2O, 1.5 percent Na_2O
- Albite—65.5 percent SiO_2, 20.6 percent Al_2O_3, 12.7 percent Na_2O, 0.5 percent CaO, 0.3 percent K_2O
- Oligoclase—66.5 percent SiO_2, 21.5 percent Al_2O_3, 10.4 percent Na_2O, 1.5 percent CaO
- Chlorite—Mg much more abundant than Fe

Accessory and trace minerals confirmed by SEM are titanite, zircon, apatite, thorite (intergrown with zircon), a titanium oxide, and monazite as minute inclusions in iron-titanium oxide; inclusions in chlorite were identified as albite, an epidote mineral, titanite, and Fe oxide having a very low Ti content.

Physical Geology of the Impact-Modified and Impact-Generated Sediments in the USGS-NASA Langley Core, Hampton, Virginia

By Gregory S. Gohn, David S. Powars, T. Scott Bruce, and Jean M. Self-Trail

Chapter C of
**Studies of the Chesapeake Bay Impact Structure—
The USGS-NASA Langley Corehole, Hampton, Virginia, and
Related Coreholes and Geophysical Surveys**
Edited by J. Wright Horton, Jr., David S. Powars, and Gregory S. Gohn

Prepared in cooperation with the
Hampton Roads Planning District Commission,
Virginia Department of Environmental Quality, and
National Aeronautics and Space Administration Langley Research Center

Professional Paper 1688

U.S. Department of the Interior
U.S. Geological Survey

Contents

Figures

Table

Physical Geology of the Impact-Modified and Impact-Generated Sediments in the USGS-NASA Langley Core, Hampton, Virginia

By Gregory S. Gohn,[1] David S. Powars,[1] T. Scott Bruce,[2] and Jean M. Self-Trail[1]

Abstract

The USGS-NASA Langley corehole penetrated a complete section of impact-modified and impact-generated sediments in the outer annular trough of the late Eocene Chesapeake Bay impact structure. The U.S. Geological Survey (USGS) and cooperators drilled the Langley corehole to a total depth of 635.1 meters (m; 2,083.8 feet (ft)) at the National Aeronautics and Space Administration (NASA) Langley Research Center in Hampton, Va.

The continuously sampled Langley core contains 390.6 m (1,281.6 ft) of impact-related sediments between the top of basement granite at 626.3 m (2,054.7 ft) depth and the base of upper Eocene postimpact sediments at 235.65 m (773.12 ft) depth. Preimpact Cretaceous and lower Tertiary sedimentary sections disrupted by the impact consisted of noncalcareous, nonglauconitic Lower Cretaceous and basal Upper Cretaceous fluvial and deltaic sediments overlain by glauconitic and calcareous Upper Cretaceous and lower Tertiary marine sediments.

Three informally defined, impact-related sedimentary units are recognized in the Langley core: crater unit A, crater unit B, and the Exmore beds. Crater unit A overlies basement granite at a depth of 626.3 m (2,054.7 ft) and consists of 183.8 m (603.0 ft) of minimally to moderately disrupted Cretaceous fluvial and deltaic sediments of the Potomac Formation. Crater unit A does not contain shocked ejecta or infiltrated exotic sediments.

Crater unit A is divided into two informal subunits: the lower beds and the upper beds. The contact between the subunits is placed at a depth of 558.1 m (1,831.0 ft). Primary (Cretaceous) sedimentary structures and cycles, including horizontal bedding and laminations, are virtually pristine in the lower beds, indicating little or no impact disruption. Similar primary structures and cycles are present in the upper beds, but massive (structureless) sands and fractured finer grained beds also are present.

Crater unit B overlies crater unit A at a depth of 442.5 m (1,451.7 ft) in the Langley core. The unit contact is placed at the base of the lowest zone of injected exotic matrix within crater unit B. Crater unit B is 173.0 m (567.7 ft) thick and consists of coherent blocks (4 millimeters to <1 m (0.16 inch to <3.3 ft) in diameter), megablocks (1 m to <25 m (<82 ft)), and megablock zones (multiple megablocks with block-on-block contacts) of Potomac Formation sediments separated by intervals of mixed native and exotic sediments called matrix zones.

The matrix zones consist of blocks of deformed Potomac Formation sediments suspended in a matrix of typically noncalcareous, muddy, pebbly, quartz-glauconite sand. The glauconite in these zones is an exotic component that represents injection of disaggregated Upper Cretaceous and Tertiary marine sediments downward into the nonglauconitic sediments of the Potomac Formation.

Crater unit B is divided into two informal subunits: the lower beds that contain glauconitic matrix only in a thin interval at their base and the upper beds that contain abundant glauconitic matrix zones. The contact between the subunits is placed at a depth of 427.7 m (1,403.3 ft).

Crater units A and B represent an autochthonous to parautochthonous sedimentary section within the impact structure's annular trough. These units present no evidence for large-scale removal of preimpact sediments by excavation flow or for shock deformation near the Langley corehole.

The basement granite, crater unit A, and the lower beds of crater unit B constitute an autochthonous section in which impact deformation was limited to local fluidization of sand beds and fracturing and faulting. Exotic sediments in this composite interval are limited to a 0.3-m-thick (1-ft-thick) interval of glauconitic matrix at the contact between crater units A and B. The upper beds of crater unit B constitute a parautochthonous section that contains widespread evidence of fracturing, slumping, and rotation of blocks and megablocks of the Potomac Formation, fluidization of sands, and injection of exotic sediments.

Inferred impact-generated deformation features in crater units A and B and their inferred causative mechanisms include the following: fractures and faults due to early tensional fracturing and (or) late-stage gravitational collapse, massive

[1]U.S. Geological Survey, Reston, VA 20192.

[2]Virginia Department of Environmental Quality, P.O. Box 10009, Richmond, VA 23240.

sand layers produced by increased pore-water pressure in sand beds or acoustic fluidization of sand beds, and dikes of disaggregated, near-surface, preimpact Cretaceous and Tertiary glauconitic sediments that were injected into an underpressured interval of the Potomac Formation.

The Exmore beds are 33.8 m (110.9 ft) thick; they overlie crater unit B and extend from 269.4 to 235.65 m (884.0 to 773.12 ft) depth in the Langley core. The Exmore beds consist of abundant clasts of unshocked, preimpact Cretaceous and Tertiary sediments and sparse shocked crystalline ejecta suspended in an unsorted and unstratified matrix of calcareous, muddy, quartz-glauconite sand and granules (polymict diamicton). A thin interval of clayey silts and fine sands (transition sediments) is present at the top of the Exmore beds above the diamicton at depths of 235.92 to 235.65 m (774.03 to 773.12 ft).

The diamicton is interpreted as debris-flow deposits produced by strong resurge currents that resulted from the late-stage gravitational collapse of the transient crater, including the water-column crater. The presence of two debris-flow units in the Exmore beds in the Langley core is inferred from the pattern of coarse-tail grading of large clasts and variations in the distribution of reworked Cretaceous fossils.

The fine-grained transition sediments represent fallout of impact-suspended sediments from the water column and the return to normal continental-shelf sedimentation. Poag (2002, *Geology,* v. 30, p. 995–998) and Poag and Norris (this volume, chap. F) interpret the presence within the transition sediments of a microspherule (microtektite) layer and an overlying biologic dead zone that lacks an indigenous fauna.

Introduction

Chesapeake Bay Impact Structure

The Chesapeake Bay impact structure is the dominant subsurface feature of the southeastern Virginia Coastal Plain and Inner Continental Shelf. It was formed about 35 million years ago by the impact of a comet fragment or asteroid on the late Eocene continental shelf of eastern North America and subsequently was buried beneath hundreds of meters of upper Eocene through Quaternary marine and paralic sediments.

The Chesapeake Bay impact structure is a complex crater that consists of an inner, highly deformed central crater (also called the inner basin) surrounded concentrically by a relatively less deformed annular trough (fig. C1) (Poag and others, 1994; Poag, 1997; Poag, Hutchinson, and others, 1999; Poag, Plescia, and Molzer, 1999; Powars and Bruce, 1999; Powars, 2000). The central crater is about 35 kilometers (km; 21.8 miles (mi)) in diameter. The annular trough extends outward from the central crater to the faulted outer margin, a radial distance of about 25 km (15.5 mi). Therefore, the outer margin (also called the outer rim) has a diameter of about 85 km (53 mi), which is the value typically cited as the size of the Chesapeake Bay impact structure.

This chapter discusses the lithologic, stratigraphic, structural, and depositional characteristics of impact-modified and impact-generated sediments of the Chesapeake Bay impact structure encountered in the USGS-NASA Langley core. The Langley corehole is located within the structure's annular trough near its southwestern margin at Hampton, Va. (fig. C1).

USGS-NASA Langley Corehole

Several coreholes were drilled into or near the annular trough of the Chesapeake Bay impact structure during the late 1980s and the 1990s (Powars and others, 1992; Powars and Bruce, 1999; Powars, 2000). The discovery of severely disrupted coastal plain deposits in these cores prompted the early investigations (Poag and others, 1991; Powars and others, 1991, 1992) that ultimately led to our present understanding of the Chesapeake Bay impact structure. However, none of these coreholes penetrated the lower part of the sedimentary section within the annular trough or the basement rocks below the sedimentary section.

In 2000, the U.S. Geological Survey (USGS) drilled a 635.1-meter (m)-deep (2,083.8-foot (ft)-deep), continuously cored test hole through the entire postimpact and impact-deformed sedimentary section and into the underlying basement rock at the National Aeronautics and Space Administration (NASA) Langley Research Center, Hampton, Va. (figs. C1, C2). This research was conducted in cooperation with the Hampton Roads Planning District Commission, the Virginia Department of Environmental Quality, the NASA Langley Research Center, and the Geology Department of the College of William and Mary (see "Acknowledgments"). Gohn and others (2001), Poag and the Chesapeake Coring Team (2001), Powars, Bruce, and others (2001), and Powers, Gohn, and others (2001) provided operational details and preliminary geologic analyses for the Langley corehole. The Langley corehole is located in the Newport News North 7.5-minute quadrangle (USGS, 1986) at lat 37°05'44.28" N., long 76°23'08.96" W. (North American Datum of 1927), at a ground-surface altitude of 2.4 m (7.9 ft) above the North American Vertical Datum of 1988.

Sediments modified or generated by the Chesapeake Bay impact are present in the Langley core between the top of basement rock at 626.3 m (2,054.7 ft) depth and the base of postimpact sediments at 235.65 m (773.12 ft) depth. This 390.6-m-thick (1,281.6-ft-thick) section is divided informally, from base to top, into crater unit A, crater unit B, and the Exmore beds. Inferences about the nature of the impact processes within the annular trough may be drawn from the patterns of sediment deformation, sediment removal, and resedimentation seen in the Langley core. This lithologic study is facilitated by the analysis of a high-resolution seismic-reflection survey conducted by the USGS at the NASA Langley Research Center (Catchings and others, this volume, chap. I).

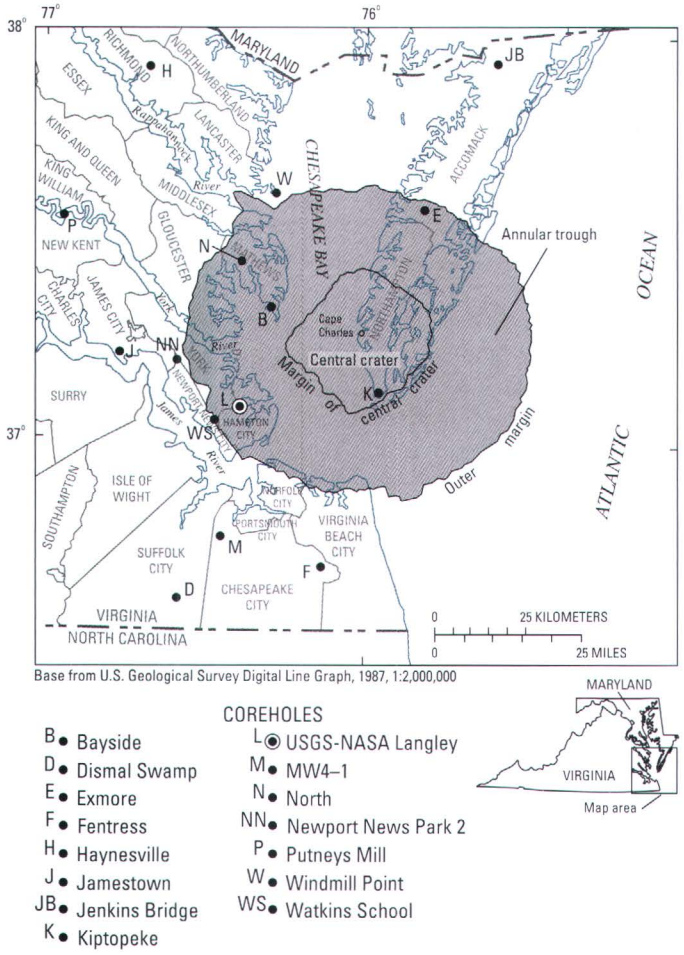

Figure C1. Regional map showing the location of the Chesapeake Bay impact structure, the USGS-NASA Langley corehole at Hampton, Va., and some other coreholes in southeastern Virginia. Locations of the central crater and outer margin are from Powars and Bruce (1999). Illustration modified from Powars, Johnson, and others (2002) and Edwards and Powars (2003).

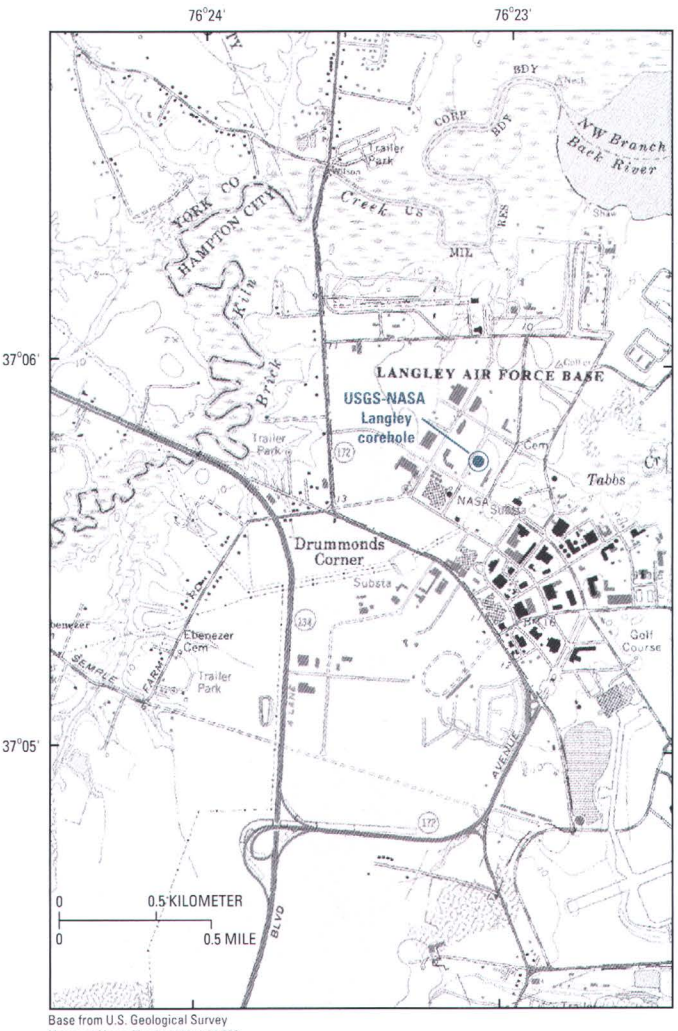

Figure C2. Detailed map showing the location of the USGS-NASA Langley corehole, Hampton, Va.

In this chapter, crater unit A, crater unit B, and the Exmore beds are discussed following a summary of the preimpact coastal plain stratigraphy of the southern Chesapeake Bay area. Horton and others (this volume, chap. B) provide an analysis of the basement rock at the bottom of the Langley core and a discussion and references for the regional geology of the pre-Cretaceous rocks below the coastal plain deposits of the impact area.

Regional Preimpact Stratigraphy

Cretaceous and lower Tertiary sediments of the Virginia Coastal Plain constituted a significant portion of the materials affected by the late Eocene Chesapeake Bay impact. Therefore, the postimpact distribution and character of these disrupted sediments within and near the impact structure constitute a major part of the complex record of impact-related deformation and sedimentation. The preimpact coastal plain units of the southern Chesapeake Bay area, as presently seen outside the impact structure, are reviewed here to provide the background needed for discussion of the impact-modified and impact-generated sediments in the Langley core.

The preimpact section of the study area consists of Lower Cretaceous, Upper Cretaceous, and lower Tertiary sedimentary units that differ significantly in their preimpact distributions and lithologic characteristics. Separate stratigraphic columns are shown in figure C3 for the areas west, south, and north (Delmarva Peninsula) of the impact structure.The Delmarva section includes data from deep drill holes in the adjacent part of the Maryland Coastal Plain north of the Chesapeake Bay

impact structure. Ward (1985), Ward and Strickland (1985), Powars and Bruce (1999), and Powars (2000) provided maps that show the distributions of preimpact and postimpact stratigraphic units in the Virginia Coastal Plain. A discussion of the preimpact stratigraphy in southeastern Virginia also is provided by Poag, Koeberl, and Reimold (2004).

Lower Cretaceous and Basal Upper Cretaceous Stratigraphy

A thick, widespread section of Lower Cretaceous and basal Upper Cretaceous fluvial and deltaic sediments is assigned to the Potomac Formation in Virginia (for example, Powars and Bruce, 1999) and the equivalent Potomac Group in Maryland (for example, Hansen, 1982). The Potomac Formation constitutes most of the impact-modified section in the Langley core.

Regionally, the Potomac Formation consists of repetitive sections of noncalcareous silty and sandy clays, clayey silts, and muddy to moderately well sorted, typically feldspathic sands, gravelly sands, and gravels (Anderson, 1948; Reinhardt, Christopher, and Owens, 1980; Owens and Gohn, 1985; Powars and Bruce, 1999). The Potomac deposits include light- to dark-gray, locally lignitic and pyritic sediments as well as color-mottled, oxidized sediments. Sedimentary structures, cyclic sedimentation patterns, and the near absence of marine fossils indicate deposition in channels, bars, flood plains, and related subenvironments within fluvial to delta-plain environments (Hansen, 1969; Reinhardt, Christopher, and Owens, 1980).

In the absence of calcareous faunas and floras, palynomorphs (primarily pollen and spores) have been the principal source of data for biostratigraphic analysis of the Potomac Formation (Brenner, 1963; Doyle and Robbins, 1977; Reinhardt, Christopher, and Owens, 1980; Doyle, 1982). These microfloras indicate Barremian(?) through early Cenomanian ages for the Potomac Formation (Group) throughout the Virginia and Maryland Coastal Plains (fig. C3). Older Lower Cretaceous sediments and Jurassic(?) sediments are present in the Maryland and Virginia sections of the Delmarva Peninsula north of the Chesapeake Bay impact structure (Brown and others, 1972; Hansen, 1982), but their presence within the impact structure is not documented, and they probably are absent from that area.

The Potomac Formation thickens from a featheredge at the western margin of the coastal plain to hundreds of meters near the modern Atlantic coast (Anderson, 1948; Hansen, 1969, 1982; Brown and others, 1972). The Potomac Formation is at least 305 m (1,000 ft) thick immediately west of the impact structure on the York-James Peninsula (Powars and Bruce, 1999) and at least 546 m (1,790 ft) thick near the southern margin of the impact structure in the Norfolk area (Brown and others, 1972). The total thickness of Lower Cretaceous and Jurassic(?) sediments north of the impact structure in Virginia is about 1,400 m (about 4,600 ft), and sections that are 1,220 m to at least 1,525 m (4,000 to 5,000 ft) thick are present farther north in Maryland (Anderson, 1948; Hansen, 1982).

Upper Cretaceous Stratigraphy

The Upper Cretaceous stratigraphic units of the southern Chesapeake Bay area consist of relatively thin sections of primarily marine sediments that are restricted in their stratigraphic and geographic extents. Common lithologies include gray and greenish-gray, fossiliferous, glauconitic quartz sands and calcareous, fossiliferous muds that contrast with the locally oxidized, nonmarine sediments of the Potomac Formation. Upper Cretaceous sediments are not present west of Chesapeake Bay and the impact structure in Virginia (Owens and Gohn, 1985; Powars and Bruce, 1999).

Unnamed upper Cenomanian beds constitute the oldest and most widespread Upper Cretaceous unit, occurring both north and south of the impact structure. South of the structure, this unit consists of numerous fining-upward repetitions of shelly, glauconitic sand and fossiliferous, burrowed muds that are overlain by micaceous, lignitic, muddy sands (Powars and others, 1992; Powars and Bruce, 1999; Powars, 2000). Collectively, these lithologies suggest deposition on the inner shelf above wave base and possibly in delta-front environments. Similar upper Cenomanian sediments are present north of the impact structure on the Delmarva Peninsula (Anderson, 1948; Hansen and Wilson, 1990; Powars and others, 1992; Powars and Bruce, 1999).

A late Cenomanian age for these beds is indicated by their palynomorphs (Doyle and Robbins, 1977; G.J. Brenner, *in* Hansen and Wilson, 1990), mollusks (Stephenson, 1948a,b; N.F. Sohl, USGS, oral commun., 1988), and ostracodes (G.S. Gohn, USGS, unpub. data). The upper Cenomanian beds thicken to the southeast in the area south of the impact structure; known thicknesses in that area range from 10.0 m (33 ft) to 64.6 m (212 ft) (Powars, 2000). North of the structure in Virginia, the upper Cenomanian beds are about 12.2 to 33.5 m (40 to 110 ft) thick (Doyle and Robbins, 1977; Hansen and Wilson, 1990; Powars and others, 1992).

Figure C3 (facing page). Regional stratigraphic columns for the Cretaceous and lower Tertiary sedimentary units in the vicinity of the Chesapeake Bay impact structure. The geologic time column is adapted from Berggren and others (1995) and Gradstein and others (1995). References for the stratigraphic units are listed in the text. Vertical bars indicate the absence of sediments.

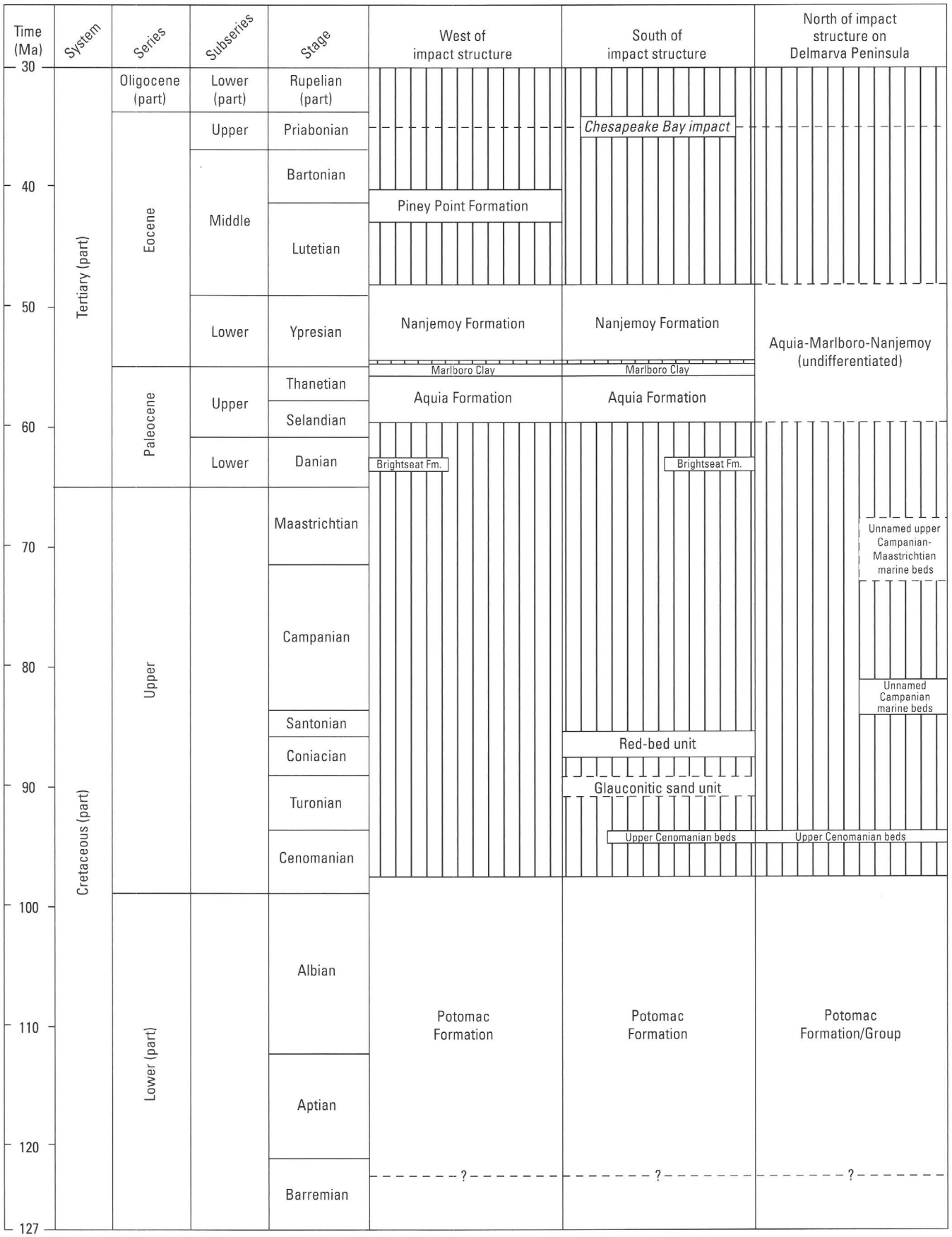
Time (Ma)
System
Series
Subseries
Stage
West of impact structure
South of impact structure
North of impact structure on Delmarva Peninsula
30
40
50
60
70
80
90
100
110
120
127
Tertiary (part)
Cretaceous (part)
Oligocene (part)
Lower (part)
Rupelian (part)
Eocene
Upper
Priabonian
Middle
Bartonian
Lutetian
Lower
Ypresian
Paleocene
Upper
Thanetian
Selandian
Lower
Danian
Upper
Maastrichtian
Campanian
Santonian
Coniacian
Turonian
Cenomanian
Lower (part)
Albian
Aptian
Barremian
Chesapeake Bay impact
Piney Point Formation
Nanjemoy Formation
Nanjemoy Formation
Aquia-Marlboro-Nanjemoy (undifferentiated)
Marlboro Clay
Marlboro Clay
Aquia Formation
Aquia Formation
Brightseat Fm.
Brightseat Fm.
Unnamed upper Campanian-Maastrichtian marine beds
Unnamed Campanian marine beds
Red-bed unit
Glauconitic sand unit
Upper Cenomanian beds
Upper Cenomanian beds
Potomac Formation
Potomac Formation
Potomac Formation/Group
?
?
?

Two informally recognized Upper Cretaceous units are present above the upper Cenomanian beds in the area south of the impact structure in Virginia; these are the glauconitic sand unit and the red-bed unit of Powars and others (1992), Powars and Bruce (1999), and Powars (2000). The glauconitic sand unit is known from two coreholes in southeastern Virginia where about 16.8 to 18.0 m (55 to 59 ft) of these marine deposits overlie the upper Cenomanian beds. No fossils have been examined from the glauconitic sand unit, but its stratigraphic position (fig. C3) suggests a Turonian age (Christopher and others, 1999).

The red-bed unit overlies the glauconitic sand unit and consists of oxidized, color-mottled muds, sands, and gravelly sands. These deposits are noncalcareous and contain mudcracks, rootlets, and paleosols that indicate continental environments of deposition similar to those inferred for the Potomac Formation.

Observed thicknesses of the red-bed unit range from 16.3 to 27.8 m (53.4 to 91.3 ft). Palynomorphs from this unit indicate a Coniacian to Santonian age (N.O. Frederiksen, USGS, written commun., 1999). The palynologic age, stratigraphic position, and lithologies of the red-bed unit suggest that it is a northward continuation of the widespread Cape Fear Formation of the Carolinas (Christopher and others, 1999).

Two additional Upper Cretaceous marine units are recognized north of the impact structure on the Delmarva Peninsula in Virginia and Maryland (fig. C3). The older of these unnamed units reaches a maximum thickness of about 15 m (about 50 ft) and contains microfossils that indicate a late Santonian(?) to early Campanian age (Anderson, 1948; Swain, 1948; R.K. Olssen, *in* Hansen and Wilson, 1990; Powars and others, 1992; G.S. Gohn, USGS, unpub. data). The presence of unnamed upper Campanian to Maastrichtian beds may be inferred from mollusks described from sediment cores of the Hammond test hole in Maryland (Stephenson, 1948b) and from reworked Maastrichtian microfossils found in impact-generated sediments of the impact structure (Powars and others, 1992). These Santonian(?) to Maastrichtian sections consist primarily of fossiliferous, fine-grained sediments (Anderson, 1948; Powars and others, 1992).

Lower Tertiary Stratigraphy

The preimpact Tertiary section of the Virginia Coastal Plain (fig. C3) consists of marine sediments of the Paleocene and Eocene Pamunkey Group (Ward, 1985); from oldest to youngest, the Pamunkey Group contains the Brightseat Formation, Aquia Formation, Marlboro Clay, Nanjemoy Formation, and Piney Point Formation. Except for the Brightseat, the formations of the Pamunkey Group are widespread in the Virginia Coastal Plain. In detailed studies, the Aquia, Nanjemoy, and Piney Point Formations typically are divided into members and (or) beds. Common lithologies include shelly limestones, muds, and muddy quartz, quartz-glauconite, and glauconite sands. Calcareous macrofossils and microfossils are moderately abundant throughout the Pamunkey Group in sections that have not been leached of their calcium carbonate. Lithologies, ages, distributions, and thicknesses of the lower Tertiary formations described in the following summary paragraphs are derived from Gibson and others (1980), Reinhardt, Newell, and Mixon (1980), Ward (1985), Ward and Strickland (1985), Mixon (1989), Hansen and Wilson (1990), Powars and others (1992), Poag and Ward (1993), Poag and Commeau (1995), Powars and Bruce (1999), and Powars (2000).

The oldest preimpact Tertiary unit is the lower Paleocene Brightseat Formation, which consists of fossiliferous, micaceous muddy fine sands. The Brightseat is generally considered to be present only in updip areas of the Virginia Coastal Plain north of the Rappahannock River. However, Powars and others (1992; also see Powars, 2000, p. 33) referred a thin section of lower Paleocene muddy, glauconitic sand in the Virginia Coastal Plain south of Chesapeake Bay and the impact structure to the Brightseat Formation on the basis of lithologic and paleontologic data (fig. C3).

The widespread upper Paleocene Aquia Formation consists of variably macrofossiliferous and microfossiliferous, muddy, glauconite and quartz-glauconite sands that extend beneath most of the Virginia Coastal Plain. The Aquia maintains a thickness in the range of 6.1 to 18.3 m (20 to 60 ft) in areas adjacent to the impact structure.

The uppermost Paleocene and lowermost Eocene Marlboro Clay is a thin but widespread unit in areas west and south of Chesapeake Bay. The Marlboro consists of distinctive, sparingly fossiliferous, gray and pale-red, kaolinitic silty clay that contrasts with the greenish glauconitic sediments of the overlying and underlying units. Thicknesses of the Marlboro are in the range of 2.4 to 5.5 m (8 to 18 ft) in areas adjacent to the western and southern margins of the impact structure.

The widespread lower Eocene Nanjemoy Formation consists of typically fossiliferous, burrowed muds and muddy fine to coarse glauconite-quartz sands. The thickness of the Nanjemoy ranges from about 12.2 to 18.3 m (40 to 60 ft) in areas near the western and southern margins of the impact structure.

The middle Eocene Piney Point Formation is composed of muddy, glauconitic, highly fossiliferous, locally calcite-cemented, quartz-glauconite sand and quartzose and glauconitic, moldic, pelecypod limestone. The Piney Point does not occur in the area south of the impact structure but is widespread in the area west of the impact structure and Chesapeake Bay. Thicknesses of 1.8 to 6.1 m (6 to 20 ft) are recorded for the Piney Point in the area adjacent to the western margin of the impact structure.

The geology of the Pamunkey Group in the Virginia part of the Delmarva Peninsula north of the impact structure is not well documented. However, data from the adjacent part of the Maryland Coastal Plain suggest that Paleocene through middle Eocene sections of marine deposits in that area are about 40 to 100 m (about 120 to 300 ft) thick (Anderson, 1948; Brown and others, 1972; Hansen, 1978; Hansen and Wilson, 1990; Poag and Commeau, 1995).

Implications for Impact Crater Analysis

The Cretaceous and lower Tertiary sedimentary section disrupted by the late Eocene Chesapeake Bay impact consisted of two lithologically distinct parts: a lower section of Lower Cretaceous and basal Upper Cretaceous nonmarine sediments and an upper section of Upper Cretaceous and lower Tertiary marine sediments. The lower section consisted of nonglauconitic, noncalcareous, locally oxidized, interbedded sands and clays, whereas the upper section consisted of glauconitic to very glauconitic, typically calcareous, sparingly oxidized, fine-grained deposits. The lithologic contrast between these two sections is a useful tool for analyzing the character and extent of impact-produced sediment disruption and mixing in the annular trough.

USGS-NASA Langley Core

Stratigraphy of the Annular Trough

Previous studies divided the sedimentary section within the annular trough of the Chesapeake Bay impact structure into two units: the megablock unit and the overlying Exmore beds (Poag, 1996, 1997; Poag, Hutchinson, and others, 1999; Powars and Bruce, 1999; Powars, 2000). Poag (1997, p. 57) considered the megablocks to be slumped blocks of fractured sedimentary rocks that were affected by the impact. His interpretations of the megablocks on seismic-reflection profiles show normal-fault-bounded, locally rotated blocks having typical dimensions of tens to hundreds of meters (Poag, 1996, 1997; Poag, Hutchinson, and others, 1999). Powers and Bruce (1999, p. 30–31) stated, on the basis of limited core data, that the megablocks consisted primarily of Lower Cretaceous fluvial and deltaic deposits (Potomac Formation).

Powers and Bruce (1999, p. 29) described the Exmore as a lithologically variable unit, which consists of shelly, glauconitic, muddy, pebbly sand that serves as a matrix between abundant clasts of preimpact sediments, sparse clasts of crystalline rock and melt rock, and sparse shocked quartz grains (also see Koeberl and others, 1996). Informal stratigraphic names previously applied to the Exmore unit include the "Exmore beds" (Powars and others, 1992), the "Exmore boulder bed" (Poag and others, 1992), the "Exmore breccia" (Poag, 1996, 1997), and the "Exmore tsunami-breccia" (Powars and Bruce, 1999; Powars, 2000). Powars, Bruce, and others (2001) referred to these deposits in the Langley core as "unit C."

In this chapter, the sedimentary section of the annular trough recovered in the Langley core is divided informally into crater unit A, crater unit B, and the Exmore beds. These units are defined on the basis of physical criteria observed in the core (fig. C4), including the lithology, size, and deformation of sediment blocks and clasts, the presence or absence of preimpact Tertiary sediments as detrital clasts, exotic blocks, or exotic matrix, and the presence or absence of fluidized sands, resedimented deposits, and shocked and (or) cataclastic crystalline-rock ejecta.

We consider the megablock sections of previous authors to be generally equivalent to crater unit A of this chapter on the basis of similarities in sediment types and postimpact stratigraphic position. Sections of crater unit B probably were assigned to the Exmore beds in previous reports because of the gross lithologic similarity of crater unit B to the Exmore beds (sediment blocks or clasts in matrix). However, the Exmore beds are more narrowly defined in this chapter, where block-in-matrix sections with a strong dominance of Potomac Formation blocks and a paucity of crystalline-rock and Tertiary sediment blocks are excluded from the Exmore and included in crater unit B.

Poag and Norris (this volume, chap. F) continue the use of a two-part subdivision (megablocks and Exmore breccia) for the sedimentary section in the Langley core (fig. C5). They indicate that their definition of the term "Exmore breccia" includes crater unit B and the Exmore beds of this chapter.

The Exmore breccia of Poag and Norris (this volume, chap. F) does not include a thin interval of fine-grained sediments that we include as the uppermost part of the Exmore beds in this chapter (fig. C5). Instead, they assign this fine-grained interval to a lower "fallout layer" and an upper "dead zone" that are located above their Exmore breccia and below the postimpact Chickahominy Formation (also see Poag, 2002). Poag and Norris (this volume, chap. F) place the fallout layer and dead zone between depths of 235.87 and 235.65 m (773.85 and 773.12 ft) in the Langley core. After reconsideration of the original core photographs and field notes for the Langley core, we consider these fine-grained sediments to extend from a depth of 235.92 m to 235.65 m (774.03 ft to 773.12 ft) (fig. C5) and refer to them as the "transition sediments" of the Exmore beds.

Terminology for Coarse-Grained Materials

Two sets of grain-size terminology are used in this chapter to describe the very large particles present in the crater materials of the Langley core. The standard Wentworth grade scale and class terms (Wentworth, 1922) are used for the Exmore beds because this unit is interpreted to consist of allogenic clastic sediments. Hence, particles having diameters longer than 4 millimeters (mm; 0.16 inch (in.)) in the Exmore beds are described as pebbles, cobbles, and boulders; the term "clast" is used to refer collectively to these size classes. The Wentworth (1922) scale also is used for primary detrital particles within the preimpact sediments.

In contrast, crater units A and B are interpreted to consist of autochthonous to parautochthonous sedimentary sections in which the formation of large constituent pieces was primarily the result of impact-induced fracturing and faulting. For these materials, the word "block" is used for particles that are 4 mm (0.16 in.) to less than 1 m (3.3 ft) in diameter. Particles that are 1 m to less than 25 m (82 ft) in diameter are called "megablocks." Particles larger than 25 m were not recognized in the

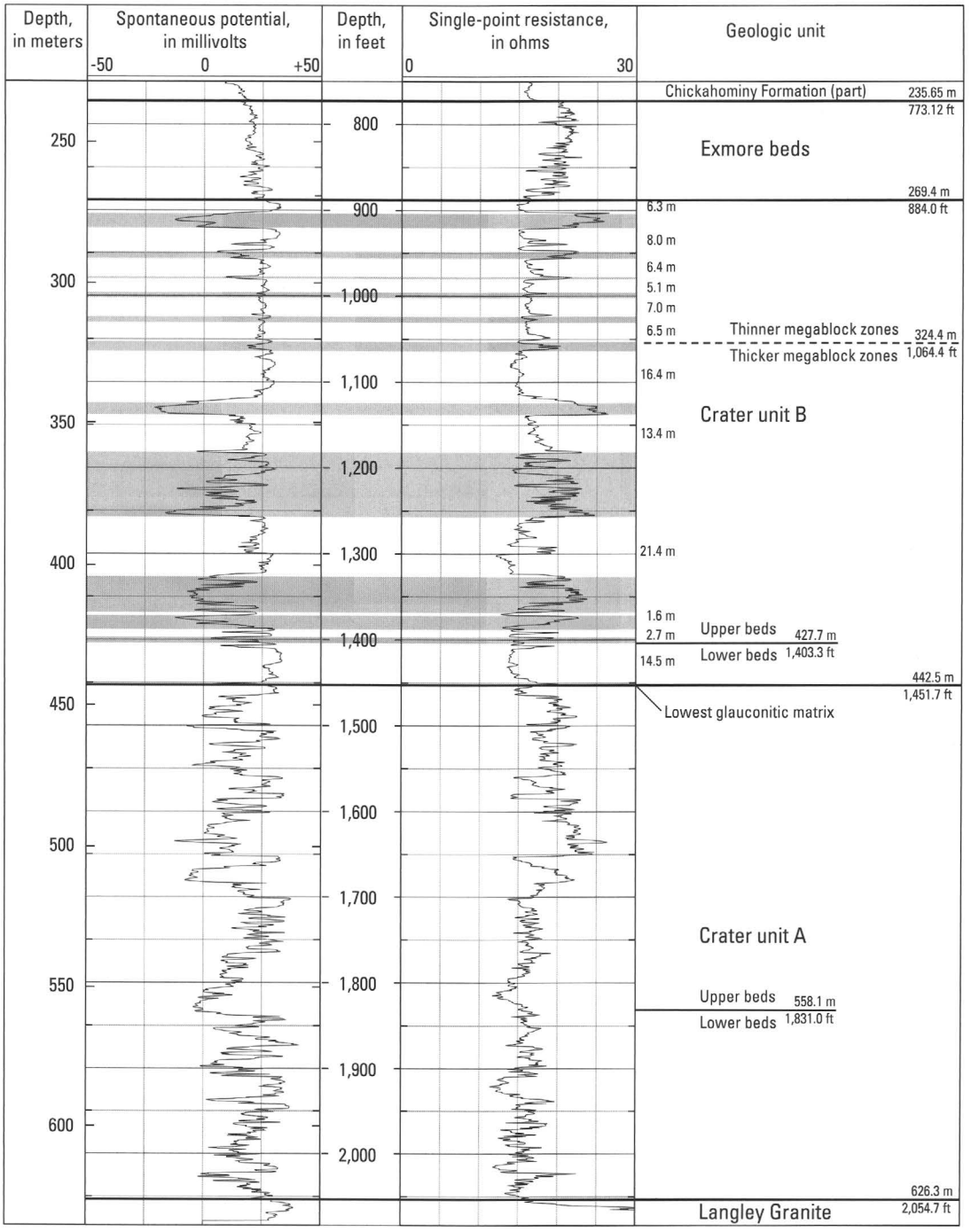

Figure C4. Summary geologic column and geophysical logs for the impact-modified sediments (crater units A and B) and impact-generated sediments (Exmore beds) in the USGS-NASA Langley core. Thicknesses of sediment megablocks in crater unit B are indicated; see also figure C7. Shaded intervals are zones of injected glauconitic matrix in crater unit B.

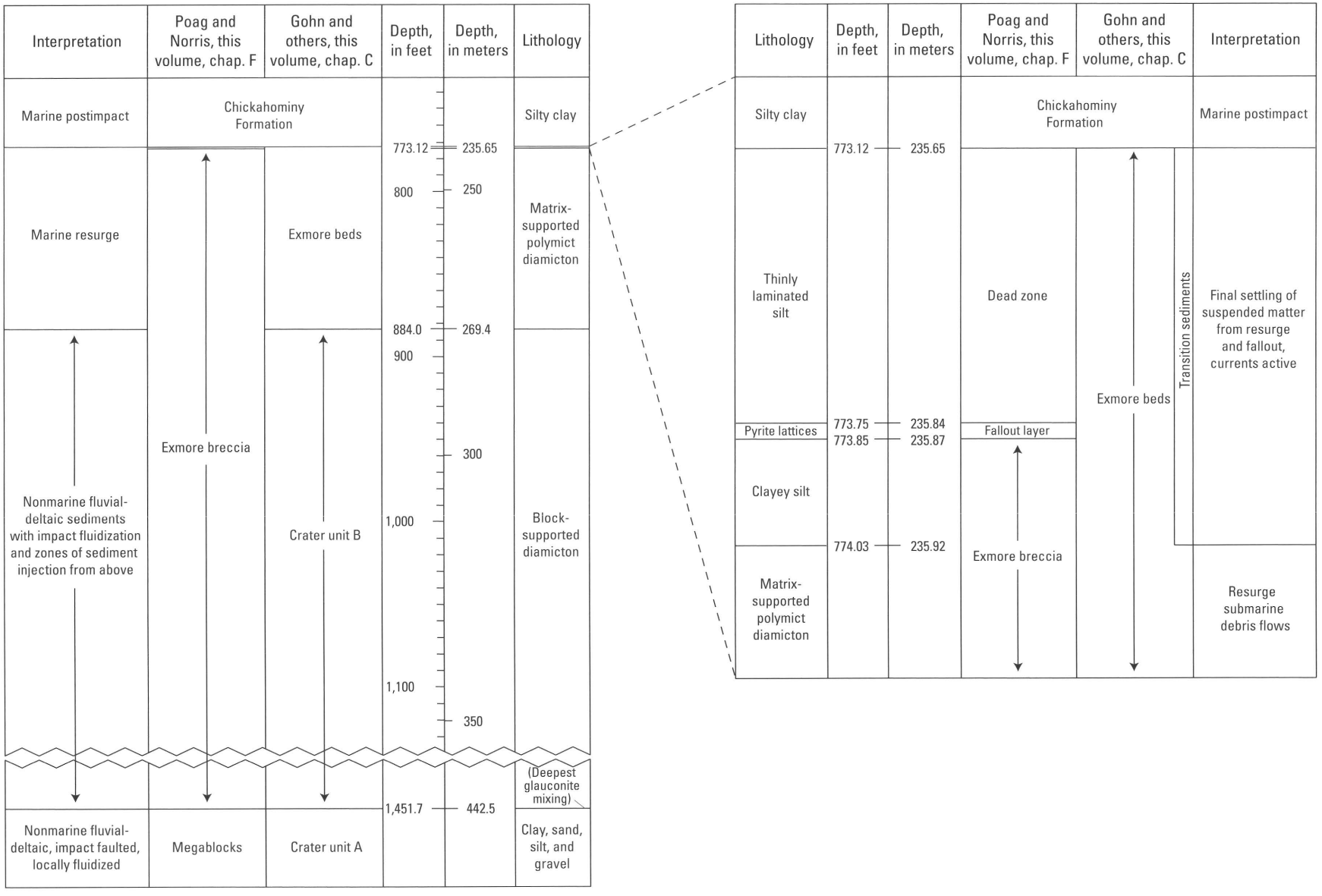

Figure C5. Correlation diagram for part of the USGS-NASA Langley core comparing informal usage of the terms "Exmore beds" and "Exmore breccia" in relation to lithology and interpretation of ocean-water resurge deposits. The stratigraphic terms defined in this chapter (Gohn and others, chap. C) are used throughout this volume except in chapter F (Poag and Norris), which follows the stratigraphy of Poag, Koeberl, and Reimold (2004). From Horton and others (this volume, chap. A, fig. A6).

Langley core, although fault-bounded blocks of greater size probably are present (Catchings and others, this volume, chap. I).

The term "megablock" in this chapter refers to constituent particles that are smaller than the fault-bounded, slumped megablocks defined by Poag (1996, 1997), Powars and Bruce (1999), and others. The term "fault blocks" might be more appropriate for the large "megablocks" (tens to hundreds of meters in diameter) described by these authors.

Crater Unit A

General Lithology and Thickness

Crater unit A comprises poorly to moderately compacted sediments of the Cretaceous Potomac Formation between depths of 626.3 m (2,054.7 ft) and 442.5 m (1,451.7 ft) in the Langley core (fig. C4); thus, it is 183.8 m (603.0 ft) thick. The basal contact of crater unit A with the underlying weathered granite is sharp and nonconformable. Approximately the basal meter (3 ft) of crater unit A contains abundant subangular to angular granite pebbles and cobbles.

Crater unit A consists of noncalcareous, nonglauconitic, silty and sandy clays, clayey silts, muddy fine sands, gravelly coarse sands, sandy quartz-feldspar-chert gravels, and sandy clay-intraclast gravels. The sands and gravelly sands are more abundant than the finer grained sediments throughout the unit. Sediment colors vary from light and dark gray to less common red and brown oxidation colors. Repetitive fining-upward sedimentary cycles with erosional bases, basal sandy gravels, and distinctive sequences of sedimentary structures and lithologies are typical of crater unit A. Shocked or cataclastic ejecta (Horton and Izett, this volume, chap. E), exotic clasts of Tertiary sediment, and exotic disaggregated Tertiary sediments were not observed in crater unit A.

The contact between crater unit A and the overlying crater unit B at a depth of 442.5 m (1,451.7 ft) is placed at the base of the lowest (deepest) occurrence of muddy, gravelly, quartz-glauconite sand (referred to as "matrix") between blocks and megablocks of Potomac Formation sediments (see following section on "Crater Unit B"). The lowest occurrence of glauconitic matrix is a useful field criterion for defining these units, and it has genetic significance with regard to the limit of impact-induced mixing of glauconitic and nonglauconitic sediments.

Crater unit A is divided into two informal subunits: the lower beds and the upper beds. Physical characteristics used to divide these subunits are the presence of highly fractured clays and thick, massive (structureless), gravelly sands in the upper beds and the paucity of these features in the lower beds. The contact between the subunits is placed at the base of the stratigraphically lowest, massive gravelly sand at 558.1 m (1,831.0 ft) depth.

Lower Beds of Crater Unit A

Undisrupted primary (Cretaceous) sedimentary features characterize the lower beds of crater unit A. Horizontal and low-angle bedding and laminations are present throughout this unit, indicating that little or no rotation of the cored section has occurred. Silty and sandy clay beds in this interval display moderate- to high-angle fractures and small faults but do not show evidence of slumping and rotation, which is common in clays of the upper beds.

Upper Beds of Crater Unit A

Primary (Cretaceous) sediment types, sedimentary structures, and sedimentary cycles in the upper beds (fig. C6*A*) are similar to those in the lower beds. However, thick intervals of massive gravelly sand also are present in the upper beds, particularly from 558.1 m to about 542.5 m (1,831.0 ft to about 1,780.0 ft) depth and from 503.4 to 486.2 m (1,651.5 to 1,595.0 ft) depth. These sands contain disseminated quartz, chert, and clay pebbles but lack stratification (fig. C6*B*). The pebbles do not occur in distinct size-graded beds or at predictable positions within sedimentary cycles, as seen in the lower beds of crater unit A. Fractured and faulted, oxidized clays from 486.2 to 482.0 m (1,595.0 to 1,581.5 ft) depth contain bedding and laminations inclined at moderate angles and overlie the higher interval of massive sand.

Crater Unit B

General Lithology and Thickness

Crater unit B is present in the Langley core from 442.5 m (1,451.7 ft) to 269.4 m (884.0 ft) depth and has a thickness of 173.0 m (567.7 ft). This unit consists, in large part, of Cretaceous sediments of the Potomac Formation that are generally similar in their primary depositional characteristics to the Potomac Formation sediments in crater unit A. However, Potomac Formation sediments in crater unit B are substantially more disrupted than those in crater unit A.

We refer to intervals in crater unit B that consist of locally derived sediment blocks suspended in a finer grained matrix of mixed exotic and locally derived sediments as "matrix zones." The matrix zones intervene between larger coherent megablocks and between intervals of multiple blocks and megablocks that we refer to as "megablock zones" (fig. C7).

Crater unit B is divided into two informal subunits: the lower beds and the upper beds. The contact between the subunits is placed at a depth of 427.7 m (1,403.3 ft); it separates Potomac Formation sediments with minimal exotic matrix in the lower beds from an overlying thicker section of Potomac Formation sediments disrupted by numerous matrix zones in the upper beds. The only matrix zone in the lower beds is present at the base of the unit from 442.5 m (1,451.7 ft) to 442.2 m (1,450.8 ft) depth.

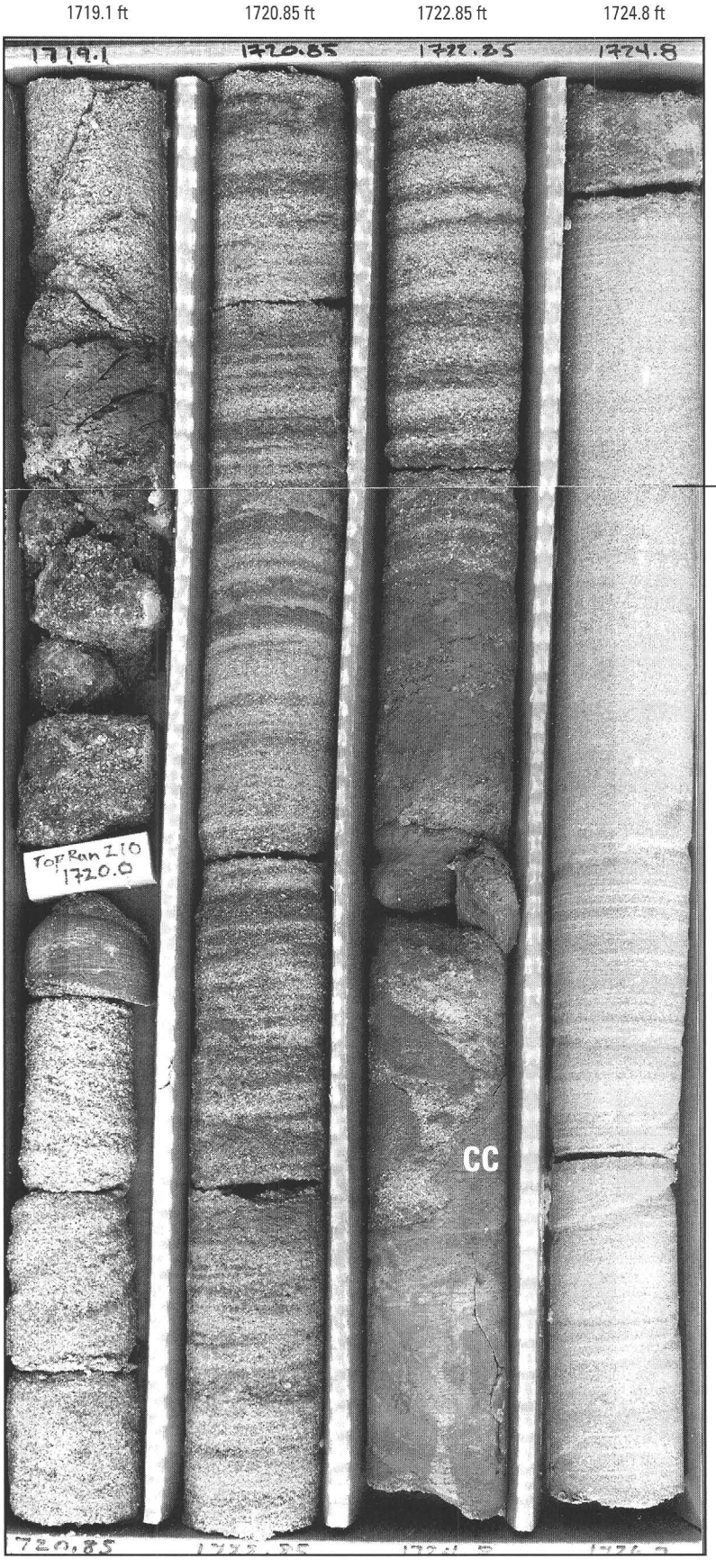

Figure C6. Photographs of the upper beds of crater unit A in the USGS-NASA Langley core. Depths handwritten on the core boxes in feet are repeated in type for clarity. Section tops are at the upper left corners of the boxes. *A,* Composite photograph of core box 173 showing horizontally laminated and cross-laminated sands, horizontally interbedded and interlaminated sands and clays, and clay-clast gravels. The clay clasts (CC) in the third tray from the left are uniform in composition and locally derived. Metric depth values for the top and bottom of box 173 are 524.0 m and 526.3 m. *B,* Photograph of core box 165 showing massive (fluidized) sand with disseminated quartz and clay pebbles. Metric depth values for the top and bottom of box 165 are 493.9 m and 496.8 m.

B

Figure C6. Continued.

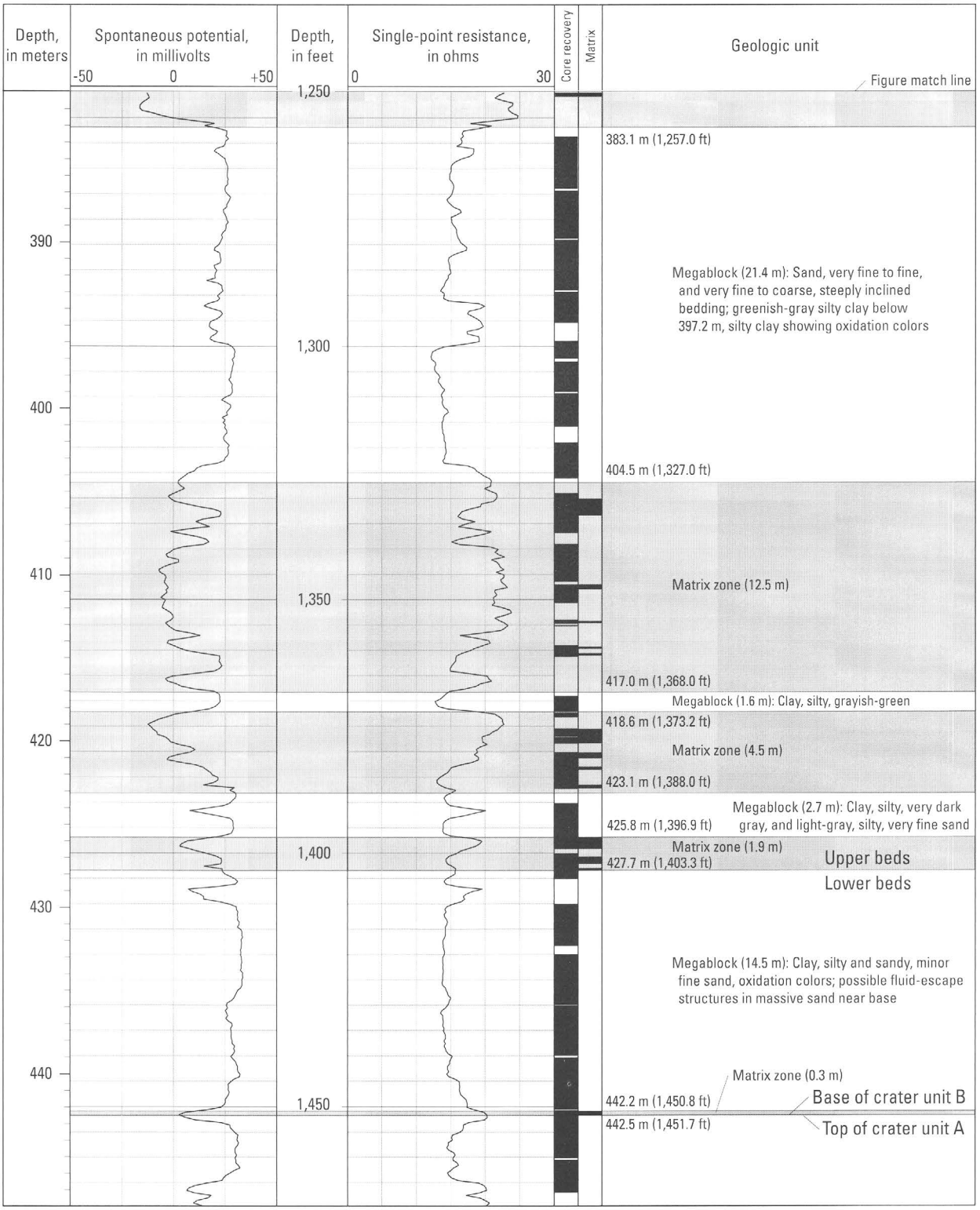

A. Lower part of crater unit B

Figure C7. Geologic column and geophysical logs for crater unit B in the USGS-NASA Langley core. Depths to contacts between blocks, megablocks, and matrix zones are listed, and thicknesses and lithologies of blocks and megablocks are indicated. Core recovery (black), individual matrix occurrences (black), and matrix zones (gray) also are indicated. The data are presented in three pages, and match lines are shown on each page. *A,* Lower part of crater unit B from 442.5 m (1,451.7 ft) to 383.1 m (1,257.0 ft) depth. *B,* Middle part of crater unit B from 383.1 m (1,257.0 ft) to 320.6 m (1,051.9 ft) depth. *C,* Upper part of crater unit B from 324.4 m (1,064.4 ft) to 269.4 m (884.0 ft) depth.

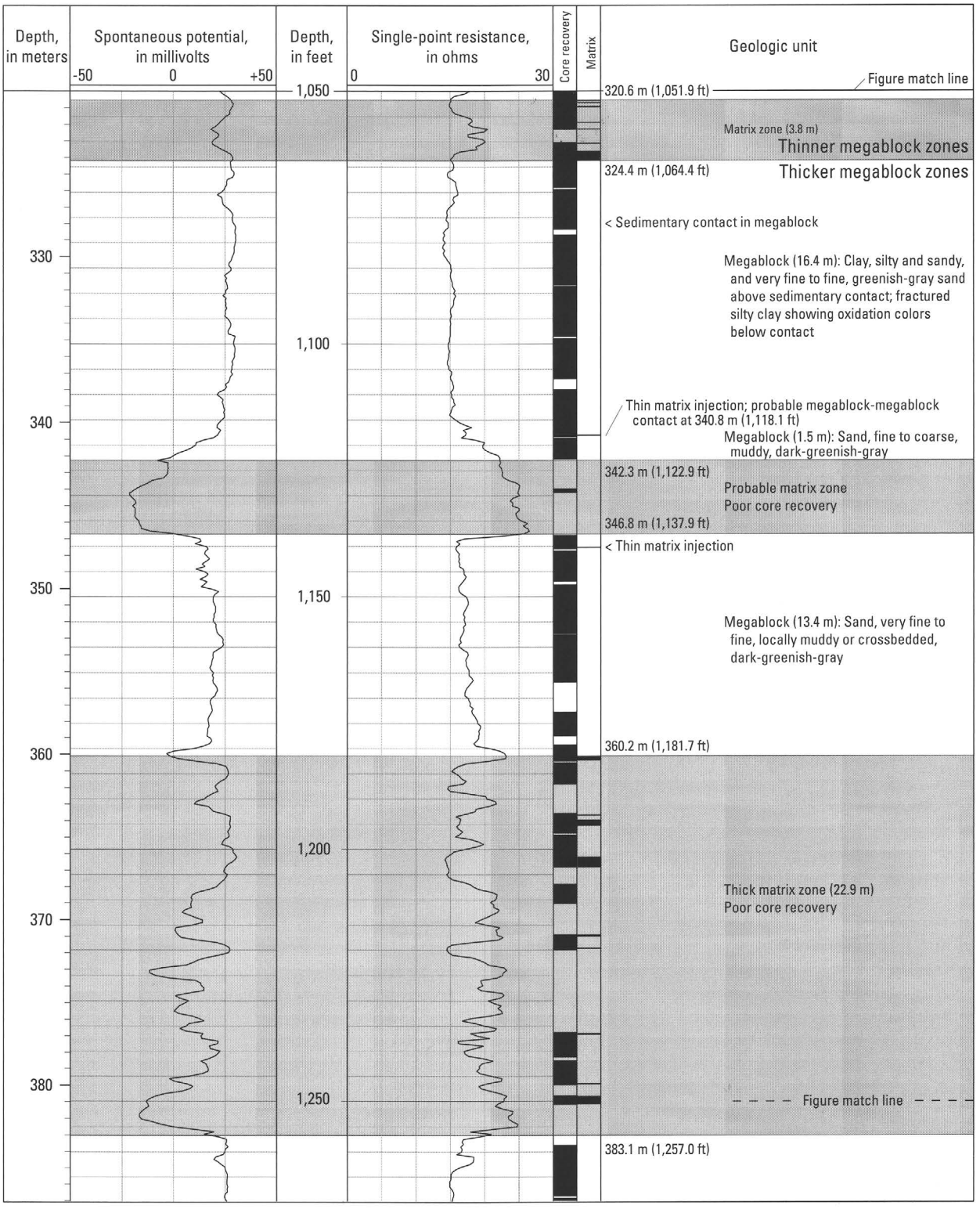

B. Middle part of crater unit B

Figure C7. Continued.

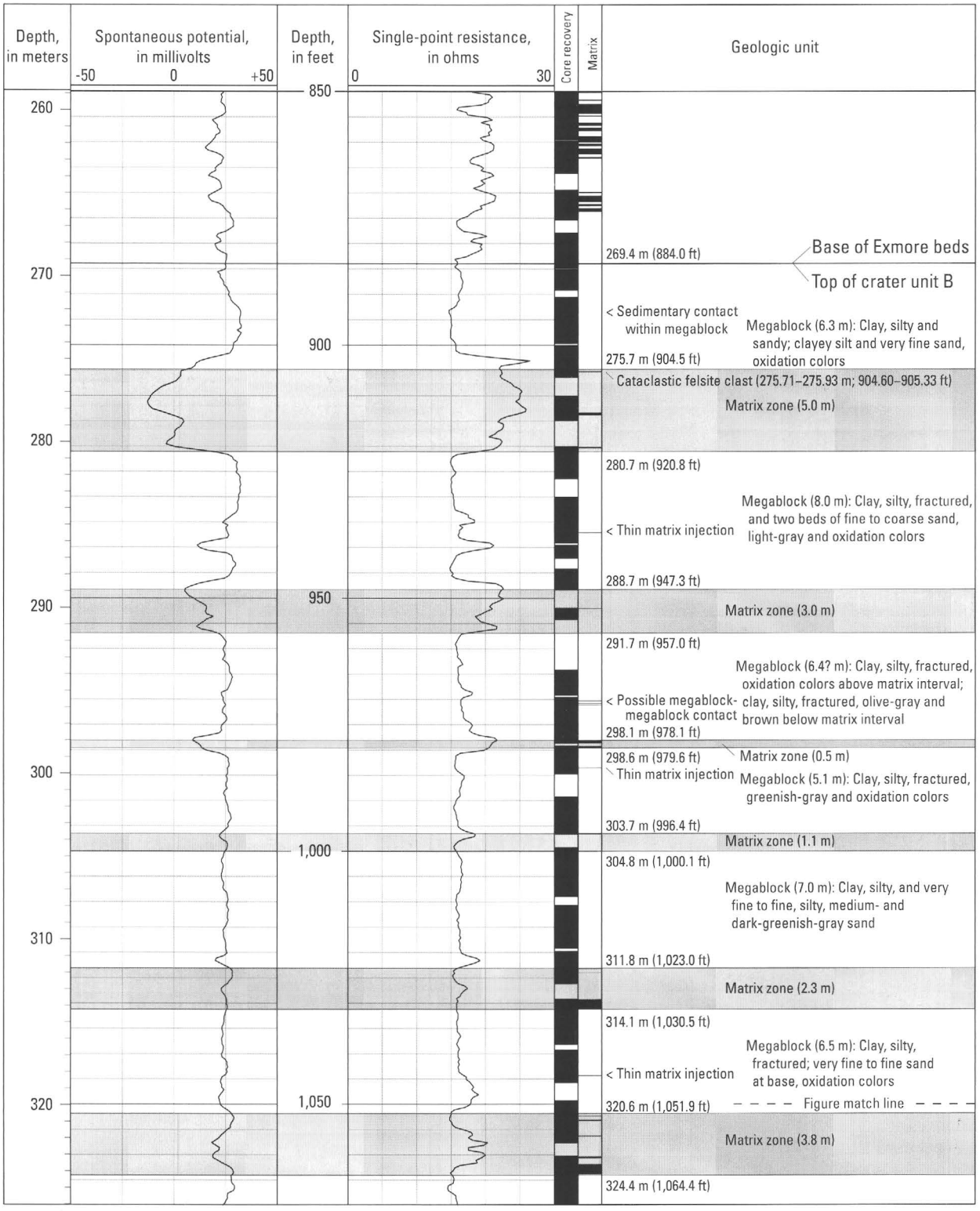

C. Upper part of crater unit B

Figure C7. Continued.

Megablocks and Megablock Zones

Definition and lithologies.—Megablocks in crater unit B consist entirely of coherent, slightly to moderately deformed pieces of the Potomac Formation. Some megablocks consist of a single lithology, whereas others contain a range of clays, silts, sands, and gravelly sands. Primary bedding, laminations, crossbedding, and erosional contacts between beds are present within many megablocks. Individual megablocks may consist primarily of multicolored oxidized sediments, light- to dark-gray sediments, or both.

A variety of structural and sedimentary features hinders the recognition of certain megablock contacts. In some sections of the Langley core, convincing examples of primary sedimentary contacts (and other stratification) within coherent megablocks are present, including cases where contrasting lithologies are separated by primary sedimentary contacts. However, planar contacts between two separate megablocks, especially contacts between two megablocks that consist of the same sediment type, can be difficult to distinguish from the sedimentary contacts within megablocks. In other examples, centimeter-scale layers of glauconitic matrix separate megablocks having similar or contrasting lithologies. In these examples, it can be difficult to distinguish a matrix-filled fracture within an otherwise coherent megablock from a block-on-block contact with a trace of matrix between two megablocks. For these reasons, we have defined megablock zones in crater unit B as composite sections of two or more Potomac Formation blocks and megablocks separated by probable block-on-block contacts. Recognized megablock contacts within megablock zones are listed in figure C7.

Nearly structureless, nonglauconitic, very fine to very coarse grained sand with a few thin intervals of disrupted relict laminations is present above the basal glauconitic matrix zone in the lower part of the lower beds from 442.2 m (1,450.8 ft) to about 439.6 m (1,442.2 ft) depth. Oxidized fine-grained sediments are present in the lower beds from about 439.6 m (1,442.2 ft) to the subunit contact at 427.7 m (1,403.3 ft).

Megablocks and megablock zones from 427.7 m (1,403.3 ft) to 340.8 m (1,118.1 ft) depth in the upper beds of crater unit B primarily consist of gray and greenish-gray, carbonaceous clays, silts, and sands (fig. C8*A*). Beds of very fine to fine and very fine to coarse sands in this interval are noncalcareous, variably muddy, and locally lignitic or gravelly. Cross laminations and crossbedding, clay laminations, burrows, and clay intraclasts are common in these sands. Thicker clay beds in this interval typically are dark gray, lignitic, silty, and sandy. Oxidized silty and sandy clays and muddy fine sands are present from 404.5 m (1,327.0 ft) to 397.2 m (1,303 ft) depth.

Megablocks and megablock zones in the upper beds of crater unit B above 340.8 m (1,118.1 ft) depth consist primarily of oxidized red, brown, and light-gray sediments (fig. C8*B*). The most common sediment type is color-mottled, noncalcareous, silty and locally sandy clay. These clays are dense and contain abundant faults with slickensides; primary bedding generally is difficult to discern. Root casts and crumbly and blocky fabrics suggest primary subaerial environments of deposition. A second sediment type in this interval is color-mottled, noncalcareous, micaceous, clayey silt and very fine sand. The sands are locally cross laminated or massive. Dominantly gray, noncalcareous, well-sorted, very fine to fine sands also are present. These sands typically are massive but locally contain clay-silt laminae and primary clay-silt intraclasts.

Thickness and distribution.—Megablocks and megablock zones in crater unit B range in thickness from about 1.5 to 21.4 m (4.9 to 70.2 ft) (fig. C7). These measured thicknesses represent the maximum apparent vertical dimension of each megablock or megablock zone.

The thicker megablocks and megablock zones (about 16.0 to 22.0 m; 52.5 to 72.2 ft) occur in the lower half of crater unit B below 324.4 m (1,064.4 ft) depth, whereas those above 324.4 m (1,064.4 ft) depth range from about 5.0 to 8.0 m (16.4 to 26.2 ft) in thickness. The change from thicker to thinner megablocks and megablock zones does not correspond to the subunit boundary between the lower and upper beds of crater unit B (fig. C4).

Structures.—Several megablocks in crater unit B display oversteepened bedding (figs. C7 and C8). Dips from 45°to about 75°are locally present, indicating significant rotation of these blocks. Fractures and faults of uncertain displacement also are typical within or bounding individual megablocks.

Matrix Zones

Definition and lithologies.—The matrix zones consist of sediment blocks from the Cretaceous Potomac Formation suspended in a matrix of disaggregated Cretaceous and Tertiary sediments (fig. C9). Megablocks, which are particles larger than 1.0 m (3.3 ft) are rare in the matrix zones. Block boundaries range from irregular and embayed to essentially smooth, and orientations range from horizontal to inclined at moderate and steep angles. Block contacts with the matrix may be sharp, slightly gradational, or broadly diffuse across a centimeter (1 cm; 0.4 in.) or more. In general, the sandier, more friable blocks show the most diffuse contacts.

Blocks in the matrix zones are strongly deformed. Their internal bedding typically is distorted or fractured and inclined at all angles from horizontal to vertical and perhaps overturned. Vertically extended and distorted bedding in partially disaggregated blocks suggests vertical fluid movement within the matrix zones.

Blocks in the matrix zones of crater unit B are locally derived pieces of the Potomac Formation. These native blocks contain a wide range of Potomac Formation sediment types that closely resemble the Potomac sediments in crater unit A and in the megablocks and megablock zones of crater unit B. Common sediment types found in the matrix-zone blocks include light- to dark-gray, noncalcareous, typically micaceous and lignitic clays and sands and noncalcareous, gray-, red-, and brown-mottled silty clays, clayey silts, muddy sands, and sandy gravels. Well-rounded quartz, quartz-feldspar, chert, and quartzite pebbles are common as disseminated particles in the matrix zones

Figure C8. Photographs of megablocks in crater unit B in the USGS-NASA Langley core. Depths handwritten on the core boxes in feet are repeated in type for clarity. Section tops are at the upper left corners of the boxes. *A*, Composite photograph of core box 124 showing steeply dipping and locally fractured, interlaminated and burrowed sands and clayey silts within a megablock in crater unit B. Metric depth values for the top and bottom of box 124 are 353.3 m and 357.5 m. *B*, Composite photograph of core box 111 showing red and brown silty clay within a megablock in crater unit B. The megablock is overlain by matrix-zone material in the left-hand tray (see dashed line). Metric depth values for the top and bottom of box 111 are 313.7 m and 316.2 m.

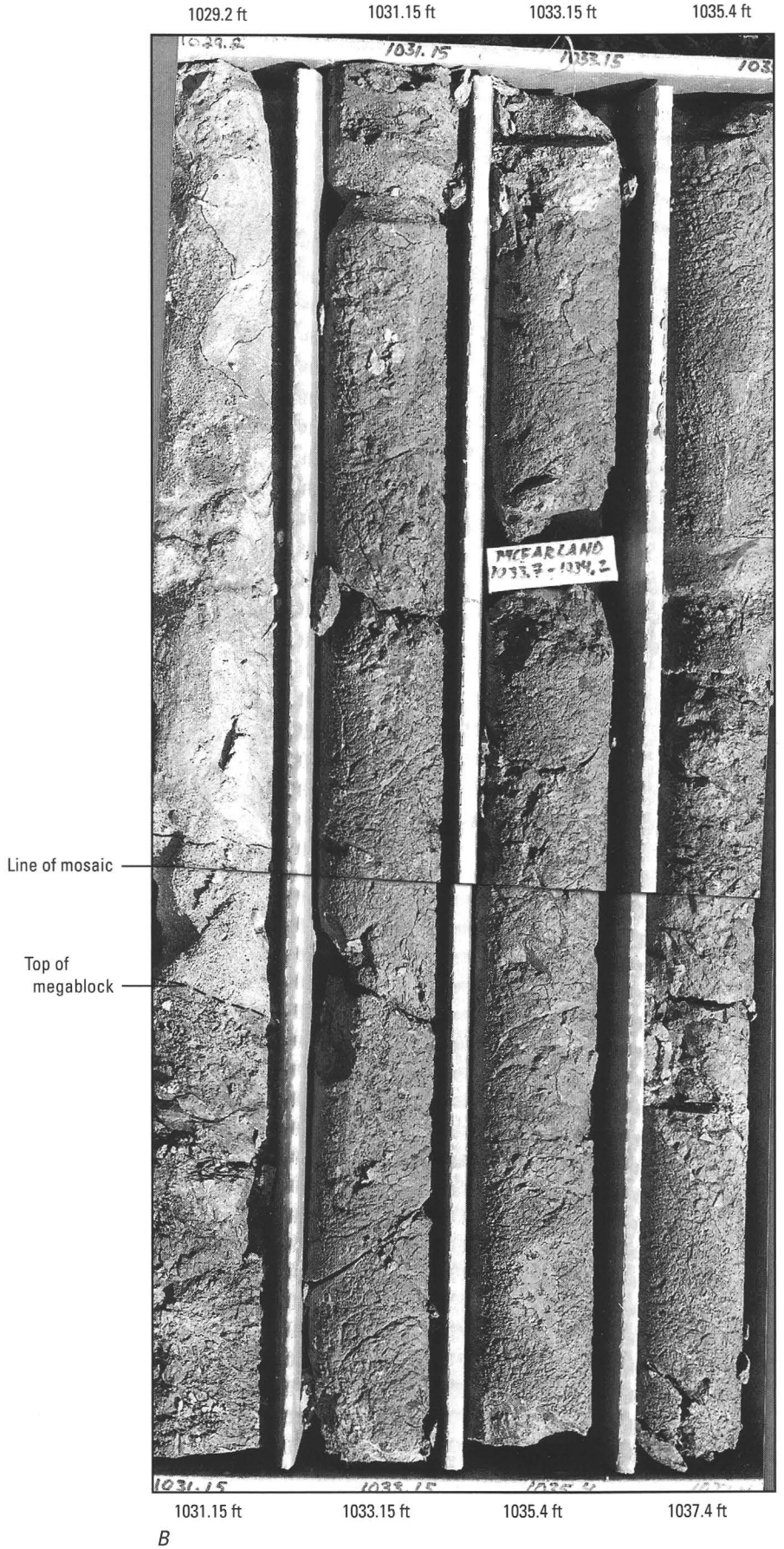

Figure C8. Continued.

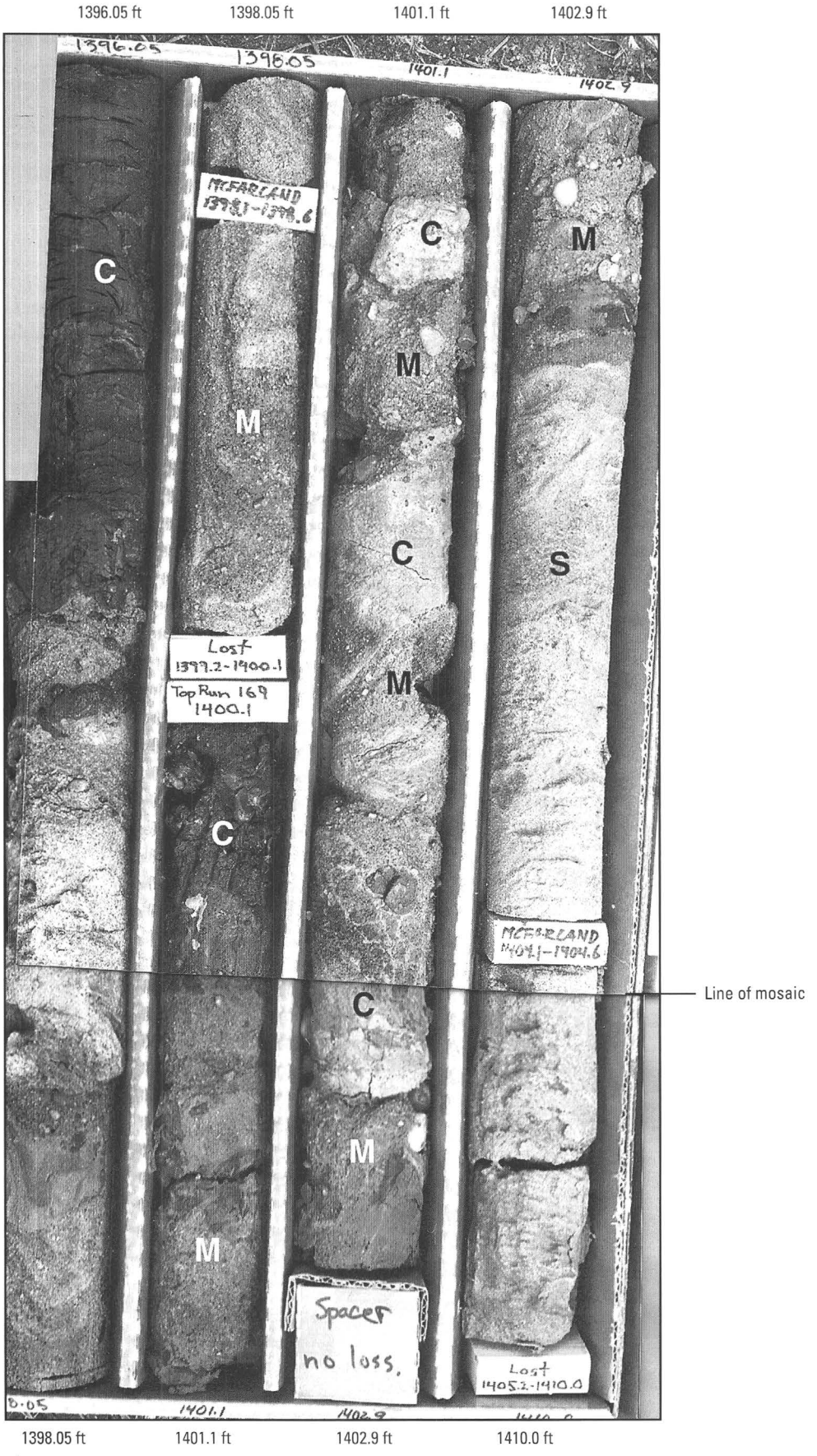

Figure C9. Photographs of matrix zones in crater unit B in the USGS-NASA Langley core. Depths handwritten on the core boxes in feet are repeated in type for clarity. Section tops are at the upper left corners of the boxes. *A*, Composite photograph of core box 144 showing blocks of sand (S) and clay (C) in glauconitic matrix (M). Metric depth values for the top and bottom of box 144 are 425.5 m and 429.8 m. *B*, Composite photograph of core box 128 showing blocks of sand (S) and clay (C) in glauconitic matrix (M). Note inclined, distorted bedding (DB). Metric depth values for the top and bottom of box 128 are 368.4 m and 377.4 m.

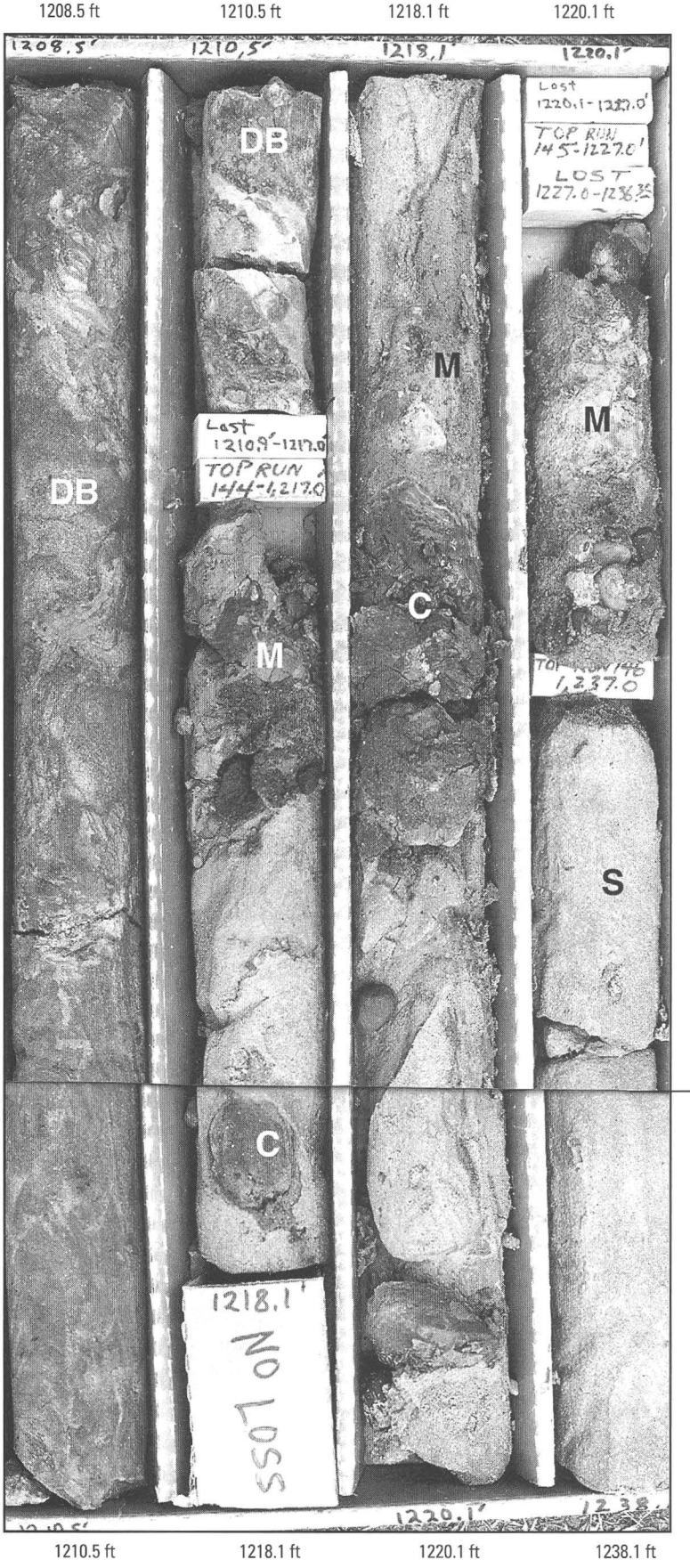

Line of mosaic

B

Figure C9. Continued.

and likely were derived locally from fluvial channel gravels in the Potomac Formation.

Almost all of the igneous- and metamorphic-rock fragments in the matrix zones also are subrounded to rounded pebbles that lack cataclastic fabrics and appear to be preimpact detrital sediments from the Potomac Formation (Horton and Izett, this volume, chap. E). A single 22-cm-long (8.7-in.-long) clast of cataclastic felsite from a depth of about 275.8 m (905.0 ft; see fig. C7*C*) contains shocked quartz and indicates the presence of rare impact ejecta in the matrix zone closest to the top of crater unit B (Horton and Izett, this volume, chap. E). This felsite clast is immediately below a 6.3-m-thick (20.7-ft-thick) megablock of oxidized Potomac Formation sediments that forms the uppermost part of crater unit B.

No exotic sediment blocks of certain Late Cretaceous or Tertiary age have been recognized in the matrix zones of crater unit B, although some greenish-gray muds and muddy fine sands potentially represent the preimpact unnamed Upper Cretaceous marine units, the Aquia Formation (upper Paleocene), and (or) the Nanjemoy Formation (lower Eocene).

The matrix between the blocks within the matrix zones consists of unsorted and unstratified, noncalcareous, muddy, quartz-glauconite sand and granules. Glauconite grains are common to abundant and are readily detected in all matrix zones. Glauconite typically is absent or extremely sparse in the preimpact Potomac Formation (Anderson, 1948; Reinhardt, Christopher, and Owens, 1980), but it is common to abundant in the Upper Cretaceous and lower Tertiary preimpact marine units in the region (see the section above on "Regional Preimpact Stratigraphy"). Hence, it appears that a substantial amount of disaggregated Upper Cretaceous and (or) Tertiary marine sediment has moved downward into the matrix zones of crater unit B. In addition to this exotic component, the matrix contains a native component of disaggregated, medium to very coarse feldspathic quartz sand and resistate pebbles derived from the sands and gravels of the Potomac Formation.

The matrix of crater unit B is similar in macroscopic appearance to the matrix between clasts in the Exmore beds above crater unit B (see the following section on the "Exmore Beds"). However, the Exmore matrix is uniformly calcareous and macrofossiliferous and microfossiliferous, whereas the matrix in crater unit B is very sparingly calcareous and fossiliferous. No macrofossil fragments or microfossils were observed during petrographic inspection of the sand fraction of 17 matrix samples from crater unit B. Fossils were found in two matrix samples processed for calcareous nannofossils or dinoflagellates, as described below

Fossils.—Ten of eleven matrix samples from crater unit B processed for calcareous nannofossils were barren (Frederiksen and others, this volume, chap. D, fig. D7). The sample from a depth of 298.5 m (979.3 ft) contains a mixed early Tertiary assemblage of uncertain origin. This sample is from a thin matrix section at the top of a coring run. As such, it was particularly susceptible to drilling-mud contamination during core recovery and handling.

Two samples from the matrix of crater unit B were processed for dinoflagellates; one was barren (Frederiksen and others, this volume, chap. D). The other matrix sample, which was from 278.4 m (913.3 ft) depth, contained a mixed early Tertiary assemblage of dinoflagellates.

Thickness and distribution.—The matrix zones range from a few centimeters (a few inches) to slightly over 20 m (65.6 ft) in thickness. Zones in the upper half of crater unit B are consistently less than 5 m (16.4 ft) thick, whereas zones thicker than 10 m (32.8 ft) are restricted to the lower half, although thinner zones also occur in the lower half of the unit. This pattern resembles the distribution of thicker and thinner megablocks and megablock zones in crater unit B. The change from thicker to thinner matrix zones does not correspond to the subunit boundary between the lower and upper beds of crater unit B.

Moderate to poor core recovery was typical of the matrix zones of crater unit B in the Langley core, particularly the thicker zones. This pattern likely results from the poorly consolidated nature of the material in these zones.

Exmore Beds

Lithology, Thickness, and Nomenclature

The Exmore beds are present between depths of 269.4 m (884.0 ft) and 235.65 m (773.12 ft) in the Langley core and have a thickness of 33.8 m (110.9 ft). The Exmore section below 235.92 m (774.03 ft) depth consists of unsorted sedimentary deposits that contain abundant pebbles, cobbles, and small boulders of preimpact sediments and rocks suspended in a finer grained matrix (fig. C10*A–D*). This interval is uniformly matrix supported except in the basal 3.0 m (9.8 ft). We refer to these unsorted deposits descriptively as the "polymict diamicton" of the Exmore beds; the term is derived from one defined by Flint and others (1960). The calcareous, laminated, clayey, quartz silt and very fine sand at the top of the Exmore beds from 235.92 m (774.03 ft) to 235.65 m (773.12 ft) depth (fig. C5) are referred to as the "transition sediments" of the Exmore beds, as noted above in the section on "Postimpact Stratigraphy of the Annular Trough." The transition sediments were not studied in detail for this chapter, and discussions of these sediments in following sections are derived primarily from Poag (2002) and Poag and Norris (this volume, chap. F).

The lower contact of the Exmore beds at 269.4 m (884.0 ft) depth separates a 6.3-m-thick (20.7-ft-thick) megablock of oxidized clayey silts and muddy very fine sands at the top of crater unit B (fig. C7*C*) from an overlying 0.5-m-thick (1.6-ft-thick) boulder of greenish-gray, muddy, very fine to coarse sand at the base of the Exmore section. The noncalcareous Potomac Formation blocks and megablocks and the sparingly calcareous matrix below this contact (crater unit B) contrast with the polymict clasts and calcareous matrix above the contact (Exmore beds). Rare exceptions to these lithologic distinctions in crater unit B are noted in the section above on "Crater Unit B."

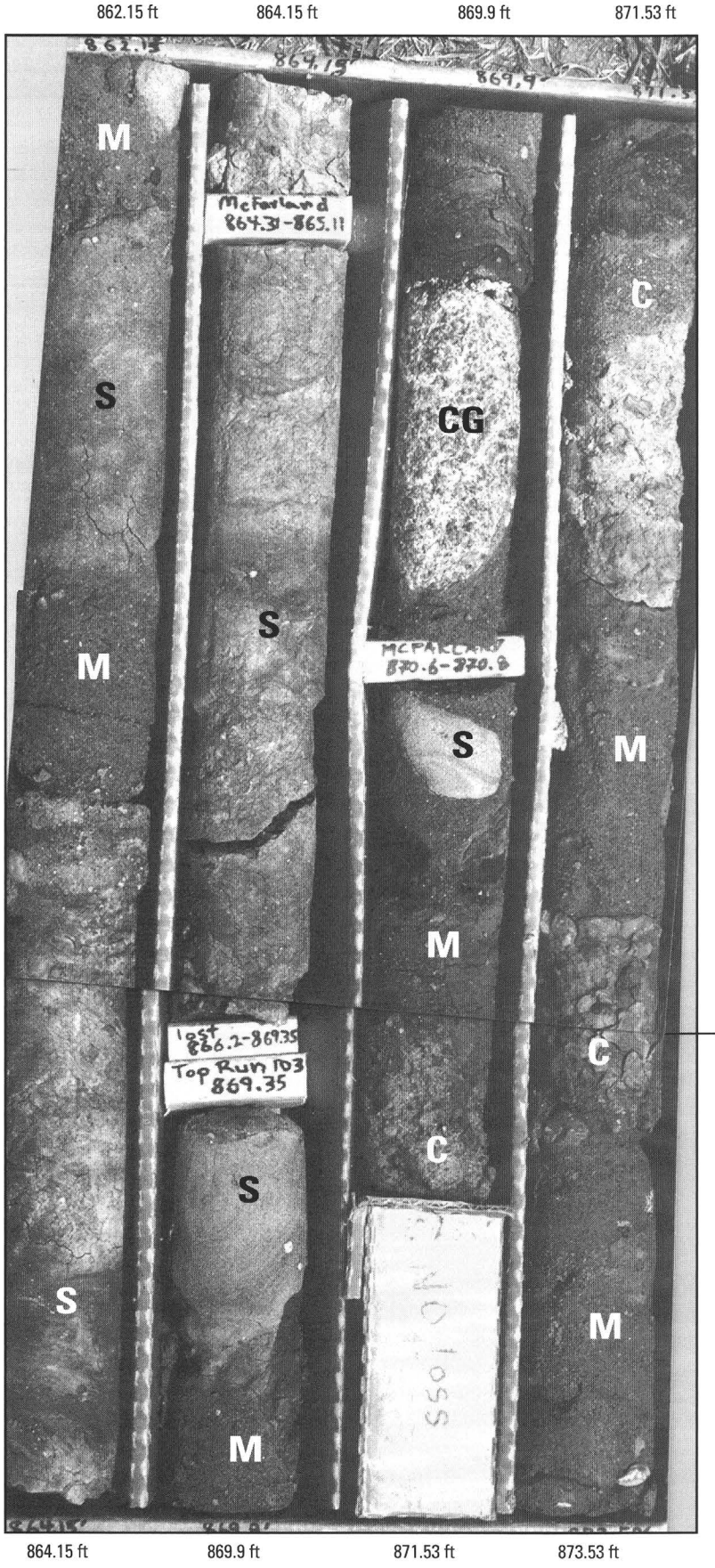

Figure C10. Photographs of the diamicton of the Exmore beds in the USGS-NASA Langley core. Depths handwritten on the core boxes in feet are repeated in type for clarity. Section tops are at the upper left corners of the boxes. *A,* Composite photograph of core box 97 showing clasts in glauconitic matrix (M). Clast types include sand (S), clay (C), and cataclastic granite (CG). Metric depth values for the top and bottom of box 97 are 262.8 m and 266.3 m. *B,* Composite photograph of core box 94 showing clasts in glauconitic matrix (M). Clast types include clay (C), calcareous quartz-glauconite sand (QGS), and cataclastic felsite (CF). Metric depth values for the top and bottom of box 94 are 255.7 m and 258.2 m. *C,* Composite photograph of core box 90 showing clasts in glauconitic matrix. Clast types include sand (S) and limestone (L). Metric depth values for the top and bottom of box 90 are 245.3 m and 248.0 m. *D,* Composite photograph of core box 87 showing clasts in glauconitic matrix. Clast types include clay (C) and clayey sand (S). Metric depth values for the top and bottom of box 87 are 236.3 m and 240.2 m.

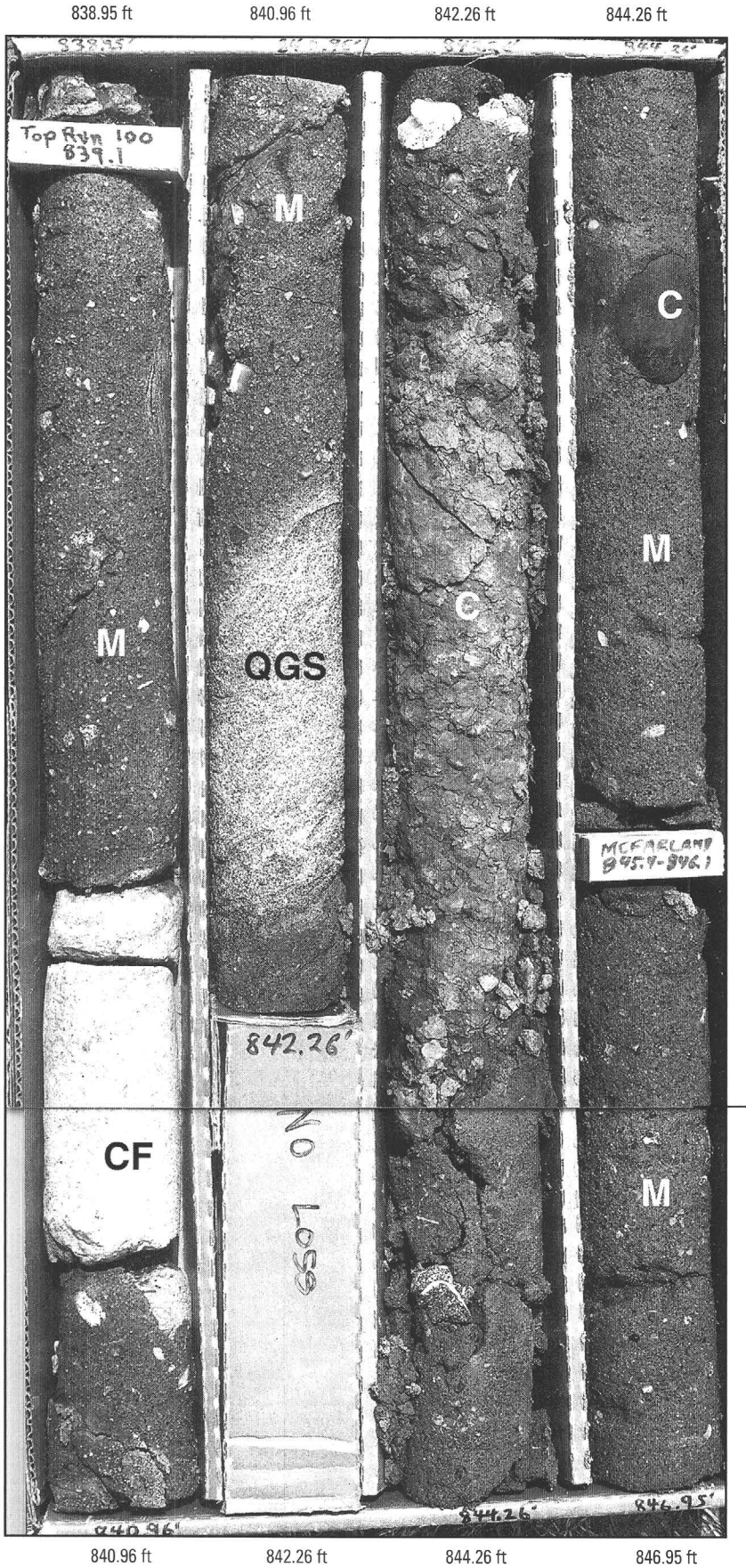

B

Figure C10. Continued.

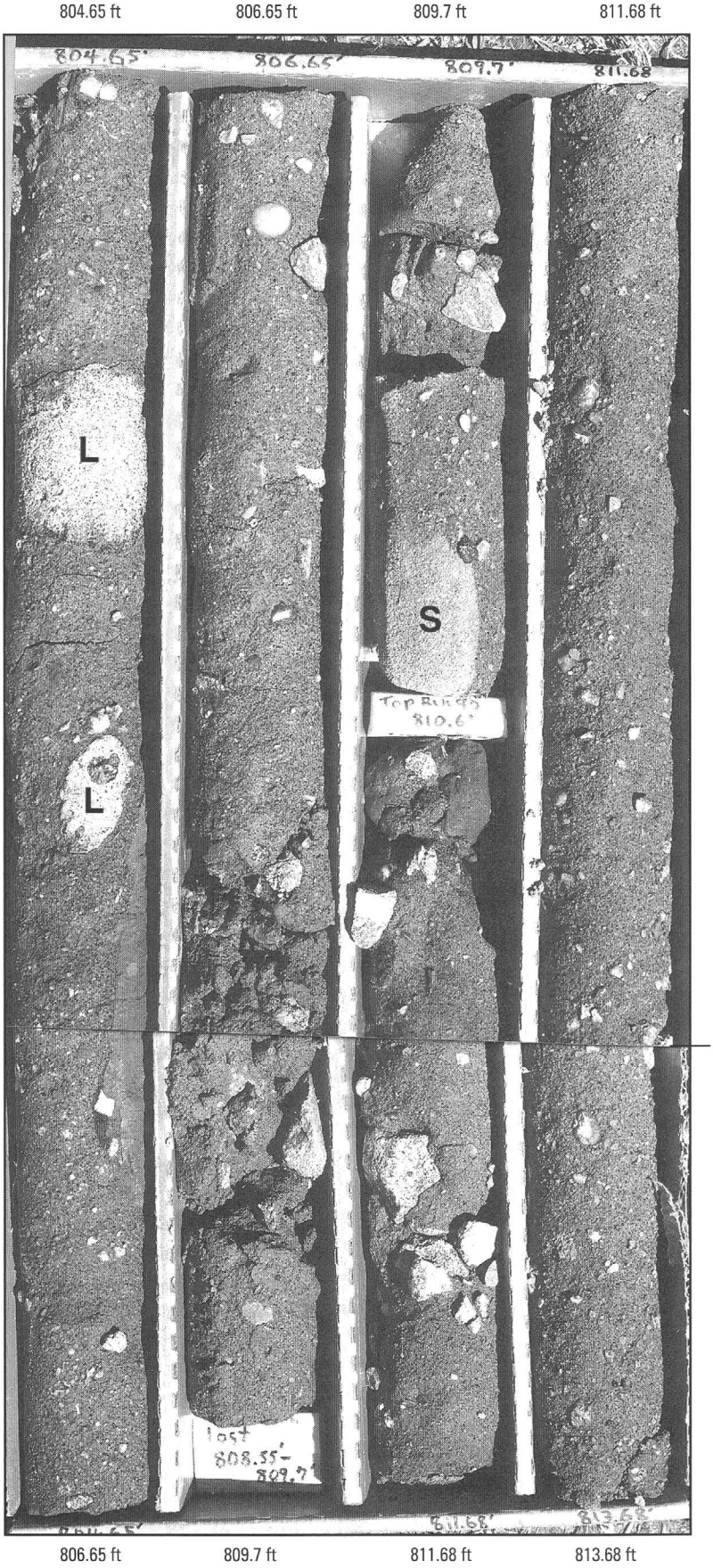

Line of mosaic

Figure C10. Continued.

Line of mosaic

Figure C10. Continued.

Lithology, Texture, and Age of the Diamicton Matrix

The matrix of the diamicton in the Exmore beds consists of unsorted and unstratified, calcareous, muddy, quartz-glauconite sand and granules smaller than 4 mm (0.16 in.). Matrix colors in fresh, wet cores vary from dark gray to dark olive gray and olive gray.

Grain-size analyses (wet sieving at 1.0-phi intervals) of 11 matrix samples from the Exmore beds indicate little variation in grain-size distribution with depth and typically poor sorting (fig. C11). Medium sand is the most abundant size fraction throughout the section (about 25 to 30 weight percent), and the total sand fraction contains about 70 to 75 weight percent of the sediment. The mud (silt and clay) fraction ranges from 18 to 25 weight percent, and the granule fraction is in the range of 2 to 9 weight percent.

Petrographic inspection of the 11 matrix samples indicates that quartz constitutes about 50 to 80 percent of the sand fraction in individual samples. The quartz is predominantly angular to subangular with some subrounded grains; sphericity of the quartz grains typically is low. Glauconite is the most abundant sand-sized mineral after quartz. The glauconite grains typically are well rounded and dark green; they contain pervasive cracks filled with clay, quartz silt, and locally pyrite. There is a distinct down-section decrease in glauconite from about 20 to 35 percent of the sand fraction in the upper part to about 5 percent in the lower part. Additional sand- and granule-sized grains include common mollusk fragments and feldspar as well as sparse white mica and microfossils, primarily benthic foraminifera and ostracodes. Pyrite is locally sparse to common as sand-sized grains, as encrustations on glauconite and carbonate grains, and as fills within benthic foraminifera tests. Shocked quartz is present but sparse in the sand fraction of the matrix (Horton and Izett, this volume, chap. E). Viewed separately from the clast fraction, the matrix may be classified petrologically as a gravelly, glauconitic arkosic wacke (Pettijohn, 1975).

The diamicton matrix in the Langley core contains palynomorphs and calcareous microfossils and nannofossils that represent a wide range of Cretaceous and early Tertiary ages (Frederiksen and others, this volume, chap. D). Similar mixed faunas and floras are present regionally in other studied sections of the Exmore beds (Poag and Aubry, 1995; Poag, 1997). Late Eocene fossils constitute the youngest assemblages in the matrix and indicate a biochronologic age that is indistinguishable from that of the overlying, postimpact Chickahominy Formation (Poag, 1997; Frederiksen and others, this volume, chap. D; Poag and Norris, this volume, chap. F; Edwards and others, this volume, chap. H).

Lithologies, Textures, and Ages of the Diamicton Clasts

The size and distribution of clasts within the diamicton of the Exmore beds were evaluated by two methods, in addition to a general inspection of the core. Line counting of clasts was conducted by tracing a straight pencil line vertically down the core exterior as presented in the core boxes. The sizes, lithologies, and depths of all particles larger than 4 mm (0.16 in.) that touched the line were recorded (fig. C12). The recorded depth for each clast represents the position of its midpoint measured along the vertical axis of the core.

To further determine the distribution of the largest clast fraction, the size, lithology, and depth of the largest clast in each 0.61-m (2.0-ft) length of core were recorded (fig. C12). For this count, the position of the clast was recorded at the midpoint of each measuring interval. This method is less accurate than the line-counting method for determining depths of clasts because clast midpoints rarely were at the interval midpoints and because some large clasts extended across measuring intervals. The depth for a clast that crossed a measuring boundary was plotted at the midpoint of the interval containing the majority of the clast. Therefore, some discrepancies exist in the plotted depths of individual large clasts that appear on the line-count graph and on the maximum-clast-size graph. It also should be noted that the clast size recorded for all clasts larger than the core diameter (nominally 6.1 cm, 2.4 in.) is the apparent maximum size along the vertical core axis.

As seen on the line-count graph (fig. C12), clasts having diameters in the range of 4 mm to 10 cm (0.16 to 3.9 in.; pebbles and small cobbles) are present throughout nearly the full vertical extent of the Exmore beds. Their apparent absence from some intervals near the bottom of the Exmore section likely results from the fact that the full volume of the core in those intervals is occupied by individual large clasts. Some core intervals also were unrecovered. The distribution of the matrix (particles less than 4 mm (0.16 in.) in diameter) throughout the Exmore beds is described in the section above (fig. C11).

Unlike the distribution of the finer grained materials, the distribution of the larger clasts has biases. On the line-count graph (fig. C12), clasts having diameters in the range of 10 cm to 1 m (3.9 in. to 3.3 ft; large cobbles and small boulders) are restricted, with one exception, to approximately the lower half of the Exmore section below a depth of about 250 m (820 ft). The only boulder larger than 1 m (3.3 ft) is present slightly above the base of the Exmore section. In contrast, clasts larger than about 2 cm (0.8 in.) are absent from the upper 2 m (6.6 ft) of the Exmore section.

These biases also are apparent on the maximum-clast-size graph (fig. C12). With one exception, the recorded maximum clast sizes range from 1 to 10 cm (0.4 to 3.9 in.; pebbles and small cobbles) above about 250 m (820 ft) depth. Below that depth, maximum clast sizes are primarily in the range from 10 cm to 1 m (3.9 in. to 3.3 ft; large cobbles and small boulders); the single boulder larger than 1 m (3.3 ft) is again recorded near the base of the unit.

The correspondence in the distribution of the larger clasts on the two graphs is expected because the small diameter of the core samples (relative to the sizes of the larger clasts) dictates that the large clasts encountered in the line count are the same clasts recorded in the maximum-clast-size count. This effect is less important above the depth of about 250 m (820 ft) but is particularly prevalent in the lower part of the diamicton, where large clasts occupy the full volume of the core.

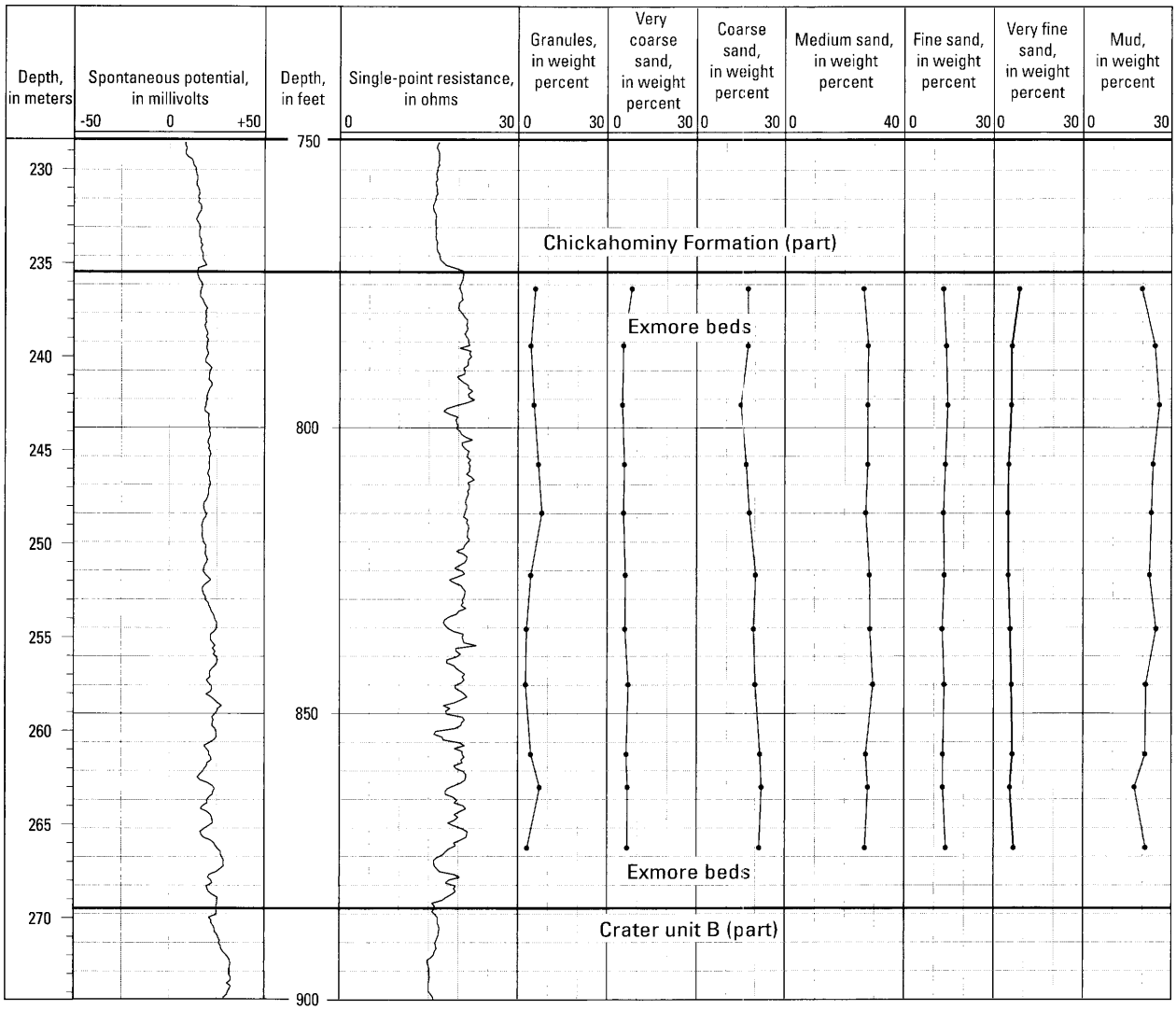

Figure C11. Graph of the grain-size distribution of 11 matrix samples from the Exmore beds in the USGS-NASA Langley core.

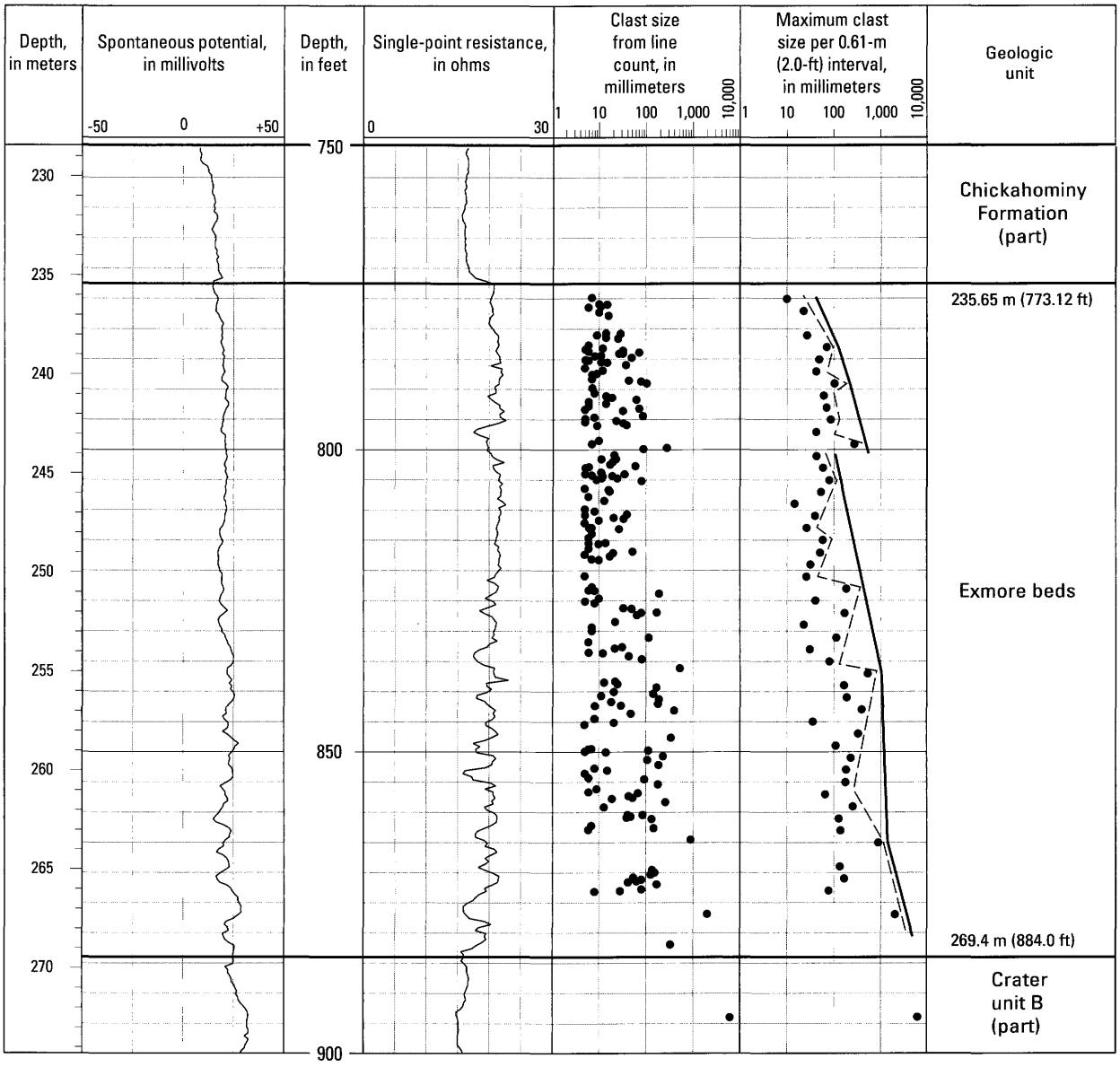

Figure C12. Graph of the grain-size distribution of clasts (>4 mm (>0.16 in.)) in the Exmore beds in the USGS-NASA Langley core. Methodology is explained in the text. The dashed line in the maximum-clast-size column highlights the local trends in maximum-clast-size distribution. The heavy line in the same column highlights the major trends in maximum-clast-size distribution.

There is considerable variation in the shape, rounding, orientation, and boundary characteristics of the clasts in the Exmore beds. Shapes of the smaller clasts vary from subspherical to elongate and irregular. The shapes of the larger clasts cannot be evaluated from the core samples. Clasts range from angular to well rounded, although most clasts are subangular to subrounded. Clast orientation appears to be random, to the degree that that parameter can be evaluated in the Langley core. Most clast boundaries are sharp except for some clasts of well-sorted sand that have diffuse boundaries across distances of less than 1 cm (0.4 in.).

There is a wide range of clast types in the Exmore beds that represents most or all of the formations affected by the Chesapeake Bay impact (fig. C3). Common sedimentary clast types include limestone, muddy sand, interbedded sand and clay, and sandy and silty clay. Individual clasts may be calcareous or noncalcareous and glauconitic or nonglauconitic; clast colors vary from gray, greenish-gray, and brownish gray to red, brown, and yellow oxidation colors.

Lithoclasts and mineral grains encountered during line counting and maximum-clast-size counting of the Exmore beds, and during general examinations of the core, have been separated on the basis of lithology into 17 categories (table C1). Fifteen categories consist of weakly to strongly compacted or cemented, siliciclastic or carbonate sediments, whereas the remaining two categories consist of igneous rocks. The lithologic categories have been numbered for ease of reference. The numbers reflect a crude preimpact stratigraphic ordering of the categories from category 1 (older) through category 17 (younger).

General geologic ages were assigned to the sediment clast categories through lithologic comparison with the undisturbed sedimentary sections outside the Chesapeake Bay impact structure in the Virginia Coastal Plain (fig. C3) (Ward, 1985; Mixon, 1989; Powars and others, 1992; Powars and Bruce, 1999; Powars, 2000). In addition, direct assessments of clast ages are available from paleontologic studies of selected Exmore clasts in the Langley core (Frederiksen and others, this volume, chap. D).

Categories 1 and 2 consist of granitic rocks and felsic volcanic rocks of pre-Mesozoic age. Horton and Izett (this volume, chap. E) discuss these clasts in detail.

Clast categories 3, 4, and 5 consist of oxidized sands, muds, and interbedded sands and muds of the Lower Cretaceous and basal Upper Cretaceous Potomac Formation. These noncalcareous, oxidized materials are readily distinguished from the gray and gray-green Upper Cretaceous and lower Tertiary marine deposits that constitute several other categories. However, some small volume of the material in categories 3 through 5 could have been derived from the Upper Cretaceous red-bed unit (possible northward extension of the Cape Fear Formation) found in the subsurface south of the impact crater (fig. C3).

Categories 6, 7, and 8 consist of angular to subrounded, single-mineral grains and chert lithoclasts that are generally in the size range from 4 to 10 mm (0.16 to 0.4 in.). The mineralogy and relatively large size of these pebbles suggest derivation from the Potomac Formation, which contains most of the gravelly preimpact deposits in the study area. Similarly, category 9 consists of well-rounded quartz, chert, and quartzite pebbles that likely represent multicycle sediments derived from fluvial channel deposits of the Potomac Formation. Very sparse, well-rounded phosphate pebbles of category 10 could also represent channel deposits of the Potomac Formation, or they could have been derived from lag deposits in the Upper Cretaceous and lower Tertiary marine section.

Clast categories 11 through 14 contain a variety of typically gray or gray-green, in part calcareous and glauconitic, marine sands and muds derived from the Upper Cretaceous and lower Tertiary formations of the impact area. Some portion of the noncalcareous gray sediments in categories 11 and 13 could represent non-oxidized sections of the Potomac Formation; in particular, gray noncalcareous sediments containing significant amounts of lignite likely represent Potomac lithologies. Category 15 consists of fragmented macrofossils, primarily mollusks, derived from the Upper Cretaceous and lower Tertiary marine deposits. Limestone clasts in categories 16 and 17 were derived from lower Tertiary formations, particularly the middle Eocene Piney Point Formation.

Table C1. Ages and lithologic categories of clasts recorded from the diamicton of the Exmore beds in the USGS-NASA Langley core during line counting and maximum-clast-size counting.

[Clasts have diameters greater than 4 millimeters (0.16 inch)]

Clast category	Age	Lithology
17	Tertiary	Limestone, shelly, cemented
16	Tertiary	Limestone, glauconitic, shelly
15	Tertiary, Cretaceous	Fossils (mollusk fragments)
14	Tertiary, Cretaceous	Mud, calcareous, gray
13	Tertiary, Cretaceous	Mud, noncalcareous, gray
12	Tertiary, Cretaceous	Sand, calcareous, gray
11	Tertiary, Cretaceous	Sand, noncalcareous, gray
10	Tertiary, Cretaceous	Rounded phosphate pebbles
9	Cretaceous	Rounded quartz and chert pebbles
8	Cretaceous	Angular quartz pebbles
7	Cretaceous	Angular chert pebbles
6	Cretaceous	Angular feldspar pebbles
5	Cretaceous	Muds, oxidized
4	Cretaceous	Sands, oxidixed
3	Cretaceous	Sands and muds, oxidized
2	Pre-Mesozoic	Igneous rocks, volcanic
1	Pre-Mesozoic	Igneous rocks, plutonic

Clast Distribution by Lithologic Category

Figures C13 and C14 show the distribution of selected clast categories in the Exmore beds of the Langley core as determined in the line count of clasts. Figure C13 shows the distribution of oxidized sand and mud clasts (categories 3, 4, and 5; table C1) that primarily represent the Potomac Formation. As such, these clasts represent material from the lower part of the preimpact sedimentary section within the impact area. Note that this category of clasts is present throughout the vertical extent of the diamicton, although vertical variations in clast size and abundance are present. Specifically, clasts in these categories are moderately abundant, and some moderately large specimens are present above a depth of about 244 m (800.5 ft). Clasts in the same categories are relatively smaller and less abundant between about 256 and 244 m (839.9 and 800.5 ft). This population of clasts achieves its greatest abundance and largest sizes between about 256 m (839.9 ft) depth and the base of the Exmore beds.

Figure C14 shows the distribution of limestone clasts (categories 16 and 17; table C1) in the diamicton of the Exmore beds. Most of these clasts represent the middle Eocene Piney Point Formation, whereas some likely represent the Paleocene Aquia Formation, the Eocene Nanjemoy Formation, and possibly the Upper Cretaceous marine units. Collectively, they represent material from the upper part of the preimpact sedimentary section within the impact area. Note that the limestone clasts also are distributed throughout most of the diamicton section, although they are distinctly less abundant below about 256 m (839.9 ft) depth, where large clasts from the Potomac Formation dominate the cored section.

Sedimentary Structures

Physical and biogenic sedimentary structures are sparse within the diamicton section of the Exmore beds. No bedding, crossbedding, burrows, or dewatering structures were observed in the matrix. Disrupted and undisrupted primary stratification and burrows are present in the interiors of some clasts but are truncated at the clast boundaries.

The size grading of the largest clasts noted above, particularly the relegation of the largest clasts to the lower part of the section, is the only pronounced sedimentary structure. This biased distribution of only the larger clasts in an otherwise unsorted deposit is referred to as coarse-tail grading (Middleton, 1967; Middleton and Hampton, 1973).

Transition Sediments

In this chapter, we consider that the transition sediments of the Exmore beds consist of three thin stratigraphic layers (fig. C5). The lowest layer consists of clayey silt between depths of 235.92 m (774.03 ft) and 235.87 m (773.85 ft). This layer is included in the Exmore breccia of Poag (2002, fig. 3) and Poag and Norris (this volume, chap. F, fig. F7).

Above this basal layer, Poag (2002) and Poag and Norris (this volume, chap. F) recognize a layer of clayey silt that contains pyritic microstructures (pyrite lattices) between depths of 235.87 m (773.85 ft) and 235.84 m (773.75 ft). Poag (2002, p. 996) described the pyrite lattices as exhibiting "smooth-walled, closely spaced, hemispherical depressions (concavities), separated from one another by curved, knife-edge partitions." Poag (2002) and Poag and Norris (this volume, chap. F) infer that the pyrite lattices originally enclosed 0.5- to 1.0-mm (0.02- to 0.04-in.) microspherules that were diagenetically removed or lost during sample processing. Poag and Norris (this volume, chap. F) refer to this layer as the "fallout layer."

Above the pyrite lattices, the upper layer consists of clayey silt laminae that are interlayered at a millimeter scale with laminae of better sorted silt and very fine sand; this section also contains sparse oval (compressed?) burrows filled with pyritic quartz sand. Poag and Norris (this volume, chap. F) refer to this upper layer as the "dead zone."

Discussion

Crater Units A and B

Principal Characteristics of Impact-Modified Sediments in the Annular Trough

Crater units A and B of the Langley core represent an impact-deformed, autochthonous to parautochthonous sedimentary section within the annular trough of the Chesapeake Bay impact structure. Observed features of inferred impact origin in this section include fractured, slumped, and rotated sediment blocks and megablocks, fluidized sand beds, and injected or infiltrated exotic sediments. The distributions of these impact features vary with depth and sediment type; the general intensity of impact deformation increases upward.

There is no evidence for large-scale removal of preimpact materials by excavation flow near the Langley corehole. The main preimpact stratigraphic units in the annular trough are the Neoproterozoic granite and the nonconformably overlying fluvial and deltaic sediments of the Cretaceous Potomac Formation. These units are deformed but preserved in recognizable stratigraphic order in the Langley core and vicinity (Horton and others, this volume, chap. B; Catchings and others, this volume, chap. I; and this chapter). Primary (Cretaceous) sedimentary structures, cycles, and lithologies typical of the Potomac Formation outside the crater (Powars and Bruce, 1999; Powars, 2000) are found throughout crater unit A and within the megablocks of crater unit B in the core. This correlation indicates that the preimpact Cretaceous sediments have not been removed and subsequently replaced by impact-generated sediments.

There also is no evidence for shock deformation within crater units A and B. The only shocked mineral grains are in a single felsite clast near the top of crater unit B that is readily interpreted as crystalline-rock ejecta injected or infiltrated into

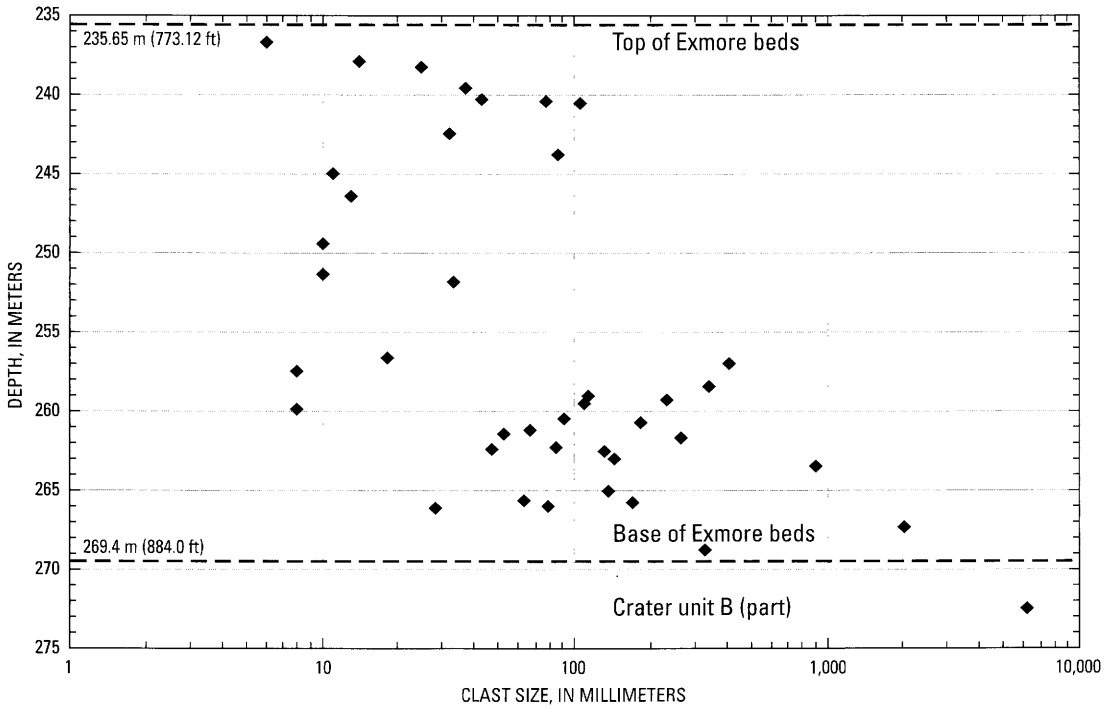

Figure C13. Graph of the distribution and size of oxidized sand and mud clasts (>4 mm (>0.16 in.)) of categories 3, 4, and 5 (table C1) in the Exmore beds in the USGS-NASA Langley core. Clasts were identified in the line count as explained in the text.

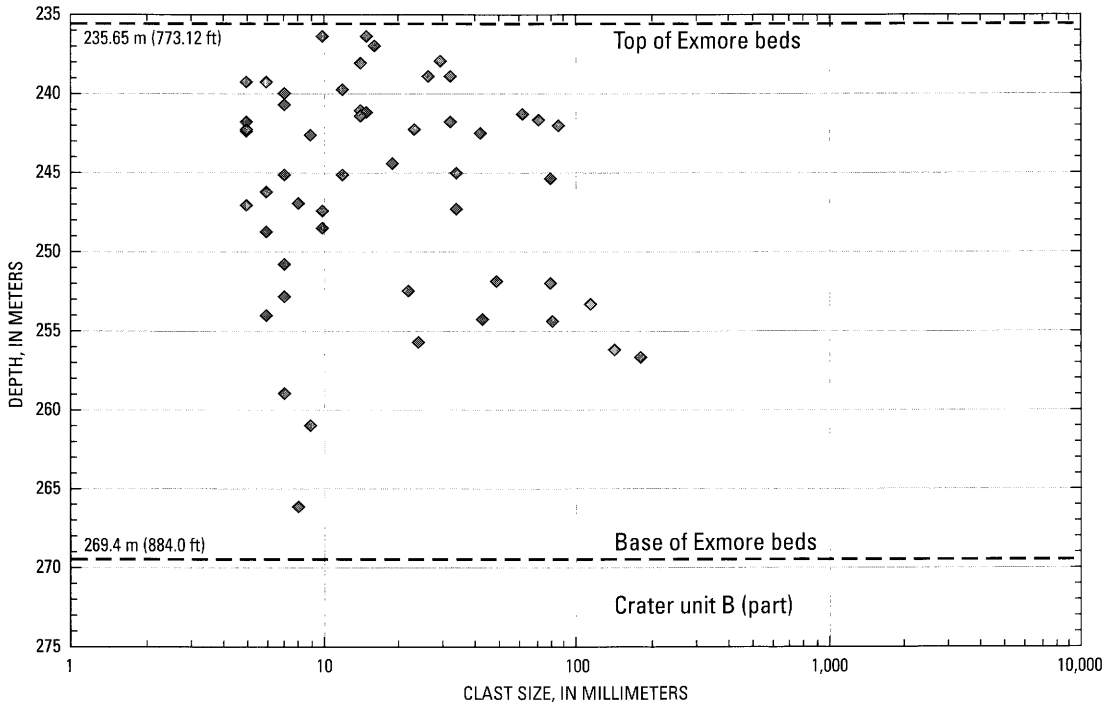

Figure C14. Graph of the distribution and size of limestone clasts (>4 mm (>0.16 in.)) of categories 16 and 17 (table C1) in the Exmore beds in the USGS-NASA Langley core. Clasts were identified in the line count as explained in the text.

the preimpact sedimentary section. Melt rock is absent from these units as well. In addition, no shock deformation or thermal effects were detected in the granite at the base of the Langley core (Horton and others, this volume, chap. B).

The basement granite, crater unit A, and the lower beds of crater unit B, all below a depth of 427.7 m (1,403.3 ft), are autochthonous materials retained at moderate depths within the annular trough and outside the zone of shock deformation and excavation flow. Significant impact deformation in this interval is limited to local in situ fluidization of sands, faulting, and fracturing. The stratigraphic order of the preimpact sediments is largely retained below 427.7 m (1,403.3 ft). Exotic sediments are present only in a single thin interval (0.3 m (1.0 ft) thick) at the boundary between crater units A and B (fig. C7*A*).

The Potomac Formation sediments in the upper beds of crater unit B above a depth of 427.7 m (1,403.3 ft) are parautochthonous materials retained at shallow depths within the annular trough and outside the zone of shock deformation and excavation flow. Fracturing, slumping, and rotation of Potomac Formation sediment blocks and megablocks, fluidization of Potomac Formation sands, and injection or infiltration of exotic sediments are widespread in this interval, and the primary stratigraphic ordering of the preimpact Potomac Formation sediments is retained only within megablocks.

Principal Impact Processes in the Annular Trough

Fracturing and Faulting

Faults and fractures are pervasive features in crater units A and B. Fractures and slickensided faults with small or uncertain displacements dip at all angles from horizontal to nearly vertical and occur in all sediment types in crater units A and B of the Langley core. These structures are irregularly spaced, although observed fault spacing generally decreases upsection. Short faults having centimeter-scale displacements are abundant in megablocks of the upper beds in crater unit B.

A complex system of short faults (tens of meters) with small, dominantly normal displacements (meters) in crater units A and B is interpreted from the migrated depth image for the Langley seismic survey adjacent to the corehole (Catchings and others, this volume, chap. I). Numerous diffractions on the unmigrated images for that survey also indicate the presence of discontinuities in this sedimentary section.

Mineralized faults, fractures, and veins are common in the granite of the Langley core; however, most of these structures probably are Mesozoic or older (Horton and others, this volume, chap. B). Partially healed, quartz-lined fractures are the best candidates for impact fractures in the cored granite, although their age remains equivocal. Catchings and others (this volume, chap. I) suggest that common diffractions on the unmigrated seismic-reflection images indicate significant numbers of discontinuities in the granite. High-angle faults that displace the contact between the granite and overlying sediments also are interpreted from the seismic images (Catchings and others, this volume, chap. I).

Two mechanisms probably account for the fracturing and faulting observed in the core and seismic images. Relatively early in the cratering process, a tensile wave moves downward into the target materials (those affected by the impact). This rarefaction results from the reflection of the direct compressive stress wave at the target's free surface, the sea floor (Melosh, 1984, 1989). The low tensile strength of most geologic materials suggests that extensive fracturing should occur by this process.

The second mechanism is the late-stage collapse of a crater. Temporary strength reduction of target materials by tensile fragmentation and (or) other mechanisms, including pore-pressure or acoustic fluidization, results in late-stage gravitational collapse of complex craters across a wide area (Melosh, 1989; Melosh and Ivanov, 1999; Collins and Melosh, 2002).

Collapse deformation in the Langley area was not uniformly distributed, however. The main feature of the Langley seismic survey is a 550-m-wide (1,805-ft-wide), stratabound collapse structure developed within the upper beds of crater unit A and crater unit B (Catchings and others, this volume, chap. I); the Langley corehole penetrated this structure near its center. Deformation within the collapse structure is distributed along the small-displacement faults noted on the seismic images rather than along bounding large-displacement normal faults. The seismic images indicate that the relatively intense deformation observed in the upper beds of crater unit B was restricted to the collapse structure to a significant extent. Hence, the pattern of deformation that characterizes crater unit A may extend closer to the surface in areas away from the collapse structure and the Langley corehole.

We were unable to distinguish faults and fractures in the Langley core produced by early tensile fracturing from faults and fractures produced during late-stage gravitational collapse. However, given the location of the corehole within the extensional collapse structure seen on the seismic images, we infer that most of the faults seen in crater units A and B of the Langley core resulted from gravitational collapse.

Fluidization of Sands

We interpret the numerous layers of structureless sand present above 558.1 m (1,831.0 ft) depth in the upper beds of crater unit A and in crater unit B as fluidized beds. Two possible mechanisms for this fluidization are increased pore-water pressure in these water-saturated sands and acoustic fluidization (Melosh, 1979, 1989; Collins and Melosh, 2002). Temporary compressive strain (densification) produced in water-saturated sands by impact-stress-wave compression would increase pore-water pressures, thereby reducing the overburden pressure and the internal friction in the sands and allowing the sand-water mixtures to flow as viscous fluids. During acoustic fluidization, alternating compressions and rarefactions in acoustic waves produced by the impact temporarily and locally reduce the overburden pressure and thereby reduce the internal frictional strength of the sand layers, allowing fluid flow (Melosh, 1979, 1989; Melosh and Ivanov, 1999; Collins and Melosh, 2002).

In either case, the widespread preservation of primary Cretaceous sedimentary structures in the sands below 558.1 m (1,831.0 ft) depth suggests that the overburden pressure remained sufficiently high to prevent fluidization below that depth near the Langley corehole. The loss of primary sedimentary structures in the fluidized sands is directly attributed to the fluid flow.

The reduction in target strength produced by fluidization in the Langley area was lithology dependent. The most susceptible sands liquefied, whereas less susceptible sands and finer grained beds remained more competent. The temporary reduction of bearing strength in the fluidized sand layers almost certainly contributed to the general collapse of beds at higher stratigraphic levels in crater unit B, particularly the fracturing, slumping, and rotation of the more competent beds. Impact-produced fractures probably acted as dewatering conduits that allowed the upward loss of pressurized pore water, thereby providing the volume accommodation required for the structural collapse of crater unit B.

Injection and Infiltration of Exotic Sediments

The matrix zones in crater unit B consist of mixed native and exotic sediments. The most obvious exotic component is the abundant glauconite sand between blocks in the matrix zones. The source of the glauconite is inferred to be the preimpact Upper Cretaceous and lower Tertiary marine sediments that are present regionally above the Potomac Formation (fig. C3).

A parautochthonous section of these marine sediments similar to the Potomac Formation sediments of crater unit B is not present in the Langley core, nor are such sections present in other cores that penetrated below the Exmore beds within the annular trough (Powars and others, 1992; Powars and Bruce, 1999). Instead, the Exmore beds routinely overlie impact-disrupted sections of the Potomac Formation.

We infer from these observations that the near-surface Cretaceous and Tertiary marine sediments, and perhaps the uppermost part of the Potomac Formation, were disaggregated into their constituent particles by the same reflected tensile wave described above as a cause of target fracturing (Melosh, 1984, 1989). The downward passage of this rarefaction also pulled apart the underlying Potomac Formation strata and allowed the downward injection of the disaggregated glauconitic sediments into the underpressured Potomac section. Sturkell and Ormö (1997) invoked this same process for the injection of clastic dikes and sills in strata adjacent to the Ordovician Lockne crater (Sweden).

In addition, some amount of disaggregated marine sediment may have been ejected as dissociated spall material due to stress wave interference in the near-surface area (Melosh, 1984, 1989), and part may have been scoured and entrained by oceanic resurge currents flowing into the collapsing crater (see the following section on the "Exmore Beds").

Exmore Beds

The diamicton section of the Exmore beds of the Langley core consists of a polymict assemblage of sediment and rock clasts suspended in an unstratified, unsorted, glauconitic, muddy and sandy matrix. The unit is dominantly matrix supported, and coarse-tail size grading of clasts is present. These textures and structures suggest sediment transport and deposition by cohesive, subaqueous debris flows (Middleton, 1967; Middleton and Hampton, 1973; Postma, 1986; Mulder and Cochonat, 1996).

The observed pattern of coarse-tail grading suggests that the diamicton of the Exmore beds consists of two debris-flow units in the Langley core (fig. C12). The core section can be divided into (1) a thick, normal coarse-tail-graded unit from the base of the Exmore to about 244 m (800 ft) depth and (2) a thinner, normal coarse-tail-graded unit from about 244 m (about 800 ft) to the top of the diamicton at 235.92 m (774.03 ft) depth. Size variations within individual lithologic categories of clasts also suggest the presence of a boundary at 244 m (800 ft) depth (fig. C13).

Frederiksen and others (this volume, chap. D) note that reworked Cretaceous calcareous nannofossils are present in diamicton matrix samples from 242.2 m (794.7 ft) depth and above but are absent from samples from 244.3 m (801.5 ft) depth and below. The nannofossil distribution indicates a change in sediment provenance and supports the presence of a depositional boundary at about 244 m (about 800 ft) depth.

Smaller scale variations in lithology also are observed in the diamicton. Figure C12 shows intervals 1 to 3 m (3.3 to 9.8 ft) thick in which maximum clast size either fines or coarsens upward. There also is a tendency for clasts to be concentrated in roughly 10-cm-thick (3.9-in.-thick) intervals within the upper part of the diamicton (fig. C10*D*). These lithologic variations likely indicate variations in flow conditions within the debris flows.

Catchings and others (this volume, chap. I) mapped four Exmore subunits (debris flows) in the vicinity of the Langley corehole on their seismic-reflection images. The three older subunits successively overstep toward the crater's center, producing a shingled appearance. Hence these three units have limited lateral distributions. The youngest subunit extends entirely across the seismic survey. Only seismic subunits Ex2 and Ex4 of Catchings and others (this volume, chap. I) are present at the Langley corehole location, where they apparently represent the two Exmore debris flows defined in the core.

We attribute the origin of the Exmore debris flows to ocean-resurge currents produced by crater collapse. During impacts on continental shelves, the collapse of the transient crater (including the water-column crater) typically includes a catastrophic collapse and resurge of the water column back into the crater (Ormö and Lindström, 2000). This process can result in severe erosion of the proximal ejecta field, the preimpact shelf deposits that underlie the ejecta field, and the crater rim, followed by deposition of the eroded materials within the collaps-

ing crater (Lindström, 1999; Ormö and Lindström, 1999, 2000; von Dalwigk and Ormö, 1999; Shuvalov and others, 2002; Tsikalas and Faleide, 2002).

Clasts in the Exmore beds of the Langley core include shocked cataclastic crystalline-rock fragments ejected from significant depths (Horton and Izett, this volume, chap. E) and coherent, unshocked Cretaceous and Tertiary sediment clasts that represent most, if not all, of the sedimentary units in the target section. The shocked ejecta likely were derived by current scour of the proximal ejecta blanket outside the collapsing crater and from direct ejecta fallback. The Tertiary sediment clasts suggest scour of the ocean floor below the level of the proximal ejecta blanket and perhaps resedimentation or direct fallback of unshocked sediment clasts ejected from the top of the preimpact sedimentary section (spall of Melosh, 1984). The Cretaceous sediment clasts likely resulted from erosion of the collapsing outer crater margin and perhaps from deep (channelized?) scouring of the adjacent shelf.

The presence of a single piece of shocked crystalline ejecta and two fossiliferous matrix samples in the upper 30 m (98.4 ft) of crater unit B suggests mixing of material from the Exmore beds and crater unit B. This mixing could represent passive infiltration of Exmore sediments into the top of crater unit B. It also could represent entrainment of blocks and megablocks of crater unit B into the base of the lowest Exmore debris flow. A third possibility is that the upper 30 m (98.4 ft) of crater unit B represents additional debris flows, perhaps generated at the collapsing outer crater margin, as suggested by the strong dominance of Potomac Formation sediment clasts (blocks) in this interval.

Wave swash during re-equilibration of sea level and the return of degraded, impact-induced tsunamis (tsunami washback) from the nearby North American shoreline may have reworked the Exmore sediments within the crater and swept fine-grained sediments from the adjacent shelf into the crater (for nonimpact examples of similar processes, see Pickering and others, 1991, and Cita and others, 1996). Possible large bedforms at the top of the Exmore section, postulated by Catchings and others (this volume, chap. I) on the basis of their seismic survey, may represent this sediment reworking.

The transition sediments at the top of the Exmore beds represent postimpact settling of fine-grained sediments suspended in the water column by impact processes. Poag (2002) and Poag and Norris (this volume, chap. F) interpret the presence of microspherules (microtektites) in a fallout layer within this section. Although microtektites were not observed directly in the Langley core, their former presence was inferred by these authors from the hemispherical molds within the pyrite lattices.

Poag (2002) and Poag and Norris (this volume, chap. F) interpret the thin interval of laminated clayey silt and very fine sand at the top of the transition sediments in the Langley core to be a biological dead zone. They base this interpretation on the absence of an indigenous microfauna in this interval (Poag and Norris, this volume, chap. F). Sparse pyritic sand-filled burrows in the dead zone may indicate the presence of a limited infauna in the dead-zone sediments, or they may represent later burrowing initiated at higher stratigraphic levels. The transition sediments represent the final stage of impact-related sedimentation before the return to normal marine-shelf sedimentation represented by the upper Eocene Chickahominy Formation.

Summary

The continuously sampled USGS-NASA Langley core and the Langley seismic-reflection survey provide a basis for describing and interpreting the impact-modified and impact-generated Cretaceous and Tertiary sediments within the outer annular trough of the Chesapeake Bay impact structure. Above the basement granite, crater unit A and the lower beds of crater unit B constitute an autochthonous section of Cretaceous sediments (Potomac Formation) that were faulted, fractured, and locally fluidized during the impact. The lowest occurrence of impact-induced fluidization of water-saturated sands is at the base of the upper beds of unit A at 558.1 m (1,831.0 ft) depth, and the lowest occurrence of injected exotic sediments is the thin matrix zone at the contact between crater units A and B at 442.5 m (1,451.7 ft) depth. The upper beds of crater unit B consist of faulted, fractured, and rotated blocks and megablocks of the Potomac Formation, fluidized sands, and matrix zones consisting of Potomac Formation blocks suspended in a finer grained matrix of mixed native and exotic sediments. The lowest occurrence of abundant injected exotic sediments is at the base of the upper beds of crater unit B at 427.7 m (1,403.3 ft) depth.

The Exmore beds consist of unshocked, preimpact Cretaceous and Tertiary sediment clasts and minor shocked and (or) cataclastic igneous-rock clasts suspended in a finer calcareous, muddy, quartz-glauconite matrix. The Exmore beds are interpreted as ocean-resurge sediments deposited by multiple debris flows as a result of the late-stage catastrophic collapse of the oceanic water column. The thin transitional beds at the top of the Exmore section record the return to normal continental shelf sedimentation.

Acknowledgments

U.S. Geological Survey (USGS) investigations of the Chesapeake Bay impact structure are conducted in cooperation with the Hampton Roads Planning District Commission, the Virginia Department of Environmental Quality, and the National Aeronautics and Space Administration (NASA) Langley Research Center. The Hampton Roads Planning District Commission and the USGS provided funds for the drilling of the USGS-NASA Langley corehole. The NASA Langley Research Center provided extensive operational and logistical support for the drilling operation. We particularly thank Joel S. Levine, John J. Warhol, Jr., and Frederick M. Thompson (all of

NASA Langley) for their enthusiastic support and assistance during the drilling operations. The Virginia Department of Environmental Quality and the Department of Geology of the College of William and Mary provided extensive operational support at the drill site.

The USGS Rocky Mountain Drilling Unit drilled the USGS-NASA Langley corehole with support from the USGS Eastern Earth Surface Processes Team's drilling crew. The USGS drill crew included Arthur C. Clark (supervisor and lead driller), Jeffery D. Eman (lead driller), Stephen J. Grant (lead driller), Donald G. Queen (operations and supply), Manuel Canabal Lopez, Eugene F. Cobbs, Eugene F. Cobbs, III, Orren C. Doss, Robert Hovland, and Michael E. Williams.

Stephen E. Curtin (USGS) and Richard E. Hodges (USGS) conducted the geophysical logging of the Langley corehole. The authors of this chapter and USGS geologists Lucy E. Edwards, Robert E. Weems, Robert G. Stamm, J. Stephen Schindler, Matthew J. Smith, and Laurel M. Bybell wrote the field descriptions of the Langley core at the drill site. The following members of the USGS also served as site geologists: Wilma B. Alemn Gonzalez, Noelia Baez Rodrìguez, Omayra Bermudez Lugo, Karl M. Dydak, Samuel V. Harvey, Robert R. Lotspeich, Rosenelsy Marrero Cuebas, Colleen T. McCartan, E. Randolph McFarland, and Thomas Weik. Matthew J. Smith (USGS) performed the laboratory grain-size analyses.

We thank Joseph P. Smoot (USGS) for helpful discussions of sedimentary structures in crater units A and B. Reviews of this report by Joseph P. Smoot, C. Scott Southworth (USGS), and J. Wright Horton, Jr. (USGS), substantially improved its content and organization.

References Cited

Anderson, J.L., 1948, Cretaceous and Tertiary subsurface geology, *in* Cretaceous and Tertiary subsurface geology—The stratigraphy, paleontology, and sedimentology of three deep test wells on the Eastern Shore of Maryland: Maryland Department of Geology, Mines and Water Resources Bulletin 2, p. 1–113, 385–441.

Berggren, W.A., Kent, D.V., Swisher, C.C., III, and Aubry, M.-P., 1995, A revised Cenozoic geochronology and chronostratigraphy, *in* Berggren, W.A., Kent, D.V., Aubry, M.-P., and Hardenbol, Jan, eds., Geochronology, time scales and global stratigraphic correlation: SEPM (Society for Sedimentary Geology) Special Publication 54, p. 129–212.

Brenner, G.J., 1963, The spores and pollen of the Potomac Group of Maryland: Maryland Department of Geology, Mines and Water Resources Bulletin 27, 215 p., 43 pls.

Brown, P.M., Miller, J.A., and Swain, F.M., 1972, Structural and stratigraphic framework and spatial distribution of permeability of the Atlantic Coastal Plain, North Carolina to New York: U.S. Geological Survey Professional Paper 796, 79 p.

Christopher, R.A., Self-Trail, J.M., Prowell, D.C., and Gohn, G.S., 1999, The stratigraphic importance of the Late Cretaceous pollen genus *Sohlipollis* gen. nov. in the Coastal Plain province: South Carolina Geology, v. 41, p. 27–44.

Cita, M.B., Camerlenghi, Angelo, and Rimoldi, Bianca, 1996, Deep-sea tsunami deposits in the eastern Mediterranean; New evidence and depositional models: Sedimentary Geology, v. 104, no. 1–4, p. 155–173.

Collins, G.S., and Melosh, H.J., 2002, Target weakening and temporary fluidization in large impact events [abs.]: Lunar and Planetary Science Conference, 33d, League City, Tex., March 11–15, 2002, Abstract 1523, available online at http://www.lpi.usra.edu/meetings/lpsc2002/pdf/1523.pdf

Doyle, J.A., 1982, Palynology of continental Cretaceous sediments, Crisfield geothermal test well, eastern Maryland, pt. 2 *of* Waste Gate Formation: Maryland Geological Survey Open-File Report 82–02–1, p. 51–87, 6 pls.

Doyle, J.A., and Robbins, E.I., 1977, Angiosperm pollen zonation of the continental Cretaceous of the Atlantic Coastal Plain and its application to deep wells in the Salisbury embayment: Palynology, v. 1, p. 43–78.

Edwards, L.E., and Powars, D.S., 2003, Impact damage to dinocysts from the late Eocene Chesapeake Bay event: Palaios, v. 18, no. 3, p. 275–285. (Also available online at http://www.bioone.org/pdfserv/i0883-1351-018-03-0275.pdf)

Flint, R.F., Sanders, J.E., and Rodgers, John, 1960, Diamictite, a substitute term for symmictite: Geological Society of America Bulletin, v. 71, no. 12, p. 1809.

Gibson, T.G., Andrews, G.W., Bybell, L.M., Frederiksen, N.O., Hansen, Thor, Hazel, J.E., McLean, D.M., Witmer, R.J., and Van Nieuwenhuise, D.S., 1980, Biostratigraphy of the Tertiary strata of the core, *in* Geology of the Oak Grove core: Virginia Division of Mineral Resources Publication 20, pt. 1, p. 14–30.

Gohn, G.S., Clark, A.C., Queen, D.G., Levine, J.S., McFarland, E.R., and Powars, D.S., 2001, Operational summary for the USGS-NASA Langley corehole, Hampton, Virginia: U.S. Geological Survey Open-File Report 01–87–A, 21 p., available online at http://pubs.usgs.gov/of/2001/of01-087/

Gradstein, F.M., Agterberg, F.P., Ogg, J.G., Hardenbol, Jan, van Veen, Paul, Thierry, Jacques, and Huang, Zehui, 1995, A Triassic, Jurassic, and Cretaceous time scale, *in* Berggren, W.A., Kent, D.V., Aubry, M.-P., and Hardenbol, Jan, eds., Geochronology, time scales and global stratigraphic correlation: SEPM (Society for Sedimentary Geology) Special Publication 54, p. 95–126.

Hansen, H.J., 1969, Depositional environments of subsurface Potomac Group in southern Maryland: American Association of Petroleum Geologists Bulletin, v. 53, no. 9, p. 1923–1937.

Hansen, H.J., 1978, Upper Cretaceous (Senonian) and Paleocene (Danian) pinchouts on the south flank of the Salisbury embayment, Maryland, and their relationship to antecedent basement structures: Maryland Geological Survey Report of Investigations 29, 36 p.

Hansen, H.J., 1982, Hydrogeologic framework and potential utilization of the brine aquifers of the Waste Gate Formation, a new unit of the Potomac Group underlying the Delmarva Peninsula, pt. 1 *of* Waste Gate Formation: Maryland Geological Survey Open File Report 82–02–1, p. 1–50.

Hansen, H.J., and Wilson, J.M., 1990, Hydrogeology and stratigraphy of a 1,515-foot test well drilled near Princess Anne, Somerset County, Maryland: Maryland Geological Survey Open File Report 91–02–5, 59 p., 2 pls.

Koeberl, Christian, Poag, C.W., Reimold, W.U., and Brandt, Dion, 1996, Impact origin of the Chesapeake Bay structure and the source of the North American tektites: Science, v. 271, no. 5253, p. 1263–1266.

Lindström, Maurits, 1999, The present status of the Lockne marine impact structure (Ordovician, Sweden) [abs.], *in* Gersonde, Rainer, and Deutsch, Alexander, eds., Oceanic impacts; Mechanisms and environmental perturbations; ESF–IMPACT Workshop, April 15–April 17, 1999, Alfred Wegener Institute for Polar and Marine Research, Bremerhaven, Germany, Abstracts: Berichte zur Polarforschung (Reports on Polar Research), v. 343, p. 54–56.

Melosh, H.J., 1979, Acoustic fluidization; A new geologic process?: Journal of Geophysical Research, v. 84, no. B13, p. 7513–7520.

Melosh, H.J., 1984, Impact ejection, spallation and the origin of meteorites: Icarus, v. 59, no. 2, p. 234–260.

Melosh, H.J., 1989, Impact cratering—A geologic process: New York, Oxford University Press, 245 p.

Melosh, H.J., and Ivanov, B.A., 1999, Impact crater collapse: Annual Review of Earth and Planetary Sciences, v. 27, p. 385–415.

Middleton, G.V., 1967, Experiments on density and turbidity currents. [Part] III, Deposition of sediment: Canadian Journal of Earth Sciences, v. 4, no. 3, p. 475–505.

Middleton, G.V., and Hampton, M.A., 1973, Sediment gravity flows; Mechanics of flow and deposition, *in* Turbidites and deep-water sedimentation; Lecture notes for a short course sponsored by the Pacific Section, Society of Economic Paleontologists and Mineralogists, and given in Anaheim, May 12, 1973: Los Angeles, Society of Economic Paleontologists and Mineralogists, Pacific Section, p. 1–38.

Mixon, R.B., ed., 1989, Geology and paleontology of the Haynesville cores—Northeastern Virginia Coastal Plain: U.S. Geological Survey Professional Paper 1489, 4 chapters, separately paged.

Mulder, Thierry, and Cochonat, Pierre, 1996, Classification of offshore mass movements: Journal of Sedimentary Research, v. 66, no. 1, p. 43–57.

Ormö, Jens, and Lindström, Maurits, 1999, Geological characteristics of marine-target craters [abs.], *in* Gersonde, Rainer, and Deutsch, Alexander, eds., Oceanic impacts; Mechanisms and environmental perturbations; ESF–IMPACT Workshop, April 15–April 17, 1999, Alfred Wegener Institute for Polar and Marine Research, Bremerhaven, Germany, Abstracts: Berichte zur Polarforschung (Reports on Polar Research), v. 343, p. 70–74.

Ormö, Jens, and Lindström, Maurits, 2000, When a cosmic impact strikes the sea bed: Geological Magazine, v. 137, no. 1, p. 67–80.

Owens, J.P., and Gohn, G.S., 1985, Depositional history of the Cretaceous series in the U.S. Atlantic Coastal Plain—Stratigraphy, paleoenvironments, and tectonic controls of sedimentation, *in* Poag, C.W., ed., Geologic evolution of the United States Atlantic margin: New York, Van Nostrand Reinhold, p. 25–86.

Pettijohn, F.J., 1975, Sedimentary rocks (3d ed.): New York, Harper & Row, 628 p.

Pickering, K.T., Soh, W., and Taira, A., 1991, Scale of tsunami-generated sedimentary structures in deep water: Journal of the Geological Society of London, v. 148, no. 2, p. 211–214.

Poag, C.W., 1996, Structural outer rim of Chesapeake Bay impact crater—Seismic and bore hole evidence: Meteoritics & Planetary Science, v. 31, no. 2, p. 218–226.

Poag, C.W., 1997, The Chesapeake Bay bolide impact; A convulsive event in Atlantic Coastal Plain evolution: Sedimentary Geology, v. 108, no. 1–4, p. 45–90.

Poag, C.W., 2002, Synimpact-postimpact transition inside Chesapeake Bay crater: Geology, v. 30, no. 11, p. 995–998.

Poag, C.W., and Aubry, M.-P., 1995, Upper Eocene impactites of the U.S. East Coast; Depositional origins, biostratigraphic framework, and correlation: Palaios, v. 10, no. 1, p. 16–43.

Poag, C.W., and the Chesapeake Coring Team, 2001, Drilling to basement inside the Chesapeake Bay crater [abs.]: Lunar and Planetary Science Conference, 32d, Houston, Tex., March 12–16, 2001, Abstract 1203, available online at http://www.lpi.usra.edu/meetings/lpsc2001/pdf/1203.pdf

Poag, C.W., and Commeau, J.A., 1995, Paleocene to middle Miocene planktic foraminifera of the southwestern Salisbury embayment, Virginia and Maryland; Biostratigraphy, allostratigraphy, and sequence stratigraphy: Journal of Foraminiferal Research, v. 25, no. 2, p. 134–155, 9 pls.

Poag, C.W., Hutchinson, D.R., Colman, S.M., and Lee, M.W., 1999, Seismic expression of the Chesapeake Bay impact crater; Structural and morphologic refinements based on new seismic data, *in* Dressler, B.O., and Sharpton, V.L., eds., Large meteorite impacts and planetary evolution; II: Geological Society of America Special Paper 339, p. 149–164.

Poag, C.W., Koeberl, Christian, and Reimold, W.U., 2004, The Chesapeake Bay crater—Geology and geophysics of a late Eocene submarine impact structure: New York, Springer-Verlag, 522 p. plus CD-ROM.

Poag, C.W., Plescia, J.B., and Molzer, P.C., 1999, Chesapeake Bay impact structure; Geology and geophysics [abs.], *in* Gersonde, Rainer, and Deutsch, Alexander, eds., Oceanic impacts; Mechanisms and environmental perturbations; ESF–IMPACT Workshop, April 15–April 17, 1999, Alfred Wegener Institute for Polar and Marine Research, Bremerhaven, Germany, Abstracts: Berichte zur Polarforschung (Reports on Polar Research), v. 343, p. 79–83.

Poag, C.W., Powars, D.S., Mixon, R.B., Edwards, L.E., Folger, D.W., Poppe, L.J., and Bruce, Scott, 1991, An upper Eocene impact-wave(?) deposit beneath Chesapeake Bay [abs.]: Geological Society of America Abstracts with Programs, v. 23, no. 5, p. A460.

Poag, C.W., Powars, D.S., Poppe, L.J., and Mixon, R.B., 1994, Meteoroid mayhem in Ole Virginny—Source of the North American tektite strewn field: Geology, v. 22, no. 8, p. 691–694.

Poag, C.W., Powars, D.S., Poppe, L.J., Mixon, R.B., Edwards, L.E., Folger, D.W., and Bruce, Scott, 1992, Deep Sea Drilling Project Site 612 bolide event—New evidence of a late Eocene impact-wave deposit and a possible impact site, U.S. East Coast: Geology, v. 20, no. 9, p. 771–774.

Poag, C.W., and Ward, L.W., 1993, Allostratigraphy of the U.S. middle Atlantic continental margin—Characteristics, distribution, and depositional history of principal unconformity-bounded Upper Cretaceous and Cenozoic sedimentary units: U.S. Geological Survey Professional Paper 1542, 81 p.

Postma, George, 1986, Classification for sediment gravity-flow deposits based on flow conditions during sedimentation: Geology, v. 14, no. 4, p. 291–294.

Powars, D.S., 2000, The effects of the Chesapeake Bay impact crater on the geologic framework and the correlation of hydrogeologic units of southeastern Virginia, south of the James River: U.S. Geological Survey Professional Paper 1622, 53 p., 1 oversize pl. (Also available online at http://pubs.usgs.gov/prof/p1622/)

Powars, D.S., and Bruce, T.S., 1999, The effects of the Chesapeake Bay impact crater on the geological framework and correlation of hydrogeologic units of the lower York-James Peninsula, Virginia: U.S. Geological Survey Professional Paper 1612, 82 p., 9 oversize pls. (Also available online at http://pubs.usgs.gov/prof/p1612/)

Powars, D.S., Bruce, T.S., Bybell, L.M., Cronin, T.M., Edwards, L.E., Frederiksen, N.O., Gohn, G.S., Horton, J.W., Jr., Izett, G.A., Johnson, G.H., Levine, J.S., McFarland, E.R., Poag, C.W., Quick, J.E., Schindler, J.S., Self-Trail, J.M., Smith, M.J., Stamm, R.G., and Weems, R.E., 2001, Preliminary geologic summary for the USGS-NASA Langley corehole, Hampton, Virginia: U.S. Geological Survey Open-File Report 01–87–B, 20 p., available online at http://pubs.usgs.gov/of/2001/of01-087/

Powars, D.S., Gohn, G.S., Catchings, R.D., McFarland, E.R., Bruce, T.S., Johnson, G.H., Izett, G.A., Emry, S.A., and Edwards, L.E., 2001, Deep corehole and seismic reflection data provide insights into crater-filling processes and the hydrogeology of the outer margin of the Chesapeake Bay impact structure, eastern Virginia Coastal Plain, USA [abs.]: Lunar and Planetary Science Conference, 32d, Houston, Tex., March 12–16, 2001, Abstract 2183, available online at http://www.lpi.usra.edu/meetings/lpsc2001/pdf/2183.pdf

Powars, D.S., Johnson, G.H., Edwards, L.E., Horton, J.W., Jr., Gohn, G.S., Catchings, R.D., McFarland, E.R., Izett, G.A., Bruce, T.S., Levine, J.S., and Pierce, H.A., 2002, An expanded Chesapeake Bay impact structure, eastern Virginia; New corehole and geophysical data [abs.]: Lunar and Planetary Science Conference, 33d, League City, Tex., March 11–15, 2002, Abstract 1034, available online at http://www.lpi.usra.edu/meetings/lpsc2002/pdf/1034.pdf

Powars, D.S., Mixon, R.B., and Bruce, Scott, 1992, Uppermost Mesozoic and Cenozoic geologic cross section, outer coastal plain of Virginia, *in* Gohn, G.S., ed., Proceedings of the 1988 U.S. Geological Survey Workshop on the Geology and Geohydrology of the Atlantic Coastal Plain: U.S. Geological Survey Circular 1059, p. 85–101.

Powars, D.S., Poag, C.W., and Bruce, Scott, 1991, Uppermost Mesozoic and Cenozoic stratigraphic framework of the central and outer coastal plain of Virginia [abs.]: Geological Society of America Abstracts with Programs, v. 23, no. 1, p. 117.

Reinhardt, Juergen, Christopher, R.A., and Owens, J.P., 1980, Lower Cretaceous stratigraphy of the core, *in* Geology of the Oak Grove core: Virginia Division of Mineral Resources Publication 20, pt. 1, p. 31–52, 1 pl.

Reinhardt, Juergen, Newell, W.L., and Mixon, R.B., 1980, Tertiary lithostratigraphy of the core, *in* Geology of the Oak Grove core: Virginia Division of Mineral Resources Publication 20, pt. 1, p. 1–13.

Shuvalov, V.V., Dypvik, H., and Tsikalas, Filippos, 2002, Numerical modeling of the Mjølnir marine impact event [abs.]: Lunar and Planetary Science Conference, 33d, League City, Tex., March 11–15, 2002, Abstract 1038, available online at http://www.lpi.usra.edu/meetings/lpsc2002/pdf/1038.pdf

Stephenson, L.W., 1948a, Cretaceous Mollusca from depths of 1894 to 1896 feet in the Bethards well, *in* Cretaceous and Tertiary subsurface geology—The stratigraphy, paleontology, and sedimentology of three deep test wells on the Eastern Shore of Maryland: Maryland Department of Geology, Mines and Water Resources Bulletin 2, p. 125–126.

Stephenson, L.W., 1948b, Tertiary and Cretaceous Mollusca from depths of 1040 to 2257 feet in the Hammond well, *in* Cretaceous and Tertiary subsurface geology—The stratigraphy, paleontology, and sedimentology of three deep test wells on the Eastern Shore of Maryland: Maryland Department of Geology, Mines and Water Resources Bulletin 2, p. 120–124.

Sturkell, E.F.F., and Ormö, Jens, 1997, Impact-related clastic injections in the marine Ordovician Lockne impact structure, central Sweden: Sedimentology, v. 44, no. 5, p. 793–804.

Swain, F.M., 1948, Ostracoda from the Hammond well, *in* Cretaceous and Tertiary subsurface geology—The stratigraphy, paleontology, and sedimentology of three deep test wells on the Eastern Shore of Maryland: Maryland Department of Geology, Mines and Water Resources Bulletin 2, p. 187–213.

Tsikalas, Filippos, and Faleide, J.I., 2002, Near-field erosional features at the Mjølnir impact crater; The role of marine sedimentary target [abs.]: Lunar and Planetary Science Conference, 33d, League City, Tex., March 11–15, 2002, Abstract 1296, available online at http://www.lpi.usra.edu/meetings/lpsc2002/pdf/1296.pdf

United States Geological Survey, 1986, [Topographic map of the] Newport News North, Virginia [7.5-minute quadrangle showing photorevisions of the 1965 map]: Reston, Va., U.S. Geological Survey, scale 1:24,000.

von Dalwigk, Ilka, and Ormö, Jens, 1999, Formation of resurge gullies at impacts at sea; The Lockne crater, Sweden [abs.], *in* Gersonde, Rainer, and Deutsch, Alexander, eds., Oceanic impacts; Mechanisms and environmental perturbations; ESF–IMPACT Workshop, April 15–April 17, 1999, Alfred Wegener Institute for Polar and Marine Research, Bremerhaven, Germany, Abstracts: Berichte zur Polarforschung (Reports on Polar Research), v. 343, p. 24–25.

Ward, L.W., 1985, Stratigraphy and characteristic mollusks of the Pamunkey Group (lower Tertiary) and the Old Church Formation of the Chesapeake Group—Virginia Coastal Plain: U.S. Geological Survey Professional Paper 1346, 78 p., 6 pls.

Ward, L.W., and Strickland, G.L., 1985, Outline of Tertiary stratigraphy and depositional history of the U.S. Atlantic Coastal Plain, *in* Poag, C.W., ed., Geologic evolution of the United States Atlantic margin: New York, Van Nostrand Reinhold, p. 87–123.

Wentworth, C.K., 1922, A scale of grade and class terms for clastic sediments: Journal of Geology, v. 30, no. 5, p. 377–392.

Paleontology of the Impact-Modified and Impact-Generated Sediments in the USGS-NASA Langley Core, Hampton, Virginia

By Norman O. Frederiksen, Lucy E. Edwards, Jean M. Self-Trail, Laurel M. Bybell, and Thomas M. Cronin

Chapter D of

Studies of the Chesapeake Bay Impact Structure—The USGS-NASA Langley Corehole, Hampton, Virginia, and Related Coreholes and Geophysical Surveys

Edited by J. Wright Horton, Jr., David S. Powars, and Gregory S. Gohn

Prepared in cooperation with the
Hampton Roads Planning District Commission,
Virginia Department of Environmental Quality, and
National Aeronautics and Space Administration Langley Research Center

Professional Paper 1688

U.S. Department of the Interior
U.S. Geological Survey

Contents

Plates

[Plates follow appendix D1]

Figures

Tables

Paleontology of the Impact-Modified and Impact-Generated Sediments in the USGS-NASA Langley Core, Hampton, Virginia

By Norman O. Frederiksen,[1] Lucy E. Edwards,[1] Jean M. Self-Trail,[1] Laurel M. Bybell,[1] and Thomas M. Cronin[1]

Abstract

Spores and pollen, dinoflagellate cysts, calcareous nannofossils, and marine ostracodes provide important information about the ages and conditions of deposition of the strata, clasts, and matrix materials that compose the impact-modified and impact-generated sediments in the USGS-NASA Langley corehole, which was drilled into the Chesapeake Bay impact crater in Hampton, Va. These sediments are divided into three parts: crater unit A (626.3 to 442.5 meters (m); 2,054.7 to 1,451.7 feet (ft)), crater unit B (442.5 to 269.4 m; 1,451.7 to 884.0 ft), and the Exmore beds (269.4 to 235.65 m; 884.0 to 773.12 ft). Crater unit A consists of relatively undisrupted strata of the Potomac Formation. One spore-pollen sample from near the top of this unit yielded a middle Albian to early Cenomanian age. All other samples from this unit were barren of spores and pollen grains.

Crater unit B is a clast-supported diamicton. Seven productive spore-pollen samples of Aptian to Cenomanian age in this unit were derived from Potomac Formation clasts. Several of the samples had mixed ages, indicating that these clasts had been contaminated by slurry sediment that penetrated the clasts during the violent movements of the material following the comet or asteroid impact or possibly during drilling. Some other clasts that contained dinocysts and nannofossils, from this unit and from the Exmore beds, were similarly contaminated. One dinocyst and one nannofossil sample from the matrix within the upper part of crater unit B were productive, and both had a mixture of Paleocene and Eocene specimens.

The Exmore beds form the matrix-supported part of the diamicton and contain the full variety of fossil types studied by the present authors—pollen, dinocysts, nannofossils, and ostracodes. Clasts within the Exmore range from Early Cretaceous to late Eocene in age. Most interesting were dinocyst, nannofossil, and ostracode species known only from the lower part of the middle Eocene, which must have been derived from previously undocumented sediments younger than the Nanjemoy Formation and older than the Piney Point Formation, and species known only from the uppermost middle Eocene and lowermost upper Eocene, which must have been derived from sediments younger than the Piney Point Formation but older than the Chickahominy Formation (the Chickahominy overlies the diamicton in the core). Units of these intermediate ages apparently were once present in the Virginia Coastal Plain but have since been eroded away or have not yet been recovered in the subsurface.

Most Potomac Formation clasts within the Exmore beds came from the upper part of the formation (Cenomanian in age). Samples from the matrix material that makes up the bulk of the Exmore beds are of mixed Late Cretaceous, Paleocene, and Eocene ages.

Many dinocyst specimens from the Exmore beds and injection zones of exotic matrix in the underlying crater unit B are fragmented, curled up, or otherwise degraded in a highly unusual manner; the degradation was probably caused by a combination of heat, pressure, and abrasion resulting from the impact. Similarly, some specimens of *Discoaster*, a genus of calcareous nannofossils, are fragmented and broken, probably from the same cause.

Introduction

This chapter documents the paleontology and biostratigraphy of part of the USGS-NASA Langley corehole, which was drilled into the Chesapeake Bay impact crater in Hampton, Va. (figs. D1, D2). The crater formed in the late Eocene, when a comet or asteroid struck the Atlantic continental shelf near the present town of Cape Charles, Va. (fig. D1; Poag and others, 1994).

The Langley corehole is approximately 8 kilometers (km; 5 miles (mi)) inside the outer margin of the buried crater and approximately 35 km (22 mi) from the center of the crater (Poag, 1997; Powars and Bruce, 1999). The corehole was drilled between July 22 and October 13, 2000, by the U.S. Geological Survey (USGS) and its partners (see "Acknowledgments"). The drill site is on the York-James Peninsula at the National Aeronautics and Space Administration (NASA) Langley Research Center in Hampton (fig. D2). The location is in the northeast quarter of the Newport News North 7.5-minute quadrangle (USGS, 1986), at lat 37°05'44.28" N., long 76°23'08.96"

[1]U.S. Geological Survey, Reston, VA 20192.

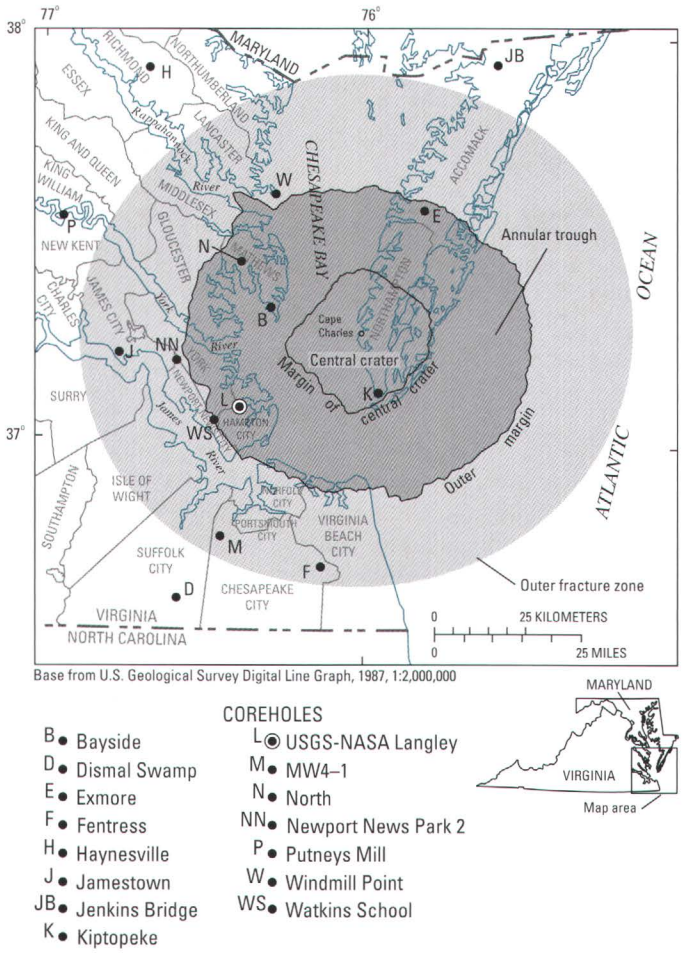

Figure D1. Regional map showing the location of the Chesapeake Bay impact structure, the USGS-NASA Langley corehole at Hampton, Va., and some other coreholes in southeastern Virginia. Locations of the central crater and outer margin are from Powars and Bruce (1999). The extent of the outer fracture zone (light gray) is based on Powars (2000) and Johnson and others (2001); the eastern part is speculative. Illustration modified from Powars, Johnson, and others (2002) and Edwards and Powars (2003).

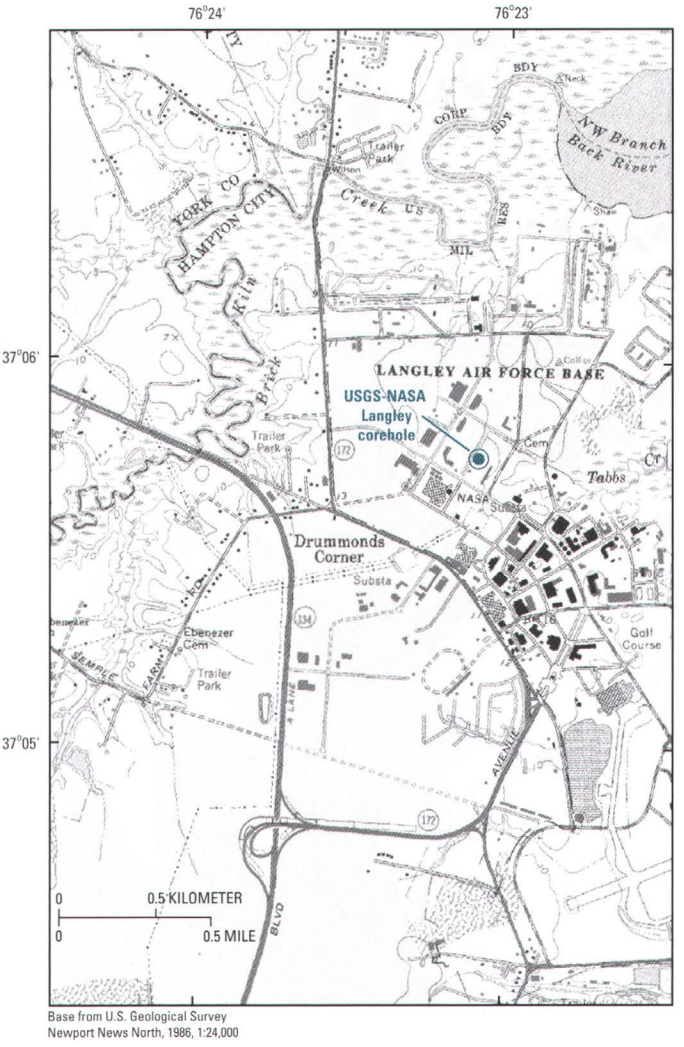

Figure D2. Detailed map showing the location of the USGS-NASA Langley corehole, Hampton, Va.

W. (North American Datum of 1927), and at a ground altitude of 2.4 meters (m; 7.9 feet (ft)) above the North American Vertical Datum of 1988.

The USGS-NASA Langley core can be divided into a number of impact-modified, impact-generated, and postimpact stratigraphic units. This chapter is concerned only with the impact-modified and impact-generated strata that form part of the crater fill. These strata are composed, in ascending order, of crater units A and B and the Exmore beds (fig. D3). These units extend from 626.3 to 235.65 m (2,054.7 to 773.12 ft) depth in the corehole. They contain strata and clasts derived from various preimpact sediments (table D1) and crystalline rocks in the region; they also contain matrix material that is composed of sands, silts, and clays.

The objectives of this study were threefold:

1. To examine various fossil groups in the impact-modified and impact-generated strata of the Langley core
2. To use the fossil data to determine the ages, provenance, and depositional environments of the strata, clasts, and matrix materials
3. To understand the dynamics involved in an impact in a shallow-marine setting

Fossils studied include palynomorphs (pollen and spores; dinoflagellate cysts, called dinocysts), calcareous nannofossils, and ostracodes. Pollen and spores are generally the only fossils found in the Lower to lower Upper Cretaceous Potomac Formation, a mainly or entirely terrigenous deposit that was affected by the impact. Dinocysts, calcareous nannofossils, foraminifera, diatoms, and ostracodes, among other marine microfossils, are present in the post-Potomac Formation, preimpact Upper Cretaceous to upper Eocene sediments of the Chesapeake Bay region.

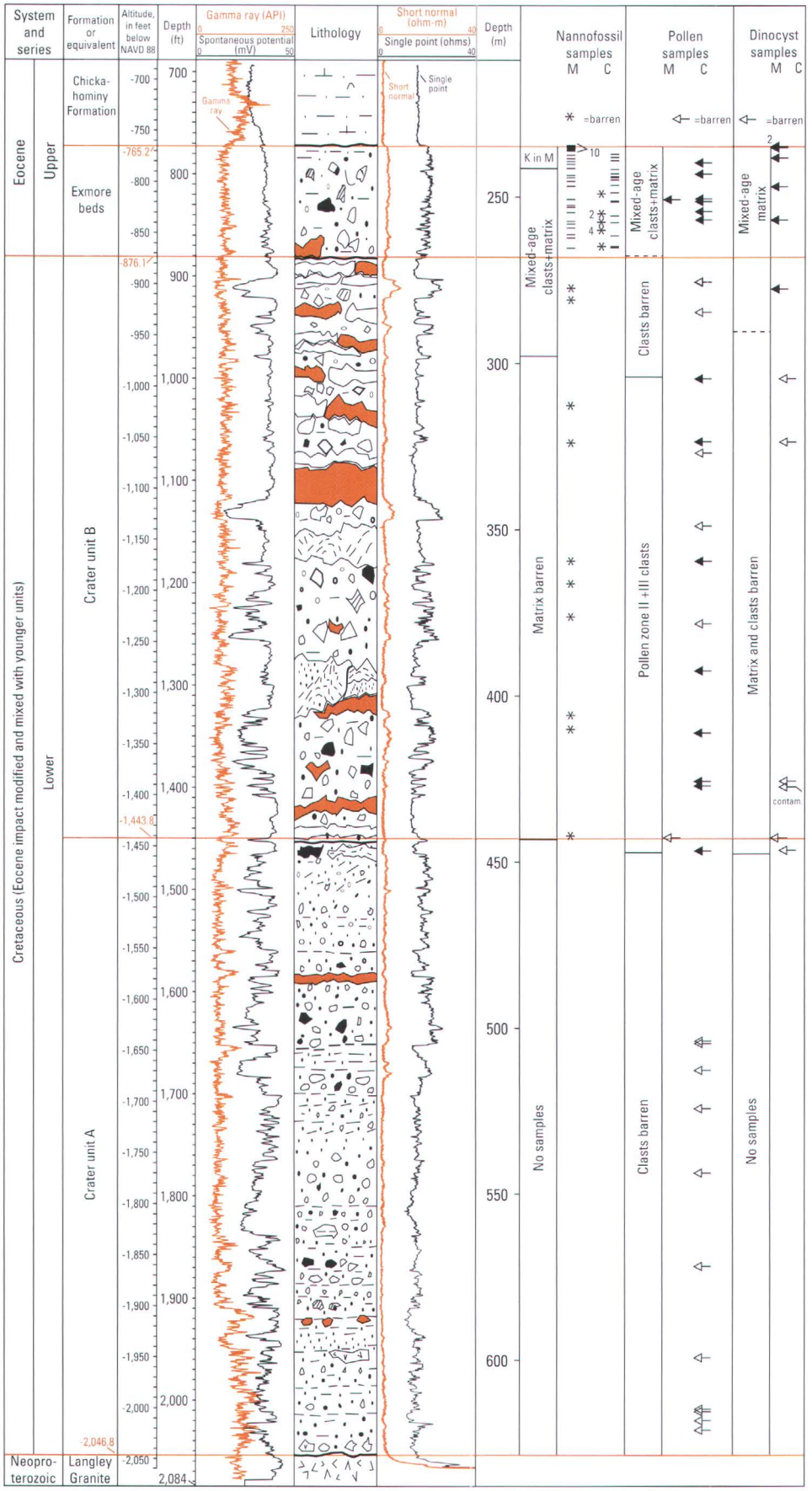

EXPLANATION

- Megablocks in crater units B and A (red clasts=very stiff oxidized clay, commonly including paleosols)
- Cobbles and boulders in Exmore beds and crater unit B
- Pebbles
- Very coarse to granular sand
- Medium to coarse sand
- Very fine sand
- Clayey silty sand
- Sandy, calcareous silt and clay
- Sandy, silty clay to sandy clayey silt
- Clay to clayey silt
- Shells
- M — Matrix
- C — Clast
- K in M — Cretaceous forms in mixed-age matrix
- Productive sample
- Barren or contaminated sample

Figure D3. Generalized lithostratigraphic column, selected geophysical logs, and a summary of the biostratigraphy of samples from crater units A and B and the Exmore beds in the USGS-NASA Langley core. Definitions: API, API units; ft, feet; m, meters; mV, millivolts; NAVD 88, North American Vertical Datum of 1988; ohm-m, ohm-meters.

Table D1. Cretaceous to middle Eocene (preimpact) stratigraphic units in Virginia.

[Units are from Teifke (1973), Meng and Harsh (1988), Olsson and others (1988), Mixon and others (1989), and Powars and Bruce (1999). These units are expected to be represented by the clasts and matrix materials in the diamicton part of the USGS-NASA Langley core, Hampton, Va.]

Unit	Age	Lithology
Piney Point Formation	Middle Eocene	Olive-gray, shelly, glauconitic sand.
Nanjemoy Formation	Early Eocene	Olive- to greenish-gray, shelly, glauconitic clay and sand.
Marlboro Clay	Latest Paleocene to earliest Eocene	Gray to reddish clay, silt, and very fine sand.
Aquia Formation	Late Paleocene	Greenish-gray, shelly, glauconitic sand.
Brightseat Formation	Early Paleocene	Olive-gray to black, partly glauconitic, clayey and silty sand.
Various names[1]	Post-Potomac Late Cretaceous	Clay and sand, partly glauconitic, and red beds.
Potomac Formation or Group (fig. D6)	Barremian(?) to early Cenomanian	Gray, pink to red, and greenish sand, silt, and clay.

[1] In Virginia, Upper Cretaceous strata are now present only in the subsurface and are more or less deeply buried (Mixon and others, 1989), but they would have been at or nearer to the surface at the time of the comet or asteroid impact. Some names attached to these Upper Cretaceous strata in Virginia include the following:
- Lower part of the Mattaponi Formation (Teifke, 1973)
- [Upper Cretaceous] undifferentiated sediments (Meng and Harsh, 1988)
- Units A, B, and C of an unnamed formation (Olsson and others, 1988)
- Upper Cretaceous deposits, undivided (Mixon and others, 1989)
- Unnamed Upper Cretaceous deposits (Powars and Bruce, 1999)

This chapter includes data from 15 productive clast and matrix samples examined for spores and pollen, 6 productive matrix samples examined for dinocysts, 47 productive clast and matrix samples examined for calcareous nannofossils, and 2 matrix samples examined for ostracodes. Depths of sampling intervals for dinocysts and spores and pollen are given in full in table D2 and figure D4, but, for expediency, generally only the midpoint of the sampling interval is stated in the text. Nannofossil samples are so small that their locations in the core are given by only single depths. Lists of spore-pollen, dinocyst, and calcareous nannofossil taxa mentioned in this chapter are given in figure D4, figure D5, and appendix D1, respectively. Photographs of selected fossils are shown in plates D1–D5.

Previous Work

The spore-pollen zonation of the Cretaceous Potomac Formation in the Middle Atlantic States was defined by Brenner (1963), Doyle and Hickey (1976), and Doyle and Robbins (1977). This zonation is tied both to lithostratigraphy and to the standard Cretaceous chronostratigraphy of Gradstein and others (1995) (fig. D6). Many articles have been published on Paleocene and Eocene pollen and dinocysts from the Middle Atlantic and Southern Atlantic States. Among those that describe the stratigraphic distributions of palynomorphs from Virginia are papers by Edwards (1984, 1989, 1996), Edwards and others (1991), and Frederiksen (1979, 1984, 1991).

Calcareous nannofossil biostratigraphy is based on the lowest and highest occurrences of species; FAD indicates a first appearance datum, and LAD indicates a last appearance datum. Ages of Cretaceous nannofossils are based on the zonation of Sissingh (1977) as modified by Perch-Nielsen (1985) and Burnett (1998). Dating of Cenozoic calcareous nannofossils is based primarily on the zonation of Martini (1971) and secondarily on the zonation of Bukry (1973) and Okada and Bukry (1980). Details about the distribution of nannofossil species in lower Tertiary formations of Virginia were provided by DiMarzio (1984) and Bybell and Gibson (1991, 1994).

Detailed information about lower Tertiary pollen, dinocysts, calcareous nannofossils, and ostracodes from the Oak Grove core in northern Virginia was given by Gibson and others (1980). Data on the lower Tertiary ostracode biostratigraphy of the Gulf and Atlantic Coastal Plains appear in Swain (1952), Pooser (1965), Hazel and others (1977, 1980), and Deck (1984).

Previous biostratigraphic studies from equivalent lithic units (impact-modified and impact-generated units) in other coreholes in the Chesapeake Bay crater have been published by Poag and Aubry (1995), Poag and Commeau (1995), and Poag (1997, 2002).

Sample Processing

Materials sampled for fossils consisted mainly of poorly sorted, partly glauconitic gray clay, silt, and very fine to coarse sand occurring in the form of matrix material, clasts, and, in the lower part of the core, marginally rotated and slumped strata and megablocks.

The early phase of processing samples for palynomorphs began in the same way for both pollen and dinocysts. One-quarter round, one-half round, or a whole piece of core was sampled over a depth interval of 3–9 centimeters (cm; 1.2–3.5 inches

(in.)) and scraped thoroughly. In the laboratory, 45–65 grams (g) of raw material was weighed and disaggregated. Each sample was treated with hydrochloric acid followed by hydrofluoric acid. Samples were then treated with nitric acid and ammonia and washed in a series of soap floats under short centrifugation.

There is an important difference in processing samples for angiosperm pollen from the Lower Cretaceous to lower Upper Cretaceous Potomac Formation as opposed to samples from younger stratigraphic units. This difference arises because angiosperm pollen grains from the Potomac Formation are generally very small, so that some of the grains will pass through even a 10-micrometer (μm) screen. In addition, Potomac Formation sediments contain large amounts of charcoal fragments. Therefore, Potomac Formation samples processed for angiosperm pollen were not sieved; following soap washes, they were separated from inorganic matter and charcoal by using a zinc chloride solution having a light specific gravity of 1.45 and designed particularly to drop out the charcoal. In contrast, zinc chloride solutions having a specific gravity of 2.0 were used for pollen samples from younger sediments, as well as for dinocyst samples. Pollen samples from younger sediments were then sieved, and the material between 10 and 200 μm was saved; dinocyst samples were sieved, and the material between 20 and 200 μm was saved. All palynomorph residues were stained with Bismark brown. Material was mounted in glycerin jelly on a glass slide with coverslip and was examined with the light microscope.

Forty nannofossil samples from the matrix portion of crater unit B and the Exmore beds and 26 nannofossil samples from clasts within the matrix were examined from the Langley core (fig. D3). For each matrix sample, a small amount of material was extracted from the central portion of a freshly broken core segment. Individual clasts were first scraped clean of drilling mud; then a small portion was removed from the center of the clast. The samples were dried in a convection oven to remove residual water, and the resultant sediments were stored in plastic vials.

To make slides, a small amount of sediment was placed in a beaker with 20 milliliters (mL) of water, stirred, and allowed to settle through the water column. An initial settling time of 1 minute (min) was used to remove the sand-sized fraction, and a second settling time of 10 min was used to concentrate the silt-sized material. Smear slides were made from the resultant slurry, and slides were affixed by using Norland Optical Adhesive 61 (NOA–61). Samples were primarily examined by using a Zeiss Photomicroscope III. Samples having exceptional preservation and abundance were further examined by using a JEOL JSM–6400 scanning-electron microscope (SEM). All palynological and nannofossil slides are stored at the U.S. Geological Survey, Reston, Va.

For ostracodes, approximately 50 g of sediment was processed by soaking the sediment overnight in tap water and washing on 63-μm sieves. Ostracodes were picked with a fine brush from the fraction >150 μm. Because so few individuals were present, all ostracodes were picked, including fragments.

Table D2. Depth of each dinocyst sample in the USGS-NASA Langley core.

[ft, feet; m, meters]

Sample	Top (ft)	Bottom (ft)	Midpoint (ft)	Midpoint (m)	Stratigraphic unit
R6110 DC	773.8	773.9	773.8	235.9	Exmore beds
R6110 DD	774.4	774.7	774.6	236.1	Exmore beds
R6110 DE	784.3	784.6	784.5	239.1	Exmore beds
R6110 DF	812.6	812.9	812.8	247.7	Exmore beds
R6110 DG	845.1	845.4	845.3	257.6	Exmore beds
R6110 DH	913.3	913.4	913.4	278.4	Crater unit B

Counting Methods for Dinocysts

One slide for each sample was examined completely for dinoflagellates and other palynomorphs. Then one or more slides were examined and counted until either 300 whole or partial specimens were noted (samples R6110 DH, DG, DF, DD, DC in table D3) or no additional slides and specimens remained (R6110 DE). All fragments that could be recognized as having dinoflagellate affinity were counted. Whole or nearly whole and fragmented specimens were placed into identifiable species, genera, or generic groups. Specimens that were not attributable to generic groups because of poor preservation were counted as "not identified to group."

Individual species could be identified in the case of some, but not all, of the whole or nearly whole specimens; most fragments could be identified only to genus level. The areoligeracean group is perhaps problematic. For whole or nearly whole specimens, most are attributable to the genus *Glaphyrocysta*. For fragmented specimens, this counting group includes chorate specimens that have solid processes but are not obviously members of the genus *Spiniferites* (pl. D2, fig. 8).

Spore-Pollen Biostratigraphy of Crater Unit A

Crater unit A extends from 626.3 to 442.5 m (2,054.7 to 1,451.7 ft) depth in the Langley core and consists of Potomac Formation strata that were disrupted very little by the impact (fig. D3). There are no matrix zones, although some fluidization of sands and fracturing of clays occurred in the upper part of the unit. There are no obvious contacts between blocks within this unit; if blocks occur in crater unit A, they are hundreds of meters in size (Gohn and others, this volume, chap. C). Potomac Formation strata in crater unit A are composed mainly of medium to very coarse sands that are barren or nearly barren of organic matter. The sands contain small numbers of clay clasts, interpreted to be primary clasts within the sand bodies, and subordinate primary clay-silt beds.

Stratigraphic unit	Crater unit A	Crater unit B							Exmore beds						
Depth (m)	446.4–446.5	426.8–426.8	425.5–425.6	411.0–411.0	392.3–392.3	359.6–359.7	323.5–323.6	304.7–304.7	268.7–268.8	257.4	255.0–255.0	251.9–252.0	251.0–251.1	243.6–243.6	240.3–240.4
Depth (ft)	1,464.5–1,464.8	1,400.1–1,400.4	1,396.1–1,396.4	1,348.3–1,348.5	1,287.0–1,287.2	1,179.8–1,180.0	1,061.5–1,061.7	999.6–999.8	881.6–881.8	844.6	836.5–836.7	826.5–826.7	823.5–823.7	799.1–799.3	788.5–788.6
Sample	R6110CB	R6110EC	R6110CA	R6110BJ	R6110BI	R6110BG	R6110BB	R6110BA	R6110AX	R6110AV	R6110AU	R6110EB	R6110AT	R6110EA	R6110AS
Matrix or clast	Clast	Clast	Clast	Clast	Clast	Clast	Clast	Clast	Clast	Clast	Clast	Matrix	Clast	Clast	Clast
Lithology	Greenish-black, lignitic, silty clay	Black, massive, noncalcareous clay	Olive-black, silty clay	Brownish-black, noncalcareous, silty clay	Very dark gray, noncalcareous, silty clay	Olive-gray, micaceous, lignitic, noncalcareous, fine sand	Olive-black, noncalcareous, silty clay	Black, noncalcareous, silty clay	Brownish-black, noncalcareous, silty clay	Brownish-black silty clay	Medium-gray to very light gray silt and very fine sand	Dark-greenish-gray, micaceous, calcareous, silty clay	Dark-olive-gray, micaceous, clayey silt	Calcareous very clayey silt	Medium-gray, micaceous, noncalcareous silty clay
Early Tertiary taxa															
Bombacacidites paulus Frederiksen 1989	.	.	.	.	.	.	.	.	.	.	.	X	.	.	.
Carya <29 µm of Frederiksen and Christopher (1978)	.	.	.	.	.	.	.	.	.	.	.	X	.	X	.
Favitricolporites baculoferus (Pflug in Thomson & Pflug 1953) Srivastava 1972	.	.	.	.	.	.	.	.	.	.	.	.	.	X	.
Insulapollenites rugulatus Leffingwell 1970	.	.	.	.	.	.	.	.	.	.	.	.	.	X	.
Interpollis microsupplingensis Krutzsch 1961	.	.	.	.	.	.	.	.	.	.	.	X	.	X	.
Intratriporopollenites pseudinstructus group of Frederiksen (1988)	.	.	.	.	.	.	.	.	.	.	.	X	.	X	.
Kyandopollenites anneratus Stover in Stover et al. 1966	.	.	.	.	.	.	.	.	.	.	.	.	.	X	.
Labrapollis globosus (Pflug in Thomson & Pflug 1953) Krutzsch 1968	.	.	.	.	.	.	.	.	.	.	.	X	.	.	.
Momipites coryloides Wodehouse 1933	.	.	.	.	.	.	.	.	.	.	.	X	.	.	.
Momipites microfoveolatus (Stanley 1965) Nichols 1973	.	.	.	.	.	.	.	.	.	.	.	X	.	X	.
Nudopollis terminalis (Pflug & Thomson in Thomson & Pflug 1953) Elsik 1968	.	.	.	.	.	.	.	.	.	.	.	X	.	X	.
Nyssa sp.	.	.	.	.	.	.	.	.	.	.	.	.	.	X	.
Platycaryapollenites swasticoidus (Elsik 1974) Frederiksen & Christopher 1978	.	.	.	.	.	.	.	.	.	.	.	X	.	.	.
Rhoipites angustus Frederiksen 1980	.	.	.	.	.	.	.	.	.	.	.	.	.	X	.
Symplocos? virginiensis group of Frederiksen (1988)	.	.	.	.	.	.	.	.	.	.	.	X	.	.	.
Thomsonipollis magnificus (Pflug in Thomson & Pflug 1953) Krutzsch 1960	.	.	.	.	.	.	.	.	.	.	.	X	.	X	.
Ulmipollenites krempii (Anderson 1960) Frederiksen 1979	.	.	.	.	.	.	.	.	.	.	.	X	.	.	.
Late Early and early Late Cretaceous taxa															
Ajatipollis sp. A of Doyle and Robbins (1977)	.	X	X	X	.	.	.	.	.	.	.	.	X	.	.
Aff. *Ajatipollis* sp. A of Doyle and Robbins (1977)	.	.	X	.	.	.	.	.	.	.	.	.	.	.	.
Appendicisporites segmentus Brenner 1963	.	.	.	.	X	.	.	.	.	.	.	.	.	.	.
Asteropollis sp. A of Doyle and Robbins (1977)	.	.	.	X	.	.	.	.	.	.	X	.	.	.	X
Cercidiphyllum type	X	.	.	.	.	.	.	.	.	.	.	.	.	.	.

Aff. *Clavatipollenites minutus* Brenner 1963 of Doyle and Robbins (1977)	X	.	.	.	.	.	.	.	.	.	.	.	.	.	.	.
Ephedripites virginiaensis Brenner 1963	.	.	.	.	P	.	.	.	.	.	.	.	.	.	.	.
"Foveotricolpites" concinnus Singh 1971	.	.	.	.	.	.	.	.	.	S	.	.	.	.	.	.
"Foveotricolporites" rhombohedralis Pierce 1961	.	.	X	.	.	.	.	.	.	.	.	.	.	.	.	X
Liliacidites sp. B of Doyle and Robbins (1977)	.	.	.	.	.	X	.	.	.	.	.	.	.	.	.	.
Liliacidites sp. D of Doyle and Robbins (1977)	.	X	.	.	.	.	.	.	.	.	.	.	.	.	.	.
Liliacidites sp. E of Doyle and Robbins (1977)	.	.	.	.	.	X	.	.	.	.	.	.	.	.	.	.
Liliacidites sp. F of Doyle and Robbins (1977)	X	.	.	.	.	X	.	.	.	.	.	.	.	.	.	.
Peromonolites reticulatus Brenner 1963	.	.	.	.	.	.	.	.	.	.	.	.	X	.	.	
Reticulatisporites arcuatus Brenner 1963	X	.	.	.	.	.	.	.	.	.	.	.	.	.	.	
"Retitricolpites" geranioides (Couper 1960) sensu Brenner 1963	.	.	.	.	.	X	.	S	.	X	.	.	.	.	.	
Cf. *"Retitricolpites" magnificus* Habib 1970 of Doyle and Robbins (1977)	.	.	.	X	.	.	.	.	.	.	.	.	.	.	.	
"Retitricolpites" prosimilis Norris 1967	.	.	X	.	.	.	.	.	.	.	.	.	.	.	.	
"Retitricolpites" vermimurus Brenner 1963	.	.	.	.	.	.	.	S	.	.	.	.	.	.	.	
"Retitricolpites" virgeus (Groot et al. 1961) Brenner 1963	.	.	.	.	.	X	.	.	.	.	.	.	.	.	.	
Rugubivesiculites reductus Pierce 1961	.	.	.	.	.	.	X	X	.	.	.	.	.	.	.	
Stephanocolpites tectorius Hedlund 1966	.	.	.	.	.	.	.	.	X	.	.	.	X	.	.	
Tricolpites albiensis Kemp 1968	.	.	.	.	S	S	.	.	.	S	.	.	.	.	.	
Cf. *Tricolpites albiensis* Kemp 1968 of Doyle and Robbins (1977)	.	.	.	X	.	.	.	.	.	.	.	.	.	.	.	
Aff. *Tricolpites albiensis* Kemp 1968 of Doyle and Robbins (1977)	.	.	X	.	.	.	.	.	.	.	.	.	.	.	.	
Tricolpites crassimurus (Groot & Penny 1960) Singh 1971	.	.	.	.	S	S	.	.	.	S	.	.	.	.	.	
Tricolpites georgensis (Brenner 1963) Burger 1970	.	.	.	.	S	X	.	X	.	S	.	.	.	.	.	
Tricolpites micromunus (Groot & Penny 1960) Burger 1970	X	.	X	.	.	X	.	.	.	.	.	.	.	.	.	
Cf. *Tricolpites micromunus* (Groot & Penny 1960) Burger 1970 of Doyle and Robbins (1977)	X	.	.	.	.	.	.	.	.	.	.	.	.	.	.	
Tricolpites nemejci Pacltová 1971	.	.	.	.	.	.	.	S	.	.	.	.	.	.	.	
Tricolpites sp. A of Doyle and Robbins (1977)	.	.	.	.	P	.	.	.	.	X	.	.	.	.	.	
Tricolporoidites bohemicus Pacltová 1971	.	.	.	S	.	.	.	.	.	.	.	.	.	.	.	
Tricolporoidites sp. A of Doyle and Robbins (1977)	.	S	X	.	.	.	.	.	.	.	.	.	.	.	.	
Aff. *Tricolporoidites* sp. A of Doyle and Robbins (1977)	.	X	.	.	.	.	.	.	.	.	.	.	.	.	.	
"Tricolporopollenites" distinctus Groot & Penny 1960	.	.	.	S	.	.	.	.	.	.	.	.	.	.	.	
Tricolporopollenites sp. A of Wolfe and others (1975)	.	X	.	.	.	.	.	.	.	.	.	.	X	.	.	
Verrumonocolpites conspicuous Pierce 1961	.	.	.	.	.	.	.	.	.	.	.	.	X	.	.	

Figure D4. Occurrence chart showing the presence of spore and pollen taxa in each productive sample from crater units A and B and the Exmore beds in the USGS-NASA Langley core. Sample positions are plotted in figure D3. Symbols: X, present; ., not present; P, probably a specimen of this species; S, similar to the species but not exactly the same.

Unit	Crater unit B	Exmore beds				
Depth (m)	278.4	257.6	247.7	239.1	236.1	235.9
Depth (ft)	913.4	845.3	812.8	784.5	774.6	773.8
Sample R6110	DH	DG	DF	DE	DD	DC
Taxon						
Achilleodinium biformoides (Eisenack 1954) Eaton 1976	.	.	X	.	.	.
Andalusiella Riegel 1974 sp. (pl. D1, fig. 20)	.	.	.	.	.	X
Apectodinium parvum (Alberti 1961) Lentin & Williams 1977 (pl. D1, figs. 17, 18)	X	.	.	.	.	.
Batiacasphaera baculata Drugg 1970 (pl. D1, fig. 2)	X	.	.	.	.	.
Carpatella cornuta Grigorovich 1969 (pl. D1, fig. 19)	.	.	.	.	X	.
Charlesdowniea coleothrypta (Williams & Downie 1966) Lentin & Vozzhennikova 1989	X	.	.	X	.	X
Cordosphaeridium funiculatum Morgenroth 1966 (pl. D1, fig. 1)	X	X	X	.	X	X
Cordosphaeridium gracile (Eisenack 1954) Davey & Williams 1966	X	.	.	.	.	X
Cordosphaeridium inodes (Klumpp 1953) Eisenack 1963	.	.	.	.	X	.
Cribroperidinium Neale & Sarjeant 1962 sp.	X	X	.	.	.	.
Deflandrea oebisfeldensis Alberti 1959	.	.	?	.	.	.
Deflandrea phosphoritica Eisenack 1938 and closely related forms (pl. D2, figs. 7, 14)	X	X	X	X	X	X
Diphyes colligerum (Deflandre & Cookson 1955) Cookson 1965	X	.	.	.	.	.
Dracodinium varielongitudum (Williams & Downie 1966) Costa & Downie 1979 (p. D1, fig. 10; pl. D2, figs. 4, 5, 6; pl. D3, figs. 1, 2, 10, 11)	X	X	X	X	X	X
Emmetrocysta Stover 1975 sp.	X	.	.	.	.	.
Eocladopyxis n. sp. A of Edwards (2001) (pl. D1, fig. 12)	X	.	.	.	.	.
Exochosphaeridium Davey et al. 1966 sp. (pl. D2, fig. 1)	.	.	X	.	.	.
Exochosphaeridium or *Operculodinium* group	X	X	.	.	.	.
Fibradinium annetorpense Morgenroth 1968 (pl. D1, figs. 7–9)	.	.	.	.	X	.
Hafniasphaera Hansen 1977 spp.	.	.	.	.	.	X
Histiocysta sp. of Stover and Hardenbol (1993) (pl. D1, figs. 3, 4)	X	X	X	X	.	.
Homotryblium tasmaniense Cookson & Eisenack 1967 (pl. D1, fig. 11)	X	.	.	.	.	.
Homotryblium tenuispinosum Cookson & Eisenack 1967	.	?	.	.	.	.
Hystrichokolpoma rigaudiae Deflandre & Cookson 1955	X	.	.	.	.	.
Hystrichokolpoma Klumpp 1953 sp.	.	X	.	.	.	.
Hystrichosphaeridium tubiferum or *Homotryblium tenuispinosum*	X	.	.	.	.	.
Impagidinium Stover & Evitt 1978 sp.	.	.	.	.	.	X
Lingulodinium machaerophorum (Deflandre & Cookson 1955) Wall 1967	X	.	.	.	.	.
Pentadinium goniferum Edwards 1982	.	.	X	.	X	X
Pentadinium laticinctum Gerlach 1961 subsp. *laticinctum* (pl. D1, fig. 16)	.	X	.	.	X	X
Pentadinium membranaceum (Eisenack 1965) Stover & Evitt 1978 (pl. D1, figs. 5, 6; pl. D2, fig. 13)	X	X	X	X	X	X
Pentadinium Gerlach 1961 spp., undifferentiated (pl. D2, figs. 9–12)	X	X	X	X	X	X
Phthanoperidinium brooksii Edwards & Bebout 1981 (pl. D1, fig. 15)	X	X	.	.	.	.
Samlandia chlamydophora Eisenack 1954	.	.	.	.	.	X
Spinidinium Cookson & Eisenack 1962 spp.	.	X	.	.	.	.
Spiniferites pseudofurcatus (Klumpp 1953) Sarjeant 1970	.	.	.	.	.	X
Spiniferites Mantell 1850 sp. (pl. D3, figs. 8, 9)	X	X	.	X	X	X
Spiniferites and *Impagidinium* group	X	X	.	.	X	.
Tectatodinium pellitum Wall 1967	X	.	.	.	.	.
Turbiosphaera or *Thalassiphora* group	X	X	X	.	X	X
Wetzeliella complex spp.	X	X	X	X	X	X
Wetzeliella hampdenensis Wilson 1967 (pl. D1, fig. 13)	.	X	.	.	.	.
Wilsonidium Lentin & Williams 1976 sp.	.	?	.	.	.	.
miscellaneous areoligeracean forms (predominantly *Glaphyrocysta* Stover & Evitt 1978 spp.) but also including miscellaneous chorate fragments (pl. D3, figs. 12–14; pl. D2, fig. 8)	X	X	X	X	X	X
miscellaneous cladopyxidiacean forms	X	X	X	.	X	.
small peridiniacean forms (pl. D1, fig. 14)	X	X	X	X	X	X

Figure D5. Occurrence chart showing the presence of dinocyst taxa in each productive matrix sample from crater unit B and the Exmore beds in the USGS-NASA Langley core. Sample positions are plotted in figure D3. Depth ranges sampled are listed in table D2; depths shown here are midpoints of the ranges. Symbols: X, present; ., not present; ?, questionably present.

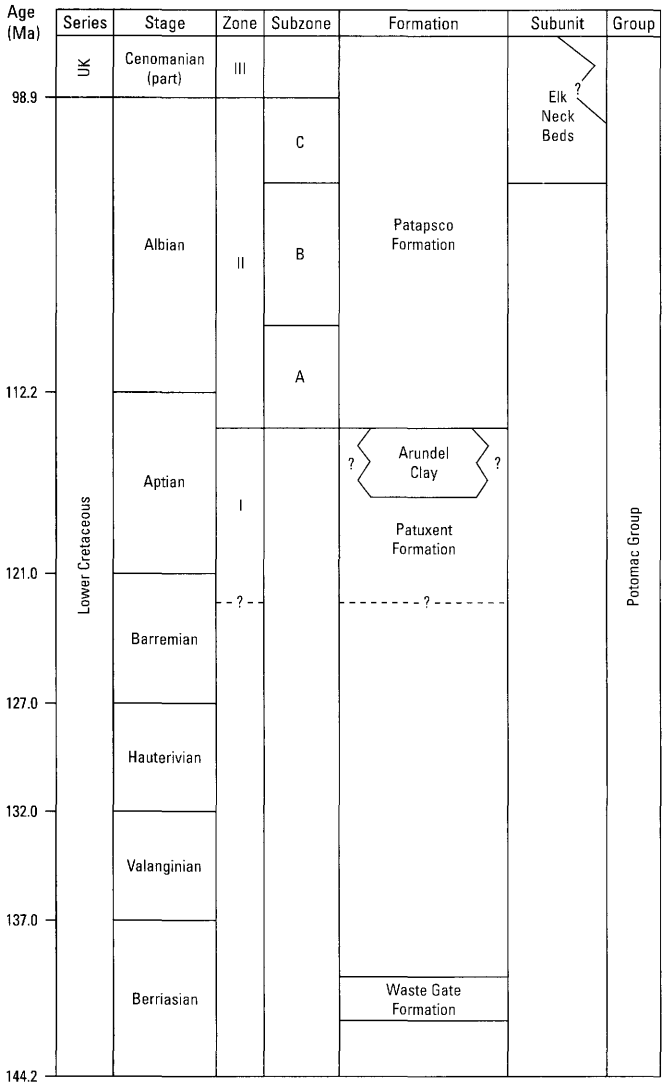

Figure D6. Correlation diagram showing stratigraphic units and palynological zones of the Potomac Group in the Middle Atlantic States. The Potomac Formation in Virginia as used in this report is equivalent to the Potomac Group in Maryland, which includes the Patapsco and Patuxent Formations and Arundel Clay, as shown above. Zonation is from Brenner (1963), Doyle and Hickey (1976), and Doyle and Robbins (1977); no zonal designation has been proposed for the spore-pollen assemblages (Doyle, 1983) of the Waste Gate Formation on the Delmarva Peninsula, east of the Chesapeake Bay. Ages of stage boundaries are from Gradstein and others (1995). UK, Upper Cretaceous.

Twelve samples of clay, silt, and sand were taken between 620.1 and 446.4 m (2,034.5 and 1,464.7 ft) in crater unit A (fig. D4; table D4); however, all samples but one were barren or nearly barren of organic matter including pollen and spores. Although the darkest strata available were sampled, all but two samples were greenish gray (the exceptions were dark red); the lack of organic matter (including pollen and spores) in these barren samples is undoubtedly due to the flood-plain strata originally having been oxidized during times of low ground-water level and then reduced during later times of high ground-water level, producing green colors of the iron minerals. However, it is assumed that all sedimentary materials within crater unit A are assignable to the Potomac Formation because no clasts or matrix materials were observed that appeared likely, on the basis of lithology, to be of post-Potomac Formation age (Gohn and others, this volume, chap. C).

The only sample from crater unit A that contained pollen and spores was the uppermost sample collected from this unit, from 446.4 m (1,464.7 ft; fig. D4). This sample was from lignitic beds; the sample was greenish black. The pollen assemblage is from Subzone IIB to Zone III, middle Albian to early Cenomanian in age. This sample was examined for dinocysts, but none were found, confirming the nonmarine origin of the sample. No palynomorph-bearing samples were obtained from the lowermost 179.8 m (589.7 ft) of crater unit A in the core, and these strata could be as old as early Aptian (fig. D6).

Biostratigraphy of Crater Unit B

Crater unit B extends from 442.5 to 269.4 m (1,451.7 to 884.0 ft; fig. D3) depth in the Langley core. Crater unit B is a sedimentary-clast diamicton in which the clast sizes vary greatly, from less than 1 cm (0.4 in.) to more than 20 m (66 ft) in diameter (Gohn and others, this volume, chap. C). This part of the diamicton is clast supported; the amount of matrix material between clasts constitutes a minor proportion of the total sediment. Clasts consist mainly of a variety of clays and sands. Zones of exotic matrix that penetrated this unit consist of muddy, fine to very coarse quartz-glauconite sand and granules. The lithology and the general absence of calcareous marine microfossils indicated at the time of drilling that most of the clasts were from the Potomac Formation.

Spores and Pollen

Thirteen samples from between 442.4 and 275.9 m (1,451.6 and 905.3 ft) in crater unit B were processed for spores and pollen (figs. D3, D4; table D4). Six of these samples were barren of palynomorphs (table D4), and these were greenish gray. Therefore, as seen also in crater unit A, prospects for obtaining spores and pollen grains from greenish samples of the Potomac Formation are rather poor. Higher in the section, abundant palynomorphs were recovered from greenish Tertiary matrix and clast samples in which the color comes from glauconite. The seven productive samples from the Potomac Formation in crater unit B were black, brownish black, or dark gray to olive black or olive gray (fig. D4).

Details about the spore-pollen assemblages found in samples from crater unit B are given in figure D4, and the ages of the assemblages are given in table D5. The seven productive clast samples from crater unit B all represented sediments derived from the Potomac Formation. The uppermost two samples could not be well dated. Among the remaining five sam-

Table D3. Quantitative composition of the dinocyst assemblage in each matrix sample from crater unit B and the Exmore beds in the USGS-NASA Langley core.

[m, meters; %, percent; W, whole; F, fragment]

Stratigraphic unit	Sample	Depth (m)	Count	% Whole or nearly whole	% Fragments	*Pentadinium* spp.		Areoligeracean group		*Deflandrea phosphoritica*		*Dracodinium varielongitudum*		Other *Wetzeliella* group		Misc. small peridiniaceans		Other identifiable forms		Not identified to group	
						W	F	W	F	W	F	W	F	W	F	W	F	W	F	W	F
Exmore beds	R6110 DC	235.9	300	22.3	77.7	16	105	11	76	11	18	20	0	4	2	1	0	3	6	1	26
Exmore beds	R6110 DD	236.1	300	6.3	93.7	5	140	2	74	0	9	5	0	2	0	1	0	4	17	0	41
Exmore beds	R6110 DE	239.1	203	22.7	77.3	5	89	0	5	19	31	8	3	9	2	2	0	1	0	2	27
Exmore beds	R6110 DF	247.7	300	15.0	85.0	14	99	3	107	6	10	4	0	12	7	1	0	5	12	0	20
Exmore beds	R6110 DG	257.6	300	21.0	79.0	8	74	6	106	6	8	3	1	14	12	12	0	12	20	2	16
Crater unit B	R6110 DH	278.4	300	23.3	76.7	3	28	12	140	4	2	5	0	10	9	16	2	19	35	1	14

ples, four or five of them contain at least some Aptian-Albian material and three contain some Cenomanian material. At least two and perhaps three of the samples contain mixed assemblages, indicating that these clasts had been contaminated by slurry sediment that penetrated the clasts during the violent movements of the material following the impact, or possibly during the drilling operation.

Dinocysts

Six samples from crater unit B were examined for the presence of dinocysts (fig. D3). Four of the samples were barren of these fossils. A fifth sample, of a clast from 426.8 m (1,400.3 ft), contained a few dinocyst specimens or fragments. However, these specimens most probably came from drilling-mud contamination, although infiltration of the sample with Tertiary material as a result of the impact event is also a possibility.

The sixth sample from crater unit B that was examined for the presence of dinocysts was a matrix sample from 278.4 m (913.4 ft; fig. D5); this sample, from near the top of crater unit B, consisted of a muddy, calcareous, quartz-glauconite sand. As in the samples from the matrix of the Exmore beds, dinocysts from 278.4 m represent a mixture of ages and show a variety of distinctive taphonomic effects. Because the matrix in the clast-supported crater unit B is genetically and lithologically continuous with the matrix in the Exmore beds, the dinocysts in the matrix from 278.4 m are discussed under "Biostratigraphy of the Exmore Beds."

Calcareous Nannofossils

Eleven matrix samples were examined from crater unit B for calcareous nannofossils, but most of these were barren (fig. D7). Only the sample from 298.5 m (979.3 ft) contained nannofossils, and the mixed assemblage in this sample consisted of species whose first occurrences (range bases) were in the early and late Paleocene and in the early, middle, and late Eocene; however, no Cretaceous species were observed.

Biostratigraphy of the Exmore Beds

The Exmore beds extend from 269.4 to 235.65 m (884.0 to 773.12 ft; fig. D3) depth in the Langley core. This unit is a matrix-supported, sedimentary-clast diamicton. Clasts in the Exmore beds generally are smaller than those in crater unit B and rarely exceed 1.0 m (3.3 ft) in diameter (Gohn and others, this volume, chap. C). Lithologically, the Exmore clasts are distinctly more heterogeneous than those in crater unit B, indicating a much larger variety of clast ages. The matrix consists mainly of muddy, calcareous, quartz-glauconite sand. Mixed sediments in the Exmore beds consist mainly of subaqueous resurge and (or) tsunami washback deposits that contain small amounts of reworked ejecta (Gohn and others, this volume, chap. C; Horton and Izett, this volume, chap. E).

Clasts appear to be of three origins (Poag, 1997; Gohn and others, this volume, chap. C):

1. Subaqueous resurge caused by the flow of seawater toward the center of the crater when the sea floor was exposed by the impact; the resurge carried with it blocks of sediment eroded from the crater rim
2. Tsunami washback derived from the return flow of huge tsunamis generated by the impact
3. Sparse fallback ejecta, consisting of blocks and unlithified sediments from the crater site that were blasted into the air, then fell back down over the region

Spores and Pollen

One matrix and six clast samples from between 268.7 and 240.4 m (881.7 and 788.6 ft) in the Exmore beds were processed for spores and pollen. All seven contained assemblages that could be dated (fig. D4). An overview of the ages of these samples is given in figure D8. The pollen assemblage from the matrix sample is compatible with an early Eocene age; however, some of the taxa have long stratigraphic ranges, and so the

Text continues on page D20.

Table D4. Depth and lithology of samples from the USGS-NASA Langley core that were collected for spore-pollen analysis but were barren of these fossils.

[m, meters; ft, feet]

Depth (m)	Depth (ft)	Sample number	Clast or matrix	Lithology
		Crater unit B		
275.9	905.2–905.3	R6110AZ	Clast	Mottled grayish-olive-green, muddy, fine to very coarse sand.
285.0–285.1	935.1–935.3	R6110BD	Clast	Light-olive-gray silty clay.
327.2–327.3	1,073.60–1,073.85	R6110BC	Clast	Greenish-gray, muddy, noncalcareous, very fine to fine sand.
349.0–349.1	1,145.00–1,145.25	R6110BE	Clast	Mottled (burrowed?) dark-greenish-gray to greenish-gray clayey sand.
378.3	1,241.0–1,241.2	R6110BH	Clast	Olive-gray noncalcareous clayey sand.
442.4–442.5	1,451.5–1,451.7	R6110ED	Matrix	Dark-greenish-gray, glauconitic, very coarse to very fine sand.
		Crater unit A		
503.4–503.5	1,651.7–1,652.0	R6110CC	Clast	Light-olive-gray, very coarse to fine, pebbly, noncalcareous sand.
504.1–504.2	1,654.0–1,654.3	R6110BK	Clast	Olive-gray, micaceous, noncalcareous, massive silty clay.
512.2	1,680.3–1,680.5	R6110EE	Clast	Greenish-black, noncalcareous silty clay.
523.7–523.8	1,718.2–1,718.4	R6110EF	Clast	Greenish-gray clay.
542.9–543.0	1,781.3–1,781.6	R6110EG	Clast	Dusky-yellowish-green, noncalcareous clayey silt.
570.9–571.0	1,872.9–1,873.2	R6110EH	Clast	Dark-greenish-gray, waxy clay.
598.3–598.4	1,963.0–1,963.2	R6110EI	Clast	Dark-greenish-gray clay.
613.7	2,013.3–2,013.6	R6110EJ	Clast	Very-dusky-red, noncalcareous silty clay.
614.6	2,016.3–2,016.5	R6110GA	Clast	Very-dusky-red, noncalcareous silty clay.
617.2	2,024.85–2,025.00	R6110EK	Clast	Dark-greenish-gray silty clay.
620.0–620.1	2,034.2–2,034.5	R6110EL	Clast	Dark-greenish-gray and dark-bluish-gray sandy clay.

Table D5. Spore-pollen ages of clast samples from crater units A and B in the USGS-NASA Langley core.

[The clasts all represent sediments derived from the Potomac Formation. Spore and pollen taxa in each clast are given in figure D4. m, meters; ft, feet]

Apparent diameter of clast		Depth		Age
(m)	(ft)	(m)	(ft)	
				Crater unit B
0.3	1	304.7	999.7	This sample contains relatively few species, which are probably long ranging; therefore, it is difficult to determine whether the assemblage is of mixed ages.
.3	1	323.6	1,061.6	Zone IIB or higher; middle Albian or younger. This sample contains only one significant species, which is long ranging. Therefore, it cannot be determined whether the assemblage includes pollen of mixed ages.
15	50	359.6	1,179.9	Probably Subzone IIB, middle Albian.
20.5	68	392.3	1,287.1	Probably Subzone IIA or IIB, probably late Aptian to middle Albian.
.5	1.5	411.0	1,348.4	This sample contains six significant species, three of them limited to Zone III, two of them apparently limited to Zone II, and one of them ranging from the upper part of Zone II to Zone III. Thus, the assemblage appears to indicate mixed ages.
2.2	6.2	425.6	1,396.2	This sample contains six significant species, two of them limited to Zone III, two species apparently limited to Zone II, and two species ranging from Zone II to Zone III. Thus, the assemblage appears to indicate mixed ages.
.15	.5	426.8	1,400.2	This sample contains only four significant species, two of them limited to Zone III, one species limited to the upper part of Zone II, and one species ranging from Zone II to Zone III. Thus, this assemblage may indicate mixed ages or may indicate a single age near the Zone II-Zone III boundary.
				Crater unit A
0.8	2.5	446.4	1,464.6	Subzone IIB to Zone III, middle Albian to early Cenomanian.

Stratigraphic unit	Depth (m)	Depth (ft)	First occurrence in early Paleocene																													
			BARREN	*Bomolithus conicus*	*Chiasmolithus consuetus*	*Chiasmolithus danicus*	*Coccolithus pelagicus*	*Cruciplacolithus asymmetricus*	*Cruciplacolithus edwardsii*	*Cruciplacolithus frequens*	*Cruciplacolithus inseadus*	*Cruciplacolithus primus*	*Cruciplacolithus tenuis*	*Cyclagelosphaera prima*	*Cyclagelosphaera reinhardtii*	*Ellipsolithus distichus*	*Ellipsolithus macellus*	*Ericsonia cava*	*Ericsonia subpertusa*	*Fasciculithus ulii*	*Hornibrookina arca*	*Markalius apertus*	*Neobiscutum parvulum*	*Prinsius bisulcus*	*Prinsius dimorphosus*	*Sphenolithus primus*	*Thoracosphaera* spp.	*Toweius pertusus*
Exmore beds	235.7	773.5	.	.	.	.	X	.	.	.	.	.	.	.	.	X	.	.	.	.	X	.	.	.	.	.	.	.	.	.	.	.
	235.8	773.8	.	.	.	.	X	.	.	.	.	.	.	X	.	.	.	.	.	X	.	.	.	.	.	.	.	X	.	.	.	.
	235.9	774.2	.	.	X	.	X	.	.	.	.	.	.	X	.	.	X	.	.	.	X	.	.	.	.	.	.	.	.	.	.	.
	236.0	774.4	.	.	X	.	X	.	.	.	.	X	.	.	.	X	X	.	X	.	X	.	.	.	.	X	.	X	.	.	.	X
	236.1	774.6	.	.	.	.	X	.	.	.	.	X	.	.	.	X	.	X	X	.	X	X	.	X	.	X	.	X	.	.	.	X
	236.12	774.7	.	.	.	.	X	X	.	.	.	X	X	.	.	X	.	.	X	.	X	X	.	.	.	.	.	X	.	.	.	X
	236.3	775.2	.	.	X	.	X	.	X	.	.	X	.	.	.	.	X	X	X	.	X	.	.	.	.	.	.	X	.	.	.	X
	236.5	775.9	.	.	X	.	X	X	X	.	.	X	.	.	.	.	X	X	X	.	X	.	.	X	.	X	.	.	.	.	.	.
	236.7	776.5	.	.	X	.	X	.	.	.	.	X	.	.	.	.	.	.	.	.	X	.	.	X	.	.	.	.	.	.	.	X
	236.9	777.4	.	.	X	.	X	.	.	X	.	.	.	.	.	X	.	.	X	.	X	.	X	.	.	X	.	X	.	.	.	X
	238.1	781.3	.	.	.	.	X	X	X	.	.	.	.	.	.	.	.	.	X	.	X	.	.	X	.	.	.	.	.	.	.	X
	239.3	785.0	.	.	X	.	X	.	.	.	.	X	.	.	X	.	X	.	X	.	X	.	.	X	.	X	X	X	.	.	.	X
	240.0	787.3	.	.	X	.	X	.	.	.	.	X	.	.	.	X	X	.	X	.	X	.	.	X	X	X	.	X	.	.	.	X
	241.0	790.8	.	.	.	.	X	.	X	.	.	X	X	.	X	X	.	.	.	.	X	.	X	X	.	X	X	X	.	.	.	X
	242.2	794.7	.	.	X	.	X	.	.	.	.	X	X	.	.	X	.	.	X	.	X	.	X	.	.	X	.	X	.	.	.	X
	244.3	801.5	.	.	X	.	X	.	X	.	.	X	.	.	.	X	.	.	X	.	X	.	.	X	.	X	.	X	.	.	.	X
	245.0	803.8	.	.	.	.	X	X	.	.	.	.	.	.	.	.	.	X	X	.	X	.	.	X	.	.	.	.	.	.	.	X
	246.0	807.0	.	.	X	.	X	.	.	.	.	.	.	.	.	.	.	.	X	.	X	X	.	X	.	X	.	X	.	.	.	X
	247.6	812.4	.	X	X	.	X	.	.	.	.	.	X	.	.	X	.	X	X	.	X	.	.	X	.	.	.	.	.	.	.	X
	251.5	825.2	.	.	.	.	X	X	.	.	.	X	.	X	.	X	.	.	X	.	X	.	.	X	.	.	.	.	.	.	.	X
	253.3	831.2	.	.	.	X	X	.	.	.	.	X	.	.	.	X	.	.	.	.	X	.	.	.	.	.	.	.	.	.	.	X
	254.0	833.2	.	.	.	.	X	.	.	.	.	.	.	.	.	X	X	.	X	.	X	.	.	X	.	X	.	X	.	.	.	X
	255.3	837.5	.	.	.	.	X	.	.	.	.	.	.	.	.	.	.	.	.	.	X	.	X	X	.	X	.	X	.	.	.	X
	258.0	846.4	.	.	.	.	X	.	.	.	.	.	.	X	.	X	X	.	X	.	X	.	X	.	.	X	.	X	.	.	.	X
	258.8	849.0	.	.	.	.	X	.	.	.	.	.	.	.	.	.	X	.	X	.	X	.	X	.	.	X	.	X	.	.	.	X
	260.0	853.0	.	.	X	.	X	.	.	.	.	.	.	X	X	X	.	X	X	.	X	.	.	X	.	X	.	X	.	.	.	X
	262.0	859.5	.	.	.	.	X	.	.	.	X	.	.	X	.	X	X	X	X	.	X	.	.	X	.	X	.	X	.	.	.	X
	263.0	863.0	.	.	X	.	X	.	.	.	.	.	.	.	.	X	.	.	X	.	X	.	.	.	.	.	.	.	.	.	.	X
	266.2	873.2	.	.	.	.	X	.	.	.	.	X	.	X	.	X	.	.	X	.	X	.	.	X	.	X	.	X	.	.	.	X
Crater unit B	278.4	913.4	X	.	.	.	.	.	.	.	.	.	.	.	.	.	.	.	.	.	.	.	.	.	.	.	.	.	.	.	.	.
	281.3	923.1	X	.	.	.	.	.	.	.	.	.	.	.	.	.	.	.	.	.	.	.	.	.	.	.	.	.	.	.	.	.
	298.5	979.3	.	.	.	.	X	.	.	.	.	.	.	.	.	.	.	.	.	.	.	X	.	.	.	X	.	.	.	.	.	.
	313.7	1,029.3	X	.	.	.	.	.	.	.	.	.	.	.	.	.	.	.	.	.	.	.	.	.	.	.	.	.	.	.	.	.
	324.1	1,063.3	X	.	.	.	.	.	.	.	.	.	.	.	.	.	.	.	.	.	.	.	.	.	.	.	.	.	.	.	.	.
	360.2	1,181.9	X	.	.	.	.	.	.	.	.	.	.	.	.	.	.	.	.	.	.	.	.	.	.	.	.	.	.	.	.	.
	366.6	1,202.9	X	.	.	.	.	.	.	.	.	.	.	.	.	.	.	.	.	.	.	.	.	.	.	.	.	.	.	.	.	.
	376.9	1,236.7	X	.	.	.	.	.	.	.	.	.	.	.	.	.	.	.	.	.	.	.	.	.	.	.	.	.	.	.	.	.
	406.1	1,332.5	X	.	.	.	.	.	.	.	.	.	.	.	.	.	.	.	.	.	.	.	.	.	.	.	.	.	.	.	.	.
	410.7	1,347.3	X	.	.	.	.	.	.	.	.	.	.	.	.	.	.	.	.	.	.	.	.	.	.	.	.	.	.	.	.	.
	442.4	1,451.5	X	.	.	.	.	.	.	.	.	.	.	.	.	.	.	.	.	.	.	.	.	.	.	.	.	.	.	.	.	.

Figure D7. Occurrence chart showing the presence of calcareous nannofossil taxa in each matrix sample from crater unit B and the Exmore beds in the USGS-NASA Langley core. Abundance and preservation data are shown on the sixth page. Symbols: X, present; ., not present; 1, a single specimen. The only productive matrix sample from crater unit B is from a thin matrix section at the top of a coring run. As such, it was susceptible to drilling-mud contamination during core recovery and handling. However, its mixed early Tertiary assemblage could be due to sediment mixing during the impact.

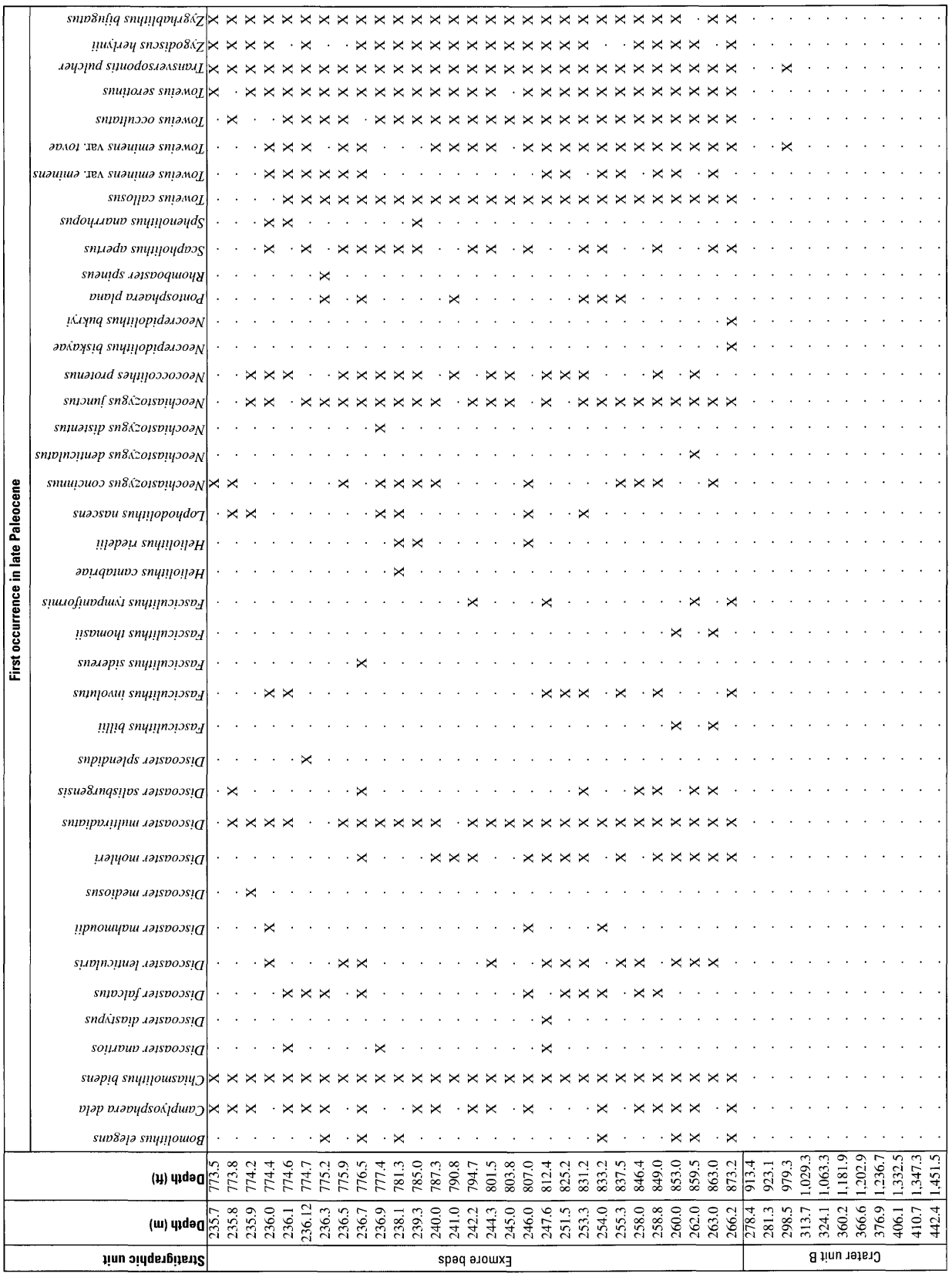

Figure D7. Continued.

Stratigraphic unit	Depth (m)	Depth (ft)	First occurrence in early Eocene																																
			Chiasmolithus eograndis	*Chiasmolithus expansus*	*Coronocyclus prionion*	*Discoaster barbadiensis*	*Discoaster deflandrei*	*Discoaster gemmifer*	*Discoaster kuepperi*	*Discoaster lodoensis*	*Discoaster septemradiatus*	*Discoaster sublodoensis*	*Ericsonia formosa*	*Helicosphaera lophota*	*Helicosphaera papillata*	*Helicosphaera seminulum*	*Holodiscolithus solidus*	*Neococcolithes dubius*	*Neococcolithes minutus*	*Pontosphaera ocellata*	*Pseudotriquetrorhabdulus inversus*	*Reticulofenestra dictyoda*	*Rhabdosphaera creber*	*Rhabdosphaera perlongus*	*Rhabdosphaera pinguis*	*Rhabdosphaera truncata*	*Rhomboaster bramlettei*	*Rhomboaster contortus*	*Rhomboaster orthostylus*	*Sphenolithus editus*	*Sphenolithus moriformis*	*Sphenolithus radians*	*Toweius? magnicrassus*	*Transversopontis obliquipons*	*Transversopontis pulcheroides*
Exmore beds	235.7	773.5	.	.	.	X	.	.	.	.	.	.	X	X	.	X	.	X	.	.	.	.	.	.	.	.	.	.	X	.	.	.	.	.	.
	235.8	773.8	.	.	.	.	.	.	X	X	.	.	X	.	.	X	.	X	.	.	.	.	X	.	.	.	.	.	X	.	.	.	.	.	X
	235.9	774.2	.	.	.	X	.	.	.	.	.	.	X	.	.	X	.	X	.	.	.	.	.	.	.	.	.	.	X	.	.	.	.	.	X
	236.0	774.4	X	X	X	.	.	X	X	.	.	.	.	X	.	.	.	X	X	.	X	X	.	.	.	X	.	.	X	.	.	.	X	.	.
	236.1	774.6	.	.	.	X	X	.	.	.	.	.	.	X	.	.	.	.	X	.	X	X	.	.	.	.	.	.	.	.	X	X	.	.	.
	236.12	774.7	.	.	.	.	.	.	.	.	.	.	.	X	.	.	.	.	X	.	X	X	.	.	.	.	X	.	.	.	.	.	.	.	.
	236.3	775.2	.	.	X	X	.	X	.	.	.	.	.	.	X	.	.	X	X	.	X	X	.	.	.	X	.	.	X	X	.	.	.	.	.
	236.5	775.9	.	.	X	.	.	.	.	.	.	X	.	.	.	X	.	.	X	X	X	X	.	.	.	X	.	.	X	.	.	.	.	.	.
	236.7	776.5	.	.	.	.	.	.	.	.	.	X	.	X	.	X	.	.	X	.	X	X	.	.	.	.	.	.	.	.	X	.	.	.	.
	236.9	777.4	.	.	.	.	.	.	.	.	.	.	.	.	.	X	.	.	X	X	X	X	.	.	.	X	.	.	X	.	.	.	.	.	.
	238.1	781.3	.	.	.	X	X	.	.	.	.	.	.	X	.	.	.	.	X	.	X	X	.	.	.	.	.	.	.	.	.	.	.	.	.
	239.3	785.0	.	.	X	.	.	.	.	.	.	.	.	.	X	X	.	.	X	.	X	X	.	.	.	.	X	.	.	.	.	X	.	.	.
	240.0	787.3	.	.	X	.	.	.	.	.	.	.	.	.	.	.	.	X	X	.	X	X	.	.	.	.	.	.	.	.	.	X	.	X	.
	241.0	790.8	.	X	.	.	.	.	.	.	.	.	.	.	.	X	X	X	X	.	X	X	.	.	.	.	.	.	.	.	.	.	.	X	.
	242.2	794.7	.	X	.	.	.	.	.	.	.	.	.	.	.	.	.	.	X	.	X	X	.	.	.	.	.	.	.	.	.	.	.	X	.
	244.3	801.5	.	.	X	X	.	.	.	.	.	.	.	.	.	.	.	X	X	.	X	X	.	.	.	.	.	.	.	.	.	.	.	X	.
	245.0	803.8	.	.	.	X	.	.	.	.	X	.	.	.	.	X	.	X	X	.	X	X	.	.	.	X	.	.	X	.	.	.	.	X	.
	246.0	807.0	.	.	.	.	.	.	.	.	.	.	.	.	.	.	.	.	X	.	X	X	.	.	X	.	.	.	X	.	.	.	.	X	.
	247.6	812.4	.	.	X	.	.	.	.	.	.	.	X	.	.	.	.	.	X	.	X	X	X	X	.	.	.	.	.	X	.	.	X	X	.
	251.5	825.2	.	.	X	.	.	.	.	.	.	.	X	.	.	.	.	.	X	.	X	X	X	.	.	.	.	.	.	.	.	.	.	X	.
	253.3	831.2	.	.	.	.	.	.	.	.	.	.	X	.	.	.	.	.	X	.	X	X	.	.	.	X	.	.	.	.	.	.	.	X	.
	254.0	833.2	.	X	.	.	X	.	.	.	.	.	X	.	.	X	X	.	X	.	.	X	.	.	.	.	X	.	X	.	.	X	.	X	.
	255.3	837.5	.	X	.	.	.	.	.	.	.	.	X	.	.	.	.	X	X	.	X	X	.	.	.	X	.	.	.	.	.	.	.	X	.
	258.0	846.4	.	X	X	.	.	.	.	.	.	.	X	.	.	X	.	X	X	.	X	X	.	.	.	.	X	.	X	.	.	.	.	X	.
	258.8	849.0	.	X	.	.	X	.	X	.	.	.	X	.	.	.	.	X	.	.	X	X	.	.	.	.	.	.	.	.	.	.	.	X	.
	260.0	853.0	.	.	.	.	X	.	X	X	.	.	X	.	.	X	.	.	X	.	X	X	.	.	.	X	.	.	.	.	.	.	.	X	.
	262.0	859.5	.	.	X	X	.	.	X	.	.	.	X	.	.	X	.	X	X	.	X	X	.	.	.	X	.	.	X	.	.	.	.	X	.
	263.0	863.0	.	X	X	.	X	.	.	.	.	.	X	.	.	.	.	.	X	.	X	X	.	.	.	.	.	.	.	.	.	.	.	X	.
	266.2	873.2	.	X	.	.	.	.	X	.	.	.	X	X	.	X	.	X	X	.	X	X	.	.	.	.	.	.	.	X	.	.	.	X	.
Crater unit B	278.4	913.4	.	.	.	.	.	.	.	.	.	.	.	.	.	.	.	.	.	.	.	.	.	.	.	.	.	.	.	.	.	.	.	.	.
	281.3	923.1	.	.	.	.	.	.	.	.	.	.	.	.	.	.	.	.	.	.	.	.	.	.	.	.	.	.	.	.	.	.	.	.	.
	298.5	979.3	.	.	.	.	.	.	.	.	.	.	X	.	.	.	.	.	.	.	.	X	.	.	.	X	.	X	.	.	X	.	.	X	.
	313.7	1,029.3	.	.	.	.	.	.	.	.	.	.	.	.	.	.	.	.	.	.	.	.	.	.	.	.	.	.	.	.	.	.	.	.	.
	324.1	1,063.3	.	.	.	.	.	.	.	.	.	.	.	.	.	.	.	.	.	.	.	.	.	.	.	.	.	.	.	.	.	.	.	.	.
	360.2	1,181.9	.	.	.	.	.	.	.	.	.	.	.	.	.	.	.	.	.	.	.	.	.	.	.	.	.	.	.	.	.	.	.	.	.
	366.6	1,202.9	.	.	.	.	.	.	.	.	.	.	.	.	.	.	.	.	.	.	.	.	.	.	.	.	.	.	.	.	.	.	.	.	.
	376.9	1,236.7	.	.	.	.	.	.	.	.	.	.	.	.	.	.	.	.	.	.	.	.	.	.	.	.	.	.	.	.	.	.	.	.	.
	406.1	1,332.5	.	.	.	.	.	.	.	.	.	.	.	.	.	.	.	.	.	.	.	.	.	.	.	.	.	.	.	.	.	.	.	.	.
	410.7	1,347.3	.	.	.	.	.	.	.	.	.	.	.	.	.	.	.	.	.	.	.	.	.	.	.	.	.	.	.	.	.	.	.	.	.
	442.4	1,451.5	.	.	.	.	.	.	.	.	.	.	.	.	.	.	.	.	.	.	.	.	.	.	.	.	.	.	.	.	.	.	.	.	.

Figure D7. Continued.

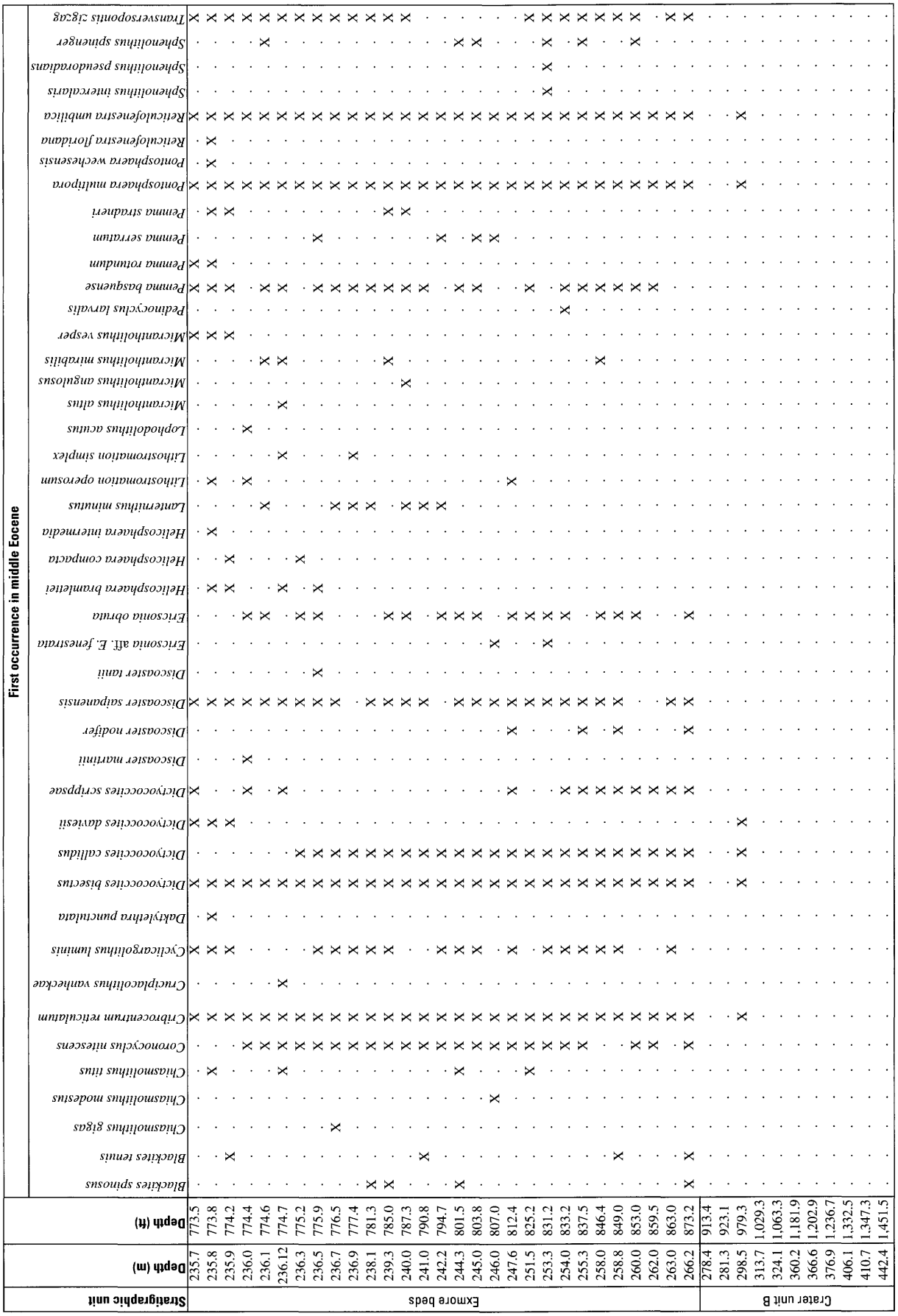

Figure D7. Continued.

Stratigraphic unit	Depth (m)	Depth (ft)	First occurrence (FO) in late Eocene								Survivor species						Unknown FOs					
			Chiasmolithus oamaruensis	*Cyclicargolithus floridanus*	*Ericsonia subdisticha*	*Helicosphaera euphratis*	*Helicosphaera reticulata*	*Helicosphaera wilcoxonii*	*Isthmolithus recurvus*	*Reticulofenestra oamaruensis*	*Biscutum constans*	*Braarudosphaera bigelowii*	*Cyclagelosphaera reinhardtii*	*Goniolithus fluckigeri*	*Markalius inversus*	*Placozygus sigmoides*	*Biscutum* spp.	*Discoaster* spp.	*Fasciculithus* spp.	*Micrantholithus* spp.	*Nannfula* spp.	*Pontosphaera* spp.
Exmore beds	235.7	773.5	X	X	.	.	.	.	X	.	.	X	.	.	.	X	.	X	.	.	.	X
	235.8	773.8	X	.	.	.	.	.	X	.	.	X	.	.	X	X	.	.	.	.	.	.
	235.9	774.2	X	X	.	.	.	.	X	.	.	X	.	.	X	.	.	.	.	.	.	.
	236.0	774.4	X	X	.	.	.	X	X	X	.	X	.	X	X	.	.	.	.	.	X	X
	236.1	774.6	.	.	.	.	.	.	X	.	X	X	.	.	X	.	.	.	.	.	.	.
	236.12	774.7	X	.	.	.	.	.	X	.	.	X	.	.	X	.	.	.	.	.	.	.
	236.3	775.2	X	.	.	.	.	.	X	.	.	X	X	.	X	.	.	.	.	.	.	X
	236.5	775.9	.	.	.	.	X	.	X	.	X	X	X	.	X	.	.	.	.	.	.	X
	236.7	776.5	X	.	.	.	.	.	X	.	X	X	.	.	X	X	.	.	.	.	.	.
	236.9	777.4	X	.	.	.	.	.	X	.	X	X	.	.	X	.	.	.	X	.	.	X
	238.1	781.3	.	.	.	.	.	.	X	.	X	X	.	.	X	.	.	.	.	.	.	X
	239.3	785.0	X	.	.	.	.	.	X	.	.	X	.	.	X	.	.	.	.	.	.	.
	240.0	787.3	X	.	.	.	.	.	X	.	.	X	.	.	X	.	.	X	X	.	.	.
	241.0	790.8	X	.	X	.	.	.	X	.	X	X	.	.	X	X	.	.	.	.	.	X
	242.2	794.7	.	.	.	.	.	.	X	.	.	X	.	.	X	.	.	.	.	.	.	.
	244.3	801.5	X	.	.	.	.	.	X	.	X	X	.	X	X	.	.	.	X	.	.	X
	245.0	803.8	X	.	.	.	.	.	X	.	.	X	.	.	.	.	.	X	.	.	.	X
	246.0	807.0	X	.	X	.	.	.	X	.	.	X	X	.	X	X	.	.	X	.	.	X
	247.6	812.4	.	.	.	.	.	.	.	.	.	X	.	.	X	.	.	.	X	.	.	X
	251.5	825.2	.	.	.	.	.	.	X	.	.	.	.	.	X	.	X	.	X	.	.	.
	253.3	831.2	X	.	.	.	.	.	X	.	.	X	.	.	X	.	X	.	X	.	.	X
	254.0	833.2	.	.	.	X	.	.	X	.	X	X	.	.	X	X	.	X	.	X	.	.
	255.3	837.5	.	X	.	.	.	.	X	.	.	X	.	.	X	.	.	.	X	.	.	.
	258.0	846.4	X	.	.	.	.	.	X	.	.	X	.	.	.	.	.	.	.	.	.	X
	258.8	849.0	X	.	.	.	.	.	X	.	.	X	X	.	X	.	.	.	.	.	.	X
	260.0	853.0	X	.	.	.	.	.	X	.	.	X	.	.	.	.	.	.	.	.	.	X
	262.0	859.5	X	.	X	.	.	.	X	.	.	.	.	.	X	.	.	X	.	.	.	.
	263.0	863.0	.	.	.	.	.	.	X	.	.	X	.	.	X	X	.	.	X	.	.	X
	266.2	873.2	.	.	.	.	.	.	X	.	X	.	.	.	X	.	.	.	.	.	.	.
Crater unit B	278.4	913.4	.	.	.	.	.	.	.	.	.	.	.	.	.	.	.	.	.	.	.	.
	281.3	923.1	.	.	.	.	.	.	.	.	.	.	.	.	.	.	.	.	.	.	.	.
	298.5	979.3	.	.	.	.	.	.	X	.	.	.	.	.	.	.	.	.	.	.	.	.
	313.7	1,029.3	.	.	.	.	.	.	.	.	.	.	.	.	.	.	.	.	.	.	.	.
	324.1	1,063.3	.	.	.	.	.	.	.	.	.	.	.	.	.	.	.	.	.	.	.	.
	360.2	1,181.9	.	.	.	.	.	.	.	.	.	.	.	.	.	.	.	.	.	.	.	.
	366.6	1,202.9	.	.	.	.	.	.	.	.	.	.	.	.	.	.	.	.	.	.	.	.
	376.9	1,236.7	.	.	.	.	.	.	.	.	.	.	.	.	.	.	.	.	.	.	.	.
	406.1	1,332.5	.	.	.	.	.	.	.	.	.	.	.	.	.	.	.	.	.	.	.	.
	410.7	1,347.3	.	.	.	.	.	.	.	.	.	.	.	.	.	.	.	.	.	.	.	.
	442.4	1,451.5	.	.	.	.	.	.	.	.	.	.	.	.	.	.	.	.	.	.	.	.

Figure D7. Continued.

Stratigraphic unit	Depth (m)	Depth (ft)	First occurrence in Late Cretaceous																																Abundance[a]	Preservation[b]
			Ahmuellerina octoradiata	*Arkhangelskiella cymbiformis*	*Broinsonia dentata*	*Calculites obscurus*	*Calculites ovalis*	*Corollithion signum*	*Cretarhabdus conicus*	*Cribrosphaerella ehrenbergii*	*Cylindralithus crassus*	*Discorhabdus ignotus*	*Eiffellithus eximius*	*Eiffellithus turriseiffelii*	*Eprolithus floralis*	*Flabellites oblonga*	*Garnerago obliquum*	*Glaukolithus diplogrammis*	*Helicolithus trabeculatus*	*Lithastrinus grillii*	*Microrhabdulus attenuatus*	*Micula decussata*	*Prediscosphaera cretacea*	*Prediscosphaera spinosa*	*Reinhardtites anthophorus*	*Repagulum parvidentatum*	*Retemediaformis* sp.	*Sollasites barringtonensis*	*Staurolithites imbricatus*	*Stovarius asymmetricus*	*Tranolithus minimus*	*Vekshinella aachena*	*Vekshinella stradneri*	*Watznaueria barnesae*		
Exmore beds	235.7	773.5	.	.	.	.	.	.	.	X	.	.	.	X	.	.	.	X	.	.	.	.	X	.	.	.	.	.	.	.	.	.	.	.	A	G
	235.8	773.8	.	.	.	.	.	.	.	.	.	X	.	X	.	.	.	.	.	.	.	.	X	.	.	.	.	.	.	.	.	.	.	.	A	M
	235.9	774.2	.	.	.	.	.	.	.	X	.	.	.	X	.	.	.	.	.	.	.	X	.	.	.	.	.	.	.	.	.	.	.	.	A	G
	236.0	774.4	.	.	.	.	.	.	.	.	.	.	.	X	.	.	.	.	.	.	X	.	X	.	.	.	.	.	.	.	.	.	.	.	C	G
	236.1	774.6	X	X	X	.	.	.	.	X	.	.	.	X	.	X	.	.	.	X	.	X	.	.	.	.	X	.	X	.	.	X	.	.	C	G
	236.12	774.7	.	.	.	.	.	.	.	.	X	X	.	.	.	.	.	.	.	.	.	X	X	.	.	.	.	.	.	.	X	.	.	.	C	G
	236.3	775.2	.	.	.	.	.	X	.	.	.	.	.	X	.	.	.	.	.	.	.	.	.	.	.	.	.	.	.	.	X	.	.	.	C	G
	236.5	775.9	.	.	.	X	X	.	X	.	.	.	.	X	.	.	X	X	.	.	.	X	X	.	.	.	X	.	.	.	.	.	.	.	C	G
	236.7	776.5	.	.	.	.	.	.	.	.	.	X	.	X	.	.	.	.	.	.	.	.	X	.	X	X	.	.	.	X	.	.	.	.	C	G
	236.9	777.4	.	.	.	.	.	.	.	X	.	.	.	X	X	.	.	.	X	.	.	.	X	.	.	.	.	.	.	.	.	.	.	.	C	G
	238.1	781.3	.	.	.	.	.	X	.	.	.	X	.	.	.	.	.	.	.	.	.	.	.	.	.	.	.	X	.	.	.	.	X	.	C	G
	239.3	785.0	.	.	.	.	.	.	.	.	.	.	.	.	.	.	.	.	X	.	.	.	X	.	.	.	.	.	.	.	.	.	.	.	C	G
	240.0	787.3	.	.	.	.	.	.	.	.	.	.	X	.	.	.	.	.	.	.	.	.	.	.	.	.	.	.	.	.	.	.	.	.	C	G
	241.0	790.8	.	.	.	.	.	.	.	.	.	.	.	.	.	.	.	X	.	.	.	.	.	X	.	.	.	.	.	.	.	.	.	.	F+	G
	242.2	794.7	.	.	.	.	.	.	.	X	.	X	.	X	.	.	.	.	.	.	.	X	.	.	.	.	.	.	.	.	.	.	.	.	C	G
	244.3	801.5	.	.	.	.	.	.	.	.	.	.	.	.	.	.	.	.	.	.	.	.	.	.	.	.	.	.	.	.	.	.	.	.	C	G
	245.0	803.8	.	.	.	.	.	.	.	.	.	.	.	.	.	.	.	.	.	.	.	.	.	.	.	.	.	.	.	.	.	.	.	.	C	G
	246.0	807.0	.	.	.	.	.	.	.	.	.	.	.	.	.	.	.	.	.	.	.	.	.	.	.	.	.	.	.	.	.	.	.	.	C	G
	247.6	812.4	.	.	.	.	.	.	.	.	.	.	.	.	.	.	.	.	.	.	.	.	.	.	.	.	.	.	.	.	.	.	.	.	A	G
	251.5	825.2	.	.	.	.	.	.	.	.	.	.	.	.	.	.	.	.	.	.	.	.	.	.	.	.	.	.	.	.	.	.	.	.	C	G
	253.3	831.2	.	.	.	.	.	.	.	.	.	.	.	.	.	.	.	.	.	.	.	.	.	.	.	.	.	.	.	.	.	.	.	.	C	G
	254.0	833.2	.	.	.	.	.	.	.	.	.	.	.	.	.	.	.	.	.	.	.	.	.	.	.	.	.	.	.	.	.	.	.	1	C	G
	255.3	837.5	.	.	.	.	.	.	.	.	.	.	.	.	.	.	.	.	.	.	.	.	.	.	.	.	.	.	.	.	.	.	.	.	C	G
	258.0	846.4	.	.	.	.	.	.	.	.	.	.	.	.	.	.	.	.	.	.	.	.	.	.	.	.	.	.	.	.	.	.	.	.	C	G
	258.8	849.0	.	.	.	.	.	.	.	.	.	.	.	.	.	.	.	.	.	.	.	.	.	.	.	.	.	.	.	.	.	.	.	.	C	G
	260.0	853.0	.	.	.	.	.	.	.	.	.	.	.	.	.	.	.	.	.	.	.	.	.	.	.	.	.	.	.	.	.	.	.	.	C	G
	262.0	859.5	.	.	.	.	.	.	.	.	.	.	.	.	.	.	.	.	.	.	.	.	.	.	.	.	.	.	.	.	.	.	.	.	C	M
	263.0	863.0	.	.	.	.	.	.	.	.	.	.	.	.	.	.	.	.	.	.	.	.	.	.	.	.	.	.	.	.	.	.	.	.	C	G
	266.2	873.2	.	.	.	.	.	.	.	.	.	.	.	.	.	.	.	.	.	.	.	.	.	.	.	.	.	.	.	.	.	.	.	.	C	G
Crater unit B	278.4	913.4	.	.	.	.	.	.	.	.	.	.	.	.	.	.	.	.	.	.	.	.	.	.	.	.	.	.	.	.	.	.	.	.		
	281.3	923.1	.	.	.	.	.	.	.	.	.	.	.	.	.	.	.	.	.	.	.	.	.	.	.	.	.	.	.	.	.	.	.	.		
	298.5	979.3	.	.	.	.	.	.	.	.	.	.	.	.	.	.	.	.	.	.	.	.	.	.	.	.	.	.	.	.	.	.	.	.	F	M
	313.7	1,029.3	.	.	.	.	.	.	.	.	.	.	.	.	.	.	.	.	.	.	.	.	.	.	.	.	.	.	.	.	.	.	.	.		
	324.1	1,063.3	.	.	.	.	.	.	.	.	.	.	.	.	.	.	.	.	.	.	.	.	.	.	.	.	.	.	.	.	.	.	.	.		
	360.2	1,181.9	.	.	.	.	.	.	.	.	.	.	.	.	.	.	.	.	.	.	.	.	.	.	.	.	.	.	.	.	.	.	.	.		
	366.6	1,202.9	.	.	.	.	.	.	.	.	.	.	.	.	.	.	.	.	.	.	.	.	.	.	.	.	.	.	.	.	.	.	.	.		
	376.9	1,236.7	.	.	.	.	.	.	.	.	.	.	.	.	.	.	.	.	.	.	.	.	.	.	.	.	.	.	.	.	.	.	.	.		
	406.1	1,332.5	.	.	.	.	.	.	.	.	.	.	.	.	.	.	.	.	.	.	.	.	.	.	.	.	.	.	.	.	.	.	.	.		
	410.7	1,347.3	.	.	.	.	.	.	.	.	.	.	.	.	.	.	.	.	.	.	.	.	.	.	.	.	.	.	.	.	.	.	.	.		
	442.4	1,451.5	.	.	.	.	.	.	.	.	.	.	.	.	.	.	.	.	.	.	.	.	.	.	.	.	.	.	.	.	.	.	.	.		

[a]Abundance: A, abundant (≥10 specimens per field of view); C, common (1–9 specimens per field of view); F, frequent (1 specimen per 1–10 fields of view).
[b]Preservation: G, good; M, moderate.

Figure D7. Continued.

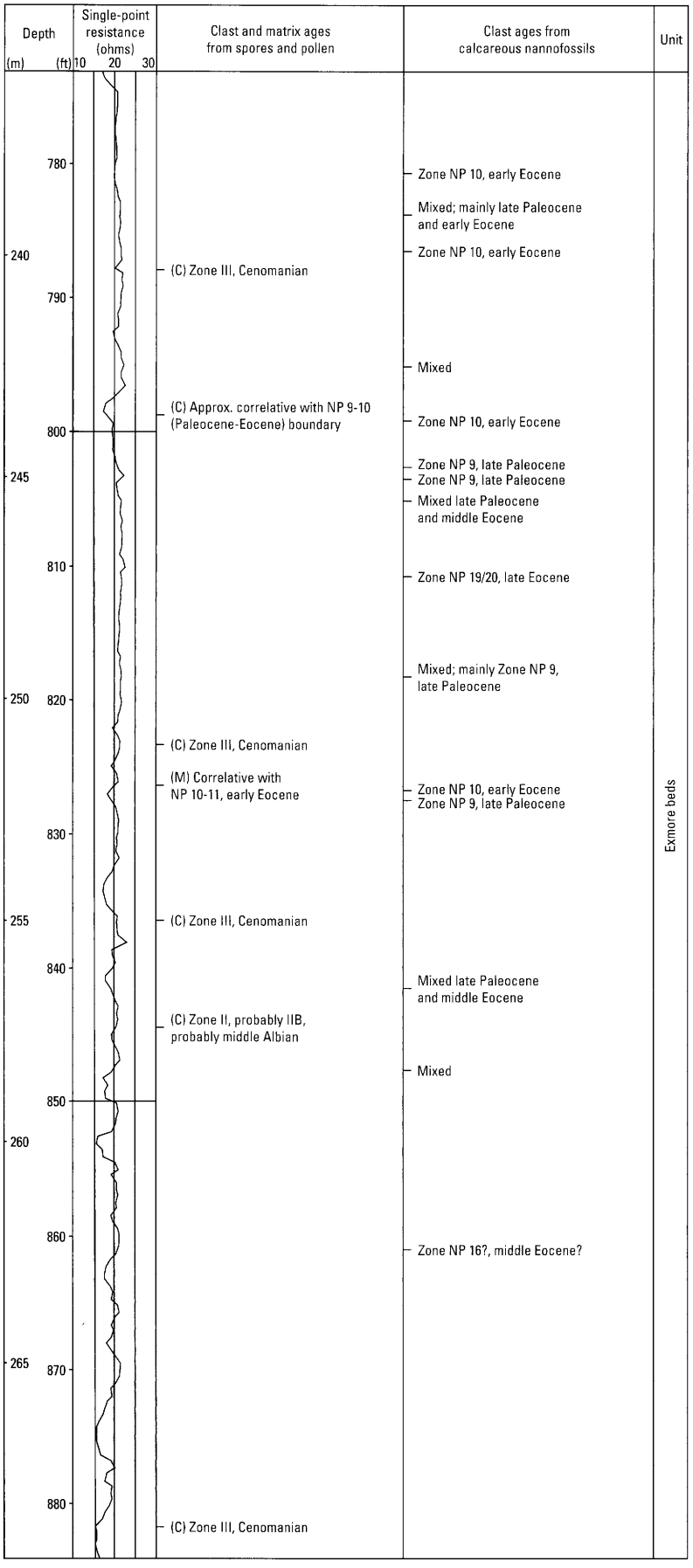

Figure D8. Single-point resistance log of the Exmore beds in the USGS-NASA Langley core, with a summary of spore-pollen ages of clast (C) and matrix (M) samples and calcareous nannofossil ages of clast samples.

assemblage might well include material of mixed ages. One of the clasts examined for pollen and spores from the Exmore beds is from near the Paleocene-Eocene boundary. The remaining five clast samples are from the Potomac Formation; one is probably from the middle Albian and four are from the lower Cenomanian. There is no evidence of any particular stratigraphic ordering of these clasts by age.

Dinocysts

Five samples from the matrix material of the Exmore beds were studied for dinoflagellate cysts (table D2; fig. D5). The four lower samples, from 257.6 to 236.1 m (845.3 to 774.6 ft), are from muddy, calcareous, quartz-glauconite sand. The uppermost sample is near the top of the Exmore and consists of massive, sandy, clayey, calcareous quartz silt. The sample from 278.4 m (913.4 ft) in the upper part of crater unit B is included in the discussion below.

Two aspects of the dinocyst assemblages need emphasis: (1) the fossils that are found represent a suite of ages, some known from typical Virginia Coastal Plain assemblages and some not previously reported from Virginia, and (2) the preservation is unusual.

Forty-six species, genera, and genera groups were identified in the matrix samples from the upper part of crater unit B and the Exmore beds (fig. D5). Most of these forms have been found in more than one of the coastal plain units that are the sources for the matrix. Biostratigraphically important forms include *Batiacasphaera baculata* (pl. D1, fig. 2), *Carpatella cornuta* (pl. D1, fig. 19), *Cordosphaeridium funiculatum* (pl. D1, fig. 1), *Dracodinium varielongitudum* (pl. D1, fig. 10; pl. D2, figs. 4–6; pl. D3, figs. 2, 10, 11), *Eocladopyxis* n. sp. A of Edwards (2001) (pl. D1, fig. 12), *Homotryblium tasmaniense* (pl. D1, fig. 11), *Pentadinium goniferum*, and *Pentadinium membranaceum* (pl. D1, figs. 5, 6; pl. D2, fig. 13).

A single, poorly preserved specimen (*Andalusiella* sp., pl. D1, fig. 20) is the only dinocyst evidence thus far of a contribution by Cretaceous units. This specimen was noted in the uppermost matrix sample from the Exmore beds (R6110 DC). Another Cretaceous specimen (*Chatangiella* sp.) was found in the overlying Chickahominy Formation of the Langley core (Edwards and others, this volume, chap. H).

Carpatella cornuta is restricted to the early Paleocene and hence has its source in the Brightseat Formation (table D1). Although no forms specifically restricted to the Aquia Formation were identified, many of the forms encountered are common in the Aquia. *Apectodinium parvum* (pl. D1, figs. 17, 18), which has previously been recorded from the Marlboro Clay (Edwards, 1996), is present in sample R6110 DH. *Dracodinium varielongitudum* and *Homotryblium tasmaniense* are early Eocene species and are common in the Nanjemoy Formation (Edwards, 1996). *Pentadinium goniferum* has a range restricted to the late part of the middle Eocene and is common in the Piney Point Formation (Edwards, 1989). *Batiacasphaera baculata* and *Cordosphaeridium funiculatum* are common in upper Eocene deposits. In summary, many of the dinocysts in the matrix material of the Exmore beds consist of late Eocene taxa that are indistinguishable from those of the Chickahominy Formation; both units have major contributions of dinocysts from the Nanjemoy Formation (lower Eocene) and Piney Point Formation (middle Eocene).

Eocladopyxis n. sp. A of Edwards (2001) has previously been reported only in Alabama and Georgia, in sediments representing the lower part of the middle Eocene (Edwards, 2001). These sediments would be younger than the Nanjemoy Formation and older than the Piney Point. A unit of this intermediate age may once have been present in the Virginia Coastal Plain but has since been eroded away or has not yet been recovered in the subsurface of the coastal plain.

Similarly, *Pentadinium membranaceum* has been reported from the uppermost middle Eocene and lowermost upper Eocene deposits in the Gulf of Mexico Coast (Edwards, 1982). The presence of this species appears to indicate the former existence of a unit younger than the Piney Point Formation but older than the Chickahominy because *P. membranaceum* has not been found in the Chickahominy. Sediments of latest middle Eocene/earliest late Eocene age contributed heavily to the tsunami washback matrix, especially near the top of the Exmore beds, as indicated by the relative abundance of *P. membranaceum* in those strata.

Phthanoperidinium brooksii (pl. D1, fig. 15) has previously been reported from offshore (Edwards and Bebout, 1981). Its presence in the Exmore beds may indicate a contribution from offshore sediments.

It is difficult to describe the dinoflagellates recovered from the Exmore matrix because the overall preservation of palynomorphs is poor. One can recognize material of dinoflagellate origin but sometimes cannot identify it to species or even to genus or family level. Fragments are much more common than whole or nearly whole specimens (table D2). Whole specimens may be folded, corroded, "curled up," "smoothed," or well preserved (Edwards and Powars, 2003). On further examination, many seemingly well preserved specimens are seen to be broken. Breakage is commonly sharp and crosses both tabulation and wall layers (pl. D2, figs. 10, 11).

In all samples, much of the organic material occurs in clumps (pl. D2, figs. 2, 3), and the clumps are distinctive in having many degrees of preservation, including opaque debris, misshapen fragments of miscellaneous plant debris, misshapen fragments of dinoflagellates, and whole, well-preserved dinoflagellate specimens. In the present study, clump size is determined by the sieve sizes used in the preparation of the slides (20–200 μm).

Many specimens have surfaces that are pitted, cratered (features that appear like broken blisters; pl. D3, figs. 4–7), or pockmarked (having distinctive radial features that have been related by previous authors (for example, Elsik, 1966, but see also Edwards and Powars, 2003) to fungal degradation; pl. D3, fig. 10). Species known to have originally smooth surfaces have been heavily corroded (pl. D2, fig. 7). Individual processes

(especially in the *Wetzeliella* group) may be broken off or may be intact but severely pitted or pocked (pl. D3, fig. 2).

Clumped specimens are often seen in unusual orientations. Clumps appear to consist of material that is welded together, although individual pieces sometimes can be teased apart with heat and a paper clip. With less heat, the individual pieces can be moved around slightly in the glycerin jelly mounting medium, but they remain loosely attached at points of contact. Under the scanning electron microscope, points of fusion can be seen (pl. D2, fig. 4). Whole or nearly whole specimens are likely to be either small, as in the *Microdinium* group (pl. D1, figs. 3, 4) and small peridiniacean group (pl. D1, fig. 14), or large and robust, such as *Deflandrea phosphoritica* (pl. D2, fig. 14) and *Dracodinium varielongitudum* (pl. D1, fig. 10).

Fragments are commonly barely recognizable as having dinoflagellate affinity. Most miscellaneous chorate fragments are of the *Glaphyrocysta* group, but a few are of the *Cordosphaeridium* group. These fragments seldom absorb the stain. Delicate meshwork is preserved in many specimens, even where processes are jaggedly broken. Processes may appear shortened (pl. D3, fig. 14).

Fragments belonging to the various species of *Pentadinium*, especially the grano-vermiculate (g/v) ones—*P. goniferum*, *P. laticinctum* (g/v forms), and *P. membranaceum* (pl. D2, figs. 9, 13)—are easy to recognize. Surface texture of these is commonly moderately to slightly subdued (pl. D2, figs. 10–12). Some have almost lost the sculpture, except in the areas that were once below the pericoel. In optical section, the sculpture appears to have been melted or fused. Specimens may be folded (pl. D2, fig. 13; pl. D3, figs. 4–7) but not compressed.

A summary of the counts made is given in table D3 and shown graphically in figures D9 and D10. The percentage of whole or nearly whole specimens (table D3; fig. D10) hovers around 15–25 percent with the notable exception of the highest sand sample (R6110 DD, second sample from the top in figure D10), in which whole specimens are 6.3 percent. The percentage of specimens not identifiable to group (the worst preservation; table D3; fig. D10) is lowest in the lowest sample and increases upward. This concentration of poorly preserved dinocysts may represent specimens from seawater that was subject to the most violent forces of impact, ejection, resurge, or tsunamis. The highest sample studied here, the uppermost Exmore silt (R6110 DC), has fewer unidentifiable specimens (better preservation) than the sand samples below it. This is the same silt that has been described as a fallout layer containing pyrite lattices (Poag, 2002; Poag and Norris, this volume, chap. F).

The matrix sample from the upper part of crater unit B and those from the lower part of the Exmore beds show higher diversity in terms of more recognizable species (fig. D5) than are in the upper part of the Exmore beds. Samples near the top of the Exmore are dominated by species of *Pentadinium* as well as *Dracodinium* and other *Wetzeliella* group forms (Eocene forms; fig. D9). These are the most robust and easy to recognize forms. Stratigraphically lower samples have more small peridiniaceans; these forms, while most are not age diagnostic, are more common in Aquia Formation (Paleocene) sediments than in other units in the coastal plain.

Sample R6110 DE (the third sample from the top in figure D9) merits mention because of its high concentration of *Deflandrea phosphoritica*. In this sample, *D. phosphoritica* makes up 24.6 percent of the specimens counted (fig. D9; table D3), which were mainly poorly preserved. This dinocyst assemblage shows that the slurry of sediments that formed exotic matrix in the upper part of crater unit B and the Exmore beds was heterogeneous. The mixture apparently resulted from differences among sediments originating as ejecta, subaqueous resurge, or tsunami washback and from differences in source beds, variable fluidization, and localized sorting of the sediments. In sample R6110 DE, preservation of the fossils may be important because *D. phosphoritica* is a rather robust species. One preservational effect that does not appear in the counts is that fewer distinct clumps of dinocysts were observed in the stratigraphically lower samples, and these clumps are smaller (pl. D2, figs. 2, 3) than clumps in the higher samples.

Calcareous Nannofossils

Samples of Matrix

Overall, preservation of calcareous nannofossils in the matrix of the Exmore beds in the Langley core is moderate to good. Unlike the dinocysts, the calcareous nannofossils do not exhibit extensive pitting or fracturing. Individual nannofossils are typically whole or have only minor fractures consistent with normal dissolution or diagenesis.

The only exception to this rule is the preservational state of rosette forms of the genus *Discoaster*. Rosette forms such as *D. multiradiatus*, *D. salisburgensis*, *D. lenticularis*, and *D. saipanensis* (pl. D4, figs. 2, 16, 17; pl. D5, fig. 12) are normally round and have between 17 and 30 rays (Wei, 1992). Overgrowth causes thickening of the rays, and dissolution causes shortening of the rays, but normally the specimens retain their round shape. However, specimens in the Exmore beds from the Langley core show distinct fracture patterns not common in rosette discoasters; the patterns result in specimens that are square or pentagonal (Self-Trail, 2003). This phenomenon was illustrated by Poag and Aubry (1995, their fig. 13) in a specimen from the Exmore beds in the Exmore core (fig. D1) that has the same distinct pentagonal appearance, although these authors did not connect the fracturing with the impact. Bybell and Self-Trail (1994) did not document this phenomenon in samples from the New Jersey Coastal Plain.

Commonly, the species present in the Exmore matrix are robust forms like *Dictyococcites bisectus*, *Isthmolithus recurvus*, and *Reticulofenestra umbilica* (pl. D5, figs. 2, 5, 7, 10, 11). These forms dominate the assemblage and commonly exhibit calcite overgrowth, although not enough to impede species identification. Forms prone to dissolution, such as *Sphenolithus* and *Fasciculithus*, are uncommon in the Exmore beds.

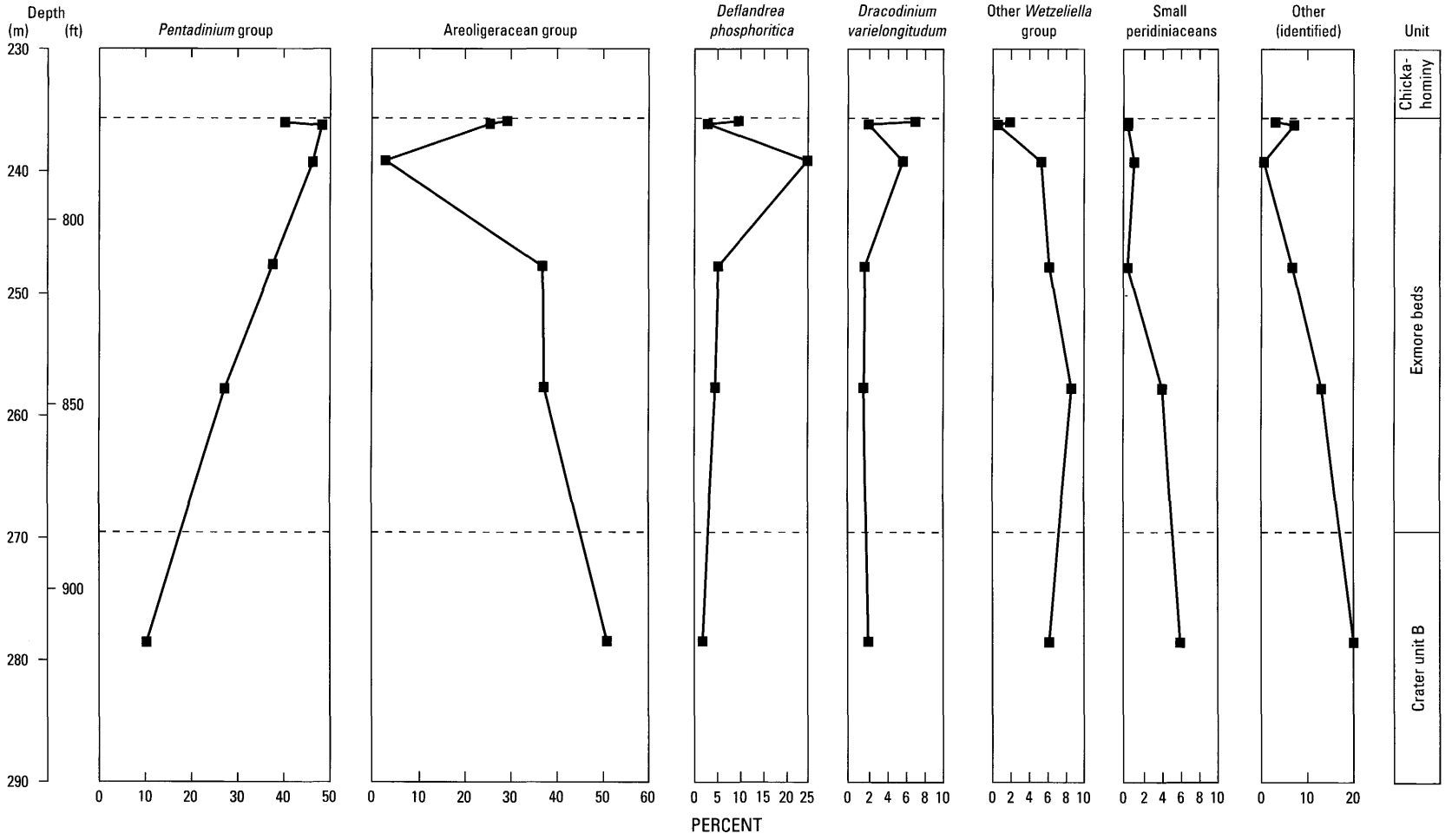

Figure D9. Graphical representation of percentages of the main dinocyst taxa in samples from crater unit B and the Exmore beds in the USGS-NASA Langley core.

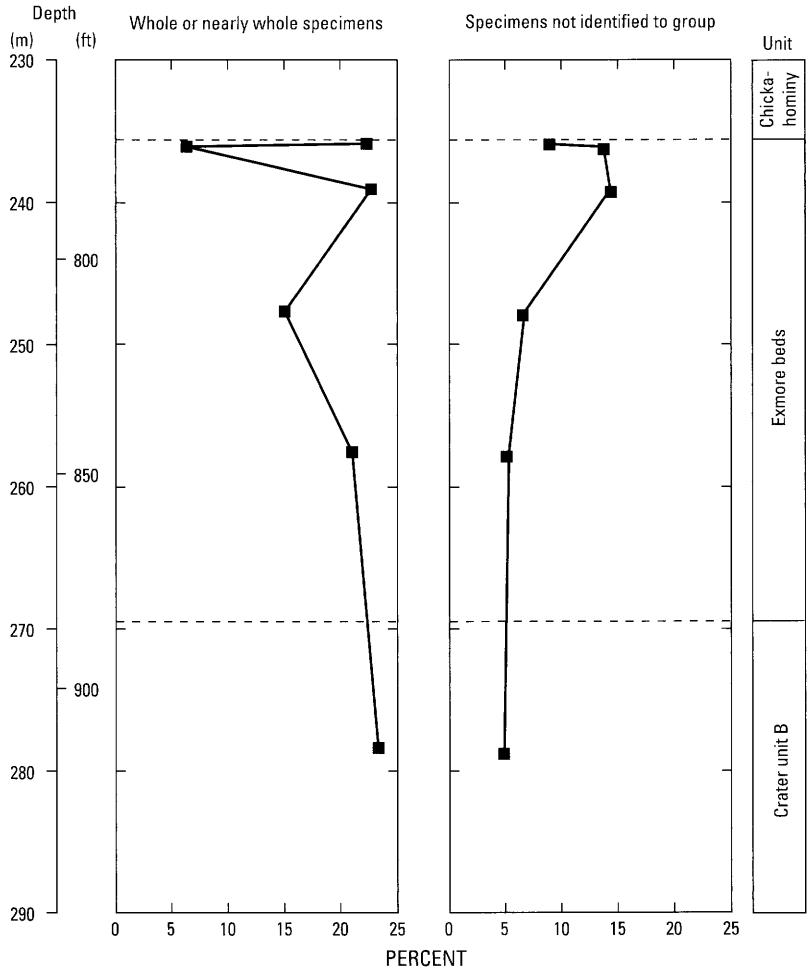

Figure D10. Graphical representation of percentages of whole dinocyst specimens and specimens not identified to group level in samples from crater unit B and the Exmore beds in the USGS-NASA Langley core. "Specimens not identified to group" includes both whole specimens and fragments.

In this study, 165 Tertiary and 32 Late Cretaceous species and genera were identified in the 30 productive matrix samples from crater unit B and the Exmore beds (fig. D7). Biostratigraphically important Tertiary forms include *Cruciplacolithus asymmetricus*, *Prinsius dimorphosus*, *Neobiscutum parvulum*, *Fasciculithus billii*, *Heliolithus riedelii*, *Heliolithus cantabriae*, *Rhomboaster contortus*, *Rhomboaster orthostylus*, *Rhomboaster bramlettei*, *Pemma basquense*, *Pemma serratum*, *Chiasmolithus gigas*, and *Isthmolithus recurvus* (pl. D5, figs. 1, 2, 3, 7). These species are present in situ in the Brightseat, Aquia, Nanjemoy, and Piney Point Formations, the Marlboro Clay, and several unnamed units in the Virginia Coastal Plain.

Cruciplacolithus asymmetricus, *P. dimorphosus*, and *N. parvulum* are restricted to lower Paleocene sediments and thus represent the Brightseat Formation. *Fasciculithus billii*, *Heliolithus cantabriae*, and *H. riedelii* are common in the upper Paleocene Aquia Formation.

Although no forms specifically restricted to the upper Paleocene-lower Eocene Marlboro Clay were identified, many of the species found span the Paleocene-Eocene boundary. Clasts lithologically similar to the Marlboro Clay are common in the matrix material; therefore, it seems likely that fossils from this formation are included in the Exmore beds.

Lower Eocene sediments are also represented by the Nanjemoy Formation. The calcareous nannofossil species *Rhomboaster contortus* and *R. orthostylus* are restricted to the Nanjemoy Formation, and *Rhomboaster bramlettei* is a common constituent of the Nanjemoy assemblages. The middle Eocene Piney Point Formation is represented by common occurrences of *P. basquense* (pl. D5, fig. 1) and *P. serratum* and by rare occurrences of *C. gigas*.

The Exmore beds are no older than Zone NP 19/20 because they contain *Isthmolithus recurvus* (pl. D5, figs. 2, 7), a nannofossil whose first appearance defines the base of this zone. The overlying Chickahominy Formation belongs to Zone NP 19/20 as indicated by the joint occurrences of *I. recurvus* and *Discoaster saipanensis*; the last appearance of the latter species defines the top of Zone NP 19/20. Therefore, the Exmore beds

must also belong to Zone NP 19/20, and the impact must have occurred during the early part of the time represented by this zone or approximately at 35.7–35.8 Ma (million years ago). Some of the material composing the Exmore beds was derived from a preimpact formation belonging to Zone NP 19/20 that apparently was once present in the Virginia Coastal Plain but has since been eroded away or has remained undetected in the subsurface. There is no recorded in situ Zone NP 19/20 material from nearby outcrops or other coreholes that is *not* Chickahominy Formation.

Biostratigraphically important Late Cretaceous forms include *Eiffellithus eximius, Eprolithus floralis, Reinhardtites anthophorus, Stovarius asymmetricus, Flabellites oblonga,* and *Lithastrinus grillii.* These species indicate that sediments of Santonian and Campanian age compose part of the Exmore beds in the Langley core. Age-equivalent sediments from North and South Carolina include the Pleasant Creek Formation (Santonian), the Shepherd Grove Formation (Santonian), the Bladen Formation (Campanian), and the Donoho Creek Formation (Campanian) (Gohn, 1992; Self-Trail and others, 2004). Calcareous nannofossils restricted to the Maastrichtian were not identified from the Exmore beds, and therefore it cannot be stated with any certainty that sediment of late Maastrichtian age (such as the Severn Formation of Maryland) contributed to the matrix material. Sediments of Late Cretaceous age are described from the Dismal Swamp, Fentress, and MW4–1 cores (fig. D1; Powars and others, 1992; Powars and Bruce, 1999; Powars, 2000) to the south of the impact crater, and these strata are most likely the sediment source for the Cretaceous calcareous nannofossil assemblages found in the Exmore beds.

Samples of Clasts

Twenty-six clasts were examined for calcareous nannofossil content from the Exmore beds in the Langley core (table D6; fig. D11). These came from a variety of formations, and the dated clasts are from late Paleocene to late Eocene in age (fig. D8). Nine of the clasts are barren and most likely of Potomac Formation lithology. Six clasts have nannofossil assemblages of more than one age and it was therefore impossible to identify the formation of origin.

Two clasts from the Aquia Formation are identified on the basis of lithology and the calcareous nannofossil assemblage. These clasts contain both *Discoaster multiradiatus* (pl. D4, figs. 2, 16) and *Transversopontis pulcher* but do not contain *Rhomboaster bramlettei* or *Rhomboaster orthostylus.* It is interesting to note that both Aquia clasts are from Zone NP 9, even though the Aquia Formation includes Zones NP 5–9. One clay clast dated as late Paleocene (Zone NP 9) is thought to be from the Marlboro Clay because of its lack of glauconite and high percentage of clay.

Clayey clasts containing a calcareous nannofossil assemblage indicative of the lower Eocene Nanjemoy Formation (Zone NP 10) are the most common (table D6). Gibson and Bybell (1994) documented the age of the Nanjemoy Formation as early Eocene (NP 10 through NP 13). However, clasts of Nanjemoy sediments recovered in the Langley core contain *Rhomboaster bramlettei* (pl. D4, fig. 15) and *Discoaster multiradiatus* (pl. D4, figs. 2, 16) but lack younger indicators such as *Rhomboaster orthostylus, Rhomboaster contortus,* and *Discoaster lodoensis,* suggesting a Zone NP 10 assignment for these clasts.

Only one clast of possible middle Eocene age (NP 16) is identified from the Langley core. This possible age is based on the co-occurrence of *Chiasmolithus solitus* (LAD at top of NP 16) and *Cribrocentrum reticulatum* (FAD in middle NP 16). However, because of poor preservation and low diversity of calcareous nannofossil species in this clast, the possibility of a mixed assemblage should not be discounted.

One clast of late Eocene age was identified from the Langley core. This clast contained *Isthmolithus recurvus* (FAD at 36 Ma) along with *Chiasmolithus oamaruensis* (FAD at 37.0 Ma) and *Cribrocentrum reticulatum* (LAD at 35 Ma). The co-occurrence of these three species places this clast within the lowermost part of Zone NP 19/20. This clast is important because it provides strong evidence for the existence of an upper Eocene, preimpact formation in the subsurface of southeastern Virginia that is heretofore unidentified from either outcrop or corehole. Additionally, the co-occurrence of *I. recurvus* and *C. reticulatum* in this sample independently restricts the time of impact to between 36 and 35 Ma.

Preservation and diversity of nannofossils in clasts within the Exmore beds vary considerably from poor to good without any apparent relation to sediment type. For example, clasts of what appear to be sediments from the Aquia or Nanjemoy Formations have nannofossil assemblages that are moderately to well preserved. Species richness is greatest in Aquia and Nanjemoy clasts and decreases in Marlboro and middle Eocene clasts. Most clasts are noncalcareous, are barren of calcareous nannofossils, and represent either a noncalcareous Marlboro Clay lithology or Cretaceous Potomac Formation clasts.

Ostracodes

Two samples from the Exmore beds in the Langley core were examined for ostracodes (not shown in fig. D3). The matrix sample from 240.8–240.9 m (790.1–790.3 ft) contains *Digmocythere russelli* (Howe and Lea 1936). This species (late Eocene and perhaps early Oligocene) is typical of the Chickahominy Formation; because the Chickahominy itself was deposited after the impact, the presence of *D. russelli* supports dinocyst and nannofossil evidence that upper Eocene pre-Chickahominy deposits existed in the region prior to the impact and perhaps still exist there.

Ostracodes from the matrix sample from 235.9 m (773.9–774.0 ft) included bairdiids, *Clithrocytheridea* sp., *Loxoconcha* sp., and *Trachyleberis* cf. *pauca* (Schmidt 1948). This is an anomalous assemblage in terms of genus-level ecology and, therefore, the ostracodes represent a mixed assemblage.

Table D6. Lithologic descriptions and diagnostic calcareous nannofossil species for each calcareous clast examined from the Exmore beds of the USGS-NASA Langley core.

[m, meters; cm, centimeter; in., inch. Some color terms are used from Goddard and others (1948)]

Depth (m)	Lithologic description	Age	Diagnostic calcareous nannofossil species (fig. D11)
238.0	Silt, clayey, micaceous, medium-gray; strong acid fizz.	Early Eocene	*Rhomboaster bramlettei* present; *R. orthostylus* absent.
238.9	Glauconite sand, medium to coarse, muddy, with matrix dike that is 3.04 cm (1.2 in.) long and 0.304 cm (0.12 in.) wide; sharp clast boundaries, full core width.	Mixed	*Discoaster multiradiatus* present with *Coronocyclus nitescens.*
239.7	Silt, clayey, micaceous, medium-gray; strong acid fizz.	Early Eocene	*Rhomboaster bramlettei* present; *R. orthostylus* absent.
242.5	Silt, clayey; clast small.	Mixed	*Toweius occultatus, Cribrocentrum reticulatum,* and *Isthmolithus recurvus* all present.
243.7	Silt, very clayey, calcareous, slightly micaceous, knobby exterior, possible microfossils; full core width; moderate acid fizz.	Early Eocene	*Rhomboaster bramlettei* present; *R. orthostylus* absent.
244.6	Clay, silty, calcareous; clast small.	Late Paleocene	*Discoaster multiradiatus, Prinsius bisulcus,* and *Transversopontis pulcher* present; *Rhomboaster bramlettei* and *R. orthostylus* absent.
245.1	Clay, silty, calcareous; clast small.	Late Paleocene	*Discoaster multiradiatus, Prinsius bisulcus,* and *Transversopontis pulcher* present; *Rhomboaster bramlettei* and *R. orthostylus* absent.
245.6	Clay, silty, dry, dark-greenish-gray (5*GY* 4/1); clast large.	Mixed	*Discoaster multiradiatus, Cribrocentrum reticulatum,* and *Reticulofenestra umbilica* all present.
247.1	Clay, silty, dark-brown; large clast.	Late Eocene	*Isthmolithus recurvus* and *Cribrocentrum reticulatum* present.
249.4	Clay, silty, waxy, dark-yellowish-brown (10*YR* 4/2); contorted.	Mixed	*Transversopontis pulcher, Cribrocentrum reticulatum,* and *Reticulofenestra umbilica* all present.
252.0	Clay, silty, micaceous, calcareous, dark-greenish-gray (5*GY* 4/1); whole core width.	Early Eocene	*Rhomboaster bramlettei* present; *R. orthostylus* absent.
252.2	Clay, silty, micaceous, calcareous, dark-greenish-gray (5*GY* 4/1); whole core width.	Late Paleocene	*Discoaster multiradiatus, Prinsius bisulcus,* and *Transversopontis pulcher* present; *Rhomboaster bramlettei* and *R. orthostylus* absent.
256.5	Sand, very fine to medium, glauconite quartz, calcite-cemented, "salt-and-pepper," light-olive-gray (5*Y* 6/1); whole core width.	Mixed	*Discoaster multiradiatus, Cribrocentrum reticulatum,* and *Pemma stradneri* all present.
258.4	Clay, silty and sandy (5 percent very fine); exterior oxidizes quickly to brown; knobby exterior; interior is greenish black (5*GY* 2/1); full core width.	Mixed	*Discoaster multiradiatus, Cribrocentrum reticulatum,* and *Dictyococcites scrippsae* all present.
262.4	Clay, silty, finely micaceous, dark-greenish-gray (5*GY* 4/1); whole core width.	Middle Eocene	*Cribrocentrum reticulatum* and *Chiasmolithus solitus* both present.

Sample	N10279	N10278	N10277	N10276	N10275	N10274	N10273	N10272	N10271	N10270	N10269	N10268	N10267	N10159
Depth (m)	266.0	265.8	265.2	262.4	261.7	261.2	260.7	259.7	258.4	257.0	256.5	255.8	254.8	252.2
Depth (ft)	872.8	872.0	870.1	861.0	858.5	857.0	855.4	852.0	847.7	843.1	841.5	839.4	835.9	827.4
Nannofossil preservation	Poor	Poor		Poor					Moderate		Moderate			Moderate
Nannofossil abundance	Rare	Rare	Barren	Frequent/Rare	Barren	Barren	Barren	Barren	Frequent	Barren	Frequent	Barren	Barren	Common
Age/zone from which the specimens were derived	Unknown	Unknown		Middle Eocene? (NP 16?)					Mixed		Mixed			Late Paleocene (NP 9)
Possible formation from which the specimens were derived	?	?	?	Unnamed	?	?	?	?	?	?	?	?	?	Marlboro Clay
Tertiary taxa														
Biscutum constans	.	.	.	.	.	.	.	.	.	.	.	.	.	.
Braarudosphaera bigelowii	.	.	.	.	.	.	.	.	.	.	.	.	.	.
Braarudosphaera spp.	.	.	.	.	.	.	.	.	.	.	.	.	.	.
Camplyosphaera dela	.	.	.	.	.	.	.	.	.	.	.	.	.	X
Chiasmolithus bidens	.	.	.	.	.	.	.	.	.	.	X	.	.	.
Chiasmolithus consuetus	.	.	.	.	.	.	.	.	.	.	.	.	.	X
Chiasmolithus oamaruensis	.	.	.	.	.	.	.	.	.	.	.	.	.	.
Chiasmolithus solitus	.	.	.	X	.	.	.	.	.	.	.	.	.	.
Coccolithus pelagicus	.	.	.	.	.	.	.	.	X	.	X	.	.	X
Coronocyclus nitescens	.	.	.	.	.	.	.	.	.	.	.	.	.	.
Coronocyclus spp.	.	.	.	.	.	.	.	.	.	.	.	.	.	X
Cribrocentrum reticulatum	.	.	.	X	.	.	.	.	X	.	X	.	.	.
Cruciplacolithus primus	.	.	.	.	.	.	.	.	.	.	.	.	.	.
Cyclagelosphaera reinhardtii	.	.	.	.	.	.	.	.	.	.	.	.	.	.
Dictyococcites bisectus	.	.	.	.	.	.	.	.	.	.	X	.	.	.
Dictyococcites callidus	.	.	.	.	.	.	.	.	.	.	.	.	.	.
Dictyococcites daviesii	.	.	.	.	.	.	.	.	.	.	.	.	.	.
Dictyococcites scrippsae	.	.	.	.	.	.	.	.	X	.	.	.	.	.
Discoaster anartios	.	.	.	.	.	.	.	.	.	.	.	.	.	X
Discoaster araneus	.	.	.	.	.	.	.	.	.	.	.	.	.	.
Discoaster falcatus	.	.	.	.	.	.	.	.	.	.	.	.	.	X
Discoaster kuepperi	.	.	.	.	.	.	.	.	.	.	.	.	.	.
Discoaster lenticularis	.	.	.	.	.	.	.	.	.	.	.	.	.	.
Discoaster mediosus	.	.	.	.	.	.	.	.	.	.	.	.	.	.
Discoaster megastypus	.	.	.	.	.	.	.	.	.	.	X	.	.	.
Discoaster mohleri	.	.	.	.	.	.	.	.	.	.	.	.	.	.
Discoaster multiradiatus	.	.	.	.	.	.	.	.	X	.	X	.	.	X
Discoaster saipanensis	.	.	.	.	.	.	.	.	.	.	.	.	.	.
Ellipsolithus distichus	.	.	.	.	.	.	.	.	.	.	X	.	.	X
Ellipsolithus macellus	.	.	.	.	.	.	.	.	.	.	.	.	.	.
Ellipsolithus spp.	.	.	.	.	.	.	.	.	.	.	.	.	.	.
Ericsonia cava	.	.	.	.	.	.	.	.	.	.	.	.	.	.
Ericsonia aff. *E. fenestra*	.	.	.	.	.	.	.	.	.	.	.	.	.	.
Ericsonia formosa	.	.	.	.	.	.	.	.	.	.	X	.	.	X
Ericsonia robusta	.	.	.	.	.	.	.	.	.	.	.	.	.	.
Ericsonia subpertusa	.	.	.	.	.	.	.	.	.	.	.	.	.	.
Fasciculithus aubertae	.	.	.	.	.	.	.	.	.	.	.	.	.	.
Fasciculithus involutus	.	.	.	.	.	.	.	.	.	.	X	.	.	.
Fasciculithus sidereus	.	.	.	.	.	.	.	.	.	.	X	.	.	X
Fasciculithus thomasii	.	.	.	.	.	.	.	.	.	.	X	.	.	X
Fasciculithus tympaniformis	.	.	.	.	.	.	.	.	.	.	.	.	.	X
Fasciculithus spp.	.	.	.	.	.	.	.	.	X	.	.	.	.	.

Figure D11. Occurrence chart showing the presence of the calcareous nannofossil taxa, age(s), and probable formations of origin for each calcareous clast sample from the Exmore beds of the USGS-NASA Langley core. Symbols: X, present, ., not present. Abundance terms are defined as follows: rare, 1 specimen per 11–50 fields of view; frequent, 1 specimen per 1–10 fields of view; common, 1–9 specimens per field of view; abundant, 10 or more specimens per field of view.

N10158	N10266	N10265	N10264	N10263	N10157	N10262	N10155	N10261	N10154	N10152	N10151
252.0	251.1	249.4	247.1	245.6	245.1	244.6	243.7	242.5	239.7	238.9	238.0
826.7	823.9	818.2	810.7	805.9	804.0	802.6	799.7	795.5	786.5	783.7	780.7
Good		Moderate	Good	Moderate	Moderate	Moderate	Moderate	Moderate	Moderate	Good	Poor
Abundant	Barren	Frequent	Common	Frequent	Common	Common	Common	Frequent	Common	Abundant	Frequent
Early Eocene (NP 10)		Mixed	Late Eocene (NP 19/20)	Mixed	Late Paleocene (NP 9)	Late Paleocene (NP 9)	Early Eocene (NP 10)	Mixed	Early Eocene (NP 10)	Mixed	Early Eocene (NP 10)
Nanjemoy Formation	?	?	Unnamed	?	Aquia Formation	Aquia Formation	Nanjemoy Formation	?	Nanjemoy Formation	?	Nanjemoy Formation
.	.	.	.	.	.	X	X	.	.	X	.
.	.	.	.	.	.	.	.	X	.	.	.
X	.	.	.	.	.	.	.	.	.	.	.
X	.	.	.	.	X	X	X	.	X	X	.
.	.	X	.	X	X	X	X	X	X	X	.
X	.	.	.	.	X	X	.	.	.	X	.
.	.	.	X	.	.	.	.	.	.	.	.
.	.	.	.	X	.	.	.	.	.	.	.
X	.	X	X	X	X	X	X	X	X	X	X
.	.	.	X	.	.	X	.	.	.	X	.
.	.	.	.	.	.	.	.	.	.	.	.
.	.	X	X	X	.	.	.	X	.	.	.
.	.	.	.	.	X	X	.	X	.	X	.
.	.	.	.	.	X	.	.	.	.	.	.
.	.	X	X	X	.	.	.	.	.	.	.
.	.	X	X	.	.	.	.	X	.	.	.
.	.	.	.	.	.	.	.	X	.	.	.
.	.	.	.	.	.	.	.	.	.	.	.
.	.	.	.	.	.	.	.	.	.	.	.
X	.	.	.	.	.	.	.	.	.	.	.
X	.	.	.	.	X	.	.	.	X	.	.
.	.	.	.	X	.	.	.	.	.	.	.
X	.	.	.	.	X	X	X	.	X	.	.
X	.	.	.	.	.	.	.	.	X	.	.
.	.	.	.	.	.	.	.	.	.	.	.
.	.	.	.	.	.	X	.	.	.	X	.
X	.	.	.	X	X	X	X	.	X	X	X
.	.	.	.	X	.	.	.	.	.	.	.
X	.	.	.	.	X	X	X	.	X	X	.
.	.	.	.	X	.	.	X	.	.	X	.
.	.	.	.	.	.	.	.	.	.	X	.
.	.	.	.	.	.	X	X	.	.	.	.
.	.	.	.	X	.	.	.	.	.	.	.
.	.	.	X	.	.	.	.	X	.	.	.
.	.	.	.	.	.	.	.	.	.	X	.
.	.	.	.	.	X	.	X	.	X	.	.
X	.	.	.	.	.	.	.	.	.	.	.
X	.	.	.	.	.	X	X	.	X	.	X
.	.	.	.	.	.	.	.	.	.	.	X
X	.	.	.	.	.	.	.	.	.	.	.
.	.	.	.	.	.	X	.	.	.	.	.
.	.	.	.	.	.	.	.	.	.	X	.

Figure D11. Continued.

Sample	N10279	N10278	N10277	N10276	N10275	N10274	N10273	N10272	N10271	N10270	N10269	N10268	N10267	N10159
Depth (m)	266.0	265.8	265.2	262.4	261.7	261.2	260.7	259.7	258.4	257.0	256.5	255.8	254.8	252.2
Depth (ft)	872.8	872.0	870.1	861.0	858.5	857.0	855.4	852.0	847.7	843.1	841.5	839.4	835.9	827.4
Nannofossil preservation	Poor	Poor		Poor					Moderate		Moderate			Moderate
Nannofossil abundance	Rare	Rare	Barren	Frequent/Rare	Barren	Barren	Barren	Barren	Frequent	Barren	Frequent	Barren	Barren	Common
Age/zone from which the specimens were derived	Unknown	Unknown		Middle Eocene? (NP 16?)					Mixed		Mixed			Late Paleocene (NP 9)
Possible formation from which the specimens were derived	?	?	?	Unnamed	?	?	?	?	?	?	?	?	?	Marlboro Clay
Helicosphaera seminulum	.	.	.	.	.	.	.	.	.	.	X	.	.	.
Hornibrookina arca	.	.	.	.	.	.	.	.	X	.	X	.	.	X
Isthmolithus recurvus	.	.	.	.	.	.	.	.	.	.	.	.	.	.
Lophodolithus nascens	.	.	.	.	.	.	.	.	.	.	.	.	.	.
Markalius inversus	.	.	.	.	.	.	.	.	.	.	X	.	.	X
Neochiastozygus concinnus	.	.	.	.	.	.	.	.	.	.	.	.	.	.
Neochiastozygus junctus	.	.	.	.	.	.	.	.	X	.	X	.	.	X
Neococcolithes dubius	.	.	.	.	.	.	.	.	.	.	.	.	.	.
Neococcolithes minutus	.	.	.	.	.	.	.	.	.	.	.	.	.	.
Neococcolithes protenus	.	.	.	.	.	.	.	.	.	.	.	.	.	X
Neocrepidolithus biskayae	.	.	.	.	.	.	.	.	.	.	.	.	.	.
Neocrepidolithus bukryi	.	.	.	.	.	.	.	.	.	.	.	.	.	.
Pemma stradneri	.	.	.	.	.	.	.	.	.	.	X	.	.	.
Pontosphaera multipora	.	.	.	X	.	.	.	.	.	.	X	.	.	.
Pontosphaera spp.	.	.	.	.	.	.	.	.	.	.	X	.	.	.
Prinsius bisulcus	.	.	.	.	.	.	.	.	.	.	.	.	.	X
Pseudotriquetrorhabdulus inversus	.	.	.	.	.	.	.	.	.	.	.	.	.	.
Reticulofenestra daviesii	.	.	.	.	.	.	.	.	X	.	.	.	.	.
Reticulofenestra dictyoda	.	.	.	X	.	.	.	.	X	.	X	.	.	.
Reticulofenestra umbilica	.	.	.	.	.	.	.	.	.	.	.	.	.	.
Rhomboaster bramlettei	.	.	.	.	.	.	.	.	.	.	.	.	.	.
Rhomboaster calcitrapa	.	.	.	.	.	.	.	.	.	.	.	.	.	.
Rhomboaster digitalis	.	.	.	.	.	.	.	.	.	.	.	.	.	.
Scapholithus apertus	.	.	.	.	.	.	.	.	.	.	X	.	.	.
Sphenolithus anarrhopus	.	.	.	.	.	.	.	.	.	.	.	.	.	.
Sphenolithus moriformis	.	.	.	.	.	.	.	.	.	.	.	.	.	.
Sphenolithus primus	.	.	.	.	.	.	.	.	X	.	X	.	.	X
Thoracosphaera spp.	.	.	.	.	.	.	.	.	.	.	.	.	.	X
Toweius callosus	.	.	.	.	.	.	.	.	.	.	X	.	.	.
Toweius eminens var. *eminens*	.	.	.	.	.	.	.	.	.	.	X	.	.	.
Toweius eminens var. *tovae*	.	.	.	.	.	.	.	.	.	.	.	.	.	.
Toweius occultatus	.	.	.	.	.	.	.	.	.	.	X	.	.	X
Toweius pertusus	.	.	.	.	.	.	.	.	X	.	X	.	.	X
Toweius serotinus	.	.	.	.	.	.	.	.	.	.	X	.	.	.
Transversopontis obliquipons	.	.	.	.	.	.	.	.	.	.	.	.	.	.
Transversopontis pulcher	.	.	.	.	.	.	.	.	X	.	X	.	.	X
Transversopontis zigzag	.	.	.	.	.	.	.	.	.	.	.	.	.	.
Zygodiscus herlynii	.	.	.	.	.	.	.	.	.	.	X	.	.	.
Zygrhablithus bijugatus	.	.	.	.	.	.	.	.	.	.	X	.	.	.
placoliths	X	X	.	.	.	.	.	.	.	.	.	.	.	.
Cretaceous taxon														
Microrhabdulus attenuatus	.	.	.	.	.	.	.	.	.	.	.	.	.	.

Figure D11. Continued.

N10158	N10266	N10265	N10264	N10263	N10157	N10262	N10155	N10261	N10154	N10152	N10151
252.0	251.1	249.4	247.1	245.6	245.1	244.6	243.7	242.5	239.7	238.9	238.0
826.7	823.9	818.2	810.7	805.9	804.0	802.6	799.7	795.5	786.5	783.7	780.7
Good		Moderate	Good	Moderate	Moderate	Moderate	Moderate	Moderate	Moderate	Good	Poor
Abundant	Barren	Frequent	Common	Frequent	Common	Common	Common	Frequent	Common	Abundant	Frequent
Early Eocene (NP 10)		Mixed	Late Eocene (NP 19/20)	Mixed	Late Paleocene (NP 9)	Late Paleocene (NP 9)	Early Eocene (NP 10)	Mixed	Early Eocene (NP 10)	Mixed	Early Eocene (NP 10)
Nanjemoy Formation	?	?	Unnamed	?	Aquia Formation	Aquia Formation	Nanjemoy Formation	?	Nanjemoy Formation	?	Nanjemoy Formation
.	.	.	.	.	.	.	.	.	.	.	.
.	.	.	.	.	X	X	.	X	.	.	.
.	.	.	X	.	.	.	.	X	.	.	.
.	.	.	.	.	X	.	.	.	.	X	.
X	.	.	.	.	.	.	X	.	X	X	X
X	.	.	.	.	.	X	X	.	.	.	.
.	.	X	.	X	X	X	X	X	X	X	X
.	.	.	.	.	.	X	.	.	.	.	.
.	.	.	.	X	.	.	.	X	.	X	.
X	.	.	.	.	X	X	X	.	X	.	.
.	.	.	.	X	.	.	.	.	.	.	.
.	.	.	.	.	X	.	.	.	.	.	.
.	.	.	.	.	.	.	.	.	.	.	.
.	.	X	X	X	.	.	.	.	.	.	.
.	.	.	.	.	X	.	.	.	.	X	.
.	.	.	.	.	X	X	.	.	.	X	.
.	.	.	X	.	.	.	.	.	.	.	.
.	.	.	.	.	.	.	.	.	.	.	.
.	.	X	X	X	.	.	.	X	.	.	.
.	.	X	X	X	.	.	.	X	.	.	.
X	.	.	.	.	.	.	X	.	X	.	X
.	.	.	.	.	.	.	X	.	.	.	.
.	.	.	.	.	.	.	.	.	.	X	.
.	.	.	.	.	.	.	.	X	.	.	.
.	.	.	.	.	X	.	.	.	.	X	.
.	.	.	.	X	.	.	.	.	.	.	.
.	.	.	.	.	X	X	X	X	X	X	X
.	.	.	.	.	X	.	.	.	.	.	.
.	.	X	.	.	X	X	.	.	.	X	.
.	.	.	.	.	.	X	X	.	.	.	.
.	.	X	.	.	.	X	X	.	X	.	X
.	.	.	.	.	X	X	X	X	X	.	.
X	.	X	.	X	X	X	X	X	X	X	X
X	.	.	.	.	.	X	.	X	X	.	X
.	.	.	X	.	.	.	.	.	.	.	.
X	.	X	.	X	X	X	X	X	X	X	.
.	.	.	.	.	.	.	.	X	.	.	.
X	.	X	.	.	X	X	.	.	X	X	.
.	.	.	.	X	X	.	.	.	.	.	.
.	.	.	.	.	.	.	.	.	.	.	.
.	.	.	.	.	.	.	X	.	.	.	.

Figure D11. Continued.

Discussion and Conclusions

Biostratigraphy of Crater Unit A

The only fossils obtained from the Potomac Formation in crater unit A in the Langley core were spores and pollen grains from a lignitic sample near the top of this unit. The pollen assemblage is from Subzone IIB to Zone III, middle Albian to early Cenomanian in age.

Biostratigraphy of Crater Unit B

Five clast samples from the Potomac Formation in crater unit B in the Langley core could be fairly well dated on the basis of spores and pollen grains. Most or all of the five samples contain at least some Aptian-Albian material, and three contain some Cenomanian material. Several of the samples contain mixed assemblages, indicating that slurry sediment may have penetrated the clasts following the impact.

Six matrix samples from crater unit B were examined for the presence of dinocysts. Only one, from near the top of this unit, appears to contain indigenous dinocysts, and these specimens represent a mixture of ages.

Only one matrix sample from crater unit B, from the upper part of that unit, contained calcareous nannofossils. The mixed assemblage in this sample consists of species having first occurrences (range bases) in various parts of the Paleocene and Eocene; however, no Cretaceous species were found.

Biostratigraphy of the Exmore Beds

The Exmore beds in the Langley core provided spores and pollen grains, dinocysts, calcareous nannofossils, and ostracodes, as well as foraminifers (Poag and Norris, this volume, chap. F). Matrix samples from this interval are generally of mixed ages, but, taken as a group, the matrix and clast samples include fossils of late Aptian to Albian, early Cenomanian, Santonian, Campanian, early Paleocene, late Paleocene, early Eocene, and late middle Eocene ages; that is, they include material derived from the Potomac Formation, the "unnamed Upper Cretaceous deposits" of Powars and Bruce (1999), the Brightseat and Aquia Formations, the Marlboro Clay, and the Nanjemoy and Piney Point Formations (table D1).

Among the dinocyst, nannofossil, and ostracode taxa in the uppermost part of crater unit B and the Exmore beds are several that are of early middle Eocene and of latest middle Eocene to earliest late Eocene ages; these ages indicate that, at the time of impact, strata existed that were younger than the Nanjemoy Formation but older than the Piney Point Formation, and younger than the Piney Point Formation but older than the Chickahominy Formation. Therefore, two stratigraphic units were present prior to the impact that are not now known to exist on the Virginia Coastal Plain. In particular, sediments younger than the Piney Point Formation but older than the Chickahominy Formation contributed heavily to the matrix of the Exmore beds. Therefore, these samples from the Langley core are very important because they provide a more detailed account than was previously available of the full array of Eocene formations in Virginia, especially those that previously existed near the surface but which now may exist only in the subsurface.

Some evidence exists for age stratification of dinocysts and calcareous nannofossils in the matrix of the upper part of crater unit B and the Exmore beds, but the evidence is somewhat contradictory. Dinocysts derived mainly from younger preimpact deposits are more common in the upper part of the Exmore beds, whereas specimens derived mainly from older Tertiary deposits are more common in the lower part of the Exmore and the uppermost part of crater unit B. Therefore, it appears that older sediments on the average were washed back into the crater before the younger sediments. Late Cretaceous nannofossils are present in the Exmore beds down to a depth of 242.1 m (794.4 ft), but they are more common near the top of the unit and decrease in abundance and diversity downsection (fig. D7); no Late Cretaceous nannofossils were found in the single nannofossil-bearing sample from crater unit B. This nannofossil distribution implies that Upper Cretaceous sediments are slightly finer grained (and therefore were slower to sink in the ocean) or perhaps came from a different source area than the Tertiary sediments.

Effects of the Comet or Asteroid Impact on the Preservation of Microfossils

Dinocysts

Dinoflagellate cysts are composed of a waxlike hydrocarbon called dinosporin. The effects of heat on palynomorphs (including dinoflagellate cysts) have been studied extensively by the petroleum industry. At temperatures between 65°C and 170°C, gas and oil are generated; above about 200°C, most organic material is carbonized (Batten, 1996, and references therein).

Dinocysts at the center of the impact would have been vaporized. Dinocysts in resurge and tsunami deposits must have been subjected to varying amounts of heat, pressure, and turbulence from the impact. Dinocysts may have been ejected into the atmosphere by the impact and settled back down over a short interval of time. One can speculate that the causes of fragmentation include both direct shock and pummeling of the dinocysts by large and small grains and clasts in the extremely turbulent synimpact depositional regime.

Foreshortened processes on some dinocyst specimens give the appearance of partial melting, not enough to destroy the shape, but sufficient to fuse fibrous areas and turn long, slender processes into shorter, squatty ones. The partial melting may have occurred in air or water or both. Folded specimens must have been heated in order to bend. Partial melting is also the

most likely explanation for the muted texture of formerly intricately sculptured surfaces. Where this sculpture is preserved below a protective outer layer, one can speculate that the outer layer offered some protection. The wall structure of many dinocysts allows pockets called pericoels. The gas or water in these pericoels must have expanded to cause the bubbles observed (pl. D3, figs. 8, 9).

Some dinocysts and other debris must have been boiled or toasted, as their shape is barely recognizable, and bubbles and craters occur without any relation to wall structure (pl. D3, figs. 4–7). Processes on some specimens appear to have been "blown off" by the force of the impact, commonly leaving pits or scars. One of the more fascinating impact-induced features is the curling of processes around a central body (pl. D3, fig. 13). The bending of the processes suggests aerodynamic or hydrodynamic shaping.

Higher in the Exmore beds, organic material appears more fragmental, but possibly more heat welded into clumps, than it does lower in the Exmore. Local differences occur among individual matrix samples, suggesting differing contributions from the various sources of the matrix material.

For all the features of dinocyst preservation described here, the most likely explanations are direct effects of the comet or asteroid that struck at approximately 35.7–35.8 Ma. Most are the product of a complex interplay of heat, shock, and abrasion. Some of these features shown may prove to be unique to impact-generated sediments. Dinocyst preservation may thus become an important tool for recognizing impact-related deposits elsewhere.

Calcareous Nannofossils

Because of the high temperatures generated by the impact, all calcareous nannofossils at ground zero, like the dinocysts, would have been vaporized. However, calcareous nannofossils in resurge and tsunami deposits would have been subjected to extreme amounts of heat and varying amounts of pressure due to the impact events. Therefore, it is interesting to note that calcareous nannofossil plates in the samples examined show little or no damage due to heat or shock. Unlike many of the dinoflagellates, which were fragmented by shock and pummeling by larger clasts, the calcareous nannofossil assemblage shows only minor fragmentation consistent with normal diagenetic processes. Only one morphotype, rosette discoasters, shows fragmentation, not common in this group, that apparently is due to the impact event.

Acknowledgments

U.S. Geological Survey (USGS) investigations of the Chesapeake Bay impact structure are conducted in cooperation with the Hampton Roads Planning District Commission, the Virginia Department of Environmental Quality, and the National Aeronautics and Space Administration (NASA) Langley Research Center. The Hampton Roads Planning District Commission and the USGS provided funds for the drilling of the USGS-NASA Langley corehole. The NASA Langley Research Center provided extensive operational and logistical support for the drilling operation. The Virginia Department of Environmental Quality and the Department of Geology of the College of William and Mary provided extensive operational support at the drill site.

Ellen Seefelt, Wilma Aleman, and Noelia Baez, all of the USGS, processed the samples for nannofossils, and Seefelt helped prepare the nannofossil plates. Colleen McCartan (USGS) processed the samples for dinocysts and helped prepare the dinocyst plates. McCartan, Aleman, and Baez processed the samples for spores and pollen grains. Chris Nytch (USGS) prepared the ostracode samples. Stephen E. Curtin (USGS) and Richard E. Hodges (USGS) provided the geophysical logs of the Langley corehole. We thank D.J. Nichols (USGS) and C.W. Poag (USGS) for reviewing the manuscript of this chapter and making helpful suggestions for its improvement.

References Cited

Batten, D.J., 1996, Palynofacies and petroleum potential, *in* Jansonius, Jan, and McGregor, D.C., eds., Palynology; Principles and applications: [College Station, Tex.] American Association of Stratigraphic Palynologists Foundation, v. 3, p. 1065–1084.

Baumann, Paul, and Roth, P.H., 1969, Zonierung des Obereozaens und Oligozaens des Monte Cagnero (Zentralapennin) mit planktonischen Foraminiferen und Nannoplankton [Zonation of the upper Eocene and the Oligocene of Cagnero Mountain (central Apennines) on the basis of planktonic foraminifera and nannoplankton]: Eclogae Geologicae Helvetiae, v. 62, no. 1, p. 303–323. (Summary in English.)

Black, Maurice, and Barnes, B., 1959, The structure of coccoliths from the English Chalk: Geological Magazine, v. 96, no. 5, p. 322–327.

Brenner, G.J., 1963, The spores and pollen of the Potomac Group of Maryland: Maryland Department of Geology, Mines and Water Resources Bulletin 27, 215 p., 43 pls.

Bukry, David, 1973, Low-latitude coccolith biostratigraphic zonation, *in* Edgar, N.T., and others, Initial reports of the Deep Sea Drilling Project, v. 15: Washington, D.C., U.S. Government Printing Office, p. 685–703.

Burnett, J.A., 1998, Upper Cretaceous, *in* Bown, P.R., ed., Calcareous nannofossil biostratigraphy: London, Chapman & Hall Press, p. 132–199.

Bybell, L.M., and Gibson, T.G., 1991, Calcareous nannofossils and foraminifers from Paleocene and Eocene strata in Maryland and Virginia *in* Gibson, T.G., and Bybell, L.M., leaders, Paleocene-Eocene boundary sedimentation in the Potomac River valley, Virginia and Maryland: International Geological Correlation Programme (IGCP) Project 308, p. 15–29.

Bybell, L.M., and Gibson, T.G., 1994, Paleogene stratigraphy of the Putneys Mill, New Kent County, Virginia, corehole: U.S. Geological Survey Open-File Report 94–217, 38 p.

Bybell, L.M., and Self-Trail, J.M., 1994, Evolutionary, biostratigraphic, and taxonomic study of calcareous nannofossils from a continuous Paleocene-Eocene boundary section in New Jersey: U.S. Geological Survey Professional Paper 1554, 74 p., 38 pls.

Crux, J.A., Hamilton, G.B., Lord, A.R., and Taylor, R.J., 1982, *Tortolithus* gen. nov. Crux and new combinations of Mesozoic calcareous nannofossils from England: INA (International Nannoplankton Association) Newsletter, v. 4, p. 98–101.

Deck, L.T., 1984, Ostracodes of the Piney Point Formation, Pamunkey River, Virginia, *in* Ward, L.W., and Krafft, Kathleen, eds., Stratigraphy and paleontology of the outcropping Tertiary beds in the Pamunkey River region, central Virginia Coastal Plain—Guidebook for Atlantic Coastal Plain Geological Association Field Trip, October 6–7, 1984: Atlantic Coastal Plain Geological Association, p. 186–191, 6 pls.

Deflandre, Georges, and Fert, Charles, 1954, Observations sur les coccolithophoridés actuels et fossiles en microscopie ordinaire et électronique: Annales de Paléontologie, v. 40, p. 115–176.

DiMarzio, J.A., 1984, Calcareous nannofossils from the Piney Point Formation, Pamunkey River, Virginia, *in* Ward, L.W., and Krafft, Kathleen, eds., Stratigraphy and paleontology of the outcropping Tertiary beds in the Pamunkey River region, central Virginia Coastal Plain—Guidebook for Atlantic Coastal Plain Geological Association Field Trip, October 6–7, 1984: Atlantic Coastal Plain Geological Association, p. 111–116, 10 pls.

Doyle, J.A., 1983, Palynological evidence for Berriasian age of basal Potomac Group sediments, Crisfield well, eastern Maryland: Pollen et Spores, v. 25, no. 3–4, p. 499–530.

Doyle, J.A., and Hickey, L.J., 1976, Pollen and leaves from the mid-Cretaceous Potomac Group and their bearing on early angiosperm evolution, *in* Beck, C.B., ed., Origin and early evolution of angiosperms: New York, Columbia University Press, p. 139–206.

Doyle, J.A., and Robbins, E.I., 1977, Angiosperm pollen zonation of the continental Cretaceous of the Atlantic Coastal Plain and its application to deep wells in the Salisbury Embayment: Palynology, v. 1, p. 43–78.

Edwards, L.E., 1982, Biostratigraphically important species of *Pentadinium* Gerlach 1961 and a likely ancestor, *Hafniasphaera goodmanii* n. sp., from the Eocene of the Atlantic and Gulf Coastal Plains: Palynology, v. 6, p. 105–117.

Edwards, L.E., 1984, Dinocysts of the Tertiary Piney Point and Old Church Formations, Pamunkey River area, Virginia, *in* Ward, L.W., and Krafft, Kathleen, eds., Stratigraphy and paleontology of the outcropping Tertiary beds in the Pamunkey River region, central Virginia Coastal Plain—Guidebook for Atlantic Coastal Plain Geological Association Field Trip, October 6–7, 1984: Atlantic Coastal Plain Geological Association, p. 124–134, 2 pls.

Edwards, L.E., 1989, Dinoflagellate cysts from the lower Tertiary formations, Haynesville cores, Richmond County, Virginia, chap. C *of* Mixon, R.B., ed., Geology and paleontology of the Haynesville cores—Northeastern Virginia Coastal Plain: U.S. Geological Survey Professional Paper 1489, p. C1–C12, 5 pls.

Edwards, L.E., 1996, Graphic correlation of the Marlboro Clay and Nanjemoy Formation (uppermost Paleocene and lower Eocene) of Virginia and Maryland, *in* Jansonius, Jan, and McGregor, D.C., eds., Palynology; Principles and applications: Salt Lake City, American Association of Stratigraphic Palynologists Foundation, v. 3, p. 989–999.

Edwards, L.E., 2001, Dinocyst biostratigraphy of Tertiary sediments from five cores from Screven and Burke Counties, Georgia, chap. G *of* Edwards, L.E., ed., Geology and paleontology of five cores from Screven and Burke Counties, eastern Georgia: U.S. Geological Survey Professional Paper 1603, p. G1–G25, 6 pls.

Edwards, L.E., and Bebout, J.W., 1981, Emendation of *Phthanoperidinium* Drugg & Loeblich 1967, and a description of *P. brooksii* sp. nov. from the Eocene of the Mid-Atlantic Outer Continental Shelf: Palynology, v. 5, p. 29–41.

Edwards, L.E, Goodman, D.K., and Witmer, R.J., 1991, Lower Tertiary (Pamunkey Group) dinoflagellate biostratigraphy, Potomac River area, Virginia and Maryland, *in* Gibson, T.G., and Bybell, L.M., leaders, Paleocene-Eocene boundary sedimentation in the Potomac River valley, Virginia and Maryland: International Geological Correlation Programme (IGCP) Project 308, p. 31–46.

Edwards, L.E., and Powars, D.S., 2003, Impact damage to dinocysts from the late Eocene Chesapeake Bay event: Palaios, v. 18, no. 3, p. 275–285. (Also available online at http://www.bioone.org/pdfserv/i0883-1351-018-03-0275.pdf)

Elsik, W.C., 1966, Biologic degradation of fossil pollen grains and spores: Micropaleontology, v. 12, no. 4, p. 515–518.

Frederiksen, N.O., 1979, Paleogene sporomorph biostratigraphy, northeastern Virginia: Palynology, v. 3, p. 129–167.

Frederiksen, N.O., 1984, Sporomorph correlation and paleoecology, Piney Point and Old Church Formations, Pamunkey River, Virginia, *in* Ward, L.W., and Krafft, Kathleen, eds., Stratigraphy and paleontology of the outcropping Tertiary beds in the Pamunkey River region, central Virginia Coastal Plain—Guidebook for Atlantic Coastal Plain Geological Association Field Trip, October 6–7, 1984: Atlantic Coastal Plain Geological Association, p. 135–149, 1 pl.

Frederiksen, N.O., 1988, Sporomorph biostratigraphy, floral changes, and paleoclimatology, Eocene and earliest Oligocene of the eastern Gulf Coast: U.S. Geological Survey Professional Paper 1448, 68 p., 16 fossil pls., 2 oversize pls.

Frederiksen, N.O., 1991, Midwayan (Paleocene) pollen correlations in the Eastern United States: Micropaleontology, v. 37, no. 2, p. 101–123, 1 pl.

Frederiksen, N.O., and Christopher, R.A., 1978, Taxonomy and biostratigraphy of Late Cretaceous and Paleogene triatriate pollen from South Carolina: Palynology, v. 2, p. 113–145.

Gartner, Stefan, Jr., and Bukry, David, 1969, Tertiary holococcoliths: Journal of Paleontology, v. 43, no. 5, p. 1213–1221.

Gibson, T.G., Andrews, G.W., Bybell, L.M., Frederiksen, N.O., Hansen, Thor, Hazel, J.E., McLean, D.M., Witmer, R.J., and Van Nieuwenhuise, D.S., 1980, Biostratigraphy of the Tertiary strata of the core, *in* Geology of the Oak Grove core: Virginia Division of Mineral Resources Publication 20, p. 14–30.

Gibson, T.G., and Bybell, L.M., 1994 [1995], Sedimentary patterns across the Paleocene-Eocene boundary in the Atlantic and Gulf Coastal Plains of the United States: Bulletin de la Société belge de Géologie, v. 103, no. 3–4, p. 237–265.

Goddard, E.N., and others, 1948, Rock-color chart: Washington, D.C., National Research Council, 6 p. (Republished by Geological Society of America, 1951; reprinted 1995.)

Gohn, G.S., 1992, Revised nomenclature, definitions, and correlations for the Cretaceous formations in USGS-Clubhouse Crossroads #1, Dorchester County, South Carolina: U.S. Geological Survey Professional Paper 1518, 39 p., 1 oversize pl.

Gradstein, F.M., Agterberg, F.P., Ogg, J.G., Hardenbol, Jan, van Veen, Paul, Thierry, Jacques, and Huang, Zehui, 1995, A Triassic, Jurassic and Cretaceous time scale, *in* Berggren, W.A., Kent, D.V., Aubry, M.-P., and Hardenbol, Jan, eds., Geochronology, time scales and global stratigraphic correlation: SEPM (Society for Sedimentary Geology) Special Publication 54, p. 95–126.

Grassé, P.P., 1952, Traité de zoologie: Paris, Masson, 1071 p.

Haq, B.U., 1968, Studies on upper Eocene calcareous nannoplankton from NW Germany: Stockholm Contributions in Geology, v. 18, no. 2, 74 p.

Hay, W.W., Mohler, H.P., Roth, P.H., Schmidt, R.R., and Boudreaux, J.E., 1967, Calcareous nannoplankton zonation of the Cenozoic of the Gulf Coast and Caribbean-Antillean area, and transoceanic correlation: Gulf Coast Association of Geological Societies Transactions, v. 17, p. 428–480.

Hazel, J.E., Bybell, L.M., Christopher, R.A., Frederiksen, N.O., May, F.E., McLean, D.M., Poore, R.Z., Smith, C.C., Sohl, N.F., Valentine, P.C., and Witmer, R.J., 1977, Biostratigraphy of the deep corehole (Clubhouse Crossroads corehole 1) near Charleston, South Carolina, chap. F *of* Rankin, D.W., ed., Studies related to the Charleston, South Carolina, earthquake of 1886—A preliminary report: U.S. Geological Survey Professional Paper 1028, p. 71–89.

Hazel, J.E., Mumma, M.D., and Huff, W.J., 1980, Ostracode biostratigraphy of the lower Oligocene (Vicksburgian) of Mississippi and Alabama: Gulf Coast Association of Geological Societies Transactions, v. 30, p. 361–378, 10 pls.

Johnson, G.H., Powars, D.S., Bruce, T.S., Beach, T.A., Harris, M.S., and Goodwin, B.K., 2001, Post-impact effects of the Eocene Chesapeake Bay impact, lower York-James Peninsula, Virginia: Virginia Geological Field Conference, 31st, Williamsburg, Virginia, October 19 and 20, 2001 [Guidebook], 40 p.

Martini, Erlend, 1971, Standard Tertiary and Quaternary calcareous nannoplankton zonation, *in* Farinacci, Anna, and Matteucci, R., eds., Proceedings of the II Planktonic Conference, Roma, 1970: Rome, Edizioni Tecnoscienza, v. 2, p. 739–785, 4 pls.

Meng, A.A., III, and Harsh, J.F., 1988, Hydrogeologic framework of the Virginia Coastal Plain: U.S. Geological Survey Professional Paper 1404–C, p. C1–C82, 4 oversize pls.

Mixon, R.B., Berquist, C.R., Newell, W.L., Johnson, G.H., Powars, D.S., Schindler, J.S., and Rader, E.K., 1989, Geologic map and generalized cross sections of the Coastal Plain and adjacent parts of the Piedmont, Virginia: U.S. Geological Survey Miscellaneous Investigations Series Map I–2033, 2 sheets, scale 1:250,000.

Okada, Hisatake, and Bukry, David, 1980, Supplementary modification and introduction of code numbers to the low-latitude coccolith biostratigraphic zonation (Bukry, 1973; 1975): Marine Micropaleontology, v. 5, no. 3, p. 321–325.

Olsson, R.K., Gibson, T.G., Hansen, H.J., and Owens, J.P., 1988, Geology of the northern Atlantic Coastal Plain; Long Island to Virginia, *in* Sheridan, R.E., and Grow, J.A., eds., The Atlantic continental margin, U.S., v. I–2 *of* The geology of North America: Boulder, Colo., Geological Society of America, p. 87–105.

Perch-Nielsen, Katharina, 1985, Mesozoic calcareous nannofossils, *in* Bolli, H.M., Saunders, J.B., and Perch-Nielsen, Katharina, eds., Plankton stratigraphy: Cambridge, U.K., Cambridge University Press, p. 329–426.

Perch-Nielsen, Katharina, Sadek, A., Barakat, M.G., and Teleb, F., 1978, Late Cretaceous and early Tertiary calcareous nannofossil and planktonic foraminifera zones from Egypt *in* Actes du VI^{e} Colloque Africain de Micropaléontologie (Tunis, Mars 1974): Tunisia Annales des Mines et de la Géologie, no. 28, v. 2, p. 337–403, 23 pls.

Piveteau, Jean, 1952, Les stades inférieurs d'organisation du Règne animal—Introduction, Généralités, Protistes, Spongiaires, Coelentérés, Bryozoaires, v. 1 *of* Traite´de paléontologie: Paris, Masson, 783 p.

Poag, C.W., 1997, The Chesapeake Bay bolide impact; A convulsive event in Atlantic Coastal Plain evolution: Sedimentary Geology, v. 108, no. 1–4, p. 45–90.

Poag, C.W., 2002, Synimpact-postimpact transition inside Chesapeake Bay crater: Geology, v. 30, no. 11, p. 995–998.

Poag, C.W., and Aubry, M.-P., 1995, Upper Eocene impactites of the U.S. East Coast; Depositional origins, biostratigraphic framework, and correlation: Palaios, v. 10, no. 1, p. 16–43.

Poag, C.W., and Commeau, J.A., 1995, Paleocene to middle Miocene planktic foraminifera of the southwestern Salisbury Embayment, Virginia and Maryland; Biostratigraphy, allostratigraphy, and sequence stratigraphy: Journal of Foraminiferal Research, v. 25, no. 2, p. 134–155, 9 pls.

Poag, C.W., Powars, D.S., Poppe, L.J., and Mixon, R.B., 1994, Meteoroid mayhem in Ole Virginny—Source of the North American tektite strewn field: Geology, v. 22, no. 8, p. 691–694.

Pooser, W.K., 1965, Biostratigraphy of Cenozoic Ostracoda from South Carolina (Arthropoda, article 8): University of Kansas Paleontological Contributions, no. 38, 80 p., 22 pls.

Powars, D.S., 2000, The effects of the Chesapeake Bay impact crater on the geologic framework and the correlation of hydrogeologic units of southeastern Virginia, south of the James River: U.S. Geological Survey Professional Paper 1622, 53 p., 1 oversize pl. (Also available online at http://pubs.usgs.gov/prof/p1622/)

Powars, D.S., and Bruce, T.S., 1999, The effects of the Chesapeake Bay impact crater on the geological framework and correlation of hydrogeologic units of the lower York-James Peninsula, Virginia: U.S. Geological Survey Professional Paper 1612, 82 p., 9 oversize pls. (Also available online at http://pubs.usgs.gov/prof/p1612/)

Powars, D.S., Johnson, G.H., Edwards, L.E., Horton, J.W., Jr., Gohn, G.S., Catchings, R.D., McFarland, E.R., Izett, G.A., Bruce, T.S., Levine, J.S., and Pierce, H.A., 2002, An expanded Chesapeake Bay impact structure, eastern Virginia; New corehole and geophysical data [abs.]: Lunar and Planetary Science Conference, 33d, League City, Tex., March 11–15, 2002, Abstract 1034, available online at http://www.lpi.usra.edu/meetings/lpsc2002/pdf/1034.pdf

Powars, D.S., Mixon, R.B., and Bruce, Scott, 1992, Uppermost Mesozoic and Cenozoic geologic cross section, outer coastal plain of Virginia, *in* Gohn, G.S., ed., Proceedings of the 1988 U.S. Geological Survey Workshop on the Geology and Geohydrology of the Atlantic Coastal Plain: U.S. Geological Survey Circular 1059, p. 85–101.

Self-Trail, J.M., 2003, Shockwave-induced fracturing of calcareous nannofossils from the Chesapeake Bay impact crater: Geology, v. 31, no. 8, p. 697–700.

Self-Trail, J.M., Prowell, D.C., and Christopher, R.A., 2004, The Collins Creek and Pleasant Creek Formations; Two new Upper Cretaceous subsurface units in the Carolina/Georgia Coastal Plain: Southeastern Geology, v. 42, no. 4, p. 237–252.

Sissingh, W., 1977, Biostratigraphy of Cretaceous calcareous nannoplankton: Geologie en Mijnbouw, v. 56, no. 1, p. 37–65.

Stover, L.E., Elsik, W.C., and Fairchild, W.W., 1966, New genera and species of early Tertiary palynomorphs from Gulf Coast: University of Kansas Paleontological Contributions, Paper 5, 11 p., 5 pls.

Stover, L.E., and Hardenbol, Jan, 1993 [1994], Dinoflagellates and depositional sequences in the lower Oligocene (Rupelian) Boom Clay Formation, Belgium: Bulletin de la Société belge de Géologie, v. 102, no. 1–2, p. 5–77, 13 pls.

Stradner, Herbert, and Edwards, A.R., 1968, Electron microscopic studies on upper Eocene coccoliths from the Oamaru Diatomite, New Zealand: Jahrbuch der Geologischen Bundesanstalt Sonderband, v. 13, 66 p.

Swain, F.M., 1952, Part 1, Cenozoic Ostracoda, chap. A *of* Ostracoda from wells in North Carolina: U.S. Geological Survey Professional Paper 234, p. 1–58, pls. 1–7.

Teifke, R.H., 1973, Stratigraphic units of the Lower Cretaceous through Miocene series (pt. 1) and Paleogeology of Early Cretaceous through Miocene time (pt. 2), *in* Geologic studies, Coastal Plain of Virginia: Virginia Division of Mineral Resources Bulletin 83, parts 1 and 2, p. 1–101, oversize pls. 1–21.

Thomson, P.W., and Pflug, H.D., 1953, Pollen und Sporen des mitteleuropäischen Tertiärs: Palaeontographica, ser. B, v. 94, 138 p.

United States Geological Survey, 1986, [Topographic map of the] Newport News North, Virginia [7.5-minute quadrangle showing photorevisions of the 1965 map]: Reston, Va., U.S. Geological Survey, scale 1:24,000.

Wei, Wuchang, 1992, Biometric study of *Discoaster multiradiatus* and its biochronological utility: Memorie di Scienze Geologiche, v. 43, p. 219–235.

Wise, S.W., Jr., and Constans, R.E., 1976, Mid-Eocene planktonic correlations; Northern Italy–Jamaica, W.I.: Gulf Coast Association of Geological Societies Transactions, v. 26, p. 144–155.

Wolfe, J.A., Doyle, J.A., and Page, V.M., 1975 [1976], The bases of angiosperm phylogeny; Paleobotany: Missouri Botanical Garden Annals, v. 62, no. 3, p. 801–824.

Appendix D1. List of Late Cretaceous and Tertiary Calcareous Nannofossil Species Present in Matrix and Clast Samples from Crater Unit B and the Exmore Beds in the USGS-NASA Langley Core, Hampton, Va.

Ahmuellerina octoradiata (Gorka 1957) Reinhardt 1964
Arkhangelskiella cymbiformis Vekshina 1959

Biscutum constans (Gorka 1957) Black *in* Black and Barnes (1959)
Blackites spinosus (Deflandre & Fert 1954) Hay & Towe 1962
Blackites tenuis (Bramlette & Sullivan 1961) Sherwood 1974
Bomolithus conicus (Perch-Nielsen 1971) Perch-Nielsen 1984
Bomolithus elegans Roth 1973
Braarudosphaera bigelowii (Gran & Braarud 1935) Deflandre 1947
Broinsonia dentata Bukry 1969

Calculites obscurus (Deflandre 1959) Prins & Sissingh *in* Sissingh (1977)
Calculites ovalis (Stradner 1963) Prins & Sissingh *in* Sissingh (1977)
Camplyosphaera dela (Bramlette & Sullivan 1961) Hay & Mohler 1967
Chiasmolithus bidens (Bramlette & Sullivan 1961) Hay & Mohler 1967
Chiasmolithus consuetus (Bramlette & Sullivan 1961) Hay & Mohler 1967
Chiasmolithus danicus (Brotzen 1969) Hay & Mohler 1967
Chiasmolithus eograndis Perch-Nielsen 1971
Chiasmolithus expansus (Bramlette & Sullivan 1961) Gartner 1970
Chiasmolithus gigas (Bramlette & Sullivan 1961) Radomski 1968
Chiasmolithus modestus Perch-Nielsen 1971
Chiasmolithus oamaruensis (Deflandre *in* Deflandre and Fert, 1954) Hay, Mohler, & Wade 1966
Chiasmolithus solitus (Bramlette & Sullivan 1961) Locker 1968
Chiasmolithus titus Gartner 1970
Coccolithus pelagicus (Wallich 1877) Schiller 1930
Corollithion signum Stradner 1963
Coronocyclus nitescens (Kamptner 1963) Bramlette & Wilcoxon 1967
Coronocyclus prionion (Deflandre & Fert 1954) Stradner *in* Stradner and Edwards (1968)
Cretarhabdus conicus Bramlette & Martini 1964
Cribrocentrum reticulatum (Gartner & Smith 1967) Perch-Nielsen 1971
Cribrosphaerella ehrenbergii (Arkhangelsky 1912) Deflandre *in* Piveteau (1952)
Cruciplacolithus asymmetricus van Heck & Prins 1987
Cruciplacolithus edwardsii Romein 1979
Cruciplacolithus frequens (Perch-Nielsen 1977) Romein 1979
Cruciplacolithus inseadus Perch-Nielsen 1969
Cruciplacolithus primus Perch-Nielsen 1977
Cruciplacolithus tenuis (Stradner 1961) Hay & Mohler *in* Hay and others (1967)
Cruciplacolithus vanheckae Perch-Nielsen 1984
Cyclagelosphaera prima (Bukry 1969) Bybell & Self-Trail 1995
Cyclagelosphaera reinhardtii (Perch-Nielsen 1968) Romein 1977
Cyclicargolithus floridanus (Roth & Hay *in* Hay and others (1967)) Bukry 1971
Cyclicargolithus luminis (Sullivan 1965) Bukry 1971
Cylindralithus crassus Stover 1966

Daktylethra punctulata Gartner *in* Gartner and Bukry (1969)
Dictyococcites bisectus (Hay & others 1966) Bukry & Percival 1971
Dictyococcites callidus Perch-Nielsen 1971
Dictyococcites daviesii (Haq 1968) Perch-Nielsen 1971
Dictyococcites scrippsae Bukry & Percival 1971
Discoaster anartios Bybell & Self-Trail 1995
Discoaster araneus Bukry 1971
Discoaster barbadiensis Tan 1927
Discoaster deflandrei Bramlette & Riedel 1954
Discoaster diastypus Bramlette & Sullivan 1961
Discoaster falcatus Bramlette & Sullivan 1961
Discoaster gemmifer Stradner 1961
Discoaster kuepperi Stradner 1959
Discoaster lenticularis Bramlette & Sullivan 1961
Discoaster lodoensis Bramlette & Sullivan 1961
Discoaster mahmoudii Perch-Nielsen 1981
Discoaster martinii Stradner 1959
Discoaster mediosus Bramlette & Sullivan 1961
Discoaster megastypus (Bramlette & Sullivan 1961) Perch-Nielsen 1984
Discoaster mohleri Bukry & Percival 1971
Discoaster multiradiatus Bramlette & Reidel 1954
Discoaster nodifer (Bramlette & Reidel 1954) Bukry 1973
Discoaster saipanensis Bramlette & Reidel 1954
Discoaster salisburgensis Stradner 1961
Discoaster septemradiatus (Klumpp 1953) Martini 1958
Discoaster splendidus Martini 1960
Discoaster sublodoensis Bramlette & Sullivan 1961

Discoaster tanii Bramlette & Riedel 1954
Discorhabdus ignotus (Gorka 1957) Perch-Nielsen 1968

Eiffellithus eximius (Stover 1966) Perch-Nielsen 1968
Eiffellithus turriseiffelii (Deflandre *in* Deflandre and Fert (1954)) Reinhardt 1965
Ellipsolithus distichus (Bramlette & Sullivan 1961) Sullivan 1964
Ellipsolithus macellus (Bramlette & Sullivan 1961) Sullivan 1964
Eprolithus floralis (Stradner 1962) Stover 1966
Ericsonia cava (Hay & Mohler 1967) Perch-Nielsen 1969
Ericsonia formosa (Kamptner 1963) Haq 1971
Ericsonia obruta Perch-Nielsen 1971
Ericsonia robusta (Bramlette & Sullivan 1961) Edwards & Perch-Nielsen 1975
Ericsonia subdisticha (Roth & Hay *in* Hay and others (1967)) Roth *in* Baumann and Roth (1969)
Ericsonia subpertusa Hay & Mohler 1967

Fasciculithus aubertae Haq & Aubry 1981
Fasciculithus billii Perch-Nielsen 1971
Fasciculithus involutus Bramlette & Sullivan 1961
Fasciculithus sidereus Bybell & Self-Trail 1995
Fasciculithus thomasii Perch-Nielsen 1971
Fasciculthus tympaniformis Hay & Mohler *in* Hay and others (1967)
Fasciculithus ulii Perch-Nielsen 1971
Flabellites oblonga (Bukry 1969) Crux *in* Crux and others (1982)

Gartnerago obliquum (Stradner 1963) Noel 1970
Glaukolithus diplogrammis (Deflandre *in* Deflandre and Fert (1954)) Reinhardt 1964
Goniolithus fluckigeri Deflandre 1957

Helicolithus trabeculatus (Gorka 1957) Verbeek 1977
Helicosphaera bramlettei (Müller 1970) Jafar & Martini 1975
Helicosphaera compacta Bramlette & Wilcoxon 1967
Helicosphaera euphratis Haq 1966
Helicosphaera intermedia Martini 1965
Helicosphaera lophota Bramlette & Sullivan 1961
Helicosphaera papillata Bukry & Bramlette 1969
Helicosphaera reticulata Bramlette & Wilcoxon 1967
Helicosphaera seminulum Bramlette & Sullivan 1961
*Helicosphaera wilcoxonii (*Gartner 1971) Jafar & Martini 1975
Heliolithus cantabriae Perch-Nielsen 1971
Heliolithus riedelii Bramlette & Sullivan 1961
Holodiscolithus solidus (Deflandre *in* Deflandre and Fert (1954)) Roth 1970
Hornibrookina arca Bybell & Self-Trail 1995

Isthmolithus recurvus Deflandre *in* Deflandre and Fert (1954)

Lanternithus minutus Stradner 1962
Lithastrinus grillii Stradner 1962
Lithostromation operosum (Deflandre *in* Deflandre and Fert (1954)) Bybell 1975
Lithostromation simplex (Klumpp 1953) Bybell 1975
Lophodolithus acutus Bukry & Percival 1971
Lophodolithus nascens Bramlette & Sullivan 1971

Markalius apertus Perch-Nielsen 1979
Markalius inversus (Deflandre *in* Deflandre and Fert (1954)) Bramlette & Martini 1964
Micrantholithus altus Bybell & Gartner 1972
Micrantholithus angulosus Stradner 1961
Micrantholithus mirabilis Locker 1965
Micrantholithus vesper Deflandre *in* Deflandre and Fert (1954)
Microrhabdulus attenuatus (Deflandre 1959) Deflandre 1963
Micula decussata Vekshina 1959

Neobiscutum parvulum (Romein 1979) Varol 1989
Neochiastozygus concinnus (Martini 1961) Perch-Nielsen 1971
Neochiastozygus denticulatus (Perch-Nielsen 1969) Perch-Nielsen 1971
Neochiastozygus distentus (Bramlette & Sullivan 1961) Perch-Nielsen 1971
Neochiastozygus junctus (Bramlette & Sullivan 1961) Perch-Nielsen 1971
Neococcolithes dubius (Deflandre 1954) Black 1967
Neococcolithes minutus (Perch-Nielsen 1967) Perch-Nielsen 1971
Neococcolithes protenus (Bramlette & Sullivan 1961) Black 1967
Neocrepidolithus biskayae Perch-Nielsen 1981
Neocrepidolithus bukryi Perch-Nielsen 1981

Pedinocyclus larvalis (Bukry & Bramlette 1969, 1971) Loeblich & Tappan 1973
Pemma basquense (Martini 1959) Bybell & Gartner 1972
Pemma rotundum Klumpp 1953

Pemma serratum (Chang 1969) Bybell & Gartner 1972
Pemma stradneri (Chang 1969) Bybell & Gartner 1972
Placozygus sigmoides (Bramlette & Sullivan 1961) Romein 1979
Pontosphaera multipora (Kamptner 1948) Roth 1970
Pontosphaera ocellata (Bramlette & Sullivan 1961) Perch-Nielsen 1984
Pontosphaera plana (Bramlette & Sullivan 1961) Haq 1971
Pontosphaera wechesensis (Bukry & Percival 1971) Aubry 1986
Prediscosphaera cretacea (Arkhangelsky 1912) Gartner 1968
Prediscosphaera spinosa (Bramlette & Martini 1964) Gartner 1968
Prinsius bisulcus (Stradner 1963) Hay & Mohler 1967
Prinsius dimorphosus (Perch-Nielsen 1969) Perch-Nielsen 1977
Pseudotriquetrorhabdulus inversus (Bukry & Bramlette 1969) Wise *in* Wise and Constans (1976)

Reinhardtites anthophorus (Deflandre 1959) Perch-Nielsen 1968
Repagulum parvidentatum (Deflandre & Fert 1954) Forchhimer 1972
Reticulofenestra daviesii (Haq 1968) Haq 1971
Reticulofenestra dictyoda (Deflandre *in* Deflandre and Fert (1954)) Stradner *in* Stradner and Edwards (1968)
Reticulofenestra floridana (Roth & Hay *in* Hay and others (1967)) Theodoridis 1984
Reticulofenestra oamaruensis (Deflandre *in* Deflandre and Fert (1954)) Stradner *in* Haq (1968)
Reticulofenestra umbilica (Levin 1965) Martini & Ritzkowski 1968
Rhabdosphaera creber Deflandre *in* Deflandre and Fert (1954)
Rhabdosphaera perlongus (Deflandre *in* Grassé (1952)) Bramlette & Sullivan 1961
Rhabdosphaera pinguis Deflandre *in* Deflandre and Fert (1954)
Rhabdosphaera truncata Bramlette & Sullivan 1961
Rhomboaster bramlettei (Brönnimann & Stradner 1960) Bybell & Self-Trail 1995
Rhomboaster calcitrapa Gartner 1971
Rhomboaster contortus (Stradner 1958) Bybell & Self-Trail 1995
Rhomboaster digitalis (Aubry 1996) Bybell & Self-Trail 1997
Rhomboaster orthostylus (Shamrai 1963) Bybell & Self-Trail 1995
Rhomboaster spineus (Shafik & Stradner 1971) Perch-Nielsen 1984

Scapholithus apertus Hay & Mohler 1967
Sollasites barringtonensis Black 1967
Sphenolithus anarrhopus Bukry & Bramlette 1969
Sphenolithus editus Perch-Nielsen *in* Perch-Nielsen and others (1978)
Sphenolithus intercalaris Martini 1976
Sphenolithus moriformis (Brönnimann & Stradner 1960) Bramlette & Wilcoxon 1967
Sphenolithus primus Perch-Nielsen 1971
Sphenolithus pseudoradians Bramlette & Wilcoxon 1967
Sphenolithus radians Deflandre *in* Grassé (1952)
Sphenolithus spinenger Bukry 1971
Staurolithites imbricatus (Gartner 1968) Burnett 1998
Stovarius asymmetricus (Bukry 1969) Perch-Nielsen 1984

Toweius callosus Perch-Nielsen 1971
Toweius eminens var. *eminens* (Bramlette & Sullivan 1961) Gartner 1971
Toweius eminens var. *tovae* (Bramlette & Sullivan 1961) Perch-Nielsen 1971
Toweius? *magnicrassus* (Bukry 1971) Romein 1979
Toweius occultatus (Locker 1967) Perch-Nielsen 1971
Toweius pertusus (Sullivan 1965) Romein 1979
Toweius serotinus Bybell & Self-Trail 1995
Tranolithus minimus (Bukry 1969) Perch-Nielsen 1984
Transversopontis obliquipons (Deflandre *in* Deflandre and Fert (1954)) Hay & others 1966
Transversopontis pulcher (Deflandre *in* Deflandre and Fert (1954)) Perch-Nielsen 1967
Transversopontis pulcheroides (Sullivan 1964) Báldi-Beke 1971
Transversopontis zigzag Roth & Hay *in* Hay and others (1967)

Vekshinella aachena Bukry 1969
Vekshinella stradneri Rood & others 1971

Watznaueria barnesae (Black *in* Black and Barnes (1959)) Perch-Nielsen 1968

Zygodiscus herlynii Sullivan 1964
Zygrhablithus bijugatus (Deflandre *in* Deflandre and Fert (1954)) Deflandre 1959

Plates D1–D5

Plate D1

Dinoflagellate Cysts from the Impact-Modified and Impact-Generated Deposits, USGS-NASA Langley Core, Hampton, Va.

[Scale bar shown applies to all photomicrographs. Sample depths and assemblages are shown in figure D5]

Figure

1. *Cordosphaeridium funiculatum* Morgenroth 1966, fragment, Exmore beds (sample R6110 DD), internal view, lower focus.
2. *Batiacasphaera baculata* Drugg 1970, fragment, crater unit B (sample R6110 DH), internal view, lower focus.

3, 4. *Histiocysta* sp. of Stover and Hardenbol (1993), crater unit B (sample R6110 DH), orientation uncertain; 3, upper focus; 4, intermediate focus.

5, 6. *Pentadinium membranaceum* (Eisenack 1965) Stover & Evitt 1978, fragment, Exmore beds (sample R6110 DC), exterior views; 5, upper focus; 6, intermediate focus.

7–9. *Fibradinium annetorpense* Morgenroth 1968, Exmore beds (sample R6110 DD), dorsal views; 7, dorsal focus; 8, intermediate focus; 9, ventral focus.

10. *Dracodinium varielongitudum* (Williams & Downie 1966) Costa & Downie 1979, crater unit B (sample R6110 DH), dorsal view, upper focus.
11. *Homotryblium tasmaniense* Cookson & Eisenack 1967, crater unit B (sample R6110 DH), antapical view, intermediate focus.
12. *Eocladopyxis* n. sp. A of Edwards (2001), fragment, crater unit B (sample R6110 DH), interior view, intermediate focus.
13. *Wetzeliella hampdenensis* Wilson 1967, Exmore beds (sample R6110 DG), ventral view, dorsal focus.
14. Miscellaneous small peridiniacean form, crater unit B (sample R6110 DH), ventral view, intermediate focus.
15. *Phthanoperidinium brooksii* Edwards & Bebout 1981, crater unit B (sample R6110 DH), dorsal view, upper focus.
16. *Pentadinium laticinctum* Gerlach 1961 subsp. *laticinctum*, fragment, Exmore beds (sample R6110 DD), external view, upper focus.

17, 18. *Apectodinium parvum* (Alberti 1961) Lentin & Williams 1977, crater unit B (sample R6110 DH), dorsal views; 17, dorsal surface; 18, intermediate focus.

19. *Carpatella cornuta* Grigorovich 1969, Exmore beds (sample R6110 DD), left-lateral view, upper focus.
20. *Andalusiella* Riegel 1974 sp., Exmore beds (sample R6110 DC), ventral view, upper focus.

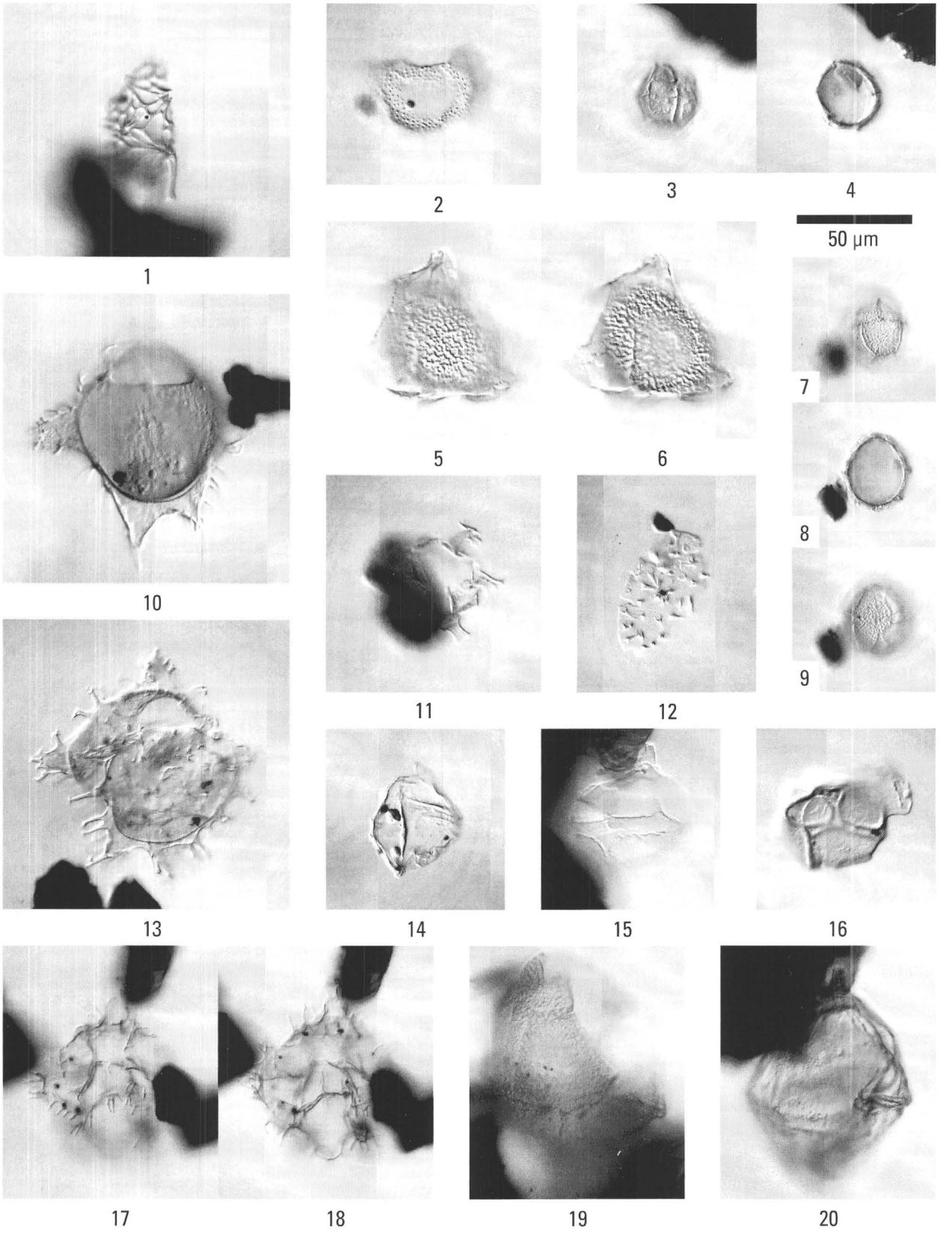

Dinoflagellate Cysts from the Impact-Modified and Impact-Generated Deposits, USGS-NASA Langley Core, Hampton, Va.

Plate D2

Dinoflagellate Cysts from the Impact-Modified and Impact-Generated Deposits, USGS-NASA Langley Core, Hampton, Va.

[Scale bar shown is 6 μm for figures 5 and 6; 30 μm for figures 4, 9, 10, and 13; 40 μm for figures 1, 7, 8, 11, 12, and 14; 150 μm for figures 2 and 3. Sample depths and assemblages are shown in figure D5]

Figure

1. *Exochosphaeridium* Davey et al. 1966 sp., Exmore beds (sample R6110 DF), oblique right-lateral view, upper focus.
2. Clump of loosely welded, acid-resistant debris, highest Exmore beds (sample R6110 DC).
3. Clump of loosely welded, acid-resistant debris, high in crater unit B (sample R6110 DH).

4–6. *Dracodinium varielongitudum* (Williams & Downie 1966) Costa & Downie 1979, Exmore beds (sample R6110 DC), scanning-electron micrographs, ventral surface; 4, entire specimen, welded to debris; 5, detail of fused processes; 6, detail of inflated (bubbled) process.

7. *Deflandrea phosphoritica* Eisenack 1938, fragment showing degraded areas and welded debris, Exmore beds (sample R6110 DF), exterior view, dorsal focus.
8. Chorate dinoflagellate fragment, an example of what was included with the areoligeracean group, Exmore beds (sample R6110 DF), exterior view, upper focus.
9. *Pentadinium* Gerlach 1961 sp., specimen showing sculptured surface, breakage, welded debris, Exmore beds (sample R6110 DC), scanning-electron micrograph, orientation uncertain.
10. *Pentadinium* Gerlach 1961 sp., specimen showing sculptured surface (highly subdued; original surface probably resembled that shown in figure 9), welded debris, Exmore beds (sample R6110 DC), scanning-electron micrograph, left-lateral view.

11, 12. *Pentadinium* Gerlach 1961 sp., fragment showing sculptured surface (highly subdued; original surface probably resembled that shown in figure 9) and optically dense endocyst, Exmore beds (sample R6110 DD), interior views; 11, high focus; 12, lower focus.

13. *Pentadinium membranaceum* (Eisenack 1965) Stover & Evitt 1978, Exmore beds (sample R6110 DC), ventral view, intermediate focus.
14. *Deflandrea* sp., probably *D. phosphoritica* Eisenack 1938, degraded specimen, Exmore beds (sample R6110 DC), ventral view, intermediate focus.

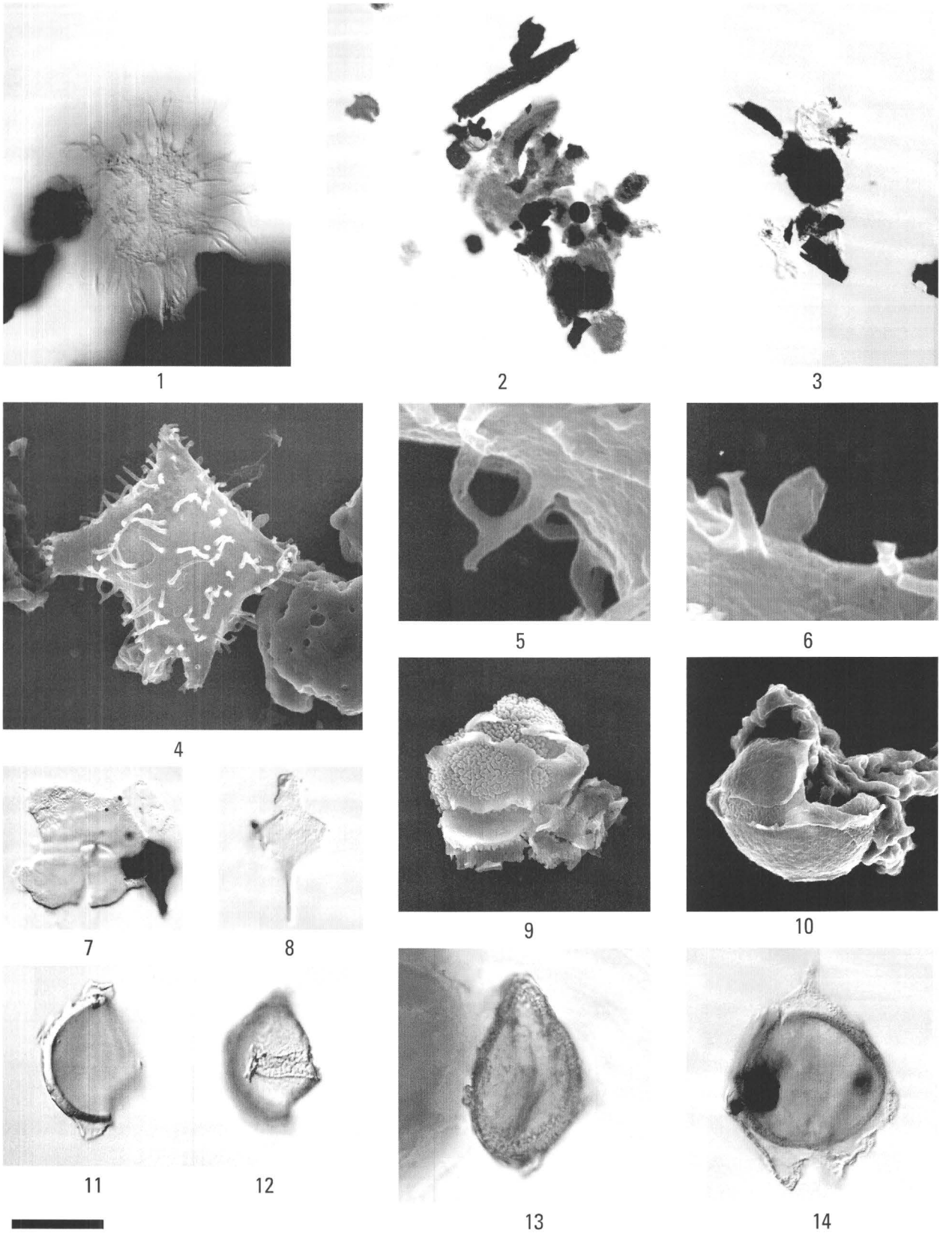

Dinoflagellate Cysts from the Impact-Modified and Impact-Generated Deposits, USGS-NASA Langley Core, Hampton, Va.

Plate D3

Dinoflagellate Cysts from the Impact-Modified and Impact-Generated Deposits, USGS-NASA Langley Core, Hampton, Va., and One Specimen from Outside the Crater, Nanjemoy Formation, Haynesville 1 Core, Richmond County, Va.

[Scale bar shown applies to all photomicrographs. Sample depths and assemblages are shown in figure D5]

Figure

1. *Dracodinium varielongitudum* (Williams & Downie 1966) Costa & Downie 1979, typical, well-preserved specimen from outside the crater, Nanjemoy Formation, Haynesville 1 core (sample R3341 A), Richmond County, Va., dorsal view, upper focus.
2. *Dracodinium varielongitudum* (Williams & Downie 1966) Costa & Downie 1979, poorly preserved specimen, crater unit B (sample R6110 DH), dorsal view, upper focus.
3. Clump of loosely welded, acid-resistant debris with *Dracodinium* or *Wetzeliella* sp., Exmore beds (sample R6110 DD), specimen in ventral view, lower focus.

4–7. *Dracodinium* Gocht 1955 or *Wetzeliella* Eisenack 1938 sp., showing folding and bubbling, Exmore beds (sample R6110 DC), probably ventral views; 4, high focus; 5, high-intermediate focus; 6, low-intermediate focus; 7, low focus. Note that only portions of the specimen are in focus in any photograph because of folding.

8, 9. *Spiniferites* Mantell 1850 sp., fragment showing inflated bases of processes (bubbles), crater unit B (sample R6110 DH); 8, high focus; 9, intermediate focus.

10. *Dracodinium varielongitudum* (Williams & Downie 1966) Costa & Downie 1979, Exmore beds (sample R6110 DG), ventral view of ventral surface. Note star-burst scars where processes once were.
11. *Dracodinium varielongitudum* (Williams & Downie 1966) Costa & Downie 1979?, degraded specimen missing endocyst, Exmore beds (sample R6110 DG), dorsal view, upper focus.
12. Miscellaneous areoligeracean form in a clump of welded debris, crater unit B (sample R6110 DH), dorsal view?, upper focus.
13. Miscellaneous areoligeracean form with curled processes, Exmore beds (sample R6110 DG), ventral view, upper focus.
14. Miscellaneous areoligeracean fragment with curled and partially melted processes, Exmore beds (sample R6110 DG), interior view, lower focus.

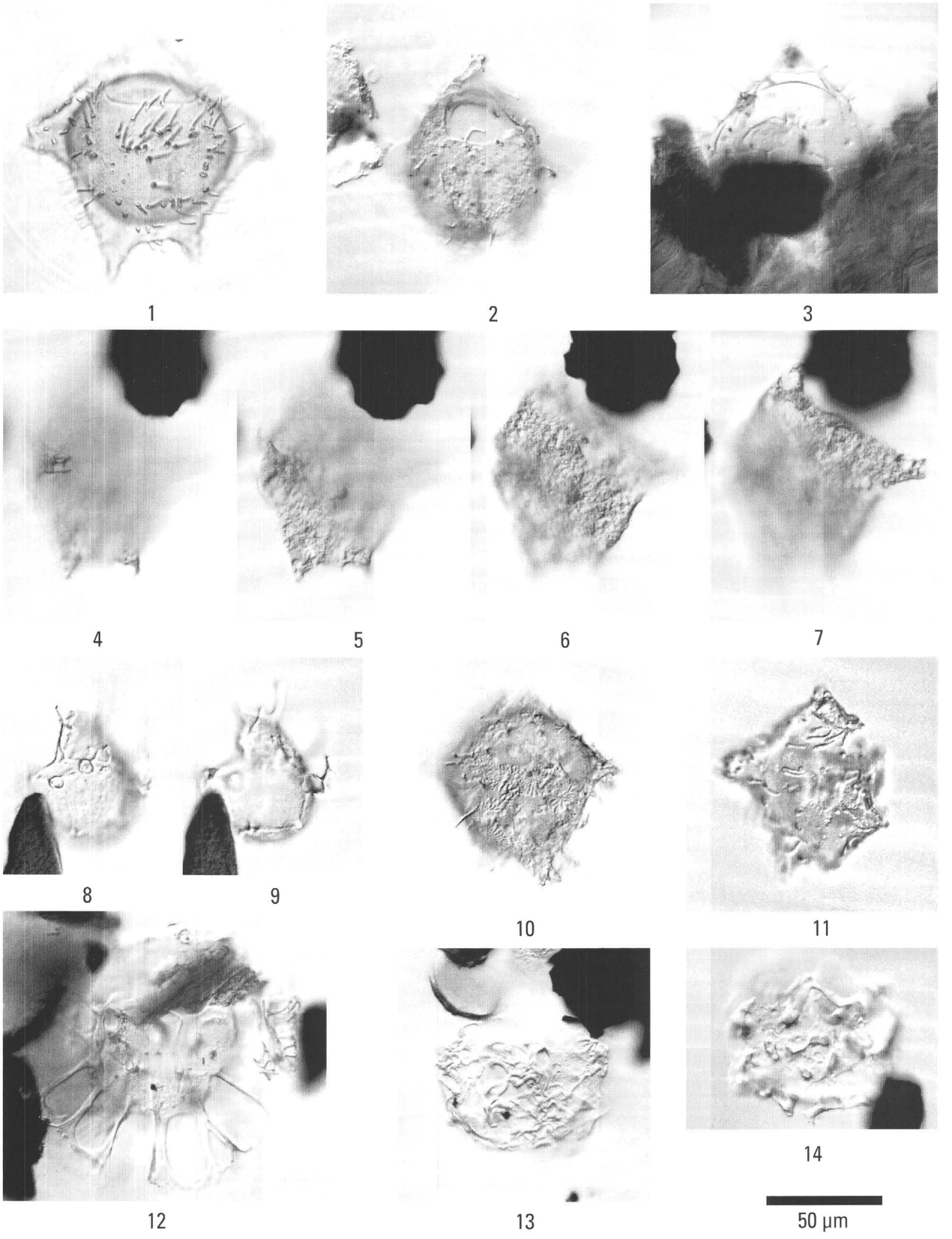

Dinoflagellate Cysts from the Impact-Modified and Impact-Generated Deposits, USGS-NASA Langley Core, Hampton, Va., and One Specimen from Outside the Crater, Nanjemoy Formation, Haynesville 1 Core, Richmond County, Va.

Plate D4

Calcareous Nannofossils from Clasts in the Exmore Beds, USGS-NASA Langley Core, Hampton, Va.

[Sample depths are given in meters (feet) below land surface. XP, cross-polarized light; PC, phase contrast; T, transmitted light; SEM, scanning-electron micrograph]

Figure

1. *Chiasmolithus bidens* (Bramlette & Sullivan 1961) Hay & Mohler 1967; 239.7 m (786.5 ft), XP.
2. *Discoaster multiradiatus* Bramlette & Reidel 1954; 243.7 m (799.7 ft), XP.
3, 4. *Camplyosphaera dela* (Bramlette & Sullivan 1961) Hay & Mohler 1967; 3, 245.0 m (804.0 ft), XP; 4, 243.7 m (799.7 ft), XP.
5. *Dictyococcites callidus* Perch-Nielsen 1971; 247.1 m (810.7 ft), XP.
6. *Neochiastozygus concinnus* (Martini 1961) Perch-Nielsen 1971; 243.7 m (799.7 ft), XP.
7. *Zygodiscus herlynii* Sullivan 1964; 245.0 m (804.0 ft), XP.
8. *Toweius serotinus* Bybell & Self-Trail 1995; 239.7 m (786.5 ft), XP.
9, 10. *Sphenolithus anarrhopus* Bukry & Bramlette 1969; 9, 245.0 m (804.4 ft), XP; 10, same specimen, 45°.
11. *Prinsius bisulcus* (Stradner 1963) Hay & Mohler 1967; 245.0 m (804.0 ft), XP.
12. *Fasciculithus involutus* Bramlette & Sullivan 1961; 243.7 m (799.7 ft), XP.
13. *Toweius callosus* Perch-Nielsen 1971; 245.0 m (804.0 ft), XP.
14. *Toweius occultatus* (Locker 1967) Perch-Nielsen 1971; 239.7 m (786.5 ft), XP.
15. *Rhomboaster bramlettei* (Brönnimann & Stradner 1960) Bybell & Self-Trail 1995; 243.7 m (799.7 ft), XP.
16. *Discoaster multiradiatus* Bramlette & Riedel 1954; 245.0 m (804.0 ft), T.
17. *Discoaster lenticularis* Bramlette & Sullivan 1961; 243.7 m (799.7 ft), SEM, distal view.
18. *Isthmolithus recurvus* Deflandre 1954; 247.1 m (810.7 ft), SEM.
19. *Reticulofenestra umbilica* (Levin 1965) Martini & Ritzkowski 1968; 247.1 m (810.7 ft), SEM, distal view.
20. *Discoaster falcatus* Bramlette & Sullivan 1961; 239.7 m (786.5 ft), PC.
21. *Pontosphaera multipora* (Kamptner 1948) Roth 1970; 247.1 m (810.7 ft), SEM, proximal view.

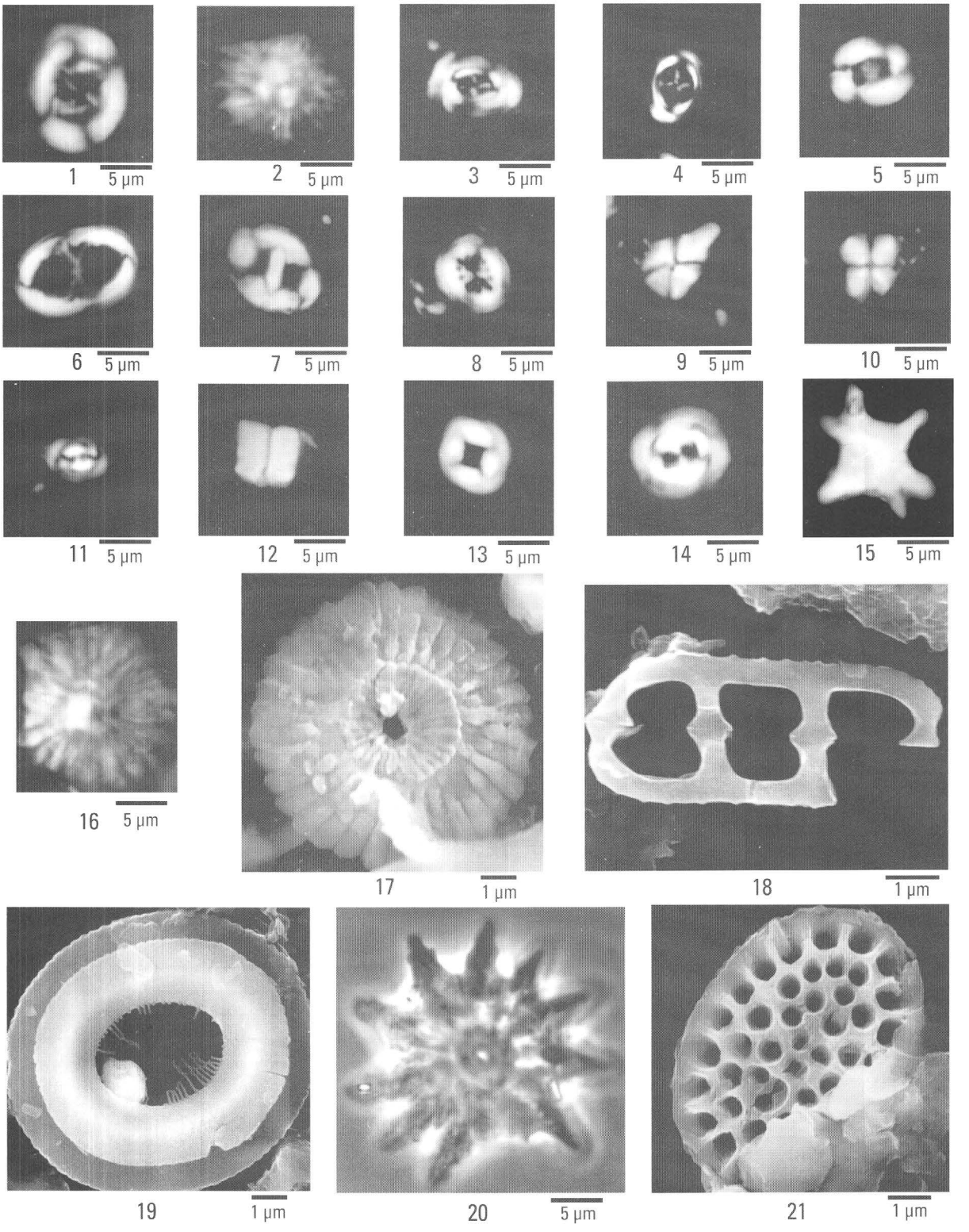

Calcareous Nannofossils from Clasts in the Exmore Beds, USGS-NASA Langley Core, Hampton, Va.

Plate D5

Calcareous Nannofossils from Matrix Material in the Exmore Beds, USGS-NASA Langley Core, Hampton, Va.

[Sample depths are given in meters (feet) below land surface. XP, cross-polarized light; SEM, scanning-electron micrograph]

Figure

1. *Pemma basquense* (Martini 1959) Bybell & Gartner 1972; 245.0 m (803.8 ft), XP.
2, 7. *Isthmolithus recurvus* Deflandre 1954; 2, 236.0 m (774.4 ft), XP; 7, 239.3 m (785.0 ft), SEM.
3. *Heliolithus riedelii* Bramlette & Sullivan 1961; 246.0 m (807.0 ft), XP.
4, 14. *Cribrocentrum reticulatum* (Gartner & Smith 1967) Perch-Nielsen 1971; 4, 236.0 m (774.4 ft), XP; 14, 260.0 m (853.0 ft), distal view, SEM.
5. *Dictyococcites bisectus* (Hay & others 1966) Bukry & Percival 1971; 245.0 m (803.8 ft), XP.
6. *Ellipsolithus macellus* (Bramlette & Sullivan 1961) Sullivan 1964; 258.0 m (846.4 ft), XP.
8. *Hornibrookina arca* Bybell & Self-Trail 1995; 260.0 m (853.0 ft), distal view, SEM.
9, 15. *Chiasmolithus oamaruensis* (Deflandre 1954) Hay, Mohler, & Wade 1966; 9, 236.0 m (774.4 ft), XP; 15, 244.3 m (801.5 ft), distal view, SEM.
10, 11. *Reticulofenestra umbilica* (Levin 1965) Martini & Ritzkowski 1968; 10, 246.0 m (807.0 ft), XP; 11, 244.3 m (801.5 ft), distal view, SEM.
12. *Discoaster multiradiatus* Bramlette & Reidel 1954; 260.0 m (853.0 ft), distal view, SEM.
13. *Cruciplacolithus primus* Perch-Nielsen 1977; 239.3 m (785.0 ft), proximal view, SEM.

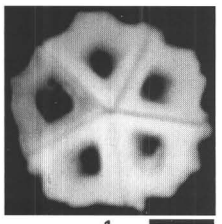

1 5 µm

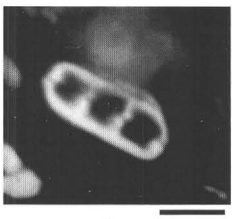

2 5 µm

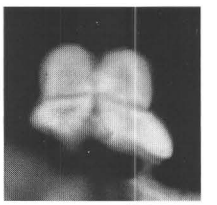

3 5 µm

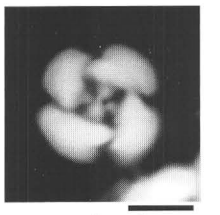

4 5 µm

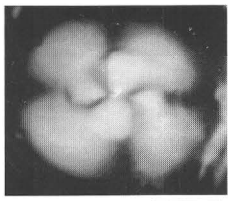

5 5 µm

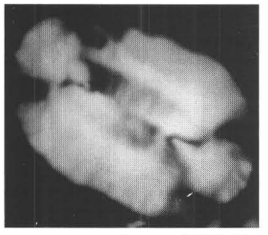

6 5 µm

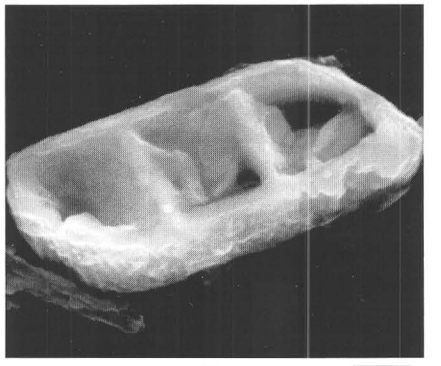

7 1 µm

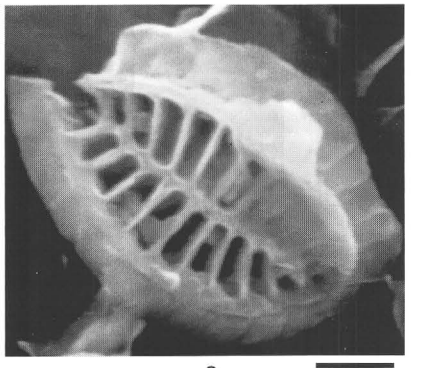

8 1 µm

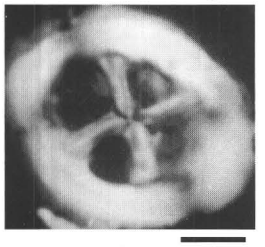

9 5 µm

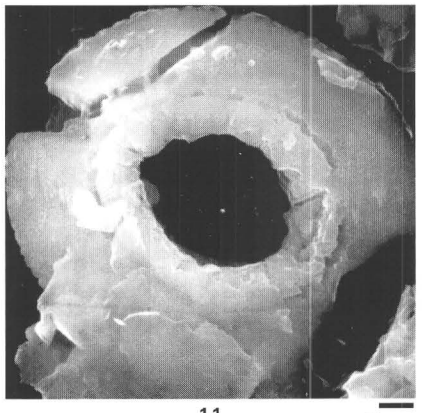

11 1 µm

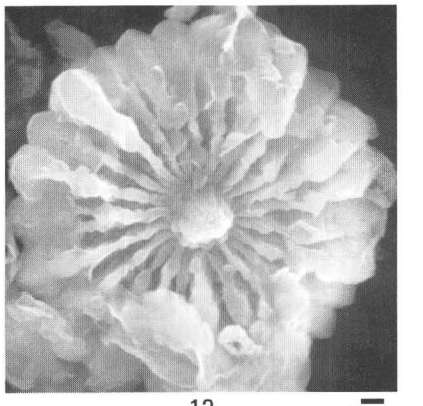

12 1 µm

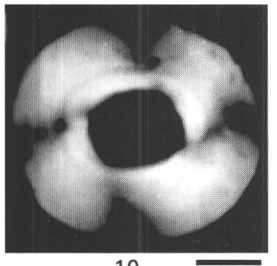

10 5 µm

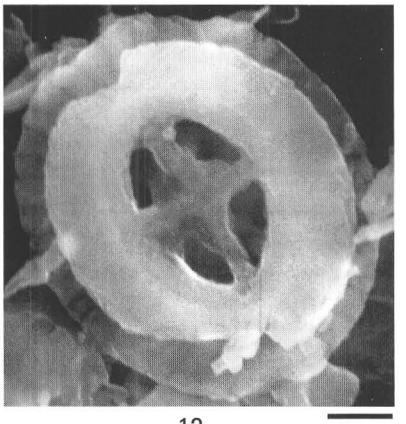

13 1 µm

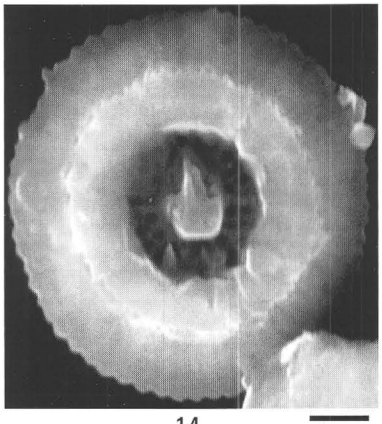

14 1 µm

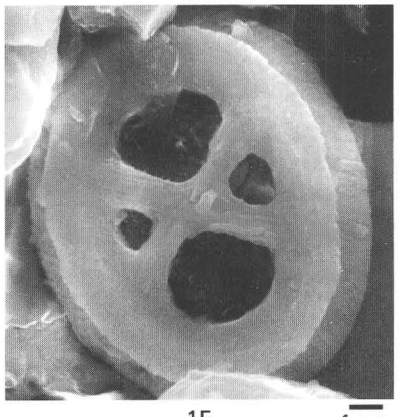

15 1 µm

Calcareous Nannofossils from Matrix Material in the Exmore Beds, USGS-NASA Langley Core, Hampton, Va.

Crystalline-Rock Ejecta and Shocked Minerals of the Chesapeake Bay Impact Structure, USGS-NASA Langley Core, Hampton, Virginia, with Supplemental Constraints on the Age of Impact

By J. Wright Horton, Jr., and Glen A. Izett

Chapter E of
Studies of the Chesapeake Bay Impact Structure—The USGS-NASA Langley Corehole, Hampton, Virginia, and Related Coreholes and Geophysical Surveys

Edited by J. Wright Horton, Jr., David S. Powars, and Gregory S. Gohn

Prepared in cooperation with the
Hampton Roads Planning District Commission,
Virginia Department of Environmental Quality, and
National Aeronautics and Space Administration Langley Research Center

Professional Paper 1688

U.S. Department of the Interior
U.S. Geological Survey

Contents

Figures

Tables

Crystalline-Rock Ejecta and Shocked Minerals of the Chesapeake Bay Impact Structure, USGS-NASA Langley Core, Hampton, Virginia, with Supplemental Constraints on the Age of Impact

By J. Wright Horton, Jr.,[1] and Glen A. Izett[2]

Abstract

The USGS-NASA Langley corehole at Hampton, Va., was drilled in 2000 as the first in a series of new coreholes drilled in the late Eocene Chesapeake Bay impact structure to gain a comprehensive understanding of its three-dimensional character. This understanding is important for assessing ground-water resources in the region, as well as for learning about marine impacts on Earth. We studied crystalline-rock ejecta and shock-metamorphosed minerals from the Langley core to determine what they reveal about the geology of crystalline rocks beneath the Atlantic Coastal Plain and how those rocks were affected by the impact.

An unusual polymict diamicton, informally called the Exmore beds (upper Eocene), is 33.8 meters (m; 110.9 feet (ft)) thick and lies at a depth of 269.4 to 235.65 m (884.0 to 773.12 ft) in the core. This matrix-supported sedimentary deposit contains clasts of Tertiary and Cretaceous sediment (ranging up to boulder size) and sparse pebbles of crystalline rock. The matrix consists of muddy sand that contains abundant quartz grains and minor glauconite and potassium feldspar.

Significantly, the sandy matrix of the Exmore beds contains sparse quartz grains (0.1 to 0.3 millimeter (0.004 to 0.012 inch) in diameter) that contain multiple sets of intersecting planar deformation features formerly referred to as shock lamellae. As many as five different sets have been observed in some quartz grains. Planar deformation features also occur in quartz grains in reworked crystalline-rock clasts in the Exmore beds. Such grains are clearly of shock-metamorphic origin. The presence of these features indicates that the quartz grains have experienced pressures greater than 6 gigapascals (GPa) and strain rates greater than 10^6/second. Thus, the shock-metamorphosed quartz grains, although rare, provide clear and convincing evidence that the Exmore beds are of hybrid impact origin. Identification of shocked quartz grains in the Langley core adds to the number of sites in the structure where their presence is confirmed.

Most of the clasts of crystalline rock that are in and just below the Exmore beds are rounded, detrital, and typical of coastal plain sediments. However, a few have angular shapes and consist of cataclastically deformed felsite having aphanitic-porphyritic to aphanitic texture and peraluminous rhyolite composition. Three of these clasts contain quartz grains that display two sets of planar deformation features of shock-metamorphic origin. Shock-metamorphosed quartz is an integral part of the cataclastic fabric in these three clasts, indicating that both the fabric and the shocked quartz were produced by the same high-energy impact event. Some felsite clasts have spherulitic textures that may be features either of an impact melt or of preimpact volcanic rocks.

A weighted-mean total-fusion $^{40}Ar/^{39}Ar$ age of 35.3±0.1 Ma (±1σ) for 19 analyses of 4 North American tektites records the age of the late Eocene Chesapeake Bay impact event.

Introduction

Purpose and Scope

The USGS-NASA Langley corehole at Hampton, Va., was drilled in 2000 as the first in a series of new coreholes drilled in the late Eocene Chesapeake Bay impact structure to gain a comprehensive understanding of its three-dimensional structure and stratigraphic framework and its influence on regional ground-water resources. We studied crystalline-rock ejecta and shock-metamorphosed minerals from the Langley core to determine what they reveal about the regional geology of crystalline rocks beneath the Atlantic Coastal Plain and how those rocks were affected by the impact. Research is in progress to expand this initial investigation to encompass samples from three coreholes completed in 2001 and 2002—the North, Bayside, and Watkins School coreholes (fig. E1).

The main purpose of this chapter is to present the results of our study of samples from the Langley core. A secondary pur-

[1]U.S. Geological Survey, Reston, VA 20192.

[2]Department of Geology, College of William and Mary, Williamsburg, VA 23187, and Emeritus, U.S. Geological Survey.

pose is to present new constraints on the age of the Chesapeake Bay impact metamorphism based on argon geochronology of North American tektites.

Study Area and Geologic Setting of the Chesapeake Bay Impact Structure

The Chesapeake Bay impact structure is near the mouth of Chesapeake Bay, where it lies buried beneath approximately 150 to 400 meters (m; 492 to 1,312 feet (ft)) of postimpact sediments of the Atlantic Coastal Plain (fig. E1); it was described in earlier reports (Poag and others, 1992, 1994; Poag, 1996, 1997, 1999; Powars and Bruce, 1999; Powars, 2000). The Chesapeake Bay impact structure is one of the largest on Earth and is one of the few fully marine impact structures that have been extensively studied by seismic reflection and drilling (Reimold and others, 2002).

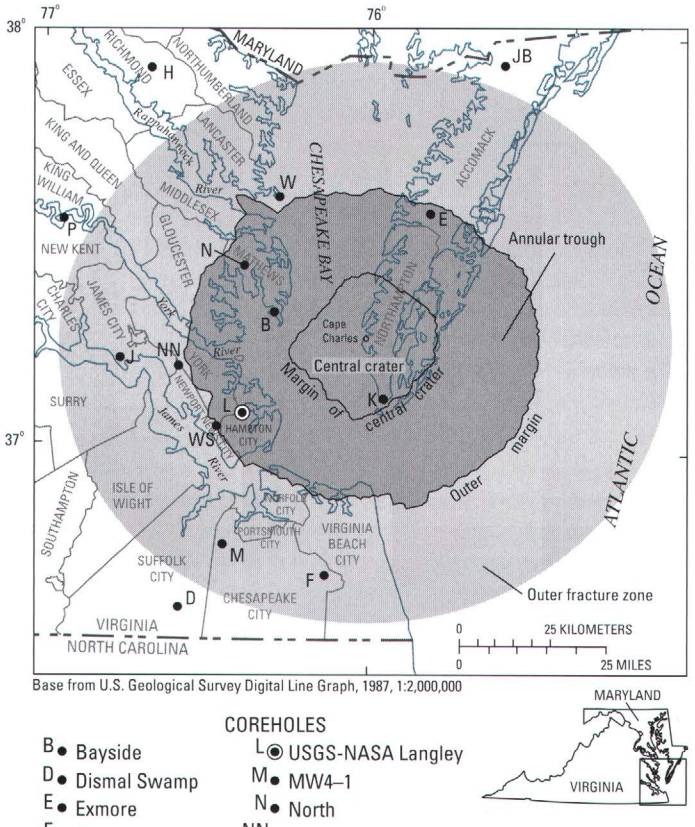

Figure E1. Regional map showing the location of the Chesapeake Bay impact structure, the USGS-NASA Langley corehole at Hampton, Va., and some other coreholes in southeastern Virginia. Locations of the central crater and outer margin are from Powars and Bruce (1999). The extent of the outer fracture zone (light gray) is based on Powars (2000) and Johnson and others (2001); the eastern part is speculative. Illustration modified from Powars, Johnson, and others (2002) and Edwards and Powars (2003).

These studies reveal that the buried structure is a complex impact crater 85 kilometers (km; 53 miles (mi)) wide. It consists of an excavated central crater, which is 30–38 km (18–24 mi) wide and 1–2 km (0.6–1.2 mi) deep, surrounded by a flat-floored annular trough, which is 21–31 km (13–19 mi) wide and contains disrupted sediments, a slumped terrace zone, and a steep gullied escarpment (Poag, 2002a; Powars, Gohn, and others, 2002; Powars, Johnson, and others, 2002). This annular trough is encircled by a 35-km-wide (22-mi-wide) outer fracture zone of concentric faults (Powars, Gohn, and others, 2002; Powars, Johnson, and others, 2002).

The innermost part of the annular trough is interpreted by some workers (Poag, Hutchinson, and others, 1999; Poag, 2002a) to be underlain by a crystalline-rock peak ring that surrounds the central crater. Geophysical interpretations suggest that the floor of the central crater contains a central peak of uplifted crystalline rock overlain by crater-fill sediments (Poag, Hutchinson, and others, 1999; Poag, Plescia, and Molzer, 1999; Poag, 2002a).

The USGS-NASA Langley corehole is located at lat 37°05'44.28" N., long 76°23'08.96" W. (North American Datum of 1927), at a ground-surface altitude of 2.4 m (7.9 ft) above the North American Vertical Datum of 1988. It is on the York-James Peninsula at the National Aeronautics and Space Administration (NASA) Langley Research Center in Hampton, Va., about 19 km (12 mi) outside the margin of the central crater and about 8 km (5 mi) inside the outer margin of the annular trough (fig. E1). The hole was drilled by the U.S. Geological Survey (USGS) and cooperators (see "Acknowledgments"). Preliminary descriptions of the core are available in Gohn, Clark, and others (2001), Gohn, Powars, and others (2001), Horton and others (2001), and Powars and others (2001).

The core contains weathered Neoproterozoic granite below 626.3 m (2,054.7 ft) depth (Horton and others, this volume, chap. B). The granite is overlain by weakly to strongly disturbed preimpact sediments (crater units A and B of Gohn and others, this volume, chap. C), followed by a polymict diamicton (the Exmore beds) and by postimpact sediments (Powars and others, this volume, chap. G).

The impact-disturbed sediments include a basal crater unit A, consisting of autochthonous, block-faulted sediments of the Cretaceous Potomac Formation, which Gohn and others (this volume, chap. C) divide into lower beds (nonfluidized) and upper beds (variably fluidized). Crater unit A is present in the Langley core between depths of 626.3 and 442.5 m (2,054.7 and 1,451.7 ft) and is 183.8 m (603.0 ft) thick.

The overlying crater unit B consists of blocks of Lower Cretaceous sediments disrupted by zones of extensive fluidization, injection, and mixing (Powars, Gohn, and others, 2002; Gohn and others, 2002 and this volume, chap. C). The base of crater unit B in the core, defined by the deepest occurrence of glauconite, is interpreted to represent the lowest zone of injection by Tertiary marine sediment from above (Gohn and others, this volume, chap. C). Crater unit B is present in the Langley core between depths of 442.5 and 269.4 m (1,451.7 and 884.0 ft) and is 173.0 m (567.7 ft) thick.

The crater-fill unit informally known as the Exmore beds (Powars and others, 1992) is a matrix-supported sedimentary deposit and contains clasts of Tertiary and Cretaceous sediment (ranging up to boulder size) and sparse pebbles of crystalline rock; the matrix consists of muddy sand that contains abundant quartz grains and minor glauconite and potassium feldspar (Gohn and others, 2002 and this volume, chap. C; Powars, Gohn, and others, 2002; this study). The unit consists mainly of rounded clasts, rather than angular fragments, in a detrital matrix and is more accurately characterized as a polymict diamicton (Gohn and others, this volume, chap. C) than a breccia (see the glossary for this chapter).

The Exmore beds have also been called the Exmore boulder bed (Poag and others, 1992), the Exmore breccia (Powars and others, 1993; Poag and others, 1994; Poag, 1996, 1997), and the Exmore tsunami-breccia (Powars and Bruce, 1999; Powars, 2000). The mixed sediments of the Exmore beds were previously interpreted as tsunami deposits (Powars and Bruce, 1999; Powars, 2000) and were reinterpreted as mainly seawater-resurge deposits (Gohn and others, this volume, chap. C).

Microfossils in the Exmore beds have mixed Cretaceous, Paleocene, and Eocene ages (Edwards and others, 2002; Frederiksen and others, this volume, chap. D). In the USGS-NASA Langley core, the Exmore beds have a thickness of 33.8 m (110.9 ft); they extend from the base of glauconitic marine sediments at 269.4 m (884.0 ft) depth to the uppermost synimpact fallout layer at 235.65 m (773.12 ft) depth (Gohn and others, this volume, chap. C).

In this chapter, we discuss shock-metamorphosed minerals and crystalline-rock clasts in and just below the Exmore beds in the USGS-NASA Langley core. Initial results of this study and related studies of other cores are summarized in several abstracts (Horton and others, 2001; Horton, Aleinikoff, and others, 2002; Horton, Kunk, and others, 2002; Horton, Gohn, and others, 2003).

General Criteria for Shock Metamorphism

Grains of quartz and other silicate minerals that contain multiple intersecting sets of closely spaced planar deformation features are commonly called "shocked" or "shock metamorphosed." They are interpreted to be formed in target rocks during hypervelocity impacts of asteroids or comet nuclei with the Earth (Grieve and others, 1996). These microstructures have been observed in rocks at known impact sites, in rocks that have undergone a high strain rate during hypervelocity shock metamorphism in laboratory experiments (Chao, 1967, 1968), and in rocks at high-yield chemical and nuclear explosion sites (Short, 1968). Quartz and feldspar in volcanic rocks produced by giant silicic pyroclastic eruptions lack these multiple sets of planar deformation features (Izett, 1990, p. 74).

Shock-metamorphic features in quartz share the following characteristics (Alexopoulos and others, 1988; French, 1998):

1. Features are planar, well to very well defined, and sharp.
2. Within each set, the planar deformation features are parallel, are generally continuous, and extend across a minimum of 75 percent of the grain.
3. Spacing between the individual planar deformation features is typically about 1 to 4 micrometers.
4. Approximately 80 percent of these features are oriented (±3° variance in orientation measurement) parallel to the basal plane c{0001} and to the rhombohedral planes $\omega\{10\bar{1}3\}$ and $\{10\bar{1}2\}$, which have poles inclined at angles of approximately 23° and 32°, respectively, to the *c* axis. The $\omega\{10\bar{1}3\}$ orientation is important because it is not a normal cleavage, twin, or growth plane and because it does not correspond to deformation features produced in low-strain-rate experiments (Alexopoulos and others, 1988).

Transmission-electron-microscopic (TEM) studies have shown that individual planar deformation features in quartz grains that have experienced low shock pressures consist mainly of planar open microfractures, dislocation bands, microgranulated laminae, and tiny voids (Chao, 1976; Chao and Goresy, 1977; Xie and Chao, 1985). Planar deformation features in quartz grains that have experienced moderate to high shock pressures consist of submicrometer-thick silica glass (Chao and Goresy, 1977; Xie and Chao, 1985).

The features characteristic of shock-deformed minerals have been variously termed "shock lamellae" (Chao, 1967), "planar features" (Carter, 1965), "planar elements" (Stöffler, 1972), "microfractures" (Chao and Goresy, 1977, p. 291), and "planar deformation features (PDFs)" (Koeberl and others, 1996). The International Union of Geological Sciences (IUGS) Subcommission on the Systematics of Metamorphic Rocks has released a proposal (Stöffler and Grieve, 2003) to standardize use of the term "planar deformation features" and to discard synonymous terms such as "shock lamellae" and "planar elements."

It has long been recognized that the presence of multiple intersecting sets of planar deformation features is the most diagnostic criterion for identifying shock metamorphism in silicate minerals. This recognition is based on extensive experimental and empirical mineralogy of impact materials (Wackerle, 1962; Carter and others, 1964; Carter, 1965, 1971; Chao, 1967, 1968; Ahrens and Rosenberg, 1968; Bunch, 1968; Engelhardt and others, 1968; McIntyre, 1968; Robertson and others, 1968; Short, 1968; Engelhardt and Bertsch, 1969; Stöffler, 1971, 1972; Grieve and others, 1996). Other important evidence of shock metamorphism can include optical mosaicism, isotropization, high-pressure mineral polymorphs such as coesite and stishovite, and macroscopic features such as shatter cones (Chao, 1968; French and Short, 1968; Grieve and others, 1977, 1996; Alexopoulos and others, 1988; Grieve, 1991).

Previous Evidence of Impact Metamorphism near Chesapeake Bay

Poag and others (1992) first reported the presence of shock-metamorphosed quartz grains in the Exmore beds in samples from the Newport News Park 2 corehole, Va. (fig. E1). Prior to publication in 1992, Larry Poppe (USGS) and Wylie Poag (USGS) sent one of us (Izett) three smear slides from the Newport News Park 2 corehole that they believed to contain shock-metamorphosed quartz grains. Izett found only two quartz grains in the three slides that contained multiple intersecting sets of planar deformation features. Neither grain was a textbook example of shocked quartz.

Subsequent studies of the Newport News Park 2 core by Izett (unpub. data, 1993) revealed clear and convincing evidence that shock-metamorphosed quartz grains, containing multiple intersecting sets of planar deformation features, were present in some samples of the Exmore beds at Newport News but in very low abundance, far less than 1 percent. Izett examined 30 immersion-oil mounts containing silicate mineral grains from the Exmore beds and found only one quartz grain that contained multiple intersecting sets of planar deformation features.

The evidence of shock metamorphism presented by Poag and others (1992), although meager, provided important physical confirmation that an asteroid or comet nucleus struck the Earth in the general region and generated the Exmore beds near the mouth of the present Chesapeake Bay. Since then, Koeberl and others (1996) presented corroborating evidence of shock metamorphism in samples from the corehole at Exmore, Va. (fig. E1). This evidence included quartz having up to six sets of planar deformation features and crystallographic orientations consistent with shock pressures of 20 to about 30 gigapascals (GPa), as well as shock-metamorphosed feldspar having as many as three sets and having microfracture patterns consistent with shock pressures of 5 to 10 GPa (Koeberl and others, 1996). Reimold and others (2002), in a continuation of that study, estimated shock pressures of 10 to 20 GPa from a small data set on the orientations and relative frequencies of planar deformation features in quartz.

Poag and others (1992) reported but did not illustrate vesicular tektite glass in samples from the Exmore, Va., corehole. More recently, Poag (2002b, p. 997) and Poag, Koeberl, and Reimold (2004, fig. 6.32) illustrated material identified as "intact glass microspherules" in thin sections of the Exmore beds from the Exmore and Newport News Park 2 coreholes. Reimold and others (2002) referred to these spherules as proximal microtektites. Further tests that are needed to confirm and characterize the suspected glass include index of refraction measurement, chemical analysis, and $^{40}Ar/^{39}Ar$ isotopic analysis. Such material has not been found in our own studies of cores from the Chesapeake Bay impact structure.

In addition to shocked minerals, marine microfossils that are interpreted to be impact damaged were recently discovered in samples of the Exmore beds from the Langley core (Edwards and Self-Trail, 2002; Edwards and others, 2002; Edwards and Powars, 2003; Self-Trail, 2003; Frederiksen and others, this volume, chap. D).

Distal impact ejecta that are inferred to be from the Chesapeake Bay impact structure include tektites and microtektites (impact glass), shocked quartz and zircon, the high-pressure silica polymorphs coesite and stishovite, and the high-pressure zircon polymorph reidite (Glass and Liu, 2001; Glass, 2002; Glass and others, 2002; Kamo and others, 2002).

Crystalline-Rock Ejecta and Shocked Minerals in the USGS-NASA Langley Core

Methods

Preparation and microscopic study of matrix samples.—Sandy matrix of the Exmore beds was sampled in the USGS-NASA Langley core at depths of 236.9 m (777.3 ft) and 250.1 m (820.6 ft). These samples were sieved, and grains having diameters less than 0.5 millimeter (mm; 0.02 inch (in.)) were prepared for microscopic examination by disaggregating the sediment in a 10-percent hydrochloric acid solution in an ultrasonic cleaning bath for at least an hour. Suspended material, consisting mostly of clay minerals, was decanted from the slurry. The residuum again was placed in an ultrasonic cleaning bath, but this time in an aqueous solution of household bleach (~30 percent). It was then treated in 5-percent hydrofluoric acid for 30 seconds to clean and enhance the visibility of any planar deformation features. Immersion-oil mounts were prepared by placing several hundred of the dried grains in 1.544 index oil without a cover glass.

Individual grains in the immersion-oil mounts that were suspected to be shock metamorphic because of their appearance under a binocular microscope were nudged out of the oil and pushed aside with a sharpened steel spindle. A selected grain was transferred into a drop of water and agitated. After the water evaporated, the grain was glue mounted (by using a mixture of 50 percent white carpenter's glue and 50 percent molasses) on the tip of a steel-wire spindle. The mounted grains were inserted into the immersion cell of a spindle stage (Wilcox, 1959).

A spindle stage is ideal for the study of shock-metamorphic features in mineral grains because planar deformation features can be rotated to the vertical, and their orientations in relation to optical directions can be measured and plotted on a stereonet. The spindle stage is also ideally suited for the measurement of the principal indices of refraction of shocked minerals. When a spindle stage is used, the precision of measuring planar features and optical directions is about ±2° (Wilcox, 1959). Techniques for preparing and manipulating quartz grains on the spindle stage and for estimating the relative abundance (percentage) of shocked grains per sample were described by Wilcox (1959) and by Izett (1990).

Preparation and microscopic study of clast samples.—The Langley core was also examined for lithic clasts composed of crystalline rock. Most of those in and just below the Exmore beds were rounded detrital pebbles. Thin sections of these rounded pebbles revealed no unusual high-strain-rate fabrics or shock-induced features (appendix E1, samples NL854.0, NL864.05).

A much smaller population of crystalline-rock clasts has angular shapes or cataclastic fabrics, and these clasts were examined in thin section (appendix E1). A standard microprobe polish was used to eliminate surface scratches in most thin sections. In other thin sections, a yellow stain (sodium cobaltinitrite) was used to distinguish potassium feldspar. Quartz grains were separated from several clasts, were processed as described in the section above, and were rotated on a spindle stage to further verify the presence or absence of shock-induced planar deformation features.

The planar deformation features can be seen readily by using a petrographic microscope and plane-polarized light, and they give the quartz grains a remarkable appearance that is very different from normal unshocked quartz. The planar microstructures are best seen when they are oriented nearly parallel to the axis of a microscope. In this orientation, they appear as parallel bright lines commonly bordered by dark lines. These closely spaced parallel planar deformation features differ from twin lamellae in that adjacent crystallographic domains do not go to extinction at different angles during rotation of the stage of a petrographic microscope. In contrast, curved discontinuous planar features (termed Böhm lamellae) that occur in quartz grains of tectonites have a much different appearance than the planar deformation features in shock-metamorphosed quartz at impact sites.

Chemical analysis of rocks.—Chemical analyses of two rock samples (discussed below) used several methods (Arbogast, 1996), including the following: wavelength-dispersive X-ray fluorescence (WDXRF) spectrometry for 10 major elements (Taggart and others, 1987; Mee and others, 1996), energy-dispersive X-ray fluorescence (EDXRF) spectrometry for 30 trace elements (Siems, 2000, 2002), instrumental-neutron-activation analysis (INAA; Baedecker and McKown, 1987) using a long-count procedure for 44 elements including rare-earth elements (Wandless, 1996), and individual determination of FeO, forms of H_2O, C as CO_2, F, and S as described by Jackson and others (1987).

Results

Shocked Quartz Grains

Quartz and potassium feldspar are the chief components of the clastic mineral grains in the Exmore beds. Most of the grains appear structureless and show normal sharp extinction when examined with a petrographic microscope using cross-polarized light. Some grains show anomalous extinction, and others exhibit Böhm lamellae. Of special importance is the fact that rare quartz grains contain multiple sets of planar deformation features. As many as five sets occur in some quartz grains. The grains are subangular, commonly 0.1 to 0.3 mm (0.004 to 0.012 in.) in diameter, and generally colorless. Spindle-stage measurements show that the planar deformation features we studied most commonly have poles inclined at about 23° to the *c* axis. This is the rhombohedral planar orientation, or the ω direction $\{10\bar{1}3\}$ in quartz.

Quartz is the only mineral in these sediment samples that has convincing shock-induced planar deformation features. No shocked feldspar grains were found, and no attempt was made to separate and examine heavy minerals such as zircon for evidence of shock metamorphism. Figure E2 and the cover of this volume show examples of shock-metamorphosed quartz grains from the Langley core.

Shock-metamorphosed quartz is scarce in samples from the Langley core. We estimate the relative abundance to be no more than one shocked grain in several thousand quartz grains, on the basis of the number of immersion-oil slides per sample and the numbers of total grains and shocked grains per slide. Consequently, point counting of grains to obtain meaningful statistics on their abundance would be impractical. Although the abundance of shocked grains is insufficient for a statistically meaningful assessment of crystallographic orientations, the orientations of planar deformation features that we measured on a spindle stage are consistent with shock metamorphism. The individual quartz grains that have confirmed shock-induced deformation features are mostly subangular and lack the rounded shapes that would indicate derivation from a detrital sedimentary target. This lack of rounding suggests that they are mainly particles of crystalline basement, or possibly fragments of smashed detrital grains, that were excavated by the impact.

Impact-Derived Clasts of Crystalline Rock

Cataclastic Fabrics and Planar Deformation Features

Cataclastic rocks are high-strain-rate rocks produced by mechanical crushing, faulting, and fracturing of existing rocks. Those found in impact structures are identical in many respects to those found in fault zones (Snoke and Tullis, 1998). They are not diagnostic as criteria for an impact origin, but they may be impact related where associated with features such as shock-metamorphosed minerals or a crater.

Lithic clasts of crystalline rock that have angular shapes or cataclastic fabrics were distributed throughout the Exmore beds in the Langley core, and one was found in the core below the Exmore beds in the upper part of crater unit B (fig. E3). Clasts larger than the nominal core diameter of 6.4 centimeters (cm; 2.5 in.) were found only in the lower half of the Exmore beds and below. Figure E4 shows some of the crystalline-rock clasts, and figure E5 shows the cataclastic microfabrics.

Figure E4*A* shows the jagged edges of a brecciated felsite clast in contact with matrix sediment of the Exmore beds, and figure E4*B* shows a clast of cataclasite (deformed felsite) with thin calcite veins along fault surfaces. Primary igneous textures are preserved in less deformed felsite clasts from the Exmore

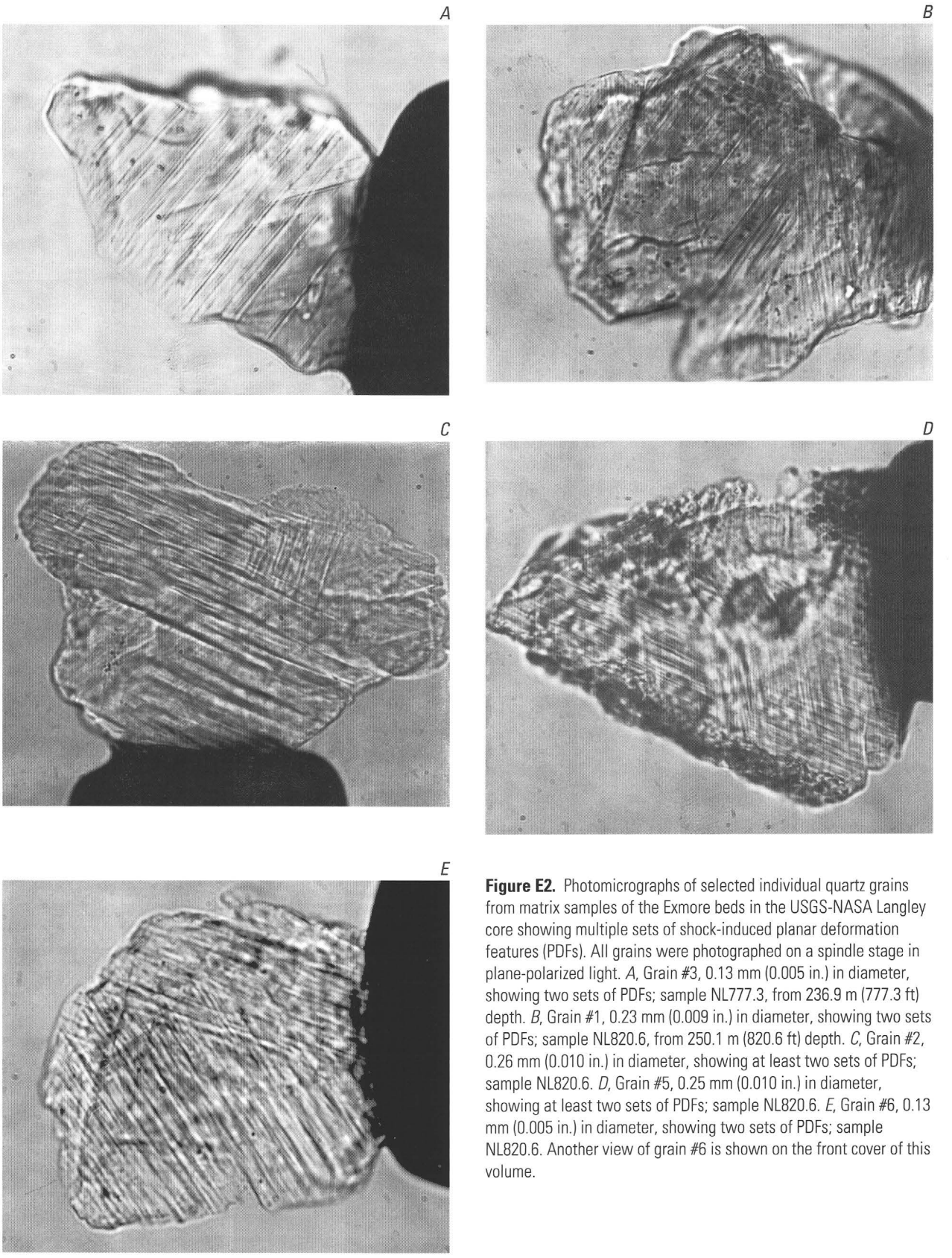

Figure E2. Photomicrographs of selected individual quartz grains from matrix samples of the Exmore beds in the USGS-NASA Langley core showing multiple sets of shock-induced planar deformation features (PDFs). All grains were photographed on a spindle stage in plane-polarized light. *A*, Grain #3, 0.13 mm (0.005 in.) in diameter, showing two sets of PDFs; sample NL777.3, from 236.9 m (777.3 ft) depth. *B*, Grain #1, 0.23 mm (0.009 in.) in diameter, showing two sets of PDFs; sample NL820.6, from 250.1 m (820.6 ft) depth. *C*, Grain #2, 0.26 mm (0.010 in.) in diameter, showing at least two sets of PDFs; sample NL820.6. *D*, Grain #5, 0.25 mm (0.010 in.) in diameter, showing at least two sets of PDFs; sample NL820.6. *E*, Grain #6, 0.13 mm (0.005 in.) in diameter, showing two sets of PDFs; sample NL820.6. Another view of grain #6 is shown on the front cover of this volume.

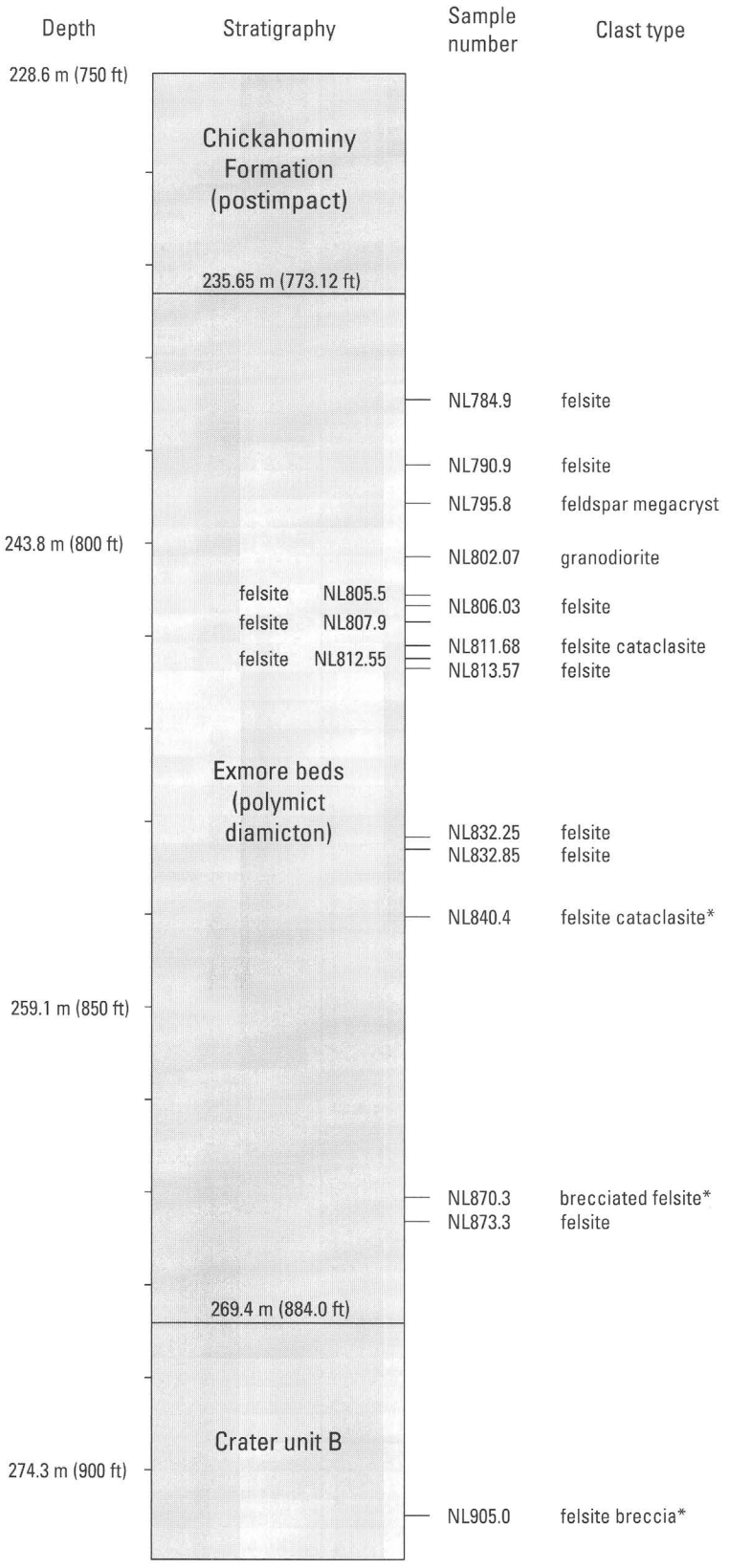

Figure E3. Stratigraphic column of part of the USGS-NASA Langley corehole showing positions of selected lithic clasts of crystalline rock. All samples interpreted as impact ejecta are from the Exmore beds, with one exception; sample NL905.0 is from crater unit B. An asterisk (*) indicates clasts larger than the nominal core diameter of 6.4 cm (2.5 in.). Sample numbers indicate depths in feet; sample descriptions are in appendix E1.

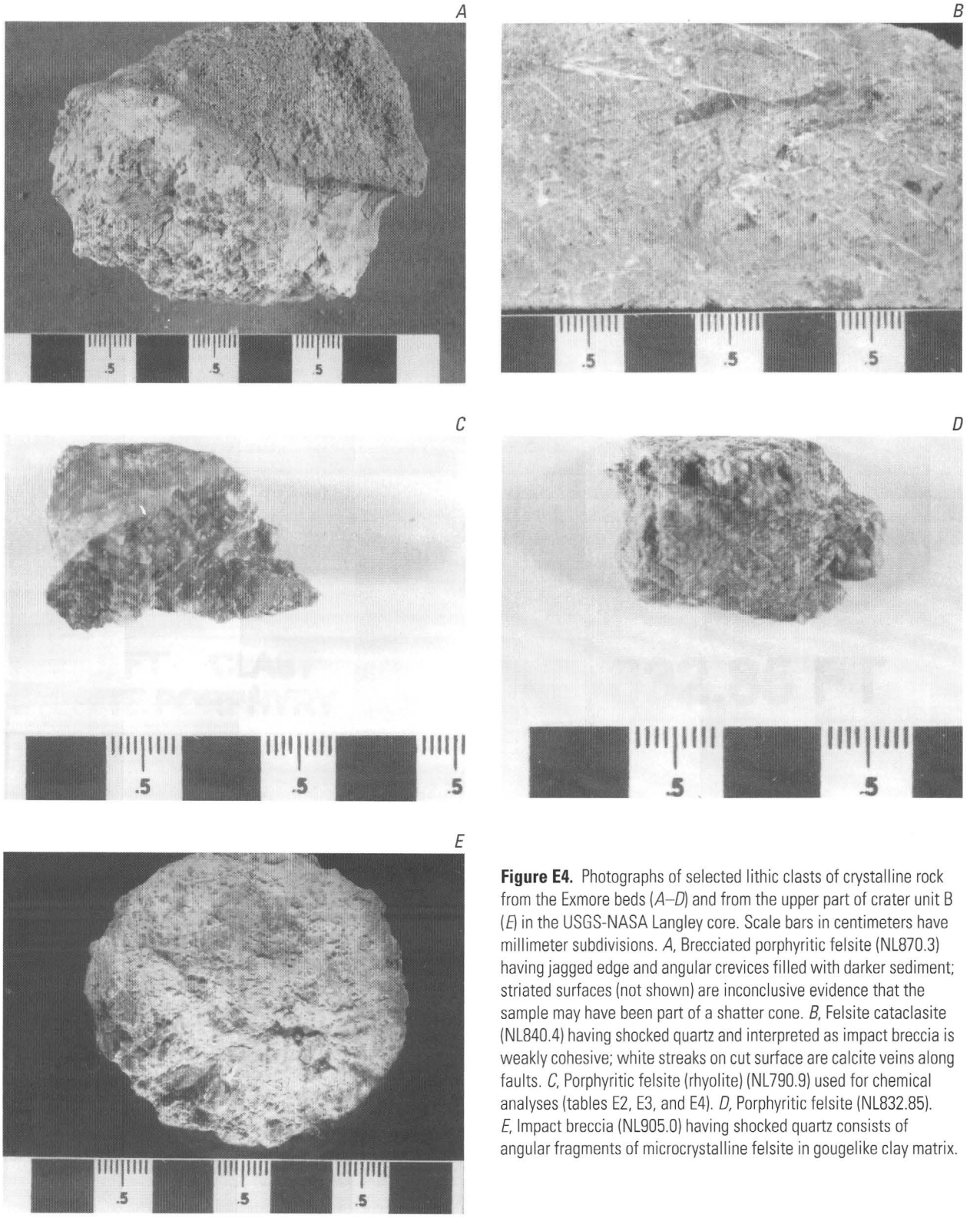

Figure E4. Photographs of selected lithic clasts of crystalline rock from the Exmore beds (*A–D*) and from the upper part of crater unit B (*E*) in the USGS-NASA Langley core. Scale bars in centimeters have millimeter subdivisions. *A*, Brecciated porphyritic felsite (NL870.3) having jagged edge and angular crevices filled with darker sediment; striated surfaces (not shown) are inconclusive evidence that the sample may have been part of a shatter cone. *B*, Felsite cataclasite (NL840.4) having shocked quartz and interpreted as impact breccia is weakly cohesive; white streaks on cut surface are calcite veins along faults. *C*, Porphyritic felsite (rhyolite) (NL790.9) used for chemical analyses (tables E2, E3, and E4). *D*, Porphyritic felsite (NL832.85). *E*, Impact breccia (NL905.0) having shocked quartz consists of angular fragments of microcrystalline felsite in gougelike clay matrix.

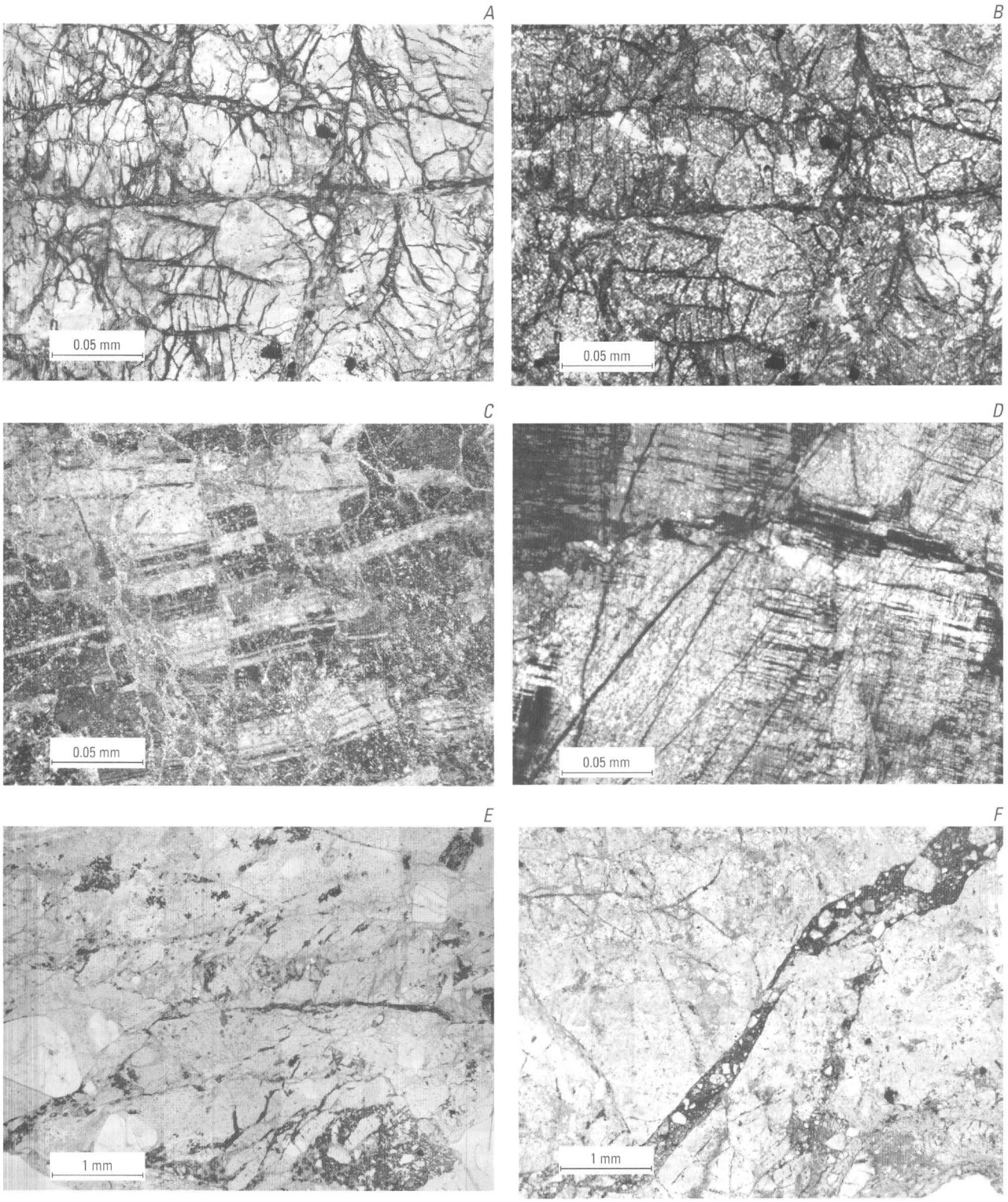

Figure E5. Photomicrographs showing cataclastic microfabrics in lithic clasts of crystalline rock from the Exmore beds in the USGS-NASA Langley core. *A*, Felsite cataclasite (NL811.68) having pervasive orthogonal sets of throughgoing microfaults and fractures, viewed in plane-polarized light. *B*, Same view as in *A* but in cross-polarized light, showing that fracture lengths greatly exceed grain size. *C*, Microfaults offsetting polysynthetic twins in plagioclase phenocryst in porphyritic felsite (NL784.9) that contains shocked quartz (fig. E6*D*), viewed in cross-polarized light. *D*, Microcline megacryst (NL795.8) crosscut by closely spaced planar microfaults oblique to perthitic exsolution lamellae, viewed in cross-polarized light. *E*, Dark microbreccia veinlets along fractures in porphyritic felsite (NL790.9), viewed in plane-polarized light. *F*, Dark vein interpreted as pseudotachylyte (frictional melt?) containing broken crystals and fragments of brecciated porphyritic felsite host (NL870.3); quartz fragments in the vein appear clean and free of planar deformation features; viewed in plane-polarized light.

beds as shown in figures E4*C* and E4*D*. The clast shown in figure E4*E* is from the upper part of crater unit B and is a brecciated felsite loosely held together by gougelike clay.

Figures E5*A* and E5*B* show a cataclasite having pervasive orthogonal sets of throughgoing microfaults and fractures. Figures E5*C* and E5*D* show examples of microfaults cutting feldspar phenocrysts (plagioclase and microcline) in clasts of igneous rock. Dark veinlets of microbreccia (fig. E5*E*) are visible in a few thin sections of porphyritic felsite. The vein in figure E5*F* appears to be a pseudotachylyte (frictional melt?), containing broken crystals and fragments of the felsite host rock.

Clasts of crystalline rock that contain shock-metamorphosed quartz are sparse in the Langley core, and three are described in appendix E1 (samples NL784.9, NL840.4, NL905.0). All of these clasts have cataclastic fabrics of which the shock-metamorphosed quartz is an integral part. Within these clasts, only a few quartz grains in any thin section have multiple sets of intersecting planar deformation features, and none were found to have more than two well-developed sets. Selected quartz grains in lithic clasts of crystalline rock are shown in figure E6. All of these have intersecting sets of parallel planar deformation features that are interpreted to be shock induced. Planar deformation features viewed in thin sections on a flat stage, as in figure E6, tend to be oblique to the microscope axis and thus not as clear in photographs as those oriented on a spindle stage (fig. E2).

Table E1 summarizes the features of clasts considered likely to be impact ejecta. Deformational features include brecciation, microfaults, shock-induced planar deformation features in quartz, and veins of pseudotachylyte or microbreccia. Some felsite clasts have porphyritic and spherulitic igneous textures.

Clast Composition

The three lithic clasts found to contain shock-induced planar deformation features in quartz consist of cataclastically deformed felsite having aphanitic-porphyritic to aphanitic texture (appendix E1). Moreover, except for one granodiorite clast (NL802.07), all of the lithic clasts having cataclastic fabrics without confirmed shocked minerals in the Langley core consist of felsite having the same characteristics (appendix E1). Thus, all of the crystalline-rock fragments confirmed or interpreted to be impact ejecta are composed of variably porphyritic felsite such as the example in figure E7. Most of the felsite clasts were considered unsuitable for chemical analyses because of calcite-filled fractures or secondary alteration.

Some of the felsite clasts have a spherulitic texture (fig. E8). Each spherulite consists of a spherical cluster of plagioclase crystals radiating from a central point, and some have potassium-feldspar-rich outer rims (yellow in stained thin sections). Spherulitic textures commonly form in volcanic glasses by devitrification (Ross and Smith, 1961) and are locally preserved in metamorphosed volcanic rocks of the southeastern United States (Allen and Wilson, 1968). Of the four felsite clasts having spherulitic devitrification texture observed in this study, only one (NL905.0) has shocked quartz (appendix E1).

Unaltered porphyritic felsite from the clast shown in figure E4*C* and figure E7 (NL790.9) and a sample of the Langley Granite (NL2083.1; Horton and others, this volume, chap. B) were chemically analyzed. The results are shown in tables E2, E3, and E4.

In LeBas and others' (1986) chemical classification of volcanic rocks based on the total alkali-silica diagram, the porphyritic felsite is classified as a rhyolite. The aphanitic matrix of the felsite is too fine grained to allow a classification based on petrographic determination of mineral percentages. The Langley Granite sample is a monzogranite in Streckeisen's (1973, 1976) classification (Horton and others, this volume, chap. B). Both the rhyolite clast and the Langley Granite sample are slightly peraluminous. They have essentially identical alumina saturation indices (A/CNK = $Al_2O_3/[CaO+Na_2O+K_2O]$, mol proportion) of 1.1 and 1.1, respectively, as well as corundum in the CIPW norms (Horton and others, this volume, chap. B). On the basis of the analytical results, the rhyolite sample NL790.9 has these minerals in the CIPW norm (weight percent): 37.7 percent quartz, 15.9 percent orthoclase, 34.8 percent albite, 3.8 percent anorthite, 2.4 percent hypersthene, 1.2 percent magnetite, 0.5 percent ilmenite, 1.7 percent corundum, and 0.25 percent apatite.

Where we have measurements of some of the same trace elements by EDXRF (table E2) and INAA (table E3), they vary in agreement. For example, concentrations of Rb agree within ~2 percent and those of Ba, Sr, and Zn agree within <20 percent. The INAA data are considered to be more accurate for the rare-earth elements and for elements in these samples that are near or below the detection limits of EDXRF, including As, Cs, Ni, Sb, U, and W.

Trace-element concentrations in the rhyolite fragment and in the Langley Granite are similar in other respects, and discrimination diagrams (not shown) for identifying the tectonic settings of granite emplacement consistently indicate a volcanic arc setting for both rocks. These include Pearce and others' (1984) diagrams for Rb and Y+Nb, for Nb and Y, for Rb and Yb+Ta, and for Ta and Yb, and Harris and others' (1986) Hf-Rb-Ta diagram.

A plot (fig. E9) of rare-earth elements (REEs) in the two samples normalized to average REE abundances in chondrites from Nakamura (1974) shows that the rhyolite (NL790.9) is lower in REEs than the Langley Granite (NL2083.1). Otherwise, the rhyolite and granite have very similar REE patterns characterized by enrichment in light REEs (rhyolite La/Lu = 10.5 x chondrite; granite La/Lu = 4.6 x chondrite), negative europium anomalies (Eu/Eu* of 0.60 and 0.63, respectively), and flat distributions of heavy REEs.

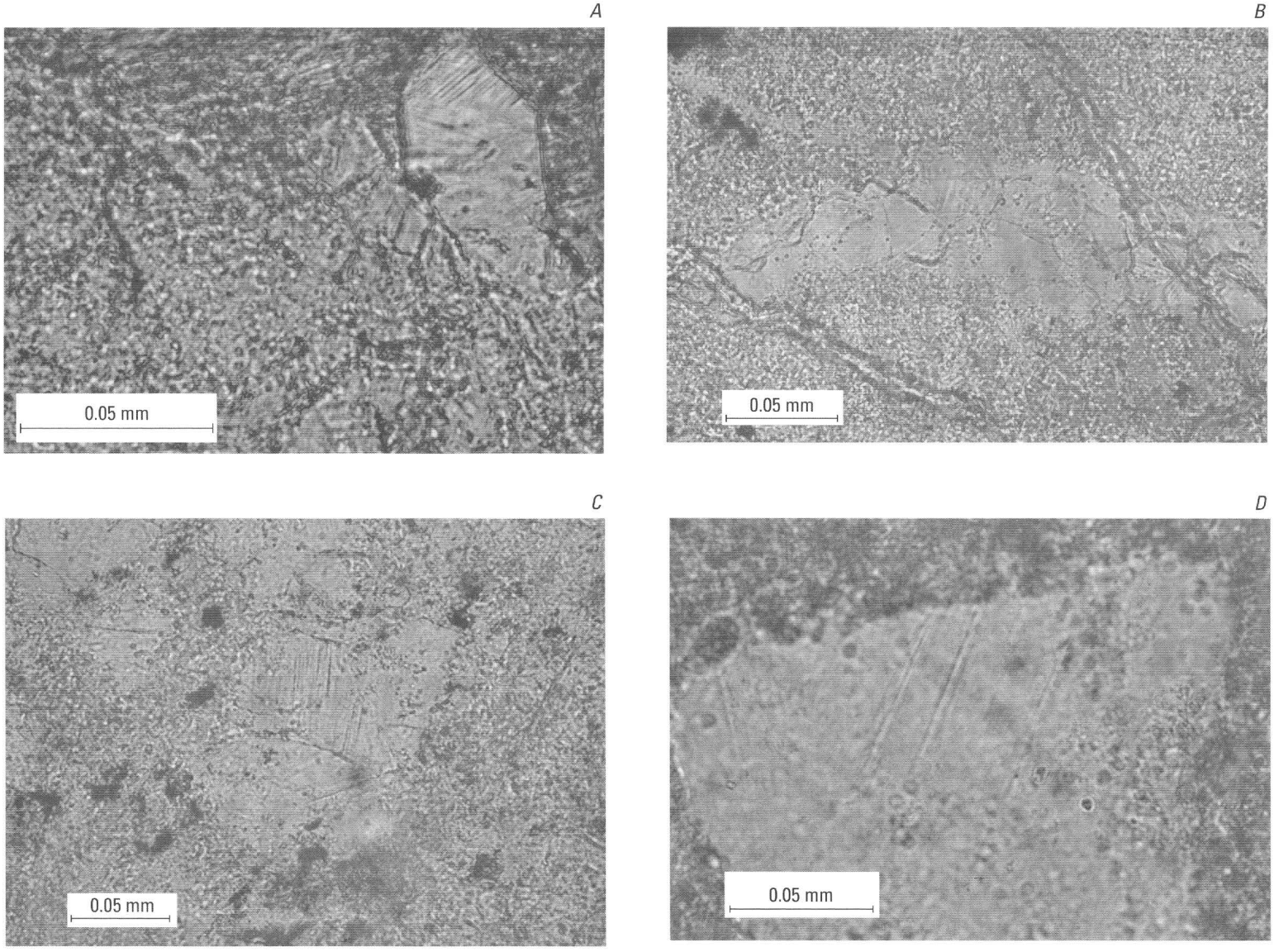

Figure E6. Photomicrographs of quartz showing intersecting sets of shock-induced planar deformation features in lithic clasts of crystalline rock from the Exmore beds in the USGS-NASA Langley core. Thin sections were photographed on a flat stage in plane-polarized light. *A*, Quartz crystal (in upper right corner) having two well-developed sets, in felsite cataclasite (NL840.4, thin section 1). *B* and *C*, Multiple quartz crystals having intersecting sets in same felsite cataclasite (NL840.4, thin section 1). *D*, Quartz phenocryst having two sets, one well developed and one poorly developed, in porphyritic felsite (NL784.9).

Table E1. Features of selected crystalline-rock clasts from the USGS-NASA Langley core that are interpreted to be possible impact ejecta.

[Samples are described in appendix E1. All samples but one are from the Exmore beds; sample NL905.0 is from crater unit B. Igneous textures: FF, flow foliation; P, porphyritic; S, spherulitic; —, none. Cataclastic or shock-induced features: B, brecciated; F, microfaults; N, not highly strained; Q, shocked quartz; V, veins of pseudotachylyte or microbreccia]

Sample number	Depth in core		Rock type	Igneous textures	Cataclastic or shock-induced features
	(meters)	(feet)			
NL784.9	239.2	784.9	Felsite	P	F, Q
NL790.9	241.1	790.9	Felsite	P	F, V
NL795.8	242.6	795.8	Feldspar megacryst	—	F
NL802.07	244.47	802.07	Granodiorite	—	N
NL805.5	245.5	805.5	Felsite	P	F
NL806.03	245.68	806.03	Felsite	P, S	N
NL807.9	246.2	807.9	Felsite	P	N
NL811.68	247.40	811.68	Felsite cataclasite	—	B, F
NL812.55	247.67	812.55	Felsite	P, S	N
NL813.57	247.98	813.57	Felsite	P	F
NL832.25	253.67	832.25	Felsite	P	N
NL832.85	253.85	832.85	Felsite	P, S	N
NL840.4	256.06–256.26	840.1–840.75	Felsite cataclasite	P	B, F, Q
NL870.3	265.27–265.36	870.3–870.6	Brecciated felsite	P	B, V
NL873.3	266.2	873.3	Felsite	FF	N
NL905.0	275.71–275.93	904.60–905.33	Felsite breccia	S	B, F, Q

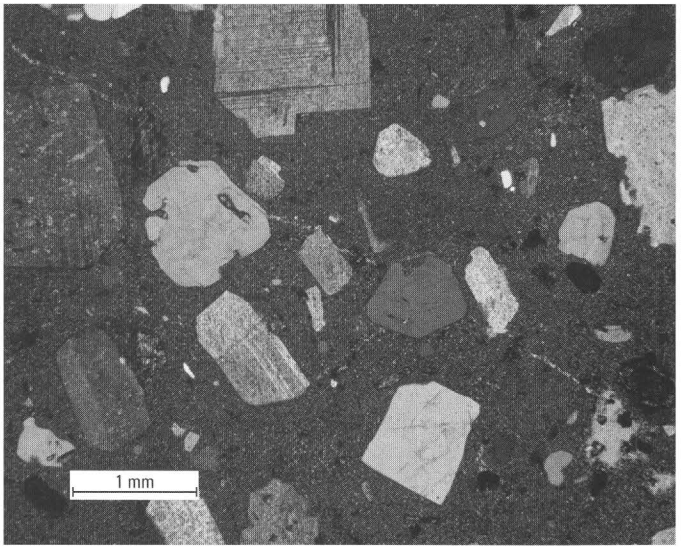

Figure E7. Photomicrograph showing the porphyritic texture in felsite (rhyolite) sample NL790.9 from the Exmore beds in the USGS-NASA Langley core; tables E2, E3, and E4 show the results of chemical analyses of this sample. Feldspar phenocrysts are euhedral to subhedral; some have embayed margins indicating magmatic corrosion. Photographed in cross-polarized light.

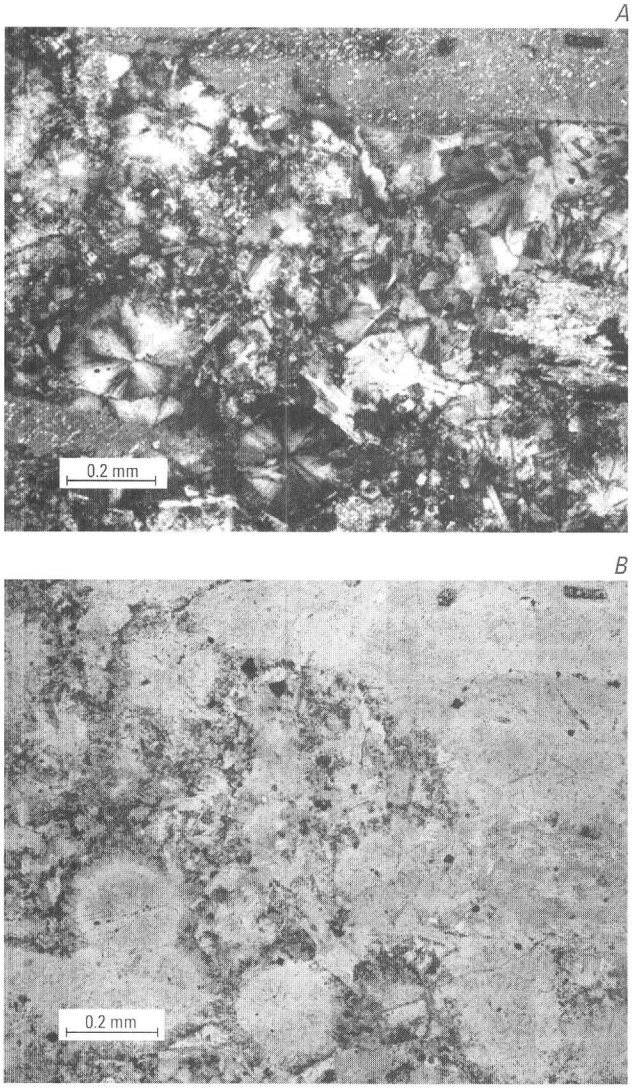

Figure E8. Photomicrographs showing spherulitic devitrification texture in felsite (NL812.55) from the Exmore beds in the USGS-NASA Langley core. *A*, Thin section in cross-polarized light. *B*, Thin section in plane-polarized light. Each spherulite is a spherical cluster of plagioclase crystals radiating from a central point as shown in *A*. Outer rims are rich in fine-grained potassium feldspar and appear gray in *B* because of a yellow sodium cobaltinitrite stain in the thin section.

Table E2. Results of X-ray fluorescence spectrometry analyses of two samples from the USGS-NASA Langley core.

[Analysts: D.F. Siems and J.E. Taggart, Jr., both of the U.S. Geological Survey. Samples are described in appendix E1]

Sample number....	**NL790.9**	**NL2083.1**
Rock type.....	**rhyolite clast**	**monzogranite**
Unit.....	**Exmore beds**	**Langley Granite**
Major oxide composition and loss on ignition (LOI) at 900°C, in weight percent [Method used: wavelength-dispersive X-ray fluorescence spectrometry (Taggart and others, 1987; Mee and others, 1996)]		
SiO_2.....	74.9	71.0
Al_2O_3.....	12.8	14.2
Fe_2O_3T*.....	1.80	2.93
MgO.....	.64	.77
CaO.....	.91	1.29
Na_2O.....	4.11	3.98
K_2O.....	2.69	3.48
TiO_2.....	.25	.38
P_2O_5.....	.11	.13
MnO.....	.06	.06
LOI.....	.99	1.24
Trace-element abundances, in parts per million [Method used: energy-dispersive X-ray fluorescence spectrometry (Siems, 2000, 2002)]		
Ag.....	<1	<1
As.....	<2	<2
Ba.....	902	668
Bi.....	<5	<5
Br.....	<1	2
Cd.....	2	<1
Ce**.....	47	61
Cr.....	7	7
Cs.....	<5	6
Cu.....	41	145
Ga.....	13	14
Ge.....	<2	<2
La**.....	29	30
Mo.....	4	4
Nb.....	8	12
Nd**.....	33	39
Ni.....	<2	4
Pb.....	28	60
Rb.....	89	123
Sb.....	<2	<2
Se.....	<1	<1
Sn.....	<2	3
Sr.....	176	156
Th.....	4	10
U.....	<4	<4
V.....	25	23
W***.....	<5	<5
Y.....	10	28
Zn.....	459	218
Zr.....	110	166

* Fe_2O_3T, total iron calculated as Fe_2O_3.
**See more accurate rare-earth-element abundances in table E3.
***W values probably reflect sample preparation procedure.

Table E3. Results of long-count instrumental-neutron-activation analyses (INAA) of two samples from the USGS-NASA Langley core.

[Analyst: J.R. Budahn of the U.S. Geological Survey. The method was described by Wandless (1996). Samples are described in appendix E1]

Sample number.....	NL790.9	NL2083.1
Rock type.....	rhyolite clast	monzogranite
Unit.....	Exmore beds	Langley Granite
Trace-element abundances, in parts per million		
As.....	1.21	0.75
Au.....	.0072	.0286
Ba.....	779	580
Co.....	2.66	3.65
Cr.....	2.88	1.78
Cs.....	1.15	1.14
Hf.....	2.99	5.23
Ni.....	2.2	3.6
Rb.....	87	121
Sb.....	.24	.18
Sc.....	3.19	5.78
Sr.....	177	185
Ta.....	.68	1.11
Th.....	6.89	9.95
U.....	1.5	2.1
W.....	1.0	.5
Zn.....	539	182
Zr.....	102	204
Rare-earth-element (REE) abundances, in parts per million		
La.....	20.3	20.4
Ce.....	38.3	50.1
Nd.....	14.7	24.0
Sm.....	2.57	5.46
Eu.....	.5	1.1
Gd.....	2.4	5.0
Tb.....	.30	.87
Ho.....	.44	1.26
Tm.....	.20	.59
Yb.....	1.27	3.8
Lu.....	.20	.55
Chondrite-normalized REE abundances (rock/chondrite) and the Eu/Eu* ratio[1]		
La.....	65.3	78.5
Ce.....	47.1	61.6
Nd.....	24.3	39.7
Sm.....	13.1	27.9
Eu.....	6.74	14.9
Gd.....	9.27	19.2
Tb.....	6.40	18.4
Ho.....	6.13	17.6
Tm.....	6.10	18.2
Yb.....	6.05	18.1
Lu.....	6.19	16.9
Eu/Eu*.....	.60	.63

[1]Eu/Eu* is the size of the europium anomaly, where Eu* is the europium concentration interpolated from surrounding elements in the REE pattern.

Table E4. Results of individual chemical analyses of two samples from the USGS-NASA Langley core.

[Analyses were done by a contractor for the U.S. Geological Survey using methods described by Jackson and others (1987). Samples are described in appendix E1. Contents of each constituent are reported in weight percent (%) except that F is in parts per million (ppm)]

Sample number.....	NL790.9	NL2083.1
Rock type.....	rhyolite clast	monzogranite
Unit.....	Exmore beds	Langley Granite
FeO (%).....	0.97	1.03
CO_2 (%).....	0.11	<0.01
CO_2 as carbonate (%)....	0.03	<0.003
S (%).....	0.18	0.42
F (ppm).....	212	358
H_2O^- (%).....	0.1	0.1
H_2O^+ (%).....	0.8	0.9

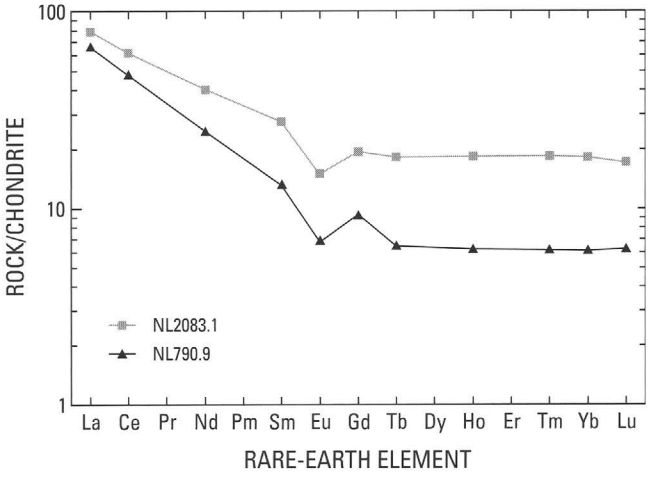

Figure E9. Rare-earth-element (REE) abundances normalized to chondrite abundances (rock/chondrite) for two samples from the USGS-NASA Langley core. The samples are a rhyolite clast (NL790.9) from the Exmore beds and a piece of the Langley Granite (NL2083.1). REE values are from table E3.

Discussion

Implications for the Chesapeake Bay Impact Event

The conclusion that multiple sets of planar deformation features in rare quartz grains from the Exmore beds are of shock-metamorphic origin is unambiguous. The presence of these features indicates that the quartz grains have experienced pressures greater than 6 GPa (Short, 1968) and strain rates greater than 10^6/second (Chao and Goresy, 1977, p. 291).

The relative proportion of shocked to unshocked quartz grains in the sediment is very low in comparison to the proportion in some other impact-related deposits (for example, see Izett, 1990, table 9), indicating that the shock-metamorphosed grains are mixed into and diluted by an enormous volume of unshocked material. This observation is consistent with the character of the Exmore beds as a mixed sedimentary deposit (Gohn and others, this volume, chap. C). The individual shocked quartz grains are mostly subangular, and they lack the rounded shapes that would indicate derivation from clastic sedimentary target deposits. Hence, we interpret them to be derived from crystalline rocks that underlie thick preimpact clastic sediments in the target region.

Although the possibility cannot be ruled out that some clasts of cataclastic rock in the Langley core could be derived from a faulted Piedmont source terrain, transported, and deposited in the outer coastal plain by purely sedimentary processes, such long-distance transport seems unlikely for clasts that are angular, internally fragmented, crumbly, and in some cases only weakly cohesive. Furthermore, shock-metamorphosed quartz is an integral part of the cataclastic fabric in some clasts. Shock metamorphism is not required to produce most of the high-strain-rate fabrics observed, but the occurrence of these fabrics together with shocked quartz strongly suggests that they were impact generated.

Using samples from earlier drill cores in the Chesapeake Bay impact structure, Reimold and others (2002) estimated shock pressures of 10–20 GPa from a small data set on the orientations and relative frequencies of planar deformation features in quartz. The Langley core has not produced enough quartz grains containing planar deformation features, or enough of these features per grain, to support a statistical study of their crystallographic orientations and relative frequencies or to estimate shock pressures by using the methods reviewed and critiqued by Grieve and others (1996).

The spherulitic texture observed in some felsite clasts (fig. E8), including one that has shocked quartz, is attributed to devitrification. Koeberl and others (1996, fig. 4B) interpreted a similar spherulitic texture as impact melt because the spherulitic matrix contained "clasts" of shocked quartz and feldspar. Alternatively, this texture could be a preimpact feature of volcanic target rocks similar to those described by Allen and Wilson (1968) in the North Carolina Piedmont. Isotopic dating of the spherulites may allow discrimination between these hypotheses.

Ejecta-derived rock fragments in the core are sparsely disseminated throughout the Exmore beds, and the largest are found near the base of the unit (fig. E3 and appendix E1). This distribution is consistent with evidence that the Exmore at this location was deposited as crudely size-graded units (Gohn and others, this volume, chap. C). We found one crystalline rock fragment containing shock-metamorphosed quartz below the Exmore beds (sample NL905.0; figs. E3 and E4*E* and appendix E1); it was in a zone of mixing about 6.4 m (21.0 ft) below the base of the Exmore. We interpret this isolated occurrence as evidence for downward injection or infiltration of sediment from the Exmore beds into the upper part of crater unit B.

Preimpact target rocks of the Chesapeake Bay impact structure are widely inferred to be the source of impact glass in tektites of the North American strewn field (Poag and others, 1994; Koeberl and others, 1996; Glass, 2002). Evidence from other strewn fields suggests that only the upper ~200 m (~650 ft) of target material was involved in the formation of tektites (Koeberl, 1994); thus, crystalline basement in the Chesapeake Bay impact structure is not as likely as the overlying preimpact sediments to be a source of the North American tektites.

The chemical compositions of tektites, including bediasites, georgiaites, and microtektites, from the North American strewn field were summarized in Koeberl (1990), Albin and others, (2000), and Koeberl and others (2001). The bulk major-element composition of the rhyolite clast (NL790.9) most closely resembles that of bediasites; it is similar in Si, Al, Mg, and Ca, lower in Ti and Fe, and higher in K and Na (volatile).

We compared the REE patterns in figure E9 with those of tektites from the North American strewn field (Albin and others, 2000, fig. 5; Huber and others, 2000, fig. 1). The REE distribution for the Langley Granite (NL2083.1) is within the range of REE distributions determined for tektites, and the rhyolite (NL790.9) is slightly depleted in REEs relative to the tektites. Both the rhyolite and the granite have patterns of light REE enrichment similar to those of the tektites, as well as flatter distributions of heavy REEs and larger negative europium anomalies than most tektites. Both the rhyolite and the Langley Granite have other trace-element concentrations (tables E2 and E3) that are clearly lower (Co, Cr, and Ni) or higher (Cu and Zn) than concentrations in the North American tektites (Koeberl, 1990, table 2; Koeberl and others, 2001, table 1).

Tektites of the North American strewn field are composed mainly of SiO_2 (microtektites averaging 70.7 percent, bediasites averaging 76.4 percent, and georgiaites averaging 81.5 percent) and Al_2O_3 (microtektites averaging 15.4 percent, bediasites averaging 13.8 percent, and georgiaites averaging 10.7 percent). Middle Eocene to Paleocene sediments in the area of the Chesapeake Bay impact structure tend to be lower in both (Koeberl, 1990, table 1; Koeberl and others, 2001, table 1). The rhyolite and granite in table E2 are comparable to the tektites in Al_2O_3 and are slightly lower in SiO_2.

Geochemical studies of these tektites show triangular arrays in oxide-oxide variation diagrams that indicate mixing of at least three source components, including a silica-rich (~90 weight percent) material such as quartz-rich sand and two com-

ponents higher in Al_2O_3 (about 16 to 18 weight percent) and in FeO (about 5.5 to 6.5 weight percent) such as shale or graywacke (Albin and others, 2000). The rhyolite and granite have intermediate compositions within the range defined by these hypothetical end members. Albin and others (2000) suggested that a crystalline basement component might explain some unusual La-Th-Sc characteristics and high Rb/Cs ratios in georgiaites. The rhyolite fragment (NL790.9) has La/Th (=2.9), Th/Sc (=2.2), and La/Sc (=6.4) ratios in the range of ratios for North American tektites and a Rb/Cs (=76) ratio higher than the ratio for the tektites. At this stage, the rhyolite is neither confirmed nor ruled out as a source for some tektites. Further geochemical studies of preimpact sediments, as well as crystalline basement and basement-derived ejecta, will be needed to link the chemistry of tektites to potential source materials.

Crystalline Terrane beneath the Coastal Plain

The crystalline rocks concealed beneath thick sedimentary deposits of the Atlantic Coastal Plain are poorly known and are considered to be one of the last frontiers of regional geology in the United States. The impact event served as a remarkable sampling tool that excavated an enormous volume of coastal plain basement rocks and scattered the fragments where they can be sampled at shallower levels.

All of the lithic clasts in the Langley core that were confirmed or suspected to be impact ejecta consist of the same rock type, a variably porphyritic felsite of rhyolitic composition. Although this felsite is petrographically distinct from the Langley Granite (Horton and others, this volume, chap. B), both rocks have similar, slightly peraluminous, bulk compositions. Similarities in REE patterns (fig. E9) and other trace-element concentrations (tables E2, E3, and E4) suggest that the rhyolite and granite magmas originated in the same volcanic arc setting. We thus infer that the undated rhyolite fragment is about the same age as the Neoproterozoic Langley Granite, which was dated at 612±10 Ma (Horton and others, this volume, chap. B). Working hypotheses for the age of spherulitic devitrification texture range from as old as Neoproterozoic (if formed in preimpact volcanic rock) to as young as late Eocene (if formed in impact glass).

The trace-element concentrations and discrimination diagrams discussed above consistently indicate that the rhyolite fragment and the Langley Granite originated in a volcanic arc setting. Thus, they are chemically distinct from Neoproterozoic granitoids that intruded Mesoproterozoic basement of the Goochland terrane in the Piedmont (see table B6 and fig. B11 of Horton and others, this volume, chap. B), which have higher concentrations of alkalis (Na_2O+K_2O >8.6 percent), Ga (>30 parts per million; ppm), Nb (>70 ppm), and Y (>89 ppm) typical of A-type granites (Owens and Tucker, 2003). Testing specific petrologic and tectonic correlations with Neoproterozoic magmatic arc terranes of the southeastern United States and studying implications for the Chesapeake Bay tectonic indenter of Archean crust proposed by Lefort and Max (1991) would require further investigation, as discussed by Horton and others (this volume, chap. B).

The relatively uniform composition of impact-derived rock fragments at the Langley corehole differs from the distribution of clast compositions at other sites in the western annular trough, where such fragments include a variety of felsic to mafic plutonic rocks as well as felsite (Horton, Aleinikoff, and others, 2002; Horton, Kunk, and others, 2002). The distinctive population of impact-derived clasts at this site suggests that the original impact ejecta were distributed unevenly, perhaps in rays. If so, the geographic distribution of impact-derived rock fragments may provide clues to the preimpact distribution of rock types and their relations in the target area.

Age of Impact Metamorphism based on Argon Dating of Tektites

Background

Estimates of the age of the Chesapeake Bay impact structure based on isotopic dating of North American tektites are widely cited (for example, by Koeberl and others, 1996). An $^{40}Ar/^{39}Ar$ geochronological study to improve the dating of those tektites, although outside the main focus of this chapter on data from the USGS-NASA Langley core, is discussed here to make the results available.

Tektites and microtektites that constitute the North American strewn field are thought to have originated by melting of near-surface sediments in the Chesapeake Bay area of Virginia, when a large asteroid or comet nucleus struck that area (Poag and others, 1994; Koeberl and others, 1996) about 35.2 to 35.8 million years ago (Obradovich and others, 1989). Tektites of this strewn field have been found mainly in upper Cenozoic gravel deposits derived from erosion of upper Eocene deposits in Georgia (georgiaites) and Texas (bediasites). Tektites less than 1.0 mm (0.039 in.) in diameter, termed microtektites, have been found in upper Eocene marine sediments in the Atlantic Ocean and Caribbean Sea.

Suess (1900) proposed the term "tektite" for small, corroded silicate glass nodules found near the Moldau River in southern Bohemia, Czechoslovakia. He suggested that the glass objects, similar in some aspects to obsidian, formed by melting of meteoritic material. Since that time, many different definitions have been proposed, emphasizing different aspects of these curious glass nodules.

Baker (1959, p. 11) defined tektites as "natural objects of impure silica glass found in thousands on the surface of certain parts of the earth, and in places buried several feet beneath surficial deposits." He noted that they occur in widely separated regions and show minor chemical composition and physical variations from place to place.

In the "Glossary of Geology" (Jackson, 1997, p. 653), a tektite was defined as "A rounded pitted jet-black to greenish or yellowish body of silicate glass of nonvolcanic origin, usually walnut-sized, found in groups in several widely separated areas of the Earth's surface [so-called strewn fields] and generally

bearing no relation to the associated [underlying] geologic formations." The definition indicated that some "have shapes strongly suggesting aerodynamic ablation during hypersonic flight."

Tektites have been studied for more than a century, and considerable physical and chemical information has been gathered (see references in O'Keefe, 1976). Chao (1963) studied several thousand tektites and noted three of their main features: (1) distinctive shapes (flanged buttons, cores, dumbbells, and elongated teardrops), (2) unique surface sculpture, and (3) color and luster. He also observed that tektites have three diagnostic microscopic characteristics: (1) universal presence of flow structure and associated strain birefringence, (2) general presence of siliceous glass inclusions (see Barnes, 1940), and (3) general absence of microlites. Ross (1962) observed that obsidians are rarely without microlites, crystallites, trichites, and Fe-oxide dust. In contrast, tektites are devoid of such materials. Aghassi (1962) and Chao (1963, p. 63) noted that tektites nearly always contain widely disseminated bubble cavities or vesicles.

Isotopic ages reported previously for the different tektite groups (Cretaceous-Tertiary (K-T) boundary, North American, Moldavite, Ivory Coast, and Australasian) were obtained in different laboratories using several different techniques (K-Ar, $^{40}Ar/^{39}Ar$, and fission track) and using diverse standards and decay constants. Fleischer and Price (1964) obtained fission-track ages (35.4, 35.3, and 27.2 Ma) for three bediasites from Texas. Albin and Wampler (1996) measured conventional K-Ar ages of georgiaites and calculated a mean age of 35.2±0.3 Ma. For North American tektites and microtektites, $^{40}Ar/^{39}Ar$ ages have been reported by Glass and others (1986, 35.4±0.6 Ma), Obradovich and others (1989, 35.5±0.3 Ma), and Glass and others (1995, 35.0±0.1 Ma). U-Pb zircon geochronology of shocked and unshocked zircons from several sites, although "not straightforward" (Kamo and others, 2002), is compatible with these results.

Argon Dating Methods

Total-fusion $^{40}Ar/^{39}Ar$ ages were determined for 19 analyses of 4 North American tektites as part of a larger $^{40}Ar/^{39}Ar$ study of all known tektite types by one of us (Izett) using the same mass spectrometer, methods, fluence monitors, and decay constants. The analytical data and ages presented in table E5 were determined in the USGS laboratory in Menlo Park, Calif., by using procedures described by Dalrymple and Lanphere (1971), Dalrymple and Duffield (1988), and Dalrymple (1989).

A technical feature of the $^{40}Ar/^{39}Ar$ method is that geologic materials of unknown age such as tektites are irradiated with fast neutrons next to a fluence-monitor mineral, or standard, having an accepted isotopic age. Thus, the method is a relative one; ages of unknown materials are relative to ages of a selected fluence-monitor mineral. The measured $^{40}Ar/^{39}Ar$ ratios of the fluence-monitor mineral are used with its known age to calculate a conversion factor, *J*, which is a measure of the fraction of ^{39}K converted to ^{39}Ar by the fast neutron reaction ($^{39}K(n,p)^{39}Ar$). The factor *J* is then used in the age equation to calculate ages for materials of unknown age. The precision of the fluence-monitor mineral calibration has a significant effect on the precision of the ages calculated for materials of unknown age.

For the North American tektites, $^{40}Ar/^{39}Ar$ ages were determined by using single fragments about 0.3 mm (0.12 in.) in diameter. The tektite fragments were irradiated in the core of the USGS TRIGA reactor. A typical irradiation packet consisted of the tektite fragments loaded into a 9-mm-diameter (0.35-in.-diameter) aluminum-foil cup and covered by a 9-mm aluminum-foil cap. The flattened pancakelike packets were sandwiched between similar packets of the neutron fluence monitor and arranged in a vertical stack in a 10-mm-diameter (0.39-in.-diameter) quartz glass tube; the position of the packets was measured. The distance between adjacent packet centers typically was about 0.3 mm (0.012 in.). The neutron fluence within the radiation package was measured by analyzing five to seven lots of two to three sanidine crystals for the fluence monitor.

We used sanidine from the Taylor Creek Rhyolite of New Mexico (Dalrymple and Duffield, 1988) as a fluence-monitor mineral because it has been shown to be uniform in K and Ar content and its isotopic age is within an acceptable range of ages for North American tektites. Dalrymple and others (1993) gave reasons for using an age of 27.92 Ma for sanidine from the Taylor Creek Rhyolite. Lanphere and Dalrymple (2000) measured an age of 513.9±2.3 Ma for the widely used MMhb–1 hornblende, which is 1.26 percent younger than the internationally adopted mean value of 520.4 Ma (Samson and Alexander, 1987). Ages reported in this chapter were first calculated using an age of 27.92 Ma for sanidine from the Taylor Creek Rhyolite of New Mexico; they were then recalculated by using an age of 28.32 Ma for sanidine from the Taylor Creek Rhyolite, which is based on the internationally adopted mean value of 520.4 Ma for MMhb–1 hornblende. All ages reported herein were calculated by using decay constants recommended by the Subcommission on Geochronology of the IUGS (Steiger and Jäger, 1977).

Results of Argon Geochronology

The individual tektite ages in table E5 are given to two decimal places, and the composite, final age is rounded to one decimal place. Errors given for individual $^{40}Ar/^{39}Ar$ ages are estimates of the analytical precision at the 1σ level and include a conservative error of 0.5 percent in *J*. The final composite age is a weighted mean $\pm\sigma_{best}$, where weighting is by the inverse of the variance (Taylor, 1982). The result is a weighted-mean total-fusion $^{40}Ar/^{39}Ar$ age of 35.3±0.1 Ma (±l σ) for 19 analyses of 4 North American tektites. We interpret this age as recording the age of the late Eocene Chesapeake Bay impact event.

Age Constraints for the Chesapeake Bay Impact

Previous estimates of the age of the Chesapeake Bay impact structure have been based either on micropaleontology

Table E5. Total-fusion $^{40}Ar/^{39}Ar$ ages of North American tektites from Washington County, Ga., and Lee County, Tex.

[Analyses by Glen A. Izett in the U.S. Geological Survey (USGS) laboratory, Menlo Park, Calif., as described in the text. Procedures used were described by Dalrymple and Lanphere (1971), Dalrymple and Duffield (1988), and Dalrymple (1989). *J*, conversion factor discussed in text; *, radiogenic]

Location	Experiment number	Catalog number[1]	*J*	$^{37}Ar/^{39}Ar$	$^{36}Ar/^{39}Ar$	$^{40}Ar/^{39}Ar^*$	$^{40}Ar^*$ (%)	Age (Ma)	Error (σ)
Georgia	94Z0379	MNGaTek	6.94E-03	0.0504	0.0015	2.7843	86.0	34.53	0.22
Georgia	94Z0380	MNGaTek	6.94E-03	0.0639	0.0012	2.7826	88.7	34.51	0.22
Georgia	94Z0382	MNGaTek	6.94E-03	0.0542	0.0002	2.7961	98.0	34.67	0.21
Georgia	94Z0383	MNGaTek	6.94E-03	0.0597	0.0035	2.7731	72.6	34.39	0.23
Georgia	94Z0384	MNGaTek	6.94E-03	0.0614	0.0022	2.7821	81.0	34.50	0.22
Texas	93Z0441	B–97	6.20E-03	0.1042	0.0003	3.1135	97.3	34.46	0.26
Texas	93Z0442	B–97	6.20E-03	0.1039	0.0003	3.1223	97.3	34.56	0.24
Texas	94Z0365	B–97	6.94E-03	0.1050	0.0001	2.7906	98.8	34.60	0.21
Texas	94Z0366	B–97	6.94E-03	0.1039	0.0001	2.8060	98.9	34.79	0.24
Texas	94Z0367	B–97	6.94E-03	0.1064	0.0001	2.7931	99.1	34.63	0.23
Texas	94Z0368	B–97	6.94E-03	0.1037	0.0001	2.8004	99.0	34.72	0.22
Texas	96Z0194	30773	7.07E-03	0.1049	0.0002	2.7590	98.3	34.83	0.21
Texas	96Z0195	30773	7.07E-03	0.1050	0.0002	2.7494	98.2	34.71	0.21
Texas	96Z0196	30773	7.07E-03	0.1062	0.0001	2.7496	98.4	34.71	0.21
Texas	97Z0516	B–74	7.09E-03	0.1348	0.0000	2.7671	99.8	35.04	0.24
Texas	97Z0517	B–74	7.09E-03	0.1386	0.0001	2.7579	99.2	34.93	0.22
Texas	97Z0518	B–74	7.09E-03	0.1396	0.0001	2.7538	99.1	34.88	0.24
Texas	97Z0519	B–74	7.09E-03	0.1365	0.0002	2.7552	97.4	34.90	0.21
Texas	97Z0520	B–74	7.09E-03	0.1384	0.0001	2.7444	98.7	34.76	0.22
						Initial weighted mean age[2]		34.8	0.1
						Recalculated weighted mean age[2]		35.3	0.1

[1]All four tektites are now in the collection of the Denver Museum of Natural History. Tektite MNGaTek was collected by R.L. Strange. Tektite 30773 came from the University of Texas Museum in Austin. Tektites B–74 and B–97 were sent by V.E. Barnes (USGS) to E.C.T. Chao (USGS).

[2]The initial weighted mean age of 34.8 Ma was calculated relative to a fluence-monitor age of 27.92 Ma for sanidine from the Taylor Creek Rhyolite; the sanidine age was based on an age for MMhb–1 hornblende of 513.9 Ma. The recalculated mean age of 35.3 Ma was determined relative to a fluence-monitor age for MMhb–1 hornblende of 520.4 Ma. The error for individual ages is ±1σ and includes a conservative error of 0.5 percent in *J;* the group error is $\pm 1\sigma_{best}$ of Taylor (1982).

within the structure or on geochronology of North American tektites from outside the structure. Studies of micropaleontology within the structure indicate that the impact event occurred in the late Eocene biochronozones P15 of planktonic foraminifera and NP 19/20 of calcareous nannofossils (Poag and Aubry, 1995; Poag, 1996, 1997). A layer of impact ejecta offshore of New Jersey at Deep Sea Drilling Project (DSDP) Site 612, although somewhat reworked, is in the same biochronozones (Poag and Aubry, 1995; Poag, 1997), and tektite material from that layer is considered to be part of the North American strewn field on the basis of geochemistry (Stecher and others, 1989). Most of the previously cited argon and fission-track dates of tektites and microtektites from the North American strewn field, including those from the DSDP 612 layer, are consistent with the biochronological data, have overlapping uncertainties, and cluster in the range of ~35 Ma to ~36 Ma. The weighted mean $^{40}Ar/^{39}Ar$ age of 35.3±0.1 Ma (±1σ) presented here for the North American tektite material is interpreted to date the late Eocene Chesapeake Bay impact event.

Conclusions

The Chesapeake Bay impact excavated unknown coastal plain basement rocks and scattered the fragments where we can sample them at shallower levels. This study of shock-metamorphosed minerals and impact-derived crystalline rock fragments in the USGS-NASA Langley core produced the following conclusions:

1. The sandy matrix of the Exmore beds contains sparse quartz grains (0.1 to 0.3 mm (0.004 to 0.012 in.) in diameter) that contain multiple sets of intersecting planar deformation features, commonly referred to as shock lamellae. As many as five different sets have been observed in some quartz grains. Planar deformation features also occur in quartz grains in reworked crystalline-rock clasts in and just below the Exmore beds. The presence of these features indicates that the quartz grains have experienced pressures greater than 6 GPa and strain rates greater than 10^6/second. The conclusion that such grains are of shock-metamorphic impact origin is unambiguous.

2. The shock-metamorphosed quartz grains, although rare, provide clear and convincing evidence that the Exmore beds are of hybrid impact origin. The identification of shocked quartz grains in the Langley core adds to the number of drill sites in Virginia where their presence in the structure is confirmed.

3. The proportion of shocked to unshocked quartz grains in the sedimentary matrix is very low in comparison to the proportion in some other impact-related deposits, indicating that the shock-metamorphosed grains are mixed into and diluted by an

enormous volume of unshocked sedimentary material. This observation is consistent with the character of the Exmore beds as a mixed sediment, which Gohn and others (this volume, chap. C) interpret as a seawater-resurge deposit.

4. Individual shock-metamorphosed quartz grains lack the rounded shapes that would indicate derivation from a clastic sedimentary target and are inferred to be mainly particles of excavated crystalline basement, or possibly smashed detrital grains.

5. Shock-metamorphosed quartz is an integral part of the cataclastic fabric in some clasts, indicating that both the fabric and the shocked quartz were produced by the same hypervelocity impact event. All of the crystalline rock fragments that contain shocked quartz also have cataclastic fabrics.

6. In this core, all of the rock fragments that are confirmed or interpreted to be reworked impact ejecta consist of variably porphyritic felsite. The chemical analysis of one sample shows it to be peraluminous rhyolite from a volcanic arc setting. The undated felsite is inferred to be Neoproterozoic in age on the basis of geochemical similarities to the dated Langley Granite of Horton and others (this volume, chap. B).

7. The monotonous population of impact-derived crystalline-rock clasts at the Langley site, in contrast to the varied populations at other sites in the western annular trough, suggests that the original impact ejecta were distributed unevenly, perhaps in rays. If so, the geographic distribution of impact-derived fragments may provide clues to the original distribution of rock types in the target area.

8. Some felsite clasts contain spherulites that are interpreted to be devitrification products, either of an Eocene impact melt or of older preimpact volcanic rock in the target area.

9. Impact-derived rock fragments are sparsely disseminated throughout the Exmore beds section of the core. Those larger than the core diameter were found in the lower half of the unit, suggesting that the Exmore at this location may consist of crudely size-graded deposits.

10. The presence of shock-metamorphosed quartz in a rock fragment several meters below the Exmore beds suggests injection or infiltration of resurge sediments from the Exmore beds (or particles from an ejecta blanket removed by resurge erosion?) into the upper part of crater unit B.

11. Trace-element geochemistry of a rhyolite fragment that is interpreted to be impact derived and a sample of the granite basement from the Langley core neither confirms nor rules out crystalline basement in the Chesapeake Bay impact structure as a partial source for some tektites of the North American strewn field.

12. A weighted-mean total-fusion $^{40}Ar/^{39}Ar$ age of 35.3±0.1 Ma (±1σ) for 19 analyses of 4 North American tektites records the age of the late Eocene Chesapeake Bay impact event.

Questions raised by this research are being addressed as our efforts expand to include samples from other coreholes (Horton, Aleinikoff, and others, 2002; Horton, Kunk, and others, 2002). Continued studies should provide insight into the character, age, and origin of rocks excavated by the impact and their relations to basement rocks sampled by deep drilling. They can provide valuable information on the regional geology of crystalline terranes beneath the Atlantic Coastal Plain, a context for understanding the Eocene impact structure, and a test of hypothetical models such as the proposed Chesapeake Bay tectonic indenter of Archean crust (Lefort and Max, 1991; Horton and others, this volume, chap. B). Isotopic dating of minerals from impact-derived clasts may yield information on thermal effects of the impact.

Acknowledgments

U.S. Geological Survey (USGS) investigations of the Chesapeake Bay impact structure are conducted in cooperation with the Hampton Roads Planning District Commission, the Virginia Department of Environmental Quality, and the National Aeronautics and Space Administration (NASA) Langley Research Center. The Hampton Roads Planning District Commission and the USGS provided funds for the drilling of the USGS-NASA Langley corehole. The NASA Langley Research Center provided extensive operational and logistical support for the drilling operation. The Virginia Department of Environmental Quality and the Department of Geology of the College of William and Mary provided extensive operational support at the drill site.

We thank Daniel J. Milton (USGS Emeritus) and Bevan M. French (Smithsonian Institution) for stimulating discussions of shock metamorphism, Yolanda Fong-Sam (USGS) for help in preparing figure E3, and James R. Budahn (USGS) for plotting the diagram in figure E9. Reviews by Jeffrey N. Grossman (USGS) and Daniel J. Milton and a partial review by Michael J. Kunk (USGS) significantly improved the manuscript.

References Cited

Aghassi, B., 1962, Bubble distribution in tektites and Libyan desert glass: Astronomical Contributions of Boston University, v. 13, p. 1–8.

Ahrens, T.J., and Rosenberg, J.T., 1968, Shock metamorphism—Experiments on quartz and feldspar, *in* French, B.M., and Short, N.M., eds., Shock metamorphism of natural materials: Baltimore, Md., Mono Book Corporation, p. 59–81.

Albin, E.F., Norman, M.D., and Roden, Michael, 2000, Major and trace element compositions of georgiaites—Clues to the source of North American tektites: Meteoritics & Planetary Science, v. 35, no. 4, p. 795–806.

Albin, E.F., and Wampler J.M., 1996, New potassium-argon ages for georgiaites and the upper Eocene Dry Branch Formation (Twiggs Clay Member); Inferences about tektite stratigraphic occurrence [abs.]: Lunar and Planetary Science Conference, 27th, Houston, Tex., March 18–22, 1996, Abstracts, pt. 1, p. 5–6.

Alexopoulos, J.S., Grieve, R.A.F., and Robertson, P.B., 1988, Microscopic lamellar deformation features in quartz—Discriminative characteristics of shock-generated varieties: Geology, v. 16, no. 9, p. 796–799.

Allen, E.P., and Wilson, W.F., 1968, Geology and mineral resources of Orange County, North Carolina: North Carolina Geological Survey Bulletin 81, 58 p., 1 oversize pl.

Arbogast, B.F., ed., 1996, Analytical methods manual for the Mineral Resource Surveys Program, U.S. Geological Survey: U.S. Geological Survey Open-File Report 96–525, 248 p.

Baedecker, P.A., and McKown, D.M., 1987, Instrumental neutron activation analysis of geochemical samples, chap. H *of* Baedecker, P.A., ed., Methods for geochemical analysis: U.S. Geological Survey Bulletin 1770, p. H1–H14.

Baker, George, 1959, Tektites: Memoirs of the National Museum of Victoria, no. 23, 313 p.

Barnes, V.E., 1940, North American tektites: University of Texas Bureau of Economic Geology Publication 3945, p. 477–583.

Bunch, T.E., 1968, Some characteristics of selected minerals from craters, *in* French, B.M., and Short, N.M., eds., Shock metamorphism of natural materials: Baltimore, Md., Mono Book Corporation, p. 413–432.

Carter, N.L., 1965, Basal quartz deformation lamellae—A criterion for recognition of impactites: American Journal of Science, v. 263, no. 9, p. 786–806.

Carter, N.L., 1971, Static deformation of silica and silicates: Journal of Geophysical Research, v. 76, no. 23, p. 5514–5540.

Carter, N.L., Christie, J.M., and Griggs, D.T., 1964, Experimental deformation and recrystallization of quartz: Journal of Geology, v. 72, no. 6, p. 687–733.

Chao, E.C.T., 1963, The petrographic and chemical characteristics of tektites, *in* O'Keefe, J.A., ed., Tektites: Chicago, University of Chicago Press, p. 51–94.

Chao, E.C.T., 1967, Shock effects in certain rock-forming minerals: Science, v. 156, no. 3772, p. 192–202.

Chao, E.C.T., 1968, Pressure and temperature histories of impact metamorphosed rocks; Based on petrographic observations, *in* French, B.M., and Short, N.M., eds., Shock metamorphism of natural materials: Baltimore, Md., Mono Book Corporation, p. 125–158.

Chao, E.C.T., 1976, The application of quantitative interference microscopy to mineralogic and petrologic investigations: American Mineralogist, v. 61, no. 3–4, p. 212–228.

Chao, E.C.T., and Goresy, Ahmed el, 1977, Shock attenuation and the implantation of Fe-Cr-Ni veinlets in the compressed zone of the 1973 Ries research deep drill core: Geologica Bavarica, v. 75, p. 289–304.

Dalrymple, G.B., 1989, The GLM continuous laser system for $^{40}Ar/^{39}Ar$ dating—Description and performance characteristics, *in* Shanks, W.C., III, and Criss, R.E., eds., New frontiers in stable isotopic research—Laser probes, ion probes, and small-sample analysis: U.S. Geological Survey Bulletin 1890, p. 89–96.

Dalrymple, G.B., and Duffield, W.A., 1988, High precision $^{40}Ar/^{39}Ar$ dating of Oligocene rhyolites from the Mogollon-Datil volcanic field using a continuous laser system: Geophysical Research Letters, v. 15, no. 5, p. 463–466.

Dalrymple, G.B., Izett, G.A., Snee, L.W., and Obradovich, J.D., 1993, $^{40}Ar/^{39}Ar$ age spectra and total-fusion ages of tektites from Cretaceous-Tertiary boundary sedimentary rocks in the Beloc Formation, Haiti: U.S. Geological Survey Bulletin 2065, 20 p.

Dalrymple, G.B., and Lanphere, M.A., 1971, $^{40}Ar/^{39}Ar$ technique of K-Ar dating; A comparison with the conventional technique: Earth and Planetary Science Letters, v. 12, no. 3, p. 300–308.

Edwards, L.E., Frederiksen, N.O., Self-Trail, J.M., and Poag, C.W., 2002, Paleontology of crater-fill deposits, Chesapeake Bay impact structure, Virginia [abs.]: Geological Society of America Abstracts with Programs, v. 34, no. 6, p. 465–466.

Edwards, L.E., and Powars, D.S., 2003, Impact damage to dinocysts from the late Eocene Chesapeake Bay event: Palaios, v. 18, no. 3, p. 275–285. (Also available online at http://www.bioone.org/pdfserv/i0883-1351-018-03-0275.pdf)

Edwards, L.E., and Self-Trail, J.M., 2002, Shocking news—Impact effects on marine microfossils, Chesapeake Bay impact structure, Virginia [abs.]: Eos, Transactions, American Geophysical Union, v. 83, no. 19, spring meeting supplement of 7 May 2002, Abstract T21A–04, p. S351.

Engelhardt, W. von, and Bertsch, W., 1969, Shock induced planar deformation structures in quartz from the Ries crater, Germany: Contributions to Mineralogy and Petrology, v. 20, no. 3, p. 203–234.

Engelhardt, W. von, Hörz, F., Stöffler, D., and Bertsch, W., 1968, Observations on quartz deformation in the breccias of West Clearwater Lake, Canada, and the Ries basin, Germany, *in* French, B.M., and Short, N.M., eds., Shock metamorphism of natural materials: Baltimore, Md., Mono Book Corporation, p. 475–482.

Fleischer, R.L., and Price, P.B., 1964, Fission track evidence for the simultaneous origin of tektites and other natural glasses: Geochimica et Cosmochimica Acta, v. 28, no. 6, p. 755–760.

French, B.M., 1998, Traces of catastrophe; A handbook of shock-metamorphic effects in terrestrial meteorite impact structures: Houston, Tex., Lunar and Planetary Institute, LPI Contribution No. 954, 120 p.

French, B.M., and Short, N.M., eds., 1968, Shock metamorphism of natural materials: Baltimore, Md., Mono Book Corporation, 644 p.

Glass, B.P., 2002, Distal impact ejecta from the Chesapeake Bay impact structure [abs.]: Geological Society of America Abstracts with Programs, v. 34, no. 6, p. 466.

Glass, B.P., Hall, C.M., and York, Derek, 1986, $^{40}Ar/^{39}Ar$ laser-probe dating of North American tektite fragments from Barbados and the age of the Eocene-Oligocene boundary: Chemical Geology (Isotope Geoscience Section), v. 59, no. 2–3, p. 181–186.

Glass, B.P., Koeberl, C., Blum, J.D., Senftle, F., Izett, G.A., Evans, B.J., Thorpe, A.N., Povenmire, H., and Strange, R.L., 1995, A muong nong-type Georgia tektite: Geochimica et Cosmochimica Acta, v. 59, no. 19, p. 4071–4082.

Glass, B.P., and Liu, Shaobin, 2001, Discovery of high-pressure $ZrSiO_4$ polymorph in naturally occurring shock-metamorphosed zircons: Geology, v. 29, no. 4, p. 371–373.

Glass, B.P., Liu, Shaobin, and Leavens, P.B., 2002, Reidite—An impact-produced high-pressure polymorph of zircon found in marine sediments: American Mineralogist, v. 87, no. 4, p. 562–565.

Gohn, G.S., Clark, A.C., Queen, D.G., Levine, J.S., McFarland, E.R., and Powars, D.S., 2001, Operational summary for the USGS-NASA Langley corehole, Hampton, Virginia: U.S. Geological Survey Open-File Report 01–87–A, 21 p., available online at http://pubs.usgs.gov/of/2001/of01-087/

Gohn, G.S., Powars, D.S., Bruce, T.S., Self-Trail, J.M., Weems, R.E., Edwards, L.E., Horton, J.W., Jr., Izett, G.A., and Johnson, G.H., 2001, Preliminary interpretation of the USGS-NASA Langley corehole, Chesapeake Bay impact structure, York-James Peninsula, Hampton, VA [abs.]: Geological Society of America Abstracts with Programs, v. 33, no. 2, p. A–24.

Gohn, G.S., Powars, D.S., Quick, J.E., Horton, J.W., Jr., and Catchings, R.D., 2002, Variation of impact response with depth and lithology, outer annular trough of the Chesapeake Bay impact structure, Virginia Coastal Plain [abs.]: Geological Society of America Abstracts with Programs, v. 34, no. 6, p. 465.

Grieve, R.A.F., 1991, Terrestrial impact—The record in the rocks: Meteoritics, v. 26, no. 3, p. 175–194.

Grieve, R.A.F., Dence, M.R., and Robertson, P.B., 1977, Cratering processes—As interpreted from the occurrence of impact melts, *in* Roddy, D.J., Pepin, R.O., and Merrill, R.B., eds., Impact and explosion cratering: New York, Pergamon, p. 791–814.

Grieve, R.A.F., Langenhorst, Falko, and Stöffler, Dieter, 1996, Shock metamorphism of quartz in nature and experiment—II, Significance in geoscience: Meteoritics, v. 31, no. 1, p. 6–35.

Harris, N.B.W., Pearce, J.A., and Tindle, A.G., 1986, Geochemical characteristics of collision-zone magmatism, *in* Coward, M.P., and Ries, A.C., eds., Collision tectonics: Geological Society of London Special Publication 19, p. 67–81.

Hobbs, B.E., Means, W.D., and Williams, P.F., 1976, An outline of structural geology: New York, John Wiley & Sons, 571 p.

Horton, J.W., Jr., Aleinikoff, J.N., Izett, G.A., Naeser, C.W., and Naeser, N.D., 2001, Crystalline rocks from the first corehole to basement in the Chesapeake Bay impact structure, Hampton, Virginia [abs.]: Geological Society of America Abstracts with Programs, v. 33, no. 6, p. A–448.

Horton, J.W., Jr., Aleinikoff, J.N., Izett, G.A., Naeser, N.D., Naeser, C.W., and Kunk, M.J., 2002, Crystalline basement and impact-derived clasts from three coreholes in the Chesapeake Bay impact structure, southeastern Virginia [abs.]: Eos, Transactions, American Geophysical Union, v. 83, no. 19, spring meeting supplement of 7 May 2002, Abstract T21A–03, p. S351. (Also available online at http://www.agu.org/meetings/waissm02.html)

Horton, J.W., Jr., Gohn, G.S., Edwards, L.E., Self-Trail, J.M., Powars, D.S., Kunk, M.J., and Izett, G.A., 2003, Recent research in the Chesapeake Bay impact crater, USA—Part 2. Reworked ejecta and impact debris [abs.]: International Conference on Large Meteorite Impacts, 3d, Noerdlingen, Germany, August 5–7, 2003, Abstract 4051, available online at http://www.lpi.usra.edu/meetings/largeimpacts2003/pdf/4051.pdf

Horton, J.W., Jr., Kunk, M.J., Naeser, C.W., Naeser, N.D., Aleinikoff, J.N., and Izett, G.A., 2002, Petrography, geochronology, and significance of crystalline basement rocks and impact-derived clasts in the Chesapeake Bay impact structure, southeastern Virginia [abs.]: Geological Society of America Abstracts with Programs, v. 34, no. 6, p. 466.

Huber, H., Koeberl, C., and Glass, B.P., 2000, Geochemical study of microtektites, bediasites, and georgiaites from the upper Eocene North American tektite strewn field [abs]: Meteoritical Society Annual Meeting, 63d, Chicago, August 28–September 1, 2000, Abstract 5255, available online at http://www.lpi.usra.edu/meetings/metsoc2000/pdf/5255.pdf

Izett, G.A., 1990, The Cretaceous/Tertiary boundary interval, Raton Basin, Colorado and New Mexico, and its content of shock-metamorphosed minerals—Evidence relevant to the K/T boundary impact-extinction theory: Geological Society of America Special Paper 249, 100 p.

Jackson, J.A., ed., 1997, Glossary of geology (4th ed.): Alexandria, Va., American Geological Institute, 769 p.

Jackson, L.L., Brown, F.W., and Neil, S.T., 1987, Major and minor elements requiring individual determination, classical whole rock analysis, and rapid rock analysis, chap. G *of* Baedecker, P.A., ed., Methods for geochemical analysis: U.S. Geological Survey Bulletin 1770, p. G1–G23.

Johnson, G.H., Powars, D.S., Bruce, T.S., Beach, T.A., Harris, M.S., and Goodwin, B.K., 2001, Post-impact effects of the Eocene Chesapeake Bay impact, lower York-James Peninsula, Virginia: Virginia Geological Field Conference, 31st, Williamsburg, Virginia, October 19 and 20, 2001 [Guidebook], 40 p.

Kamo, S.L., Krogh, T.E., Glass, B.P., and Liu, S., 2002, U-Pb study of shocked zircons from the North American microtektite layer [abs.]: Lunar and Planetary Science Conference, 33d, League City, Tex., March 11–15, 2002, Abstract 1643, available online at http://www.lpi.usra.edu/meetings/lpsc2002/pdf/1643.pdf

Koeberl, Christian, 1990, The geochemistry of tektites—An overview: Tectonophysics, v. 171, no. 1–4, p. 405–422.

Koeberl, Christian, 1994, Tektite origin by hypervelocity asteroidal or cometary impact—Target rocks, source craters, and mechanisms, *in* Dressler, B.O., Grieve, R.A.F., and Sharpton, V.L., eds., Large meteorite impacts and planetary evolu-

tion: Geological Society of America Special Paper 293, p. 133–151.

Koeberl, Christian, Kruger, F.J., and Poag, C.W., 2001, Geochemistry of surficial sediments near the Chesapeake Bay impact structure and the search for source rocks of the North American tektites [abs.]: Lunar and Planetary Science Conference, 32d, Houston, Tex., March 12–16, 2001, Abstract 1333, available online at http://www.lpi.usra.edu/meetings/lpsc2001/pdf/1333.pdf

Koeberl, Christian, Poag, C.W., Reimold, W.U., and Brandt, Dion, 1996, Impact origin of the Chesapeake Bay structure and the source of the North American tektites: Science, v. 271, no. 5253, p. 1263–1266.

Lanphere, M.A., and Dalrymple, G.B., 2000, First-principles calibration of ^{38}Ar tracers—Implications for the ages of $^{40}Ar/^{39}Ar$ fluence monitors: U.S. Geological Survey Professional Paper 1621, 10 p.

LeBas, M.J., LeMaitre, R.W., Streckeisen, Albert, and Zanettin, Bruno, 1986, A chemical classification of volcanic rocks based on the total alkali-silica diagram: Journal of Petrology, v. 27, p. 745–750.

Lefort, J.P., and Max, M.D., 1991, Is there an Archean crust beneath Chesapeake Bay?: Tectonics, v. 10, no. 1 p. 213–226.

McIntyre, D.B., 1968, Impact metamorphism at Clearwater Lake, Quebec, *in* French, B.M., and Short, N.M., eds., Shock metamorphism of natural materials: Baltimore, Md., Mono Book Corporation, p. 363–366.

Mee, J.S., Siems, D.F., and Taggart, J.E., Jr., 1996, Major element analysis by wavelength dispersive X-ray fluorescence spectrometry, *in* Arbogast, B.F., ed., Analytical methods manual for the Mineral Resource Surveys Program, U.S. Geological Survey: U.S. Geological Survey Open-File Report 96–525, p. 236–242.

Nakamura, Noboru, 1974, Determination of REE, Ba, Fe, Mg, Na and K in carbonaceous and ordinary chondrites: Geochimica et Cosmochimica Acta, v. 38, no. 5, p. 757–775.

Obradovich, J.D., Snee, L.W., and Izett, G.A., 1989, Is there more than one glassy impact layer in the late Eocene? [abs.]: Geological Society of America Abstracts with Programs, v. 21, no. 6, p. A134.

O'Keefe, J.A., 1976, Tektites and their origin: New York, Elsevier, 254 p.

Owens, B.E., and Tucker, R.D., 2003, Geochronology of the Mesoproterozoic State Farm Gneiss and associated Neoproterozoic granitoids, Goochland terrane, Virginia: Geological Society of America Bulletin, v. 115, no. 8, p. 972–982.

Passchier, C.W., and Trouw, R.A.J., 1996, Microtectonics: New York, Springer-Verlag, 289 p.

Pearce, J.A., Harris, N.B.W., and Tindle, A.G., 1984, Trace element discrimination diagrams for the tectonic interpretation of granitic rocks: Journal of Petrology, v. 25, no. 4, p. 956–983.

Poag, C.W., 1996, Structural outer rim of Chesapeake Bay impact crater—Seismic and bore hole evidence: Meteoritics & Planetary Science, v. 31, no. 2, p. 218–226.

Poag, C.W., 1997, The Chesapeake Bay bolide impact; A convulsive event in Atlantic Coastal Plain evolution: Sedimentary Geology, v. 108, no. 1–4, p. 45–90.

Poag, C.W., 1999, Chesapeake invader; Discovering America's giant meteorite crater: Princeton, N.J., Princeton University Press, 183 p.

Poag, C.W., 2002a, Structure and morphology of the Chesapeake Bay submarine impact crater [abs.]: Geological Society of America Abstracts with Programs, v. 34, no. 6, p. 465.

Poag, C.W., 2002b, Synimpact-postimpact transition inside Chesapeake Bay crater: Geology, v. 30, no. 11, p. 995–998.

Poag, C.W., and Aubry, M.-P., 1995, Upper Eocene impactites of the U.S. East Coast; Depositional origins, biostratigraphic framework, and correlation: Palaios, v. 10, no. 1, p. 16–43.

Poag, C.W., Hutchinson, D.R., Colman, S.M., and Lee, M.W., 1999, Seismic expression of the Chesapeake Bay impact crater; Structural and morphologic refinements based on new seismic data, *in* Dressler, B.O., and Sharpton, V.L., eds., Large meteorite impacts and planetary evolution; II: Geological Society of America Special Paper 339, p. 149–164.

Poag, C.W., Koeberl, Christian, and Reimold, W.U., 2004, The Chesapeake Bay crater—Geology and geophysics of a late Eocene submarine impact structure: New York, Springer-Verlag, 522 p. plus CD-ROM.

Poag, C.W., Plescia, J.B., and Molzer, P.C., 1999, Chesapeake Bay impact structure; Geology and geophysics [abs.], *in* Gersonde, Rainer, and Deutsch, Alexander, eds., Oceanic impacts; Mechanisms and environmental perturbations; ESF–IMPACT Workshop, April 15–April 17, 1999, Alfred Wegener Institute for Polar and Marine Research, Bremerhaven, Germany, Abstracts: Berichte zur Polarforschung (Reports on Polar Research), v. 343, p. 79–83.

Poag, C.W., Powars, D.S., Poppe, L.J., and Mixon, R.B., 1994, Meteoroid mayhem in Ole Virginny—Source of the North American tektite strewn field: Geology, v. 22, no. 8, p. 691–694.

Poag, C.W., Powars, D.S., Poppe, L.J., Mixon, R.B., Edwards, L.E., Folger, D.W., and Bruce, Scott, 1992, Deep Sea Drilling Project Site 612 bolide event—New evidence of a late Eocene impact-wave deposit and a possible impact site, U.S. East Coast: Geology, v. 20, no. 9, p. 771–774.

Powars, D.S., 2000, The effects of the Chesapeake Bay impact crater on the geologic framework and the correlation of hydrogeologic units of southeastern Virginia, south of the James River: U.S. Geological Survey Professional Paper 1622, 53 p., 1 oversize pl. (Also available online at http://pubs.usgs.gov/prof/p1622/)

Powars, D.S., and Bruce, T.S., 1999, The effects of the Chesapeake Bay impact crater on the geological framework and correlation of hydrogeologic units of the lower York-James Peninsula, Virginia: U.S. Geological Survey Professional

Paper 1612, 82 p., 9 oversize pls. (Also available online at http://pubs.usgs.gov/prof/p1612/)

Powars, D.S., Bruce, T.S., Bybell, L.M., Cronin, T.M., Edwards, L.E., Frederiksen, N.O., Gohn, G.S., Horton, J.W., Jr., Izett, G.A., Johnson, G.H., Levine, J.S., McFarland, E.R., Poag, C.W., Quick, J.E., Schindler, J.S., Self-Trail, J.M., Smith, M.J., Stamm, R.G., and Weems, R.E., 2001, Preliminary geologic summary for the USGS-NASA Langley corehole, Hampton, Virginia: U.S. Geological Survey Open-File Report 01–87–B, 20 p., available online at http://pubs.usgs.gov/of/2001/of01-087/

Powars, D.S., Gohn, G.S., Edwards, L.E., Catchings, R.D., Bruce, T.S., Johnson, G.H., and Poag, C.W., 2002, Lithostratigraphic framework of the crater-fill deposits; Western annular trough, Chesapeake Bay impact crater [abs.]: Geological Society of America Abstracts with Programs, v. 34, no. 6, p. 465.

Powars, D.S., Johnson, G.H., Edwards, L.E., Horton, J.W., Jr., Gohn, G.S., Catchings, R.D., McFarland, E.R., Izett, G.A., Bruce, T.S., Levine, J.S., and Pierce, H.A., 2002, An expanded Chesapeake Bay impact structure, eastern Virginia; New corehole and geophysical data [abs.]: Lunar and Planetary Science Conference, 33d, League City, Tex., March 11–15, 2002, Abstract 1034, available online at http://www.lpi.usra.edu/meetings/lpsc2002/pdf/1034.pdf

Powars, D.S., Mixon, R.B., and Bruce, Scott, 1992, Uppermost Mesozoic and Cenozoic geologic cross section, outer coastal plain of Virginia, *in* Gohn, G.S., ed., Proceedings of the 1988 U.S. Geological Survey Workshop on the Geology and Geohydrology of the Atlantic Coastal Plain: U.S. Geological Survey Circular 1059, p. 85–101.

Powars, D.S., Poag, C.W., and Mixon, R.B., 1993, The Chesapeake Bay "impact crater," stratigraphic and seismic evidence [abs.]: Geological Society of America Abstracts with Programs, v. 25, no. 6, p. A–378.

Reimold, W.U., Koeberl, Christian, and Poag, C.W., 2002, Chesapeake Bay impact crater; Petrographic and geochemical investigations of the impact breccia fill [abs.]: Geological Society of America Abstracts with Programs, v. 34, no. 6, p. 466.

Robertson, P.B., Dence, M.R., and Vos, M.A., 1968, Deformation in rock-forming minerals from Canadian craters, *in* French, B.M., and Short, N.M., eds., Shock metamorphism of natural materials: Baltimore, Md., Mono Book Corporation, p. 433–452.

Ross, C.S., 1962, Microlites in glassy volcanic rocks: American Mineralogist, v. 47, p. 723–740.

Ross, C.S., and Smith, R.L., 1961, Ash-flow tuffs—Their origin, geologic relations, and identification: U.S. Geological Survey Professional Paper 366, 81 p.

Samson, S.D., and Alexander, E.C., Jr., 1987, Calibration of the interlaboratory $^{40}Ar/^{39}Ar$ dating standard MMhb-1: Chemical Geology (Isotope Geoscience Section), v. 66, no. 1–2, p. 27–34.

Self-Trail, J.M., 2003, Shockwave-induced fracturing of calcareous nannofossils from the Chesapeake Bay impact crater: Geology, v. 31, no. 8, p. 697–700.

Short, N.M., 1968, Nuclear-explosion-induced microdeformation of rocks—An aid to the recognition of meteorite impact structures, *in* French, B.M., and Short, N.M., eds., Shock metamorphism of natural materials: Baltimore, Md., Mono Book Corporation, p. 185–210.

Siems, D.F., 2000, The determination of 30 elements in geological materials by energy-dispersive X-ray fluorescence spectrometry: U.S. Geological Survey Open-File Report 00–475, 13 p.

Siems, D.F., 2002, The determination of 30 elements in geological materials by energy-dispersive X-ray fluorescence spectrometry, chap. U *of* Taggart, J.E., Jr., ed., Analytical methods for chemical analysis of geologic and other materials, U.S. Geological Survey: U.S. Geological Survey Open-File Report 02–223, p. U1–U11, available online at http://pubs.usgs.gov/of/2002/ofr-02-0223/U27edsfinal_U.pdf

Snoke, A.W., and Tullis, Jan, 1998, An overview of fault rocks, *in* Snoke, A.W., Tullis, Jan, and Todd, V.R., eds., Fault-related rocks—A photographic atlas: Princeton, N.J., Princeton University Press, p. 3–18.

Stecher, Ole, Ngo, H.H., Papanastassiou, D.A., and Wasserburg, G.J., 1989, Nd and Sr isotopic evidence for the origin of tektite material from DSDP Site 612 off the New Jersey coast: Meteoritics, v. 24, no. 2, p. 89–98.

Steiger, R.H., and Jäger, E., comps., 1977, Subcommission on Geochronology—Convention on the use of decay constants in geo- and cosmochronology: Earth and Planetary Science Letters, v. 36, no. 3, p. 359–362.

Stöffler, Dieter, 1971, Progressive metamorphism and classification of shocked and brecciated crystalline rocks at impact craters: Journal of Geophysical Research, v. 76, no. 23, p. 5541–5551.

Stöffler, Dieter, 1972, Deformation and transformation of rock-forming minerals by natural and experimental shock processes. I. Behavior of minerals under shock compression: Fortschritte der Mineralogie, v. 49, p. 50–113.

Stöffler, Dieter, and Grieve, R.A.F., 2003, Impactites—A proposal on behalf of the IUGS Subcommission on the Systematics of Metamorphic Rocks, Web version of 30.04.2003, paper 11 *of* Towards a unified nomenclature of metamorphic petrology: 9 p., available online at http://www.bgs.ac.uk/scmr/docs/paper_12/scmr_paper_12_1.pdf

Streckeisen, A.L., chairman, 1973, Plutonic rocks—Classification and nomenclature recommended by the IUGS Subcommission on the Systematics of Igneous Rocks: Geotimes, v. 18, no. 10, p. 26–30.

Streckeisen, A.L., 1976, To each plutonic rock its proper name: Earth-Science Reviews, v. 12, no. 1, p. 1–33.

Suess, F.E., 1900, Die Herkunft der Moldavite und verwandter Gläser: Austria, Geologische Reichsanstalt, Jahrbuch, v. 50, no. 2, p. 193–382.

Taggart, J.E., Jr., Lindsay, J.R., Scott, B.A., Vivit, D.V., Bartel, A.J., and Stewart, K.C., 1987, Analysis of geologic materials by wavelength-dispersive X-ray fluorescence spectrometry, chap. E *of* Baedecker, P.A., ed., Methods for geochemical analysis: U.S. Geological Survey Bulletin 1770, p. E1–E19.

Taylor, J.R., 1982, An introduction to error analysis—The study of uncertainties in physical measurements: Mill Valley, Calif., University Science Books, 270 p.

Wackerle, Jerry, 1962, Shock-wave compression in quartz: Journal of Applied Physics, v. 33, p. 922–937.

Wandless, G.A., 1996, Instrumental neutron activation by long count, *in* Arbogast, B.F., ed., Analytical methods manual for the Mineral Resource Surveys Program, U.S. Geological Survey: U.S. Geological Survey Open-File Report 96–525, p. 218–227.

Wilcox, R.E., 1959, Use of the spindle stage for determination of principal indices of refraction of crystal fragments: American Mineralogist, v. 44, no. 11–12, p. 1272–1293.

Xie, Xiande, and Chao, E.C.T., 1985, The variation range of optical constants and distribution characteristics of shock lamellae in shock-metamorphosed quartz: Geochemistry (English Language Edition), v. 4, no. 2, p. 97–113.

Glossary

A

allochthonous impact breccia "Impact breccia in which component materials have been displaced from their point of origin." (Stöffler and Grieve, 2003, p. 5)

B

breccia "A coarse-grained clastic rock, composed of angular broken rock fragments held together by a mineral cement or in a fine-grained matrix . . . " (Jackson, 1997, p. 82)

C

cataclasite "A fine-grained, cohesive cataclastic rock, normally lacking a penetrative foliation or microfabric, formed during fault movement. The fracture of rock and mineral components is a significant factor in the generation of a cataclasite, and it may play a significant role in the continued deformation of the rock." (Jackson, 1997, p. 99)

cataclastic "Pertaining to the structure produced in a rock by the action of severe mechanical stress during dynamic metamorphism; characteristic features include the bending, breaking, and granulation of the minerals." (Jackson, 1997, p. 100)

cataclastic rock "A rock . . . containing angular fragments that have been produced by the crushing and fracturing of preexisting rocks as a result of mechanical forces in the crust." (Jackson, 1997, p. 100)

D

diamictite "A comprehensive, nongenetic term . . . for a nonsorted or poorly sorted, noncalcareous, terrigenous sedimentary rock that contains a wide range of particle sizes." (Jackson, 1997, p. 175)

diamicton "A general term . . . for the nonlithified equivalent of a diamictite." (Jackson, 1997, p. 175)

E

ejecta *See* impact ejecta.

F

fabric "The complete spatial and geometrical configuration of all those components that make up the rock. It covers terms such as texture, structure, and preferred orientation." (Hobbs and others, 1976, p. 73)

G

gouge "Non-consolidated fractured rock, commonly very fine-grained, formed by brittle deformation at a shallow crustal level along a fault." (Passchier and Trouw, 1996, p. 259)

H

hypervelocity impact "The impact of a projectile onto a surface at a velocity such that the stress waves produced on contact are orders of magnitude greater than the static bulk compressive strength of the target material. The minimum required velocities vary for different materials, but are generally 1–10 km/sec, and about 4–5 km/sec for most crystalline rocks." (Jackson, 1997, p. 312)

I

impact breccia "Monomict or polymict breccia, which occurs around, inside, and below impact craters." (Stöffler and Grieve, 2003, p. 5)

impact ejecta "Solid, liquid, and vaporized rock ejected ballistically from an impact crater." (Stöffler and Grieve, 2003, p. 4)

impact pseudotachylyte "Pseudotachylite [sic] produced by impact metamorphism; dike-like breccia formed by frictional melting in the basement of impact craters; may contain unshocked and shocked mineral and lithic clasts in a fine-grained aphanitic matrix." (Stöffler and Grieve, 2003, p. 6)

"Some workers attribute impact-related pseudotachylyte formation to shock melting . . . whereas others believe it is primarily the product of frictional melting incurred during gravitational collapse of the impact-generated transient cavity . . . Regardless of origin, all pseudotachylytes are high-strain-rate features." (Snoke and Tullis, 1998, p. 9)

M

microfabric "The fabric of a rock as seen under a microscope." (Jackson, 1977, p. 406)

monomict impact breccia "Cataclasite produced by impact and generally displaying weak or no shock metamorphism; occurs in the (par)autochthonous floor of an impact crater or as

clast (up to the size of blocks and megablocks) within allochthonous impact breccias." (Stöffler and Grieve, 2003, p. 5)

P

planar deformation features "Submicroscopic amorphous lamellae occurring in shocked minerals as multiple sets of planar lamellae (optical discontinuities under the petrographic microscope) parallel to rational crystallographic planes; indicative of shock metamorphism; synonymous with the terms "planar elements" and "shock lamellae" which should be discarded." (Stöffler and Grieve, 2003, p. 7)

planar fractures "Fractures occurring in shocked minerals as multiple sets of planar fissures parallel to rational crystallographic planes, which are not usually observed as cleavage planes under normal geological (non-shock) conditions." (Stöffler and Grieve, 2003, p. 7)

planar microstructures "Collective term comprising shock-induced planar fractures and planar deformation features." (Stöffler and Grieve, 2003, p. 7)

polymict "Said of a clastic sedimentary rock composed of many mineral or rock types." (Jackson, 1997, p. 501)

polymict impact breccia "Breccia with clastic matrix or crystalline matrix (derived from the crystallization of impact melt) containing lithic and mineral clasts of different degree of shock metamorphism excavated by an impact from different regions of the target rock section, transported, mixed, and deposited inside or around an impact crater or injected into the target rocks as dikes." (Stöffler and Grieve, 2003, p. 5)

pseudotachylyte "Dark brittle fault rock occurring in veins and fractures in host rocks with low porosity. Pseudotachylyte is thought to form by local melting of a host rock along a fault in response to seismic activity on the fault and associated local generation of frictional heat." (Passchier and Trouw, 1996, p. 262)

Also spelled pseudotachylite. *See* impact pseudotachylyte.

S

shock metamorphism "Metamorphism of rocks or minerals caused by shock wave compression due to impact of a solid body or due to the detonation of high-energy chemical or nuclear explosives." (Stöffler and Grieve, 2003, p. 3)

shocked Term used for brevity in places for "shock metamorphosed." (Izett, 1990, p. 3)

spherulite "A rounded or spherical mass of acicular crystals, commonly of feldspar, radiating from a central point. Spherulites may range in size from microscopic to several centimeters in diameter . . . Most commonly formed by the devitrification of volcanic glass." (Jackson, 1997, p. 612)

spherulitic "Volcanic igneous texture dominated by spherulites or spherical bodies of radiating mineral fibers." (Jackson, 1997, p. 612)

T

target rocks "Rock(s) exposed at the site of an impact before crater formation." (Stöffler and Grieve, 2003, p. 4)

tektite "Impact glass formed at terrestrial impact craters from melt ejected ballistically and deposited sometimes as aerodynamically shaped bodies in a strewn field outside the continuous ejecta blanket; the size of tektites ranges from the submillimeter range (MICROTEKTITES, generally found in deep sea sediments) to the subdecimeter range, rarely to decimeters." (Stöffler and Grieve, 2003, p. 6)

Appendix E1. Descriptions of Matrix and Clast Samples from the Exmore Beds and Crater Unit B in the USGS-NASA Langley Core

Samples from the USGS-NASA Langley core that are described in this chapter are identified by the letters NL followed by a number indicating depth in feet. The clasts examined are nonlineated and nonfoliated except in sparse, very narrow shear zones and in one clast (NL873.3) where oriented grains are interpreted as igneous flow foliation. Positions of selected clasts are plotted on the stratigraphic column in figure E3. Sample descriptions in this appendix are ordered from highest to lowest sample depth.

Sample NL777.3

[About 10 immersion-oil slides + quartz on spindle stage (fig. E2*A*)]

Depth.—236.9 m (777.3 ft); core box 87.

Sample type.—Sandy sediment of the matrix.

Host unit.—Exmore beds (polymict diamicton).

Description.—About 10 immersion-oil slides, each containing several hundred grains, were examined of residue from the core at 236.9 m (777.3 ft) depth by using an optical petrographic microscope. Three shocked quartz grains were examined by using a spindle stage. One grain (0.23 mm (0.009 in.) in diameter, not photographed) showed five sets of intersecting planar deformation features on rotation through 180°. A second grain, 0.24 mm (0.009 in.) in diameter, had three sets of intersecting planar deformation features. A third grain, 0.13 mm (0.005 in.) in diameter, had two sets of intersecting planar deformation features (fig. E2*A*). Two of these grains with multiple planar deformation features were photographed, and optic measurements were made. No feldspar grains showed convincing planar deformation features.

Sample NL784.9

[1 thin section (figs. E5*C* and E6*D*) + quartz on spindle stage]

Depth.—239.2 m (784.9 ft); core box 87.

Rock type.—Porphyritic felsite, containing microfaults.

Host unit.—Exmore beds (polymict diamicton).

Dimensions.—4.0x1.8x2.5 cm (1.6x0.71x0.98 in.), whole clast.

Description.—The subangular clast of porphyritic felsite is medium light gray to greenish gray and nonfoliated. It consists of feldspar phenocrysts (~25 percent) in a microcrystalline matrix (~75 percent). Feldspar phenocrysts are medium to coarse grained (2–7 mm (0.079–0.28 in.) long). In thin section, plagioclase phenocrysts appear euhedral to subhedral, and some are highly fractured and internally faulted. Twinning and grain boundaries of some phenocrysts are offset by abundant microfaults. One large quartz grain (near the label end of the thin section) has two sets of intersecting planar deformation features, a strong set and a weaker set, which does not extend across the whole grain (fig. E6*D*). Other grains show no evidence of shock metamorphism. Quartz grains from the residue of this sample were examined in immersion-oil slides and on a spindle stage; one grain was discovered to have two sets of planar deformation features.

Sample NL790.9

[1 thin section (figs. E5*E* and E7) + chemical analysis (tables E2, E3, and E4)]

Depth.—241.1 m (790.9 ft); core box 88.

Rock type.—Porphyritic felsite (rhyolite), with faults and microbreccia veins.

Host unit.—Exmore beds (polymict diamicton).

Dimensions.—3.0x2.0x1.5 cm (1.2x0.79x0.59 in.), whole clast (fig. E4*C*).

Description.—The angular clast of porphyritic felsite is greenish gray and nonfoliated. It consists of feldspar phenocrysts in an aphanitic matrix. In thin section, feldspar phenocrysts appear euhedral to subhedral, and some have embayed margins (fig. E7) or matrix-filled pits indicating magmatic corrosion. A throughgoing fault (near the center of the thin section) and smaller anastomosing faults contain narrow microbreccia veins. One quartz phenocryst has a single set of Böhm lamellae, which are not highly planar or uniform. No planar deformation features were found, but some quartz phenocrysts have mosaic texture.

Sample NL795.8

[1 thin section (fig. E5*D*)]

Depth.—242.6 m (795.8 ft); core box 88.

Rock type.—Microcline megacryst, strained and microfaulted.

Host unit.—Exmore beds (polymict diamicton).

Dimensions.—2.4x1.3x1.0 cm (0.94x0.51x0.39 in.), partial clast bounded by core.

Description.—The subangular clast is very light gray, and a single feldspar crystal extends the full length of the clast. The thin section shows a large microcline crystal, which is internally microfaulted and highly strained.

Sample NL802.07

[1 thin section]

Depth.—244.47 m (802.07 ft); core box 89.

Rock type.—Granodiorite.

Host unit.—Exmore beds (polymict diamicton).

Dimensions.—2.3x2.3x1.4 cm (0.91x0.91x0.55 in.), whole clast.

Description.—The angular clast is granodiorite according to the classification of Streckeisen (1976); it is fine to medium grained, pale red, and nonfoliated. In thin section, the rock is nonfoliated, inequigranular to porphyritic having euhedral to subhedral plagioclase phenocrysts; the thin section is composed of plagioclase (~55 percent), quartz (~30 percent), potassium feldspar (~10 percent), clinozoisite (<1 percent), magnetite (<1 percent), secondary chlorite (~5 percent), and secondary carbonate. The potassium feldspar occurs mainly as granophyric intergrowths with quartz and plagioclase. Clinozoisite and chlorite indicate metamorphic or hydrothermal (deuteric?) alteration. Euhedral comb quartz crystals occur along the edge of a small cavity now filled with secondary calcite. Evidence of high strain is limited to a narrow ductile shear zone along the edge of the sample (in thin section) and to a parallel veinlet of strained quartz grains. No evidence of shock metamorphism is seen.

Sample NL805.5

[1 thin section]

Depth.—245.5 m (805.5 ft); core box 90.

Rock type.—Porphyritic felsite, containing microfaults.

Host unit.—Exmore beds (polymict diamicton).

Dimensions.—2.0x1.3x1.3 cm (0.79x0.51x0.51 in.), clast.

Description.—The angular clast of weathered porphyritic felsite is nonfoliated and consists of medium-grained, subhedral to angular, white feldspar phenocrysts in an aphanitic, pale-red clayey matrix. In thin section, feldspar megacrysts are internally microfaulted; some have mosaic texture and extreme undulatory extinction.

Sample NL806.03

[1 thin section]

Depth.—245.68 m (806.03 ft); core box 90.

Rock type.—Porphyritic felsite having spherulitic texture.

Host unit.—Exmore beds (polymict diamicton).

Dimensions.—2.4x1.5x1.0 cm (0.94x0.59x0.39 in.), whole clast.

Description.—The subangular clast of porphyritic felsite is fine grained, light brownish gray, and nonfoliated. In thin section, the felsite has a pervasive spherulitic texture composed mainly of plagioclase and quartz, with secondary clay minerals having a spotty potassium stain.

Sample NL807.9

[1 thin section]

Depth.—246.2 m (807.9 ft); core box 90.

Rock type.— Porphyritic felsite.

Host unit.—Exmore beds (polymict diamicton).

Dimensions.—1.7x1.5x0.9 cm (0.67x0.59x0.35 in.), clast.

Description.—The angular clast of porphyritic felsite is fine grained, grayish red, and nonfoliated. In thin section, the felsite consists of plagioclase phenocrysts 1–2 mm (0.039–0.079 in.) long in an aphanitic matrix. The yellow sodium cobaltinitrite stain indicates that fine-grained potassium feldspar makes up about 25 percent of the matrix. Minor constituents include an epidote mineral (~2 percent) and opaque minerals (~1 percent). No high-strain fabrics are evident.

Sample NL811.68

[3 thin sections (fig. E5*A,B*) + quartz on spindle stage]

Depth.—247.40 m (811.68 ft); core box 90.

Rock type.—Cataclasite (deformed felsite).

Host unit.—Exmore beds (polymict diamicton).

Dimensions.—3.2x2.0x1.1 cm (1.3x0.79x0.43 in.), whole clast.

Description.—The subangular clast of fine-grained cataclasite formed by deformation of felsite is leucocratic, light gray, and nonfoliated, and it has disseminated sulfide crystals. Striated surfaces are inconclusive evidence that the sample may have been part of a shatter cone (Daniel J. Milton, USGS Emeritus, oral commun., 2001). Thin sections show highly microfaulted and brecciated but cohesive felsite consisting of plagioclase phenocrysts in an aphanitic feldspar-quartz matrix. Plagioclase phenocrysts are crosscut by microfaults and have highly undulatory extinction and mosaic texture. Calcite-filled fractures are abundant. A few quartz grains have a suspicious brown color in thin section but lack planar deformation features. One potassium feldspar crystal has weak, nonthroughgoing lamellae, which are interesting but inconclusive.

Sample NL812.55

[1 thin section (fig. E8)]

Depth.—247.67 m (812.55 ft); core box 90.

Rock type.—Porphyritic felsite having spherulitic texture.

Host unit.—Exmore beds (polymict diamicton).

Dimensions.—1.9x0.9x0.4 cm (0.75x0.35x0.16 in.), whole clast.

Description.—The angular clast of porphyritic felsite is grayish red and nonfoliated. Calcite-filled fractures are visible in hand sample. In thin section, the felsite consists of euhedral plagioclase phenocrysts (~30 percent) in a finer grained matrix dominated by feldspar-quartz spherulites. The yellow stain for potassium is concentrated in the outer margins of spherulites and in mesostasis. Some clear, euhedral plagioclase laths appear to have grown across earlier spherulites. Minor constituents include opaque minerals (~2 percent), secondary calcite (~5 percent) and chlorite (~5 percent). The thin section does not contain the calcite-filled fractures, and no other cataclastic features were observed.

Sample NL813.57

[1 thin section]

Depth.—247.98 m (813.57 ft); core box 90.

Rock type.—Porphyritic felsite.

Host unit.—Exmore beds (polymict diamicton).

Dimensions.—1.2x1.0x0.8 cm (0.47x0.39x0.31 in.), whole clast.

Description.—The angular clast of porphyritic felsite has tiny disseminated sulfide (pyrite?) crystals and secondary calcite in fractures. In thin section, the felsite consists of plagioclase phenocrysts in an aphanitic feldspar-quartz matrix. Embayed margins of some feldspar phenocrysts indicate magmatic corrosion. Microfaults and fractures are filled by polygonal quartz and by calcite.

Sample NL820.6

[About 10 immersion-oil slides + quartz on spindle stage (fig. E2*B, C,D,E*)]

Depth.—250.1 m (820.6 ft); core box 91.

Sample type.—Sandy sediment of the matrix.

Host unit.—Exmore beds (polymict diamicton).

Description.—About 10 immersion-oil slides, each containing several hundred grains, were examined of residue from the core at 250.1 m (820.6 ft) by using an optical petrographic microscope. Six of the quartz grains examined by using a spindle stage were observed to have two or more sets of intersecting planar deformation features (fig. E2*B,C,D,E*), indicating that the grains had experienced shock metamorphism. These grains ranged in diameter from 0.13 to 0.26 mm (0.005 to 0.010 in.).

Sample NL832.25

[1 thin section]

Depth.—253.67 m (832.25 ft); core box 92.

Rock type.—Porphyritic felsite.

Host unit.—Exmore beds (polymict diamicton).

Dimensions.—1.7x1.2x1.0 cm (0.67x0.47x0.39 in.), clast.

Description.—The angular clast of porphyritic felsite is grayish red and nonfoliated. In thin section, it consists of euhedral to subhedral plagioclase phenocrysts in an aphanitic quartz-feldspar matrix. The yellow sodium cobaltinitrite stain indicates that potassium feldspar is disseminated in the groundmass. Many euhedral plagioclase phenocrysts are rimmed by potassium feldspar coronas. A volcaniclastic origin is suggested by the possible contained igneous rock fragment as well as by the angularity of grains in the groundmass. No high-strain fabrics were observed.

Sample NL832.85

[1 thin section]

Depth.—253.85 m (832.85 ft); core box 92.

Rock type.—Porphyritic felsite.

Host unit.—Exmore beds (polymict diamicton).

Dimensions.—3.4x2.2x1.7 cm (1.3x0.87x0.67 in.), partial clast bounded by core (fig. E4*D*).

Description.—The angular clast of porphyritic felsite is porphyritic-aphanitic, mottled grayish red and grayish green, and nonfoliated. The thin section shows phenocrysts of plagioclase and quartz, and the aphanitic matrix has a mild yellow sodium cobaltinitrite stain, indicating that it contains disseminated potassium feldspar. Minor constituents include opaque minerals and secondary calcite, both disseminated and in veinlets. Some of the matrix has a spherulitic texture. No high-strain fabrics were observed.

Sample NL840.4

[2 thin sections (fig. E6*A,B,C*) + quartz on spindle stage]

Depth (entire clast).—256.06–256.26 m (840.1–840.75 ft) (ends were left in the core box).

Depth (sampled part).—256.11–256.23 m (840.25–840.65 ft); core box 94. The depth in the sample number, 840.4 ft, is within the sampled part of the clast.

Rock type.—Cataclasite (deformed felsite), pervasively microfaulted, brecciated, and weakly cohesive (fig. E4*B*).

Host unit.—Exmore beds (polymict diamicton).

Dimensions.—12-cm-long (4.7-in.-long) central part of clast bounded by the core having a nominal diameter of 6.4 cm (2.5 in.).

Description.—The very light gray, very fine grained clast is larger than the core diameter, and so its shape is undetermined; the top and bottom of the clast are irregular. It consists of porphyritic-aphanitic felsite, which is pervasively microfaulted, brecciated, and weakly cohesive. Two thin sections show that the rock consists mainly of euhedral to subhedral plagioclase phenocrysts in a matrix of aphanitic quartz and plagioclase, and they show very little of the yellow sodium cobaltinitrite stain indicating potassium. Some plagioclase phenocrysts are offset by crosscutting microfaults. Secondary calcite (about 5 percent) is disseminated through the rock and also commonly fills fractures. A sulfide mineral (pyrite?) occurs as tiny disseminated crystals. Numerous crosscutting microfaults and fractures extend short distances and disappear in the microcrystalline groundmass. Calcite-filled fractures up to 1 mm (0.039 in.) thick are conspicuous; some of this calcite is strained, suggesting continued fault slip. Many quartz grains in thin section 1 have at least two sets of intersecting planar deformation features, indicating shock metamorphism.

Sample NL854.0

[1 thin section]

Depth.—260.3 m (854.0 ft); core box 95.

Rock type.—Diabase pebble (detrital).

Host unit.—Exmore beds (polymict diamicton).

Dimensions.—4.5x3.5x2.8 cm (1.8x1.4x1.1 in.), whole clast.

Description.—The subrounded pebble of fine-grained diabase (Early Jurassic?) is medium gray and nonfoliated. It has randomly oriented plagioclase laths and an intergranular texture. It resembles typical Early Jurassic diabases in the Appalachian Piedmont, except that it contains 1–2 percent magnetite as equant megacrysts 1.0–1.5 mm (0.039–0.059 in.) across. In thin section, the diabase consists of plagioclase (~60 percent), orthopyroxene (relict and chemically weathered to clay, ~25 percent), miscellaneous clay weathering products (~15 percent), and a secondary carbonate mineral (<1 percent); no relict olivine was found. No high-strain fabrics or possible impact effects were observed.

Sample NL864.05

[1 thin section]

Depth.—263.36 m (864.05 ft); core box 96.

Rock type.—Quartz pebble (detrital).

Host unit.—Exmore beds (polymict diamicton).

Dimensions.—2.3x1.7x1.3 cm (0.91x0.67x0.51 in.), whole clast.

Description.—The well-rounded quartz pebble is very light gray and nonfoliated. The quartz is polycrystalline. In thin section, the quartz grains have irregular interlocking grain boundaries, no obvious preferred orientation, and no unusual undulatory extinction or any other evidence of high strain.

Sample NL870.3

[1 thin section (fig. E5*F*)]

Depth (entire clast).—265.27–265.36 m (870.3–870.6 ft); core box 97.

Depth (sample).—265.27–265.33 m (870.3–870.5 ft) (the remainder was left in the core box).

Rock type.—Brecciated porphyritic felsite containing pseudotachylyte(?).

Host unit.—Exmore beds (polymict diamicton).

Dimensions.— 8.0-cm-long (3.1-in.-long) partial clast (fig. E4*A*) bounded by the core having a nominal diameter of 6.4 cm (2.5 in.).

Description.—The partial clast of brecciated porphyritic felsite is very fine grained, light gray, nonfoliated, and crumbly; it appears weathered. The clast is larger than the core diameter, and so its shape is undetermined; the top is subhorizontal, and the bottom dips about 60°. Striated fractures on the top surface (in the core box) are inconclusive evidence that the sample may have been part of a shatter cone (Daniel J. Milton, USGS Emeritus, oral commun., 2001). The thin section shows a highly brecciated porphyritic felsite having abundant microfractures, including some offsetting twins in plagioclase phenocrysts. A pseudotachylyte(?) vein (about 0.2 mm (0.0079 in.) thick) was injected into a tension fracture having matching grain fragments on opposite walls. The vein contains some large clean quartz grains. Even quartz in and adjacent to the pseudotachylyte(?) vein appears clean and free of planar deformation features. No shock-metamorphosed minerals were found.

Sample NL873.3

[1 thin section]

Depth.—266.2 m (873.3 ft); core box 97.

Rock type.—Felsite having igneous flow foliation.

Host unit.—Exmore beds (polymict diamicton).

Dimensions.—2.3x1.4x1.1 cm (0.91x0.55x0.43 in.), whole clast.

Description.—The angular clast of felsite is grayish black, appears flinty, and does not fizz in hydrochloric acid. The thin section shows sparse, matrix-supported feldspar phenocrysts in a very fine grained groundmass of feldspar and quartz with diffuse spots of opaque oxide. Alignment of tiny plagioclase laths in the matrix may be an igneous flow foliation. No cataclastic fabrics were observed.

Sample NL905.0

[5 thin sections + quartz on spindle stage]

Depth (entire clast).—275.71–275.93 m (904.60–905.33 ft); core box 101.

Depth (sample).—275.80– 275.84 m (904.85–905.00 ft) (the remainder was left in the core box).

Rock type.—Monomict felsite breccia (impact breccia).

Host unit.—Crater unit B (upper part) of Gohn and others (this volume, chap. C).

Dimensions.—22-cm-long (8.7-in.-long) clast bounded by the core having a nominal diameter of 6.4 cm (2.5 in.).

Description.—The clast is larger than the core diameter, and so its shape is undetermined; the top surface dips ~10°, and the bottom dips ~50°. It is a monomict breccia composed of angular, grayish-red, cherty microcrystalline felsite fragments separated by white gougelike clay between the fragments and in fractures. The clay matrix lacks primary cohesion and crumbles when wet. Thin sections show pervasive brecciation. Angular fragments of microcrystalline felsite resemble chert and consist mainly of very fine grained plagioclase and quartz; the yellow stain for potassium is dispersed on clay-sized particles. Some spherulitic texture is present. Microfaults offset twins in plagioclase. The clay matrix contains a few round, green glauconite pellets along the margins and in cracks, indicating some mixing with coastal plain sedimentary material. A few quartz grains in thin section 3 and thin section 5 have two convincing sets of intersecting shock-induced planar deformation features; some other quartz grains have one visible set of parallel planar deformation features.

Stratigraphy and Paleoenvironments of Early Postimpact Deposits at the USGS-NASA Langley Corehole, Chesapeake Bay Impact Crater

By C. Wylie Poag and Richard D. Norris

Chapter F of
**Studies of the Chesapeake Bay Impact Structure—
The USGS-NASA Langley Corehole, Hampton, Virginia, and
Related Coreholes and Geophysical Surveys**

Edited by J. Wright Horton, Jr., David S. Powars, and Gregory S. Gohn

Prepared in cooperation with the
Hampton Roads Planning District Commission,
Virginia Department of Environmental Quality, and
National Aeronautics and Space Administration Langley Research Center

Professional Paper 1688

U.S. Department of the Interior
U.S. Geological Survey

Contents

Plates

[Plates follow References Cited]

Figures

Tables

Stratigraphy and Paleoenvironments of Early Postimpact Deposits at the USGS-NASA Langley Corehole, Chesapeake Bay Impact Crater

By C. Wylie Poag[1] and Richard D. Norris[2]

Abstract

The USGS-NASA Langley corehole was drilled into the Chesapeake Bay impact crater in Hampton, Va. We used whole and split cores, seismic-reflection surveys (multichannel and single channel), downhole geophysical logs (spontaneous potential and gamma ray), micropaleontology (planktonic and benthic foraminifera and bolboformids), and stable-isotope records ($\delta^{18}O$, $\delta^{13}C$) to interpret the lithic, biotic, paleoenvironmental, and geophysical properties contained in, or represented by, the late synimpact and early postimpact deposits (fallout layer, dead zone, and Chickahominy Formation) overlying the Exmore breccia in the USGS-NASA Langley core.

The initial postimpact deposit in the Langley core (resting above a fallout layer) is a dead zone, barren of indigenous foraminifera, which represents an interval of hostile sea-floor paleoenvironments; the interval length was between less than 1,000 years and 8,000 years. Full recovery of the benthic foraminiferal community was rapid once amenable conditions were reestablished at the beginning of Chickahominy time.

Planktonic foraminifera and bolboformids show that biochronozones P15 and P16-P17 of the late Eocene are represented by the Chickahominy Formation in the Langley corehole. These are the same biochronozones previously documented in the Chickahominy Formation from inside the Chesapeake Bay impact crater at the Exmore and Kiptopeke core sites.

The benthic foraminiferal assemblages of the Chickahominy Formation are encompassed in a single biozone (*Cibicidoides pippeni* Zone), which is represented by 126 calcareous and agglutinated species in the Chickahominy Formation in the Langley core. The *Cibicidoides pippeni* Zone can be divided into five subbiozones (*Bathysiphon, Bulimina jacksonensis, Lagenoglandulina virginiana, Uvigerina dumblei,* and *Bolivina tectiformis* Subzones). The most abundant and stratigraphically most persistent species represented in the *Cibicidoides pippeni* assemblage indicate a paleodepth of about 300 meters (~1,000 feet) for the Chickahominy sea floor, which exhibited oxygen deprivation and high flux rates of organic carbon.

At the Langley corehole, the spontaneous-potential and gamma-ray curves allow recognition of four or five lithic subunits, which correlate approximately with those similarly distinguished in three other intracrater coreholes (North, Bayside, Kiptopeke). Lithically, the Chickahominy Formation in the Langley corehole differs from its equivalents in the other three coreholes, however, by having greater permeability and a greater volume of glauconite near the base of the formation.

The late Eocene paleoclimate, as expressed by the postimpact $\delta^{18}O$ record at the Langley corehole, was characterized by three negative excursions of $\delta^{18}O$ (interpreted to represent pulses of atmospheric warmth). A significant negative excursion of $\delta^{13}C$ in the upper part of the Chickahominy Formation is consistent with a net global decrease in carbon burial. These same isotopic successions have been previously recorded in the Kiptopeke corehole, as well as at many other locations around the globe. The isotope record provides evidence that the Chesapeake Bay impact and other late Eocene impacts may have exerted a long-term influence on global climate changes, which culminated in the well-known early Oligocene mass extinction event.

Introduction

The Chesapeake Bay impact crater formed in the late Eocene when a hypervelocity impactor struck the Atlantic continental shelf near the present town of Cape Charles, Va. The impactor was either a comet or an asteroid, but in this chapter, it is referred to by the generic term "bolide." To obtain geological information about the impact and the resultant crater, the U.S. Geological Survey (USGS) and its partners drilled the USGS-NASA Langley corehole in 2000 (see "Acknowledgments").

The USGS-NASA Langley core site is located at lat 37°05'44.28" N., long 76°23'08.96" W. (North American Datum of 1927), at the National Aeronautics and Space Administration (NASA) Langley Research Center in Hampton, Va. The core site is approximately 5 kilometers (km; 3 miles (mi))

[1]U.S. Geological Survey, Woods Hole, MA 02543.
[2]Scripps Institution of Oceanography, La Jolla, CA 92093.

inside the southwestern rim (in the outer part of the annular trough) of the Chesapeake Bay impact crater (figs. F1, F2). Here the Chickahominy Formation is 52.37 meters (m; 171.8 feet (ft)) thick and represents apparently continuous sediment accumulation for most of the final ~2.1 million years (m.y.) of the late Eocene Epoch.

The principal objectives of this study were (1) to establish the immediate effects of the Chesapeake Bay bolide impact on the local benthic biota and to characterize the transition from synimpact to postimpact deposition at the USGS-NASA Langley core site; (2) to qualitatively evaluate the biostratigraphy of principally the benthic foraminiferal assemblages in the Chickahominy Formation in the USGS-NASA Langley core and then to compare the evaluations with the results from previous investigations; and (3) to interpret the postimpact paleoenvironments of the Chickahominy Formation as represented at the USGS-NASA Langley core site.

Methods

We used downhole geophysical logs and cores (whole and split sections) to analyze the general lithostratigraphic aspects of the fallout layer, dead zone, and Chickahominy Formation. To study the foraminiferal suites, we took 66 samples (~85 cubic centimeters each) spaced ~1 m (3 ft) apart (table F1) and prepared them in a standard manner (wet sieved on a 63-micrometer (μm) screen after 15 minutes of boiling in a solution of sodium hexametaphosphate). Oven-dried samples were examined by optical and scanning-electron microscopy. We identified benthic foraminiferal species from available literature where possible (Cushman, 1935; Cushman and Cederstrom, 1945; Charletta, 1980; Jones, 1990), but we also used many provisory trivial names (enclosed in quotation marks in fig. F20, pl. F2, and tables F4–F9) for stratigraphic purposes. These names were previously published by Poag, Koeberl, and Reimold (2004), who studied Chickahominy foraminifera from the Kiptopeke corehole. Because this was not a taxonomic investigation, we did not thoroughly assess the validity or priority of all formal taxonomic names we applied.

We performed stable-isotope analyses for oxygen and organic carbon on the same samples used for foraminiferal analysis (table F2). We used monospecific samples (~3–20 individuals of the benthic foraminifer *Cibicidoides pippeni*) from the >63-μm grain-size fraction. We performed mass spectrometry using a Finnigan MAT 252 instrument with an online automated carbonate reaction Kiel device (Woods Hole Oceanographic Institution). Analytical precision based on repeated analysis of standards (NBS–19, Carrara Marble, and B–1 marine carbonate) was better than ±0.03 per mil (‰) for $\delta^{13}C$ and 0.08‰ for $\delta^{18}O$ relative to the Peedee belemnite (PDB) standard.

We used the magnetobiochronological framework (synthesis of radioisotopes, geomagnetic polarity, planktonic foraminifera, and calcareous nannofossils) of Berggren and others (1995) to guide interpretation and correlation of our biostratigraphic and stable-isotope results (fig. F3).

Previous Work

Several previous studies have documented the physical and biotic characteristics of deposits that record the transition from synimpact sedimentation (fallout zone) to postimpact sedimentation (dead zone and Chickahominy Formation) at sites within and outside the Chesapeake Bay impact crater (Poag, 1997a; Powars and Bruce, 1999; Poag, 2002; Poag, Koeberl, and Reimold, 2004). An initial qualitative stratigraphic study of Chickahominy foraminiferal assemblages was carried out more than 50 years ago (Cushman and Cederstrom, 1945). No subsequent microfossil investigations of the Chickahominy were initiated until cores became available from the Chesapeake Bay impact crater.

After this long hiatus, several new qualitative studies of benthic foraminifera, planktonic foraminifera, and bolboformids were published (Poag and Aubry, 1995; Poag and Commeau, 1995; Poag, 1997a; Poag, Koeberl, and Reimold, 2004; fig. F4). In addition, Poag, Koeberl, and Reimold (2004) presented a *quantitative* stratigraphic analysis and paleoenvironmental interpretation of the Chickahominy benthic foraminiferal assemblages (fig. F5) from the Kiptopeke corehole, located inside the peak ring, near the center of the crater (fig. F1). Poag, Mankinen, and Norris (2003) analyzed the paleomagnetic and stable-isotope records ($\delta^{18}O$ and $\delta^{13}C$) of the Chickahominy Formation at Kiptopeke (figs. F5, F6) and correlated them with other upper Eocene sections around the globe. Poag (2002) and Poag, Koeberl, and Reimold (2004) provided initial assessments of the transition from fallout layer to dead zone to Chickahominy Formation in the USGS-NASA Langley core (fig. F7). Poag, Koeberl, and Reimold (2004, p. 391) extended this evaluation to the Kiptopeke core.

The reader should note that in this chapter, we use the stratigraphic framework and terminology of Poag, Koeberl, and Reimold (2004), in which the brecciated sedimentary crater-fill deposits (underlain by either displaced sedimentary megablocks or crystalline basement rocks, and overlain by the fallout layer) are designated as the *Exmore breccia.* By this designation, the Exmore breccia embraces all but the very top of the *Exmore beds* (as applied in all other chapters of this volume) and includes crater unit B as well (see Gohn and others, this volume, chap. C).

Fallout Layer

Poag (2002) and Poag, Koeberl, and Reimold (2004) showed that at the USGS-NASA Langley corehole, the 52.37-m-thick (171.8-ft-thick) Chickahominy Formation is separated from the Exmore breccia by two thin deposits (3–19 centimeters

Text continues on page F13.

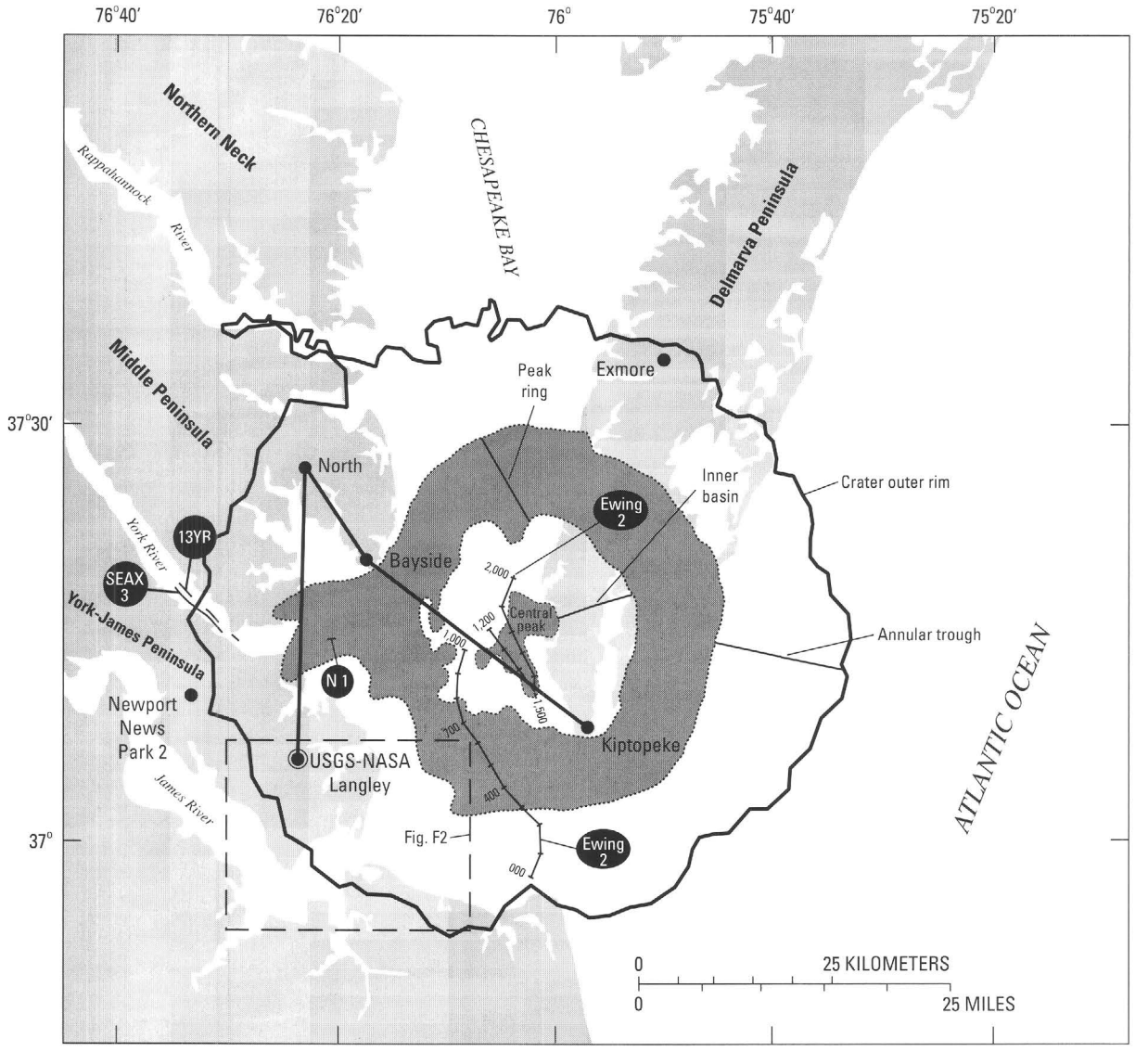

EXPLANATION

400 — Ewing 2 — Trackline for seismic-reflection profile; numbered ticks indicate shotpoints; circled label indicates profile name (derived from the ship name) and number

Line connecting four coreholes for which geophysical logs are compared in figure F18

Figure F1. Regional map showing location of the USGS-NASA Langley corehole, four other intracrater coreholes, and one extracrater corehole relative to the principal morphological features of the Chesapeake Bay impact crater. Parts of the crater are defined differently in this chapter than in the other chapters in this volume. Tracklines for most seismic-reflection profiles are labeled as defined in figure F2; N1 indicates a short segment of trackline Neecho 1 (fig. F15); 13YR indicates a multichannel profile furnished by Texaco, Inc. (fig. F9). A detailed map of the USGS-NASA Langley site is shown in figure F2.

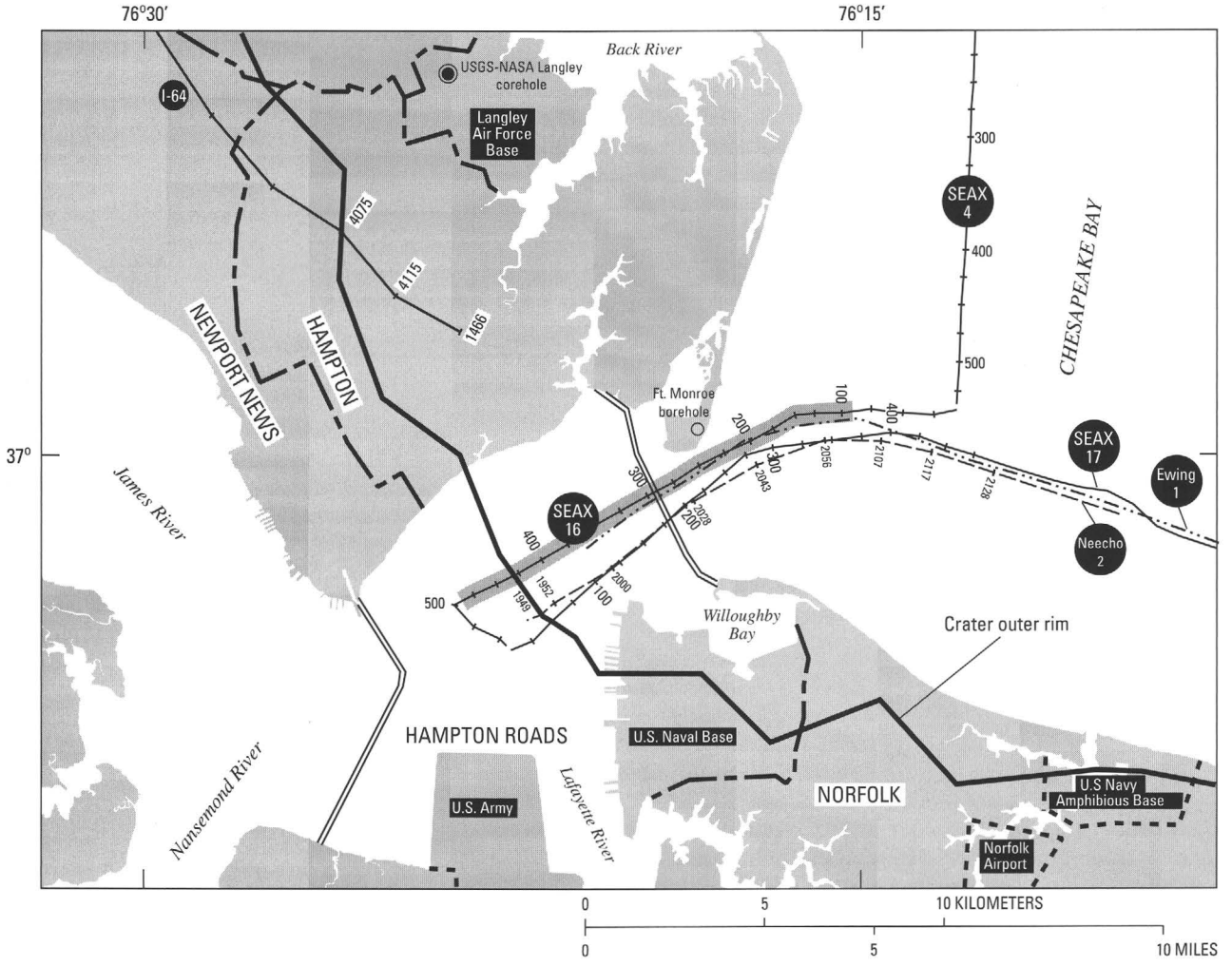

Figure F2. Detailed map showing location of the USGS-NASA Langley corehole, the Fort Monroe borehole, and nearby lines for seismic-reflection profiles. Different line styles are used to differentiate closely spaced tracklines. Offshore profile labels indicate the name of the ship used to collect the profile: Research Vessel (R.V.) *Seaward Explorer* (SEAX); *Neecho*; R.V. *Maurice Ewing*. The shaded segment of profile SEAX 16 is shown in figure F12. I–64 indicates a USGS onshore seismic profile parallel to U.S. Interstate Highway 64. Numbers on I–64, SEAX, and *Ewing* lines are seismic shotpoints; numbers on *Neecho* trackline designate time of day in hours (military time).

Table F1. Numbers and depths of samples collected for analysis of benthic foraminifera in early postimpact deposits in the USGS-NASA Langley core.

[Depths were measured in the field; the datum is ground level. m, meters; ft, feet]

Sample number	Top of sample (m)	Base of sample (m)	Top of sample (ft)	Base of sample (ft)
Drummonds Corner beds				
66	183.00	183.06	600.40	600.60
Chickahominy Formation				
65	183.28	183.34	601.30	601.50
64	183.54	183.60	602.15	602.35
63	183.70	183.76	602.70	602.90
62	184.62	184.68	605.70	605.90
61	185.53	185.59	608.70	608.90
60	186.45	186.60	611.70	611.90
59	187.36	187.42	614.70	614.90
58	188.28	188.34	617.70	617.90
57	189.19	189.25	620.70	620.90
56	190.10	190.16	623.70	623.90
55	191.05	191.13	626.80	627.00
54	191.96	192.02	629.80	630.00
53	192.85	192.91	632.70	632.90
52	193.76	193.82	635.70	635.90
51	194.58	194.64	638.40	638.60
50	195.38	195.44	641.00	641.20
49	196.35	196.41	644.20	644.40
48	197.27	197.33	647.20	647.40
47	198.18	198.24	650.20	650.40
46	199.25	199.31	653.70	653.90
45	200.01	200.07	656.20	656.40
44	201.84	201.90	662.20	662.40
43	202.75	202.81	665.20	665.40
42	203.67	203.73	668.20	668.40
41	204.58	204.64	671.20	671.40
40	205.50	205.56	674.20	674.40
39	206.29	206.35	676.80	677.00
38	207.26	207.32	680.00	680.20
37	208.24	208.30	683.20	683.40
36	209.12	209.18	686.10	686.30
35	210.04	210.10	689.10	689.30
34	210.98	211.04	692.20	692.40
33	211.90	211.96	695.20	695.40
32	212.84	212.90	698.30	698.50
31	213.70	213.76	701.10	701.30
30	214.82	214.88	704.80	705.00
29	215.80	215.86	708.00	708.20
28	216.56	216.62	710.50	710.70
27	219.46	219.52	720.00	720.20
26	220.37	220.43	723.00	723.20
25	221.41	221.47	726.40	726.60
24	222.20	220.26	729.00	729.20
23	223.18	223.24	732.20	732.40
22	224.06	224.12	735.10	735.30
21	224.93	224.99	737.96	738.16

Table F1. Numbers and depths of samples collected for analysis of benthic foraminifera in early postimpact deposits in the USGS-NASA Langley core.—Continued

Sample number	Top of sample (m)	Base of sample (m)	Top of sample (ft)	Base of sample (ft)
Chickahominy Formation—Continued				
20	225.86	225.92	741.00	741.20
19	226.74	226.80	743.90	744.10
18	227.69	227.75	747.00	747.20
17	228.60	228.66	750.00	750.20
16	229.51	229.57	753.00	753.20
15	230.46	230.52	756.10	756.30
14	231.44	231.50	759.30	759.50
13	232.26	232.32	762.00	762.20
12	233.16	233.22	764.95	765.15
11	234.12	234.18	768.10	768.30
10	234.91	234.94	770.70	770.80
9	235.49	235.52	772.60	772.70
8	235.58	235.63	772.90	773.05
Dead zone [The contact between the dead zone and the Chickahominy Formation is near the middle of sample 7 at 235.65 m (773.12 ft), and the contact between the dead zone and the fallout layer is within sample 4 at ~235.84 m (~773.75 ft) (fig. F7)]				
7	235.63	235.67	773.05	773.20
6	235.67	235.72	773.20	773.35
5	235.79	235.82	773.60	773.70
4	235.82	235.85	773.70	773.80
Fallout layer				
3	235.85	235.87	773.80	773.85
Exmore breccia				
2	235.87	235.88	773.85	773.90
1	235.88	235.92	773.90	774.00

Table F2. Stable-isotope data derived from carbonate tests of *Cibicidoides pippeni* extracted from samples of the Chickahominy Formation and the Drummonds Corner beds in the USGS-NASA Langley core.

[Depths are in meters (m) to the tops of samples; depths in feet are in table F1. Delta values for oxygen and organic carbon isotopes are in parts per mil (‰). No data were available for samples 61 and 23 (table F1) from depths of 185.53 m and 223.18 m]

Depth (m)	$\delta^{13}C$ (‰)	$\delta^{18}O$ (‰)	Depth (m)	$\delta^{13}C$ (‰)	$\delta^{18}O$ (‰)	Depth (m)	$\delta^{13}C$ (‰)	$\delta^{18}O$ (‰)	Depth (m)	$\delta^{13}C$ (‰)	$\delta^{18}O$ (‰)
183.00	–7.182	+0.325	195.38	–0.637	–0.124	210.04	–0.954	–0.003	225.86	+0.096	+0.036
183.28	–0.621	+0.184	196.35	–0.286	+0.110	210.98	–0.719	+0.235	226.74	–0.328	+0.275
183.54	–0.616	+0.264	197.27	–0.726	+0.064	211.90	–0.708	–0.001	227.69	+0.073	–0.013
183.70	–0.640	+0.241	198.18	–1.090	+0.111	212.84	–1.190	–0.035	228.60	–0.121	+0.012
184.62	–0.710	+0.344	199.25	–0.765	+0.035	213.70	–0.900	–0.077	229.51	–0.341	–0.029
186.45	–0.938	+0.170	200.01	–0.671	+0.224	214.82	–0.864	–0.078	230.46	–0.407	–0.204
187.36	–0.782	+0.131	201.84	–0.946	+0.334	215.80	–1.066	–0.272	231.44	–0.236	–0.014
188.28	–0.753	–0.044	202.75	–1.329	+0.019	216.56	–0.897	+0.227	232.26	+0.004	–0.029
189.19	–0.526	+0.073	203.67	–0.785	+0.118	219.46	–0.948	+0.201	233.16	–0.189	–0.173
190.10	–0.860	–0.116	204.58	–0.773	–0.276	220.37	–0.975	+0.406	234.12	–0.040	+0.073
191.05	–0.837	–0.047	205.50	–0.736	+0.286	221.41	–1.005	+0.123	234.91	–1.543	–0.246
191.96	–0.704	–0.002	206.29	–0.706	–0.052	222.20	–1.069	+0.087	235.49	–0.702	+0.124
192.85	–0.159	+0.172	207.26	–0.903	–0.149	224.06	–0.172	+0.039	235.58	–0.603	–0.173
193.76	–0.806	+0.013	208.24	–0.922	–0.148	224.93*	–0.106	+0.278			
194.58	–0.449	+0.174	209.12	–0.793	+0.114	224.93*	–0.070	+0.214			

*Two analyses were performed for sample 21 from 224.93 m.

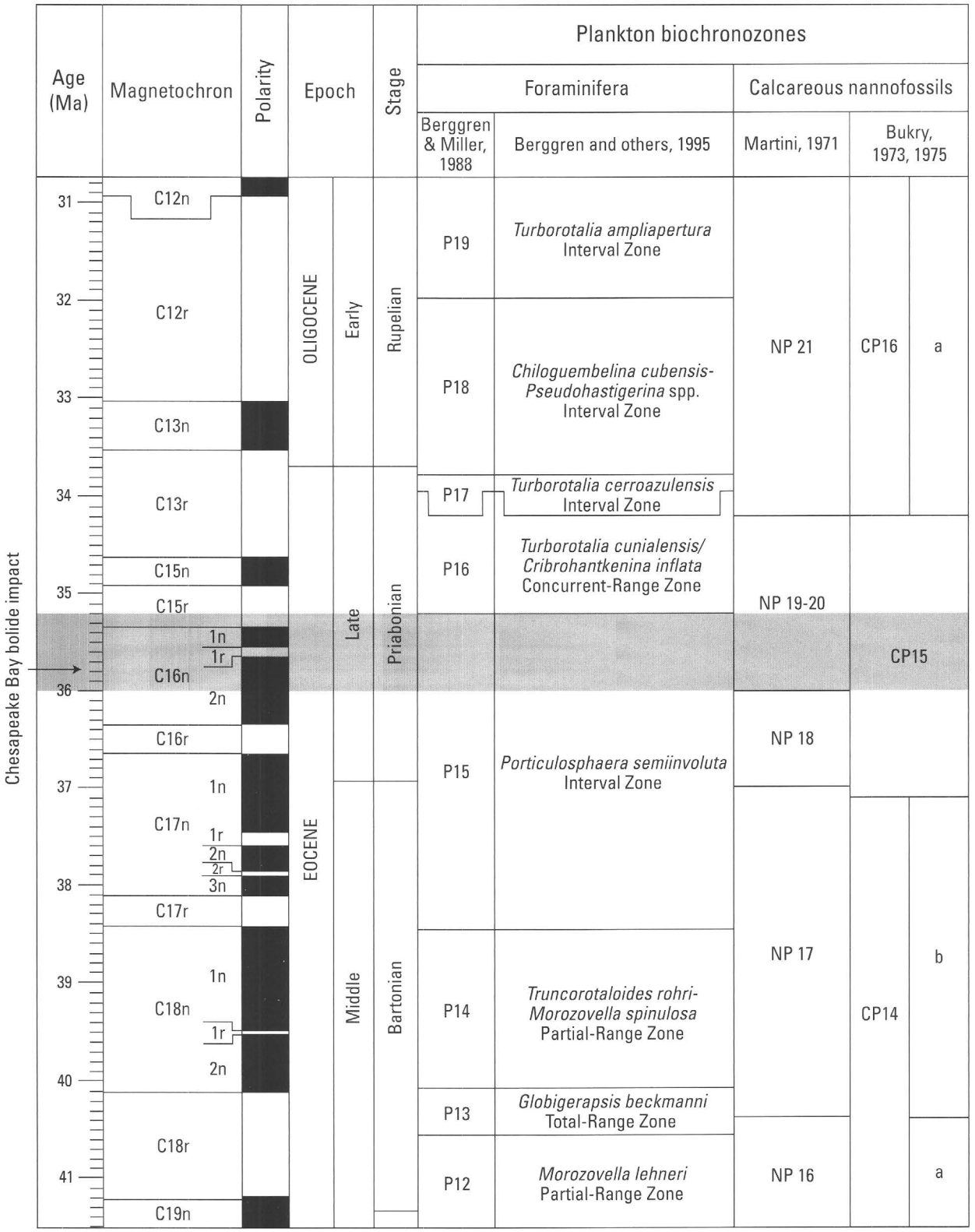

Figure F3. Correlation chart showing magnetobiochronology used in this chapter (modified from Berggren and others, 1995). The shaded band indicates the biochronologic resolution for the age of the Chesapeake Bay impact. The band is the interval of overlap between the top of the planktonic foraminiferal biochronozone P15 and the base of the calcareous nannofossil biochronozone NP 19-20 (35.2–36 Ma). The arrow marks the age of the Chesapeake Bay impact as extrapolated from sediment-accumulation-rate data from the Kiptopeke corehole (modified from Poag, Koeberl, and Reimold, 2004).

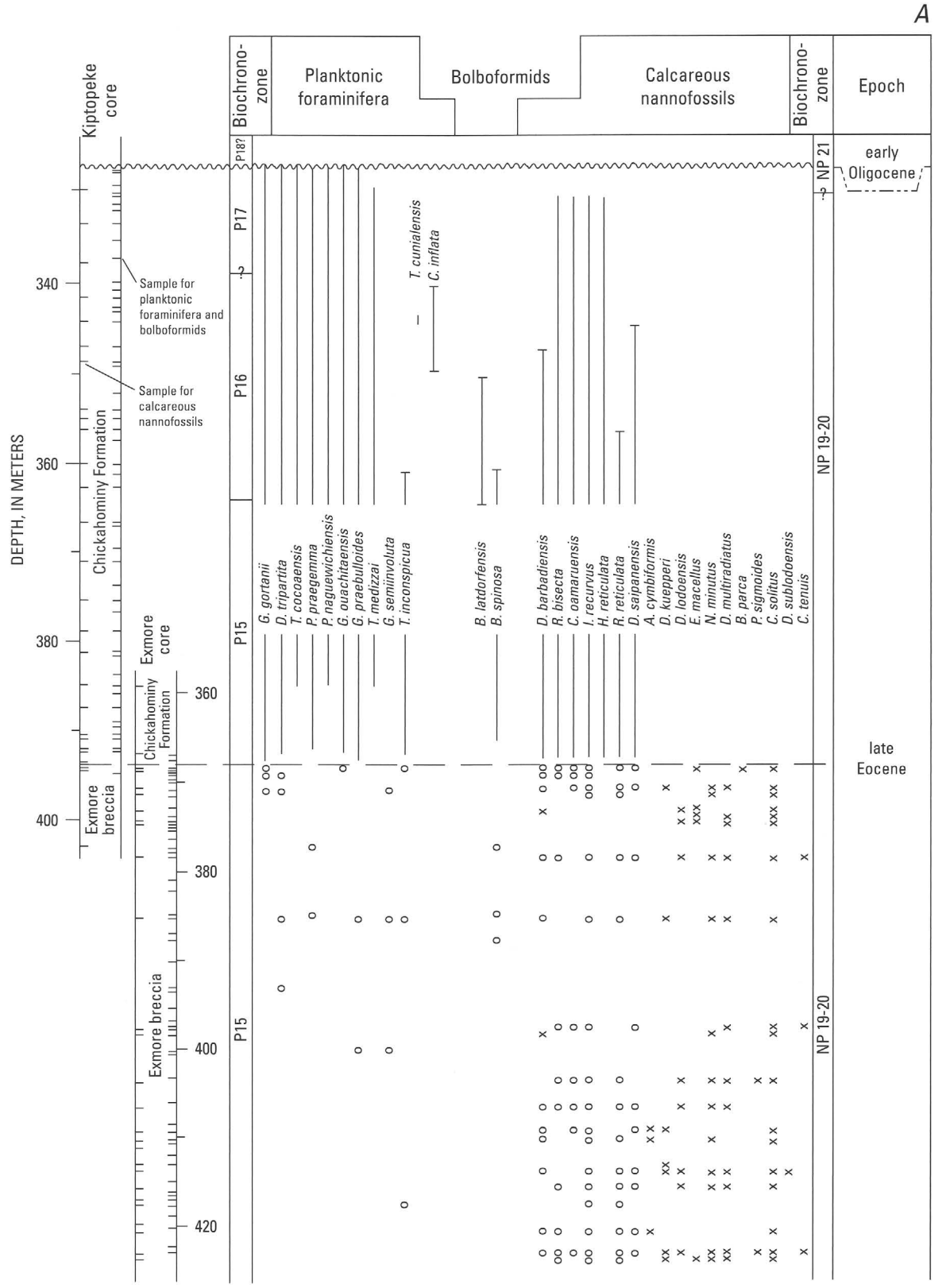

Figure F4. Chart summarizing ranges of principal planktonic foraminifera, bolboformids, and calcareous nannofossils identified in the Chickahominy Formation and the underlying Exmore breccia from the Kiptopeke and Exmore coreholes (from Poag and Aubry, 1995). *A,* Species ranges. *B,* Species names used in figure F4*A*. Ticks inside the core diagrams indicate sample depths for planktonic foraminifera and bolboformids (right) and calcareous nannofossils (left). Symbols for stratigraphically mixed specimens found within the Exmore breccia: o=indigenous late Eocene specimens; x=allogenic specimens (older than late Eocene).

B, Species names used in figure F4*A*

Planktonic Foraminifera

Cribrohantkenina inflata (Howe) 1928
Dentoglobigerina tripartita (Koch) 1926
Globigerina gortanii (Borsetti) 1959
Globigerina ouachitaensis Howe and Wallace, 1932
Globigerina praebulloides Blow, 1959
Globigerinatheka semiinvoluta (Keijzer) 1945
Praetenuitella praegemma Li, 1987
Pseudohastigerina naguewichiensis (Myatyliuk) 1950
Testacarinata inconspicua (Howe) 1939
Testacarinata medizzai (Toumarkine and Bolli) 1975
Turborotalia cocoaensis (Cushman) 1928
Turborotalia cunialensis (Toumarkine and Bolli) 1970

Bolboformids

Bolboforma latdorfensis Spiegler, 1991
Bolboforma spinosa Daniels and Spiegler, 1974

Calcareous Nannofossils

Arkhangelskiella cymbiformis Vekshina, 1959
Broinsonia parca (Stradner, 1963)
Chiasmolithus oamaruensis (Deflandre, 1954)
Chiasmolithus solitus (Bramlette and Sullivan, 1961)
Cruciplacolithus tenuis (Stradner, 1961)
Discoaster barbadiensis (Tan, 1927)
Discoaster kuepperi Stradner, 1959
Discoaster lodoensis Bramlette and Sullivan, 1961
Discoaster multiradiatus Bramlette and Riedel, 1954
Discoaster saipanensis Bramlette and Riedel, 1954
Discoaster sublodoensis Bramlette and Sullivan, 1961
Ellipsolithus macellus (Bramlette and Sullivan, 1961)
Helicosphaera reticulata Bramlette and Wilcoxon, 1967
Isthmolithus recurvus Deflandre, 1954
Neococcolithes minutus (Perch-Nielsen, 1967)
Placozygus sigmoides (Bramlette and Sullivan, 1961)
Reticulofenestra bisecta (Hay, Mohler, and Wade, 1966)
Reticulofenestra reticulata (Gartner and Smith, 1967)

Figure F4. Continued.

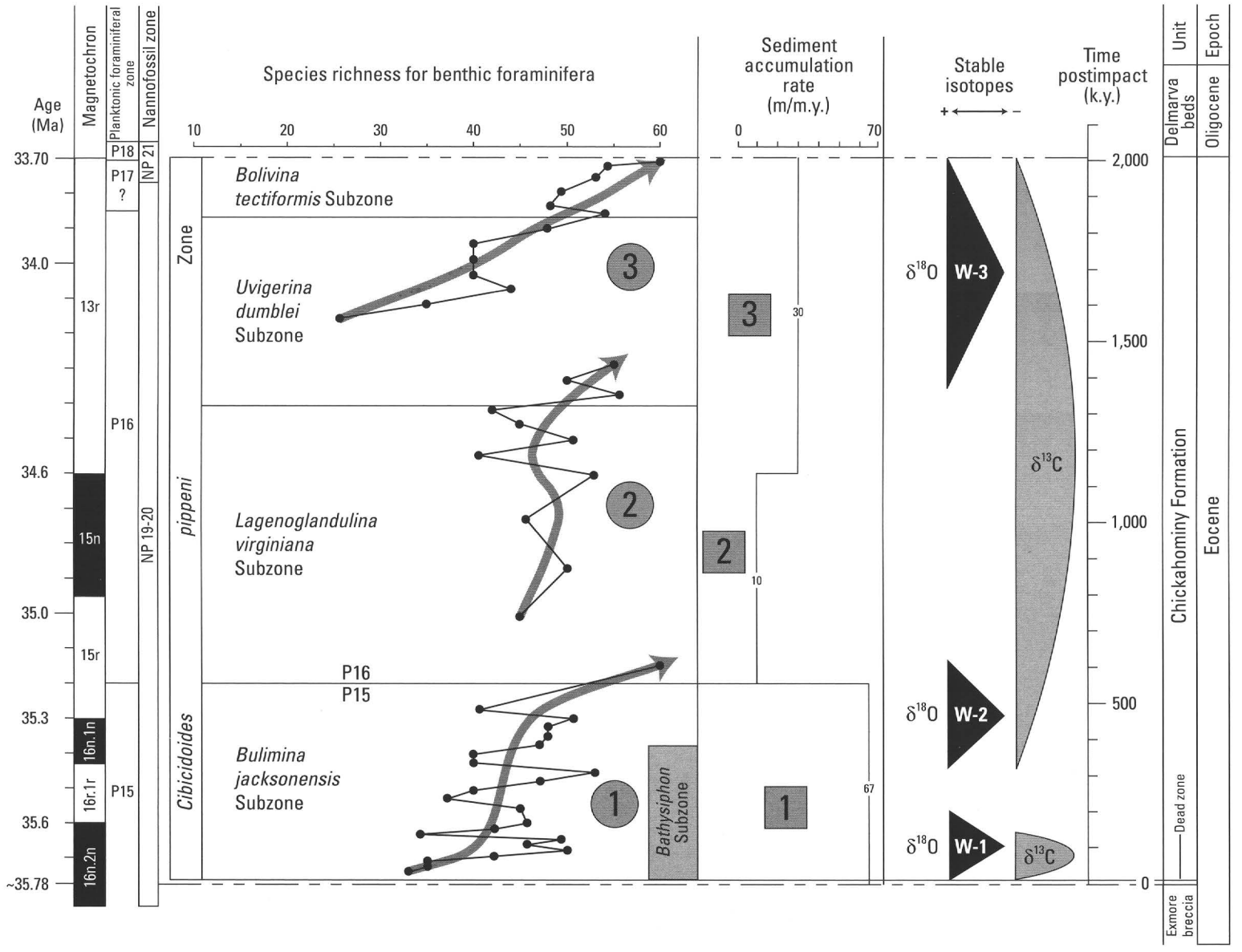

Figure F5. Chart summarizing correlations among magnetostratigraphy, planktonic foraminiferal and calcareous nannofossil zones, benthic foraminiferal subzones, species-richness cycles, sediment accumulation rates, and stable-isotope records ($\delta^{18}O$, $\delta^{13}C$) in the Chickahominy Formation in the Kiptopeke corehole (modified from Poag, Koeberl, and Reimold, 2004, fig. 13.10). W–1, W–2, W–3=pulses of warm global climate based on $\delta^{18}O$; species richness=number of benthic foraminiferal species identified in a sample. Scale at right indicates time in thousands of years (k.y.) postimpact. The three species-richness cycles (numbers in circles) differ slightly from the three depositional episodes (numbers in squares) determined from sediment accumulation rates (Poag, Koeberl, and Reimold, 2004, table 13.1).

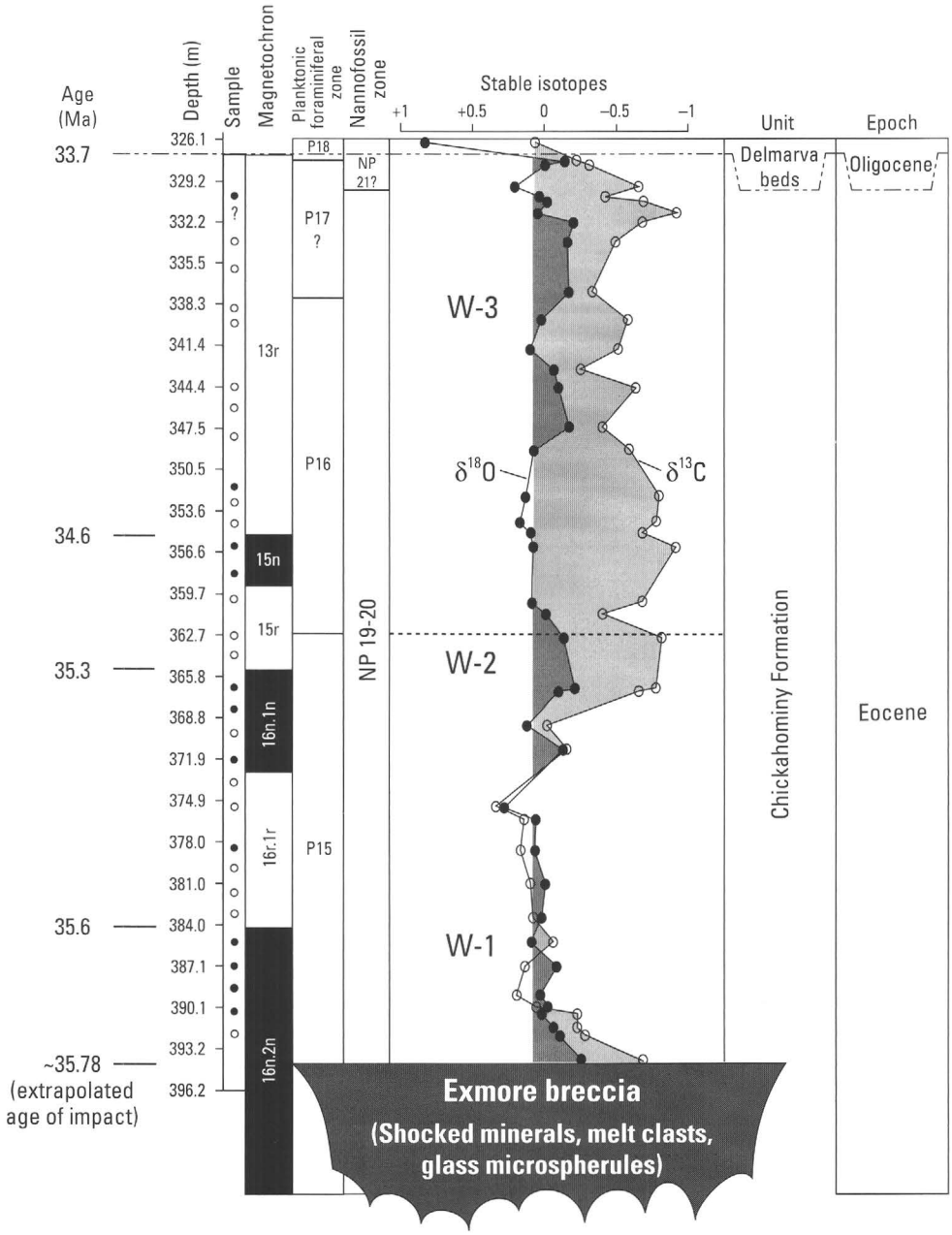

Figure F6. Chart summarizing correlations among magnetostratigraphy, biozones, and stable-isotope records ($\delta^{18}O$, $\delta^{13}C$) for the Chickahominy Formation in the Kiptopeke corehole (modified from Poag, Mankinen, and Norris, 2003). Age of impact was extrapolated by using the sediment accumulation rate of 67 m/m.y. shown in figure F5. In the sample column, open circles indicate reversed polarity; filled circles indicate normal polarity. W–1, W–2, W–3=pulses of warm global climate based on $\delta^{18}O$.

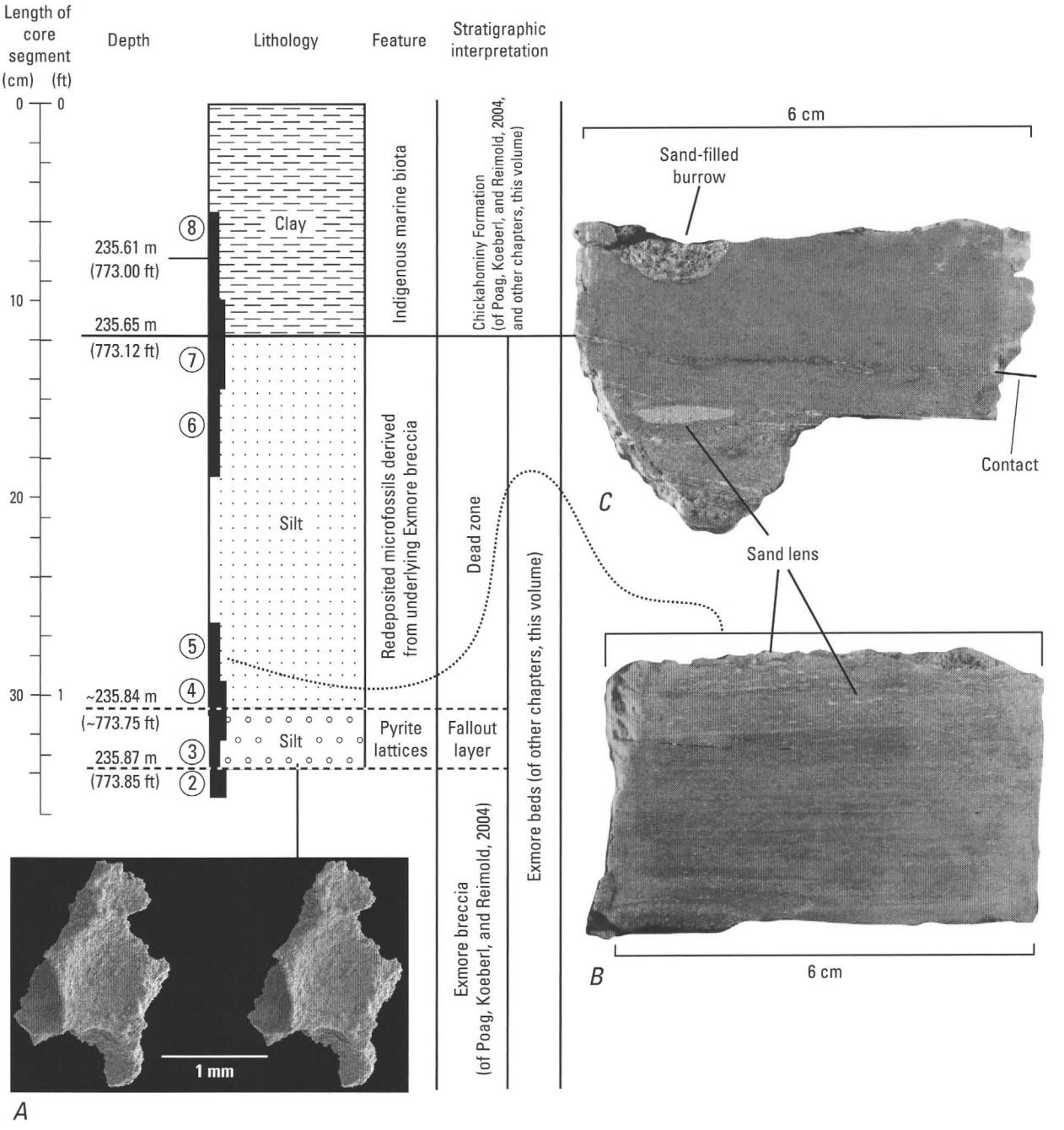

Figure F7. Core log showing stratigraphic interpretation of sediments across the transition from the Exmore breccia to the Chickahominy Formation in the USGS-NASA Langley corehole and images of sampled sediment (modified from figs. 3 and 4 of Poag, 2002). Each solid rectangle at left of the lithology column indicates the position of a sample taken for this study (circled numbers are sample numbers listed in table F1). *A*, Stereopair of scanning-electron micrographs illustrating fragment of pyrite lattice (modified from Poag, 2002, fig. 4). Note hemispherical concavities separated by knife-edge partitions; Poag (2002) inferred that the concavities originally contained glass microspherules, which constituted the fallout layer from the Chesapeake Bay impact. *B*, Split-core sample (sample 5) from near the base of the dead zone (see leader), showing a repetitious succession of submillimeter-scale horizontal laminae of sand, silt, and clay. Photograph from Poag (2002, fig. 3). *C*, Split-core sample (sample 7) containing boundary between clay of the Chickahominy Formation (above) and the dead zone (below). Photograph from Poag (2002, fig. 3). Note coarse sand in the Chickahominy burrow and fine sandy laminae and lenses in the dead zone. Note also that our stratigraphic interpretations of this core interval follow those of Poag, Koeberl, and Reimold (2004). Thus, we recognize the fallout layer and dead zone as a composite transitional interval that separates the Exmore breccia (Exmore beds, in part, of other chapters in this volume) from the Chickahominy Formation.

(cm) or 1.2–7.5 inches (in.) thick) that record the synimpact-postimpact transition. This critical depositional shift began with accumulation of a thin (~3 cm; 1.2 in.) layer of silty clay, containing dozens of well-preserved fragments of pyrite microstructures (fig. F7*A*). The microstructures exhibit smooth-walled, closely spaced, hemispherical pits or depressions, approximately 0.5–1.0 millimeter (mm; 0.02–0.04 in.) in diameter, which are separated from each other by curved, knife-edge partitions. Poag and the Chesapeake Coring Team (2001), Poag, Gohn, and Powers (2001), Poag (2002), and Poag, Koeberl, and Reimold (2004) concluded that the pyrite microstructures originally were parts of a larger pyrite lattice, which had encased a layer of stacked glass microspherules (microtektites) derived from shock-melted silica droplets. Those authors inferred that the glass microspherules had been part of a fallout layer, which originally accumulated in quiet-water conditions following abatement of massive impact-generated turbulence over the crater.

Poag (2002) and Poag, Koeberl, and Reimold (2004) placed the base of the fallout layer at 235.87 m (773.85 ft; fig. F7) in the Langley core. Poag (2002) interpreted the fallout layer to be part of the Exmore breccia (other authors in the present volume assign it to the Exmore beds), whereas Poag, Koeberl, and Reimold (2004) considered the fallout layer to be part of a silt-rich unit that separates the sand-rich Exmore breccia from the clay-rich Chickahominy Formation.

Dead Zone

Above the fallout layer, Poag (2002) and Poag, Koeberl, and Reimold (2004) described a dark-gray, laminated, clayey silt unit, ~0.19 m (~0.63 ft) thick in the Langley core, which they designated as a dead zone (fig. F7). The silt appears to be devoid of indigenous microfossils, though specimens reworked from the Exmore breccia are abundant in thin white laminae and millimeter-scale lenses of micaceous, fine to very fine sand (fig. F7*B,C*). Pyritized burrow casts also are particularly common in the dead zone. Poag (2002) and Poag, Koeberl, and Reimold (2004) interpreted the dead zone to be the initial postimpact marine sedimentary unit, and they inferred quiet-water deposition from the undisturbed geometry of the repetitive, submillimeter-scale, horizontal laminae of sand, silt, and clay. Poag (2002) and Poag, Koeberl, and Reimold (2004) placed the conformable lower contact of the dead zone at 235.84 m (773.75 ft) in the Langley core. The upper boundary of the dead zone is a sharp contact with the base of the Chickahominy Formation at 235.65 m (773.12 ft; fig. F7*C*).

Chickahominy Formation

Lithic Characteristics

Poag, Koeberl, and Reimold (2004) described fresh cores of the Chickahominy Formation from several coreholes in the Chesapeake Bay impact crater as typically composed of gray-green clay that weathers to yellowish olive brown and contains variable amounts of finely comminuted glauconite and muscovite (see also Powars and others, this volume, chap. G). The clay is silty to sandy, is richly fossiliferous, and commonly displays fine to coarse (frequently faint) lamination. The biota are mainly marine microfossils (benthic and planktonic foraminifera, calcareous nannofossils, bolboformids, ostracodes, dinoflagellates, radiolarians), but they also include common to abundant remains or evidence of invertebrates (echinoid spines, solitary corals, thin bivalves, scaphopods, pyritized burrow casts) and vertebrates (fish skeletal debris and teeth; see also Edwards and others, this volume, chap. H).

Sediments subjacent to the upper boundary of the Chickahominy Formation are usually intensely burrowed; those near the lower boundary are moderately burrowed. Larger burrows are filled with coarser material (sand) than the Chickahominy itself (clay) and can be identified as far as 2 m (6.6 ft) into the Chickahominy. Burrows at the top of the Chickahominy are filled with glauconitic quartz sand and microfossils reworked downward from the overlying Oligocene Drummonds Corner beds (Langley core) or Delmarva beds (Kiptopeke core). At the base of the Chickahominy Formation, the smallest, most abundant burrows are filled with framboidal pyrite. The largest burrows in this basal interval are filled with quartz sand and mixed microfossil assemblages reworked upward from the Exmore breccia. The presence of the sand-filled burrows causes the upper and lower sediments in the Chickahominy section to fracture and crumble upon drying, in contrast to most of the remainder of the unit, which maintains its dense, massive character.

Seismic Signature

Integrating the lithic core records and downhole geophysical records allows precise correlation between the lithic boundaries of the Chickahominy Formation and their reflection signatures on seismic-reflection profiles (Poag, 1997a; Poag and others, 1999; Poag, Koeberl, and Reimold, 2004). Normally, a significant impedance contrast exists between the relatively consolidated (dense) clay of the Chickahominy Formation and the unconsolidated sands of the overlying unit, which in different areas is the lower Oligocene Drummonds Corner beds or the lower Oligocene Delmarva beds (Powars and others, 1992; Powars and Bruce, 1999; Powars and others, this volume, chap. G). This impedance contrast produces an easily recognized high-amplitude reflection at the upper boundary of the Chickahominy Formation (fig. F8), which can be traced over the entire crater and extends a short distance outside the crater rim.

The lower boundary of the Chickahominy also is characterized by a strong impedance contrast and a resultant high-amplitude reflection where clay of the Chickahominy Formation contacts the underlying unconsolidated silts and sands of the Exmore breccia (figs. F8, F9). Even on profiles where the boundary reflections are weak (fig. F9), the large number of intersections between profiles (Poag and others, 1999; Poag, Koeberl, and Reimold, 2004) assures recognition of both the

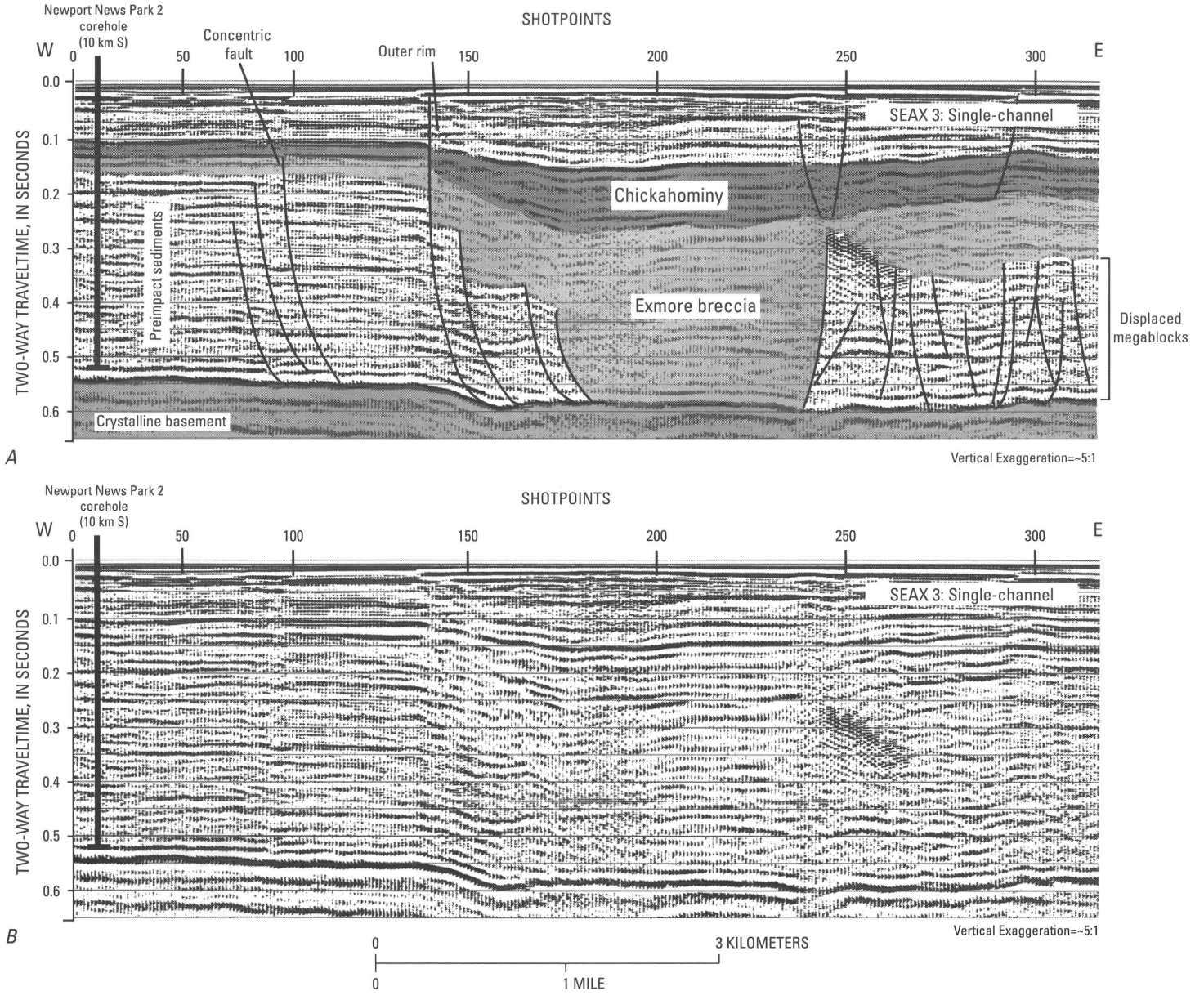

Figure F8. Segment of single-channel seismic-reflection profile SEAX 3 collected by the U.S. Geological Survey (USGS) in collaboration with the National Geographic Society (NGS) in 1996. This profile is one of two parallel seismic-reflection profiles collected in the York River, northwest of the USGS-NASA Langley corehole; it shows that the Chickahominy Formation sags and thickens as it crosses the outer rim of the Chesapeake Bay impact crater. See figure F1 for location of profile. *A,* Interpreted segment of single-channel profile SEAX 3 (from Poag, Koeberl, and Reimold, 2004, fig. 4.9A). *B,* Uninterpreted version of *A.*

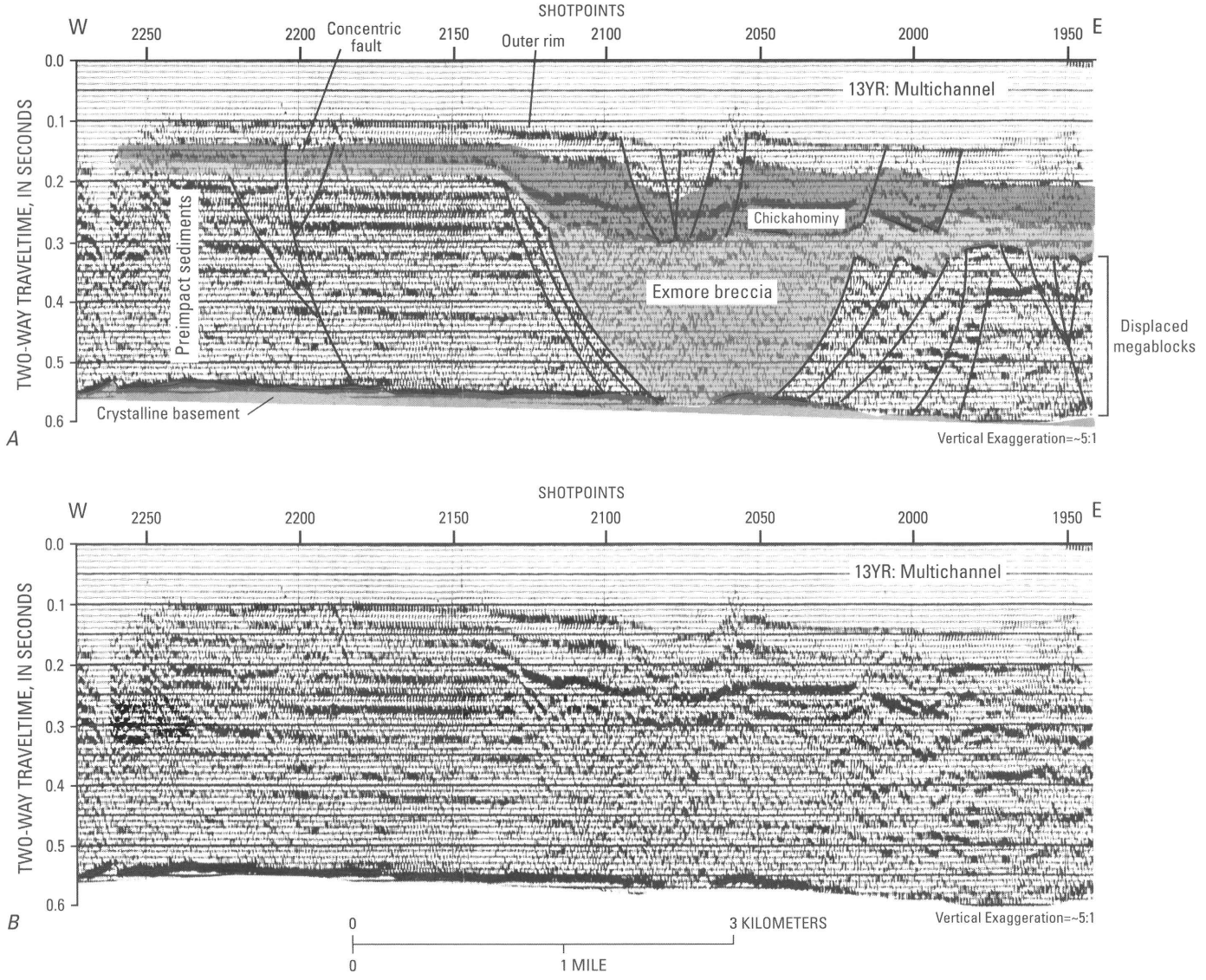

Figure F9. Segment of multichannel seismic-reflection profile 13YR collected by Teledyne Exploration Co. for Texaco, Inc., and Exxon Exploration Co. in 1986 in the York River. It shows that the Chickahominy Formation sags and thickens as it crosses the outer rim of the Chesapeake Bay impact crater. See figure F1 for location of profile. *A,* Interpreted segment of multichannel profile13YR (from Poag, Koeberl, and Reimold, 2004, fig. 4.9B). *B,* Uninterpreted version of *A.*

upper and lower boundaries of the Chickahominy Formation. In the thickest sections of the Chickahominy, internal seismic reflections indicate the probability of meter-scale bedding. In short, the seismostratigraphic signature of the Chickahominy is easy to recognize and to trace over the crater, and, therefore, its present structure (fig. F10), thickness (fig. F11), and distribution can be accurately mapped.

Geometry and Distribution

The structure, morphology, and distribution of the Chickahominy Formation have been influenced strongly by the original irregular geometry of the upper surface of the Exmore breccia and by a long-term subsidence differential between the unconsolidated, water-saturated impact breccia inside the crater and the semiconsolidated, preimpact sedimentary column outside the crater (Poag, Koeberl, and Reimold, 2004). Differential subsidence is partly responsible (along with original bathymetric differences between the crater basin and its peripheral lithotopes) for a much thicker section of Chickahominy inside the crater than outside the crater (figs. F1, F11). In addition, continued differential subsidence during the roughly 34 million years (m.y.) of post-Eocene time, in concert with differential compaction of the underlying breccia, has caused the Chickahominy Formation to sag irregularly over the crater rim (table F3). Thus, the Chickahominy thickens and sags as it crosses into the annular trough and inner basin, just as the underlying Exmore breccia does (figs. F8, F9, F12, F13, F14). Likewise, the Chickahominy mimics the geometry of the underlying Exmore breccia by arching up and thinning over the peak ring and central peak (figs. F13, F14).

Inside the crater, the Chickahominy Formation is ~20 m to >220 m (66 to >720 ft) thick and averages ~100–120 m (330–390 ft) (fig. F11). The thickness varies greatly because the unit fills various pits and troughs in the upper surface of the breccia, which were accentuated by postimpact differential compaction. In general, the formation is thickest where the underlying Exmore breccia is thickest (where the basement surface is deepest) and thins where the Exmore breccia is thinnest (where the basement shallows).

The Chickahominy Formation thickens from 20 m to >90 m (66 to >290 ft) where it crosses the western part of the outer rim, from 20 m to >150 m (66 to >490 ft) across the northern part of the outer rim, and from 20 m to >160 m (66 to >520 ft) across the eastern and southern parts (fig. F11; table F3). The thickest part of the formation (>220 m; >720 ft) occupies the western sector of the inner basin. We have no seismic data for the eastern sector of the inner basin, but a gravity model (Poag, Koeberl, and Reimold, 2004) indicates a similar thickness of Chickahominy there.

The Chickahominy thins over broad areas of the western, northern, and southern sectors of the annular trough; the two locations having the thinnest sections are the area over the southwestern crest of the peak ring and the area over the central peak (figs. F11, F13, F14). The Chickahominy thins rapidly to <10 m (<33 ft) within a few kilometers outside the crater rim, and it is too thin to trace beyond that point on the seismic profiles (fig. F11). The formation is less than 10 m (33 ft) thick in most of the noncored boreholes that have penetrated it outside the crater (Brown and others, 1972; Powars and Bruce, 1999).

Faults and Fault Systems

In addition to producing thickening, thinning, and sagging of the Chickahominy Formation, differential compaction of the Exmore breccia also has created a series of normal-offset faults and fault systems within the postimpact sedimentary section, which break the Chickahominy Formation into discrete fault blocks (figs. F8, F9, F12, F13, F14, F15; Poag, Koeberl, and Reimold, 2004). The throw on most faults decreases upsection, indicating that they are growth faults along which long-term continuous or intermittent movement has occurred (fig. F15). The USGS-NASA Langley corehole crossed a minor branch of one of the postimpact compaction faults, which slices through the Chickahominy Formation at 229.9 m (754.4 ft) depth (fig. F16).

The two most prominent systems of compaction faults are expressed on the seismic profiles as complex intervals of disrupted and offset reflections that derive from distinct grabens located along the outer margins of the annular trough and inner basin (figs. F8, F9, F12, F13). Because these graben structures are present on almost every seismic profile that crosses the outer rim and (or) the outer wall of the inner basin, we infer that they represent parts of two nearly continuous concentric graben systems (ring grabens) that encircle the crater just inside the outer rim and the peak ring (fig. F17).

In addition to the two ring grabens documented on the seismic profiles, more than 700 individual faults and fault clusters (small grabens, horsts, or normal faults) are scattered in mainly concentric orientations throughout the Chickahominy Formation (Poag, Koeberl, and Reimold, 2004; see fig. F17 of this chapter).

Biostratigraphy

Poag and Aubry (1995) established the general biostratigraphic framework for the Chickahominy Formation on the basis of planktonic foraminifera, calcareous nannofossils, and bolboformids from the Kiptopeke core (fig. F4). They concluded that the lower part of the Chickahominy embraces planktonic foraminiferal biochronozone P15 and the upper part represents biochronozone P16-P17. An erosional surface at the top of the Chickahominy Formation is presumed to result from removal of the base of Zone P18, an interval that would represent roughly 0.1 m.y. The P15 zonal marker *Globigerinatheka semiinvoluta* has not been found in the Chickahominy Formation, but specimens of this species are present in the Exmore breccia of the Kiptopeke core. Their presence in the breccia

Text continues on page F26.

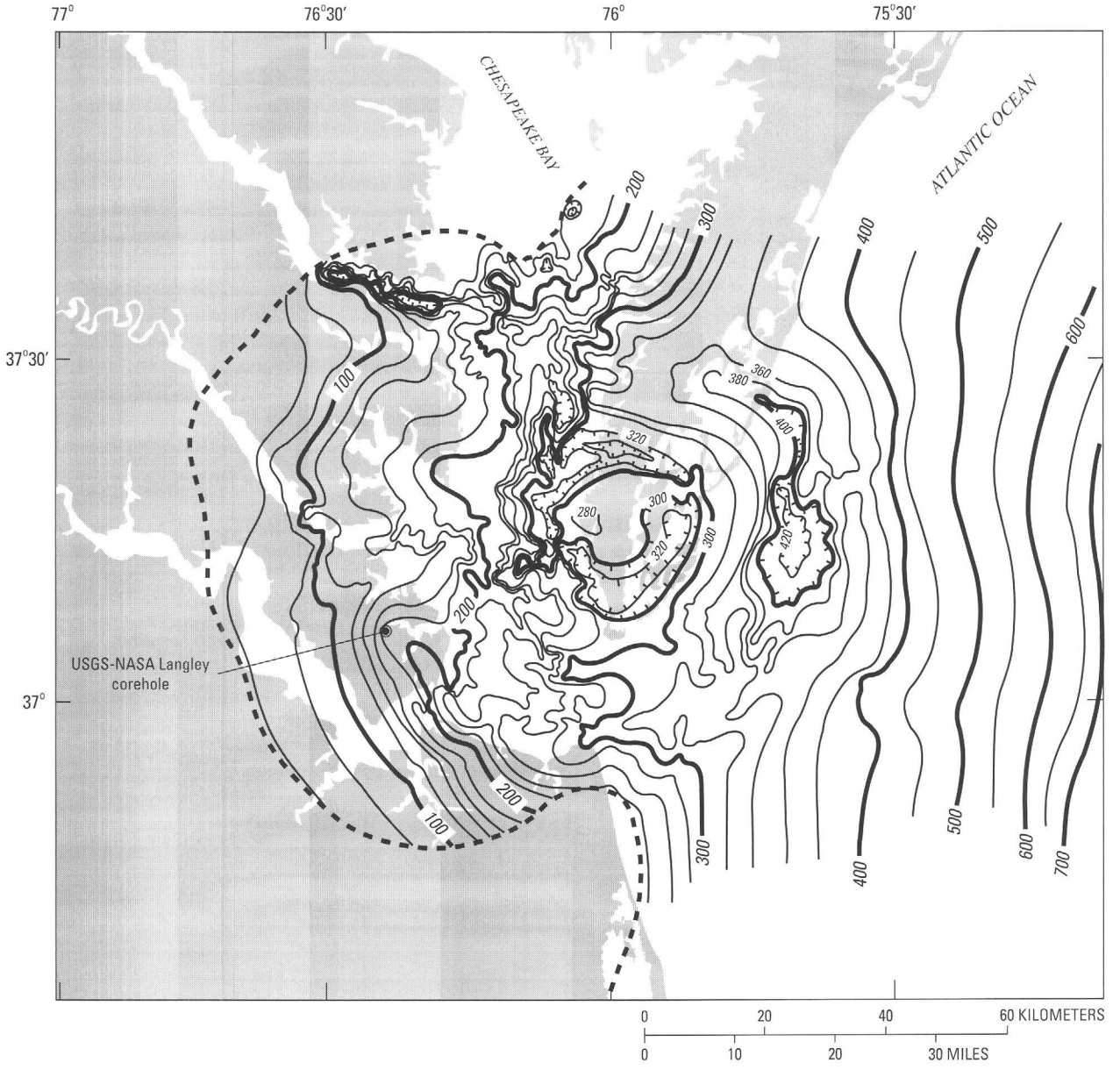

Figure F10. Structure map representing depth to the top of the Chickahominy Formation in the area of the Chesapeake Bay impact crater (fig. F1). Contour intervals are 20 and 50 m (66 and 164 ft); hachured contours indicate depressions. Dashed line is the approximate landward (updip) limit of the Chickahominy Formation. The map is from Poag, Koeberl, and Reimold (2004, fig. 7.8).

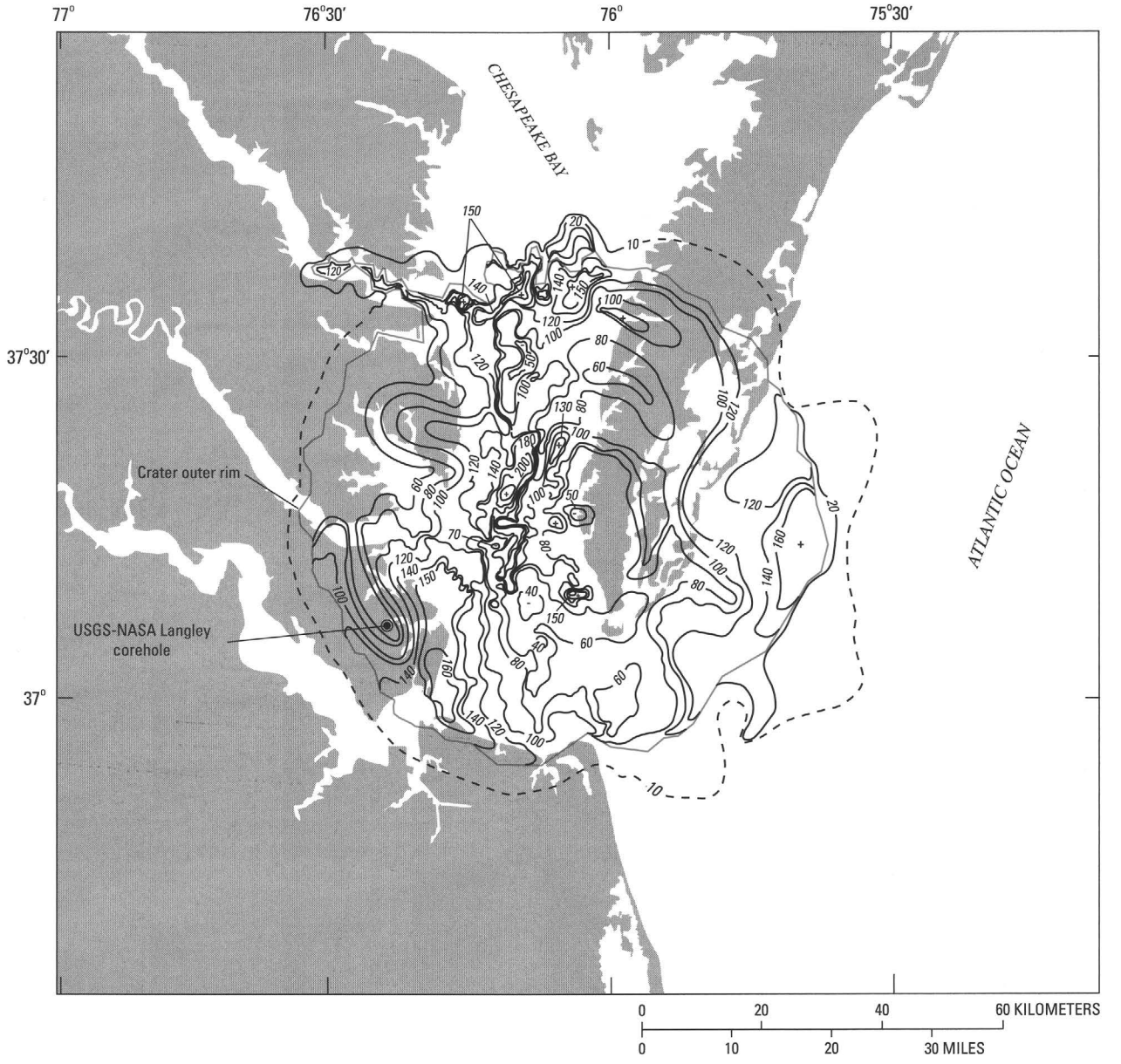

Figure F11. Isopach map of the Chickahominy Formation in the area of the Chesapeake Bay impact crater (fig. F1). Contour intervals are 10 and 20 m (33 and 66 ft); the 10-m contour (dashed where inferred) shows that the Chickahominy extends outside the crater. In places, the outer rim of the crater (red) coincides with various contours. The map is from Poag, Koeberl, and Reimold (2004, fig. 7.9).

Table F3. Elevation, sag, and thickness data for the Chickahominy Formation where it crosses the outer rim of the Chesapeake Bay impact crater.

[Data derived from 25 seismic-reflection profiles and Poag, Koeberl, and Reimold (2004); a few selected profiles are shown in this report (figs. F8, F9, F12). Elevation is depth in meters (m) below sea level (bsl) to the top of the Chickahominy Formation]

Profile name and number	Elevation outside rim (m bsl)	Elevation inside rim (m bsl)	Amount of sag (m)	Thickness outside rim (m)	Thickness inside rim (m)	Thickness increase	
						(m)	(%)
SEAX 2	100	175	75	25	110	85	340
SEAX 3 (fig. F8)	85	120	35	10	90	80	800
Texaco 13YR (fig. F9)	75	120	45	10	90	80	800
SEAX 16 (fig. F12)	110	190	80	15	80	65	433
SEAX 17	125	170	45	10	100	90	900
Neecho 3	110	170	60	10	70	60	600
Texaco 11–PR	120	220	100	40	100	60	150
Texaco 9–CB–F	120	210	90	40	100	60	150
SEAX 12	140	180	40	20	140	120	600
SEAX 13	150	200	50	15	110	95	633
Texaco 10–RR	180	230	50	10	140	130	1,300
Texaco 1–CB	175	200	25	10	90	80	800
SEAX 4	150	180	30	20	100	80	400
SEAX 10	175	220	45	10	130	120	1,200
SEAX 11	160	180	20	10	120	110	1,100
SEAX 5	220	240	20	10	120	110	1,100
SEAX 6	220	270	50	15	70	55	367
SEAX 8	255	310	55	15	60	45	300
SEAX 9	280	320	40	15	100	85	567
SEAX 19	365	390	25	10	120	110	1,100
SEAX 22	370	390	20	10	100	90	900
SEAX 25	350	380	30	30	150	120	400
SEAX 27	315	320	5	20	130	110	550
SEAX 1	365	405	40	20	150	130	650
Ewing 3	310	340	30	25	130	105	420
Average	201	245	44	17	108	91	662

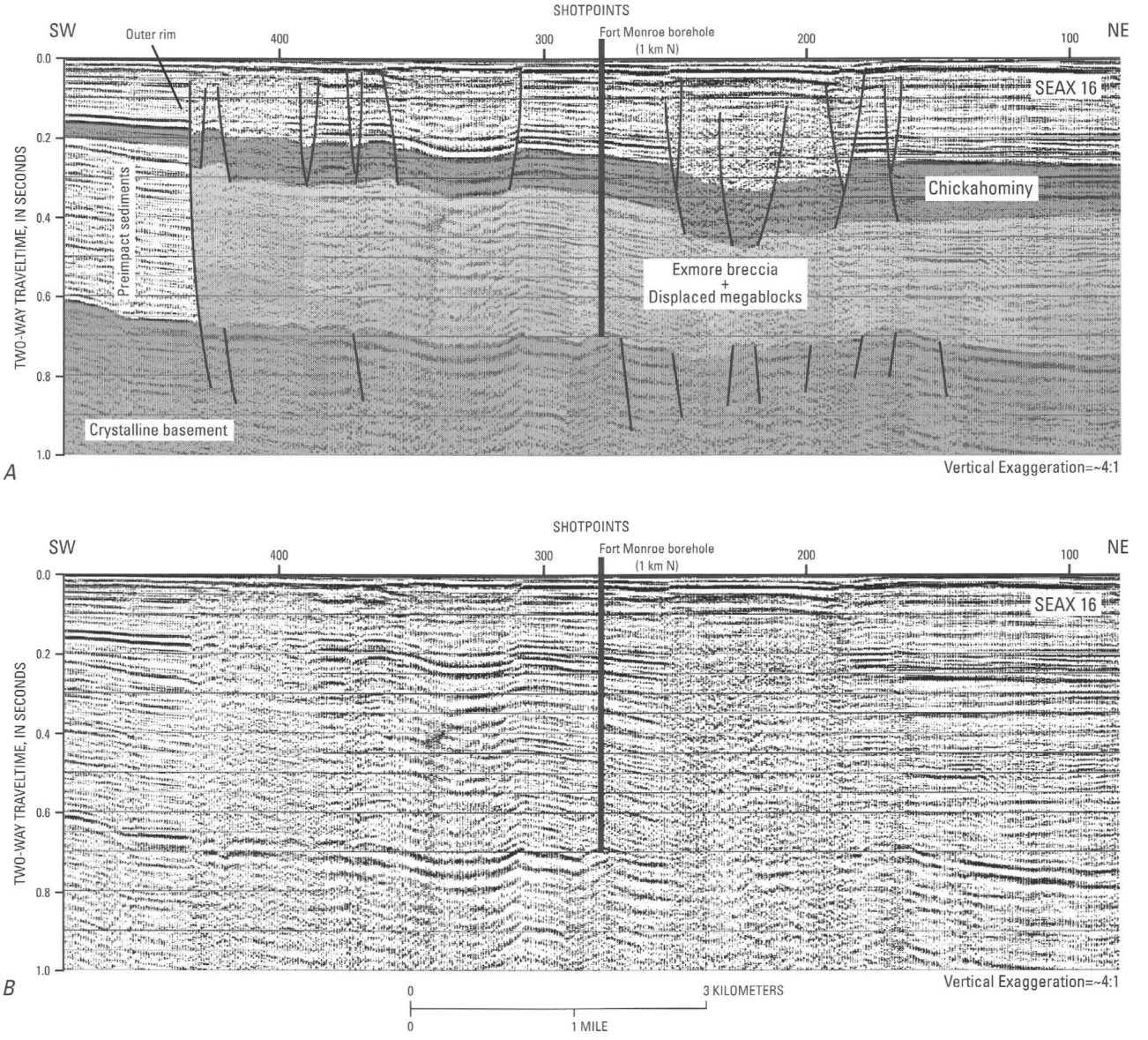

Figure F12. Segment of single-channel seismic-reflection profile SEAX 16 collected by the USGS and the NGS in 1996 in the mouth of the James River. See figure F2 for location of profile. *A,* Interpreted segment of single-channel profile SEAX 16 (from Poag, Koeberl, and Reimold, 2004, fig. 4.11). *B,* Uninterpreted version of *A.*

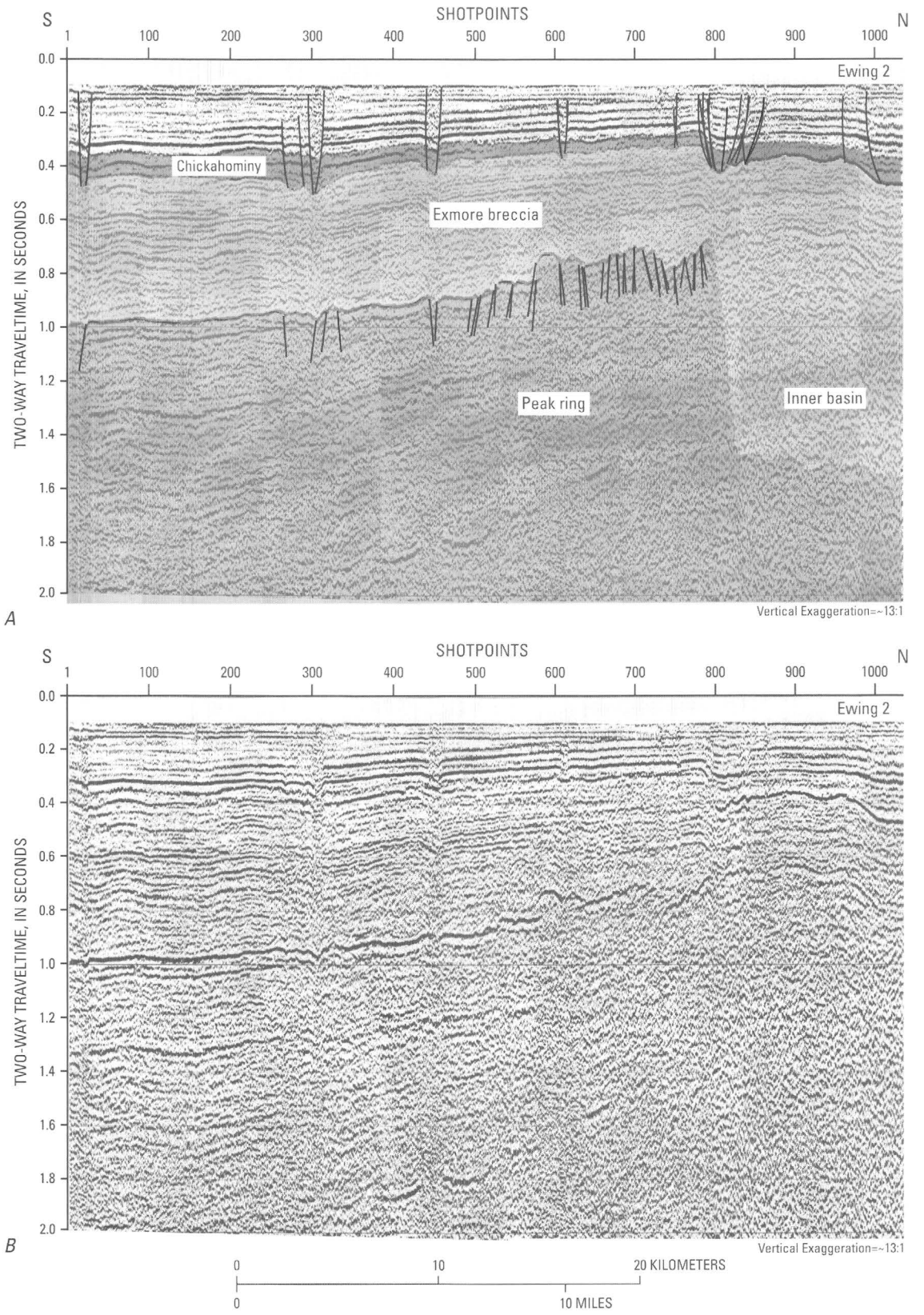

Figure F13. First segment of two-channel seismic-reflection profile Ewing 2 collected in 1998 by the USGS in collaboration with the Lamont-Doherty Earth Observatory (LDEO). The profile segment crosses the peak ring of the Chesapeake Bay impact crater. Note that the Chickahominy Formation thins and rises structurally over basement highs. See figure F1 for location of profile. *A*, Interpreted segment of two-channel profile Ewing 2 (from Poag, Koeberl, and Reimold, 2004, fig. 4.26A). *B*, Uninterpreted version of *A*.

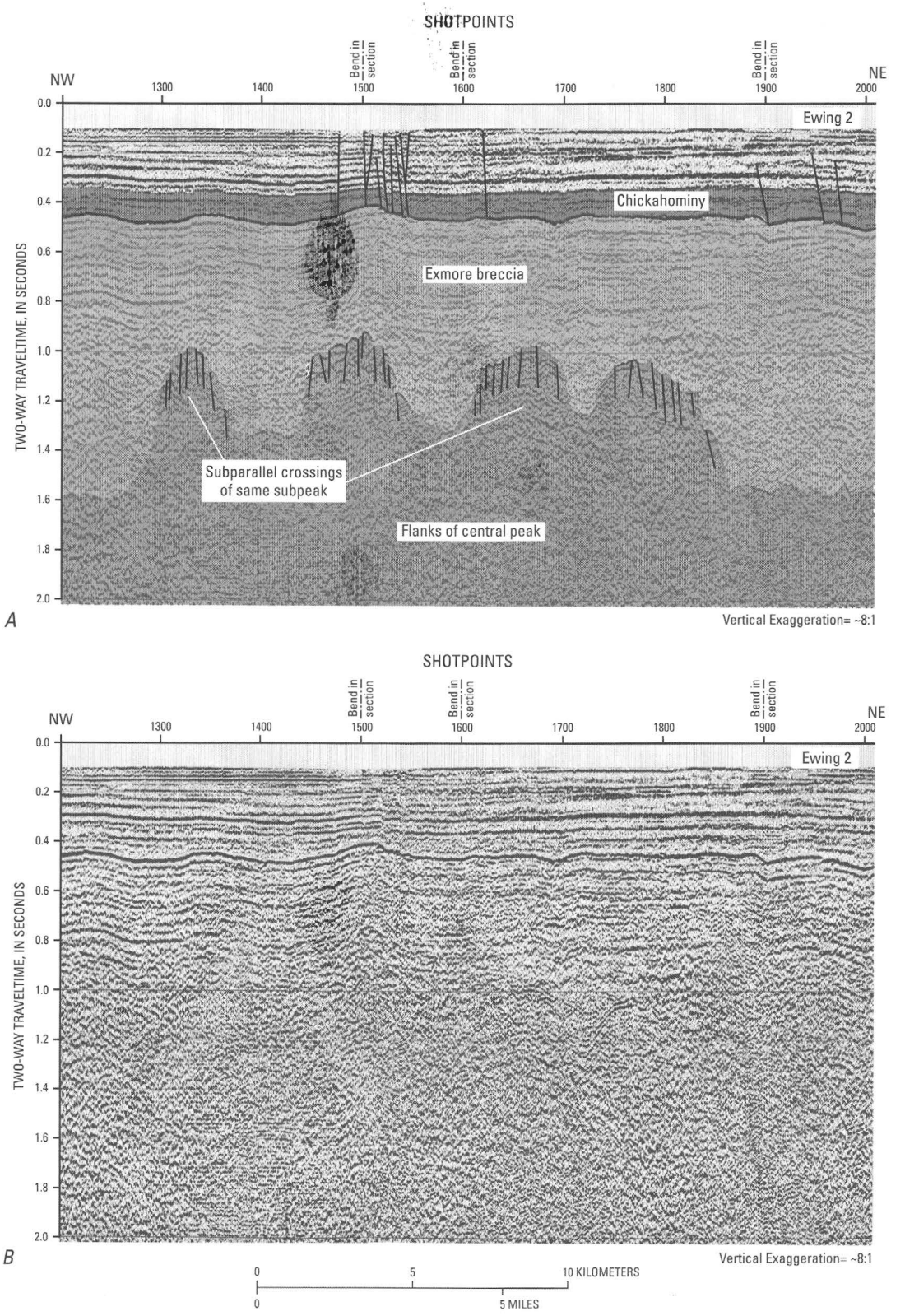

Figure F14. Second segment of two-channel seismic-reflection profile Ewing 2 collected in 1998 by the USGS in collaboration with the Lamont-Doherty Earth Observatory (LDEO). The profile segment crosses the flanks of the central peak of the Chesapeake Bay impact crater. Note that the Chickahominy Formation thins and rises structurally over basement highs. See figure F1 for location of profile. *A,* Interpreted segment of two-channel profile Ewing 2 (from Poag, Koeberl, and Reimold, 2004, fig. 4.32). *B,* Uninterpreted version of *A.*

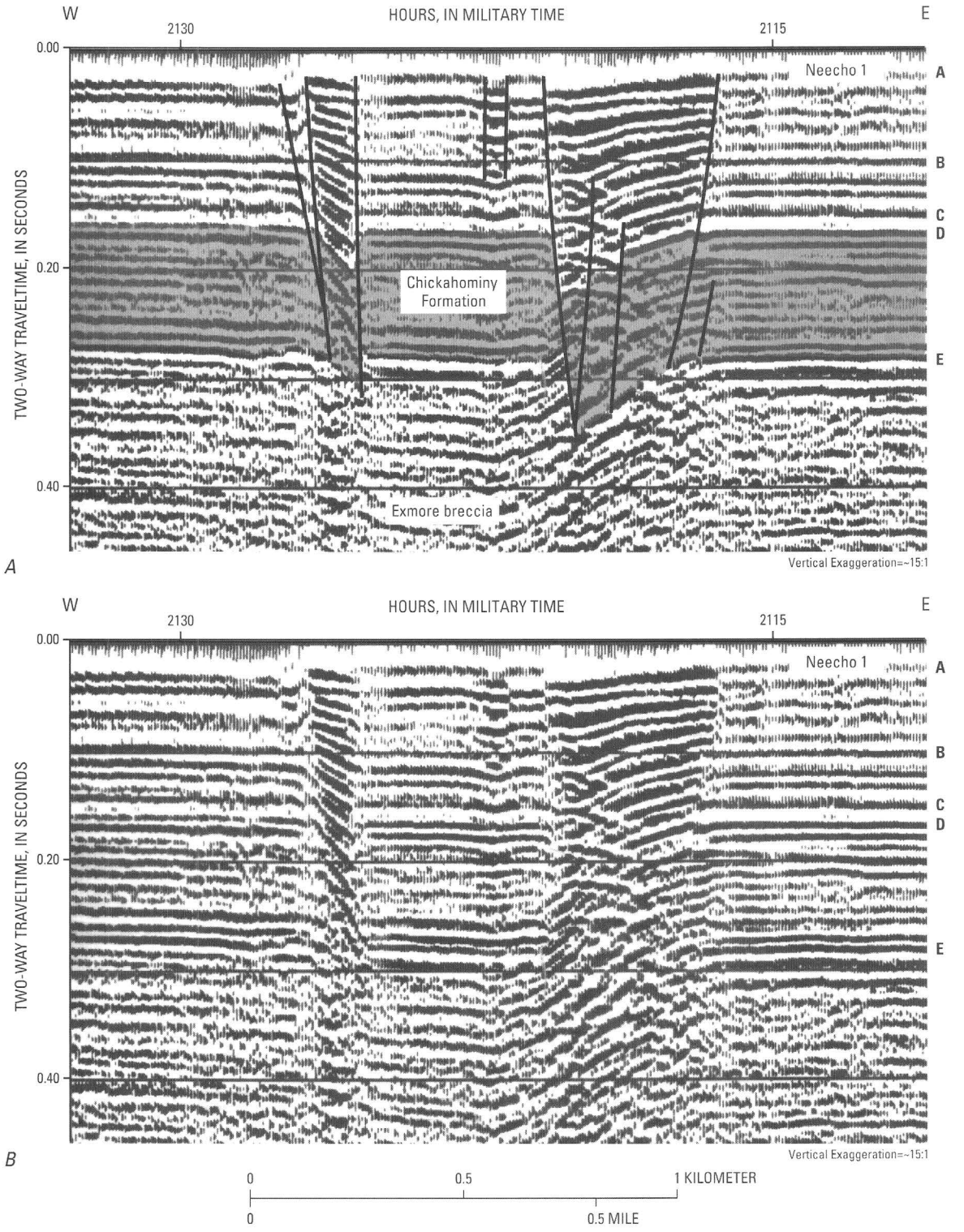

Figure F15. Segment of multichannel seismic-reflection profile Neecho 1 collected near the mouth of the York River by the USGS in 1982. The profile shows stratal offsets due to postimpact faults extending from the Chickahominy Formation. Letters A–E indicate seismic reflections traced across the profile to demonstrate upward decrease in fault throw. See figure F1 for location of profile. *A,* Interpreted segment of multichannel profile Neecho 1 (from Poag, Koeberl, and Reimold, 2004, fig. 7.12C). *B,* Uninterpreted version of *A.*

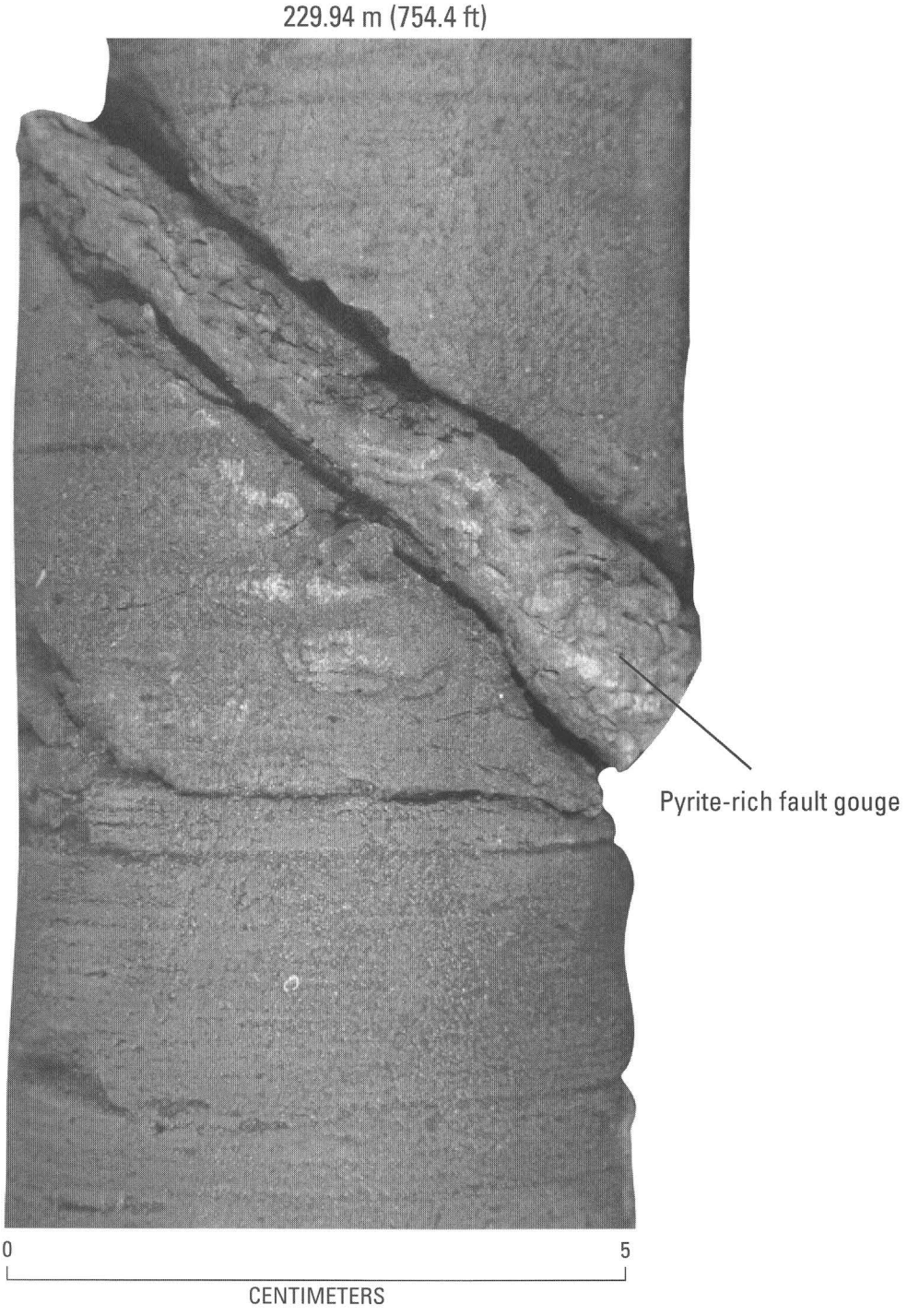

Figure F16. Photograph of a core segment of the Chickahominy Formation from the USGS-NASA Langley corehole showing a minor branch of the postimpact fault system. Leader indicates pyrite-rich fault gouge. Photograph by C.W. Poag (from Poag, Koeberl, and Reimold, 2004, fig. 7.10).

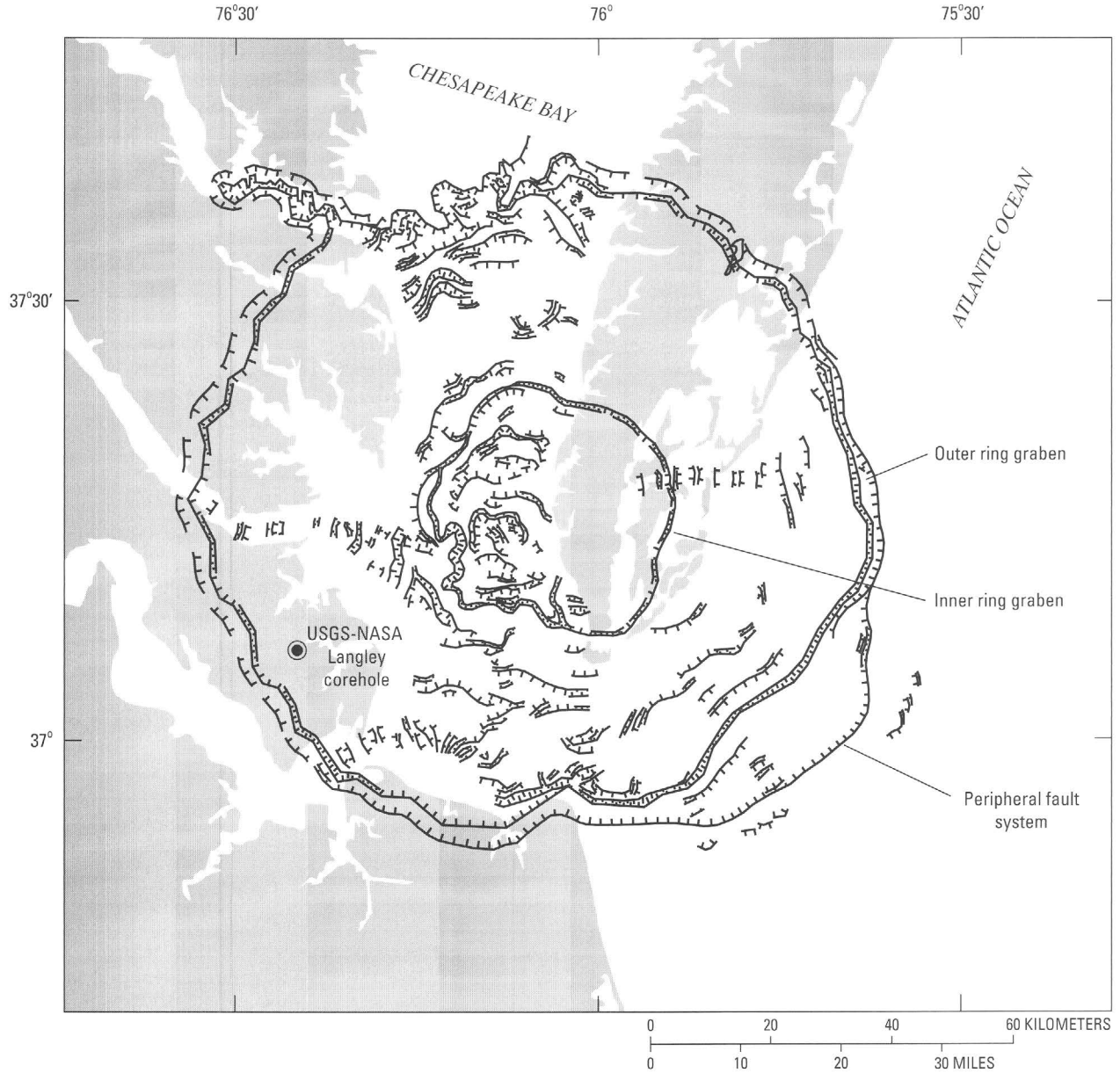

Figure F17. Map showing the general distribution of postimpact compaction faults (ticks on downthrown side) that cut the Chickahominy Formation at the Chesapeake Bay impact crater, as interpreted from seismic-reflection data. From Poag, Koeberl, and Reimold (2004, fig. 7.11).

indicates that sediment belonging to Zone P15 had been deposited prior to the impact.

The presence of *Turborotalia cunialensis* and *Cribrohantkenina inflata* in the Chickahominy at Kiptopeke is evidence that Zone P16 is represented in that core. The P15-P16 *biozonal* boundary was not recognized at Kiptopeke, however. Instead, Poag and Aubry (1995) identified the P15-P16 *biochronozone* on the basis of a thin concurrent-range biozone defined by the highest occurrence of *Bolboforma spinosa* and the lowest occurrence of *Bolboforma latdorfensis* (fig. F4; see also Poag, Koeberl, and Reimold, 2004). This bolboformid biozone has been established as approximately correlative with the P15-P16 biozonal boundary at Deep Sea Drilling Project (DSDP) Site 612 on the New Jersey Continental Slope (Poag and Aubry, 1995).

Poag, Koeberl, and Reimold (2004) also analyzed the stratigraphic distribution of benthic foraminifera in the Chickahominy Formation at Kiptopeke. They identified one calcareous benthic foraminiferal biozone (*Cibicidoides pippeni*) and four calcareous benthic foraminiferal subbiozones (*Bulimina jacksonensis, Lagenoglandulina virginiana, Uvigerina dumblei,* and *Bolivina tectiformis*) based on the stratigraphic ranges (presence-absence) of the nominate calcareous benthic foraminiferal species (fig. F5; pl. F1).

Poag, Koeberl, and Reimold (2004) defined the calcareous benthic foraminiferal zonation as follows:

- ***Cibicidoides pippeni* Taxon-Range Biozone**. That part of the Chickahominy Formation embracing the stratigraphic range of the nominate species. *Cibicidoides pippeni* appears to have a more extensive stratigraphic range in other localities, however, such as the Gulf of Mexico Coast and Caribbean (Van Morkhoven, Berggren, and Edwards, 1986) than it has at Kiptopeke.

- ***Bulimina jacksonensis* Interval Subbiozone**. That part of the Chickahominy Formation embracing the partial stratigraphic range of the nominate species between its lowest occurrence and the lowest occurrence of *Lagenoglandulina virginiana.*

- ***Lagenoglandulina virginiana* Interval Subbiozone**. That part of the Chickahominy Formation embracing the partial stratigraphic range of the nominate species between its lowest occurrence and the lowest occurrence of *Uvigerina dumblei.*

- ***Uvigerina dumblei* Interval Subbiozone**. That part of the Chickahominy Formation embracing the partial range of the nominate species between its lowest occurrence and the lowest occurrence of *Bolivina tectiformis.*

- ***Bolivina tectiformis* Taxon-Range Subbiozone.** That part of the Chickahominy Formation embracing the total range of the nominate species.

Poag, Koeberl, and Reimold (2004) also recognized a fifth subbiozone on the basis of agglutinated benthic foraminiferal taxa (fig. F5; pl. F1):

- ***Bathysiphon* Abundance Subbiozone**. That part of the Chickahominy Formation at the base of the *Bulimina jacksonensis* Subbiozone that contains the peak development (maximum specimen abundance and species diversity) of a suite of agglutinated benthic foraminifera in which *Bathysiphon* sp. is a notable (persistent and relatively abundant) constituent.

The USGS-NASA Langley Core

Lithostratigraphy

In the USGS-NASA Langley core, the Chickahominy Formation appears visually to be relatively uniform in composition. It is mainly a dense, dark-greenish-gray, highly fossiliferous marine clay (especially rich in microfossils); the unit is 52.37 m (171.8 ft) thick (see Powars and others, this volume, chap. G). On closer examination, the lithology is seen to be variable. For example, the relative amount of quartz silt and sand, mica flakes, and finely comminuted glauconite (as observed in washed foraminiferal samples) is not uniform through the cored section. Also, the unit is heavily burrowed at its top contact. The largest burrows contain sand and microfossils reworked downward from the overlying Oligocene Drummonds Corner beds. Fewer burrows are present at the base of the Chickahominy. The basal burrows contain sand and stratigraphically mixed microfossils reworked upward from the underlying Exmore breccia. Smaller burrows filled with framboidal pyrite are scattered throughout the formation but are more densely concentrated in some intervals than in others.

Log Correlations

Comparisons of downhole spontaneous-potential (SP) logs from the USGS-NASA Langley corehole and three other intracrater coreholes (North, Bayside, Kiptopeke; fig. F1) are useful in deciphering the thickness and distribution of lithofacies within the Chickahominy section. The logs from North, Bayside, and Kiptopeke indicate that the Chickahominy is notably less permeable (*negative* deflection of the SP curve) than the units that bound it (fig. F18). The Chickahominy section in the Langley corehole is an exception, however. There, the SP log is *positively* deflected relative to the log of the underlying Exmore breccia, which we infer to indicate greater permeability. Nevertheless, at all four core sites, the Chickahominy Formation can be partitioned into four principal subunits (SP–1 through SP–4) on the basis of log-defined SP deflections (relative permeability; fig. F18); a fifth subunit (SP–5) is recognized only at Kiptopeke.

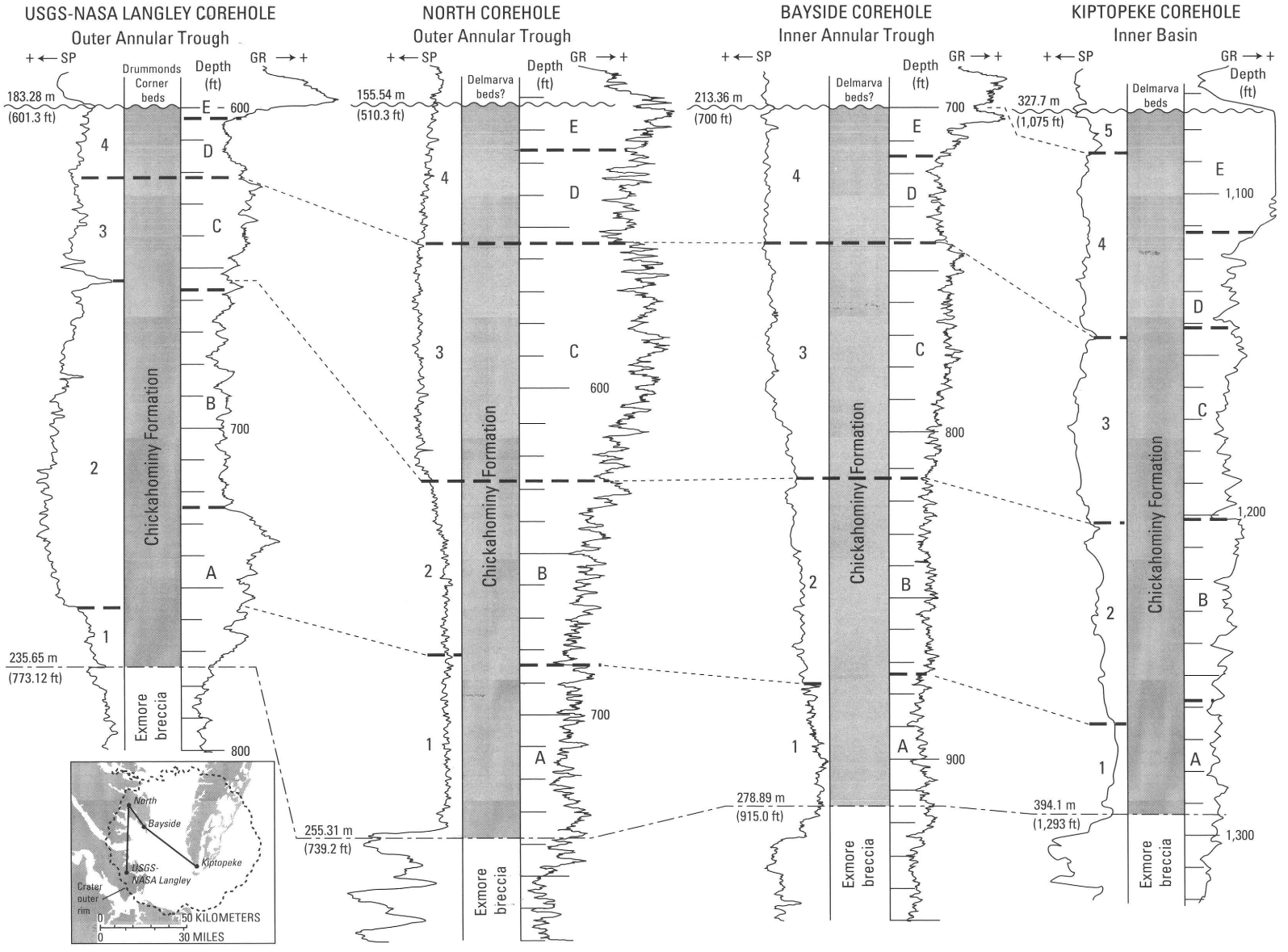

Figure F18. Downhole spontaneous-potential (SP) and gamma-ray (GR) logs, emphasizing log-defined lithic subunits within the Chickahominy Formation in the USGS-NASA Langley corehole and their correlations with subunits in the North, Bayside, and Kiptopeke coreholes (fig. F1). From Poag, Koeberl, and Reimold (2004, fig. 7.7A). Stratigraphic resolution is too coarse to show the dead zone. Vertical scales represent drill depths in feet. Negative deflections of the SP curves are interpreted to represent decreased permeability. Positive deflections of the GR curves are interpreted to represent increased amounts of clay or glauconite.

Subunits SP–1 through SP–5 are described below in ascending order:

- **Subunit SP–1.** At each site, subunit SP–1 (at the base) is characterized by the strongest negative deflections (lowest permeability).
- **Subunit SP–2.** At North, Bayside, and Kiptopeke, subunit SP–2 is characterized by SP values that become gradually more positive upcore (increasing permeability). In the Langley corehole, on the other hand, the positive SP deflection is abrupt at the base of SP–2, reaches highest values for this corehole, and then tapers off negatively, before declining steeply (becoming less permeable) at the top of SP–2 (fig. F18).
- **Subunit SP–3.** The log deflection in subunit SP–3 is more positive (greater permeability) than the deflection in SP–2 at North, Bayside, and Kiptopeke but is more negative (less permeability) than the deflection in SP–2 in the Langley corehole.
- **Subunit SP–4.** In subunit SP–4, the SP curve deflects negatively relative to the curve for SP–3 at North, Kiptopeke, and Langley but shows a relatively positive deflection at Bayside (fig. F18).
- **Subunit SP–5.** A fifth subunit (SP–5) at the top of the Chickahominy Formation can be recognized only at Kiptopeke. In subunit SP–5, the SP log deflects notably in the positive direction upsection.

Downhole gamma-ray (GR) logs, which reflect mainly the relative amount of clay and (or) glauconite in the Chickahominy Formation, provide a somewhat stronger definition of downhole lithic changes than do the SP curves (fig. F18); positive deflections of a GR log are interpreted to represent increased amounts of clay or glauconite. The GR curves at all four sites indicate a fivefold subdivision (GR–A through GR–E) of the Chickahominy. The upward succession of relative GR values, like that of the SP values, is similar at North, Bayside, and Kiptopeke.

Subunits GR–A through GR–E are described below in ascending order:

- **Subunit GR–A.** The basal GR subunit (GR–A) displays the greatest negative values at North, Bayside, and Kiptopeke, but in stark contrast, GR–A gives unusually high positive values at the Langley corehole.
- **Subunit GR–B.** Subunit GR–B shows upwardly increasing positive values at North and Kiptopeke, uniformly slightly higher values than GR–A at Bayside, and uniformly more negative values than GR–A at Langley (fig. F18).
- **Subunit GR–C.** In subunit GR–C, the GR values continue to increase positively upward at the Langley, North, and Bayside coreholes but decrease slightly before increasing again at Kiptopeke.
- **Subunit GR–D.** In subunit GR–D, GR values become negative at all sites relative to those of subunit GR–C.
- **Subunit GR–E.** Maximum positive GR values are reached at the top of the Chickahominy Formation in subunit GR–E at all four core sites (fig. F18).

The complex correlations of SP and GR subunits among different coreholes, combined with the marked stratigraphic variability within individual coreholes, are the results of laterally and vertically shifting Chickahominy lithotopes and suggest that the subunit boundaries are not likely to be synchronous from corehole to corehole. The most consistent intracorehole correlation is between SP–3 and GR–C, whose upper and lower boundaries coincide (or nearly coincide) at all four sites (fig. F18). There also is good correlation between SP–1 and GR–A and between SP–2 and GR–B at North, Bayside, and Kiptopeke, but these correlations break down at Langley. At the top of the Chickahominy section, SP–4 is equivalent to GR–D and GR–E, except at Kiptopeke, where SP–5 correlates with the top of GR–E.

In general, the logs indicate that during the early stages of Chickahominy deposition, the sedimentary regime at the USGS-NASA Langley site was distinctly different than that of the other three core sites. This difference is particularly manifested by subunit SP–2 (199–232 m; 653–760 ft) in the Langley corehole, which not only contains more sand-sized sediment than the basal (SP–1) and upper (SP–3, SP–4) subunits at Langley, but also contains much more sand-sized sediment than equivalent subunits farther downdip at the North corehole or farther toward the center of the crater at the Bayside and Kiptopeke coreholes (fig. F18). Moreover, the basal part of SP–2 at Langley also contains far more glauconite (subunit GR–A) than equivalent sections at the other three core sites (fig. F18).

Biostratigraphy

Planktonic Framework

In our Chickahominy samples from the USGS-NASA Langley core, we identified most of the same species of planktonic foraminifera and bolboformids (fig. F19) reported by Poag and Aubry (1995) for the Kiptopeke core. The planktonic foraminiferal succession in the Langley core is not sufficient to place the biozonal boundaries accurately, however, and so we followed Poag and Aubry (1995) and used the *Bolboforma spinosa-Bolboforma latdorfensis* biozone boundary to place the P15-P16 biochronozone boundary; in the Langley core, the boundary is between samples 24 and 25 at ~221.80 m (~727.70 ft) depth. See Edwards and others (this volume, chap. H) for stratigraphic distribution of additional planktonic microfossil groups.

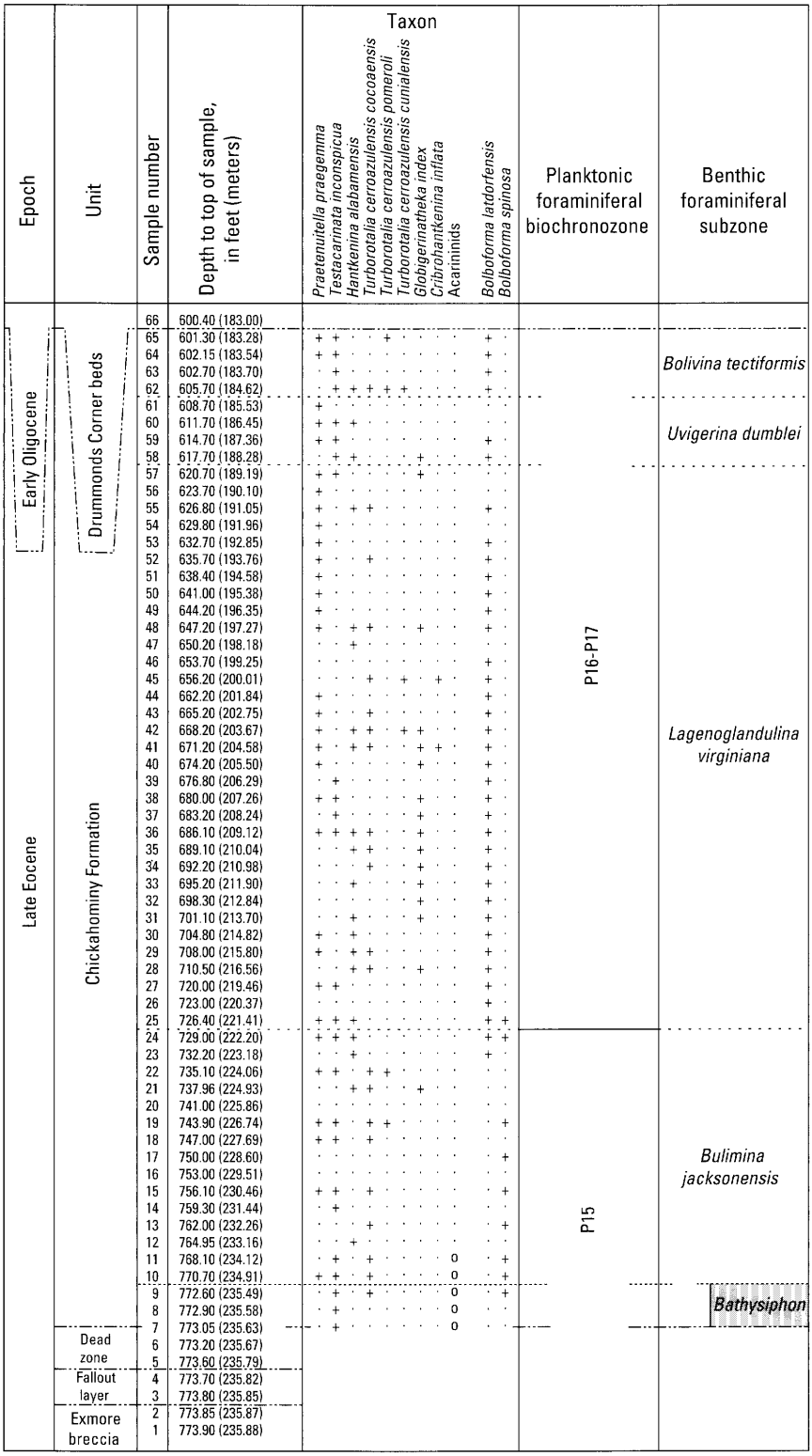

Figure F19. Chart showing planktonic biochronostratigraphic framework (based on occurrences of key planktonic foraminifera and bolboformids) for the Chickahominy Formation in the USGS-NASA Langley corehole correlated with benthic foraminiferal subzones. Symbols: +=present, .=absent, o= reworked specimen. Note that the contact between the dead zone and the Chickahominy Formation is near the middle of sample 7, whose top is at 235.63 m (773.05 ft) depth; the contact between the dead zone and the fallout layer is within sample 4 at ~235.84 m (~773.75 ft) (fig. F7). See also Edwards and others (this volume, chap. H).

Benthic Foraminifera

As in the Kiptopeke core, abundant benthic foraminiferal assemblages are present in the Chickahominy Formation samples from the Langley core and can be stratigraphically divided into the same *Cibicidoides pippeni* Zone and its five subzones (tables F4–F8; pl. F1; figs. F19, F20, and F21). Correlation of the benthic foraminiferal biozones of the Langley core with those of the Kiptopeke core is straightforward, but notable variations in the thickness of equivalent benthic subzones between the two core sites indicate that not all benthic subzone boundaries are isochronous horizons. Thickness disparities are particularly notable for the *Bulimina jacksonensis* and *Lagenoglandulina virginiana* Subzones, for example. The *Lagenoglandulina virginiana* Subzone is 12.6 m (41.3 ft) thick at Kiptopeke but is nearly three times as thick (33.07 m; 108.5 ft) at Langley. The benthic boundary that most closely approximates an isochronous boundary is that which separates the *Bulimina jacksonensis* Subzone from the *Lagenoglandulina virginiana* Subzone, because it is coincident with the planktonic foraminiferal P15-P16 zonal boundary at both Kiptopeke and Langley (fig. F22).

Age-Depth Model

Poag, Mankinen, and Norris (2003) and Poag, Koeberl, and Reimold (2004) used three biochronological datums and three magnetochronological datums to construct an age-depth model for the Kiptopeke core (fig. F23). Poag, Koeberl, and Reimold (2004) interpreted the two strongest deflections in the depth-age curve at Kiptopeke to represent significant changes in sediment accumulation rate (figs. F5, F22). We reassessed the Kiptopeke age-depth model and derived slightly different accumulation-rate values (fig. F23), but we identified the same two major shifts at the same stratigraphic horizons reported by Poag, Koeberl, and Reimold (2004).

At the Langley corehole, we are limited to the three biochronological datums: the base and top of the *Cibicidoides pippeni* Zone (35.78 Ma and 33.7 Ma, respectively) and the P15-P16 planktonic zonal boundary (35.2 Ma; Berggren and others, 1995; see fig. F3 of this chapter). We infer that erosion removed the base of planktonic foraminiferal chronozone Zone P18 from the very top of the intensely burrowed Chickahominy section; the lost record may have represented ~0.1 m.y. By using these datums, we identified a minor shift in sediment accumulation rate at the P15-P16 boundary at 221.8 m (~727.70 ft) depth (fig. F19), where the rate increases from 24 m/m.y. to 26 m/m.y. (78.7 ft/m.y. to 85.3 ft/m.y.). Given the imprecision of identifying stratigraphic boundaries on the basis of presence-absence data in core material and the relatively coarse sampling intervals, however, the differences between these two accumulation rates may not be significant. On the other hand, the largest rate shift at Kiptopeke takes place at the same stratigraphic level (P15-P16 boundary; fig. F22).

Even if the rate shift were significant, the resultant two-part sediment-accumulation record at the Langley corehole contrasts markedly with the three-part accumulation record at Kiptopeke (Poag, Koeberl, and Reimold, 2004; see figs. F5, F22, F23 of this chapter). The accumulation rate at Kiptopeke started out at an average of 56 m/m.y. (183.7 ft/m.y.) in the lowest 32 m (105 ft), decreased to 9 m/m.y. (29.5 ft/m.y.) in the succeeding 5 m (16.4 ft), and then increased to 32 m/m.y. (105 ft/m.y.) in the upper 27 m (88.6 ft). Even though the stratigraphic level of the sediment-accumulation-rate shift at the Langley site is coeval with the largest rate shift at Kiptopeke (fig. F22), the latter shift is a six-fold *decrease*, rather than a minor *increase*.

If one assumes that the sediment accumulation rate did not vary significantly between successive datums at the Langley site, then one can derive a rough estimate of the duration of each benthic foraminiferal subzone and the postimpact age of each benthic subzonal boundary (fig. F21). These estimates would support the hypothesis that some benthic subzonal boundaries are diachronous between the Langley and Kiptopeke coreholes. Such diachroneity would be further supported by comparing these boundary positions graphically (fig. F24). In the graphic correlation, the top of the *Bulimina jacksonensis* Subzone appears to be the only unequivocally isochronous benthic horizon, because its plot coincides with that of the planktonic P15-P16 boundary at both sites. The top of the *Uvigerina dumblei* Subzone plots close to the line of isochroneity, however, and may be truly isochronous, given the coarse sample spacing at both sites. The other two benthic foraminiferal subzonal boundaries are significantly distant from the line of isochroneity. One must keep in mind, however, that the SP and GR logs strongly indicate that the rate of sediment accumulation during Chickahominy time at the Langley site varied considerably, though perhaps not in concert with the rate changes at Kiptopeke. Clearly an analysis of the paleomagnetic record (or some other reliable set of datums) is needed at the Langley site to provide a more detailed record of sediment accumulation rates there.

Species Richness

In their study of Chickahominy benthic foraminifera in the Kiptopeke core, Poag, Koeberl, and Reimold (2004) demonstrated quantitatively that species richness (number of species represented in a sample) varied cyclically in approximate concert with the three intervals of distinctly different sediment accumulation rates (fig. F5). In the USGS-NASA Langley core, we find no equivalent cycles of species richness (fig. F25). Instead, there is a twofold subdivision, with higher average species richness (56) below 201.84 m (662.20 ft) and lower average species richness (47) above this level. This richness shift does not correspond to any obvious biostratigraphic boundary but takes place near the middle of the *Lagenoglandulina virginiana* Subzone. Most of the interval of higher average species richness corresponds, however, to the section of greatest positive SP deflection (SP–2; greatest permeability) in the Chickahominy Formation in the Langley corehole (fig. F18). In contrast, the

Text continues on page F43.

Table F4. Important benthic foraminiferal species of the *Cibicidoides pippeni* Zone in the Chickahominy Formation in the USGS-NASA Langley core.

[The benthic foraminiferal assemblages of the Chickahominy Formation are encompassed in a single biozone, the *Cibicidoides pippeni* Zone, which is represented by 126 calcareous and agglutinated species in the Chickahominy Formation (postimpact) in the USGS-NASA Langley core (fig. F20). Species listed in this table are those whose specimens are persistently present and (or) abundant in the *Cibicidoides pippeni* Zone in the Langley core. An asterisk (*) indicates species that were also present during the earliest late Eocene (preimpact) in the region later affected by the Chesapeake Bay impact. The *Cibicidoides pippeni* Zone was defined for the Kiptopeke core and preimpact species were identified by Poag, Koeberl, and Reimold (2004, tables 13.2 and 13.3). Quotation marks indicate provisory trivial names used by Poag, Koeberl, and Reimold (2004)]

*Bulimina jacksonensis**
*Caucasina marylandica**
*Charltonina madrugaensis**
*Cibicidoides pippeni**
*Epistominella minuta**
*Globobulimina ovata**
*Globulina gibba**
*Grigelis annulospinosa**
Grigelis cookei
Grigelis "elongata"
*Guttulina hantkeni**
*Guttulina irregularis**
*Gyroidinoides byramensis**
*Gyroidinoides planatus**
Hanzawaia blanpiedi
Lenticulina americana
*Lenticulina virginiana**
Loxostomina vicksburgensis f. "spinosa"*
*Marginulina cocoaensis**
*Melonis planatus**
Nodosaria capitata
Nodosaria cooperensis
*Oridorsalis umbonatus**
Proxyfrons virginiana
Sigmoidella plummerae
*Spiroplectinella mississippiensis**
*Stilostomella cocoaensis**
*Uvigerina gardnerae**
Vaginulina longiforma

Table F5. Important calcareous benthic foraminiferal species of the *Bulimina jacksonensis* Subzone in the Chickahominy Formation in the USGS-NASA Langley core.

[Species listed are those whose specimens are persistently present and (or) abundant in this subzone or are restricted (or nearly so) to this subzone. Quotation marks indicate provisory trivial names used by Poag, Koeberl, and Reimold (2004)]

Bolivina gardnerae	*Lenticulina americana*
Bolivina gracilis	*Lenticulina* "carinata"
Bolivina jacksonensis	*Loxostomina vicksburgensis* f. "spinosa"
Bolivina "praevirginiana"	*Marginulina cocoaensis*
Bolivina striatella	*Marginulina karreriana*
Bulimina jacksonensis	*Melonis planatus*
Caucasina marylandica	*Nodosaria capitata*
Charltonina madrugaensis	*Nodosaria cooperensis*
Cibicidoides "chickahominyanus"	*Nuttallides* sp.
Cibicidoides pippeni	*Oridorsalis umbonatus*
Epistominella minuta	*Parafrondicularia cookei*
Globobulimina ovata	*Sigmoidella plummerae*
Globulina gibba	*Spiroplectinella mississippiensis*
Grigelis annulospinosa	*Stilostomella* "aduncocostata"
Grigelis cookei	*Stilostomella cocoaensis*
Grigelis "elongata"	*Trifarina cooperensis*
Grigelis "tubulosa"	*Uvigerina gardnerae*
Grigelis "tumerosa"	*Valvulineria texana*
Guttulina hantkeni	
Guttulina irregularis	
Gyroidinoides aequilateralis	
Gyroidinoides byramensis	
Gyroidinoides planatus	
Hanzawaia blanpiedi	
Hoeglundina elegans	

Table F6. Important benthic foraminiferal species of the *Lagenoglandulina virginiana* Subzone in the Chickahominy Formation in the USGS-NASA Langley core.

[Species listed are those whose specimens are persistently present and (or) abundant in this subzone or are restricted (or nearly so) to this subzone. Quotation marks indicate provisory trivial names used by Poag, Koeberl, and Reimold, (2004)]

Bolivina "carinocostata"	*Lagenoglandulina virginiana*
Bolivina jacksonensis	*Lenticulina americana*
Bulimina cooperensis	*Lenticulina* "carinata"
Bulimina jacksonensis	*Lenticulina crassilimbata*
Caucasina marylandica	*Lenticulina virginiana*
Ceratobulimina perplexa	*Loxostomina vicksburgensis* f. "spinosa"
Charltonina madrugaensis	*Marginulina cocoaensis*
Cibicidoides pippeni	*Marginulina karreriana*
Epistominella minuta	*Melonis planatus*
Frondovaginulina tenuissima	*Nodosaria capitata*
Globobulimina ovata	*Nodosaria cooperensis*
Globulina gibba	*Nodosaria vertebralis*
Grigelis annulospinosa	*Nuttallides* sp.
Grigelis cookei	*Oridorsalis umbonatus*
Grigelis "elongata"	*Proxyfrons virginiana*
Grigelis "tubulosa"	*Sigmoidella plummerae*
Grigelis "tumerosa"	*Siphonina tenuicarinata*
Guttulina hantkeni	*Spiroplectinella mississippiensis*
Guttulina irregularis	*Stilostomella cocoaensis*
Gyroidinoides aequilateralis	*Uvigerina gardnerae*
Gyroidinoides byramensis	*Uvigerina jacksonensis* f. alata
Gyroidinoides planatus	*Uvigerina jacksonensis* f. typica
Hanzawaia blanpiedi	*Valvulineria texana*
Hoeglundina elegans	*Vasiglobulina alabamensis*
Hopkinsina danvillensis	

Table F7. Important benthic foraminiferal species of the *Uvigerina dumblei* Subzone in the Chickahominy Formation in the USGS-NASA Langley core.

[Species listed are those whose specimens are persistently present and (or) abundant in this subzone or are restricted (or nearly so) to this subzone. Quotation marks indicate provisory trivial names used by Poag, Koeberl, and Reimold (2004)]

Bolivina "carinocostata"	*Lenticulina virginiana*
Bulimina jacksonensis	*Loxostomina vicksburgensis* f. "spinosa"
Buliminellita curta	*Marginulina cocoaensis*
Caucasina marylandica	*Marginulina karreriana*
Charltonina madrugaensis	*Massilina decorata*
Cibicidina mauricensis	*Melonis planatus*
Cibicidoides pippeni	*Nodosaria cooperensis*
Epistominella minuta	*Nodosaria vertebralis*
Globobulimina ovata	*Oridorsalis umbonatus*
Globulina gibba	*Proxyfrons virginiana*
Grigelis annulospinosa	*Saracenaria hantkeni*
Grigelis cookei	*Sigmoidella plummerae*
Grigelis "elongata"	*Siphonina tenuicarinata*
Grigelis "tumerosa"	*Spiroplectinella mississippiensis*
Guttulina irregularis	*Stilostomella cocoaensis*
Gyroidinoides aequilateralis	*Uvigerina gardnerae*
Gyroidinoides byramensis	*Valvulineria texana*
Gyroidinoides planatus	
Hanzawaia blanpiedi	
Hoeglundina elegans	
Hopkinsina danvillensis	
Lagenoglandulina virginiana	
Lenticulina americana	
Lenticulina americana f. "spinosa"	
Lenticulina "carinata"	

Table F8. Important benthic foraminiferal species of the *Bolivina tectiformis* Subzone in the Chickahominy Formation in the USGS-NASA Langley core.

[Species listed are those whose specimens are persistently present and (or) abundant in this subzone or are restricted (or nearly so) to this subzone. Quotation marks indicate provisory trivial names used by Poag, Koeberl, and Reimold (2004)]

Bolivina regularis	*Loxostomina vicksburgensis* f. "spinosa"
Bolivina tectiformis	*Marginulina cocoaensis*
Bulimina jacksonensis	*Massilina decorata*
Buliminellita curta	*Melonis planatus*
Cassidulinoides braziliensis	*Nodosaria capitata*
Caucasina marylandica	*Nodosaria cooperensis*
Charltonina madrugaensis	*Nodosaria vertebralis*
Cibicidina mauricensis	*Oridorsalis umbonatus*
Cibicidoides pippeni	*Proxyfrons virginiana*
Epistominella minuta	*Sigmoidella plummerae*
Globobulimina ovata	*Siphonina tenuicarinata*
Globulina gibba	*Spiroplectinella mississippiensis*
Grigelis cookei	*Stilostomella* "aduncocostata"
Grigelis "elongata"	*Stilostomella cocoaensis*
Grigelis "tumerosa"	*Uvigerina gardnerae*
Guttulina hantkeni	*Vaginulina longiforma*
Gyroidinoides byramensis	
Gyroidinoides planatus	
Hanzawaia blanpiedi	
Hopkinsina danvillensis	
Lagenoglandulina virginiana	
Lenticulina americana	
Lenticulina americana f. "spinosa"	
Lenticulina "carinata"	
Lenticulina virginiana	

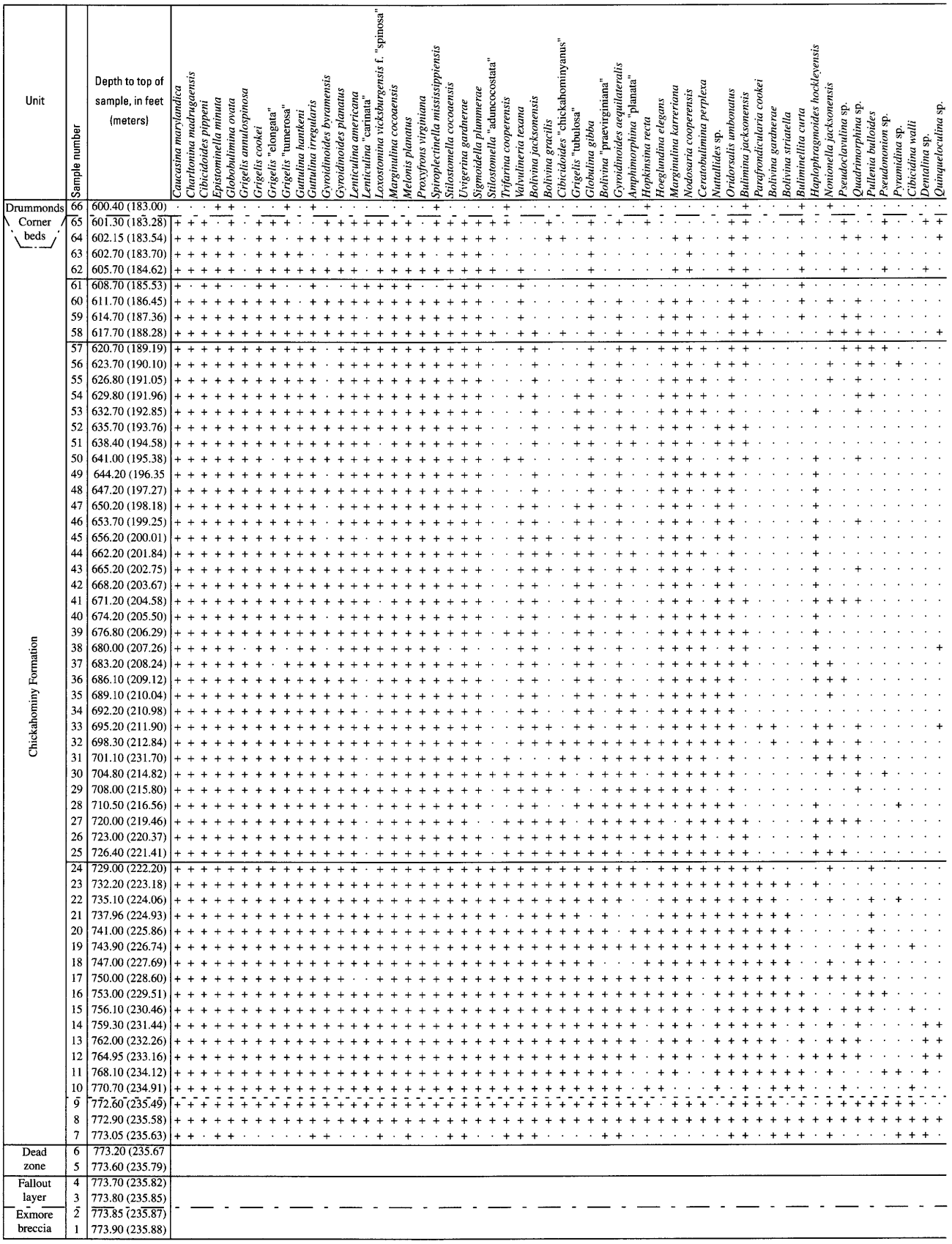

Figure F20. Occurrence chart showing the presence of benthic foraminifera identified in the Chickahominy Formation in the USGS-NASA Langley core. Symbols: +=present, . =absent. The placement of the P15-P16 planktonic foraminiferal biochronozone boundary was approximated by the overlapping ranges of *Bolboforma latdorfensis* and *Bolboforma spinosa* (fig. F19). Note that the contact between the dead zone and the Chickahominy Formation is near the middle of sample 7, whose top is at 235.63 m (773.05 ft) depth.

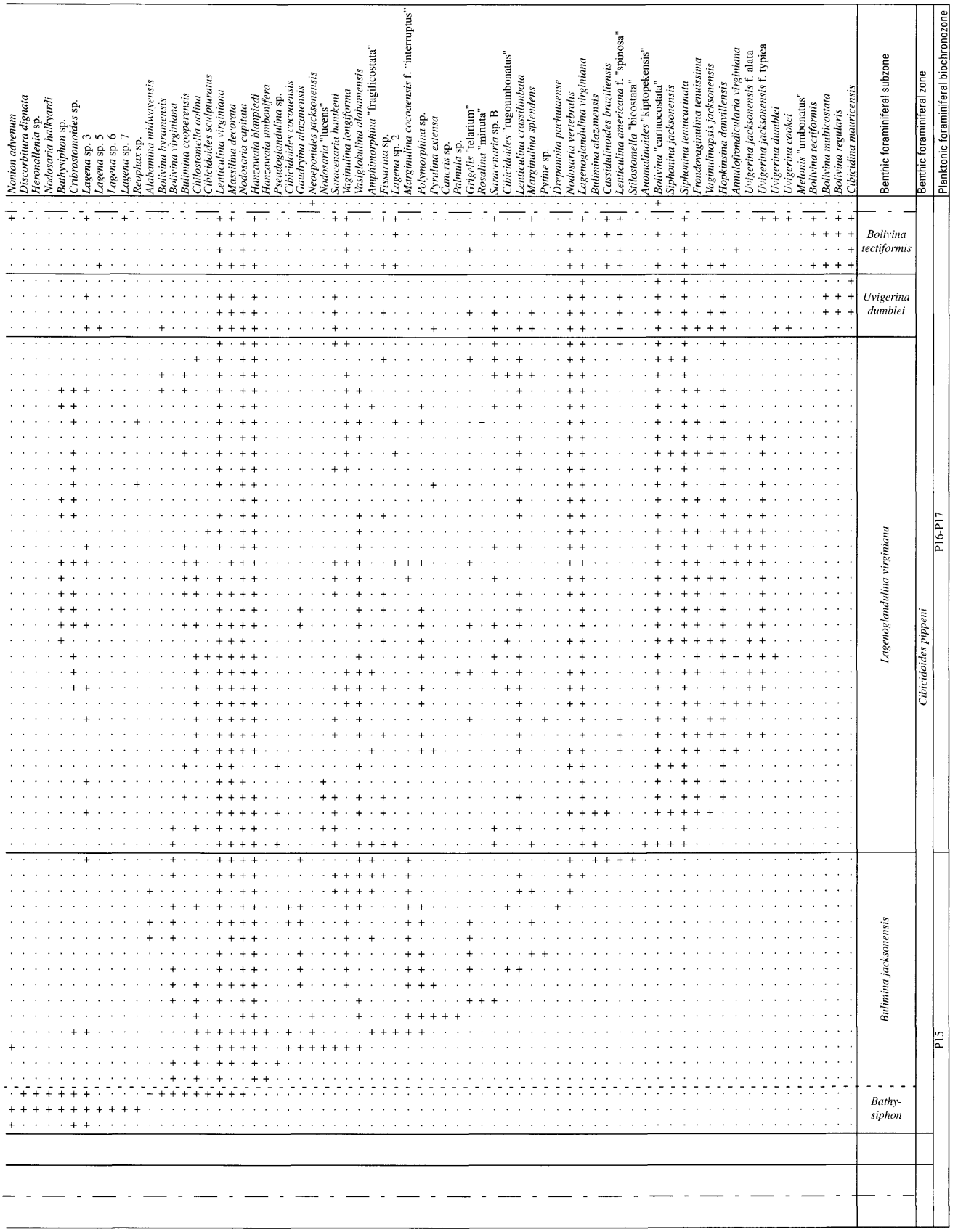

Figure F20. Continued.

Kiptopeke core

Zone	Subzone	Boundary depth (m)	Postimpact age	Approximate duration (k.y.)
		327.7	2.10 m.y.	
Cibicidoides pippeni	*Bolivina tectiformis*			134
		332.0	1.98 m.y.	
	Uvigerina dumblei			506
		348.2	1.47 m.y.	
	Lagenoglandulina virginiana			837
		360.8	596 k.y.	
	Bulimina jacksonensis			593
		370.3	426 k.y.	
	Bathysiphon			423
		394.0	3 k.y.	
Dead zone				<1–3
		394.2	0.0 y.	

USGS-NASA Langley core[1]

Zone	Subzone	Boundary depth (m)	Postimpact age	Approximate duration (k.y.)
		183.28	2.10 m.y.	
Cibicidoides pippeni	*Bolivina tectiformis*			69
		185.07	2.02 m.y.	
	Uvigerina dumblei			141
		188.73	1.88 m.y.	
	Lagenoglandulina virginiana			1,272
		221.80	604 k.y.	
	Bulimina jacksonensis			577
		235.19	27 k.y.	
	Bathysiphon			19
		235.65	8 k.y.	
Dead zone				<1–8
		235.84	0.0 y.	

[1]If the rate at the Langley core site was 24 m/m.y., then 1 m of sediment accumulated in 42 k.y. If the rate at the Langley core site was 26 m/m.y., then 1 m of sediment accumulated in 39 k.y.

Figure F21. Chart showing boundary depths, postimpact ages, and approximate durations of five benthic foraminiferal subzones recognized in the Chickahominy Formation at the Kiptopeke and USGS-NASA Langley core sites. The time scale for the Kiptopeke core was derived from magnetochronology, biochronology, and sediment accumulation rates recalculated from those shown in figure F5. The time scale for the USGS-NASA Langley core was derived from biochronology and sediment accumulation rates.

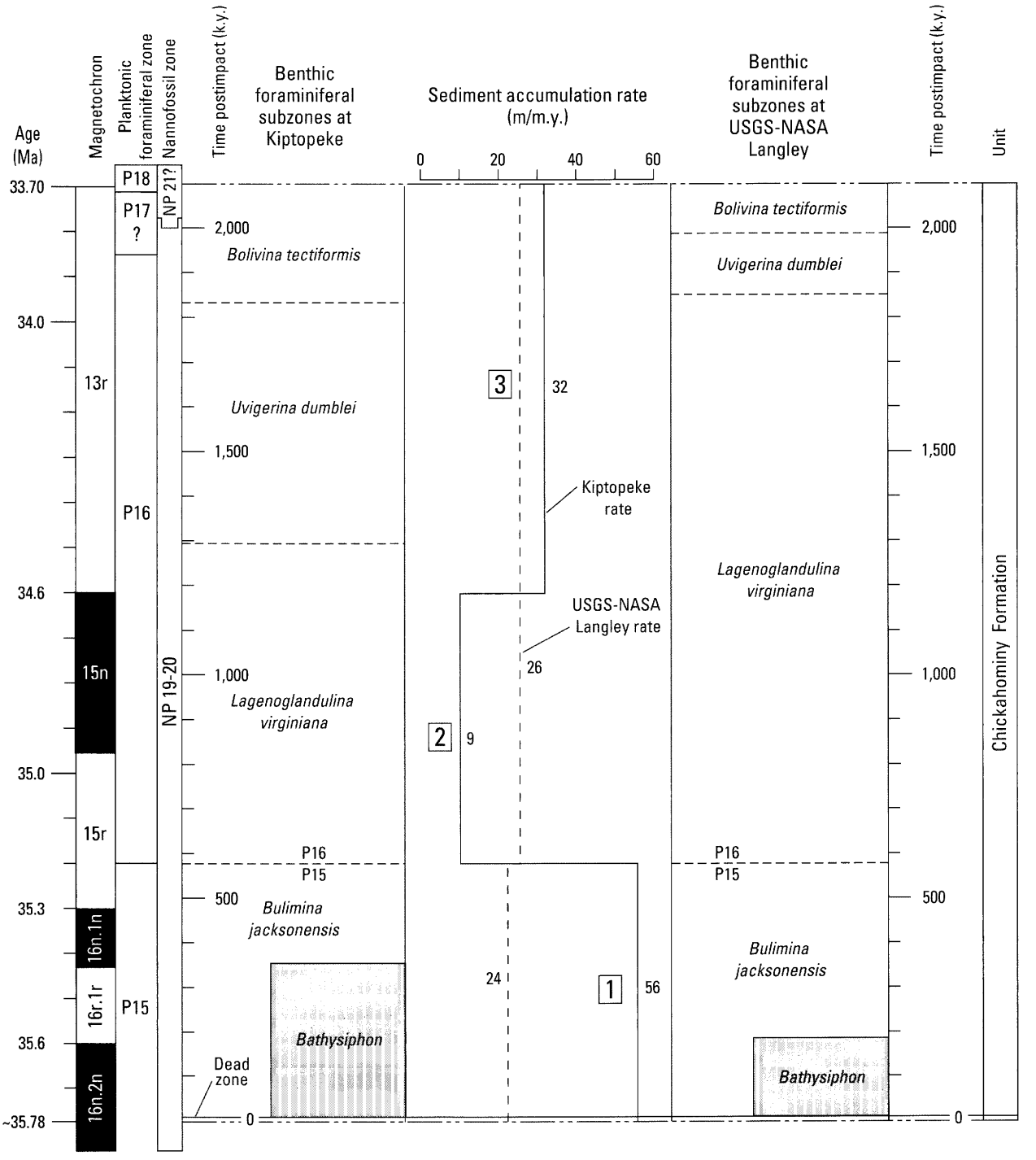

Figure F22. Chart showing geochronological correlation of benthic foraminiferal subzones and sediment accumulation rates for the Chickahominy Formation in the USGS-NASA Langley corehole compared with those in the Kiptopeke corehole (modified from Poag, Koeberl, and Reimold, 2004). Scale at right indicates time in thousands of years (k.y.) postimpact; see figure F5. Note that the top of the *Bulimina jacksonensis* Subzone (coincident with the planktonic foraminiferal P15-P16 biochronozone boundary) is the only benthic subzone boundary (other than the base and top of the Chickahominy section) that is isochronous between these two core sites. Numbers 1, 2, and 3 in squares indicate the three depositional episodes at Kiptopeke; the sediment accumulation rates for these episodes are revised from rates shown in figure F5 and reported by Poag, Koeberl, and Reimold (2004, table 13.1).

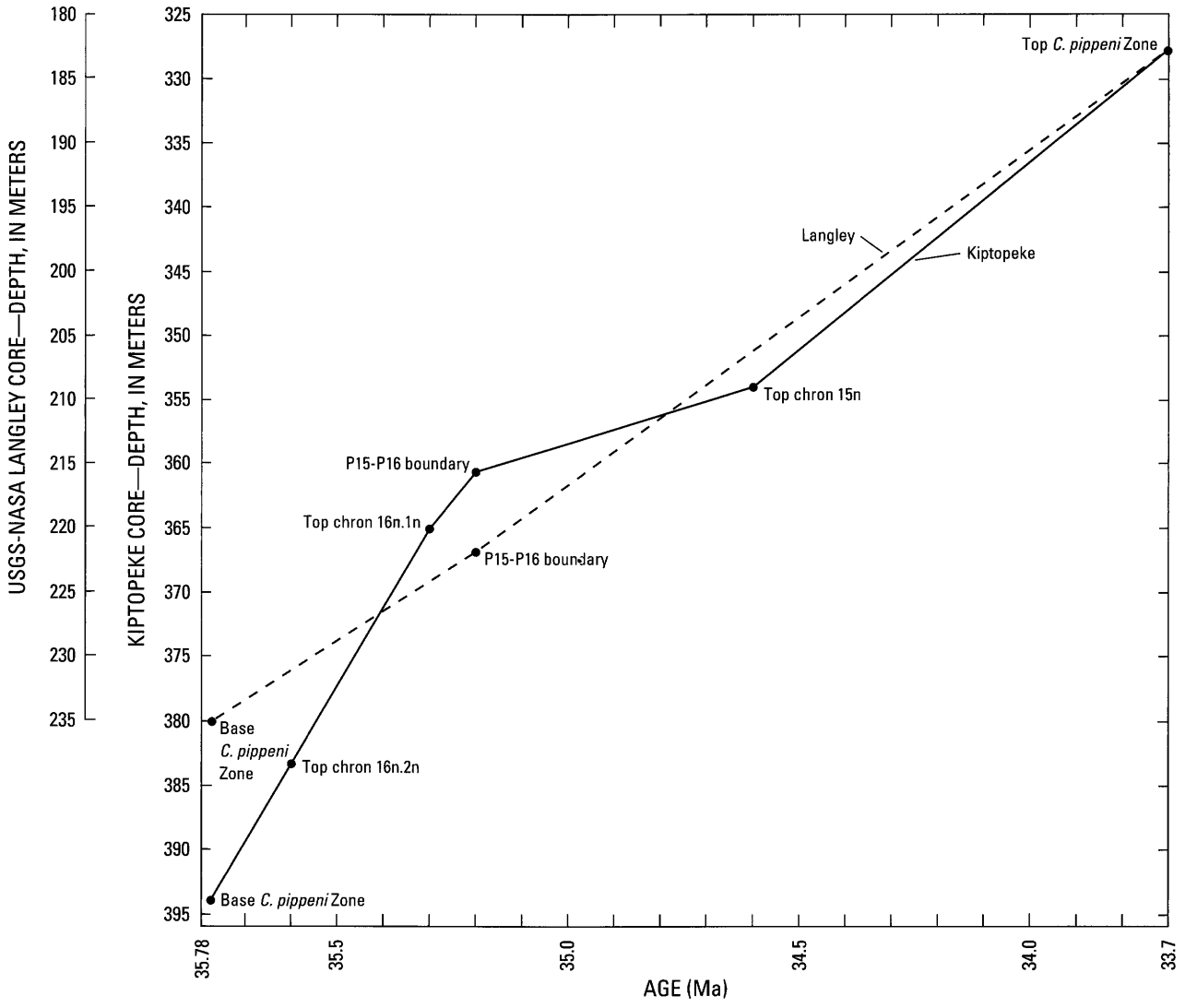

Figure F23. Graph showing depth-age models for the Chickahominy Formation in the Kiptopeke and USGS-NASA Langley cores. Kiptopeke data are from Poag, Koeberl, and Reimold (2004, p. 392, 393). The Langley model shows fewer control points because magnetochron boundaries in the Langley core have not been determined. The time scale is from figure F22.

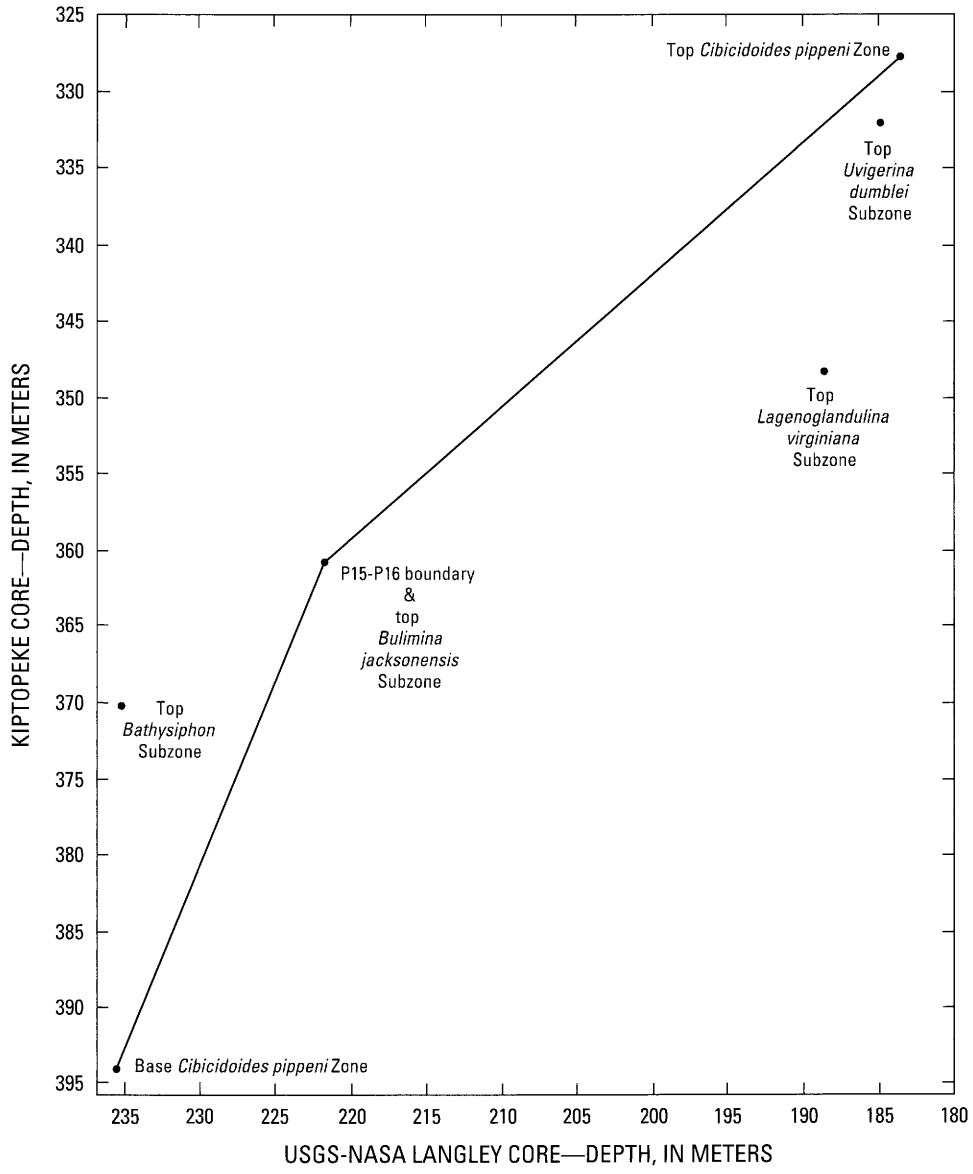

Figure F24. Graph showing correlation of three correlative stratigraphic boundaries in the Kiptopeke and USGS-NASA Langley cores. The bend in the line of correlation results from the marked shift in sediment accumulation rate at the P15-P16 boundary in the Kiptopeke core (see fig. F22). The top boundaries of the *Bathysiphon, Lagenoglandulina virginiana,* and *Uvigerina dumblei* Subzones plot well away from the line of correlation, which indicates that the subzone boundaries are not isochronous horizons between these two core sites.

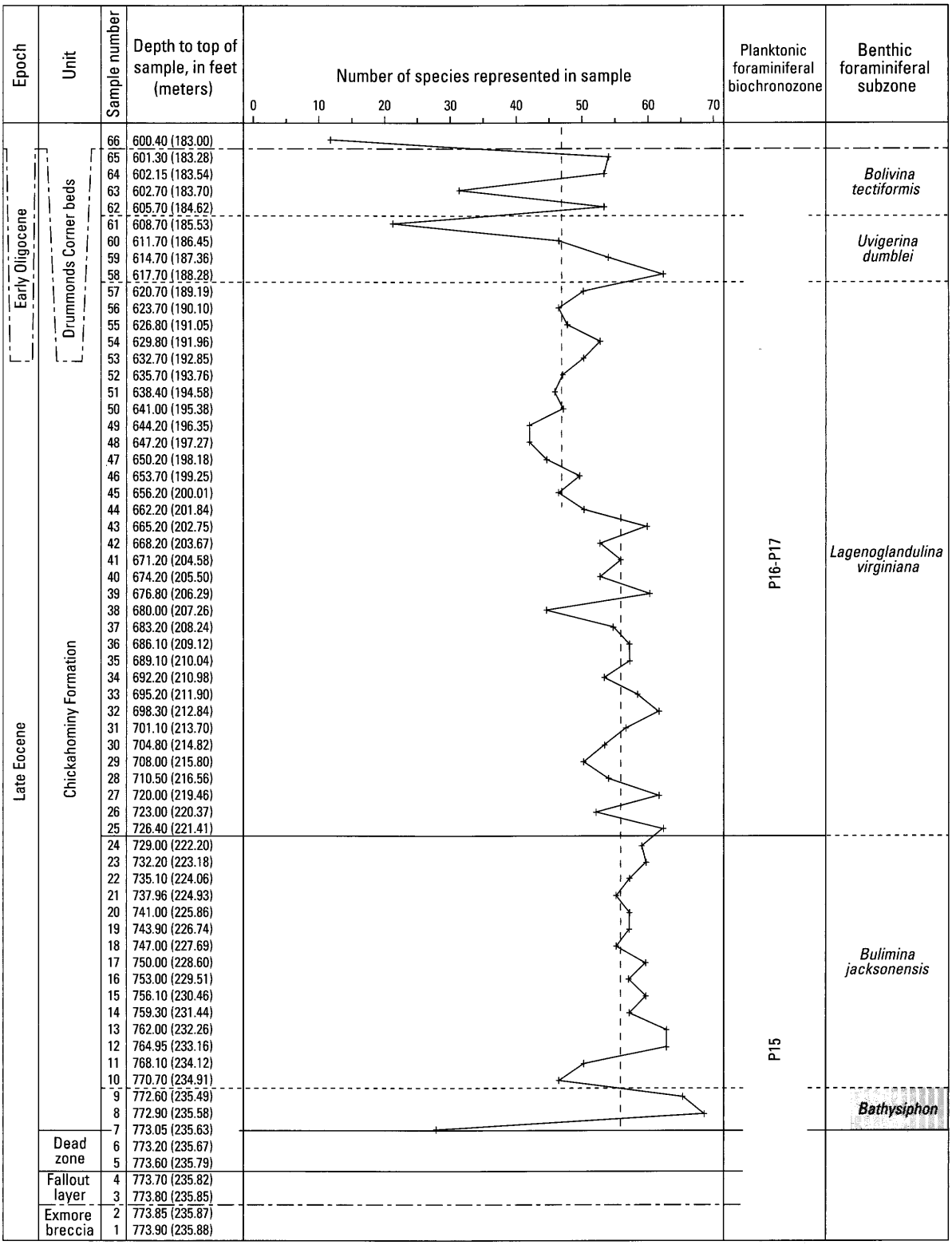

Figure F25. Graph showing species-richness curve (number of species represented in sample) for the Chickahominy Formation in the USGS-NASA Langley core. Occurrence data are from figure F20. P15-P16 is the planktonic foraminiferal biochronozone boundary approximated by the overlapping ranges of *Bolboforma latdorfensis* and *Bolboforma spinosa*. Note that the average species richness (indicated by dashed vertical lines) shifts to persistently lower values in samples higher than the middle of the *Lagenoglandulina virginiana* Subzone. Note also that the contact between the dead zone and the Chickahominy Formation is near the middle of sample 7, whose top is at 235.63 m (773.05 ft) depth.

highest values for species richness (65, 67) occur at the base of the section (fig. F25), where permeability is lowest (SP–1; fig. F18). The two highest values of species richness at the base of the section can be explained by the added presence of several species of agglutinated foraminifera that constitute the *Bathysiphon* Subzone.

Stable-Isotope Analyses

Poag (1997b) hypothesized that an impact-generated pulse of warm climate could be recognized in late Eocene marine and terrestrial records. Poag, Mankinen, and Norris (2003) supported that idea with stable-isotope ($\delta^{18}O$) analyses from the Chickahominy Formation at Kiptopeke. The Kiptopeke $\delta^{18}O$ record showed three pulses of relatively warm climate in the late Eocene, rather than a single long-lasting pulse (figs. F5, F26). The amplitude of the $\delta^{18}O$ variation is ~0.2‰–0.3‰ and suggests temperature variations of ~1°C or slightly more. The first pulse (W–1) was identified at the base of the Chickahominy and probably lasted 0–200 k.y. postimpact; a second pulse (W–2) was identified in the middle of the Chickahominy (350–600 k.y. postimpact), and a third (W–3), at the top of the Chickahominy (1,400–2,000 k.y. postimpact; figs. F5, F26). Poag, Mankinen, and Norris (2003) correlated these three pulses with a similar tripartite subdivision of the global record of late Eocene climate. Poag, Mankinen, and Norris (2003) interpreted the $\delta^{18}O$ record as an indication of impact-generated climatic warming maintained by a 2-m.y.-long late Eocene comet shower, which had previously been inferred from an unusual abundance of extraterrestrial ^{3}He within the Eocene-Oligocene boundary stratotype at Massignano, Italy (Farley and others, 1998).

The $\delta^{18}O$ record in the USGS-NASA Langley core is nearly identical to that of the Kiptopeke core (fig. F26) and shows the same three principal negative excursions identified by Poag, Mankinen, and Norris (2003). This similarity reinforces Poag's (1997b) hypothesis that a relatively warm late Eocene climate (see also Kobashi and others, 2001; Pearson and others, 2001) was initiated or reinforced by the Chesapeake Bay and Popigai (northern Siberia, Russia) impacts and was maintained during the following ~2 m.y. by a prolonged succession of impacts during the comet shower.

Poag, Mankinen, and Norris (2003) also analyzed the $\delta^{13}C$ record at Kiptopeke and found a small (single-point) negative excursion associated with the basal Chickahominy warm pulse and another, much larger and longer lasting negative excursion, nearly coincident with biochronozone P16-P17 (figs. F5, F26). We found an identical pair of negative excursions in the Chickahominy record in the USGS-NASA Langley core (fig. F26). The stratigraphically highest negative $\delta^{13}C$ excursion has been documented at several other sites around the globe and indicates a significant net decrease in global carbon burial. This negative $\delta^{13}C$ excursion also promises to provide good correlations in areas where other stratigraphic data may be weak or missing (Poag, Mankinen, and Norris, 2003). The positive extensive $\delta^{13}C$ excursion in the lower part of the Chickahominy Formation can be interpreted as a net exhumation of carbon (decrease in global carbon storage). The single-point negative $\delta^{13}C$ excursion at the base of the Chickahominy section at Langley matches that at Kiptopeke, giving support to its validity, but additional sampling in the basal section is needed for corroboration.

Paleoenvironmental Interpretations

Postimpact Microfaunal Recovery

Poag (2002) interpolated the maximum duration of the dead zone at the USGS-NASA Langley site to be <1–10 k.y. by extrapolating the sediment accumulation rate of 21 m/m.y. (68.9 ft/m.y.) in the lower part of the Langley core. We slightly reduced the maximum duration estimate to ~8 m.y. by using a sediment accumulation rate of 24 m/m.y. (78.7 ft/m.y.). Poag, Koeberl, and Reimold (2004) took only one sample in the dead zone at Kiptopeke and were not able to measure the thickness of the dead zone there because the core had been disrupted between the time it was drilled (1989) and the time it was sampled (1992).

Samples analyzed above the dead zone at Kiptopeke (Poag, Koeberl, and Reimold, 2004) show relatively slow repopulation of that site by the *Cibicidoides pippeni* assemblage (*Bulimina jacksonensis* subassemblage). The Kiptopeke *Bulimina jacksonensis* subassemblage did not reach preimpact species richness (as documented by Poag, Koeberl, and Reimold, 2004) until 3.4 m (11.1 ft) above the top of the dead zone (at 390.5 m; 1,281 ft), which is equivalent to ~36 k.y. postimpact, if one uses the basal Kiptopeke sediment accumulation rate of 67 m/m.y. (220 ft/m.y.) (Poag, Koeberl, and Reimold, 2004; see original and revised rates in figs. F5 and F22 of this chapter). In contrast, the *Cibicidoides pippeni* assemblage (*Bulimina jacksonensis* subassemblage) reoccupied the USGS-NASA Langley site immediately following deposition of the dead zone, appearing in the top third of sample 7 (235.63–235.65 m; 773.06–773.13 ft depth), which is the base of the Chickahominy Formation (figs. F7, F19, and F20; table F1). Though the precision of these rate calculations is low, the relative difference suggests that postimpact paleoenvironments normalized faster near the western rim of the crater (at Langley) than farther toward the crater center (inside the peak ring at Kiptopeke; fig. F1).

Paleobathymetry

The USGS-NASA Langley and Kiptopeke core sites occupied the middle part of a broad, gently sloping continental shelf before the impact (Poag, 1997b). After the impact, the two sites were inside the crater, a partly filled, subcircular excavation, whose upper surface formed a depression or closed basin in the sea floor. Presumably, the depression was somewhat deeper in the center than along the periphery, but the bathymetric differ-

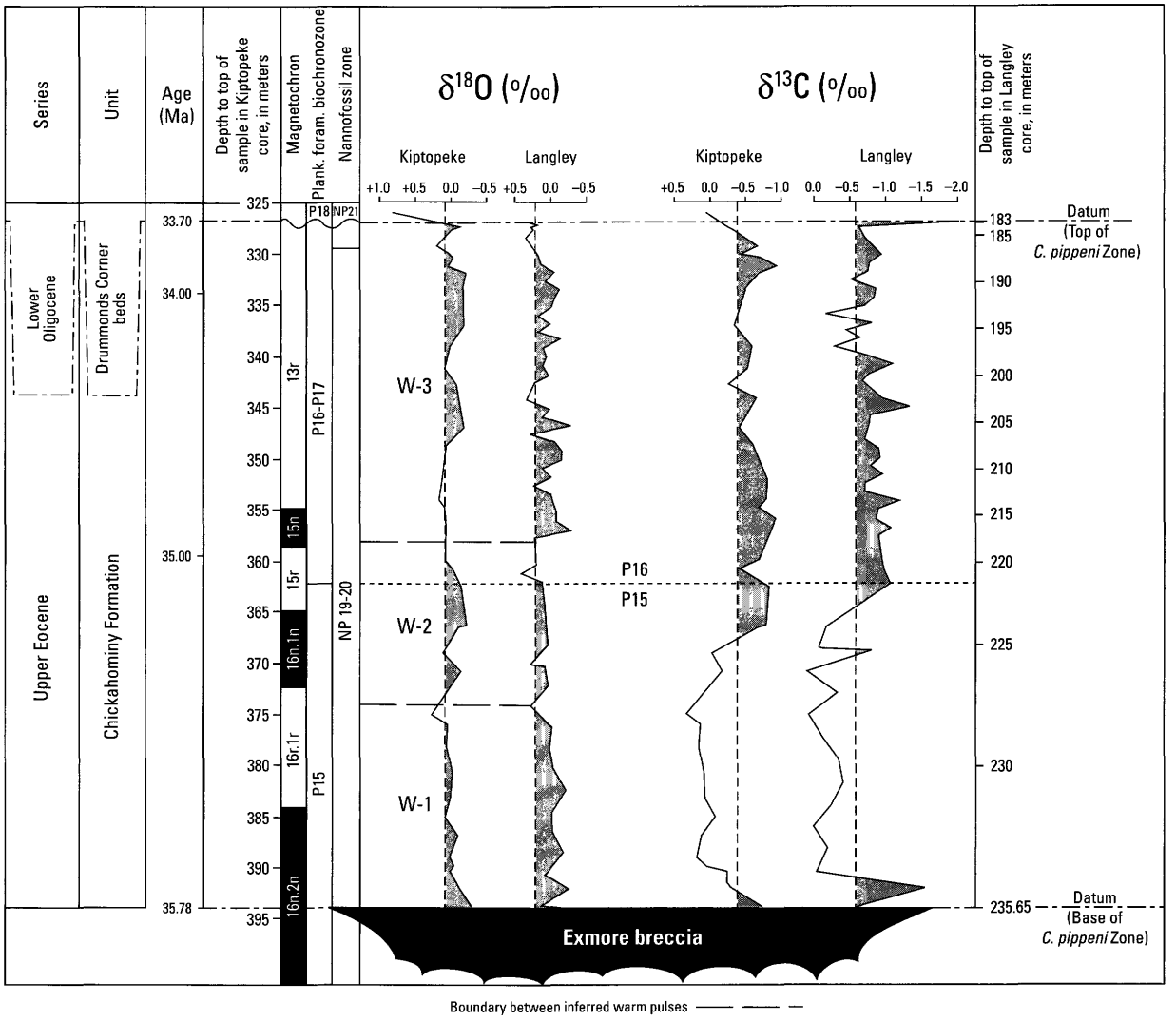

Figure F26. Diagram showing correlation of stable-isotope records from the Chickahominy Formation in the USGS-NASA Langley core with those in the Kiptopeke core. P15-P16 is the planktonic foraminiferal biochronozone boundary approximated by the overlapping ranges of *Bolboforma latdorfensis* and *Bolboforma spinosa*. W–1, W–2, and W–3 are warm pulses inferred from relatively negative $\delta^{18}O$ values. The lower part of the depth scale for the USGS-NASA Langley core and corresponding segments of isotope curves have been uniformly stretched because the part of the Chickahominy Formation below the P15-P16 boundary is much thicker at Kiptopeke than at Langley; the stretching enables the three isochronous correlation horizons (base and top of *Cibicidoides pippeni* Zone and P15-P16 biochronozone boundary) to be displayed as horizontal lines on this diagram. The vertical dashed lines and shading are provided to aid the reader in visualizing the grouping of positive and negative excursions of the isotope data.

ence, if any, is beyond the resolution of the current foraminiferal analysis.

Nearly all the Chickahominy species at Kiptopeke and Langley have modern counterparts; in fact, some are still extant (Poag, Koeberl, and Reimold, 2004). Most of these modern species are abundant (individually and in similar species associations) in outer neritic to upper bathyal marine biotopes, and the fossil counterparts indicate paleodepths of 150–500 m (~500–~1,600 ft) (table F9; Charletta, 1980; Poag, 1981; Van Morkhoven, Berggren, and Edwards, 1986). Many of the Chickahominy species at Kiptopeke and Langley (such as *Bulimina jacksonensis*, *Siphonina tenuicarinata*, *Hoeglundina elegans*, *Turrilina robertsi*, *Bolivina byramensis*, *Grigelis* spp., *Stilostomella* spp.) also occur in other widely distributed Paleogene outer neritic-bathyal deposits (Beckmann, 1954; Tjalsma and Lohmann, 1983; Van Morkhoven, Berggren, and Edwards, 1986). From these data, Poag, Koeberl, and Reimold (2004) estimated that the paleodepth at Kiptopeke was ~300 m (~1,000 ft) during deposition of the Chickahominy Formation. We infer that the paleodepth was essentially identical at Langley.

Benthic Habitats

Most of the predominant genera and species in the Chickahominy benthic foraminiferal assemblages from the Langley and Kiptopeke cores have modern counterparts that are notable for opportunistic life strategies and tolerance of (or preference for) oxygen-depleted (disoxic, microxic, anoxic) muds rich in organic detritus (Poag, Koeberl, and Reimold, 2004). Among the best documented of these modern taxa are the calcareous genera that predominate in the *Cibicidoides pippeni* assemblage: *Epistominella*, *Bolivina*, *Bulimina*, *Globobulimina*, *Uvigerina*, and *Buliminella* (modern counterpart of *Caucasina*) (Phleger and Soutar, 1973; Douglas and Heitman, 1979; Mackensen and Douglas, 1989; Jorissen and others, 1992; Kaminski and others, 1995; Sen Gupta and others, 1996; Bernhard and Sen Gupta, 1999; Loubere and Fariduddin, 1999; table F9; pls. F1, F2). Most of the members of the Chickahominy *Bathysiphon* Subassemblage also are typical inhabitants of oxygen-depleted, nutrient-rich substrates (Gooday, 1994; Kaminski and others, 1995).

Nutrient Supply

There is considerable evidence from the modern oceans that the geographic distribution, test size, and abundance (absolute and relative) of certain benthic foraminiferal species and genera are strongly correlative with the flux of organic detritus to the sea floor (Caralp, 1989; Corliss and Fois, 1990; Corliss and Silva, 1993; Pfannkuche, 1993; Linke and others, 1995; Gooday, 1996). This correlation exists because outer neritic, bathyal, and abyssal benthic foraminifera are dependent upon the flux of labile organic carbon for their food source (Gooday, 1994; Loubere and Fariduddin, 1999).

Most of the predominant Chickahominy calcareous genera (and those of the *Bathysiphon* subassemblage) at the Langley and Kiptopeke core sites have modern counterparts that are most abundant, and often have largest test sizes, in organic-matter-rich muds, which commonly also are oxygen depleted (Poag, Koeberl, and Reimold, 2004). The Chickahominy assemblages also are notable for unusually large test sizes, especially among the lenticulinids, nodosariids, and stilostomellids.

Of special note in the Chickahominy assemblages is an association of small, smooth, thin-walled, hyaline, opportunistic genera, such as *Epistominella*, which in modern oceans live epifaunally within aggregates of phytodetritus (a gelatinous matrix containing the remains of phytoplankton and zooplankton) on the sea floor (Gooday, 1993, 1994). These species have opportunistic feeding strategies and grow explosively into large concentrations during peak development of phytodetritus. Among the predominant Chickahominy taxa, species of *Epistominella* and *Caucasina* are probably representative of this lifestyle (pl. F2, figs. 1, 6).

Paleoenvironmental Summary

Overall, the Chickahominy benthic foraminiferal associations documented in the USGS-NASA Langley corehole represent consistently diverse, species-rich communities living within the upper 10 cm (4 in.) of fine-grained substrates, in paleodepths of ~300 m (~1,000 ft), generally typified by high flux rates of organic carbon and by oxygen deficiency. The development of five successive subassemblages, however, points to marked temporal changes in environmental properties other than paleodepth. The principal variable properties that we have considered are sediment delivery rates, permeability (volume of sand-sized particles), glauconite content, marked to subtle changes in substrate chemistry and nutrient flux, and broad-scale shifts in climate indicated by $\delta^{18}O$ variations and in the local and global carbon budget indicated by $\delta^{13}C$ variations. However, coincident temporal changes in the measured or calculated values of these properties do not necessarily establish a one-to-one cause-and-effect relationship.

For example (indicated by stars in fig. F27), a change in the composition of benthic foraminiferal assemblages at the boundary between the *Bulimina jacksonensis* and *Lagenoglandulina virginiana* Subzones coincides (or nearly coincides) with shifts in several properties, including a minor increase in rate of sediment accumulation, a brief positive excursion in $\delta^{18}O$, a sustained negative excursion in $\delta^{13}C$ (increased burial of carbon), a significant positive deflection in the SP curve (peak in permeability), and a negative deflection in the GR curve (reduction in glauconite content). A major paleoceanographic change also took place at that level, as indicated by the changes in planktonic foraminifera and bolboformid assemblages.

Similar correlations at this horizon apply to the Kiptopeke corehole (fig. F27), though the depositional lithofacies there (indicated by differences in geophysical logs) were quite different from those at Langley, and some of the log-derived lithic

Table F9. Benthic foraminiferal species used for interpretation of Chickahominy paleoenvironments at the USGS-NASA Langley and Kiptopeke core sites.

[Core sites are shown in figure F1. Species names in quotation marks are provisory. Abbreviations in the microhabitat column for infaunal depths: s=shallow (depth below sediment-water interface of 0–2 cm; 0–0.8 in.), i=intermediate (depth of 2–4 cm; 0.8–1.6 in.), d=deep (depth of 4–10 cm; 1.6–3.9 in.). Table from Poag, Koeberl, and Reimold (2004, table 13.9)]

Species	Test construction	Microhabitat	Oxygen/ nutrient tolerance	Preferred paleodepth	Opportunist
Ammobaculites sp.	agglutinated	infaunal	low/high	outer neritic-upper bathyal	
Amphimorphina "fragilicostata"	calcite	infaunal	low/high	outer neritic-upper bathyal	
Amphimorphina "planata"	calcite	infaunal	low/high	outer neritic-upper bathyal	
Bathysiphon sp.	agglutinated	epifaunal	low/high	bathyal-abyssal	
Bolivina byramensis	calcite	s infaunal	low/high	outer neritic-upper bathyal	
Bolivina gardnerae	calcite	s infaunal	low/high	outer neritic-upper bathyal	yes
Bolivina gracilis	calcite	i-d infaunal	low/high	outer neritic-upper bathyal	
Bolivina jacksonensis	calcite	i-d infaunal	low/high	outer neritic-upper bathyal	yes
Bolivina multicostata	calcite	s infaunal	low/high	outer neritic-upper bathyal	
Bolivina plicatella	calcite	s infaunal	low/high	outer neritic-upper bathyal	
Bolivina "postvirginiana"	calcite	s infaunal	low/high	outer neritic-upper bathyal	yes
Bolivina "praevirginiana"	calcite	s infaunal	low/high	outer neritic-upper bathyal	
Bolivina regularis	calcite	i-d infaunal	low/high	outer neritic-upper bathyal	
Bolivina striatella	calcite	s infaunal	low/high	outer neritic-upper bathyal	
Bolivina tectiformis	calcite	s infaunal	low/high	outer neritic-upper bathyal	
Bolivina virginiana	calcite	s infaunal	low/high	outer neritic-upper bathyal	yes
Bulimina alazanensis	calcite	i-d infaunal	low/high	outer neritic-upper bathyal	
Bulimina cooperensis	calcite	i-d infaunal	low/high	outer neritic-upper bathyal	
Bulimina jacksonensis	calcite	i-d infaunal	low/high	outer neritic-upper bathyal	yes
Caucasina marylandica	calcite	phytodetrital	low/high	outer neritic-upper bathyal	yes
Charltonina madrugaensis	calcite	d infaunal	low/high	outer neritic-upper bathyal	yes
Cibicidoides pippeni	calcite	epifaunal	high/low	outer neritic-upper bathyal	
Cribrostomoides sp.	agglutinated	s infaunal	low/high	outer neritic-upper bathyal	
Cyclammina cancellata	agglutinated	s infaunal	low/high	outer neritic-upper bathyal	
Dorothia sp.	agglutinated	d infaunal	low/high	outer neritic-upper bathyal	
Epistominella minuta	calcite	epifaunal	low/high	outer neritic-upper bathyal	yes
Gaudryina alazanensis	agglutinated	d infaunal	low/high	outer neritic-upper bathyal	
Globobulimina ovata	aragonite?	i-d infaunal	low/high	outer neritic-upper bathyal	
Globocassidulina subglobosa	calcite	phytodetrital	low/high	outer neritic-upper bathyal	
Grigelis annulospinosa	calcite	infaunal	low/high	outer neritic-upper bathyal	
Grigelis cookei	calcite	infaunal	low/high	outer neritic-upper bathyal	
Grigelis "curvicostata"	calcite	infaunal	low/high	outer neritic-upper bathyal	
Grigelis "elongata"	calcite	infaunal	low/high	outer neritic-upper bathyal	
Grigelis "elongostriata"	calcite	infaunal	low/high	outer neritic-upper bathyal	
Grigelis "gigas"	calcite	infaunal	low/high	outer neritic-upper bathyal	
Grigelis "tubulosa"	calcite	infaunal	low/high	outer neritic-upper bathyal	
Grigelis "tumerosa"	calcite	infaunal	low/high	outer neritic-upper bathyal	
Gyroidinoides aequilateralis	calcite	s infaunal	low/high	outer neritic-upper bathyal	
Gyroidinoides byramensis	calcite	s infaunal	low/high	outer neritic-upper bathyal	
Gyroidinoides octocameratus	calcite	s infaunal	low/high	outer neritic-upper bathyal	
Gyroidinoides planatus	calcite	s infaunal	low/high	outer neritic-upper bathyal	
Hoeglundina elegans	aragonite	epifaunal	low/high	outer neritic-upper bathyal	
Marginulina cocoaensis	calcite	infaunal	low/high	outer neritic-upper bathyal	
Marginulina karreriana	calcite	infaunal	?/?	outer neritic-upper bathyal	

Table F9. Benthic foraminiferal species used for interpretation of Chickahominy paleoenvironments at the USGS-NASA Langley and Kiptopeke core sites.—Continued

Species	Test construction	Microhabitat	Oxygen/ nutrient tolerance	Preferred paleodepth	Opportunist
Melonis planatus	calcite	i-d infaunal	low/high	outer neritic-upper bathyal	
Nodosaria capitata	calcite	infaunal	low/high	outer neritic-upper bathyal	
Nodosaria pustulosa	calcite	infaunal	low/high	outer neritic-upper bathyal	
Nodosaria saggitula	calcite	infaunal	low/high	outer neritic-upper bathyal	
Nodosaria soluta	calcite	infaunal	low/high	outer neritic-upper bathyal	
Nodosaria vertebralis	calcite	infaunal	low/high	outer neritic-upper bathyal	
Oridorsalis umbonatus	calcite	epifaunal	low/high	outer neritic-upper bathyal	
Reophax sp.	agglutinated	i-d infaunal	low/high	inner neritic-upper bathyal	
Spiroplectinella mississippiensis	agglutinated	d infaunal	low-high	outer neritic-upper bathyal	
Stilostomella "aduncocostata"	calcite	infaunal	low/high	outer neritic-upper bathyal	
Stilostomella annulospinosa	calcite	infaunal	low/high	outer neritic-upper bathyal	
Stilostomella "bicostata"	calcite	infaunal	low/high	outer neritic-upper bathyal	
Stilostomella cocoaensis	calcite	infaunal	low/high	outer neritic-upper bathyal	
Stilostomella "exilispinata"	calcite	infaunal	low/high	outer neritic-upper bathyal	
Stilostomella "juvenocostata"	calcite	infaunal	low/high	outer neritic-upper bathyal	
Stilostomella "multispiculata"	calcite	infaunal	low/high	outer neritic-upper bathyal	
Technitella sp.	agglutinated	infaunal	low/high	outer neritic-upper bathyal	
Turrilina robertsi	calcite	infaunal	low/high	outer neritic-upper bathyal	
Uvigerina cookei	calcite	s infaunal	low/high	outer neritic-upper bathyal	
Uvigerina dumblei	calcite	s infaunal	low/high	outer neritic-upper bathyal	
Uvigerina gardnerae	calcite	s infaunal	low/high	outer neritic-upper bathyal	yes
Uvigerina jacksonensis	calcite	s infaunal	low/high	outer neritic-upper bathyal	
Uvigerina spinicostata	calcite	s infaunal	low/high	outer neritic-upper bathyal	

boundaries and benthic foraminiferal subzonal boundaries are shown to be diachronous. For example, application of the depth-age model indicates that subunits SP–2 and SP–3 at Kiptopeke are equivalent geochronologically to SP–2 at Langley. This correlation implies further that SP–4 and SP–5 at Kiptopeke are equivalent to SP–3 and SP–4, respectively, at Langley. Likewise, the depth-age model indicates that log subunits GR–A and GR–B at Kiptopeke are equivalent to GR–A at Langley, requiring consequent reassignment of GR–C (now GR–B) and the combination of GR–D and GR–E (now GR–C) at Kiptopeke.

On the other hand, however, significant shifts in some of these same physico-chemical properties take place near the middle of the *Lagenoglandulina virginiana* Subzone (indicated by filled triangles in fig. F27) without a corresponding change in the benthic foraminiferal populations (other than an upward shift in average species diversity).

Summary and Conclusions

The transition from synimpact to postimpact deposition at the USGS-NASA Langley core site began with an airfall of shock-melted glass microspherules, which collected as a fallout layer, 3 cm (1.2 in.) thick, in tranquil conditions on the floor of the 300-m-deep (~1,000-ft-deep) crater basin. Marine deposition resumed at the site, but hostile bottom conditions prevented a normal marine benthic community from migrating into the crater. Instead, a succession of submillimeter-scale clay, silt, and sand laminae accumulated, in which the sand laminae contained reworked specimens of microfossils (mainly foraminifera and ostracodes). The reworked specimens apparently were derived from the apron of Exmore breccia that surrounded the crater rim. The hostile conditions lasted no more than ~8 k.y. (the duration could have been less than 1 k.y.) and were replaced by fertile, clay-dominated marine lithotopes that supported a rich assemblage of benthic microbiota whose fossils are found in cores of the Chickahominy Formation.

Upon visual examination, the Chickahominy Formation in the USGS-NASA Langley core appears to be a uniform, massive marine clay unit that is 52.37 m (171.8 ft) thick. Likewise, acoustic impedance properties of the Chickahominy yield a generally uniform signature on seismic-reflection profiles. This seismic signature enables us to easily trace the Chickahominy over the entire impact crater, to determine the structural geometry of its upper surface, and to extrapolate its stratigraphic thickness in areas where no cores are available.

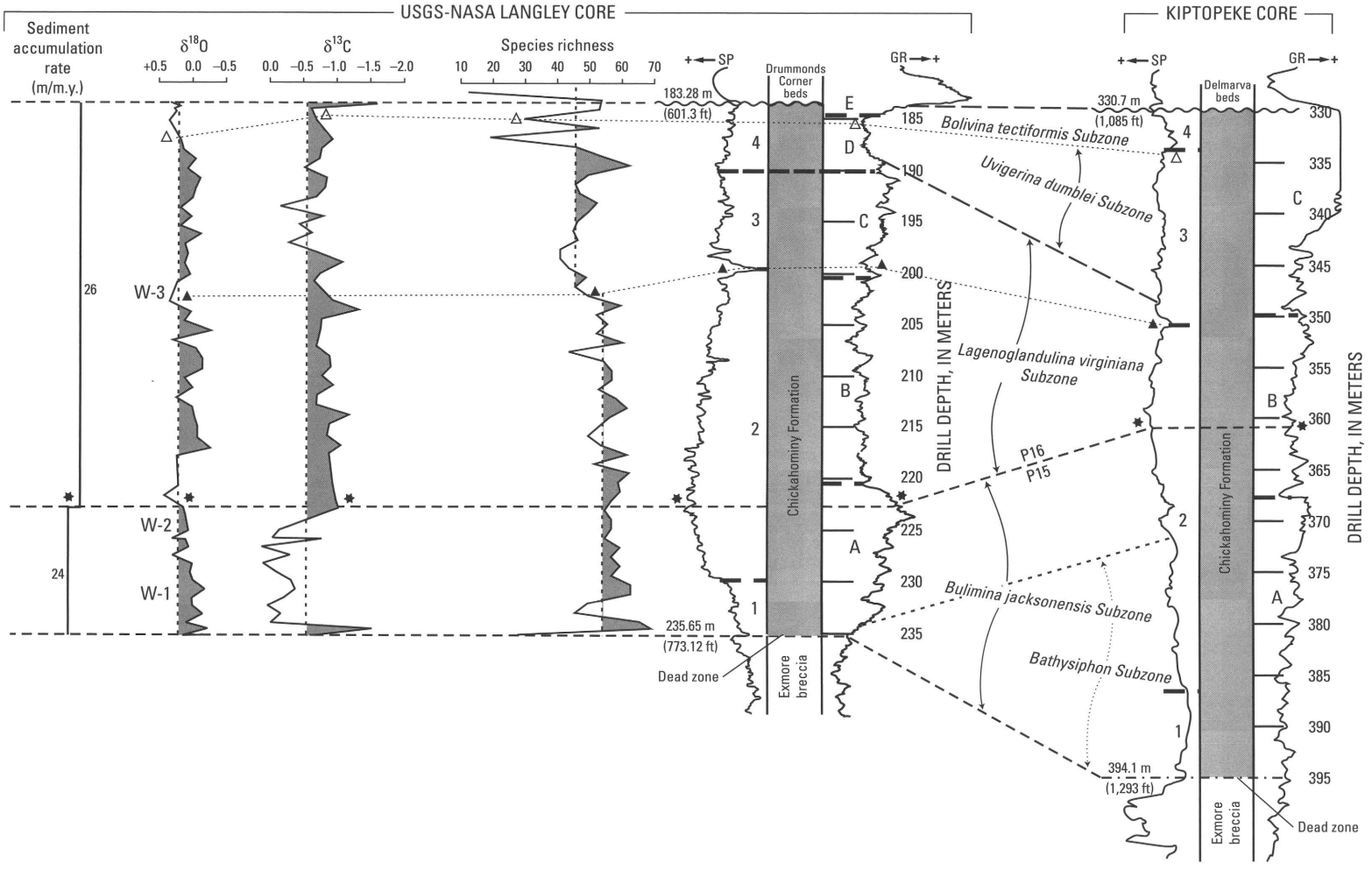

Figure F27. Chart showing correlations of principal properties of the Chickahominy Formation studied in the USGS-NASA Langley corehole with geophysical logs and benthic foraminiferal stratigraphy from the Kiptopeke corehole. The best (closest to isochronous) correlations (indicated by stars) are among the upward increase in sediment accumulation rate, the positive excursion in $\delta^{18}O$, the negative excursion in $\delta^{13}C$, the maximum positive deflection in the spontaneous-potential (SP) curve (peak in permeability), and the maximum positive deflection in the gamma-ray (GR) curve (peak in glauconite content) at Langley and the top of the *Bulimina jacksonensis* Subzone (coincident with the P15-P16 boundary) at Langley and Kiptopeke. A secondary (approximate) correlation (indicated by filled triangles) exists among the upward species-richness decrease, the major negative deflection of the SP curve (permeability decrease), and the moderate positive shift in the GR curve (glauconite increase) near the middle of the *Lagenoglandulina virginiana* Subzone at Langley and the boundary between subunits SP–2 and SP–3 at Kiptopeke. Another possible secondary correlation (indicated by open triangles) exists at the top of the Chickahominy section among the positive $\delta^{18}O$ deflection, the negative $\delta^{13}C$ deflection, the increase in stratigraphic variability of species richness, and the negative deflection in the GR curve (glauconite decrease) at Langley and the top of the *Uvigerina dumblei* Subzone at both Langley and Kiptopeke.

The Chickahominy can be stratigraphically subdivided rather easily, however, on the basis of downhole geophysical logs and foraminifera (both planktonic and benthic). The spontaneous-potential (SP) log curve allows a fourfold subdivision, whereas the gamma-ray (GR) log curve defines a fivefold subdivision. These subdivisions can be also recognized in the North, Bayside, and Kiptopeke coreholes, but not all subunit boundaries can be considered coeval at the different core sites. In the middle of the formation, the SP and GR unit boundaries are closely correlative from corehole to corehole, but lithic boundary correlations are poor at the top and base of the Chickahominy. On the basis of these log characteristics, the Chickahominy in the USGS-NASA Langley corehole is anomalous with regard to the unit in the other three intracrater coreholes, mainly because of the unusually great permeability and thickness of subunit SP–2 and the significantly greater glauconite volume in subunit GR–A. Another anomaly in the USGS-NASA Langley corehole is the fact that the basal part of the Chickahominy is significantly more permeable than the top part of the underlying Exmore breccia, whereas, the opposite relationship characterizes the transition in the other three coreholes.

The planktonic foraminiferal record at the USGS-NASA Langley site yields no clear subdivision of the Chickahominy. Elements of Zones P15, P16, and P17 are present but not in enough abundance or stratigraphic persistence to identify their mutual boundary. We, therefore, identified the approximate P15-P16 biochronozonal boundary by proxy, by using the short overlap interval between the highest occurrence of *Bolboforma spinosa* and the lowest occurrence of *Bolboforma latdorfensis*.

A suite of 126 benthic foraminiferal species in the Chickahominy Formation in the Langley core represents a single, easily recognizable biozone (*Cibicidoides pippeni* Zone), which embraces five distinct subbiozones (from base to top, the *Bathysiphon, Bulimina jacksonensis, Lagenoglandulina virginiana, Uvigerina dumblei,* and *Bolivina tectiformis* Subzones). Both planktonic and benthic zonations correlate well with equivalent zonations in the Kiptopeke core, but only one of the benthic boundaries (top of the *Bulimina jacksonensis* Subzone) appears to be isochronous.

The dominant benthic foraminiferal assemblages in the Chickahominy Formation at Langley contain both calcareous and agglutinated species, whose modern counterparts and ancient equivalents have been studied in many other localities. The key paleoenvironmental indicators point to epifaunal and shallow infaunal microhabitats characterized by oxygen deprivation and high flux rates of organic matter to the sea floor. At the USGS-NASA Langley site, the *Cibicidoides pippeni* assemblage reoccupied the crater floor a relatively short time (<1 to 8 k.y.) after tumultuous deposition of the Exmore breccia had abated.

Stable-isotope records derived from the benthic foraminifer *Cibicidoides pippeni* show three negative excursions in $\delta^{18}O$ (interpreted as pulses of warm paleoclimate) and two negative excursions in $\delta^{13}C$ (interpreted as variations in the global burial of carbon). This stable-isotope record matches that previously documented at Kiptopeke and supports the hypothesis of Poag (1997b) that the Chesapeake Bay and Popigai (Russia) bolide impacts significantly influenced the long-term atmospheric dynamics of the late Eocene-early Oligocene time interval and may have helped trigger a globally recognized mass extinction event in the early Oligocene.

Acknowledgments

U.S. Geological Survey (USGS) investigations of the Chesapeake Bay impact structure are conducted in cooperation with the Hampton Roads Planning District Commission, the Virginia Department of Environmental Quality, and the National Aeronautics and Space Administration (NASA) Langley Research Center. The Hampton Roads Planning District Commission and the USGS provided funds for the drilling of the USGS-NASA Langley corehole. The NASA Langley Research Center provided extensive operational and logistical support for the drilling operation. The Virginia Department of Environmental Quality and the Department of Geology of the College of William and Mary provided extensive operational support at the drill site.

We thank the other members of the Chesapeake coring team for acquiring and sampling the USGS-NASA Langley core, Stephen E. Curtin (USGS) and Richard E. Hodges (USGS) for providing the geophysical logs of the Langley, North, and Bayside coreholes, Texaco, Inc., for providing multichannel seismic-reflection profiles, Judith Commeau (USGS) and Louie Kerr (Marine Biological Laboratory) for providing scanning-electron microscopy, and Emily Denham (USGS) for preparing the samples for analysis. We are indebted to the National Geographic Society for funding the collection of single-channel seismic profiles, to the Woods Hole Oceanographic Institution for use of its mass spectrometer, and to the Marine Biological Laboratory (Woods Hole, Mass.) for use of its scanning-electron-microscope facilities. Lucy E. Edwards, Harry J. Dowsett, J. Wright Horton, Jr., David S. Powars, and Gregory S. Gohn, all of the USGS, reviewed early versions of the manuscript of this chapter.

References Cited

Bandy, O.L., 1949, Eocene and Oligocene foraminifera from Little Stave Creek, Clarke County, Alabama: Bulletins of American Paleontology, v. 32, no. 131, 210 p.

Beckmann, J.P., 1954, Die Foraminferen der Oceanic Formation (Eocaen-Oligocaen) von Barbados, Kl. Antillen: Eclogae Geologicae Helvetiae, v. 46, no. 2, p. 301–412, 15 pls. (In German with English summary.)

Berggren, W.A., Kent, D.V., Swisher, C.C., III, and Aubry, M.P., 1995, A revised Cenozoic geochronology and chronostratigraphy, *in* Berggren, W.A., Kent., D.V., Aubry, M.-P., and Hardenbol, Jan, eds., Geochronology, time scales, and global stratigraphic correlation: SEPM (Society for Sedimentary Geology) Special Publication 54, p. 129–212.

Berggren, W.A., and Miller, K.G., 1988, Paleogene tropical planktonic foraminiferal biostratigraphy and magnetobiochronology: Micropaleontology, v. 34, no. 4, p. 362–380.

Bernhard, J.M., and Sen Gupta, B.K., 1999, Foraminifera of oxygen-depleted environments, *in* Sen Gupta, B.K., ed., Modern foraminifera: Boston, Kluwer Academic Publishers, p. 201–216.

Brown, P.M., Miller, J.A., and Swain, F.M., 1972, Structural and stratigraphic framework and spatial distribution of permeability of the Atlantic Coastal Plain, North Carolina to New York: U.S. Geological Survey Professional Paper 796, 79 p.

Bukry, David, 1973, Low-latitude coccolith biostratigraphic zonation, *in* Edgar, N.T., and others, Initial reports of the Deep Sea Drilling Project, v. 15: Washington. D.C., U.S. Government Printing Office, p. 685–703.

Bukry, David, 1975, Coccolith and silicoflagellate biostratigraphy, northwestern Pacific Ocean, Deep Sea Drilling Project, Leg 32, *in* Initial reports of the Deep Sea Drilling Project, v. 32: College Station, Tex., Texas A&M University, Ocean Drilling Program, p. 677–701.

Caralp, M.H., 1989, Abundance of *Bulimina exilis* and *Melonis barleeanum*; Relationship to the quality of marine organic matter: Geo-Marine Letters, v. 9, no. 1, p. 37–43.

Charletta, A.C., 1980, Eocene benthic foraminiferal paleoecology and paleobathymetry of the New Jersey continental margin: New Brunswick, N.J., Rutgers, the State University of New Jersey, Ph.D. thesis, 82 p.

Corliss, B.H., and Fois, Elisabetta, 1990, Morphotype analysis of deep-sea benthic foraminifera from the northwest Gulf of Mexico: Palaios, v. 5, no. 6, p. 589–605.

Corliss, Bruce, and Silva, K.A., 1993, Rapid growth of deep-sea benthic foraminifera: Geology, v. 21, no. 11, p. 991–994.

Cushman, J.A., 1925, Eocene foraminifera from the Cocoa Sand of Alabama: Contributions from the Cushman Laboratory for Foraminiferal Research, v. 1, p. 65–70.

Cushman, J.A., 1926, Some fossil Bolivinas from Mexico: Contributions from the Cushman Laboratory for Foraminiferal Research, v. 1, p. 81–84.

Cushman, J.A., 1933, New foraminifera from the Upper Jackson Eocene of the southeastern coastal plain of the United States: Contributions from the Cushman Laboratory for Foraminiferal Research, v. 9, p. 1–21.

Cushman, J.A., 1935, Upper Eocene foraminifera of the southeastern United States: U.S. Geological Survey Professional Paper 181, 88 p.

Cushman, J.A., and Applin, E.R., 1926, Texas Jackson foraminifera: American Association of Petroleum Geologists Bulletin, v. 10, no. 2, p. 154–189, 6 pls.

Cushman, J.A., and Bermúdez, P.T., 1948, Some Paleocene foraminifera from the Madruga Formation of Cuba: Contributions from the Cushman Laboratory for Foraminiferal Research, v. 24, p. 68–75.

Cushman, J.A., and Cederstrom, D.J., 1945, An upper Eocene foraminiferal fauna from deep wells in York County, Virginia: Virginia Geological Survey Bulletin 67, 58 p., 6 pls.

Cushman, J.A., and Garrett, J.B., 1938, Three new rotaliform foraminifera from the lower Oligocene and upper Eocene of Alabama: Contributions from the Cushman Laboratory for Foraminiferal Research, v. 14, p. 62–66.

Cushman, J.A., and Todd, R., 1946, A foraminiferal fauna from the Byram Marl at its type locality: Contributions from the Cushman Laboratory for Foraminiferal Research, v. 22, p. 76–102.

Douglas, R.G., and Heitman, H.L., 1979, Slope and basin benthic foraminifera of the California borderland, *in* Doyle, L.J., and Pilkey, O.H., eds., Geology of continental slopes: Society of Economic Paleontologists and Mineralogists Special Publication 27, p. 231–246.

Farley, K.A., Montanari, A., Shoemaker, E.M., and Shoemaker, C.S., 1998, Geochemical evidence for a comet shower in the late Eocene: Science, v. 280, no. 5367, p. 1250–1253.

Gooday, A.J., 1993, Deep-sea benthic foraminiferal species which exploit phytodetritus; Characteristic features and controls on distribution: Marine Micropaleontology, v. 22, no. 3, p. 187–205.

Gooday, A.J., 1994, The biology of deep-sea foraminifera; A review of some advances and their applications to paleoceanography: Palaios, v. 9, no. 1, p. 14–31.

Gooday, A.J., 1996, Epifaunal and shallow infaunal foraminiferal communities at three abyssal NE Atlantic sites subject to differing phytodetritus input regimes: Deep-Sea Research, v. 43, p. 1395–1421.

Jones, M.H., 1990, Middle Eocene foraminifera from the Piney Point Formation of the Virginia and Maryland Coastal Plain: Norfolk, Va., Old Dominion University, masters thesis, 243 p.

Jorissen, F.J., Barmawidjaja, D.M., Puskaric, S., and van der Zwaan, G.J., 1992, Vertical distribution of benthic foraminifera in the northern Adriatic Sea; The relation with the organic flux: Marine Micropaleontology, v. 19, no. 1–2, p. 131–146.

Kaminski, M.A., Boersma, Ann, Tyszka, Jaroslaw, and Holbourn, A.E.L., 1995, Response of deep-water agglutinated foraminifera to dysoxic conditions in the California borderland basins, *in* Kaminski, M.A., Geroch, Stanislaw, and Gasinski, M.A., eds., Proceedings of the Fourth International Workshop on Agglutinated Foraminifera, Krakow, Poland,

September 12–19, 1993: Grzybowski Foundation Special Publication 3, p. 131–140, 1 pl.

Kobashi, Takuro, Grossman, E.L., Yancey, T.E., and Dockery, D.T., III, 2001, Reevaluation of conflicting Eocene tropical temperature estimate; Molluskan oxygen isotope evidence for warm low latitudes: Geology, v. 29, no. 11, p. 983–986.

Linke, P., Altenbach, A.V., Graf, G., and Heeger, T., 1995, Response of deep-sea benthic foraminifera to a simulated sedimentation event: Journal of Foraminiferal Research, v. 25, no. 1, p. 75–82.

Loubere, P., and Fariduddin, M., 1999, Benthic foraminifera and the flux of organic carbon to the seabed, *in* Sen Gupta, B.K., ed., Modern foraminifera: Boston, Kluwer Academic Publishers, p. 181–199.

Mackensen, Andreas, and Douglas, R.G., 1989, Down-core distribution of live and dead deep-water benthic foraminifera in box cores from the Weddell Sea and the California continental borderland: Deep-Sea Research, v. 36, no. 6, p. 879–900.

Martini, Erlend, 1971, Standard Tertiary and Quaternary calcareous nannoplankton zonation, *in* Farinacci, Anna, and Matteucci, R., eds., Proceedings of the II Planktonic Conference, Roma, 1970: Rome, Edizioni Tecnoscienza, v. 2, p. 739–785, 4 pls.

Nogan, D.S., 1964, Foraminifera, stratigraphy, and paleoecology of the Aquia Formation of Maryland and Virginia: Cushman Foundation for Foraminiferal Research Special Publication 7, 50 p.

Olsson, R.K., 1960, Foraminifera of latest Cretaceous and earliest Tertiary age in the New Jersey Coastal Plain: Journal of Paleontology, v. 34, no. 1, p. 1–58.

Orbigny, Alcide d', 1846, Foraminifères fossiles du bassin tertiare de Vienne: Paris, 312 p.

Pearson, P.N., Ditchfield, P.W., Singano, Joyce, Harcourt-Brown, K.G., Nicholas, C.J., Olsson, R.K., Shackleton, N.J., and Hall, M.A., 2001, Warm tropical sea surface temperatures in the Late Cretaceous and Eocene epochs: Nature, v. 413, no. 6855, p. 481–487.

Pfannkuche, O., 1993, Benthic response to the sedimentation of particulate organic matter at the BIOTRANS station, 47°N, 20°W: Deep-Sea Research, v. 40, p. 135–139.

Phleger, F.B, and Soutar, Andrew, 1973, Production of benthic foraminifera in three east Pacific oxygen minima: Micropaleontology, v. 19, no. 1, p. 110–115.

Plummer, H.J., 1927, Foraminifera of the Midway Formation in Texas: Texas University Bulletin 2644, 205 p., 15 pls.

Poag, C.W., 1981, Ecologic atlas of benthic foraminifera of the Gulf of Mexico: Woods Hole, Mass., Marine Science International, 174 p.

Poag, C.W., 1997a, The Chesapeake Bay bolide impact; A convulsive event in Atlantic Coastal Plain evolution: Sedimentary Geology, v. 108, no. 1–4, p. 45–90.

Poag, C.W., 1997b, Roadblocks on the kill curve; Testing the Raup hypothesis: Palaois, v. 12, no. 6, p. 582–590.

Poag, C.W., 2002, Synimpact-postimpact transition inside Chesapeake Bay crater: Geology, v. 30, no. 11, p. 995–998.

Poag, C.W., and Aubry, M.-P., 1995, Upper Eocene impactites of the U.S. East Coast; Depositional origins, biostratigraphic framework, and correlation: Palaios, v. 10, no. 1, p. 16–43.

Poag, C.W., and the Chesapeake Coring Team, 2001, Drilling to basement inside the Chesapeake Bay crater [abs.]: Lunar and Planetary Science Conference, 32d, Houston, Tex., March 12–16, 2001, Abstract 1203, available online at http://www.lpi.usra.edu/meetings/lpsc2001/pdf/1203.pdf.

Poag, C.W., and Commeau, J.A., 1995, Paleocene to middle Miocene planktonic foraminifera of the southwestern Salisbury embayment, Virginia and Maryland; Biostratigraphy, allostratigraphy, and sequence stratigraphy: Journal of Foraminiferal Research, v. 25, no. 2, p. 134–155, 9 pls.

Poag, C.W., Gohn, G.S., and Powars, D.S., 2001, From shocked basement to fallout spherules; The coring record at the Chesapeake Bay crater [abs.]: Geological Society of America Abstracts with Programs, v. 33, no. 6, p. A–433.

Poag, C.W., Hutchinson, D.R., Colman, S.M., and Lee, M.W., 1999, Seismic expression of the Chesapeake Bay impact crater; Structural and morphologic refinements based on new seismic data, *in* Dressler, B.O., and Sharpton, V.L., eds., Large meteorite impacts and planetary evolution; II: Geological Society of America Special Paper 339, p. 149–164.

Poag, C.W., Koeberl, Christian, and Reimold, W.U., 2004, The Chesapeake Bay crater—Geology and geophysics of a late Eocene submarine impact structure: New York, Springer-Verlag, 522 p. plus CD-ROM.

Poag, C.W., Mankinen, E., and Norris, R.D., 2003, Late Eocene impacts; Geologic record, correlation, and paleoenvironmental consequences, *in* Prothero, D.R., Ivany, L.C., and Nesbitt, E.R., eds., From greenhouse to icehouse; The marine Eocene-Oligocene transition: New York, Columbia University Press, p. 495–510.

Powars, D.S., and Bruce, T.S., 1999, The effects of the Chesapeake Bay impact crater on the geologic framework and the correlation of hydrogeologic units of the lower York-James Peninsula, Virginia: U.S. Geological Survey Professional Paper 1612, 82 p., 9 oversize pls. (Also available online at http://pubs.usgs.gov/prof/p1612/).

Powars, D.S., Mixon, R.B., and Bruce, Scott, 1992, Uppermost Mesozoic and Cenozoic geologic cross section, outer coastal plain of Virginia, *in* Gohn, G.S., ed., Proceedings of the 1988 U.S. Geological Survey Workshop on the Geology and Geohydrology of the Atlantic Coastal Plain: U.S. Geological Survey Circular 1059, p. 85–101.

Sen Gupta, B.K., Turner, R.E., and Rabalais, N.N., 1996, Seasonal oxygen depletion in continental-shelf waters of Louisi-

ana; Historical record of benthic foraminifers: Geology, v. 24, no. 3, p. 227–230.

Tjalsma, R.C., and Lohmann, G.P., 1983, Paleocene-Eocene bathyal and abyssal benthic foraminifera from the Atlantic Ocean: Micropaleontology Special Publication 4, 90 p., 22 pls.

Van Morkhoven, F.P.C.M., Berggren, W.A., and Edwards, A.S., 1986, Cenozoic cosmopolitan deep-water benthic foraminifera: Bulletin des Centres de Recherches Exploration-Production Elf-Aquitaine, Mémoire 11, 421 p.

Plates F1, F2

Plate F1

Nominate Species for Benthic Foraminiferal Zone and Subzones Recognized in the Chickahominy Formation

[Scale bars are 100 micrometers (μm). These species are represented in the Chickahominy Formation in all cores obtained from the Chesapeake Bay impact crater. Sites where cores were obtained are shown in figure F1. Plate from Poag, Koeberl, and Reimold (2004, fig. 13.3)]

Figure
1. *Cibicidoides pippeni* (Cushman and Garrett) 1938. Chickahominy Formation, Exmore core, umbilical view.
2. *Bulimina jacksonensis* Cushman 1925. Chickahominy Formation, Exmore core, lateral view.
3. *Lagenoglandulina virginiana* (Cushman and Cederstrom) 1945. Chickahominy Formation, Newport News Park 2 core, lateral view.
4. *Uvigerina dumblei* Cushman and Applin 1926. Chickahominy Formation, Exmore core, lateral view.
5. *Bolivina tectiformis* Cushman 1926. Chickahominy Formation, Exmore core, lateral view.
6. *Bathysiphon* sp. Chickahominy Formation, Kiptopeke core, lateral view.

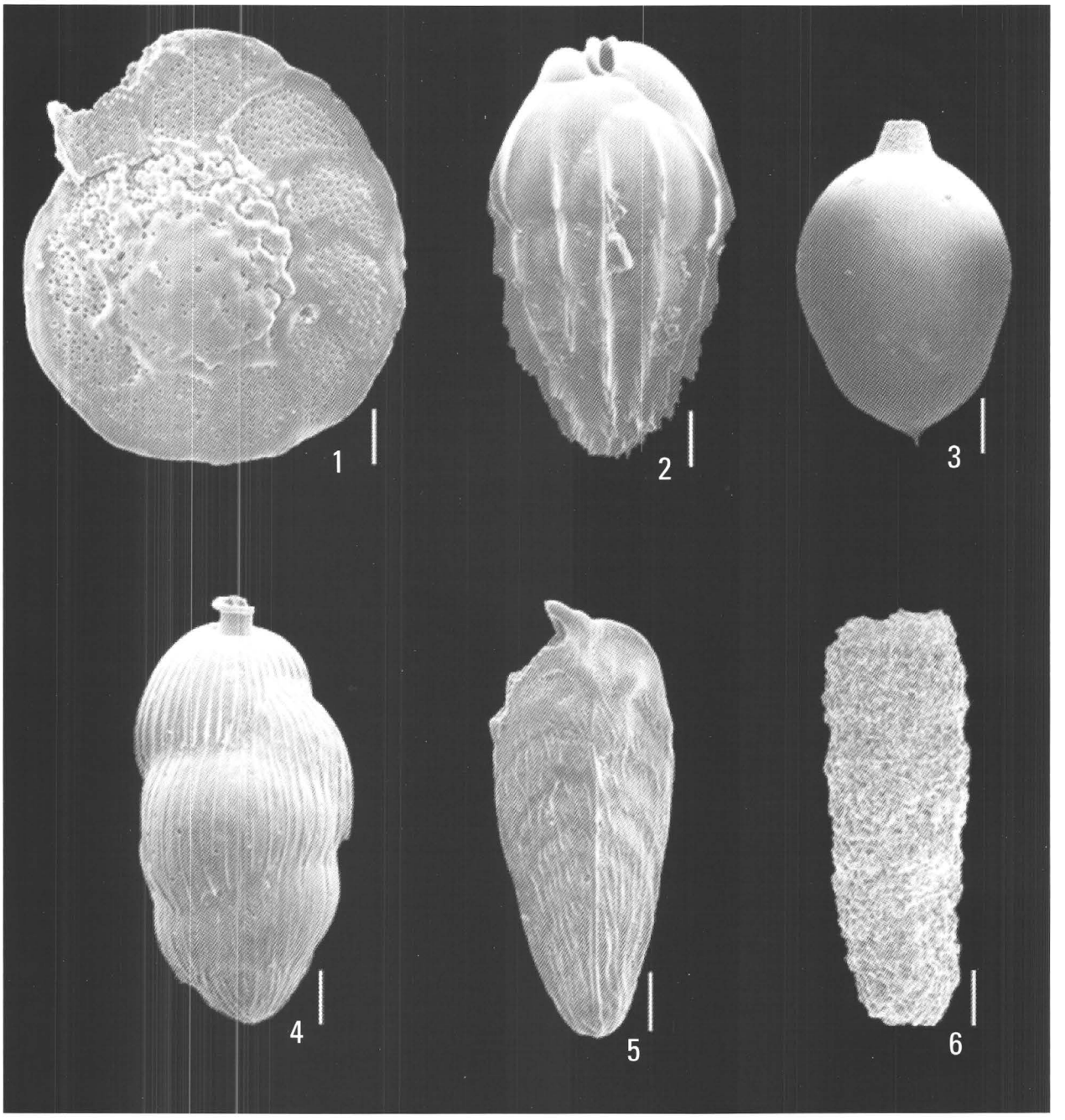

Nominate Species for Benthic Foraminiferal Zone and Subzones Recognized in the Chickahominy Formation

Plate F2

Important Benthic Foraminiferal Species from the Chickahominy Formation Used for Paleoenvironmental Interpretations

[Scale bars are 100 μm. Illustrated specimens are from the Exmore core; specimens of the same species in the Kiptopeke and USGS-NASA Langley cores are used for paleoenvironmental interpretations (table F9). The Exmore, Kiptopeke, and Langley corehole locations are shown in figure F1. Plate from Poag, Koeberl, and Reimold (2004, fig. 13.7). Quotation marks indicate provisory trivial name]

Figure

1. *Epistominella minuta* Olsson 1960. Chickahominy Formation, Exmore core, umbilical view.
2. *Charltonina madrugaensis* (Cushman and Bermúdez) 1948. Chickahominy Formation, Exmore core, umbilical view.
3. *Gyroidinoides aequilateralis* (Plummer) 1927. Chickahominy Formation, Exmore core, umbilical view.
4. *Gyroidinoides byramensis* (Cushman and Todd) 1946. Chickahominy Formation, Exmore core, umbilical view.
5. *Uvigerina gardnerae* Cushman 1926. Chickahominy Formation, Exmore core, lateral view.
6. *Caucasina marylandica* (Nogan) 1964. Chickahominy Formation, Exmore core, lateral view.
7. *Bolivina gracilis* Cushman and Applin 1926. Chickahominy Formation, Exmore core, lateral view.
8. *Bolivina virginiana* Cushman and Cederstrom 1945. Chickahominy Formation, Exmore core, lateral view.
9. *Bolivina* "praevirginiana." Chickahominy Formation, Exmore core, lateral view.
10. *Globobulimina ovata* (d'Orbigny) 1846. Chickahominy Formation, Exmore core, lateral view.
11. *Grigelis cookei* (Cushman) 1933. Chickahominy Formation, Exmore core, lateral view, final two chambers.
12. *Grigelis annulospinosa* (Bandy) 1949. Chickahominy Formation, Exmore core, lateral view.
13. *Stilostomella* "exilispinata." Chickahominy Formation, Exmore core, lateral view.
14. *Stilostomella cocoaensis* (Cushman) 1925. Chickahominy Formation, Exmore core, lateral view.

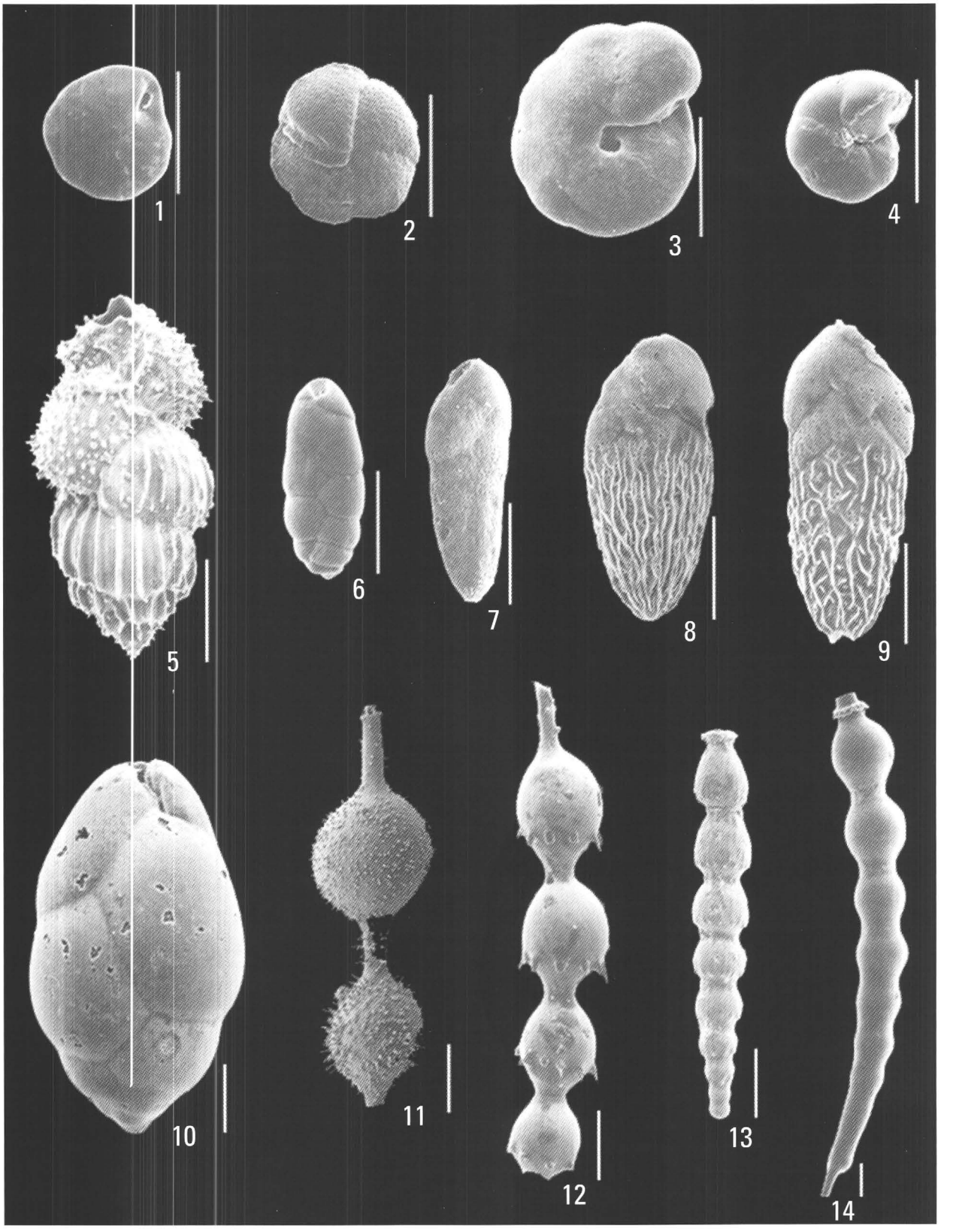

Important Benthic Foraminiferal Species from the Chickahominy Formation Used for Paleoenvironmental Interpretations

Physical Stratigraphy of the Upper Eocene to Quaternary Postimpact Section in the USGS-NASA Langley Core, Hampton, Virginia

By David S. Powars, T. Scott Bruce, Lucy E. Edwards,
Gregory S. Gohn, Jean M. Self-Trail, Robert E. Weems,
Gerald H. Johnson, Matthew J. Smith, and Colleen T. McCartan

Chapter G of
**Studies of the Chesapeake Bay Impact Structure—
The USGS-NASA Langley Corehole, Hampton, Virginia, and
Related Coreholes and Geophysical Surveys**

Edited by J. Wright Horton, Jr., David S. Powars, and Gregory S. Gohn

Prepared in cooperation with the
Hampton Roads Planning District Commission,
Virginia Department of Environmental Quality, and
National Aeronautics and Space Administration Langley Research Center

Professional Paper 1688

U.S. Department of the Interior
U.S. Geological Survey

Contents

Figures

Tables

Physical Stratigraphy of the Upper Eocene to Quaternary Postimpact Section in the USGS-NASA Langley Core, Hampton, Virginia

By David S. Powars,[1] T. Scott Bruce,[2] Lucy E. Edwards,[1]
Gregory S. Gohn,[1] Jean M. Self-Trail,[1] Robert E. Weems,[1]
Gerald H. Johnson,[3] Matthew J. Smith,[1] and Colleen T. McCartan[1]

Abstract

In 2000 a corehole at the National Aeronautics and Space Administration (NASA) Langley Research Center, Hampton, Va., was continuously cored through the entire coastal plain section into crystalline basement rock by the U.S. Geological Survey (USGS) and its cooperators; a high-resolution seismic-reflection and seismic-refraction survey across the York-James Peninsula was simultaneously conducted. The core and land-based seismic data were needed to interpret the Chesapeake Bay impact crater's effects on the geological and hydrogeological framework of the lower York-James Peninsula. This kind of information is required to determine the location of the crater's buried outer margin escarpment.

The USGS-NASA Langley corehole reached a total depth of 635.1 meters (m; 2,083.8 feet (ft)); the hole penetrated 235.65 m (773.12 ft) of postimpact sediments overlying 390.63 m (1,281.6 ft) of synimpact debris and 8.9 m (29.1 ft) of crystalline basement rock. The synimpact and postimpact stratigraphic units of the new corehole correlate well with units interpreted by Powars and Bruce (1999, USGS Professional Paper 1612) from geophysical logs and descriptions of cuttings from a preexisting test well that was located about 520 m (1,700 ft) east of the new corehole.

The postimpact deposits recovered in the USGS-NASA Langley core include, in ascending order, the following units: the very clayey, calcareous Chickahominy Formation (upper Eocene); the glauconitic, phosphatic, and partly shelly lithologies of both the Drummonds Corner beds (a newly recognized upper lower Oligocene stratigraphic unit) and the Old Church Formation (upper Oligocene); the shelly and sandy beds of the Calvert Formation (lower Miocene); the primarily siliciclastic, fine-grained part of the Calvert Formation (middle Miocene), the St. Marys Formation (upper Miocene), and the lower part of the Eastover Formation (upper Miocene); the siliciclastic, locally glauconitic, fine- to coarse-grained, fossiliferous upper part of the Eastover (upper Miocene) and the Yorktown Formation (lower and upper Pliocene); and the fluvial to estuarine Tabb Formation (upper Pleistocene).

The land-based seismic-reflection survey was run adjacent to the Langley corehole to correlate velocities and reflectors with the lithology of the core. The seismic profile also shows that most of the synimpact crater debris consists of highly fractured and fault-bounded, blocky material with distinctive anisotropy and reflection patterns. The overlying postimpact deposits show disruption zones suggesting fracturing and faulting; the scale of deformation in the postimpact deposits is orders of magnitude less than the scale of deformation within the synimpact deposits. Recovery of several angled fractures with slickensides and a fault filled with gouge within the postimpact section provides supportive evidence for their signature on the seismic images. These postimpact fractures and faults may be related to continued compaction and megablock movement. The existence of a preimpact James River structural zone along the southern and southwestern margin of the crater has an apparent additive effect to synimpact and postimpact structural adjustments of the region.

The structural depression of the crater has greatly influenced the postimpact depositional history, sedimentary patterns, and stratigraphic relations of the units that have buried it. Initially the crater's depression transformed parts of the preimpact inner neritic (shallow) shelf depositional environment into a bathyal (deep) depositional environment. Postimpact loading and compaction, possibly along with structural adjustments, have helped the crater to maintain a persistent bathymetric low so that postimpact stratigraphic units dip into and thicken

[1]U.S. Geological Survey, Reston, VA 20192.
[2]Virginia Department of Environmental Quality, P.O. Box 10009, Richmond, VA 23240.
[3]Department of Geology, College of William and Mary, Williamsburg, VA 23187.

toward the center of the crater. This low has resulted in the deposition and preservation of postimpact stratigraphic units (upper Eocene, Oligocene, and lower Miocene) that are found only within the Chesapeake Bay impact structure. Delineation of the types of structural features and stratigraphic affinities created by the impact is essential to development of the hydrogeologic framework to be used in the modeling of the ground-water flow system and regional water quality of the Virginia Coastal Plain.

Introduction

The discovery of a large impact crater beneath the Chesapeake Bay and its apparent effects on the regional ground-water resources has prompted a revision of the structural, stratigraphic, and hydrogeologic framework of a large part of the Virginia Coastal Plain (Powars and Bruce, 1999). The revision process began with the analysis of borehole and marine seismic-reflection data that revealed the existence of a large crater (Powars and others, 1993; Poag, Powars, Mixon, and Bruce, 1994; Poag, Powars, Poppe, and Mixon, 1994). This analysis was followed by structural and stratigraphic documentation of the 85-kilometer-wide (53-mile-wide) Chesapeake Bay impact crater (Koeberl and others, 1996; Poag, 1996, 1997, 2000; Poag and others, 1999; Powars and Bruce, 1999; Powars, 2000). Recently, Johnson, Powars, and others (1998, 2001), Powars (2000), and Powars, Johnson, and others (2002) have presented evidence for an outer fracture zone that surrounds the crater and that is as much as 35 kilometers (km; 22 miles (mi)) wide (fig. G1). The whole structure is referred to as the Chesapeake Bay impact structure and is located beneath the lower Chesapeake Bay, its adjacent peninsulas, and a small part of the Atlantic Ocean east of the lower part of the Delmarva Peninsula. The approximate center of the crater is beneath the town of Cape Charles, Va., as shown in figure G1.

The Chesapeake Bay impact structure formed approximately 35.7 to 35.8 million years ago (Ma) (Horton and others, this volume, chap. A) when a large comet or asteroid crashed into shallow continental shelf waters of the western Atlantic Ocean, penetrated several hundred meters of unconsolidated, seaward-dipping, water-saturated sediments, and blasted a hole into the crystalline basement rocks. At this time during the late Eocene, the Earth was warmer than it is today, and sea level was about a hundred meters (about 300 feet) higher than it is today. The Virginia coastline was located somewhere on the Piedmont, west of the present Fall Zone, and the land was covered by a tropical forest.

The explosion caused by the impact created an initial water-column splash that probably reached the upper atmosphere (H.J. Melosh, University of Arizona, Tucson, oral commun., 2002). The impact produced an inverted, sombrero-shaped, complex crater that was immediately filled by a forceful resurge of ocean water containing chaotically mixed submarine debris (similar to debris in the Lockne impact crater in Sweden described by von Dalwigk and Ormö, 2001), rim-collapse material, and fluidized and slumped material. The initial resurge was followed by trains of debris-loaded tsunamis; their deposits were capped by the settling out of suspended and fallout particles. Younger postimpact sedimentary deposits have buried the crater since this catastrophic event. Walled terraces, central peaks, and flat floors characterize complex craters (Melosh, 1989), and the Chesapeake Bay impact crater appears to have all these features buried at depth.

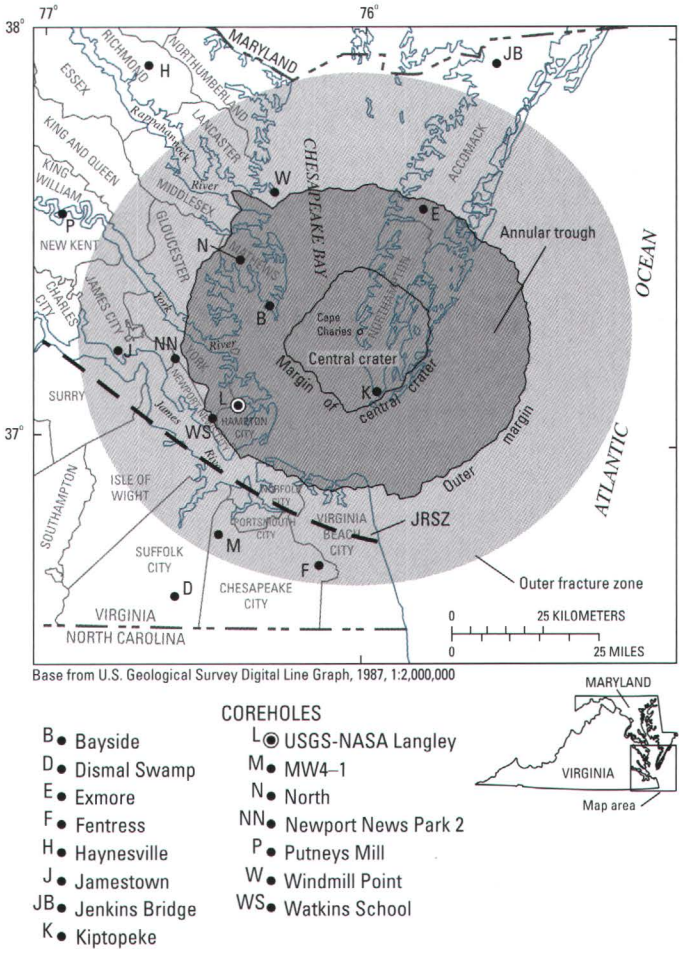

Figure G1. Regional map showing the location of the Chesapeake Bay impact structure, the USGS-NASA Langley corehole at Hampton, Va., and some other coreholes in southeastern Virginia. Locations of the central crater and outer margin are from Powars and Bruce (1999). The extent of the outer fracture zone (light gray) is based on Powars (2000) and Johnson, Powars, and others (2001); the eastern part is speculative. Illustration modified from Powars, Johnson, and others (2002) and Edwards and Powars (2003). JRSZ, James River structural zone of Powars (2000).

The regional ground-water flow paths apparently were altered by truncation and disruption of preimpact aquifers, by emplacement of the synimpact deposits, and by subsequent postimpact deposition of mostly very fine grained deposits in the crater's structural low. Powars and others (1994) and Bruce and Powars (1995) recognized that the western part of the buried crater generally coincided with Virginia's inland saltwater wedge as mapped by Cederstrom (1943, 1945a,b,c, 1957). Cederstrom suggested that the wedge was created by differential flushing of a sediment-filled Eocene basin. The present interpretation is that the buried crater created a large region where seawater has not been flushed from the coastal plain sediments in and around the crater. The western outer margin of the crater appears to act as a mixing (transition) zone separating ground water of high salinity (brackish) inside the outer margin from lower salinity water outside the outer margin (Powars and Bruce, 1999). It should be emphasized that this salinity transition area is a zone and that brackish water is found west of the crater's margin in some of the sediments within the outer fracture zone (for details, see McFarland and Bruce, this volume, chap. K). Until the crater was discovered, there was no satisfactory explanation for the anomalous saltwater wedge (which is better defined as a bulge because it rises to shallow depths) (Powars and others, 1994; Powars and Bruce, 1999) or the region's stratigraphic and structural complexities.

The location and geometry of the outer margin of the Chesapeake Bay impact crater beneath the lower York-James Peninsula are poorly defined. Additional data are needed to locate and delineate the outer margin precisely. Hydrologic data (such as flow direction, water quality, and permeability within the crater) are limited. Information about the depositional processes associated with such a large impactor into water-saturated, unconsolidated sediments is sparse. The societal need for water across the Hampton Roads region has led several municipalities to develop brackish-water desalination plants just outside the crater, but geologic and hydrologic information is needed to model more accurately and evaluate the ground-water flow and the potential for movement of salty water into well fields in the vicinity of the impact crater.

To further investigate the geology and hydrology of this structure, in the year 2000, the U.S. Geological Survey (USGS) and cooperating institutions (see "Acknowledgments") drilled a deep corehole in the southwestern part of the structure's annular trough and completed high-resolution seismic-reflection and seismic-refraction surveys (Catchings, Powars, and others, 2001, 2002; Catchings, Saulter, and others, 2001; Catchings and others, this volume, chap. I) and audio-magnetotelluric surveys (Pierce, this volume, chap. J) across its southwestern margin. A suite of geophysical borehole logs was obtained, including a sonic velocity log for correlation with the seismic data.

The deep corehole, called the USGS-NASA Langley corehole, was drilled on the York-James Peninsula at the National Aeronautics and Space Administration (NASA) Langley Research Center in Hampton, Va., within the northeast quarter of the Newport News North 7.5-min quadrangle (USGS, 1986) (figs. G2 and G3). The site is a short distance north of Langley Boulevard and southwest of Building 1190 in an open grassy area. The coordinates for the Langley corehole, as determined by using a high-accuracy Global Positioning System, are lat 37°05'44.28" N., long 76°23'08.96" W. (North American Datum of 1927); the hole was begun at a ground-surface altitude of 2.4 meters (m; 7.9 feet (ft)) above the North American Vertical Datum of 1988 (NAVD 88). The Langley corehole has a total depth of 635.1 m (2,083.8 ft).

The core site is approximately 8 km (5 mi) inside the outer margin of the buried Chesapeake Bay impact structure as mapped in the Hampton-Newport News area by Powars and Bruce (1999), and it is approximately 36.8 km (22.9 mi) from the center of the impact structure at Cape Charles, Va. The surficial geology at the core site represents shallow paleo-Chesapeake Bay floor sediments deposited in the late Pleistocene when sea level was 5.5 m (18 ft) above today's level. These bay-floor deposits formed a flat topographic surface that Coch (1971) named the Hampton Flat; its associated shoreline, the Big Bethel scarp, is 4 km (2.5 mi) west of the drill site (see Horton and others, this volume, chap. A, fig. A4).

The stratigraphic interval sampled by the USGS-NASA Langley corehole is physically distinguished by three primary geologic units (presented below with thickness and boundary altitudes relative to the NAVD 88):

- Crystalline rock (Neoproterozoic peraluminous granite), 8.9 m (29.1 ft) thick, between altitudes of –632.74 and –623.87 m (–2,075.9 and –2,046.8 ft); see Horton and others (this volume, chap. B)
- Impact-modified and impact-generated crater debris, 390.63 m (1,281.6 ft) thick, between altitudes of –623.87 and –233.23 m (–2,046.8 and –765.2 ft); see Gohn and others (this volume, chap. C), Frederiksen and others (this volume, chap. D), and Horton and Izett (this volume, chap. E)
- Postimpact shallow-marine and coastal plain deposits, 235.65 m (773.12 ft) thick, between –233.32 m (–765.2 ft) and the top of the corehole at +2.4 m (+7.9 ft); see this chapter (G) and Edwards and others (this volume, chap. H) and Poag and Norris (this volume, chap. F)

A variety of paleontological data for the USGS-NASA Langley core confirmed Powars and Bruce's (1999) stratigraphic interpretation of the 1974 NASA Langley test well located only about 520 m (about 1,700 ft) east of the Langley corehole (comparison shown in fig. G4). The USGS-NASA Langley corehole provides key information for understanding the formative processes that occurred in the Chesapeake Bay impact structure's southwestern annular trough.

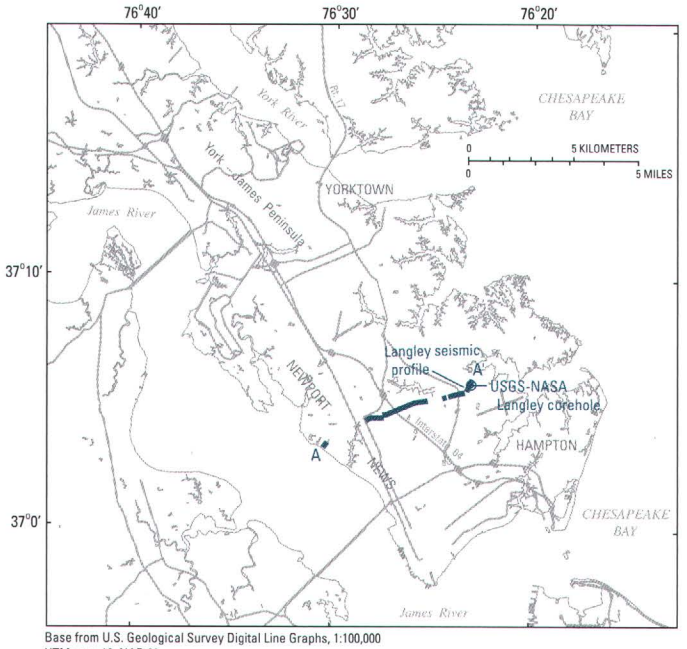

Base from U.S. Geological Survey Digital Line Graphs, 1:100,000
UTM zone 18, NAD 83

Figure G2. Map of the lower York-James Peninsula showing the location of the USGS-NASA Langley corehole and the land-based high-resolution seismic transect (black line; gaps show areas skipped). The final segment of the transect, the 1-km-long (0.62-mi-long) Langley seismic profile, is described by Catchings and others (this volume, chap. I).

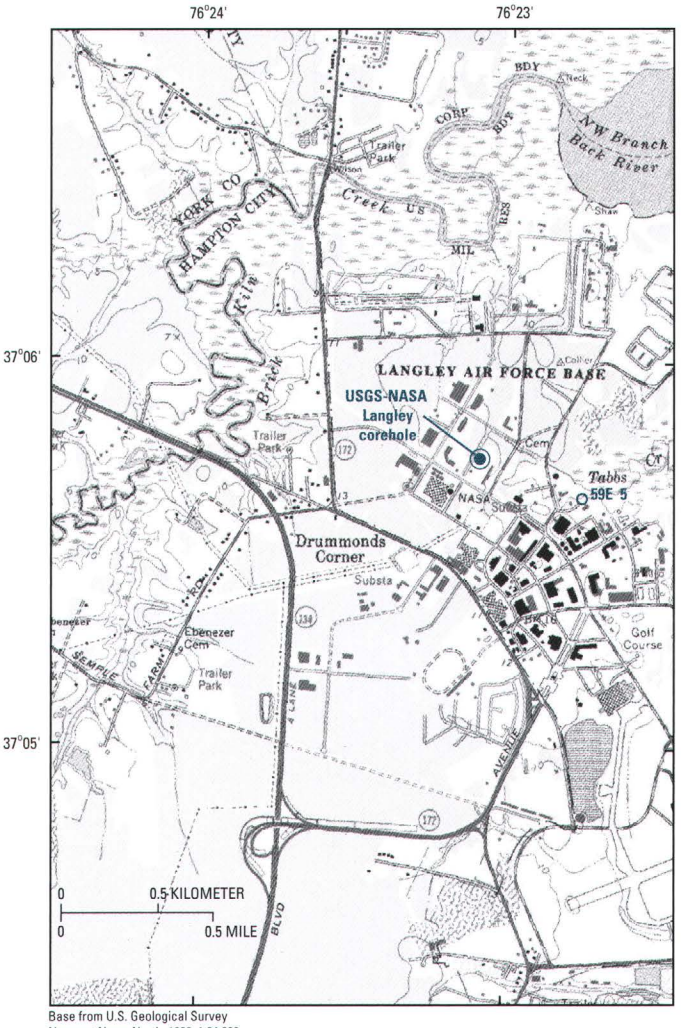

Base from U.S. Geological Survey
Newport News North, 1986, 1:24,000

Figure G3. Detailed map showing the location of the USGS-NASA Langley corehole (59E 31) and the 1974 NASA Langley test well (59E 5) at the NASA Langley Research Center, Hampton, Va.

Figure G4 (facing page). Stratigraphic columns and geophysical logs for the USGS-NASA Langley corehole (*A*, this report) and the 1974 NASA Langley test well (*B*, Powars and Bruce, 1999). See figure G3 for hole locations. Colors in bands indicate equivalent units.

Purpose and Scope

This chapter describes the physical geology of the 235.65 m (773.12 ft) of postimpact deposits penetrated in the USGS-NASA Langley corehole and summarizes the paleontological data (Edwards and others, this volume, chap. H). Lithic descriptions of the Langley core are provided in appendix G1. The lithostratigraphy of the core is correlated with borehole geophysical logs and the land-based high-resolution seismic-reflection data to characterize the physical properties of the stratigraphic units and their geophysical signatures. The correlation of the core and borehole geophysical logs provides the supportive evidence required for accurate interpretation of earlier water-well geophysical logs and descriptions of borehole cuttings. This information makes possible a better understanding of the Chesapeake Bay impact structure's effects on the geological and hydrological framework of southeastern Virginia over approximately the last 35.7 to 35.8 million years (m.y.).

Recent Previous Investigations

Table G1 lists some of the products that have come from the combined efforts of the U.S. Geological Survey, the Hampton Roads Planning District Commission, and the Virginia Department of Environmental Quality from 1987 through the year 2002. These publications have greatly changed our understanding of the subsurface geologic and hydrologic framework of southeastern Virginia.

Methods of Investigation

Compilation of Lithologic Data from Core

Compilation of the onsite graphical representation and written descriptions of the lithology of the USGS-NASA Langley core was supplemented by additional postdrill inspection

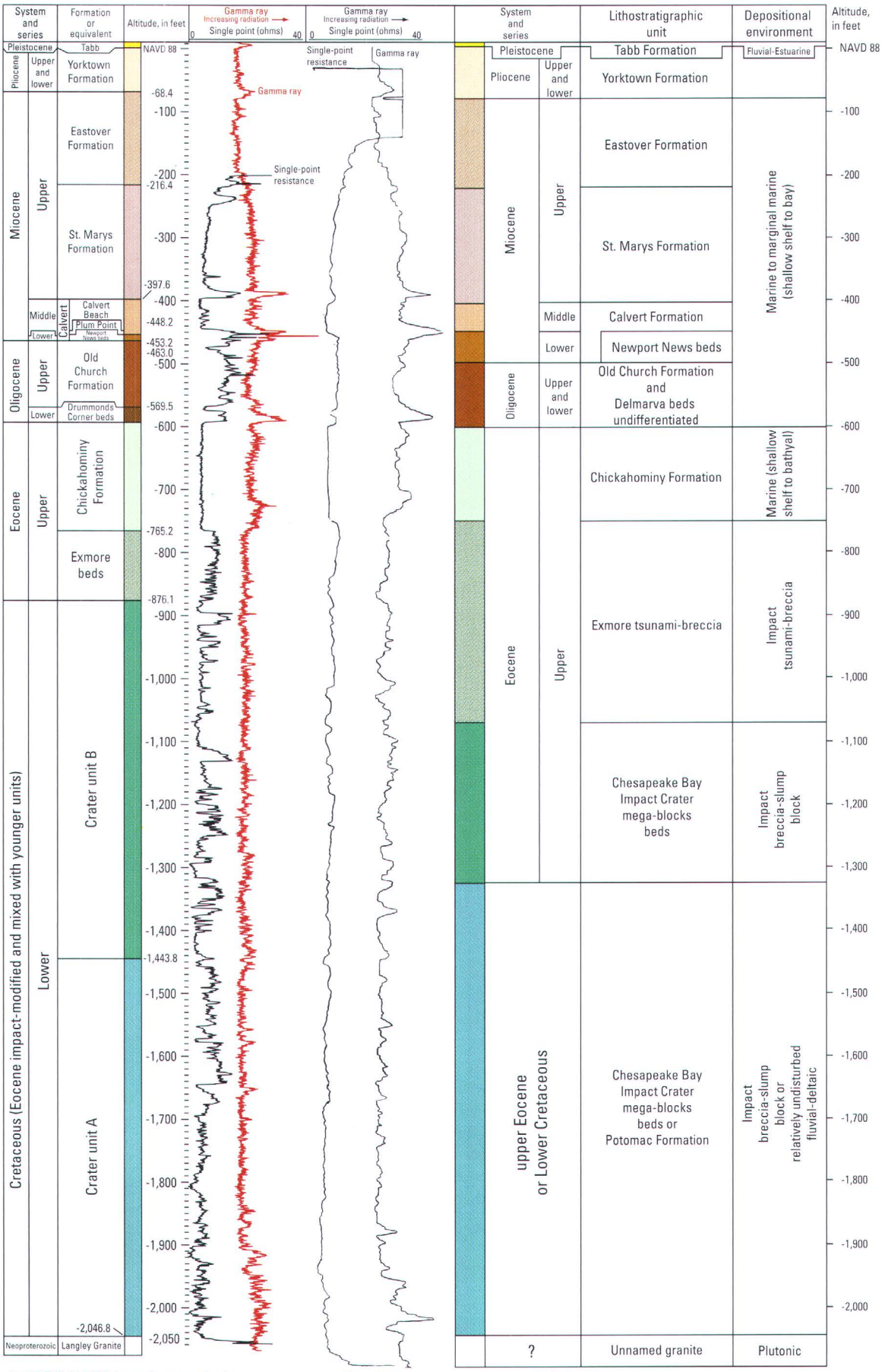

A. USGS-NASA Langley corehole (59E 31), 2000

B. NASA Langley test well (59E 5), 1974

Table G1. Key Chesapeake Bay impact crater publications from 1987 through 2002.

[Many of the listed publications result from cooperative work by the U.S. Geological Survey, the Hampton Roads Planning District Commission, and the Virginia Department of Environmental Quality. Publications are listed by year within each group]

Contributions to regional geologic framework, 1987–2000
Powars, Mixon, Edwards, Andrews, and Ward, 1987
Powars, Mixon, Edwards, Poag, and Bruce, 1990
Poag, Powars, Mixon, Edwards, Folger, Poppe, and Bruce, 1991
Powars, Poag, and Bruce, 1991
Poag, Poppe, Powars, and Mixon, 1992
Poag, Powars, Poppe, Mixon, Edwards, Folger, and Bruce, 1992
Powars, Mixon, and Bruce, 1992
Poag and Aubry, 1995
Poag and Commeau, 1995
Powars and Bruce, 1999
Powars, 2000
Crater discovery, 1993–94
Powars, Poag, and Mixon, 1993
Poag, Powars, Mixon, and Bruce, 1994
Poag, Powars, Poppe, and Mixon, 1994
Crater's association with Virginia's inland saltwater wedge, 1994–2002
Powars, Bruce, Poag, and Mixon, 1994
Bruce and Powars, 1995
Powars, Bruce, and Johnson, 1998
Powars and Bruce, 1999
Powars, 2000
McFarland, 2002
McFarland and Bruce, 2002
Crater's structural and stratigraphic effects on postimpact deposits and geomorphology, 1993–2000
Powars, Poag, and Mixon, 1993
Poag, Powars, Mixon, and Bruce, 1994
Poag, Powars, Poppe, and Mixon, 1994
Johnson and Powars, 1996
Koeberl, Poag, Reimold, and Brandt, 1996
Poag, 1996, 1997, 2000
Riddle, Vaughn, Lucey, Kruse, Johnson, and Hobbs, 1996
Johnson, Kruse, Vaughn, Lucey, Hobbs, and Powars, 1998
Johnson, Powars, Bruce, Vaughn, Lucey, and Kruse, 1998
Powars, Bruce, and Johnson, 1998
Poag, Hutchinson, Colman, and Lee, 1999
Powars and Bruce, 1999
Powars, 2000
Powars, Edwards, Bruce, and Johnson, 2000

Table G1. Key Chesapeake Bay impact crater publications from 1987 through 2002.—Continued

Preliminary descriptions of the USGS-NASA Langley corehole data, 2001
Gohn, Clark, Queen, Levine, McFarland, and Powars, 2001
Powars, Bruce, Bybell, Cronin, Edwards, and others, 2001
Interpretations of the crater's structure and synimpact and postimpact crater-filling processes, 2001–2002
Catchings, Powars, Gohn, Goldman, Gandhok, and Johnson, 2001
Catchings, Saulter, Powars, Goldman, Dingler, Gohn, Schindler, and Johnson, 2001
Gohn, Powars, Bruce, Self-Trail, Weems, Edwards, Horton, Izett, and Johnson, 2001
Horton, Aleinikoff, Izett, Naeser, and Naeser, 2001
Johnson, Powars, Bruce, Beach, Harris, and Goodwin, 2001
Poag and the Chesapeake Coring Team, 2001
Powars, Gohn, Catchings, McFarland, Bruce, Johnson, Izett, Emry, and Edwards, 2001
Powars, Gohn, Edwards, Bruce, Catchings, Emry, Johnson, Levine, Poag, and Pierce, 2001
Powars, Johnson, Bruce, and Edwards, 2001
Catchings, Powars, Gohn, and Goldman, 2002
Gohn, Powars, Bruce, Quick, and Catchings, 2002
Gohn, Powars, Quick, Horton, and Catchings, 2002
Horton, Aleinikoff, Izett, Naeser, Naeser, and Kunk, 2002
Horton, Kunk, Naeser, Naeser, Aleinikoff, and Izett, 2002
Johnson, Powars, and Bruce, 2002
Poag, 2002a,b,c
Poag, Gohn, and Powars, 2002
Poag, Plescia, and Molzer, 2002
Powars, Edwards, Bruce, and Johnson, 2002
Powars, Gohn, Bruce, Johnson, Catchings, Frederiksen, Edwards, Self-Trail, and Pierce, 2002
Powars, Gohn, Edwards, Catchings, Bruce, Johnson, and Poag, 2002
Powars, Johnson, Edwards, Horton, Gohn, Catchings, McFarland, Izett, Bruce, Levine, and Pierce, 2002

(10x hand lens and binocular microscope) and sampling. A variety of paleontological data (Edwards and others, this volume, chap. H) provided confirmation of preliminary stratigraphic assignments and the guidance for the stratigraphic assignment and recognition of units. Colors are described with reference to the color charts of Munsell Color Company (1988) and Goddard and others (1948). This chapter mostly uses depth from the surface of the corehole in meters followed by feet in parentheses. Depth and altitude are provided on the stratigraphic columns.

Analysis of Borehole Geophysical Logs

Stephen E. Curtin (USGS) and Richard E. Hodges (USGS) ran a suite of geophysical logs in the USGS-NASA Langley borehole using a Century logging system with a Model 8043 multi-tool probe. Different suites of geophysical logs were run on several different dates to different depths. The deepest suite of logs reached 634.9 m (2,083 ft), almost the total depth of the hole (635.1 m; 2,083.8 ft); this suite included natural-gamma-ray, multipoint-resistivity, 6-ft lateral-resistivity, caliper, acoustic televiewer (ATV), induction-resistivity, single-point-resistance, spontaneous-potential, and sonic velocity logs. Other suites included long-normal-resistance and short-normal-resistance logs. Borehole geophysical logs, especially the resistivity and natural-gamma-ray logs, were interpreted by establishing geophysical signatures for the various lithic units observed in the core. The lithostratigraphy in this chapter is largely based on interpretation of the lithic descriptions and geophysical logs supplemented by paleontological data (Edwards and others, this volume, chap. H).

Correlation with High-Resolution Seismic Images

Both marine- and land-based seismic data reveal numerous faults that displace the top of basement and overlying sediments in the annular trough and the outer fracture zone (Poag and others, 1999; Powars and others, 2003). The existence of a preimpact James River structural zone (fig. G1) along the southern and southwestern margin of the crater has an apparent additive effect to synimpact and postimpact structural adjustments of the region (Powars, 2000). A 1-km-long (0.62-mi-long), high-resolution, land-based seismic image (Catchings and others, this volume, chap. I, fig. I9) was collected adjacent to the USGS-NASA Langley corehole to allow correlation with the core and geophysical logs (especially the sonic velocity log). Figure G5 shows how the seismic reflections correlate directly with the corehole stratigraphy and geophysical logs. Abrupt shifts in the sonic velocity log correspond to density changes across lithic contacts and produce high-amplitude positive seismic reflections (black in fig. G5). Within the postimpact units, lower amplitude positive reflections appear to relate to subtle changes in lithology, which are also reflected in most of the geophysical logs (the Chickahominy Formation is a good example of very subtle lithic changes creating noticeable changes in seismic reflections; see fig. G5).

The high-resolution seismic-reflection data having a common-depth-point (CDP) interval of 2.5 m (8.2 ft) indicate that most of the synimpact crater debris consists of highly fractured and fault-bounded blocks of Lower Cretaceous fluvial-deltaic deposits (Catchings and others, this volume, chap. I; Gohn and others, this volume, chap. C). The overlying postimpact deposits also show fracturing and faulting, but the deformation is an order of magnitude less than the deformation within the synimpact deposits. The postimpact stratigraphic units at and near the Langley site have relatively horizontal continuous reflections typical of marine strata; the stratigraphic units with contrasting lithologies (primarily sand vs. clay) appear to have distinct seismic signatures and positive reflections at their contacts (fig. G5; see also Catchings and others, this volume, chap. I, figs. I9 and I11).

Figure G5 shows that the contact between the synimpact and postimpact deposits is marked by an abrupt major change in the velocity, from high (top synimpact) to low (first postimpact); this velocity change creates the positive seismic reflection at the top of the synimpact sediments. The upper part of the synimpact deposits clearly shows three strong positive reflections and, when correlated with the marine seismic data, indicates that Powars and Bruce's (1999) seismic interpretation of the first postimpact unit, the Chickahominy Formation, actually represents the uppermost synimpact deposits.

All the marine seismic images across the crater's western annular trough show that most of the postimpact sediments have a low dip toward the central crater (fig. G6) and that numerous extensional collapse structures disrupt synimpact and postimpact sediments (Poag and others, 2003). Most of the collapse structures are bounded by zones of faulting that appear to extend down into the basement, and some appear to be rooted by detachment zones within the slumping sedimentary section. Powars and others (2003) suggested that these structures appear to be concentrated into three structural rings in the annular trough and that their inner edges are at about 8, 15, and 22 km (5, 9, and 14 mi) from the margin of the central crater. The high-resolution seismic survey (Catchings and others, this volume, chap. I) shows that the Langley corehole is almost centered on one of these extensional collapse structures; at the corehole site, only the synimpact sediments beneath the multiple tsunami and postimpact sediments appear to be significantly deformed.

Physical Stratigraphy of Postimpact Deposits in the USGS-NASA Langley Corehole

The postimpact deposits in the USGS-NASA Langley core consist of 235.65 m (773.12 ft) of upper Eocene to Quaternary deposits that buried the crater and the synimpact deposits. Except for some Pleistocene fluvial-estuarine deposits, the postimpact deposits are primarily marine shallow-shelf clays,

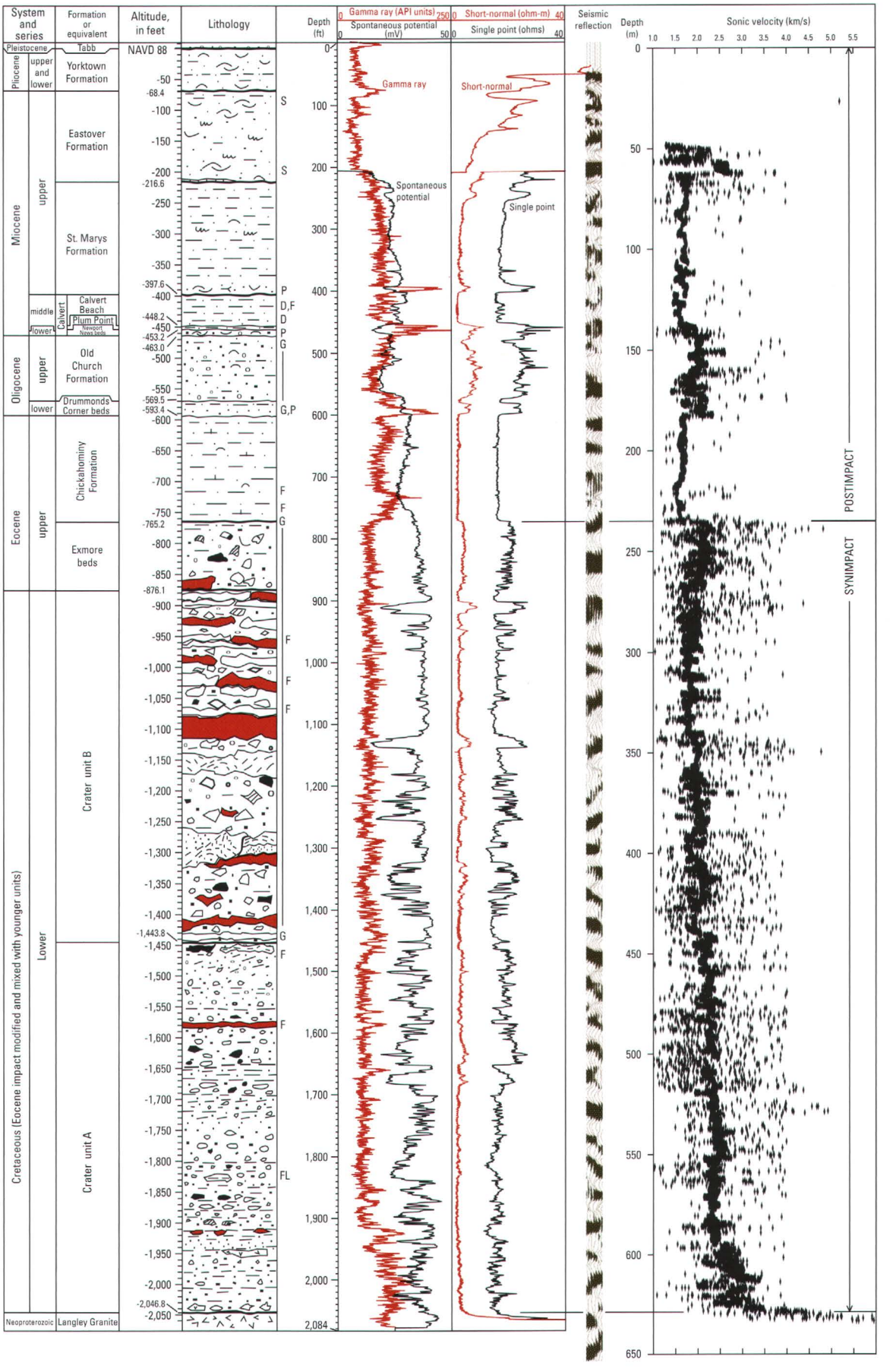
System and series
Formation or equivalent
Altitude, in feet
Lithology
Depth (ft)
Gamma ray (API units)
Spontaneous potential (mV)
Short-normal (ohm-m)
Single point (ohms)
Seismic reflection
Depth (m)
Sonic velocity (km/s)
Pleistocene
Pliocene
upper and lower
Tabb
Yorktown Formation
Miocene
upper
Eastover Formation
St. Marys Formation
middle
lower
Calvert
Calvert Beach
Plum Point
Newport News beds
Oligocene
upper
lower
Old Church Formation
Drummonds Corner beds
Eocene
upper
Chickahominy Formation
Exmore beds
Cretaceous (Eocene impact modified and mixed with younger units)
Lower
Crater unit B
Crater unit A
Neoproterozoic
Langley Granite
NAVD 88
Gamma ray
Spontaneous potential
Short-normal
Single point
POSTIMPACT
SYNIMPACT

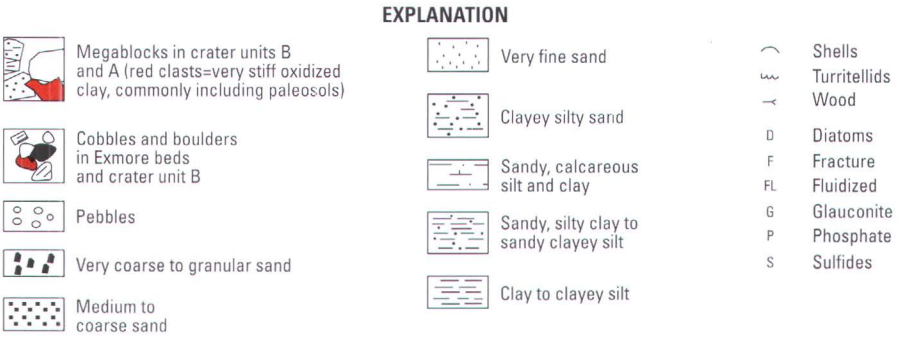

Figure G5 (above and facing page). Stratigraphic column for the USGS-NASA Langley corehole showing correlation with high-amplitude positive seismic reflections and geophysical logs, including gamma-ray, spontaneous-potential, single-point-resistance, short-normal-resistance, and sonic velocity logs. The seismic-reflection column is from Catchings and others (this volume, chap. I, fig. I9); high-amplitude positive reflections are black. Definitions: ft, feet; km/s, kilometers per second; m, meters; mV, millivolts; NAVD 88, North American Vertical Datum of 1988; ohm-m, ohm-meters.

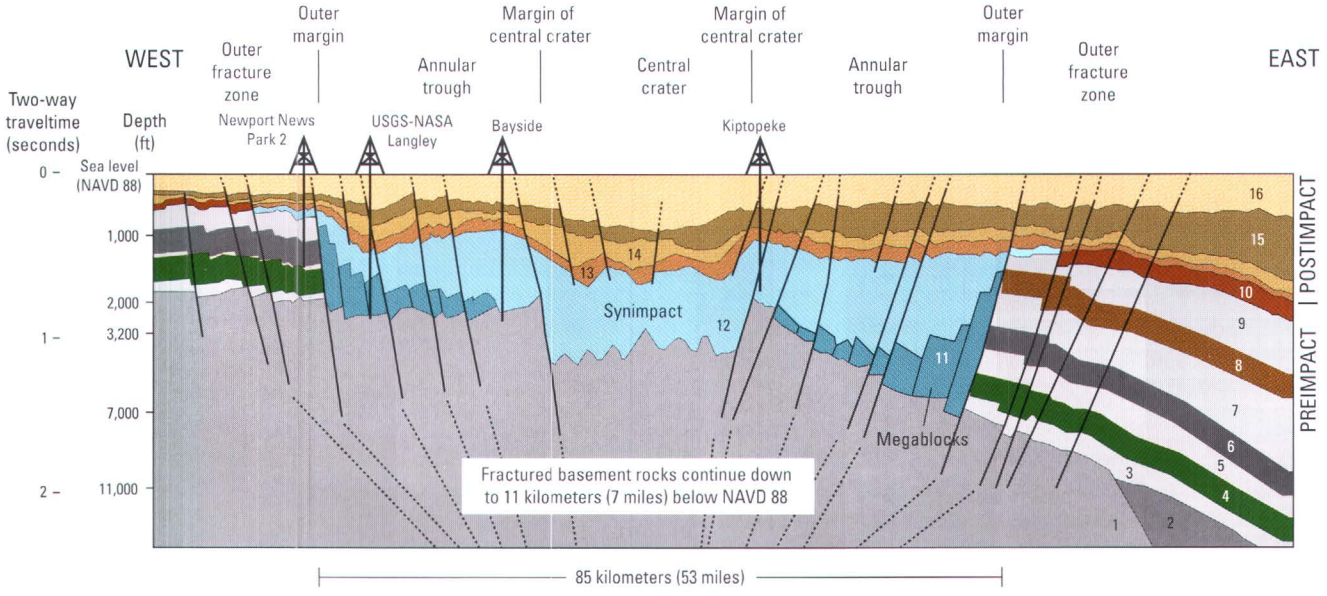

LAYERS

1 Crystalline basement
2 Norfolk rift basin (Triassic)
3–9 Preimpact Cretaceous deposits
10 Preimpact lower Tertiary deposits
11 Synimpact slumped megablocks
12 Synimpact resurge deposits mixed with slumped megablocks
13 Uppermost synimpact deposits and postimpact upper Eocene clays and silts
14 Postimpact Oligocene to lower Miocene deposits
15 Postimpact middle Miocene deposits
16 Postimpact upper Miocene to Holocene deposits

Figure G6. Generalized cross section of the buried Chesapeake Bay impact structure; postimpact sediment geometry and distribution are generalized from scaled marine seismic images and corehole stratigraphic data modified from Powars and Bruce (1999). Corehole locations are shown in figure G1.

silts, and very fine to very coarse sands that may include diatomaceous, glauconitic, shelly, and thin calcium-carbonate-cemented intervals. Microfauna, macrofauna, and flora indicate marine to restricted-marine paleoenvironments.

Correlation of the postimpact units with a 1-km-long (0.62-mi-long) high-resolution seismic-reflection profile at the NASA Langley Research Center indicates (1) that the postimpact stratigraphic units here produce relatively horizontal continuous reflections typical of marine strata, (2) that a good correlation exists between positive black reflections and lithic changes that correspond to stratigraphic contacts, and (3) that stratigraphic units having different lithologies are indicated by obvious to subtle changes in the seismic character of the reflections (seismic signature). Some disturbed zones (fractures and faults) are present in the postimpact section, but they are much less common than in the underlying synimpact deposits.

The postimpact stratigraphic record in the Langley core shows numerous cycles of deposition, erosion, and periods of high and low sedimentation rates. These cycles were created by the interactions among global sea level, sediment supply, accommodation, regional to local tectonic activity, and impact (structural subsidence or uplift) influences. Because the impact was on a dipping shallow shelf, it created a unique depositional environment with a deepwater circular basin surrounded mostly by a shallow-shelf setting. For the first few million years, a bathyal depositional environment existed inside the crater.

In the Langley corehole, which is located on the southwestern updip side of the outer annular trough, the bathyal deposits are mostly overlain by postimpact deposits that represent transgressive and highstand depositional environments in inner to middle neritic water depths; these postimpact deposits include evidence for periods of continuous deposition and for other periods punctuated by changes resulting in numerous unconformities. Such unconformities are generally created when sea level rises and high-energy waves erode and rework the previous highstand deposits. The most resistant material (bone, teeth, phosphate, wood, and shells) is generally concentrated into the basal lag deposit formed after a rise in sea level. Most of the unconformable contacts between postimpact stratigraphic units in the Langley core are marked by sandy basal lag deposits that sharply overlie and are burrowed down into much finer grained clay and silt deposited during a previous highstand.

Postimpact deposits in the USGS-NASA Langley core include, in ascending order, the following units: the very clayey, calcareous Chickahominy Formation (upper Eocene); the glauconitic, phosphatic, and partly shelly lithologies of both the Drummonds Corner beds (upper lower Oligocene) and the Old Church Formation (upper Oligocene); the shelly and sandy beds of the Calvert Formation (lower Miocene); the primarily siliciclastic, fine-grained part of the Calvert Formation (middle Miocene), the St. Marys Formation (upper Miocene), and the lower part of the Eastover Formation (upper Miocene); the siliciclastic, locally glauconitic, fine- to coarse-grained, fossiliferous upper part of the Eastover Formation (upper Miocene) and the Yorktown Formation (lower and upper Pliocene); and the fluvial to estuarine Tabb Formation (upper Pleistocene). The stratigraphy of the Langley core's postimpact sedimentary units above the synimpact sedimentary debris is provided in table G2 and figure G7, and the lithology is described in appendix G1. The ages indicated for these units are derived primarily from biostratigraphic analyses of microfossils from the Langley core (Edwards and others, this volume, chap. H).

Chickahominy Formation (Upper Eocene)

The upper Eocene Chickahominy Formation is the oldest postimpact deposit found above synimpact deposits throughout the southern Chesapeake Bay area. In the Langley core, the Chickahominy Formation extends from a sharp but conformable contact with the underlying Exmore beds at 235.65 m (773.12 ft) (fig. G8) upward to a burrowed contact with the overlying upper lower Oligocene Drummonds Corner beds at 183.3 m (601.3 ft) (fig. G9); accordingly, the Chickahominy section in the Langley core is 52.3 m (171.8 ft) thick.

At the lower contact, very tight clay with scattered horizontal thin (millimeter-scale) silt to very fine sand laminae of the Exmore beds contains only reworked, mixed-age microfossils and is overlain by massive silty clay of the Chickahominy, which contains in situ and reworked macrofossils and microfossils. The silt-laminated clay represents the final settling of sediments disturbed by the impact and, thus, constitutes the uppermost part of the synimpact Exmore beds (for more details, see figure G9; Poag and Norris, this volume, chap. F; and Edwards and others, this volume, chap. H).

The upper contact of the Chickahominy is lithologically sharp and strongly burrowed. Coarse-grained phosphatic and glauconitic quartz sand of the Drummonds Corner beds fills burrows that extend down 0.7 m (2.2 ft) into the silty clay of the Chickahominy.

The Chickahominy Formation in the Langley core consists primarily of homogeneous, generally bioturbated, very compact, massive to thin-bedded, olive-gray, clayey silt to silty clay, which contains abundant microfossils and scattered macrofossils. It contains variable amounts of fine-sand- to silt-sized, primarily black to dark-green glauconite, mica, finely crystalline iron sulfides, and coarser grained pyrite. The Chickahominy section in the Langley core is generally similar lithologically to other Chickahominy sections found throughout the region (Powars and Bruce, 1999).

A pyrite-filled fracture dipping moderately at about 45° was found in the core at 230.0 to 229.9 m (754.7 to 754.4 ft) depth (fig. G10). This is the first core sample that recovers actual fractures and faults seen in the seismic-reflection images of the postimpact section (for example, in Poag and others, 1999, and Powars and Bruce, 1999). Several other similarly

Table G2. Stratigraphic contact depths and thicknesses of the postimpact sediments in the USGS-NASA Langley core.

Stratigraphic unit	Top (m)	Top (ft)	Base (m)	Base (ft)	Thickness (m)	Thickness (ft)	Series
Lynnhaven Member of Tabb Formation	0.0	0.0	2.2	7.2	2.2	7.2	upper Pleistocene
Yorktown Formation	2.2	7.2	23.3	76.3	21.1	69.1	Pliocene
Eastover Formation	23.3	76.3	68.4	224.5	45.2	148.2	upper Miocene
St. Marys Formation	68.4	224.5	123.6	405.5	55.2	181.0	upper Miocene
Calvert Formation	123.6	405.5	143.5	470.9	19.9	65.4	lower and middle Miocene
Calvert Beach Member	123.6	405.5	139.0	456.1	15.4	50.6	middle Miocene
Plum Point Member	139.0	456.1	140.5	461.1	1.5	5.0	middle Miocene
Newport News beds	140.5	461.1	143.5	470.9	3.0	9.8	lower Miocene
Old Church Formation	143.5	470.9	176.0	577.4	32.5	106.5	upper Oligocene
Drummonds Corner beds	176.0	577.4	183.3	601.3	7.3	23.9	upper lower Oligocene
Chickahominy Formation	183.3	601.3	235.65	773.12	52.3	171.8	upper Eocene

angled fractures with slickensides were found in the Chickahominy section of the Langley core (fig. G10).

The fine-grained Chickahominy section is represented by a distinctive, flat, low-value signature on borehole resistivity logs (fig. G7); it is easily differentiated from the irregular, higher resistivity signature typical of the underlying Exmore beds (except for the thin, 0.27-m-thick (0.9-ft-thick) capping fine-grained interval in the Exmore beds discussed above). The irregular, higher resistivity signature of the overlying, much sandier Drummonds Corner beds also is relatively easy to distinguish from the flat resistivity signature of the Chickahominy. The contact with the overlying Drummonds Corner beds also is marked on the natural-gamma-ray log by an increase in radioactivity in the phosphatic basal lag deposits of the Drummonds Corner beds relative to the values recorded for the Chickahominy section (fig. G7). Variations in the natural-gamma-ray log within the Chickahominy strata reflect differences in the phosphate and glauconite content (Poag and Norris, this volume, chap. F), and the resistivity logs reflect differences in the content of silt-clay and sandy silt. The lower part (about 12 m (40 ft)) of the Chickahominy has relatively high gamma-ray-log values indicating increased phosphate. This higher gamma-ray signature for the lower Chickahominy is prevalent in all of the corehole and water-well logs from the southwestern outer annular trough and the surrounding outer fracture zone.

A distinctive suite of microfossils is found in the Chickahominy Formation, indicating a late Eocene age for this unit, which is based on calcareous nannofossil Zones NP 19/20 and NP 21 and planktonic foraminiferal Zones P15, P16, and P17 (Edwards and others, this volume, chap. H; Poag and Norris, this volume, chap. F). The Chickahominy section in the Langley core represents continuous bathyal deposition from the cessation of synimpact deposition at 35.2±0.3 Ma (age based on argon-40/argon-39 plateau ages of tektites inferred to result from the Chesapeake Bay impact; Obradovich and others, 1989; Poag, Powars, Poppe, and Mixon, 1994) to 35.3±0.1 Ma (age from Horton and Izett, this volume, chap. E) to 33.7 Ma or before (age from the time scale of Berggren and others, 1995). The lower contact of the Chickahominy is conformable, whereas the upper contact is an unconformity that represents a hiatus of 3.8 m.y. (Edwards and others, this volume, chap. H).

Paleoenvironmental analysis of the Chickahominy fauna and flora in the Langley core (see Poag and Norris, this volume, chap. F; and Edwards and others, this volume, chap. H) indicates that the Chickahominy sediments were deposited in a quiet-water, low-oxygen, marine environment with water depths of approximately 300 m (984 ft). The deepest water paleodepth detected from the fossil assemblages appears to be at a depth of 221.7 m (727.4 ft) in the core.

Drummonds Corner Beds (Upper Lower Oligocene)

Lower Oligocene deposits are present in the Langley core from the unconformable contact with the Chickahominy strata at 183.3 m (601.3 ft) depth to a burrowed unconformity with the overlying upper Oligocene Old Church Formation at 176.0 m (577.4 ft) depth (figs. G9, G11, and G12). The Drummonds Corner beds (upper lower Oligocene) are herein described and informally named to distinguish them from the stratigraphically older and lithically similar lower Oligocene Delmarva beds of Powars and others (1992).

Oligocene units in general, and lower Oligocene units in particular, are poorly known from the Virginia Coastal Plain.

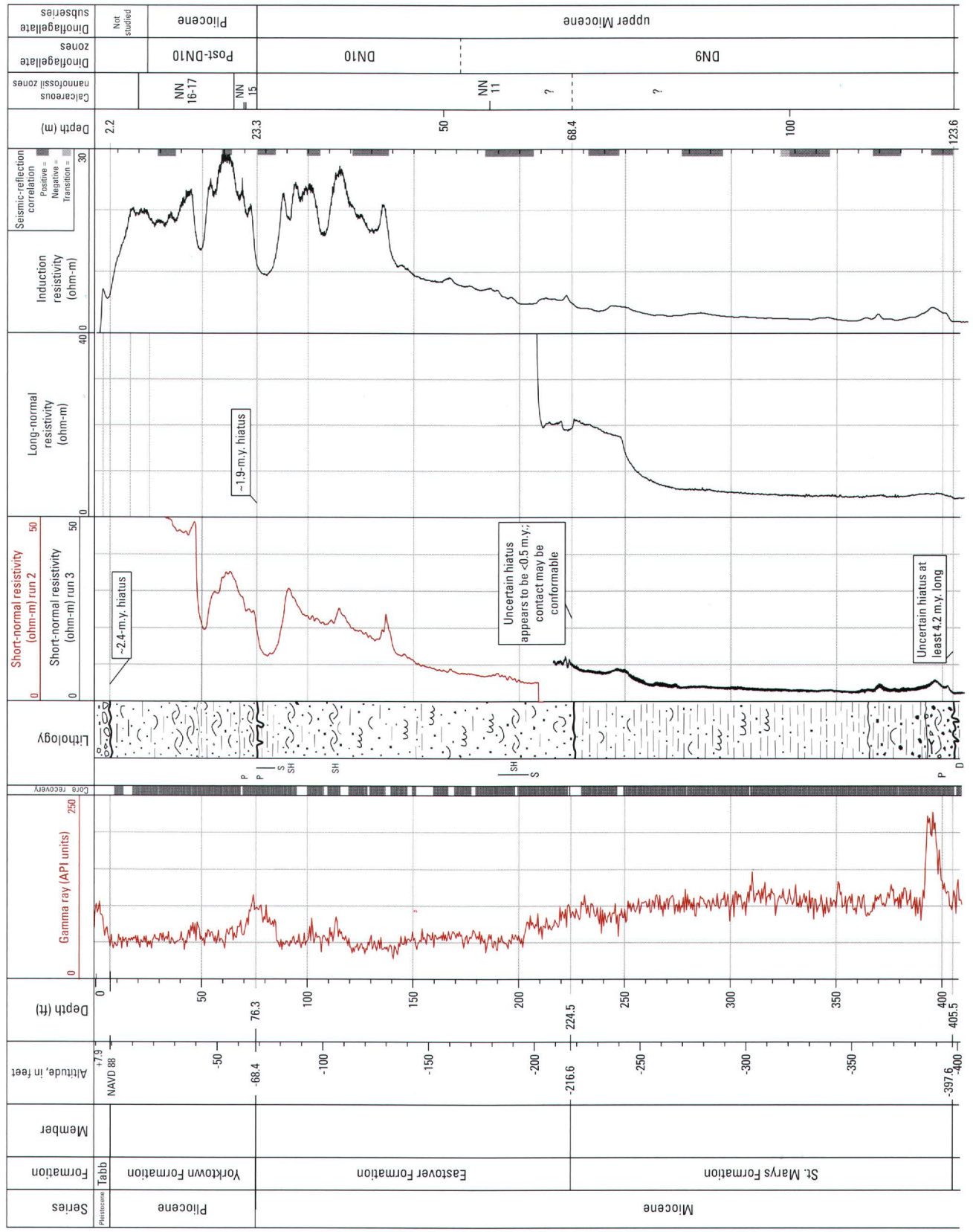

Figure G7. Lithostratigraphic column and selected geophysical logs of the postimpact section of the USGS-NASA Langley corehole showing major lithic breaks. Key nannofossil and dinoflagellate age data and hiatus lengths are from Edwards and others (this volume, chap. H). Definitions: ft, feet; m, meters; m.y., million years; NAVD 88, North American Vertical Datum of 1988; ohm-m, ohm-meters.

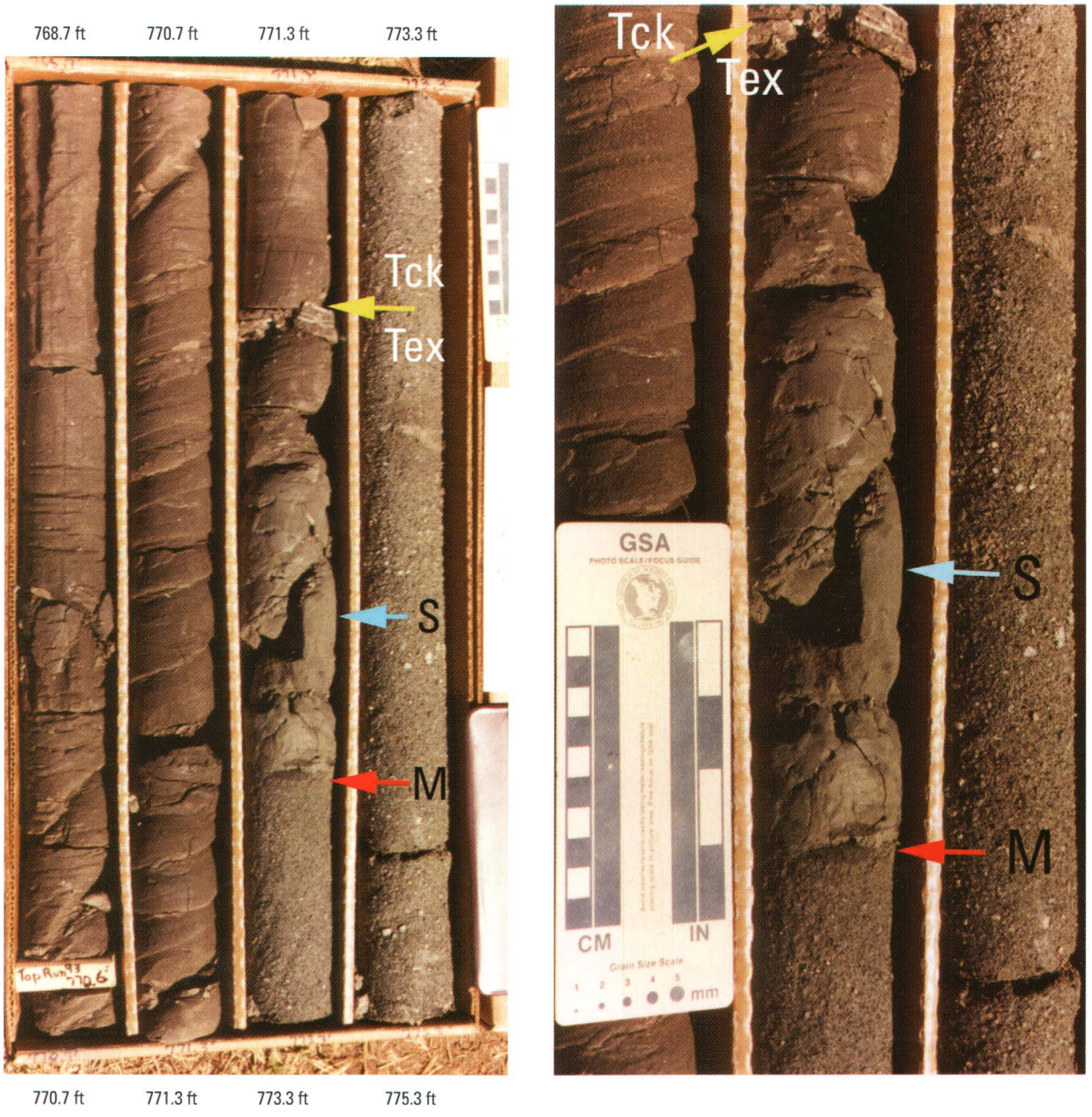

Figure G8. Photographs of the USGS-NASA Langley core showing the conformable contact at 235.65 m (773.12 ft) depth (top arrow) between the synimpact Exmore beds (Tex) and the overlying Chickahominy Formation (Tck). The photograph on the right is a closeup view of part of the core shown in the photograph on the left. In this core, the top of the Exmore beds includes a thin, fine-grained interval that is 0.27 m (0.9 ft) thick. Millimeter-scale pyrite lattices (labeled S for sulfides) were described by Poag (2002b) near the top of a 0.085-m-thick (0.28-ft-thick) basal silt layer between depths of 236.0 and 235.9 m (774.03 and 773.75 ft). Above the basal silt layer, the sediments abruptly change to very tight gray clay (which changes to dark-green-gray clay in the uppermost 0.19 m (0.63 ft)); the clay contains scattered horizontal, very thin (millimeter-scale) silt to very fine sand laminae and a few burrows(?) filled by coarser grained "Exmore matrix"; apparently, the matrix was moved from below by an early postimpact burrowing organism. The silt layer overlies the typical polymict matrix of the Exmore beds (labeled M); note dark-gray clast at contact. Top of core is at upper left. Depths handwritten on the core boxes in feet are repeated in type for clarity.

Figure G9. Composite and closeup photographs of the USGS-NASA Langley core showing the burrowed contact interval between the Chickahominy Formation (Tck) and the unconformably overlying Drummonds Corner beds (Tdc). This unconformity represents a 3.8-m.y. hiatus. The photograph on the right is a closeup view of part of the core shown in the photograph on the left; the core was slightly turned between photographs. Fine-grained marine sediments of the Chickahominy are overlain by quartz-glauconite sand of the Drummonds Corner beds. The arrow is at the formation contact at 183.3 m (601.3 ft) depth. Top of core is at upper left. Nominal core diameter is 6.1 centimeters (cm; 2.4 inches (in.)). Depths handwritten on the core boxes in feet are repeated in type for clarity.

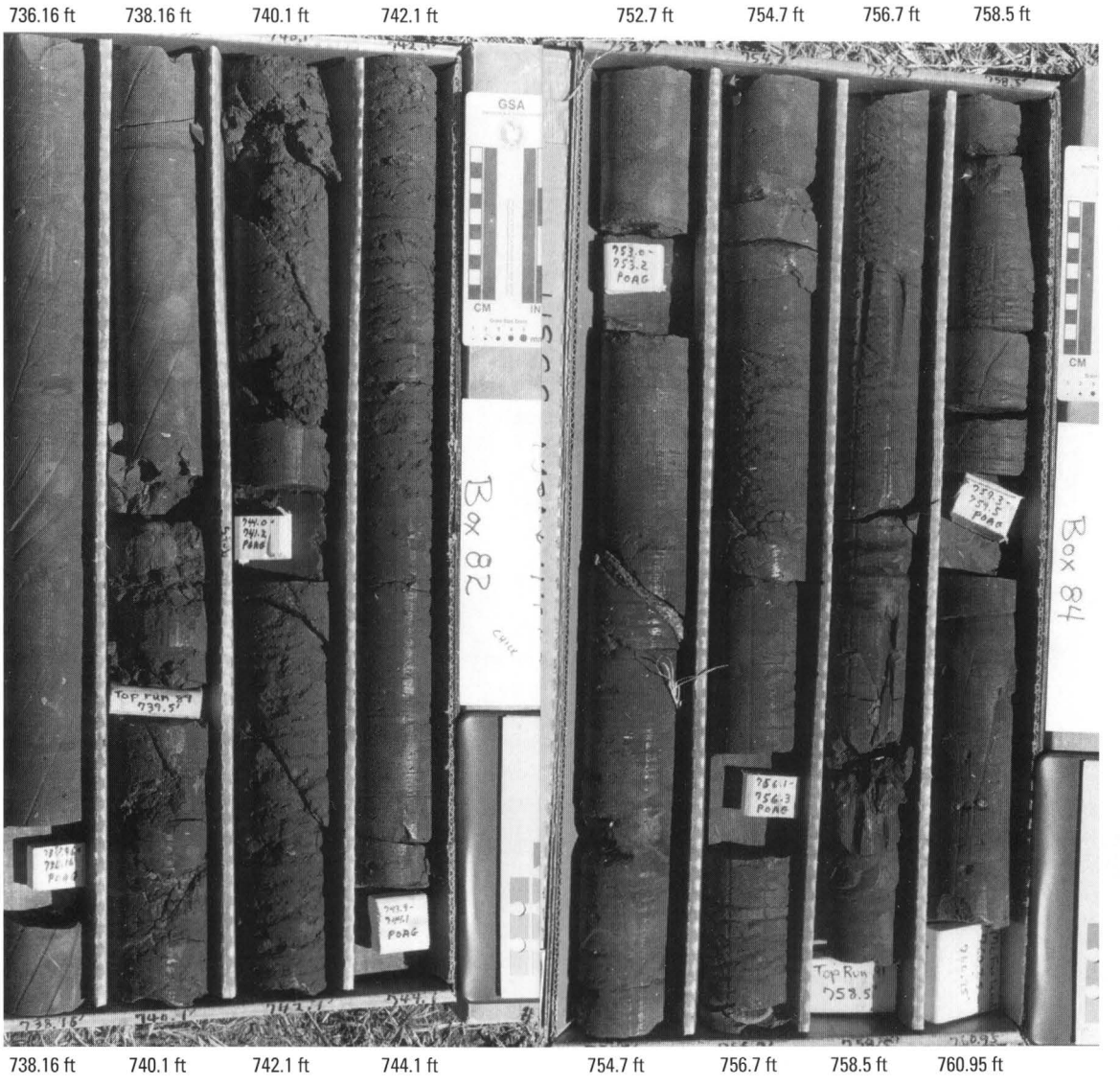

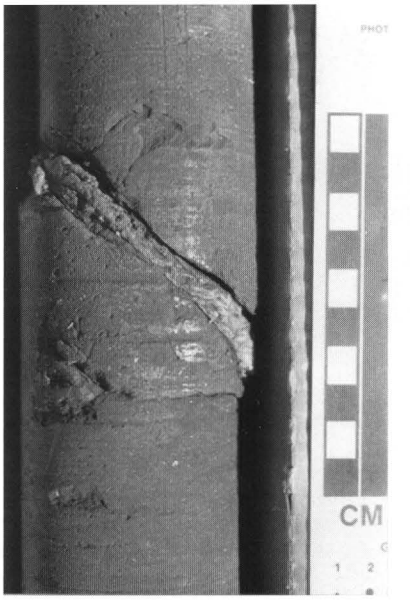

Figure G10. Photographs of the USGS-NASA Langley core showing fractures at 45°–55° angles with slickensides and a pyritized fault gouge filling of a moderately dipping fault in the Chickahominy Formation. The photograph on the bottom is a closeup view of part of the core shown in the photograph above. The fractured interval is between 225.4 and 226.2 m (739.5 and 742.0 ft) depth; the fault shown in the closeup goes from 230.0 to 229.9 m (754.7 to 754.4 ft) depth. The fault corresponds to a change in the resistivity logs (fig. G7) at that depth. Depths handwritten on the core boxes in feet are repeated in type for clarity.

Figure G11. Composite photograph of the USGS-NASA Langley core from depths of 179.8 to 182.3 m (590.0 to 598.2 ft) showing highly burrowed, muddy to coarser grained quartz-glauconitic basal sands of the Drummonds Corner beds. Top of core is at upper left; core in upper left corner of box is from 3.4 m (11.3 ft) above the basal contact. Nominal core diameter is 6.1 cm (2.4 in.). Depths handwritten on the core boxes in feet are repeated in type for clarity.

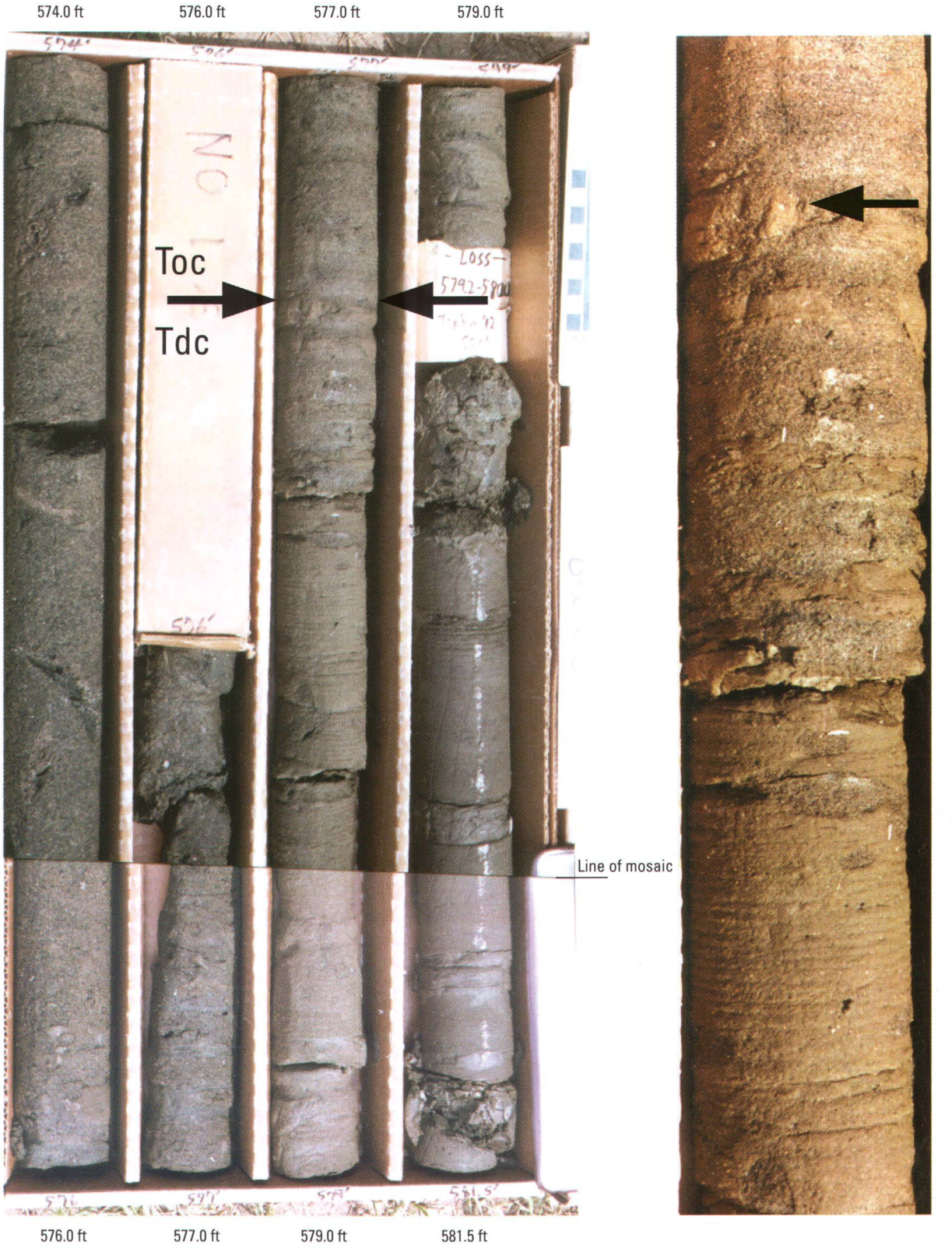

Figure G12. Composite and closeup photographs of the USGS-NASA Langley core showing (at the arrows) the unconformable burrowed contact at 176.0 m (577.4 ft) depth between the muddy finer grained sediments of the uppermost Drummonds Corner beds (Tdc) and the overlying much coarser grained quartz-glauconitic sands of the Old Church Formation (Toc). Top of core is at upper left. Nominal core diameter is 6.1 cm (2.4 in.). Depths handwritten on the core boxes in feet are repeated in type for clarity. Color differences between the composite and closeup photographs are due to lighting changes.

The first report of lower Oligocene sediments was the description of the informal Delmarva beds by Powars and others (1992) from the Exmore core, Northampton County, Va. They reported (p. 95) "as much as" 12.5 m (41 ft) of lower Oligocene sediments overlain by 13.7 m (45 ft) of incompletely recovered sediments that they tentatively assigned to the Old Church Formation. Powars and Bruce (1999) and Powars (2000) recognized the Delmarva beds in additional cores and wells in the Virginia Coastal Plain. However, in these sections, they included material that would now be placed in the Drummonds Corner beds and that in places overlies thin deposits correlative with the original Delmarva beds. In addition, the upper part of the Oligocene section in the Exmore core that they assigned to the Old Church Formation would now be placed in the Drummonds Corner beds. Powars and Bruce (1999) observed that the lower 5.2 m (17 ft) of their Old Church Formation in the Exmore core was early Oligocene in age, not late Oligocene, and suggested that this material should be included with the Delmarva beds (although they did not include it in the Delmarva beds in their tables).

In the subsurface of the Virginia Coastal Plain, we now recognize three Oligocene units; from oldest to youngest, they are the Delmarva beds, the Drummonds Corner beds, and the Old Church Formation. Determination of the biostratigraphy of all three units is complicated by the prevalence of fossil reworking within the postimpact crater section.

The lowest unit, the Delmarva beds, is present in only a few cores and is placed in the lower part of the lower Oligocene represented by planktonic foraminiferal Zones P18–P20 (undifferentiated, Powars and others, 1992). The Delmarva beds also contain palynomorphs that are restricted to the lower part of the Rupelian Stage (including the acritarch *Ascostomocystis potana,* according to L.E. Edwards, USGS, unpub. data, 1987 and 2004; the assignment of *A. potana* to the Rupelian follows Stover and Hardenbol (1993)).

The middle unit, the Drummonds Corner beds, is placed in the upper part of the lower Oligocene. It is placed in foraminiferal Zone P21a (Powars and others, 1992; Powars and Bruce, 1999) and in calcareous nannofossil Zone NP 24. It also contains palynomorphs whose overlapping ranges indicate placement in the upper part of the Rupelian Stage (Edwards and others, this volume, chap. H). Both the Delmarva beds and the Drummonds Corner beds are glauconitic, phosphatic sands and silts.

The upper unit, the Old Church Formation, is placed in the upper Oligocene (calcareous nannofossil Zone NP 24 and perhaps Zone NP 25). It contains palynomorphs that indicate placement in the upper part of the upper Oligocene (to lowest Miocene) and is therefore in the Chattian Stage (Edwards and others, this volume, chap. H).

In the Langley core, the upper lower Oligocene Drummonds Corner beds consist of microfossiliferous, quartz-glauconite sand near their base that becomes muddier upward, as indicated by the resistivity logs (fig. G7). At its base, the unit consists of very poorly sorted sand with scattered phosphate pebbles that sharply overlies and is burrowed down into the much finer grained Chickahominy strata. Figure G11 illustrates dense burrows characteristic of the Drummonds Corner beds.

Biostratigraphic analysis of the Drummonds Corner beds indicates that this unit is early Oligocene or early late Oligocene; it contains calcareous nannofossils that indicate assignment to Zone NP 24. Hence, these deposits are no older than early Oligocene (29.9 Ma) and no younger than early late Oligocene (28.5 Ma). The basal unconformity of the Drummonds Corner beds represents a 3.8-m.y. hiatus. The time span of the hiatus at the upper unconformity is uncertain, as both the Drummonds Corner beds and overlying Old Church Formation are within the same calcareous nannofossil zone (Edwards and others, this volume, chap. H); the hiatus is probably less than 0.5 m.y. long.

Paleoenvironmental analysis indicates that the Drummonds Corner beds represent deposition in shallower water and more nearshore environments than existed during deposition of the underlying Chickahominy deposits. The fish teeth in the Drummonds Corner beds are from species that are common to a subtropical climate (Edwards and others, this volume, chap. H).

Old Church Formation (Upper Oligocene)

In the Langley core, the interval from the contact at 176.0 m (577.4 ft) depth to the contact at 143.5 m (470.9 ft) depth is assigned to the Old Church Formation (figs. G12, G13, and G14). This 32.5-m-thick (106.5-ft-thick) section consists of intensely burrowed, poorly sorted, gray-olive to dark-green and black, shelly, microfossiliferous, fine to very coarse, glauconitic and phosphatic quartz sand generally in a clay-silt matrix. These beds locally include better sorted, finer grained, sandy clay-silts or thin, sandy, indurated layers. Granules of quartz, glauconite, and phosphate are scattered throughout along with minor amounts of pyrite, carbonaceous material (including wood), and occasional very small teeth from sharks. The burrows vary in size and orientation and include clay-lined, clay-filled, and sand-filled types.

The Old Church section consists of six fining-upward packages (fig. G13*A*). Burrowed sand-over-clay contacts are visible in the core at depths of 161.2 m (529.0 ft), 160.2 m (525.5 ft), 155.8 m (511.0 ft), and 154.5 m (507 ft); two are shown in figure G13*B*. Another contact is inferred to be present at 166.1 m (545.0 ft) because of the resistivity log (fig. G7). These fining-upward packages are represented on the resistivity log by upward decreases in resistivity that track the upward gradation from lower, better sorted sands to higher, clayey and silty sands.

Dinoflagellates and calcareous nannofossils indicate placement in calcareous nannofossil Zones NP 24 and NP 25 or their chronozones and, hence, a late Oligocene age for the Old

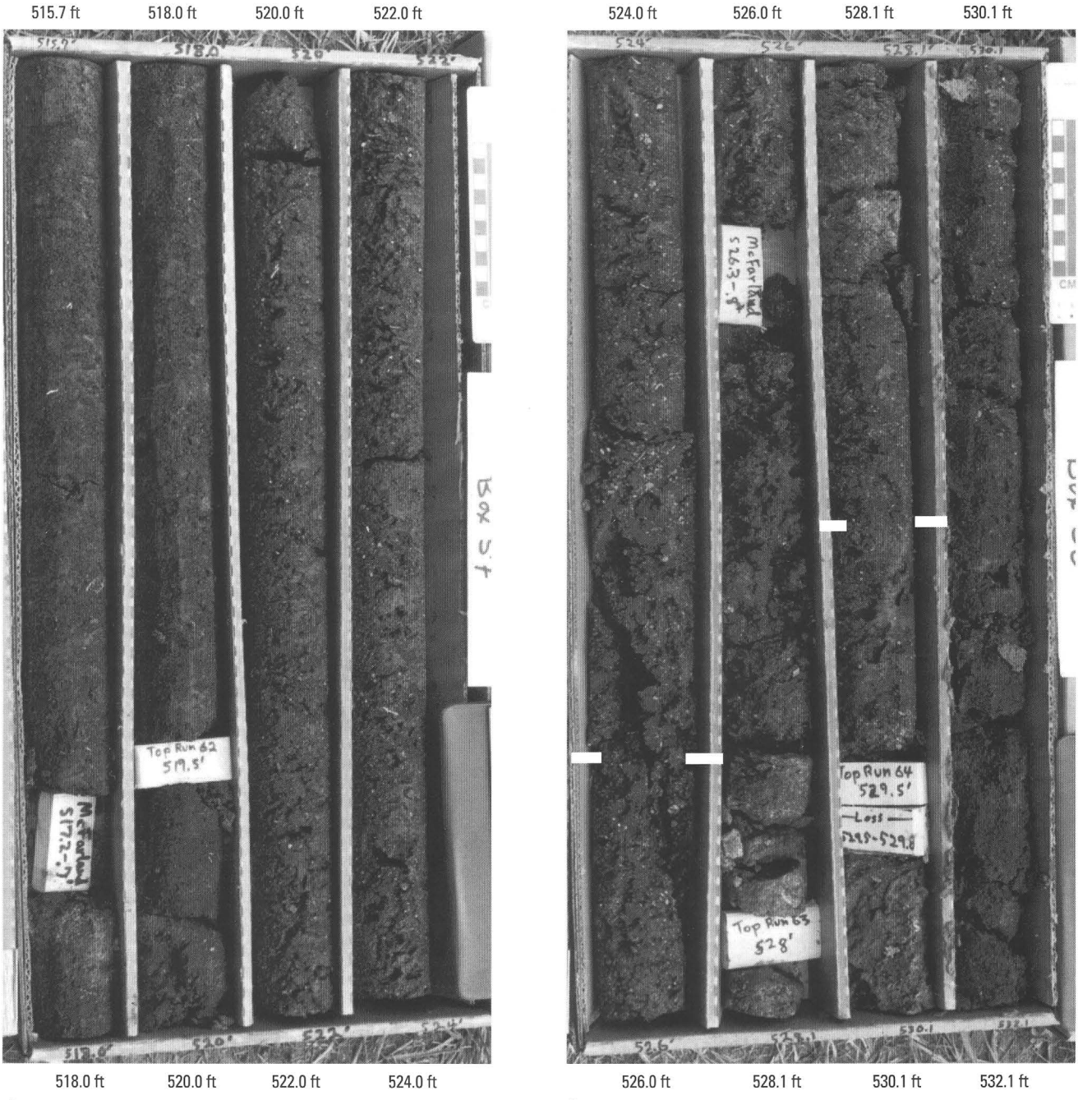

Figure G13. Photographs of the USGS-NASA Langley core showing fining-upward subunits typical of the Old Church Formation in the Langley core. Top of core is at upper left. *A*, Transition upward at about 158 m (520 ft) depth from sandier to muddier sediments within one of the subunits. *B*, Subtle lithic contacts (short lines) between subunits at 161.2 and 160.2 m (529.0 and 525.5 ft) depth, where much coarser grained quartz-glauconitic sands are overlying and burrowed down into muddy, finer grained matrix-supported sediments. Depths handwritten on the core boxes in feet are repeated in type for clarity.

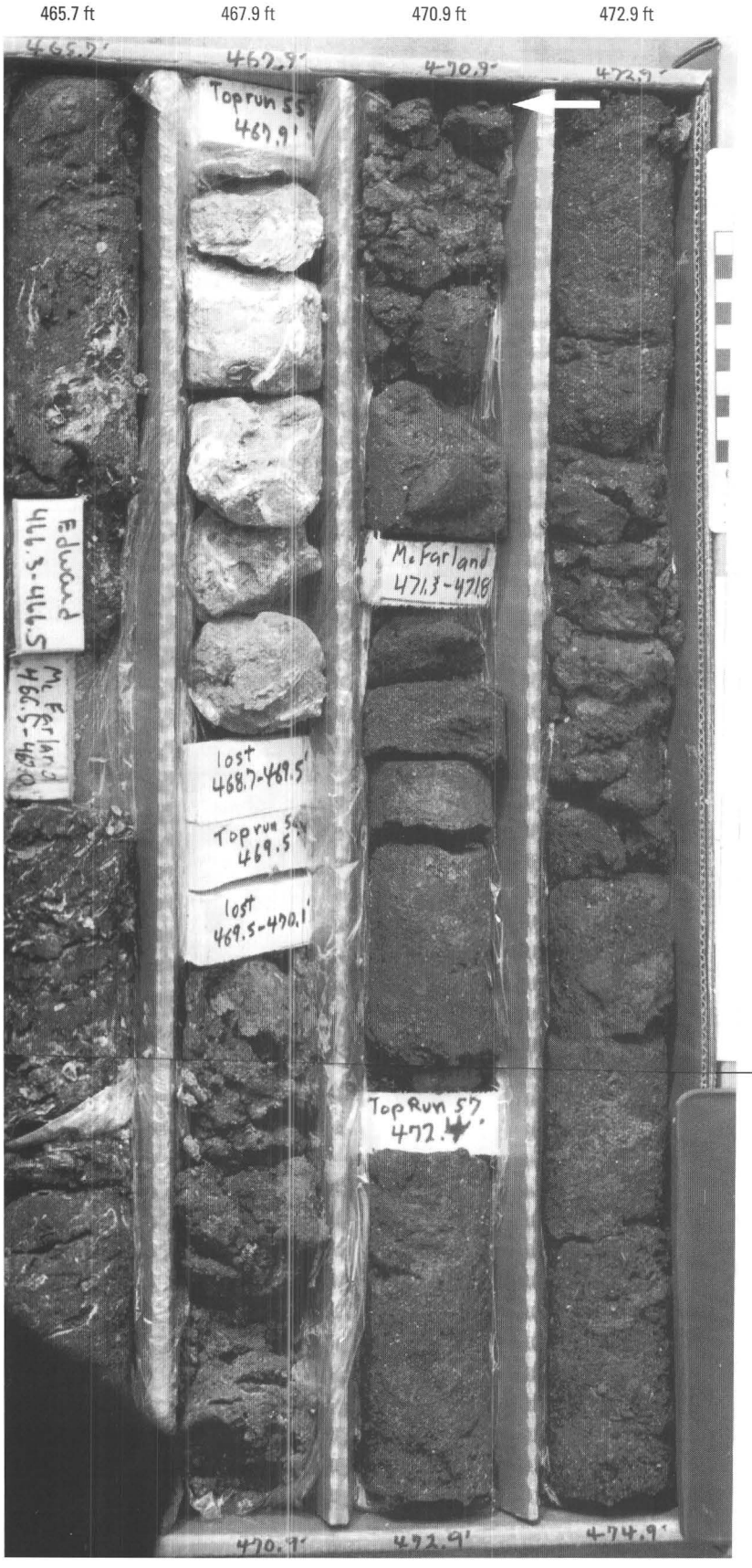

Figure G14. Composite photograph of the USGS-NASA Langley core showing the unconformable contact at 143.5 m (470.9 ft) depth (arrow) between fine-grained marine deposits of the Old Church Formation and overlying shelly and locally cemented marine sediments of the Newport News beds of the Calvert Formation. Top of core is at upper left. Nominal core diameter is 6.1 cm (2.4 in.). Depths handwritten on the core boxes in feet are repeated in type for clarity.

Church Formation. The type section of the Old Church is in Zone NP 25 according to Bybell and Gibson (1994). The duration of the interval represented by the lower unconformity is uncertain but not more than 0.5 m.y.; the upper unconformity represents at least a 3.9-m.y. hiatus (Edwards and others, this volume, chap. H).

Paleoenvironmental analysis of the Old Church fauna and flora in the Langley core indicates that this unit was deposited in nearshore to middle-outer shelf water depths in a subtropical to tropical climate.

Calvert Formation (Lower and Middle Miocene)

The lower and middle Miocene Calvert Formation is present from 143.5 m (470.9 ft) depth to 123.6 m (405.5 ft) depth in the Langley core (figs. G14, G15, and G16). The Calvert Formation in the Langley core can be subdivided (in ascending order) into the lower Miocene Newport News beds, a middle Miocene portion of the Plum Point Member, and the middle Miocene Calvert Beach Member.

Newport News Beds (Lower Miocene)

Lower Miocene sediments unconformably overlie the glauconitic and phosphatic sand of the Old Church Formation in the Langley core between depths of 143.5 and 140.5 m (470.9 and 461.1 ft); they have a thickness of 3.0 m (9.8 ft). These lower Miocene sediments consist of partially indurated to indurated, poorly sorted, bioclastic, very coarse phosphatic quartz sand that is assigned to the Newport News beds of the Calvert Formation (Powars and Bruce, 1999) (figs. G14 and G15). Coarse phosphatic sand of the Plum Point Member of the Calvert Formation unconformably overlies the Newport News beds.

Differentiation of these thin, shelly, Miocene sand units from each other and from the Old Church Formation is facilitated by the analysis of the geophysical logs. Basal transgressive lag deposits of marine units typically concentrate uranium- and thorium-bearing phosphatic material (nodules, sharks' teeth, bone) that create "spikes" or "hot kicks" (high values) on natural-gamma-ray logs. These lag deposits also produce "sand kicks" (high values) on resistivity logs. Figure G7 shows this geophysical signature opposite the basal lag deposits of all stratigraphic units from the lower Oligocene Drummonds Corner beds to the upper Miocene St. Marys Formation.

Calcareous nannofossils and dinoflagellates indicate an early Miocene age for the Newport News beds in the Langley core and assignment to calcareous nannofossil Zones NN 2–4 and dinoflagellate subzone DN2b (Edwards and others, this volume, chap. H). De Verteuil (1997) calibrated subzone DN2b at 20.0 to 19.4 Ma. Powars and Bruce (1999) reported a strontium-isotope date of 20.1 Ma for shells in correlative strata from the nearby Newport News Park 2 corehole. Data indicate (Edwards and others, this volume, chap. H) that the basal unconformity represents at least a 3.9-m.y. hiatus and that the upper unconformity represents an apparent 2.7-m.y. hiatus.

The fauna and flora indicate deposition of the Newport News beds in nearshore to shallow-shelf water depths during a paleoclimate period that was somewhat warmer than the present climate at the Langley site.

Plum Point Member (Middle Miocene Part)

In the Langley core, the Plum Point Member of the Calvert Formation consists of a 1.5-m-thick (5.0-ft-thick), unconformity-bounded, fining-upward interval of shelly, poorly sorted, muddy, fine to very coarse phosphatic quartz sand that grades upward into a 0.3-m-thick (1.0-ft-thick) section of bioturbated, microfossiliferous silt and silty clay. The lower contact at 140.5 m (461.1 ft) depth is at the top of the partially indurated shelly sand of the Newport News beds (fig. G15). The truncated upper contact at 139.0 m (456.1 ft) depth (fig. G15) is between clayey silt to silty clay of the Plum Point Member and very coarse sand with sharks' teeth in the overlying Calvert Beach Member. Burrows filled with Calvert Beach sand penetrate the top of the Plum Point Member.

The Plum Point Member in the Langley core is middle Miocene in age and is assigned to calcareous nannofossil Zones NN 3–5 and to dinoflagellate Zone DN4. The lower unconformity represents an apparent 2.7-m.y. hiatus, and the upper unconformity represents a hiatus of 1.1 to 1.6 m.y. (for details, see Edwards and others, this volume, chap. H). The lower Miocene portion of the Plum Point Member that was present in the Exmore core (Powars and Bruce, 1999) is not present at the Langley site.

Paleoenvironmental analysis of fossil assemblages from the Plum Point Member in the Langley core indicates deposition in nearshore to shallow-shelf water depths and a paleoclimate somewhat warmer than the present climate at the Langley site.

Calvert Beach Member (Middle Miocene)

The Calvert Beach Member of the Calvert Formation in the Langley core is an unconformity-bounded marine unit that consists of dark-greenish-gray to olive-gray, homogeneous, massive to thinly bedded, microfossiliferous, silty clay to clayey silt. Diatoms and foraminifera are abundant and relatively easy to see with a 10x hand lens. Most of the section contains only sparse grains of very fine, angular quartz and pyrite and small percentages of wood fragments, sponge spicules, fish scales, and vertebrae. The Calvert Beach Member is present from depths of 139.0 to 123.6 m (456.1 to 405.5 ft) in the Langley core (figs. G15 and G16). It overlies the middle Miocene Plum Point Member of the Calvert Formation and underlies the upper Miocene St. Marys Formation.

The basal 1.8 m (6 ft) of the Calvert Beach Member fines upward from very coarse phosphatic and glauconitic quartz sand with sharks' teeth, bone, and clay-filled and sand-filled

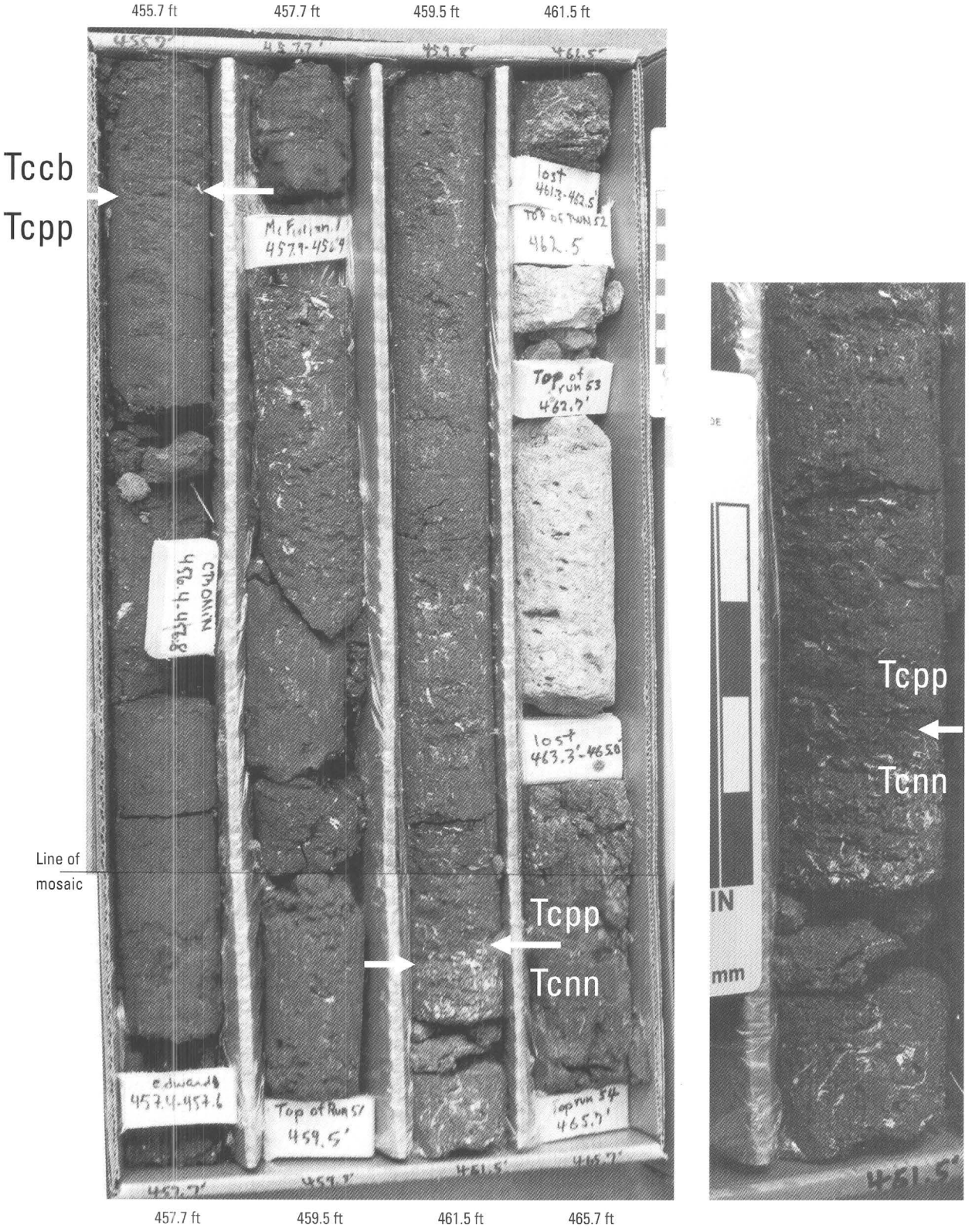

Figure G15. Composite and closeup photographs of the USGS-NASA Langley core showing unconformable Miocene contacts within the Calvert Formation at the top and base of the Plum Point Member. Arrows indicate the contact at 140.5 m (461.1 ft) depth between the Newport News beds (Tcnn, lower Miocene) and the overlying Plum Point Member (Tcpp, middle Miocene). Arrows also indicate the contact at 139.0 m (456.1 ft) depth between the Plum Point Member and the overlying Calvert Beach Member (Tccb, middle Miocene). Top of core is at upper left. The photograph at right is a closeup of the middle Miocene-lower Miocene contact (arrow) shown in the large photograph. Depths handwritten on the core boxes in feet are repeated in type for clarity.

Figure G16. Composite photograph of the USGS-NASA Langley core showing the location of the burrowed contact at 123.6 to 123.9 m (405.5 to 406.8 ft) depth between the finer grained middle Miocene Calvert Beach Member (Tccb) of the Calvert Formation (tray at right) and the overlying basal sands of the upper Miocene St. Marys Formation (Tsm). The contact must be within the core-loss interval indicated by arrows. Sandy burrows of the St. Marys extend down into the top 0.15 m (0.5 ft) of the recovered clay-silt of the Calvert strata. Top of core is at upper left. Nominal core diameter is 6.1 cm (2.4 in.). Depths of the top and bottom of the core box in feet are shown in type.

burrows to dark-gray, poorly sorted, clayey and silty, fine sand. This basal sand sharply overlies and is burrowed into a thin, much finer grained, sandy clay-silt layer at the top of the truncated Plum Point strata.

A 0.4-m (1.3-ft) core loss in the coring run from 124.0 to 121.8 m (406.8 to 399.5 ft) depth apparently lost the Calvert Beach-St. Marys contact, and so there is some uncertainty about the exact depth of this contact. However, the resistivity and natural-gamma-ray logs clearly indicate that the contact is at 123.6 m (405.5 ft) depth (figs. G7 and G16), which corresponds to the lowest sand recovered in this core run. This lowest sand is exactly where the drillers noted a drilling chatter that indicated vibrations caused by cutting shells or cemented layers or phosphatic bones and teeth or chunks of wood or very well sorted tight sand. There was a physical gap in the core when it first came out of the retrieval (inner) barrel separating the base of the sand at 123.6 m (405.5 ft) from much finer grained, sandy clayey silt (top of Calvert Beach Member); the silt contains small burrows filled with greenish-black, coarser sand (basal sand of the St. Marys Formation) that penetrate less than 0.3 m (1 ft) downward. The site geologist and drillers agreed that the 0.4-m (1.3-ft) missing interval was from this physical gap and therefore placed the loss at 123.6 to 124.0 m (405.5 to 406.8 ft). On the basis of the lowest sand recovered and the geophysical logs, the contact is placed at 123.6 m (405.5 ft).

The resistivity and gamma-ray logs reflect the lithic changes that occur at the upper and lower contacts. These contacts are typical marine unconformities with lag deposits of coarse phosphatic quartz sand that overlie and are burrowed into finer grained sediments below the contact. The homogeneous, fine-grained lithology of most of the Calvert Beach Member creates a low-value, flat-resistivity-log signature similar to that of the Chickahominy Formation. The gamma-ray, resistivity, and sonic logs show a major shift to higher values related to the transition from the finer grained silty clay to clayey silt of the Calvert Beach Member to its very thin basal coarse sand and the underlying coarse sand of the truncated Plum Point Member. Except for the two sand lag deposits in the lower part of the St. Marys Formation, the next shelly sand encountered upward in the Langley core occurs at about 42.7 m (140 ft) depth within the Eastover Formation.

Dinoflagellates, diatoms, and silicoflagellates indicate a middle Miocene age for the Calvert Beach Member. Calcareous nannofossils suggest a slightly younger latest middle Miocene to early late Miocene age. The base of this 15.4-m-thick (50.6-ft-thick) unit is calibrated at 14.1 Ma or a younger age (first appearance of the dinocyst *Habibacysta tectata*, according to de Verteuil and Norris, 1996); the age of the top of the unit is no younger than the top of Zone DN6 (12.7 Ma). The lower unconformity appears to represent a hiatus of 1.1 to 1.6 m.y. (Edwards and others, this volume, chap. H). The duration of the interval represented by the upper unconformity is uncertain; it is at least 4.0 m.y. in the Langley core, and stratigraphic analysis of the Newport News Park 2 core indicates that the hiatus could be as much as 4.2 m.y. long (Powars and Bruce, 1999).

The Calvert Beach Member represents a shallow-shelf to nearshore depositional environment similar to the environment for the Plum Point Member at the Langley site. Paleontologic data indicate nutrient upwelling during sedimentation and a slight to moderate cooling upward trend toward reduced paleotemperatures.

St. Marys Formation (Upper Miocene)

The upper Miocene St. Marys Formation is present from the top of the Calvert Formation at 123.6 m (405.5 ft) depth in the Langley core to a contact with the upper Miocene Eastover Formation within a poorly recovered interval at 68.4 m (224.5 ft) depth (figs. G16, G17, and G18). A deflection of the resistivity curve at 68.3 m (224 ft) from lower resistivities in the silty clays of the upper St. Marys to higher resistivities in the basal sands of the Eastover Formation supports this contact pick.

The basal 4.6 m (15.0 ft) of the St. Marys consists of greenish-black, variably shelly, woody, pyritic, very fine to medium phosphatic quartz sand with sparse fish vertebrae and teeth and faint low-angled crossbeds at the base that grades upward into a finer sand and then by 117.0 m (384.0 ft) depth becomes an olive-gray to dark-greenish-gray clayey silt to silty clay (fig. G17). The other 50.6 m (166.0 ft) of the unit consists generally of homogeneous, massive, dense, well-sorted, dark-greenish-gray to grayish-olive-green, variably micaceous and calcareous, very clayey silt to very fine sandy clay and silt. This section contains rare to moderately abundant shells, rare to abundant burrows, abundant iron sulfide (pyrite and chalcopyrite, grains to nodules to burrow fillings and linings), finely disseminated organic material, rare scattered sponge spicules, and a trace of glauconite.

Powars and Bruce (1999) reported that beneath the lower York-James Peninsula, the St. Marys exhibits a gradational change from a lower clayey facies to an upper, sandy, shelly facies. These lithological changes are reflected in the Langley corehole resistivity logs by the gradual upward change from lower to higher resistivities at 79.2 m (260 ft) depth, but these values are lower than the resistivity of the overlying sandier Eastover (fig. G7). As described by Powars and Bruce (1999), the lower clayey facies commonly contains two fining-upward sequences that have thin, shelly, phosphatic, sandy basal lag deposits that are less than 1.5 m (5 ft) thick. These lag deposits may be represented in the Langley core by 2.9-m-thick (9.4-ft-thick) sandier beds at 113.8–110.9 m (373.4–364.0 ft) depth and the 4.6-m-thick (15.0-ft-thick) basal sands.

The upper sand lacks the shells but has abundant wood and phosphate grains. The core description of the basal St. Marys agrees well with the gamma-ray-log and resistivity-log signatures that indicate the more phosphatic and sandier nature of the sediments at 1.5 m (5 ft) and 3.0 m (10 ft), respectively, above the basal contact (fig. G7). The upper lag deposits above the contact at 113.8 m (373.4 ft) are also reflected in the resistivity logs with a positive kick (deflection to the right), and the gamma-ray log is low (deflected to the left), reflecting the scar-

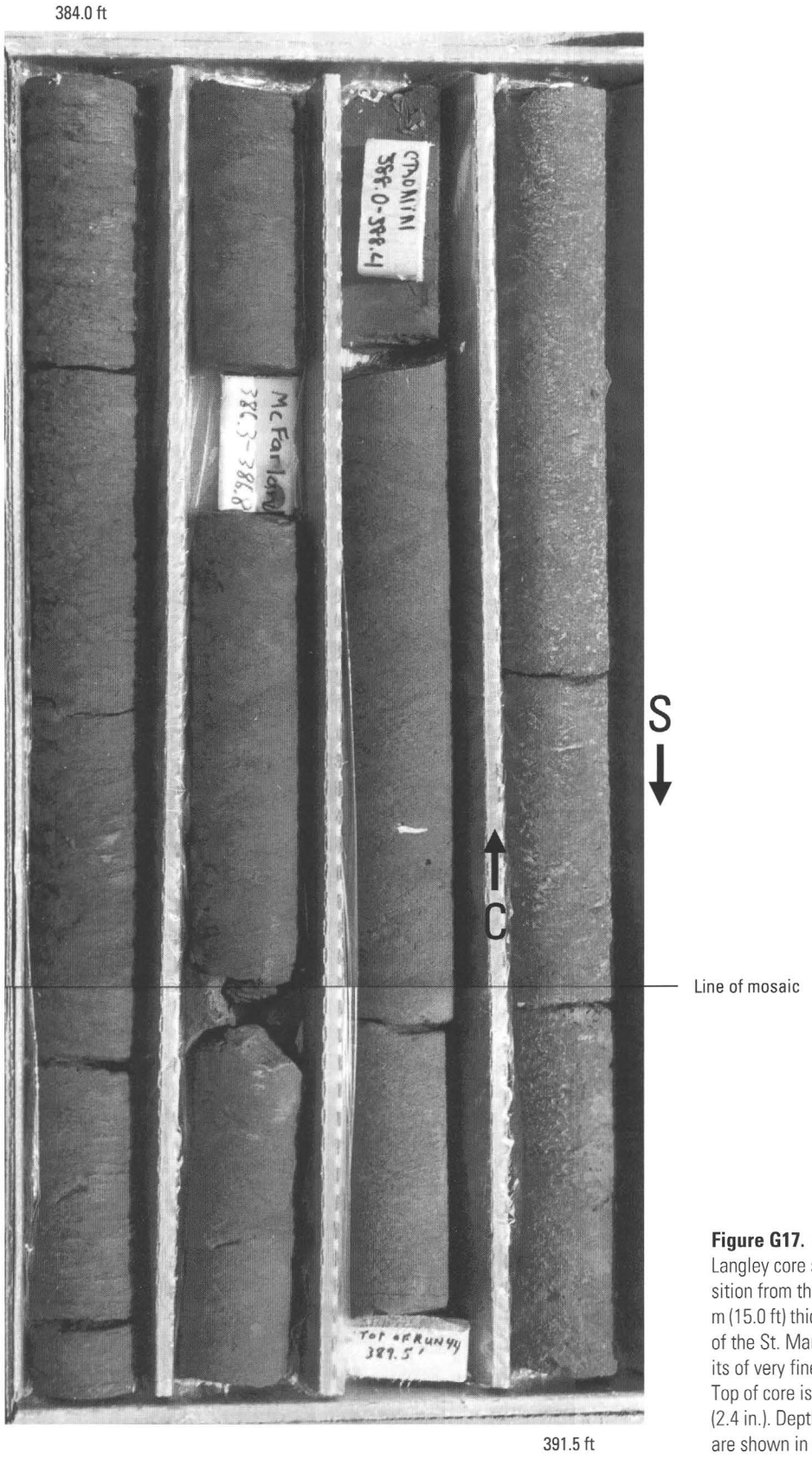

Figure G17. Composite photograph of the USGS-NASA Langley core showing the St. Marys Formation and the transition from the top of its sandy (S) basal beds, which are 4.6 m (15.0 ft) thick, to silty clay (C), which is the typical lithology of the St. Marys. White wisps in core at far right are deposits of very fine to medium quartz sand in a clay-silt matrix. Top of core is at upper left. Nominal core diameter is 6.1 cm (2.4 in.). Depths of the top and bottom of the core box in feet are shown in type.

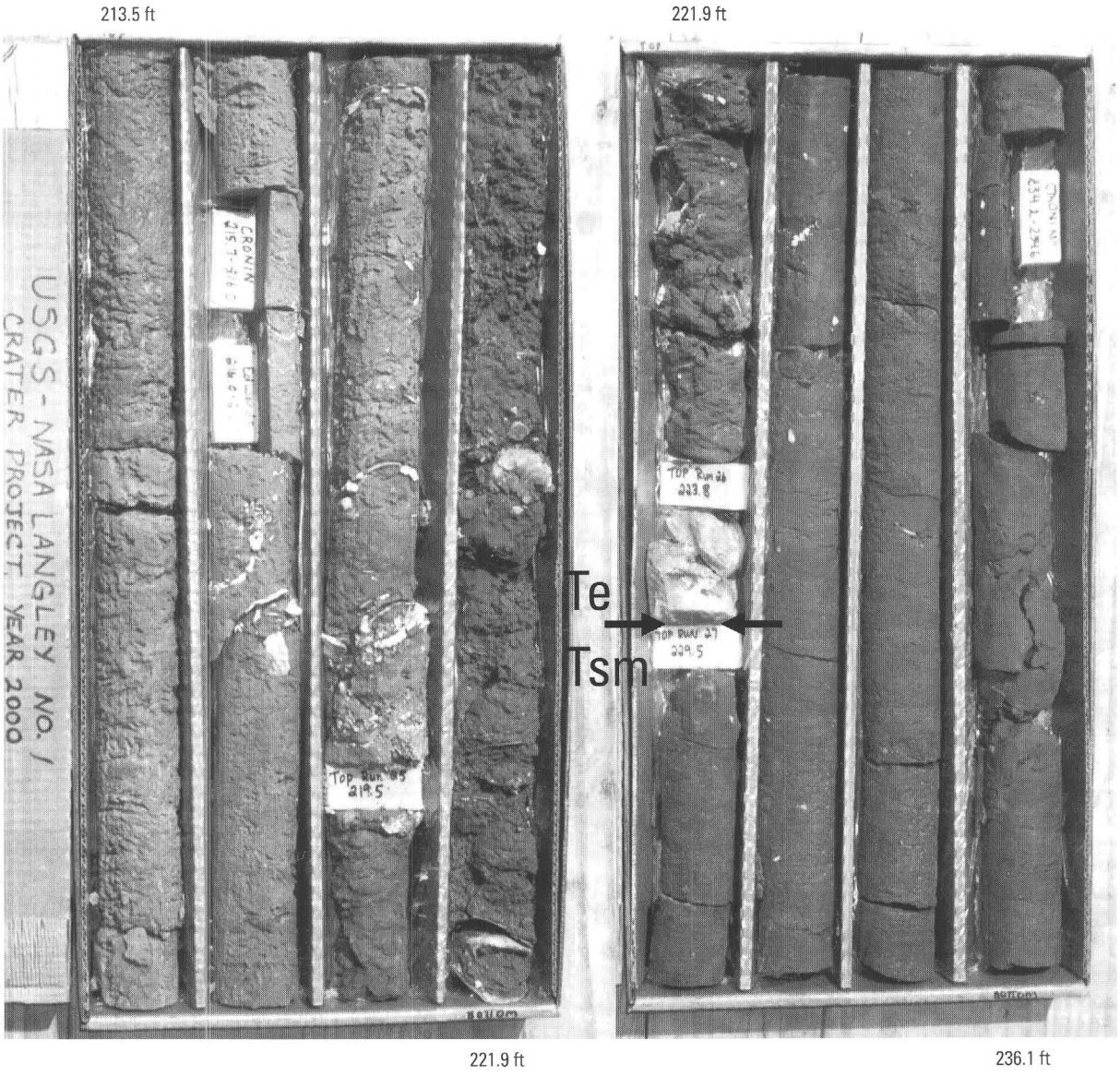

Figure G18. Photograph of the USGS-NASA Langley core showing core loss (arrows) of the presumably unconformable contact between the St. Marys Formation (Tsm) and the overlying light-colored calcite-cemented hard bed at the base of the Eastover Formation (Te). On the basis of geophysical logs, the contact is placed at 68.4 m (224.5 ft) depth and is interpreted as the base of hard bed. Top of core is at upper left. Nominal core diameter is 6.1 cm (2.4 in.). Depths of the top and bottom of the core boxes in feet are shown in type.

city of phosphate. Figure G17 shows the upward transition from the sandier beds to the silty clay beds at 119.5 to 118.6 m (392.0 to 389.0 ft) depth. Above the St. Marys, a shelly, sandy basal lag deposit at the base of the Eastover Formation lacks phosphatic material and, therefore, has a high resistivity-log signature and a low gamma-ray-log signature.

Foraminifera are the most common microfossils in the St. Marys Formation in the Langley core, and they become more abundant downward in the lower 38.1 m (125 ft) of the unit. The macrofossils are mostly clams, oysters, and *Turritella*. As in most cores across the region, *Turritella* fossils dominate the lower to middle part of the St. Marys strata from about 97.5 to 88.3 m (320.0 to 290.0 ft) depth in the Langley core; zones of concentration are at 95.1 to 94.5 m (312 to 310 ft) and 92.4 to 90.1 m (303 to 295.5 ft) depth.

Biostratigraphic analysis of the St. Marys Formation in the Langley core indicates a late Miocene age. The St. Marys is placed in dinoflagellate Zone DN9 (calibrated at 8.7–7.4 Ma according to de Verteuil and Norris, 1996), which continues into the basal Eastover (Edwards and others, this volume, chap. H). All nannofossil samples were either barren or nondiagnostic; however, Powars and Bruce (1999) reported that strontium-isotope analysis of shell material from the nearby Newport News Park 2 corehole indicates that the age of the St. Marys strata ranges from about 6.7 to 5.5 Ma, which is equivalent to the biochronozone of foraminiferal Zone N17. The lower unconformity represents at least a 4.0-m.y. hiatus, as the base of the St. Marys Formation is 8.7 Ma or younger. The upper contact may be conformable or may be a minor unconformity that represents a hiatus of less than 0.5 m.y. (Edwards and others, this volume, chap. H).

Analysis of the fauna and flora in the St. Marys Formation in the Langley core indicates a marine inner to outer shelf depositional environment with cool-water upwelling and a relatively small seasonality in temperatures. Ostracodes in the upper St. Marys indicate a temperate paleoclimate during sedimentation.

Eastover Formation (Upper Miocene)

The upper Miocene Eastover Formation is present in the Langley core from its contact with the underlying St. Marys Formation at 68.4 m (224.5 ft) depth to an unconformable contact with the overlying Yorktown Formation at 23.3 m (76.3 ft) depth (figs. G18 and G19). The base of the Eastover is within a poorly recovered 2.0-m-thick (6.7-ft-thick) interval and is placed at the base of a 0.06-m-thick (0.2-ft-thick), medium-gray, calcite-cemented, shelly sand bed that contains a few uncemented sand-filled burrows or borings. Only this indurated bed was recovered from the drill run from 68.2 to 70.0 m (223.8 to 229.5 ft) depth; it is represented by a thin, sharp high-resistivity kick at 68.4 m (224.5 ft) depth on the short-normal resistivity log (fig. G7). Another thin, sharp resistivity kick is seen on the short-normal log just slightly higher at 67.8 m (222.3 ft) depth, but this correlates with a recovered very shelly sand bed.

The contact with the overlying Yorktown Formation was completely recovered. Very shelly (large blackened oysters) and glauconitic quartz sand of the basal Yorktown sharply overlies and is burrowed at least 0.24 m (0.8 ft) down into dense, plastic, slightly sandy, silty clay of the Eastover Formation. These burrows vary from clay lined to sand filled and range from 0.12 to 0.24 m (0.4 to 0.8 ft) in width. High values on the gamma-ray and resistivity logs mark the position above the contact of the basal sand of the Yorktown Formation.

The Eastover Formation consists primarily of dark-greenish-gray to grayish-olive-gray to grayish-olive-green, bioturbated, locally macrofossiliferous, clayey and silty, very fine to medium quartz sands. Most of the Eastover apparently lacks bedding because of the high degree of bioturbation, as indicated by the mottled texture. However, some intervals have a wide variety of sparse to abundant burrows, including clay-lined sand-filled, sand-filled, clay-filled, and back-filled burrows of various sizes and orientations. The upper 3.0 m (10.0 ft) of the Eastover consists of sparingly fossiliferous, silty and sandy clay that has very thin bedding. A thin interval of laminated silty clay to clayey silt is present from 46.1 to 46.0 m (151.2 to 151.0 ft) depth.

The Eastover contains variable amounts (trace to 10 percent) of very fine grained to medium-grained, dark-green to black glauconite, which is most abundant in the upper 11.9 m (39.0 ft) of the unit. The glauconite percentage increases downward from 26.2 to 27.3 m (86.0 to 89.5 ft) depth. The glauconite is commonly concentrated in burrows. Sulfides are visible at 64.3 m (from 211.1 to 210.9 ft), from 63.8 to 61.2 m (209.3 to 200.8 ft), and from 27.1 to 23.3 m (89.0 to 76.3 ft) as irregular patches, as very fine to fine spheres, or as core surfaces that turned yellow when they dried.

No microfossils are visible in the top 10.3 m (33.7 ft), and microfossils are sparse to very sparse in the rest of the Eastover Formation. Echinoid spines are sparse throughout most of the section but are abundant from 51.8 to 48.8 m (170.0 to 160.0 ft).

The Eastover is sparsely to abundantly shelly and includes shells concentrated into layers forming shell hashes (storm deposits, marked SH in fig. G7) that are found at the following depths: 28.7 to 27.1 m (94.0 to 89.0 ft), 37.5 to 34.4 m (123.0 to 113.0 ft), 41.6 to 38.2 m (136.5 to 125.2 ft), and 61.2 to 56.8 m (200.7 to 186.2 ft). *Isognomon*, a tabular mollusk with a pearly luster, is a common species in the Eastover Formation. It is present from 64.0 to 27.4 m (210.0 to 90.0 ft) depth in the Eastover section of the Langley core, but it is not present in the overlying Yorktown Formation or in the underlying St. Marys Formation. *Turritella* is common to abundant from 58.2 to 37.8 m (191.0 to 124.0 ft).

Powars and Bruce (1999) reported that, across the region, the lower part of the Eastover Formation consists of a more clayey, fine-grained facies with characteristically low resistivity-log signatures that show an upward-coarsening trend into

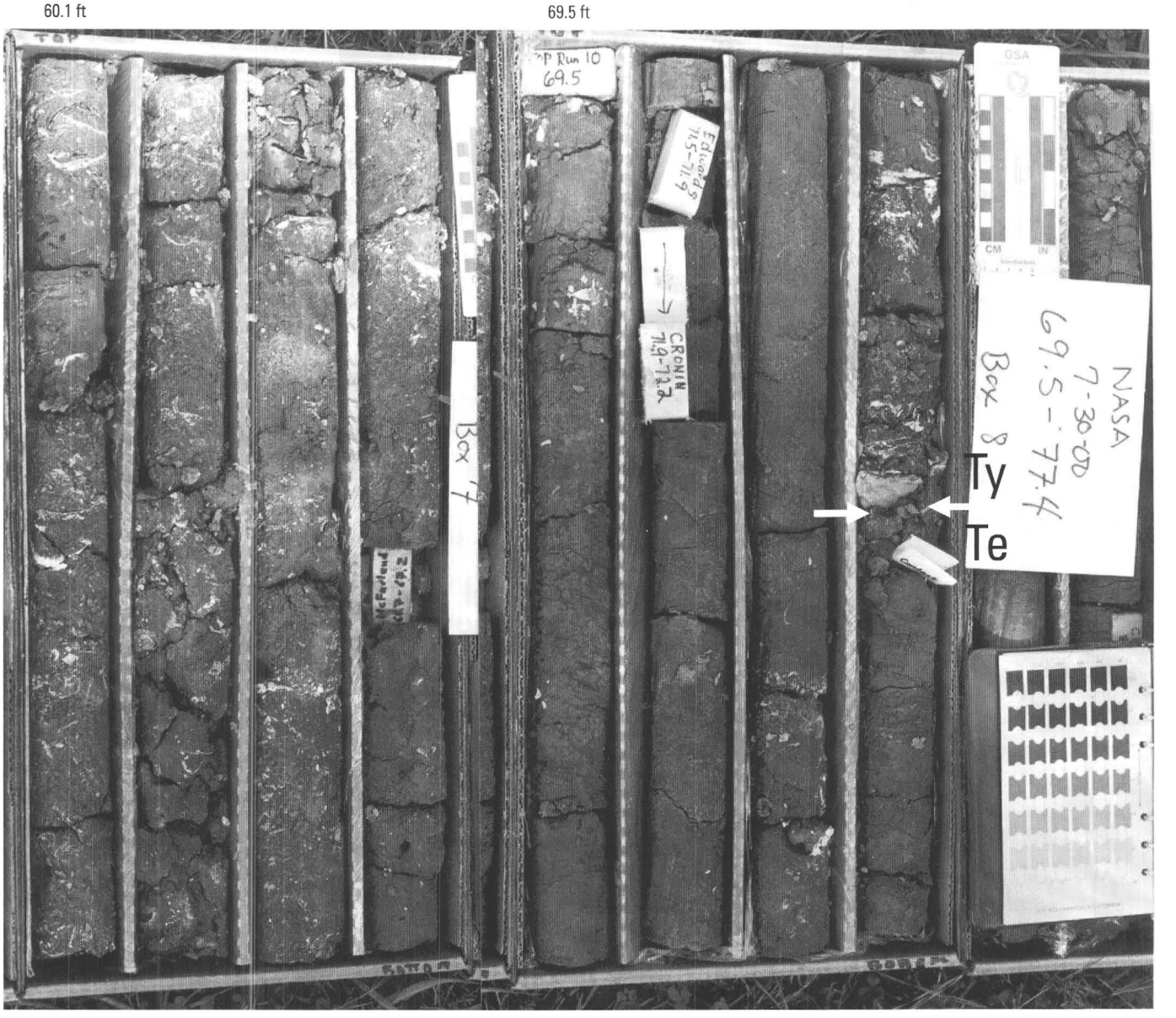

Figure G19. Photograph of the USGS-NASA Langley core showing the unconformable contact at 23.3 m (76.3 ft) depth (arrows) between the Eastover Formation (Te, lower right) and the overlying Yorktown Formation (Ty). Top of core is at upper left. Depths of the top and bottom of the core boxes in feet are shown in type.

an upper shelly, coarse-grained facies with characteristically high resistivities. This configuration of Eastover strata also is found in the Langley core, with a gradual decrease in the clay and silt fraction from about 64.0 m (210.0 ft) depth upward to about 42.7 m (140.0 ft) and a corresponding change in resistivity values.

Biostratigraphic analysis indicates a late Miocene age for the Eastover Formation in the Langley core (Edwards and others, this volume, chap. H). The only clearly datable calcareous nannofossil sample comes from the lower part of the unit at 56.9 m (186.6 ft) and is assigned to Zone NN 11. The dinoflagellate data place the unit in Zones DN9 and DN10. The DN9-DN10 boundary is present in the lower part of the unit and is calibrated at 7.4 Ma (de Verteuil and Norris, 1996). This boundary is bracketed by samples at 59.9 to 52.4 m (196.5 to 171.8 ft) depth and correlates to near the top of calcareous nannofossil Zone NN 11. The top of Zone DN10 is calibrated at 5.9 Ma. Powars and Bruce (1999) reported strontium-isotope dates from shells in the correlative strata from the nearby Newport News Park 2 corehole; those dates suggest that part of the Eastover Formation ranges from 6.2 Ma to 5.5 Ma, equal to the upper part of calcareous nannofossil Zone NN 11.

The Eastover Formation's lower contact with the St. Marys Formation is not precisely dated at this point and may be a conformable contact or a minor unconformity representing a hiatus of less than 0.5 m.y. The unconformity between the Eastover Formation and the overlying Yorktown Formation represents at least a 1.9-m.y. hiatus (see Edwards and others, this volume, chap. H).

Macrofauna and microfauna and microflora in the Langley core indicate that the Eastover Formation was deposited in a shallow-shelf to nearshore, marine environment. The molluscan genera are similar to modern subtropical to warm temperate marine-shelf assemblages that live in nearshore shallow-water environments with diverse substrates. The Eastover ostracode assemblages suggest progressively diminished upwelling and a temperate climate in an inner-middle neritic shelf setting.

Yorktown Formation (Pliocene)

Marine sediments of the Pliocene Yorktown Formation are present from 23.3 to 2.2 m (76.3 to 7.2 ft) depth in the Langley core (figs. G19 and G20). The Yorktown deposits unconformably overlie similar shallow-marine deposits of the Eastover Formation. The Yorktown consists of calcareous, muddy, very fine to fine quartz sand containing common macrofossils and microfossils.

As is common at most of the other marine unconformities, the basal shelly sand of the Yorktown corresponds to a high resistivity-log deflection and a high natural-gamma-ray-log deflection (fig. G7). The contact with the underlying sandy clay of the uppermost Eastover is marked by a sharp reduction of resistivity values opposite the Eastover section.

The upper contact of the Yorktown is lithologically sharp between the dark-gray, noncalcareous (where leached by ground water) to calcareous, fine-grained sediments of the Yorktown and the oxidized medium to coarse sand of the basal part of the overlying upper Pleistocene Tabb Formation. Because core recovery was poor in this contact interval, five auger holes were made nearby. The original 2.6-m-deep (8.5-ft-deep) hand-auger hole was made in apparently undisturbed forest land about 18 m (60 ft) north-northwest of the core site. This hole provided detailed data on the Yorktown and Pleistocene sediments and the nature of the contact between them.

The Yorktown in the Langley core is composed principally of grayish-olive to greenish-gray, very fine to fine sand, silt, and clay and whole and broken shells. Quartz, aragonite, and calcite are the most abundant minerals; lesser amounts of glauconite, phosphate, and mica are present. Much of the medium to coarse sand and all of the coarser clasts are composed of aragonite and calcite. Shell material from the upper 12 cm (0.4 ft) of the Yorktown in the auger hole is partially to wholly leached.

Bedding in the Yorktown part of the core is indistinct, and variations in texture and shell content are gradational. Laminae of well-rounded and sorted fine quartzose sand occur sporadically in the core. The basal 0.5 m (1.6 ft) of the Yorktown shows a increase in shell material downward to the contact at 23.3 m (76.3 ft) (see fig. G19). Beds with shell concentrations occur at depth intervals of 19.7 to 16.8 m (64.5 to 55 ft) and 13.2 to 12.3 m (43.4 to 40.2 ft) and at about 6.7 m (22 ft). Almost all shell material, even in the shell-rich zones, is matrix supported. Although larger planar shells and shell fragments in the core are subhorizontal, especially in fossil-rich intervals, most of the other shell material is randomly oriented.

Much of the Yorktown Formation in the Langley core has been bioturbated. The fauna is dominated by gastropods, most commonly *Crepidula fornicata*, and bivalves. Scaphopods, bryozoans, barnacles, and corals are less common. Echinoid spines and plates, sponge spicules, ostracodes, and foraminifera are also found in the finer fractions. Examination of the macrofossils from the basal part of the Yorktown Formation reveals reworked Eastover fossils mixed with Yorktown fossils. A reworked Oligocene or Miocene dinocyst was found at 7.3 m (24 ft) above the contact (Edwards and others, this volume, chap. H, fig. H11).

The mollusk and ostracode data suggest that the lowest part of the Yorktown, the Sunken Meadow Member (Zone 1 of Mansfield, 1943), is missing at this site and that most of the section contains several Pliocene age-diagnostic ostracodes that place it in the *Orionina vaughani* Assemblage Zone (see Edwards and others, this volume, chap. H). This zone correlates with the Rushmere, Morgarts Beach, and Moorehouse Members (undifferentiated) of the Yorktown Formation (Ward and Blackwelder, 1980; equivalent to Mollusk Zone 2 of Mansfield, 1943).

From a subtle contact at 20.4 m (66.9 ft) downward to the top of the Eastover, the nearly 3 m (9.7 ft) of sediment contains

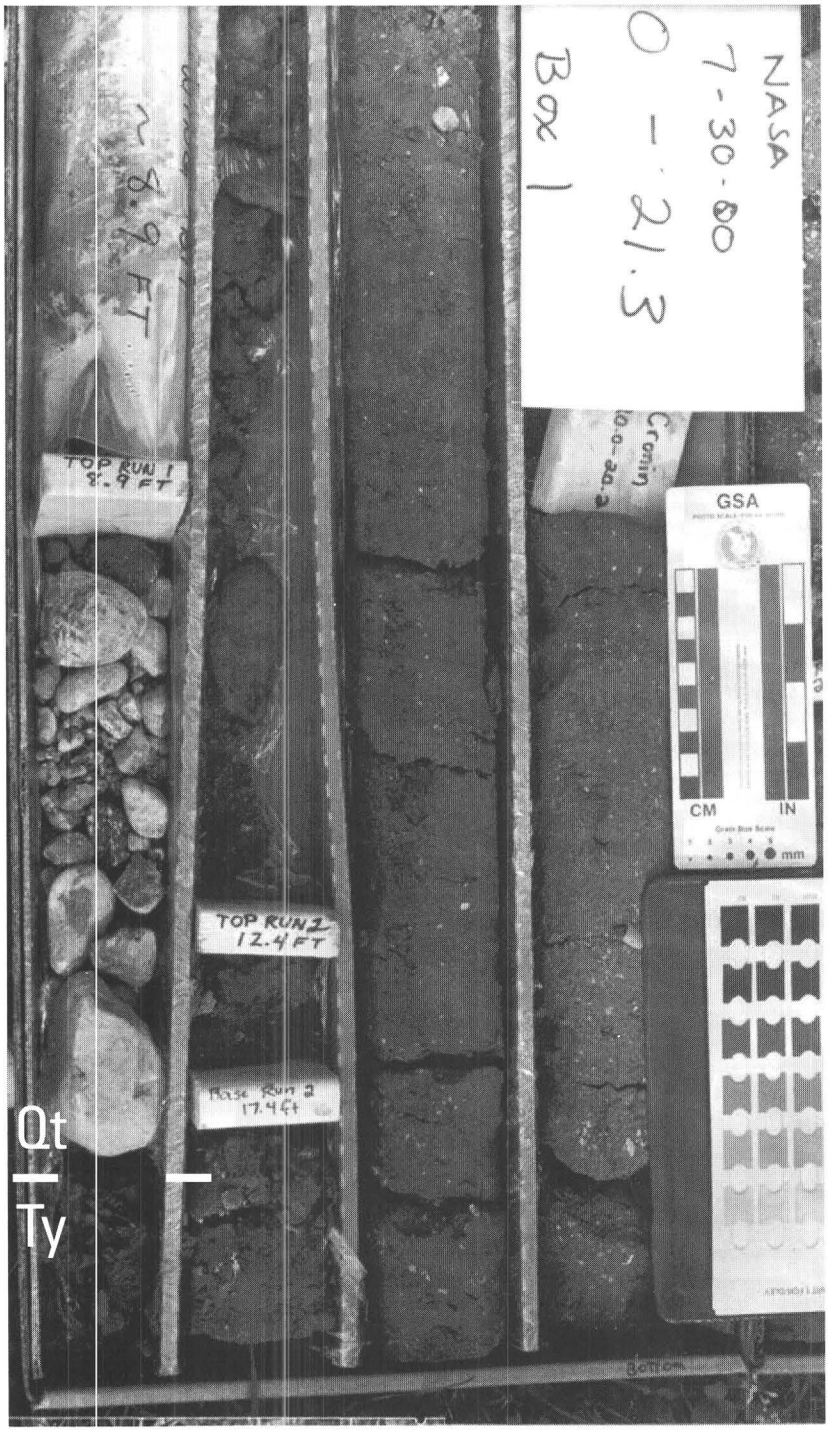

Figure G20. Photograph of the USGS-NASA Langley core showing the contact (short white lines) between cobbles of the Tabb Formation (Qt, upper Pleistocene) and the underlying dark, finer grained, marine strata of the Yorktown Formation (Ty, Pliocene). The contact is apparently disturbed as cobbles are pushed down a few feet below the contact. The contact was found at a depth of 2.2 m (7.2 ft) in the original nearby auger hole. Top of core is at upper left.

no diagnostic macrofossils or ostracodes; however, the calcareous nannofossils from this interval indicate an early Pliocene age, and the dinoflagellate assemblage includes a *Selenopemphix armageddonensis,* which is generally found in the Miocene but is also reported in the Pliocene. Below this subtle contact at 20.4 m (66.9 ft), the lack of mollusks that are typically found in the Sunken Meadow Member argues against this interval being assigned to the Sunken Meadow Member; however, the nannofossil data indicate that the interval could represent the Sunken Meadow Member. Above this subtle contact at 20.4 m (66.9 ft), several age-diagnostic mollusks were found, including *Chesapecten madisonius,* that indicate assignment to Zone 2 of Mansfield (1943).

The upper part of the Yorktown Formation (Zone 2 of Mansfield, 1943) was deposited under shallow-marine conditions on an unstable continental shelf (Johnson, Kruse, and others, 1998). At the time, the Langley area was surrounded on the north, west, and south by a series of large, discontinuous, arcuate, planar and crossbedded bioclastic sand shoals. There is insufficient evidence to establish their presence to the east in the eastern half of the annular trough of the Chesapeake Bay impact structure. These shoals limited the influx of terrigeneous sediment (silicate minerals) into the Langley area to silt, fine sand, and clay; skeletal carbonates and glauconite were indigenous. Because there is only one lithic break at 20.4 m (66.9 ft) within the Yorktown, sedimentation rates appear to have been relatively constant during deposition. The uppermost Yorktown has been removed by erosion at the Langley site. Ornamentation on most whole fossils in the Yorktown part of the core is well preserved, suggesting relatively rapid burial and low energy conditions. Furthermore, many species present in the Langley core favor or tolerate turbid waters and muddy bottoms. The presence of large species of the gastropod *Scaphella* and other subtropical forms in the upper part of the Yorktown south of the James River (G. Stephens, fossil collector, and G.H. Johnson, College of Willliam and Mary, oral commun., 1995) indicates significantly warmer conditions than today during the deposition of the Yorktown Formation.

Microfossil and macrofossil data acquired before the Langley corehole was drilled (Ward and Blackwelder, 1980; Gibson, 1983; Hazel, 1983; Cronin and others, 1984; Dowsett and Wiggs, 1992) indicate that the Yorktown is early and early late Pliocene in age (regionally the Yorktown has been reported to contain foraminiferal zones N18, N19, and N20). The age of the Yorktown from outcrops in southeastern Virginia extends from 4.0 Ma to 3.0 Ma according to Dowsett and Wiggs (1992). Analysis of calcareous nannofossil samples from the Langley core indicates (1) that the lower part of the Yorktown below about 20.4 m (66.9 ft) is no younger than early Pliocene (no younger than Zone NN 15) and (2) that the upper part of the Yorktown above 20.4 m (66.9 ft) is assignable to Zone NN 16-17 and, thus, is latest early or late Pliocene in age (Edwards and others, this volume, chap. H). The unconformity at the base of the Yorktown in the Langley core represents at least a 1.9-m.y. hiatus, and the upper unconformity represents about a 2.4-m.y. hiatus (Edwards and others, this volume, chap. H).

Tabb Formation (Upper Pleistocene)

In the Langley core, sediments of Pleistocene age are present from the unconformable contact with the Yorktown (fig. G20) to the top of the corehole section (land surface). These surficial sediments are assigned to the Lynnhaven Member of the Tabb Formation.

The Tabb-Yorktown contact was found in the Langley core at 3.4 m (11.0 ft) depth by Powars, Bruce, and others (2001); however, during the coring operation, pebbles and cobbles in the Tabb were pushed downward into the water-saturated, weathered Yorktown by the bit, yielding a highly disturbed sedimentary sequence in the core barrel. Five adjacent supplemental auger holes suggest that the Tabb-Yorktown contact must be higher. In the original auger hole, the contact between the Tabb and Yorktown is placed at a depth of 2.2 m (7.2 ft) and is marked by a change from a light-brown (10*YR* 6/20), well-rounded and sorted, medium to coarse, quartzose sand (Tabb) above to a strong-brown (7.5*YR* 5/6), nonfossiliferous, leached silty fine sand below. The contact is sharp to gradational over 1.8 cm (0.7 in.) and is burrowed in places.

The Tabb Formation of late Pleistocene age is the surficial stratigraphic unit on the eastern part of the York-James Peninsula (Johnson, 1976; Johnson and others, 1987; Mixon and others, 1989). In this region, it is subdivided into three members: the oldest and topographically highest Sedgefield Member, the intermediate Lynnhaven Member, and the youngest and lowest Poqouson Member. The Lynnhaven Member of the Tabb Formation is the mapped surficial unit at the Langley corehole (Johnson, 1972; Johnson and others, 1987; Mixon and others, 1989).

In the original auger hole near the Langley corehole, the Lynnhaven has a basal medium to coarse sand (34 cm (1.1 ft) thick) described above. From lowest to highest, the following layers appear above the basal sand:

- Silty clay mottled brownish yellow (18 cm (0.6 ft) thick)
- Silty clay containing well-rounded pebbles to cobbles and fining upward (18 cm (0.6 ft) thick)
- Silty clay with scattered medium and coarse sand grains and a surficial friable silt that grades upward into the next layer (58 cm (1.9 ft) thick)
- Silty clay (91.4 cm (3.0 ft) thick) (top of Pleistocene)
- Leaf litter (5 cm (2 in.) thick) (Holocene)

Except for burrows, the Lynnhaven is nonfossiliferous at Langley. The only reported fossil in this unit on the York-James Peninsula is *Crassostrea virginica* recovered from the A.B. Southall pit at the toe of the Big Bethel scarp, about 4 km (2.5 mi) west northwest of the Langley corehole (Johnson, 1976).

The Tabb Formation is considered to be late Pleistocene in age and may have been deposited in oxygen-isotope Stage 5c. Radiometric, thermoluminescence, and amino-acid age estimates on materials from the Tabb are equivocal. The Lynnhaven Member has been correlated with part of the Sandbridge Formation, Kempsville Formation, and other formations in the central Atlantic Coastal Plain (Johnson and others, 1987).

During the deposition of the Lynnhaven Member of the Tabb Formation, sea level was about +5.5 m (+18 ft) relative to present mean sea level (NAVD 88). Lynnhaven sediments were deposited in brackish waters of an ancestral Chesapeake Bay. This bay was bounded on the east by the Eastern Shore and on the west by the York-James Peninsula. It was open to the northern Chesapeake region, partially restricted on the southwest by the eastward extension of the Big Bethel scarp, and open to the south and southeast. The York River discharged fine sand, silt, and clay into this bay. The coarse clasts present in this member at Langley were derived from erosion of the Shirley Formation (middle Pleistocene) and the Sedgefield Member (lower upper Pleistocene) of the Tabb Formation. In addition to the fine sediment delivered by the York River, erosion of the upper parts of the Yorktown, Shirley, and Sedgefield Member of the Tabb yielded most of the fines in the Langley core.

Conclusions

The USGS-NASA Langley core, together with geophysical surveys, provides essential sedimentary and structural data needed for the further refinement of the geological framework of the region and clearly documents the crater's existence and effects on the regional geologic framework. This kind of information is required for the development of an accurate representation of the hydrological framework in the subsurface, which is needed for ground-water modeling.

The postimpact deposits consist of 235.65 m (773.12 ft) of upper Eocene to Quaternary deposits that buried the crater and the synimpact deposits. Except for some Pleistocene fluvial-estuarine deposits, all of the postimpact deposits are marine clays, silts, and very fine to very coarse sands that may include diatomaceous, glauconitic, shelly, and rare thin calcium-carbonate-cemented intervals. The creation of a persistent bathymetric low due to the crater's deep depression and postimpact loading and compaction have resulted in the deposition of several postimpact stratigraphic units that are preserved within the Chesapeake Bay impact structure and nowhere else beneath the Virginia Coastal Plain (Powars and Bruce, 1999; Powars, 2000). These units are the Chickahominy Formation (upper Eocene), Delmarva beds (lower Oligocene), Drummonds Corner beds (upper lower Oligocene), and Newport News beds (lower Miocene).

The postimpact sediments in the Langley core are primarily fine grained and contain about 149.6 m (491 ft) of mostly very fine to fine sand, silt, and clay and about 85.9 m (282 ft) of fine to medium sand with scattered coarser grains (commonly muddy). The Chickahominy Formation, the Calvert Formation excluding the Newport News beds, the St. Marys Formation, and the lower part of the Eastover Formation are all primarily fine grained, whereas the Drummonds Corner beds, the Newport News beds, the upper part of the Eastover Formation, the Yorktown Formation, and the Tabb Formation are generally sandier and make up the aquifer layers in this part of the system. In the western part of the crater's annular trough, there appears to be a constant layering of the finer grained postimpact layers (confining units) with the sandier layers (aquifers) according to the regional core data reported by Powars and Bruce (1999).

Correlation of the postimpact units with the seismic data indicates that the postimpact stratigraphic units appear to have some distinct seismic signatures and are clearly fractured and faulted, but to a much lesser degree than the underlying synimpact deposits. The seismic images also show that most of the postimpact deposits have a small dip toward the inner basin.

This investigation provides some of the foundation data needed to more accurately model the directions of ground-water flow and the potential for movement of salty water to well fields in the vicinity of the impact crater. As ground-water use increases in the Hampton Roads region and public water utilities increasingly tap into brackish-water aquifers as sources of drinking water, additional information about the Chesapeake Bay impact crater will be needed for future management of these ground-water resources.

Acknowledgments

U.S. Geological Survey (USGS) investigations of the Chesapeake Bay impact structure are conducted in cooperation with the Hampton Roads Planning District Commission, the Virginia Department of Environmental Quality, and the National Aeronautics and Space Administration (NASA) Langley Research Center. The Hampton Roads Planning District Commission and the USGS provided funds for the drilling of the USGS-NASA Langley corehole. The NASA Langley Research Center provided extensive operational and logistical support for the drilling operation. The Virginia Department of Environmental Quality and the Department of Geology of the College of William and Mary provided extensive operational support at the drill site.

The USGS Rocky Mountain Drilling Unit drilled the USGS-NASA Langley corehole with support from the USGS Eastern Earth Surface Processes Team's drilling crew. The USGS drill crew included Arthur C. Clark (supervisor and lead driller), Jeffery D. Eman (lead driller), Stephen J. Grant (lead driller), Donald G. Queen (operations and supply), Manuel Canabal Lopez, Eugene F. Cobbs, Eugene F. Cobbs, III, Orren C. Doss, Robert Hovland, and Michael E. Williams.

Stephen E. Curtin (USGS) and Richard E. Hodges (USGS) conducted the geophysical logging of the Langley corehole.

The authors of this chapter and USGS geologists Robert G. Stamm, J. Stephen Schindler, and Laurel M. Bybell wrote the field descriptions of the Langley core at the drill site. The following members of the USGS also served as site geologists: Wilma B. Alemán Gonzalez, Noelia Baez Rodríguez, Omayra Bermudez Lugo, Karl M. Dydak, Samuel V. Harvey, Robert R. Lotspeich, Rosenelsy Marrero Cuebas, Colleen T. McCartan, E. Randolph McFarland, and Thomas Weik. Core photographs in this chapter were taken by the first author (Powars).

Reviews of the manuscript by Wayne L. Newell (USGS) and J. Stephen Schindler (USGS) substantially improved this chapter.

References Cited

Berggren, W.A., Kent, D.V., Swisher, C.C., III, and Aubry, M.-P., 1995, A revised Cenozoic geochronology and chronostratigraphy, *in* Berggren, W.A., Kent, D.V., Aubry, M.-P., and Hardenbol, Jan, eds., Geochronology, time scales and global stratigraphic correlation: SEPM (Society for Sedimentary Geology) Special Publication 54, p. 129–212.

Bruce, T.S., and Powars, D.S., 1995, Inland salt water wedge in the coastal plain aquifers of Virginia [abs.]: Virginia Water Resources Conference, Richmond, Va., April 17–18, 1995, Abstracts, p. 7–8.

Bybell, L.M., and Gibson, T.G., 1994, Paleogene stratigraphy of the Putneys Mill, New Kent County, Virginia, corehole: U.S. Geological Survey Open-File Report 94–217, 38 p.

Catchings, R.D., Powars, D.S., Gohn, G.S., and Goldman, M.R., 2002, High-resolution seismic reflection survey of the southwestern margin of the Chesapeake Bay impact structure, Virginia [abs.]: Eos, Transactions, American Geophysical Union, v. 83, no. 19, spring meeting supplement of 7 May 2002, Abstract T21A–05, p. S352. (Also available online at http://www.agu.org/meetings/waissm02.html)

Catchings, R.D., Powars, D.S., Gohn, G.S., Goldman, M.R., Gandhok, G., and Johnson, G.H., 2001, Subsurface images of the annular trough of the Chesapeake Bay impact structure, Virginia, from seismic reflection/refraction data [abs.]: Lunar and Planetary Science Conference, 32d, Houston, Tex., March 12–16, 2001, Abstract 1937, available online at http://www.lpi.usra.edu/meetings/lpsc2001/pdf/1937.pdf

Catchings, R.D., Saulter, D.E., Powars, D.S., Goldman, M.R., Dingler, J.A., Gohn, G.S., Schindler, J.S., and Johnson, G.H., 2001, High-resolution seismic reflection/refraction images near the outer margin of the Chesapeake Bay impact crater, York-James Peninsula, southeastern Virginia: U.S. Geological Survey Open-File Report 01–407, 18 p., available only online at http://geopubs.wr.usgs.gov/open-file/of01-407/

Cederstrom, D.J., 1943, Chloride in ground water in the coastal plain of Virginia: Virginia Geological Survey Bulletin 58, 36 p.

Cederstrom, D.J., 1945a, Geology and ground-water resources of the coastal plain in southeastern Virginia: Virginia Geological Survey Bulletin 63, 384 p.

Cederstrom, D.J., 1945b, Selected well logs in the Virginia Coastal Plain north of James River: Virginia Geological Survey Circular 3, 81 p.

Cederstrom, D.J., 1945c, Structural geology of southeastern Virginia: American Association of Petroleum Geologists Bulletin, v. 29, no. 1, p. 71–95.

Cederstrom, D.J., 1957, Geology and ground-water resources of the York-James Peninsula, Virginia: U.S. Geological Survey Water-Supply Paper 1361, 237 p.

Coch, N.K., 1971, Geology of the Newport News South and Bowers Hill quadrangles, Virginia: Virginia Division of Mineral Resources Report of Investigations 28, 26 p., 2 oversize maps.

Cronin, T.M., Bybell, L.M., Poore, R.Z., Blackwelder, B.W., Liddicoat, J.C., and Hazel, J.E., 1984, Age and correlation of emerged Pliocene and Pleistocene deposits, U.S. Atlantic Coastal Plain: Palaeogeography, Palaeoclimatology, Palaeoecology, v. 47, no. 1–2, p. 21–51.

de Verteuil, Laurent, 1997, Palynological delineation and regional correlation of lower through upper Miocene sequences in the Cape May and Atlantic City boreholes, New Jersey Coastal Plain: Proceedings of the Ocean Drilling Program, Scientific Results, v. 150X, p. 129–145.

de Verteuil, Laurent, and Norris, Geoffrey, 1996, Miocene dinoflagellate stratigraphy and systematics of Maryland and Virginia: Micropaleontology, v. 42, Supplement, 172 p., 18 pls.

Dowsett, H.J., and Wiggs, L.B., 1992, Planktonic foraminiferal assemblage of the Yorktown Formation, Virginia, USA: Micropaleontology, v. 38, no.1, p. 75–86.

Edwards, L.E., and Powars, D.S., 2003, Impact damage to dinocysts from the late Eocene Chesapeake Bay event: Palaios, v. 18, no. 3, p. 275–285. (Also available online at http://www.bioone.org/pdfserv/i0883-1351-018-03-0275.pdf)

Gibson, T.G., 1983, Key foraminifera from upper Oligocene to lower Pleistocene strata of the central Atlantic Coastal Plain, *in* Ray, C.E., ed., Geology and paleontology of the Lee Creek Mine, North Carolina; I: Smithsonian Contributions to Paleobiology, no. 53, p. 355–453, 22 pls.

Goddard, E.N., and others, 1948, Rock-color chart: Washington, D.C., National Research Council, 6 p. (Republished by Geological Society of America, 1951; reprinted 1984.)

Gohn, G.S., Clark, A.C., Queen, D.G., Levine, J.S., McFarland, E.R., and Powars, D.S., 2001, Operational summary for the USGS-NASA Langley corehole, Hampton, Virginia: U.S. Geological Survey Open-File Report 01–87–A, 21 p., available online at http://pubs.usgs.gov/of/2001/of01-087/

Gohn, G.S., Powars, D.S., Bruce, T.S., Quick, J.E., and Catchings, R.D., 2002, Geologic constraints on modeling of complex-crater collapse; Data from the Chesapeake Bay impact structure, Virginia [abs.]: Eos, Transactions, American Geophysical Union, v. 83, no. 19, spring meeting supplement of 7 May 2002, Abstract T21A–07, p. S352. (Also available online at http://www.agu.org/meetings/waissm02.html)

Gohn, G.S., Powars, D.S., Bruce, T.S., Self-Trail, J.M., Weems, R.E., Edwards, L.E., Horton, J.W., Jr., Izett, G.A., and Johnson, G.H., 2001, Preliminary interpretation of the USGS-NASA Langley corehole, Chesapeake Bay impact structure, York-James Peninsula, Hampton, VA [abs.]: Geological Society of America Abstracts with Programs, v. 33, no. 2, p. A–24.

Gohn, G.S., Powars, D.S., Quick, J.E., Horton, J.W., Jr., and Catchings, R.D., 2002, Variation of impact response with depth and lithology, outer annular trough of the Chesapeake Bay impact structure, Virginia Coastal Plain [abs.]: Geological Society of America Abstracts with Programs, v. 34, no. 6, p. 465.

Hazel, J.E., 1983, Age and correlation of the Yorktown (Pliocene) and Croatan (Pliocene and Pleistocene) Formations at the Lee Creek Mine, *in* Ray, C.E., ed., Geology and paleontology of the Lee Creek Mine, North Carolina; I: Smithsonian Contributions to Paleobiology, no. 53, p. 81–199, 38 pls.

Horton, J.W., Jr., Aleinikoff, J.N., Izett, G.A., Naeser, C.W., and Naeser, N.D., 2001, Crystalline rocks from the first corehole to basement in the Chesapeake Bay impact structure, Hampton, Virginia [abs.]: Geological Society of America Abstracts with Programs, v. 33, no. 6, p. A–448.

Horton, J.W., Jr., Aleinikoff, J.N., Izett, G.A., Naeser, N.D., Naeser, C.W., and Kunk, M.J., 2002, Crystalline basement and impact-derived clasts from three coreholes in the Chesapeake Bay impact structure, southeastern Virginia [abs.]: Eos, Transactions, American Geophysical Union, v. 83, no. 19, spring meeting supplement of 7 May 2002, Abstract T21A–03, p. S351. (Also available online at http://www.agu.org/meetings/waissm02.html)

Horton, J.W., Jr., Kunk, M.J., Naeser, C.W., Naeser, N.D., Aleinikoff, J.N., and Izett, G.A., 2002, Petrography, geochronology, and significance of crystalline basement rocks and impact-derived clasts in the Chesapeake Bay impact structure, southeastern Virginia [abs.]: Geological Society of America Abstracts with Programs, v. 34, no. 6, p. 466.

Johnson, G.H., 1972, Geology of the Yorktown, Poquoson West, and Poquoson East quadrangles, Virginia: Virginia Division of Mineral Resources Report of Investigations 30, 57 p., 3 oversize pls.

Johnson, G.H., 1976, Geology of the Mulberry Island, Newport News North, and Hampton quadrangles, Virginia: Virginia Division of Mineral Resources Report of Investigations 41, 72 p., 3 oversize pls.

Johnson, G.H., Kruse, S.E., Vaughn, A.W., Lucey, J.K., Hobbs, C.H., III, and Powars, D.S., 1998, Postimpact deformation associated with the late Eocene Chesapeake Bay impact structure in southeastern Virginia: Geology, v. 26, no. 6, p. 507–510.

Johnson, G.H., and Powars, D.S., 1996, Effects of Chesapeake Bay impact structure on late Cenozoic stratigraphic sequences and landscapes, southeastern Virginia [abs.]: Geological Society of America Abstracts with Programs, v. 28, no. 7, p. A–119.

Johnson, G.H., Powars, David, and Bruce, Scott, 2002, Stratigraphic and paleontologic complexities in late Cenozoic deposits around the Chesapeake Bay impact structure in eastern Virginia [abs.], *in* Abstract volume; The Cape Fear Arch, transition between the north and southern Atlantic Coastal Plain—Fourth Bald Head Island Conference on Coastal Plains Geology, Kure Beach, N.C., November 16–19, 2002: Wilmington, N.C., University of North Carolina at Wilmington, p. 24.

Johnson, G.H., Powars, D.S., Bruce, T.S., Beach, T.A., Harris, M.S., and Goodwin, B.K., 2001, Post-impact effects of the Eocene Chesapeake Bay impact, lower York-James Peninsula, Virginia: Virginia Geological Field Conference, 31st, Williamsburg, Virginia, October 19 and 20, 2001 [Guidebook], 40 p.

Johnson, G.H., Powars, D.S., Bruce, Scott, Vaughn, A.W., Lucey, J.K., and Kruse, S.E., 1998, Relationship of Yorktown Formation lithofacies to post-impact deformation on the terrace zone, southeastern VA [abs.]: Geological Society of America Abstracts with Programs, v. 30, no. 4, p. 19.

Johnson, G.H., Ward, L.W., and Peebles, P.C., 1987, Stratigraphy and paleontology of Pliocene and Pleistocene deposits of southeastern Virginia, *in* Whittecar, G.R., ed., Geological excursions in Virginia and North Carolina—Geological Society of America, Southeastern Section, 36th Annual Meeting, 1987, Guidebook, Field Trips nos. 1–7: Norfolk, Va., Old Dominion University, Department of Geological Sciences, p. 189–218.

Koeberl, Christian, Poag, C.W., Reimold, W.U., and Brandt, Dion, 1996, Impact origin of the Chesapeake Bay structure and the source of the North American tektites: Science, v. 271, no. 5253, p. 1263–1266.

Mansfield, W.C., 1943 [1944], Stratigraphy of the Miocene of Virginia and the Miocene and Pliocene of North Carolina, *in* Gardner, Julia, Part 1, Pelecypoda, chap. A *of* Mollusca from the Miocene and lower Pliocene of Virginia and North Carolina: U.S. Geological Survey Professional Paper 199, p. 1–19.

McFarland, E.R., 2002, Hydrochemical evidence for the origin of the elevated ground-water salinity in the Chesapeake Bay impact structure, southeastern Virginia [abs.]: Geological Society of America Abstracts with Programs, v. 34, no. 6, p. 466.

McFarland, E.R., and Bruce, Scott, 2002, Distribution, origin, and relations to flow of salty ground water along the western margin of the Chesapeake Bay impact structure in eastern Virginia [abs.]: Eos, Transactions, American Geophysical Union, v. 83, no. 19, spring meeting supplement of 7 May 2002, Abstract T21A–08, p. S352. (Also available online at http://www.agu.org/meetings/waissm02.html)

Melosh, H.J., 1989, Impact cratering—A geologic process: New York, Oxford University Press, 245 p.

Mixon, R.B., Berquist, C.R., Newell, W.L., Johnson, G.H., Powars, D.S., Schindler, J.S., and Rader, E.K., 1989, Geological map and generalized cross sections of the Coastal Plain and adjacent parts of the Piedmont, Virginia: U.S. Geological

Survey Miscellaneous Investigations Series Map I–2033, 2 sheets, scale 1:250,000.

Munsell Color Company, 1988, Munsell soil color charts: Baltimore, Md., 20 p.

Obradovich, J.D., Snee, L.W., and Izett, G.A., 1989, Is there more than one glassy impact layer in the late Eocene? [abs.]: Geological Society of America Abstracts with Programs, v. 21, no. 6, p. A134.

Poag, C.W., 1996, Structural outer rim of Chesapeake Bay impact crater—Seismic and bore hole evidence: Meteoritics & Planetary Science, v. 31, no. 2, p. 218–226.

Poag, C.W., 1997, The Chesapeake Bay bolide impact; A convulsive event in Atlantic Coastal Plain evolution: Sedimentary Geology, v. 108, no. 1–4, p. 45–90.

Poag, C.W., 2000, Nature and distribution of deposits derived from the Chesapeake Bay submarine impact [abs.]: Geological Society of America Abstracts with Programs, v. 32, no. 7, p. A–163.

Poag, C.W., 2002a, Structure and morphology of the Chesapeake Bay submarine impact crater [abs.]: Geological Society of America Abstracts with Programs, v. 34, no. 6, p. 465.

Poag, C.W., 2002b, Synimpact-postimpact transition inside Chesapeake Bay crater: Geology, v. 30, no. 11, p. 995–998.

Poag, C.W., 2002c, Tsunamis and hypercanes; Late-stage impact depositional systems at Chesapeake Bay [abs.]: Eos, Transactions, American Geophysical Union, v. 83, no. 19, spring meeting supplement of 7 May 2002, Abstract T21A–06, p. S352. (Also available online at http://www.agu.org/meetings/waissm02.html)

Poag, C.W., and Aubry, M.-P., 1995, Upper Eocene impactites of the U.S. East Coast; Depositional origins, biostratigraphic framework, and correlation: Palaios, v. 10, no. 1, p. 16–43.

Poag, C.W., and the Chesapeake Coring Team, 2001, Drilling to basement inside the Chesapeake Bay crater [abs.]: Lunar and Planetary Science Conference, 32d, Houston, Tex., March 12–16, 2001, Abstract 1203, available online at http://www.lpi.usra.edu/meetings/lpsc2001/pdf/1203.pdf

Poag, C.W., and Commeau, J.A., 1995, Paleocene to middle Miocene planktic foraminifera of the southwestern Salisbury embayment, Virginia and Maryland; Biostratigraphy, allostratigraphy, and sequence stratigraphy: Journal of Foraminiferal Research, v. 25, no. 2, p. 134–155, 9 pls.

Poag, C.W., Gohn, G.S., and Powars, D.S., 2002, Chesapeake Bay impact crater; Seismostratigraphy and lithostratigraphy of displaced sedimentary megablocks [abs.]: Lunar and Planetary Science Conference, 33d, League City, Tex., March 11–15, 2002, Abstract 1019, available online at http://www.lpi.usra.edu/meetings/lpsc2002/pdf/1019.pdf

Poag, C.W., Hutchinson, D.R., Colman, S.M., and Lee, M.W., 1999, Seismic expression of the Chesapeake Bay impact crater; Structural and morphologic refinements based on new seismic data, *in* Dressler, B.O., and Sharpton, V.L., eds., Large meteorite impacts and planetary evolution; II: Geological Society of America Special Paper 339, p. 149–164.

Poag, C.W., Plescia, J.B., and Molzer, P.C., 2002, Ancient impact structures on modern continental shelves; The Chesapeake Bay, Montagnais, and Toms Canyon craters, Atlantic margin of North America: Deep-Sea Research Part II—Topical Studies in Oceanography, v. 49, no. 6, p. 1081–1102.

Poag, C.W., Poppe, L.J., Powars, D.S., and Mixon, R.B., 1992, Distribution, volume, and depositional origin of upper Eocene bolide-generated sediments along the U.S. East Coast [abs.]: Geological Society of America Abstracts with Programs, v. 24, no. 7, p. A172–A173.

Poag, C.W., Powars, D.S., Mixon, R.B., and Bruce, S., 1994, Convulsive events in Atlantic Coastal Plain evolution—Effects of the Chesapeake Bay bolide impact [abs.]: Geological Society of America Abstracts with Programs, v. 26, no. 7, p. A–152.

Poag, C.W., Powars, D.S., Mixon, R.B., Edwards, L.E., Folger, D.W., Poppe, L.J., and Bruce, S., 1991, An upper Eocene impact-wave(?) deposit beneath Chesapeake Bay [abs.]: Geological Society of America Abstracts with Programs, v. 23, no. 5, p. A460.

Poag, C.W., Powars, D.S., Poppe, L.J., and Mixon, R.B., 1994, Meteoroid mayhem in Ole Virginny—Source of the North American tektite strewn field: Geology, v. 22, no. 8, p. 691–694.

Poag, C.W., Powars, D.S., Poppe, L.J., Mixon, R.B., Edwards, L.E., Folger, D.W., and Bruce, Scott, 1992, Deep Sea Drilling Project Site 612 bolide event—New evidence of a late Eocene impact-wave deposit and a possible impact site, U.S. East Coast: Geology, v. 20, no. 9, p. 771–774.

Powars, D.S., 2000, The effects of the Chesapeake Bay impact crater on the geologic framework and the correlation of hydrogeologic units of southeastern Virginia, south of the James River: U.S. Geological Survey Professional Paper 1622, 53 p., 1 oversize pl. (Also available online at http://pubs.usgs.gov/prof/p1622/)

Powars, D.S., and Bruce, T.S., 1999, The effects of the Chesapeake Bay impact crater on the geological framework and correlation of hydrogeologic units of the lower York-James Peninsula, Virginia: U.S. Geological Survey Professional Paper 1612, 82 p., 9 oversize pls. (Also available online at http://pubs.usgs.gov/prof/p1612/)

Powars, D.S., Bruce, T.S., Bybell, L.M., Cronin, T.M., Edwards, L.E., Frederiksen, N.O., Gohn, G.S., Horton, J.W., Jr., Izett, G.A., Johnson, G.H., Levine, J.S., McFarland, E.R., Poag, C.W., Quick, J.E., Schindler, J.S., Self-Trail, J.M., Smith, M.J., Stamm, R.G., and Weems, R.E., 2001, Preliminary geologic summary for the USGS-NASA Langley corehole, Hampton, Virginia: U.S. Geological Survey Open-File Report 01–87–B, 20 p., available online at http://pubs.usgs.gov/of/2001/of01-087/

Powars, D.S., Bruce, T.S., and Johnson, G.H., 1998, Stratigraphic, structural, and hydrogeological complexities related to the outer rim of the Chesapeake Bay impact crater [abs.]: Geological Society of America Abstracts with Programs, v. 30, no. 7, p. A–279.

Powars, D.S., Bruce, Scott, Poag, C.W., and Mixon, R.B., 1994, Virginia's Coastal Plain inland salt water wedge—A geohydrologic response to the Chesapeake Bay bolide impact

[abs.]: Geological Society of America Abstracts with Programs, v. 26, no. 7, p. A–410.

Powars, D.S., Edwards, L.E., Bruce, T.S., and Johnson, G.H., 2000, Structural and stratigraphic complexities in the coastal plain of Virginia [abs.]: Geological Society of America Abstracts with Programs, v. 32, no. 7, p. A–458.

Powars, D.S., Edwards, L.E., Bruce, T.S., and Johnson, G.H., 2002, "Wet target" effects on the syn-impact partial filling and post-impact burial of the Chesapeake Bay impact crater, southeastern Virginia [abs.]: Geological Society of America Abstracts with Programs, v. 34, no. 6, p. 544.

Powars, D.S., Gohn, G.S., Bruce, T.S., Johnson, G.H., Catchings, R.D., Frederiksen, N.O., Edwards, L.E., Self-Trail, J.M., and Pierce, H.A., 2002, Distribution and origin of impact-generated debris; Western annular trough, Chesapeake Bay impact crater [abs.]: Eos, Transactions, American Geophysical Union, v. 83, no. 19, spring supplement of 7 May 2002, abstract T21A–02, p. S351. (Also available online at http://www.agu.org/meetings/waissm02.html)

Powars, D.S., Gohn, G.S., Catchings, R.D., Horton, J.W., Jr., and Edwards, L.E., 2003, Recent research in the Chesapeake Bay impact crater, USA—Part 1. Structure of the western annular trough and interpretation of multiple collapse structures [abs.]: International Conference on Large Meteorite Impacts, 3d, Noerdlingen, Germany, August 5–7, 2003, Abstract 4053, available online at http://www.lpi.usra.edu/meetings/largeimpacts2003/pdf/4053.pdf

Powars, D.S., Gohn, G.S., Catchings, R.D., McFarland, E.R., Bruce, T.S., Johnson, G.H., Izett, G.A., Emry, S.R., and Edwards, L.E., 2001, Deep corehole and seismic reflection data provide insights into crater-filling processes and the hydrogeology of the outer margin of the Chesapeake Bay impact structure, eastern Virginia Coastal Plain, USA [abs.]: Lunar and Planetary Science Conference, 32d, Houston, Tex., March 12–16, 2001, Abstract 2183, available online at http://www.lpi.usra.edu/meetings/lpsc2001/pdf/2183.pdf

Powars, D.S., Gohn, G.S., Edwards, L.E., Bruce, T.S., Catchings, R.D., Emry, S.R., Johnson, G.H., Levine, J.S., Poag, C.W., and Pierce, H.A., 2001, Structure and composition of the southwestern margin of the buried Chesapeake Bay impact structure, Virginia [abs.]: Geological Society of America Abstracts with Programs, v. 33, no. 6, p. A–203.

Powars, D.S., Gohn, G.S., Edwards, L.E., Catchings, R.D., Bruce, T.S., Johnson, G.H., and Poag, C.W., 2002, Lithostratigraphic framework of the crater-fill deposits; Western annular trough, Chesapeake Bay impact crater [abs.]: Geological Society of America Abstracts with Programs, v. 34, no. 6, p. 465.

Powars, D.S., Johnson, G.H., Bruce, T.S., and Edwards, L.E., 2001, The relation between the Chesapeake Bay impact structure and the structure and stratigraphy of Cenozoic deposits in eastern Virginia [abs.]: Geological Society of America Abstracts with Programs, v. 33, no. 2, p. A–76.

Powars, D.S., Johnson, G.H., Edwards, L.E., Horton, J.W., Jr., Gohn, G.S., Catchings, R.D., McFarland, E.R., Izett, G.A., Bruce, T.S., Levine, J.S., and Pierce, H.A., 2002, An expanded Chesapeake Bay impact structure, eastern Virginia; New corehole and geophysical data [abs.]: Lunar and Planetary Science Conference, 33d, League City, Tex., March 11–15, 2002, Abstract 1034, available online at http://www.lpi.usra.edu/meetings/lpsc2002/pdf/1034.pdf

Powars, D.S., Mixon, R.B., and Bruce, Scott, 1992, Uppermost Mesozoic and Cenozoic geologic cross section, outer coastal plain of Virginia, *in* Gohn, G.S., ed., Proceedings of the 1988 U.S. Geological Survey Workshop on the Geology and Geohydrology of the Atlantic Coastal Plain: U.S. Geological Survey Circular 1059, p. 85–101.

Powars, D.S., Mixon, R.B., Edwards, L.E., Andrews, G.W., and Ward, L.W., 1987, Evidence for Paleocene and lower Eocene pinch-outs on the north flank of the Norfolk arch, Eastern Shore of Virginia [abs.]: Geological Society of America Abstracts with Programs, v. 19, no. 2, p. 124.

Powars, D.S., Mixon, R.B., Edwards, L.E., Poag, C.W., and Bruce, Scott, 1990, Cross section of Cretaceous and Cenozoic strata, Norfolk arch to Salisbury basin, outer coastal plain of Virginia [abs.]: Geological Society of America Abstracts with Programs, v. 22, no. 4, p. 57.

Powars, D.S., Poag, C.W., and Bruce, Scott, 1991, Uppermost Mesozoic and Cenozoic stratigraphic framework of the central and outer coastal plain of Virginia [abs.]: Geological Society of America Abstracts with Programs, v. 23, no. 1, p. 117.

Powars, D.S., Poag, C.W., and Mixon, R.B., 1993, The Chesapeake Bay "impact crater," stratigraphic and seismic evidence [abs.]: Geological Society of America Abstracts with Programs, v. 25, no. 6, p. A–378.

Riddle, P.C., Vaughn, A.W., Lucey, J.K., Kruse, S.E., Johnson, G.H., and Hobbs, C.H., III, 1996, Geophysical studies of near-surface deformation associated with the Chesapeake Bay impact structure, southeastern Virginia [abs.]: Geological Society of America Abstracts with Programs, v. 28, no. 7, p. A–119.

Stover, L.E., and Hardenbol, Jan, 1993 [1994], Dinoflagellates and depositional sequences in the lower Oligocene (Rupelian) Boom Clay Formation, Belgium: Bulletin de la Société belge de Géologie, v. 102, no. 1–2, p. 5–77.

United States Geological Survey, 1986, [Topographic map of the] Newport News North, Virginia [7.5-min quadrangle showing photorevisions of the 1965 map]: Reston, Va., U.S. Geological Survey, scale 1:24,000.

von Dalwigk, Ilka, and Ormö, Jens, 2001, Formation of resurge gullies at impacts at sea; The Lockne crater, Sweden: Meteoritics & Planetary Science, v. 36, no. 3, p. 359–369.

Ward, L.W., and Blackwelder, B.W., 1980, Stratigraphic revision of upper Miocene and lower Pliocene beds of the Chesapeake Group, middle Atlantic Coastal Plain: U.S. Geological Survey Bulletin 1482–D, p. D1–D61, 5 pls.

Appendix G1. Lithic Summary of the Postimpact Section of the USGS-NASA Langley Core

Depth to base, in meters (feet)	Thickness, in meters (feet)	Lithology
	0.6 (2.1)	GRAVEL, clay, silt, sand, and cobbles up to 9.1 centimeters (cm; 3.6 inches (in.)) in diameter; quartz, quartzite, chert; dark yellowish orange (10*YR* 6/6).
Note: Nearby auger holes indicate that the base of the Pleistocene is at 2.2 meters (m; 7.2 feet (ft)) depth.		
		Tabb Formation, Lynnhaven Member (upper Pleistocene)
3.4 (11.0)	----------sharp unconformable contact ----------	
		Yorktown Formation (Pliocene)
	11.7 (38.5)	SAND (very fine to fine), muddy; primarily quartz and trace glauconite (1 percent glauconite and phosphate in upper 1 m (3 ft); less than 20 percent mollusk fragments throughout section, with an exception in the interval at 12.3–13.2 m (40.2–43.4 ft) depth containing 50–70 percent shell fragments and whole valves (pelecypods dominate with occurrence of scaphopods, turritellids, gastropods, and echinoid spines); very sparse to common microfauna throughout section; soft, poorly compacted, bioturbated; basal contact sharp with sand-filled burrows extending down 0.5 m (1.7 ft) into the silty clay below; dark greenish gray (5*GY* 4/1) in upper 0.5 m (1.7 ft), grayish olive green (5*GY* 3/2) throughout remaining interval.
15.1 (49.5)	----------sharp burrowed contact ----------	
	1.6 (5.3)	CLAY, silty, slightly sandy (very fine) increasing downward with lowest 0.5 m (1.7 ft) interbedded silty clay and micaceous, silty very fine to fine sand; 5 percent quartz sand, trace glauconite, 1 percent white mica; mollusk fragments (ranging from common to abundant), sparse echinoid spines; texture mottling due to bioturbation; grayish olive green (5*GY* 3/2).
16.7 (54.8)	----------gradational contact across 0.03 m (0.1 ft) ----------	
	3.7 (12.1)	SAND (very fine to fine), very muddy; quartz, glauconite (up to 1 percent), calcareous matrix, mollusk fragments (ranging from common to abundant), sparse echinoid spines, sponge borings, and microfauna; bioturbated, soft to slightly compacted; grayish olive green (5*GY* 3/2).
20.4 (66.9)	----------subtle sharp contact----------	
	2.9 (9.4)	SAND (very fine), muddy; quartz, trace glauconite, white mica, abundant sulfides from 21.3 to 22.5 m (70 to 74 ft) depth; sparse microfauna, mollusk fragments (1 percent, very fine to fine), pelecypods (large fragments present and increasing downward at 22.0 m (72.2 ft) depth and from 22.8 to 23.3 m (74.8 to 76.4 ft) depth), abundant fragments (up to 5 cm (2 in.)) of blackened oysters in basal 0.1 m (0.4 ft); soft, poorly compacted, massive, texture mottled, bioturbated; dark greenish gray (5*GY* 4/1).

Depth to base, in meters (feet)	Thickness, in meters (feet)	Lithology
		Yorktown Formation (Pliocene)
23.3 (76.3)		----------sharp, burrowed unconformable contact----------
		Eastover Formation (upper Miocene)
	3.0 (10.0)	CLAY, silty, sandy (very fine, 5 percent); trace glauconite (gradually increases downward to 5 percent at 26.2 m (85.9 ft), 1 percent white mica, quartz sand (increases downward), up to 3 percent sulfide spheres and irregular masses to abundant sulfides, finely crystalline irregular masses of pyrite occur as alteration on glauconite; faintly texture mottled, bioturbated (dark, sand-filled burrows, 1.3–2.5 cm (0.5–1.0 in.) wide, from 23.3 to 23.6 m (76.4 to 77.4 ft) depth); very thin bedding from 23.9 to 24.0 m (78.5 to 79 ft) depth; dark greenish gray (*5GY* 4/1).
26.3 (86.3)		----------gradational contact ----------
	42.1 (138.2)	SAND (very fine to medium), muddy to slightly muddy; most of the lower part of the Eastover from about 64.0 m (210.0 ft) depth upward to 42.7 m (140.0 ft) depth is a muddier fine-grained facies; generally up to 1 percent glauconite (3–5 percent in the interval of 33.4–35.1 m (109.5–115.1 ft) depth), up to 1 percent mica, quartz sand, abundant sulfides in top 0.8 m (2.7 ft); locally sparse microfauna, mollusks (sand sized to whole valve) are present variably up to 70 percent (pectens, oysters, scaphopods, and turritellids), *Isognomon* is scattered to abundant from 27.4 to 64.0 m (90.0 to 210.0 ft) depth, *Turritella* is common to abundant from 37.8 to 58.2 m (124.0 to 191.0 ft) depth, pectens are concentrated into layers forming a shell hash of stacked(?) storm deposits from 27.1 to 28.7 m (89.0 to 94.0 ft) depth, other shell hashes are at depths of 34.4–37.5 m (113.0–123.0 ft), 38.2–41.6 m (125.2–136.5 ft), and 56.8–61.2 m (186.2–200.7 ft), echinoid spines are sparse throughout most of the section but are abundant from 51.8 to 48.8 m (170.0 to 160.0 ft) depth; soft, poorly compacted, thoroughly bioturbated with sand-filled, clay-filled, and back-filled burrows, texture mottled, laminated (laminae 1 millimeter (mm) thick) shelly and carbonaceous clayey silt to silty clay from 46.0 to 46.1 m (151.0 to 151.2 ft) depth; color ranges from dark greenish gray (*5GY* 4/1) to grayish olive green (*5GY* 3/2). The base of the Eastover is within a poorly recovered 2.0-m-thick (6.7-ft-thick) interval and is placed at the base of a 0.06-m-thick (0.2-ft-thick), calcite-cemented, sand hard bed; contact placement is based on correlation with a kick at 68.4 m (224.5 ft) depth on the short-normal resistivity log (fig. G7); mollusk shell fragments and molds present, possible burrows/borings represented by uncemented sand tubes, medium gray (*N5*).
		Eastover Formation (upper Miocene)
68.4 (224.5)		------ contact not recovered; may be conformable or a minor unconformity-----
		St. Marys Formation (upper Miocene)

Depth to base, in meters (feet)	Thickness, in meters (feet)	Lithology
	42.5 (139.5)	CLAY, silty, sandy (above 100.6 m (330.0 ft) depth very fine to fine), ranging from 2 to 15 percent, subrounded to subangular quartz, well to moderately sorted; increase in clay and microfauna below 79.2 m (260 ft) depth, increase in shells and shell material from 85.3 to 88.4 m (280 to 290 ft) depth, shells dominated by *Turritella* from 88.3 to 97.5 m (290 to 320 ft) depth, foraminifera sand at 100.6–103.5 m (330.0–339.6 ft) depth, no quartz; foraminifera sand from 103.5–110.9 m (339.6–364.0 ft) depth with sparse quartz (very fine to fine) and faint thin laminations; up to 3 percent glauconite throughout section (no occurrence at 97.4–103.5 m (319.5–339.6 ft) depth), up to 5 percent white mica, pyrite occurrence varies from trace to frequent (scattered pyritized burrows noted below 82.1 m (269.4 ft) depth, and pebble-sized pyrite chunks with reduction rims present at 103.5–106.5 m (339.6–349.4 ft) depth, trace irregular masses of sulfide noted at 70.0–76.0 m (229.6–249.3 ft) depth, up to 5 percent dark heavy minerals noted at 76.0–88.2 m (249.3–289.4 ft) depth, scattered acicular gypsum crystals noted below 106.5 m (349.4 ft) depth; sparse microfauna (benthic foraminifera and ostracodes), rare sponge spicules noted below 82.5 m (270.7 ft) depth, very sparse echinoid spines noted between 88.2 and 91.3 m (289.4 and 299.5 ft) and below 106.5 m (349.4 ft) depth, 1 percent plant fragments noted at 76.0–91.3 m (249.3–299.5 ft) depth, a fish tooth noted below 94.3 m (309.3 ft) depth, fish bone fragments between 100.4 m (329.4 ft) and 103.5 m (339.6 ft) depth; moderately dense and compact, texture mottled and bioturbated; top 4.6 m (15.1 ft) are olive gray (5*Y* 4/1), below 73.0 m (239.5 ft) depth, color ranges from grayish olive green (5*GY* 3/2) to dark greenish gray (5*GY* 4/1).
110.9 (364.0)	----------gradational contact----------	
	2.9 (9.4)	SILT to SAND, clayey, sandy (very fine to medium); quartz (subrounded to angular), trace glauconite, white and brown mica (sparse increasing downward to abundant), pyrite (sparse increasing downward to abundant), trace acicular gypsum crystals, and abundant phosphate; rare mollusks, rare echinoid spines, sparse foraminifera, rare fish bones and teeth, a pyrite-filled tube fragment, and abundant wood chips; moderately dense and compacted, texture mottled and bioturbated; ranging from grayish olive green (5*GY* 3/2) to grayish olive (10*Y* 4/2). Subtly coarsens downward to subtle contact with underlying clay.
113.8 (373.4)	----------subtle sharp contact----------	
	2.2 (7.1)	CLAY, silty, sandy (very fine to medium); rare quartz, abundant white mica, and abundant pyrite; scattered thin mollusk shells (clams), abundant foraminifera, and abundant wood chips; faintly laminated; grayish olive green (5*GY* 3/2).
116.0 (380.5)	----------gradational contact----------	
	3.5 (11.5)	SILT, clayey, sandy (very fine to medium); quartz, 1 percent glauconite, moderately abundant white mica, and abundant pyrite; sparse clam shells, locally abundant foraminifera, rare sponge spicules, scattered wood chips, and rare bone chips; texture mottled, bioturbated; grayish olive green (5*GY* 3/2).
119.5 (392.0)	----------gradational contact----------	

Depth to base, in meters (feet)	Thickness, in meters (feet)	Lithology
	4.1 (13.5)	SAND (very fine to medium, primarily very fine to fine), silty, clayey; dominant quartz (subangular to angular), up to 1 percent glauconite, 1–2 percent phosphate; mollusk (mostly clam) shell fragments abundant, foraminifera moderately abundant, few sponge spicules present, some wood pieces present, and sparse fish vertebrae and teeth; texture mottled and bioturbated, grading down to faintly crossbedded very fine to coarse sand; color darkens downsection, olive gray (5*Y* 3/2) to dark greenish gray (10*Y* 3/1) to greenish black (10*Y* 2.5/1).
		St. Marys Formation (upper Miocene)
123.6 (405.5)	----------sharp, burrowed unconformable contact ----------	
		Calvert Formation, Calvert Beach Member (middle Miocene)
	15.4 (50.6)	SILT, clayey, with scattered grains of sand of various mineralogies; quartz (very fine to fine), mica (very fine), pyrite (very fine to coarse), trace glauconite (very fine to coarse), and sparse rounded phosphate grains of sand size; common to abundant foraminifera, rare pyritized diatoms at top becoming more common downward, rare fish scales and vertebrae, and rare wood chips; thinly laminated, breaks apart into shalelike chips; becomes a MUDDY SAND (very fine to medium) in basal 0.6 m (2.1 ft) and has increased phosphate, abundant burrows filled by clean coarse to very coarse sand, some burrows filled by clay and silt, and includes tiny shell fragments, scattered fish vertebrae, sharks' teeth, rays' teeth and bone (phosphatized), mostly dark-greenish-gray (10*Y* 4/1) with a small portion of dark-olive-gray (5*Y* 3/2) material noted near the middle of the section and for the finer grained burrows in the basal sand.
		Calvert Formation, Calvert Beach Member (middle Miocene)
139.0 (456.1)	----------irregular, sharp, burrowed unconformable contact ----------	
		Calvert Formation, Plum Point Member (middle Miocene)
	0.3 (1.0)	SILT, clayey, few scattered very fine to fine sand grains, rare foraminifera; dark olive gray (5*Y* 3/2).
139.3 (457.1)	----------gradational contact----------	
	1.2 (4.0)	SAND (fine to medium with scattered coarse to very coarse grains increasing downward to contact) varies from grain-to-grain contact to grains floating in clay-silt matrix; mostly quartz (subangular to subrounded) and mica (fine to very coarse), scattered sand-sized phosphate; abundant shells, rare foraminifera; dark olive gray (5*Y* 3/2).
		Calvert Formation, Plum Point Member (middle Miocene)
140.5 (461.1)	----------sharp, burrowed unconformable contact----------	
		Calvert Formation, Newport News beds (lower Miocene)

Depth to base, in meters (feet)	Thickness, in meters (feet)	Lithology
	3.0 (9.8)	SAND to SHELLY SAND (fine to very coarse, primarily medium to coarse) varies from grain-to-grain contact to grains floating in clay-silt matrix; poorly sorted; primarily clear quartz (very angular to well rounded) with some smoky and blue quartz, 20–30 percent glauconite and phosphate; coarsens down to contact becoming a fine sand with scattered small pebbles; abundant shells throughout the section (in places a shell hash), shells concentrated in two separate lithified calcium-carbonate-cemented zones, each about 0.4 m (1.3 ft) thick and located near the top and bottom of the section, also semilithified at very top, scattered foraminifera; dark olive gray (5*Y* 3/2) except for the lithified segments, which are olive gray (5*Y* 4/2).
		Calvert Formation, Newport News beds (lower Miocene)
143.5 (470.9)		----------sharp unconformable contact----------
		Old Church Formation (upper Oligocene)
	32.5 (106.5)	SIX FINING-UPWARD SEQUENCES, range from 1.1 m (3.5 ft) to 11.0 m (36.1 ft) in thickness, each grades upward from better sorted sands to clay-silt-matrix-supported sands, with burrowed sand-over-clay contacts at depths of 154.5 m (507.0 ft), 155.8 m (511.0 ft), 160.2 m (525.5 ft), and 161.2 m (529.0 ft) and one contact indicated by the resistivity log at 166.1 m (545.0 ft) (fig. G7). SAND (very fine to very coarse), variable clay-silt matrix, scattered granules to small pebbles; poorly sorted, very angular to well rounded, varies from grain-to-grain contact to grains supported in clay-silt matrix (top of cycle); few scattered, indurated thin layers and patches below 149.2 m (489.5 ft) depth; abundant quartz (up to pebble size of 0.7 cm (0.3 in.)), abundant glauconite, scattered phosphate (up to pebble size of 0.5 cm (0.2 in.)), and scattered white mica flakes present below 170.7 m (560.0 ft) depth and scattered throughout with minor amounts of pyrite, carbonaceous material, and occasional very small sharks' teeth; foraminifera ranging from rare to abundant and diverse (more abundant in finer grained upper parts of the sequences), sediment-back-filled and clay-lined burrows present throughout; scattered mollusk shells and shell fragments (increase in basal sands of each sequence), small pecten at 160.0 m (524.9 ft) depth, sponge spicules present near 161.5 m (529.9 ft) depth, echinoid spines present near 162.7 m (533.8 ft) depth, and wood clast (1 cm x 3 mm (0.4 x 0.1 in.)) at 161.0 m (528.2 ft) depth; faintly bedded, by clay-silt matrix, but mostly bioturbated, scattered lenses and patches of calcite-cemented sand present near 161.0 m (528.2 ft) and below 169.0 m (554.5 ft) depth; color varies from olive (5*Y* 5/3) near top, to dark olive gray (5*Y* 3/2), olive gray (5*Y* 4/2), and black (5*Y* 2.5/1)/(5*Y* 2.5/2) below, to very dark gray (5*Y* 3/1) near bottom.
		Old Church Formation (upper Oligocene)
176.0 (577.4)		----------sharp, burrowed unconformable contact----------
		Drummonds Corner beds (upper lower Oligocene)

Depth to base, in meters (feet)	Thickness, in meters (feet)	Lithology
	2.4 (8.0)	SILT, very clayey, sandy (very fine to fine); scattered quartz and white mica (decreasing downward), moderately abundant phosphate and glauconite, phosphate content increasing downward to abundant; moderately abundant foraminifera increasing downward to abundant, abundant burrows (some concentrated near upper boundary and filled with sand from overlying Old Church Formation), very effervescent with hydrochloric acid application; thinly bedded (1 cm (0.4 in.)) to laminated (millimeter scale); colors ranging from olive gray (5*Y* 3/2) to grayish olive green (10*Y* 4/2).
178.4 (585.4)	----------gradational contact----------	
	4.9 (15.9)	SAND (very fine to very coarse, primarily a very fine to medium sand), silty, moderately clayey, abundant phosphate, lesser quartz and glauconite (both are subrounded to rounded); abundant foraminifera, highly burrowed; faint bedding; coarsens down to 2.2 m (7.1 ft) of basal sand with scattered granules and small quartz pebbles (up to 0.05 cm (0.02 in.)), increased phosphate, and sparse clam and snail shells; olive gray (5*Y* 3/2) with mottling (due to burrows) of olive black (5*Y* 2/1).
		Drummonds Corner beds (upper lower Oligocene)
183.3 (601.3)	----------sharp, burrowed unconformable contact----------	
		Chickahominy Formation (upper Eocene)
	52.3 (171.8)	CLAYEY SILT to SILTY CLAY throughout section with very rare sand (very fine) and silt near the top, but gradually increasing to sparse further downward; quartz, rare to sparse glauconite (silt to very fine sand sized), glauconite-rich lenses with slight increase in phosphate, quartz, and silt from 221.1 to 223.8 m (725.5 to 734.4 ft) depth overlie 0.06-m-thick (0.2-ft-thick), black (*N*1) clay layer with very dark gray (5*Y* 3/1) clayey-silt-filled burrows; throughout section rare to abundant occurrence of pyrite grains (very fine to fine), nodules, and pyrite-filled shells, sparse rounded phosphate (fine to medium) with scattered occurrence from 221.1 m (725.5 ft) depth down to basal contact; massive to laminated (millimeter scale) top 8.9 m (29.2 ft) becoming more massive with faintly visible thin bedding (1 mm to 1 cm (0.04 to 0.4 in.)) (mica flakes and shells aligned on bedding planes); matrix is very effervescent with application of hydrochloric acid, sparse to abundant foraminifera increasing downward, sparse to abundant shells (clams, scaphopods, echinoid spines, and thin-shelled oysters), increase in shell content from depths of 192.0–195.4 m (630.0–641.0 ft) and 204.5–223.8 m (671.0–734.4 ft), rare fish teeth and scales, scattered wood chips from 207.3 to 213.7 m (680.0 to 701.0 ft) depth, burrows scattered throughout section, abundant phosphate-rich sand-filled burrows from the overlying Drummonds Corner beds extending down 0.7 m (2.2 ft) into the top of the silty clay; in the lower 7.0 m (23.1 ft) increase in quartz silt with rare very fine to fine sand grains; in the lower 16.2 m (53.0 ft) are inclined fracture planes with slickensides at 219.6 m (720.5 ft) depth, several between 225.4 and 226.2 m (739.5 and 742.0 ft) depth, and a fault dipping moderately (about 45°) at 230.0–229.9 m (754.7–754.4 ft) depth (with slickensides and pyritized fault gouge; color varies from olive gray (5*Y* 4/1) to dark greenish gray (5*G* 4/1) to very dark gray (5*Y* 3/1).

Depth to base, in meters (feet)	Thickness, in meters (feet)	Lithology
		Chickahominy Formation (upper Eocene)
235.65 (773.12)	------BASE OF POSTIMPACT DEPOSITS--------sharp conformable contact--	
		Exmore beds (upper Eocene)
	0.19 (0.63)	SILTY CLAY, laminated (millimeter scale) with scattered horizontal silt to very fine sand laminae and a few burrows (including one with the typical Exmore matrix); gray changing upward to dark greenish gray.
235.84 (773.75)	----------sharp contact----------	
	0.085 (0.28)	SILT, clayey; millimeter-scale pyrite lattice at the top from 235.84 to 235.87 m (773.75 to 773.85 ft) depth; medium olive gray (5*Y* 5/1).
235.92 (774.03)	----------sharp contact----------	
		MATRIX-SUPPORTED SEDIMENTARY-CLAST DIAMICTON (typical Exmore beds)

Paleontology of the Upper Eocene to Quaternary Postimpact Section in the USGS-NASA Langley Core, Hampton, Virginia

By Lucy E. Edwards, John A. Barron, David Bukry, Laurel M. Bybell, Thomas M. Cronin, C. Wylie Poag, Robert E. Weems, and G. Lynn Wingard

Chapter H of
Studies of the Chesapeake Bay Impact Structure—The USGS-NASA Langley Corehole, Hampton, Virginia, and Related Coreholes and Geophysical Surveys

Edited by J. Wright Horton, Jr., David S. Powars, and Gregory S. Gohn

Prepared in cooperation with the
Hampton Roads Planning District Commission,
Virginia Department of Environmental Quality, and
National Aeronautics and Space Administration Langley Research Center

Professional Paper 1688

U.S. Department of the Interior
U.S. Geological Survey

Contents

Plates

[Plates follow appendix H2]

Figures

Tables

Paleontology of the Upper Eocene to Quaternary Postimpact Section in the USGS-NASA Langley Core, Hampton, Virginia

By Lucy E. Edwards,[1] John A. Barron,[2] David Bukry,[2] Laurel M. Bybell,[1] Thomas M. Cronin,[1] C. Wylie Poag,[3] Robert E. Weems,[1] and G. Lynn Wingard[1]

Abstract

The USGS-NASA Langley corehole was drilled in 2000 in Hampton, Va. The core serves as a benchmark for the study of calcareous nannofossils, dinoflagellates, diatoms and silicoflagellates, mollusks, ostracodes, planktonic foraminifera and bolboformids, and vertebrate remains in the upper Eocene, Oligocene, Miocene, and Pliocene sediments in southeastern Virginia. These sediments were deposited after the comet or asteroid impact that produced the Chesapeake Bay impact structure.

The Chickahominy Formation was deposited rapidly in outer neritic to upper bathyal marine environments during the last 2 million years of the late Eocene. The Drummonds Corner beds are newly recognized in the Langley core. These beds appear to represent shallower water or more nearshore deposition than the underlying Chickahominy deposits. Paleontology indicates an age in the later part of the early Oligocene, with a sharp floral and faunal break between the Drummonds Corner beds and the underlying Chickahominy Formation. Late Oligocene sedimentation is represented by the Old Church Formation.

The record of early and middle Miocene deposition in the Langley core is incomplete. The Calvert Formation records brief episodes of deposition in three members, which are separated by unconformities and are called the informal Newport News beds, the Plum Point Member, and the Calvert Beach Member.

A second episode of rapid deposition at the Langley site is preserved as the upper Miocene St. Marys and Eastover Formations. The Eastover is overlain unconformably by the Yorktown Formation, which is both late early and early late Pliocene. The highest unit, the Tabb Formation (Pleistocene), was not studied paleontologically.

Continued movement along faults and fractures of the crater and nearby region may have enhanced the contributions of older material into the various units filling the Chesapeake Bay impact crater, as suggested by the conspicuous reworking of microfossils in many of the samples from the upper Eocene and younger units in the USGS-NASA Langley core.

Introduction

At about 35–36 Ma (about 35 million–36 million years ago), a comet or asteroid hit in shallow marine waters where the Eastern Shore of Virginia is now located (see Horton and others, this volume, chap. A). The USGS-NASA Langley corehole (fig. H1) is near the outer margin of the crater produced by this late Eocene impact. It was drilled during the summer and fall of 2000 in the city of Hampton, Va. Drilling was done by the U.S. Geological Survey (USGS) and its partners (see "Acknowledgments"). The synimpact deposits recovered from the Langley core are discussed in chapters C and D, this volume. Here, we discuss the paleontology of the 235.65 meters (m; 773.12 feet (ft)) of sediments that were deposited subsequent to the impact (table H1; fig. H2).

The lithostratigraphy of the postimpact sediments is described in detail by Powars and others (this volume, chap. G). Upper Eocene, lower Oligocene, and upper Oligocene sediments from the Maryland-Virginia Coastal Plain are unknown or poorly known in outcrop. The Langley core provides an exceptional opportunity to detail the paleontology of these sediments. Miocene, Pliocene, and Pleistocene units have been recognized for nearly 200 years and have been studied extensively in outcrops in Virginia, Maryland, and Delaware. The Langley core provides the opportunity to relate some of these classic stratigraphic units to microfossil and megafossil studies of the

[1]U.S. Geological Survey, Reston, VA 20192.
[2]U.S. Geological Survey, Menlo Park, CA 94205.
[3]U.S. Geological Survey, Woods Hole, MA 02543.

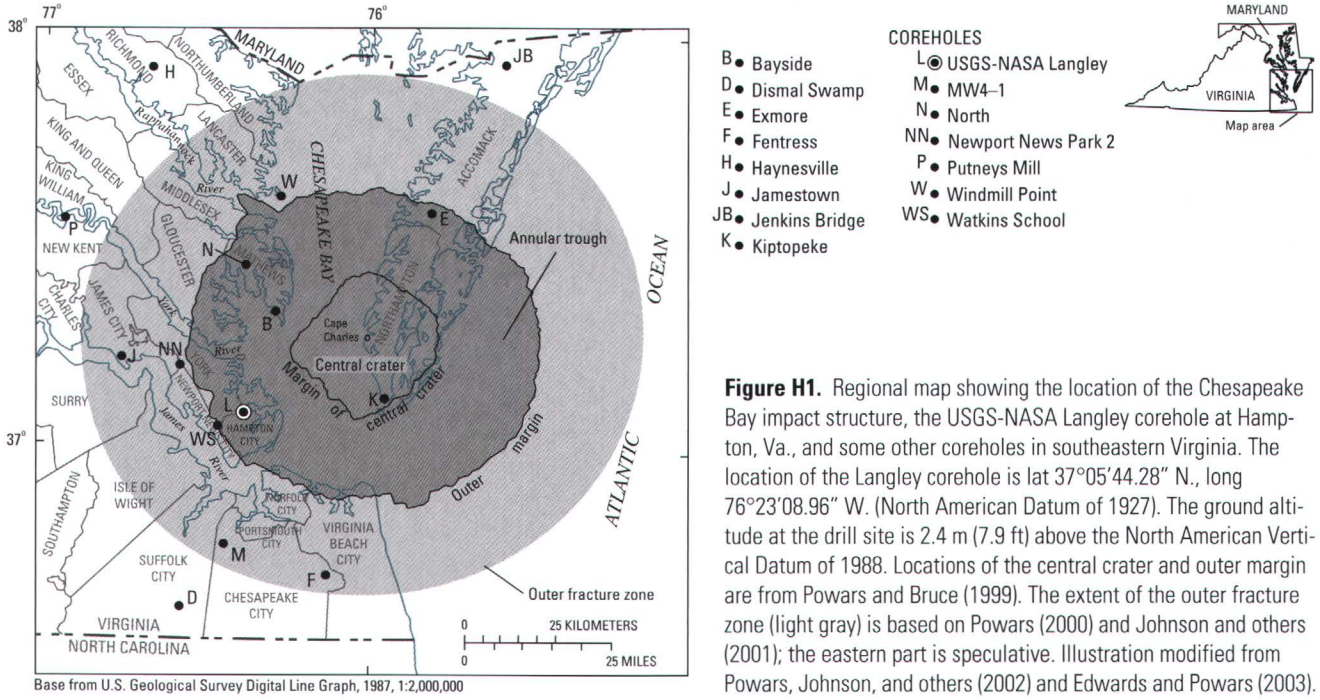

Base from U.S. Geological Survey Digital Line Graph, 1987, 1:2,000,000

Figure H1. Regional map showing the location of the Chesapeake Bay impact structure, the USGS-NASA Langley corehole at Hampton, Va., and some other coreholes in southeastern Virginia. The location of the Langley corehole is lat 37°05'44.28" N., long 76°23'08.96" W. (North American Datum of 1927). The ground altitude at the drill site is 2.4 m (7.9 ft) above the North American Vertical Datum of 1988. Locations of the central crater and outer margin are from Powars and Bruce (1999). The extent of the outer fracture zone (light gray) is based on Powars (2000) and Johnson and others (2001); the eastern part is speculative. Illustration modified from Powars, Johnson, and others (2002) and Edwards and Powars (2003).

Table H1. Postimpact stratigraphic units discussed in this chapter.

Age	Stratigraphic unit	Known from outcrops?	Recognized in Langley core?	Thickness in Langley core	
				(meters)	(feet)
Holocene	Alluvium, swamp, beach deposits	Yes	No	–	–
Pleistocene	Tabb Formation	Yes	Yes	2.2	7.2
Pleistocene	Shirley Formation	Yes	No	–	–
Pleistocene	Chuckatuck Formation	Yes	No	–	–
Pleistocene	Charles City Formation	Yes	No	–	–
Pliocene-Pleistocene	Windsor Formation	Yes	No	–	–
Pliocene	Bacons Castle Formation	Yes	No	–	–
Pliocene	Chowan River Formation	Yes	No	–	–
Pliocene	Yorktown Formation	Yes	Yes	21.1	69.1
Miocene	Eastover Formation	Yes	Yes	45.1	148.2
Miocene	St. Marys Formation	Yes	Yes	55.2	181.0
Miocene	Choptank Formation	Yes	No	–	–
Miocene	Calvert Formation*	Yes	Yes	19.9	65.4
Oligocene	Old Church Formation	Yes; few, very thin	Yes	32.5	106.5
Oligocene	Drummonds Corner beds	No; first reported in Langley core	Yes	7.3	23.9
Oligocene	Delmarva beds	No; subsurface only	No	–	–
Eocene	Chickahominy Formation	No; subsurface only	Yes	52.4	171.82

*Three members of the Calvert Formation are mentioned in this chapter; they record brief episodes of deposition, are separated by unconformities, and are called the informal Newport News beds, the Plum Point Member, and the Calvert Beach Member.

core. Table H1 provides a summary of the stratigraphic units discussed in this chapter.

Paleontologic studies of the postimpact sediments in the USGS-NASA Langley core included work on calcareous nannofossils, dinoflagellates and acritarchs, diatoms and silicoflagellates, mollusks, ostracodes, planktonic foraminifera and bolboformids, and vertebrate remains. Complete taxonomic names are given in appendix H1. Photographs of selected fossils are shown in plates H1–H9. After summaries of previous work, lithostratigraphy, and methods, this chapter contains paleontologic interpretations for each postimpact unit in the Langley core.

Previous Work and Zonations Used

Beginning in the early 19th century, the exposures along the Chesapeake Bay and the riverbanks of Maryland and Virginia have been studied by many researchers, including Thomas Say (1822, 1824), T.A. Conrad (for example, 1832, 1833), W.B. Rogers (1884), W.B. Clark (1895), G.C. Martin (1904), and Clark and Miller (1912). In 1890, G.D. Harris did an extensive study of the bluffs at Yorktown, Va. (published in Ward, 1993). Multidisciplinary studies of the subsurface Virginia Coastal Plain include work on the Oak Grove core (Gibson and others, 1980), the Haynesville cores (Mixon, 1989), and the Fentress, Dismal Swamp, and Exmore cores (Powars and others, 1992). Paleontological data from the Chesapeake Bay impact structure are included in Powars and Bruce (1999) and Powars (2000).

Time scale.—In this chapter, we use the time scale of Berggren and others (1995). Correlation of the time scale with the relevant calcareous nannofossil, dinoflagellate, diatom, silicoflagellate, mollusk, and planktonic foraminifera zones is shown in figure H3.

Calcareous nannofossils.—The calcareous nannofossil zonation used for the upper 236 m (773 ft) of Cenozoic strata in the USGS-NASA Langley core is based upon the zonation of Martini (1971). Calcareous nannofossil biostratigraphy is based on the highest and lowest occurrences of species; FAD indicates a first appearance datum, and LAD indicates a last appearance datum. Important Cenozoic nannofossil datums are given in appendix H2.

Dinoflagellates and acritarchs.—Although there are no widely accepted worldwide zonations for the dinoflagellate cysts (dinocysts) of the Tertiary, two local zonations for the Salisbury embayment of the Atlantic Coast have been published. Edwards (1996) erected six named zones that cover the latest Paleocene to early Eocene. De Verteuil and Norris (1996) erected 10 named and numbered zones (DN1–DN10) that cover the Miocene. Miscellaneous microfossils called acritarchs are studied with dinocysts.

Diatoms and silicoflagellates.—Siliceous microfossils (including diatoms and silicoflagellates) have been documented for more than 100 years from the middle Miocene of the mid-Atlantic coastal region in both outcrop and core material. Earlier studies were largely descriptive, whereas the biostratigraphic studies of the past 20 years (see summaries in Andrews, 1988, and Abbott, 1984) have concentrated on correlating regional zonal schemes with deep-sea zonations and with the geological time scale.

Mollusks.—Mansfield (1943) published his research on the stratigraphy of the Miocene and Pliocene strata of Virginia in Gardner's (1943) work on the molluscan fauna. L.W. Ward and B.W. Blackwelder began extensive work on the physical stratigraphy and molluscan biostratigraphy of the mid-Atlantic Coastal Plain in the 1970s, publishing revisions of the Eocene through Pliocene units (Ward and others, 1978; Ward and Blackwelder, 1980) and establishing molluscan faunal zones (Blackwelder, 1981; Ward, 1992).

Ostracodes.—In contrast to the Gulf of Mexico region, where detailed ostracode zonations exist (see Poag, 1974; Hazel and others, 1980), only a few isolated Eocene-Oligocene ostracode faunas from the Chesapeake Bay region have been described and illustrated in the published literature (for example, Swain, 1951; Deck, 1985). Therefore, the papers of Pooser (1965) and Hazel and others (1980) and references therein were used for species identification of Eocene-Oligocene faunas. The papers of Valentine (1971), Hazel (1983), and Cronin (1990) were used for taxonomy of Miocene and Pliocene faunas. The ostracodes from the classic Miocene Calvert Cliffs of Maryland were described by Ulrich and Bassler (1904), and their taxonomy was updated by Forester (1980).

Planktonic foraminifera and bolboformids.—Previous studies of planktonic foraminifera and bolboformids from cores within or near the Chesapeake Bay impact crater include those by Poag and Aubry (1995), Poag and Commeau (1995), and Poag (1997).

Vertebrates.—No vertebrate biostratigraphic zonation has been erected yet for upper Eocene and Oligocene stratigraphic units in the Atlantic Coastal Plain. The only published vertebrate reports on this general part of the stratigraphic column in the Atlantic Coastal Plain are papers on the selachians of the upper Oligocene or lower Miocene Trent Formation of North Carolina (Case, 1980), late Eocene selachians of south-central Georgia (Case, 1981), and selachians and otoliths from the middle Eocene Piney Point Formation and upper Oligocene Old Church Formation (Müller, 1999).

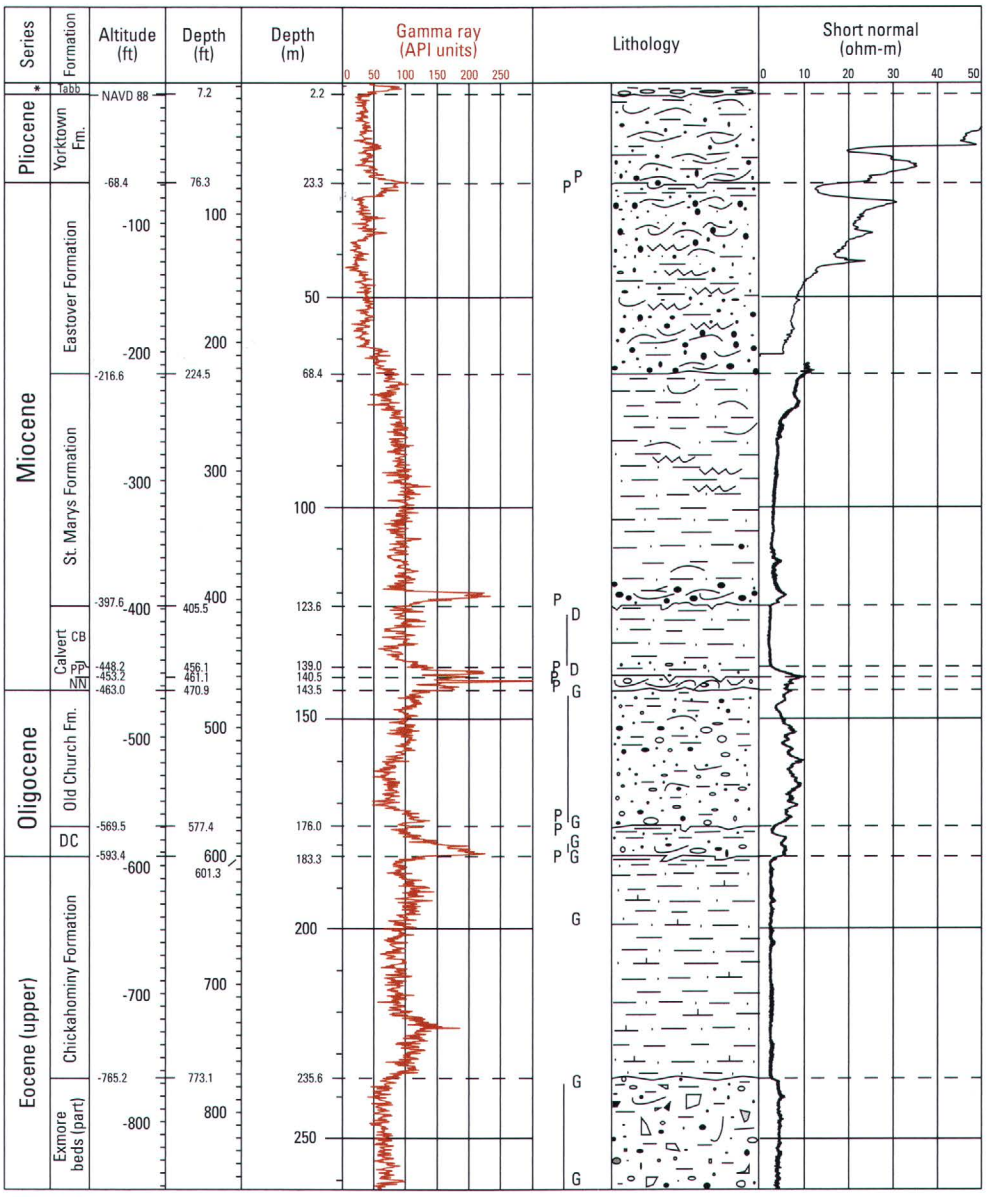

*Pleistocene.

Figure H2. Stratigraphic column of postimpact units in the USGS-NASA Langley core showing selected geophysical logs, generalized lithology, and locations of samples studied for fossils. Calcareous nannofossil zonation (NP, NN numbers) is from Martini (1971), dinoflagellate zonation (DN) is from de Verteuil and Norris (1996) and de Verteuil (1997), diatom zonation, (*D. penelliptica* = *Delphineis penelliptica* Zone) is from Abbott (1980), silicoflagellate zonation (*C. t.* = *Corbisema triacantha* Zone; *D. s.* = *Distephanus stauracanthus* Subzone; *D. sch.* = *Distephanus schulzii* Subzone) is from Bukry (1981) and Perch-Nielsen (1985), molluscan zonation (M) is based on Blackwelder (1981) and Ward (1992), ostracode zonation is from Hazel (1971), and planktonic foraminiferal zonation (P) is from Berggren and Miller (1988). The Calvert Formation contains the informal Newport News beds (NN), the Plum Point Member (PP), and the Calvert Beach Member (CB). Definitions: DC = Drummonds Corner beds; ft = feet; m = meters; NAVD 88, North American Vertical Datum of 1988; ohm-m = ohm-meters.

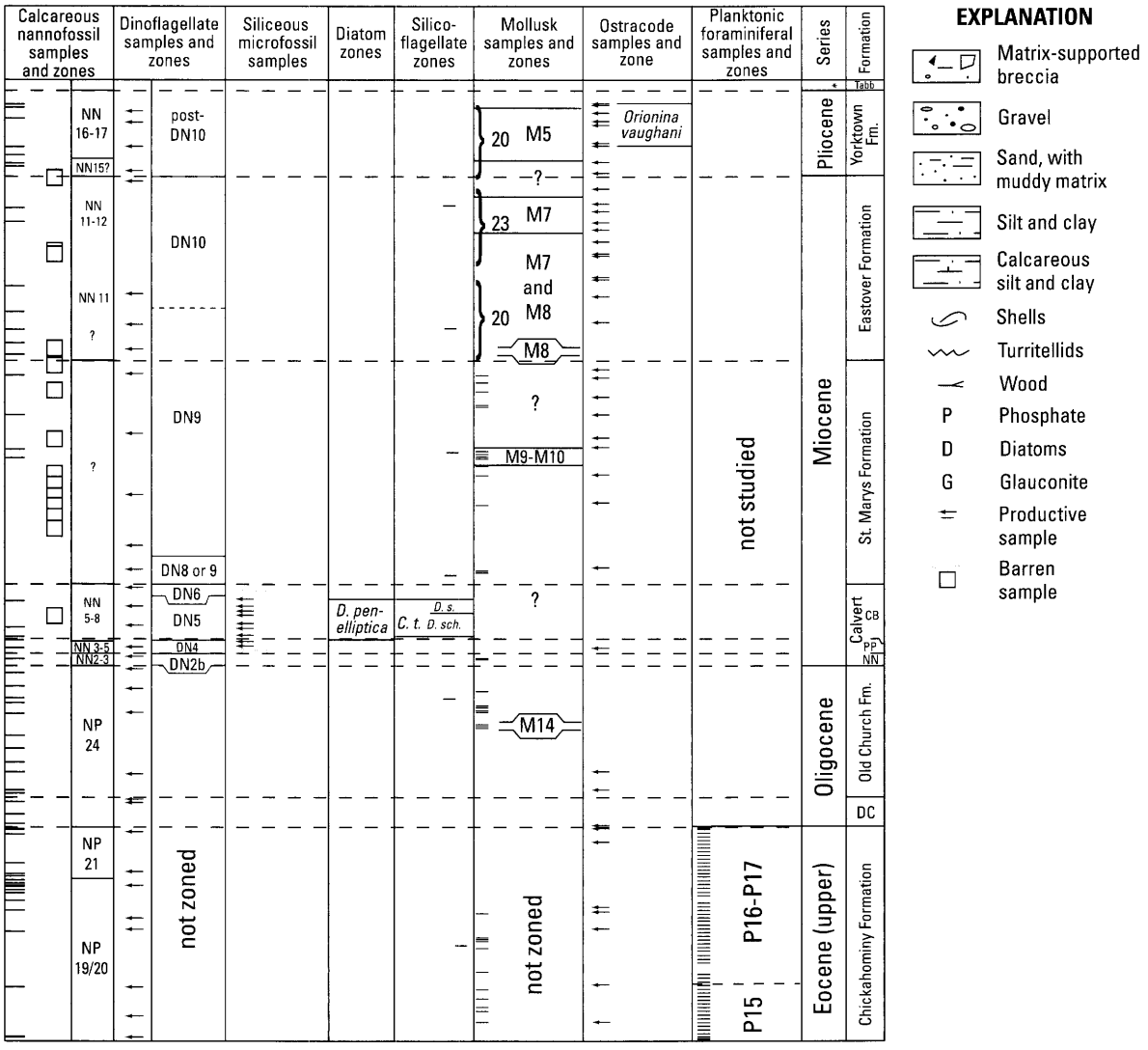

EXPLANATION

- Matrix-supported breccia
- Gravel
- Sand, with muddy matrix
- Silt and clay
- Calcareous silt and clay
- Shells
- Turritellids
- Wood
- P — Phosphate
- D — Diatoms
- G — Glauconite
- Productive sample
- Barren sample

Figure H2. Continued.

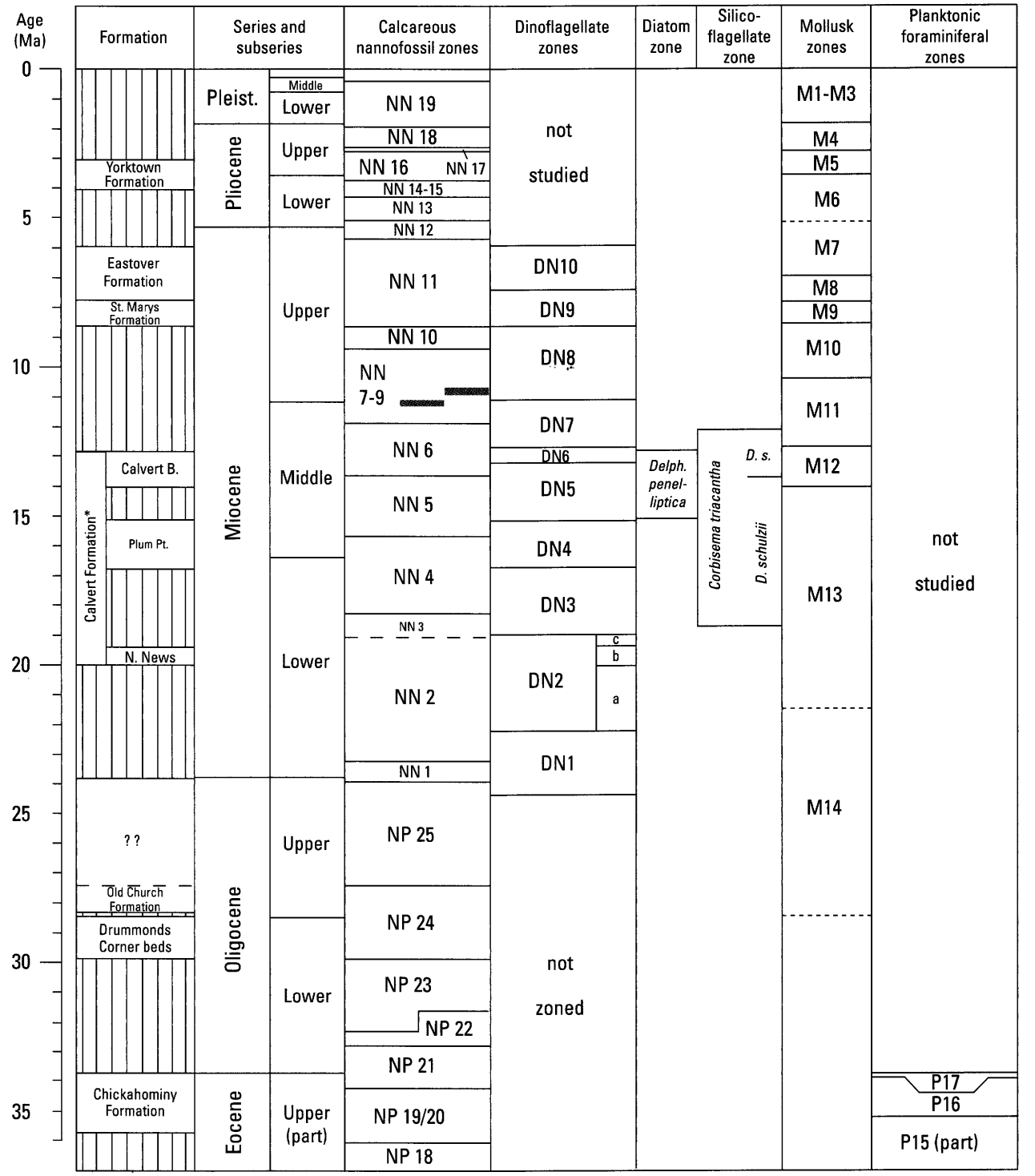

* The Calvert Formation contains the informal Newport News beds, the Plum Point Member, and the Calvert Beach Member.

Lithostratigraphy of Postimpact Deposits in the USGS-NASA Langley Corehole

The physical geology of the postimpact sediments in the USGS-NASA Langley core is described in detail by Powars and others (this volume, chap. G). A brief overview is given here.

The base of the Chickahominy Formation in the Langley core represents the beginning of in-place postimpact deposition. This contact is placed at a depth of 235.65 m (773.12 ft) in the core, where massive, calcareous, marine silty clay bearing in-place microfossils overlies a horizontally laminated quartz-glauconitic silt bearing mixed and altered microfossil assemblages. The Chickahominy Formation is a thick section of calcareous clay representing late Eocene deposition.

The Chickahominy Formation is overlain by a shallower marine unit, informally termed the Drummonds Corner beds. These quartz-glauconite sands are placed in the upper part of the lower Oligocene. The lower contact of the Drummonds Corner beds is unconformable and heavily burrowed; it is at a depth of 183.3 m (601.3 ft).

Figure H3 (facing page). Correlation chart for the stratigraphic units and zonations used in the study of the postimpact deposits in the USGS-NASA Langley core. Tabb Formation is not shown. Time scale in Ma (millions of years before present) is from Berggren and others (1995). Calcareous nannofossil zonation is from Martini (1971). Calcareous nannofossil zones NN 7, NN 8, and NN 9 are grouped here. Berggren and others (1995, p. 191) noted inconsistent correlations with the magnetic polarity record, and they presented two separate correlation possibilities for Zone NN 8 (shown in gray). Dinoflagellate zonation and correlations with the time scale of Berggren and others (1995) are from de Verteuil and Norris (1996). Diatom zone is from Abbott (1980). Silicoflagellate zone and subzones are from Bukry (1981) and Perch-Nielsen (1985); abbreviations are defined in figure H2. Mollusk zones are based on Blackwelder (1981) and Ward (1992). Correlation of M zones with DN zones for the Miocene portion of the section is based on de Verteuil and Norris (1996). No data exist to correlate M14, established by Ward (1992), with either DN zones or time; the dashed line indicates an estimate of its placement based on the lithostratigraphic units in which Ward found M14 mollusks. The boundary between M6 and M7 is tentatively placed at the Miocene-Pliocene boundary where Ward (1992) placed it in his stratigraphic section, but no data exist to correlate the M7-M6 boundary with time or DN zones. M1, M2, and M3 of Blackwelder (1981) represent little time and are not present in the Langley core; therefore, they are grouped together in this section. Planktonic foraminiferal zonation is from Berggren and others (1995).

Both the Chickahominy Formation and the Drummonds Corner beds are known only from the subsurface. The Chickahominy Formation was first described from wells in York County, Va. (Cushman and Cederstrom, 1945). The Drummonds Corner beds are newly recognized in the Langley core, although they most likely have been encountered in previously drilled cores in Virginia (Powars and others, this volume, chap. G). They are stratigraphically higher than beds that were informally called the Delmarva beds in the Exmore corehole (fig. H1), located to the northeast of the Langley corehole. No sediments equivalent to the Delmarva beds are recognized in the Langley core.

The Drummonds Corner beds are overlain in the Langley core by the Old Church Formation, a glauconitic, phosphatic quartz sand of late Oligocene age. The lower contact of the Old Church is at a depth of 176.0 m (577.4 ft). The Old Church was first recognized in outcrop by Ward (1985), where it is less than 2 m (6 ft) thick. It has also been recognized in the subsurface (Mixon and others, 1989; Powars and Bruce, 1999; Powars, 2000) and is 32.5 m (106.5 ft) thick at the USGS-NASA Langley corehole site inside the impact structure.

Overlying the Old Church Formation in the Virginia Coastal Plain are Miocene and Pliocene units that may include, in ascending order, the Calvert, Choptank, St. Marys, Eastover, Yorktown, Chowan River, and Bacons Castle Formations (table H1). These are typically overlain by one or more Quaternary units. The Calvert Formation is well represented at Calvert Cliffs along the western shore of the Chesapeake Bay in Maryland and has been studied for over a century (Shattuck, 1902, 1904). The Calvert is typically fine grained and is locally diatomaceous.

In studying the Langley core, we recognize three units within the Calvert Formation (in ascending order from a depth of 143.5 m (470.9 ft)): the informal Newport News beds and two formally named members, the Plum Point Member and the Calvert Beach Member. The Newport News beds consist of 3.0 m (9.8 ft) of shelly sands of early Miocene age. The Plum Point and Calvert Beach Members consist of microfossiliferous silts and silty clays, 1.5 m (5.0 ft) and 15.4 m (50.6 ft) thick, respectively, of middle Miocene age.

The Calvert Beach Member of the Calvert Formation is overlain unconformably by the upper Miocene St. Marys Formation. Except for a basal shelly, phosphatic, quartz sand, the St. Marys consists of calcareous clayey silt to sandy clay and silt. The St. Marys Formation in the Langley core extends from 123.6 to 68.4 m (405.5 to 224.5 ft) depth. The Choptank Formation, which lies between the Calvert and St. Marys Formations elsewhere, is not recognized in the Langley core.

The St. Marys Formation in the Langley core is overlain by the upper Miocene Eastover Formation, which has a shelly, sandy basal lag and consists of clayey, silty sands. The Pliocene Yorktown Formation overlies the Eastover Formation at a heavily burrowed contact; the contact depth is 23.3 m (76.3 ft).

The Yorktown in this core is a calcareous, muddy sand that has abundant macrofossils and microfossils.

The Yorktown is overlain unconformably by 2.2 m (7.2 ft) of oxidized muddy Quaternary gravel and sand of the Lynnhaven Member of the Tabb Formation. The Tabb elsewhere has been dated as late Pleistocene (Rader and Evans, 1993). The upper Pliocene Chowan River and Bacons Castle Formations are not recognized in the Langley core, nor are additional Quaternary units.

Methods

Selected samples from postimpact sediments in the USGS-NASA Langley core were studied for calcareous nannofossils (Bybell), dinoflagellates and acritarchs (Edwards), diatoms (Barron), silicoflagellates (Bukry), mollusks (Wingard), ostracodes (Cronin), planktonic foraminifera and bolboformids (Poag; see also Poag and Norris, this volume, chap. F), and vertebrate remains (Weems). Most samples for the various fossil groups studied were taken at the drill site. Calcareous nannofossils, dinoflagellates, mollusks, and ostracodes were studied from most or all postimpact stratigraphic units. Diatoms, silicoflagellates, planktonic foraminifera and bolboformids, and vertebrates were studied from one or a few stratigraphic units. Benthic foraminifera from the Chickahominy Formation are discussed by Poag and Norris (this volume, chap. F). For the purpose of formal names of species and genera, calcareous nannofossils, dinoflagellates, diatoms, silicoflagellates, and bolboformids are classified as plants. Mollusks, ostracodes, foraminifera, and vertebrates are classified as animals. Complete taxonomic names are given in appendix H1.

For precision, endpoint depths of sampling intervals for some fossils are given in feet to the number of decimal places recorded at the time of sampling. For small samples, their locations in the core are given by only single depths.

Calcareous nannofossil samples.—Seventy-one Cenozoic calcareous nannofossil samples were examined from the upper 235.65 m (773.12 ft) of the Langley core. The sample spacing was determined by the ease or difficulty in establishing the age of the units being examined. Deeper water units with abundant calcareous nannofossils throughout were examined with a greater sample spacing than shallower water units. Sample depth in meters is a direct conversion of the sample depth in feet for the entire small sample.

For all calcareous nannofossil samples, a small amount of sediment was extracted from the central portion of a core segment (freshly broken where possible). The samples were dried in a convection oven to remove residual water, and the dry sediment was placed in vials for long-term storage in the calcareous nannofossil laboratory at the USGS in Reston, Va. Semiconsolidated or consolidated samples were ground with a mortar and pestle.

A small portion of each sample was placed in a beaker, stirred, and settled through 20 milliliters (mL) of water. An initial settling time of 1 minute (min) was used to remove the coarse fraction, and a second settling time of 10 min was used to remove the fine fraction. Smear slides were prepared from the remaining suspended material. Coverslips were attached to the slides by using Norland Optical Adhesive 61 (NOA–61), a clear adhesive that bonds glass to glass and cures when exposed to ultraviolet radiation.

Samples were primarily examined by using a Zeiss Axiophot 2 microscope. A few samples with good preservation and abundance were further examined by using a JEOL JSM–6400 scanning-electron microscope (SEM).

Dinoflagellate and acritarch samples.—Samples taken from the Langley core for dinoflagellate and acritarch studies were thoroughly scraped onsite. Sample depth in meters represents the midpoint of the interval sampled.

In the laboratory, up to 80 grams (g) of raw material was weighed and disaggregated. Each sample was treated with hydrochloric acid followed by hydrofluoric acid. Residues from the acid treatments were sieved at 10 and 200 micrometers (μm) and then separated by using a zinc chloride solution having a specific gravity of 2.0. Samples were checked under a microscope to determine if an oxidation and or ultrasonic treatment were needed, and if so, one or both of these steps were performed. All samples were resieved at 10 μm and, if enough residue remained, 20 μm. Samples were then stained with Bismark brown and mounted in glycerin jelly on a glass slide with coverslip. Slides were examined by using a light microscope.

Diatom and silicoflagellate samples.—Samples from between 125.7 and 140.4 m (412.4 and 460.6 ft) depth in the Langley core were collected for the study of diatoms and silicoflagellates. Sample depth in meters represents the midpoint of the interval sampled.

The samples were prepared by boiling them in hydrogen peroxide and later in a dilute solution of hydrochloric acid. Samples were settled for a minimum of 4 hours before excess liquid was decanted off and replaced with distilled water. This washing process was repeated four times until the suspended liquid was of neutral pH. One or two strewn slides were prepared for each sample (cover glass size 22x40 millimeters (mm)) and examined in entirety under the light microscope (at 500x for diatoms and 250x for silicoflagellates). The total silicoflagellates were counted for each slide and tabulated as percentages.

Mollusk samples.—The Langley core was examined for molluscan fauna. Occurrences of large recognizable species and any molluscan remains were noted. Fossiliferous samples were collected at selected intervals for processing and further examination. Sample depth in meters represents the direct conversion of the sample depth in feet; if a range is given, values represent endpoints in both feet and meters.

Samples were washed, the fraction >850 μm was retained, and molluscan fauna specimens recovered were sorted and

identified. Generic assignments for extant groups were updated on the basis of Turgeon and others (1998).

Ostracode samples.—For ostracode samples of the Langley core, sample depth in meters represents the midpoint of the interval sampled. Approximately 50 g of sediment from each sample was processed by soaking sediment overnight in tap water and washing through 63-μm sieves. Ostracodes were picked with a fine brush from the fraction >150 μm. Because the number of individuals was limited in most units, all ostracodes were picked, including fragments. In contrast, some samples from the Eastover and Yorktown Formations contained abundant ostracodes, and about 300 individuals were picked.

Planktonic foraminifera and bolboformid samples.—For planktonic foraminifera and bolboformid samples from the Langley core, sample depth in feet and meters represents the top of the interval sampled. Samples were prepared in a standard manner (wet sieved on a 63-μm screen after 15 min of boiling in a solution of sodium hexametaphosphate). Identification is based on available literature and personal collections of Poag.

Vertebrate samples.—Because the Langley core is relatively narrow and volumetrically small, the chance of recovering any large vertebrate material was virtually nil (unless a large bone or tooth were to be sectioned during coring). Occasional bones and teeth substantially smaller than the diameter of the core could be expected, and such vertebrate remains were isolated by sieving sediment from two units (Chickahominy Formation and Drummonds Corner beds). Sample depth in meters represents the direct conversion of the sample depth in feet; if a range is given, values represent endpoints in both feet and meters.

Paleontology

Chickahominy Formation

The Chickahominy Formation at 235.65–183.3 m (773.12–601.3 ft) depth in the Langley core was studied for calcareous nannofossils (fig. H4, in pocket), dinoflagellates (fig. H5), mollusks (fig. H6, in pocket), ostracodes (fig. H7), planktonic foraminifera and bolboformids (fig. H8), and vertebrates (fig. H9). All fossil groups indicate placement in the upper Eocene. This 52-m-thick (172-ft-thick) unit represents approximately 2 million years (m.y.) of depositional accumulation. As explained below, the environment of deposition was marine. Benthic foraminifera indicate outer neritic to upper bathyal paleodepths; a nutrient-rich, oxygen-depleted environment is likely.

Calcareous nannofossils.—Eighteen samples from the Chickahominy Formation in the Langley core were examined for calcareous nannofossil content (fig. H4). Most of the samples contained abundant calcareous nannofossils with good preservation. The remainder contained common or abundant nannofossils with moderate preservation. Calcareous nannofossil assemblages were sufficient in number of specimens, diversity of taxa, and preservational state to allow placement of samples within one specific zone.

Samples from 235.0 to 196.4 m (770.9 to 644.5 ft) indicate placement in upper Eocene Zone NP 19/20 based on the presence of *Isthmolithus recurvus* (FAD defines base of Zone NP 19/20; see appendix H2) and *Discoaster saipanensis* (LAD defines the top of Zone NP 19/20), which occur in all samples within this depth range (fig. H4). *Cribrocentrum reticulatum* and *Discoaster barbadiensis* have LADs very near the top of Zone NP 19/20. *Cribrocentrum reticulatum* has its highest occurrence at 222.7 m (730.5 ft), and *D. barbadiensis* has its highest occurrence at 209.0 m (685.8 ft). Therefore, the interval between 222.7 and 196.4 m (730.5 and 644.5 ft) is placed in the very uppermost part of Zone NP 19/20, in what is assumed to be an expanded section.

Samples from 195.5 to 183.6 m (641.5 to 602.5 ft) are placed within Zone NP 21 on the basis of the absence of *D. saipanensis* (LAD defines the top of Zone NP 19/20) and the presence of *Cyclococcolithus formosus* (LAD defines the top of Zone NP 21). According to Berggren and others (1995), Zone NP 21 spans the Eocene-Oligocene boundary. Calcareous nannofossils do not clearly indicate whether the Zone NP 21 material in the Langley core is within the upper Eocene or lower Oligocene part of this zone. However, a late Eocene age is more likely because both *Chiasmolithus titus* and *Blackites tenuis* are present in parts of this interval. These two species have their LADs in the lower part of Zone NP 21. Additional evidence for a late Eocene age is the absence of a noticeable unconformity in the core between the uppermost Zone NP 19/20 material, which is very late Eocene, and the Zone NP 21 material.

The boundary between calcareous nannofossil Zone NP 19/20 and Zone NP 21 was calibrated at 34.2 Ma by Berggren and others (1995) for low and middle latitudes (fig. H3). In the Langley core, this boundary is bracketed by closely spaced samples from 196.4 and 195.5 m (644.5 and 641.5 ft).

Poag and Aubry (1995) reported an assignment of Zone NP 19/20 for Chickahominy Formation samples examined from the Exmore and Kiptopeke coreholes, which are also located within the Chesapeake Bay impact crater (fig. H1).

Dinoflagellates and acritarchs.—Eight samples from the Chickahominy Formation in the Langley core yielded highly diverse dinoflagellate assemblages of late Eocene age (fig. H5); selected specimens are shown in plates H1–H3. Sample depths range from 235.2 to 185.2 m (771.6 to 607.5 ft). Preservation ranges from fair to good.

Typical late Eocene species present include *Areosphaeridium diktyoplokus*, *Batiacasphaera baculata*, *Batiacasphaera compta*, *Trigonopyxidia fiscellata*, and *Cordosphaeridium funiculatum*. Species that are present in the Chickahominy but not to the top of the unit include *Charlesdowniea variabilis* (highest occurrence is in sample R6110 DA, 230.2 m=755.2–755.5 ft), *Diphyes colligerum* (highest occurrence is in sample R6110 AO, 209.3 m=686.4–686.8 ft), *Rhombodinium perfora-*

Unit	Chickahominy Formation								DC beds		Old Church Formation			
Depth to midpoint (m)	235.2	230.2	222.7	209.3	206.7	198.8	195.1	185.2	178.0	177.3	171.1	155.8	150.0	144.9
Depth range (ft)	771.4–771.6	755.2–755.5	730.3–730.7	686.4–686.8	677.9–678.3	652.0–652.4	639.9–640.3	607.5–607.9	583.8–584.1	581.5–581.9	561.0–561.4	511.0–511.4	492.0–492.2	475.4–475.7
Taxon / Sample number R6110	DB	DA	AR	AO	AN	AL	AK	AI	AH	AG	AF	AD	AB	AA
Achilleodinium biformoides	.	.	X	X	X	X	X	X	X	X	R	.	.	.
Apteodinium spiridoides	.	.	.	.	.	.	.	.	.	.	X	.	.	.
Areosphaeridium diktyoplokus	.	.	.	.	X	.	.	X	.	.	.	.	.	.
Batiacasphaera baculata	.	.	X	X	X	.	X	X	.	.	.	.	.	.
Batiacasphaera compta	.	.	X	X	X	.	X	X	.	.	R	.	.	.
Batiacasphaera hirsuta	.	.	.	.	.	.	.	.	?	.	.	.	.	.
Batiacasphaera sphaerica	.	.	.	.	.	.	.	.	.	.	.	X	.	X
Charlesdowniea coleothrypta	.	X	X	X	X	X	X	X	.	.	.	.	.	.
Charlesdowniea variabilis	X	X	.	.	.	.	.	.	.	.	.	.	.	.
Chiropteridium galea	.	.	.	.	.	.	.	.	.	.	X	X	X	X
Chiropteridium lobospinosum	.	.	.	.	.	.	.	.	X	X	X	X	X	X
Cleistosphaeridium placacanthum	X	.	X	X	X	X	X	X	X	X	X	X	X	X
Cordosphaeridium cantharellus	.	.	X	X	X	X	X	X	X	X	X	X	.	.
Cordosphaeridium fibrospinosum	.	.	.	X	.	.	.	.	.	.	.	.	.	.
Cordosphaeridium funiculatum	X	X	X	X	X	X	X	X	.	.	R	.	R	.
Cordosphaeridium gracile	.	.	.	X	X	.	.	.	.	.	.	.	.	.
Corrudinium incompositum	.	.	X	.	.	.	X	?	.	.	.	.	.	.
Corrudinium sp.	.	.	.	.	.	.	.	.	.	.	.	X	.	.
Cribroperidinium spp.	X	X	X	X	X	X	X	X	.	.	X	.	X	X
Cyclopsiella vieta	.	?	X	.	.	.	X	.	.	X	.	.	.	.
Cyclopsiella sp.	.	.	.	.	.	.	.	.	.	X	.	.	.	.
Dapsilidinium pseudocolligerum	.	.	X	X	X	X	X	X	X	X	X	X	X	X
Deflandrea phosphoritica and forms intermediate with *D. heterophlycta*	X	X	X	X	X	X	X	X	.	.	R?	.	.	.
Deflandrea phosphoritica (incl. *D. phosphoritica* var. *spinulosa*)	.	.	.	.	.	.	.	.	.	.	X	X	X	X
Dinopterygium cladoides sensu Morgenroth (1966)	.	.	X	.	X	X	X	X	X	X	.	X	.	.
Diphyes colligerum	.	.	.	X	.	.	.	.	.	.	.	.	.	.
Distatodinium ellipticum	.	.	.	.	X	?	.	X	.	.	.	.	.	.
Distatodinium spp.	.	.	X	.	.	.	X	.	.	X	X	X	.	.
Dracodinium varielongitudum	R	.	.	.	.	.	.	.	.	.	.	.	.	.
Ennaedocysta sp. or spp.	.	.	X	X	X	X	X	X	.	.	R	.	.	.
Eocladopyxis peniculata	.	.	.	.	.	.	.	.	.	.	R	.	.	.
Heteraulacacysta porosa	.	X	?	.	X	.	?	X	.	.	R	.	.	.
Histiocysta sp. of Stover and Hardenbol (1993 [1994])	.	X	.	X	X	.	X	X	.	.	.	.	.	.
Homotryblium aculeatum	.	.	.	X	X	.	.	.	.	.	.	.	.	.
Homotryblium plectilum	.	.	.	X	X	.	.	.	X	.	X	.	.	X
Homotryblium vallum	.	.	.	.	.	.	.	.	X	X	X	.	.	X
Hystrichokolpoma cinctum	.	.	.	.	.	.	X	.	X	X	X	X	.	.
Hystrichokolpoma rigaudiae	.	.	X	X	X	X	X	X	X	.	.	X	.	X
Hystrichostrogylon aff. *coninckii* of De Coninck (1995)	.	.	.	.	.	.	.	X	.	.	.	.	.	.
Kallosphaeridium capulatum	.	.	.	.	X	.	.	X	.	.	.	.	.	.
Lejeunecysta hyalina	.	.	X	.	.	.	.	.	.	.	.	.	.	.
Lejeunecysta spp.	.	.	.	.	X	.	.	X	X	?	.	.	.	X

Lentinia serrata	.	.	.	.	X	.	.	.	.	.	.	.	.	.	
Lingulodinium machaerophorum (incl. *L. siculum*)	.	.	X	X	X	X	X	X	X	X	X	X	X	X	
Lophocysta? sp. indet. of De Coninck (1986)	.	.	.	X	.	X	.	.	.	.	.	.	.	.	
Membranophoridium aspinatum	.	.	.	.	X	.	.	.	X	X	X	.	X	.	
Nematosphaeropsis pusulosa	.	.	X	.	.	.	X	X	.	.	.	.	.	.	
Operculodinium centrocarpum	.	.	.	.	.	X	.	.	X	.	.	.	.	.	
Operculodinium divergens	.	.	.	.	.	X	.	.	.	.	.	.	.	.	
Operculodinium? *placitum*	.	.	.	.	.	X	.	.	.	.	.	.	.	.	
Operculodinium spp.	.	X	.	.	X	.	X	X	.	.	.	X	X	X	
Palaeocystodinium golzowense	X	X	X	X	X	X	X	X	X	X	X	X	.	X	
Pentadinium imaginatum	.	.	.	.	.	.	.	.	.	.	.	.	X	.	
Pentadinium laticinctum subsp. *laticinctum*	X	X	X	X	X	X	X	X	X	.	.	.	.	.	
Pentadinium laticinctum (grano-vermiculate forms)	.	X	.	X	X	X	X	X	X	gr	X	X	.	.	
Pentadinium membranaceum	R?	.	.	.	.	.	.	.	.	.	.	.	.	.	
Pentadinium sp. I of Edwards (1986)	.	.	.	.	.	.	.	.	.	.	.	X	.	.	
Phthanoperidinium comatum	.	.	X	.	X	.	.	X	.	.	.	.	.	.	
Reticulatosphaera actinocoronata	.	.	.	.	.	.	.	.	X	X	X	.	.	.	
Rhombodinium perforatum	.	.	X	.	X	.	.	.	.	.	.	.	.	.	
Rottnestia borussica	.	X	.	.	?	.	.	.	.	.	.	.	.	.	
Samlandia chlamydophora	.	X	X	X	X	.	.	.	.	.	.	.	.	.	
Samlandia chlamydophora sensu Stover and Hardenbol (1993 [1994])	.	.	.	.	.	X	X	X	.	.	.	.	.	.	
Saturnodinium pansum	.	.	.	.	.	.	.	.	.	.	?	X	X	.	
Saturnodinium sp.	.	.	X	X	X	.	X	X	.	X	R	.	? (R)	.	
Selenopemphix brevispinosa subsp. *brevispinosa*	.	.	X	.	.	.	.	.	.	.	.	.	.	.	
Selenopemphix nephroides	.	.	.	X	.	X	.	.	.	.	.	.	.	.	
Selenopemphix sp.	.	.	.	.	.	.	.	X	.	.	.	.	.	.	
Spiniferites mirabilis	.	.	.	.	.	.	.	.	.	X	X	X	.	.	
Spiniferites pseudofurcatus	X	.	X	X	X	X	X	X	X	X	X	.	.	X	
Spiniferites spp.	.	.	X	X	X	X	X	X	X	X	X	X	X	X	
Tectatodinium pellitum	.	X	.	X	.	.	X	X	X	.	X	.	.	X	
Thalassiphora delicata	.	.	.	.	.	.	X	.	.	.	.	.	.	.	
Thalassiphora pelagica	.	.	X	X	X	X	X	X	X	X	X	.	.	.	
Thalassiphora reticulata	.	.	.	.	X	.	.	.	.	.	.	.	.	.	
Trigonopyxidia fiscellata	X	.	X	.	.	.	X	X	.	.	R	.	.	.	
Tuberculodinium vancampoae	.	.	.	.	.	.	.	.	.	.	X	X	.	X	
Wetzeliella symmetrica	.	.	.	.	.	.	.	.	X		.	.	.	.	
Wetzeliella sp.	X	.	X	.	.	.	.	.	.	X	X	.	.	.	
new genus?, new species (apical archeopyle, areolig. group, with ectophragm)	.	.	.	.	.	.	.	.	.	.	.	.	.	X	
miscellaneous areoligeracean forms (mostly *Glaphyrocysta* spp.)	X	X	X	X	.	X	.	.	X	.	X	.	.	.	
miscellaneous peridiniacean forms	.	X	X	X	X	.	X	X	.	.	.	X	X	.	
additional reworked specimens (Cretaceous, Paleocene, Eocene)	R	R	R	.	R	.	R	R	R	?	R	.	.	.	
Preservation	fair	fair	fair	good	good	good	fair	fair	fair	good	var.	poor	poor	poor	

Figure H5. Occurrence chart showing the presence of dinoflagellates in samples from the Chickahominy Formation, Drummonds Corner (DC) beds, and Old Church Formation in the USGS-NASA Langley core. Selected specimens are shown in plates H1–H4. Definitions: X=present, ?=questionably present, R=present but presumably reworked, R?=questionably reworked, ?(R)=questionably identified, reworked if identification is correct, gr=identified to group only, .=not present, var.=variable.

Genus/species (Depth)	228.8 m (750.6–750.8 ft)	221.7 m (727.2–727.6 ft)	207.9 m (682.0–682.4 ft)	203.7 m (668.1–668.2 ft)	202.6 m (664.6–665.0 ft)	186.7 m (612.4–612.7 ft)	183.4 m (601.7–601.9 ft)	182.5 m (598.7–599.0 ft)	173.8 m (570.2–570.4 ft)	169.2 m (555.0–555.4 ft)	139.2 m (456.4–456.8 ft)	120.2 m (394.2–394.6 ft)	104.2 m (341.6–342.0 ft)	97.2 m (318.8–319.1 ft)	90.6 m (297.0–297.2 ft)	88.1 m (289.1–289.3 ft)	82.4 m (270.0–270.4 ft)	78.1 m (256.3–256.5 ft)	73.4 m (240.6–240.8 ft)	71.3 m (233.9–234.1 ft)	59.6 m (195.5–195.9 ft)	53.3 m (174.9–175.2 ft)	49.3 m (161.5–161.8 ft)	48.8 m (160.0–160.2 ft)	43.3 m (141.8–142.0 ft)	42.7 m (140.1–140.3 ft)	39.7 m (130.1–130.3 ft)	36.8 m (120.5–120.8 ft)	35.0 m (114.8–115.0 ft)	32.1 m (105.3–105.6 ft)	30.5 m (99.9–100.2 ft)	26.7 m (87.5–87.7 ft)	22.8 m (74.7–74.9 ft)	20.3 m (66.5–66.7 ft)	16.1 m (52.8–53.1 ft)	15.4 m (50.5–50.7 ft)	10.8 m (35.4–35.6 ft)	9.7 m (31.7–32.0 ft)	8.0 m (26.1–26.3 ft)	6.1 m (20.0–20.2 ft)	5.6 m (18.4–18.6 ft)
Unit	Chickahominy Formation							DC	OC		PP	St. Marys Formation									Eastover Formation												Yorktown Formation								
Acanthocythereis sp.	.	X	.	.	.	.	.	.	.	.	.	.	.	.	.	.	.	.	.	.	.	.	.	.	.	.	.	.	.	.	.	.	.	.	.	.	.	.	.	.	.
Actinocythereis captionis	.	.	.	.	.	.	.	.	.	.	.	.	.	.	.	.	.	.	.	.	.	.	.	.	.	.	.	.	.	.	.	.	.	.	.	.	.	.	.	X?	X
Actinocythereis cf. *A. dacyi*	.	X	.	X	.	.	.	.	.	.	.	.	.	.	.	.	.	.	.	.	.	.	.	.	.	.	.	.	.	.	.	.	.	.	.	.	.	.	.	.	.
Actinocythereis dawsoni	.	.	.	.	.	.	.	.	.	.	.	.	.	.	.	.	.	.	.	.	X?	.	.	.	.	.	.	.	.	.	.	.	.	X	X	.	.	.	X	.	.
Actinocythereis exanthemata	.	.	.	.	.	.	.	.	X?	.	.	X?	.	.	X?	X	.	X?	.	.	X?	X?	.	X?	X?	.	.	.	.	.	.	.	.	.	.	X?	.	.	.	.	.
Actinocythereis cf. *A. stenzeli*	.	.	X	.	.	.	.	.	.	.	.	.	.	.	.	.	.	.	.	.	.	.	.	.	.	.	.	.	.	.	.	.	.	.	.	.	.	.	.	.	.
Actinocythereis thompsoni	.	.	.	.	.	.	.	.	X	.	.	.	.	.	.	.	.	.	.	.	.	.	.	.	.	.	.	.	.	.	.	.	.	.	.	.	.	.	.	.	.
Actinocythereis sp.	.	.	.	.	.	.	.	X	X	X	.	.	.	.	.	.	.	.	.	.	.	.	.	.	.	.	.	.	.	.	.	.	.	.	.	.	.	.	.	.	.
Alatacythere ivani	.	.	.	.	X	X	X	.	.	.	.	.	.	.	.	.	.	.	.	.	.	.	.	.	.	.	.	.	.	.	.	.	.	.	.	.	.	.	.	.	.
Argilloecia sp.	.	X	.	.	.	.	.	.	.	.	.	.	.	.	.	.	.	.	.	.	.	.	.	.	.	.	.	.	.	.	.	.	.	.	.	.	.	.	.	.	.
Aurila laevicula	.	.	.	.	.	.	.	.	.	.	.	.	.	.	.	.	.	.	.	.	.	.	.	.	.	.	.	.	.	.	.	.	.	.	X	.	.	.	.	.	.
Bensonocythere americana	.	.	.	.	.	.	.	.	.	.	.	.	.	.	.	.	.	.	.	.	.	.	.	.	.	.	.	.	.	.	.	.	.	X	X	.	X	X	X	X	X
Bensonocythere blackwelderi	.	.	.	.	.	.	.	.	.	.	.	.	.	.	.	.	.	.	.	.	.	.	.	.	.	.	.	.	.	.	.	.	.	.	X	.	X	X	X	X	X
Bensonocythere bradyi	.	.	.	.	.	.	.	.	.	.	.	.	.	.	.	.	.	.	.	.	.	.	.	.	.	.	.	.	.	.	.	.	.	.	.	.	.	.	X	.	X
Bensonocythere calverti	.	.	.	.	.	.	.	.	.	.	.	.	.	.	.	.	.	.	.	.	.	.	.	.	.	.	.	.	.	.	.	.	.	.	.	.	.	.	.	X?	.
Bensonocythere ricespitensis	.	.	.	.	.	.	.	.	.	.	.	.	.	.	.	.	.	.	.	.	.	.	.	.	.	.	.	.	.	.	.	.	.	.	.	.	.	.	X?	.	X
Bensonocythere rugosa	.	.	.	.	.	.	.	.	.	.	.	.	.	.	.	.	.	.	.	.	.	.	.	.	.	.	.	.	.	.	.	.	.	.	.	.	X	X	X	.	.
Bensonocythere trapezoidalis	.	.	.	.	.	.	.	.	.	.	.	.	.	.	.	.	.	.	.	.	.	.	.	.	.	.	.	.	.	.	.	.	.	X?	.	.	.	.	.	.	.
Bensonocythere spp.	.	.	.	.	.	.	.	.	.	.	.	.	.	.	.	.	.	.	.	.	.	X	X	.	.	.	.	.	.	.	.	.	.	.	.	X	.	.	.	.	.
Buntonia sp.	.	X	.	.	.	.	.	.	.	.	.	.	.	.	.	.	.	.	.	.	.	.	.	.	.	.	.	.	.	.	.	.	.	.	.	.	.	.	.	.	.
Campylocythere laeva	.	.	.	.	.	.	.	.	.	.	.	.	.	.	.	.	.	.	.	.	.	.	.	.	.	.	.	.	.	.	.	.	.	X	X	X	X	X	X	X	X
Cytherella spp.	.	.	X	.	.	.	X	X	.	.	.	.	.	X	.	X	.	X	.	X	.	.	.	.	.	.	.	.	.	.	.	.	.	.	.	.	.	.	.	.	.
Cytheridea subovalis	.	.	.	.	.	.	.	.	X	.	.	X?	X?	.	.	X	.	X	.	.	X	.	.	.	X	.	.	.	.	.	.	X?	.	.	.	.	.	.	.	.	.
Cytheridea virginiensis	.	.	.	.	.	.	.	.	.	.	.	.	.	.	.	.	.	.	.	.	.	.	.	.	.	.	.	.	.	.	.	.	.	.	.	X	X	X	.	.	X
Cytheridea n. sp.	.	.	.	.	.	.	.	.	.	.	.	.	.	.	X	X	.	.	X	X	.	.	.	.	.	.	.	.	.	.	.	.	.	.	.	.	.	.	.	.	.
Cytheromorpha macroincisa	.	.	.	.	.	.	.	.	.	.	.	.	.	.	.	.	.	.	.	.	.	.	.	.	.	.	.	.	.	.	.	.	.	.	X	X	X	.	.	.	.
Cytheromorpha warneri	.	.	.	.	.	.	.	.	.	.	.	X	.	.	.	.	.	X	X	X	.	.	.	.	.	.	.	X	.	.	.	.	.	.	X	.	X	X	X	.	X
Cytheropteron talquinensis	.	.	.	.	.	.	.	.	.	.	.	.	.	.	.	X	.	X	X	.	X	.	X	X	.	.	.	.	.	.	.	.	.	.	X	.	X	X	X	X	X
Cytheropteron yorktownensis	.	.	.	.	.	.	.	.	.	.	.	.	.	.	.	.	.	.	.	.	.	.	.	.	.	.	.	.	.	.	.	.	.	.	X	X	X	X	.	X	X
Cytheropteron sp.	.	.	.	.	.	.	.	.	.	.	.	.	.	.	.	.	.	X	.	.	.	.	.	.	.	.	.	.	.	.	.	.	.	.	.	.	.	.	.	.	.
Cytherura coryelli	.	.	.	.	.	.	.	.	.	.	.	.	.	.	.	.	.	.	.	.	X	.	.	.	.	.	.	.	.	.	.	.	.	.	.	.	.	X	.	.	.
Cytherura howei	.	.	.	.	.	.	.	.	.	.	.	.	.	.	.	.	.	.	.	.	.	.	.	.	.	.	.	.	.	.	.	.	.	X	X	.	.	.	.	.	.
Cytherura reticulata	.	.	.	.	.	.	.	.	.	.	.	.	.	.	.	.	.	.	.	.	.	.	.	.	.	.	.	.	.	.	.	.	.	.	X	.	.	X	.	.	.
Digmocythere russelli	.	X	.	.	X	X	X	.	.	.	.	.	.	.	.	.	.	.	.	.	.	.	.	.	.	.	.	.	.	.	.	.	.	.	.	.	.	.	.	.	.
Echinocythereis miniscula	.	.	.	.	.	.	.	.	.	.	.	.	.	.	.	X	.	X	.	.	X	.	.	.	.	.	.	.	.	.	.	.	.	.	.	.	.	.	.	.	.
Echinocythereis sp.	.	.	.	.	.	.	.	.	X	.	.	.	.	.	.	.	.	.	.	.	.	.	.	.	.	.	.	.	.	.	.	.	.	.	.	.	.	.	.	.	.
Eucythere gibba	.	.	.	.	.	.	.	.	.	.	.	.	.	.	.	.	.	.	.	.	.	.	.	.	.	.	.	.	.	.	.	.	.	.	.	.	X	X	.	.	.
Haplocytheridea n. sp.	.	.	.	.	.	.	.	X	.	.	.	.	.	.	.	.	.	.	.	.	.	.	.	.	.	.	.	.	.	.	.	.	.	.	.	.	.	.	.	.	.
Hemicytheridea cf. *H. montgomeryensis*	.	X	.	.	.	.	.	.	.	.	.	.	.	.	.	.	.	.	.	.	.	.	.	.	.	.	.	.	.	.	.	.	.	.	.	.	.	.	.	.	.
Henryhowella evax	X	X	.	.	X	X	.	.	.	.	.	X	.	.	.	X	.	.	.	.	.	.	.	.	.	.	.	.	.	.	.	.	.	.	X	.	.	.	.	.	.
Hulingsina americana	.	.	.	.	.	.	.	.	.	.	.	.	.	.	.	.	.	.	.	.	.	.	.	.	.	.	.	.	.	.	.	.	.	X	.	.	.	X	.	.	X
Hulingsina calvertensis	.	.	.	.	.	.	.	.	.	.	.	.	.	.	.	.	.	.	.	.	X	X	X	X	.	.	.	.	.	.	.	.	.	.	.	.	.	.	.	.	.
Hulingsina rugipustulosa	.	.	.	.	.	.	.	.	.	.	.	.	.	.	.	.	.	.	.	.	.	.	.	.	.	.	.	.	.	.	.	.	.	.	X	X	.	X	X	X	X
Hulingsina spp.	.	.	.	.	.	.	.	.	X	.	.	.	.	.	X	X	.	.	.	.	.	.	.	.	X	.	.	.	.	.	X	.	.	.	X	X	X	X	X	X	X
Krithe sp.	.	X	.	.	.	.	.	.	.	.	.	.	.	.	.	.	.	.	.	.	.	.	.	.	.	.	.	.	.	.	.	.	.	.	.	.	.	.	.	.	.
Leguminocythereis sp.	.	.	.	.	.	.	X	.	.	.	.	.	.	.	.	.	.	.	.	.	.	.	.	.	.	.	.	.	.	.	.	.	.	.	.	.	.	.	.	.	.

Leguminocythereis cf. *L. scarabaeus*	.	X	.	.	.	.	.	.	.	.	.	.	.	.	.	.	.	.	.	.	.	.	.	.	.	.	.	.	.	.	.	.	.	.	.	.	.	.	.	.	.
Loxoconcha florencensis	.	.	.	.	.	.	.	.	.	.	.	.	.	.	.	.	.	.	.	.	X	.	X	X	.	.	.	.	.	.	.	.	.	X	.	.	.	.	.	.	.
Loxoconcha reticularis	.	.	.	.	.	.	.	.	.	.	.	.	.	.	.	.	.	.	.	.	.	.	.	.	.	.	.	.	.	.	.	.	.	.	.	X	X	X	X	X	X
Loxoconcha aff. *L. granulata*	.	.	.	.	.	.	.	.	.	.	.	.	.	.	.	.	.	.	.	.	.	.	.	.	.	.	.	.	.	.	.	.	.	.	.	.	.	X	X	X	X
Loxoconcha sp.	.	.	.	.	.	.	.	.	.	.	.	X	.	.	.	X	.	X	.	.	.	.	.	.	.	.	.	.	.	.	.	.	.	.	X	X	.	.	.	.	.
Malzella conradi	.	.	.	.	.	.	.	.	.	.	.	.	.	.	.	.	.	.	.	.	.	.	.	.	.	.	.	.	.	.	.	.	.	X	X	X	X	X	X	X	X
Malzella evexa	.	.	.	.	.	.	.	.	.	.	.	.	.	.	.	.	.	.	.	.	.	.	.	.	.	.	.	.	.	.	.	.	.	.	X	X	X	X	X	X	X
Microcytherura choctawhatcheensis	.	.	.	.	.	.	.	.	.	.	.	.	.	.	.	.	.	.	.	.	.	.	.	.	.	.	.	.	.	.	.	.	.	.	X	X	X	X	X	X	X
Microcytherura shattucki	.	.	.	.	.	.	.	.	.	.	.	.	.	.	.	.	.	.	.	.	.	.	.	X	.	.	.	.	.	.	.	.	.	.	.	.	.	.	.	.	.
Microcytherura similis	.	.	.	.	.	.	.	.	.	.	.	.	.	.	.	.	.	.	.	.	.	.	.	.	.	.	.	.	.	.	.	.	.	X	X	.	X	X	X	X	X
Muellerina blowi	.	.	.	.	.	.	.	.	.	.	.	.	.	.	.	.	.	.	.	.	.	.	.	.	.	.	.	.	.	.	.	.	.	.	.	.	.	X	.	X	X
Muellerina lienenklausi	.	.	.	.	.	.	.	.	X	X	.	.	X	.	X	X	X	X	X	.	.	X	.	.	.	.	.	.	.	.	.	.	.	.	.	.	.	.	.	.	.
Muellerina micula	.	.	.	.	.	.	.	.	.	.	.	.	X	.	.	X?	.	X	.	.	X?	.	X	X	.	.	.	.	.	.	X	.	.	.	.	.	.	.	.	.	.
Muellerina ohmerti	.	.	.	.	.	.	.	.	.	.	.	.	.	.	.	.	.	.	.	.	.	.	.	.	.	.	.	.	.	.	.	.	.	X	.	.	X	X	X	X	X
Muellerina wardi	.	.	.	.	.	.	.	.	.	.	.	.	.	.	.	.	.	.	.	.	.	.	.	.	.	.	.	.	.	.	.	.	.	.	X	X	X	X	X	X	X
Munseyella sp.	.	.	.	.	.	.	.	.	.	.	.	.	.	.	.	.	.	X	.	.	.	.	.	.	.	.	.	.	.	.	.	.	.	.	.	.	.	.	.	.	.
Murrayina barclayi	.	.	.	.	.	.	.	.	.	.	.	.	.	.	.	X	.	.	X	X?	X	X	.	.	.	.	.	.	.	.	.	.	.	.	.	.	X	.	X	X	X
Murrayina macleani	.	.	.	.	.	.	.	.	.	.	.	.	.	.	.	.	.	X	.	X	.	X	X	.	.	.	.	.	.	.	.	.	.	.	.	.	X	.	.	.	.
Murrayina radiata	.	.	.	.	.	.	.	.	.	.	.	.	.	.	.	.	.	.	.	.	X?	.	X?	.	.	.	.	.	.	.	.	.	.	.	.	.	.	.	.	.	.
Neonesidea laevicula	.	.	.	.	.	.	.	.	.	.	.	.	.	.	.	.	.	.	.	.	.	.	.	.	.	.	.	.	.	.	.	.	.	.	.	.	X	X	.	X	X
Orionina vaughani	.	.	.	.	.	.	.	.	.	.	.	.	.	.	.	.	.	.	.	.	.	.	.	.	.	.	.	.	.	.	.	.	.	.	X	X	X	X	X	X	X
Paracytheridea altila	.	.	.	.	.	.	.	.	.	.	.	.	.	.	.	.	.	.	.	.	.	.	.	.	.	.	.	.	.	.	.	.	.	.	X	X	X	X	X	X	X
Paracytheridea cf. *P. mucra*	.	.	.	.	.	.	.	.	.	.	.	.	.	.	.	.	.	.	.	.	.	.	.	.	.	.	.	.	.	.	.	.	.	.	.	.	X	X	X	X	X
Paracytheridea rugosa	.	.	.	.	.	.	.	.	.	.	.	.	.	.	.	.	.	.	.	.	.	.	X?	.	.	.	.	.	.	.	.	.	.	.	.	.	.	.	.	.	.
Paradoxostoma sp.	.	.	.	.	.	.	.	.	.	.	.	.	.	.	.	.	.	.	.	.	.	.	.	.	.	.	.	.	.	.	.	.	.	.	.	X	.	.	.	.	.
Proteoconcha gigantea	.	.	.	.	.	.	.	.	.	.	.	.	.	.	.	.	.	.	.	.	.	.	.	.	X	.	.	.	.	.	.	.	.	.	.	.	.	.	.	.	.
Proteoconcha tuberculata	.	.	.	.	.	.	.	.	.	.	.	.	.	.	.	.	.	.	.	.	.	.	.	.	.	.	.	.	.	.	.	.	.	.	X	.	.	.	X	X	X
Pseudocytheretta burnsi	.	.	.	.	.	.	.	.	.	.	.	.	.	.	.	X	.	.	X	X	X	X	X	X	X	.	X	.	.	X	.	.	.	.	X	X	X	X	X	X	X
Pseudocytheretta plebeia	.	.	.	.	.	.	.	.	.	.	.	.	.	.	.	.	.	X?	.	.	.	.	.	.	.	.	.	.	.	.	.	.	.	.	.	.	.	.	.	.	.
Pterygocythereis americana	.	.	.	.	.	.	.	X	.	.	.	.	.	.	.	.	.	.	.	.	.	.	.	.	.	.	.	.	.	.	.	.	.	.	.	.	.	.	.	.	.
Pterygocythereis inexpectata	.	.	.	.	.	.	.	.	.	.	.	.	.	.	.	.	.	.	.	.	X	X	X	X	.	.	.	.	.	.	.	.	.	X	.	.	.	.	.	.	.
Puriana carolinensis	.	.	.	.	.	.	.	.	.	.	.	.	.	.	.	.	.	.	.	.	.	.	.	.	.	.	.	.	.	.	.	.	.	.	.	.	.	.	.	.	X
Puriana rugipunctata	.	.	.	.	.	.	.	.	.	.	.	.	.	.	.	.	.	.	.	.	.	.	.	.	.	.	.	.	.	.	.	.	.	.	.	.	.	X	X	X	X
Sahnia sp.	.	.	.	.	.	.	.	.	.	.	.	.	.	.	.	.	.	.	.	.	.	.	X	.	.	.	.	.	.	.	.	.	.	X	.	.	.	.	.	.	.
Thaerocythere schmidtae	.	.	.	.	.	.	.	.	.	.	.	.	.	.	.	.	.	.	.	.	.	.	.	.	.	.	.	.	.	.	.	.	.	X	.	.	.	.	.	.	.
Trachyleberidea blanpiedi	.	.	.	.	.	X	.	.	.	.	.	.	.	.	.	.	.	.	.	.	.	.	.	.	.	.	.	.	.	.	.	.	.	.	.	.	.	.	.	.	.
indeterminate	.	.	X	.	.	.	.	.	.	.	X	.	.	.	.	.	.	.	.	.	.	.	.	.	.	X	.	.	.	.	.	X	X	.	.	.	.	.	.	.	.
Preservation	P	VG	F	P	F	G	F	P	F	F	P	F	R	F	F	E	R	E	VG	VG	VG	VG	VG	G	P	F	P	F	P	P	F	P	P	F	E	E	E	E	E	E	E
Zone	none available																																?	?	*Orionina vaughani*						
Inferred age		late Eocene	late Eocene	?	Eocene-Oligocene	late Eocene-early Olig.	Oligocene	Oligocene	late Olig.-early Miocene	late Olig.-early Miocene	?	late Miocene	late Miocene	late Miocene		late Miocene	late Miocene	late Miocene	late Miocene	late Miocene	late Miocene	late Miocene	late Miocene			late Miocene		late Miocene			late Miocene			early-middle Pliocene	middle Pliocene			middle Pliocene		middle Pliocene	middle Pliocene

Figure H7. Occurrence chart showing the presence of ostracodes in samples from the USGS-NASA Langley core; samples are from the Chickahominy Formation, Drummonds Corner beds (DC), Old Church Formation (OC), Plum Point Member (PP) of the Calvert Formation, and St. Marys, Eastover, and Yorktown Formations. One sample (35 m=114.8–115.0 ft depth) is barren, and three others (139.2 m=456.4–456.8 ft; 42.7 m=140.1–140.3 ft; 22.8 m=74.7–74.9 ft) have only poorly preserved indeterminate specimens. Occurrence symbols: X=present, X?=species identity uncertain; .=not present. Preservation symbols: E=excellent, VG=very good, G=good, F=fair, P=poor, R=rare.

Series	Unit	Depth to top of sample (ft)	Depth to top of sample (m)	Taxon: *Testacarinata inconspicua*	*Turborotalia cerroazulensis cocoaensis*	*Praetenuitella praegemma*	*Hantkenina alabamensis*	*Turborotalia cerroazulensis pomeroli*	*Globigerinatheka index*	*Cribrohantkenina inflata*	*Turborotalia cerroazulensis cunialensis*	Acarininids (reworked)	*Bolboforma spinosa*	*Bolboforma ladorfensis*	Planktonic foraminiferal biochronozone
Upper Eocene	Chickahominy Formation	601.30	183.28	X	.	X	.	X	.	.	.	.	.	X	
		602.15	183.54	X	.	X	.	.	.	.	.	.	.	X	
		602.70	183.70	X	.	.	.	.	.	.	.	.	.	X	
		605.70	184.62	X	X	.	X	X	.	.	X	.	.	X	
		608.70	185.53	.	.	X	.	.	.	.	.	.	.	.	
		611.70	186.45	X	.	X	X	.	.	.	.	.	.	.	
		614.70	187.36	X	.	X	.	.	.	.	.	.	.	X	
		617.70	188.28	X	.	.	X	.	X	.	.	.	.	X	
		620.70	189.19	X	.	X	.	.	X	.	.	.	.	.	
		623.70	190.10	.	.	X	.	.	.	.	.	.	.	.	
		626.80	191.05	.	X	X	X	.	.	.	.	.	.	X	
		629.80	191.96	.	.	X	.	.	.	.	.	.	.	.	
		632.70	192.85	X	.	X	.	.	.	.	.	.	.	X	
		635.70	193.76	X	X	X	.	.	.	.	.	.	.	X	
		638.40	194.58	.	.	X	.	.	.	.	.	.	.	X	
		641.00	195.38	.	.	X	.	.	.	.	.	.	.	X	
		644.20	196.35	X	.	X	.	.	.	.	.	.	.	X	
		647.20	197.27	X	X	X	X	.	X	.	.	.	.	X	
		650.20	198.18	.	.	.	X	.	.	.	.	.	.	.	
		653.70	199.25	.	.	.	.	.	.	.	.	.	.	X	
		656.20	200.01	.	X	.	.	.	.	X	X	.	.	X	P16-P17
		662.20	201.84	.	.	X	.	.	.	.	.	.	.	X	
		665.20	202.75	.	X	X	.	.	.	.	.	.	.	X	
		668.20	203.67	.	X	X	X	.	X	.	X	.	.	X	
		671.20	204.58	.	X	X	X	.	X	X	.	.	.	X	
		674.20	205.50	.	.	X	.	.	X	.	.	.	.	X	
		676.80	206.29	X	.	.	.	.	.	.	.	.	.	X	
		680.00	207.26	X	.	X	.	.	X	.	.	.	.	X	
		683.20	208.24	X	.	.	.	.	X	.	.	.	.	X	
		686.10	209.12	X	X	X	X	.	X	.	.	.	.	X	
		689.10	210.04	.	X	.	X	.	X	.	.	.	.	X	
		692.20	210.98	.	X	.	.	.	X	.	.	.	.	X	
		695.20	211.90	.	.	.	X	.	X	.	.	.	.	X	
		698.30	212.84	.	.	.	.	.	X	.	.	.	.	X	
		701.10	213.70	.	.	.	X	.	X	.	.	.	.	X	
		704.80	214.82	.	.	X	X	.	.	.	.	.	.	X	
		708.00	215.80	.	X	X	X	.	.	.	.	.	.	X	
		710.50	216.56	.	X	.	X	.	X	.	.	.	.	X	
		720.00	219.46	X	.	X	.	.	.	.	.	.	.	X	
		723.00	220.37	.	.	.	.	.	.	.	.	.	.	X	
		726.40	221.41	X	.	X	X	.	.	.	.	.	X	X	
		729.00	222.20	X	.	X	X	.	.	.	.	.	X	X	
		732.20	223.18	.	.	.	X	.	.	.	.	.	.	X	
		735.10	224.06	X	X	X	.	X	.	.	.	.	.	.	
		737.96	224.93	.	X	.	X	.	X	.	.	.	.	.	
		741.00	225.86	.	.	.	.	.	.	.	.	.	.	.	
		743.90	226.74	X	X	X	.	X	.	.	.	.	X	.	
		747.00	227.69	X	X	X	.	.	.	.	.	.	.	.	
		750.00	228.60	.	.	.	.	.	.	.	.	.	X	.	
		753.00	229.51	.	.	.	.	.	.	.	.	.	.	.	
		756.10	230.46	X	X	X	.	.	.	.	.	.	X	.	P15
		759.30	231.44	X	.	.	.	.	.	.	.	.	.	.	
		762.00	232.26	.	X	.	.	.	.	.	.	.	X	.	
		764.95	233.16	.	.	.	X	.	.	.	.	.	.	.	
		768.10	234.12	X	X	.	.	.	.	.	.	X	X	.	
		770.70	234.91	X	X	X	.	.	.	.	.	X	X	.	
		772.60	235.49	X	X	.	.	.	.	.	.	X	X	.	
		772.90	235.58	X	.	.	.	.	.	.	.	X	.	.	
		773.05	235.63	X	.	.	.	.	.	.	.	X	.	.	

Figure H8. Occurrence chart showing the presence of key planktonic foraminifera and bolboformids in samples of the Chickahominiy Formation in the USGS-NASA Langley core. Zones are based on Berggren and others (1995). Symbols: X=present, .=not present.

Taxon	Chickahominy Formation		Drummonds Corner beds
	211.7 m (694.7 ft)	197.9 m (649.4 ft)	182.5 m (598.5–599.3 ft)
Sharks:			
Scyliorhinus gilberti	.	X	.
Squalus sp.	.	.	X
Rays:			
Dasyatis sp.	.	.	X
Bony fishes:			
Acanthocybium proosti	X	.	.
Diaphyodus wilsoni	.	.	X
Trichiurides sagittidens	.	.	X

Figure H9. Occurrence chart showing the presence of teeth of sharks, rays, and bony fishes in samples of the Chickahominy Formation and the Drummonds Corner beds in the USGS-NASA Langley core. The teeth are shown in plate H9. Symbols: X=present, .=not observed.

tum (highest occurrence is in sample R6110 AN, 206.7 m= 677.9–678.3 ft), and *Thalassiphora reticulata* (highest occurrence is in sample R6110 AN). Species that are present but not in the lowest sample include *Membranophoridium aspinatum* (lowest occurrence is in sample R6110 AN) and *Dapsilidinium pseudocolligerum* (lowest occurrence is in sample R6110 AR, 222.7 m=730.3–730.7 ft).

Dinocysts from the Chickahominy Formation in the Langley core can be compared with dinocysts from the Eocene-Oligocene boundary stratotype at Massignano, Italy. The form that Brinkhuis (1994) called *Escharisphaeridia* sp. is clearly *Batiacasphaera compta*. The highest occurrence of this form makes a good proxy for the Eocene-Oligocene boundary at the boundary stratotype. Because this species ranges to the top of the Chickahominy, the entire Chickahominy is Eocene, although the presence of *Operculodinium divergens* (in sample R6110 AL) suggests that this sample (and higher samples) is near the boundary. The Chickahominy dinoflagellate samples show striking similarities with the dinoflagellates reported from the Bassevelde Sands of the Zelzate Formation in Belgium (De Coninck, 1986, 1995).

Mollusks.—Molluscan remains are relatively sparse in the Chickahominy Formation in the Langley core (fig. H6). Seven taxa are represented in the lower portion of the formation, from 232.3 to 205.6 m (762.2 to 674.4 ft) depth, including several species of pectens, *Astarte* sp., *Dentalium* sp., *Nucula* sp., and *Nuculana* sp. (pl. H6, figs. 4–6). From 205.6 to 183.3 m (674.4 to 601.3 ft), molluscan remains are rare to absent in each sample, and no recognizable forms are present.

Ostracodes.—Before discussing the ostracode assemblages from the Eocene-Oligocene interval in the Langley core, it is first necessary to discuss the limitations on assigning ages. First, the preservation in some samples is marginal in terms of the valves themselves (commonly broken) and the abundances are low, usually less than 10 specimens except at 221.7 m (727.2–727.6 ft), 186.7 m (612.4–612.7 ft), and 173.8 m (570.2–570.4 ft). Such preservation precludes detailed examination of populations and morphologic variability in potentially age-diagnostic species until additional samples and cores are analyzed.

The second factor is the absence of a formal ostracode biostratigraphic zonation for the mid-Atlantic region. In contrast to the Gulf of Mexico region, where detailed ostracode zonations exist (see Poag, 1974; Hazel and others, 1980), only a few isolated Eocene-Oligocene ostracode faunas from the Chesapeake Bay region have been described and illustrated in the published literature (for example, Swain, 1951; Deck, 1985). Therefore, we must proceed on the assumption, which may not be valid for some species, that their stratigraphic ranges are isochronous in the Gulf and mid-Atlantic coastal regions.

The third factor is the taxonomic status of species in several relatively important genera (*Actinocythereis*, *Cytheridea*, *Leguminocythereis*), which will require additional comparative study in the future. These factors mean that any age interpretation based on the ostracodes must be done in conjunction with biostratigraphic data from other fossil groups.

In spite of these limitations, the ostracodes from the Langley core provide some age indications. The assemblages from the Chickahominy Formation include the key species *Actinocythereis* cf. *A. dacyi*, *A.* cf. *A. stenzeli*, *Alatacythere ivani*, *Digmocythere russelli*, *Leguminocythereis* cf. *L. scarabaeus*, and *Trachyleberidea blanpiedi*. Together these species suggest a late Eocene to early Oligocene age. These species are common guide fossils for the Jacksonian and Vicksburgian provincial stages of the Gulf of Mexico Coast (Hazel and others, 1980) and also occur in the Santee Formation and Cooper Group of

South Carolina (Pooser, 1965; Hazel and others, 1977) and subsurface units in North Carolina (Swain, 1951). Distinctive ostracodes from the middle Claibornian to middle Jacksonian described by Deck (1985) from the middle Eocene Piney Point Formation have not been found in the Langley core.

Planktonic foraminifera and bolboformids.—The stratigraphic record of late Eocene planktonic foraminifera and bolboformids from the Chickahominy Formation inside the Chesapeake Bay crater has previously been established in the Kiptopeke and Exmore coreholes (Poag and Aubry, 1995; Poag and Commeau, 1995; Poag, 1997). Poag and Aubry (1995) demonstrated that these two Chickahominy sections are biostratigraphically correlative with an upper Eocene chalk section cored by the Deep Sea Drilling Project (DSDP) at Site 612 on the continental slope of New Jersey (Poag, Watts, and others, 1987).

The planktonic foraminiferal suite at these cored sites is a typical late Eocene association (Zones P15–P17 as defined by Berggren and others, 1995), composed of the following key species:

Cribrohantkenina inflata
Globigerina gortanii
Globigerina medizzai
Globigerina ouachitaensis
Globigerina praebulloides
Globigerina tripartita
Globigerinatheka index
Globigerinatheka semiinvoluta
Hantkenina alabamensis
Praetenuitella praegemma
Pseudohastigerina naguewichiensis
Testacarinata inconspicua
Turborotalia cerroazulensis cerroazulensis
Turborotalia cerroazulensis cocoaensis
Turborotalia cerroazulensis cunialensis
Turborotalia cerroazulensis pomeroli

It is difficult to recognize the P15-P16 and P16-P17 biozonal boundaries in the two previously studied Chickahominy sections because the requisite taxa (*Globigerinatheka semiinvoluta, Cribrohantkenina inflata*, and *Turborotalia cerroazulensis cunialensis*) are scarce and (or) sporadically present. Poag and Aubry (1995) found, however, that the highest occurrence of *Bolboforma spinosa* overlaps briefly the lowest occurrence of *Bolboforma latdorfensis* approximately at the P15-P16 boundary (lowest occurrence of *Turborotalia cerroazulensis cunialensis*) at DSDP Site 612. They, therefore, used this bolboformid overlap interval as a proxy for the P15-P16 boundary at their two Chickahominy sites.

At the USGS-NASA Langley corehole site, above the top of the Exmore beds, a succession of 59 samples, spaced approximately 1 m (about 3 ft) apart, reveals typical Chickahominy planktonic foraminiferal and bolboformid assemblages, nearly identical to those of the Kiptopeke and Exmore coreholes. The presence of the following key species indicates the late Eocene age of the Chickahominy Formation (fig. H8):

Cribrohantkenina inflata
Globigerinatheka index
Hantkenina alabamensis
Praetenuitella praegemma
Testacarinata inconspicua
Turborotalia cerroazulensis cocoaensis
Turborotalia cerroazulensis cunialensis
Turborotalia cerroazulensis pomeroli

As at the Kiptopeke and Exmore sites, the late Eocene planktonic foraminiferal biozonal boundaries cannot be recognized in the USGS-NASA Langley corehole. However, the position of the P15-P16 biochronozonal boundary can be approximated at 221.8 m (727.7 ft) by the *Bolboforma latdorfensis-Bolboforma spinosa* overlap interval (fig. H8). Berggren and others (1995) placed the P15-P16 boundary at 35.2 Ma.

Vertebrates.—A fragmentary tooth of *Acanthocybium proosti* (USNM 519553; pl. H9, fig. 5), an extinct species of wahoo (Weems, 1999), was recovered from the Chickahominy Formation at 211.7 m (694.7 ft) depth in the Langley core (fig. H9). The stout, roughly triangular shape of the tooth and the basal cross section that has one side nearly planar and the other strongly arched are characteristic of this species. Living wahoos typically are found in tropical waters and tend to prefer open ocean environments (Wheeler, 1975). Although wahoos generally are near-surface inhabitants, teeth of dead animals could readily have drifted downward through the crater water column and been buried at great depth far from the normal depths inhabited by this fish. *Acanthocybium proosti* is known from the lower Eocene Nanjemoy Formation (Weems, 1999), and so its presence in the upper Eocene Chickahominy Formation in the Langley core represents a range extension for this species. No wahoo remains have been reported yet from the middle Eocene Piney Point Formation.

A well-preserved tooth of *Scyliorhinus gilberti* (USNM 519554; pl. H9, fig. 4), an extinct species of catshark, was recovered from the Chickahominy Formation at 197.9 m (649.4 ft). This species is known in Europe from upper Eocene beds (Kent, 1999), and so its presence here is not unexpected. Many species of living catsharks prefer deep water (Kent, 1999), so it is most interesting that this is the only shark specimen to show up in the presumably deepwater depositional environment of this formation.

Paleoenvironmental information.—The benthic foraminiferal assemblage (Poag and Norris, this volume, chap. F) indicates a Chickahominy sea floor of about 300 m (984 ft) paleodepth (outer neritic to upper bathyal, 150–500 m), with restricted oxygen availability and high flux rates of organic carbon.

Although the emphasis of the dinoflagellate studies was biostratigraphic, it is interesting to note that specimens of the nearshore genus *Homotryblium* are present in only two of the

samples in the middle of the Chickahominy (209.3–206.7 m= 686.4–678.3 ft) (fig. H5).

The numbers of molluscan specimens present are too low to determine anything definitive about the environment. However, the Nuculacea and *Dentalium* present are indicative of deep and (or) quiet water. The *Dentalium* are large (length greater than 5 centimeters (cm), or about 2 inches (in.)) and relatively well preserved for fossils having their fragile construction and aragonitic composition; the preservation implies little to no transport.

The ostracodes present suggest that the environment of deposition of the Chickahominy Formation was mainly outer neritic to upper bathyal; the record of the deepest water environment for the formation is at 221.7 m (727.2–727.6 ft), where *Krithe* and *Argilloecia* occur. These taxa may also reflect slope-to-shelf upwelling of cooler slope waters.

Of the two vertebrate teeth found at different levels in the Chickahominy, one species suggests a deepwater environment, whereas the other is nektonic and could readily have had its remains sink into a deepwater depositional basin from the overlying near-surface nektonic environment. Although these two occurrences are far too sparse to constitute proof of a deepwater environment for the Chickahominy Formation, they are fully compatible with such an interpretation.

Other paleontological information.—Both calcareous nannofossil samples and dinoflagellate samples throughout the Chickahominy Formation contain sporadic specimens reworked from older units. All dinoflagellate samples include rare specimens that appear to have been altered (for example, folded or partially melted, as described in Powars and Edwards, 2003; Frederiksen and others, this volume, chap. D).

Implications of sediment accumulation rates in the Chickahominy.—Two zone boundaries and the Eocene-Oligocene boundary were used to set limits on the sediment accumulation rate in the Chickahominy Formation based on the time scale of Berggren and others (1995). The P15/P16-P17 boundary at 35.2 Ma is placed at 221.8 m (727.7 ft) and the NP 19-20/NP 21 boundary at 34.2 Ma is placed between samples at 196.4 and 195.5 m (644.5 and 641.5 ft). Because the highest samples in the Chickahominy are still within the Eocene, the top of the Chickahominy at a depth of 183.3 m (601.3 ft) must be assigned an age of 33.7 Ma or older. By using these points, the possible lines that can be constructed are quite limited (fig. H10). Sediment accumulation rates must be in the range of 25–27 m/m.y. (82–89 ft/m.y.) The top of the Chickahominy is nearly coincident with the Eocene-Oligocene boundary. Using slightly different assumptions, but the same tie point at the P15/P16-P17 boundary, Poag and Norris (this volume, chap. F) arrive at almost the same sedimentation rates.

One can project the base of the Chickahominy at 235.65 m (773.12 ft) into the time scale of Berggren and others (1995), using these zone boundaries and sediment accumulation rates to yield a value of 35.7–35.8 Ma for the time of impact (fig. H10). This value is based ultimately on the geomagnetic reversal time scale of Cande and Kent (1995), which is calibrated to numeric ages at 33.7±0.4 and 46.8±0.5 Ma. Thus, 35.7–35.8 Ma does not differ significantly from ages of tektites given by Horton and Izett (this volume, chap. E).

Drummonds Corner Beds

The Drummonds Corner beds at 183.3–176.0 m (601.3–577.4 ft) depth in the Langley core were studied for calcareous nannofossils (fig. H4, in pocket), dinoflagellates (fig. H5), ostracodes (fig. H7), and vertebrates (fig. H9). Molluscan remains in the Drummonds Corner beds are highly weathered and not identifiable. Dinoflagellates indicate placement in the upper part of the lower Oligocene. Calcareous nannofossils indicate placement in Zone NP 24, which includes parts of both the lower and upper Oligocene. Together, these two fossil groups indicate calibration to 29.9–28.5 Ma (base of Zone NP 24 and top of lower Oligocene according to Berggren and others, 1995). Thus, this 7.3-m-thick (23.9-ft-thick) unit represents 1.4 m.y. or less of deposition.

Calcareous nannofossils and dinoflagellates show a sharp floral change, and ostracodes show a sharp faunal change, between the Drummonds Corner beds and the underlying Chickahominy Formation. Fossils representing the lower part of the lower Oligocene are not present. The Drummonds Corner beds appear to represent shallower water or more nearshore deposition than the underlying Chickahominy deposits. The inferred climate is subtropical.

Calcareous nannofossils.—Only three samples were examined for calcareous nannofossils from the Drummonds Corner beds in the Langley core; they are from depths of 182.6, 180.1, and 177.2 m (599.1, 591.0, and 581.5 ft). Calcareous nannofossils were abundant in all three samples and had moderate to good preservation. The unit is tentatively placed within Zone NP 24. *Reticulofenestra umbilicus* (LAD defines the top of Zone NP 22) is absent from these samples, placing the unit in Zone NP 23 or higher. *Helicosphaera recta* (first appears in Zone NP 24) is present in the lower two samples, as is *Sphenolithus predistentus* (LAD within Zone NP 24). The absence of these two species in the uppermost sample at 177.2 m (581.5 ft) may be due to the somewhat poorer preservation of this sample. The absence of *Sphenolithus distentus* (ranges from Zone NP 23 to Zone NP 24) and *Sphenolithus ciperoensis* (FAD defines the base of Zone NP 24) from this interval, which contains other sphenoliths, cannot be explained. Berggren and others (1995) calibrated the lower boundary of Zone NP 24 at 29.9 Ma and the upper boundary of this zone at 27.5 Ma (fig. H3).

Dinoflagellates and acritarchs.—Two samples were examined for dinocysts from the Drummonds Corner beds in the Langley core (fig. H5). The samples are from depths of 178.0 and 177.3 m (583.8–584.1 and 581.5–581.9 ft). Preseva-tion ranges from fair to good.

The dinocysts indicate that the age of this unit is "mid" Oligocene (late Rupelian, the latter part of the early Oligocene). Dinoflagellate species that have their lowest occurrences in the Drummonds Corner beds include *Chiropteridium lobospinosum*, *Homotryblium vallum* (pl. H3, fig. 6), *Reticulatosphaera*

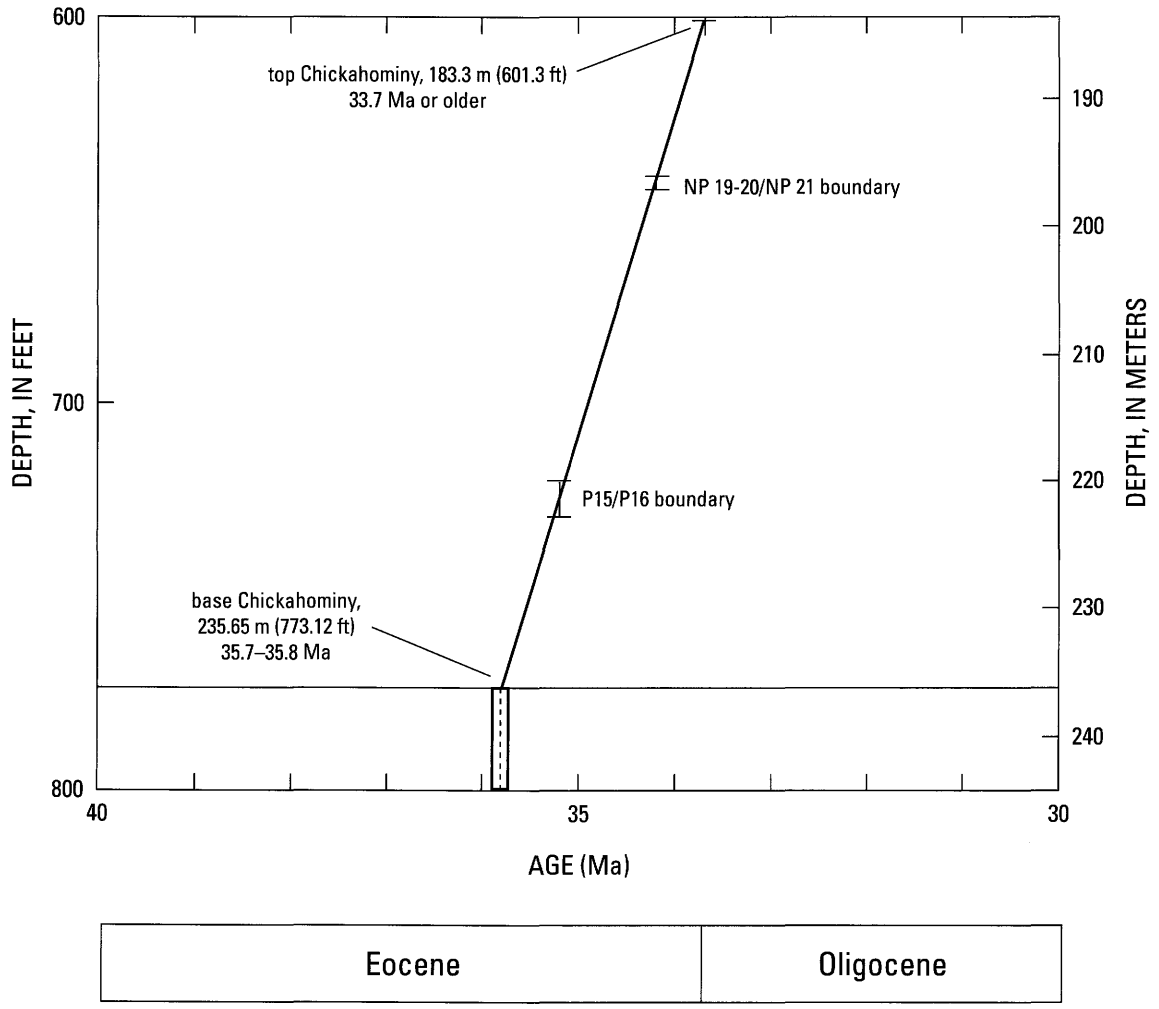

Figure H10. Age-depth plot for the Chickahominy Formation in the USGS-NASA Langley core. Time scale is from Berggren and others (1995).

actinocoronata (pl. H3, fig. 9), *Spiniferites mirabilis*, and *Wetzeliella symmetrica*. Both *Chiropteridium lobospinosum* and *Homotryblium vallum* have their lowest occurrences in the upper part of the lower Oligocene, within calcareous nannofossil Zone NP 23. *Achilleodinium biformoides* (p. H3, fig. 5) has its highest occurrence near the top of the lower Oligocene; it is present in both samples of the Drummonds Corner beds. Both samples lack *Tuberculodinium vancampoae*, which has its lowest occurrence in the upper part of the upper Oligocene and is present in the overlying Old Church Formation samples.

Ostracodes.—Ostracodes are extremely sparse and poorly preserved in the Drummonds Corner beds in the Langley core (fig. H7). The possible occurrence of a form resembling *Pterygocythereis americana* at 182.5 m (598.7–599.0 ft) in the Drummonds Corner beds is unusual in lower Oligocene sediments of this region (see discussion in Hazel, 1967), where it usually occurs in sediments of latest Oligocene or early Miocene age. Further work must confirm this identity and compare the Langley material with *P. howei*.

Vertebrates.—A sample of sediment from 182.5 m (598.5–599.3 ft) depth in the Drummonds Corner beds of the Langley core was sieved for vertebrate remains. Teeth from four species of fish were found (pl. H9), three of which suggest that the depositional environment was shallow coastal waters. The only mutual overlap in the climatic preference of the living representatives of these four species is in the modern subtropical climatic zone.

A tooth of *Squalus* sp. (USNM 519557; pl. H9, fig. 1*J*) documents the presence of a dogfish shark in this unit. Dogfish sharks are typically deepwater species that frequently range into shallower water (Kent, 1999).

A male tooth referable to *Dasyatis* sp. (USNM 519558; pl. H9, fig. 2*J*) documents the presence of whiptail stingrays in the lower Oligocene Drummonds Corner beds. The genus has been reported from beds as old as Cretaceous in North America (Cap-

petta, 1987), and so its presence is not surprising. Living *Dasyatis* prefer coastal subtropical to tropical waters.

A tooth of *Trichiurides sagittidens* (USNM 519556; pl. H9, fig. 3) documents the presence of a cutlassfish in this unit. Among fossil cutlassfishes, the presence of a deep, conical pulp cavity in the base of the tooth is characteristic of this genus. The tooth is not discernibly different from similar teeth noted from the Nanjemoy Formation (Weems, 1999) and from upper Eocene beds in Georgia (Dennis Parmley, Georgia College and State University, written commun., 2001). Modern trichiurids inhabit tropical to warm temperate seas and generally are found at shallow to moderate depths (Wheeler, 1975).

A small round and flattened tooth with a shallow and broadly open pulp cavity seems referable to an extinct drumfish. In the Eocene, *Diaphyodus wilsoni* is the only known representative of this group in eastern North America (Westgate, 1989), and so the present tooth (USNM 519555; pl. H9, fig. 6) is referred to this species in the absence of any features that would debar it. Presumably *Diaphyodus* gave rise to the living genus of drumfish, *Pogonias*. The timing of this evolutionary transition has not been documented, but specimens clearly referable to *Pogonias* are not known from beds older than Miocene at the present time. Living drumfishes are bottom dwellers that live in coastal waters and eat mollusks and crustaceans with their specialized crushing dentitions. They inhabit temperate to subtropical waters at the present time (Wheeler, 1975).

Paleoenvironmental information.—The presence of relatively nearshore dinoflagellate genera, such as *Homotryblium* and *Chiropteridium*, suggests that the Drummonds Corner beds represent shallower water deposition than the underlying Chickahominy Formation. The ostracodes suggest that the environment of deposition was most likely middle-outer neritic, where species of *Pterygocythereis* typically live today in the mid-Atlantic region. Fish teeth collectively suggest a subtropical climate.

Other paleontological information.—Lower Tertiary reworking is noticeable in the Drummonds Corner beds. The lowest dinoflagellate sample (R6110 AH, 178.0 m, 583.8–584.1 ft) shows a single specimen of *Hafniasphaera septata*. Reworked lower Tertiary calcareous nannofossils include specimens of *Chiasmolithus titus*, *Isthmolithus recurvus*, and *Markalius inversus*.

Old Church Formation

The Old Church Formation at 176.0–143.5 m (577.4–470.9 ft) depth in the Langley core was studied for calcareous nannofossils (fig. H4, in pocket), dinoflagellates (fig. H5), mollusks (fig. H6, in pocket), and ostracodes (fig. H7). Dinoflagellates indicate placement in the upper part of the upper Oligocene (to lowest Miocene), and calcareous nannofossils indicate placement in Zone NP 24. Although Zone NP 24 includes parts of both the lower and upper Oligocene, the Old Church sediments represent the upper part of the zone; the lower part of Zone NP 24 is found in the underlying Drummonds Corner beds. Because the presence of the dinoflagellate *Tuberculodinium vancampoae* sets a maximum age late in the late Oligocene, and because the placement of the uppermost sample in calcareous nannofossil Zone NP 24 is based on a single specimen, we allow the possibility that the Old Church includes both NP 24 and NP 25 (queried interval in fig. H3). According to Berggren and others (1995), the total time span of the upper Oligocene part of Zones NP 24 plus NP 25 is 28.5–23.9 Ma. This 32.5-m-thick (106.5-ft-thick) unit represents 4.6 m.y. or less of deposition. A paleoenvironment of middle-outer neritic, subtropical, is suggested.

Calcareous nannofossils. —Eleven samples were examined from the Old Church Formation from 175.3 to 145.4 m (575.0 to 477.1 ft). All of the samples contained abundant to common calcareous nannofossils with good to moderate preservation (fig. H4).

The entire interval can be placed within Zone NP 24 because of the presence of *Sphenolithus ciperoensis* (FAD defines the base of Zone NP 24) in the lowest sample at 175.3 m (575.0 ft) and *Sphenolithus distentus* (LAD defines the top of Zone NP 24) in the top sample at 145.4 m (477.1 ft). The presence of only one specimen of *S. distentus* at 151.0 and 145.4 m (495.4 and 447.1 ft) is not strong evidence for this material being placed in Zone NP 24 rather than Zone NP 25. However, *Helicosphaera compacta* (LAD in Zone NP 24) is still present at 167.5 m (549.6 ft), and *Transversopontis zigzag* (LAD also in Zone NP 24) is questionably present up to 164.0 m (538.1 ft). *Helicosphaera truempyi* (FAD in the uppermost part of Zone NP 24) first appears at 148.7 m (487.9 ft). Combining this evidence indicates that the Old Church Formation in the Langley core is most likely in Zone NP 24. Zone NP 24 spans the early-late Oligocene boundary (Berggren and others, 1995). The calcareous nannofossils cannot determine whether this material in the Langley core is of early or late Oligocene age, although late Oligocene is more likely because Zone NP 24 sediments are present in the underlying Drummonds Corner beds.

Dinoflagellates and acritarchs. —Four samples were examined for dinocysts from the Old Church Formation in the Langley core (fig. H5); selected specimens are shown in plates H3 and H4. The samples are from depths of 171.1 to 144.9 m (581.0 to 475.4 ft). The preservation in all but the lowest is poor.

The lower three samples are late Oligocene, as indicated by the overlapping ranges of *Tuberculodinium vancampoae* (lowest occurrence in the late Oligocene) and *Saturnodinium pansum* (highest occurrence in calcareous nannofossil Zone NP 25 according to de Verteuil and Norris, 1996). The highest sample (R6110 AA, 144.9 m=475.4–475.7 ft) does not contain *S. pansum*, and it contains no other species that restrict its possible age more precisely than late Oligocene or earliest Miocene.

Mollusks.—Calcitic molluscan remains are present from 169.5 to 148.7 m (556 to 488 ft) depth in the Old Church Formation of the Langley core, and most of the mollusks are concentrated in the segment from 159.7 to 153.9 m (524 to 505 ft) (fig. H6). The absence of aragonitic mollusks indicates extensive leaching, which is consistent with Ward's (1985, p. 51) description of the type Old Church. The calcitic remains include

an *Anomia* sp., fragments of *Ecphora* sp., and five distinct species of pectens (pl. H6, figs. 1, 3). Several of the pectens may be undescribed, but two of the species (pectinid cf. *Chlamys brooksvillensis* Mansfield and pectinid cf. *Chlamys* aff. *C. vaun wythei* Hertlein Mansfield) bear a resemblance to specimens described by Mansfield (1937) from the lower Oligocene Suwannee Limestone of Florida (age refined by Brewster-Wingard and others, 1997). *Rebeccapecten berryae*, present in a single sample at 159.3–159.4 m (522.7–522.9 ft), was reported by Ward (1992) from zone M14, Oligocene to lowermost Miocene.

Ostracodes.—Ostracodes are extremely sparse and poorly preserved in the two samples obtained from the Old Church Formation in the Langley core (fig. H7). The lowest occurrences of *Hulingsina*, *Echinocythereis* (perhaps *E. clarkana* Ulrich and Bassler 1904), and *Cytheridea subovalis* in the Old Church Formation suggest a possible age equivalent to the upper part of the Cooper Group (now Ashley Formation), which Hazel and others (1977) correlated with the Chickasawhayan. These taxa typically first appear in the uppermost Oligocene and lower Miocene sediments of the Atlantic Coastal Plain.

Paleoenvironmental information.—The present-day environment of the dinoflagellate *Tuberculodinium vancampoae* is nearshore and subtropical to tropical. Its occurrence in the Old Church may suggest similar conditions. The ostracodes present suggest that the environment of deposition for the Old Church Formation was most likely middle-outer neritic, where species of *Echinocythereis* typically live today in the mid-Atlantic region. Because of the extensive leaching, the molluscan fauna cannot provide any paleoenvironmental information.

Other paleontological information.—Paleontology supports the presence of a considerable lag bed at the base of the Old Church Formation. The lowest dinoflagellate sample (R6110 AF, 171.1 m, 561.0–561.4 ft) shows a noteworthy component of reworked material from a variety of different ages, including late Eocene (time of impact), early Eocene or Paleocene, and Paleocene. Folding of specimens and curling of processes were noted on some Eocene specimens in which an impact origin is most likely. Dinoflagellate assemblages from higher in the Old Church include rare impact-related specimens. Reworked calcareous nannofossils (scattered specimens of *Isthmolithus recurvus*) are also recorded in the lower part of the Old Church.

Calvert Formation

The Calvert Formation at 143.5–123.6 m (470.9–405.5 ft) depth in the Langley core was divided into the lower Miocene Newport News beds (informal unit) and the middle Miocene Plum Point Member and Calvert Beach Member (fig. H3). The Fairhaven Member of the Calvert Formation, known from outcrops and subsurface studies in Virginia and Maryland, is not recognized in the Langley core.

Newport News Beds

The Newport News beds of the Calvert Formation at 143.5–140.5 (470.9–461.1 ft) depth in the Langley core were studied for calcareous nannofossils (fig. H4, in pocket) and dinoflagellates (fig. H11). Molluscan remains were not studied, as the Newport News beds in the core contain only scattered oyster shells and fragments (fig. H6, in pocket). No siliceous microfossils were found. Dinoflagellates and calcareous nannofossils indicate placement in the lower Miocene. Dinoflagellate biostratigraphy places this unit in the lower Miocene subzone DN2b, which de Verteuil (1997) calibrated at 19.4–20.0 Ma. Thus, this 3.0-m-thick (9.8-ft-thick) unit represents approximately 0.6 m.y. or less of deposition.

Calcareous nannofossils.—Only one calcareous nannofossil sample was examined from the Newport News beds, from 142.1 m (466.3 ft) depth in the Langley core (fig. H4). Nannofossils were common with good preservation. This sample was placed in the lower Miocene Zone NN 2–3 on the basis of the presence of *Helicosphaera ampliaperta* (FAD within Zone NN 2) and the absence of *Sphenolithus heteromorphus* (FAD in Zone NN 4), which does occur in the overlying sample at 139.3 m (457.0 ft). However, none of Martini's (1971) zone-defining species was found in the sample from the Newport News beds.

Dinoflagellates and acritarchs.—A single sample (R6110 Z, 142.2 m=466.3–466.5 ft depth in the Langley core) was examined for dinocysts from the Newport News beds of the Calvert Formation (fig. H11). Two specimens are shown in plate H4 (figs. 1 and 5). Preservation is good.

This sample is assigned to the lower Miocene Zone DN2 of de Verteuil and Norris (1996), and more specifically to subzone DN2b of de Verteuil (1997), on the basis of the co-occurrence of *Cordosphaeridium cantharellus* (highest occurrence defines top of subzone DN2b) and *Exochosphaeridium insigne* (lowest occurrence defines base of subzone DN2b). Specimens of *Chiropteridium* spp. and *Homotryblium plectilum* may be reworked, or their occurrences here may represent upward range extensions.

Paleoenvironmental information.—The high-diversity dinocyst assemblage suggests normal marine surface-water conditions; some nearshore species are present. The presence of *Tuberculodinium vancampoae* may indicate subtropical to tropical temperatures somewhat warmer than the present Chesapeake Bay.

Plum Point Member

The Plum Point Member of the Calvert Formation at 140.5–139.0 m (461.1–456.1 ft) depth in the Langley core was studied for calcareous nannofossils (fig. H4, in pocket) and dinoflagellates (fig. H11). Only indeterminate diatoms (fig. H12) and ostracodes (fig. H7) and highly weathered mollusks and pieces of *Isognomon* sp. are reported. Dinoflagellates and calcareous nannofossils indicate placement in the middle Miocene. According to the time scale of de Verteuil and Norris

(1996), the time represented by middle Miocene dinoflagellate Zone DN4 is 16.7–15.2 Ma. Thus, this 1.5-m-thick (5.0-ft-thick) unit represents approximately 1.5 m.y. or less of deposition.

Calcareous nannofossils.—Only one calcareous nannofossil sample was examined from the Plum Point Member, from 139.3 m (457.0 ft) depth in the Langley core (fig. H4). Calcareous nannofossils were abundant with moderate preservation. This sample is placed in the middle Miocene Zones NN 3–5 on the basis of the presence of *Sphenolithus heteromorphus* (LAD defines the top of Zone NN 5; FAD within Zone NN 3).

Dinoflagellates and acritarchs.—A single sample (R6110 Y, 139.4 m=457.4–457.6 ft depth in the Langley core) was examined for dinocysts from the Plum Point Member (fig. H11). Four specimens are shown in plate H4 (figs. 4, 7, 9, and 10). Preservation is fair.

The sample was determined to be latest early (Burdigalian) or early middle Miocene (Langhian). This sample is assigned to Zone DN4 of de Verteuil and Norris (1996) on the basis of the co-occurrence of *Distatodinium paradoxum* (highest occurrence defines the top of DN4) and *Labyrinthodinium truncatum* (lowest occurrence defines the base of DN4). A single specimen of *Habibacysta tectata* (lowest occurrence within DN5) may be a downhole contaminant. The early-middle Miocene boundary is near, but may not be coincident with, the base of Zone DN4. De Verteuil and Norris (1996) also placed the Plum Point Member of the Calvert Formation in Zone DN4.

Diatoms and silicoflagellates.—Two samples of the Plum Point Member in the Langley core were examined for siliceous microfossils (figs. H12, H13). No silicoflagellates were reported in these samples.

In the sample from 140.5 m (460.8–460.9 ft) depth, diatoms are rare and poorly preserved. *Paralia sulcata,* a robust diatom ranging from the Cretaceous to the present, is the only form identified. The sample from 139.4 m (457.3–457.4 ft) also contained poorly preserved diatoms, mostly *Paralia sulcata.* The lack of age-diagnostic diatoms in these two samples prevents their assignment to a diatom zone.

Mollusks.—The Plum Point Member in the Langley core has abundant evidence of highly weathered aragonitic mollusks and pieces of *Isognomon* sp. No samples of the member were collected for mollusk analysis.

Ostracodes.—Only indeterminate ostracodes are reported from the Plum Point Member in the Langley core (fig. H7).

Paleoenvironmental information.—The high-diversity dinocyst assemblage suggests normal marine surface-water conditions; some nearshore species are present. The presence of the dinoflagellate *Tuberculodinium vancampoae* may indicate subtropical to tropical temperatures somewhat warmer than the present Chesapeake Bay. The sparse molluscan fauna is unusual for the Calvert Formation and does not provide any paleoenvironmental information.

Calvert Beach Member

The Calvert Beach Member of the Calvert Formation at 139.0–123.6 m (456.1–405.5 ft) depth in the Langley core was studied for calcareous nannofossils (fig. H4, in pocket), dinoflagellates (fig. H11), diatoms (fig. H12), and silicoflagellates (fig. H13). No molluscan remains were observed in the Calvert Beach Member, and no samples were studied for ostracodes. Dinoflagellates, diatoms, and silicoflagellates indicate placement in the middle Miocene for material up to 128.0 m (419.9 ft) depth. Calcareous nannofossils include specimens of the genus *Catinaster*, which would suggest, in the absence of dinoflagellate, diatom, and silicoflagellate data, a slightly younger age (Zone NN 8 in the latest middle or early late Miocene). Fossils of all groups are sparse or absent in the upper part of this unit. The base of this 15.4-m-thick (50.6-ft-thick) unit is calibrated at 14.1 Ma or younger (base of the dinocyst *Habibacysta tectata*, according to de Verteuil and Norris, 1996); the age of the top of the unit is no younger than the top of Zone DN 6 (12.7 Ma according to de Verteuil and Norris, 1996).

Calcareous nannofossils.—Four calcareous nannofossil samples were examined from the Calvert Beach Member in the Langley core (fig. H4). The two upper samples, from 131.4 and 127.9 m (431.2 and 419.5 ft), could not be dated because one was barren of calcareous nannofossils and the other sample contained only rare, nondiagnostic species.

The bottom two samples, from 136.6 and 134.4 m (448.0 and 440.9 ft), contained common calcareous nannofossils with good preservation. Each of these samples contained several specimens of at least two morphologies that are assigned to the genus *Catinaster*. Two of these specimens have been observed with the scanning-electron microscope (SEM); they are similar to *Catinaster coalitus* and *Catinaster mexicanus*, but they differ enough that they may represent one or more new species. Additional SEM searches for these *Catinaster* specimens are planned, and they may clarify these identifications. Although the earliest reported occurrence of the genus *Catinaster* (Peleo-Alampay and others, 1998) is *C. coalitus*, whose base defines the base of Zone NN 8, it cannot be assumed that these specimens must indicate a Zone NN 8 age, particularly when other fossil groups place this interval within the middle Miocene. The presence of *Discoaster exilis* (LAD in Zone NN 8) in these two samples indicates an age no younger than Zone NN 8 age.

Dinoflagellates and acritarchs.—Three samples were examined for dinocysts from the upper middle Miocene part of the Calvert Formation between depths of 134.5 and 125.0 m (441.4 and 409.9 ft) in the Langley core (fig. H11). Four specimens are shown in plates H4 (figs. 8, 11, and 12) and H5 (fig. 1). Preservation is fair to poor.

The two lower samples are assigned to the upper part of Zone DN5 of de Verteuil and Norris (1996) on the basis of the co-occurrence of *Habibacysta tectata* (lowest occurrence about midway within DN5) and *Cleistosphaeridium placacanthum* (highest occurrence defines the top of DN5). According to the correlation charts in de Verteuil and Norris (1996), these sam-

Formation	Calvert Formation					St. Marys Formation					Eastover Formation				Yorktown Formation			
Member	NN	PP	Calvert Beach															
Depth to midpoint (m)	142.2	139.4	134.5	129.6	125.0	120.4	114.5	102.2	86.9	72.2	66.1	59.9	52.4	24.8	21.9	16.0	9.6	7.3
Depth range (ft)	466.3–466.5	457.4–457.6	441.0–441.4	425.2–425.4	409.9–410.2	394.8–395.2	375.5–375.8	335.0–335.4	285.0–285.3	236.8–237.2	216.6–216.9	196.4–196.7	171.6–172.0	81.2–81.6	71.5–71.9	52.4–52.8	31.4–31.7	23.8–24.1
Sample number R6110	Z	Y	X	W	V	U	T	R	O	L	K	J	I	F	E	D	C	B
Taxon / Zonation of de Verteuil and Norris (1996), de Verteuil (1997)	DN2b	DN4	DN5	DN5	DN6	DN8/9	DN9	DN9	DN9	DN9	DN9	DN9	DN10	DN10	post DN10			
Achomosphaera andalousiensis	.	.	.	.	.	X	X	X	.		X	X	X	X	.	.	.	.
Achomosphaera sp.	.	.	.	.	.	.	.	.	.	.	.	.	.	X	X	.	.	.
Amiculasphaera umbracula	.	.	.	.	.	.	.	.	.	.	.	.	.	.	.	.	X	?
Apteodinium spiridoides	X	X	.	.	.	.	.	.	.	.	.	.	.	.	.	1R	.	.
Apteodinium tectatum	X	X	.	.	.	.	.	.	.	.	.	.	.	.	.	.	.	.
Ataxiodinium confusum	.	.	.	.	.	.	.	.	.	.	.	.	.	.	.	.	X	.
Barssidinium evangelineae (including *B. pliocenicum*)	.	.	.	.	.	X	X	X	.	.	.	X	X	X	.	X	.	X
Batiacasphaera sphaerica	X	X	.	.	X	.	.	.	.	.	X	.	.	.	.	.	.	.
Bitectatodinium tepikiense/Bitectatodinium raedwaldii	.	.	.	.	.	.	.	.	.	.	.	X	.	X	.	X	X	.
Brigantedinium cariacoense	.	.	X	.	.	.	.	.	.	.	.	.	X	.	X	.	.	.
Cerebrocysta poulsenii	X	X	.	.	X	.	.	.	.	.	.	.	.	.	.	.	.	.
Cerebrocysta satchelliae	X	.	.	.	.	.	.	.	.	.	.	.	.	.	.	.	.	.
Chiropteridium spp.	R?	.	.	.	.	.	? (R)	.	.	.	.	.	.	.	.	.	.	.
Cleistosphaeridium placacanthum	X	X	X	X	.	.	.	.	.	.	.	.	.	.	.	.	.	.
Cordosphaeridium cantharellus	X	.	.	.	.	.	.	.	.	.	.	.	.	.	.	.	.	.
Cousteaudinium aubryae	.	?	.	.	.	.	.	.	.	.	.	.	.	.	.	.	.	.
Cribroperidinium tenuitabulatum	X	.	.	.	.	.	.	.	.	.	.	.	.	.	.	.	.	.
Cyclopsiella lusatica	X	X	.	.	.	.	.	.	.	.	.	.	.	.	.	.	.	.
Dapsilidinium pseudocolligerum	X	.	.	.	.	.	.	.	.	.	.	.	.	.	.	.	.	.
Distatodinium paradoxum	.	X	.	.	.	.	.	.	.	.	.	.	.	.	.	.	.	.
Erymnodinium delectabile	.	.	.	.	.	.	.	X	.	.	X	X	X	X	.	.	.	.
Exochosphaeridium insigne	X	.	.	.	.	.	.	.	.	.	.	.	.	.	.	.	.	.
Filisphaera microornata	.	.	.	.	.	.	.	.	.	.	.	.	.	X	.	.	.	.
Geonettia clineae	.	.	.	.	.	.	.	X	.	.	.	.	.	.	.	.	.	.
Habibacysta tectata	.	C?	X	X	X	X	X	X	.	X	X	X	X	X	.	.	X	.
Heteraulacacysta sp.	X	.	.	.	.	.	.	.	.	.	.	.	.	.	.	.	.	.
Homotryblium plectilum	R?	.	.	.	.	.	.	.	.	.	.	.	.	.	.	.	.	.
Hystrichokolpoma rigaudiae	X	X	X	X	.	.	.	.	.	.	.	.	.	.	.	.	.	.
Hystrichosphaeropsis obscura	.	X	X	X	X	X	X	X	X	X	X	X	.	.	.	.	.	.
Impagdinium pallidum	.	.	.	.	.	?	.	.	.	.	.	.	.	.	.	.	.	.
Impagidinium antecarcerum	.	.	.	.	.	.	.	.	.	.	.	.	.	X	.	.	.	.
Impagidinium maculatum of Santarelli (1997)	.	.	.	.	.	X	X	.	.	.	.	.	.	.	.	.	.	.
Impagidinium paradoxum	.	.	X	X	.	.	.	.	.	.	.	.	.	.	.	.	X	.
Impagidinium sphaericum	.	.	.	.	.	.	.	.	.	.	.	.	.	.	X	.	.	.
Impagidinium spp. (including *I.* sp. cf. *strialatum*)	X	X	.	X	.	.	.	X	X	X	X	X	.	.	.	.	.	X
Invertocysta lacrymosa	.	.	X	.	.	X	X	.	.	.	X	.	X	.	X	X	X	.
Invertocysta tabulata	.	.	?	.	.	.	.	.	.	.	.	.	.	.	.	.	.	.

Invertocysta sp. indet.	?	X	.	.	.	.	.	.	.	.	.	X	.	.	.	X	.	.	
Labyrinthodinium truncatum subsp. *modicum*	.	X	X	.	.	.	.	.	.	.	.	.	.	.	.	.	.	.	
Labyrinthodinium truncatum subsp. *truncatum*	.	X	X	X	X	X	X	X	X	X	X	X	X	.	.	.	.	.	
Lejeunecysta spp.	X	X	X	X	X	.	X	X	.	.	X	X	X	X	X	X	.	X	
Lingulodinium machaerophorum	X	X	X	X	X	.	X	X	.	.	X	.	X	.	.	X	.	.	
Melitasphaeridium choanophorum	.	X	X	X	X	.	X	X	.	.	X	.	.	X	.	.	.	.	
Membranilarnaci? *picena*	X	.	.	.	.	.	.	.	.	.	.	.	.	.	.	.	.	.	
Nematosphaeropsis rigida	.	.	.	.	.	.	.	.	.	.	.	.	.	X	X	.	.	.	
Nematosphaeropsis sp.	.	.	.	.	.	.	.	.	.	.	.	.	.	.	.	X	.	.	
Operculodinium centrocarpum	X	X	.	.	.	.	.	.	.	.	.	.	X	X	X	X	X	.	
Operculodinium centrocarpum sensu Wall (1967)	.	.	.	.	.	.	.	.	.	.	.	.	.	.	.	.	.	X	
Operculodinium piaseckii	.	.	X	X	X	X	X	X	X	X	X	X	.	.	.	.	.	.	
Operculodinium tegillatum	.	.	.	.	.	.	.	.	.	.	.	.	.	.	.	.	.	?	
Operculodinium spp.	.	.	X	X	X	X	X	X	X	X	X	X	.	.	.	.	.	.	
Palaeocystodinium golzowense	X	X	X	X	X	.	.	.	.	.	.	.	.	.	.	.	.	.	
Pentadinium sp. cf. *P. laticinctum granulatum*	X	X	X	X	X	.	.	.	.	.	.	.	.	.	.	.	.	.	
Pentadinium sp. I of Edwards (1986)	X	.	.	.	.	.	.	.	.	.	.	.	.	.	.	.	.	.	
Polysphaeridium zoharyi/*Homotryblium vallum*	.	X	.	.	.	.	.	.	.	.	.	.	.	.	.	X	.	.	
Pyxidiella? *simplex*	.	.	.	.	.	X	.	.	.	.	.	.	.	.	.	.	.	.	
Reticulatosphaera actinocoronata	X	X	X	X	X	X	X	X	.	.	.	X	X	X	.	.	.	.	
Selenopemphix armageddonensis	.	.	.	.	.	.	.	.	.	.	.	.	X	X	X	.	.	.	
Selenopemphix brevispinosa	.	X	.	X	X	.	.	.	.	.	X	.	.	X	.	X	.	.	
Selenopemphix brevispinosa /S. dionaeacysta	.	.	.	.	.	.	.	.	.	.	.	.	.	.	X	.	.	.	
Selenopemphix dionaeacysta	.	.	.	.	.	X	.	X	.	.	.	.	.	.	.	.	.	.	
Selenopemphix nephroides	.	.	.	.	.	.	.	.	.	.	X	.	.	.	X	.	.	.	
Selenopemphix quanta	.	.	.	X	.	.	X	.	.	.	.	.	.	X	.	.	.	X	
Spiniferites mirabilis	.	X	X	X	.	.	.	X	.	.	X	X	.	.	.	X	.	.	
Spiniferites pseudofun'atus	X	X	X	.	.	X	.	.	.	.	.	.	.	.	.	.	.	.	
Spiniferites spp.	X	X	X	X	X	X	X	X	X	X	X	X	X	X	X	X	X	X	
Sumatradinium druggii	.	.	X	X	X	.	.	.	.	.	.	.	.	.	.	.	.	.	
Sumatradinium soucouyantiae	X	X	X	X	X	1R?	.	.	.	.	.	.	.	.	.	.	.	.	
Sumatradinium? sp. (fragment)	.	.	.	.	.	.	.	.	.	?	.	.	.	.	.	.	.	.	
Tectatodinium pellitum	X	X	X	.	X	.	X	.	.	X	.	.	X	X	X	X	X	X	
Trinovantedinium ferugnomatum	.	.	.	.	.	.	.	X	.	.	.	.	.	.	.	.	.	.	
Trinovantedinium glorianum	.	.	.	.	X	.	.	X	.	.	.	.	.	X	.	.	.	.	
Trinovantedinium harpagonium	.	.	X	.	.	.	.	.	.	.	.	.	.	.	.	.	.	.	
Trinovantedinium papula	.	.	.	.	X	.	.	.	.	.	X	.	X	.	.	.	.	.	
Trinovantedinium spp.	.	.	.	.	.	.	X	.	.	.	.	.	X	.	.	.	.	.	
Trinovantedinium? *xylochoporum*	X	.	.	X	.	.	.	.	.	.	.	.	.	.	.	.	.	.	
Tuberculodinium vancampoae	X	X	X	.	.	X	X	.	.	.	X	X	.	.	X	X	X	.	
Unipontidinium aquaeductum	.	.	X	.	.	.	.	.	.	.	.	.	.	.	.	.	.	.	
freshwater alga *Pediastrum*	.	.	.	.	.	.	X	X	X	X	X	.	.	.	.	X	.	X	
Preservation	good	fair	fair	poor	poor	fair	good	fair	poor	poor	fair	good	good	good	fair	fair	good	good	

Figure H11. Occurrence chart showing the presence of dinoflagellates and acritarchs in samples from the Calvert, St. Marys, Eastover, and Yorktown Formations in the USGS-NASA Langley core. The Calvert Formation contains the informal Newport News beds (NN), the Plum Point Member (PP), and the Calvert Beach Member. Selected specimens are shown in plates H4 and H5. Symbols: X= present, 1=single specimen, ?=questionably present, R=present but presumably reworked, R?=questionably reworked, ?(R)=questionably identified, reworked if identification is correct, C?=questionably a contaminant, .=not present.

Zone	?		*Delphineis penelliptica* Zone (middle Miocene)								?
Unit	PP		Calvert Beach Member								
Taxon / Depth (ft) / Depth (m)	140.5 m (460.8–460.9 ft)	139.4 m (457.3–457.4 ft)	138.4 m (454.0–454.1 ft)	136.9 m (449.0–449.2 ft)	135.3 m (443.7–443.9 ft)	133.8 m (439.0–439.1 ft)	131.9 m (432.8–433.0 ft)	130.8 m (429.1–429.3 ft)	129.6 m (425.2–425.4 ft)	128.0 m (419.9–420.0 ft)	125.9 m (413.1–413.3 ft)
Abundance	VR	R	C	A	A	A	A	A	A	C	VR
Preservation	P	P	M	M	G	G	G	G	G	M	M
Actinocyclus ellipticus	.	.	.	.	.	.	.	.	.	R	.
Actinocyclus ingens	.	.	R	F	F	F	R	R	R	F	VR
Actinocyclus octonarius	.	.	F	F	F	R	R	R	F	F	.
Actinoptychus senarius	.	R	.	R	F	R	R	F	R	R	.
Actinoptychus thumii	.	.	.	.	.	.	.	.	R	.	.
Actinoptychus virginicus	.	.	.	R	R	R	.	R	.	.	.
Annellus californicus	.	.	R	.	.	.	R	.	.	.	.
Azpeitia vetustissimus	.	.	R	R	R	R	R	R	R	R	.
Cavitatus miocenicus	.	.	.	.	.	R	R	R	.	.	.
Cladogramma dubium	.	.	.	R	.	R	.	.	.	.	.
Coscinodiscus apiculatus	.	.	R	F	R	R	R	R	R	F	.
Coscinodiscus curvatulus	.	.	.	R	.	.	.	R		R	.
Coscinodiscus lewisianus	.	.	.	.	R	.	.	R	.	.	.
Coscinodiscus marginatus	.	.	F	R	R	R	R	R	R	R	.
Coscinodiscus oculus-iridis	.	R	.	.	.	R	R	R	R	R	.
Coscinodiscus radiatus	.	.	R	R	R	R	R	R	R	R	.
Coscinodiscus rothii	.	.	.	.	.	R	.	R	R	.	.
Cosmiodiscus elegans	.	.	.	.	.	.	.	R	.	.	.
Craspedodiscus coscinodiscus	.	R	R	.	.	.	F	R	.	.	.
Cymatogonia amplyoceras	.	.	.	R	R	.	.	.	.	.	.
Delphineis angustata	.	.	.	.	.	.	.	.	R	.	VR
Delphineis biseriata	.	.	.	R	R	R	F	F	R	.	.
Delphineis novaecesarea	.	.	.	.	R	.	F	R	R	.	.
Delphineis penelliptica	.	.	.	R	F	F	F	F	F	R	VR
Denticulopsis simonsenii	.	.	.	R	.	R	R	R	R	R	.
Goniothecium rogersii	.	.	.	.	.	.	.	.	.	R	.
Melosira westii	.	.	F	F	F	R	F	F	C	C	.
Navicula pennata	.	.	.	.	.	.	R	R	.	.	.
Paralia complexa	.	.	F	F	R	R	.	R	.	R	.
Paralia sulcata	R	F	C	A	A	C	A	A	C	C	VR
Pleurosigma affine var. *marylandica*	.	.	.	.	.	R	R	R	R	R	.
Pyxidicula cruciata	.	.	R	R	R	R	R	F	R	R	.
Rhaphoneis gemmifera	.	.	.	R	R	R	.	.	R	R	.
Rhaphoneis lancelettula	.	.	.	.	.	.	.	.	R	R	.
Stellarima sp.	.	.	.	.	.	.	R	.	.	.	.
Stephanopyxis corona	.	.	R	.	R	.	.	.	R	.	.
Stephanopyxis grunowii	.	.	R	.	R	R	R	.	R	.	.
Stephanopyxis turris	.	.	R	.	.	R	R	R	R	R	.
Stephanopyxis sp. cf. *S. lineata*	.	.	R	.	.	.	.	R	R	.	.
Thalassionema nitzschioides	.	.	F	F	F	R	F	F	F	R	VR
Thalassiosira leptopus	.	.	.	.	.	.	R	.	.	.	.
Thalassiosira praeyabei	.	.	.	.	.	.	R	.	.	.	.
Thalassiothrix longissima	.	.	.	.	.	R	R	R	R	R	VR
Triceratium condecorum	.	.	.	R	R	.	R	.	R	.	.
Xanthiopyxis spp.	.	.	R	R	F	R	F	F	F	R	.
TABULAR GLASSY MINERALS	A	A	.	.	.	.	.	.	.	.	.

Figure H12. Occurrence chart showing the presence of diatoms in samples from the Miocene Plum Point Member (PP) and Calvert Beach Member of the Calvert Formation in the USGS-NASA Langley core. The diatom zone is from Abbott (1980). Abundance definitions: A= abundant (more than one specimen per field of view); C=common (at least one specimen per three fields of view); F=few (at least one specimen per vertical traverse having a length of 22 mm); R=rare (fewer occurrences than few but more than two specimens per slide); VR=very rare (only one or two specimens per slide); .= not present. Preservation abbreviations: P= poor, M=moderate, G=good.

Unit	Depth (ft)	Depth (m)	Specimens	Ts	Taxon																					Subzones of the middle Miocene *Corbisema triacantha* Zone
					Bachmannocena circulus	*Bachmannocena elliptica elliptica*	*Bachmannocena elliptica miniformis*	*Bachmannocena triangula*	*Caryocha* sp.	*Corbisema triacantha*	*Dictyocha brevispina ausonia*	*Dictyocha brevispina brevispina*	*Dictyocha fibula* (large)	*Dictyocha fibula* (small)	*Dictyocha pulchella*	*Distephanus crux crux*	*Distephanus crux parvus*	*Distephanus crux scutulatus*	*Distephanus longispinus*	*Distephanus speculum speculum*	*Distephanus speculum triommata*	*Distephanus stauracanthus*	*Distephanus stradneri*	*Distephanus* sp. aff. *D. schauinslandii*	
CB	407.4–407.6	124.2	0		.	.	.	.	.	.	.	.	.	.	.	.	.	.	.	.	.	.	.	.	.	
CB	413.1–413.3	125.9	0		.	.	.	.	.	.	.	.	.	.	.	.	.	.	.	.	.	.	.	.	.	
CB	419.9–420.0	128.0	50	51	2	.	.	4	2	4	.	8	.	2	6	40	10	.	12	4	.	6	.	.	*D. stauracanthus*
CB	425.2–425.4	129.6	100	52	.	.	.	.	1	1	1	.	4	.	.	56	26	4	.	.	1	1	3	2	*D. stauracanthus*
CB	429.1–429.3	130.8	200	55	.	2	.	.	1	1	2	2	3	.	1	41	23	12	12	1	.	.	3	.	*D. schulzii*
CB	432.8–433.0	131.9	260	45	.	.	7	.	1	1	3	.	3	.	.	37	34	3	4	8	1	.	1	.	*D. schulzii*
CB	439.0–439.1	133.8	100	56	.	1	.	.	1	2	2	.	13	.	.	48	18	1	3	3	.	.	7	.	*D. schulzii*
CB	443.7–443.9	135.3	100	56	.	.	.	.	2	1	.	.	13	.	.	42	28	.	3	1	.	.	10	.	*D. schulzii*
CB	449.0–449.2	136.9	30		.	.	.	x	.	.	x	.	.	.	.	X	x	.	x	.	.	.	.	.	
CB	454.0–454.1	138.4	0		.	.	.	.	.	.	.	.	.	.	.	.	.	.	.	.	.	.	.	.	
PP	457.3–457.4	139.4	0		.	.	.	.	.	.	.	.	.	.	.	.	.	.	.	.	.	.	.	.	
PP	460.8–460.9	140.5	0		.	.	.	.	.	.	.	.	.	.	.	.	.	.	.	.	.	.	.	.	
NN	467.0–467.1	142.4	0		.	.	.	.	.	.	.	.	.	.	.	.	.	.	.	.	.	.	.	.	

Figure H13. Occurrence chart showing the presence of silicoflagellates from the Miocene Calvert Formation in the USGS-NASA Langley core. Units of the Calvert Formation that were sampled are the Newport News beds (NN), Plum Point Member (PP), and Calvert Beach Member (CB). All the silicoflagellate-bearing samples are in the middle Miocene *Corbisema triacantha* Zone. Ts values are relative values; higher values represent relatively warmer temperatures. The specimen count for each sample is listed; species abundances are given as percentages. Any sub-50 sample count is shown as a species checklist (small x) with the one most numerous species indicated by a large X.

ples should be equivalent biostratigraphically to the Calvert Beach Member of the Calvert Formation.

The highest sample (R6110 V) is assigned to Zone DN6 of de Verteuil and Norris (1996) on the basis of the absence of *Cleistosphaeridium placacanthum* (highest occurrence defines the top of DN5). The sample contains *Pentadinium* sp. (highest occurrence within DN7, but rare above DN6) and a single specimen of *Trinovantedinium glorianum* (lowest occurrence within DN6). Although this sample is technically above the highest occurrence of *C. placacanthum*, its flora is otherwise quite similar to that in the sample below. In de Verteuil and Norris' (1996) original publication, their highest middle Miocene sample (Calvert Formation) in the Exmore core was also lacking *C. placacanthum*.

Diatom biostratigraphy.—Samples of the Calvert Beach Member in the Langley core were studied for siliceous microfossils (figs. H12, H13). The presence of *Delphineis penelliptica*, *Denticulopsis simonsenii* (=*D. hustedtii*), and *Coscinodiscus lewisianus*, along with the absence of *Thalassiosira grunowii* (=*Coscinodiscus plicatus*) and *Delphineis ovata*, in the diatom assemblages of samples from 136.9 m (449.0–449.2 ft) through 128.0 m (419.9–420.0 ft) places them in the *Delphineis penelliptica* Partial Range Zone (IV) of Abbott (1978) (Abbott, 1980). It is presumed that the more poorly preserved interval represented by the sample from 138.4 m (454.0–454.1 ft) also correlates with the *D. penelliptica* Zone, because the background diatom assemblage is the same.

Abbott's (1980) *Delphineis penelliptica* Zone is documented in offshore cores from Atlantic Margin Coring Project (AMCOR) Sites 6022 (lat 31°08.75' N., long 80°31.05' W., water depth 32 m (105 ft)) and 6011 (lat 39°43.5' N., long 73°58.6' W., water depth 22.3 m (73 ft)) and therefore would seem to have wide application along the U.S. East Coast. Abbott (1984) emphasized the importance of the first occurrence of *T. grunowii* in both onshore and offshore sections along the U.S. Atlantic margin and stated that it falls within strata assigned to planktonic foraminiferal Zone N11. This taxon was not found in the samples studied from the Langley core.

According to Abbott (1984), the first occurrence of *Denticulopsis simonsenii* coincides with the base of Zone N11 along the U.S. East Coast, whereas the last occurrence of *C. lewisianus* occurs within the lower half of Zone N12. The first occurrence of *D. simonsenii*, a cool-water species, is dated at about 14.2 Ma in California and in the Southern Ocean, so presumably this age would be a maximum age for the diatom-bear-

ing section studied from the Langley core. The last occurrence of the warm-water diatom *C. lewisianus* in the equatorial Pacific is dated at 12.93 Ma, establishing a minimum age for the section studied. Although Burckle (1996) favored a somewhat younger age (about 12.1 Ma) for the last occurrence of *C. lewisianus* in the equatorial Pacific, Burckle may have confused some specimens of *C. lewisianus* with *Actinocyclus ellipticus* var. *spiralis*, a morphologically similar taxon that ranges above the true last occurrence of *C. lewisianus* (Barron, 1985). The entire interval (14.1–12.93 Ma) represented by samples from 138.4 to 128.0 m (454.0–454.1 to 419.9–420.0 ft) is correlated with planktonic foraminiferal Zone N10 and is correlated with the uppermost part of calcareous nannofossil Zone CN4 and the lowermost part of CN5a according to Berggren and others (1995).

The diatom assemblage appears to correlate entirely with the *Coscinodiscus lewisianus* Zone of Burckle (1996). However, if the last occurrence of *C. lewisianus* in the sample from 130.8 m (429.1–429.3 ft) represents a true last occurrence datum level, then samples from 129.6 m (425.2–425.4 ft) and 128.0 m (419.9–420.0 ft) would be assignable to the overlying *Rhizosolenia barboi/Delphineis penelliptica* Zone of Burckle (1996).

The diatom assemblage would also appear to correlate with the middle to upper part of Andrews' (1988) East Coast Diatom Zone (ECDZ) 5, the *Delphineis novaecesarea* Partial Range Zone because of the presence of *Actinoptychus virginicus*, *Delphineis penelliptica,* and *D. novaecesarea* and the absence of *Rhaphoneis magnapunctata, R. clavata,* and *Thalassiosira grunowii*. As such, it is an assemblage that coincides with that of Shattuck's (1904) bed "14" to lower "15" of the Calvert Formation in the Scientist Cliffs area of Calvert County, Md. (Andrews, 1988). Such a correlation is in agreement with de Verteuil and Norris (1996), who correlated ECDZ 5 with dinoflagellate zone DN5.

Diatom correlation with other East Coast sections.—The diatom assemblage in the Calvert Beach Member of the Calvert Formation in the Langley core resembles those of other reports on the U.S. East Coast. It is very similar to that of the Coosawhatchie Clay Member of the Hawthorn Formation of South Carolina as described by Ernissee and others (1977); however, the absence of *Thalassiosira grunowii* (=*C. plicatus*) in the Langley core material suggests that it is slightly older than the Coosawhatchie Clay. Similarly, the diatom assemblage closely resembles the diatom assemblage of the Choptank Formation from Calvert County, Md., described by Andrews (1976), but it lacks *Rhaphoneis diamantella*, a marker taxon for Andrews' (1988) East Coast Diatom Zone 7 and, therefore, it appears to be older.

Andrews and Abbott (1985) also documented a similar diatom assemblage from the Hawthorn Formation of Thomas County, Ga.; however, the lack of *Denticulopsis simonsenii* in the Hawthorn suggests that that assemblage was slightly older than that studied from the Langley core, a conclusion that is also supported by the presence of *Rhaphoneis magnapunctata* in the former and its absence from the latter (Andrews, 1988).

Silicoflagellates.—The first occurrence of *Distephanus stauracanthus* in the sample from 129.6 m (425.2–425.4 ft) depth in the Langley core (fig. H13) is correlated with the lowermost part of calcareous nannofossil Subzone CN5a in the equatorial Pacific according to Barron and others (1985), a correlation slightly younger than that of Perch-Nielsen (1985) and Ernissee and others (1977), who placed this silicoflagellate datum at the CN4-CN5 zonal boundary. Either way, it appears that the equivalent of the CN4-CN5 boundary, dated at 13.6 Ma by Berggren and others (1995), would fall in the upper part of the section studied.

Langley core silicoflagellate floras of the *Corbisema triacantha* Zone are dominated (50 to 82 percent) by *Distephanus crux crux* and *D. crux parvus* and contain sparse (2 to 12 percent) *Bachmannocena*, *Caryocha*, and *Corbisema*. Silicoflagellates are abundant in only one sample, from 131.9 m (432.8–433.0 ft), where *B. elliptica miniformis* and *D. speculum speculum* indicate strongest nutrient upwelling. The silicoflagellate section in the Langley core extends from 136.9 to 128.0 m (449.0–449.2 to 419.9–420.0 ft); the zonal guide species in this short, 9-m-thick (29-ft-thick) Langley section, *C. triacantha* and *D. stauracanthus*, have been reported together with mid-Miocene coccoliths of Subzone CN5a in a 27-m (90-ft) section at DSDP Site 470 in the Pacific off northern Mexico (Bukry, 1981). The silicoflagellate relative paleotemperature values (Ts column in fig. H13) for the Langley samples are moderate and show slight cooling upwards.

Nearly identical *Distephanus stauracanthus* Subzone floras have been described from cores of mid-Miocene strata from southern New Jersey (Bukry, 1990). There, well ACOW 1 (lat 39°19'52" N., long 74°25'89" W.), south of Atlantic City, contains a 71-m (234-ft) interval assigned to the subzone by the presence of *C. triacantha* and *D. stauracanthus*. The floras are also dominated by the *D. crux* group. Sample 658, near the bottom of the subzone in ACOW 1, has the overlap of *D. stauracanthus* with diatom guide *Coscinodiscus lewisianus*. This overlap might occur in the unsampled interval between 129.6 and 128.0 m (425.3 and 420.0 ft) in the Langley core, if the last *C. lewisianus* in the sample from 130.8 m (429.1–429.3 ft) represents a true last occurrence datum (fig. H12).

In noting the co-occurrence of *D. stauracanthus* and *C. lewisianus* in the Coosawhatchie Clay Member of the Hawthorn Formation in South Carolina and its equivalent in Georgia, Ernissee and others (1977) emphasized that the overlap of these two taxa is substantial in the equatorial Pacific, a conclusion that is also supported at DSDP Site 470 in the Pacific off northern Mexico (Barron, 1981a; Bukry, 1981). Ernissee and others (1977) indicated that the first *Distephanus stauracanthus* occurs below the first occurrence of the diatom *T. grunowii* (= *Coscinodiscus plicatus*) in an interval correlated with the lowermost part of calcareous nannofossil Zone NN 6 (=CN5a). In contrast to the correlations of Abbott (1978, 1984), Ernissee and others (1977) showed that *Thalassiosira grunowii* first occurs near the middle of NN 6 (=CN5a), a correlation supported in the equatorial Pacific (Barron, 1981b). It would, therefore, appear that the top of the biosiliceous section studied in the sample

from 128 m (419.9–420.0 ft) correlates with the lower portion of calcareous nannofossil Subzone CN5a (=NN 6) and that the last occurrence of *C. lewisianus* in the sample from 130.8 m (429.1–429.3 ft) does not represent a true last occurrence datum.

Paleoenvironmental information.—Strong nutrient upwelling is indicated for the sample at 131.9 m (432.8–433.0 ft) because of the presence of *Bachmannocena elliptica miniformis* and *Distephanus speculum speculum*. The silicoflagellate relative paleotemperature Ts values for the Langley samples are moderate and show slight cooling upwards (fig. H13).

Middle Miocene correlation of the Calvert Beach Member of the Calvert Formation.—Dinoflagellate, diatom, and silicoflagellate biostratigraphy all indicate placement of the Calvert Beach Member of the Calvert Formation in the middle Miocene. Dinoflagellate placement is in the upper half of Zone DN5 and in Zone DN6 of de Verteuil and Norris (1996). Diatoms indicate the *Delphineis penelliptica* Partial Range Zone (IV) of Abbott 1978 (Abbott, 1980) and *Coscinodiscus lewisianus* Zone of Burckle (1996). Silicoflagellates indicate placement in the *Distephanus schulzii* and *Distephanus stauracanthus* Subzones of the *Corbisema triacantha* Zone.

In the absence of dinoflagellate, diatom, and silicoflagellate data to the contrary, the presence of specimens of the calcareous nannofossil genus *Catinaster* would have indicated a latest middle or early late Miocene age. A similar anomalous occurrence of *Catinaster* was noted by the shipboard scientific party for Ocean Drilling Program (ODP) Leg 150, Site 905, offshore New Jersey (Mountain, Miller, Blum, and others, 1994, p. 277). Aubry (1996, p. 436) attributed the Leg 150 occurrence to core contamination. The number of occurrences of *Catinaster* in the Langley core suggests that contamination is not the cause; rather, the lowest occurrence of genus *Catinaster* may be within the middle Miocene, possibly at 13–14 Ma.

St. Marys Formation

The St. Marys Formation at 123.6–68.4 m (405.5–224.5 ft) depth in the Langley core was studied for dinoflagellates (fig. H11), mollusks (fig. H6, in pocket), and ostracodes (fig. H7). Although 13 samples were examined for calcareous nannofossils from this formation, most of the samples were barren of calcareous nannofossils, and the rest contained no age-diagnostic species. Dinoflagellates place the unit in Zone DN9, although the lowest sample is possibly in DN8. Both zones are upper Miocene. The unit is 55.2 m (181.0 ft) thick and represents less than 1.3 m.y of deposition. The base of this unit is calibrated at the base of Zone DN9 (8.7 Ma according to de Verteuil and Norris, 1996). The top of the St. Marys is still within DN9 (and thus older than 7.4 Ma according to de Verteuil and Norris, 1996). As discussed below, both mollusks and ostracodes indicate intervals representing episodes of upwelling within the St. Marys Formation.

Dinoflagellates and acritarchs.—Five samples were examined for dinocysts from the St. Marys Formation in the Langley core (fig. H11). The sample depths range from 120.4 to 72.2 m (395.2 to 236.8 ft). Three specimens are shown in plate H5 (figs. 2, 3, and 7). Preservation ranges from good to poor.

These five samples are placed in the upper Miocene (Tortonian) Zone DN9 on the basis of the presence of *Barssidinium evangelineae* (lowest occurrence at or near the base of DN9) and *Hystrichosphaeropsis obscura* (highest occurrence defines the top of DN9). The lowest St. Marys sample (R6110 U) contains a single, poorly preserved specimen of *Sumatradinium soucouyantiae* (highest occurrence defines the top of DN8), and thus it alternatively could be placed in uppermost Zone DN8. The absence of *Palaeocystodinium golzowense* (highest occurrence at the top of DN8) favors the interpretation of *S. soucouyantiae* as reworked.

Mollusks.—The St. Marys Formation at 123.6–68.4 m (405.5–224.5 ft) depth within the Langley core contains 15 recognizable molluscan taxa (fig. H6) scattered throughout the unit. The dominant taxa are *Turritella plebeia plebeia*, *T. plebeia carinata*, and *T. subvariabilis*, and these are concentrated in zones around 95.1–94.5 m (312–310 ft) and 92.3–90.1 m (303–295.5 ft). The preservation of *Turritella subvariabilis* within the Langley core does not allow separation of this species into subspecies. Ward (1992) listed the stratigraphic ranges of these species of *Turritella* as shown in table H2.

The presence of *Turritella plebeia plebeia* and *Turritella subvariabilis* in the St. Marys is in agreement with Ward (1992); however, the occurrence of *T. plebeia carinata* is outside the published range. *Turritella plebeia carinata* is distinctive (see specimen from Eastover Formation on pl. H7, figs. 11, 12, for representative form), well preserved, and relatively abundant in the St. Marys in the Langley core, and so the most likely explanation is that the subsurface St. Marys contains species not seen in outcrop and, therefore, extends the stratigraphic range of *T. plebeia carinata*.

Ostracodes.—Although the ostracodes from the classic Miocene Calvert Cliffs of Maryland were described by Ulrich and Bassler (1904) and their taxonomy was updated by Forester (1980), the detailed stratigraphic distribution of species is still only generally known. Nonetheless, the Langley core samples between 120.2 m (394.2–394.6 ft) and 71.3 m (233.9–234.1 ft) contain typical St. Marys assemblages that include *Actinocythereis exanthemata*, *Muellerina lienenklausi*, *Murrayina barclayi*, and *Murrayina macleani* (fig. H7). It should be noted that an apparently undescribed species of *Cytheridea* occurs in this interval and that the specimens of *A. exanthemata* are more reticulated than is typical of this species. The lowest occurrence of *Pseudocytheretta burnsi* in the upper St. Marys at 88.1 m (289.1–289.3 ft) may prove to be a noteworthy marker for the transition between the St. Marys and the overlying Eastover Formation.

Paleoenvironmental information.—Both mollusks and ostracodes indicate intervals of upwelling within the St. Marys Formation.

The abundance of *Turritella* in the St. Marys Formation indicates favorable conditions for this group during the time of deposition. Allmon (1988), in a summary of living turritelline

Table H2. Stratigraphic ranges and mollusk zones of selected *Turritella* species reported by Ward (1992) from the U.S. middle Atlantic Coastal Plain.

Taxon	Formation	Age	Mollusk zone
Turritella plebeia plebeia	Eastover Formation St. Marys Formation Choptank Formation Calvert Formation	Lower middle Miocene to upper Miocene	M7–M13
Turritella plebeia carinata	Eastover Formation (Claremont Manor Member)	Upper Miocene	M8
Turritella subvariabilis subvariabilis	St. Marys Formation (Windmill Point beds)	Lower upper Miocene	M9
Turritella subvariabilis bohaski	St. Marys Formation (Little Cove Point beds)	Lower upper Miocene	M10
Turritella subvariabilis dianae	Choptank Formation (Drumcliff Member)	Middle middle Miocene	M12

ecology, concluded that they are most commonly found at depths of less than 100 m (330 ft) and in fully marine water, although some species can tolerate salinities less than 35 parts per thousand (ppt). Typically they are found in waters between 15°C and 20°C, although they can range from 2°C to 27°C. Living *Turritella* frequently occur in areas of coastal upwelling, and most high-density populations of *Turritella* are found landward of these upwelling zones (Allmon, 1988). The dense zones of *Turritella* within the St. Marys may be indicative of coastal upwelling. The other molluscan species in the St. Marys indicate marine shelf conditions but do not provide any further details on depositional environment.

Ostracodes indicate that the depositional environment for the St. Marys Formation (120.2 –71.3 m; 394.6–233.9 ft) was inner-middle neritic, although the consistent occurrence, often in abundance, of *Cytherella* may signify outer neritic conditions, upwelling cooler water, or both. Seasonality in temperatures was relatively small.

Other paleontological information.—Rare dinoflagellate specimens that appear to have been altered by the impact (curled processes as described in Frederiksen and others, this volume, chap. D) were found in the St. Marys Formation (R6110 T, 114.5 m=375.5–375.8 ft) and thus are possibly, but not necessarily, reworked.

Eastover Formation

The Eastover Formation at 68.4–23.3 m (224.5–76.3 ft) depth in the Langley core was studied for dinoflagellates (fig. H11), mollusks (fig. H6, in pocket), and ostracodes (fig. H7). All calcareous nannofossil samples but one were either barren or very questionably datable. The single clearly datable nannofossil sample at 56.9 m (186.6 ft) is in Zone NN 11 (fig. H4). Dinoflagellates place the unit in Zones DN9 and DN10. Both zones are upper Miocene. The boundary between DN9 and DN10 is bracketed by samples at 52.4 and 59.9 m (171.6–172.0 and 196.4–196.7 ft). The DN9-DN10 boundary is calibrated at 7.4 Ma, and the top of DN10 is at 5.9 Ma (de Verteuil and Norris, 1996). The unit is 45.1 m (148.2 ft) thick.

Calcareous nannofossils.—Twelve samples from 67.3 to 23.8 m (220.8 to 78.2 ft) depth in the Langley core were examined for calcareous nannofossils from the Eastover Formation. Most of the samples were barren or contained only rare calcareous nannofossils. However, a sample from 56.9 m (186.6 ft) contained frequent calcareous nannofossils, and the presence of *Discoaster berggrenii* (FAD and LAD within Zone NN 11) restricts this sample to the late Miocene Zone NN 11.

The sample from 31.4 m (103.0 ft) contains a questionable occurrence of *Discoaster intercalaris* (Zones NN 11–12 in range). If it is this species, then the samples from 50.6 to 31.4 m (166.1 to 103.0 ft) can be no older than Zone NN 11 because they overlie samples of this zone, and no younger than Zone NN 12 because *D. intercalaris* does not occur above Zone NN 12. If the specimen is not *D. intercalaris,* then the upper part of the Eastover cannot be dated any closer than Zones NN 11–15 on the basis of calcareous nannofossils.

Dinoflagellates and acritarchs.—Four samples from the Eastover Formation were examined for dinocysts. The sample depths range from 66.1 to 24.8 m (216.9 to 812 ft) in the Langley core. All are upper Miocene. Selected specimens are shown in plate H5 (figs. 4–6, 8–11). Preservation ranges from fair to good.

The lower two samples are assigned to Zone DN9 on the basis of the presence of *Hystrichosphaeropsis obscura*, the highest occurrence of which defines the top of DN9. The two higher samples are assigned to the upper upper Miocene Zone DN10 on the basis of the presence of *Selenopemphix armageddonensis* (lowest occurrence at or near the base of DN10) and *Erymnodinium delectabile* (highest occurrence defines the top of DN10) and the absence of *Hystrichosphaeropsis obscura* (highest occurrence defines the top of DN9). The presence of *Labyrinthodinium truncatum* (lowest occurrence at or near the top of DN9) in sample R6110 I (52.4 m=171.6–172.0 ft depth)

suggests that this sample should fall near the DN9-DN10 boundary, as this species is not known to range very far into DN10. The uppermost sample also contains *Filisphaera microornata* (lowest occurrence at or near the base of DN10).

Mollusks.—The molluscan assemblages within the Eastover Formation in the Langley core are relatively diverse, containing 46 recognizable molluscan taxa (fig. H6, pl. H7). The dominant forms are *Anomia* sp., *Lirophora vredenburgi*, *Nucula proxima*, *Isognomon* sp., *Turritella* spp., and pectens. Two segments within the Eastover portion of the core contain more concentrated and diverse molluscan remains: 61.2–56.8 m (200.7–186.2 ft) and 41.6–34.4 m (136.5–113 ft).

Ward (1992) designated molluscan interval zones M7 and M8 (upper part of the upper Miocene) within the Eastover Formation, which correlate with the Cobham Bay and Claremont Manor Members of the Eastover. *Ecphora gardnerae whiteoakensis*, present in the sample from 66.8 m (219 ft), is restricted to M8 (Ward, 1992). The segment of the core from 58.8 to 37.2 m (193 to 122 ft) contains a mixture of specimens from zones M7 and M8 (Ward, 1992): *Turritella plebeia carinata* (M8), *Chesapecten middlesexensis* (M7–M8), *Anadara carolinensis* (M7–M8), *Spisula rappahannockenis* (M7–M8), and *Lirophora vredenburgi* (M7). The co-occurrence of *Turritella plebeia carinata* and *Lirophora vredenburgi* indicates either that the ranges of one or both species need to be revised or that the Langley core preserves Eastover beds that lie stratigraphically between the Cobham Bay and the Claremont Manor Members as they are known in outcrop. In addition, *Turritella subvariabilis*, typical of zones M9–M12 in the St. Marys Formation (see discussion above), is present from 44.0 to 38.6 m (144.5 to 126.5 ft). The very worn and weathered condition of *Turritella subvariabilis* implies that reworking may have occurred in this segment of the Eastover. From 37.1 m (121.6 ft) to the top of the Eastover at 23.3 m (76.3 ft), the sediments contain two species of mollusks restricted to the M7 zone of Ward (1992)—*Carolinapecten urbannaensis* and *Lirophora vredenburgi*.

Fragments of *Isognomon* sp. occur throughout the Eastover sediments in the Langley core but are densely concentrated from 62.5 to 59.7 m (205 to 196 ft) and from 42.7 to 41.8 m (140.1 to 137.0 ft). Ward (1992) described *Isognomon* as being abundant in the Eastover Formation, occurring in thin beds in the Claremont Manor Member and in thick beds (up to 1.8 m (6 ft) thick) in the Cobham Bay Member.

Ostracodes.—The lower Eastover Formation in the Langley core is marked by the first occurrence of the ostracodes *Loxoconcha florencensis* and *Hulingsina calvertensis* and the genus *Bensonocythere*. *Microcytherura shattucki* is a distinctive species that seems to be a useful indicator of the upper Miocene of the region, though it occurs only rarely. *Pterygocythereis inexpectata* first occurs in the lower Eastover; additional work is needed on the stratigraphic ranges of intermediate forms between *P. americana* and *P. inexpectata* (see Forester, 1980).

Paleoenvironmental information.—The molluscan pelecypod genera present in the Eastover Formation in the Langley core are similar to an assemblage from a modern subtropical to warm-temperate, relatively shallow, marine shelf having diverse substrates, analogous to the modern Gulf Coast of Florida (Brewster-Wingard and others, 2001; for modern environmental information, see the U.S. Geological Survey's (2004) South Florida Information Access databases at http://sofia.usgs.gov/flaecohist/). The absence of a diverse gastropod assemblage implies that the waters were cooler than the modern Florida coast or that there was an absence of subaquatic vegetation or both. The sample from 32.5 m (106.5–106.6 ft) contains a single specimen of *Truncatella*, which belongs to a group that lives just above high tide and is typically found in nearshore deposits (Emerson and Jacobson, 1976). Ostracodes suggest that the depositional environment for the Eastover Formation was inner-middle neritic.

Other paleontological information.—As in other Virginia cores, the dinocyst DN9-DN10 boundary in the Langley core does not exactly coincide with the St. Marys-Eastover contact. In the Langley core, this boundary is placed well up into the Eastover Formation (bracketed by samples at 52.4 and 59.9 m (171.6–172.0 and 196.4–196.7 ft). Sedimentation appears to have been essentially continuous.

Yorktown Formation

The Yorktown Formation at 23.3–2.2 m (76.3–7.2 ft) depth in the Langley core was studied for calcareous nannofossils (fig. H4, in pocket), dinoflagellates (fig. H11), mollusks (fig. H6, in pocket), and ostracodes (fig. H7). Fossils place the Yorktown in the Pliocene, both lower Pliocene and lower part of the upper Pliocene. Neither the mollusks nor the ostracodes record the presence of the oldest Yorktown known from other localities. Mollusks from zone M6 and ostracodes corresponding to the Sunken Meadow Member (Zone 1 of Mansfield, 1943) were not found. The Yorktown Formation in the Langley core is 21.1 m (69.1 ft) thick. We have used calibration points of 3.0 and 4.0 Ma for the upper and lower boundaries of the Yorktown, respectively, following Dowsett and Wiggs (1992). This calibration is based on the presence of the foraminifera *Dentoglobigerina altispira*, *Sphaeroidinellopsis*, and *Globorotalia puncticulata,* not in the Langley core, but in outcrops they studied nearby in southeastern Virginia.

Calcareous nannofossils.—Seven samples from 21.3 to 6.0 m (70.0 to 19.7 ft) depth in the Langley core were examined for calcareous nannofossils from the Yorktown Formation (fig. H4). These samples had abundant to common calcareous nannofossils with good to poor preservation. However, these samples were very difficult to date because, although the samples contained many specimens, the diversity was low, and there were few age-diagnostic species.

The lowest two samples, from 21.3 and 20.5 m (70.0 and 67.2 ft), are placed questionably in Zone NN 15 because they contain *Sphenolithus abies* (LAD near the top of Zone NN 15) and the Yorktown elsewhere has never been found older than Zone NN 15. *Reticulofenestra pseudoumbilicus* (LAD defines the top of Zone NN 15) is present only in the lowest sample at

21.3 m (70.0 ft), which also supports a NN 15 call for only the lowest part of the Yorktown in the Langley core. The absence of this species from the sample at 20.5 m (67.2 ft), which contains *S. abies,* is unexplained.

Although the samples in the interval from 18.2 to 16.5 m (59.8 to 54.2 ft) do not have any *Sphenolithus abies* or *Pseudoemiliania lacunosa*, it is more likely that they are in Zones NN 16–17 because *S. abies* is clearly present in the two underlying samples at 20.5 and 21.3 m (67.2 and 70.0 ft), and because its absence in the interval from 18.2 m (59.8 ft) and above is considered to be more diagnostic than the absence of *P. lacunosa*.

The upper three samples from 9.6 to 6.0 m (31.4 to 19.7 ft) are placed in Zones NN 16–17 because they do not have any sphenoliths, and they do contain *Pseudoemiliania lacunosa* (FAD in upper part of Zone NN 15) and *Discoaster asymmetricus* (LAD in Zone NN 17).

Dinoflagellates and acritarchs.—Four samples from 21.9 to 7.3 m (71.9 to 24.1 ft) depth in the Langley core were examined for dinoflagellates from the Yorktown Formation. Dinoflagellate samples from the Yorktown are most likely Pliocene. Two specimens are shown in plate H5 (figs. 12–15). Preservation ranges from fair to good.

The lowest dinoflagellate sample from the Yorktown Formation is similar to those of the underlying Eastover Formation, with the significant exception of the absence of *Erymnodinium delectabile,* the highest occurrence of which defines the top of Zone DN10. The top of DN10 is just below the top of the Miocene. The lowest Yorktown sample (R6110 E) additionally contains *Selenopemphix armageddonensis*, which is typically a late Miocene form but is known to range into the Pliocene.

The presence of *Ataxiodinium confusum* in sample R6110 C (9.6 m=31.4–31.7 ft depth) is diagnostic. The reported range of this species is approximately Zones NN 12–16 (lower Pliocene and lower part of the upper Pliocene). *Invertocysta lacrymosa*, also present in this sample, has its highest occurrence in the upper Pliocene. The highest Yorktown sample is most likely Pliocene as it contains *Barssidinium evangelineae* (or *Barssidinium pliocenicum*), which does not range into the Pleistocene or may range only slightly into it. Sample R6110 D (16.0 m=52.4–52.8 ft depth) has material reworked from the Oligocene or Miocene.

Mollusks.—The Yorktown Formation in the Langley core contains 52 identifiable molluscan taxa identified from the sediments examined (fig. H6; pl. H6, fig. 2; pl. H8). The dominant species are *Turritella alticostata, Yoldia laevis, Nuculana acuta, Pitar sayana, Nucula proxima,* and *Crepidula fornicata. Tectonatica pusilla* and *Parvilucina crenulata*, two minute species, are abundant in some samples. Molluscan remains are scattered throughout the unit, but concentrations are increased in the segments at 19.7–16.8 m (64.5–55 ft), 13.1–12.5 m (43–41 ft), and about 6.7 m (22 ft).

No molluscan species representative of mollusk zone M6 (lower Pliocene) from the lower part of the Yorktown were identified in the Langley core. *Chesapecten madisonius, Turritella alticostata, Striarca centenaria*, and *Astarte undulata* of M5 (lower Pliocene to mid-upper Pliocene) (Blackwelder, 1981) were present in the sediments. A number of molluscan species identified by Harris (Harris *in* Ward, 1993) from the type Yorktown sections are present in the core: *Acteocina candei, Astarte concentrica, Chesapecten madisonius, Crepidula fornicata, Cyclocardia granulata, Nucula proxima, Nuculana acuta, Pitar sayana, Striarca centenaria, Turritella alticostata,* and *Yoldia laevis*.

Ostracodes.—The lowest Yorktown Formation ostracode sample in the Langley core (22.8 m (74.7–74.9 ft) depth) cannot be assigned to an ostracode zone. The next higher sample at 20.3 m (66.5–66.7 ft) contains ostracode species that place it within the middle part of the Pliocene but do not restrict it to either of the *Pterygocythereis inexpectata* or *Orionina vaughani* Zones of Hazel (1971). Ostracodes corresponding to the Sunken Meadow Member (Zone 1 of Mansfield, 1943) were not found.

The Yorktown Formation samples between 16.1 m (52.8–53.1 ft) and 5.6 m (18.4–18.6 ft) contain the most abundant and diverse ostracode assemblages in the core. These faunas typically contain age-diagnostic Pliocene species described in detail in Hazel (1977, 1983), Cronin and Hazel (1980), and Cronin (1990), whose taxonomy and biostratigraphy of Yorktown ostracodes supersede those of earlier workers (Malkin, 1953; Swain, 1974). The Yorktown beds above 16.1 m in the Langley core represent the *Orionina vaughani* ostracode assemblage zone, and they include several age-diagnostic Pliocene species such as *Orionina vaughani* and several species of *Muellerina* and *Bensonocythere*. Elsewhere in Virginia, the *Orionina vaughani* Zone is represented by the Rushmere, Morgarts Beach, and Moorehouse Members of the Yorktown of Ward and Blackwelder (1980).

The Yorktown ostracode assemblages indicate a pattern of progressively warmer water temperatures and (or) shallower water during this mid-Pliocene transgression that has been well documented in previous studies in Virginia and in the age-equivalent Raysor and Duplin Formations in South Carolina (Hazel, 1971; Cronin, 1988). This transition is exemplified by the shift from assemblages dominated by cool-mild temperate taxa (such as *Actinocythereis dawsoni, Thaerocythere, Cytheromorpha warneri,* and *Cytherura howei*) to those dominated by warm temperate and marginally subtropical conditions. The progressive appearances of the following warmer water taxa are noteworthy: *O. vaughani, Proteoconcha tuberculata, Paracytheridea altila,* and *Hulingsina* spp., at 16.1 m (52.8–53.1 ft), *Loxoconcha reticularis* at 15.4 m (50.5–50.7 ft), *Neonesidea laevicula* and *Paracytheridea* cf. *P. mucra* at 10.8 m (35.4–35.6 ft), and *Puriana rugipunctata* and *P. carolinensis* at 9.7 m (31.7–32.0 ft).

Paleoenvironmental information.—The abundant Nuculacea and *Crepidula* within the Yorktown sediments in the Langley core indicate a shallow, quiet-water environment, possibly back barrier or bay. Many of the other molluscan taxa (Lucinidae, Arcidae, *Astarte* spp., *Tellina* spp., *Chione cancellata*) require near-normal marine salinities but could be found in an open bay system or shallow shelf. The *Turritella* typically sug-

gest marine conditions and possible upwelling (Allmon, 1988; see discussion above under "St. Marys Formation").

The ostracodes indicate a nearly complete record of the *Orionina vaughani* Zone of the Yorktown in the Langley core; during depositon of this zone, paleoceanographic changes led to large-scale faunal changes and useful age-diagnostic stratigraphic ranges. The progressive warming during the late Miocene through middle Pliocene, indicated by the northward migration of subtropical ostracode taxa and the corresponding decrease in temperate taxa, has been discussed as a manifestation of the growing influence of the Gulf Stream-North Atlantic drift system, which probably intensified as the Central American Isthmus formed (Cronin and Dowsett, 1996). The broader significance of the middle Pliocene warmth indicated by the Yorktown ostracodes is discussed in Cronin (1991).

The presence of the dinoflagellate *Tuberculodinium vancampoae* may indicate temperatures somewhat warmer than the present Chesapeake Bay. Low numbers of offshore genera, such as *Invertocysta* and *Impagidinium*, are present.

Tabb Formation

The upper 2.2 m (7.2 ft) of the Langley core is assigned to the Lynnhaven Member of the Tabb Formation (Powars and others, this volume, chap. G). The unit consists of oxidized, muddy and sandy gravel that grades upward to oxidized muddy sand. No fossils were recovered from this unit in the Langley core.

Discussion

The combination of the various fossil data allows the construction of a depth-age plot for the Langley core (fig. H14). Minimum sediment accumulation rates are shown here, as only zone boundaries are plotted even where a unit may not span an entire zone. The steep slope on the plot clearly shows an initial rapid sedimentation throughout the deposition of the Chickahominy Formation, reflecting the filling or partial filling of the crater. Sediment accumulation rates slowed in the Oligocene and early and middle Miocene, where sea-level changes caused unconformities that punctuate the record. Deposition of the St. Marys and Eastover Formations reflects a second episode of rapid sedimentation. Gaps in the plot below the Yorktown and Tabb Formations also reflect unconformities punctuating the record.

The Miocene lithostratigraphic units discussed in this chapter have been divided into members in the classic outcrops in Virginia and Maryland (Shattuck, 1904; Dryden and Overbeck, 1948; Gernant, 1970; Ward and Blackwelder, 1980; Ward, 1984; see de Verteuil and Norris, 1996, for further discussion); the members are listed in table H3. In the USGS-NASA Langley core, these members reflect the sedimentary history of the crater-fill. For the lower and middle Calvert Formation, three of the four formal and informal members are recognized here. None are very thick in the Langley core. The upper middle Miocene Choptank Formation is not present in the Langley core. As figure H14 shows, the lower and middle Miocene sediment record at the Langley corehole is dominated by large gaps in the recovered record. In contrast, the upper Miocene St. Marys and Eastover Formations show rapid accumulation of a thick sedimentary record. We do not distinguish individual members of these formations at the Langley corehole, because they show nearly continuous sediment accumulation and thus reveal a more complete record than sections in which the members were defined.

Reworking of microfossils is a notable feature of many of the samples from the Langley core. For the Chickahominy Formation, all dinoflagellate samples studied thus far contain rare specimens that have been folded, partially melted, or otherwise altered by the impact, as described by Frederiksen and others (this volume, chap. D). Altered dinoflagellates were also recognized in the Old Church and St. Marys Formation. The finding of these specimens in postimpact sediments as young as the late Miocene supports the idea of continued exhumation of impact-generated sediments, especially around the buried rim of the Chesapeake Bay impact structure (Johnson and others, 1998).

Summary and Conclusions

The USGS-NASA Langley core provides an exceptional opportunity to describe the paleontology of upper Eocene, lower Oligocene, and upper Oligocene sediments of the Chickahominy Formation, the Drummonds Corner beds, and the Old Church Formation. These units are unknown to poorly known in outcrop. The Chickahominy Formation in the Langley core is a 52-m-thick (172-ft-thick) unit that represents approximately 2 m.y. of depositional accumulation in outer neritic to upper bathyal marine environments during the late Eocene.

The Drummonds Corner beds are newly recognized in the Langley core. This 7.3-m-thick (23.9-ft-thick) unit represents 1.4 m.y. or less of deposition. Paleontology indicates an age in the later part of the early Oligocene, with a sharp floral and faunal break between the Drummonds Corner beds and the underlying Chickahominy Formation. The Drummonds Corner beds appear to represent shallower water or more nearshore deposition than the underlying Chickahominy deposits.

The Old Church Formation is 32.5 m (106.5 ft) thick in the Langley core and represents 4.6 m.y. or less of deposition. It contains a more complete upper Oligocene record than is known from outcrops or shallow cores. A paleoenvironment of middle-outer neritic, subtropical, is suggested.

In contrast to the underlying units, the Miocene, Pliocene, and Pleistocene units have been recognized and studied extensively in outcrops in Virginia, Maryland, and Delaware. The Langley core provides the opportunity to relate some of these classic stratigraphic units to microfossil and megafossil studies of the core. Other regional stratigraphic units are not present at this site.

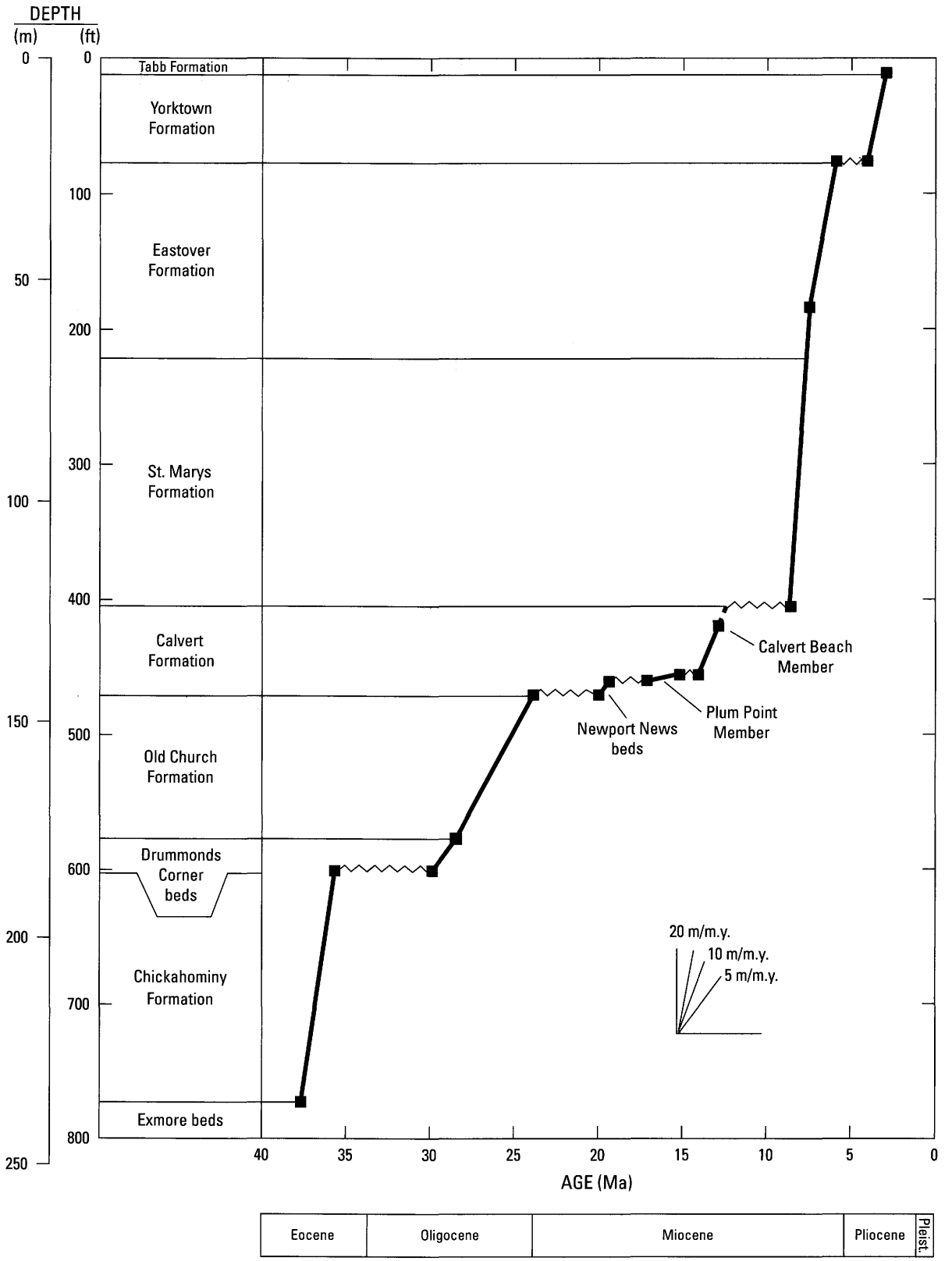

Figure H14. Age-depth plot for the postimpact sediments in the USGS-NASA Langley core. Time scale is from Berggren and others (1995). Calibration points are discussed in text. Sediment accumulation rates represent minimum values.

Table H3. Miocene lithostratigraphic units in the classic outcrops in Virginia and Maryland and in the USGS-NASA Langley core, Hampton, Va.

Formation	Member or informal subunit in outcrops	Member or informal subunit in Langley core	Thickness in Langley core (m)	Thickness in Langley core (ft)	Comment
Eastover			45.1	148.2	The Eastover Formation is undivided in the Langley core and contains a more complete record than outcrops where the members were established
	Cobham Bay Member	Not differentiated	–	–	
	Claremont Manor Member	Not differentiated	–	–	
St. Marys			55.2	181.0	The St. Marys Formation is undivided in the Langley core and contains a more complete record than outcrops where the members were established
	Windmill Point beds	Not differentiated	–	–	
	Little Cove Point beds	Not differentiated	–	–	
Choptank			–	–	The Choptank Formation is absent from the Langley core
	Conoy Member[1]	Absent	–	–	
	Boston Cliffs Member	Absent	–	–	
	Drumcliff Member	Absent	–	–	
	St. Leonard Member	Absent	–	–	
Calvert			–	–	
	Calvert Beach Member	Calvert Beach Member	15.4	50.6	
	Plum Point Member	Plum Point Member	1.5	5.0	
	Fairhaven Member	Absent	–	–	
	Popes Creek Sand Member[2]	Newport News beds[2]	3.0	9.8	

[1]Placement of the Conoy Member in the Choptank Formation follows the usage of de Verteuil and Norris (1996).

[2]We follow Powars and Bruce (1999) in placing the lower part of the Calvert Formation in the Langley core in the informal Newport News beds. This unit may not be precisely correlative with the lowest named member of the Calvert Formation (Popes Creek Sand Member) in Maryland.

The Calvert Formation in the Langley core is represented by the lower Miocene Newport News beds and the middle Miocene Plum Point and Calvert Beach Members. Each member is bounded above and below by unconformities.

The St. Marys Formation represents 55.2 m (181.0 ft) and the Eastover Formation represents 45.1 m (148.2 ft) of late Miocene sedimentation. The unconformity-bounded members of these two formations cannot be distinguished florally or faunally in the Langley core because this core represents a more complete, and probably more continuous, section than is found in the areas where their members were described.

The Yorktown Formation is 21.1 m (69.1 ft) thick, and its fossils provide a record of a warm interval in the middle of the Pliocene. The Pleistocene Tabb Formation was not studied paleontologically.

The biostratigraphic study of the Langley core includes calcareous nannofossils, dinoflagellates and acritarchs, diatoms and silicoflagellates, mollusks, ostracodes, planktonic foraminifera and bolboformids, and vertebrate remains. This core will likely prove to be a benchmark for correlations among the various fossil groups in the upper Eocene, Oligocene, Miocene, and Pliocene sediments in southeastern Virginia.

Patterns in the rate of sediment accumulation indicate at least two episodes of rapid filling at the site of the Langley core: late Eocene and late Miocene. In contrast, the record of early and middle Miocene deposition at the site is punctuated by unconformities.

Reworking of microfossils, especially dinoflagellates, is a notable feature of many samples from the upper Oligocene to Pliocene units in the USGS-NASA Langley core. Some of the reworked specimens show impact-related damage, as described by Edwards and Powars (2003) and Frederiksen and others (this volume, chap. D). Other reworked specimens clearly postdate the impact. Continued exhumation along faults may have enhanced the contributions of older material into the various units filling the Chesapeake Bay impact crater (see also discussions in Powars and others, this volume, chap. G, and Catchings and others, this volume, chap. I).

Acknowledgments

U.S. Geological Survey (USGS) investigations of the Chesapeake Bay impact structure are conducted in cooperation with the Hampton Roads Planning District Commission, the Virginia Department of Environmental Quality, and the National Aeronautics and Space Administration (NASA) Lang-

ley Research Center. The Hampton Roads Planning District Commission and the USGS provided funds for the drilling of the USGS-NASA Langley corehole. The NASA Langley Research Center provided extensive operational and logistical support for the drilling operation. The Virginia Department of Environmental Quality and the Department of Geology of the College of William and Mary provided extensive operational support at the drill site.

We especially thank the USGS drilling crew of Manuel Canabal Lopez, Arthur C. Clark, Eugene F. Cobbs, Eugene F. Cobbs, III, Orren C. Doss, Jeffery D. Eman, Stephen J. Grant, Robert Hovland, Donald G. Queen, and Michael E. Williams for spectacular core recovery. Stephen E. Curtin (USGS) and Richard E. Hodges (USGS) provided the geophysical logs of the Langley corehole.

We thank Nancy Durika and Colleen McCartan (USGS) for processing dinoflagellate samples. Colleen McCartan also prepared dinoflagellate plates. James Murray (USGS) assisted in sample collection, processed all molluscan samples, and prepared the plates of mollusks. Carleigh Trappe (USGS) assisted in the preparation of the digital images of mollusks. Barron and Bukry thank Scott Starratt (USGS) for processing of siliceous microfossils. Christopher J. Nytch (USGS) processed material for ostracodes. We thank Emily Denham (USGS) for processing of foraminifera. Rob Stamm and Ellen Seefelt (both USGS) assisted with scanning-electron microscope work. Norman O. Frederiksen and Jean M. Self-Trail (both USGS) reviewed an earlier version of the manuscript and aided in difficult interpretations.

References Cited

Abbott, W.H., 1978, Correlation and zonation of Miocene strata along the Atlantic margin of North America using diatoms and silicoflagellates: Marine Micropaleontology, v. 3, no. 1, p. 15–34.

Abbott, W.H., 1980, Diatoms and stratigraphically significant silicoflagellates from the Atlantic Margin Coring Project and other Atlantic margin sites: Micropaleontology, v. 26, no. 1, p. 49–80.

Abbott, W.H., 1984, Progress in the recognition of Neogene diatom datums along the U.S. Atlantic Coast: Palaeogeography, Palaeoclimatology, Palaeoecology, v. 47, no. 1–2, p. 5–20.

Allmon, W.D., 1988, Ecology of Recent turritelline gastropods (Prosobranchia, Turritellidae); Current knowledge and paleontological implications: Palaios, v. 3, no. 3, p. 259–284.

Andrews, G.W., 1976, Miocene marine diatoms from the Choptank Formation, Calvert County, Maryland: U.S. Geological Survey Professional Paper 910, 26 p.

Andrews, G.W., 1988, A revised marine diatom zonation for Miocene strata of the Southeastern United States: U.S. Geological Survey Professional Paper 1481, 29 p.

Andrews, G.W., and Abbott, W.H., 1985, Miocene diatoms from Hawthorn Formation, Thomas County, Georgia: Bulletins of American Paleontology, v. 87, no. 321, 109 p.

Aubry, Marie-Pierre, 1996, Data report; Eocene to upper Miocene calcareous nannofossil stratigraphy: Proceedings of the Ocean Drilling Program, Scientific Results, v. 150, p. 435–437.

Bachmann, Alfred, and Ichikawa, W., 1962, The silicoflagellides in the Wakura Beds, Nanao City, Prefecture Ishikawa, Japan: Science Reports of the Kanazawa University, v. 8, no. 1, p. 161–175.

Barron, J.A., 1981a, Late Cenozoic diatom biostratigraphy and paleoceanography of the middle-latitude eastern North Pacific, Deep Sea Drilling Project Leg 63, *in* Yeats, R.S., and others, Initial reports of the Deep Sea Drilling Project, v. 63: College Station, Tex., Texas A&M University, Ocean Drilling Program, p. 507–538.

Barron, J.A., 1981b, Middle Miocene diatom biostratigraphy of DSDP Site 77B in the eastern equatorial Pacific: Geoscience Journal (India), v. 2, no. 2, p. 137–144.

Barron, J.A., 1985, Late Eocene to Holocene diatom biostratigraphy of the equatorial Pacific Ocean, Deep Sea Drilling Project Leg 85, *in* Mayer, L.A., and others, Initial reports of the Deep Sea Drilling Project, v. 85: College Station, Tex., Texas A&M University, Ocean Drilling Program, p. 413–456.

Barron, J.A., Nigrini, C.A., Pujos, Annick, Saito, Tsunemasa, Theyer, Fritz, Thomas, Elkin, and Weinreich, Norbert, 1985, Synthesis of biostratigraphy, central equatorial Pacific, Deep Sea Drilling Project Leg 85, refinement of Oligocene to Quaternary biochronology, *in* Mayer, L.A., and others, Initial reports of the Deep Sea Drilling Project, v, 85: College Station, Tex., Texas A&M University, Ocean Drilling Program, p. 905–934.

Berggren, W.A., Kent, D.V., Swisher, C.C., III, and Aubry, M.-P., 1995, A revised Cenozoic geochronology and chronostratigraphy, *in* Berggren, W.A., Kent, D.V., Aubry, M.-P., and Hardenbol, Jan, eds., Geochronology, time scales and global stratigraphic correlation: SEPM (Society for Sedimentary Geology) Special Publication 54, p. 129–212.

Berggren, W.A., and Miller, K.G., 1988, Paleogene tropical planktonic foraminiferal biostratigraphy and magnetobiochronology: Micropaleontology, v. 34, no. 4, p. 362–380.

Blackwelder, B.W., 1981, Late Cenozoic stages and molluscan zones of the U.S. middle Atlantic Coastal Plain: Paleontological Society Memoir 12, 34 p.

Brewster-Wingard, G.L., Scott, T.M., Edwards, L.E., Weedman, S.D., and Simmons, K.R., 1997, Reinterpretation of the peninsular Florida Oligocene; An integrated stratigraphic approach: Sedimentary Geology, v. 108, no. 1–4, p. 207–228.

Brewster-Wingard, G.L., Stone, J.R., and Holmes, C.W., 2001, Molluscan faunal distribution in Florida Bay, past and present; An integration of down-core and modern data: Bulletins of American Paleontology, no. 361, p. 199–231.

Brinkhuis, Henk, 1994, Late Eocene to early Oligocene dinoflagellate cysts from central and northeast Italy: Utrecht, Netherlands, Rijksuniversiteit te Utrecht, Ph.D. thesis, 169 p.

Bukry, David, 1981, Silicoflagellate stratigraphy of offshore California and Baja California, Deep Sea Drilling Project Leg 63, *in* Yeats, R.S., and others, Initial reports of the Deep Sea Drilling Project, v. 63: College Station, Tex., Texas A&M University, Ocean Drilling Program, p. 539–557.

Bukry, David, 1990, Remarks on calcareous and siliceous nannoplankton biostratigraphy for some Cretaceous and Tertiary core samples from southern New Jersey: U.S. Geological Survey Open-File Report 90–278, 22 p.

Burckle, L.H., 1996, Diatom biostratigraphy. Leg 150: Proceedings of the Ocean Drilling Program, Scientific Results, v. 150, p. 17–35.

Cande, S.C., and Kent, D.V., 1995, Revised calibration of the geomagnetic polarity timescale for the Late Cretaceous and Cenozoic: Journal of Geophysical Research, v. B100, no. 4, p. 6093–6095.

Cappetta, Henri, 1987, Chondrichthyes; II. Mesozoic and Cenozoic Elasmobranchii: New York, Gustav Fischer Verlag, 193 p.

Case, G.R., 1980, A selachian fauna from the Trent Formation, lower Miocene (Aquitanian) of eastern North Carolina: Palaeontographica, Abteilung A: Palaeozoologie-Stratigraphie, v. 171, no. 1–3, p. 75–103, 10 pls.

Case, G.R., 1981, Late Eocene selachians from south-central Georgia: Palaeontographica, Abteilung A: Palaeozoologie-Stratigraphie, v. 176, no. 1–3, p. 52–79, 9 pls.

Clark, W.B., 1895, Contributions to the Eocene fauna of the middle Atlantic slope: Johns Hopkins University Circular 15, p. 3–6.

Clark, W.B., and Miller, B.L., 1912, The physiography and geology of the Coastal Plain province of Virginia: Virginia Geological Survey Bulletin 4, 274 p.

Conrad, T.A., 1832, Fossil shells of the Tertiary formations of North America, v. 1: Philadelphia, Pa., Judah Dobson, p. 1–20.

Conrad, T.A., 1833, On some new fossil and Recent shells of the United States: American Journal of Science and Arts, v. 23, art. XVII, p. 339–346.

Cronin, T.M., 1988, Evolution of marine climates of the U.S. Atlantic Coast during the past four million years: Philosophical Transactions of the Royal Society of London, Series B, v. 318, no. 1191, p. 661–678.

Cronin, T.M., 1990, Evolution of Neogene and Quaternary marine Ostracoda, United States Atlantic Coastal Plain; Evolution and speciation in Ostracoda, IV, chap. C *of* Studies related to the Charleston, South Carolina, earthquake of 1886—Neogene and Quaternary lithostratigraphy and biostratigraphy: U.S. Geological Survey Professional Paper 1367, p. C1–C43, 17 pls.

Cronin, T.M., 1991, Pliocene shallow water paleoceanography of the North Atlantic Ocean based on marine ostracodes: Quaternary Science Reviews, v. 10, no. 2–3, p. 175–188.

Cronin, T.M., and Dowsett, H.J., 1996, Biotic and oceanographic response to the Pliocene closing of the Central American Isthmus, *in* Jackson, J.B.C., Budd, A.F., and Coates, A.C., eds., Evolution and environment in tropical America: Chicago, University of Chicago Press, p. 76–104.

Cronin, T.M., and Hazel, J.E., 1980, Ostracode biostratigraphy of Pliocene and Pleistocene deposits of the Cape Fear Arch region, North and South Carolina, chap. B *of* Shorter contributions to paleontology, 1979: U.S. Geological Survey Professional Paper 1125, p. B1–B25.

Cushman, J.A., and Cederstrom, D.J., 1945, An upper Eocene foraminiferal fauna from deep wells in York County, Virginia: Virginia Geological Survey Bulletin 67, 58 p., 6 pls.

De Coninck, Jan, 1986, Organic walled phytoplankton from the Bartonian and Eo-Oligocene transitional deposits of the Woensdrecht borehole, southern Netherlands: Mededelingen Rijks Geologische Dienst, v. 40, no. 2, 49 p., 11 pls.

De Coninck, Jan, 1995, Organic-walled phytoplankton as biostratigraphic indicators in Tertiary marine sand in Oret, Entre-Sambre-et-Meuse, Belgium: Bulletin de la Société belge de Géologie, v. 104, no. 1–2, p. 151–161, 4 pls. (In French; summary in English.)

de Verteuil, Laurent, 1997, Palynological delineation and regional correlation of lower through upper Miocene sequences in the Cape May and Atlantic City boreholes, New Jersey Coastal Plain: Proceedings of the Ocean Drilling Program, Scientific Results, v. 150X, p. 129–145.

de Verteuil, Laurent, and Norris, Geoffrey, 1996, Miocene dinoflagellate stratigraphy and systematics of Maryland and Virginia: Micropaleontology, v. 42, Supplement, 172 p., 18 pls.

Deck, L.T., 1985, The Piney Point Formation along the Pamunkey River, Virginia Coastal Plain: Virginia Minerals, v. 31, no. 2, p. 23–27, 1 pl.

Deflandre, Georges, 1959, Sur les nannofossiles calcaires et leur systématique: Revue de Micropaleontologie, v. 3, p. 127–152.

Deflandre, Georges, and Fert, Charles, 1954, Observations sur les coccolithophoridés actuels et fossiles en microscopie ordinaire et électronique: Annales de Paléontologie, v. 40, p. 115–176.

Dowsett, H.J., and Wiggs, L.B., 1992, Planktonic foraminiferal assemblage of the Yorktown Formation, Virginia, USA: Micropaleontology, v. 38, no. 1, p. 75–86.

Dryden, A.L., Jr., and Overbeck, R.M., 1948, Geology of Charles County, *in* The physical features of Charles County: Maryland Department of Geology, Mines and Water Resources [Report 13], p. 6–17.

Edwards, L.E., 1986, Late Cenozoic dinoflagellate cysts from South Carolina, U.S.A., *in* Wrenn, J.H., Duffield, S.L., and Stein, J.A., eds., Papers from the First Symposium on Neogene Dinoflagellate Cyst Biostratigraphy: American Association of Stratigraphic Palynologists Contribution Series, no. 17, p. 47–58.

Edwards, L.E., 1996, Graphic correlation of the Marlboro Clay and Nanjemoy Formation (uppermost Paleocene and lower

Eocene) of Virginia and Maryland, *in* Jansonius, Jan, and McGregor, D.C., eds., Palynology; Principles and applications: [College Station, Tex.,] American Association of Stratigraphic Palynologists Foundation, v. 3, p. 989–999.

Edwards, L.E., and Powars, D.S., 2003, Impact damage to dinocysts from the late Eocene Chesapeake Bay event: Palaios, v. 18, no. 3, p. 275–285. (Also available online at http://www.bioone.org/pdfserv/i0883-1351-018-03-0275.pdf)

Emerson, W.K., and Jacobson, M.K., 1976, The American Museum of Natural History guide to shells—Land, freshwater, and marine, from Nova Scotia to Florida: New York, Alfred A. Knopf Publishers, 482 p., 40 pls.

Ernissee, J.J., Abbott, W.H., and Huddlestun, P.F., 1977, Microfossil correlation of the Coosawhatchie Clay (Hawthorn Formation, Miocene) of South Carolina, and its equivalent in Georgia: Marine Micropaleontology, v. 2, no. 2, p. 105–119.

Forester, R.M., 1980, A systematic revision of the ostracode species described by Ulrich and Bassler and by Malkin from the Chesapeake Group in Maryland and Virginia: U.S. Geological Survey Professional Paper 1128, 25 p., 7 pls.

Gardner, Julia, 1943 [1944], Part 1, Pelecypoda, chap. A *of* Mollusca from the Miocene and lower Pliocene of Virginia and North Carolina: U.S. Geological Survey Professional Paper 199, p. 1–178, pls. 1–23.

Gernant, R.E., 1970, Paleoecology of the Choptank Formation (Miocene) of Maryland and Virginia: Maryland Geological Survey Report of Investigations 12, 90 p., 1 pl.

Gibson, T.G., Andrews, G.W., Bybell, L.M., Frederiksen, N.O., Hansen, Thor, Hazel, J.E., McLean, D.M., Witmer, R.J., and Van Nieuwenhuise, D.S., 1980, Biostratigraphy of the Tertiary strata of the core, *in* Geology of the Oak Grove core: Virginia Division of Mineral Resources Publication 20, p. 14–30.

Hay, W.W., Mohler, H.P., Roth, P.H., Schmidt, R.R., and Boudreaux, J.E., 1967, Calcareous nannoplankton zonation of the Cenozoic of the Gulf Coast and Caribbean-Antillean area, and transoceanic correlation: Gulf Coast Association of Geological Societies Transactions, v. 17, p. 428–480.

Hazel, J.E., 1967, Classification and distribution of the Recent Hemicytheridae and Trachyleberididae (Ostracoda) off northeastern North America: U.S. Geological Survey Professional Paper 564, 49 p., 11 pls.

Hazel, J.E., 1971, Ostracode biostratigraphy of the Yorktown Formation (upper Miocene and lower Pliocene) of Virginia and North Carolina: U.S. Geological Survey Professional Paper 704, 13 p.

Hazel, J.E., 1977, Distribution of some biostratigraphically diagnostic ostracodes in the Pliocene and lower Pleistocene of Virginia and northern North Carolina: U.S. Geological Survey Journal of Research, v. 5, no. 3, p. 373–388.

Hazel, J.E., 1983, Age and correlation of the Yorktown (Pliocene) and Croatan (Pliocene and Pleistocene) Formations at the Lee Creek Mine: Smithsonian Contributions to Paleobiology, no. 53, p. 81–199, 38 pls.

Hazel, J.E., Bybell, L.M., Christopher, R.A., Frederiksen, N.O., May, F.E., McLean, D.M., Poore, R.Z., Smith, C.C., Sohl, N.F., Valentine, P.C., and Witmer, R.J., 1977, Biostratigraphy of the deep corehole (Clubhouse Crossroads corehole 1) near Charleston, South Carolina, chap. F *of* Rankin, D.W., ed., Studies related to the Charleston, South Carolina, earthquake of 1886—A preliminary report: U.S. Geological Survey Professional Paper 1028, p. 71–89.

Hazel, J.E., Mumma, M.D., and Huff, W.J., 1980, Ostracode biostratigraphy of the lower Oligocene (Vicksburgian) of Mississippi and Alabama: Gulf Coast Association of Geological Societies Transactions, v. 30, p. 361–378, 10 pls.

Johnson, G.H., Kruse, S.E., Vaughn, A.W., Lucey, J.K., Hobbs, C.H., III, and Powars, D.S., 1998, Postimpact deformation associated with the late Eocene Chesapeake Bay impact structure in southeastern Virginia: Geology, v. 26, no. 6, p. 507–510.

Johnson, G.H., Powars, D.S., Bruce, T.S., Beach, T.A., Harris, M.S., and Goodwin, B.K., 2001, Post-impact effects of the Eocene Chesapeake Bay impact, lower York-James Peninsula, Virginia: Virginia Geological Field Conference, 31st, Williamsburg, Virginia, October 19 and 20, 2001 [Guidebook], 40 p.

Kent, B.W., 1999, Sharks from the Fisher/Sullivan site, *in* Weems, R.E., and Grimsley, G.J., eds., Early Eocene vertebrates and plants from the Fisher/Sullivan site (Nanjemoy Formation), Stafford County, Virginia: Virginia Division of Mineral Resources Publication 152, p. 11–38, 3 pls.

Malkin, D.S., 1953, Biostratigraphic study of Miocene Ostracoda of New Jersey, Maryland, and Virginia: Journal of Paleontology, v. 27, no. 6, p. 761–799.

Mansfield, W.C., 1937, Mollusks of the Tampa and Suwannee Limestones of Florida: Florida Geological Survey Bulletin 15, 334 p., 23 pls.

Mansfield, W.C., 1943 [1944], Stratigraphy of the Miocene of Virginia and the Miocene and Pliocene of North Carolina, *in* Gardner, Julia, Part 1, Pelecypoda, chap. A *of* Mollusca from the Miocene and lower Pliocene of Virginia and North Carolina: U.S. Geological Survey Professional Paper 199, p. 1–19.

Martin, G.C., 1904, Mollusca, Gastropoda, *in* Systematic paleontology of the Miocene deposits of Maryland: Maryland Geological Survey, Miocene volume (text), p. 131–270.

Martini, Erlend, 1971, Standard Tertiary and Quaternary calcareous nannoplankton zonation, *in* Farinacci, Anna, and Matteucci, R., eds., Proceedings of the II Planktonic Conference, Roma, 1970: Rome, Edizioni Tecnoscienza, v. 2, p. 739–785, 4 pls.

Mixon, R.B., ed., 1989, Geology and paleontology of the Haynesville cores—Northeastern Virginia Coastal Plain: U.S. Geological Survey Professional Paper 1489, 4 chapters, separately paged.

Mixon, R.B., Powars, D.S., Ward, L.W., and Andrews, G.W., 1989, Lithostratigraphy and molluscan and diatom biostratigraphy of the Haynesville cores—Outer coastal plain of Virginia, chap. A *of* Mixon, R.B., ed., Geology and paleontology

of the Haynesville cores—Northeastern Virginia Coastal Plain: U.S. Geological Survey Professional Paper 1489, p. A1–A48, 1 oversize pl.

Morgenroth, Peter, 1966, Mikrofossilien und Konkretionen des nordwesteuropäischen Untereozäns: Palaeontographica, Abteilung B: Palaeophytologie, v. 119, no. 1–3, p. 1–53, pls. 1–11.

Mountain, G.S., and others, 1994, Site 905: Proceedings of the Ocean Drilling Program, Part A: Initial Reports, v. 150, p. 255–308.

Müller, A., 1999, Ichthyofaunen aus dem atlantischen Tertiär der USA: Leipzig, Leipziger Geowissenschaften, 9/10, p. 1–360.

Peleo-Alampay, A.M., Bukry, David, Liu, Li, and Young, J.R., 1998, Late Miocene calcareous nannofossil genus *Catinaster*; Taxonomy, evolution and magnetobiochronology: Journal of Micropaleontology, v. 17, pt. 1, p. 71–85, 3 pls.

Perch-Nielsen, Katharina, 1985, Silicoflagellates, *in* Bolli, H.M., Saunders, J.B., and Perch-Nielsen, Katharina, eds., Plankton stratigraphy: Cambridge, U.K., Cambridge University Press, p. 811–846.

Poag, C.W. 1974, Ostracode biostratigraphy and correlation of the Chickasawhay Stage (Oligocene) of Mississippi and Alabama: Journal of Paleontology, v. 48, no. 2, p. 344–356.

Poag, C.W., 1997, The Chesapeake Bay bolide impact; A convulsive event in Atlantic Coastal Plain evolution: Sedimentary Geology, v. 108, no. 1-4, p. 45–90.

Poag, C.W., and Aubry, M.-P., 1995, Upper Eocene impactites of the U.S. East Coast; Depositional origins, biostratigraphic framework, and correlation: Palaios, v. 10, no. 1, p. 16–43.

Poag, C.W., and Commeau, J.A., 1995, Paleocene to middle Miocene planktic foraminifera of the southwestern Salisbury embayment, Virginia and Maryland; Biostratigraphy, allostratigraphy, and sequence stratigraphy: Journal of Foraminiferal Research, v. 25, no. 2, p. 134–155, 9 pls.

Poag, C.W., and others, 1987, Initial reports of the Deep Sea Drilling Project, v. 95: Washington, D.C., U.S. Government Printing Office, 817 p.

Pooser, W.K., 1965, Biostratigraphy of Cenozoic Ostracoda from South Carolina (Arthropoda, article 8): University of Kansas Paleontological Contributions, no. 38, 80 p., 22 pls.

Powars, D.S., 2000, The effects of the Chesapeake Bay impact crater on the geologic framework and the correlation of hydrogeologic units of southeastern Virginia, south of the James River: U.S. Geological Survey Professional Paper 1622, 53 p., 1 oversize pl. (Also available online at http://pubs.usgs.gov/prof/p1622/)

Powars, D.S., and Bruce, T.S., 1999, The effects of the Chesapeake Bay impact crater on the geological framework and correlation of hydrogeologic units of the lower York-James Peninsula, Virginia: U.S. Geological Survey Professional Paper 1612, 82 p., 9 oversize pls. (Also available online at http://pubs.usgs.gov/prof/p1612/)

Powars, D.S., Johnson, G.H., Edwards, L.E., Horton, J.W., Jr., Gohn, G.S., Catchings, R.D., McFarland, E.R., Izett, G.A., Bruce, T.S., Levine, J.S., and Pierce, H.A., 2002, An expanded Chesapeake Bay impact structure, eastern Virginia; New corehole and geophysical data [abs.]: Lunar and Planetary Science Conference, 33d, League City, Tex., March 11–15, 2002, Abstract 1034, available online at http://www.lpi.usra.edu/meetings/lpsc2002/pdf/1034.pdf

Powars, D.S., Mixon, R.B., and Bruce, Scott, 1992, Uppermost Mesozoic and Cenozoic geologic cross section, outer coastal plain of Virginia, *in* Gohn, G.S., ed., Proceedings of the 1988 U.S. Geological Survey Workshop on the Geology and Geohydrology of the Atlantic Coastal Plain: U.S. Geological Survey Circular 1059, p. 85–101.

Rader, E.K., and Evans, N.H., 1993, Geologic map of Virginia; Expanded explanation: Charlottesville, Va., Virginia Division of Mineral Resources, 163 p.

Rogers, W.B., 1884, A reprint of annual reports and other papers on the geology of the Virginias: New York, D. Appleton and Co., 832 p.

Santarelli, Andrea, 1997, Dinoflagellate cysts and astronomical forcing in the Mediterranean upper Miocene [doctoral thesis]: Rijksuniversiteit te Utrecht, LPP (Laboratorium voor Palaeobotanie en Palynologie) Contributions Series, no. 6, 141 p.

Say, Thomas, 1822, An account of some of the marine shells of the United States: Journal of the Academy of Natural Sciences of Philadelphia, v. 2, pt. 2, p. 221–248.

Say, Thomas, 1824, An account of some of the fossil shells of Maryland: Journal of the Academy of Natural Sciences of Philadelphia, v. 4, pt. 1, p. 124–155.

Shattuck, G.B., 1902, The Miocene problem of Maryland [abs.]: Science, new series, v. 15, p. 906.

Shattuck, G.B., 1904, The Miocene deposits of Maryland; Geological and paleontological relations, with a review of earlier investigations, *in* Systematic paleontology of the Miocene deposits of Maryland: Maryland Geological Survey, Miocene volume (text), p. xxxiii–cxxxvii.

Stover, L.E., and Hardenbol, Jan, 1993 [1994], Dinoflagellates and depositional sequences in the lower Oligocene (Rupelian) Boom Clay Formation, Belgium: Bulletin de la Société belge de Géologie, v. 102, no. 1–2, p. 5–77.

Stradner, Herbert, and Edwards, A.R., 1968, Electron microscopic studies on upper Eocene coccoliths from the Oamaru Diatomite, New Zealand: Jahrbuch der Geologischen Bundesanstalt Sonderband, v. 13, 66 p.

Swain, F.M., 1951 [1952], Ostracoda from wells in North Carolina: U.S. Geological Survey Professional Paper 234, issued as two separate chapters, A, Part 1, Cenozoic Ostracoda (p. 1–58, pls. 1–7) and B, Part 2, Mesozoic Ostracoda (p. 59–93, pls. 8–9).

Swain, F.M., 1974, Some upper Miocene and Pliocene(?) Ostracoda of Atlantic coastal region for use in hydrogeologic studies: U.S. Geological Survey Professional Paper 821, 50 p., 13 pls.

Turgeon, D.D., Quinn, J.F., Jr., Bogan, A.E., Coan, E.V., Hochberg, F.G., Lyons, W.G., Mikkelsen, P.M., Neves, R.J., Roper, C.F.E., Rosenberg, G., Roth, B., Scheltema, A., Thompson, F.G., Vecchione, M., and Williams, J.D., 1998,

Common and scientific names of aquatic invertebrates from the United States and Canada; Mollusks (2d ed.): American Fisheries Society Special Publication 26, 526 p., 1 CD-ROM.

Ulrich, E.O., and Bassler, R.S., 1904, Ostracoda, Bryozoa, *in* Systematic paleontology of the Miocene deposits of Maryland: Maryland Geological Survey, Miocene volume (text), p. 98–130.

U.S. Geological Survey, 2004, South Florida Ecosystem History Project, part of the South Florida Information Access Web site: U.S. Geological Survey Web site at http://sofia.usgs.gov/flaecohist/ (Accessed June 30, 2004.)

Valentine, P.C., 1971, Climatic implication of a late Pleistocene ostracode assemblage from southeastern Virginia, chap. D *of* Contributions to paleontology: U.S. Geological Survey Professional Paper 683, p. D1–D28, 4 pls.

Wall, David, 1967, Fossil microplankton in deep-sea cores from the Caribbean Sea: Paleontology, v. 10, no. 1, p. 95–123, pls. 14–16.

Ward, L.W., 1984, Stratigraphy of outcropping Tertiary beds along the Pamunkey River, central Virginia Coastal Plain *in* Ward, L.W., and Krafft, Kathleen, eds., Stratigraphy and paleontology of the outcropping Tertiary beds in the Pamunkey River region, central Virginia Coastal Plain—Guidebook for Atlantic Coastal Plain Geological Association Field Trip, October 6–7, 1984: Atlantic Coastal Plain Geological Association, p. 11–77, 12 pls.

Ward, L.W., 1985, Stratigraphy and characteristic mollusks of the Pamunkey Group (lower Tertiary) and the Old Church Formation of the Chesapeake Group—Virginia Coastal Plain: U.S. Geological Survey Professional Paper 1346, 78 p., 6 pls.

Ward, L.W., 1992, Molluscan biostratigraphy of the Miocene middle Atlantic Coastal Plain of North America: Virginia Museum of Natural History Memoir 2, 159 p., 26 pls.

Ward, L.W., 1993, The G.D. Harris 1890 manuscript on the stratigraphy of the Miocene and Pliocene beds at Yorktown, Virginia: Paleontological Research Institution Special Publication 20, 118 p.

Ward, L.W., and Blackwelder, B.W., 1980, Stratigraphic revision of the upper Miocene and lower Pliocene beds of the Chesapeake Group, middle Atlantic Coastal Plain, chap. D *of* Contributions to stratigraphy: U.S. Geological Survey Bulletin 1482, p. D1–D61.

Ward, L.W., Lawrence, D.R., and Blackwelder, B.W., 1978, Stratigraphic revision of the middle Eocene, Oligocene, and lower Miocene—Atlantic Coastal Plain of North Carolina, chap. F *of* Contributions to straigraphy: U.S. Geological Survey Bulletin 1457, p. F1–F23.

Weems, R.E., 1999, Actinopterygian fishes from the Fisher/Sullivan site, *in* Weems, R.E., and Grimsley, G.J., eds., Early Eocene vertebrates and plants from the Fisher/Sullivan site (Nanjemoy Formation), Stafford County, Virginia: Virginia Division of Mineral Resources Publication 152, p. 53–100, 12 pls.

Westgate, J.W., 1989, Lower vertebrates from an estuarine facies of the middle Eocene Laredo Formation (Claiborne Group), Webb County, Texas: Journal of Vertebrate Paleontology, v. 9, no. 3, p. 282–294.

Wheeler, A.C., 1975, Fishes of the world; An illustrated dictionary: New York, Macmillan Publishing Company, 366 p.

Wise, S.W., Jr., and Constans, R.E., 1976, Mid-Eocene planktonic correlations; Northern Italy–Jamaica, W.I.: Gulf Coast Association of Geological Societies Transactions, v. 26, p. 144–155.

Appendix H1. Full Taxonomic Citations for Taxa Mentioned in Chapter H

Selected samples from postimpact sediments in the USGS-NASA Langley core were studied for calcareous nannofossils (Bybell), dinoflagellates (Edwards), diatoms (Barron), silicoflagellates (Bukry), mollusks (Wingard), ostracodes (Cronin), planktonic foraminifera and bolboformids (Poag; see also Poag and Norris, this volume, chap. F, for information on benthic foraminifera), and vertebrate remains (Weems). For the purpose of formal names of species and genera, calcareous nannofossils, dinoflagellates, diatoms, silicoflagellates, and bolboformids are classified as plants. Mollusks, ostracodes, foraminifera, and vertebrates are classified as animals. Complete taxonomic names are given below.

Calcareous Nannofossils

Amaurolithus tricorniculatus (Gartner 1967) Gartner & Bukry 1975

Blackites spinosus (Deflandre & Fert 1954) Hay & Towe 1962
Blackites tenuis (Bramlette & Sullivan 1961) Sherwood 1974
Blackites Hay & Towe 1962 spp.
Braarudosphaera bigelowii (Gran & Braarud 1935) Deflandre 1947

Calcidiscus leptoporus (Murray & Blackman 1898) Loeblich & Tappan 1978
Calcidiscus macintyrei (Bukry & Bramlette 1969) Loeblich & Tappan 1978
Catinaster coalitus Martini & Bramlette 1963
Catinaster mexicanus Bukry 1971
Catinaster Martini & Bramlette 1963 spp.
Cepekiella lumina (Sullivan 1965) Bybell 1975
Ceratolithus rugosus Bukry & Bramlette 1968
Chiasmolithus altus Bukry & Percival 1971
Chiasmolithus bidens (Bramlette & Sullivan 1961) Hay & Mohler 1967
Chiasmolithus oamaruensis (Deflandre *in* Deflandre and Fert, 1954) Hay et al. 1966
Chiasmolithus titus Gartner 1970
Chiasmolithus Hay et al. 1966 spp.
Coccolithus eopelagicus (Bramlette & Riedel 1954) Bramlette & Sullivan 1961
Coccolithus pelagicus (Wallich 1877) Schiller 1930
Coronocyclus nitescens (Kamptner 1963) Bramlette & Wilcoxon 1967
Cribrocentrum reticulatum (Gartner & Smith 1967) Perch-Nielsen 1971
Cruciplacolithus Hay & Mohler, *in* Hay and others 1967 spp.
Cyclococcolithus formosus Kamptner 1963
Cyclococcolithus Kamptner 1954 spp.
Dictyococcites antarcticus Haq 1976
Dictyococcites bisectus (Hay et al. 1966) Bukry & Percival 1971
Dictyococcites scrippsae Bukry & Percival 1971
Discoaster asymmetricus Gartner 1969
Discoaster barbadiensis Tan Sin Hok 1927
Discoaster berggrenii Bukry 1971
Discoaster brouweri Tan Sin Hok 1927
Discoaster deflandrei Bramlette & Riedel 1954
Discoaster distinctus Martini 1958
Discoaster druggii Bramlette & Wilcoxon 1967
Discoaster exilis Martini & Bramlette 1963
Discoaster hamatus Martini & Bramlette 1963
Discoaster intercalaris Bukry 1971
Discoaster kugleri Martini & Bramlette 1963
Discoaster musicus Stradner 1959
Discoaster nodifer (Bramlette & Riedel 1954) Bukry 1973
Discoaster pentaradiatus Tan Sin Hok 1927
Discoaster quinqueramus Gartner 1969
Discoaster saipanensis Bramlette & Riedel 1954
Discoaster signus Bukry 1971
Discoaster surculus Martini & Bramlette 1963
Discoaster tanii Bramlette & Riedel 1954
Discoaster variabilis Martini & Bramlette 1963
Discoaster woodringii Bramlette & Riedel 1954
Discoaster Tan Sin Hok 1927 spp.

Ellipsolithus macellus (Bramlette & Sullivan 1961) Sullivan 1964
Ericsonia fenestrata (Deflandre & Fert 1954) Stradner *in* Stradner and Edwards, 1968
Ericsonia obruta Perch-Nielsen 1971

Gephyrocapsa Kamptner 1943 spp.
Goniolithus fluckigeri Deflandre 1957

Helicosphaera ampliaperta Bramlette & Wilcoxon 1967
Helicosphaera bramlettei (Müller 1970) Jafar & Martini 1975
Helicosphaera carteri (Wallich 1877) Kamptner 1954
Helicosphaera compacta Bramlette & Wilcoxon 1967
Helicosphaera euphratis Haq 1966
Helicosphaera intermedia Martini 1965
Helicosphaera minuta Müller 1981
Helicosphaera obliqua Bramlette & Wilcoxon 1967
Helicosphaera paleocarteri Theodoridis 1984
Helicosphaera recta (Haq 1966) Jafar & Martini 1975
Helicosphaera reticulata Bramlette & Wilcoxon 1967
Helicosphaera sellii (Bukry & Bramlette 1969) Jafar & Martini 1975
Helicosphaera seminulum Bramlette & Sullivan 1961
Helicosphaera truempyi Biolzi & Perch-Nielsen 1982

Helicosphaera wilcoxonii (Gartner 1971) Jafar & Martini 1975
Helicosphaera Kampter 1954 spp.

Isthmolithus recurvus Deflandre *in* Deflandre and Fert, 1954

Lithostromation operosum (Deflandre *in* Deflandre and Fert, 1954) Bybell 1975
Lithostromation perdurum Deflandre 1942
Lithostromation simplex (Klumpp 1953) Bybell 1975
Lithostromation Deflandre 1942 spp.

Markalius inversus Bramlette & Martini 1964

Neochiastozygus concinnus (Martini 1961) Perch-Nielsen 1971
Neococcolithes Sujkowski 1931 spp.

Pedinocyclus larvalis Bukry & Bramlette 1971
placoliths
Pontosphaera alta Roth 1970
Pontosphaera enormis (Locker 1967) Perch-Nielsen 1984
Pontosphaera multipora (Kamptner *ex* Deflandre 1959) Roth 1970
Pontosphaera pygmaea (Locker 1967) Bystrická & Lehotayova 1974
Pontosphaera segmenta (Bramlette & Percival 1971) Knuttel 1986
Pontosphaera wechesensis (Bukry & Percival 1971) Aubry 1986
Pontosphaera Lohmann 1902 spp.
Pseudoemiliania lacunosa (Kamptner 1963) Gartner 1969
Pseudotriquetrorhabdulus inversus (Bukry & Bramlette 1969) Wise *in* Wise and Constans, 1976

Reticulofenestra abisecta (Müller 1970) Roth & Thierstein 1972
Reticulofenestra daviesii (Haq 1968) Haq 1971
Reticulofenestra dorinocoides (Black & Barnes 1961) Kothe 1986
Reticulofenestra floridana (Roth & Hay *in* Hay and others, 1967) Theodoridis 1984
Reticulofenestra lockeri Müller 1970
Reticulofenestra pseudolockeri Juráková 1974
Reticulofenestra pseudoumbilicus (Gartner 1967) Gartner 1969
Reticulofenestra umbilicus (Levin 1965) Martini & Ritzkowski 1968
Reticulofenestra Hay et al. 1966 spp.
Rhabdosphaera vitrea (Deflandre *in* Deflandre and Fert, 1954) Bramlette & Sullivan 1961
Rhabdosphaera Haeckel 1894 spp.
Rhomboaster bramlettei (Brönnimann & Stradner 1960) Bybell & Self-Trail 1995

Scyphosphaera Lohmann 1902 spp.
Sphenolithus abies Deflandre *in* Deflandre and Fert, 1954
Sphenolithus belemnos Bramlette & Wilcoxon 1967
Sphenolithus ciperoensis Bramlette & Wilcoxon 1967
Sphenolithus distentus (Martini 1965) Bramlette & Wilcoxon 1967
Sphenolithus heteromorphus Deflandre 1953
Sphenolithus moriformis (Brönnimann & Stradner 1960) Bramlette & Wilcoxon 1967
Sphenolithus neoabies Bukry & Bramlette 1969
Sphenolithus predistentus Bramlette & Wilcoxon 1967
Sphenolithus pseudoradians Bramlette & Wilcoxon 1967
Sphenolithus Deflandre 1952 spp.
Syracosphaera clathrata Roth & Hay *in* Hay and others, 1967

Transversopontis pulcher (Deflandre *in* Deflandre and Fert, 1954) Perch-Nielsen 1967
Transversopontis pulcheroides (Sullivan 1964) Báldi-Beke 1971
Transversopontis zigzag Roth & Hay *in* Hay and others, 1967
Triquetrorhabdulus carinatus Martini 1965

Zygrhablithus bijugatus (Deflandre *in* Deflandre and Fert, 1954) Deflandre 1959

Dinoflagellates and Acritarchs

Achilleodinium biformoides (Eisenack 1954) Eaton 1976
Achomosphaera andalousiensis Jan du Chêne 1977
Achomosphaera Evitt 1963 sp.
Amiculasphaera umbracula Harland 1979
Apteodinium spiridoides Benedek 1972
Apteodinium tectatum Piasecki 1980
Areosphaeridium diktyoplokus (Klumpp 1953) Eaton 1971
Ataxiodinium confusum Versteegh & Zevenboom 1995

Barssidinium evangelineae Lentin et al. 1994 [may include *Barssidinium pliocenicum* (Head 1993) Head 1994]
Batiacasphaera baculata Drugg 1970
Batiacasphaera compta Drugg 1970
Batiacasphaera hirsuta Stover 1977
Batiacasphaera sphaerica Stover 1977
Bitectatodinium tepikiense Wilson 1973/*Bitectatodinium raedwaldii* Head 1997
Brigantedinium cariacoense (Wall 1967) Lentin & Williams 1993

Cerebrocysta poulsenii de Verteuil & Norris 1996
Cerebrocysta satchelliae de Verteuil & Norris 1996
Charlesdowniea coleothrypta (Williams & Downie 1966) Lentin & Vozzhennikova 1989
Charlesdowniea variabilis (Bujak 1980) Lentin & Vozzhennikova 1989
Chatangiella Vozzhennikova 1967
Chiropteridium galea (Maier 1959) Sarjeant 1983
Chiropteridium lobospinosum Gocht 1960
Chiropteridium Gocht 1960 spp.
Cleistosphaeridium placacanthum (Deflandre & Cookson 1955) Eaton et al. 2001
Cordosphaeridium cantharellus (Brosius 1963) Gocht 1969

Cordosphaeridium fibrospinosum Davey & Williams 1966
Cordosphaeridium funiculatum Morgenroth 1966
Cordosphaeridium gracile (Eisenack 1954) Davey & Williams 1966
Corrudinium incompositum (Drugg 1970) Stover & Evitt 1978
Corrudinium Stover & Evitt 1978 sp.
Cousteaudinium aubryae de Verteuil & Norris 1996
Cribroperidinium tenuitabulatum (Gerlach 1961) Helenes 1984
Cribroperidinium Neale & Sarjeant 1962 spp.
Cyclopsiella lusatica (Krutzsch 1970) Strauss & Lund 1992
Cyclopsiella vieta Drugg & Loeblich 1967
Cyclopsiella Drugg & Loeblich 1967 sp.

Damassadinium californicum (Drugg 1967) Fensome et al. 1993
Dapsilidinium pseudocolligerum (Stover 1977) Bujak et al. 1980
Deflandrea phosphoritica and forms intermediate with *D. heterophlycta*
Deflandrea phosphoritica Eisenack 1938 [including *D. phosphoritica* var. *spinulosa*]
Deflandrea Eisenack 1938 sp.
Dinopterygium cladoides sensu Morgenroth (1966)
Diphyes colligerum (Deflandre & Cookson 1955) Cookson 1965
Distatodinium ellipticum (Cookson 1965) Eaton 1976
Distatodinium paradoxum (Brosius 1963) Eaton 1976
Distatodinium Eaton 1976 spp.
Dracodinium varielongitudum (Williams & Downie 1966) Costa & Downie 1979

Ennaedocysta Stover & Williams 1995 sp. or spp.
Eocladopyxis peniculata Morgenroth 1966
Erymnodinium delectabile (de Verteuil & Norris 1992) Lentin et al. 1994
Escharisphaeridia Erkmen & Sarjeant 1980 sp.
Exochosphaeridium insigne de Verteuil & Norris 1996
Exochosphaeridium Davey et al. 1966? sp.

Filisphaera microornata (Head et al. 1989) Head 1994

Geonettia clineae de Verteuil & Norris 1996
Glaphyrocysta semitecta (Bujak 1980) Lentin & Williams 1981 [grouped as miscellaneous areoligeracean forms (*Glaphyrocysta* spp.) in figure H5]
Glaphyrocysta Stover & Evitt 1978 spp.

Habibacysta tectata Head et al. 1989
Hafniasphaera septata (Cookson & Eisenack 1967) Hansen 1977
Heteraulacacysta porosa Bujak 1980
Heteraulacacysta Drugg & Loeblich 1967 sp.
Histiocysta sp. of Stover and Hardenbol (1993)
Homotryblium aculeatum Williams 1978
Homotryblium plectilum Drugg & Loeblich 1967
Homotryblium vallum Stover 1977
Hystrichokolpoma cinctum Klumpp 1953
Hystrichokolpoma rigaudiae Deflandre & Cookson 1955
Hystrichosphaeropsis obscura Habib 1972
Hystrichostrogylon aff. *coninckii* of De Coninck (1995)

Impagdinium pallidum Bujak 1984
Impagidinium antecarcerum de Verteuil & Norris 1996
Impagidinium maculatum (Cookson & Eisenack 1961) Stover & Evitt 1978 sensu Santarelli (1997)
Impagidinium paradoxum (Wall 1967) Stover & Evitt 1978
Impagidinium sphaericum (Wall 1967) Lentin & Williams 1981
Impagidinium Stover & Evitt 1978 spp. [including cf. *I. strialatum* (Wall 1967) Stover & Evitt 1978]
Invertocysta lacrymosa Edwards 1984
Invertocysta tabulata Edwards 1984
Invertocysta Edwards 1984 spp.
Isabelidinium Lentin & Williams 1977 sp.

Kallosphaeridium capulatum Stover 1977

Labyrinthodinium truncatum Piasecki 1980 subsp. *modicum* de Verteuil & Norris 1996
Labyrinthodinium truncatum Piasecki 1980 subsp. *truncatum*
Lejeunecysta hyalina (Gerlach 1961) Artzner & Dörhöfer 1978
Lejeunecysta Artzner & Dörhöfer 1978 spp.
Lentinia serrata Bujak 1980
Lingulodinium machaerophorum (Deflandre & Cookson 1955) Wall 1967 [including *Lingulodinium siculum*]
Lophocysta? sp. indet. of De Coninck (1986)

Melitasphaeridium choanophorum (Deflandre & Cookson 1955) Harland & Hill 1979
Membranilarnacia? *picena* Biffi & Manum 1988
Membranophoridium aspinatum Gerlach 1961

Nematosphaeropsis pusulosa (Morgenroth 1966) Stover & Evitt 1978
Nematosphaeropsis rigida Wrenn 1988
Nematosphaeropsis Deflandre & Cookson 1955 sp.
new genus?, new species [apical archeopyle, areoligeracean group, with ectophragm]

Operculodinium? *placitum* Drugg & Loeblich 1967
Operculodinium centrocarpum (Deflandre & Cookson 1955) Wall 1967
Operculodinium centrocarpum sensu Wall (1967)
Operculodinium divergens (Eisenack 1954) Stover & Evitt 1978
Operculodinium piaseckii Strauss & Lund 1992
Operculodinium tegillatum Head 1997
Operculodinium Wall 1967 spp.

Palaeocystodinium golzowense Alberti 1961
Pentadinium imaginatum (Benedek 1972) Stover & Hardenbol 1993

Pentadinium laticinctum Gerlach 1961 [grano-vermiculate forms]
Pentadinium laticinctum Gerlach 1961 subsp. *laticinctum*
Pentadinium membranaceum (Eisenack 1965) Stover & Evitt 1978
Pentadinium Gerlach 1961 sp.
Pentadinium sp. cf. *P. laticinctum granulatum* Gocht 1969
Pentadinium sp. I of Edwards (1986)
Phthanoperidinium comatum (Morgenroth 1966) Eisenack & Kjellstrom 1971
Polysphaeridium zoharyi (Rossignol 1962) Bujak et al. 1980/ *Homotryblium vallum* Stover 1977
Pyxidiella? *simplex* Harland 1979

Reticulatosphaera actinocoronata (Benedek 1972) Bujak & Matsuoka 1986
Rhombodinium perforatum (Jan du Chêne & Châteauneuf 1975) Lentin & Williams 1977
Rottnestia borussica (Eisenack 1954) Cookson & Eisenack 1961

Samlandia chlamydophora Eisenack 1954
Samlandia chlamydophora sensu Stover and Hardenbol (1993)
Saturnodinium pansum (Stover 1977) Brinkhuis et al. 1992
Saturnodinium Brinkhuis et al. 1992 sp.
Selenopemphix armageddonensis de Verteuil & Norris 1992
Selenopemphix brevispinosa Head et al. 1989
Selenopemphix brevispinosa Head et al. 1989 subsp. *brevispinosa*
Selenopemphix brevispinosa/*S. dionaeacysta* Head et al. 1989
Selenopemphix dionaeacysta de Verteuil & Norris 1992
Selenopemphix nephroides Benedek 1972
Selenopemphix quanta (Bradford 1975) Matsuoka 1985
Selenopemphix Benedek 1972 sp.
Spiniferites mirabilis (Rossignol 1964) Sarjeant 1970
Spiniferites pseudofurcatus (Klumpp 1953) Sarjeant 1970
Spiniferites Mantell 1850 spp.
Sumatradinium druggii Lentin et al. 1994
Sumatradinium soucouyantiae de Verteuil & Norris 1996
Sumatradinium Lentin & Williams 1976 sp.? [fragment]

Tectatodinium pellitum Wall 1967
Thalassiphora delicata Williams & Downie 1966
Thalassiphora pelagica (Eisenack 1954) Eisenack & Gocht 1960
Thalassiphora reticulata Morgenroth 1966
Trigonopyxidia fiscellata De Coninck 1986
Trinovantedinium ferugnomatum de Verteuil & Norris 1992
Trinovantedinium glorianum (Head et al. 1989) de Verteuil & Norris 1992
Trinovantedinium harpagonium de Verteuil & Norris 1992
Trinovantedinium papula de Verteuil & Norris 1992
Trinovantedinium Reid 1977 spp.
Trinovantedinium? *xylochoporum* de Verteuil & Norris 1992
Tuberculodinium vancampoae (Rossignol 1962) Wall 1967
Turbiosphaera Archangelsky 1969 sp.
Unipontidinium aquaeductum (Piasecki 1980) Wrenn 1988

Wetzeliella gochtii Costa & Downie 1976
Wetzeliella symmetrica Weiler 1956
Wetzeliella Eisenack 1938 sp.

miscellaneous areoligeracean forms
miscellaneous peridiniacean forms
freshwater alga *Pediastrum* Meyen 1829

Diatoms

Actinocyclus ellipticus Grunow
Actinocyclus ellipticus var. *spiralis* Barron
Actinocyclus ingens Rattray
Actinocyclus octonarius Ehrenberg
Actinoptychus senarius (Ehrenberg) Ehrenberg
Actinoptychus thumii (Schmidt) Hanna
Actinoptychus virginicus (Grunow) Andrews
Annellus californicus Tempère
Azpeitia vetustissima (Pantocsek) P.A. Sims

Cavitatus miocenicus (Schrader) Akiba et Yanagisawa
Cladogramma dubium Lohman
Coscinodiscus apiculatus Ehrenberg
Coscinodiscus curvatulus Grunow
Coscinodiscus lewisianus Greville
Coscinodiscus marginatus Ehrenberg
Coscinodiscus oculus-iridis Ehrenberg
Coscinodiscus plicatus Grunow
Coscinodiscus radiatus Ehrenberg
Coscinodiscus rothii (Ehrenberg) Grunow
Cosmiodiscus elegans Greville
Craspedodiscus coscinodiscus Ehrenberg
Cymatogonia amplyoceras (Ehrenberg) Hanna

Delphineis angustata (Pantocsek) Andrews
Delphineis biseriata (Grunow) Andrews
Delphineis novaecesarea (Kain et Schulze) Andrews
Delphineis ovata Andrews
Delphineis penelliptica Andrews
Denticulopsis hustedtii (Simonsen et Kanaya) Simonsen
Denticulopsis simonsenii (Mertz) Akiba

Goniothecium rogersii Ehrenberg

Melosira westii W. Smith

Navicula pennata Schmidt

Paralia complexa (Lohman) Andrews
Paralia sulcata (Ehrenberg) Cleve
Pleurosigma affine var. *marylandica* Grunow
Pyxidicula cruciata Ehrenberg

Rhaphoneis clavata Andrews
Rhaphoneis diamantella Andrews
Rhaphoneis gemmifera Ehrenberg
Rhaphoneis lancelettula Grunow
Rhaphoneis magnapunctata Andrews

Stellarima sp.
Stephanopyxis corona (Ehrenberg) Grunow
Stephanopyxis grunowii Grove et Sturt
Stephanopyxis turris (Greville) Ralfs
Stephanopyxis sp. cf. *S. lineata* (Ehrenberg) Forti

Thalassionema nitzschioides Grunow
Thalassiosira grunowii Akiba et Yanagisawa
Thalassiosira leptopus (Grunow) Hasle et Fryxell
Thalassiosira praeyabei (Schrader) Akiba et Yanagisawa
Thalassiothrix longissima Cleve et Grunow
Triceratium condecorum Ehrenberg

Xanthiopyxis spp.

Silicoflagellates

Bachmannocena circulus (Ehrenberg) Locker
Bachmannocena elliptica elliptica (Ehrenberg) Bukry
Bachmannocena elliptica miniformis (Bachmann et Papp) Bukry
Bachmannocena triangula (Ehrenberg) Locker

Caryocha sp. Bukry et Monechi
Corbisema triacantha (Ehrenberg) Hanna

Dictyocha brevispina ausonia (Deflandre) Bukry
Dictyocha brevispina brevispina (Lemmermann) Bukry
Dictyocha fibula Ehrenberg
Dictyocha pulchella Bukry
Distephanus crux crux (Ehrenberg) Haeckel
Distephanus crux parvus (Bachmann) Bukry
Distephanus crux scutulatus Bukry
Distephanus longispinus (Schulz) Bukry et Foster
Distephanus schulzii (Deflandre *in* Bachmann et Ichikawa) Ciesielski et al.
Distephanus speculum speculum (Ehrenberg) Haeckel
Distephanus speculum triommata (Ehrenberg) Bukry
Distephanus stauracanthus (Ehrenberg) Haeckel
Distephanus stradneri (Jerkovic) Bukry
Distephanus sp. aff. *D. schauinslandii* Lemmermann

Mollusks

Pelecypoda

Amiantis? sp.
Anadara carolinensis (juv.) (Dall, 1895)?
Anisodonta? sp.
Anomia sp.
Astarte concentrica Conrad 1834
Astarte exalta Conrad, 1841
Astarte undulata Say 1824
Astarte spp. (worn)

Brachidontes sp.

carditid fragments
Carolinapecten urbannaensis (Mansfield 1929)
Chama sp.
Chesapecten madisonius (Say 1824)
Chesapecten middlesexensis (Mansfield 1936)
Chesapecten sp.
Chione cancellata (Linne 1767)
Clinocardium laqueatum (Conrad 1830)
Clinocardium sp.
corbulid fragments
Crassinella lunulata (Conrad 1834)
Crassinella sp.
Crassostrea sp.
Cyclocardia granulata (Say 1824)

Dosinia sp.

Eucrassatella sp. (juv.)

Glycymeris pectinata (Gmelin 1791)

Isognomon sp.

Leptomactra delumbis (Conrad 1832)
Leptonacea
Lirophora vredenburgi Ward 1992
Lirophora sp.
Lucina floridana Conrad 1833
Lucinisca cribraria (Say 1824)
Lucinoma contracta (Say 1824)

Macrocallista sp.
Mercenaria sp.
Musculus lateralis (Say 1822)? [?=*M. virginicus* Conrad 1867]
Mya wilsoni Ward 1992?

Nucula proxima Say 1822
Nucula sp.
Nuculana acuta (Conrad 1832)
Nuculana sp.

ostreid fragments and juv.

Pandora sp. cf. *P. dalli* Gardner
Panopea sp.
Parvilucina crenulata (Conrad 1840)
pectinid cf. "*Pecten*" *choctavensis* Aldrich 1895
pectinid cf. *Chlamys brooksvillensis* Mansfield 1937

pectinid cf. *Chlamys* aff. *C. vaun wythei* Hertlein Mansfield 1937
pectinid cf. *Placopecten* sp. (juv.)
pectinid fragments
Pitar sayana (Conrad 1833)
Placopecten sp.
Pleuromeris sp.

Raisa arata (Say 1824)
Rebeccapecten berryae Ward 1992

Solen sp.
Spisula rappahannockensis Gardner 1944
Spondylus sp.
Striarca centenaria (Say 1824)

Tellina spp.

Yoldia laevis (Say 1824)

Scaphopoda

Dentalium sp.

Gastropoda

Acteocina candei (d'Orbigny 1842)

Cadulus sp.
Calliostoma sp.
Cochliolepsis sp.
Crepidula fornicata (Linne 1758)
Crepidula plana Say 1822

Diodora sp. cf. *D. auroraensis* Ward and Blackwelder 1987

Ecphora gardnerae whiteoakensis Ward and Gilinsky 1988
Ecphora sp. (fragments)
Epitonium junceum Gardner 1948
Epitonium sp.
Eulima dalli (Gardner and Aldrich 1919)
Eupleura caudata (Say 1822)

Lunatia heros (Say 1822)
Lunatia sp.

Mitrella communis (Conrad 1862)

Nassarius marylandica (Martin 1904)
Nassarius peralta (Conrad 1868)
Nassarius spp.

Odostomia sp.
Olivella sp.

pyramidellids
"*Scalaspira*" *strumosa* (Conrad 1832)

Tectonatica pusilla (Say 1822)
Teinostoma tectispira Pilsbry 1953
Teinostoma sp.
Terebra? sp.
Truncatella sp.
Turbonilla sp.
Turritella alticostata Conrad 1834
Turritella plebeia Say 1824
Turritella plebeia carinata Gardner 1948
Turritella plebeia plebeia Say 1824
Turritella subvariabilis d'Orbigny 1852
Turritella subvariabilis bohaski Ward 1992
Turritella subvariabilis dianae Ward 1992
Turritella subvariabilis subvariabilis d'Orbigny 1852
Turritella sp.

Ostracodes

Acanthocythereis sp.
Actinocythereis captionis Hazel 1983
Actinocythereis dawsoni (Brady 1870)
Actinocythereis exanthemata (Ulrich and Bassler 1904)
Actinocythereis thompsoni Howe and Law 1936
Actinocythereis cf. *A. dacyi* (Howe and Law 1936)
Actinocythereis cf. *A. stenzeli* (Stephenson 1946)
Actinocythereis sp.
Alatacythere ivani Howe 1951
Argilloecia sp.
Aurila laevicula Edwards 1944

Bensonocythere americana Hazel 1967
Bensonocythere blackwelderi Hazel 1983
Bensonocythere bradyi Hazel 1983
Bensonocythere calverti (Ulrich and Bassler 1904)
Bensonocythere ricespitensis Hazel 1983
Bensonocythere rugosa Hazel 1983
Bensonocythere trapezoidalis (Swain 1974)
Bensonocythere spp.
Buntonia sp.

Campylocythere laeva Edwards 1944
Cytherella spp.
Cytheridea subovalis (Ulrich and Bassler 1904)
Cytheridea virginiensis (Malkin 1953)
Cytheridea n. sp.
Cytheromorpha macroincisa Hazel 1983
Cytheromorpha warneri Howe and Spurgeon 1935
Cytheropteron talquinensis Puri 1954
Cytheropteron yorktownensis (Malkin 1953)
Cytheropteron sp.
Cytherura coryelli Malkin 1953
Cytherura howei (Puri 1954)
Cytherura reticulata Edwards 1944

Digmocythere russelli Howe and Lea 1936

Echinocythereis clarkana Ulrich and Bassler 1904
Echinocythereis miniscula (Ulrich and Bassler 1904)
Echinocythereis sp.
Eucythere gibba Edwards 1944

Haplocytheridea n. sp.
Hemicytheridea cf. *H. montgomeryensis* Howe and Chambers 1935
Henryhowella evax (Ulrich and Bassler 1904)
Hulingsina americana (Cushman 1906)
Hulingsina calvertensis Forester 1980
Hulingsina rugipustulosa (Edwards 1944)
Hulingsina spp.

Krithe sp.

Leguminocythereis cf. *L. scarabaeus* Howe and Law 1936
Leguminocythereis sp.
Loxoconcha florencensis Cronin 1990
Loxoconcha reticularis Edwards 1944
Loxoconcha aff. *L. granulata* Sars 1865
Loxoconcha sp.

Malzella conradi (Howe and McGuirt 1953)
Malzella evexa Hazel 1985
Microcytherura choctawhatcheensis (Puri 1954)
Microcytherura shattucki (Ulrich and Bassler 1904)
Microcytherura similis (Malkin 1953)
Muellerina blowi Hazel 1983
Muellerina lienenklausi (Ulrich and Bassler 1904)
Muellerina micula (Ulrich and Bassler 1904)
Muellerina ohmerti Hazel 1983
Muellerina wardi Hazel 1983
Munseyella sp.
Murrayina barclayi Mclean 1957
Murrayina macleani Swain 1974
Murrayina radiata (Malkin 1953)

Neonesidea laevicula (Edwards 1944)

Orionina vaughani (Ulrich and Bassler 1904)

Paracytheridea altila Edwards 1944
Paracytheridea rugosa Edwards 1944
Paracytheridea aff. *P. mucra* Edwards 1944
Paradoxostoma sp.
Proteoconcha gigantea Plusquelec and Sandberg 1969
Proteoconcha tuberculata Puri 1960
Pseudocytheretta burnsi (Ulrich and Bassler 1904)
Pseudocytheretta plebeia (Ulrich and Bassler 1904)
Pterygocythereis americana (Ulrich and Bassler 1904)
Pterygocythereis howei (Hill 1954)
Pterygocythereis inexpectata (Blake 1929)
Puriana carolinensis Hazel 1983
Puriana rugipunctata (Ulrich and Bassler 1904)

Sahnia sp.

Thaerocythere schmidtae (Malkin 1953)
Trachyleberidea blanpiedi Howe and Law 1936

Planktonic Foraminifera

Cribrohantkenina inflata (Howe 1928)

Globigerina gortanii (Borsetti 1959)
Globigerina medizzai Toumarkine and Bolli 1975
Globigerina ouachitaensis Howe and Wallace 1932
Globigerina praebulloides Blow 1959
Globigerina tripartita Koch 1926
Globigerinatheka index (Finlay 1939)
Globigerinatheka semiinvoluta (Keijzer 1945)

Hantkenina alabamensis Cushman 1925

Praetenuitella praegemma Li 1987
Pseudohastigerina naguewichiensis Myatliuk 1950

Testacarinata inconspicua (Howe 1939)
Turborotalia cerroazulensis cerroazulensis (Cole 1928)
Turborotalia cerroazulensis cocoaensis (Cushman 1928)
Turborotalia cerroazulensis cunialensis (Toumarkine and Bolli 1970)
Turborotalia cerroazulensis pomeroli (Toumarkine and Bolli 1970)

Bolboformids

Bolboforma latdorfensis Spiegler 1991
Bolboforma spinosa Daniels and Spiegler 1974

Vertebrates

Acanthocybium proosti (Storms 1897)

Dasyatis Rafinesque 1810 sp.
Diaphyodus wilsoni Westgate 1989

Scyliorhinus gilberti Casier 1946
Squalus Linnaeus 1758 sp.

Trichiurides sagittidens Winkler 1874

Appendix H2. Useful Cenozoic Calcareous Nannofossil Datums

The following calcareous nannofossil species can be used to date sediments of late Eocene to late Pliocene age. Many, but not all, of these species are present in the USGS-NASA Langley core. FAD is a first appearance datum, and LAD is a last appearance datum. Zonal markers for the NP and NN zones of Martini (1971) are indicated with an asterisk (*). Bybell has found the remaining species to be biostratigraphically useful in the U.S. Gulf of Mexico and Atlantic Coastal Plains.

LAD **Discoaster brouweri*—top of Zone NN 18, late Pliocene

LAD **Discoaster pentaradiatus*—top of Zone NN 17, late Pliocene
LAD *Discoaster asymmetricus*—within Zone NN 17, late Pliocene

LAD **Discoaster surculus*—top of Zone NN 16, late Pliocene

LAD **Reticulofenestra pseudoumbilicus*—top of Zone NN 15, early Pliocene
FAD *Pseudoemiliania lacunosa*—within upper part of Zone NN 15, early Pliocene

LAD **Amaurolithus tricorniculatus*—top of Zone NN 14, early Pliocene
FAD **Discoaster asymmetricus*—base of Zone NN 14, early Pliocene

FAD **Ceratolithus rugosus*—base of Zone NN 13, early Pliocene

LAD **Discoaster quinqueramus*—top of Zone NN 11, late Miocene
LAD *Discoaster berggrenii*—within Zone NN 11, late Miocene
FAD *Discoaster berggrenii*—near base of Zone NN 11, late Miocene
FAD **Discoaster quinqueramus*—base of Zone NN 11, late Miocene

LAD **Discoaster hamatus*—top of Zone NN 9, late Miocene
FAD **Discoaster hamatus*—base of Zone NN 9, late Miocene

LAD *Discoaster exilis*—within Zone NN 8; middle or late Miocene
FAD **Catinaster coalitus*—base of Zone NN 8; middle or late Miocene

FAD **Discoaster kugleri*—base of Zone NN 7, middle Miocene

LAD **Sphenolithus heteromorphus*—top of Zone NN 5, middle Miocene

LAD **Helicosphaera ampliaperta*—top of Zone NN 4, middle Miocene
FAD *Discoaster variabilis*—near base of Zone NN 4; may occur sporadically within Zone NN 3, early Miocene

LAD **Sphenolithus belemnos*—top of Zone NN 3, early Miocene
FAD *Sphenolithus heteromorphus*—within Zone NN 3, early Miocene
FAD **Sphenolithus belemnos*—base of Zone NN 3, early Miocene

LAD **Triquetrorhabdulus carinatus*—top of Zone NN 2, early Miocene
FAD *Helicosphaera ampliaperta*—within Zone NN 2, early Miocene
FAD **Discoaster druggii*—base of Zone NN 2, early Miocene

LAD *Zygrhablithus bijugatus*—near bottom of Zone NN 1, early Miocene
LAD *Dictyococcites bisectus*—near bottom of Zone NN 1, early Miocene

LAD **Helicosphaera recta*—top of Zone NP 25, late Oligocene
LAD *Sphenolithus ciperoensis*—near top of Zone NP 25, late Oligocene
LAD *Chiasmolithus altus*—within Zone NP 25, late Oligocene

LAD **Sphenolithus distentus*—top of Zone NP 24, late Oligocene
LAD *Transversopontis zigzag*—within Zone NP 24, late Oligocene
LAD *Helicosphaera compacta*—within Zone NP 24, late Oligocene
FAD *Helicosphaera recta*—lower Zone NP 24, early Oligocene
FAD **Sphenolithus ciperoensis*—base of Zone NP 24, early Oligocene

FAD *Sphenolithus distentus*—within Zone NP 23, early Oligocene

LAD **Reticulofenestra umbilicus*—top of Zone NP 22, early Oligocene
LAD *Chiasmolithus oamaruensis*—within Zone NP 22, early Oligocene
FAD *Chiasmolithus altus*—within Zone NP 22, early Oligocene

LAD **Cyclococcolithus formosus*—top of Zone NP 21, early Oligocene
LAD *Isthmolithus recurvus*—within Zone NP 21, early Oligocene

LAD **Discoaster saipanensis*—top of Zone NP 19/20, late Eocene
LAD *Discoaster barbadiensis*—near top of Zone NP 19/20, late Eocene
LAD *Cribrocentrum reticulatum*—very near top of Zone NP 19/20, late Eocene
FAD **Isthmolithus recurvus*—base of Zone NP 19/20, late Eocene

Plates H1–H9

Plate H1

Dinoflagellate Cysts from the Chickahominy Formation in the USGS-NASA Langley Core, Hampton, Va.

[Scale bar shown applies to all photomicrographs. Sample depths and assemblages are shown in figure H5]

Figure

1. *Areosphaeridium diktyoplokus* (Klumpp 1953) Eaton 1971, Chickahominy Formation (sample R6110 AN), possible ventral view, upper focus.
2. *Batiacasphaera baculata* Drugg 1970, Chickahominy Formation (sample R6110 AO), orientation uncertain, upper focus.
3. *Batiacasphaera compta* Drugg 1970, Chickahominy Formation (sample R6110 AR), orientation uncertain, upper focus.
4. *Cordosphaeridium funiculatum* Morgenroth 1966, Chickahominy Formation (sample R6110 AR), orientation uncertain, upper focus.

5, 6. *Histiocysta* sp. of Stover and Hardenbol (1993 [1994]), Chickahominy Formation (sample R6110 AN), ventral views; 5, upper focus; 6, lower focus.

7. *Glaphyrocysta semitecta* (Bujak 1980) Lentin & Williams 1981 [grouped as miscellaneous areoligeracean forms (*Glaphyrocysta* spp.) in figure H5], Chickahominy Formation (sample R6110 AR), ventral view, intermediate focus.
8. *Dapsilidinium pseudocolligerum* (Stover 1977) Bujak et al. 1980, Chickahominy Formation (sample R6110 AL), orientation uncertain, upper focus.

9, 10. *Saturnodinium* Brinkhuis et al. 1992 sp., Chickahominy Formation (sample R6110 AO), possible antapical view; 9, upper focus; 10, intermediate focus.

11. *Trigonopyxidia fiscellata* De Coninck 1986, Chickahominy Formation (sample R6110 AR), dorsal view, dorsal surface.
12. *Rhombodinium perforatum* (Jan du Chêne & Châteauneuf 1975) Lentin & Williams 1977, Chickahominy Formation (sample R6110 AN), ventral view, intermediate focus.
13. *Operculodinium divergens* (Eisenack 1954) Stover & Evitt 1978, Chickahominy Formation (sample R6110 AL), possible right-lateral view, upper focus.

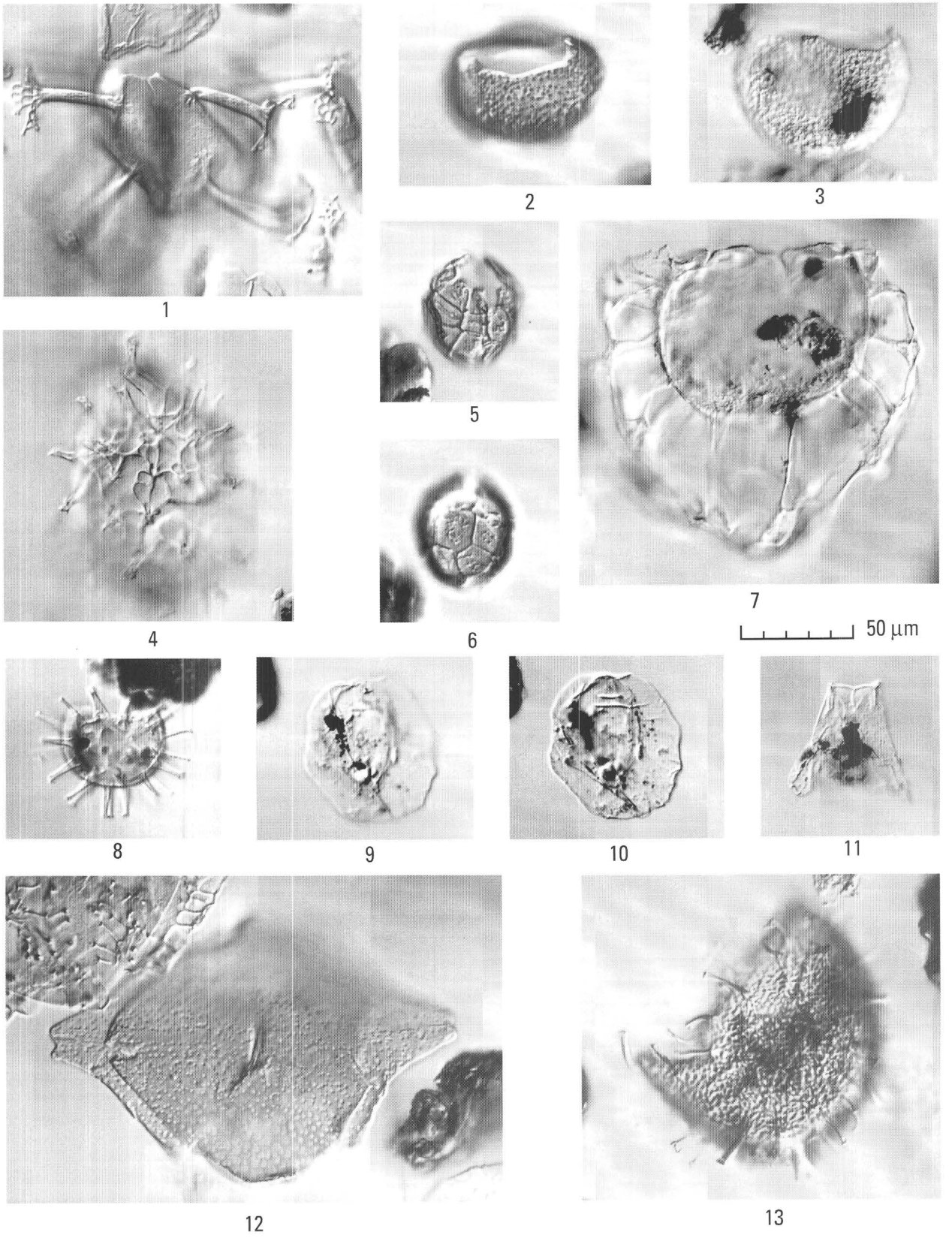

Dinoflagellate Cysts from the Chickahominy Formation in the USGS-NASA Langley Core, Hampton, Va.

Plate H2

Dinoflagellate Cysts from the Chickahominy Formation in the USGS-NASA Langley Core, Hampton, Va.

[Scale bar shown applies to all photomicrographs. Sample depths and assemblages are shown in figure H5]

Figure

1, 2. *Samlandia chlamydophora* sensu Stover and Hardenbol (1993 [1994]), Chickahominy Formation (sample R6110 AL), dorso-left-lateral views; 1, upper focus; 2, intermediate focus.

3. Miscellaneous areoligeracean form (*Glaphyrocysta* Stover & Evitt 1978 sp.), showing curling of processes around the central body, Chickahominy Formation (sample R6110 DA), presumably reworked from impact, possible dorsal view, intermediate focus.

4, 5. *Thalassiphora reticulata* Morgenroth 1966, Chickahominy Formation (sample R6110 AN), ventral views; 4, ventral surface; 5, dorsal surface.

6. Miscellaneous chorate form, *Exochosphaeridium* Davey et al. 1966? sp., showing curling of processes around the central body, Chickahominy Formation (R6110 AK), presumably reworked from impact, dorso-right-lateral view, intermediate focus.

7, 8. *Turbiosphaera* Archangelsky 1969 sp., Chickahominy Formation (sample R6110 AR), reworked, dorso-left-lateral views; 7, upper focus; 8, intermediate focus.

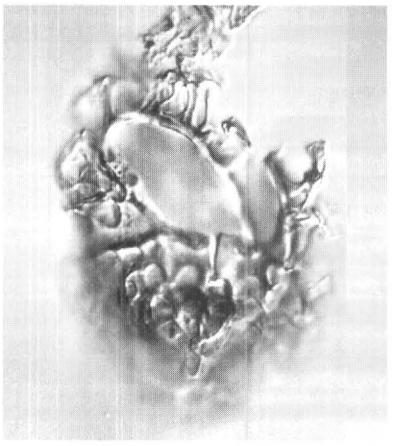

1

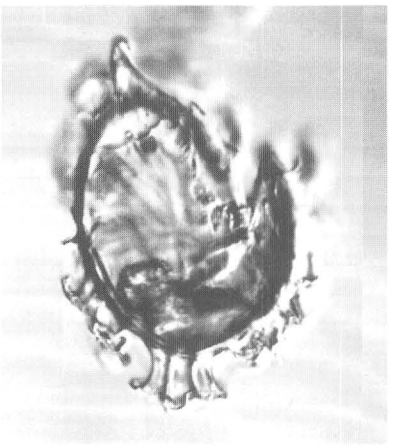

2

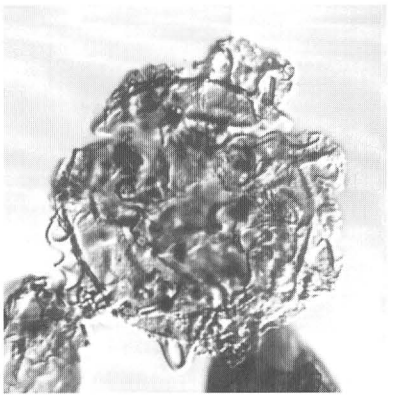

3

50 µm

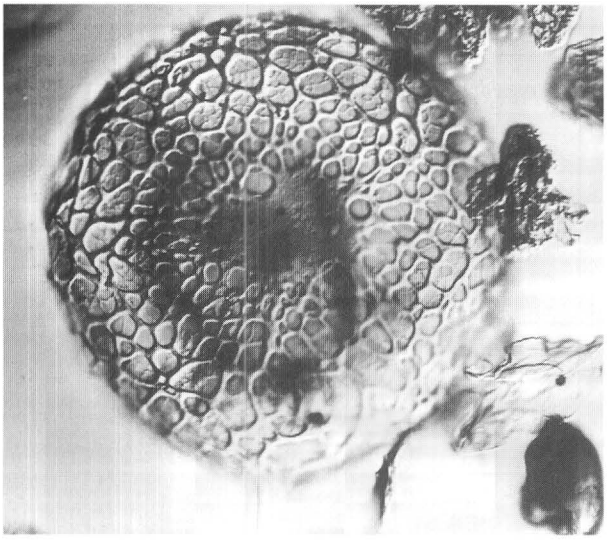

4

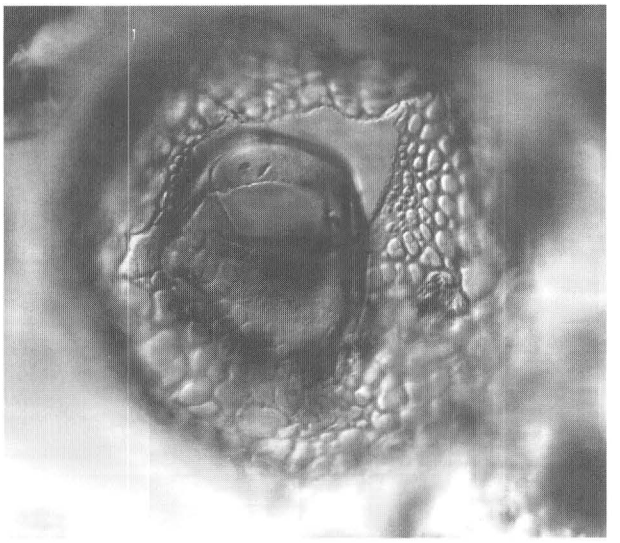

5

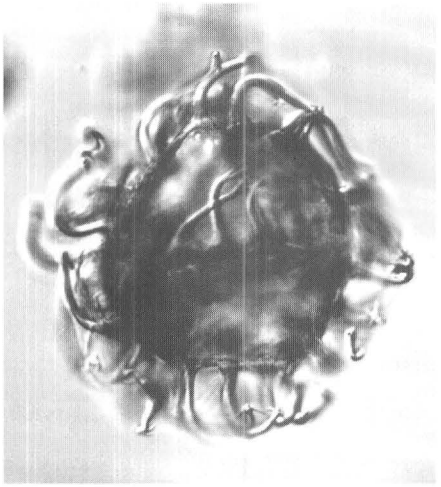

6

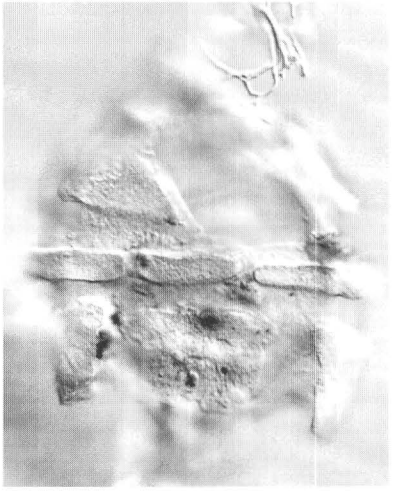

7

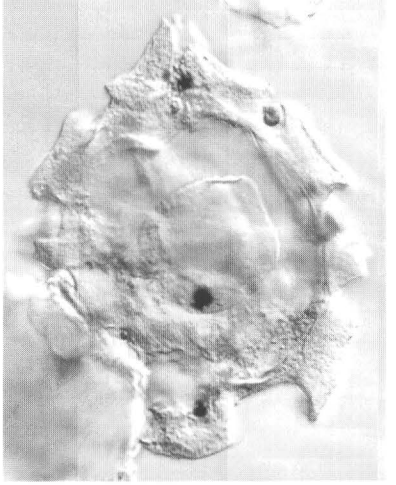

8

Dinoflagellate Cysts from the Chickahominy Formation in the USGS-NASA Langley Core, Hampton, Va.

Plate H3

Dinoflagellate Cysts from the Chickahominy Formation, Drummonds Corner Beds, and Old Church Formation in the USGS-NASA Langley Core, Hampton, Va.

[Scale bar shown applies to all photomicrographs. Sample depths and assemblages are shown in figure H5]

Figure

1. *Deflandrea* Eisenack 1938 sp., Chickahominy Formation (sample R6110 AN), presumably reworked from impact, dorsal view, dorsal surface.
2. *Cordosphaeridium gracile* (Eisenack 1954) Davey & Williams 1966, Chickahominy Formation (sample R6110 AN), presumably reworked from impact, fragment showing bent processes, upper focus.
3. *Chatangiella* Vozzhennikova 1967 or *Isabelidinium* Lentin & Williams 1977, Chickahominy Formation (sample R6110 DB), presumably reworked from impact, folded specimen, dorsal view, dorsal surface.
4. *Chiropteridium lobospinosum* Gocht 1960, Old Church Formation (sample R6110 AD), dorsal view, dorsal surface.
5. *Achilleodinium biformoides* (Eisenack 1954) Eaton 1976, Drummonds Corner beds (sample R6110 AH), dorsal view, dorsal surface.
6. *Homotryblium vallum* Stover 1977, Drummonds Corner beds (sample R6110 AH), oblique interior view of antapex.
7. *Chiropteridium galea* (Maier 1959) Sarjeant 1983, Old Church Formation (sample R6110 AD), dorsal view, intermediate focus.
8. *Membranophoridium aspinatum* Gerlach 1961, Old Church Formation (sample R6110 AF), ventral view, ventral surface.
9. *Reticulatosphaera actinocoronata* (Benedek 1972) Bujak & Matsuoka 1986, Drummonds Corner beds (sample R6110 AH), orientation uncertain, upper focus.

10, 14. *Trigonopyxidia fiscellata* De Coninck 1986, Old Church Formation (sample R6110 AF), presumably reworked from impact, folded specimen, left-lateral views; 10, upper focus; 14, lower focus.

11. *Tuberculodinium vancampoae* (Rossignol 1962) Wall 1967, Old Church Formation (sample R6110 AF), orientation uncertain, upper focus.

12, 13. *Saturnodinium pansum* (Stover 1977) Brinkhuis et al. 1992, Old Church Formation, possible antapical views; 12, (sample R6110 AD) upper focus; 13, (sample R6110 AB) detail of margin.

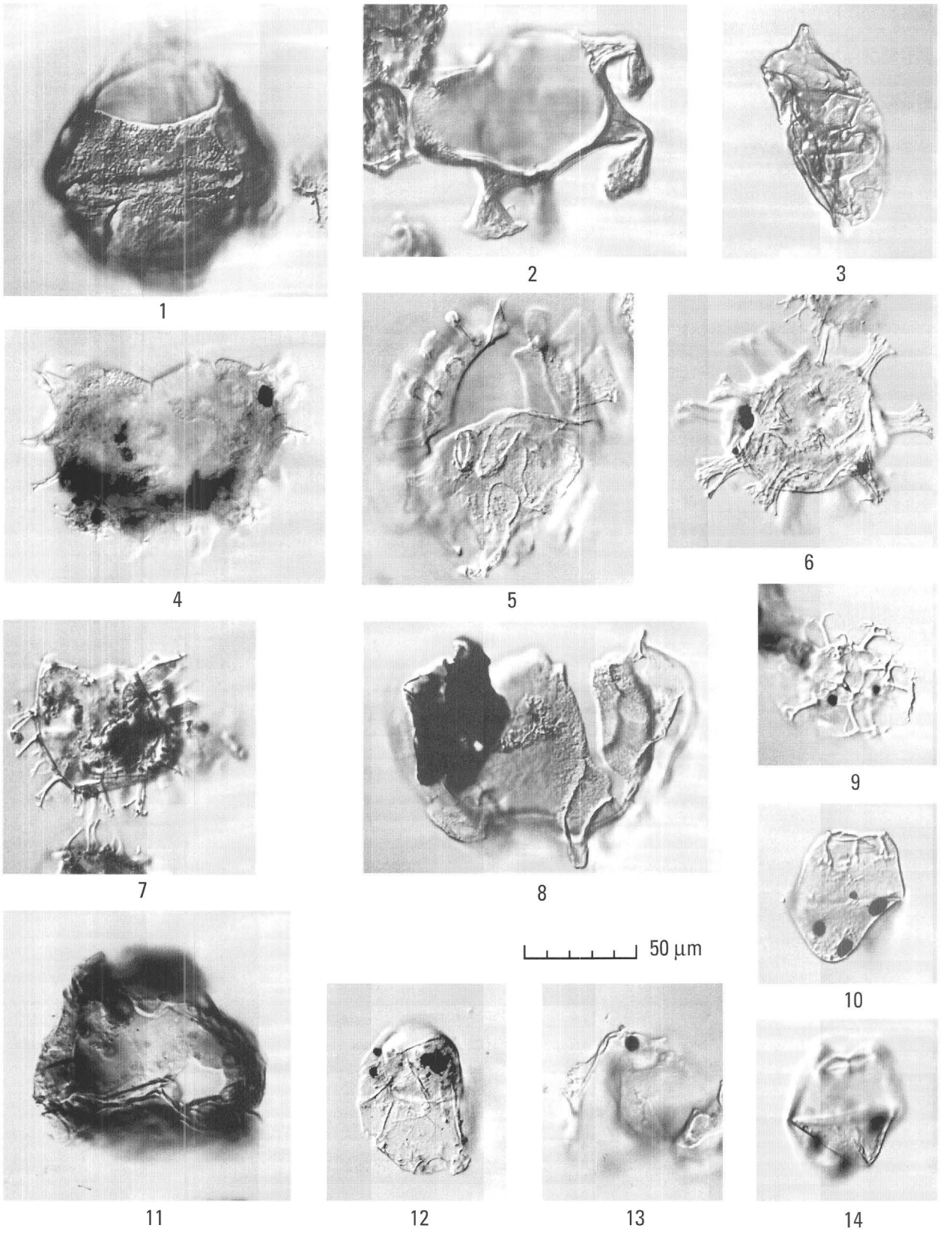

Dinoflagellate Cysts from the Chickahominy Formation, Drummonds Corner Beds, and Old Church Formation in the USGS-NASA Langley Core, Hampton, Va.

Plate H4

Dinoflagellate Cysts from the Old Church and Calvert Formations in the USGS-NASA Langley Core, Hampton, Va.

[Scale bar shown applies to all photomicrographs. Sample depths and assemblages are shown in figures H5 and H11]

Figure

1. *Exochosphaeridium insigne* de Verteuil & Norris 1996, Newport News beds of the Calvert Formation (sample R6110 Z), ventral view, intermediate focus.
2. New genus?, new species (apical archeopyle), Old Church Formation (sample R6110 AA), ventral view, ventral focus.
3. *Damassadinium californicum* (Drugg 1967) Fensome et al. 1993 operculum, Old Church Formation (sample R6110 AF), reworked, apical view, upper focus.
4. *Labyrinthodinium truncatum* Piasecki 1980 subsp. *modicum* de Verteuil & Norris 1996, Plum Point Member of the Calvert Formation (sample R6110 Y), apical view, intermediate focus.
5. *Apteodinium spiridoides* Benedek 1972, Newport News beds of the Calvert Formation (sample R6110 Z), dorsal view, dorsal surface.
6. *Wetzeliella gochtii* Costa & Downie 1976, Old Church Formation (sample R6110 AF), dorsal view, dorsal surface.
7. *Distatodinium paradoxum* (Brosius 1963) Eaton 1976, Plum Point Member of the Calvert Formation (sample R6110 Y), orientation uncertain, upper focus.
8. *Habibacysta tectata* Head et al. 1989, Calvert Beach Member of the Calvert Formation (sample R6110 W), dorso-left-lateral view, upper focus.
9. *Sumatradinium soucouyantiae* de Verteuil & Norris 1996, Plum Point Member of the Calvert Formation (sample R6110 Y), orientation uncertain, intermediate focus.
10. *Apteodinium spiridoides* Benedek 1972, Plum Point Member of the Calvert Formation (sample R6110 Y), oblique ventral view, upper focus. Many of the specimens of *A. spiridoides* in this sample have the distinctive, somewhat circular ornament shown in this specimen that is atypical for the species.
11. *Pentadinium* sp. cf. *P. laticinctum granulatum* Gocht 1969, Calvert Beach Member of the Calvert Formation (sample R6110 V), ventral view, ventral surface.
12. *Cleistosphaeridium placacanthum* (Deflandre & Cookson 1955) Eaton et al. 2001, Calvert Beach Member of the Calvert Formation (sample R6110 W), oblique ventral view, upper focus.

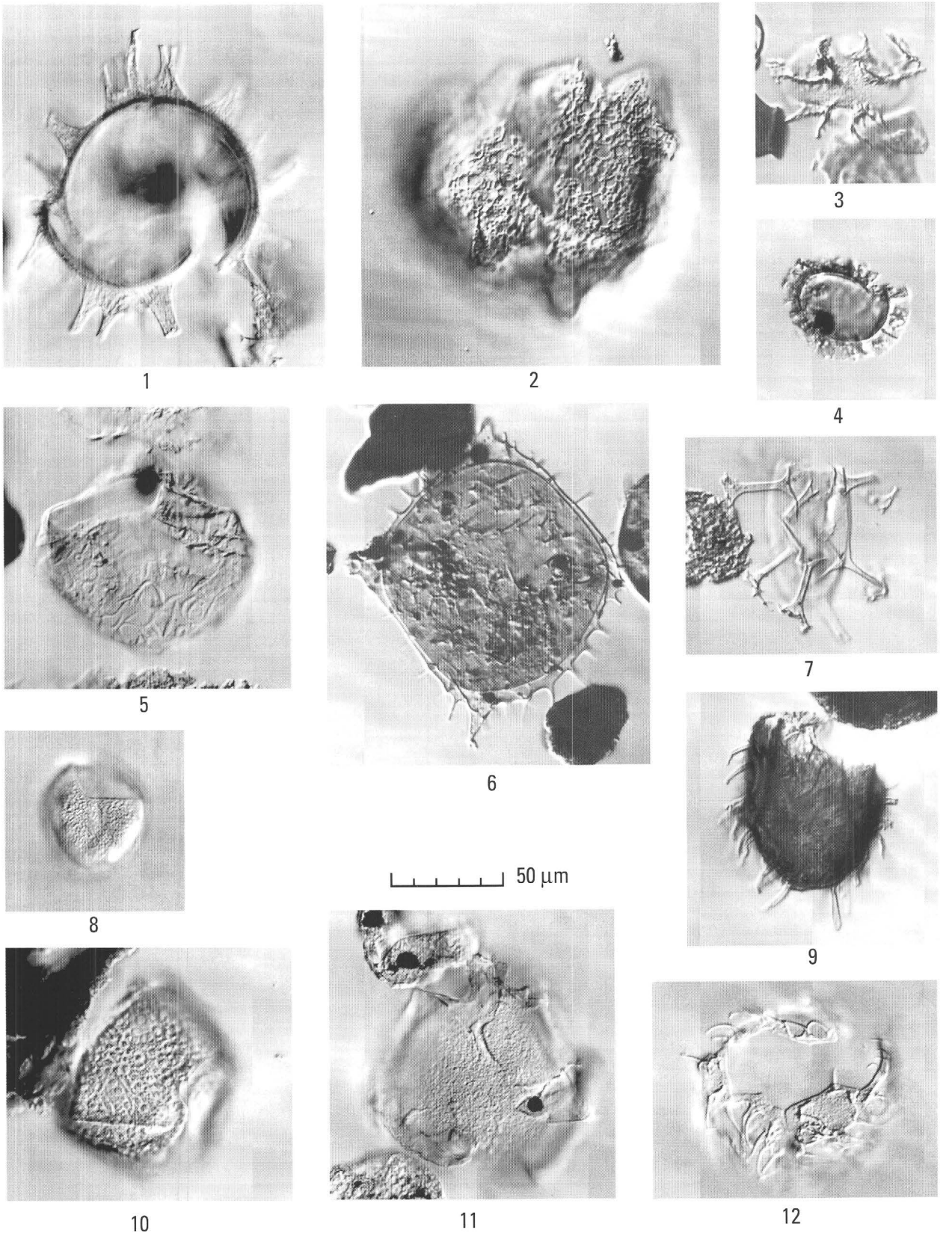

Dinoflagellate Cysts from the Old Church and Calvert Formations in the USGS-NASA Langley Core, Hampton, Va.

Plate H5

Dinoflagellate Cysts from the Calvert, St. Marys, Eastover, and Yorktown Formations in the USGS-NASA Langley Core, Hampton, Va.

[Scale bar shown applies to all photomicrographs. Sample depths and assemblages are shown in figure H11]

Figure

1. *Trinovantedinium harpagonium* de Verteuil & Norris 1992, Calvert Beach Member of the Calvert Formation (sample R6110 X), dorsal view, dorsal surface.
2. *Geonettia clineae* de Verteuil & Norris 1996, St. Marys Formation (sample R6110 R), orientation uncertain, upper focus.
3. *Hystrichosphaeropsis obscura* Habib 1972, St. Marys Formation (sample R6110 L), right-lateral view, upper focus.
4. *Erymnodinium delectabile* (de Verteuil & Norris 1992) Lentin et al. 1994, Eastover Formation (sample R6110 I), dorsal view, dorsal surface.
5. *Barssidinium evangelineae* Lentin et al. 1994, Eastover Formation (sample R6110 F), ventral view, ventral surface.
6. *Achomosphaera andalousiensis* Jan du Chêne 1977, Eastover Formation (sample R6110 I), orientation uncertain, upper focus.
7. Miscellaneous chorate form (*Spiniferites* Mantell 1850? sp.), showing curling of processes around the central body, St. Marys Formation (sample R6110 T), possibly reworked from impact, orientation uncertain, intermediate focus.
8. *Invertocysta lacrymosa* Edwards 1984, Eastover Formation (sample R6110 K), possible ventral view, intermediate focus.
9. *Labyrinthodinium truncatum* Piasecki 1980 subsp. *truncatum,* Eastover Formation (sample R6110 K), orientation uncertain, intermediate focus.
10. *Selenopemphix armageddonensis* de Verteuil & Norris 1992, Eastover Formation (sample R6110 F), possible apical view, intermediate focus.
11. *Filisphaera microornata* (Head et al. 1989) Head 1994, Eastover Formation (sample R6110 F), dorsal view, dorsal surface.

12–14. *Ataxiodinium confusum* Versteegh & Zevenboom 1995, Yorktown Formation (sample R6110 C), dorsal views; 12, dorsal surface; 13, intermediate focus; 14, ventral surface.

15. *Bitectatodinium tepikiense* Wilson 1973, Yorktown Formation (sample R6110 D), ventral view, dorsal surface.

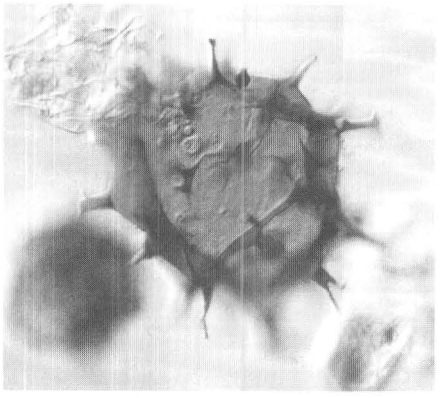

1

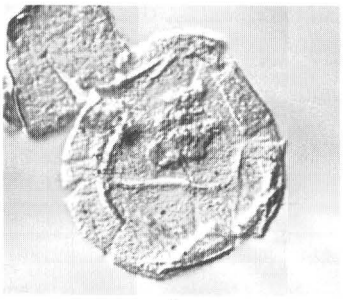

2

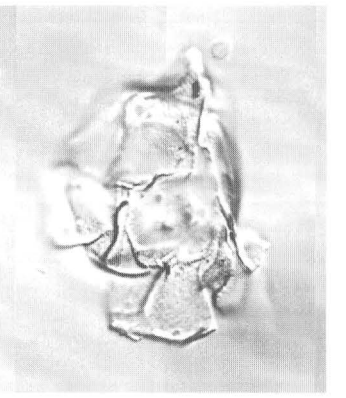

3

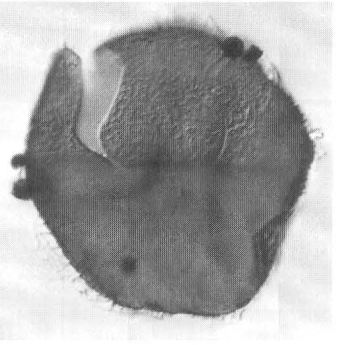

4

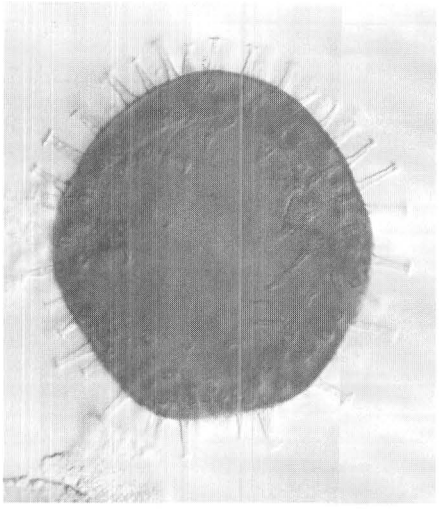

5

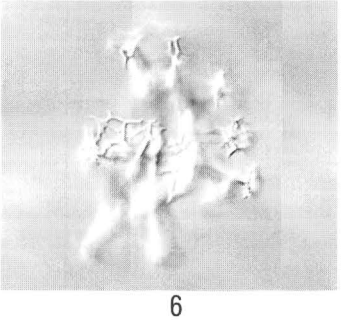

6

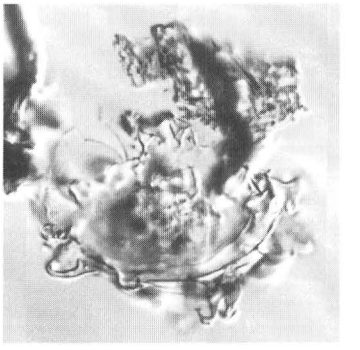

7

50 µm

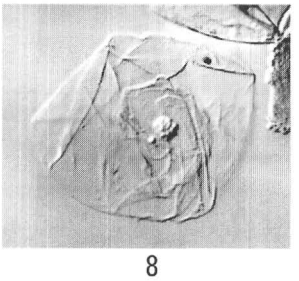

8

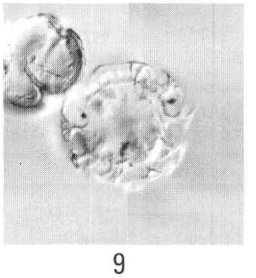

9

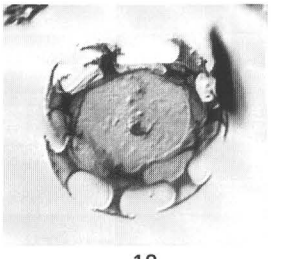

10

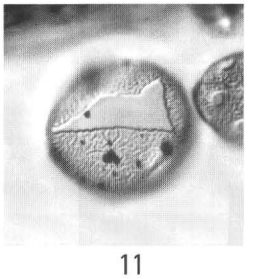

11

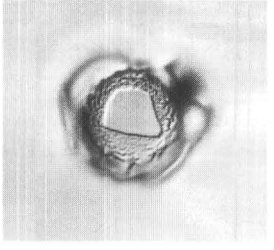

12

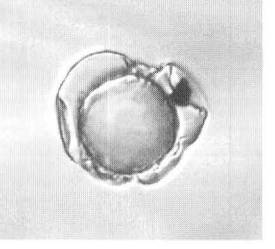

13

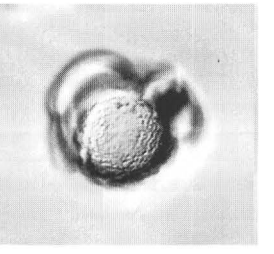

14

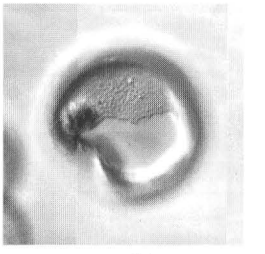

15

Dinoflagellate Cysts from the Calvert, St. Marys, Eastover, and Yorktown Formations in the USGS-NASA Langley Core, Hampton, Va.

Plate H6

Representative Mollusca from the Chickahominy, Old Church, and Yorktown Formations in the USGS-NASA Langley Core, Hampton, Va.

[Scale bars are 1 cm. Assemblage data are in figure H6, in pocket]

Figure

1. Pectinid cf. *Chlamys brooksvillensis* Mansfield 1937, 155.5 m (510.1–510.2 ft), Old Church Formation, exterior view.
2. *Cyclocardia granulata* (Say 1824), 19.5–19.6 m (64.0–64.2 ft), Yorktown Formation, exterior view.
3. Pectinid cf. "*Pecten*" *choctavensis* Aldrich 1895, 151.1 m (495.6–495.7 ft), Old Church Formation, exterior view.
4. *Dentalium* sp., 211.8–211.9 m (695.0–695.1 ft), Chickahominy Formation, shell is compressed and surrounding matrix was retained.
5. *Nuculana* sp., 205.6 m (674.5 ft), Chickahominy Formation, aragonitic "ghost" of shell in surrounding matrix.
6. *Rebeccapecten berryae* Ward 1992?, 212.08 m (695.8 ft), Chickahominy Formation, exterior view of aragonitic "ghost" of shell in surrounding matrix.

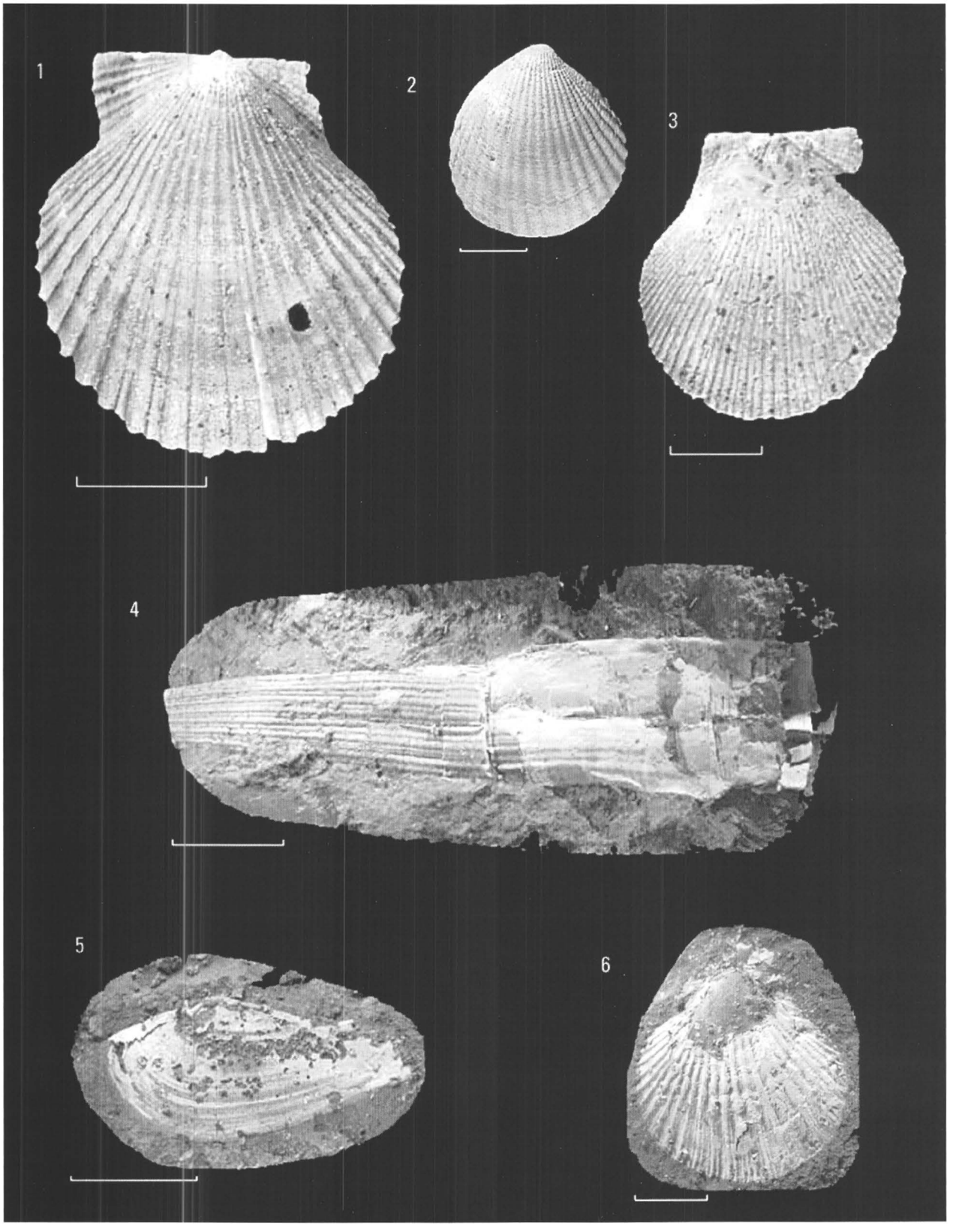

Representative Mollusca from the Chickahominy, Old Church, and Yorktown Formations in the USGS-NASA Langley Core, Hampton, Va.

Plate H7

Representative Mollusca from the Eastover and St. Marys Formations in the USGS-NASA Langley Core, Hampton, Va.

[Scale bars are 1 cm unless otherwise noted. Assemblage data are in figure H6, in pocket]

Figures

1, 3. *Lirophora vredenburgi* Ward 1992, Eastover Formation; 1, 54.9 m (180.1–180.2 ft), exterior view of right valve, scale bar is 1 cm; 3, 37.1 m (121.6–121.7 ft), interior view of left valve, scale bar is 1 mm.

2, 4. *Nucula proxima* Say 1822, 66.8 m (219.1–219.3 ft), Eastover Formation, right valve; 2, interior view; 4, exterior view. Scale bars are 1 mm.

5, 6. *Mitrella communis* (Conrad 1862), 66.8 m (219.1–219.3 ft), Eastover Formation; 5, back view; 6, apertural view. Scale bars are 1 mm.

7. *Ecphora gardnerae whiteoakensis* Ward and Gilinsky 1988, 66.8 m (219.1–219.3 ft), Eastover Formation, apical whorls of broken specimen.

8. *Nassarius peralta* (Conrad 1868), 66.8 m (219.1–219.3 ft), Eastover Formation, back view, scale bar is 1 mm.

9. *Nassarius* sp., 66.8 m (219.1–219.3 ft), Eastover Formation, apertural view, scale bar is 1 mm.

10. *Turbonilla* sp., 66.8 m (219.1–219.3 ft), Eastover Formation, apertural view, scale bar is 1 mm.

11, 12. *Turritella plebeia carinata* Gardner 1948, 38.3–38.4 m (125.8–126.0 ft), Eastover Formation, apertural views, scale bars are 1 mm.

13. *Lunatia heros* (Say 1822)?, 66.8 m (219.1–219.3 ft), Eastover Formation, back view of specimen with broken body whorl and encrusting bryozoan.

14. *Carolinapecten urbannaensis* (Mansfield 1929), 28.3 m (92.7–93.0 ft), Eastover Formation, exterior view of specimen with damaged ventral margin.

15. *Chesapecten middlesexensis* (Mansfield 1936), 38.3–38.4 m (125.8–126.0 ft), Eastover Formation, exterior view of juvenile specimen.

16. *Turritella plebeia plebeia* Say 1824, 74.5 m (244.4–244.5 ft), St. Marys Formation, apertural view.

17. *Turritella subvariabilis* d'Orbigny 1852, 43.3 m (142.0–142.1 ft), Eastover Formation, apertural view. Worn and pitted condition of shell may indicate that the specimen is reworked.

18. *Parvilucina crenulata* (Conrad 1840), 66.8 m (219.1–219.3 ft), Eastover Formation, exterior view of left valve, scale bar is 1 mm.

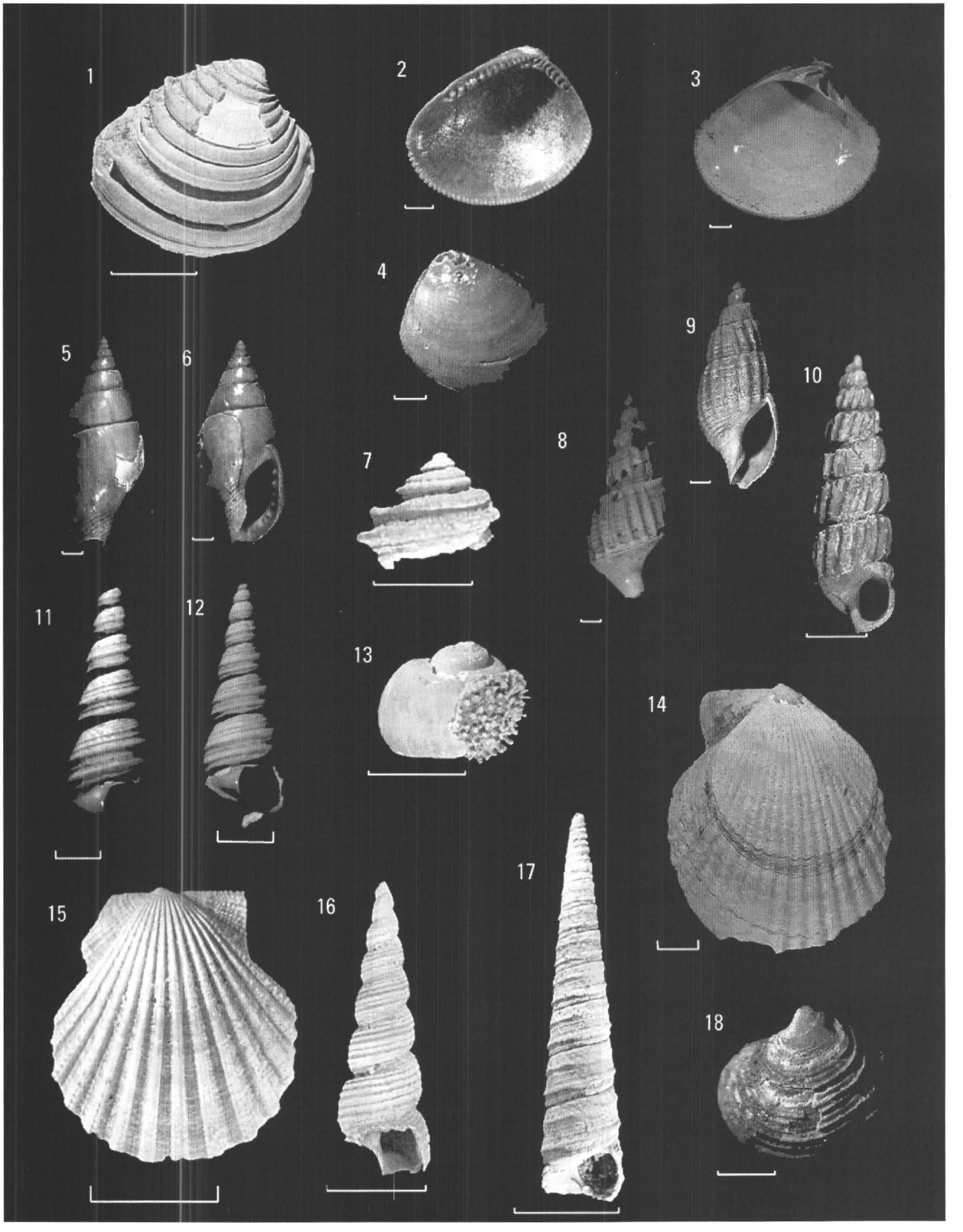

Representative Mollusca from the Eastover and St. Marys Formations in the USGS-NASA Langley Core, Hampton, Va.

Plate H8

Representative Mollusca from the Yorktown Formation in the USGS-NASA Langley Core, Hampton, Va.

[Scale bars are 1 mm unless otherwise noted. Assemblage data are in figure H6, in pocket]

Figures

1, 2. *Nuculana acuta* (Conrad 1832), 6.5 m (21.3–21.5 ft), right valve; 1, interior view; 2, exterior view.

3. *Epitonium junceum* Gardner 1948, 8.6–8.7 m (28.3–28.4 ft), apertural view, scale bar is 5 mm.

4. *Cadulus* sp., 6.5 m (21.3–21.5 ft).

5. *Eulima dalli* (Gardner and Aldrich 1919), 6.5 m (21.3–21.5 ft), apertural view.

6, 7. *Tectonatica pusilla* (Say 1822), 6.5 m (21.3–21.5 ft); 6, back view; 7, apertural view.

8. *Crassinella lunulata* (Conrad 1834), 6.5 m (21.3–21.5 ft), exterior of right valve.

9. *Acteocina candei* (d'Orbigny 1842), 6.5 m (21.3–21.5 ft), apertural view.

10, 11. *Parvilucina crenulata* (Conrad 1840), 6.5 m (21.3–21.5 ft); 10, exterior view of right valve; 11, interior view of left valve.

12. *Striarca centenaria* (Say 1824), 19.5–19.6 m (64.0–64.2 ft), exterior view of left valve with broken ventral margin, scale bar is 1 cm.

13, 14. *Musculus lateralis* (Say 1822)? [possibly synonymous with *M. virginicus* Conrad 1867], 17.3 m (56.6–56.7 ft); 13, interior view of left valve; 14, exterior view of right valve.

15. *Turritella alticostata* Conrad 1834, 6.5 m (21.3–21.5 ft), apertural view, scale bar is 1 cm.

16, 17. *Yoldia laevis* (Say 1824), 6.5 m (21.3–21.5 ft), left valve; 16, exterior view; 17, interior view.

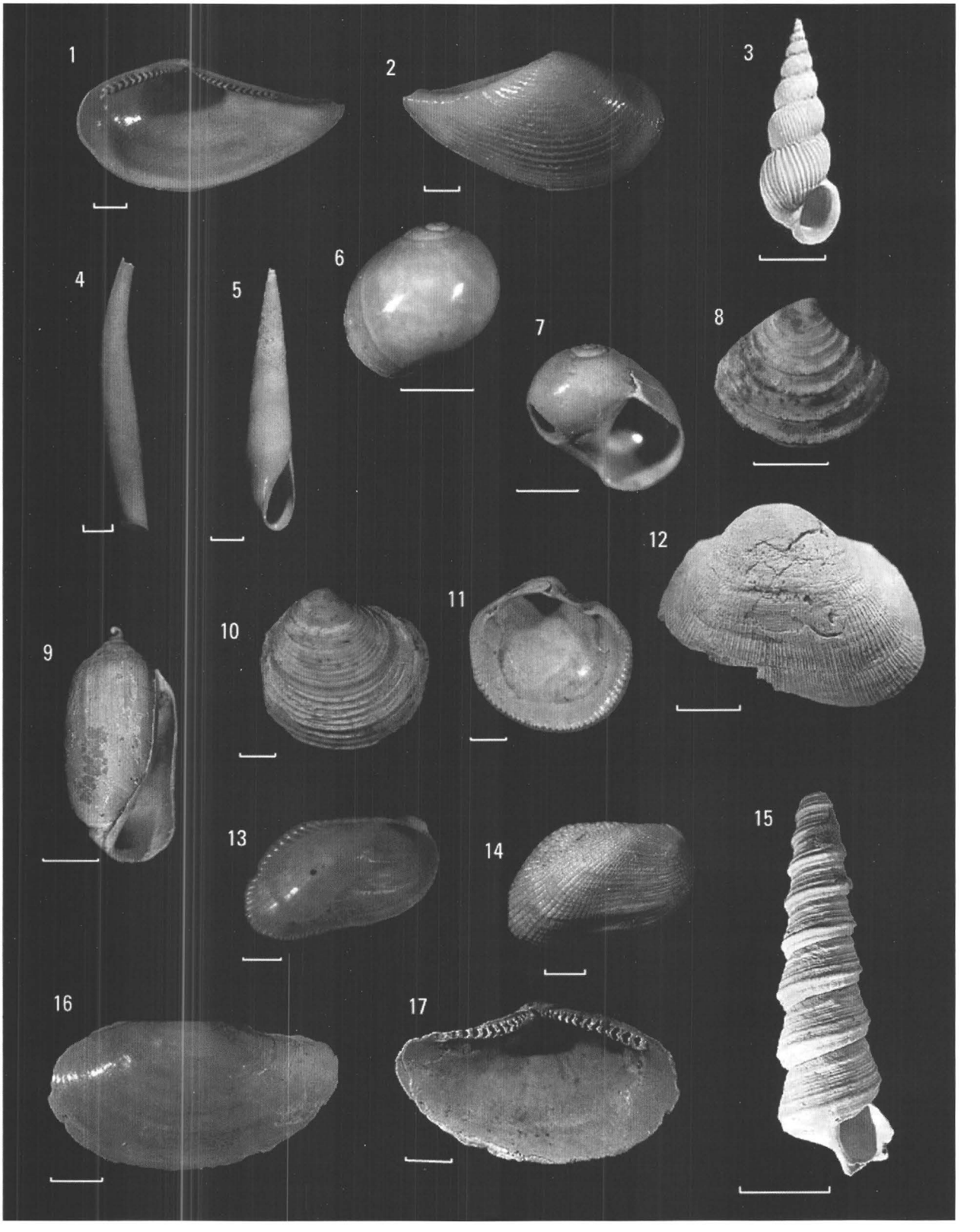

Representative Mollusca from the Yorktown Formation in the USGS-NASA Langley Core, Hampton, Va.

Plate H9

Late Eocene and Early Oligocene Fish Teeth from the USGS-NASA Langley Core, Hampton, Va.

[USNM, U.S. National Museum of Natural History, Washington, D.C. Scale bars are 1 mm. Sample depths are in figure H9]

Figure

1. *Squalus* Linnaeus 1758 sp. (USNM 519557), Drummonds Corner beds, lower Oligocene.
2. *Dasyatis* Rafinesque 1810 sp. (USNM 519558), Drummonds Corner beds, lower Oligocene.
3. *Trichiurides sagittidens* Winkler 1874 (USNM 519556), Drummonds Corner beds, lower Oligocene.
4. *Scyliorhinus gilberti* Casier 1946 (USNM 519554), Chickahominy Formation, upper Eocene.
5. *Acanthocybium proosti* (Storms 1897) (USNM 519553), Chickahominy Formation, upper Eocene.
6. *Diaphyodus wilsoni* Westgate 1989 (USNM 519555), Drummonds Corner beds, lower Oligocene.

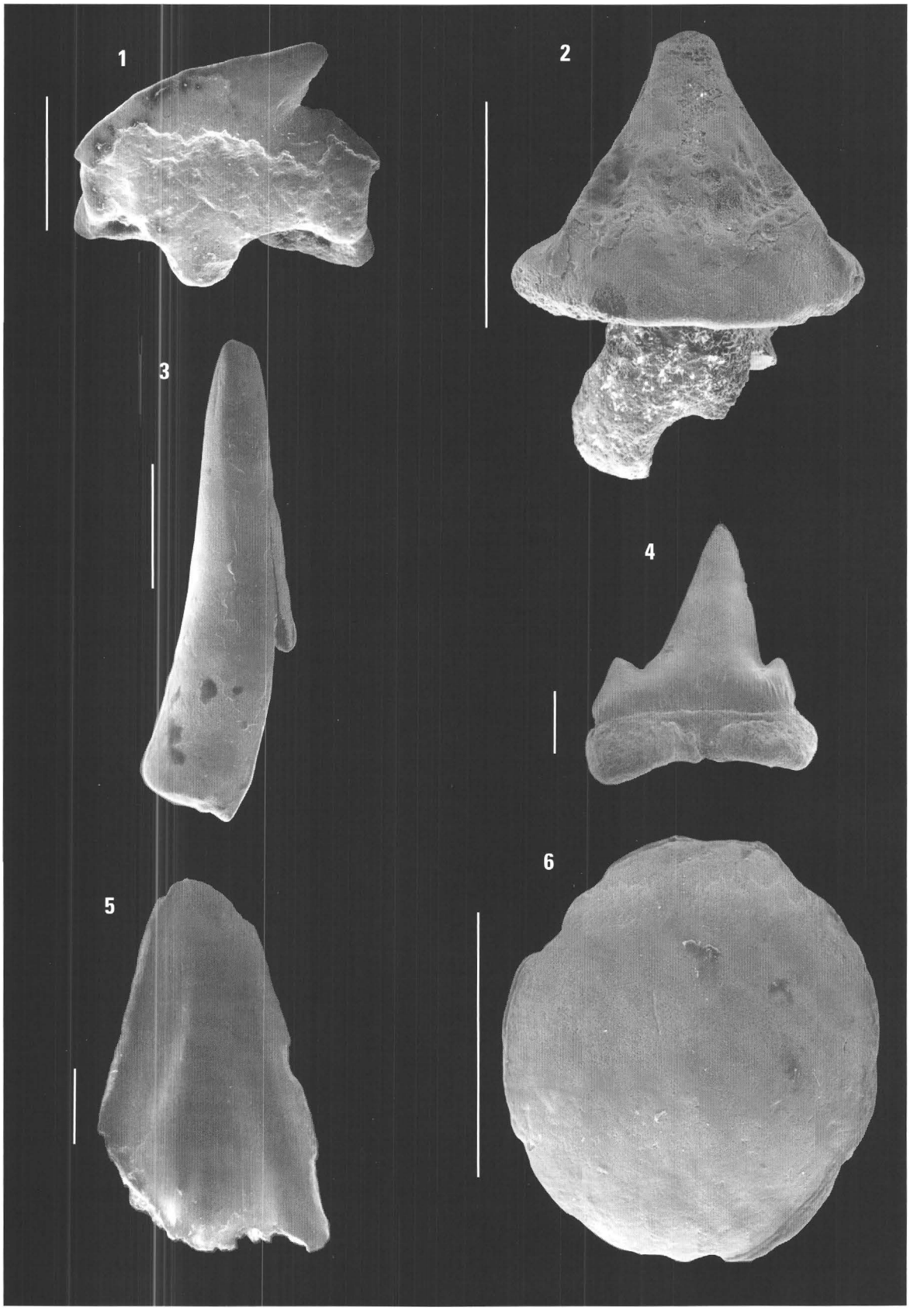

Late Eocene and Early Oligocene Fish Teeth from the USGS-NASA Langley Core, Hampton, Va.

High-Resolution Seismic-Reflection Image of the Chesapeake Bay Impact Structure, NASA Langley Research Center, Hampton, Virginia

By Rufus D. Catchings, David S. Powars, Gregory S. Gohn, and Mark R. Goldman

Chapter I of
**Studies of the Chesapeake Bay Impact Structure—
The USGS-NASA Langley Corehole, Hampton, Virginia, and
Related Coreholes and Geophysical Surveys**

Edited by J. Wright Horton, Jr., David S. Powars, and Gregory S. Gohn

Prepared in cooperation with the
Hampton Roads Planning District Commission,
Virginia Department of Environmental Quality, and
National Aeronautics and Space Administration Langley Research Center

Professional Paper 1688

U.S. Department of the Interior
U.S. Geological Survey

Contents

Figures

Tables

High-Resolution Seismic-Reflection Image of the Chesapeake Bay Impact Structure, NASA Langley Research Center, Hampton, Virginia

By Rufus D. Catchings,[1] David S. Powars,[2] Gregory S. Gohn,[2] and Mark R. Goldman[1]

Abstract

A 1-kilometer-long (0.62-mile-long) seismic reflection and refraction profile collected at the National Aeronautics and Space Administration (NASA) Langley Research Center, Hampton, Va., provides a detailed image of part of the annular trough of the buried, 35-million-year-old Chesapeake Bay impact structure. This profile passes within 5 meters (m; 16.4 feet (ft)) of a 635.1-m-deep (2,083.8-ft-deep), continuously cored and geophysically logged test hole at the Langley Center (the USGS-NASA Langley corehole). High-resolution seismic-reflection images (having a common-depth-point spacing of 2.5 m (8.2 ft)) of the upper 1,000 m (3,281 ft) along the seismic profile were generated by using refraction velocities and corehole sonic velocities to convert from time sections to depth sections.

Time-distance, unmigrated depth-distance, and migrated depth-distance images show lateral variations in the geologic units observed in the USGS-NASA Langley corehole. A high-amplitude reflection at 630 to 625 m (2,067 to 2,051 ft) depth on the migrated depth image correlates with the top of weathered granite (the Langley Granite) at 626.3 m (2,054.7 ft) in the Langley core. Additional high-amplitude reflections below that depth likely represent a weathering profile developed in the upper part of the granite. Diffractions on the unmigrated images suggest that the granite contains numerous inhomogeneities that may consist of mineral veins and mineralized faults and fractures, as seen in the granite cores.

Above the granite, crater unit A (minimally to moderately disturbed sands and clays of the Cretaceous Potomac Formation) is characterized by semicontinuous, horizontal and moderately inclined reflections that are broken by pervasive, subvertical, small-offset faults. Sediments of the lower beds of crater unit A below 558.1 m (1,831.0 ft) in the core have horizontal bedding and are nearly pristine. Above that depth, the upper beds of crater unit A contain thick fluidized sand intervals and fractured clay-silt beds. The contact between the granite and crater unit A is essentially horizontal on the migrated depth profile and shows minor relief produced by a few steeply dipping faults.

Above crater unit A, the lower beds of crater unit B are lithologically similar to the upper beds of crater unit A and display similar impact-generated deformation. In the migrated depth image, crater unit A and the lower beds of crater unit B are combined into one unit. A thin zone (0.3 m (1.0 ft) thick) of injected glauconitic sediment at the base of the lower beds (at 442.5 m (1,451.7 ft) depth) is the only occurrence of exotic material in the lower beds of crater unit B in the core.

The upper beds of crater unit B (above 427.7 m (1,403.3 ft) depth) are represented by discontinuous, locally weak, isolated, or inclined reflections on the migrated depth image. In the core, the upper beds of crater unit B are divided into megablocks and megablock zones that consist of fragmented sediments of the Potomac Formation. The megablocks are separated by matrix zones that consist of smaller blocks of sediments of the Potomac Formation suspended in a matrix of native disaggregated sediments of the Potomac Formation and injected, exotic disaggregated, glauconitic Upper Cretaceous and lower Tertiary marine sediments. Angular relationships and offsets of reflections across the high-relief contact between the upper beds of crater unit B and the underlying combined crater unit A and the lower beds of crater unit B suggest that the contact is a dip-slip fault locally.

Above a contact with crater unit B at a depth of 269.4 m (884.0 ft), the Exmore beds are represented by strong, continuous and discontinuous, overstepping reflections that suggest division of the Exmore into four laterally discontinuous depositional subunits. Two of these subunits are present near the Langley corehole on the seismic images and are recognized in the core (Gohn and others, this volume, chap. C). In the Langley core, the Exmore beds consist of clasts of Cretaceous and Tertiary preimpact sediments and cataclastic, shocked,

[1]U.S. Geological Survey, Menlo Park, CA 94025.
[2]U.S. Geological Survey, Reston, VA 20192.

pre-Mesozoic igneous rocks suspended in a matrix of calcareous, muddy, quartz-glauconite sand and granules that contains shocked quartz.

The dipping, truncated, and disrupted reflections within crater units A and B are interpreted to represent a 550-m-wide (1,805-ft-wide), stratabound collapse structure. This structure does not affect the underlying basement granite or the lower beds of crater unit A, nor does it affect the base of the Exmore beds above crater unit B. The collapse structure is not bounded laterally by major normal faults. Instead, structural displacements appear to be distributed among abundant short, small-offset faults and intervals of fluidized sediment. Fluidized sands above 558 m (1,831 ft) depth in crater unit A are interpreted as a low-strength zone that accommodated the widespread, late-stage, gravitational collapse of the impact structure. The proposed Langley collapse structure may be analogous to stratabound grabens in the outer zone of the Silverpit crater (North Sea).

The Exmore beds are interpreted as impact-generated, ocean-resurge deposits. The upper contact of the Exmore section is a wavy, semicontinuous reflection that may represent large bedforms produced by resurge currents or returning impact-generated tsunamis, or it may represent the unmodified blocky or hummocky top of the final Exmore debris flow. Typically continuous, nearly horizontal reflections characterize the upper Eocene to Pleistocene postimpact section of dominantly marine sediments.

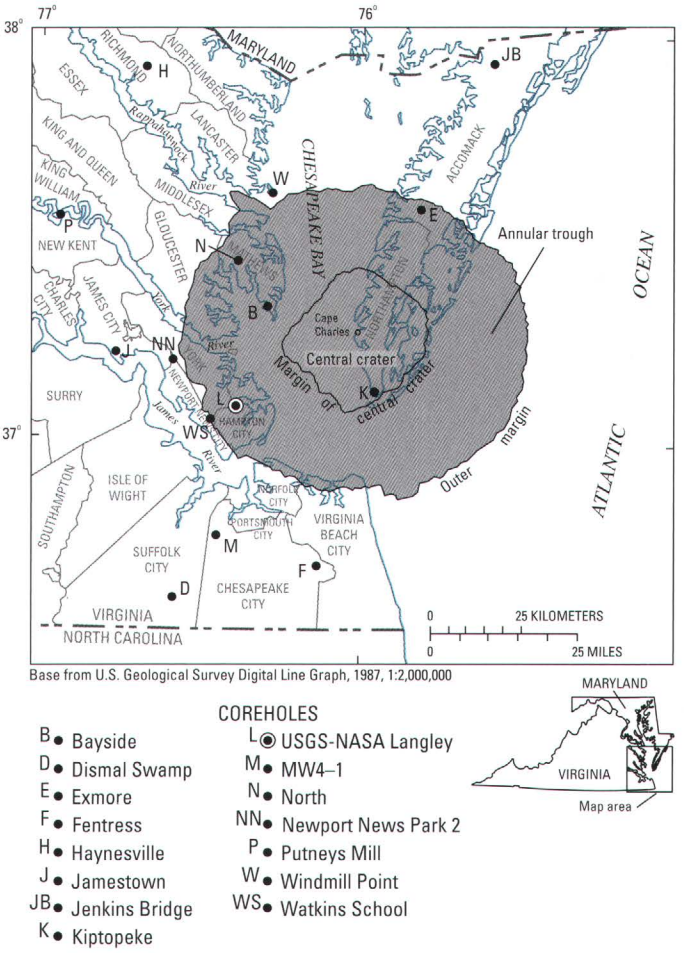

Figure I1. Regional map showing the location of the Chesapeake Bay impact structure, the USGS-NASA Langley corehole at Hampton, Va., and some other coreholes in southeastern Virginia. Locations of the central crater and outer margin are from Powars and Bruce (1999). Illustration modified from Powars, Johnson, and others (2002) and Edwards and Powars (2003).

Introduction

The Chesapeake Bay impact structure is among the largest and best preserved of the known impact craters on Earth (Poag, 1997). It is 85 kilometers (km; 53 miles (mi)) wide. This late Eocene structure lies buried beneath postimpact continental-margin sediments of the Virginia Coastal Plain and adjacent inner continental shelf (fig. I1) (Poag and others, 1994; Poag, 1997; Powars and Bruce, 1999). The center of the structure is beneath the town of Cape Charles, Va., on the Delmarva Peninsula.

Marine seismic-reflection surveys played a major role in the discovery and subsequent study of the Chesapeake Bay impact structure in the 1990s. Poag and others (1999) used over 1,200 km (746 mi) of multichannel and single-channel reflection profiles to interpret the location, major structures, and morphology of this complex crater (also see Poag and others, 1994; Poag, 1996, 1997; and Powars and Bruce, 1999). Stratigraphic and structural interpretations of the seismic profiles were substantially enhanced by the availability of stratigraphic and lithologic data from continuously cored test holes in nearby onshore areas (Powars and others, 1992; Powars and Bruce, 1999).

In 2000, the U.S. Geological Survey (USGS) and cooperating agencies (see "Acknowledgments") conducted a high-resolution seismic reflection and refraction survey and drilled a continuously cored test hole (the USGS-NASA Langley corehole) near the outer margin of the Chesapeake Bay impact structure on the York-James Peninsula (fig. I2). The objectives of these studies were to acquire the structural, stratigraphic, lithologic, petrologic, and hydrologic data needed to assess the effect of the impact structure on the regional ground-water flow regime and to infer the formative processes and geologic history of the impact structure (Gohn, Bruce, and others, 2001).

The seismic survey traversed the southern York-James Peninsula in a northeast to southwest direction at a high angle to the local trend of the impact structure's outer margin (fig. I2). The survey extended from the National Aeronautics and Space Administration (NASA) Langley Research Center on the northeast through the cities of Hampton and Newport News to the James River. The full length of the survey was 13.6 km (8.5 mi); however, substantial data gaps required by the densely populated urban setting reduced the actual surveyed distance to approximately 9 km (5.6 mi). To maintain straight-line

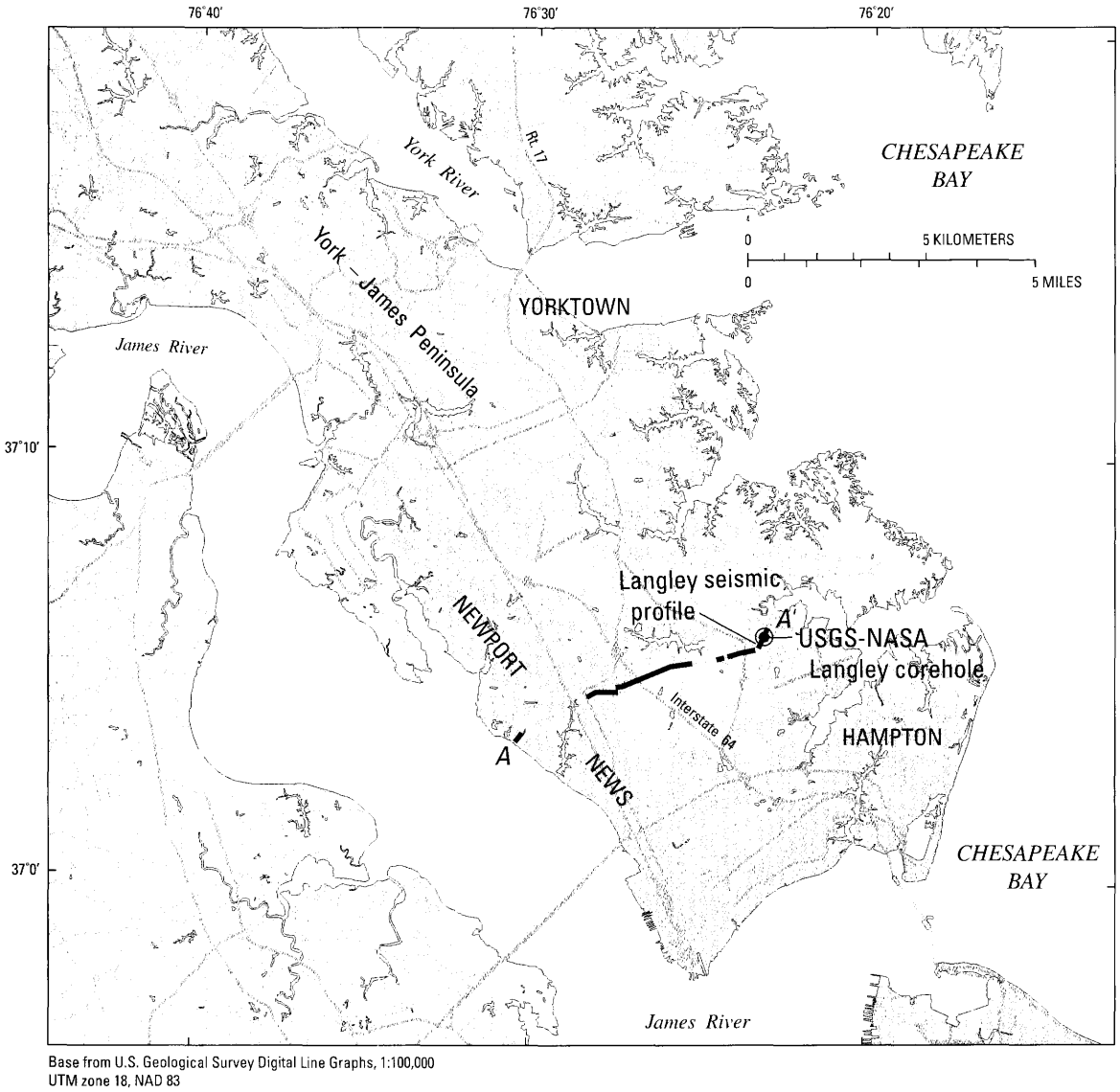

Figure I2. Map showing the location of the 1-km-long (0.62-mi-long) Langley seismic profile and the USGS-NASA Langley corehole in relation to the entire 13.6-km-long (8.5-mi-long) York-James seismic transect (*A*–*A*'). See figure I1 for the regional setting.

segments, the seismic transect was divided into nine individual seismic profiles that ranged in length from about 250 meters (m; 820 feet (ft)) to more than 2,650 m (8,694 ft, or 1.65 mi).

The USGS-NASA Langley corehole was completed to a total depth of 635.1 m (2,083.8 ft) at the NASA Langley Research Center (Gohn, Clark, and others, 2001; Powars and others, 2001). The corehole penetrated the full thickness of postimpact, impact-generated, and impact-modified sediments and bottomed in underlying granite (fig. I3). A single-transmitter, dual-receiver sonic tool was run the full length of the Langley corehole to record acoustic interval-transit times. The resulting sonic log provided much of the velocity information that was used to process the seismic-reflection data.

Core and geophysical-log depths originally were recorded in feet at the drill site. Core and log depths given in meters in this chapter are calculated from the corresponding measured depths in feet and are correlated with the seismic data, which were acquired in metric units.

This chapter presents a stratigraphic and structural interpretation of a 1-km-long (0.62-mi-long), seismic reflection and refraction profile surveyed across the NASA Langley Research Center (fig. I2). This survey passed through the Langley drill site within 5 m (16.4 ft) of the corehole, thereby providing the opportunity to integrate the core geologic data and corehole geophysical data with the seismic data. The Langley seismic profile is the northeasternmost segment of the 13.6-km-long (8.5-mi-long) York-James seismic survey.

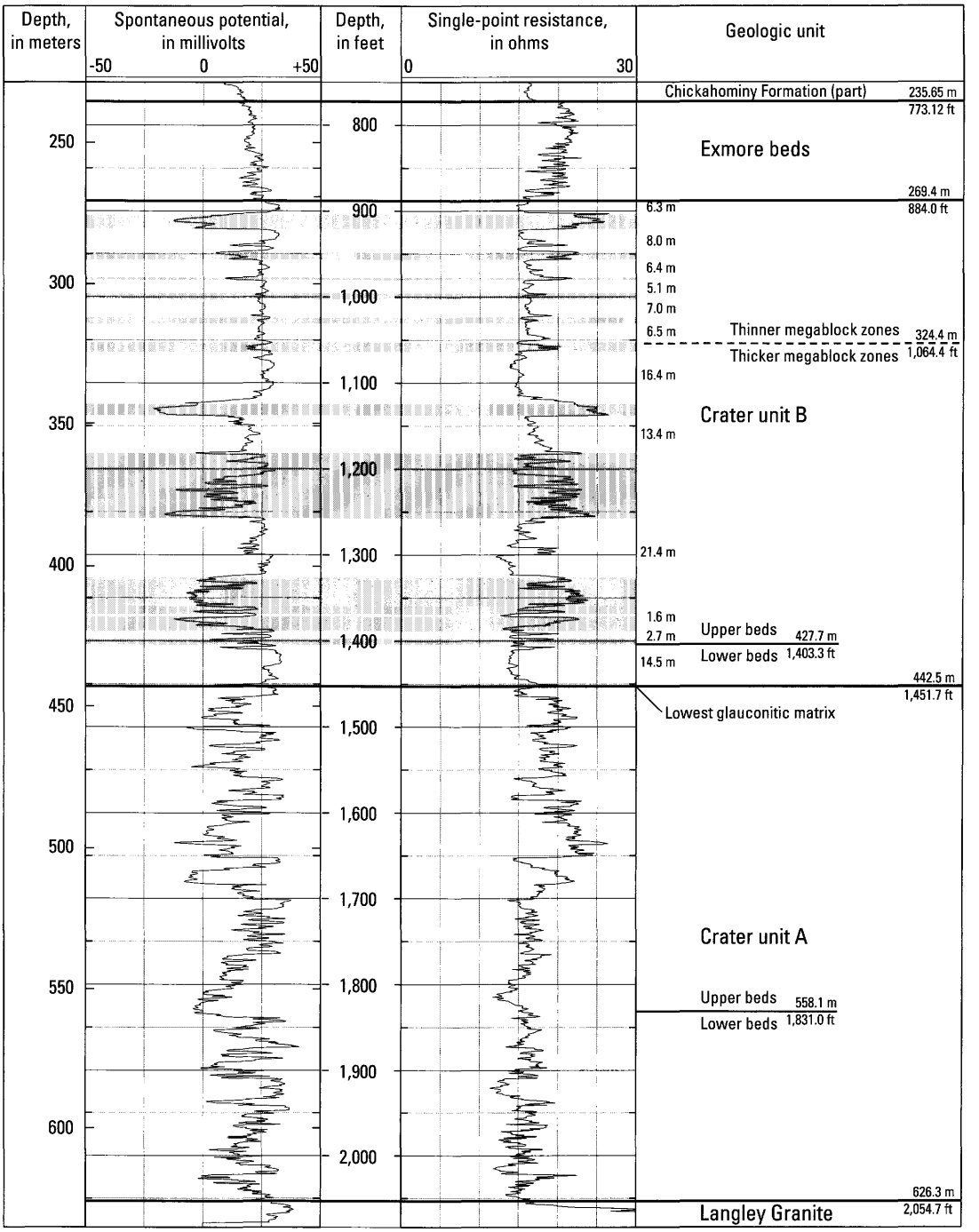

Figure I3. Summary geologic column and geophysical logs for the impact-modified sediments (crater units A and B) and impact-generated sediments (Exmore beds) in the USGS-NASA Langley core. Thicknesses of sediment megablocks in crater unit B are indicated. Shaded intervals are zones of injected glauconitic matrix in crater unit B. Figure from Gohn and others (this volume, chap. C, figs. C4 and C7).

Chesapeake Bay Impact Structure

The Chesapeake Bay impact structure is a complex crater developed in a multilayered marine target (Poag and others, 1994, 1999; Poag, 1997; Powars and Bruce, 1999; Powars, 2000). It was formed about 35 million years ago by the impact of a comet fragment or asteroid on the late Eocene continental shelf (fig. I1). Target materials below the atmosphere included an oceanic water column (<340 m (<1,115 ft) deep), a seaward-thickening Cretaceous and lower Tertiary sedimentary section (about 400 m to about 1,500 m (about 1,300 ft to about 4,900 ft) thick), and an underlying basement of igneous and metamorphic rocks (Poag, 1997; Powars and Bruce, 1999; Gohn and others, this volume, chap. C; Horton and others, this volume, chap. A, chap. B). The structure lies beneath a seaward-dipping and seaward-thickening wedge of postimpact, middle to upper Cenozoic sediments. The postimpact section is about 250 m (820 ft) thick on the lower York-James Peninsula (Powars and Bruce, 1999; Gohn and others, this volume, chap. C) and thickens eastward to at least 396 m (1,300 ft) at the southern tip of the Delmarva Peninsula (Powars and Bruce, 1999).

The average diameter of the Chesapeake Bay impact structure, as illustrated by Poag (1997), Poag and others (1999), and Powars and Bruce (1999), is about 85 km (53 mi). The outer margin bounds an approximately 25-km-wide (15.5-mi-wide) annular trough that surrounds the structure's 35-km-wide (22-mi-wide), complexly deformed central crater. The seismic profile discussed in this chapter is located within the southwestern part of the annular trough of the Chesapeake Bay impact structure and is referred to as the "Langley seismic profile" (or survey).

Seismic Survey

Data Acquisition

The Langley seismic survey was conducted entirely on the premises of the NASA Langley Research Center at Hampton, Va., in September 2000. The Langley profile is 1,000 m (3,281 ft) long and trends approximately northeast to southwest (fig. I2). Acquisition parameters are shown in table I1.

Seismic sources were generated by a combination of explosions and seisgun blanks. We used the larger explosive sources to ensure propagation of seismic energy in the urban Hampton-Newport News area. Explosions were generated by 0.11-kilogram (0.25-pound) charges of ammonium nitrate at depths of approximately 3 m (10 ft). The explosions were spaced approximately every 25 m (82 ft) along the seismic profile, except near cultural features. Most seismic sources were generated by 400-grain, 8-gauge Betsy Seisgun blanks at depths of about 0.3 m (1 ft). The seisgun sources were spaced every 5 m (16.4 ft); however, seisgun sources were not generated at the locations of explosion shots. Thus, the effective spacing for seismic sources (explosions and blanks combined) was 5 m (16.4 ft) along the seismic profile.

Shot timing for the 0.11-kilogram (0.25-pound) explosions was determined by synchronized master clocks that are accurate to approximately 1 millisecond (ms). The master clocks controlled both the shot timing and the turn-on times for the seismographs. Shot timing for the Betsy Seisgun sources was determined electronically at the seismic source when the hammer electronically closed contact with the Betsy Seisgun, which also sent an electronic signal to the seismographs. Seismic sources were co-located (at 1-m (3.3-ft) lateral offset) with the geophones so that uphole times also were available for timing. To maintain a consistent start time, we removed 2 ms and 20 ms from the uphole times of explosive and seisgun sources, respectively. The consistent start time and calculated static corrections allowed data from both types of sources to be stacked together.

The seismic sources were recorded on an array of four Geometrics Strataview RX–60 seismographs, each with 60 channels. Along the Langley seismic profile, the setup of the seismic acquisition array allowed for 202 shots and 202 recording sites (geophones), which allows for a theoretical fold of 202 when the data are stacked. All 202 recording sites were utilized; however, because of cultural features (such as roadways and pipelines), 15 shotpoints were not utilized, and the resulting actual maximum fold was 187. We used 40-hertz (Hz), single-element, vertical-component Mark Products L–40A geophones to record the seismic signal. Approximately 5 seconds (s) of data were recorded for each shot at a sampling rate of 0.5 ms. The data were stored on the hard drive of the Geometrics Strataview RX–60 computers during field acquisition and were later downloaded to 4-millimeter (mm) tape for permanent storage in SEG-Y format (Barry and others, 1975).

Prior to acquiring the data, we measured distances between shotpoints with a meter tape and prepared shotholes at those locations. Individual recording sites also were predetermined and flagged to obtain the proper spacing. After the data were acquired, we used a high-precision differential Global Positioning System to measure the recording sites and shotpoint locations to accuracies of approximately 0.01 m (0.03 ft).

Data Processing

The long offset (about 1,000 m (3,281 ft) maximum) and multiple sources permitted both reflection and refraction data to be simultaneously acquired. We used two types of seismic data processing—seismic-refraction tomographic inversion and reflection-image processing. In refraction-data processing, we used the tomographic inversion method developed by Hole (1992), whereby first arrivals on each seismic trace were modeled to obtain detailed velocities along the profile.

Table I1. Acquisition parameters for the Langley seismic profile, Hampton, Va.

[ft, feet; Hz, hertz; kg, kilograms; lb, pounds; m, meters; ms, milliseconds; s, seconds]

Parameter	Description
Profile length	1,000 m (3,281 ft)
Timing	Electronic
Seismic sources	
Overall shot spacing	5 m (16.4 ft)
Explosion spacing	25 m (82 ft)
Explosion depth	3 m (10 ft)
Explosion type	0.11-kg (0.25-lb) charge of ammonium nitrate
Seisgun spacing	5 m (16.4 ft)
Seisgun depth	0.3 m (1 ft)
Seisgun type	400-grain, 8-gauge Betsy Seisgun
Seismic recording data	
Geophone spacing	5 m (16.4 ft)
Geophone type	40-Hz, single-element, vertical-component Mark Products L–40A geophone
Recording system	Array of 4 Geometrics Strataview RX–60 seismographs, each with 60 channels
Number of active channels	202
Sample rate	0.5 ms
Acquisition filters	None
Trace length	5 s

Table I2. Processing parameters for the Langley seismic profile, Hampton, Va.

[ft, feet; Hz, hertz; m, meters; m/s; meters per second; ms, milliseconds]

Parameter	Description
Maximum fold	187
Common-depth-point spacing	2.5 m (8.2 ft)
Deconvolution	21 ms/200 ms
Automatic gain control (AGC)	
Prestack	300 ms
Poststack	100 ms
Bandpass filtering	
Prestack	25–50–600–1,200 Hz
Poststack	30–60–600–1,200 Hz
Frequency-distance (F-K) filtering	
F-K acceptance level	>1,000 m/s
F-K rejection level	1–200 Hz
Migration	
Angle	25°
Aperture	400 m
Frequency	400 Hz

Approximately 40,000 first arrivals were used to develop the velocity model, and all first-arrival measurements were checked for reciprocity between shot and receiver pairs. However, lower velocity sediments underlying higher velocity sediments at depths of about 50 m (164 ft) limited measurement of refraction velocities to the upper 50 m (164 ft). From about 50 m (164 ft) to about 635 m (2,083.3 ft), velocities were determined from the sonic velocity (interval transit time) log measured within the USGS-NASA Langley corehole located near the center of the seismic profile. The models are described in the next section.

Seismic-reflection data were processed by generally following the procedure outlined by Brouwer and Helbig (1998). Parameters used in processing are shown in table I2. Processing steps included the following: geometry installation, independent trace editing (to remove noisy traces or data from malfunctioning geophones), timing corrections, elevation static corrections, automatic-gain-control (AGC) bandpass filtering, frequency-distance (F-K) filtering, velocity analysis (from refractions and sonic log), normal-move-out correction, stretch muting, common-depth-point (CDP) stacking, Kirchoff prestack depth migration, poststack AGC, poststack bandpass filtering, poststack deconvolution, and time-to-depth conversion (for unmigrated data).

Seismic Data and P-Wave Velocity Models

All shots, whether seisgun or explosive, propagated the entire length of the recording array. A typical explosive shot record is shown in figure I4. Numerous clear reflections are observed from about 0 ms to about 700 ms, and first-arrival refractions are observed along the length of the Langley profile.

Compressional wave (P-wave) velocities in the upper 50 m (164 ft) range from about 800 meters per second (m/s; 2,625 feet per second (ft/s)) to about 1,700 m/s (5,577 ft/s) and are laterally continuous with minor variations (fig. I5*A*). A relatively low velocity gradient is apparent below about 50 m (164 ft) depth (fig. I5*B*).

Corehole sonic velocities were calculated from acoustic interval-transit times acquired approximately every 3 centimeters (0.1 ft) in the Langley corehole by the interval-transit-time

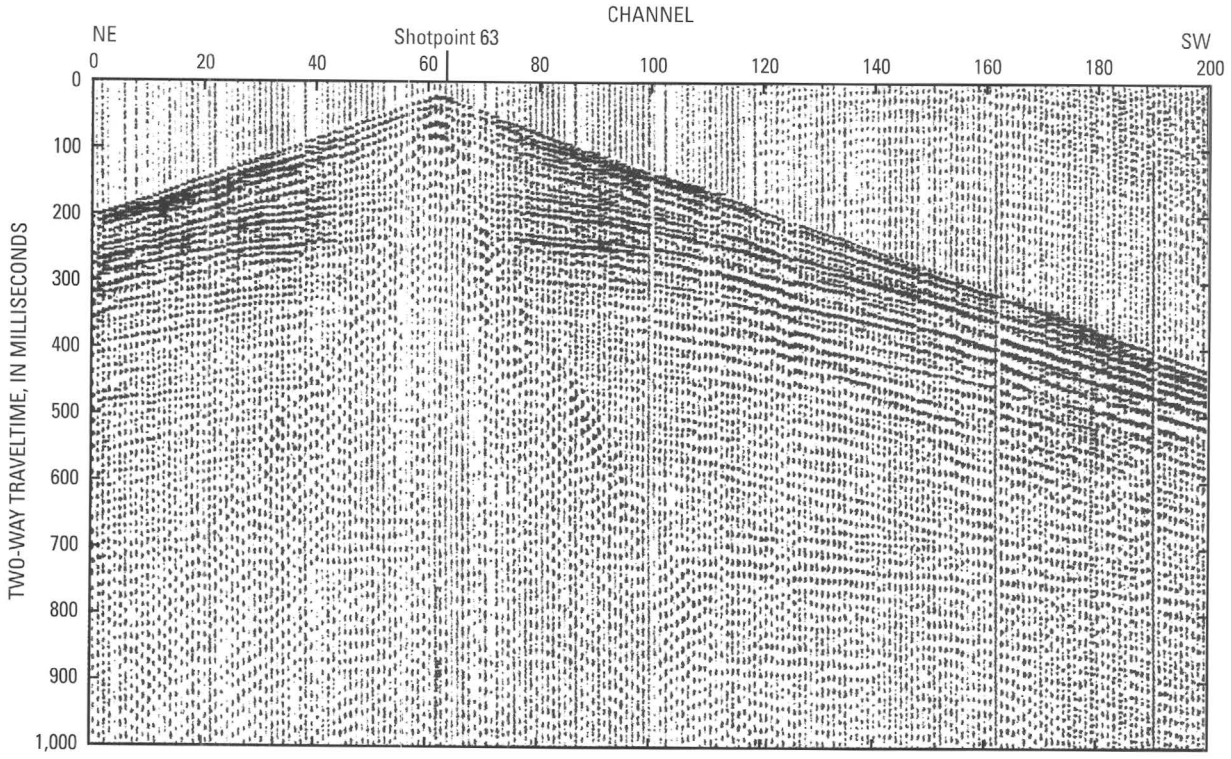

Figure I4. Explosion shot gather at shotpoint 63 from the Langley seismic profile showing the reflective nature of the subsurface from the surface to about 700 ms and the clear first-arrival refractions. A channel was located at each shotpoint.

sonde (fig. I5*B*). Appreciable scatter in the data suggests a range of velocities at all depths and (or) measurement errors that likely resulted in part from "cycle skipping" produced by excessive signal attenuation. We selected representative velocities within the range of scatter as shown in figure I5*B*.

In general, the sonic measurements suggest that velocities are relatively low (less than 2,500 m/s, or 8,202 ft/s) for most of the subsurface above basement. The data show a high-velocity cap at about 50 to 62 m (164 to 203 ft) depth, where velocities range from about 2,500 m/s (8,202 ft/s) to about 3,000 m/s (9,843 ft/s). From about 60 m (197 ft) to about 140 m (459 ft) depth, average velocities range between about 1,500 m/s (4,921 ft/s) and about 2,000 m/s (6,562 ft/s), and the overall trend is toward a slight negative gradient. This lower velocity or the negative gradient limits the surface-based refraction measurements. From about 140 m (459 ft) to about 180 m (591 ft) depth and from about 235 m (771 ft) to 275 m (902 ft) depth, relatively higher velocities also are observed (about 2,000 to 2,200 m/s, or 6,562 to 7,218 ft/s), but these velocities are generally lower than those at 60 m (197 ft) depth. The relatively low velocities between about 60 m (197 ft) depth and crystalline basement near 625 m (2,051 ft) depth prevent surface-based refracted energy from returning to the surface. In crustal-scale refraction seismology, lower velocity materials that underlie higher velocity materials are commonly referred to as low-velocity zones, shadow zones, or velocity inversions.

Seismic-Reflection Images

We stacked shot gathers along the Langley profile to produce seismic-reflection images of the upper 1,000 m (3,281 ft) of section. Common-depth-point (CDP) traces are located every 2.5 m (8.2 ft) along the seismic profile. Time-distance, unmigrated depth-distance, and migrated depth-distance plots were generated (figs. I6, I7, and I8). Depths were calculated by assuming the velocity profile shown in figure I5. The data are plotted as positive polarity.

Vertical resolution of the seismic images depends on the velocities and frequencies used to generate the images. Velocities generally range from about 800 m/s (2,625 ft/s) to about 3,000 m/s (9,843 ft/s) in the upper 600 m (1,969 ft), and frequencies range from about 30 to 600 Hz. When the one-quarter wavelength criteria (Waters, 1981) are used, the minimum thickness of imaged reflectors ranges between about 1 m (3.3 ft) and 15 m (49.2 ft).

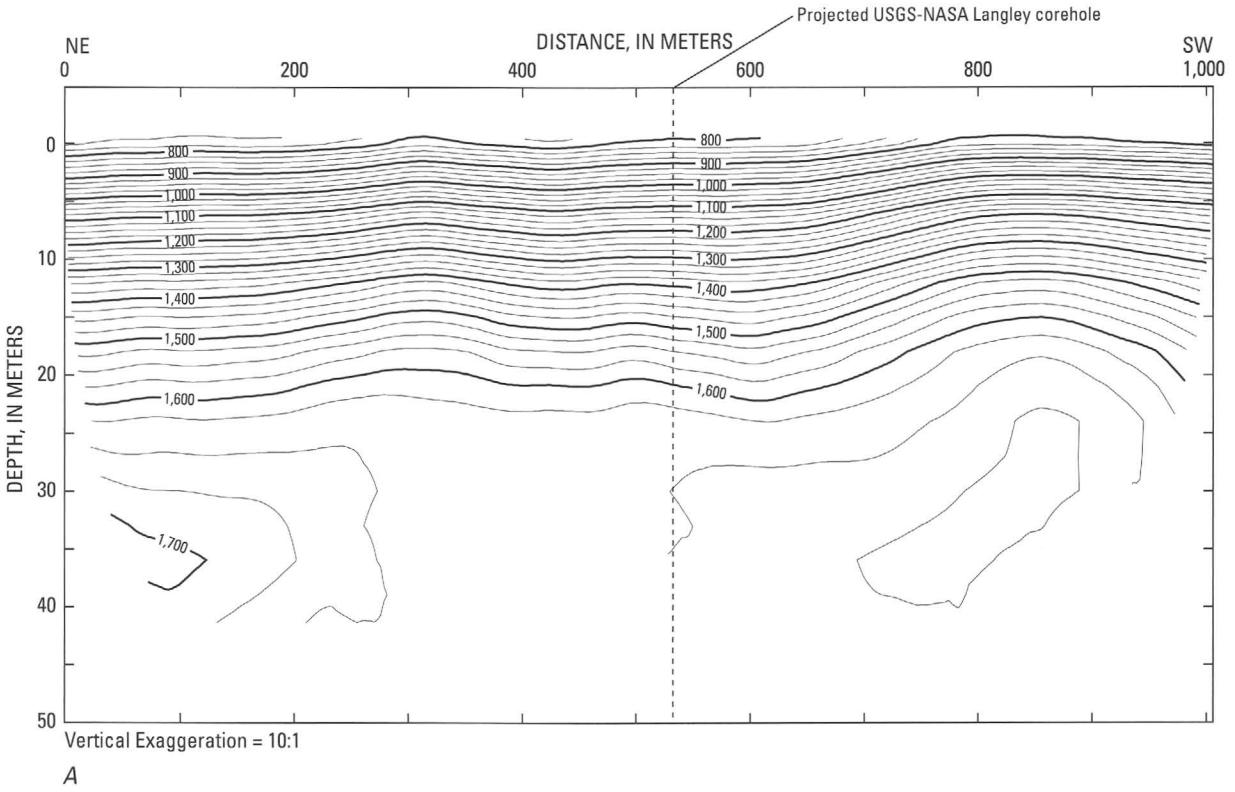

Figure I5. Velocity model from the Langley seismic profile and velocity log from the USGS-NASA Langley corehole. *A,* Two-dimensional velocity model along the Langley profile derived from inversion of first-arrival refractions. Contours show P-wave velocities in meters per second. *B,* One-dimensional velocity model (solid line) derived from the sonic velocity (interval transit time) log collected in the Langley corehole. The left track displays every second data point in the corehole dataset. The right track displays every tenth data point in the dataset. The stratigraphy of the corehole section is shown on the left: Ple, Pleistocene; DC, Drummonds Corner beds; NP, Neoproterozoic; LG, Langley Granite.

The three seismic images show numerous reflections across their full depth of 1,000 m (3,281 ft). Reflections above 635.1 m (2,083.8 ft) depth are correlated with the geologic units identified in the USGS-NASA Langley core (Gohn and others, this volume, chap. C; Poag and Norris, this volume, chap. F; Powars and others, this volume, chap. G).

Time-distance image.—Numerous reflections are observed along the Langley profile from about 25 ms to about 740 ms (fig. I6). Although the entire section is reflective above 740 ms, the nature of the reflections varies appreciably within differing time intervals. Laterally continuous reflections are particularly pronounced from about 25 ms to 50 ms and from about 200 ms to about 400 ms. However, reflections between about 400 ms and about 670 ms are largely laterally discontinuous, except for several clear southwest-dipping reflections on the northeastern half of the profile and less obvious northeast-dipping reflections on the southwestern half of the profile. The fewest laterally coherent reflections occur from about 740 ms to about 1,000 ms.

Most reflections above 670 ms indicate slight vertical displacement along the profile, and small diffractions are apparent on the section. An apparent vertical offset in reflections at 700 ms (meter 550 of the profile) also shows diffracted energy originating at the location of the offset. Such diffractions usually can be attributed to lateral velocity variations caused by faulting and fracturing that result in abrupt truncations of layers (Anstey, 1977).

Unmigrated depth-distance image.—We converted the time-distance seismic image (fig. I6) to an unmigrated depth-distance seismic image (fig. I7) by using the combined refraction and sonic velocity model (fig. I5). In stacking, velocities in the upper 50 m (164 ft) varied laterally as determined by the refraction velocity model, but we used laterally constant velocities from the sonic log below 50 m (164 ft) depth. The depth-distance image shows laterally continuous reflections in the depth ranges from about 0 m to 50 m (about 0 ft to 164 ft), 150 m to 325 m (about 492 ft to 1,066 ft), and 625 m to 800 m (about 2,051 ft to 2,625 ft). From about 325 m to about 625 m (about 1,066 ft to about 2,051 ft) depth, the subsurface is less reflective, and reflections are laterally discontinuous. Southwesterly and northeasterly dipping reflections also are apparent, as observed in the time section (fig. I6). Reflections below about 625 m (2,051 ft) appear much thicker and higher in amplitude than those higher

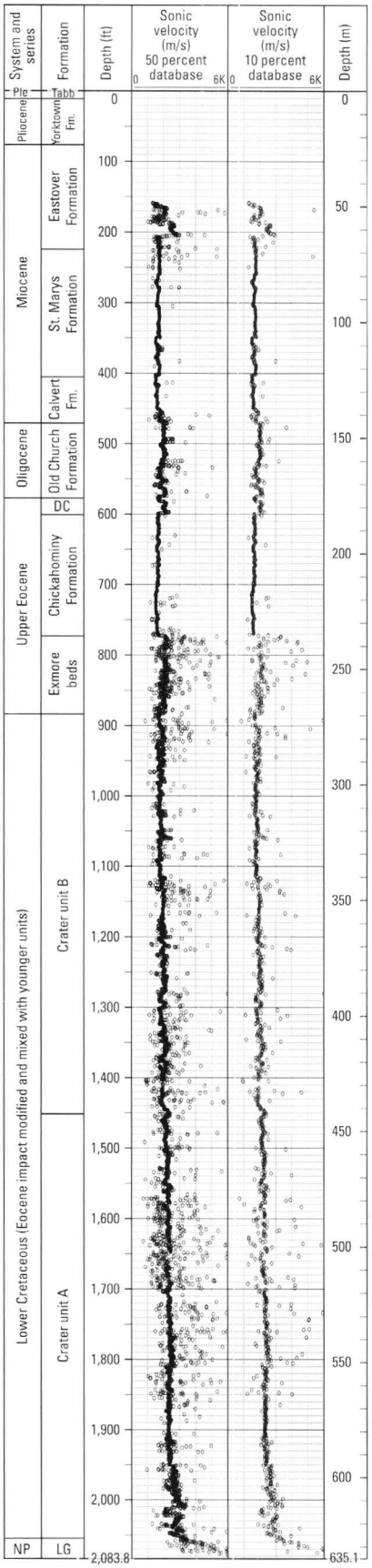

B

Figure I5. Continued.

in the section. Slight vertical offsets are apparent, as observed on the time section, and these offsets correlate with diffracted energy, suggestive of faulting and fracturing.

Migrated depth-distance image.—We used Kirchoff prestack depth migration to collapse the diffracted energy observed on the time and depth sections. The resulting migrated depth-distance section (fig. I8) shows much the same reflectivity pattern as the unmigrated depth section (fig. I7); however, numerous small offsets in reflectors are apparent where the diffracted energy was collapsed. Although there are some small offsets in layers above about 325 m (1,066 ft) depth and at 625 m (2,051 ft) depth, a far greater number of small offsets (faults or fractures) are observed from about 325 m to about 625 m (about 1,066 ft to about 2,051 ft) depth. Migration also shows that the dipping reflections between 325 m and 625 m (1,066 ft to 2,051 ft) depth merge into subhorizontal reflections near the northeastern and southwestern ends of the profile. Migration allows a more accurate placement of the top of basement.

Geologic Interpretation of Seismic Images

Coastal Plain Basement

We interpret the top of basement rocks as the nearly continuous, wavy, high-amplitude reflection that varies in depth between 630 m and 625 m (2,067 ft and 2,051 ft) on the migrated depth image (figs. I9, I10, and I11). These depths are in good agreement with the top of weathered granite found at 626.3 m (2,054.7 ft) depth in the Langley core (fig. I3); this granite is named the Langley Granite by Horton and others (this volume, chap. B). Granite was recovered to the bottom of the Langley corehole at a depth of 635.1 m (2,083.8 ft). This cored section consists of variably weathered, pale-red, medium-grained, homogeneous granite of Neoproterozoic age (Horton and others, this volume, chap. B).

The time-distance and depth-distance sections (figs. I6 and I7) show at least three major reflections at and below the top of the granite. We interpret the shallowest reflection as the sediment-weathered rock contact, the second reflection as the weathered rock-to-unweathered rock transition, and the third reflection as a reverberation arising from the weathered and unweathered contacts. These reflections are widely spaced on the unmigrated and migrated depth sections because of the high basement velocities used to convert from time to depth. This interpretation suggests that the weathered rock is about 40 m (131 ft) thick. The recovered 8.9-m-long (29.1-ft-long) granite core is strongly weathered and crumbly in its upper part but grades down to partially weathered, hard granite in the basal 0.9 m (3 ft) of the core (Horton and others, this volume, chap. B). Weathering along mineral veins and mineralized fractures and faults observed in the core (Horton and others, this volume, chap. B) may be a contributing factor to the large thickness of the weathering zone inferred from the seismic images.

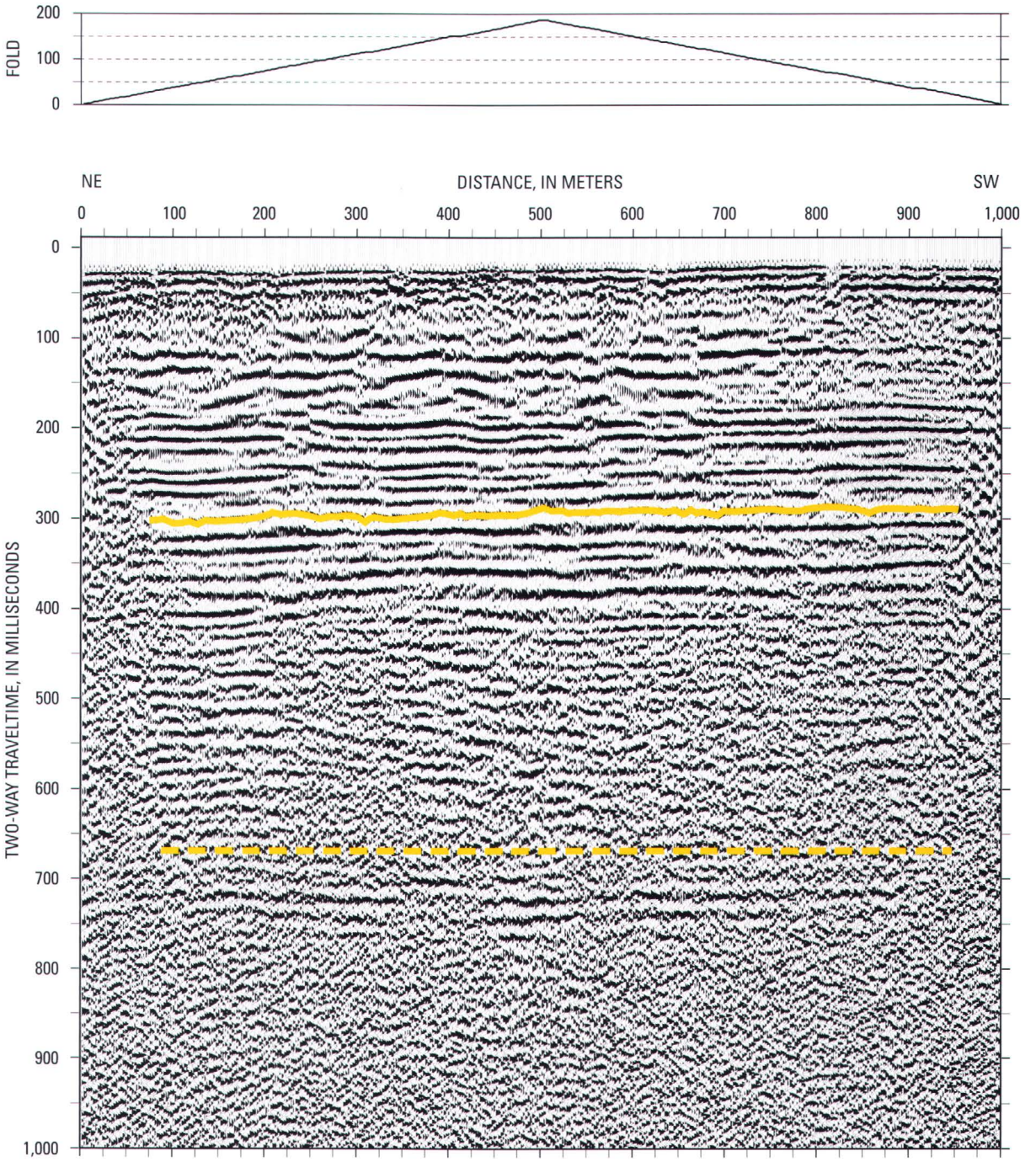

Figure I6. Time-distance seismic-reflection image for the Langley profile. The lower highlighted boundary (at about 670 ms) is between crystalline basement rocks (the Langley Granite in the USGS-NASA Langley core) and overlying preimpact sediments. The upper highlighted boundary (at about 300 ms) is between preimpact and synimpact sediments and overlying postimpact sediments. The seismic sources were energetic enough to provide signals from depths of about 1 km (0.6 mi) along part of the seismic profile with a fold of only 1.

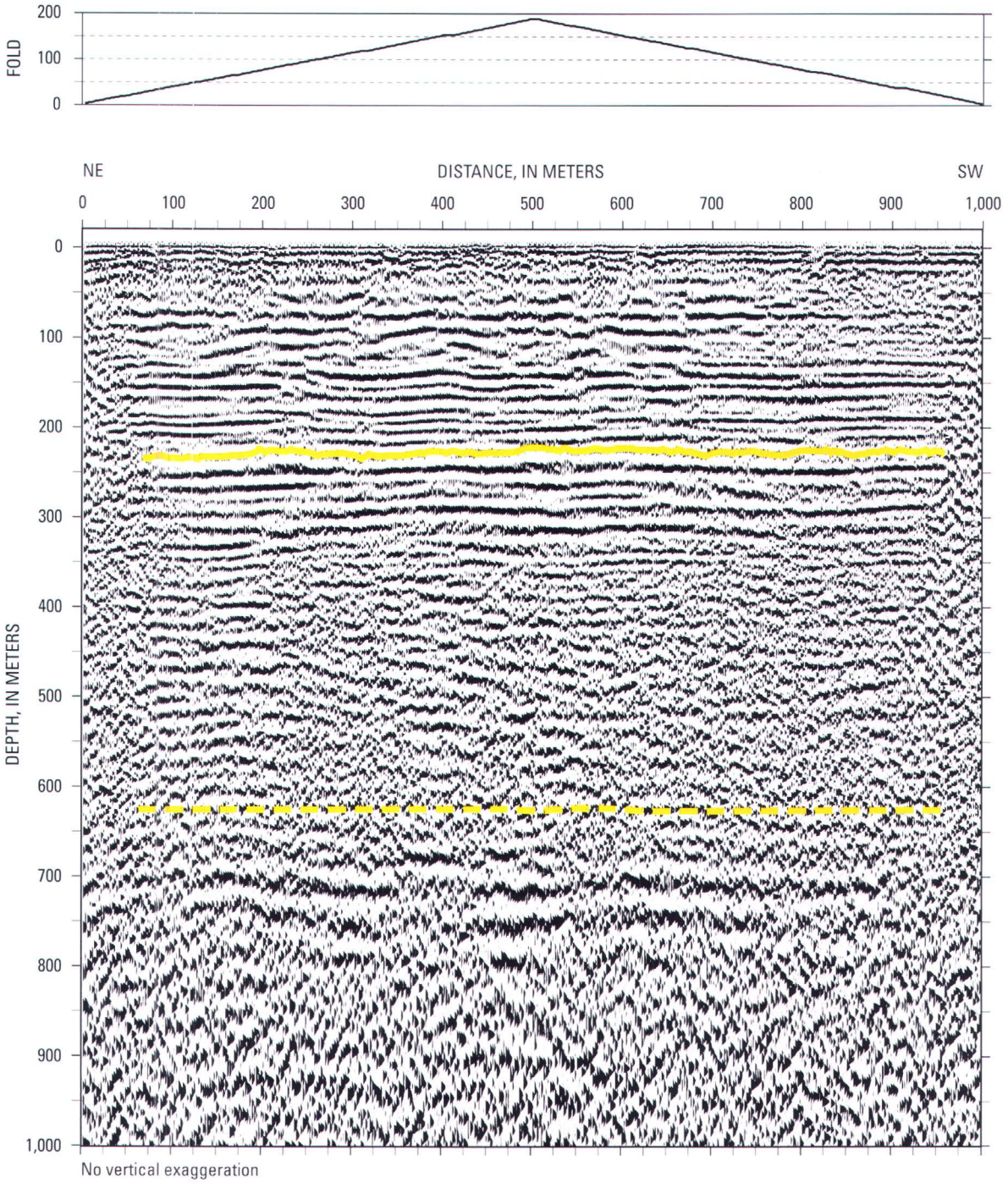

Figure I7. Unmigrated depth-distance seismic-reflection image for the Langley profile. The lower highlighted boundary (at about 625 m, 2,051 ft) is between crystalline basement rocks (the Langley Granite in the USGS-NASA Langley core) and overlying preimpact sediments. The upper highlighted boundary (at about 240 m, 787.4 ft) is between preimpact and synimpact sediments and overlying postimpact sediments.

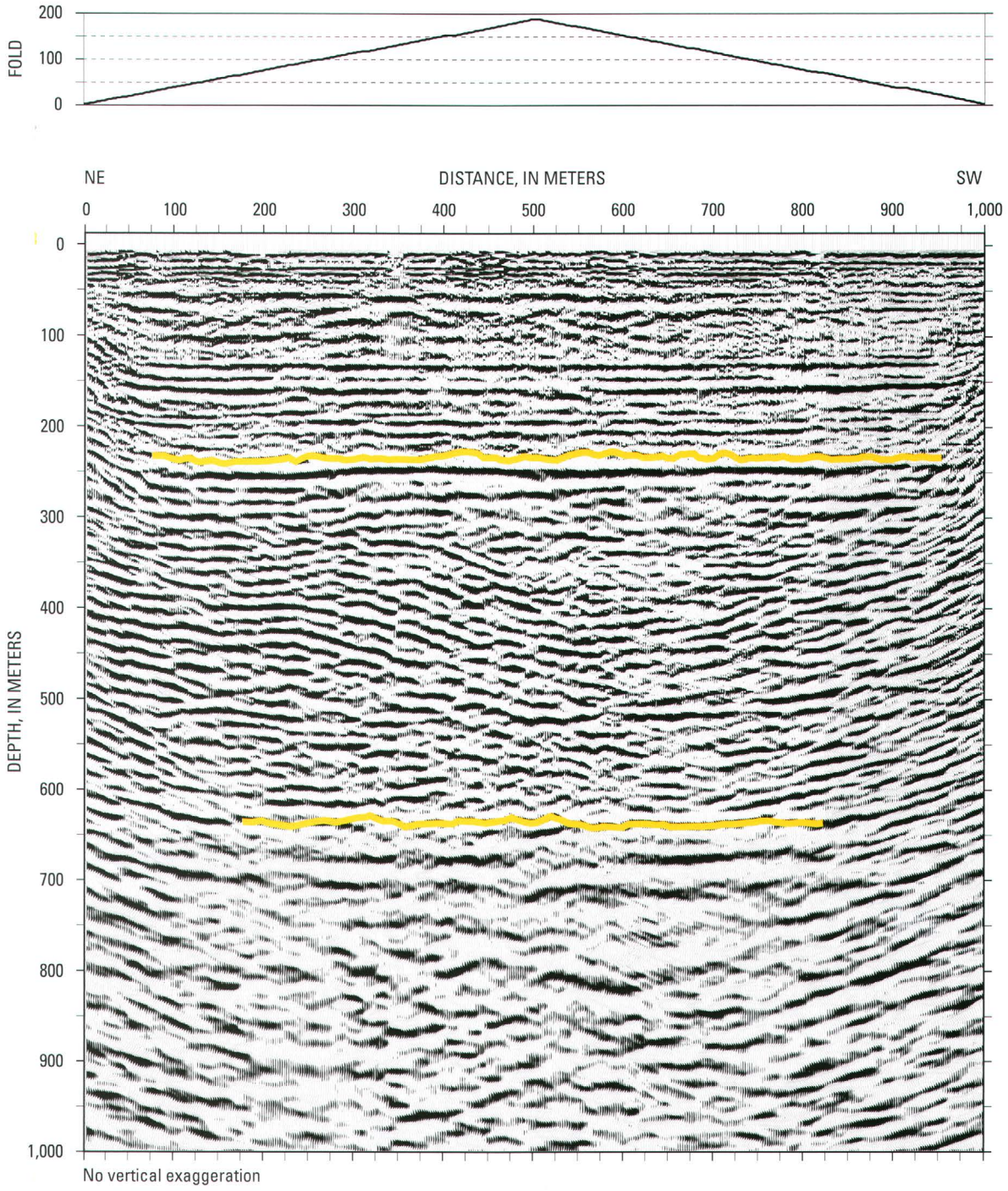

Figure I8. Migrated depth-distance seismic-reflection image for the Langley profile. Highlighted boundaries as in figure I7. Migration allows a more accurate placement of the top of basement than in the unmigrated section.

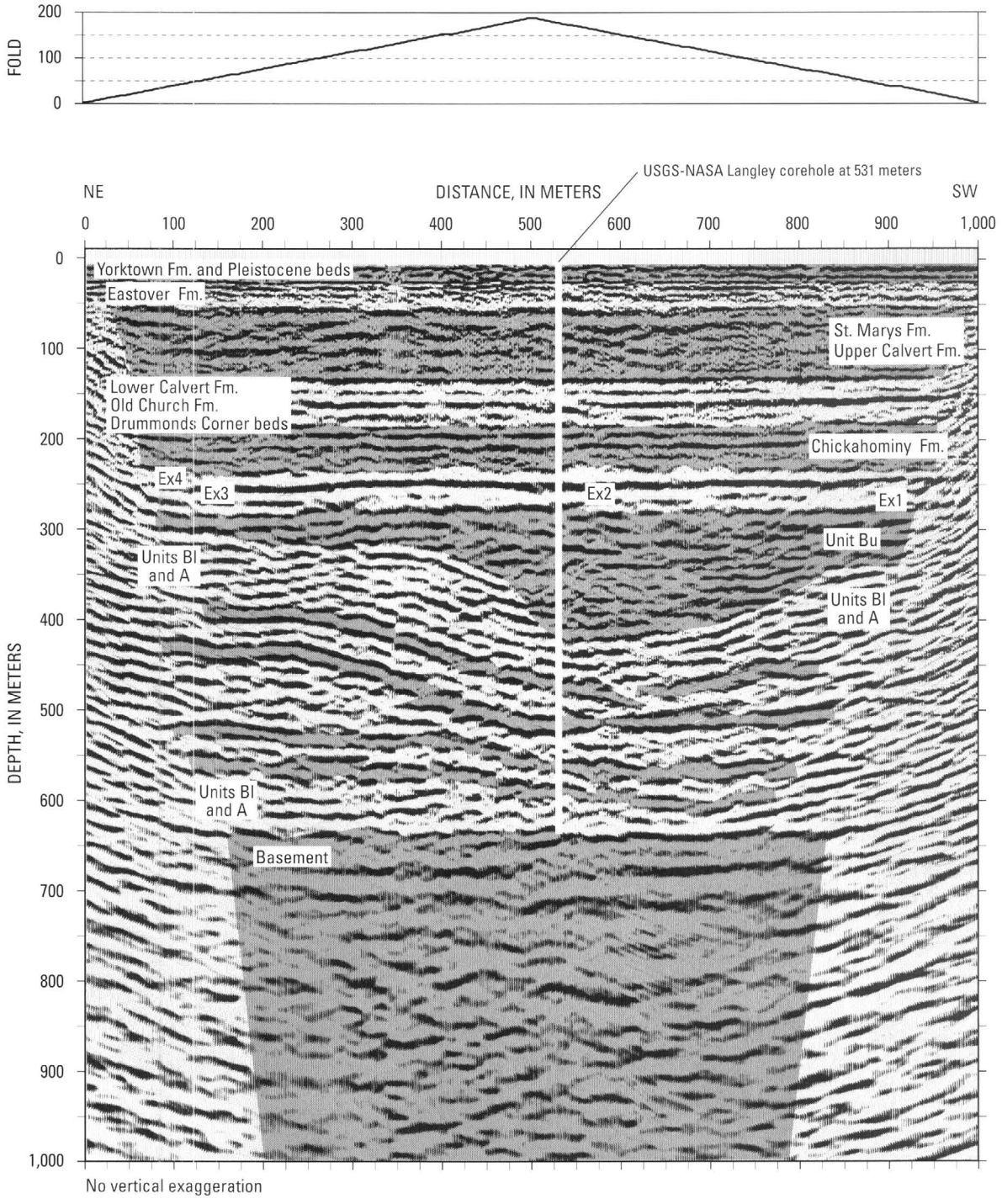

Figure I9. Interpreted migrated depth image for the Langley profile showing the major impact-related and postimpact seismic-stratigraphic units discussed in the text. Unit designations: A, crater unit A; BI, lower beds of crater unit B; Bu, upper beds of crater unit B; Ex1, Ex2, Ex3, and Ex4, seismically defined subunits of the Exmore beds; Fm., formation.

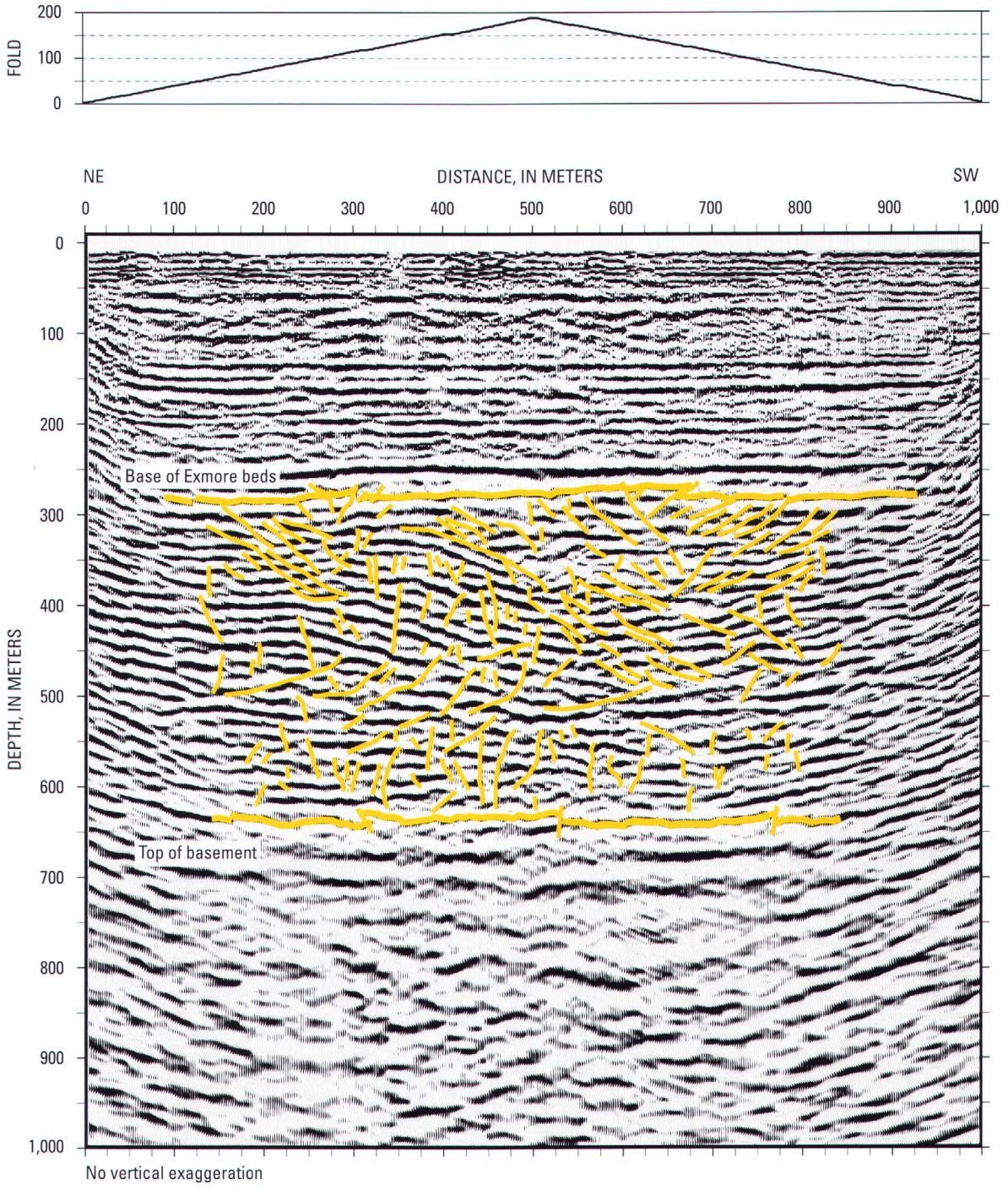

Figure I10. Interpreted migrated depth image for the Langley profile showing the distribution of small-offset faults (short yellow lines) in crater units A and B between highlighted boundaries representing the top of basement rocks and the base of the Exmore beds.

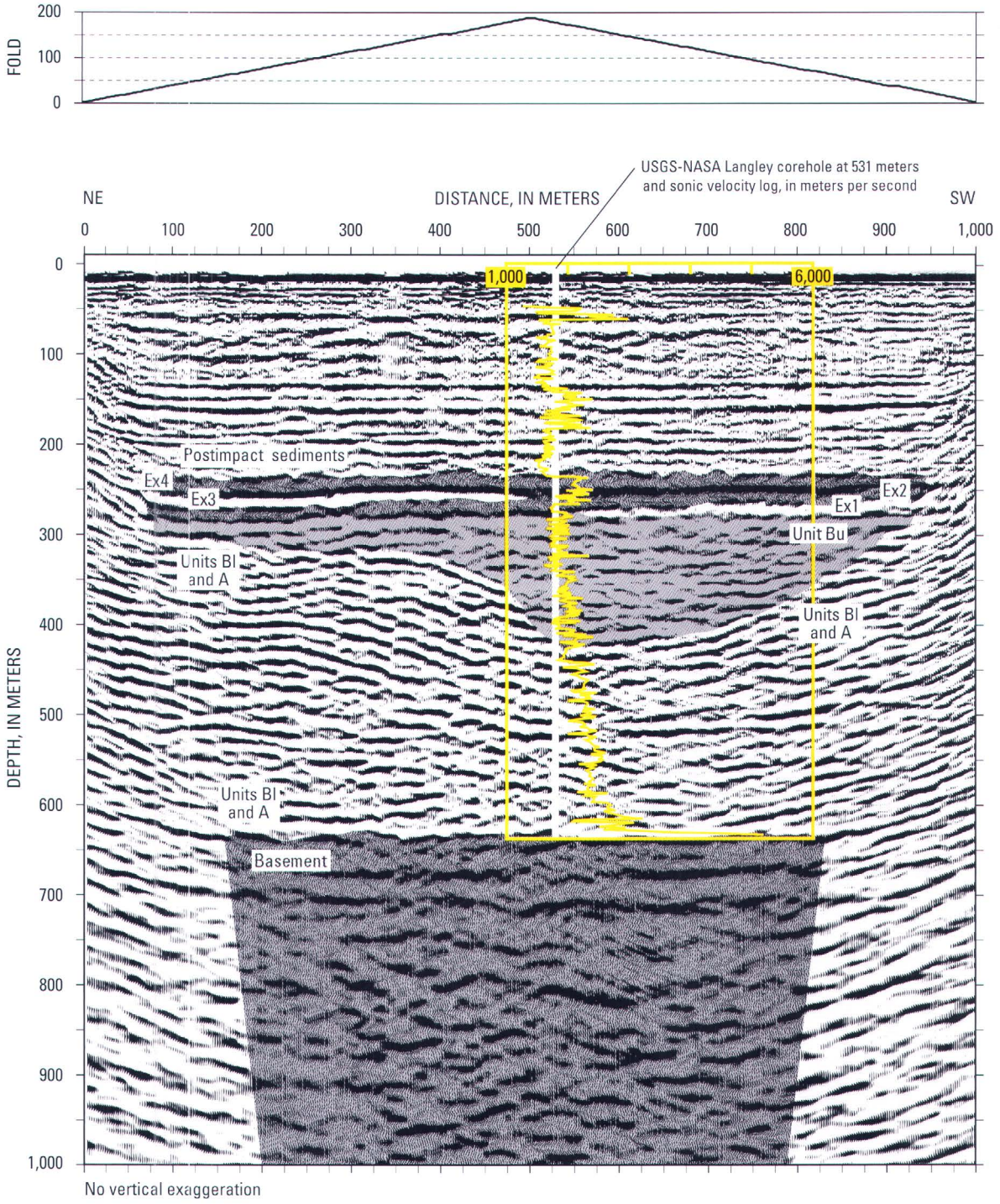

Figure I11. Interpreted migrated depth image for the Langley profile showing the seismic-stratigraphic units and generalized sonic velocity data acquired in the USGS-NASA Langley corehole (fig. I5*B*). Sonic velocities range from about 1,500 to about 5,500 meters per second (m/s). Note that the seismically defined subunits of the Exmore beds (Ex1, Ex2, Ex3, and Ex4) are variably shaded.

Horizontal, discontinuous, wavy, high-amplitude reflections characterize most of the basement section on the migrated depth image (fig. I9). Diffractions on the time-distance and depth-distance images (figs. I6 and I7) suggest that the basement section contains numerous inhomogeneities. In addition, inferred high-angle faults of uncertain extent displace the top of basement by less than 10 m (33 ft) at several places on the migrated depth image (fig. I10).

The granite core from the Langley corehole is too short to address the source of the horizontal, wavy reflections. However, the common mineral veins and mineralized fractures and faults in the core dip at all angles from vertical to horizontal and could be the source of the diffractions seen on the unmigrated images (Horton and others, this volume, chap. B). The granite is assumed to extend significantly below the base of the rocks depicted in the seismic images.

Impact-Modified Sediments

Core Stratigraphy

The impact-modified sedimentary section in the Langley core primarily consists of Lower Cretaceous and basal Upper Cretaeous fluvial sediments of the Potomac Formation. This variably deformed section is divided informally into crater unit A and overlying crater unit B (Frederiksen and others, this volume, chap. D; Gohn and others, this volume, chap. C). The unit contact is placed at the base of the lowest occurrence of injected exotic glauconitic sediments at 442.5 m (1,451.7 ft) depth (fig. I3). The contact between crater unit B and the overlying Exmore beds is placed at a depth of 269.4 m (884.0 ft). Reflections within crater units A and B (figs. I6, I7, I8, I9, and I10) are interpreted to represent primary bedding within the Potomac Formation.

Crater unit A is divided into two subunits in the Langley core—the lower beds and the upper beds (Gohn and others, this volume, chap. C). The subunit contact is placed at a depth of 558.1 m (1,831.0 ft) (fig. I3). The lower beds consist of nearly pristine sands, silts, and clays of the Potomac Formation, in which primary horizontal stratification is well preserved, clay-silt beds are only moderately fractured, and primary sedimentary structures and cycles typical of the Potomac Formation outside the impact structure are intact. In the upper beds, however, zones of structureless fluidized sand up to 17 m (55.8 ft) thick and strongly fractured clay-silt layers are present locally. Crater unit A does not contain igneous-rock or sediment ejecta, shocked quartz grains, or exotic preimpact Tertiary sediments (Gohn and others, this volume, chap. C; Horton and Izett, this volume, chap. E).

Crater unit B also is divided informally into lower beds and upper beds; the contact is at 427.7 m (1,403.3 ft) depth (fig. I3). The lower beds consist of locally fluidized and fractured sediments of the Potomac Formation similar to those found in the upper beds of crater unit A. Exotic injected glauconitic sediments are present only in a 0.3-m-thick (1.0-ft-thick) zone at the base of the lower beds of crater unit B (fig. I3).

The upper beds of crater unit B in the core consist of megablocks (1 m to 25 m (3.3 ft to 82.0 ft) in diameter) and megablock zones (intervals of multiple megablocks with block-on-block contacts) of fragmented sediments of the Potomac Formation (Gohn and others, this volume, chap. C). Fractures and steeply dipping primary stratification are common within the megablocks and indicate postdepositional movement and rotation.

The megablocks and megablock zones are separated by intervals consisting of blocks of sediment of the Potomac Formation (4 mm to 1 m (0.16 inch to 3.3 ft) in diameter) suspended in a muddy, sandy, and gravelly matrix of native disaggregated sediments of the Potomac Formation and downward-injected, exotic, disaggregated, glauconitic Upper Cretaceous and Tertiary marine sediments. Gohn and others (this volume, chap. C) refer to these lithologically heterogeneous intervals as matrix zones. The presence of exotic Upper Cretaceous and Tertiary marine sediments is inferred from the large amount of glauconite sand in the matrix zones; glauconite is very sparse in the Potomac Formation but is very common in the preimpact Upper Cretaceous and Tertiary sections (Powars and Bruce, 1999; Gohn and others, this volume, chap. C). Shocked quartz has not been found in the upper beds of crater unit B, except in one piece of igneous-rock ejecta found near the top of the unit, and exotic lithoclasts of preimpact Upper Cretaceous and Tertiary marine sediments are absent (Gohn and others, this volume, chap. C; Horton and Izett, this volume, chap. E).

Seismic Images

Semicontinuous, horizontal and moderately dipping reflections between depths of about 625 m (2,051 ft) and about 420 m (1,378 ft) near the corehole represent crater unit A and the lower beds of crater unit B (unit Bl) of the Langley core (figs. I3 and I9). Thicker combined sections of these units are present northeast and southwest of the corehole.

Horizontal reflections in crater units A and Bl near the northeastern end of the profile dip to the southwest at moderate apparent angles beginning between meters 250 and 300 of the distance scale and continuing past meter 500 to the vicinity of the corehole, where their dip angles generally flatten (fig. I9). Similarly, subhorizontal reflections in crater units A and Bl near the southwestern end of the profile dip to the northeast at moderate apparent angles beginning near meters 750 to 800 of the seismic profile (distance scale) and continuing to near the corehole, where their dip angles also decrease. (The outermost zones of unusually steep dips on figure I9 are artifacts of the migration process.) Within the interval of dipping reflections, apparent dip angles tend to decrease downsection from about 25° in the upper part of the interval to less than 10° near the base of the interval. Structural relief on the order of 75 m (246 ft) is apparent for some dipping reflections in the northeastern part of the structure. Four pairs of high-amplitude reflections in combined units A and Bl are shaded in figure I9 to illustrate the unit's internal structure.

The upper contact of combined crater units A and Bl mimics their internal structure (fig. I9). This contact is near a depth of 300 m (984 ft) at the northeastern end of the profile but dips downward, and cuts stratigraphically downsection, to a depth of about 420 m (1,378 ft) near the corehole. From there, the contact is interpreted to rise in elevation to the southwest. The position of the top of combined crater units A and Bl is not readily determined southwest of meter 800 (distance scale) on the migrated depth image; the position of this contact in this area is drawn provisionally in figure I9. Approximately 120 m (394 ft) of relief are present along this surface. In contrast, the lower contact of crater unit A with the basement granite is horizontal and has only minor relief.

Vertical to moderately dipping faults that have short lengths (tens of meters) and small displacements on the order of a few meters to 10 m (33 ft) are apparent throughout combined crater units A and Bl on the migrated depth image. The complexity of the faulting does not permit a unique interpretation of fault locations and displacements; our interpretation is shown in figure I10. Individual faults typically offset one to four reflections. The lateral spacing of these faults is irregular but may be as small as about 10 m (33 ft). Normal and reverse faults are present in this fault population, and similar faults having smaller displacements below the resolution of the seismic image also may be present.

In our interpretation (fig. I10), there is a change in fault dip angles at or near the contact between the lower beds and the upper beds of crater unit A, which is placed at 558.1 m (1,831.0 ft) depth in the Langley core. Fault dip angles above this depth typically are moderate, although some steeply dipping faults also are present; below this depth, steeply dipping faults predominate. Faults in crater units A and B of the Langley core include vertical to moderately dipping dip-slip faults and a few horizontal faults (Gohn and others, this volume, chap. C; Horton and others, this volume, chap. B).

The upper beds of crater unit B (unit Bu) are represented by a planar-convex interval of discontinuous and locally weak, isolated, and (or) inclined reflections on the migrated depth image (fig. I9). There is a general trend toward greater continuity of individual reflections within crater unit Bu from the center to the ends of the seismic profile. The small-offset faults seen in crater units A and Bl also are observed in crater unit Bu (fig. I10).

The high-relief contact between combined crater units A and Bl and overlying crater unit Bu is defined on the migrated depth image by angular relationships and offsets between reflections, except near meter 600 of the profile southwest of the Langley corehole where the reflections appear conformable or paraconformable (fig. I9). The truncation and offset of reflections at the contact suggest that it locally consists of low- to moderate-angle dip-slip faults.

Impact-Generated Sediments

Variations of the informal name "Exmore beds" have been applied to the impact-generated polymict sedimentary breccias that underlie the postimpact, upper Eocene Chickahominy Formation and typically cap the impactite section of the Chesapeake Bay impact structure (Powars and others, 1992; Poag, 1997; Powars and Bruce, 1999). We place the lower and upper contacts of the Exmore beds at approximately 270 m (886 ft) and 235 m (771 ft) depths, respectively, in the center of the migrated depth section (fig. I9), in agreement with the contacts of the Exmore beds in the Langley core at depths of 269.4 m (884.0 ft) and 235.65 m (773.12 ft) (Gohn and others, this volume, chap. C).

In the Langley core, the Exmore beds consist of pebbles, cobbles, and boulders (typically smaller than 1 m (3.3 ft) in diameter) suspended in an unsorted and unstratified matrix of calcareous, muddy, very fine to very coarse sand and granules. The clasts primarily consist of sediment lithoclasts derived from the preimpact Cretaceous and lower Tertiary formations of the area (Powars and Bruce, 1999; Gohn and others, this volume, chap. C). The sand fraction of the matrix consists primarily of quartz and glauconite. Shocked and (or) cataclastic igneous-rock lithoclasts also are present, and shocked quartz grains are present but sparse in the Exmore matrix (Horton and Izett, this volume, chap. E).

We interpret the Exmore beds to consist of four subunits on the migrated depth profile (figs. I9 and I11). Exmore subunits 1, 2, and 3 are bounded by inclined, overlapping reflections that progressively overstep the underlying reflection from southwest to northeast toward the crater's center. Therefore, the base of the Exmore beds is a composite surface within the limits of the Langley profile as a result of the overstepping contacts. The base of Exmore subunit 4 is the high-amplitude reflection near 250 m (820 ft) depth, along which subunit 4 overlies subunits 2 and 3. The upper contact of the Exmore beds with the overlying fine-grained sediments of the Chickahominy Formation is a wavy, semicontinuous reflection.

Postimpact Sediments

A provisional analysis of the distribution of individual and composite postimpact stratigraphic units on the migrated depth image is illustrated in figure I9. The postimpact section extends from the top of the Exmore beds at about 235 m (771 ft) depth to the top of the image. The corresponding section in the Langley core consists of 235.65 m (773.12 ft) of upper Eocene through Pliocene marine sediments and Pleistocene paralic deposits (Edwards and others, this volume, chap. H; Powars and others, this volume, chap. G).

The postimpact units are characterized by horizontal, semicontinuous and continuous reflections at their boundaries and internally. Fine-grained shelf deposits of the upper Eocene Chickahominy Formation above the Exmore beds are overlain by a composite section of glauconitic or shelly sediments of the

Oligocene Drummonds Corner beds and Old Church Formation and the lower Miocene part of the Calvert Formation (fig. I9). That section is overlain by a composite section of middle Miocene siliceous clay-silts of the upper part of the Calvert Formation and overlying upper Miocene calcareous clay-silts of the St. Marys Formation. Shelly, clayey silts and muddy fine sands of the upper Miocene Eastover Formation overlie the St. Marys. Above the Eastover, a composite unit consisting of shelly, muddy fine sands of the Pliocene Yorktown Formation and thin, sandy, estuarine(?) Pleistocene sediments completes the postimpact section.

Wavy reflections within specific stratigraphic intervals in the postimpact section may result from lateral velocity variations produced by lateral lithologic changes. These wavy reflections are best developed in the undifferentiated upper Calvert-St. Marys section.

Discussion

Collapse Structure

We interpret the major structural feature observed on the Langley seismic images (figs. I6, I7, I8, I9, I10, and I11) as a stratabound, extensional collapse structure. This structure is defined on the seismic images by the dipping (downward-displaced), truncated reflections in crater units A and B and in the Langley core by the style and intensity of sediment disruption in those units. The structure is confined vertically to the sedimentary section of the impact structure's annular trough. Deformation of this magnitude is not present along the low-angle, low-relief contact of crater unit B with the Exmore beds above the collapse structure nor below the structure along the subhorizontal, low-relief top of the granite or within the lower beds of crater unit A (fig. I9). The variable dip directions and variable and relatively steep apparent dip angles of bedding (reflections) within the collapse structure are not typical of the Atlantic Coastal Plain, where seaward dips of less than 1° are normal (Olsson and others, 1988).

The lateral boundaries of the collapse structure cannot be located precisely. Major normal faults apparently do not bound the collapsed section; instead, the displacements required by the structure are distributed among numerous small-displacement, subvertical faults (fig. I10), possible bedding-parallel faults, and fluidized sand layers. The structure is interpreted to be about 550 m (1,805 ft) in maximum width between meters 225 (738 ft) and 775 (2,543 ft) of the seismic profile (fig. I9).

We suggest that fluidized sand beds in crater unit A at 558 m (1,831 ft) depth and above (Gohn and others, this volume, chap. C) provided the necessary low-strength zone in the lower part of the collapsed interval. Upward loss of formation water from the fluidized sands through the pervasive network of small-offset faults (fig. I10), in combination with sand grain compaction, would have provided the accommodation space needed in the lower part of the collapse structure.

An inferred detachment zone near 558 m (1,831 ft) depth separates fluidized sands and fractured clays in the upper beds of crater unit A and in crater unit B from the lower beds of crater unit A and the underlying granite, in which no unequivocal evidence for impact deformation is observed in the Langley core (Gohn and others, this volume, chap. C; Horton and others, this volume, chap. B). The apparent dip angles of reflections in crater unit A also decrease significantly at this approximate depth (fig. I9), and the observed change in the predominant dip angles of the small-displacement faults also occurs at this depth (fig. I10).

The collapse structure described in this chapter may be analogous to fault-bounded grabens in the early Tertiary Silverpit impact structure of the North Sea, described by Stewart and Allen (2002). Stratabound grabens delimited by steep, facing normal faults are the major structures in the outermost zone (zone 3) of the Silverpit impact structure. Cretaceous sedimentary strata between the grabens appear relatively undeformed and horizontal, which is also the case for most of the strata seen on our seismic transect on the York-James Peninsula. The Silverpit grabens have widths (hundreds of meters) and vertical structural displacements (tens of meters) similar to those of the Langley collapse structure. Differences in lateral boundary structures between the normal-fault-bounded Silverpit grabens and the distributed structural displacements of the Langley collapse structure may result from differences in sediment compaction and lithification between Cretaceous chalks at Silverpit and Cretaceous sands and clays of the Potomac Formation at Langley.

Stewart and Allen (2002) suggested that overpressured chalk layers in a chalk-clay sequence provided detachment zones at depths equal to the lower terminations of the graben-bounding normal faults at Silverpit. They also suggested that fractures acted as dewatering conduits that produced the volume accommodation needed at the bottoms of the grabens.

In plan view, the Silverpit grabens and other normal faults define a concentric multi-ring structural pattern in the outer part of the 20-km-wide (12-mi-wide) Silverpit impact structure (Stewart and Allen, 2002). Powars and others (2003) have suggested the possibility of a similar concentric structural pattern in the Chesapeake Bay impact structure. Confirmation of the Chesapeake Bay crater-Silverpit crater analogy ultimately will require a three-dimensional grid of reflection profiles near Langley or elsewhere within the annular trough of the Chesapeake Bay impact structure.

The annular troughs of complex impact craters result from late-stage, gravity-driven collapse across an area that is significantly wider than the short-lived transient crater opened by excavation and downward displacement of materials at the center of the impact (Melosh, 1989; Melosh and Ivanov, 1999; Morgan and others, 2000). The stratabound collapse structure seen on the Langley seismic images is interpreted as representative of this late stage of impact crater evolution.

Exmore Beds

During impacts into marine targets, late-stage gravitational collapse may be accompanied or closely followed by the catastrophic resurge of water-sediment-ejecta mixtures into the collapsing crater, resulting in local erosion and extensive sediment deposition (Tsikalas and others, 1998; Ormö and Lindström, 2000; von Dalwigk and Ormö, 2001; Shuvalov and others, 2002; Tsikalas and Faleide, 2002). The Exmore beds in the Langley core display vertical variations in fossil assemblages and lithoclast size and composition that suggest two depositional units with different provenances produced by resurge sedimentation (Frederiksen and others, this volume, chap. D; Gohn and others, this volume, chap. C). Two of the four seismically defined subunits of the Exmore beds shown on the migrated depth image (figs. I9 and I11) likely represent the depositional units observed in the core.

The base of seismic subunit 4 of the Exmore beds is a strong, continuous reflection located at about 250 m to 245 m (820 ft to 804 ft) depth near the Langley corehole (fig. I9). Gohn and others (this volume, chap. C) recognize a depositional boundary at about 244 m (about 800 ft) depth in the core on the basis of size grading (coarse-tail-grading) of the larger lithoclasts. Frederiksen and others (this volume, chap. D) note that reworked Cretaceous calcareous nannofossils are present in the Exmore matrix only at and above 242.1 m (794.4 ft) depth, suggesting differences in sediment sources for the deposits above and below that sample depth. The close proximity in depth of these three boundaries suggests the correlation of the two depositional units defined in the core with Exmore subunits 2 and 4 interpreted on the migrated depth image (fig. I11).

The upper contact of the Exmore beds is a wavy, nearly continuous reflection with about 10 m (33 ft) of relief, as seen on the migrated depth image (figs. I9 and I11). We speculate that this irregular surface may represent large bedforms, either megaripples or hummock-and-swale bed topography. These features could have resulted from low-density ocean-resurge currents or wave-interference patterns produced by collapse of the transient water-column crater or by the return of impact-generated tsunamis from the nearby North American shoreline. Alternatively, this irregular surface may represent the essentially unmodified hummocky or blocky upper surface of the final Exmore debris flow (for non-impact examples, see Prior and others, 1984, and Mulder and Cochonat, 1996). Wavy reflections in the postimpact Chickahominy Formation may represent the draping of fine-grained marine sediments over the irregular upper surface of the Exmore beds.

Summary

Complementary data from the seismic reflection and refraction survey and the corehole at the NASA Langley Research Center allowed us to describe and interpret the stratigraphy and impact deformation of preimpact rocks and sediments and the deposition of synimpact sediments within part of the annular trough of the Chesapeake Bay impact structure. A stratabound collapse structure within the preimpact sedimentary section of the annular trough is interpreted to have formed during widespread, late-stage gravitational collapse of the impact structure. Observed deformation features increase upward in the preimpact section, including fracturing of clays, fluidization of sands, and injection of previously overlying Upper Cretaceous and Tertiary marine sediments. Fluidized sands within the lower part of the sedimentary section probably provided a detachment interval and accommodation space in the lower part of the collapse structure. The Exmore beds are interpreted as ocean-resurge deposits that consist of multiple depositional units with differing provenances. Resurge currents or returning impact-generated tsunamis may have modified the upper surface of the Exmore beds.

Acknowledgments

U.S. Geological Survey (USGS) investigations of the Chesapeake Bay impact structure are conducted in cooperation with the Hampton Roads Planning District Commission, the Virginia Department of Environmental Quality, and the National Aeronautics and Space Administration (NASA) Langley Research Center. The Hampton Roads Planning District Commission and the USGS provided funds for the drilling of the USGS-NASA Langley corehole. The Virginia Department of Environmental Quality and the Department of Geology of the College of William and Mary provided extensive operational support at the drill site. The NASA Langley Research Center provided extensive operational and logistical support for the drilling of the USGS-NASA Langley corehole and for the York-James seismic survey. We especially thank Joel S. Levine, John J. Warhol, Jr., and Frederick M. Thompson (all of NASA-Langley), for their enthusiastic support during these operations.

We thank Dominion Virginia Power for access to their right-of-way in Hampton and Newport News. We also thank the members of the USGS seismic field crew, whose hard work and dedication made this research possible: Joe Catchings, Chris Crosby, Gini Gandhok, Shawn Hanson, Ron Kaderabek, Bryan Kerr, Lora Kiger, Colleen McCartan, Lela Preshad, Jose Rodriguez, Ben Sleeter, and Matthew Smith. The USGS Rocky Mountain Drilling Unit (Arthur C. Clark, supervisor and lead driller) drilled the USGS-NASA Langley corehole with support from the USGS Eastern Earth Surface Processes Team's drilling crew. Stephen E. Curtin (USGS) and Richard E. Hodges (USGS) conducted the geophysical logging of the Langley corehole. We thank Nicholas M. Ratcliffe (USGS) and Thomas M. Brocher (USGS) for their reviews of this chapter, which substantially improved its organization and content.

References Cited

Anstey, N.A., 1977, Seismic interpretation; The physical aspects: Boston, International Human Resources Development Corporation, 637 p.

Barry, K.M., Cavers, D.A., and Kneale, C.W., 1975, Recommended standards for digital tape formats: Geophysics, v. 40, no. 2, p. 344–352.

Brouwer, Jan, and Helbig, Klaus, 1998, Shallow high-resolution reflection seismics, v. 19 *of* Helbig, Klaus, and Treitel, Sven, eds., Handbook of geophysical exploration; Section 1, Seismic exploration: New York, Elsevier, 391 p.

Edwards, L.E., and Powars, D.S., 2003, Impact damage to dinocysts from the late Eocene Chesapeake Bay event: Palaios, v. 18, no. 3, p. 275–285. (Also available online at http://www.bioone.org/pdfserv/i0883-1351-018-03-0275.pdf)

Gohn, G.S., Bruce, T.S., Catchings, R.D., Emry, S.R., Johnson, G.H., Levine, J.S., McFarland, E.R., Poag, C.W., and Powars, D.S., 2001, Integrated geologic, hydrologic, and geophysical investigations of the Chesapeake Bay impact structure, Virginia, USA; A multi-agency program [abs.]: Lunar and Planetary Science Conference, 32d, Houston, Tex., March 12–16, 2001, Abstract 1901, available online at http://www.lpi.usra.edu/meetings/lpsc2001/pdf/1901.pdf

Gohn, G.S., Clark, A.C., Queen, D.G., Levine, J.S., McFarland, E.R., and Powars, D.S., 2001, Operational summary for the USGS-NASA Langley corehole, Hampton, Virginia: U.S. Geological Survey Open-File Report 01–87–A, 21 p., available only online at http://pubs.usgs.gov/of/2001/of01-087/

Hole, J.A., 1992, Nonlinear high-resolution three-dimensional seismic travel time tomography: Journal of Geophysical Research, v. 97, no. B5, p. 6553–6562.

Melosh, H.J., 1989, Impact cratering—A geologic process: New York, Oxford University Press, 245 p.

Melosh, H.J., and Ivanov, B.A., 1999, Impact crater collapse: Annual Review of Earth and Planetary Sciences, v. 27, p. 385–415.

Morgan, J.V., Warner, M.R., Collins, G.S., Melosh, H.J., and Christeson, G.L., 2000, Peak-ring formation in large impact craters; Geophysical constraints from Chicxulub: Earth and Planetary Science Letters, v. 183, no. 3–4, p. 347–354.

Mulder, Thierry, and Cochonat, Pierre, 1996, Classification of offshore mass movements: Journal of Sedimentary Research, v. 66, no. 1, p. 43–57.

Olsson, R.K., Gibson, T.G., Hansen, H.J., and Owens, J.P., 1988, Geology of the northern Atlantic Coastal Plain; Long Island to Virginia, *in* Sheridan, R.E., and Grow, J.A., eds., The Atlantic continental margin, U.S., v. I–2 *of* The geology of North America: Boulder, Colo., Geological Society of America, p. 87–105.

Ormö, Jens, and Lindström, Maurits, 2000, When a cosmic impact strikes the sea bed: Geological Magazine, v. 137, no. 1, p. 67–80.

Poag, C.W., 1996, Structural outer rim of Chesapeake Bay impact crater; Seismic and bore hole evidence: Meteoritics & Planetary Science, v. 31, no. 2, p. 218–226.

Poag, C.W., 1997, The Chesapeake Bay bolide impact; A convulsive event in Atlantic Coastal Plain evolution: Sedimentary Geology, v. 108, no. 1–4, p. 45–90.

Poag, C.W., Hutchinson, D.R., Colman, S.M., and Lee, M.W., 1999, Seismic expression of the Chesapeake Bay impact crater; Structural and morphologic refinements based on new seismic data, *in* Dressler, B.O., and Sharpton, V.L., eds., Large meteorite impacts and planetary evolution; II: Geological Society of America Special Paper 339, p. 149–164.

Poag, C.W., Powars, D.S., Poppe, L.J., and Mixon, R.B., 1994, Meteoroid mayhem in Ole Virginny—Source of the North American tektite strewn field: Geology, v. 22, no. 8, p. 691–694.

Powars, D.S., 2000, The effects of the Chesapeake Bay impact crater on the geologic framework and the correlation of hydrogeologic units of southeastern Virginia, south of the James River: U.S. Geological Survey Professional Paper 1622, 53 p., 1 oversize pl. (Also available online at http://pubs.usgs.gov/prof/p1622)

Powars, D.S., and Bruce, T.S., 1999, The effects of the Chesapeake Bay impact crater on the geological framework and correlation of hydrogeologic units of the lower York-James Peninsula, Virginia: U.S. Geological Survey Professional Paper 1612, 82 p., 9 oversize pls. (Also available online at http://pubs.usgs.gov/prof/p1612)

Powars, D.S., Bruce, T.S., Bybell, L.M., Cronin, T.M., Edwards, L.E., Frederiksen, N.O., Gohn, G.S., Horton, J.W., Jr., Izett, G.A., Johnson, G.H., Levine, J.S., McFarland, E.R., Poag, C.W., Quick, J.E., Schindler, J.S., Self-Trail, J.M., Smith, M.J., Stamm, R.G., and Weems, R.E., 2001, Preliminary geologic summary for the USGS-NASA Langley corehole, Hampton, Virginia: U.S. Geological Survey Open-File Report 01–87–B, 20 p., available only online at http://pubs.usgs.gov/of/2001/of01-087/

Powars, D.S., Gohn, G.S., Catchings, R.D., Horton, J.W., Jr., and Edwards, L.E., 2003, Recent research in the Chesapeake Bay impact crater, USA—Part 1. Structure of the western annular trough and interpretation of multiple collapse structures [abs.]: International Conference on Large Meteorite Impacts, 3d, Noerdlingen, Germany, August 5–7, 2003, Abstract 4053, available online at http://www.lpi.usra.edu/meetings/largeimpacts2003/pdf/4053.pdf

Powars, D.S., Johnson, G.H., Edwards, L.E., Horton, J.W., Jr., Gohn, G.S., Catchings, R.D., McFarland, E.R., Izett, G.A., Bruce, T.S., Levine, J.S., and Pierce, H.A., 2002, An expanded Chesapeake Bay impact structure, eastern Virginia; New corehole and geophysical data [abs.]: Lunar and Planetary Science Conference, 33d, League City, Tex., March 11–15, 2002, Abstract 1034, available online at http://www.lpi.usra.edu/meetings/lpsc2002/pdf/1034.pdf

Powars, D.S., Mixon, R.B., and Bruce, Scott, 1992, Uppermost Mesozoic and Cenozoic geologic cross section, outer coastal plain of Virginia, *in* Gohn, G.S., ed., Proceedings of the 1988

U.S. Geological Survey Workshop on the Geology and Geohydrology of the Atlantic Coastal Plain: U.S. Geological Survey Circular 1059, p. 85–101.

Prior, D.B., Bornhold, B.D., and Johns, M.W., 1984, Depositional characteristics of a submarine debris flow: Journal of Geology, v. 92, no. 6, p. 707–727.

Shuvalov, V.V., Dypvik, H., and Tsikalas, F., 2002, Numerical modeling of the Mjølnir marine impact event [abs.]: Lunar and Planetary Science Conference, 33d, League City, Tex., March 11–15, 2002, Abstract 1038, available online at http://www.lpi.usra.edu/meetings/lpsc2002/pdf/1038.pdf

Stewart, S.A., and Allen, P.J., 2002, A 20-km-diameter multi-ringed impact structure in the North Sea: Nature, v. 418, no. 6897, p. 520–523.

Tsikalas, Filippos, and Faleide, J.I., 2002, Near-field erosional features at the Mjølnir impact crater; The role of marine sedimentary target [abs.]: Lunar and Planetary Science Conference, 33d, League City, Tex., March 11–15, 2002, Abstract 1296, available online at http://www.lpi.usra.edu/meetings/lpsc2002/pdf/1296.pdf

Tsikalas, Filippos, Gudlaugsson, S.T., and Faleide, J.I., 1998, Collapse, infilling, and postimpact deformation at the Mjølnir impact structure, Barents Sea: Geological Society of America Bulletin, v. 110, no. 5, p. 537–552.

von Dalwigk, Ilka, and Ormö, Jens, 2001, Formation of resurge gullies at impacts at sea; The Lockne crater, Sweden: Meteoritics & Planetary Science, v. 36, no. 3, p. 359–369.

Waters, K.H., 1981, Reflection seismology; A tool for energy resource exploration (2d ed.): New York, John Wiley and Sons, 453 p., 4 pls.

Audio-Magnetotelluric (AMT) Soundings across the Margin of the Chesapeake Bay Impact Structure, York-James and Middle Peninsulas, Virginia

By Herbert A. Pierce

Chapter J of
**Studies of the Chesapeake Bay Impact Structure—
The USGS-NASA Langley Corehole, Hampton, Virginia, and
Related Coreholes and Geophysical Surveys**

Edited by J. Wright Horton, Jr., David S. Powars, and Gregory S. Gohn

Prepared in cooperation with the
Hampton Roads Planning District Commission,
Virginia Department of Environmental Quality, and
National Aeronautics and Space Administration Langley Research Center

Professional Paper 1688

U.S. Department of the Interior
U.S. Geological Survey

Contents

Figures

Table

Audio-Magnetotelluric (AMT) Soundings across the Margin of the Chesapeake Bay Impact Structure, York-James and Middle Peninsulas, Virginia

By Herbert A. Pierce[1]

Abstract

The Chesapeake Bay impact structure is a roughly circular subsurface feature created about 35 million years ago when a comet fragment or asteroid impacted the continental shelf near the present-day mouth of the Chesapeake Bay. Interpretation of seismic and other data suggests that the central crater is about 35 to 40 kilometers (km; 22 to 25 miles (mi)) wide and contains a central uplift. The central crater is surrounded by an annular trough that is about 25 km (16 mi) wide. The annular trough is surrounded by an outer fracture zone that is about 35 km (22 mi) wide.

During 2000 and 2001, 18 audio-magnetotelluric (AMT) soundings were collected across the western outer margin of the annular trough in two locations as part of the Chesapeake Bay impact crater study. These tensor AMT soundings provided estimates of impedances across the outer margin of the impact structure. From the impedances, resistivities and phases as a function of frequency were calculated. They were inverted as a function of depth, and electrical cross sections were constructed to provide an image of the electrical response associated with the structure.

The cross sections show a nearly vertical resistivity high at the outer margin of the annular trough. The bottoms of the electrical sections show a subhorizontal resistive layer interpreted to be the basement rocks buried by conductive sedimentary rocks. Polar plots of the tensor impedances were calculated, and the principal impedance directions indicate fracture orientations roughly parallel to the outer margin. The maximum depth of investigation for the soundings and sections is about 1,000 meters (m; about 3,300 feet (ft)) except inside the outer margin near Mathews, Va., where low-resistivity sediments limit the depth of exploration in some places to 300 m (980 ft).

[1]U.S. Geological Survey, Reston, VA 20192.

Introduction

The Chesapeake Bay impact structure is a subsurface feature of the eastern Virginia Coastal Plain and inner continental shelf (Powars and Bruce, 1999; Powars, 2000). It was formed about 35 million years ago by a comet fragment or asteroid impact on the late Eocene continental shelf. The feature was buried beneath several hundred meters of upper Eocene through Quaternary marine and paralic sediments.

The structure has a central crater that underlies the southern Delmarva Peninsula. The margin of the central crater separates the central crater from the less deformed annular trough and is about 35 to 40 kilometers (km; 22 to 25 miles (mi)) in diameter. A small central uplift within the central crater is inferred from geophysical evidence (Poag, Hutchinson, and others, 1999; Poag, Plescia, and Molzer, 1999).

The annular trough extends from the margin of the central crater outward to the faulted outer margin, a radial distance of about 25 km (16 mi) (Poag, 1996). The outer margin has a diameter between 85 and 90 km (53 and 56 mi). The annular trough is surrounded by an outer fracture zone that is about 35 km (22 mi) wide (Powars, 2000; Horton and others, this volume, chap. A, fig. A1).

The Chesapeake Bay impact structure resulted from a wet-target impact; the target included water-saturated sediments and a seawater column (Horton and others, this volume, chap. A). Crater collapse was probably accompanied by the catastrophic resurge of water-sediment-ejecta mixtures toward the center of the crater, which resulted in local erosion of the outer crater margin and adjacent sediments and deposition within the crater (Gohn and others, this volume, chap. C). These sediments were reworked by wave swash and impact-generated tsunamis as the sea returned to equilibrium (Gohn and others, this volume, chap. C). The Exmore beds are interpreted to be the sedimentary deposits produced by the inward-flowing resurge of bottom currents following collapse of the water column and perhaps by the return of impact-produced tsunamis (Gohn and others, this volume, chap. C).

During 2000 and 2001, 18 audio-magnetotelluric soundings were collected across the western outer margin of the annular trough in two locations (figs. J1 and J2, table J1). The work was part of the Chesapeake Bay impact crater study conducted by the U.S. Geological Survey (USGS) and its partners (see "Acknowledgments"). The purpose of the electromagnetic soundings was to test the ability of the audio-magnetotelluric technique to image the electrical nature of the outer margin of the Chesapeake Bay impact structure. Specifically, this work was designed to help map the outer margin, measure the magnitude of electrical anisotropy, and provide impedance strike directions. Because most of the impact structure is covered by the lower Chesapeake Bay, these soundings were focused on the western outer margin, collapse structures in the annular trough, and the underlying crystalline basement rocks. The data from the soundings supplement data from seismic surveys and deep coreholes, including the USGS-NASA Langley corehole (fig. J2) discussed in other chapters of this volume.

Audio-Magnetotelluric Methods

Audio-magnetotelluric (AMT) soundings are made to determine variations in the electrical resistivity of the earth with depth (Cagniard, 1950, 1953; Wait, 1962; Keller and Frischknecht, 1966; Hoover and Long, 1976; Hoover and others, 1976, 1978; Dmitriev and Berdichevsky, 1979; Vozoff, 1986, 1991). The AMT method uses natural-source multifrequency electromagnetic signals that result from lightning or atmospheric disturbances ("sferics") as an energy source. For this survey, a controlled-source transmitter was used to supplement natural source energy when signal strength was low. Low levels of natural source energy in the middle frequency band of the instrument can cause errors in the impedance estimates.

AMT soundings consist of electrical and magnetic field measurements over a range of frequencies from 5 to 100,000 hertz (Hz) with fixed receiver and transmitter locations. The distribution of currents induced in the earth depends on the earth's electrical resistivity, the earth's magnetic permeability, and the frequency measured. Because low-frequency signals penetrate to greater depths than high-frequency signals, measurements of the electromagnetic response at several frequencies contain information on the variation of resistivity with depth. In this study, a series of soundings were stitched together to form two profiles or lines approximately normal to the outer margin structure.

Field Work

AMT tensor soundings collected during the spring of 2000 on the York-James Peninsula (fig. J2) were recorded by using an Electromagnetic Instruments, Inc. (EMI), 10-channel MT1 system. For each station location, approximately 55 AMT frequencies were recorded for each of the two directions (*Ex* and *Ey*) from 4 to 23,250 Hz.

The soundings collected during the spring of 2001 on the Middle Peninsula (fig. J2) were recorded by using a Geometrics EH4 system. Approximately 40 AMT frequencies were collected with this system for each of the two directions from 10 to 100,000 Hz. The magnetic field sensors, electrical field sensors, buffers, and preamplifiers for both systems were manufactured by EMI.

Tensor Audio-Magnetotelluric Soundings

The impedance tensor (Z) is frequency dependent and is obtained from vector measurements of the electrical and magnetic fields. The AMT method measures both orthogonal magnetic and electrical fields (*Hx, Hy, Ex,* and *Ey*) so that the impedance can be described as a complex tensor to account for anisotropy.

The AMT impedance tensor (Z) contains four complex components that relate the measured electrical (E) and magnetic (H) fields:

$$\begin{bmatrix} Ex \\ Ey \end{bmatrix} = \begin{bmatrix} Zxx & Zxy \\ Zyx & Zyy \end{bmatrix} \times \begin{bmatrix} Hx \\ Hy \end{bmatrix} \quad (1)$$

The impedances are computed from spectra collected in the field by using a magnetic (H) field reference where $<AB^*>$ is a complex value formed from the real and imaginary parts of AB. The quantity $<AA^*>$ is an autopower and is real valued. Both the scalar and tensor impedance values are frequency averaged from the spectral data.

$$Zxx = \frac{<ExHx^*><HyHy^*> - <ExHy^*><HyHx^*>}{<HxHx^*><HyHy^*> - <HxHy^*><HyHx^*>} \quad (2)$$

$$Zxy = \frac{<ExHx^*><HxHy^*> - <ExHy^*><HxHx^*>}{<HyHx^*><HxHy^*> - <HyHy^*><HxHx^*>} \quad (3)$$

$$Zyx = \frac{<EyHx^*><HyHy^*> - <EyHy^*><HyHx^*>}{<HxHx^*><HyHy^*> - <HxHy^*><HyHx^*>} \quad (4)$$

$$Zyy = \frac{<EyHx^*><HxHy^*> - <EyHy^*><HxHx^*>}{<HyHx^*><HxHy^*> - <HyHy^*><HxHx^*>} \quad (5)$$

All of the soundings collected use local *Hx* and *Hy* fields as reference (Gamble and others, 1979a,b).

The apparent resistivities and phases are computed from the four components of the impedance tensor (*Zxx, Zxy, Zyx,* and *Zyy*). Apparent resistivities $\rho(f)$ and corresponding phases $\phi(f)$ are computed by using:

$$\rho_{ij} = \frac{1}{5f}|Z_{ij}|^2 \quad (6)$$

$$\phi_{ij} = \tan^{-1}\left(\frac{im\{Z_{ij}\}}{re\{Z_{ij}\}}\right) \quad (7)$$

where *im* is the imaginary part and *re* is the real part of Z.

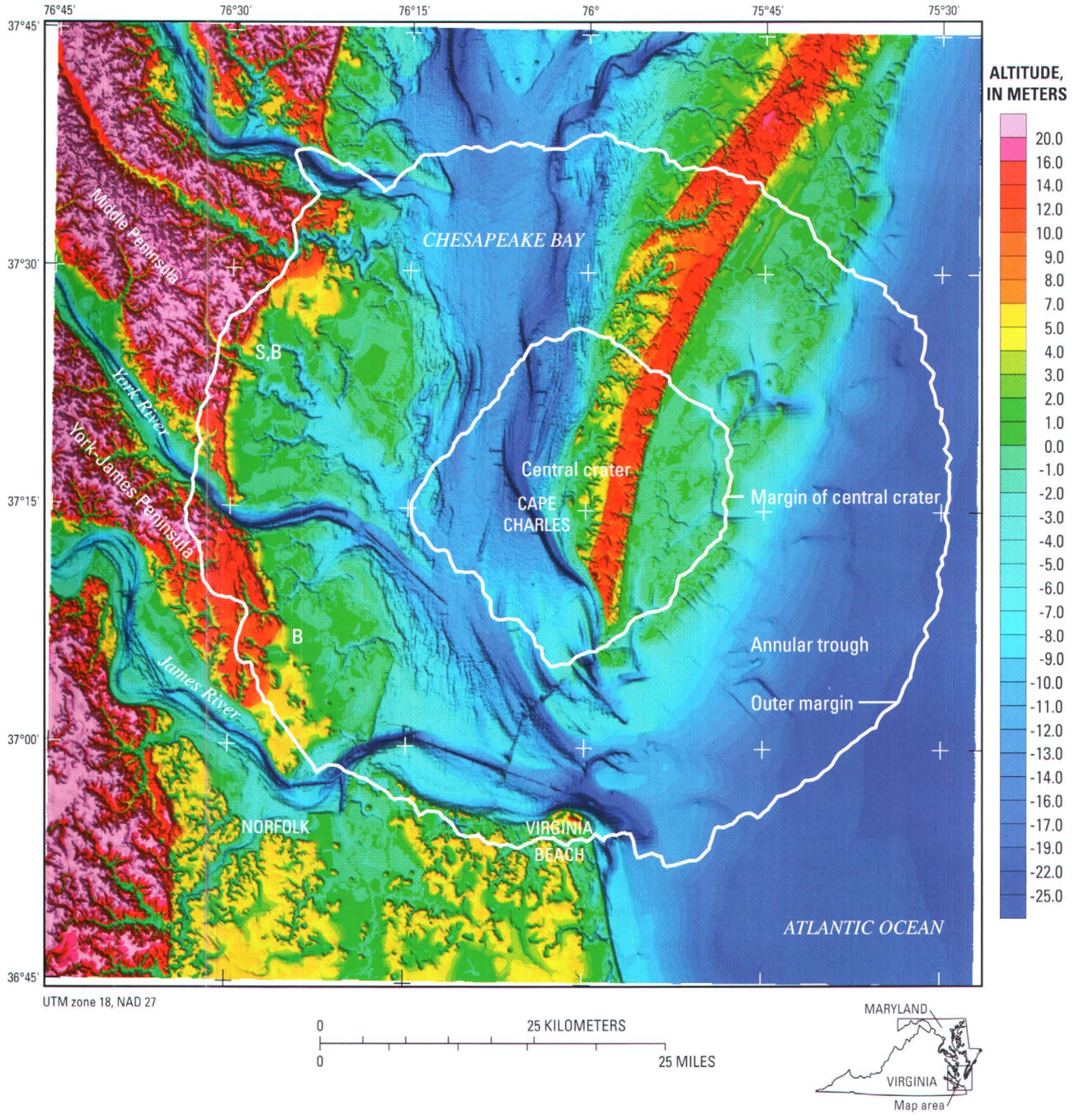

Figure J1. Color shaded-relief map of the part of Virginia near the mouth of Chesapeake Bay showing the location of the subsurface Chesapeake Bay impact structure. The land part of the map is from the U.S. Geological Survey's National Elevation Dataset digital elevation model (DEM). The bathymetry is from the National Oceanic and Atmospheric Administration (NOAA), National Geophysical Data Center (NGDC), U.S. coastal relief model. The original data resolution of the DEM grid was 30 m (98 ft), but data were regridded to 60 m (197 ft) and merged with the NOAA bathymetric data. The Suffolk-Big Bethel (S, B) scarp is visible in the center-left portion of the map; the resolution is not sufficient to identify the Harpersville scarp (Johnson and others, 2001). All three scarps are shown in Horton and others (this volume, chap. A, fig. A4). Locations of the central crater and outer margin of the Chesapeake Bay impact structure are from Powars and Bruce (1999). The AMT data indicate that the Suffolk-Big Bethel scarp is coincident with the westernmost edge of the outer margin of the impact structure across the Middle Peninsula. The Big Bethel scarp on the York-James Peninsula does not coincide with the location of the outer margin suggested by the AMT data, which is the same location suggested by Powars and Bruce (1999). The scarp is about 2.5 km (about 1.6 mi) northeast of the resistivity high interpreted to be the outer margin according to the AMT data and Powars and Bruce (1999).

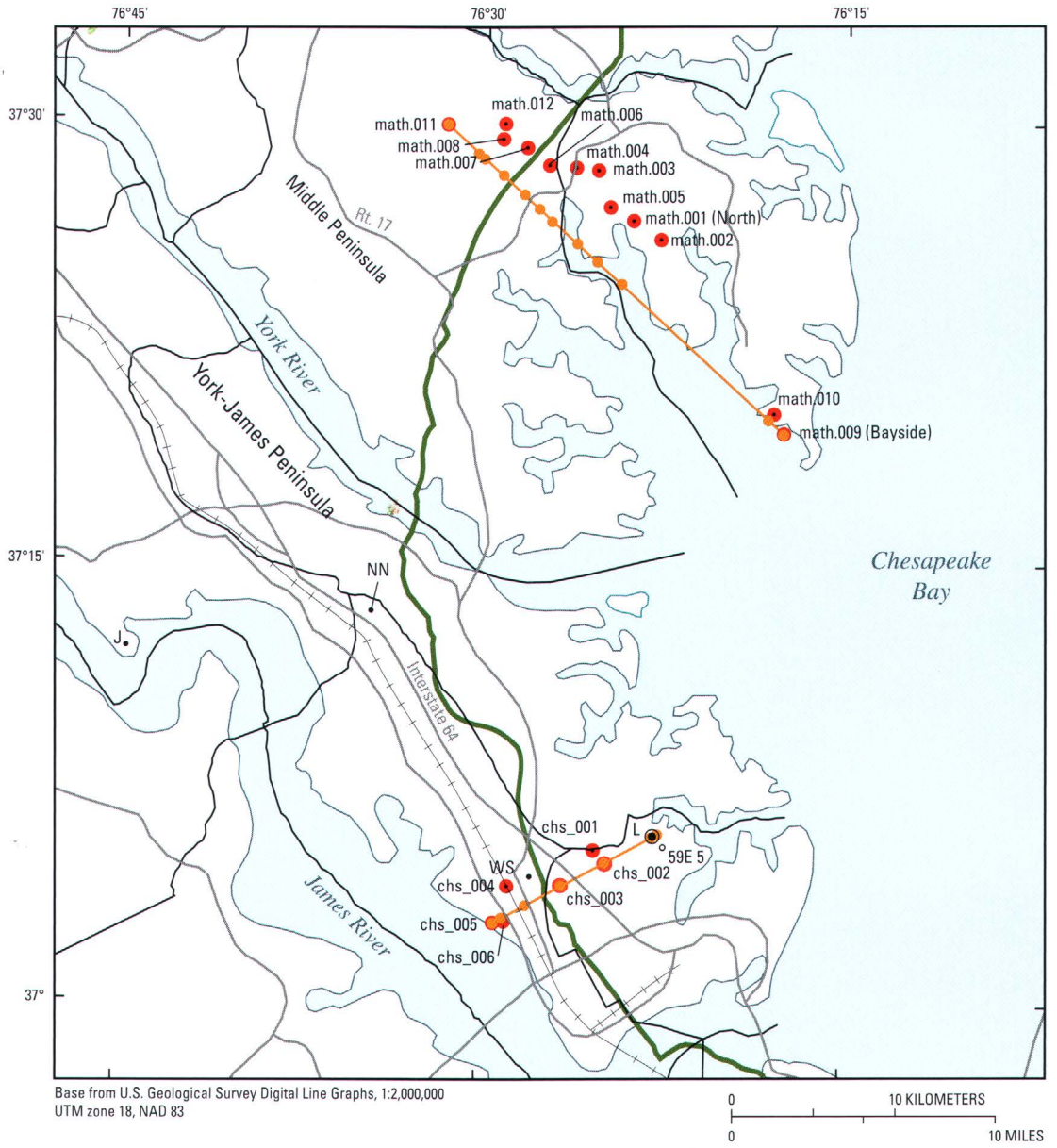

EXPLANATION

Political boundary

Road

Railroad

Outer margin of the Chesapeake Bay impact crater

chs_004 AMT station

Projection of AMT station to section line

COREHOLES AND WELL

J • Jamestown

L ◉ USGS-NASA Langley

NN • Newport News Park 2

WS • Watkins School

59E 5 ○ NASA Langley test well drilled in 1974

Figure J2. Map of the York-James and Middle Peninsulas, Va., showing the locations of 18 AMT stations, part of the outer margin of the Chesapeake Bay impact structure, and coreholes and a well that provided comparison data. Station coordinates and altitudes are given in table J1. Stations having the prefix "chs" were the sites of data collection in 2000 on the York-James Peninsula near the USGS-NASA Langley corehole (L) and the NASA Langley test well drilled in 1974 (59E 5). Stations having the prefix "math" were the sites of data collection in 2001 on the Middle Peninsula near Mathews, Va.; the Bayside corehole coincides with station math.009, and the North corehole coincides with station math.001. Data from the stations were projected onto two electrical section lines; see figs. J7 and J8.

Table J1. Station identifiers, locations, and altitudes for AMT soundings collected in 2000 on the York-James Peninsula (station prefix "chs") and in 2001 on the Middle Peninsula (station prefix "math"), Va.

[Station locations are plotted in figure J2, which is a Universal Transverse Mercator (UTM) projection. Latitude and longitude are in decimal degrees north and west, respectively. UTM coordinates are in meters with a central meridian of –75° and base latitude of 0° (zone 18). Altitude is in meters above mean sea level]

Station	Latitude (°N)	Longitude (°W)	UTM (Northing)	UTM (Easting)	Altitude (m)
chs_001	37.08833	76.42000	4105411	373794	6
chs_002	37.08056	76.41167	4104538	374521	5
chs_003	37.06806	76.44194	4103192	371809	8
chs_004	37.06889	76.47528	4103329	368847	9
chs_005	37.04639	76.48833	4100851	367648	9
chs_006	37.04667	76.48111	4100872	368290	10
math.001	37.44550	76.39810	4145008	376326	8
math.002	37.43471	76.37904	4143786	377994	5
math.003	37.47383	76.42304	4148185	374167	6
math.004	37.47524	76.43845	4148362	372807	5
math.005	37.45307	76.41448	4145869	374889	11
math.006	37.47662	76.45684	4148539	371183	32
math.007	37.48608	76.47239	4149611	369824	24
math.008	37.49088	76.48927	4150166	368340	31
math.009	37.32557	76.29249	4131569	385486	1
math.010	37.33648	76.29958	4132788	384874	2
math.011	37.49886	76.52779	4151107	364949	23
math.012	37.49949	76.48795	4151120	368472	21

Once the phases and resistivities are estimated from the impedances, a Bostick depth transform (Bostick, 1977) is used to transform frequency domain apparent resistivity data into a resistivity-versus-depth sounding. The Bostick depth transforms are calculated for each frequency by using:

$$\rho_{Bostick} = \rho \times \frac{(1+M)}{(1-M)}, \text{ where } M = \frac{d\log(\rho)}{d\log(\rho)} \quad (8)$$

M equals the slope of the apparent resistivity curve on a log-log plot. The slope is estimated by using a finite difference approximation. Another way M can be calculated is to use the Hilbert transform relationship (Sheriff and Geldart, 1982; Sutarno and Vozoff, 1991) between the apparent resistivity ρ and its phase ϕ in degrees translated into the first quadrant and clipped to the range $0° \le \phi \le 90°$:

$$M = 1 - \left(\frac{\phi}{45}\right) \quad (9)$$

and

$$D_{meters} = \sqrt{\frac{\rho}{2\pi f \mu_0}} \quad (10)$$

where D_{meters} is depth in meters, and μ_0 is magnetic permeability of free space.

The cross sections can be generated by using the rotationally invariant arithmetic average derived from the full tensor impedances. Arithmetic electrical sections can be computed by using the following formula:

$$Z_{arithmetic} = \frac{(Zxy + Zyx)}{2} \quad (11)$$

If the geologic structure is two dimensional, then the tensor Z can be rotated to the angle corresponding to the strike of the geology to get a rotated tensor Z'. For Z', $Z'xy$ and $Z'yx$ are maximized and $Z'xx$ and $Z'yy$ are minimized. The angle θ_0 that maximizes:

$$Z'xy^2 + Z'yx^2 \quad (12)$$

is the principal direction of Z. The principal direction of Z, or the *Zstrike,* is evaluated for each frequency. The way the *Zstrike* is calculated results in four possible solutions at 90° intervals, or two possible geologic strike directions. Because we did not use a vertical magnetic coil, tipper information was unavailable; thus, the choice between these solutions was based on geologic information. A series of impedance polar diagrams with the *Zstrike* calculated for each frequency indicates how the geologic strike varies with frequency.

Results

AMT soundings were made to determine variations in the electrical resistivity of the earth with depth (Spies and Frischknecht, 1991) along two electrical section lines. Both AMT sounding lines cross the curvilinear Suffolk-Big Bethel scarp (Johnson and others, 2001) on the York-James and Middle Peninsulas of the Chesapeake Bay as seen in the digital terrain (shaded-relief) map (fig. J1). The locations where the AMT soundings were collected and lines of electrical sections generated from them are plotted in figure J2. These lines constructed from the AMT stations were designed to cross normal to the outer margin of the annular trough adjacent to the high-resolution seismic profile (Catchings and others, this volume, chap. I) and close to several wells used for ground truth.

Raw AMT resistivity and phase curves were edited, interpolated, and inverted by using the Bostick depth transform. The inverted soundings map the location of the outer margin as a resistivity high. The transition between low-resistivity Lower Cretaceous sediments and the resistive though weathered Paleozoic and Proterozoic crystalline basement is a resistivity gradient. In general, apparent resistivity patterns seen in the sections agree with the geology, induction well logs, and seismic-reflection data. The electrical sections provide an image showing the location of the outer margin of the impact structure and basement contact.

The series of soundings carried out during 2000 and 2001 show similar results, although details of the electrical sections generated from the individual soundings differ in several ways. The soundings collected during the spring of 2000 on the York-James Peninsula were recorded by using an EMI 10-channel receiver. In practice, the receiver requires a total of seven channels per tensor AMT sounding. Channels one through four were *Ex, Ey, Hx,* and *Hy.* The fifth channel, *Hz,* was collected as a null because vertical magnetic sensor data were not collected. Channels six and seven record the remote data channels *Rx* and *Ry.* In this case, data from *Hx* and *Hy* were written to channels six and seven to provide a local reference (*Rx* and *Ry*).

The soundings collected during the spring of 2001 on the Middle Peninsula of the Chesapeake were recorded by using a four-channel Geometrics EH4 receiver. The four channels were *Ex, Ey, Hx,* and *Hy.* The local magnetic reference (*Rx* and *Ry*) was computed by using *Hx* and *Hy* channels.

All the soundings were collected in areas where cultural interference is a problem. Powerlines, roads, sewerlines, and other cultural artifacts make recording difficult, and the setup is subject to assessment of the effects caused by local interfering signals. Electromagnetic signals recorded in urban or suburban settings are typically noisy, and caution must be used to interpret the electrical sections.

To limit the noise generated by cultural effects, both receivers used a 60-Hz notch filter to remove effects caused by the local power grid. For the EMI MT1 system used during 2000, coherency filtering removed signals that had a coefficient of coherence less than 0.8. The Geometrics EH4 system, used during 2001, had a two-stage filter. The EH4 used cutoffs for the coefficient of coherence at 0.3 for the first stage and 0.5 for the second stage. Signal amplitudes were monitored, and any that saturated the receiver amplifiers were rejected. Time series that had more than seven saturations were also rejected. Assessments were made of the sounding locations before and after data collection. Sites were chosen so that stations were 100 m (330 ft) away from known powerlines. The first AMT station collected on the York-James Peninsula, chs_001, was rejected because one electrical field line straddled a buried power conduit that interfered with and degraded the natural-source curves.

Discussion

Both AMT profiles show a zone of higher resistivities coincident with the outer margin. Unedited AMT resistivity plots for each station on the York-James Peninsula transect are shown in figure J3. Unedited AMT resistivity plots for each station on the Middle Peninsula are shown on figure J4. Unedited AMT phase plots for each station on the York-James Peninsula transect are shown in figure J5. Unedited AMT phase plots for each station on the Middle Peninsula are shown on figure J6. Some of the stations display scattered data points and points with large error bars. These problems are to be expected for any electromagnetic survey conducted in an urban area. Fortunately, many frequencies were collected, and the interpreter could deactivate frequencies with large error bars. The resistivity and phase curves were then edited, smoothed, and interpolated prior to inversion and interpretation.

Figure J7 shows the electrical cross section for the York-James Peninsula. This Bostick inversion uses the single *Ex* field and corresponding *Hy* field. The outer margin of the annular trough here is interpreted to coincide with the resistivity high near AMT station chs_004. Neoproterozoic granite (Horton and others, this volume, chap. B) was drilled beneath the sediments at altitudes of –623.9 m (–2,046.8 ft) in the USGS-NASA Langley corehole and –633.7 m (–2,079 ft) in the NASA Langley test well 59E 5 (fig. J7). Seismic-reflection data also show a strong reflector near these altitudes (Catchings and others, this volume, chap. I, fig. I7). The contact between basement rocks and overlying Cretaceous sediments was placed in figure J7 on the basis of borehole resistivity data and core-sample data, which were extrapolated laterally by using the electrical section.

The high resistivities displayed in figure J7 beneath AMT station chs_005 are anomalous and not understood. This station is close to the James River and is near a country club's main building and restaurant at the southwest end of line. Data for

station chs_005 may be compromised by the land-water boundary or by cultural effects. The resistivity high may represent basement rock that is shallower than that drilled in the USGS-NASA Langley corehole and that is related to Powars' (2000) proposed James River structural zone.

Above the basement and just inside (northeast) of the outer margin, the Cretaceous sediments are thought to be large blocks slumped toward the center of the crater and covered by the Exmore beds (Gohn and others, this volume, chap. C) and postimpact sediments (Powars and others, this volume, chap. G). The resolution in this section is not sufficient to map individual blocks.

Figure J8 shows the resistivity profile on the Middle Peninsula near Mathews, Va. This profile is the directionally invariant arithmetic average calculated (equation 11) from the two measured directions *Ex* and *Ey*. The outer margin of the impact structure along this line coincides approximately with the Suffolk-Big Bethel scarp (Johnson and others, 2001) and stations math.006 and math.007, where a resistivity high extends from basement toward the surface. Resistivities in the sediments are low on both sides of the high interpreted as the outer margin and limit the depth of exploration in some places to 300 m (980 ft). The Bayside corehole (which coincides with station math.009) was drilled during 2001 and penetrated the granitic basement rocks at an altitude of –707.7 m (–2,321.7 ft). The deepest part of the AMT profile reaches the basement in several places, and the basement's top appears to be uneven.

Southeast of stations math.006 and math.007, slumped Cretaceous megablocks are thought to lie above the basement and below the Exmore beds and postimpact sediments. The inverted AMT data do not have the resolution necessary to map individual slumped blocks.

Although the high-resistivity zone that appears near the outer margin on both electrical sections (figs. J7 and J8) is not well understood, it provides enough resistivity contrast to map the outer margin at least on the western and southwestern side of the Chesapeake Bay impact structure. The resistivity high may be caused by freshwater discharging from the Lower Cretaceous sediments at the outer margin, by cementation along the fault zone, or by compaction of the sediments as a result of the impact event. Gubins and Strangway (1978) found similar results while working on the Dumas and Viewfield astroblemes in Saskatchewan: "AMT soundings show in general that these structures are highly resistive in a conductive medium." They also proposed that "to account for the structures being resistive[,] ground water in pore-spaces and fractures must be negligible."

The outer margin of the Chesapeake Bay impact structure is a concentric fault zone that cuts Cretaceous sediments (Poag, 1996). If the westernmost side of the fault zone is normal to the west-to-east regional ground-water flow, then the marginal fault may have provided a permeable zone where water fresher than the brackish water in Chesapeake Bay discharged from the Lower Cretaceous sediments. The resistivity high associated with the marginal fault zone may be caused by the ongoing discharge of freshwater. Alternatively, the resistivity high could be an artifact of the paleo-ground-water flow system; that is, water flowing through the higher permeability material along the ring fracture during the last 35 million years deposited minerals such as SiO_2 and $CaCO_3$ and partially cemented the rocks along and near the fractures. The high could also be caused by some combination of the two processes and impact-related compaction. Further research is needed to resolve this problem.

If the geology is close to a two-dimensional feature such as a vertical fault or vertical contact between different rocks, then the impedance tensor *Z* can be rotated to the angle corresponding to the strike of geologic structures (such as fractures) at each frequency to get a rotated tensor *Z'*. Figures J9 and J10 show polar plots of ellipses generated when the *Zxy* tensor impedances are maximized (aqua ellipses) and the corresponding *Zxx* tensor impedances are minimized (pink ellipses). The angle for each frequency that maximizes $(Z'xy^2 + Z'yx^2)$ is called the principal direction of *Z* and is related to the geologic strike. Interpreting the strike directions requires care because the way the strike is calculated results in a 90° ambiguity; the direction it points corresponds to either a minimum or maximum of *Zxy*.

In homogeneous and isotropic (one-dimensional) geologic settings, polar plots of *Zxy* become circular, and the principal strike angle becomes mathematically unresolvable. Where the geology is two dimensional, the *Zxy* plot becomes elliptical, and the *Zxx* plot approaches a minimum. As the sounding depth of investigation or physical location of the sounding approaches a complex three-dimensional geologic structure, the *Zxx* impedance (pink ellipse) cannot be minimized (figs. J9 and J10). Where the geology is moderately complex, the polar plots take on a peanut shape. Where the geology is extremely complex, the polar plots appear first as bowties and then as large cloverleaves. This type of response can also occur where the data are compromised by coherent noise. Cultural noise and land-water boundary conditions near Chesapeake Bay also contribute to the occasional problems in calculating the principal impedance strike direction.

In general, the principal directions of *Z*, or strike of geologic structures, for the York-James Peninsula are to the northwest (fig. J9). The principal directions of *Z* for the Middle Peninsula are to the northeast (fig. J10). These directions are consistent with fractures parallel to a circular impact structure having a northwest strike on the York-James Peninsula and a northeast strike on the Middle Peninsula (fig. J1).

Text continues on p. J16.

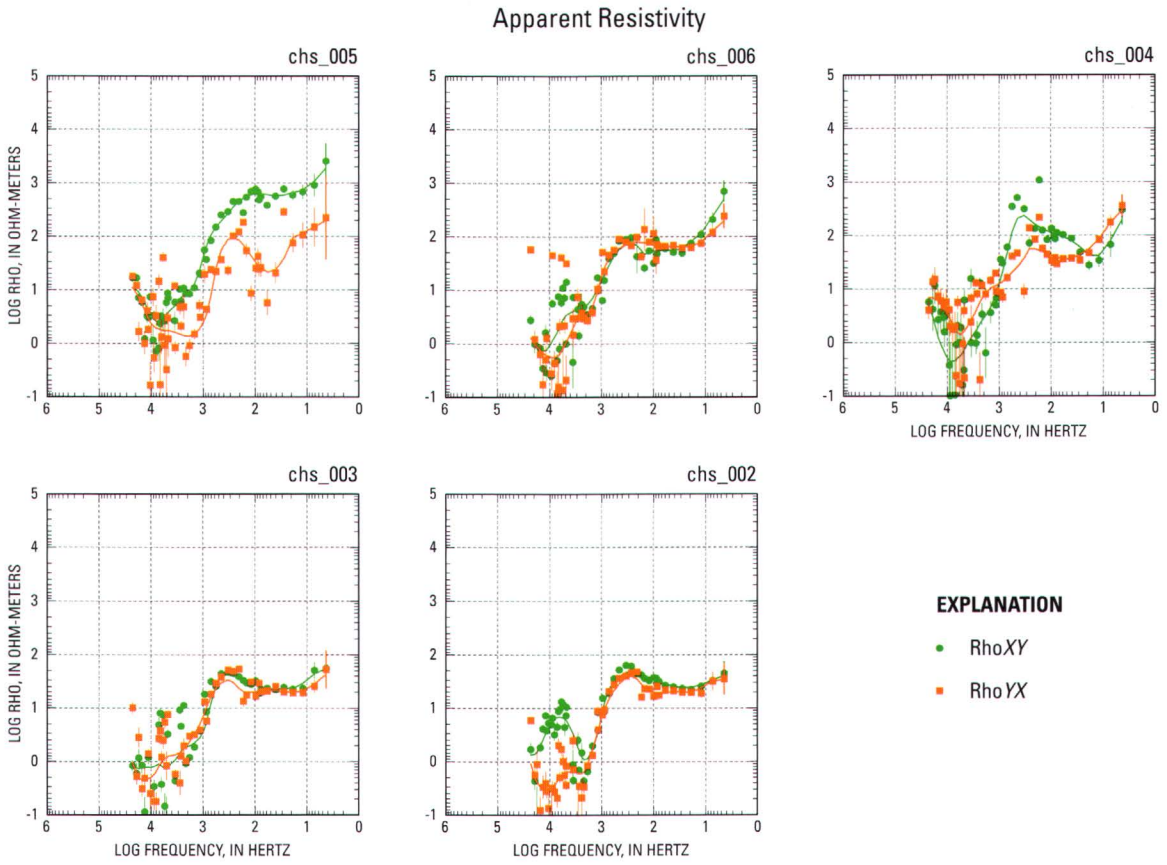

Figure J3. Raw apparent resistivity (ρ, rho) plots of the AMT data collected across the York-James Peninsula, Va., during the spring of 2000. Station locations are shown in figure J2. Data from station chs_001 were rejected because of interference from a buried power conduit. Vertical lines are error bars showing the variance computed by using the method of Gamble and others (1979a). Variables: rho*XY*, resistivity with the electrical (*E*) field in the *x*-direction and the magnetic (*H*) field in the *y*-direction; rho*YX*, resistivity with *E* in the *y*-direction and *H* in the *x*-direction.

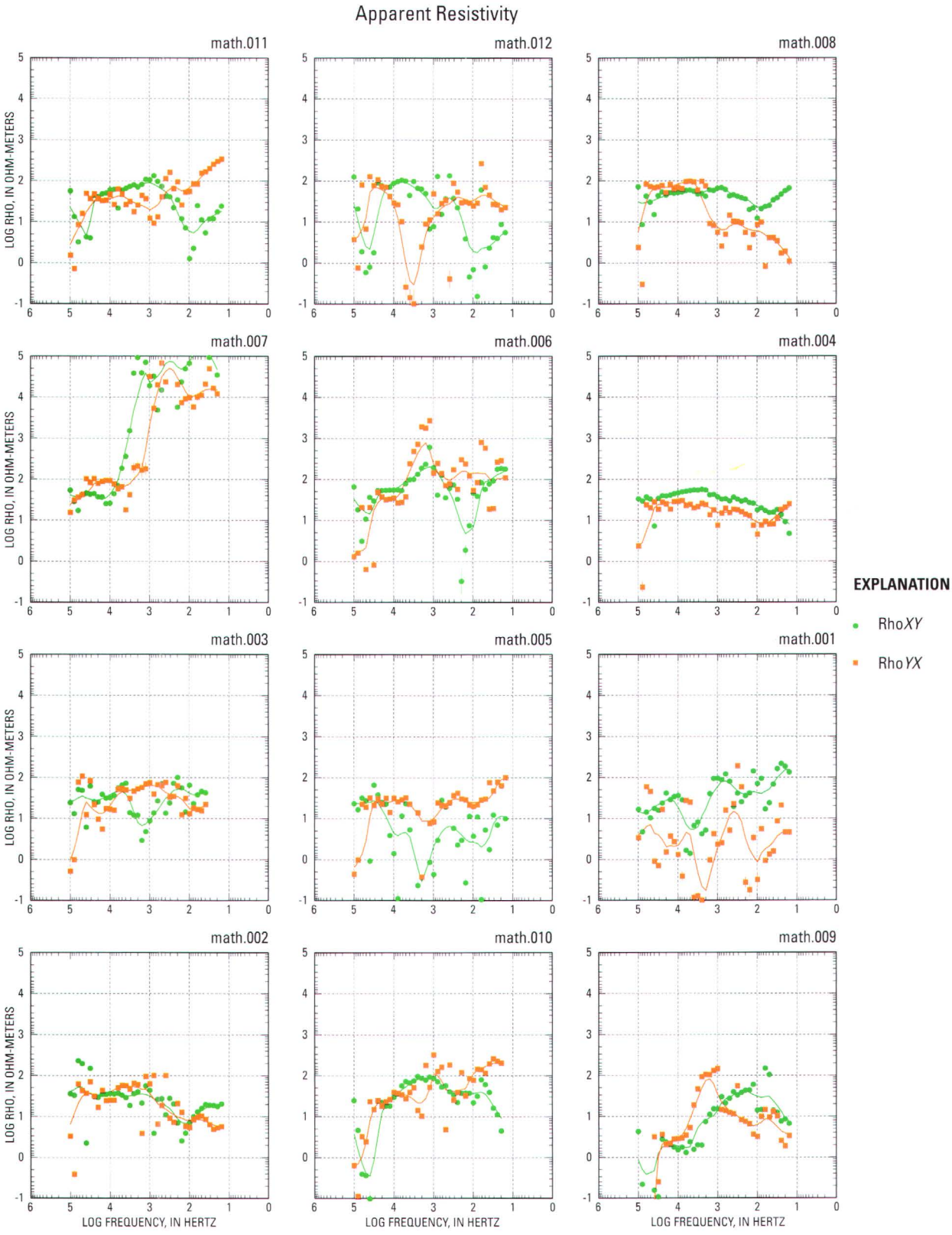

Figure J4. Raw apparent resistivity (ρ, rho) plots of the AMT data collected on the Middle Peninsula near Mathews, Va., during the spring of 2001. Station locations are shown in figure J2, and the sequence of stations along the line of section dictates the order of graphs in this figure. Vertical lines are error bars showing the variance computed by using the method of Gamble and others (1979a). Variables: rho*XY*, resistivity with the electrical (*E*) field in the *x*-direction and the magnetic (*H*) field in the *y*-direction; rho*YX*, resistivity with *E* in the *y*-direction and *H* in the *x*-direction.

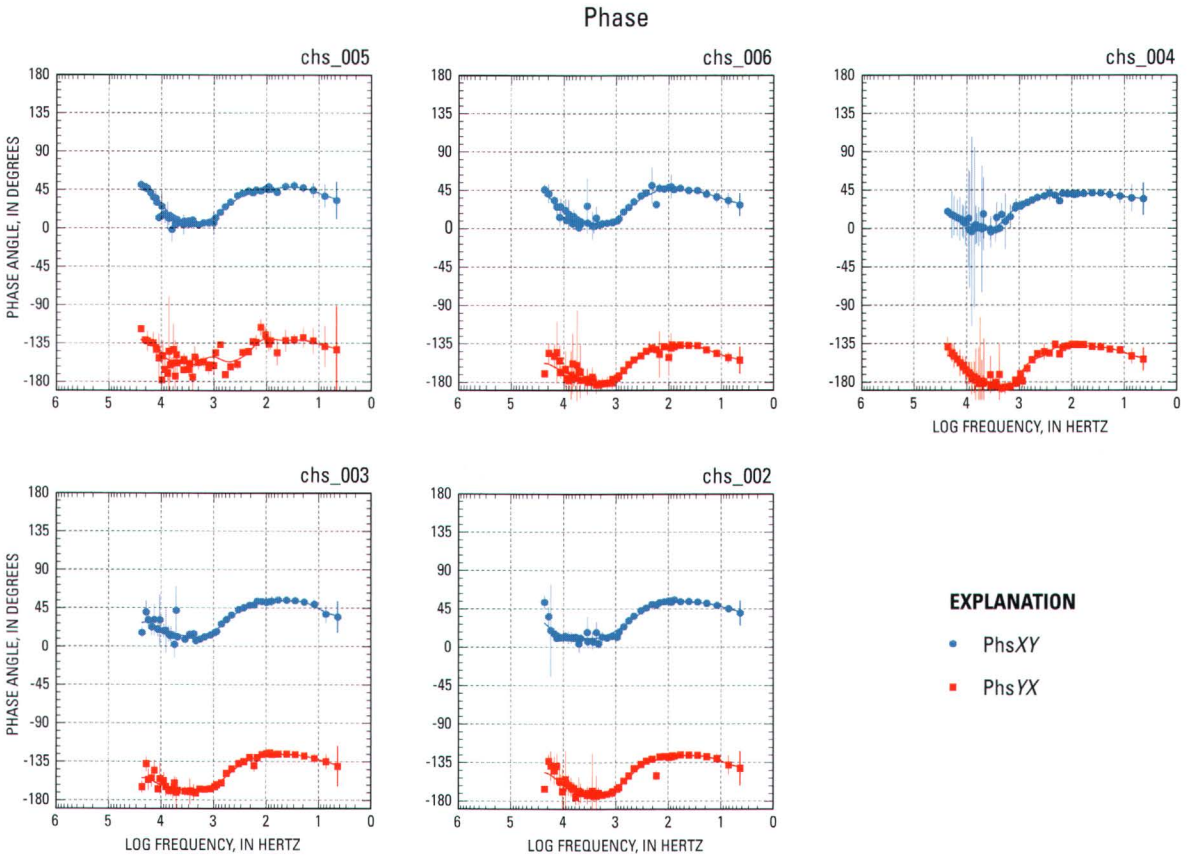

Figure J5. Raw phase (phs) plots of the AMT data collected across the York-James Peninsula, Va., during the spring of 2000. Station locations are shown in figure J2. Data from station chs_001 were rejected because of interference from a buried power conduit. Vertical lines are error bars showing the variance computed by using the method of Gamble and others (1979a). Variables: phs*XY*, phase of the two directions with the electrical (*E*) field in the *x*-direction and the magnetic (*H*) field in the *y*-direction; phs*YX*, phase of the two directions with *E* in the *y*-direction and *H* in the *x*-direction.

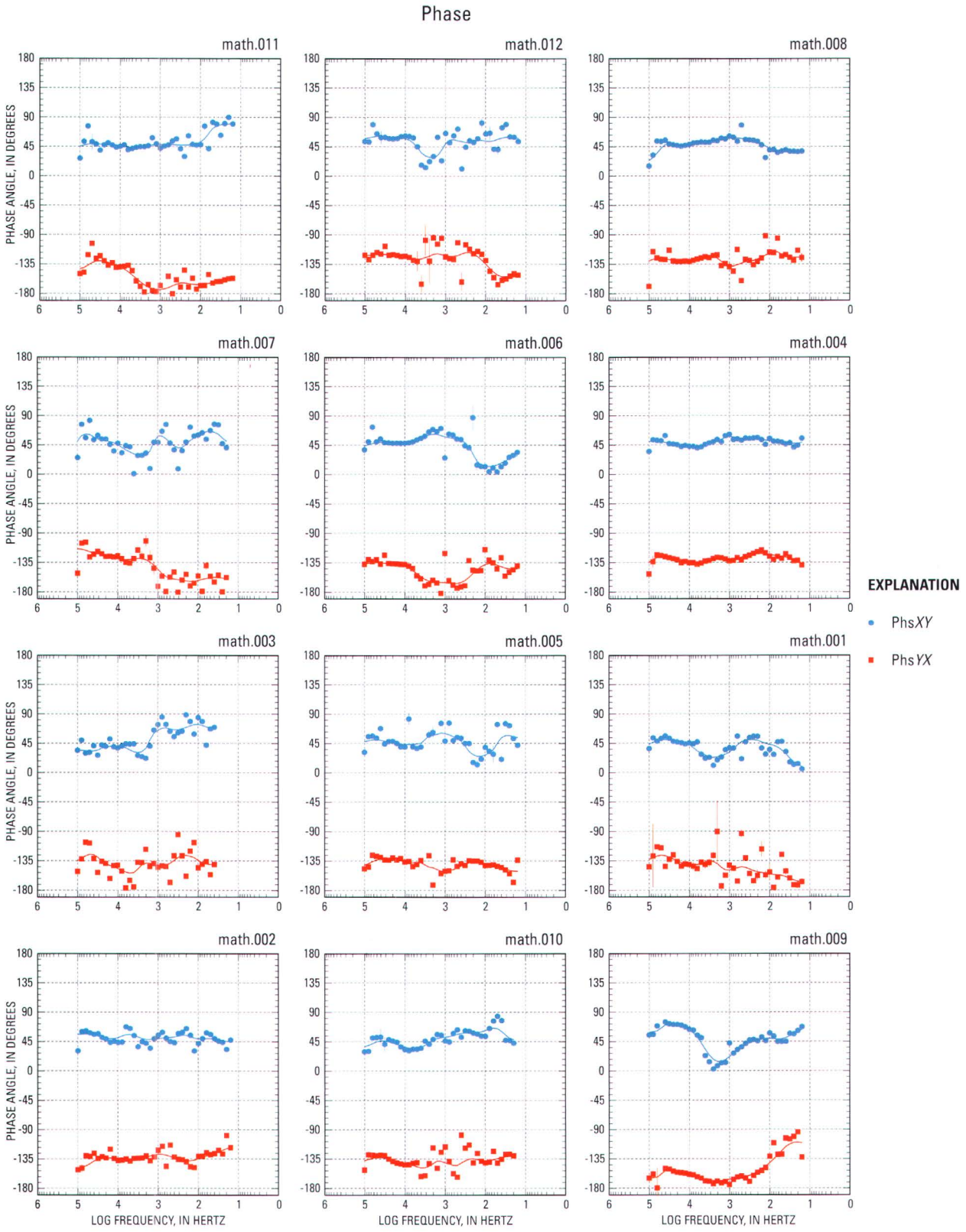

Figure J6. Raw phase (phs) plots of the AMT data collected on the Middle Peninsula near Mathews, Va., during the spring of 2001. Station locations are shown in figure J2, and the sequence of stations along the line of section dictates the order of graphs in this figure. Vertical lines are error bars showing the variance computed by using the method of Gamble and others (1979a). Variables: phs*XY*, phase of the two directions with the electrical (*E*) field in the *x*-direction and the magnetic (*H*) field in the *y*-direction; phs*YX*, phase of the two directions with *E* in the *y*-direction and *H* in the *x*-direction.

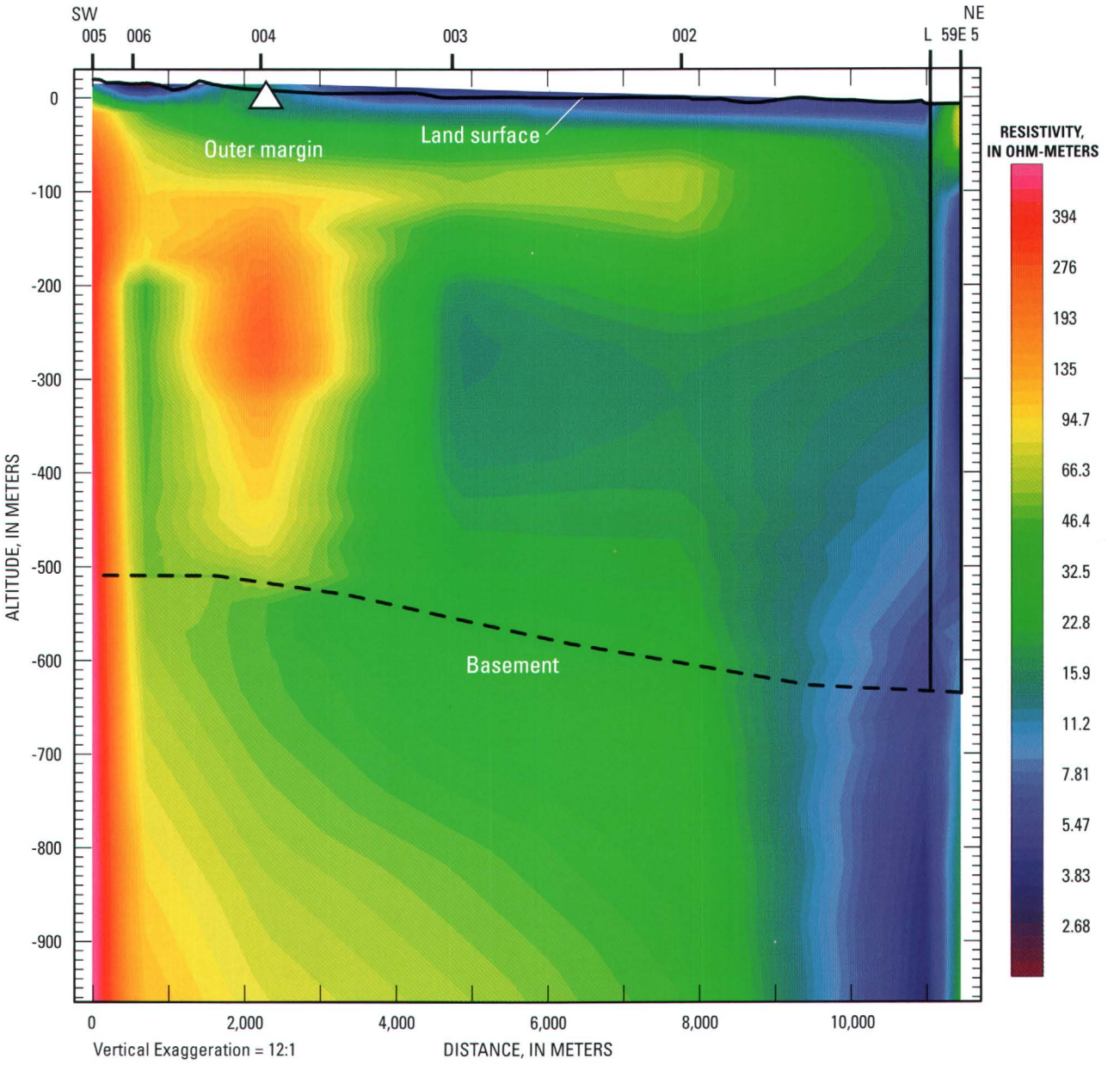

Figure J7. Bostick inverted electrical resistivity section with the electrical (*E*) field in the *x*-direction and the magnetic (*H*) field in the *y*-direction across the York-James Peninsula, Va. The strike of the section is N. 61° E. AMT station locations are shown in figure J2; to save space, the station numbers 002–006 across the top of the section lack the prefix "chs_." The two stations at the right side of the section are at the National Aeronautics and Space Administration (NASA) Langley Research Center in Hampton, Va.: the USGS-NASA Langley corehole (L), which was drilled in 2000, and the NASA Langley test well (59E 5), which was drilled in 1974; see Powars and others (this volume, chap. G, fig. G4). The resistivity data from the two holes at Langley were generated from induction borehole log data (the 2000 log is given by Powars and others, this volume, chap. G, fig. G7; the 1974 log is unpub. data on file at the Richmond, Va., office of the USGS). The altitude is shown in meters below mean sea level. The contact at the top of basement rocks is based upon the granite contacts drilled in the 1974 and 2000 wells extrapolated to the southwest. The depth of granite in the 1974 well was given by Johnson (1975, table 1) as 636 m (2,088 ft), which was corrected to an altitude of –633.7 m (–2,079 ft) (D.S. Powars, USGS, written commun., 2005); the depth of granite in the 2000 well (Horton and others, this volume, chap. B) was converted to an altitude of –623.9 m (–2,046.8 ft). The interpreted location of the outer margin of the Chesapeake Bay impact structure coincides with the resistivity high near station chs_004.

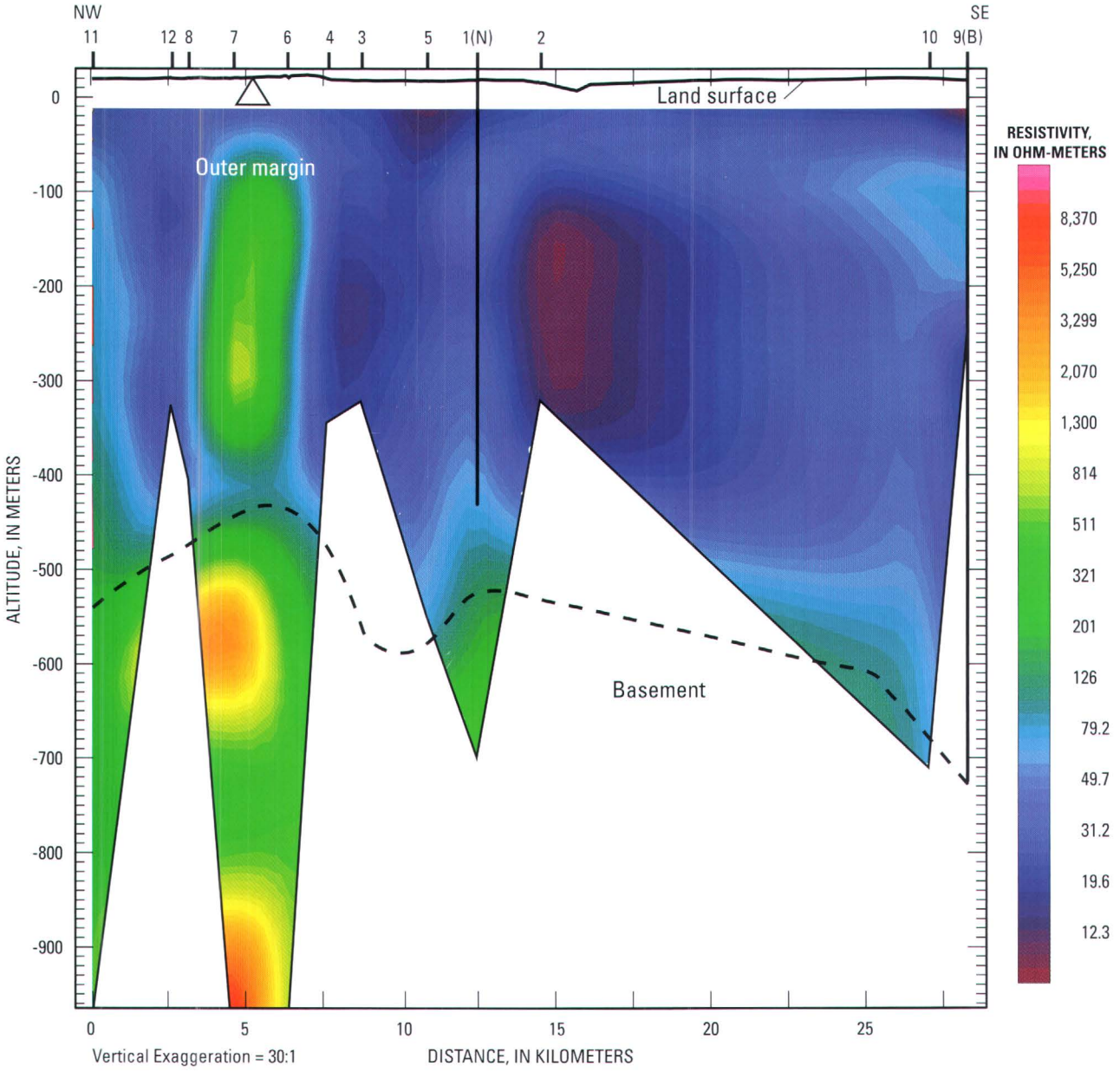

Figure J8. Bostick depth section showing a plot of arithmetic average resistivities computed from the two directions (*Ex* and *Ey*) across the Middle Peninsula, Va. The strike of the section is S. 46° E. AMT station locations are shown in figure J2; to save space, the station numbers across the top of the section lack the prefix "math.0." The altitude is shown in meters below mean sea level. Depth of the colored resistivity cross section is limited by low resistivities encountered in the near surface. The North (N) corehole coincides with AMT station math.001, and the Bayside (B) corehole coincides with AMT station math.009; both coreholes were drilled by the USGS in 2001. The Bayside corehole penetrated the Cretaceous sediment contact with the granite basement at an altitude of –707.7 m (–2,321.7 ft). The bottom of the North corehole at an altitude of –430.5 m (–1,412.5 ft) did not penetrate the granite basement. The dashed line is the basement contact interpreted by using the Bayside and North coreholes as ground truth. The interpreted location of the outer margin of the Chesapeake Bay impact structure coincides with the resistivity high measured at AMT stations math.006 and math.007 and with the Suffolk-Big Bethel scarp identified in figure J1.

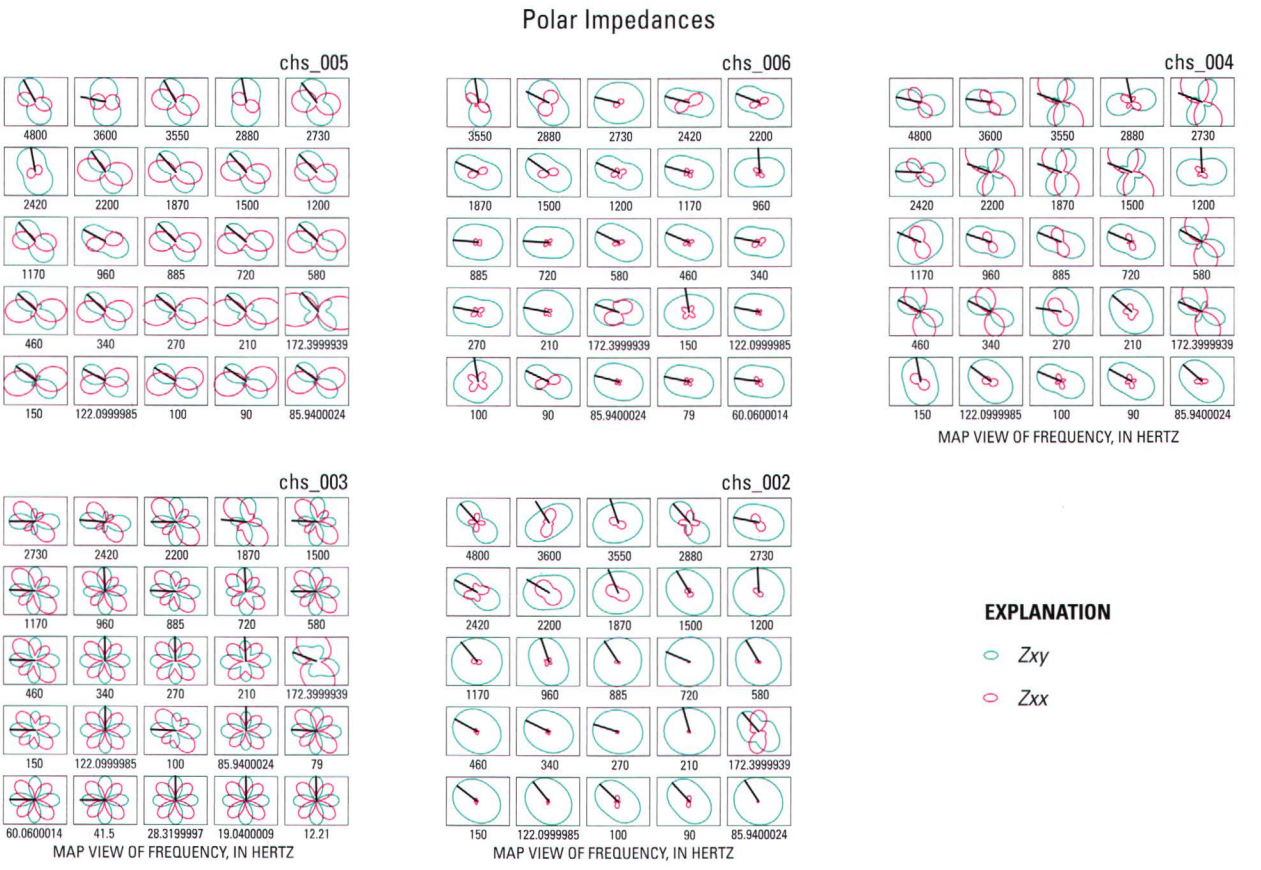

Figure J9. Polar impedance and impedance strike plots for the stations (fig. J2) where AMT data were collected across the York-James Peninsula, Va., during the spring of 2000. For each station, data are plotted for 25 different frequencies selected to show the largest spread. *Zxy* tensor impedances (aqua ellipses) are maximized, and corresponding *Zxx* tensor impedances (pink ellipses) are minimized. The black line that originates at the center of each polar-plot ellipse represents the principal impedance strike direction. North is at the top of the page.

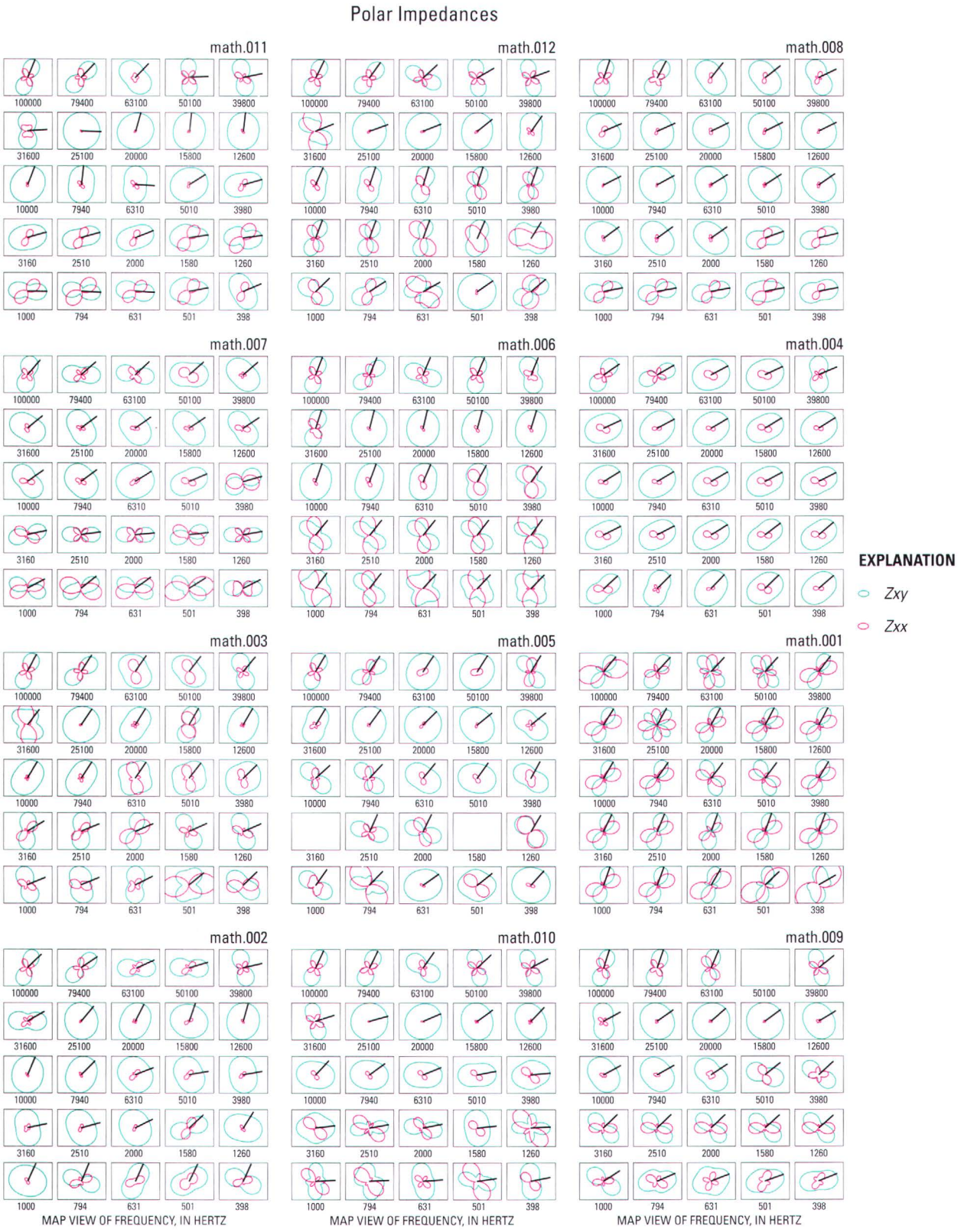

Figure J10. Polar impedance and impedance strike plots for the stations (fig. J2) where AMT data were collected on the Middle Peninsula near Mathews, Va., during the spring of 2001. For each station, data are plotted for 25 different frequencies to show the largest spread. Blank plots indicate inactive frequencies. *Zxy* tensor impedances (aqua ellipses) are maximized, and corresponding *Zxx* tensor impedances (pink ellipses) are minimized. The black line that originates at the center of each polar-plot ellipse represents the principal impedance strike direction. North is at the top of the page.

Conclusions

A resistivity contrast in sediments near the outer margin of the Chesapeake Bay impact structure measured on both the York-James Peninsula and the Middle Peninsula AMT profiles can be used to map the location of the outer margin of the impact structure. The reason the resistivity contrast exists and is associated with the outer margin is not clearly understood but may be attributed to a combination of freshwater intrusion, cementation, or impact-related compaction. Although electromagnetic readings in urban and suburban areas are typically noisy, useful resistivity profiles can be obtained in these areas if care is taken in selecting station locations.

In places, the depth of exploration was great enough to map the lateral contact between Cretaceous sediments and Proterozoic and Paleozoic basement rocks. The basement contact, however, was close to the limit of the technique's resolution and depth of exploration, especially near Mathews, Va.; in that area, low resistivities in the near-surface sediments limited the depth of exploration. Three-dimensional structures in Cretaceous sediments above the basement contact and within the annular trough probably lack contrasts in resistivity and thus could not be imaged well enough to suggest shapes such as slumped megablocks.

Polar plots generated for AMT stations on the York-James Peninsula indicate that the strike is to the northwest. Polar plots for AMT stations on the Middle Peninsula indicate a strike to the northeast. The principal directions for the impedance strike trends are generally consistent with fractures parallel to the curvilinear trend of the outer margin, with exceptions for stations near the brackish water in Chesapeake Bay.

Acknowledgments

U.S. Geological Survey (USGS) investigations of the Chesapeake Bay impact structure are conducted in cooperation with the Hampton Roads Planning District Commission, the Virginia Department of Environmental Quality, and the National Aeronautics and Space Administration (NASA) Langley Research Center. I extend a special thanks to Matt Smith (USGS), Professor Gerald H. Johnson (of the Department of Geology of the College of William and Mary), Professor Rick Berquist (of the Department of Geology of the College of William and Mary), and his students, Tim Russel and Heidi Romine, without whose field help this work would have been much harder.

References Cited

Bostick, F.X., Jr., 1977, A simple and almost exact method of MT analysis, *in* Workshop on Electrical Methods in Geothermal Exploration: Salt Lake City, Utah, University of Utah, p. 175–177. (Prepared under USGS contract 14–08–0001–G–359.)

Cagniard, Louis, 1950, Procédé de prospection géophysique [Procedure of geophysical prospecting]: French patent no. 1025683, 6 p., available online at http://l2.espacenet.com/espacenet/bnsviewer?CY=ep&LG=en&DB=EPD&PN=FR1025683&ID=FR+++1025683A++I+

Cagniard, Louis, 1953, Basic theory of the magneto-telluric method of geophysical prospecting: Geophysics, v. 18, no. 3, p. 605–635.

Dmitriev, V.I., and Berdichevsky, M.N., 1979, The fundamental model of magnetotelluric sounding: Proceedings of the IEEE (Institute of Electrical and Electronics Engineers), v. 67, no. 7, p. 1034–1044.

Gamble, T.D., Goubau, W.M., and Clarke, J., 1979a, Error analysis for remote reference magnetotellurics: Geophysics, v. 44, no. 5, p. 959–968.

Gamble, T.D., Goubau, W.M., and Clarke, J., 1979b, Magnetotellurics with a remote magnetic reference: Geophysics, v. 44, no. 1, p. 53–68.

Gubins, A., and Strangway, D.W., 1978, Magnetic and audio frequency magnetotelluric (AMT) investigations at the Dumas and Viewfield, Saskatchewan astroblemes [abs.]: Eos, Transactions, American Geophysical Union, v. 59, no. 12, p. 1036.

Hoover, D.B., Frischknecht, F.C., and Tippens, C.L., 1976, Audiomagnetotelluric sounding as a reconnaissance exploration technique in Long Valley, California: Journal of Geophysical Research, v. 81, no. 5, p. 801–809.

Hoover, D.B., and Long, C.L., 1976, Audio-magnetotelluric methods in reconnaissance geothermal exploration: United Nations Symposium on the Development and Use of Geothermal Resources, 2d, San Francisco, Calif., 20–29 May 1975, Proceedings, v. 2, p. 1059–1064.

Hoover, D.B., Long, C.L., and Senterfit, R.M., 1978, Some results from audiomagnetotelluric investigations in geothermal areas: Geophysics, v. 43, no. 7, p. 1501–1514.

Johnson, G.H., Powars, D.S., Bruce, T.S., Beach, T.A., Harris, M.S., and Goodwin, B.K., 2001, Post-impact effects of the Eocene Chesapeake Bay impact, lower York-James Peninsula, Virginia: Virginia Geological Field Conference, 31st, Williamsburg, Virginia, October 19 and 20, 2001 [Guidebook], 40 p.

Johnson, S.S., 1975, Bouger gravity in southeastern Virginia: Virginia Division of Mineral Resources Report of Investigations 39, 42 p.

Keller, G.V., and Frischknecht, F.C., 1966, Electrical methods in geophysical prospecting: London, Pergamon Press, 519 p.

Poag, C.W., 1996, Structural outer rim of Chesapeake Bay impact crater—Seismic and bore hole evidence: Meteoritics & Planetary Science, v. 31, no. 2, p. 218–226.

Poag, C.W., Hutchinson, D.R., Colman, S.M., and Lee, M.W., 1999, Seismic expression of the Chesapeake Bay impact crater; Structural and morphologic refinements based on new seismic data, *in* Dressler, B.O., and Sharpton, V.L., eds., Large meteorite impacts and planetary evolution; II: Geological Society of America Special Paper 339, p. 149–164.

Poag, C.W., Plescia, J.B., and Molzer, P.C., 1999, Chesapeake Bay impact structure; Geology and geophysics [abs.], *in* Gersonde, Rainer, and Deutsch, Alexander, eds., Oceanic impacts; Mechanisms and environmental perturbations; ESF–IMPACT Workshop, April 15–April 17, 1999, Alfred Wegener Institute for Polar and Marine Research, Bremerhaven, Germany, Abstracts: Berichte zur Polarforschung (Reports on Polar Research), v. 343, p. 79–83.

Powars, D.S., 2000, The effects of the Chesapeake Bay impact crater on the geologic framework and the correlation of the hydrogeologic units of southeastern Virginia, south of the James River: U.S. Geological Survey Professional Paper 1622, 53 p., 1 oversize pl. (Also available online at http://pubs.usgs.gov/prof/p1622)

Powars, D.S., and Bruce, T.S., 1999, The effects of the Chesapeake Bay impact crater on the geological framework and correlation of hydrogeologic units of the lower York-James Peninsula, Virginia: U.S. Geological Survey Professional Paper 1612, 82 p., 9 oversize pls. (Also available online at http://pubs.usgs.gov/prof/1612)

Sheriff, R.E., and Geldart, L.P., 1982, History, theory, and data acquisition, v. 1 *of* Exploration seismology: Cambridge, U.K., Cambridge University Press, 253 p.

Spies, B.R., and Frischknecht, F.C., 1991, Electromagnetic sounding, *in* Nabighian, M.N., and Corbett, J.D., eds., Electromagnetic methods in applied geophysics: Society of Exploration Geophysicists Investigations in Geophysics no. 3, v. 2 (Applications), pt. A, p. 285–422.

Sutarno, Doddy, and Vozoff, Keeva, 1991, An application of regression *M*-estimation with the Hilbert transform to magnetotelluric data processing: Exploration Geophysics, v. 22, no. 2, p. 383–389.

Vozoff, Keeva, 1986, Magnetotelluric methods: Society of Exploration Geophysicists Geophysics Reprint Series no. 5, 763 p.

Vozoff, Keeva, 1991, The magnetotelluric method, *in* Nabighian, M.N., and Corbett, J.D., eds., Electromagnetic methods in applied geophysics: Society of Exploration Geophysicists Investigations in Geophysics no. 3, v. 2 (Applications), pt. A, p. 641–712.

Wait, J.R., 1962, Theory of magnetotelluric fields: U.S. National Bureau of Standards Journal of Research, Radio Propagation, v. 66D, p. 509–541.

Distribution, Origin, and Resource-Management Implications of Ground-Water Salinity along the Western Margin of the Chesapeake Bay Impact Structure in Eastern Virginia

By E. Randolph McFarland and T. Scott Bruce

Chapter K of
**Studies of the Chesapeake Bay Impact Structure—
The USGS-NASA Langley Corehole, Hampton, Virginia, and
Related Coreholes and Geophysical Surveys**

Edited by J. Wright Horton, Jr., David S. Powars, and Gregory S. Gohn

Prepared in cooperation with the
Hampton Roads Planning District Commission,
Virginia Department of Environmental Quality, and
National Aeronautics and Space Administration Langley Research Center

Professional Paper 1688

U.S. Department of the Interior
U.S. Geological Survey

Contents

Figures

Table

Distribution, Origin, and Resource-Management Implications of Ground-Water Salinity along the Western Margin of the Chesapeake Bay Impact Structure in Eastern Virginia

By E. Randolph McFarland[1] and T. Scott Bruce[2]

Abstract

Stratified unconsolidated sediments that compose a regionally extensive system of aquifers and confining units beneath the Virginia Coastal Plain contain saltwater approximately 50 kilometers (30 miles) landward of its normally expected position along the coast. Part of the Chesapeake Bay impact structure (formed by the collision of a large asteroid or comet) underlies the Virginia Coastal Plain. The impact severely disrupted preexisting sediments, and its effects are still influencing the regional ground-water flow. Geologic and hydrologic evidence indicates that the impact structure contains seawater emplaced during a regional inundation approximately 2 million years ago, along with much older seawater and evaporative brine emplaced potentially as far back as the impact event 35 million years ago.

With emergence of the coastal plain and resumption of ground-water recharge during the past 2 million years, freshwater flushing displaced residual seawater across the region but was impeded across the impact structure by the clayey Chickahominy Formation. Flushing took place laterally along the crater outer margin through underlying crater-fill sediments, followed by upward leakage and surface discharge to areas outside of the crater. Saltwater within the impact structure maintained its present position even as flushing outside of the impact structure extended in places nearly to the edge of the continental shelf during the Pleistocene glacial maximum of 18,000 years ago. Sea level has since risen to its present position, and the residual seawater has merged with the modern ocean along an inverted and unstable transition zone along the western margin of the impact structure that separates fresh ground water to the west from saltwater to the east.

During the past century, hydraulic gradients have been greatly increased and flow has been redirected landward across regional cones of depression centered on industrial pumping centers located outside of the impact structure. Saltwater intrusion across regional distances from the impact structure has not taken place, however, because most of the ground water now present was emplaced prior to the onset of heavy pumping. Because saltwater within the impact structure maintained its present position for millennia during freshwater flushing prior to pumping, a potentially very long timeframe could be required for regional saltwater intrusion to occur even under present gradients.

In contrast, localized saltwater movement along the western margin of the impact structure is possible across relatively short distances because of municipal withdrawals being made from within the saltwater transition zone. Major increases in withdrawal and desalinization of brackish ground water from the transition zone are being projected to address rapidly growing demands for public supplies during the coming several decades. Water-supply planning is challenged, however, by future increases in ground-water salinity that are difficult to estimate because of complex hydrogeologic controls and withdrawal-induced effects within the transition zone. A detailed local-scale characterization of hydrologic conditions along the western margin will be critical to assessment of the potential for saltwater movement.

[1]U.S. Geological Survey, Richmond, VA 23228.
[2]Virginia Department of Environmental Quality, P.O. Box 10009, Richmond, VA 23240.

Introduction

Part of the Chesapeake Bay impact structure underlies the coastal plain of eastern Virginia (fig. K1). The structure was produced approximately 35 million years ago by the collision of a large asteroid or comet (Powars and Bruce, 1999). The area that became eastern Virginia was covered by the Atlantic Ocean at the time of impact. The discovery of the buried structure in the 1990s has led to a new understanding of regional ground-water flow.

Coastal plain aquifers are a heavily used water resource in Virginia (Hammond and Focazio, 1995). Large and increasing withdrawals have resulted in significant and continuing water-level declines (Hammond and others, 1994a,b,c) and have altered ground-water flow directions to create the potential for saltwater intrusion. In order to characterize and understand the hydrologic function of the aquifer system, a regional-scale hydrogeologic framework (Meng and Harsh, 1988) and ground-water flow model (Harsh and Laczniak, 1990) of the Virginia Coastal Plain were developed by U.S. Geological Survey (USGS) scientists during the early 1980s under the Regional Aquifer-System Analysis (RASA) Program. The framework and model were adopted by the Virginia Department of Environmental Quality (VDEQ) as a means to organize ground-water information and to evaluate the potential effects of proposed and existing withdrawals on ground-water levels and flows (McFarland, 1998).

In the RASA model, the Virginia Coastal Plain was depicted as a seaward-dipping and seaward-thickening, stratified sequence of unconsolidated sediments that made up a regionally extensive, vertically layered system of aquifers and confining units (fig. K2). The old model was based on the following ideas: (1) The unconfined aquifer at the land surface was recharged by infiltration of rainwater, some of which leaked downward through underlying confining units to recharge deeper confined aquifers. (2) Water flowed laterally through the aquifers toward the coast. (3) Upon encountering more dense saltwater, flow was diverted back to the surface as upward leakage and was discharged to Chesapeake Bay and the Atlantic Ocean.

Ground-water management efforts need to keep pace with changing demands on the resource and with current knowledge of the aquifer system. The amounts and locations of ground-water withdrawals have changed from those that were incorporated in the RASA model. In addition, recent efforts to further characterize the aquifer system have identified significant features that are not adequately represented in the original framework and model. Among these, the Chesapeake Bay impact structure requires changes to previous conceptualizations of the aquifer system as having a relatively simple layered configuration. The preexisting composition and structure of sediments within the impact area are now known to have been severely disrupted by the force of the collision, resulting in a complex stratigraphic and structural configuration. Strata affected by the impact were partly to entirely truncated across a crater and replaced by a chaotic mix of crater-fill sediments. The configuration of the outer regions of the impact structure is theorized to be controlled by a complex array of faults.

USGS and VDEQ scientists are investigating the Chesapeake Bay impact event and its effects on the geologic history of the region. Concomitantly, USGS and VDEQ researchers are analyzing geologic, hydrologic, and geophysical data to revise the hydrogeologic framework of the Virginia Coastal Plain, including the impact structure. In addition, a comprehensive assessment is being made of the quantities and distribution of ground-water withdrawals. All of these components are planned to contribute to an in-depth analysis and revision of the ground-water flow model.

In addition to the above studies, research is being done to obtain a better understanding of the processes affecting the distribution of saltwater within the aquifers. Parts of some aquifers across eastern Virginia have been known for many decades to contain saltwater approximately 50 kilometers (30 miles) landward of its expected position along the coast (Sanford, 1913; see fig. K1 of this chapter). The zone of saltwater is termed the "inland saltwater wedge"; it predates large ground-water withdrawals and was formed under unstressed conditions. Although localized increases in chloride concentration of several percentage points have been observed at various times during the history of ground-water development (Smith, 1999), regional saltwater intrusion has not taken place despite stress-induced water-level declines and altered flow directions. The western margin of the saltwater wedge is now recognized to coincide with the western margin of the Chesapeake Bay impact structure (Powars and Bruce, 1999). Thus, the impact structure has been inferred to play some role in the origin of the saltwater wedge and in controlling its response to pumping stresses.

Although some explanations for the presence of the saltwater wedge have been suggested both prior to (Cederstrom, 1943) and following (Powars and Bruce, 1999) the discovery of the impact structure, no definitive findings have been previously documented. Knowledge of processes controlling the salinity distribution is needed to support sound management of the ground-water resource. In addition to historically lowered water levels and altered flow directions that create the potential for saltwater intrusion, recent trends of increasing ground-water withdrawals within areas of elevated salinity (with subsequent desalinization treatment) pose the likelihood of additional effects on the salinity distribution. Hence, a clear understanding of the origin and emplacement of the saltwater is needed to predict its future response to numerous and diverse stresses on the flow system.

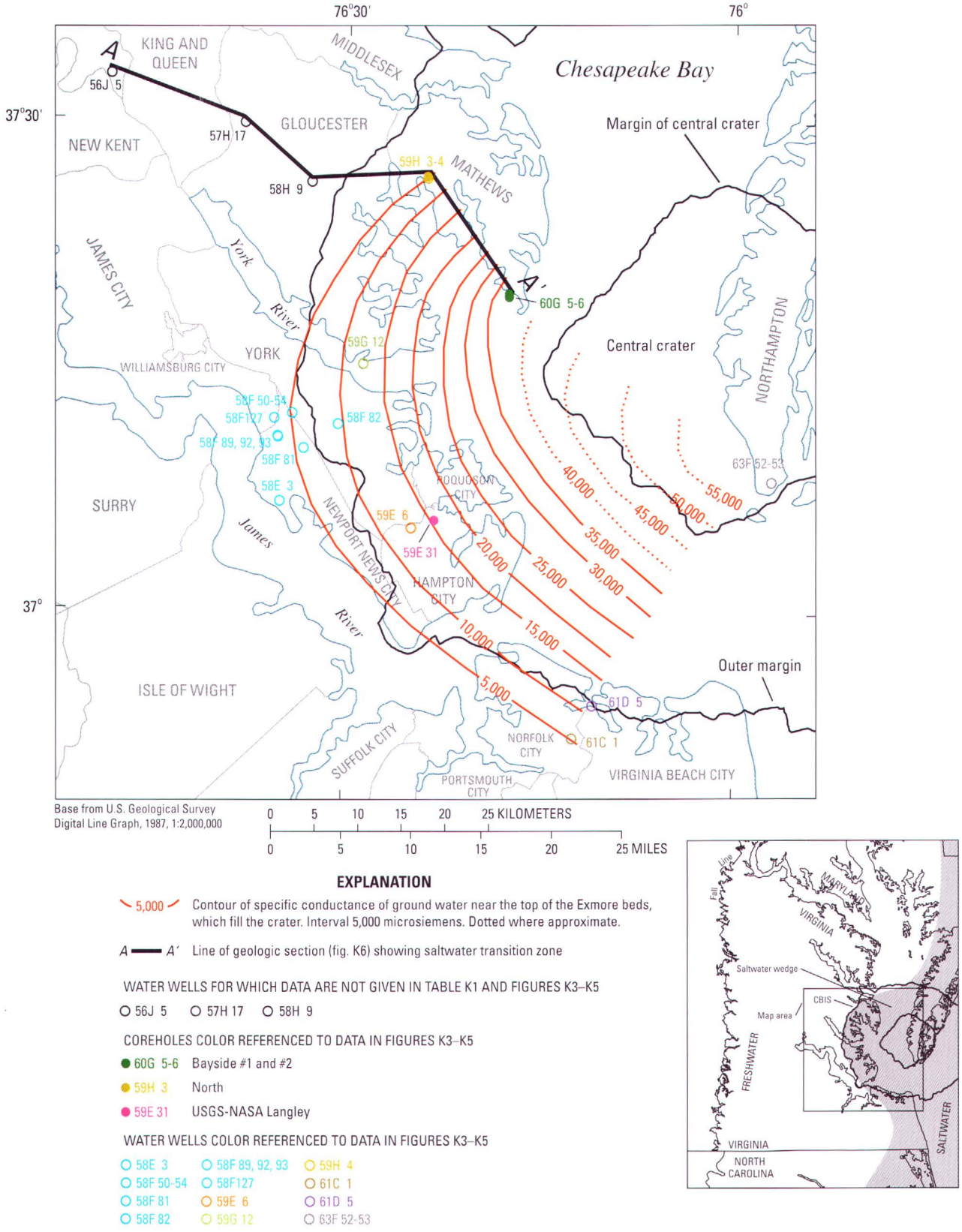

Figure K1. Map showing locations of sediment-core sites (coreholes) and well sites and ground-water specific conductance near the top of the Exmore beds along the western margin of the Chesapeake Bay impact structure (CBIS) in the Virginia Coastal Plain. Site locations are color referenced to sample data shown in figures K3–K5; chemical data for samples from these sites are in table K1 (at end of this chapter). Three open black circles indicate wells for which data are plotted in section *A–A'* in figure K6; no data for these wells are given in table K1 or figures K3–K5. Crater margins from Powars and Bruce (1999) and Powars (2000). Index map shows the distribution of fresh (unshaded) and salty (shaded) ground water and the location of the saltwater wedge.

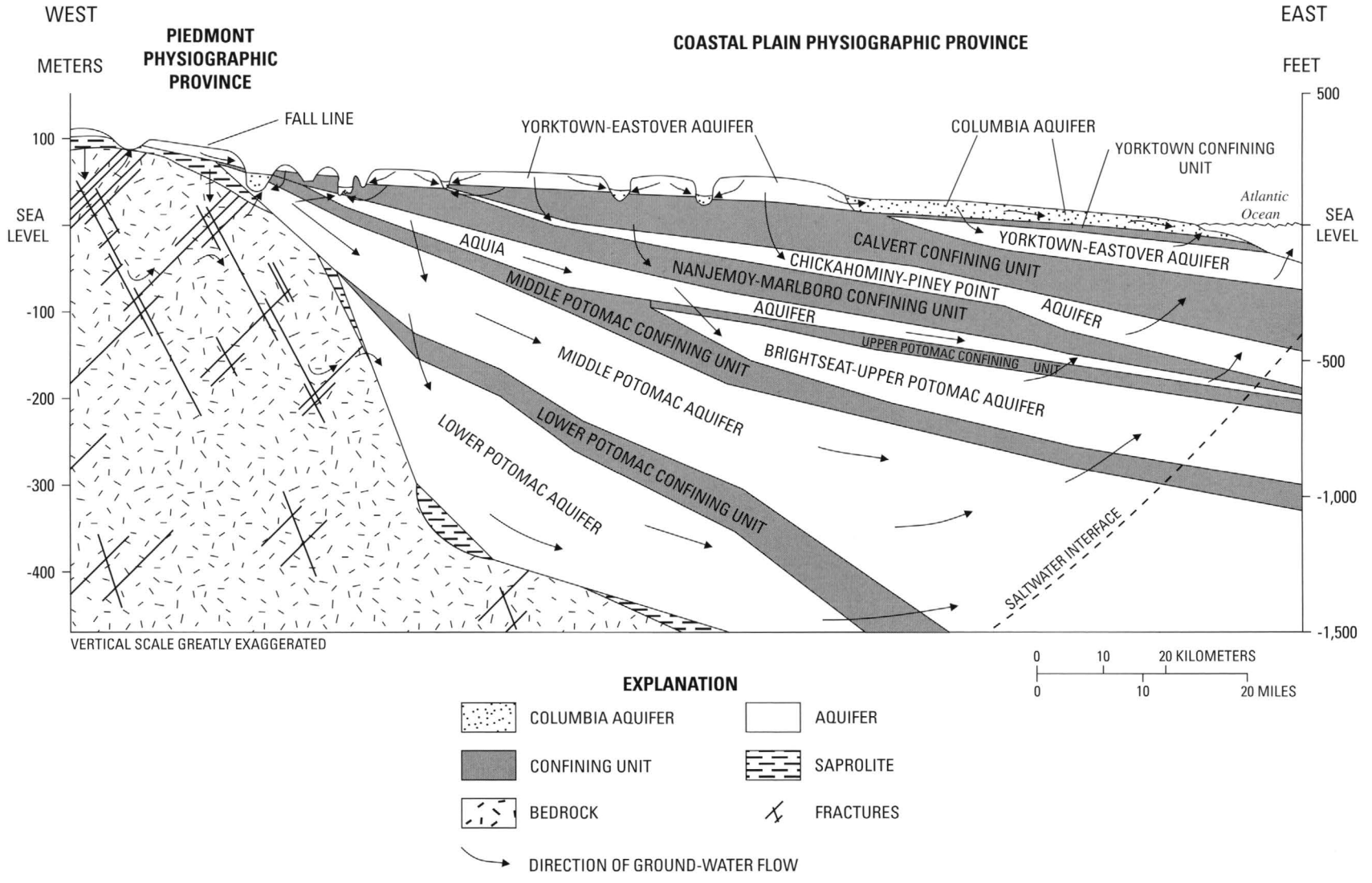

Figure K2. Conceptual hydrogeologic section representing the Virginia Coastal Plain Province as vertically layered aquifers and confining units. Modified from Harsh and Laczniak (1990). This section illustrates concepts held before the discovery of the Chesapeake Bay impact structure.

Purpose and Scope

As part of studies of the geology of the Chesapeake Bay impact structure, continuous sediment cores were obtained at three locations along the western margin of the impact structure during 2000–2001 (fig. K1, table K1 at end of this chapter): USGS-NASA Langley corehole (site 59E 31), North corehole (site 59H 3), and Bayside coreholes 1 and 2 (sites 60G 5 and 60G 6). In order to interpret various aspects of the impact event and its effects on the geologic history of the region, detailed analyses are being performed of the USGS-NASA Langley core; they focus on stratigraphy and structure (Gohn and others, this volume, chap. C; Poag and Norris, this volume, chap. F; Powars and others, this volume, chap. G), petrology (Horton and others, this volume, chap. B; Horton and Izett, this volume, chap. E), and paleontology (Frederiksen and others, this volume, chap. D; Edwards and others, this volume, chap. H). In addition, to delineate the extent and configuration of the impact structure, the Langley core data are being used with borehole and surface geophysical data (Catchings and others, this volume, chap. I; Pierce, this volume, chap. J).

USGS and VDEQ scientists are collecting ground-water quality data and additional information for the area having elevated salinity in ground water along the western margin of the Chesapeake Bay impact structure in the coastal plain of eastern Virginia. As part of this effort, ground water was extracted from samples of the Langley, North, and Bayside cores and was analyzed. Additional existing ground-water quality data collected from 19 nearby water-well sites also have been examined (table K1).

This chapter, K, presents data from chemical analyses of ground water extracted from sediment cores and collected from water wells, describes the distribution of the data areally and with depth, and delineates the configuration of the saltwater transition zone. The origin of the saltwater is assessed by relating possible sources of the salinity to chemical evidence. Lastly, ideas on the origin of the salinity are used to identify possible effects of present and future ground-water withdrawal on the salinity distribution.

Methods

Sediment-Core Water

Continuous sediment cores were obtained at three locations along the western margin of the Chesapeake Bay impact structure during 2000–2001 (fig. K1): USGS-NASA Langley, North, and Bayside coreholes. Hydraulic-rotary drilling with wire-line coring was performed to obtain cores having a nominal diameter of 6.4 centimeters (cm; 2.5 inches (in.)); the cores provide nearly complete sediment profiles from land surface into underlying basement bedrock to depths of nearly 730 meters (m; 2,400 feet (ft)). Thicknesses of overlying sediment of more than 700 m (2,300 ft) were penetrated and include pre-impact formations, crater-fill sediments, and overlying postimpact formations.

Comprehensive sampling of 163 subsections (about 15 cm (6 in.) long) of sediment core was performed during drilling operations at all three sites to provide high-resolution detail of vertical changes in ground-water salinity and related chemistry. Sample collection and processing followed procedures developed by Manheim and others (1994). Care was taken with field procedures to preclude conditions that could potentially alter the chemistry of ground water retained in the core sediment, including invasion of drilling mud into the sediment or evaporation of ground water from the sediment.

Following retrieval of core in lengths as great as 3 m (10 ft) from the borehole, sample subsections were collected only from core that was promptly extruded from the core barrel, and any delayed core was left unsampled. In addition, only clearly intact intervals of core were selected, and any deformed or suspect intervals were avoided. Upon extrusion, each sample subsection was quickly measured and sliced from the core prior to rinsing the remaining core to remove drilling mud. The subsection was placed on a clean, dry plastic cutting board, where drilling mud and the outer approximately 1 cm (0.5 in.) of core sediment were sliced away with a clean, dry knife. The resulting innermost diameter of the subsection was then isolated in an air-tight glass jar for storage and transfer from the field to the laboratory for further processing.

Upon transfer from the field, each sample was initially processed by disaggregating the sediment in its glass jar to homogenize it with the retained ground water. Ground water was then extracted from the sediment by using high-pressure squeezing techniques (Manheim and others, 1994). A portion of sediment was placed inside a hand-sized steel cylinder-and-piston device, from which the water was forced under a 12-ton hydraulic press into a small syringe. Typically, several milliliters of water were obtained by each extraction.

All water samples were analyzed for specific conductance immediately upon extraction. Subsequently, selected samples underwent additional analysis. Concentrations of chloride in 36 samples, bromide in 26 samples, and iodide in 27 samples from all three core sites were determined by colorimetry by the USGS National Water-Quality Laboratory (NWQL). Hydrogen (deuterium) and oxygen stable-isotope ratios, calculated relative to Vienna Standard Mean Ocean Water (Fritz and Fontes, 1980), in 15 samples from all three core sites were determined by mass spectrometry by the USGS Isotope Research Laboratory. Isotope ratios of chlorine-36 to total chloride ($^{36}Cl/Cl$) in 12 samples from the USGS-NASA Langley core site were determined by accelerator mass spectrometry by the Purdue Rare Isotope Measurement Laboratory (PRIME Lab).

Well Water

Existing ground-water quality data collected from water wells near the western margin of the Chesapeake Bay impact structure were retrieved from the USGS water-quality database (http://waterdata.usgs.gov/va/nwis/qw). Table K1 shows data for 44 samples collected at 19 water-well sites during 1967–2002. Multiple samples were collected from some wells by zone testing within the borehole during drilling. Specific conductance was determined for all 44 samples, chloride concentrations were determined for 42 samples, bromide concentrations were determined for 28 samples from 13 wells, and iodide concentrations were determined for 9 samples from 2 wells. Hydrogen (deuterium) and oxygen stable-isotope ratios were determined for samples from two wells, one of which was also analyzed to determine the $^{36}Cl/Cl$ ratio, as described above for the samples of sediment-core water.

Ground-Water Salinity

The dissolved constituents in ground water in the area of the Chesapeake Bay impact structure are dominated by sodium cations and chloride anions (Focazio and others, 1993). Other constituents are present at generally much smaller concentrations. Chloride is the constituent of greatest concern for management of the ground-water resource in the Virginia Coastal Plain. Water having a chloride concentration below the U.S. Environmental Protection Agency's (1990) secondary maximum contaminant level of 250 milligrams per liter (mg/L) is commonly referred to as "fresh." Water having chloride concentrations between those of freshwater and seawater (19,000 mg/L according to Hem, 1985) is referred to as "brackish"; such brackish water is widespread in the major water-supply aquifers of the eastern part of the Virginia Coastal Plain. Water having a chloride concentration above that of seawater is called "brine."

Distribution

Chemical data (table K1) were compiled on ground water extracted during 2000–2001 from sediment cores obtained along the western margin of the Chesapeake Bay impact structure and on ground water collected during 1967–2002 from existing water wells in adjacent areas. Corehole and well-site locations collectively span the western and southwestern parts of the impact structure (fig. K1). All three core sites (site numbers 59E 31, 59H 3, and 60G 5–6) are within the estimated structural boundary described as the crater's outer margin (Powars and Bruce, 1999; Powars, 2000). The wells are generally located near the crater's outer margin, and most are outside it. Two wells (63F 52–53) are within the estimated central crater and are closer to the center of the impact structure than any of the other sites. Although well-sample collection times span 35 years, regionally significant changes in ground-water quality have not been observed (Smith, 1999), and the well data generally represent current conditions.

Sediment-Core-Water and Well-Water Chemistry

Chloride concentrations were determined for selected samples of water extracted from sediment cores and for all but two of the samples collected from wells (table K1). Specific conductance was measured in all samples from both cores and wells. Chloride concentration is strongly correlated with specific conductance (correlation coefficient greater than 0.95) in samples for which both determinations were made, ranging from relatively small values through the specific conductance and chloride concentration of seawater of 45,000 microsiemens (μS), and 19,000 mg/L (Hem, 1985), respectively, and higher. Because the dominant constituents of the water are sodium cations and chloride anions, and because specific conductance is related to total dissolved solids, specific conductance can provide a reliable surrogate for chloride concentration in samples for which chloride concentration was not determined. Thus, trends among the much larger number of specific conductance values indicate similar trends among chloride concentrations and can provide greater detail on the spatial distribution of salinity than the chloride concentrations alone.

In eastern Virginia, the specific conductance of ground water generally increases from the western margin of the Chesapeake Bay impact structure toward its center (fig. K1). Specific conductance also generally increases with depth (fig. K3), in a few instances exceeding that of seawater by as much as 35 percent and thus indicating that the ground water is brine. Variations from the generally downward increasing trend are also apparent, however, across some intervals at all three of the core sites and among the group of wells centered on northern Newport News (shown in blue in figures K1 and K3). As noted above, chloride concentrations likely are similarly distributed.

Specific conductance exhibits a greater degree of small-scale variation at the USGS-NASA Langley core site (site number 59E 31) than at the other sample locations (fig. K3), possibly as a result of closely spaced short-interval samples. Because the USGS-NASA Langley core was the first for this study to be sampled for water extraction, the sample interval required to adequately characterize the salinity distribution was unknown. Accordingly, samples of the USGS-NASA Langley core were collected from almost every retrieved length of core, approximately every 3 m (10 ft). On the basis of these initial results, more widely spaced samples from approximately every 15–30 m (50–100 ft) were later collected from the North (59H 3) and Bayside (60G 5–6) cores.

Identical sample-collection procedures were followed for all three cores (see "Methods") to prevent intrusion of drilling fluid into the sediment and contamination of the retained

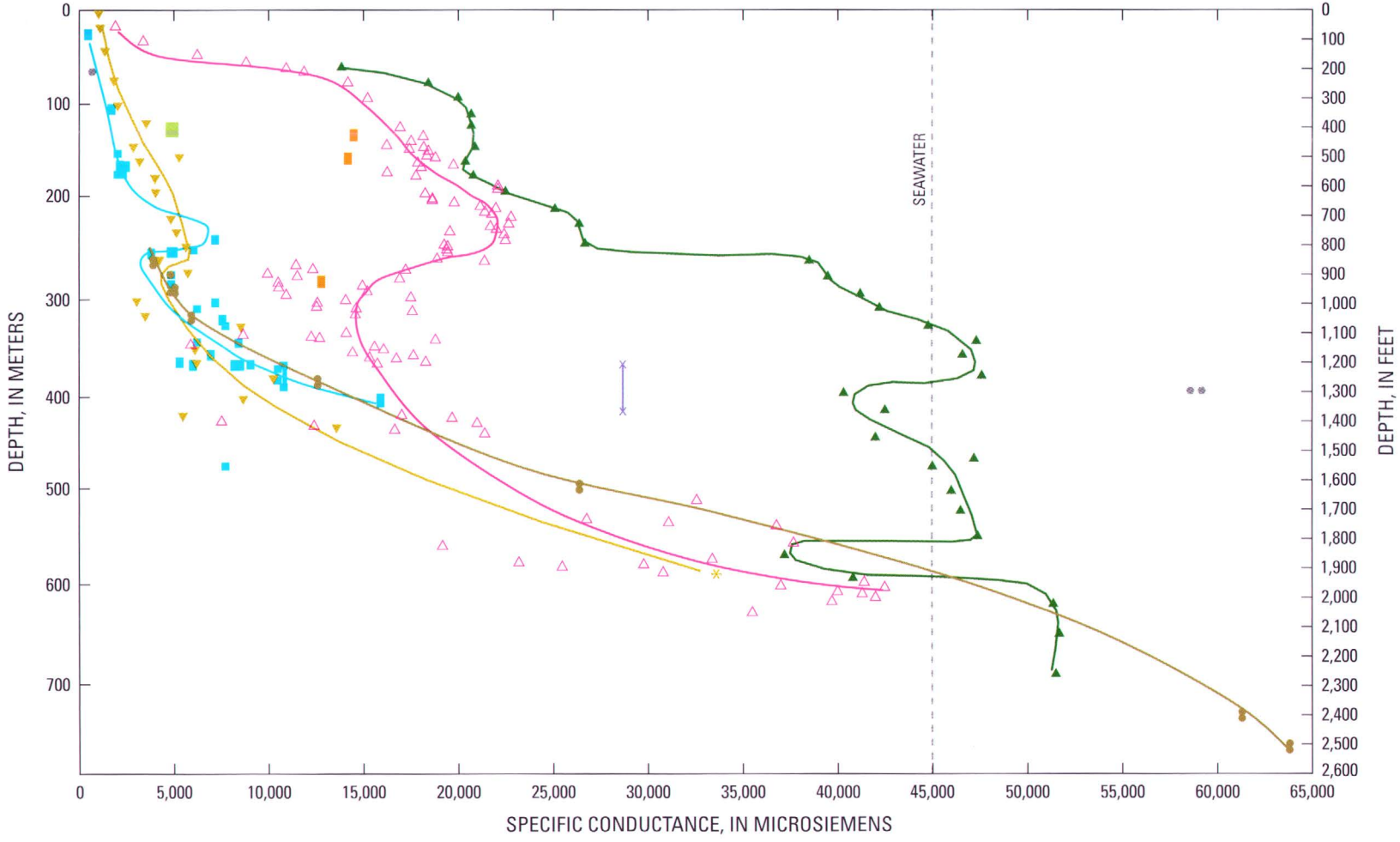

Figure K3. Graph showing the relation of specific conductance of sediment-core water and well water to depth below land surface along the western margin of the Chesapeake Bay impact structure in the Virginia Coastal Plain. Sample intervals are color referenced to sample locations shown in figure K1. Corresponding curves indicate general trends with depth. Samples shown in blue represent closely spaced wells centered on northern Newport News. Other colors represent single locations.

ground water. The validity of the procedures is confirmed by the lack of bias between the specific conductance of samples from the USGS-NASA Langley core of fine-grained, low-permeability sediments (which are very unlikely to be contaminated) and the specific conductance of coarser grained, higher permeability sediments.

Subsets of the Langley data based on farther spaced samples generally exhibit decreased variability of specific conductance and have distributions that are similar to those at North and Bayside. The well samples also were vertically spaced relatively far apart and were collected across screen intervals generally of several meters (table K1), which are long compared to the core-sample intervals. Thus, small-scale variations in specific conductance possibly exist at the other sample locations but are not exhibited by samples that are farther spaced and—in the case of the wells—have longer collection intervals.

Concentrations of bromide and iodide also were determined for selected samples of water extracted from sediment cores and for some samples collected from wells (table K1). Bromide concentrations generally are smaller than chloride concentrations by approximately three orders of magnitude, and iodide concentrations are smaller than chloride concentrations by four to five orders of magnitude. The relation of the ratio of bromide concentration to chloride concentration (Br/Cl) to depth below land surface was examined (fig. K4). The bromide concentration of seawater is 65 mg/L according to Hem (1985), and the Br/Cl ratio of seawater is 0.003; most of the samples exhibit Br/Cl ratios that exceed that of seawater by an average of approximately 24 percent, although four ratios are below that of seawater. The iodide concentration of seawater is 0.06 mg/L according to Hem (1985), and the iodide-to-chloride concentration ratio (I/Cl) of seawater is 3.2×10^{-6}; the I/Cl ratios for the samples generally range from one to two orders of magnitude above that of seawater (table K1).

Stable-isotope ratios, in per mil relative to Vienna Standard Mean Ocean Water (Fritz and Fontes, 1980), of the hydrogen isotope deuterium (expressed as δD) and oxygen (expressed as $\delta^{18}O$) were determined for 15 samples of water extracted from sediment cores and for 2 samples from wells (table K1). All values of both ratios are negative, indicating depletion of the heavy isotopes of the elements relative to the lighter isotopes. Hence, all the samples are isotopically lighter than modern seawater, which has a value of zero for both ratios. The δD values are strongly correlated with the $\delta^{18}O$ values, although two distinct relations are apparent in the graph of the data shown in figure K5: most samples indicate freshwater-seawater mixing, whereas several samples indicate evaporation. In addition, samples with the most negative values have a relatively small specific conductance, whereas less negative samples (including three samples of brine) have a large specific conductance.

Isotope ratios of chlorine-36 to total chloride ($^{36}Cl/Cl$) are shown as <1 in table K1 for 12 samples from the USGS-NASA Langley core (site 59E 31) because the ratios were below the analytical detection limit of 10^{-15}. The $^{36}Cl/Cl$ ratio of one sample from a well (site 63F 52) had a low value of 12.1×10^{-15}. The $^{36}Cl/Cl$ ratio of modern seawater is below 10^{-15} (Phillips and others, 1986). The well sample also differed from the core-water samples in being generally deeper, approximately 395.3 m (1,297 ft) to 401.4 m (1,317 ft) compared to 45.9 m (150.5 ft) to 599.2 m (1,965.8 ft), and in exhibiting a greater specific conductance of 58,600 μS compared to 6,260 to 42,500 μS.

Configuration of the Saltwater Transition Zone

Initial understanding of the physical principles governing the nature of the transition from freshwater to saltwater in coastal aquifers has been widely attributed to Ghyben (1888) and Herzberg (1901). In a homogeneous unconfined aquifer under hydrostatic conditions, freshwater is separated from the more dense seawater by a landward-sloping interface. Subsequent workers have expounded significantly on the original concept. Hubbert (1940) elaborated that with steady-state outflow to the sea, the interface is displaced seaward. Henry (1960) described the transition as a dispersive mixing zone rather than a sharp boundary, which Pinder and Cooper (1970) further characterized with transient movement in a confined aquifer.

Meisler (1989) provided a comprehensive analysis of the distribution of ground-water salinity and the processes controlling it in the Atlantic Coastal Plain from New Jersey through North Carolina. A relatively broad transition zone between freshwater and saltwater was described. Large-scale salinity variations (both areally and with depth) were attributed to variations in flow rates among different parts of the aquifer system and to variable sea-level fluctuations across the region. For the Virginia Coastal Plain, Larson (1981) described similar relations between fresh and brackish ground water in the upper few hundred meters of sediment.

The eastward- and downward-increasing specific conductance of ground water along the western margin of the Chesapeake Bay impact structure reflects a broad and generally landward-dipping transition zone between fresh ground water to the west and saltwater to the east (fig. K6). An inversion of part of the transition zone is exhibited across an interval where the vertical trend is reversed. The presence of relatively deep freshwater along the inverted interval possibly is reflected by anomalously large earth resistivities detected along the crater outer margin by using audio-magnetotelluric methods (Pierce, this volume, chap. J). The salinity inversion was described by Meisler (1989, p. D9) as a deep "freshwater wedge" that extends north of the lower Chesapeake Bay (that is, north of the impact structure) and east beneath the Atlantic coast; it becomes more broad and thick beneath the upper Chesapeake Bay, the Delmarva Peninsula, and the continental shelf off New Jersey, where it attains depths as great as 150 to 460 m (500 to 1,500 ft) below sea level. The salinity inversion also has been locally observed south of the impact structure, but apparently it does

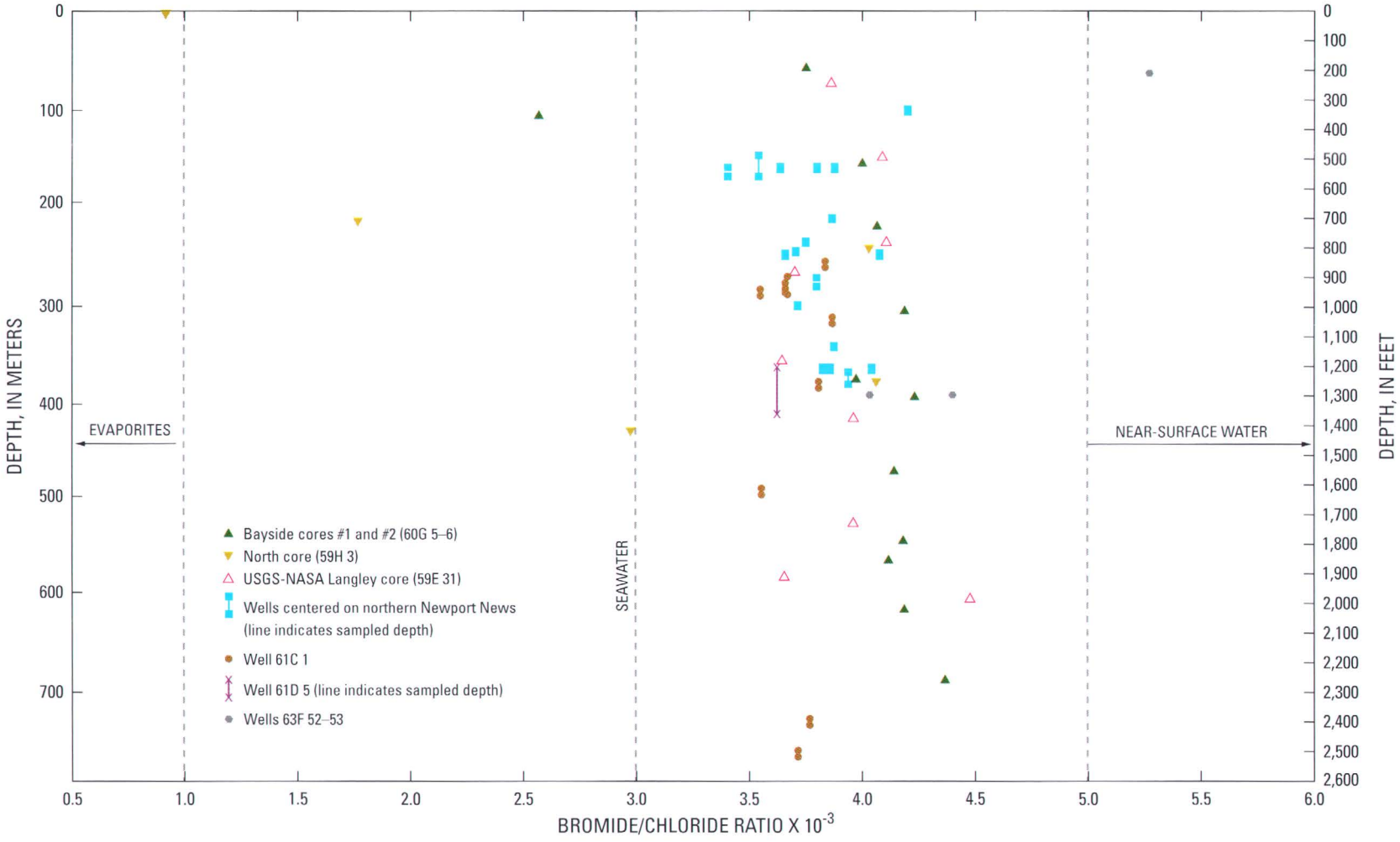

Figure K4. Graph showing relation of the ratios of bromide concentration to chloride concentration (Br/Cl) of sediment-core water and well water to depth below land surface along the western margin of the Chesapeake Bay impact structure in the Virginia Coastal Plain. Sample intervals are color referenced to sample locations shown in figure K1. Data from table K1.

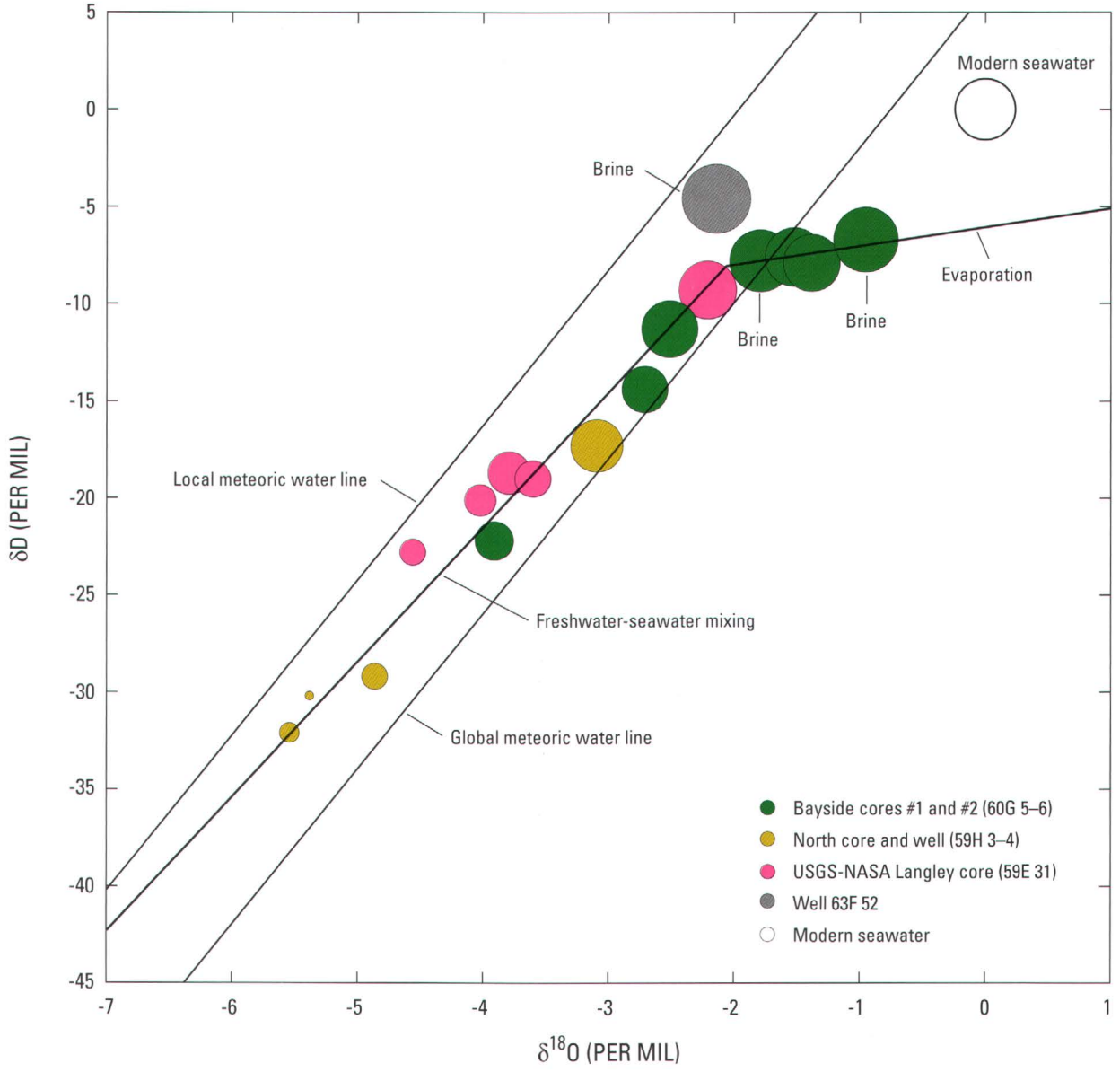

Figure K5. Graph showing the relation between hydrogen (δD) and oxygen ($\delta^{18}O$) isotope ratios and specific conductance of sediment-core water and well water along the western margin of the Chesapeake Bay impact structure in the Virginia Coastal Plain. Sample symbols are color referenced to sample locations shown in figure K1. One well (63F 52) is within the central crater. Symbol diameter is proportional to sample specific conductance; that of modern seawater is 45,000 microsiemens (Hem, 1985). Brines have a specific conductance higher than that of seawater. Global meteoric water line from Coplen (1993). Local meteoric water line from Dunkle and others (1993).

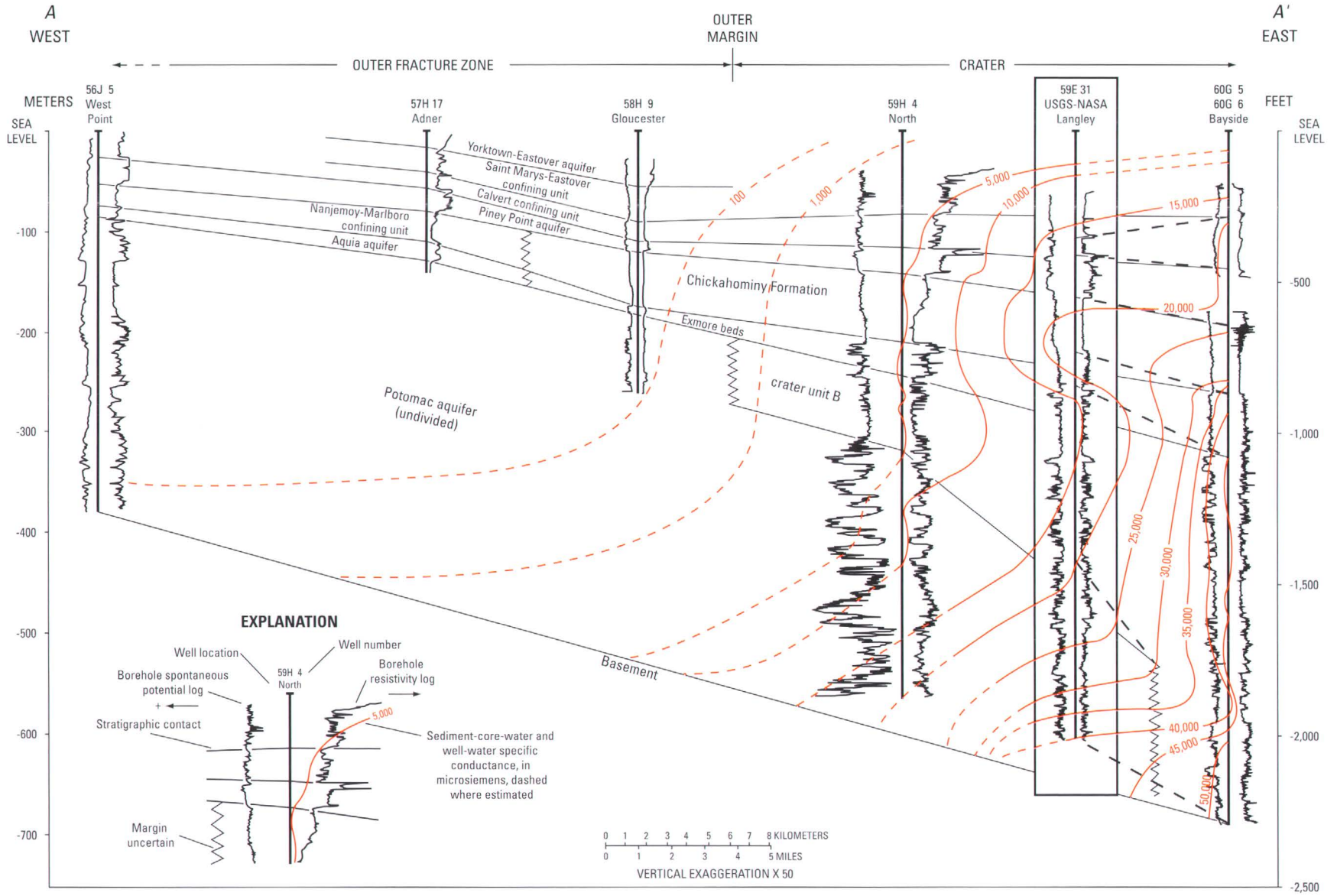

Figure K6. Simplified preliminary composite section across the western margin of the Chesapeake Bay impact structure showing the configuration of the saltwater transition zone as indicated by specific conductance contours. The line of section *A–A'* is shown in figure K1. The USGS-NASA Langley corehole (site 59E 31) is projected onto the section line. The westward distribution of specific conductance is estimated from Focazio and others (1993).

not extend into the North Carolina Coastal Plain (Winner and Coble, 1996).

Areally, the coincidence of elevated ground-water specific conductance with the western margin of the Chesapeake Bay impact structure (fig. K1) is consistent with the aforementioned descriptions of the saltwater transition zone in eastern Virginia as being an inland saltwater wedge. In three dimensions, the transition zone exhibits a convoluted configuration. Additionally within the broad regional trend, dispersive mixing is indicated by small-scale variations in specific conductance (fig. K3), as observed where closely spaced samples were collected from the USGS-NASA Langley core (site 59E 31). Similar variations possibly exist toward the center of the impact structure, where the saltiest water may be present in isolated pockets. Because of the scarcity of data, however, small-scale variations in salinity are unknown across this area.

Origin

Diverse processes can potentially affect the chemical composition of ground water in coastal aquifers. Among these, Jones and others (1999) listed mixing, ion exchange, diagenesis, and oxidation-reduction reactions. Back (1966) provided a comprehensive analysis of the geochemistry of ground water in the northern Atlantic Coastal Plain to characterize controls on ground-water composition. On the regional scale, the chemical composition of ground water evolves eastward with time along flow paths; it initially undergoes carbonate dissolution, followed by exchange of calcium for sodium on clays, and finally mixing with seawater near the coast. In this study, only partial chemical data are available for all of the ground-water samples, and a complete geochemical analysis is beyond the scope of this chapter. As demonstrated below, however, the available data are useful in inferring the relative likelihood of various mechanisms that have been suggested to explain the elevated salinity of ground water in eastern Virginia.

Sources of Salinity

At least three hypotheses can be considered to explain the origin and emplacement of the inland saltwater wedge in eastern Virginia: differential flushing, diffusion of solutes from basement evaporite deposits, and membrane filtration by clays. The hypotheses are summarized below.

Differential flushing.—Cederstrom (1943) described the area of the then-unknown impact structure as a "structural depression" where stratigraphic dips steepen, and around which ground water was proposed to flow in a "differential flushing" manner that has left residual seawater retained in the now-recognized crater-fill sediments. Regional inundation of the coastal plain by the Atlantic Ocean was thought to have initially saturated the sediments with seawater. A coincidence of faults with the saltwater wedge has been noted; Rogers and Spencer (1971) suggested that the faults promoted migration of seawater into the deepest sediments. Upon re-emergence of the coastal plain and resumption of recharge with meteoric water, seawater would have been gradually flushed from the sediments by freshwater.

The observed salinity distribution alone, however, provides only circumstantial evidence for differential flushing. Chemical data that could indicate the source of the salinity and hydrologic information to demonstrate the behavior of the flow system also are needed to support more definitive conclusions. The resource-management implication of differential flushing is that, given adequate knowledge of the flow system, withdrawal amounts and locations could be configured to enhance movement of fresh ground water and to minimize the spread of saltwater.

Diffusion of solutes from basement evaporite deposits.—As an alternative to the differential flushing hypothesis, Manheim and Horn (1968) and Meisler (1989) cited upward diffusion of solutes from the dissolution of basement evaporite deposits as having produced at least some of the saltwater in the Atlantic Coastal Plain sediments, particularly where brines have been observed. Differential flushing alone can account only for brackish ground water. In the context of present knowledge, the Chesapeake Bay impact structure is seen as a possible conduit for evaporite solutes to produce the saltwater wedge. Because the source of salinity is within basement bedrock, however, it remains unclear whether diffusion or advection in the area of the impact structure would have dominated solute transport under the unstressed flow conditions in which the saltwater wedge was formed.

As with the differential flushing hypothesis, information to indicate the source of the salinity and to demonstrate the behavior of the flow system is needed. The resource-management implication of evaporite solutes as the dominant source of salinity depends on whether diffusion or advection is the dominant transport mechanism. Because diffusion is probably much slower than advection, the amounts and locations of withdrawals would potentially have little effect on the distribution of salinity if diffusion were to remain dominant under present-day stressed flow conditions.

Membrane filtration by clays.—A third potential mechanism to explain the saltwater wedge is salinity production from membrane filtration by clays. Russel (1933) first suggested that under pressure a reversed osmotic movement of water can be induced between particles of clay from areas of high salinity toward areas of lower salinity. Because the clay particles are electrically charged, they repel and impede the movement of dissolved ions, causing the remaining solution to become more concentrated with time. Bredehoeft and others (1963) hypothesized that the requisite large hydraulic gradients could arise in sedimentary basins having sufficiently uplifted margins, and Hanshaw and Coplen (1973) demonstrated with laboratory studies that the process is theoretically possible. Specifically for the Virginia Coastal Plain, Larson (1981) cited membrane filtration along with the previously described mechanisms among

various possible explanations for the presence of elevated ground-water salinity. Powars and Bruce (1999) theorized that loading, compaction, and dewatering of crater-fill sediments within the Chesapeake Bay impact structure could have produced the saltwater wedge, presumably by membrane filtration.

Although the above-cited studies treated membrane filtration with reasoned speculation, an overview by Hanor (1983) indicated that its role in the production of saltwater had not been clearly demonstrated. Further, the feasibility of membrane filtration appears to be problematic in light of some observations. Manheim and Horn (1968) pointed out that regionally along the Atlantic coast, present-day hydraulic gradients are far below those required to achieve a significant degree of filtration. Within the Chesapeake Bay impact structure during the geologic past, hydraulic gradients likely were not appreciably greater than those existing at present even during basin compaction, because the basin margins would not have been sufficiently uplifted. Recently, Neuzil (2000) demonstrated that very low porosities of approximately 0.05 are required for appreciable membrane efficiency. By contrast, preliminary estimates of porosities of sediment core from the Chesapeake Bay impact structure range from 0.21 to 0.54 (E.R. McFarland, unpub. data, 2004).

Chemical Evidence

The composition of natural waters can be interpreted with respect to controlling chemical processes to infer the origin and history of the water and source(s) of its solutes. On a theoretical basis, either differential flushing or dissolution of evaporites appears to be a possible alternative mechanism for formation of the saltwater wedge associated with the Chesapeake Bay impact structure. In contrast, current information casts significant doubt on membrane filtration as a plausible mechanism to explain the saltwater wedge. Accordingly, formation of the saltwater wedge from either differential flushing or dissolution of evaporites was further assessed by using ground-water concentration ratios of bromide to chloride, stable hydrogen and oxygen isotopes, and chlorine-36 to total chloride.

Ratios of the concentrations of bromide and chloride ions (Br/Cl) in ground water have received increasingly widespread application to differentiate various sources of salinity (Davis and others, 1998). For example, Andreasen and Fleck (1997) used Br/Cl ratios to identify intrusion of brackish water from Chesapeake Bay into the Aquia aquifer in the Maryland Coastal Plain. This and other studies generally have compared Br/Cl ratios of ground water with those that are characteristic of various sources of salinity. Modern seawater has a Br/Cl ratio of approximately 0.003. Bromide can be enriched relative to seawater in organic matter and also in precipitation as a result of the kinetics of evaporation from the ocean surface (B.F. Jones, U.S. Geological Survey, oral commun., 2002). As a result of contributions from these sources, water near land surface (surface water and shallow ground water) is enriched in bromide and has Br/Cl ratios of 0.005 or greater. Organic matter within deeper coastal plain sediments can be an additional potential source of bromide to ground water.

Bromide also is partitioned during precipitation of evaporite minerals such that the minerals are depleted in bromide and have Br/Cl ratios below 0.001 as a result of different solubilities among the various halide minerals; the remaining solution is proportionately enriched in bromide and has Br/Cl ratios as great as 0.02. Conversely, solutions resulting from the dissolution of evaporite minerals are depleted in bromide and have correspondingly low Br/Cl ratios below 0.001.

Most of the ground-water samples from along the western margin of the Chesapeake Bay impact structure have Br/Cl ratios above that of seawater by an average of approximately 24 percent (fig. K4). The ratios exhibit no clear trend with areal location or depth, although a few samples deviate from the rest. Similarly, no trend of Br/Cl ratios with chloride concentration is apparent because chloride concentration generally increases with depth.

Most of the Br/Cl ratios in figure K4 are consistent with the chloride having originated from seawater that was enriched with bromide by roughly 24 percent but are too high to be consistent with dissolution of evaporite minerals. Among the four samples having Br/Cl ratios below that of seawater, only one sample has a ratio value below 0.001 (fig. K4); such a low ratio usually indicates that the chloride originated from dissolution of evaporites. This sample was collected from the North core (site 59H 3) at a shallow depth of approximately 4.3 m (14 ft) (table K1) beneath a graveled commuter parking lot, where most of the chloride probably originated from pavement de-icing salts.

Some of the chloride in the three remaining samples having Br/Cl ratios below that of seawater also possibly originated partly from dissolution of small amounts of evaporite minerals deposited with the sediments at these particular depths; the chloride is probably not from basement evaporite deposits because of the isolated occurrence of the samples and the lack of known evaporites in the nearby basement. Evaporite minerals are not expected to remain in the sediments because observed salinities are well below their saturation points. Although halite has been observed in a core from Kiptopeke, Virginia (Powars and Bruce, 1999), it likely was precipitated in the sediment after drilling as the core dried and high-salinity water evaporated.

The Br/Cl ratios indicate that the observed range of ground-water salinity likely resulted from various mixtures of seawater with freshwater having much less chloride. Although the parent seawater possibly had a Br/Cl ratio greater than that of the modern ocean, enrichment of bromide relative to modern seawater in most of the samples also could have resulted from (1) decay of organic material from near-surface sources and (or) at depth in the sediments and (or) (2) precipitation of evaporite minerals as a result of evaporation of the parent seawater. Additional evidence as discussed below indicates that both mechanisms are probable.

Various forms of organic matter are widespread within the Virginia Coastal Plain sediments and have likely contributed to enrichment of bromide in ground water relative to seawater. Organic matter, particularly nearshore marine vegetation, is even more enriched in iodide than in bromide relative to seawater; the iodide concentration of seawater is 0.06 mg/L (Hem, 1985). Iodide-to-chloride concentration ratios of the sediment-core-water and well-water samples range approximately from one to two orders of magnitude greater than that of seawater (table K1); the I/Cl ratios reflect a much greater enrichment of iodide than of bromide. Thus, bromide and iodide have undergone different degrees of enrichment in ground water that are consistent with their relative amounts in organic matter, which is probably their dominant source.

Enrichment of bromide from organic matter possibly is indicated by the greatest Br/Cl ratio value of 0.0053 (fig. K4) from well 63F 53 on the Virginia Eastern Shore (fig. K1). This sample is from a relatively shallow depth in the Yorktown-Eastover aquifer and has a correspondingly small specific conductance of 684 µS (table K1). By contrast, the much deeper well 63F 52 in the Exmore beds at the same location exhibits a much higher specific conductance of 59,200 µS but a lower Br/Cl ratio of 0.00403; the Br/Cl ratio is similar to the ratios of most of the other samples from various locations and spanning a range of depths and specific conductances. Thus, the highest Br/Cl value in well 63F 53 is isolated and possibly reflects local conditions. The Yorktown-Eastover aquifer in some parts of Virginia contains large amounts of organic matter as bedded peat. The peat beds locally are as thick as several meters but are generally discontinuous laterally; their proximity to well 63F 53 is unknown. Although iodide concentrations and other information are not available to demonstrate that bromide was enriched in well 63F 53 from organic matter, the peat is at least one possible source.

In addition to decay of organic matter, a probable source of bromide enrichment in ground water along the western margin of the Chesapeake Bay impact structure is the precipitation of evaporite minerals as a result of evaporation of the seawater. Surface evaporation of modern seawater results first in precipitation of calcium carbonate (calcite and (or) aragonite) followed by calcium sulfate (gypsum) (Drever, 1988). Concentrations of both chloride and bromide in the resulting brine increase above that of the parent seawater, and calcium and sulfate are relatively depleted, but the Br/Cl ratio remains unchanged. Not until 90 percent of the water is removed does halite (NaCl) begin to precipitate; the consequent removal of chloride causes the Br/Cl ratio of the remaining water to increase.

Some of the ground-water samples show evidence for evaporation of seawater. Deep samples from the Bayside core (site 60G 5–6) and from wells 61C 1 and 63F 52 (fig. K1) have specific conductance values that exceed that of seawater by as much as 35 percent (fig. K3) and thereby constitute brine. Because mixtures of freshwater and seawater cannot produce brine, its presence elsewhere in the Atlantic Coastal Plain has been cited (Manheim and Horn, 1968; Meisler, 1989) to indicate dissolution of evaporites as the source of salinity. Br/Cl ratios from the brine samples here, however, lie in the same range as ratios of the less concentrated samples (fig. K4) and indicate bromide enrichment rather than the bromide depletion that would have resulted from evaporite dissolution. An alternative to evaporite dissolution is evaporation of seawater to have produced the brine and to have precipitated halite and thereby enriched bromide in the brine. The salinity required to reach halite precipitation, however, is roughly 30 times that of the most concentrated brine observed. Although such a "super brine" has not yet been found within the impact structure, mixing with less concentrated water (originating as freshwater and (or) seawater) following the initial formation of the brine would likely have diluted it back down to observed salinities.

The mechanism of evaporation of seawater whereby the resulting brine would enter the ground-water system has not yet been clearly demonstrated. In some present-day arid regions, ground water is closely associated with seawater evaporating from restricted coastal supratidal sabkha environments (Drever, 1988). Whether such conditions have ever existed in the area of the Chesapeake Bay impact structure, however, is unknown. Alternatively, evaporation associated with the impact event 35 million years ago has been demonstrated to be theoretically possible, as a result of hydrothermal activity associated with the dissipation of residual heat retained in the sediments following the impact (Sanford, 2003). Although very rapid vaporization of seawater from the intense heat of the blast seems likely, heat-conduction calculations indicate that maximum temperatures greater than 400°C in the crater-fill sediments would have not been reached until 10,000 years after the impact and that associated brine generation would have likely continued for another million years.

In addition to Br/Cl ratios, stable-isotope ratios of hydrogen and oxygen have been applied toward understanding diverse origins and histories of ground water (Coplen, 1993), and they provide additional insight on the formation of the salt-water wedge associated with the Chesapeake Bay impact structure. Relations between δD and $\delta^{18}O$ values of sediment-core water and well water from along the western margin of the impact structure (fig. K5) indicate that mixing of freshwater and seawater and possibly evaporation of seawater have taken place. Most of the samples follow a relatively steep trend line that is between the local and global meteoric water lines, which reflect the fractionation of the isotopes between atmospheric moisture and precipitation. Because fresh ground water originates as isotopically light precipitation, the trend for most samples represents various mixtures of freshwater (having the most negative δD and $\delta^{18}O$ values) with isotopically heavier seawater (less negative values). Mixing is also reflected by specific conductance increasing in the direction of less negative values.

In addition, a few of the deepest samples from the Bayside core (site 60G 5–6) having specific conductance values near and above that of seawater appear to deviate from the others and

possibly follow a second, less steep trend that is characteristic of water having undergone evaporation. Additional samples are needed from elsewhere within the impact structure, particularly near the center of the crater where the greatest salinities are expected, to determine whether stable-isotope ratios show any further indication of evaporation.

In addition to Br/Cl and stable-isotope ratios, the ratios of chlorine-36 to total chloride ($^{36}Cl/Cl$) have been applied to differentiate various sources of ground-water salinity and to estimate ground-water age where the chloride is of primarily meteoric origin (Phillips and others, 1986). For example, Purdy and others (1996) used ground-water $^{36}Cl/Cl$ ratios from the Aquia aquifer in the Maryland Coastal Plain to determine ground-water ages as great as 100,000 years. Importantly, concentrations of total chloride in the Aquia aquifer in Maryland are only a few milligrams per liter, and most of the chloride is of meteoric origin. Although significant amounts of cosmogenic ^{36}Cl are produced in the atmosphere, seawater represents a very large reservoir of much older chloride in which most of the ^{36}Cl has decayed and cannot be used to estimate age.

Thirteen samples of ground water from the Chesapeake Bay impact structure were analyzed for $^{36}Cl/Cl$ ratios. Twelve of the samples are from the USGS-NASA Langley core (site 59E 3, fig. K1); for all twelve Langley samples, the $^{36}Cl/Cl$ ratios are below the analytical detection limit of 10^{-15}, and they are consistent with earlier results in indicating that most of the chloride originated from seawater.

Only the remaining sample from well 63F 52 in the Exmore beds on the Virginia Eastern Shore (in the central crater, fig. K1) has a $^{36}Cl/Cl$ ratio above the detection limit; its value is 12.1×10^{-15} (table K1). The high concentration of total chloride (23,000 mg/L) in well 63F 52 indicates that the chloride is probably of seawater rather than meteoric origin and is not the source of the ^{36}Cl. More likely, ground water in well 63F 52 is old enough for secondary ^{36}Cl to have accumulated in the subsurface as a result of decay of solid-phase uranium in the sediments.

Formation of the Inland Saltwater Wedge

Values of Br/Cl ratios, δD, $\delta^{18}O$, and $^{36}Cl/Cl$ ratios for ground-water samples indicate that seawater was the source of salinity along the western margin of the Chesapeake Bay impact structure and that evaporation of seawater produced the observed brine. The seawater and brine have mixed with freshwater to produce the observed range of ground-water salinities. Thus, the results of this study support Cederstrom's (1943) original hypothesis that the saltwater wedge resulted from differential flushing of residual seawater.

Seawater has been emplaced throughout the Atlantic Coastal Plain sediments during regional inundations by the Atlantic Ocean. Large parts of the Virginia Coastal Plain were repeatedly inundated during the Tertiary Period between 2 million and 65 million years ago, as recorded by sediments of that age. The most recent marine deposits are of Pliocene age and formed approximately 2 million to 4 million years ago. Regionally extensive younger sediments are largely of fluvial origin. Although several additional inundations took place as recently as 115,000 years ago during interglacial periods of the Pleistocene Epoch, sea levels then were higher by at most 6 m (20 ft) because the climate was not significantly warmer than today's climate (Bradley, 1999); only areas near the Chesapeake Bay impact structure were inundated.

In addition to geological evidence, hydrologic information suggests a relatively old age for seawater still present in the crater-fill sediments. The youngest ground water in the Virginia Coastal Plain is in the fresh-to-brackish zone outside of the crater and has ages as great as 40,000 years determined from carbon-14 analyses (D.L. Nelms, U.S. Geological Survey, oral commun., 2001). Within the crater, ground-water δD and $\delta^{18}O$ values are uniformly negative (fig. K5), indicating that the hydrogen and oxygen isotopic composition of the original seawater is lighter than that of modern seawater. By contrast, seawater of the most recent geologic past during the Pleistocene Epoch was generally heavier than modern seawater because of the cooler climate. Thus, the original seawater likely predates the Pleistocene and has been buried since at least the last regional inundation of 2 million to 4 million years ago, when the climate was warmer than present. Further evidence indicates that potentially much older seawater from previous inundations could be present. The $^{36}Cl/Cl$ ratio of 12.1×10^{-15} in well 63F 52 (table K1) is based on ^{36}Cl that probably was produced by decay of solid-phase uranium in the sediments, which could take several million years or more depending on their uranium content. In addition, calculated estimates of solute advection and diffusion rates indicate that at least some seawater, along with hydrothermally produced brine, likely remains in the crater fill from the time of the impact (Sanford, 2003).

Areal ground-water recharge resumed following emergence of the Atlantic Coastal Plain from the last regional inundation during the Pliocene Epoch. The consequent flow of fresh ground water since then has to varying degrees flushed residual seawater from the coastal plain sediments, thereby affecting the position and configuration of the saltwater transition zone. At the extreme during the last Pleistocene glacial maximum of 18,000 years ago, sea levels were as far as 120 m (390 ft) lower than present (Bradley, 1999), and the Atlantic shore was located several tens of kilometers eastward of its present position. Freshwater flushing extended nearly to the edge of the continental shelf and was vigorously driven by fresh ground-water heads that were high relative to the low sea level. Warming since then has resulted in sea level rising to its present location.

The manner in which differential flushing of the residual seawater has taken place across the Chesapeake Bay impact structure can be inferred from the relation of the saltwater transition zone to the configuration of various geologic units along the western margin of the impact structure (fig. K6). Specifi-

cally, the vertical salinity inversion along the crater outer margin coincides with the interval occupied by the Chickahominy Formation and underlying crater-fill sediments (crater unit B and Exmore beds as described by Gohn and others, this volume, chap. C). Preexisting sediments were highly disrupted by the impact and were chaotically mixed and deposited under very high energy conditions immediately following the impact in a large crater that was formed by the blast. Among these, crater unit B consists of clast-supported boulder-sized and larger blocks of preexisting formations that were violently rolled, swept, or hurled into the crater. The overlying and thinner Exmore beds consist of matrix-supported cobbles and smaller fragments floating in densely packed and poorly sorted sand that was washed in by tsunamis to further fill the crater. Lastly, the Chickahominy Formation consists of very fine grained clay that was deposited under low-energy conditions in a deep marine basin left by the impact; it is preserved only in the immediate vicinity of the crater. Undisrupted preimpact sediments outside of the crater are truncated against these units along the crater outer margin, and postimpact sediments overlie all earlier units. A complex array of faults is theorized to influence the configuration of the margin between preimpact and crater-fill sediments and to also propagate upward through postimpact sediments and laterally into preimpact sediments across an outer fracture zone (Johnson and others, 1998).

The configuration of the saltwater transition zone (fig. K6) indicates that differential flushing has taken place in a complex three-dimensional fashion across the western margin of the Chesapeake Bay impact structure. The salinity inversion along the crater outer margin indicates that flushing of saltwater has been impeded across the clayey Chickahominy Formation, beneath which greater flushing has taken place through the more sandy crater fill. The lithologic compositions of these units suggest that permeabilities and ground-water flow rates could be directly related to their contrasting degrees of flushing. Coincidentally, sediments that comprise the Chickahominy Formation as currently recognized appear to have been represented in the RASA ground-water flow model as part of the Nanjemoy-Marlboro confining unit (Harsh and Laczniak, 1990; see fig. K2 of this chapter). As a necessary feature to successfully calibrate the model, the distribution of vertical-leakance values assigned to the Nanjemoy-Marlboro confining unit decreases abruptly approximately across the now-known crater outer margin. Hence, the hydraulic effect of the impact structure had apparently been manifest in this analysis even though the investigators were unaware of its presence. Preliminary analyses since undertaken in developing a revised model of the Virginia Coastal Plain demonstrate explicitly the likelihood that differential flushing across the impact structure formed the saltwater wedge (Heywood, 2003).

The differential flushing exhibited along the crater outer margin does not appear to persist across the entire impact structure. Farther into the impact structure, the specific conductance of ground water increases abruptly to that of seawater (45,000 μS) and greater at depth (fig. K6). In addition, no large salinity inversion is apparent, and the saltwater transition zone assumes a nearly vertical orientation across most of the sediments. Apparently little or no flushing of saltwater has taken place through sediments across the inner part of the impact structure. Possibly lesser permeabilities in the crater fill toward the center of the impact structure and (or) the greater density of the saltwater create a barrier to flow. Estimates of solute advection and diffusion rates (Sanford, 2003) indicate that saltwater in the deepest part of the impact structure at its center likely has undergone essentially no flushing since being emplaced at the time of the impact.

For differential flushing to provide a complete explanation, the means by which ground water is discharged from the flow system must be identified. Across the eastward downgradient part of the Virginia Coastal Plain, upward leakage and discharge to Chesapeake Bay, its major tributaries, and the Atlantic Ocean are the primary means by which water exits the flow system (fig. K2) (Harsh and Laczniak, 1990). The configuration of the saltwater transition zone across the crater outer margin, however, indicates that little or no upward leakage and associated flushing have taken place from the crater fill through the overlying Chickahominy Formation (fig. K6). Neither does ground water that flushed differentially along the outer margin appear to continue across the impact structure toward the ocean. The only other apparent exit is by lateral flow around the outer margin, followed by upward leakage and surface discharge to areas outside of the crater where the Chickahominy Formation is not present (fig. K7).

The complex array of faults theorized to span the margin of the Chesapeake Bay impact structure likely exerts some control on differential flushing, although in what manner is largely unknown. Given the unconsolidated nature of the sediments, most faults would likely not exist as open fractures along which enhanced flow could take place. Permeability within the sediments could potentially be either increased or decreased along faulted intervals, depending on how the sediments had been altered at the intergranular scale. At a minimum, some faults probably juxtapose adjacent aquifers and confining units that would otherwise have continuous extents. Effects of faulting on fluid migration in evolving sedimentary basins can potentially be highly variable both spatially and temporally (Stover and others, 2001), depending on specific relations among faults, the strata they penetrate, and the distribution of fluid pressure. These relations within the impact structure have likely changed since the time of the impact, as the structure has evolved with ongoing sediment deposition, subsidence, and fault propagation. In addition to effects on lateral flow around the crater outer margin, faults across the outer fracture zone could potentially facilitate ground-water discharge by enhancing upward leakage in areas outside of the crater.

Lateral flow and flushing possibly have taken place preferentially toward the north side of the impact structure rather than toward the south, as indicated by the area of elevated spe-

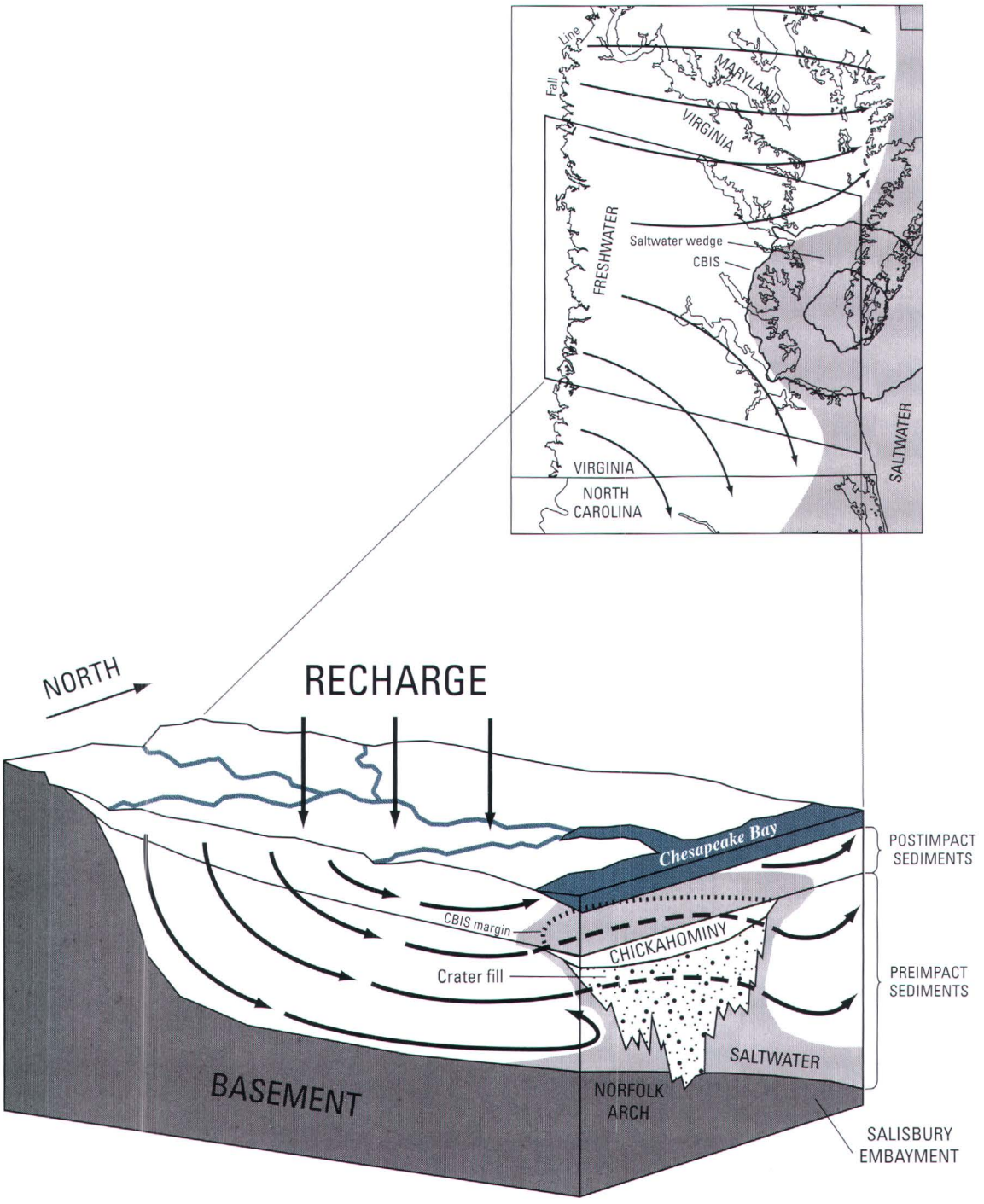

Figure K7. Schematic block diagram representing hypothetical differential ground-water flow directions (arrows) across the Chesapeake Bay impact structure (CBIS) prior to large ground-water withdrawals. The map shows the location of the saltwater wedge and of the region represented in the block diagram. The dashed lines in the block diagram indicate flow diverted around and behind the impact structure (dotted line).

cific conductance, which is shifted southward several kilometers relative to the position of the crater (fig. K1). Several controls on ground-water flow possibly have acted in combination to cause preferential northward flow. First, recharge during the Pleistocene Epoch possibly was enhanced across the northern part of the Atlantic Coastal Plain as a result of a large amount of infiltration associated with glacial outwash and a strong seaward gradient from the elevated and nearby Fall Line. Second, depth of basement and sediment thickness markedly increase northward from the impact structure into the Salisbury embayment (fig. K7), possibly providing the most transmissive path for lateral flow around the impact structure. The salinity inversion along the crater outer margin broadens, thickens, and deepens northeastward beneath Chesapeake Bay, the Delmarva Peninsula, and the continental shelf off New Jersey and is a relict feature of vigorous Pleistocene flushing (Meisler, 1989).

In contrast to flow north of the impact structure, southward lateral flow along the crater outer margin could be relatively constrained. Climate was warm enough even during the Pleistocene Epoch that glacial outwash was not present to provide an enhanced source of infiltration. The Fall Line is also farther inland and at a lower elevation, thereby reducing the seaward gradient. In addition, the basement is increasingly shallow across the Norfolk arch and into North Carolina (fig. K7), and so sediment thicknesses and transmissivities are less. Hydraulic continuity of the sediments also could be interrupted to the south across a zone roughly aligned with the James River (Powars, 2000), along which numerous stratigraphic discontinuities have been discerned. The salinity inversion along the crater outer margin does not appear to continue as far south as North Carolina (Winner and Coble, 1996), possibly as a result of constraints on lateral flow and flushing.

Flushing by fresh ground water of residual seawater from coastal plain sediments has continued to the present, from its onset during the emergence of the coastal plain at the end of the Pliocene Epoch, through its peak with the lowest sea level during the last Pleistocene glacial maximum of 18,000 years ago. The climate has warmed since then, sea level has risen to its present position, and seawater has re-inundated the continental shelf as well as the Pleistocene-age valley of the Susquehanna River, thereby forming Chesapeake Bay. Consequently, the saltwater transition zone has migrated landward during the past 18,000 years, and flushing at present is less vigorous than at its maximum.

With the rise in sea level to its present position, seawater has begun to reenter sediments underlying the re-inundated continental shelf and Chesapeake Bay, but at a rate slower than sea-level rise because the seawater advance has been relatively rapid compared to ground-water flow rates. As a result, the Atlantic Ocean and Chesapeake Bay have ridden over a volume of freshwater now stalled beneath saltier shallow ground water, thereby producing the salinity inversion that extends from the continental shelf off New Jersey southwestward beneath the Delmarva Peninsula and Chesapeake Bay and along the western margin of the Chesapeake Bay impact structure. Hence, the configuration of the saltwater transition zone represents an unstable transient condition in which the overriding seawater is not in equilibrium hydrodynamically with underlying fresh ground water. Solute-transport modeling of inundation of thick, relatively low-permeability sediments demonstrates how rapid inundation can produce a poorly mixed saltwater transition zone overlying a freshwater zone (Kooi and others, 2000). Sea level would have to maintain its present position for some period for the saltwater transition zone to attain a stable equilibrium configuration. Alternatively, should the climate continue to warm and sea level to rise, seawater will inundate additional areas and ride over and stall a greater volume of fresh ground water, thereby further propagating the salinity inversion.

Resource-Management Implications

Ground-water withdrawals in the Virginia Coastal Plain have increased during the past century to roughly 150 million gallons per day. A major part of this withdrawal has historically occurred at industrial pumping centers located outside of the Chesapeake Bay impact structure. Regional cones of depression centered on the industrial withdrawals exhibit water-level declines as great as 60 m (200 ft) and presently dominate the head distribution across the entire Virginia Coastal Plain (Hammond and others, 1994a,b,c). As a result, hydraulic gradients have been greatly increased and flow has been largely redirected landward from the saltwater wedge associated with the impact structure. The industrial withdrawals have been maintained at relatively stable rates for several decades. In addition, withdrawals for public supplies have been increasing in rapidly growing metropolitan areas positioned along the western margin of the impact structure and underlain by the saltwater transition zone. Desalinization of brackish ground water is being actively developed in these areas as a means to address growing water demands expected during the coming several decades.

Regional Saltwater Intrusion

The present withdrawal-induced head distribution has imposed a potential for saltwater intrusion across most of the Virginia Coastal Plain during much of the past century. The saltwater wedge, however, was recognized even earlier and prior to the onset of large ground-water withdrawals (Sanford, 1913). Thus, the saltwater wedge cannot be attributed to withdrawal-induced intrusion and must have formed under earlier, largely unstressed conditions. Conversely, intrusion in the form of landward expansion of the saltwater wedge across regional distances has not occurred (Smith, 1999) despite several decades of heavy pumping.

Diverse geologic and hydrologic evidence indicates that the saltwater wedge originated from seawater that was emplaced throughout the Virginia Coastal Plain sediments dur-

ing regional inundation as recently as approximately 2 million years ago, along with much older seawater and evaporative brine within the Chesapeake Bay impact structure that was emplaced potentially as far back as the impact event 35 million years ago. With emergence of the coastal plain and resumption of ground-water recharge during the past 2 million years, residual seawater has been displaced by varying degrees by freshwater flushing, which at its most vigorous extended nearly to the edge of the continental shelf during the Pleistocene glacial maximum of 18,000 years ago. Because the saltwater wedge is still present today, it must have persisted during this maximum emergence even while some adjacent areas were being so vigorously flushed as to emplace freshwater far beyond the impact structure across most of the continental shelf. Preliminary simulation analyses demonstrate that saltwater within the impact structure maintained its present position during the Pleistocene emergence even as freshwater was being emplaced on all sides (Heywood, 2003). Since then, sea level has risen to its present position and the residual seawater has merged with the modern ocean.

Insufficient time has elapsed from the onset of heavy pumping to achieve the degree of regional flow under present gradients needed for significant landward expansion of the saltwater wedge. Despite greatly increased gradients and altered flow directions, the actual movement of ground water under stressed conditions has been relatively little throughout the Virginia Coastal Plain. Ground-water ages range from tens of thousands of years across much of the area outside of the Chesapeake Bay impact structure to several millions of years or more within the impact structure, and most of the ground water now present was emplaced prior to large withdrawals. Because of the preponderance of storative fine-grained sediments, much of the water withdrawn during the past century has apparently been derived from the release of old water from storage and not from flow across regional distances to pumping wells. As a result, ground-water salinity remains fundamentally as it was distributed under unstressed conditions.

The amount of time needed to induce sufficient flow in response to present gradients to cause landward expansion of the saltwater wedge across regional distances is unknown. Some details of the future behavior of the flow system under stressed conditions, however, could impose important controls. Conceivably, a threshold in terms of the duration and (or) magnitude of withdrawal could be reached beyond which removal from storage no longer provides most of the withdrawn water, and regional flow under present gradients becomes dominant. In addition, the hydraulic sluggishness of the Chesapeake Bay impact structure that enabled the saltwater wedge to persist during Pleistocene emergence could be expected to likewise lead to a lack of response to strong landward gradients. Predictive numerical simulation of regional flow and solute transport is one means to assess if and how the saltwater wedge could expand significantly landward in response to present and (or) projected pumping stresses, but it is beyond the scope of this chapter. Because the saltwater wedge has apparently maintained its present extent for millennia, our subjective judgment is that landward expansion across regional distances even under withdrawal-induced gradients could require a very long timeframe by human standards.

Saltwater Movement along the Western Margin

Although the saltwater wedge has not expanded regionally in response to large industrial withdrawals located outside of the Chesapeake Bay impact structure, relatively small changes in ground-water salinity have occurred along the western margin of the impact structure in association with co-located municipal withdrawals (Smith, 1999), some of which are of brackish ground water. The saltwater transition zone is positioned along the western margin of the impact structure and exhibits a convoluted configuration resulting from a large salinity inversion formed by complex differential flushing across and around crater-fill sediments (figs. K6 and K7). Additionally at the meter scale, the salinity distribution across the western margin exhibits a large degree of spatial variability (fig. K3). Although some large-scale controls on prepumping differential flushing along the western margin are apparent, such as the distribution of contrasting sediment lithologies, many small-scale hydrogeologic details, such as possible effects of faults, remain unknown.

In addition to hydrogeologic controls on the salinity distribution that have existed since unstressed conditions, localized effects now imposed by withdrawals located along the western margin are likewise unknown but possibly are even more complex. Many of these primarily municipal withdrawals have historically been episodic, ranging in duration from several months to several years to supplement surface-water supplies during prolonged drought, and have been interrupted by extended periods of no withdrawal (Focazio and Speiran, 1993). Manifold hydraulic interactions are likely among closely spaced wells operated by different municipalities and having diverse pumping histories. Within the coming decade, municipal withdrawal and desalinization of brackish ground water along the western margin are expected to increase significantly in response to population growth; municipal withdrawals may become as large as the industrial withdrawals located far inland from the western margin.

Unlike regional landward expansion of the saltwater wedge, localized saltwater movement along the western margin is possible within a relatively short timeframe. Withdrawals are increasing from wells placed directly within the saltwater transition zone where the salinity distribution is locally highly variable. At this scale, solute transport paths and traveltimes are relatively short. Were ground water within several tens of meters of a particular well to have a different salinity than that in which the well is first constructed, the salinity of the withdrawn water could potentially change within a period of several years after

the onset of pumping. Under these conditions, saltwater movement could take place not only laterally through an aquifer but also vertically between aquifers (Smith, 1999).

The potential for localized withdrawal-induced redistribution of salinity within the saltwater transition zone poses a challenge to planning for increasing ground-water withdrawal by municipalities located along the western margin. Desalinization of brackish ground water is being increasingly relied on as a means to provide for the rapidly growing water demand. Future localized changes in the ground-water salinity distribution, however, could be difficult to assess. Similar to assessing regional landward expansion of the saltwater wedge, predictive numerical simulation of localized flow and solute transport along the western margin is one means to assess if and how salinity changes could occur in response to present and projected pumping from within the saltwater transition zone. Historically, these withdrawals have been difficult to project for the complex array of various municipal well systems that operate with a high degree of temporal and spatial variability and in response to unpredictable climate-driven demands (Focazio and Speiran, 1993). Significant uncertainty associated with a simplified simulation of solute transport across part of the western margin (Smith, 1999) resulted from limited information on withdrawal histories, as well as local-scale details of the configuration and hydraulic properties of aquifers and confining units, and on the spatial distribution and temporal changes in ground-water salinity.

Because hydrogeologic controls and withdrawal-induced effects within the saltwater transition zone are complex, a detailed local-scale characterization of hydrologic conditions will be critical to support any meaningful future assessment of the potential for saltwater movement along the western margin. Adequate spatial delineation of aquifer and confining-unit configurations and hydraulic properties, and of the distribution and changes in salinity, will require very densely arrayed data on sediment stratigraphy and structure (including the effects of faults) and ground-water levels, large-magnitude aquifer pumping tests, and long-term ground-water quality monitoring. Similarly, detailed histories of ground-water withdrawal will be needed. If ground water becomes a major component of the total water supply along the western margin, then future withdrawals could be more consistent and less episodic than past usage and, thus, easier to model.

Summary and Conclusions

The Chesapeake Bay impact structure in eastern Virginia is encompassed by a regionally extensive and heavily used aquifer system. Large and increasing withdrawals have resulted in significant and continuing water-level declines and have altered ground-water flow directions to create the potential for saltwater intrusion. The discovery of the impact structure requires changes to previous conceptualizations of the aquifer system as having a relatively simple layered configuration. To provide a basis for ground-water management decisions, the USGS and VDEQ are revising the hydrogeologic framework and an associated ground-water flow model of the entire Virginia Coastal Plain.

The impact structure has been inferred to play a role in controlling the salinity distribution in eastern Virginia. For this study, chemical analyses were performed on samples of ground water extracted from three sediment cores and collected from wells along the western margin of the impact structure. Increasing specific conductance values and increasing concentrations of chloride with depth reflect a broad but generally landward-dipping transition zone across the western margin that separates fresh ground water to the west from saltwater to the east. Areal coincidence of the transition zone with the western margin of the impact structure is consistent with earlier descriptions of the transition zone in eastern Virginia as comprising an inland saltwater wedge. Dispersive mixing is exhibited by small-scale variations in specific conductance where closely spaced samples were collected.

Ratios of bromide to chloride, iodide to chloride, and chlorine-36 to total chloride and stable hydrogen and oxygen isotope ratios indicate mixing of freshwater and seawater and support differential flushing of residual seawater among various competing hypotheses to explain the presence of the inland saltwater wedge. In addition, evaporation of seawater probably produced some ground water having specific conductance values that exceed that of seawater by as much as 35 percent; the mechanisms may have been (1) evaporation in restricted coastal environments under arid conditions, (2) rapid vaporization caused by the impact event, and (or) (3) evaporation caused by residual heat and associated hydrothermal activity following the impact.

The saltwater wedge originated from seawater emplaced throughout the Virginia Coastal Plain sediments during a regional inundation as recently as approximately 2 million years ago and from much older seawater and evaporative brine within the impact structure that were emplaced potentially as far back as the impact event 35 million years ago. With emergence of the coastal plain and resumption of ground-water recharge during the past 2 million years, residual seawater has been displaced to varying degrees by freshwater flushing.

Freshwater flushing across the crater outer margin was impeded by the clayey Chickahominy Formation, beneath which greater flushing took place through crater-fill sediments, and little or no flushing took place farther into the impact structure. As a result, water exited the flow system by lateral flow and flushing around the outer margin, followed by upward leakage and surface discharge to areas outside of the crater and possibly enhanced by faults. Within the impact structure, the saltwater wedge maintained its present position even during the Pleistocene glacial maximum of 18,000 years ago, while the most vigorous flushing outside of the impact structure extended

nearly to the edge of the continental shelf. Since then, sea level has risen to its present position and the residual seawater has merged with the modern ocean along an inverted and hydrodynamically unstable transition zone.

A potential for saltwater intrusion across most of the Virginia Coastal Plain has been imposed during much of the past century by regional cones of depression centered on industrial pumping centers located outside of the Chesapeake Bay impact structure. The saltwater wedge predates the onset of heavy pumping, however, and has not since expanded across regional distances because most of the ground water now present was emplaced prior to large withdrawals. Predictive numerical simulation could be undertaken to assess whether a potentially very long timeframe could be required for regional expansion of the saltwater wedge.

Localized saltwater movement along the western margin of the impact structure could take place as a result of increasing withdrawals being made directly from the saltwater transition zone. Assessment of the potential for saltwater movement along the western margin represents significant technical challenges because of complex hydrogeologic controls and withdrawal-induced effects within the transition zone. Predictive simulation would require a detailed local-scale characterization of aquifer and confining-unit configurations and hydraulic properties, the distribution and changes in salinity, and withdrawal histories.

Acknowledgments

The authors are grateful to USGS field personnel who provided support in collecting the many core samples for ground-water chemical analysis, including Wilma Aleman, Laurel Bybell, Lucy Edwards, Gregory Gohn, Samuel Harvey, Russell Lotspeich, Colleen McCartan, David Powars, Jean Self-Trail, Mathew Smith, and Robert Weems. Thanks are also extended to Frank Manheim and John Bratton of the USGS for assistance with core-sample collection and processing techniques and to Glenda Brown and Ted Struzeski of the USGS National Water-Quality Laboratory (NWQL), Tyler Coplen of the USGS Isotope Research Laboratory, and David Elmore of the Purdue Rare Isotope Measurement Laboratory (PRIME Lab) for sample analysis. Helpful guidance with data analysis and interpretation was provided by JK Bohlke, Tyler Coplen, Blair Jones, Isaac Winograd, Ward Sanford, and James Landmeyer of the USGS, especially the last two who also provided reviews of this chapter.

Gratitude is also expressed to the National Aeronautics and Space Administration (NASA) Langley Research Center, the Virginia Department of Transportation, and the Mathews County Land Conservancy for access to coring sites. Lastly, many thanks are due to drillers and owners of water-supply wells who have provided well-log, construction, water-level, and water-quality data, particularly Sydnor Hydrodynamics, Inc., who has historically provided many highly useful geophysical well logs.

References Cited

Andreasen, D.C., and Fleck, W.B., 1997, Use of bromide:chloride ratios to differentiate potential sources of chloride in a shallow, unconfined aquifer affected by brackish-water intrusion: Hydrogeology Journal, v. 5, no. 2, p. 17–26.

Back, William, 1966, Hydrochemical facies and ground-water flow patterns in northern part of the Atlantic Coastal Plain: U.S. Geological Survey Professional Paper 498–A, p. A1–A42.

Bradley, R.S., 1999, Paleoclimatology; Reconstructing climates of the Quaternary: New York, Academic Press, 613 p.

Bredehoeft, J.D., Blyth, C.R., White, W.A., and Maxey, G.B., 1963, Possible mechanism for concentration of brines in subsurface formations: American Association of Petroleum Geologists Bulletin, v. 47, no. 2, p. 257–269.

Cederstrom, D.J., 1943, Chloride in ground water in the coastal plain of Virginia: Virginia Geological Survey Bulletin 58, 36 p.

Coplen, T.B., 1993, Uses of environmental isotopes, *in* Alley, W.M., ed., Regional ground-water quality: New York, Van Nostrand Reinhold, p. 227–254.

Davis, S.N., Whittemore, D.O., and Fabryka-Martin, June, 1998, Uses of chloride/bromide ratios in studies of potable water: Ground Water, v. 36, no. 2, p. 338–350.

Drever, J.I., 1988, The geochemistry of natural waters (2d ed.): Englewood Cliffs, N.J., Prentice-Hall, 437 p.

Dunkle, S.A., Plummer, L.N., Busenberg, E., Phillips, P.J., Denver, J.M., Hamilton, P.A., Michel, R.L., and Coplen, T.B., 1993, Chlorofluorocarbons (CCl_3F and CCl_2F_2) as dating tools and hydrologic tracers in shallow groundwater of the Delmarva Peninsula, Atlantic Coastal Plain, United States: Water Resources Research, v. 29, no. 12, p. 3837–3860.

Focazio, M.J., and Speiran, G.K., 1993, Estimating net drawdown resulting from episodic withdrawals at six well fields in the Coastal Plain physiographic province of Virginia: U.S. Geological Survey Water-Resources Investigations Report 93–4159, 21 p., 7 oversize pls.

Focazio, M.J., Speiran, G.K., and Rowan, M.E., 1993, Quality of ground water in the Coastal Plain physiographic province of Virginia: U.S. Geological Survey Water-Resources Investigations Report 92–4175, 20 p.

Fritz, P., and Fontes, J.C., 1980, Introduction, *in* The terrestrial environment, A, v. 1 *of* Fritz, P., and Fontes, J.C., eds., Handbook of environmental isotope geochemistry: Amsterdam, Elsevier, p. 1–19.

Ghyben, W.B., 1888, Nota in verband met de voorgenomen putboring nabij Amsterdam [Notes on the probable results of the

proposed well drilling near Amsterdam]: Koninklijk Instituut van Ingenieurs Tijdschrift 1888–89, p. 8–22.

Hammond, E.C., and Focazio, M.J., 1995, Water use in Virginia; Surface-water and ground-water withdrawals during 1992: U.S. Geological Survey Fact Sheet 94–057, 2 p.

Hammond, E.C., McFarland, E.R., and Focazio, M.J., 1994a, Potentiometric surface of the Brightseat-upper Potomac aquifer in Virginia, 1993: U.S. Geological Survey Open-File Report 94–370, 1 p.

Hammond, E.C., McFarland, E.R., and Focazio, M.J., 1994b, Potentiometric surface of the lower Potomac aquifer in Virginia, 1993: U.S. Geological Survey Open-File Report 94–373, 1 p.

Hammond, E.C., McFarland, E.R., and Focazio, M.J., 1994c, Potentiometric surface of the middle Potomac aquifer in Virginia, 1993: U.S. Geological Survey Open-File Report 94–372, 1 p.

Hanor, J.S., 1983, Fifty years of development of thought on the origin and evolution of subsurface sedimentary brines, *in* Boardman, S.J., ed., Revolution in the earth sciences; Advances in the past half-century: Dubuque, Iowa, Kendall/Hunt, p. 99–111.

Hanshaw, B.B., and Coplen, T.B., 1973, Ultrafiltration by a compacted clay membrane; II. Sodium ion exclusion at various ionic strengths: Geochimica et Cosmochimica Acta, v. 37, no. 10, p. 2311–2327.

Harsh, J.F., and Laczniak, R.J., 1990, Conceptualization and analysis of ground-water flow system in the coastal plain of Virginia and adjacent parts of Maryland and North Carolina: U.S. Geological Survey Professional Paper 1404–F, p. F1–F100. (Also available online at http://water.usgs.gov/pubs/pp/pp1404-f/)

Hem, J.D., 1985, Study and interpretation of the chemical characteristics of natural water (3d ed.): U.S. Geological Survey Water-Supply Paper 2254, 263 p. (Also available online at http://water.usgs.gov/pubs/wsp/wsp2254/)

Henry, H.R., 1960, Salt water intrusion into coastal aquifers: International Association of Scientific Hydrology Publication 52, p. 478–487.

Herzberg, Alexander, 1901, Die Wasserversorgung einiger Nordseebader [The water supply of parts of the North Sea Coast]: Journal für Gasbeleuchtung und verwandte Beleuchtungsarten sowie für Wasserversorgung, v. 44, p. 815–819; v. 45, p. 842–844.

Heywood, C.E., 2003, Influence of the Chesapeake Bay impact structure on ground-water flow and salinity in the Atlantic Coastal Plain aquifer system of Virginia, *in* Proceedings of MODFLOW and More 2003; Understanding through Modeling: Golden, Colo., International Ground Water Modeling Center, p. 871–875.

Hubbert, M.K., 1940, The theory of ground-water motion: Journal of Geology, v. 48, no. 8, pt. 1, p. 785–944.

Johnson, G.H., Kruse, S.E., Vaughn, A.W., Lucey, J.K., Hobbs, C.H., III, and Powars, D.S., 1998, Postimpact deformation associated with the late Eocene Chesapeake Bay impact structure in southeastern Virginia: Geology, v. 26, no. 6, p. 507–510.

Jones, B.F., Vengosh, A., Rosenthal, E., and Yechieli, Y., 1999, Geochemical investigations, *in* Bear, Jacob, Cheng, A.H.-D., Sorek, Shaul, Ouazar, Driss, and Herrera, Ismael, eds., Seawater intrusion in coastal aquifers; Concepts, methods, and practices: Dordrecht, The Netherlands, Kluwer Academic Publishers, p. 43–63.

Kooi, H., Groen, J., and Leijnse, A., 2000, Modes of seawater intrusion during transgressions: Water Resources Research, v. 36, no. 12, p. 3581–3589.

Larson, J.D., 1981, Distribution of saltwater in the coastal plain aquifers of Virginia: U.S. Geological Survey Open-File Report 81–1013, 25 p., 2 oversize pls.

Manheim, F.T., Brooks, E.G., and Winters, W.J., 1994, Description of a hydraulic sediment squeezer: U.S. Geological Survey Open-File Report 94–584, 39 p.

Manheim, F.T., and Horn, M.K., 1968, Composition of deeper subsurface waters along the Atlantic continental margin: Southeastern Geology, v. 9, no. 4, p. 215–236.

McFarland, E.R., 1998, Design, revisions, and considerations for continued use of a ground-water-flow model of the coastal plain aquifer system in Virginia: U.S. Geological Survey Water-Resources Investigations Report 98–4085, 49 p. (Also available online at http://va.water.usgs.gov/online_pubs/WRIR/98-4085/g-wfmcpasys_va.html)

Meisler, Harold, 1989, The occurrence and geochemistry of salty ground water in the northern Atlantic Coastal Plain: U.S. Geological Survey Professional Paper 1404–D, p. D1–D51, 6 oversize pls.

Meng, A.A., III, and Harsh, J.F., 1988, Hydrogeologic framework of the Virginia Coastal Plain: U.S. Geological Survey Professional Paper 1404–C, p. C1–C82, 4 oversize pls. (Also available online at http://pubs.water.usgs.gov/pp1404-C/)

Neuzil, C.E., 2000, Osmotic generation of "anomalous" subsurface fluid pressures in geological environments: Nature, v. 403, no. 6766, p. 182–184.

Phillips, F.M., Bentley, H.W., and Elmore, David, 1986, Chlorine-36 dating of old ground water in sedimentary basins, *in* Hitchon, Brian, Bachu, Stefan, and Sauveplane, C.M., eds., Hydrogeology of sedimentary basins; Application to exploration and exploitation [Proceedings of the Third Canadian/American Conference on Hydrogeology, Banff, Alberta, Canada, June 22–26, 1986]: Dublin, Ohio, National Water Well Association, p. 143–150.

Pinder, G.F., and Cooper, H.H., Jr., 1970, A numerical technique for calculating the transient position of the saltwater front: Water Resources Research, v. 6, no. 3, p. 875–882.

Powars, D.S., 2000, The effects of the Chesapeake Bay impact crater on the geologic framework and the correlation of hydrogeologic units of southeastern Virginia, south of the James River: U.S. Geological Survey Professional Paper 1622, 53 p., 1 oversize pl. (Also available online at http://pubs.usgs.gov/prof/p1622/)

Powars, D.S., and Bruce, T.S., 1999, The effects of the Chesapeake Bay impact crater on the geological framework and

correlation of hydrogeologic units of the lower York-James Peninsula, Virginia: U.S. Geological Survey Professional Paper 1612, 82 p., 9 oversize pls. (Also available online at http://pubs.usgs.gov/prof/p1612/)

Purdy, C.B., Helz, G.R., Mignerey, A.C., Kubnuk, P.W., Elmore, David, Sharma, Pankaj, and Hemmick, Thomas, 1996, Aquia aquifer dissolved Cl^- and $^{36}Cl/Cl$; Implications for flow velocities: Water Resources Research, v. 32, no. 5, p. 1163–1171.

Rogers, W.S., and Spencer, R.S., 1971, Ground-water quality and structural control in southeastern Virginia: Geological Society of America Bulletin, v. 82, no. 8, p. 2313–2318.

Russel, W.L., 1933, Subsurface concentration of chloride brines: American Association of Petroleum Geologists Bulletin, v. 17, p. 1213–1228.

Sanford, Samuel, 1913, The underground-water resources of the Coastal Plain province of Virginia: Virginia Geological Survey Bulletin 5, 361 p.

Sanford, Ward, 2003, Heat flow and brine generation following the Chesapeake Bay bolide impact: Journal of Geochemical Exploration, v. 78–79, p. 243–247.

Smith, B.S., 1999, The potential for saltwater intrusion in the Potomac aquifers of the York-James Peninsula, Virginia: U.S. Geological Survey Water-Resources Investigations Report 98–4187, 24 p.

Stover, S.C., Ge, Shemin, Weimer, Paul, and McBride, B.C., 2001, The effects of salt evolution, structural development, and fault propagation on late Mesozoic-Cenozoic oil migration; A two-dimensional fluid-flow study along a megaregional profile in the northern Gulf of Mexico basin: American Association of Petroleum Geologists Bulletin, v. 85, no. 11, p. 1945–1966.

U.S. Environmental Protection Agency, 1990, Secondary maximum contaminant levels (section 143.3 of part 143, National secondary drinking water regulations): U.S. Code of Federal Regulations, Title 40, Parts 100 to 149, revised as of July 1, 1990, p. 674.

Winner, M.D., Jr., and Coble, R.W., 1996, Hydrogeologic framework of the North Carolina Coastal Plain: U.S. Geological Survey Professional Paper 1404–I, p. I1–I106, 24 oversize pls.

Table K1. Chemical Data for Sediment-Core Water and Well Water along the Western Margin of the Chesapeake Bay Impact Structure in Eastern Virginia

Table K1 contains data on ground water extracted during 2000–2001 from sediment cores obtained along the western margin of the Chesapeake Bay impact structure and on ground water collected during 1967–2002 from existing water wells in adjacent areas (fig. K1). All three core sites (site numbers 59E 31 (USGS-NASA Langley), 59H 3 (North), and 60G 5–6 (Bayside)) are within the crater's outer margin. Seventeen wells are near the crater's outer margin, and most of them are outside it. Two wells (63F 52–53) are within the central crater and are closer to the center of the impact structure than any of the other sites. Although well-sample collection times span 35 years, the well data generally represent current conditions.

Sampling and analytical techniques are described in the section on "Methods." Selected samples of sediment-core water were analyzed as follows:

- Concentrations of chloride, bromide, and iodide were determined by colorimetry by Glenda Brown and Ted Struzeski of the USGS National Water-Quality Laboratory (NWQL)
- Stable-isotope ratios, in per mil relative to Vienna Standard Mean Ocean Water (Fritz and Fontes, 1980), of the hydrogen isotope deuterium (expressed as δD) and oxygen (expressed as $\delta^{18}O$) were determined by mass spectrometry by Tyler Coplen of the USGS Isotope Research Laboratory
- Isotope ratios of chlorine-36 to total chloride ($^{36}Cl/Cl$) were determined by accelerator mass spectrometry by David Elmore of the Purdue Rare Isotope Measurement Laboratory (PRIME Lab)

Existing ground-water quality data collected from water wells during 1967–2002 were retrieved from the USGS water-quality database (http://waterdata.usgs.gov/va/nwis/qw).

Table K1. Chemical data for sediment-core water and well water along the western margin of the Chesapeake Bay impact structure in eastern Virginia.

[µS, microsiemens; mg/L, milligrams per liter; conc., concentration; Br/Cl, bromide to chloride; I/Cl, iodide to chloride; δD, delta deuterium; $\delta^{18}O$, delta oxygen-18; ‰, per mil; $^{36}Cl/Cl$, chlorine-36 to total chloride; $^{36}Cl/Cl$ ratios shown as <1 indicate ratios below the analytical detection limit of 10^{-15}; blank entries indicate no data]

Sample or well number	Depth to sample top (meters)	Depth to sample top (feet)	Depth to sample bottom (meters)	Depth to sample bottom (feet)	Geologic formation	Specific conductance (µS)	Chloride conc. (mg/L)	Bromide conc. (mg/L)	Br/Cl ratio ($x10^{-3}$)	Iodide conc. (mg/L)	I/Cl ratio ($x10^{-5}$)	δD (‰)	$\delta^{18}O$ (‰)	$^{36}Cl/Cl$ ratio ($x10^{-15}$)	Remarks
USGS-NASA Langley core pore water (well number 59E 31, drilled in 2000)															
1	15.6	51.3	15.8	51.8	Yorktown	1,918									Shelly fine sand
5	31.8	104.3	31.9	104.8	Eastover	3,390	216								Medium sand; poor cohesion
10	45.8	150.2	45.9	150.7	Eastover	6,260								<1	Medium sand; poor cohesion
12	53.1	174.2	53.2	174.7	Eastover	8,820						–22.8	–4.56		Medium sand; poor cohesion
14	59.7	195.9	59.9	196.4	Eastover	10,950								<1	Silty very fine sand
15	63.2	207.5	63.4	208.0	Eastover	11,890									Fine to medium sand
17	74.5	244.4	74.6	244.9	Saint Marys	14,200	3,960	15.3	3.87	0.377	9.52				Silty very fine sand
22	90.7	297.6	90.9	298.1	Saint Marys	15,230									Clay and shell
29	111.1	364.6	111.3	365.1	Saint Marys	16,450								<1	Clay
33	120.9	396.5	121.0	397.0	Saint Marys	16,950									Silty fine sand
36	130.1	426.8	130.2	427.3	Calvert	18,150									Silty fine sand
38	135.8	445.5	135.9	446.0	Calvert	17,530									Clayey fine sand
39	139.6	457.9	139.7	458.4	Calvert	16,240									Silty fine sand and shell
40	142.2	466.5	142.3	467.0	Calvert	18,180									Silty fine to medium sand, shell
41	143.7	471.3	143.8	471.8	Old Church	17,450									Glauconitic/phosphatic sand
42	145.8	478.4	146.0	478.9	Old Church	18,420									Glauconitic/phosphatic sand
43	150.7	494.5	150.9	495.0	Old Church	18,370	5,360	21.9	4.09	0.725	13.5				Glauconitic/phosphatic sand
44	152.5	500.3	152.6	500.8	Old Church	18,810									Glauconitic/phosphatic sand
45	157.6	517.2	157.8	517.7	Old Church	17,850									Glauconitic/phosphatic sand
46	160.4	526.2	160.5	526.7	Old Church	19,770									Glauconitic/phosphatic sand
47	162.8	534.0	162.9	534.5	Old Church	18,070									Glauconitic/phosphatic sand
48	167.6	549.9	167.8	550.4	Old Church	16,270									Glauconitic/phosphatic sand
49	171.3	562.0	171.5	562.5	Old Church	17,800									Glauconitic/phosphatic sand
51	181.7	596.0	181.8	596.5	Drummonds Corner beds	22,100									Glauconitic/phosphatic sand
52	184.9	606.6	185.0	607.1	Chickahominy	22,100									Dense clay
53	189.7	622.3	189.8	622.8	Chickahominy	18,270								<1	Dense clay
54	194.7	638.9	194.9	639.4	Chickahominy	18,640									Dense clay
55	196.8	645.8	197.0	646.3	Chickahominy	18,640									Dense clay
56	199.1	653.1	199.2	653.6	Chickahominy	19,800									Dense clay
57	203.3	667.1	203.5	667.6	Chickahominy	21,200									Dense clay
58	205.0	672.6	205.2	673.1	Chickahominy	22,000									Dense clay
59	209.4	687.1	209.6	687.6	Chickahominy	21,400									Dense clay

Table K1. Chemical data for sediment-core water and well water along the western margin of the Chesapeake Bay impact structure in eastern Virginia.—Continued

[µS, microsiemens; mg/L, milligrams per liter; conc., concentration; Br/Cl, bromide to chloride; I/Cl, iodide to chloride; δD, delta deuterium; $\delta^{18}O$, delta oxygen-18; ‰, per mil; $^{36}Cl/Cl$, chlorine-36 to total chloride; $^{36}Cl/Cl$ ratios shown as <1 indicate ratios below the analytical detection limit of 10^{-15}; blank entries indicate no data]

Sample or well number	Depth to sample top		Depth to sample bottom		Geologic formation	Specific conductance (µS)	Chloride conc. (mg/L)	Bromide conc. (mg/L)	Br/Cl ratio ($x10^{-3}$)	Iodide conc. (mg/L)	I/Cl ratio ($x10^{-5}$)	δD (‰)	$\delta^{18}O$ (‰)	$^{36}Cl/Cl$ ratio ($x10^{-15}$)	Remarks
	(meters)	(feet)	(meters)	(feet)											
USGS-NASA Langley core pore water (well number 59E 31, drilled in 2000)—Continued															
98	339.5	1,113.7	339.6	1,114.2	Crater unit B	12,700									Clay clast
99	341.5	1,120.5	341.7	1,121.0	Crater unit B	18,820									Sand clast
100	347.0	1,138.3	347.1	1,138.8	Crater unit B	5,930									Sand clast
101	348.3	1,142.7	348.4	1,143.2	Crater unit B	15,610									Clayey sand clast
102	351.2	1,152.2	351.3	1,152.7	Crater unit B	16,100									Sand clast
103	354.2	1,162.2	354.4	1,162.7	Crater unit B	14,440									Sand clast
104	357.7	1,173.7	357.9	1,174.2	Crater unit B	17,660									Clayey sand clast
105	359.8	1,180.3	359.9	1,180.8	Crater unit B	15,340	6,180	22.5	3.65	0.0233	0.377				Sand clast
106	360.8	1,183.7	360.9	1,184.2	Crater unit B	16,760									Clayey fine sand clast
107	364.4	1,195.6	364.6	1,196.1	Crater unit B	18,330									Clayey sand clast
108	365.9	1,200.5	366.1	1,201.0	Crater unit B	15,750								<1	Sand clast
109	419.3	1,375.7	419.5	1,376.2	Crater unit B	17,060	5,620	22.3	3.96	0.169	3.00				Sand and clay
110	422.5	1,386.1	422.6	1,386.6	Crater unit B	19,700									Silty fine sand clast
111	426.1	1,398.1	426.3	1,398.6	Crater unit B	7,550									Medium to coarse sand clast
112	428.0	1,404.1	428.1	1,404.6	Crater unit B	21,000									Medium sand clast
113	430.7	1,413.0	430.8	1,413.5	Crater unit B	12,420									Clay clast
114	434.6	1,426.0	434.8	1,426.5	Crater unit B	16,670						–19.0	–3.60		Clayey fine sand clast
115	438.7	1,439.2	438.8	1,439.7	Crater unit B	21,400								<1	Silty fine sand clast
116	507.9	1,666.5	508.0	1,666.7	Crater unit A	32,600								<1	Sand
117	527.7	1,731.4	527.8	1,731.6	Crater unit A	26,800	9,850	39.0	3.96	0.703	7.13				Clay
118	531.1	1,742.6	531.2	1,742.8	Crater unit A	31,100									Sand
119	534.0	1,752.0	534.1	1,752.2	Crater unit A	36,800									Sand
120	552.2	1,811.6	552.3	1,812.0	Crater unit A	37,700									Medium sand
121	555.3	1,822.0	555.5	1,822.5	Crater unit A	19,180									Medium to coarse sand
122	569.0	1,866.8	569.2	1,867.3	Crater unit A	33,400								<1	Medium to coarse sand
123	572.3	1,877.5	572.4	1,878.0	Crater unit A	23,200									Medium to coarse sand
124	574.5	1,885.0	574.7	1,885.5	Crater unit A	29,800									Medium to coarse sand
125	576.7	1,892.0	576.8	1,892.5	Crater unit A	25,500									Medium sand
126	582.8	1,912.0	582.9	1,912.5	Crater unit A	30,800	12,200	44.5	3.66	1.18	9.67				Clay
127	593.1	1,945.9	593.3	1,946.4	Crater unit A	41,400						–9.30	–2.21		Silty fine to medium sand
128	596.6	1,957.5	596.8	1,958.0	Crater unit A	37,000									Medium sand
129	599.1	1,965.5	599.2	1,966.0	Crater unit A	42,500								<1	Medium to coarse sand
130	602.9	1,978.0	603.0	1,978.5	Crater unit A	40,000									Medium to coarse sand
131	605.1	1,985.4	605.3	1,985.9	Crater unit A	41,300	18,000	80.7	4.48	1.80	9.98				Medium to coarse sand
132	608.7	1,997.0	608.8	1,997.5	Crater unit A	42,000									Medium to coarse sand
133	613.1	2,011.5	613.3	2,012.0	Crater unit A	39,700									Clayey fine to medium sand
134	624.8	2,050.0	624.9	2,050.3	Crater unit A	35,500									Clayey medium sand

Table K1. Chemical data for sediment-core water and well water along the western margin of the Chesapeake Bay impact structure in eastern Virginia.—Continued

[µS, microsiemens; mg/L, milligrams per liter; conc., concentration; Br/Cl, bromide to chloride; I/Cl, iodide to chloride; δD, delta deuterium; $\delta^{18}O$, delta oxygen-18; ‰, per mil; $^{36}Cl/Cl$, chlorine-36 to total chloride; $^{36}Cl/Cl$ ratios shown as <1 indicate ratios below the analytical detection limit of 10^{-15}; blank entries indicate no data]

Sample or well number	Depth to sample top (meters)	Depth to sample top (feet)	Depth to sample bottom (meters)	Depth to sample bottom (feet)	Geologic formation	Specific conductance (µS)	Chloride conc. (mg/L)	Bromide conc. (mg/L)	Br/Cl ratio ($x10^{-3}$)	Iodide conc. (mg/L)	I/Cl ratio ($x10^{-5}$)	δD (‰)	$\delta^{18}O$ (‰)	$^{36}Cl/Cl$ ratio ($x10^{-15}$)	Remarks
USGS-NASA Langley core pore water (well number 59E 31, drilled in 2000)—Continued															
60	211.1	692.5	211.4	693.5	Chickahominy	21,800									Dense clay
61	214.4	703.5	214.7	704.5	Chickahominy	22,800									Dense clay
62	221.3	725.9	221.4	726.4	Chickahominy	22,700									Dense clay
63	224.3	735.9	224.5	736.4	Chickahominy	21,700									Dense clay
64	227.0	744.6	227.1	745.1	Chickahominy	22,000								<1	Dense clay
65	229.5	752.8	229.6	753.3	Chickahominy	19,570									Dense clay
66	232.6	763.0	232.8	763.7	Chickahominy	22,400						–18.7	–3.79		Dense clay
67	238.2	781.6	238.4	782.3	Exmore beds	22,500	6,480	26.6	4.11	0.634	9.77				Matrix
68	243.0	797.4	243.2	797.9	Exmore beds	19,250									Matrix
69	244.8	803.1	244.9	803.6	Exmore beds	19,480									Matrix
71	248.6	815.6	248.8	816.3	Exmore beds	19,410									Matrix
72	250.7	822.6	250.9	823.3	Exmore beds	19,440									Matrix
73	253.4	831.4	253.6	832.1	Exmore beds	18,870									Matrix
74	257.7	845.4	257.9	846.1	Exmore beds	18,900									Matrix
75	260.0	853.1	260.3	853.9	Exmore beds	21,400								<1	Matrix
76	263.7	865.1	263.9	865.9	Exmore beds	11,470									Clay clast
78	267.9	879.1	268.2	879.8	Exmore beds	12,380									Clay clast
79	269.1	882.8	269.2	883.3	Exmore beds	17,260	6,340	23.5	3.71	0.661	10.4				Sand clast
80	272.7	894.7	272.9	895.5	Crater unit B	9,970									Clay clast
81	275.0	902.2	275.2	903.0	Crater unit B	11,530									Clay clast
82	278.0	912.0	278.2	912.8	Crater unit B	16,930									Medium to coarse sand clast
83	281.9	925.0	282.2	925.7	Crater unit B	10,530									Clay clast
84	285.3	936.0	285.4	936.5	Crater unit B	14,960									Clayey sand clast
85	286.9	941.2	287.1	942.0	Crater unit B	10,550									Clay clast
86	291.0	954.7	291.2	955.4	Crater unit B	15,220									Clayey sand clast
87	294.5	966.3	294.8	967.1	Crater unit B	10,960									Clay clast
88	297.9	977.2	298.0	977.7	Crater unit B	17,500									Clayey sand clast
89	300.0	984.2	300.1	984.7	Crater unit B	14,090									Silty fine sand clast
90	302.9	993.8	303.1	994.5	Crater unit B	12,590						–20.1	–4.02		Clay clast
91	307.1	1,007.4	307.3	1,008.2	Crater unit B	12,550	4,740								Clay clast
92	308.8	1,013.1	308.9	1,013.6	Crater unit B	14,630									Clay clast
93	311.9	1,023.2	312.0	1,023.7	Crater unit B	17,610									Sand clast
94	315.1	1,033.7	315.2	1,034.2	Crater unit B	14,580								<1	Clay clast
95	334.0	1,095.7	334.1	1,096.2	Crater unit B	14,100									Clay clast
96	336.1	1,102.7	336.3	1,103.2	Crater unit B	8,680									Clayey sand clast
97	338.2	1,109.7	338.4	1,110.2	Crater unit B	12,260									Clay clast

Table K1. Chemical data for sediment-core water and well water along the western margin of the Chesapeake Bay impact structure in eastern Virginia.—Continued

[µS, microsiemens; mg/L, milligrams per liter; conc., concentration; Br/Cl, bromide to chloride; I/Cl, iodide to chloride; δD, delta deuterium; $\delta^{18}O$, delta oxygen-18; ‰, per mil; $^{36}Cl/Cl$, chlorine-36 to total chloride; $^{36}Cl/Cl$ ratios shown as <1 indicate ratios below the analytical detection limit of 10^{-15}; blank entries indicate no data]

Sample or well number	Depth to sample top (meters)	Depth to sample top (feet)	Depth to sample bottom (meters)	Depth to sample bottom (feet)	Geologic formation	Specific conductance (µS)	Chloride conc. (mg/L)	Bromide conc. (mg/L)	Br/Cl ratio ($x10^{-3}$)	Iodide conc. (mg/L)	I/Cl ratio ($x10^{-5}$)	δD (‰)	$\delta^{18}O$ (‰)	$^{36}Cl/Cl$ ratio ($x10^{-15}$)	Remarks
Bayside #1 core pore water (well number 60G 5, drilled in 2001)—Continued															
165	107.6	353.0	107.7	353.5	Calvert	20,700	7,200	18.5	2.57	1.00	13.9				Clayey silt
166	119.2	391.0	119.3	391.5	Calvert	20,700									Silty fine sand
167	141.4	464.0	141.6	464.5	Calvert	20,900									Silty fine sand
169	156.6	513.7	156.7	514.2	Calvert	20,400	7,110	28.5	4.00	1.02	14.4				Silty fine sand
170	171.2	561.7	171.4	562.2	Old Church	20,800									Glauconitic sand
171	187.8	616.0	187.9	616.5	Old Church	22,500									Glauconitic sand
172	205.6	674.5	205.7	675.0	Old Church	25,100									Glauconitic sand
173	221.4	726.5	221.6	727.0	Chickahominy	26,400	11,200	45.5	4.07	1.66	14.8				Dense clay
174	241.9	793.5	242.0	794.0	Chickahominy	26,700						−14.4	−2.71		Dense clay
175	259.8	852.4	260.0	852.9	Chickahominy	38,500	13,700								Dense clay
176	276.1	905.7	276.2	906.2	Chickahominy	39,500						−11.3	−2.51		Dense clay
177	294.1	965.0	294.3	965.5	Exmore beds	41,200									Matrix
179	308.6	1,012.6	308.8	1,013.1	Exmore beds	42,200	16,500	69.2	4.19	2.51	15.2				Matrix
180	327.4	1,074.3	327.6	1,074.8	Exmore beds	44,800									Matrix
181	343.1	1,125.5	343.2	1,126.0	Exmore beds	47,300						−7.80	−1.79		Matrix
Bayside #2 core pore water (well number 60G 6, drilled in 2001)															
182	357.3	1,172.4	357.5	1,172.9	Exmore beds	46,600									Matrix
183	379.1	1,243.8	379.3	1,244.3	Exmore beds	47,600	18,600	74.0	3.97	1.05	5.67				Silty sand clast
184	397.2	1,303.0	397.3	1,303.5	Exmore beds	40,300	14,700	62.2	4.23	2.09	14.2				Sand clast
185	414.8	1,361.0	415.0	1,361.5	Exmore beds	42,500									Clay clast
186	443.2	1,454.0	443.3	1,454.5	Exmore beds	42,000						−7.60	−1.52		Clay clast
187	465.0	1,525.5	465.1	1,526.0	Exmore beds	47,200									Silty sand clast
188	473.4	1,553.0	473.5	1,553.5	Exmore beds	45,000	18,900	78.4	4.14	1.49	7.87				Clay clast
189	498.6	1,635.7	498.7	1,636.2	Exmore beds	46,000									Clay clast
190	519.4	1,704.0	519.5	1,704.5	Exmore beds	46,500									Sand clast
191	545.3	1,789.2	545.5	1,789.7	Exmore beds	47,400	18,800	78.6	4.18	2.61	13.9				Sand clast
192	565.3	1,854.5	565.4	1,855.0	Exmore beds	37,200	14,200	58.4	4.12	1.19	8.37				Clay clast
193	588.9	1,932.1	589.1	1,932.6	Exmore beds	40,800						−7.90	−1.38		Silty sand clast
194	615.9	2,020.7	616.1	2,021.2	Exmore beds	51,400	21,800	91.4	4.19	2.92	13.4				Sand clast
195	647.1	2,123.0	647.2	2,123.5	Exmore beds	51,700						−6.70	−0.95		Sand clast
197	688.7	2,259.4	688.8	2,259.9	Exmore beds	51,500	21,500	93.8	4.37	1.30	6.06				Indurated sand

Table K1. Chemical data for sediment-core water and well water along the western margin of the Chesapeake Bay impact structure in eastern Virginia.—Continued

[µS, microsiemens; mg/L, milligrams per liter; conc., concentration; Br/Cl, bromide to chloride; I/Cl, iodide to chloride; δD, delta deuterium; $\delta^{18}O$, delta oxygen-18; ‰, per mil; $^{36}Cl/Cl$, chlorine-36 to total chloride; $^{36}Cl/Cl$ ratios shown as <1 indicate ratios below the analytical detection limit of 10^{-15}; blank entries indicate no data]

Sample or well number	Depth to sample top (meters)	Depth to sample top (feet)	Depth to sample bottom (meters)	Depth to sample bottom (feet)	Geologic formation	Specific conductance (µS)	Chloride conc. (mg/L)	Bromide conc. (mg/L)	Br/Cl ratio ($x10^{-3}$)	Iodide conc. (mg/L)	I/Cl ratio ($x10^{-5}$)	δD (‰)	$\delta^{18}O$ (‰)	$^{36}Cl/Cl$ ratio ($x10^{-15}$)	Remarks
North core pore water (well number 59H 3, drilled in 2001)															
136	4.2	13.7	4.3	14.2	Eastover	1,031	99.6	0.091	0.92	0.163	16.4				Silty very fine sand
137	19.2	62.9	19.3	63.4	Eastover	1,101						–30.2	–5.38		Medium sand; poor cohesion
138	43.2	141.7	43.3	142.2	Eastover	1,369									Fine to medium shelly sand
139	74.0	242.7	74.1	243.2	Saint Marys	1,842	229								Clay
140	99.8	327.5	100.0	328.0	Calvert	2,050									Clayey fine sand
141	118.2	387.9	118.4	388.4	Calvert	3,560	304								Clayey fine sand
142	142.6	468.0	142.8	468.5	Old Church	2,860									Glauconitic/phosphatic sand
143	153.2	502.5	153.3	503.0	Old Church	5,300	434								Glauconitic/phosphatic sand
144	157.9	517.9	158.0	518.4	Chickahominy	3,190	394								Dense clay
145	175.0	574.0	175.1	574.5	Chickahominy	4,020									Dense clay
146	189.6	622.0	189.7	622.5	Chickahominy	4,050									Dense clay
147	217.5	713.5	217.6	714.0	Chickahominy	4,870	945	1.67	1.77	0.133	14.1				Dense clay
148	231.4	759.1	231.5	759.6	Exmore beds	5,140						–32.1	–5.54		Matrix
149	246.1	807.5	246.3	808.0	Exmore beds	5,660	1,230	4.96	4.03	0.279	22.7				Matrix
150	259.6	851.7	259.8	852.2	Crater unit B	4,240	1,100								Clay clast
151	273.3	896.7	273.5	897.2	Crater unit B	5,740									Sand clast
152	302.7	993.0	302.8	993.5	Crater unit B	3,040	761								Clay clast
154	318.5	1,044.8	318.6	1,045.3	Crater unit B	3,490									Clay clast
155	329.2	1,080.1	329.4	1,080.6	Crater unit A	8,560									Sand clast
156	353.0	1,158.0	353.1	1,158.5	Crater unit A	6,120									Sand
157	367.1	1,204.5	367.3	1,205.0	Crater unit A	6,210									Silty very fine sand
158	383.1	1,256.8	383.2	1,257.3	Crater unit A	10,250	3,130	12.7	4.06	0.396	12.7				Sand
159	404.4	1,326.7	404.5	1,327.2	Crater unit A	8,680						–29.2	–4.86		Sand
160	421.5	1,383.0	421.7	1,383.5	Crater unit A	5,500	1,400			0.231	16.5				Sand
161	433.6	1,422.5	433.7	1,423.0	Crater unit A	13,620	4,650	13.8	2.98	0.560	12.1				Sand
Bayside #1 core pore water (well number 60G 5, drilled in 2001)															
162	58.5	192.0	58.7	192.5	Eastover	13,870	3,600	13.5	3.75	0.230	6.40				Silty fine sand
163	75.0	246.0	75.1	246.5	Saint Marys	18,420						–22.2	–3.91		Clayey sand
164	90.2	296.0	90.4	296.5	Saint Marys	20,000									Silty clay

Table K1. Chemical data for sediment-core water and well water along the western margin of the Chesapeake Bay impact structure in eastern Virginia.—Continued

[μS, microsiemens; mg/L, milligrams per liter; conc., concentration; Br/Cl, bromide to chloride; I/Cl, iodide to chloride; δD, delta deuterium; $\delta^{18}O$, delta oxygen-18; ‰, per mil; $^{36}Cl/Cl$, chlorine-36 to total chloride; $^{36}Cl/Cl$ ratios shown as <1 indicate ratios below the analytical detection limit of 10^{-15}; blank entries indicate no data]

Sample or well number	Depth to sample top (meters)	Depth to sample top (feet)	Depth to sample bottom (meters)	Depth to sample bottom (feet)	Geologic formation	Specific conductance (μS)	Chloride conc. (mg/L)	Bromide conc. (mg/L)	Br/Cl ratio ($x10^{-3}$)	Iodide conc. (mg/L)	I/Cl ratio ($x10^{-5}$)	δD (‰)	$\delta^{18}O$ (‰)	$^{36}Cl/Cl$ ratio ($x10^{-15}$)	Remarks
							Water wells								
58E 3	160.0	525	166.1	545		2,140	420								Mulberry Island, 1978
58F 50	364.2	1,195	367.3	1,205		5,300	2,100								Lee Hall, 1984
58F 50	367.3	1,205	370.3	1,215		6,000	2,000								Lee Hall, 1986
58F 50	367.3	1,205	370.3	1,215		8,190	2,400	9.7	4.0						Lee Hall, 1996
58F 50	367.3	1,205	370.3	1,215		8,520	2,410	9.31	3.86						Lee Hall, 1997
58F 51	249.9	820	253.0	830		5,000	1,300								Lee Hall, 1984
58F 51	249.9	820	253.0	830		4,860	1,300	5.3	4.1						Lee Hall, 1986
58F 51	251.5	825	254.5	835		3,800	1,400								Lee Hall, 1996
58F 52	160.6	527	163.7	537		2,400	540								Lee Hall, 1984
58F 52	160.6	527	163.7	537		2,200	500								Lee Hall, 1986
58F 52	160.6	527	163.7	537		2,430	490	1.9	3.9						Lee Hall, 1996
58F 52	160.6	527	163.7	537		2,460	502	1.91	3.80						Lee Hall, 1997
58F 53	101.5	333	104.5	343		1,700	160								Lee Hall, 1984
58F 53	101.5	333	104.5	343		1,686	150	0.63	4.2						Lee Hall, 1996
58F 54	23.8	78	26.8	88		460	17								Lee Hall, 1984
58F 81	213.4	700	214.9	705		5,740	1,500	5.8	3.9						Filtration plant, 1995
58F 81	247.5	812	249.0	817		6,040	1,700	6.3	3.7						Filtration plant, 1995
58F 81	303.0	994	304.5	999		7,180	2,100	7.8	3.7						Filtration plant, 1995
58F 81	345.0	1,132	346.6	1,137		8,430	2,400	9.3	3.9						Filtration plant, 1995
58F 81	372.5	1,222	384.7	1,262		10,490	3,300	13	3.9						Filtration plant, 1995
58F 82	237.7	780	239.3	785		7,190	2,000	7.5	3.7						Remote site, 1995
58F 82	367.3	1,205	368.8	1,210		9,050	2,600	10	3.8						Remote site, 1995
58F 89	310.1	1,017.4	344.7	1,131		6,230									Skiffes Creek, 1998
58F 92	161.5	530	170.7	560		2,300	470	1.6	3.4						Skiffes Creek, 1996
58F 93	274.9	902	284.1	932		4,870	1,300	4.93	3.80						Skiffes Creek, 2000
58F127	149.0	489	170.7	560		2,030	387	1.37	3.54						Skiffes Creek, 2000

Table K1. Chemical data for sediment-core water and well water along the western margin of the Chesapeake Bay impact structure in eastern Virginia.—Continued

[µS, microsiemens; mg/L, milligrams per liter; conc., concentration; Br/Cl, bromide to chloride; I/Cl, iodide to chloride; δD, delta deuterium; $\delta^{18}O$, delta oxygen-18; ‰, per mil; $^{36}Cl/Cl$, chlorine-36 to total chloride; $^{36}Cl/Cl$ ratios shown as <1 indicate ratios below the analytical detection limit of 10^{-15}; blank entries indicate no data]

Sample or well number	Depth to sample top (meters)	Depth to sample top (feet)	Depth to sample bottom (meters)	Depth to sample bottom (feet)	Geologic formation	Specific conductance (µS)	Chloride conc. (mg/L)	Bromide conc. (mg/L)	Br/Cl ratio ($x10^{-3}$)	Iodide conc. (mg/L)	I/Cl ratio ($x10^{-5}$)	δD (‰)	$\delta^{18}O$ (‰)	$^{36}Cl/Cl$ ratio ($x10^{-15}$)	Remarks
Water wells—Continued															
59E 6	127.4	418	132.0	433		14,500	4,800								Big Bethel, 1984; shell & sand
59E 6	151.8	498	156.4	513		14,200	4,700								Big Bethel, 1984; black sand
59E 6	279.5	917	284.1	932		12,800	4,400								Big Bethel, 1984; coarse sand
59G 12	120.4	395	128.0	420		5,050	1,110								Gloucester Point, 1969
59G 12	120.4	395	128.0	420		4,780	1,100								Gloucester Point, 1972
59H 4	584.3	1,917	584.3	1,917		33,600						–17.3	–3.09		North, 2002
61C 1	258.5	848	264.6	868		3,900	964	3.7	3.8	0.4	41				Moores Bridge, 1967
61C 1	274.3	900	292.6	960		4,840	1,280	4.7	3.7	0.1	7.8				Moores Bridge, 1967
61C 1	287.4	943	293.5	963		5,080	1,380	4.9	3.6	0.4	29				Moores Bridge, 1968
61C 1	316.1	1,037	322.2	1,057		5,940	1,680	6.5	3.9	0.4	24				Moores Bridge, 1968
61C 1	382.5	1,255	389.2	1,277		12,600	4,200	16	3.8	0.8	19				Moores Bridge, 1968
61C 1	491.9	1,614	498.0	1,634		26,400	9,560	34	3.6	2.1	22				Moores Bridge, 1968
61C 1	728.8	2,391	735.2	2,412		61,300	26,000	98	3.8	3.7	14				Moores Bridge, 1968
61C 1	761.7	2,499	768.1	2,520		63,800	26,900	100	3.72	3.7	14				Moores Bridge, 1968
61D 5	367.9	1,207	416.7	1,367		28,700	10,200	36.8	3.63						Ferry Road, 2000
63F 52	395.3	1,297	401.4	1,317	Exmore beds	59,200	23,000	92.8	4.03						Kiptopeke, 1997; top of breccia
63F 52	395.3	1,297	401.4	1,317	Exmore beds	58,600	22,500	99	4.4	9.27	41.2	–4.6	–2.14	12.1	Kiptopeke, 2002; top of breccia
63F 53	64.0	210	67.1	220	Yorktown-Eastover aquifer	684	62.6	0.33	5.3						Kiptopeke, 1997; postimpact

A. Preimpact target

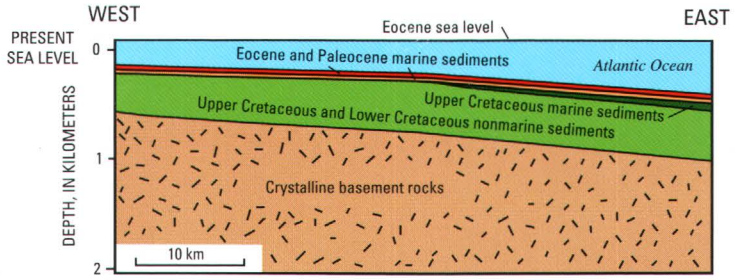

B. Contact compression followed by excavation

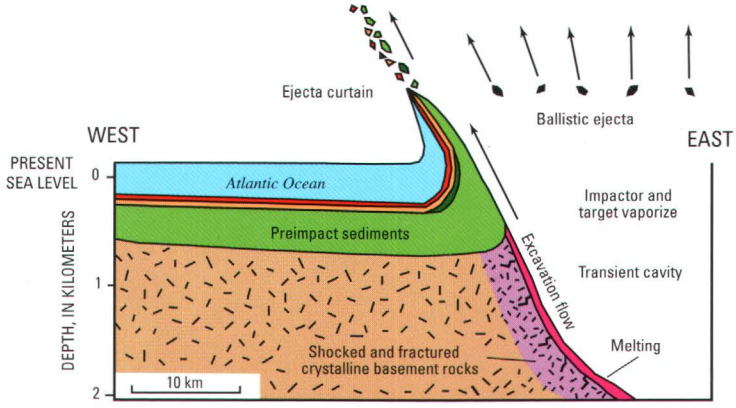

C. Crater modification (collapse, slump blocks, and water resurge)

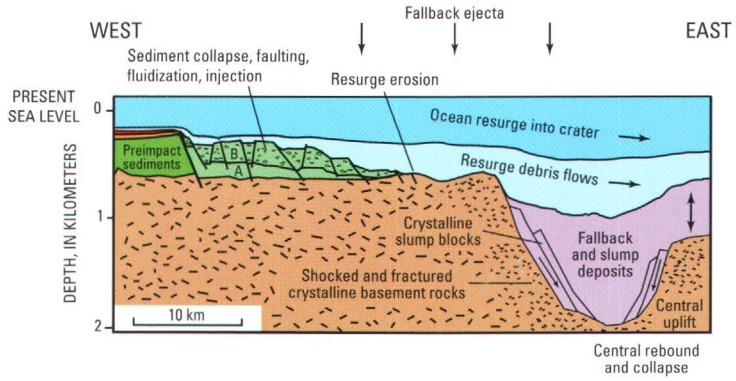

D. Postimpact burial

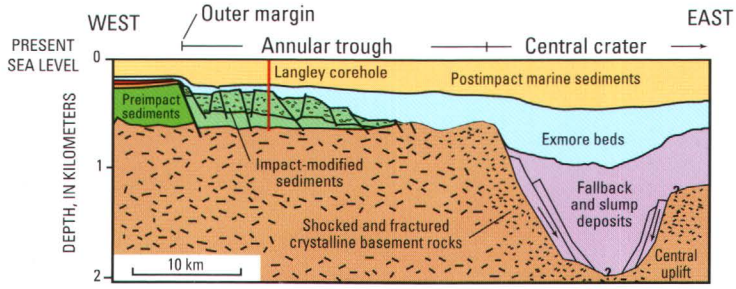

ISBN 0-607-98598-4